



*pharmaceutics*

# Advanced Blood-Brain Barrier Drug Delivery

---

Edited by

William M. Pardridge

Printed Edition of the Special Issue Published in *Pharmaceutics*

# **Advanced Blood-Brain Barrier Drug Delivery**



# Advanced Blood-Brain Barrier Drug Delivery

Editor

**William M. Pardridge**

MDPI • Basel • Beijing • Wuhan • Barcelona • Belgrade • Manchester • Tokyo • Cluj • Tianjin



*Editor*

William M. Pardridge  
Department of Medicine  
UCLA  
Los Angeles  
United States

*Editorial Office*

MDPI  
St. Alban-Anlage 66  
4052 Basel, Switzerland

This is a reprint of articles from the Special Issue published online in the open access journal *Pharmaceutics* (ISSN 1999-4923) (available at: [www.mdpi.com/journal/pharmaceutics/special\\_issues/abb](http://www.mdpi.com/journal/pharmaceutics/special_issues/abb)).

For citation purposes, cite each article independently as indicated on the article page online and as indicated below:

LastName, A.A.; LastName, B.B.; LastName, C.C. Article Title. <i>Journal Name</i> <b>Year</b> , <i>Volume Number</i> , Page Range.
--

**ISBN 978-3-0365-6417-3 (Hbk)**

**ISBN 978-3-0365-6416-6 (PDF)**

Cover image courtesy of ArmaGen, Inc

© 2023 by the authors. Articles in this book are Open Access and distributed under the Creative Commons Attribution (CC BY) license, which allows users to download, copy and build upon published articles, as long as the author and publisher are properly credited, which ensures maximum dissemination and a wider impact of our publications.

The book as a whole is distributed by MDPI under the terms and conditions of the Creative Commons license CC BY-NC-ND.

# Contents

<b>About the Editor</b> . . . . .	vii
<b>Preface to “Advanced Blood-Brain Barrier Drug Delivery”</b> . . . . .	ix
<b>William M. Pardridge</b> Advanced Blood–Brain Barrier Drug Delivery Reprinted from: <i>Pharmaceutics</i> <b>2022</b> , <i>15</i> , 93, doi:10.3390/pharmaceutics15010093 . . . . .	1
<b>William M. Pardridge</b> A Historical Review of Brain Drug Delivery Reprinted from: <i>Pharmaceutics</i> <b>2022</b> , <i>14</i> , 1283, doi:10.3390/pharmaceutics14061283 . . . . .	7
<b>Ruben J. Boado</b> IgG Fusion Proteins for Brain Delivery of Biologics via Blood–Brain Barrier Receptor-Mediated Transport Reprinted from: <i>Pharmaceutics</i> <b>2022</b> , <i>14</i> , 1476, doi:10.3390/pharmaceutics14071476 . . . . .	185
<b>Hiroyuki Sonoda, Kenichi Takahashi, Kohtaro Minami, Toru Hirato, Tatsuyoshi Yamamoto and Sairei So et al.</b> Treatment of Neuronopathic Mucopolysaccharidoses with Blood–Brain Barrier-Crossing Enzymes: Clinical Application of Receptor-Mediated Transcytosis Reprinted from: <i>Pharmaceutics</i> <b>2022</b> , <i>14</i> , 1240, doi:10.3390/pharmaceutics14061240 . . . . .	213
<b>Weijun Ou, Yuu Ohno, Joshua Yang, Devaraj V. Chandrashekar, Tamara Abdullah and Jiahong Sun et al.</b> Efficacy and Safety of a Brain-Penetrant Biologic TNF- Inhibitor in Aged APP/PS1 Mice Reprinted from: <i>Pharmaceutics</i> <b>2022</b> , <i>14</i> , 2200, doi:10.3390/pharmaceutics14102200 . . . . .	229
<b>Sahar Roshanbin, Ulrika Julku, Mengfei Xiong, Jonas Eriksson, Eliezer Masliah and Greta Hultqvist et al.</b> Reduction of SYN Pathology in a Mouse Model of PD Using a Brain-Penetrating Bispecific Antibody Reprinted from: <i>Pharmaceutics</i> <b>2022</b> , <i>14</i> , 1412, doi:10.3390/pharmaceutics14071412 . . . . .	249
<b>Emily Clarke, Pawel Stocki, Elizabeth H. Sinclair, Aziz Gauhar, Edward J. R. Fletcher and Alicja Krawczun-Rygmaczewska et al.</b> A Single Domain Shark Antibody Targeting the Transferrin Receptor 1 Delivers a TrkB Agonist Antibody to the Brain and Provides Full Neuroprotection in a Mouse Model of Parkinson’s Disease Reprinted from: <i>Pharmaceutics</i> <b>2022</b> , <i>14</i> , 1335, doi:10.3390/pharmaceutics14071335 . . . . .	265
<b>Alvaro Yogi, Greg Hussack, Henk van Faassen, Arsalan S. Haqqani, Christie E. Delaney and Eric Brunette et al.</b> Brain Delivery of IGF1R5, a Single-Domain Antibody Targeting Insulin-like Growth Factor-1 Receptor Reprinted from: <i>Pharmaceutics</i> <b>2022</b> , <i>14</i> , 1452, doi:10.3390/pharmaceutics14071452 . . . . .	281
<b>Julia V. Georgieva, Moriah Katt, Zhou Ye, Benjamin J. Umlauf, Cody J. Wenthur and Eric V. Shusta</b> The 46.1 Antibody Mediates Neurotensin Uptake into the CNS and the Effects Depend on the Route of Intravenous Administration Reprinted from: <i>Pharmaceutics</i> <b>2022</b> , <i>14</i> , 1706, doi:10.3390/pharmaceutics14081706 . . . . .	299

<b>Macarena Sánchez-Navarro and Ernest Giralt</b> Peptide Shuttles for Blood–Brain Barrier Drug Delivery Reprinted from: <i>Pharmaceutics</i> <b>2022</b> , <i>14</i> , 1874, doi:10.3390/pharmaceutics14091874 . . . . .	<b>317</b>
<b>Johanna Huttunen, Santosh Kumar Adla, Magdalena Markowicz-Piasecka and Kristiina M. Huttunen</b> Increased/Targeted Brain (Pro)Drug Delivery via Utilization of Solute Carriers (SLCs) Reprinted from: <i>Pharmaceutics</i> <b>2022</b> , <i>14</i> , 1234, doi:10.3390/pharmaceutics14061234 . . . . .	<b>331</b>
<b>Sana Latif and Young-Sook Kang</b> Blood–Brain Barrier Solute Carrier Transporters and Motor Neuron Disease Reprinted from: <i>Pharmaceutics</i> <b>2022</b> , <i>14</i> , 2167, doi:10.3390/pharmaceutics14102167 . . . . .	<b>373</b>
<b>Toshiki Kurosawa, Yuma Tega, Yasuo Uchida, Kei Higuchi, Hidetsugu Tabata and Takaaki Sumiyoshi et al.</b> Proteomics-Based Transporter Identification by the PICK Method: Involvement of TM7SF3 and LHFPL6 in Proton-Coupled Organic Cation Antiport at the Blood–Brain Barrier Reprinted from: <i>Pharmaceutics</i> <b>2022</b> , <i>14</i> , 1683, doi:10.3390/pharmaceutics14081683 . . . . .	<b>389</b>
<b>Patrick T. Ronaldson and Thomas P. Davis</b> Transport Mechanisms at the Blood–Brain Barrier and in Cellular Compartments of the Neurovascular Unit: Focus on CNS Delivery of Small Molecule Drugs Reprinted from: <i>Pharmaceutics</i> <b>2022</b> , <i>14</i> , 1501, doi:10.3390/pharmaceutics14071501 . . . . .	<b>409</b>
<b>Maj Schneider Thomsen, Kasper Bendix Johnsen, Krzysztof Kucharz, Martin Lauritzen and Torben Moos</b> Blood–Brain Barrier Transport of Transferrin Receptor-Targeted Nanoparticles Reprinted from: <i>Pharmaceutics</i> <b>2022</b> , <i>14</i> , 2237, doi:10.3390/pharmaceutics14102237 . . . . .	<b>437</b>
<b>Yu Sakurai, Himeka Watanabe, Kazuma Nishio, Kohei Hashimoto, Atsuki Harada and Masaki Gomi et al.</b> pH-Responsive Lipid Nanoparticles Achieve Efficient mRNA Transfection in Brain Capillary Endothelial Cells Reprinted from: <i>Pharmaceutics</i> <b>2022</b> , <i>14</i> , 1560, doi:10.3390/pharmaceutics14081560 . . . . .	<b>455</b>
<b>Ulrich Bickel</b> Modeling Blood–Brain Barrier Permeability to Solutes and Drugs In Vivo Reprinted from: <i>Pharmaceutics</i> <b>2022</b> , <i>14</i> , 1696, doi:10.3390/pharmaceutics14081696 . . . . .	<b>467</b>

# About the Editor

## **William M. Pardridge**

William M. Pardridge, M.D., is a Distinguished Professor Emeritus, University of California, and was Founder of ArmaGen, Inc., and The Lipogene Company, Inc. Dr. Pardridge has worked on the blood–brain barrier (BBB) since 1970 and is the author of over 500 publications and the inventor of over 70 issued patents in the BBB field. He is the inventor of the BBB molecular Trojan horse technology, which has enabled the re-engineering of multiple classes of biologics as BBB-penetrating recombinant IgG fusion proteins for the treatment of brain disorders, and of the Trojan horse liposome technology for non-invasive, non-viral plasmid DNA gene therapy of the brain. He first developed the field of BBB genomics in 2001. His research interests cover carrier-mediated transport, receptor-mediated transport, non-viral gene therapy of the brain, plasma protein-mediated transport, and mathematical models of BBB transport.





# Preface to “Advanced Blood-Brain Barrier Drug Delivery”

This Special Issue of *Pharmaceutics*, “Advanced Blood-Brain Barrier Drug Delivery”, comprises 17 articles, which cover five areas of brain drug delivery, including receptor-mediated transport (RMT), carrier-mediated transport (CMT), active efflux transport (AET), Trojan horse lipid nanoparticles (LNP), and the in vivo measurement of drug transport across the blood–brain barrier (BBB). The articles on RMT describe the genetic engineering of IgG fusion proteins, wherein the IgG domain targets an endogenous peptide receptor at the BBB. The IgG domain of the fusion protein acts as a molecular Trojan horse to ferry the fused biologic agent into the brain, which alone does not cross the BBB. Endogenous CMT systems for the brain drug delivery of small molecules include the GLUT1 glucose transporter, the LAT1 large neutral amino acid transporter, and others. AET systems at the BBB cause the active efflux of small-molecule drugs from brain to blood, and include carriers in the Solute Carrier (SLC) and the ATP binding cassette (ABC) transporter super-families. Trojan horse LNPs are formulated to access RMT systems at the BBB for the brain delivery of mRNA or plasmid DNA. Articles in this Special Issue critically evaluate the in vivo measurement of drug transport into brain.

**William M. Pardridge**

*Editor*



Editorial

# Advanced Blood–Brain Barrier Drug Delivery

William M. Pardridge 

Department of Medicine, University of California, Los Angeles (UCLA), Los Angeles, CA 90095, USA;  
wpardrid@ucla.edu

This Special Issue of *Pharmaceutics*, “Advanced Blood–Brain Barrier Drug Delivery,” comprises 16 articles or reviews, which cover a cross-section of brain drug delivery for either small-molecule or large-molecule therapeutics. The areas covered include (i) receptor-mediated transport (RMT); (ii) carrier-mediated transport (CMT); (iii) active efflux transport (AET); (iv) lipid nanoparticles (LNP); and (v) in vivo methods for the measurement of blood–brain barrier (BBB) drug transport. Many areas of brain drug delivery are not covered in a designated article but are reviewed in this issue [1]. These areas include drug delivery into the cerebrospinal fluid (CSF) via an intrathecal injection into either the lumbar or ventricular CSF; trans-nasal drug delivery; intra-cerebral brain drug delivery with either intra-cerebral implants or convection enhanced diffusion; BBB disruption via the intra-carotid arterial infusion of noxious agents or the intravenous injection of micro-bubbles in association with focused ultrasound; exosomes; stem cells; or the lipidization of polar small molecules. These latter brain drug delivery technologies have specific limitations, which, to date, have prevented the scalable translation to human neurotherapeutics, as reviewed in this volume [1].

The RMT of biologics across the BBB requires attachment of the biologic to a peptide or peptidomimetic monoclonal antibody (MAb) that binds to a specific endogenous receptor expressed on the luminal membrane of the brain capillary endothelium that forms the BBB. The targeted receptor normally serves to mediate the transport of an endogenous peptide from blood to brain, such as the insulin receptor (IR), transferrin receptor 1 (TfR1), insulin-like growth factor (IGF) 1 receptor (IGF1R), or leptin receptor (LEPR) [1]. The peptide or MAb acts as a molecular Trojan horse to ferry the biologic agent across the BBB via RMT on the endogenous peptide receptor at the brain endothelium. This Special Issue includes seven articles that describe the use of MAb-based Trojan horses targeting the IR, TfR1, IGF1R, or an orphan receptor [2–8], and one article on the use of peptides as a BBB Trojan horse [9].

The review by Boado [2] describes the genetic engineering of IgG fusion proteins that target either the murine TfR1 for mouse investigations, or the human insulin receptor (HIR) for either brain uptake studies in Old World primates such as the Rhesus monkey, or in human clinical trials. Boado [2] describes the genetic engineering, expression, and validation of TfRMAB and HIRMAb fusion proteins for all four classes of protein biologic drugs: lysosomal enzymes, neurotrophins, decoy receptors, and therapeutic antibodies. In the case of the BBB delivery of a therapeutic antibody, the transporter antibody and the therapeutic antibody are combined to produce a bispecific antibody (BSA) [2]. The first clinical trial of a BBB Trojan horse was reported in 2018, which described the 52-week treatment of children with MPSI with weekly intravenous (IV) infusions of a fusion protein of the HIRMAb and the lysosomal enzyme that is mutated in MPSI,  $\alpha$ -L-iduronidase (IDUA), and this HIRMAb-IDUA fusion protein is designated valanafusp alfa [2].

The review by Sonoda et al. [3] describes the genetic engineering of a fusion protein, designated pabinafusp alfa, which is formed by a fusion of the mature human iduronate 2-sulfatase (IDS) lysosomal enzyme to the carboxyl terminus of the heavy chain (HC) of a TfRMAB specific for the human TfR1. IDS is mutated in MPS II (Hunter syndrome), where

**Citation:** Pardridge, W.M. Advanced Blood–Brain Barrier Drug Delivery. *Pharmaceutics* **2023**, *15*, 93.  
<https://doi.org/10.3390/pharmaceutics15010093>

Received: 1 November 2022  
Accepted: 6 December 2022  
Published: 27 December 2022



**Copyright:** © 2022 by the author. Licensee MDPI, Basel, Switzerland. This article is an open access article distributed under the terms and conditions of the Creative Commons Attribution (CC BY) license (<https://creativecommons.org/licenses/by/4.0/>).

the accumulation of glycosaminoglycans (GAG) in the brain leads to cognitive impairment early in the life of subjects with mutations in the human IDS gene. Pabinafusp alfa treatment of humans with MPSII results in a decrease in GAG levels in CSF [3]. Pabinafusp alfa received regulatory approval in Japan in 2021 [3] and is the first Trojan horse fusion protein to be granted market approval for the treatment of a human disease of the brain.

Decoy receptor therapeutics, such as etanercept, are engineered by fusion of the carboxyl terminus of a soluble extracellular domain (ECD) of a membrane receptor to the amino terminus of a human IgG Fc. Etanercept binds, sequesters, and suppresses the action of the pro-inflammatory cytokine, TNF $\alpha$ . TNF $\alpha$  plays a pro-inflammatory role in AD, but etanercept cannot be used to treat AD because it does not cross the BBB [2]. However, the human TNFR ECD can be re-engineered for BBB penetration and for the treatment of AD with the genetic engineering and application of an IgG-TNFR fusion protein [4]. Ou et al. [4] describe the chronic treatment of 1-year-old double transgenic APP/PS1 AD mice with 2–3 mg/kg of either etanercept or the TfrMab-TNFR fusion protein administered by intra-peritoneal injection three times a week for 10 weeks. The TfrMab-TNFR fusion protein, but not etanercept, reduced the A $\beta$  peptide content, thioflavin-S positive A $\beta$  plaques, and insoluble oligomeric A $\beta$  in the brain, in parallel with an increase in A $\beta$  plaque-associated phagocytic microglia [4]. Chronic treatment of the AD mice with the TfrMab-TNFR fusion protein caused no abnormalities in either hematologic parameters in blood or iron dysregulation in the brain [4].

PD is associated with the deposition in the brain of insoluble aggregates derived from the  $\alpha$ -synuclein (SYN) protein, and a MAb that disaggregates SYN plaque is a potential treatment of PD. However, therapeutic antibodies do not cross the BBB [1]. In order to produce a new treatment for PD, a BSA was engineered from the 8D3 mouse TfrMab and the Syn-02 antibody, as described by Roshanbin et al. [5]. The Syn-02 antibody binds SYN aggregates but not soluble SYN monomers [5]. A single chain Fv (ScFv) form of the 8D3 TfrMab was fused to the carboxyl terminus of each light chain (LC) of an engineered form of the Syn-02 antibody [5]. L61 transgenic mice that over-express the human SYN protein develop aggregates in the brain by 3 months of age [5]. L61/SYN transgenic mice were treated with 10 mg/kg of either the Syn-2 antibody alone or the 8D3-Syn-02 BSA on days 1, 2, and 4, and then euthanized on day 5. This short course of treatment resulted in a modest decrease in the brain levels of SYN oligomers. Future studies describing a longer duration of treatment are warranted for this novel approach to the reduction in insoluble SYN aggregates in the brain in PD.

The works of Boado [2], Sonoda et al. [3], Ou et al. [4], and Roshanbin et al. [5] developed classical dual-domain antibodies comprised of both an HC and an LC, each with a variable region. In contrast, single-domain antibodies (sdAb)—also called a nanobody owing to their small size of 15 kDa—are formed only by a variable region of the heavy chain (VH). The two sources of sdAbs are sharks, where the shark VH is designated as a variable new antigen receptor (VNAR) antibody, and camelids (e.g., llama), where the camelid VH is designated a VHH. In this Special Issue, the study of Clarke et al. [6] describe the genetic engineering of a BSA comprising a therapeutic antibody and a shark VNAR. Yogi et al. [7] describe the genetic engineering of a fusion protein derived from a camelid VHH and the neuroactive peptide, neurotensin.

Clarke et al. [6] describe the genetic fusion of the 29D7 TrkB agonist antibody and a single-domain shark VNAR antibody against the Tfr1, and designated TXB4. The TXB4-TrkB BSA retained high-affinity binding (low nM KD) to both the transporter target, the Tfr1, and to the therapeutic target, TrkB [6]. The therapeutic efficacy of the TXB4-TrkB BSA was assessed in a murine 6-hydroxydopamine model of PD. Mice were treated with phosphate buffered saline (PBS) or 2.5–5 mg/kg of the TXB4-TrkB BSA at days –1 and +7 relative to toxin administration. This dose of toxin in the mouse produces a partial lesion, and the number of cells in the substantia nigra immunoreactive with an antibody against tyrosine hydroxylase (TH) was reduced by 27% on the lesioned side compared to the non-lesioned side in the PBS treated mice. However, there was only a 3% reduction

in striatal TH on the lesioned side, relative to the contralateral or non-lesioned side, in the PD mice treated with the TXB4-TrkB BSA [6]. Since the BSA was administered 24 h before neurotoxin injection, future work can examine the neuroprotective effects of delayed treatment with the TxB4-TrkB fusion protein following toxin administration.

Yogi et al. [7] describe the isolation of a camelid VHH following llama immunization with the human IGF1R ECD. The optimal VHH was isolated and designated IGF1R5, and humanized following standard protocols [7]. Humanization of the IGF1R5 VHH resulted in several amino acid substitutions across all four of its framework regions (FR), and its humanized form was designated IGF1R5-H2 [7]. This humanization had a significant impact on the affinity of the VHH binding to the IGF1R, which was measured by surface plasmon resonance. The *in vivo* transport was measured in the rat model for the non-humanized IGF1R5:Fc. The CSF/serum ratio of the antibody was 0.3%, and the brain concentration of the antibody was 11 nM at 24 h following the IV administration of 15 mg/kg of the fusion protein [7]. After the intravenous injection of 5–20 mg/kg of the VHH-Fc fusion protein, a fusion protein of neurotensin and the IGF1R5-human Fc produced a reduction in core body temperature [7].

The work of Boado [2], Sonoda et al. [3], Ou et al. [4], Roshanbin et al. [5], Clarke et al. [6], and Yogi et al. [7] targeted known RMT systems at the BBB, e.g., the IR, Tfr1, or IGF1R. To discover orphan RMT systems at the BBB, in this Special Issue, Georgieva et al. [8] describe their work with the 46.1 antibody. This antibody was generated following screening of a human single chain Fv (ScFv) phage library with cultured brain microvascular endothelial cells, which were produced following the retinoic acid differentiation of induced pluripotent stem cells. The lead candidate ScFv antibody, designated 46.1, was isolated and fused to the amino terminus of rabbit IgG Fc [8], which produces a bivalent antibody of ~100 kDa in size. In a pharmacologic application of the 46.1 orphan receptor antibody, Georgieva et al. [8] describe the genetic engineering of a fusion protein of 46.1 ScFv-Fc and mature neurotensin, which is a 13 amino acid (AA) neuropeptide released from a larger precursor. The biologic activity of the fusion protein *in vivo* was measured by a core body temperature assay and a phencyclidine-induced hyper-locomotor activity assay [8]. The 46.1 ScFv-Fc-neurotensin fusion protein was pharmacologically active in both assays in mice following the IV injection of 20 mg/kg into the retro-orbital vein. The pharmacologic effect in either assay was reduced or not observed following tail vein injection [8].

The articles in this Special Issue used a monoclonal antibody as the BBB molecular Trojan horse to shuttle the fused biologic agent from blood to brain via endogenous RMT systems at the BBB. Peptides that target RMT systems at the BBB can also be used as drug delivery vectors, and Sanchez-Navarro and Giralt [9]—also in this issue—provide a comprehensive review of BBB shuttle peptides. Two classes of peptide are reviewed: synthetic peptides and peptides isolated from phage display [9]. The most widely studied synthetic peptides include (a) peptides with sequences overlapping with AA 130–152 of human apolipoprotein E (apoE), which are low-affinity ligands for the low density lipoprotein receptor (LDLR) or the LDLR-related protein 1 (LRP1); (b) a peptide overlapping with AA 3371–3409 of human apolipoprotein B (apoB), which is a low-affinity ligand for LDLR; (c) angiopep-2, a 19 AA peptide that is a low-affinity ligand for LRP1; and (d) a 29 AA peptide corresponding to a sequence from the rabies virus glycoprotein (RVG), which is a ligand for the nicotinic acetylcholine receptor (nAChR) [9]. However, the immunohistochemical detection of LDLR, LRP1, or the nAChR in the brain shows that these receptors are expressed on brain cells beyond the BBB and not on the brain endothelium *in vivo* [1]. Therefore, ligands targeting the LDLR, LRP1, or nAChR are unlikely to mediate RMT across the BBB, and alternative transport pathways should be evaluated. Since all of these peptides are strongly cationic with isoelectric points (pI) of 9–10, they may undergo cationic charge-dependent absorptive-mediated transport (AMT) across the BBB [1]. Potential peptide shuttles derived from screening phage peptide libraries are reviewed in this Special Issue [9]. In a typical peptide phage display library, a 15-mer random AA sequence is incorporated in the amino terminus of the bacteriophage P3 minor

coat protein [9]. The phage coat protein is a large protein of >400 AA in length, and the activity of the 15 AA sequence that is embedded in the large p3 protein may differ from the shuttle activity of the 15 AA sequence as a free peptide [1].

Small molecules are often assumed to penetrate the BBB owing to the small size of the drug. However, ~98% of all small molecules do not cross the BBB [1]. Small molecule drugs that penetrate the BBB have a MW < 400 Da, form <8 hydrogen bonds with water, and lack an affinity for a BBB active efflux transporter (AET), such as p-glycoprotein. In the past, medicinal chemists have attempted to increase the BBB transport of drugs by blocking polar functional groups on the drug, a process referred to as ‘lipidization.’ However, lipidization of polar drugs by medicinal chemistry rarely leads to new BBB penetrating drugs, since this increases the MW of the drug and renders it unstable in the blood. An alternative approach to the use of medicinal chemistry to enhance the BBB transport of small-molecule drugs is to modify the drug so that it both (a) retains pharmacologic activity, and (b) has a modest to high affinity for transport via one of several CMT systems at the BBB. In this Special Issue, the article by Huttunen et al. [10] is the most comprehensive review, to date, on the use of medicinal chemistry for designing drugs that reach the brain via CMT across the BBB. All of the CMT systems reviewed by the authors [10] are members of the Solute Carrier (SLC) gene family. The problem lies in the complexity of the SLC family of transporters, as there are >400 genes in >60 families of SLC transporters [1]. Therefore, it is crucial to identify which SLC transporter functions at the luminal membrane of the brain capillary endothelium. Based on the available literature data, Huttunen et al. [10] recommend targeting certain SLC transporters, including ASCT1; the alanine-serine-cysteine transporter (SLC1A); the GLUT1 glucose transporter (SLC2A); the CAT1 cationic amino acid transporter, the LAT1 large neutral amino acid transporter (SLC7A); the MCT1 and MCT8 monocarboxylic acid transporters (SLC16A); the OATP2B1 and OATP1A2 organic anion transporters (SLC21A/SLCO); the OCT1-3 and OCTN1-2 organic anion and organic cation transporters (SLC22A); and the SNAT3 glutamine transporter (SLC38A). In addition, certain vitamins undergo CMT across the BBB via other members of the SLC gene family [1] and are potential targets for medicinal chemists [10].

The SLC transporters at the BBB may be up- or down-regulated in disease, and in this Special Issue, Latif and Kang [11] review the changes in certain SLC transporters at the BBB in motor neuron disease. They review changes in amyotrophic lateral sclerosis for certain SLC transporters, including the ASCT1/2, LAT1, CAT1, MCT1, the carnitine carrier, OCTN2, and the high-affinity choline transporter (CHT1). Regarding BBB choline transport, the more important transporter at the BBB is shown to be the lower affinity choline transporter-like protein 1 (CTL1, SLC44A1) [11].

Not all small-molecule transporters at the BBB may be members of the SLC gene family. In this Special Issue, Kurosawa et al. [12] use new methodology to identify potential candidates for the protein-coupled organic cation ( $H^+$ /OC) transporter. To identify potential candidates for the BBB organic cation transporter, the authors [12] develop a new methodology, the proteomics-based identification of transporters by crosslinking substrate using the keyhole (PICK) method. This new methodology identified the TM7SF3 transmembrane 7 superfamily member 3 and the LHFPL tetraspan subfamily 6 proteins as potential candidates for the  $H^+$ /OC transporter. Human TM7SF3 is a widely expressed glycosylated membrane protein comprising seven transmembrane regions and 570 AA, including a 21 AA signal peptide (NP\_057635). Human LHFPL is a membrane protein comprising four transmembrane regions and 236 AA, with no predicted signal peptide sequence, no predicted N-linked glycosylation sites, and an alanine-rich amino terminus (NP\_945351).

Certain BBB transporters mediate the transport of endogenous ligands or drugs in the brain-to-blood direction, and they are active efflux transporters (AET). In this Special Issue, Ronaldson and Davis [13] review the major AETs at the BBB—which are transporters derived from both the SLC and ATP-binding cassette (ABC) gene families—and emphasize the differential expression of transporters in the multiple cells that comprise the neuro-

vascular unit, including the capillary endothelium, capillary pericyte, the astrocyte endfeet or neuronal endings that contact the capillary basement membrane, and peri-vascular cells such as microglia [13]. There are seven ABC gene families, ABCA through ABCG, which encompass ~50 transporters. The most widely studied ABC transporters at the BBB are p-glycoprotein (ABCB1), breast cancer resistance protein, BCRP (ABCG2), and multidrug resistance protein MRP1-6 (ABCC1-C6) [13]. SLC transporters also contribute to the active efflux from the brain to blood of ligands and drugs, including members of the SLC21 family (now named the SLCO family), and include OATP1A2, and the mouse homologue, Oatp1a4 [13].

Nanoparticles comprise the sector in the field of brain drug delivery with the greatest number of publications [1]. Nanoparticles are a diverse group of formulations and include lipid nanoparticles (LNP)—which include cationic polyplexes (also called cationic liposomes)—and pegylated liposomes [1]. A review of the literature shows that nanoparticles, per se, do not cross the BBB, unless the nanoparticle is modified by conjugation of a Trojan horse ligand to its surface [1]. In this Special Issue, Thomsen et al. [14] describe the BBB transport of Trojan horse gold nanoparticles or Trojan horse LNPs, where the Trojan horse that mediates BBB transport is a TfRMAB. The BBB transport of Trojan horse LNPs in vivo is monitored using 2-photon microscopy [14].

Trojan horse LNPs are particularly suited to the BBB delivery of large nucleic acids such as mRNA or plasmid DNA. In this Special Issue, Sakurai et al. [15] describe the delivery of mRNA to cultured brain endothelial cells with LNPs, formulated without a Trojan horse, and encapsulating mRNA encoding for green fluorescent protein. The production of the LNPs described by the authors [15] is very similar to the production of the COVID-19 mRNA vaccines, which uses the ethanol dilution method for nucleic acid encapsulation within LNPs. The delivery of mRNA to cells with the pegylated liposome type of LNPs produced by Sakurai et al. [15] was only tested in cell culture, not in vivo, as these LNPs were formulated without a surface Trojan horse. However, when a TfRMAB or HIRMAb Trojan horse is conjugated to the surface of the LNP, the Trojan horse LNPs, also called Trojan horse liposomes (THL), enable the delivery of plasmid DNA to the brain in vivo [1]. Plasmid DNA encoding either reporter genes or therapeutic genes has been encapsulated in Trojan horse LNPs and administered IV in rats, mice, and monkeys [1]. THLs encapsulated with plasmid DNA encoding specific genes exert therapeutic effects in vivo in rodent models of brain cancer, PD, and Niemann-Pick type C1 disease [1].

BBB drug delivery is frequently measured in vitro with models of cultured endothelium, and these BBB models are discussed in detail in this Special Issue [1]. A critical examination of the in vitro models shows that they should supplement, not replace, in vivo measurements of BBB drug delivery. The in vitro BBB models are leaky owing to the marked down-regulation of BBB-specific gene expression when the brain endothelium is cultured in vitro [1]. The in vivo methods for the measurement of BBB drug delivery, compartmental model approaches, and the  $K_{p,uu}$  parameter are reviewed in this Special Issue by Bickel [16]. In a steady state, the  $K_{p,uu}$  parameter is the ratio of unbound drug concentration in brain interstitial fluid, relative to the unbound (bioavailable) drug concentration in plasma, which is equal to the ratio of the unidirectional clearance (CL) of influx, relative to the unidirectional clearance of efflux [16].

Continued progress in the field of brain drug delivery is important because of the rate-limiting role played by the BBB in the development of new drugs to treat diseases of the brain and spinal cord. Only ~2% of small molecules cross the BBB, and biologic drugs (recombinant proteins, RNA and DNA therapeutics) do not cross the BBB in the absence of a BBB delivery technology. Owing to the difficulty in the development of scalable BBB delivery technology that can be successfully translated to clinical medicine, the majority of brain drug delivery approaches either avoid the BBB (e.g., drug delivery to CSF, intracerebral drug delivery, trans-nasal drug delivery), or disrupt the BBB [1]. BBB disruption leads to the brain uptake of plasma proteins and to a sterile inflammatory reaction in the brain [1]. The alternative approach to brain drug delivery is to target the endogenous small



and large-molecule transport pathways that normally function at the BBB. RMT pathways, which serve to deliver certain peptides to the brain (e.g., insulin or transferrin), can be targeted with molecular Trojan horses and IgG fusion proteins for the brain delivery of biologics. CMT pathways, which serve to deliver nutrients and vitamins to the brain, can be targeted for the brain delivery of small-molecule drugs. An understanding of the molecular and cellular biology of the endogenous transport pathways at the BBB is the key to the future development of brain drug delivery technologies.

**Institutional Review Board Statement:** Not applicable.

**Informed Consent Statement:** Not applicable.

**Data Availability Statement:** Not applicable.

**Conflicts of Interest:** The author declares no conflict of interest.

## References

1. Pardridge, W.M. A Historical Review of Brain Drug Delivery. *Pharmaceutics* **2022**, *14*, 1283. [CrossRef]
2. Boado, R.J. IgG Fusion Proteins for Brain Delivery of Biologics via Blood-Brain Barrier Receptor-Mediated Transport. *Pharmaceutics* **2022**, *14*, 1476. [CrossRef]
3. Sonoda, H.; Takahashi, K.; Minami, K.; Hirato, T.; Yamamoto, T.; So, S.; Tanizawa, K.; Schmidt, M.; Sato, Y. Treatment of Neuronopathic Mucopolysaccharidoses with Blood-Brain Barrier-Crossing Enzymes: Clinical Application of Receptor-Mediated Transcytosis. *Pharmaceutics* **2022**, *14*, 1240. [CrossRef] [PubMed]
4. Ou, W.; Ohno, Y.; Yang, J.; Chandrashekar, D.V.; Abdullah, T.; Sun, J.; Murphy, R.; Roules, C.; Jagadeesan, N.; Cribbs, D.H.; et al. Efficacy and Safety of a Brain-Penetrant Biologic TNF-alpha Inhibitor in Aged APP/PS1 Mice. *Pharmaceutics* **2022**, *14*, 2200. [CrossRef]
5. Roshanbin, S.; Julku, U.; Xiong, M.; Eriksson, J.; Masliah, E.; Hultqvist, G.; Bergstrom, J.; Ingelsson, M.; Syvanen, S.; Sehlin, D. Reduction of alphaSYN Pathology in a Mouse Model of PD Using a Brain-Penetrating Bispecific Antibody. *Pharmaceutics* **2022**, *14*, 1412. [CrossRef] [PubMed]
6. Clarke, E.; Stocki, P.; Sinclair, E.H.; Gauhar, A.; Fletcher, E.J.R.; Krawczun-Rygmaczewska, A.; Duty, S.; Walsh, F.S.; Doherty, P.; Rutkowski, J.L. A Single Domain Shark Antibody Targeting the Transferrin Receptor 1 Delivers a TrkB Agonist Antibody to the Brain and Provides Full Neuroprotection in a Mouse Model of Parkinson's Disease. *Pharmaceutics* **2022**, *14*, 1335. [CrossRef]
7. Yogi, A.; Hussack, G.; van Faassen, H.; Haqqani, A.S.; Delaney, C.E.; Brunette, E.; Sandhu, J.K.; Hewitt, M.; Sulea, T.; Kemmerich, K.; et al. Brain Delivery of IGF1R5, a Single-Domain Antibody Targeting Insulin-like Growth Factor-1 Receptor. *Pharmaceutics* **2022**, *14*, 1452. [CrossRef] [PubMed]
8. Georgieva, J.V.; Katt, M.; Ye, Z.; Umlauf, B.J.; Wenthur, C.J.; Shusta, E.V. The 46.1 Antibody Mediates Neurotensin Uptake into the CNS and the Effects Depend on the Route of Intravenous Administration. *Pharmaceutics* **2022**, *14*, 1706. [CrossRef] [PubMed]
9. Sanchez-Navarro, M.; Giralt, E. Peptide Shuttles for Blood-Brain Barrier Drug Delivery. *Pharmaceutics* **2022**, *14*, 1874. [CrossRef] [PubMed]
10. Huttunen, J.; Adla, S.K.; Markowicz-Piasecka, M.; Huttunen, K.M. Increased/Targeted Brain (Pro)Drug Delivery via Utilization of Solute Carriers (SLCs). *Pharmaceutics* **2022**, *14*, 1234. [CrossRef] [PubMed]
11. Latif, S.; Kang, Y.S. Blood-Brain Barrier Solute Carrier Transporters and Motor Neuron Disease. *Pharmaceutics* **2022**, *14*, 2167. [CrossRef] [PubMed]
12. Kurosawa, T.; Tega, Y.; Uchida, Y.; Higuchi, K.; Tabata, H.; Sumiyoshi, T.; Kubo, Y.; Terasaki, T.; Deguchi, Y. Proteomics-Based Transporter Identification by the PICK Method: Involvement of TM7SF3 and LHFPL6 in Proton-Coupled Organic Cation Antiport at the Blood-Brain Barrier. *Pharmaceutics* **2022**, *14*, 1683. [CrossRef] [PubMed]
13. Ronaldson, P.T.; Davis, T.P. Transport Mechanisms at the Blood-Brain Barrier and in Cellular Compartments of the Neurovascular Unit: Focus on CNS Delivery of Small Molecule Drugs. *Pharmaceutics* **2022**, *14*, 1501. [CrossRef] [PubMed]
14. Thomsen, M.S.; Johnsen, K.B.; Kucharz, K.; Lauritzen, M.; Moos, T. Blood-Brain Barrier Transport of Transferrin Receptor-Targeted Nanoparticles. *Pharmaceutics* **2022**, *14*, 2237. [CrossRef] [PubMed]
15. Sakurai, Y.; Watanabe, H.; Nishio, K.; Hashimoto, K.; Harada, A.; Gomi, M.; Suzuki, M.; Oyama, R.; Handa, T.; Sato, R.; et al. pH-Responsive Lipid Nanoparticles Achieve Efficient mRNA Transfection in Brain Capillary Endothelial Cells. *Pharmaceutics* **2022**, *14*, 1560. [CrossRef] [PubMed]
16. Bickel, U. Modeling Blood-Brain Barrier Permeability to Solutes and Drugs In Vivo. *Pharmaceutics* **2022**, *14*, 1696. [CrossRef] [PubMed]

**Disclaimer/Publisher's Note:** The statements, opinions and data contained in all publications are solely those of the individual author(s) and contributor(s) and not of MDPI and/or the editor(s). MDPI and/or the editor(s) disclaim responsibility for any injury to people or property resulting from any ideas, methods, instructions or products referred to in the content.

Review

# A Historical Review of Brain Drug Delivery

William M. Pardridge 

Department of Medicine, University of California, Los Angeles (UCLA), Los Angeles, CA 90095, USA; wpardrid@ucla.edu

**Abstract:** The history of brain drug delivery is reviewed beginning with the first demonstration, in 1914, that a drug for syphilis, salvarsan, did not enter the brain, due to the presence of a blood–brain barrier (BBB). Owing to restricted transport across the BBB, FDA-approved drugs for the CNS have been generally limited to lipid-soluble small molecules. Drugs that do not cross the BBB can be re-engineered for transport on endogenous BBB carrier-mediated transport and receptor-mediated transport systems, which were identified during the 1970s–1980s. By the 1990s, a multitude of brain drug delivery technologies emerged, including trans-cranial delivery, CSF delivery, BBB disruption, lipid carriers, prodrugs, stem cells, exosomes, nanoparticles, gene therapy, and biologics. The advantages and limitations of each of these brain drug delivery technologies are critically reviewed.

**Keywords:** blood–brain barrier; endothelium; receptor-mediated transport; carrier-mediated transport; genetic engineering; IgG fusion proteins; nanoparticles; liposomes

## Contents

1. Introduction
  - 1.1. Blood–Brain Barrier and Blood–CSF Barrier
  - 1.2. History of the Blood–Brain Barrier
  - 1.3. History of Brain Drug Delivery
2. Invasive Drug Delivery to Brain
  - 2.1. CSF Delivery
    - 2.1.1. CSF Microcirculation and Microcirculation
    - 2.1.2. Drug Transfer from CSF to Blood
    - 2.1.3. Lumbar CSF Delivery
    - 2.1.4. Ventricular CSF Delivery
  - 2.2. Intra-Cerebral Delivery
    - 2.2.1. Intra-Cerebral Implants
    - 2.2.2. Convection-Enhanced Diffusion
3. Trans-Nasal Drug Delivery to Brain
  - 3.1. Drainage of CSF from Brain to Nose
  - 3.2. Drug Delivery from Nose to Brain
  - 3.3. Clinical Trials of Trans-Nasal Drug Delivery to Brain
4. Brain Drug Delivery with Blood–Brain Barrier Disruption (BBBD)
  - 4.1. BBBD Following Intra-Carotid Arterial Infusion
    - 4.1.1. BBBD with Intra-Arterial Hyper-Osmolar Solutions
    - 4.1.2. BBBD with Intra-Arterial Bradykinin Analogs
  - 4.2. BBBD with Intravenous Microbubbles/Focused Ultrasound
  - 4.3. Miscellaneous forms of BBBD
    - 4.3.1. BBBD with Tight Junction Modulators
    - 4.3.2. BBBD with Adenosine Analogs
    - 4.3.3. BBBD with Anti-Bacterial Antibodies
    - 4.3.4. BBBD with Intra-Arterial Polycations
    - 4.3.5. BBBD with Intra-Arterial Amphipathic Agents
    - 4.3.6. BBBD and Free Radicals
    - 4.3.7. BBBD and Electromagnetic Radiation

**Citation:** Pardridge, W.M. A Historical Review of Brain Drug Delivery. *Pharmaceutics* **2022**, *14*, 1283. <https://doi.org/10.3390/pharmaceutics14061283>

Academic Editor: Inge S. Zuhorn

Received: 10 May 2022

Accepted: 7 June 2022

Published: 16 June 2022

**Publisher's Note:** MDPI stays neutral with regard to jurisdictional claims in published maps and institutional affiliations.



**Copyright:** © 2022 by the author. Licensee MDPI, Basel, Switzerland. This article is an open access article distributed under the terms and conditions of the Creative Commons Attribution (CC BY) license (<https://creativecommons.org/licenses/by/4.0/>).

5. Cell-Mediated Transport
  - 5.1. Stem Cells for Brain Drug Delivery
  - 5.2. Exosomes for Brain Drug Delivery
6. Brain Drug Delivery of Small Molecules
  - 6.1. Lipid-Mediated Transport of Small Molecules
    - 6.1.1. Approved Small Molecules for the CNS
    - 6.1.2. Mechanism of Small Molecule Diffusion through the BBB
    - 6.1.3. Lipid-Soluble Pro-Drugs
    - 6.1.4. Conjugation of Hydrophilic Drugs to Hydrophobic Carriers
  - 6.2. Carrier-Mediated Transport of Small Molecules
    - 6.2.1. GLUT1 Glucose Carrier
    - 6.2.2. LAT1 Large Neutral Amino Acid Carrier
    - 6.2.3. CAT1 Cationic Amino Acid Carrier
    - 6.2.4. MCT1 Monocarboxylic Acid Carrier
    - 6.2.5. CNT2 Purine Nucleoside Carrier and Adenine Carrier
    - 6.2.6. CTL1 Choline Carrier
    - 6.2.7. Vitamin Carriers
    - 6.2.8. Thyroid Hormone Carriers
    - 6.2.9. Organic Cation Carrier
  - 6.3. Active Efflux Transport of Small Molecules
    - 6.3.1. Brain-to-Blood Efflux
    - 6.3.2. ABC Efflux Transporters
    - 6.3.3. SLC Efflux Transporters
7. Absorptive-Mediated Transport of Cationic Proteins or Lectins
  - 7.1. Cationic Proteins
    - 7.1.1. Cationized Proteins
    - 7.1.2. Endogenous Cationic Proteins
    - 7.1.3. Cell-Penetrating Peptides
  - 7.2. Lectins
  - 7.3. Toxicity of Cationic Proteins and Lectins
    - 7.3.1. Toxicity of Cationic Proteins
    - 7.3.2. Toxicity of Lectins
8. Receptor-Mediated Transport of Peptides and Monoclonal Antibodies
  - 8.1. Receptor-Mediated Transporters at the Blood–Brain Barrier
    - 8.1.1. Insulin Receptor
    - 8.1.2. Transferrin Receptor
    - 8.1.3. IGF Receptor
    - 8.1.4. Leptin Receptor
    - 8.1.5. LRP1 Receptor
    - 8.1.6. LDL Receptor
    - 8.1.7. Nicotinic Acetylcholine Receptor
    - 8.1.8. Basigin/CD147
    - 8.1.9. Miscellaneous Receptors
  - 8.2. Trojan Horse Delivery Via Blood–Brain Barrier Receptor-Mediated Transport (RMT)
    - 8.2.1. Peptide-Based RMT Trojan Horses
    - 8.2.2. Monoclonal Antibody-Based RMT Trojan Horses
  - 8.3. IgG Fusion Proteins for Blood–Brain Barrier Delivery of Biologics
    - 8.3.1. Lysosomal Enzymes
    - 8.3.2. Neurotrophins
    - 8.3.3. Decoy Receptors
    - 8.3.4. Bispecific Antibodies
  - 8.4. Avidin-Biotin Technology
    - 8.4.1. Peptide Radiopharmaceuticals for Brain Imaging
    - 8.4.2. Antisense Radiopharmaceuticals for Brain Imaging
    - 8.4.3. IgG–Avidin Fusion Proteins
9. Nanoparticles
  - 9.1. Nanoparticle Formulations

- 9.2. Polymer-Based Nanoparticles
  - 9.2.1. Polymeric Nanoparticles
  - 9.2.2. Dendrimers
  - 9.2.3. Micelles
  - 9.2.4. Albumin Nanoparticles
- 9.3. Lipid-Based Nanoparticles
  - 9.3.1. Liposomes
  - 9.3.2. Solid Lipid Nanoparticles
- 9.4. Non-Polymeric Nanoparticles
  - 9.4.1. Carbon Nanotubes
  - 9.4.2. Graphene Oxide, Fullerenes, and Quantum Dots
  - 9.4.3. Metallic Nanoparticles
- 9.5. Mediated Blood–Brain Barrier Delivery of Functionalized Nanoparticles
  - 9.5.1. Carrier-Mediated Transport of Nanoparticles
  - 9.5.2. Absorptive-Mediated Transport of Nanoparticles
  - 9.5.3. Receptor-Mediated Transport of Nanoparticles
  - 9.5.4. Brain Delivery of Nanoparticles with BBB Avoidance Strategies
- 9.6. Nanoparticle Clinical Trials for the Brain
- 9.7. Nanoparticle Neurotoxicology
- 10. Gene Therapy of the Brain
  - 10.1. Viral Gene Therapy
    - 10.1.1. Lentivirus-Transfected Stem Cells
    - 10.1.2. Adenovirus
    - 10.1.3. Herpes Simplex Virus
    - 10.1.4. Adeno-Associated Virus
  - 10.2. Non-Viral Gene Therapy of Brain
    - 10.2.1. Cationic Liposomes and Cationic Polyplexes
    - 10.2.2. Pegylated Liposomes
    - 10.2.3. Trojan Horse Liposomes
- 11. Blood–Brain Barrier Transport Methodology
  - 11.1. Physiologic Model of Free Drug in Brain and Plasma
  - 11.2. Free Drug in Plasma and Role of Plasma Protein Binding
  - 11.3. Measurement of Free Drug in Brain
    - 11.3.1. CSF as a Measure of Free Drug in Brain
    - 11.3.2. Free Drug in Brain with Cerebral Microdialysis
    - 11.3.3. Free Drug in Brain In Vitro with Brain Slices or Homogenates
  - 11.4. Measurement of  $PS^{influx}$ 
    - 11.4.1. Brain Uptake index Method
    - 11.4.2. Internal Carotid Artery Perfusion Method
    - 11.4.3. Capillary Depletion Method
    - 11.4.4. Intravenous Injection Methods
  - 11.5. Measurement of  $PS^{efflux}$ 
    - 11.5.1. Brain Uptake index Method
    - 11.5.2. Brain Efflux index Method
  - 11.6. Measurement of Drug Sequestration in Brain In Vivo
  - 11.7. In Vitro BBB Models
    - 11.7.1. Isolated Brain Microvessels
    - 11.7.2. In Vitro Models of BBB Transport in Cell Culture
  - 11.8. BBB Transport Methods from Perspective of Pharmaceutical Industry
- 12. Summary
- 13. Perspective
- Abbreviations
- References

## 1. Introduction

The driving force in the evolution of brain drug delivery technology is the blood–brain barrier (BBB) and the limitation this barrier creates in the development of new drugs for the brain. More than 98% of small molecule drugs do not cross the BBB [1], as illustrated

in Figure 1, which shows the selective organ uptake in the mouse of histamine, a small molecule drug with a molecular weight (MW) of just 111 Daltons (Da).

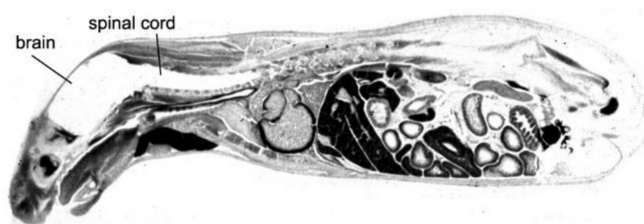


**Figure 1. The blood–brain barrier to small molecules.** Whole body autoradiography of mouse following the IV injection of [ $^{14}\text{C}$ ]-histamine shows the lack of transport of this small molecule drug into brain and spinal cord. Reprinted with permission from [2], Copyright© 1986 American College of Physicians.

Following intravenous (IV) administration, histamine penetrates all of the organs of the body except for the brain and spinal cord (Figure 1). The fraction of large molecule biologics that do not cross the BBB is essentially 100%. Therefore, brain drug development, in the absence of brain drug delivery technology, is limited to the <2% of small molecules that penetrate the BBB via lipid-mediated free diffusion [1]. In order to develop new drugs for brain disease from either water-soluble small molecule drugs, or from biologics (recombinant proteins or nucleic acid pharmaceuticals), a multitude of brain drug delivery technologies have emerged over the last 40 years. These technologies can be broadly classified as:

- *Invasive brain drug delivery:* the BBB is circumvented by drug injection into either the cerebrospinal fluid (CSF) following intrathecal or trans-nasal administration, or by trans-cranial direct injection of drug into brain tissue by either intra-cerebral implants or convection-enhanced diffusion (CED).
- *BBB disruption brain drug delivery:* the brain capillary endothelial tight junctions that form the BBB are disrupted by either the intra-arterial infusion of noxious agents, or by the intravenous injection of micro-bubbles followed by sonication of brain.
- *Trans-vascular brain drug delivery:* the non-disrupted brain capillary endothelial barrier is traversed following the re-engineering of the pharmaceutical so as to gain access to multiple carrier-mediated transporters (CMT) for small molecules, or receptor-mediated transporters (RMT) for biologics. This category also includes the development of co-drugs that inhibit active efflux transporters (AET) at the BBB, such as p-glycoprotein (P-gp), as well as the free diffusion of lipid-soluble small molecules.

Within each of these 3 spheres, different parallel approaches have emerged to the point where brain drug delivery science has now evolved into a complex maze of competing technologies. This maze is nearly impenetrable by the artisan who practices outside the field of brain drug delivery, or even within a competing brain delivery area. The complexity of modern brain drug delivery science is illustrated by the outline in Figure 2.

Prior to an analysis of each of the brain drug delivery technologies shown in Figure 2, the different anatomic locations of the BBB, at the brain capillary endothelium, and the blood–CSF barrier, at the choroid plexus, are reviewed. The presence of a barrier between blood and brain was discovered in 1900, and the limitation this barrier plays on brain drug delivery can be dated to 1914.

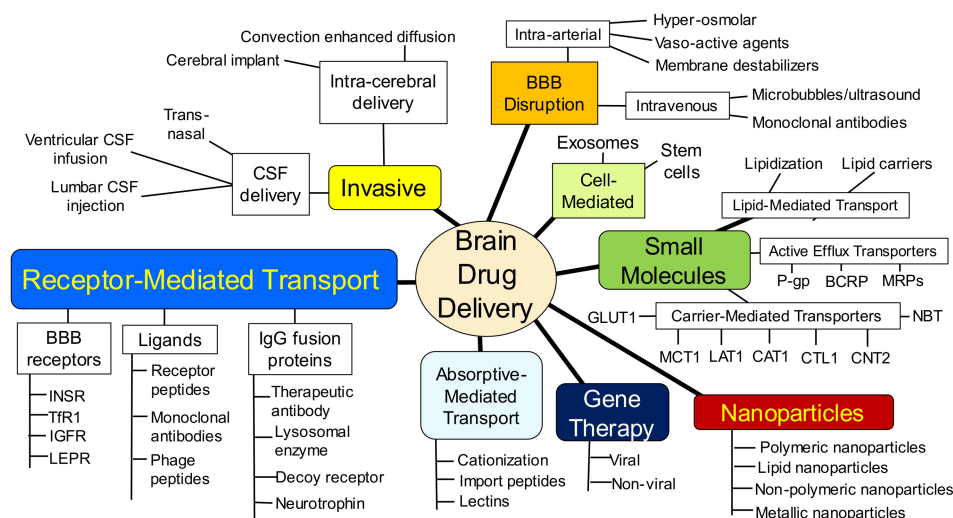
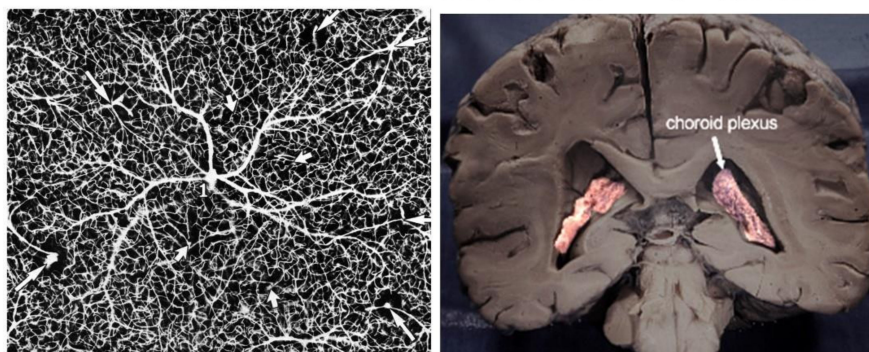


**Figure 2. Overview of brain drug delivery technologies.** These multiple delivery technologies can be broadly classified into 3 categories: (i) invasive brain drug delivery, which includes transcranial intra-thecal drug delivery into CSF, intra-cerebral implants, or convection-enhanced diffusion; (ii) BBB disruption brain drug delivery, which includes either the intra-carotid arterial infusion of noxious agents, or the intravenous injection of microbubbles coupled with focal external sonication of the brain; (iii) trans-vascular brain drug delivery, which includes receptor-mediated transport, carrier-mediated transport, active efflux transport, and lipid-mediated transport.

### 1.1. Blood–Brain Barrier and Blood–CSF Barrier

The BBB and the blood–CSF barrier are functionally and anatomically distinct barriers within the brain. The different anatomical locations of the BBB and the blood–CSF barrier are viewed in Figure 3. The BBB, at the brain microvascular endothelium, is shown in the left panel, and the blood–CSF barrier, at the choroid plexus, is shown in the right panel of Figure 3. The BBB at the brain capillary is formed by endothelial high resistance tight junctions that eliminate any paracellular pathway of solute movement from blood-to-brain extracellular space (ECS) [3]. Minimal pinocytosis within brain capillary endothelium removes any non-specific transcellular pathway of solute transport from blood to brain [4]. The blood–CSF barrier is formed by the epithelial cells of the choroid plexus [5], which lines the floor of each of the 4 cerebral ventricles, including both lateral ventricles shown in Figure 3 (right panel). The blood–CSF barrier is leaky relative to the BBB, as reflected by the electrical resistance across these two barriers. The electrical resistance across the choroid plexus epithelial barrier is only 26 ohm·cm<sup>2</sup> [6]. In contrast, the electrical resistance across pial vessels on the surface of the brain is 1600 ohm·cm<sup>2</sup> [7]. However, pial vessels express tight junctional complexes less developed than those in parenchymal vessels, and pial vessels are more permeable than parenchymal capillaries [8,9]. The electrical resistance across the endothelium of capillaries within brain parenchyma is estimated to be 8000 ohm·cm<sup>2</sup> [10], which is 300-fold higher than the resistance across the blood–CSF barrier [11]. Owing to the relative leakiness of the blood–CSF barrier, serum proteins readily move from plasma to CSF, as reflected by the high CSF/plasma ratio of IgG, which is ~0.2% [12]. In contrast, the brain/plasma IgG ratio in for the parenchyma of brain is <0.01% [13].

## Separate Barriers in Brain: *Blood-brain barrier and blood-CSF barrier*



- |   |   |
|---|---|
| <ul style="list-style-type: none"> <li>• Blood-brain barrier localized to capillary endothelium within brain parenchyma</li> <li>• Electrical resistance = <math>8000 \Omega \cdot \text{cm}^2</math></li> <li>• Brain/plasma IgG &lt;0.01 %</li> </ul> | <ul style="list-style-type: none"> <li>• Blood-CSF barrier localized to choroid plexus epithelium within brain ventricles</li> <li>• Electrical resistance = <math>26 \Omega \cdot \text{cm}^2</math></li> <li>• Brain/plasma IgG ~0.2 %</li> </ul> |
|---|---|

**Figure 3. Blood–brain barrier vs. blood–CSF barrier.** (Left) Inverted India ink labeling of microvasculature of human cerebral cortex, which is from [14] with permission, Copyright© 1981 Elsevier. (Right) Coronal section of human brain showing the choroid plexus lining the floor of both lateral ventricles. Adapted from [15], Copyright© 2020 licensed under Creative Commons Attribution License (CC-BY).

The brain capillary endothelium, which forms the permeability barrier between blood and brain parenchyma, is buttressed on the blood side by the endothelial glycocalyx, and on the brain side by the capillary basement membrane and the astrocyte endfeet that terminate on the basement membrane [16]. The thickness of the endothelium is 300 nm from the luminal to the abluminal endothelial membranes [17]. The thickness of the glycocalyx ranges from 100 nm, as measured by electron microscopy [18], to 400 nm, as measured by two-photon microscopy [19]. The glycocalyx covers about 40% of the surface area of the endothelial luminal membrane [20]. The capillary basement membrane covers the entire abluminal endothelial membrane and has a thickness ranging from 20 nm to 200 nm [21]. The basement membrane invests both the abluminal surface of the endothelium and the pericyte, which sits on the abluminal surface of the endothelium. Astrocyte endfeet terminate on the capillary basement membrane [21]. Electron microscopy of cryo-fixed brain shows the astrocyte endfeet cover about 63% of the basement membrane surface [22]. As discussed below, electron microscopy of brain shows that horseradish peroxidase (HRP), a 40 kDa protein, after injection into the brain, moves freely through the brain extracellular space (ECS), through the astrocyte endfeet, and through the capillary basement membrane to reach the abluminal surface of the capillary endothelium [3].

### 1.2. History of the Blood–Brain Barrier

The first known recognition of a restrictive permeability of the blood vessels in brain was reported by Ridley in 1695, as reviewed by Liddelow [23] and Thakur et al. [24]. The restricted uptake of acidic vital dyes by brain as compared to peripheral organs was demonstrated by Ehrlich in the 19th century [23]. Acidic vital dyes were systemically injected in rabbits and all the organs were stained by the dye with the exception of the central nervous system (CNS). However, these observations were attributed to lack of adsorption of the dyes to brain tissue, and not to any barrier between blood and brain. In 1900, Lewandowsky reported experiments on the intravenous and intrathecal injection of sodium ferrocyanide, as reviewed by Liddelow [23] and Macinowski [25]. Lewandowsky observed ferrocyanide effects on the CNS following intrathecal injection but not after intravenous administration, and first used the term, *blut-thirn-schranke*, or blood–brain

barrier, to characterize the selective permeability properties of the cerebral capillaries. In 1913, Goldman repeated Ehrlich's observations that the brain was not stained by acidic dyes following intravenous injection in rabbits, but observed the brain was stained by the dye following intrathecal administration, and Goldman's findings were summarized in the English literature by Mott in 1913 [26]. At this time, the prevailing view was that nutrients in blood passed first into the CSF and then into brain. Within this view, any barrier between blood and brain must necessarily lie at the choroid plexus, as reflected by Mott's commentary on Goldman's experiments:

- "Vital stains possess an affinity for the nervous system, and specially for the ganglion cells. If they are introduced by means of subcutaneous or intravenous injections, they are kept back by the plexus."
- "From the plexus choroideus the cerebro-spinal fluid receives important metabolic products, which are carried to the nerve substance by the fluid."

However, in 1916, McIntosh and Fildes [27] reported their findings on the intravenous injection of basic vital dyes, methylene blue and neutral red, which do cross the BBB. They observed the brain stained with no parallel staining of the CSF, and made the following conclusions:

- "Certain dye substances can pass directly from the blood to the brain substance proper without being found in the cerebrospinal fluid, while others fail to penetrate into the brain."
- Certain substances "do not possess the necessary solubility to allow them to pass from the blood-vessels into the brain substance. Their relative inefficiency has nothing to do with their absence from the cerebrospinal fluid".

By 1916, McIntosh and Fildes [27] clearly localized the BBB to the brain capillary, not the choroid plexus, and recognized that CSF was not an intermediate compartment between blood and brain.

The ambiguity in regard to location of the BBB, i.e., brain capillary vs. choroid plexus, was reinforced by Stern working in the 1920s, who used the term, *barrier-hemato-encephalique*, or BBB, but concluded the BBB was localized to the choroid plexus [28]. However, by the 1940s, workers such as Broman in 1941 [29], and Friedemann in 1942 [30] observed that the location of the BBB was clearly at the brain capillary wall, and not the choroid plexus. Friedemann [30] wrote, "this paper deals exclusively with the distribution of substances between blood and CNS. As will be shown, distribution between blood and CSF is an entirely different problem and remains outside the scope of this review." In 1946, Krough [31] observed that Broman had shown the BBB was localized to the brain capillary endothelium.

Consensus on the location of the BBB was elusive, as Hassin [32] wrote in 1948 that "the cerebrospinal fluid represents the tissue fluids of the brain", and that the "hemato-encephalique barrier (if one must consider such) is the Virchow-Robin spaces". Hassin, in 1948, reinforced the 1913 view of Mott [26] that CSF was an intermediate compartment as nutrients passed from blood to brain. The reluctance to even accept a specific location of the BBB was presented by Dobbing in 1961 [33], who disputed the concept of a specific BBB, and proposed the use of the term, "brain barrier system". This concept of 'brain barrier systems' is still used today [34], so as to lump together the BBB and blood-CSF barrier as a single system.

The anatomical location of the BBB was unambiguously localized to the brain capillary endothelium by the 1969 work of Brightman and Reese [3]. The brain was examined with electron microscopic histochemistry following the intravenous or intrathecal administration of horseradish peroxidase (HRP), a protein of 40 kDa, or lanthanum, an electron dense trivalent cation [3]. Following intravenous injection, the transport of lanthanum from blood to brain was blocked by the endothelial tight junctions on the luminal side of the brain capillary endothelium, as shown in Figure 4 (left panel).



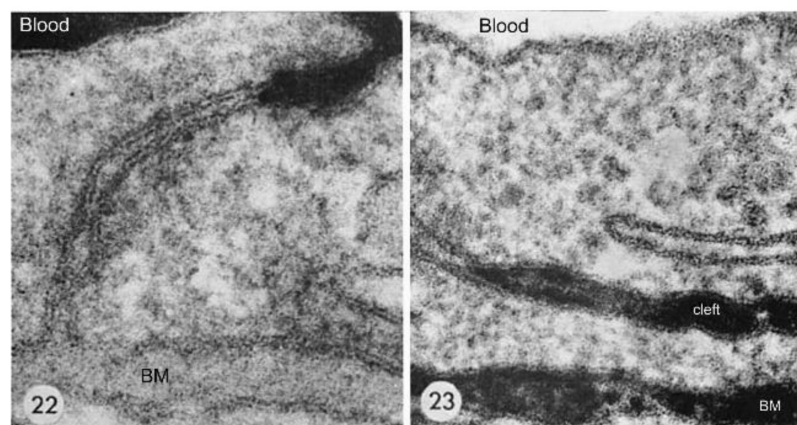


**Figure 4. Brain capillary endothelial tight junctions.** (Left) Electron microscopy of mouse brain following the intravenous injection of lanthanum, which is retained in the blood volume of brain at the top of the figure. (Right) Electron microscopic histochemistry of mouse brain following the intrathecal injection of HRP. This 40 kDa protein moves freely through the brain ECS, through the astrocyte endfeet, through the capillary basement membrane (BM), and into abluminal clefts formed between adjacent endothelial cells. Reproduced from [3], Copyright© 1969 under Creative Commons Attribution License (Share Alike 4.0 Unported).

The endothelial tight junctions eliminated any para-cellular pathway for solute-free diffusion across the endothelium. In addition, no lanthanum was observed within intracellular vesicles, indicating the pinocytotic transcellular pathway found in endothelia of peripheral tissues is nearly eliminated within the brain capillary endothelium [4]. Following the intrathecal administration of HRP, the 40 kDa protein was observed to move freely through the brain ECS, and to traverse the microvascular astrocyte endfeet and capillary basement membrane (Figure 4, right panel). However, further passage of HRP was blocked by the endothelial tight junction at the abluminal side of the capillary (Figure 4, right panel). After decades of controversy, this seminal work finally clarified unequivocally the location of the BBB as residing in the capillary endothelial cells, as suggested by several authors decades before. The anatomic basis of the endothelial barrier was the presence of high resistance tight junctions between endothelial cells. A total of 98% of all listings in PubMed under the search term, ‘blood–brain barrier,’ has been generated since the 1969 publication of Brightman and Reese [3].

### 1.3. History of Brain Drug Delivery

The first indication that the BBB would be a problem in brain drug development occurred in 1914, at the beginning of the synthetic pharmaceutical era. In 1913, Ehrlich described the production of salvarsan and neosalvarsan, which were the first commercial anti-microbial agents, and were marketed by Hoechst for the treatment of syphilis [35]. Salvarsan was a mixture of dimer and trimer complexes of neosalvarsan, which was a polar organic arsenical compound [36]. The first organo-arsenical compound, atoxyl, was synthesized in 1859, and used to treat trypanosomiasis [37]. Ehrlich determined the structure of atoxyl, and he and his colleague, Hata, synthesized salvarsan, and the more soluble, less toxic neosalvarsan, for the treatment of syphilis [37]. However, the syphilitic spirochete invades the brain to cause neurosyphilis, as described by Wile in 1916 [38]. Within a year of Ehrlich’s publication, McIntosh and Fildes [39], in 1914, showed that salvarsan and neosalvarsan do not enter brain from blood in the rabbit following IV administration. They made the following observations:

- “After intravenous injections of salvarsan and neosalvarsan in man and animals no arsenic can be found in the brain.”
- “This phenomenon is not due to a lack of affinity between the brain and the drugs, but to an inability on the part of the drugs to penetrate into the substance of the brain.”

Therefore, in 1914, the problem of the blood–brain barrier and brain drug delivery was born. The most serious effect of syphilis, neurosyphilis, could not be treated by neosalvarsan, owing to the lack of transport of this drug across the BBB.

By the 1950s, drugs such as tricyclic antidepressants and chlorpromazine were developed for affective disorders of the brain [40,41]. These drugs crossed the BBB by free diffusion owing to high lipid solubility and low MW, in the range of 280–320 Da, as discussed in Section 6.1. The role of lipid solubility in BBB transport of small molecules was demonstrated by Oldendorf, in 1972, with the description of the comparative brain uptake of heroin, codeine, and morphine [42]. While lipid-soluble, low-MW drugs crossed the BBB and could be developed for certain brain disorders; drugs that lacked these characteristics were not effective, owing to lack of penetration of the BBB. This was exemplified by methotrexate, which was developed as a treatment for leukemic infiltration of the meninges. Methotrexate was not effective in the CNS following IV administration, so the drug was delivered directly into the CSF compartment by lumbar CSF injection [43].

The first brain drug delivery technology was developed by Ommaya in 1963 [44], which was an implantable reservoir for catheter infusion of drug into the CSF of a lateral ventricle. Ommaya developed the reservoir to facilitate chronic treatment of bacterial meningitis with intrathecal antibiotic [44]. However, the Ommaya reservoir was not widely adopted, owing to the technical issues related to device implantation and maintenance. The next brain drug delivery system that was developed, albeit inadvertently, was the treatment of Parkinson's disease (PD) with L-DOPA, as reviewed by Hornykiewicz in 1966 [45]. It was known that PD was associated with striatal dopamine deficiency, and that treatment of PD with dopamine, per se, was not effective. However, the dopamine precursor, L-DOPA, which is a large neutral amino acid, was effective in the treatment of PD. L-DOPA acted as a prodrug, as it was converted into dopamine in brain following the enzymatic action of aromatic amino acid decarboxylase (AADC). The use of L-DOPA was an 'accidental' brain drug delivery approach, as the efficacy of L-DOPA was not immediately linked to a BBB transport mechanism [45]. Nearly 10 years later, in 1975, Wade and Katzman [46], using the Brain Uptake Index (BUI) technique of Oldendorf [47,48], demonstrated that brain uptake of L-DOPA was mediated by a BBB neutral amino acid transport system. BBB transport of L-DOPA was saturable, and was inhibited by other large neutral amino acids [46]. The next brain drug delivery technology was introduced in 1979, which aimed to deliver drugs to brain following BBB disruption. The intra-carotid arterial infusion of hyperosmolar 25% (1.4 M) mannitol enhanced brain uptake of methotrexate in dogs [49]. Trans-nasal drug delivery to CSF was introduced as a means to bypass the BBB in 1982. Progesterone was administered to monkeys by intra-nasal or IV administration, and CSF levels of the steroid were reported to be higher following intra-nasal administration [50].

Over the 20-year period of 1980–2000, multiple brain drug delivery approaches were developed. Trans-cranial approaches were developed by 1994, and used intra-cerebral implants, including polymers [51] or genetically engineered fibroblasts [52], or convection-enhanced diffusion [53]. Cationic vectors were developed including cationized albumin [54], and cationic cell-penetrating peptides (CPP), such as tat [55] or penetratin [56]. Lipid carriers, such as docosahexaenoic acid (DHA), were developed [57]. Receptor-mediated transcytosis of receptor ligands through the BBB was proposed in 1986 [58], followed by the development of monoclonal antibodies (MAbs) targeting either the BBB transferrin receptor [59,60] or insulin receptor [61]. The model active efflux transporter (AET) is p-glycoprotein (Pgp), and the high expression of Pgp at the brain capillary was demonstrated in 1989 [62]. Nanotechnology for the brain was introduced with liposomes in 1990 [63], nanoparticles in 1995 [64], and dendrimers in 2004 [65]. BBB disruption with the IV administration of microbubbles coupled with focused ultrasound (FUS) was developed in 2001 [66], and exosomes were introduced for brain drug delivery in 2011 [67].

A literature search in PubMed, using the keyword, ‘brain drug delivery’ yielded a total of 19,087 citations, and over 80% of these citations cover the 20 areas in Table 1.

**Table 1.** Brain drug delivery citations in PubMed.

No.	Delivery Technology Keyword <sup>a</sup>	Citations	No.	Delivery Technology Keyword <sup>a</sup>	Citations
1	Nanoparticles (1995)	4169	11	Cationic (1987)	437
2	Ultrasound (2001)	1472	12	p-glycoprotein (1989)	382
3	Cerebral implant (1994)	1417	13	Transferrin receptor (1991)	373
4	Liposomes (1990)	1285	14	Dendrimers (2004)	364
5	Nasal (1982)	1024	15	Carrier-mediated transport (1975)	327
6	Lipid carrier (1996)	814	16	Cell-penetrating peptide (2000)	263
7	Cerebrospinal fluid (1963)	666	17	Exosomes (2011)	224
8	BBB disruption (1979)	627	18	Tat (1994)	155
9	Small molecules (1954)	598	19	Insulin receptor (1995)	134
10	Receptor-mediated transport (1986)	566	20	Convection-enhanced diffusion (1994)	124

<sup>a</sup> PubMed search term is ‘brain drug delivery and keyword’, and each of the 20 keywords is listed in Table. The first year of publication of the brain drug delivery technology is given in parenthesis next to the technology keyword.

The PubMed search was refined with the search term, ‘brain drug delivery and keyword’, where 20 different keywords were used, as listed in Table 1. The brain drug delivery technologies are ranked according to the number of citations in PubMed, and range from 124 citations for CED, to 4160 citations for nanoparticles (Table 1). These top 20 keywords account for 81% of the 19,807 citations for brain drug delivery. Nanoparticles, ultrasound, cerebral implants, and nasal delivery account for 42% of all brain drug delivery citations. The remainder of this review will discuss these 20 brain drug delivery technologies listed in Table 1. The relative efficacy and toxicity of each technology will be reviewed, as well as the extent to which, despite decades of experimentation, the technology has failed to lead to FDA approval, or even clinical trials for brain diseases in humans.

## 2. Invasive Drug Delivery to Brain

### 2.1. CSF Delivery

#### 2.1.1. CSF Macrocirculation and Microcirculation

There is 140 mL of CSF in the human CNS, and this fluid is produced at the choroid plexus that lines the four cerebral ventricles (four lateral ventricles, third ventricle, fourth ventricle) [11]. The CSF is absorbed into the peripheral blood, primarily across the arachnoid villi into the superior sagittal sinus of the venous system [68]. This ‘macrocirculation’ of the CSF is relatively rapid and turns over every ~5 h or ~5 times each day in the human brain [11]. The CSF production rate in the 2 g rat brain is 3.4 uL/min [69], and in the 1400 g human brain, it is 350 uL/min [70]. There is also a ‘microcirculation’ within the interstitial fluid (ISF) of brain, as originally described by Cserr et al. [71]. Following the intra-cerebral injection of either 900 Da polyethylene glycol (PEG) or the 68 kDa albumin, both molecules exited the brain at a flow rate of 0.2 uL/min in the rat [71]. Since the rate of clearance was independent of MW, the mechanism of exodus was convection via peri-vascular pathways [71]. Ultimately, the tracers were transferred to blood via intermediate compartments composed of either CSF or the lymphatics. Qualitatively, the ISF microcirculation could provide a conduit for drug entry into brain parenchyma from the CSF. However, quantitatively, the ISF microcirculation is slow compared to the CSF macrocirculation. The rate of fluid flow in brain via the CSF macrocirculation, 3.4 uL/min in the rat [69], is nearly 20-fold higher than the rate of fluid flow via the ISF microcirculation, 0.2 uL/min, in the rat [71]. The comparative kinetics of the CSF microcirculation and the ISF microcirculation comport with the results of many studies that show solutes move from CSF to brain parenchyma slowly by diffusion, and not via more rapid convection pathways, as discussed below.

Transfer of solute between CSF and brain parenchyma via fluid convection is also called the glymphatic pathway. Early work in support of the convection pathway was reported by Wagner et al. in 1974 [72] and Rennels et al. in 1985 [73], and these investiga-

tions suggested the ISF microcirculation may proceed at high rates such that this pathway could provide for rapid transfer of solutes in CSF to the deep parenchyma of brain. In these studies, HRP was injected into the lateral ventricle of a rat [72] or cat [73], and brain was removed just 10 min after the intra-cerebroventricular (ICV) injection. Histochemistry showed broad distribution of the HRP deep into brain parenchyma. However, these findings appear to be artifacts following the ICV injection of very large volumes of the HRP solution. In the rat study [72], a volume of 35  $\mu\text{L}$  of 7% HRP was injected into one lateral ventricle as a bolus. This volume is 300% greater than the volume of the lateral ventricle in the rat, which is 12  $\mu\text{L}$  [74]. In the cat study [73], a volume of 1000  $\mu\text{L}$  of 4% HRP was injected. This volume is 800% greater than the volume of the lateral ventricle in the cat, which is 130  $\mu\text{L}$  [75]. In both studies, it was necessary to cannulate either the contralateral ventricle [72], or the cisterna magna [73], to reduce the high pressure introduced by these high-volume injections. As discussed below, multiple studies on the passage of drugs from CSF to brain parenchyma do not support a quantitatively significant role of the convection pathway under conditions of normal pressure in the CSF compartment.

In support of the convection pathway for drug delivery from CSF to brain parenchyma, extensive distribution of a therapeutic MAb into brain parenchyma of the primate was observed following ICV administration of the antibody [13]. However, this study actually supports the classical diffusion pathway. The MAb against the beta secretase-1 was continuously infused 24/7 for 42 consecutive days into the left lateral ventricle of a primate at a rate of 0.4 mL/day. At the end of the 42-day continuous infusion, the brain was removed and the MAb concentration was measured in multiple regions of brain by ELISA. Immunohistochemistry (IHC) showed the MAb was distributed to both sides of the brain, but MAb entry into brain parenchyma was confined to gray matter, with no MAb visible in white matter [13]. The lack of MAb penetration into white matter is inconsistent with a convection pathway, as perivascular flow occurs preferentially in white matter [76]. The MAb concentration in the contralateral motor cortex, which is near the CSF surface, is nearly 30-fold greater than the MAb concentration in the contralateral putamen, a deep parenchyma structure. If convection into brain was the prominent pathway, then the concentration in motor cortex and putamen should be comparable. Quantitative considerations indicate that diffusion, not convection, is the principal mechanism of MAb distribution from CSF to brain parenchyma following ICV infusion for 42 consecutive days. Given a MAb diffusion coefficient in brain of  $0.6 \times 10^{-6} \text{ cm}^2/\text{s}$  [77], and a time for diffusion of 42 days ( $3.6 \times 10^6 \text{ s}$ ), the diffusion diameter is 30 mm. The width of the primate brain is 40 mm [11]. Therefore, diffusion alone would be expected to cover 75% of the primate brain following a 42-day constant ICV infusion.

Support for the classical diffusion pathway of solute movement from CSF to brain comes from a variety of studies. In 1969, Brightman and Reese [3] injected HRP into the lateral ventricle of the mouse brain, and removed the brain at either 10 min or 90 min for histochemistry. The use of different fixation protocols showed the movement of HRP into brain tissue occurred *in vivo*, and was not a post-mortem artifact. The distribution of HRP at 10 min and 90 min is shown in Figure 5A.

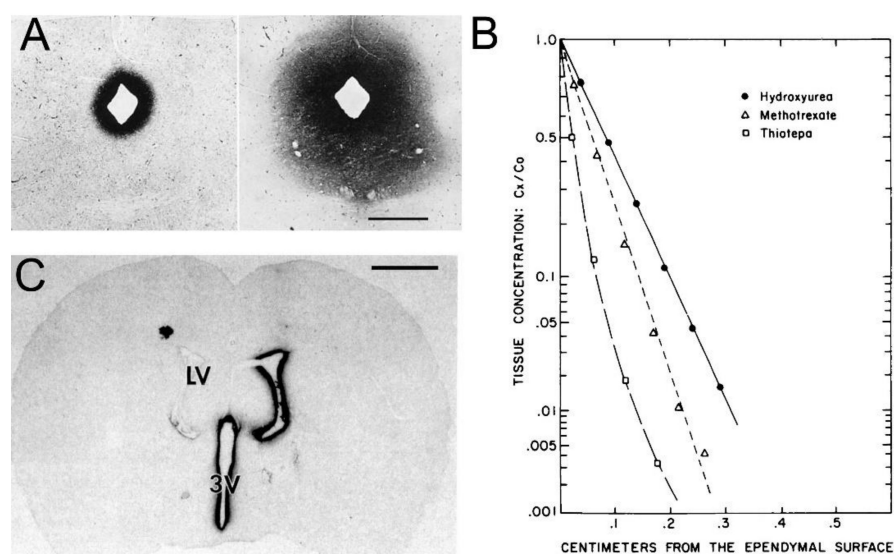


**Figure 5. Limited drug delivery to brain via the ventricular CSF.** (A) Peroxidase histochemistry of mouse brain removed at either 10 min (left) or 90 min (right) after ICV administration of HRP. The magnification bar is 0.7 mm. Reproduced from [3], Copyright© 1969 under Creative Commons Attribution License (Share Alike 4.0 Unported). (B) Brain concentrations of hydroxyurea (MW = 76 Da), methotrexate (MW = 454 Da), and thiotepa (MW = 189 Da) at 1–4 mm, removed from ependymal surface at 60 min following drug injection into the lateral ventricle of the Rhesus monkey. Reproduced with permission from [78], Copyright© 1975 Am. Soc. Pharm. Exp. Ther. (C) Film autoradiography of a coronal section of rat brain removed 24 h after injection into one lateral ventricle (LV) of [<sup>125</sup>I]-BDNF. The magnification bar is 2 mm; 3V = third ventricle. Reproduced with permission from [79], Copyright© 1994 Elsevier.

The HRP diffused 0.2 mm and 0.7 mm into peri-aqueductal brain at 10 min and 90 min, respectively (Figure 5A). Given a brain diffusion coefficient for HRP of  $0.6 \times 10^{-6} \text{ cm}^2/\text{s}$ , it is expected that HRP would diffuse 0.2 mm and 0.7 mm in 10 min and 90 min, respectively [11]. Therefore, the distribution of HRP into brain shown in Figure 5A can be accounted for solely on the basis of diffusion. In 1970, Levin and colleagues showed the concentration of inulin was decreased 10-fold at just 1–2 mm from the CSF surface in rabbits, cats, dogs, and monkeys [80]. In 1975, Blasberg et al. [78] injected small molecules (thiotepa, hydroxyurea, methotrexate) into the lateral ventricle of the Rhesus monkey, and removed the brain 60 min after ICV injection. Drug concentration was measured at 1 mm intervals removed from the CSF surface. Drug concentration in brain decreases logarithmically, and is just 1% of the CSF concentration at 1–2 mm removed from the ependymal surface (Figure 5B). The logarithmic decline in brain drug concentration is consistent with a diffusion model, not a convection model, of drug distribution from CSF to brain. Moreover, diffusion is inefficient as a drug delivery mechanism, and the drug concentration in brain is decreased 99% at just 1–2 mm from the ependymal surface (Figure 5B). In 1994, Yan et al. [79] injected [<sup>125</sup>I]-brain-derived neurotrophic factor (BDNF) into the lateral ventricle of the rat. The brain was removed 24 h later, and coronal sections were analyzed with film autoradiography. The study shows that BDNF distributes only to the ependymal surface of the lateral ventricle ipsilateral to the injection and to the third ventricle. BDNF diffusion into brain parenchyma from the CSF compartment is limited to a distance of only 0.2 mm. The failure to observe BDNF in the contralateral brain is due to the unidirectional flow of CSF from the lateral ventricle to the third ventricle to the fourth ventricle and into the spinal canal and over the convexities of the cerebrum. The only path for distribution to the contralateral ventricle following an ICV injection in one lateral ventricle is reflux through the foramen of Monro from the third ventricle to the contralateral lateral ventricle. There may be minimal reflux during diastole [81], but this does not result in significant drug

distribution to the contralateral ventricle as shown in Figure 5C. The distribution in brain of [ $^{125}$ I]-insulin-like growth factor (IGF)-1 following an ICV injection of the peptide was also determined by film autoradiography, and a result identical to that shown in Figure 5C was reported [82]. In summary, the data in Figure 5 show that drug movement from CSF to brain parenchyma is limited by diffusion, which is fundamentally incompatible with a quantitatively significant role for the convection or glymphatic pathway.

### 2.1.2. Drug Transfer from CSF to Blood

The paradox of intrathecal drug delivery to brain, i.e., drug injection into the CSF compartment, is that this route delivers drug to blood, not to brain parenchyma. The studies described in Figure 5 show that the ICV route only delivers drug to the ependymal surface of brain lining the CSF flow tracts. In parallel with the slow entry of drug into brain, there is a rapid movement of drug from CSF to blood following ICV drug administration. This fast CSF-to-blood transfer occurs as the entire CSF volume is absorbed into the venous blood ~5 times per day. In 1965, Fishman and Christy [83] studied the distribution of corticosteroids in blood following an intrathecal injection, and they concluded, “the intraspinal route of administration of free steroid is, in effect, equivalent to no more than a prolonged intravenous injection”. Additionally, in the 1960s, Reed and Woodbury [84] showed the plasma profile of iodide in rats was identical within 5 min of administration either as an IV injection or as an intrathecal injection in the cisterna magna. In 1984, Aird [85] showed that the dose of barbiturate that induced anesthesia in dogs was identical whether the drug was administered by injection into the blood or the CSF of the cisterna magna. After CSF injection, the drug rapidly moved to the blood, and then entered brain following transport across the BBB. Aird [85] concluded, “the relative effectiveness of intrathecal agents should be evaluated by comparing maintenance doses for a given central effect, when produced by both intrathecal and IV route”. That is, a clinical trial testing the CNS efficacy of a drug following intrathecal injection should include a control group wherein the drug was administered by IV injection. This point is illustrated for an Ommaya reservoir clinical trial discussed in Section 2.1.4. Other examples of the rapid movement of drug from CSF to blood include:

- The intrathecal injection of an interferon resulted in drug distribution to the surface of the brain, and to the blood, but not into brain parenchyma [86].
- The effect of intrathecal cholecystokinin (CCK) on food intake was found to be caused by CCK action in peripheral organs following CCK transfer from CSF to blood [87].
- Drug was injected into CSF in rats implanted with an intra-cerebral dialysis fiber; however, the drug did not appear in the dialysate of brain following ICV administration [88].
- Liver glycosaminoglycans (GAG) were reduced in the Type IIIB Mucopolysaccharidosis (MPSIIIB) mouse following the intrathecal injection of N-acetyl- $\alpha$ -glucosaminidase (NAGLU), the enzyme that is mutated in MPSIIIB [89], owing to enzyme movement from CSF to liver via the blood.
- The rapid movement of a monoclonal antibody (MAb) from CSF to liver, via the blood, was demonstrated by positron emission tomography (PET) in humans following the administration of the [ $^{124}$ I]-8H9 MAb via an Ommaya reservoir. Whole body PET scans at 24 h after intrathecal injection showed the antibody was present in liver, but not within the parenchyma of brain [90].

### 2.1.3. Lumbar CSF Drug Delivery

Some drugs are FDA approved for CNS conditions following drug injection into the lumbar CSF. As noted by Aird [85], intrathecal drug delivery can be effective for conditions that affect the *surface* of the brain or spinal cord, which is contiguous with the CSF flow tract. Intrathecal morphine is effective for pain [91], because opioid receptors are expressed on the surface of the spinal cord [92]. Intrathecal baclofen is used to treat spinal spasticity [93],

as gamma aminobutyric acid (GABA)-B receptors are expressed on the surface of the spinal cord [94].

Lumbar injection of nusinersen is FDA approved for treatment of spinal muscular atrophy (SMA) [95]. Nusinersen is a 2'-O-methoxyethyl phosphorothioate antisense oligodeoxynucleotide (ASO), which modulates alternative splicing of the survival motor neuron (SMN)-2 gene [96]. SMA is a disease of spinal cord motor neurons, and these neurons lie near the surface of the spinal cord [97]. Nusinersen is not representative of drug distribution in the spinal cord following intrathecal administration. Nusinersen has a very long residence time in CSF with a  $T_{1/2}$  of 191 days in the mouse [96]. The molecular basis for this long residence time in CSF is not clear but appears to be related to the sulfur moiety of the phosphorothioate ASO. A phosphorodiamidate ASO, which is a sulfur-free ASO, is less effective in vivo, although both the phosphorothioate ASO and the phosphorodiamidate ASO are equally effective in cell culture [96]. Based on the FDA approval of intrathecal nusinersen for a disease of the surface of the spinal cord, other ASOs entered CNS clinical trials for treatment of the parenchyma of brain or spinal cord by drug injection into the lumbar CSF. Tominersen is an ASO targeting the huntingtin mRNA of Huntington's disease (HD), and tofersen is an ASO targeting the superoxide dismutase 1 (SOD1) mRNA of SOD1 dependent amyotrophic lateral sclerosis (ALS) [98]. Since these ASOs do not cross the BBB, and since no antisense BBB delivery technology was developed by the drug sponsors, both tominersen and tofersen were delivered to brain by intrathecal injection into the lumbar CSF [98]. The phase 3 trials of both tominersen and tofersen ended in clinical failures, which is attributed to the poor penetration of drug into brain parenchyma following drug injection into CSF. The nusinersen model for treatment of the surface of the spinal cord by lumbar CSF injection could not be replicated for treatment of the parenchyma of brain by lumbar CSF injection.

In an effort to treat the brain in genetic lysosomal storage disease, the recombinant lysosomal enzyme was delivered to brain by intrathecal injection into the lumbar CSF. Injection of recombinant iduronate 2-sulfatase (IDS), the enzyme that is mutated in MPSII (Hunter syndrome), into the lumbar CSF resulted in a reduction in CSF GAGs, but had no improvement on cognitive function [99]. Chronic injection of N-sulfoglucosamine sulfohydrolase (SGSH), the enzyme mutated in MPSIIIA (Sanfilippo A syndrome), caused a reduction in CSF heparan sulfate [100], but had no effect on cognitive function in this disease, and the clinical trial was terminated [101].

Drug development for a brain disease, which is not restricted to the surface of the brain or spinal cord, by intrathecal drug delivery to brain is a futile effort, because drug is only distributed to the surface of the brain following drug injection into CSF (Figure 5). The futility arises not from the process of CNS drug discovery, but rather from the use of an ineffective brain drug delivery technology.

#### 2.1.4. Ventricular CSF Drug Delivery

The Ommaya reservoir was developed in 1963 [44] as an alternative to repeat intrathecal injections. A reservoir is implanted in the subcutaneous tissue of the skull and a catheter connects the reservoir to the CSF compartment of one lateral ventricle. An Ommaya reservoir delivery approach can be expected to treat diseases of the surface of the brain, which are contiguous with the CSF flow tract, such as meningitis, or meningeal infiltration in acute leukemia, and the first application of the Ommaya reservoir was the treatment of cryptococcal meningitis [44]. In 1975, Shapiro et al. [102] compared the CSF concentration of the chemotherapeutic agent, methotrexate, in CSF following IV administration, injection in the lumbar CSF, or injection in the ventricular CSF using an Ommaya reservoir. Administration of methotrexate via an Ommaya reservoir connected to the lateral ventricle provided for a more consistent delivery of methotrexate to the ventricular CSF than was afforded by drug injection into the lumbar CSF [102]. Previously, in 1962, Rieselbach et al. [103] showed in primates that the lumbar injections of large volumes, e.g., 10% of the CSF volume, were necessary in order to achieve consistent drug distribution into the subarachnoid space around

both cerebral hemispheres. The injection of chemotherapeutic agents into the ventricular CSF with an Ommaya reservoir is still current practice, particularly for childhood brain tumors [104].

The Ommaya reservoir was originally designed to treat acute diseases of the surface of the brain following injection of the antibiotic or chemotherapeutic agent into the ventricular CSF. However, given the legacy misconception that CSF is equivalent to the ECS of brain, as discussed in Section 1, it was natural to broaden the application of the Ommaya reservoir to the treatment of chronic disease of the brain parenchyma. Setting aside the invasive nature, and clinical complications of this delivery system [105], the physiology of drug transfer from CSF to brain would argue against the viability of treating intra-parenchymal brain disease by chronic ICV drug administration. First, investigations over many decades show that drug in CSF distributes only to the CSF surface of the brain as illustrated in Figure 5, and discussed in Section 2.1.1. Second, drug injected into the CSF rapidly moves to the peripheral blood, where the drug can exert pharmacologic actions in peripheral organ, which could be falsely attributed to a CNS site of action, as discussed in Section 2.1.2. As originally emphasized by Aird [85] in 1984, any examination of the pharmacologic effect of intrathecal drug administration should include a side-by-side evaluation of drug effects following IV infusion. Predictably, with one exception discussed below, ICV drug administration has not achieved FDA approval for the treatment of brain parenchyma of chronic disease. Patients with acquired immune deficiency syndrome (AIDS) and multifocal leukoencephalopathy were treated with cytarabine, a highly polar small molecule, by weekly injections into the ventricular CSF with an Ommaya reservoir, but without a clinical benefit [106]. Glial-derived neurotrophic factor (GDNF) was administered to PD patients by the ICV route, but without a clinical effect on the disease [107]. A potential toxicity may arise from the ICV administration of neurotrophic factors. This mode of brain drug delivery produces a very high drug concentration at the ependymal surface of brain, as shown in Figure 5C. The repeat ICV injection of basic fibroblast growth factor (bFGF) causes a reactive astrogliosis along the ependymal surface [108]. The chronic ICV infusion of nerve growth factor (NGF) stimulates axonal sprouting and Schwann cell hyperplasia within the pial-arachnoid surface of brain [109].

In 2017, the FDA approved the first, and only, treatment of parenchymal brain disease where the drug is administered with a chronically implanted Ommaya reservoir in a lateral ventricle. Recombinant tripeptidyl tripeptidase 1 (TPP1, cerliponase alfa) was approved for the treatment of Ceroid Lipofuscinosis 2 (CLN2) disease following ICV enzyme infusion in a lateral ventricle [110]. CLN2 disease is a lysosomal storage disorder caused by mutations in the TPP1 gene, and is characterized by childhood neurodegeneration, language delay, motor abnormalities, seizures, blindness, and early death [111]. The cDNA encoding for human TPP1 was cloned and expressed in CHO cells in 2001 [112]. However, intravenous Enzyme Replacement Therapy (ERT) with recombinant TPP1 was not initiated for CLN2 disease, because TPP1 does not cross the BBB [113]. So as to develop a treatment of the brain in CLN2 disease, the TPP1 proenzyme was infused in children with CLN2 disease into a lateral ventricle with a chronically implanted Ommaya reservoir every 2 weeks at a dose of 300 mg of enzyme in a volume of 10 mL over a 4 h period [110]. This infusion volume exceeds the entire volume of the lateral ventricle, which is 8.5 mL in adult humans, as discussed in Section 10.1.4. The control group in this pivotal clinical trial was not intravenous ERT, but rather historical controls [110]. The trial should have been designed with an intravenous ERT treatment group, because the TPP1 enzyme in CSF rapidly is exported to blood [114]. TPP1, similar to other lysosomal enzymes, is mannose 6-phosphorylated (M6P), and is a ligand for the M6P receptor (M6PR) [112], which is widely expressed in peripheral tissues [115]. Owing to the high expression of the M6PR in peripheral tissues, recombinant TPP1 is rapidly taken up by peripheral tissues, and is cleared from plasma with a  $T_{1/2}$  of just 12 min [113]. Lipofuscin granules, the lysosomal inclusion bodies that accumulate in CLN disease, are formed in peripheral organs including skeletal muscle [116]. Therefore, following the ICV injection, the TPP1 enzyme moves from



CSF to plasma followed by uptake into peripheral organs via the M6PR. This process could contribute to the improved motor function of children with CLN2 disease as compared to historical controls that expressed no TPP1 enzyme [110]. Such speculation would have been obviated by a clinical trial design that compared ICV drug delivery with intravenous drug delivery, as opposed to historical controls [110]. The admonitions of Fishman and Christy in 1965 [83], and of Aird in 1984 [85], that an intrathecal drug injection is similar to an IV infusion, were not heeded in the trial design of TPP1 in CLN2 disease [110]. To date, recombinant TPP1 for CLN2 is the only treatment that is FDA approved for any chronic CNS disease of brain parenchyma wherein the drug is infused in a chronically implanted Ommaya reservoir in a lateral ventricle [117].

## 2.2. Intra-Cerebral Delivery

### 2.2.1. Intra-Cerebral Implants

An alternative to intrathecal drug delivery to brain is a trans-cranial intra-cerebral injection of drug encapsulated in a polymer or released from a genetically engineered cell line. However, similar to intrathecal drug delivery, the limiting factor in intra-cerebral delivery is diffusion. The brain concentration of drug that enters the parenchyma via diffusion decreases logarithmically with each mm of diffusion distance [118], as illustrated in Figure 5. The maximal effective diffusion distance for small or large molecules in brain is 0.2–2 mm, and this is irrespective of the mechanism of delivery including intra-cerebral implants, ICV administration, intra-cerebral micro-dialysis or intra-cerebral micro-infusion [118].

There is an FDA-approved treatment for brain cancer, carmustine or Gliadel<sup>®</sup>, which is an intra-cerebral implant form of brain drug delivery. Carmustine is a dime-sized wafer of a water-soluble polymer embedded with a small molecule chemotherapeutic alkylating agent, 1,3-bis(2-chloroethyl)-1-nitroso urea (BCNU) [51,119]. The polymer is 20% 1,3-bis(p-carboxyphenoxy) propane and 80% sebacic acid, which is a C-8 dicarboxylic acid found in castor oil. The carmustine polymeric/BCNU wafer is placed in the brain cavity created by the neurosurgical extirpation of the bulk of the cancer, and was first tested in recurrent malignant glioma [120], followed by trials that placed the wafer in the brain cavity at the first surgical resection for malignant glioma [121,122]. Statistical analysis showed the carmustine wafer increases survival in malignant glioma by 10 weeks from 11.6 months to 13.9 months [123]. Subsequent to the 1996 FDA approval of carmustine, no similar intra-cerebral implants for brain cancer, or any other brain disease, have reached regulatory approval. This intra-cerebral implant approach to brain drug delivery cannot escape the physical limitations of diffusion, and the fact that brain 2 mm or more away from the implant is exposed to very little drug released from the wafer [118,119].

The intra-cerebral implant method of brain drug delivery has also been tested following the intra-cerebral injection of genetically modified cells. Rat fibroblasts permanently transfected with a lentivirus encoding for prepro brain-derived neurotrophic factor (BDNF) were implanted in the substantia nigra of rats 1 week prior to the intra-striatal injection of the neurotoxin, 1-methyl-4-phenylpyridinium (MPP+) [52]. MPP+ injection creates an experimental model of PD, which involves neurodegeneration of the nigral-striatal tract in brain. The intra-cerebral implant of the BDNF secreting cells doubled the number of surviving neurons in the nigral-striatal tract [52]. The C2C12 mouse myoblast line was permanently transfected with a gene encoding for human GDNF and encapsulated in a 5 mm rod composed of poly(ethyl-sulfone), followed by implantation in the striatum of the rat, and the diffusion of GDNF from the rod was followed by immunohistochemistry [124]. GDNF was detected within 2 mm of the rod [124]. This distance, 2 mm, may be significant for the 2 g rat brain, but would not cover much volume in the 1400 g human brain. Neural stem cells have been permanently transfected with a variety of neurotrophic factors, and intra-cerebral cell-mediated drug delivery to brain has been reviewed [125].

In an attempt to counter the limited drug distribution in brain following diffusion from a single intra-cerebral injection depot, multi-pronged catheter bundles were described

in 1988 [126]. A bundle of four catheters was developed, and 17–25 such bundles were implanted in the brain of patients with malignant glioma for infusion over 10–14 days of the alkylating agent, cisplatin. With this approach, a total of 68–100 sites of infusion in the brain was created [126]. There has been renewed interest in the multiple catheter approach to intra-cerebral brain drug delivery, as reviewed below for convection-enhanced diffusion.

### 2.2.2. Convection-Enhanced Diffusion

Convection-enhanced diffusion (CED) was developed to overcome the limitations imposed by diffusion on intra-cerebral drug delivery [53]. A catheter is implanted in the brain and fluid flow through the catheter is driven by an external pump, which is implanted in the abdomen. The intent was for drug to move through the brain ECS by convection, rather than diffusion. In the initial evaluation, [ $^{111}\text{In}$ ]-transferrin (Tf) was infused bilaterally by CED in the corona radiata in the cat [53]. The catheter was placed in the white matter of the corona radiata as it was believed that bulk flow in brain would take place preferentially in parallel to the myelin tracts of white matter. Film autoradiography showed a mean radial spread of the Tf through brain of 3 mm [53], which would be equivalent to a volume of  $\sim 100\text{ mm}^3$ . In contrast, the volume of the putamen of the human brain is  $6000\text{ mm}^3$  on each side of the brain [127]. These early findings with CED foretold a potential problem in adequate drug distribution to brain in human clinical trials using CED to deliver neurotrophins to the striatum, as discussed below.

CED was used for brain delivery of cationic liposomes encapsulating herpes simplex virus (HSV)-1 encoding thymidine kinase in patients with recurrent glioblastoma multiforme (GBM) [128]. Patients were administered IV ganciclovir for 2 weeks starting 4 days after the HSV1 administration by CED. This small open label trial of eight patients did not advance to a phase 3 trial [129]. A phase 3 double-blind, placebo-controlled randomized clinical trial (RCT) was performed with the bilateral administration of recombinant GDNF to the putamen of patients with PD [130]. A total of 34 patients were randomized to CED groups that received either GDNF or placebo. The pump was placed in the abdomen and a subcutaneous catheter terminated in the posterior dorsal putamen on both sides of the brain [130]. The trial was unblinded after determining the Unified Parkinson Disease Rating Scale (UPDRS) in all patients after 6 months of CED. There was no significant difference between the UPDRS scores of the GDNF or placebo treated subjects with CED brain drug delivery [130].

A Rhesus monkey study using CED delivery of GDNF to brain illustrated the limitations of the CED approach for brain drug delivery [131]. GDNF ( $14\text{ }\mu\text{g}/\text{day}$ ) was infused into the right putamen of adult Rhesus monkeys at a rate of  $144\text{ }\mu\text{L}/\text{day}$  for 7 consecutive days. The CED catheter was connected to a pump implanted subcutaneously in the abdomen [131]. After 7 days of CED, the brain was removed, and the distribution of GDNF in brain was determined by immunohistochemistry (IHC) and by ELISA. The IHC was performed on serial sections of brain to compute the volume of distribution of GDNF in brain following CED in the primate. These results showed the neurotrophin distributed in a brain volume ranging from  $87\text{--}360\text{ mm}^3$  [131]. This volume of distribution is comparable to the volume of distribution of transferrin following CED in the cat, which was  $\sim 100\text{ mm}^3$  [53]. As discussed above, this distribution volume is small compared to the volume of the putamen, which is  $6000\text{ mm}^3$  on each side of the human brain [127]. The brain concentration of GDNF was measured by ELISA for each mm of distance removed from the CED catheter [131]. The brain concentration of GDNF decreases exponentially with each mm of distance removed from the CED catheter, which indicates the neurotrophin is penetrating brain tissue by diffusion, not convection. The brain GDNF concentrations are shown in Figure 6A.

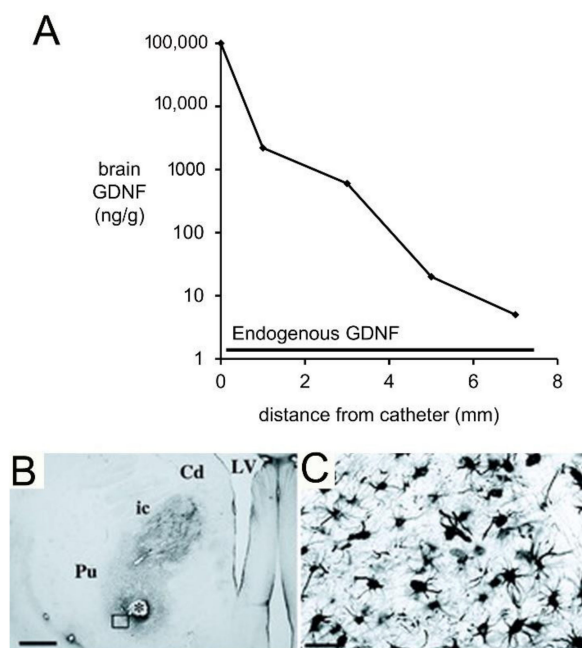


**Figure 6. Brain drug delivery by convection-enhanced diffusion.** (A) Concentration of GDNF in primate brain at 1–7 mm removed from the CED catheter. Derived from data reported by Salvatore et al. [131] and reproduced with permission from [132], Copyright© 2010 Taylor and Francis. Original GDNF concentrations, in pg per mg protein, were converted to ng per gram brain, based on 100 mg protein per gram brain [133]. (B,C) Glial fibrillary acidic protein (GFAP) immunohistochemistry of monkey brain following CED administration of GDNF. Magnification bar is 1 mm in (B) and 50 microns in (C). Reproduced with permission [134], Copyright© 2003 John Wiley & Sons.

The data in Figure 6A show the region of brain most proximal to the catheter is exposed to GDNF concentrations that are log orders higher than the endogenous concentration of GDNF. High concentrations of GDNF may cause aberrant neuronal sprouting in brain [135]. CED of GDNF in the primate brain causes a local astrogliosis, as shown by GFAP immunohistochemistry (Figure 6B,C). It is not clear if this astrogliosis is due to the high local GDNF concentration, or if it is due to the CED delivery system.

CED was evaluated in a multi-centered randomized clinical trial of recurrent GBM treated with either a post-operative placement of carmustine wafer or the post-operative CED administration of cintredexin besudotox, which is a fusion protein of interleukin-13 and a mutated truncated form of the *Pseudomonas aeruginosa* exotoxin A [136]. CED of the toxin provided no clinical benefit and the target of a 2 cm penumbra around the CED catheter was met in only 20% of the patients [136]. The majority of infusions in the patients did not produce a significant coverage of the affected area [137]. A total of 15 CED clinical trials have been performed as of 2019 [129] without any advancement to drug approval. In an attempt to increase drug distribution in brain following CED, a variety of new approaches have been proposed, including the use of CED together with ultrasound [138], CED with newly designed catheters to enable the infusion of high volumes [139], the use of special catheters that infuse fluid simultaneously through 4 parallel ports [140], and the concurrent use of CED with pulsed electric currents applied to brain [141]. Real time MRI has been useful for the identification of reflux along the cannula, leakage of the infusate, and ventricular compression associated with CED [142].

### 3. Trans-Nasal Drug Delivery to Brain

The first report of drug movement from the nasal cavity to CSF was described 40 years ago [50]. Since then, over 1000 publications have evaluated drug delivery to brain and CSF via the nasal route (Table 1). However, to date, there is not a single FDA-approved drug for treatment of the brain parenchyma that is administered by the intra-nasal route [143].

To understand why 40 years of research on nasal delivery in animals has not translated to humans, it is useful to consider species differences in the anatomy of the nasal-cribriform plate. Species differences in the nasal cavity anatomy are consistent with the much greater role of olfaction in animals as compared to humans, as reflected in the number of olfactory receptor (OR) genes. OR genes comprise the largest multi-gene family in the mammalian genome, and constitute 4–5% of the mammalian proteome [144]. There are about 2000 OR genes in the rat [145], about 1000 OR genes in the mouse, but only about 400 OR genes in humans [144]. The olfactory region of the nasal mucosa, which is the site where drug must penetrate the nasal mucosa to enter olfactory CSF, constitutes 50% of the nasal cavity surface area in the rat, but only 3% of the nasal cavity surface area in humans [146]. Another factor limiting the translation of nasal drug delivery from animals to humans is the fact that the vast majority of preclinical investigations on nasal drug delivery to brain are performed with experimental designs that produce local nasal injury and membrane disruption, owing to the nasal instillation of very large volumes of drug. The introduction of >100  $\mu\text{L}$  in the human nostril causes local injury to the nasal mucosa [147,148]. The volume of the nasal cavity in humans is 20 mL, but is only 0.4 mL in the rat, and only 0.03 mL in the mouse [148]. Therefore, by extrapolation, the nasal administration of a volume greater than 1% of the volume of the nasal cavity can induce local injury. A nasal administration volume of 1% of the nasal cavity volume would be 4  $\mu\text{L}$  in the rat and 0.3  $\mu\text{L}$  in the mouse. A review of the literature discussed below shows that the nasal administration volumes in preclinical nasal drug delivery research are 1–2 log orders higher than these injury related volume thresholds.

### 3.1. Drainage of CSF from Brain to Nose

There is evidence from animal models that CSF drains from the subarachnoid space of brain into the nasal mucosa, and then to the lymphatic system. The anatomy of the olfactory nerves and arachnoid, cribriform plate, and nasal mucosa is shown in Figure 7A.

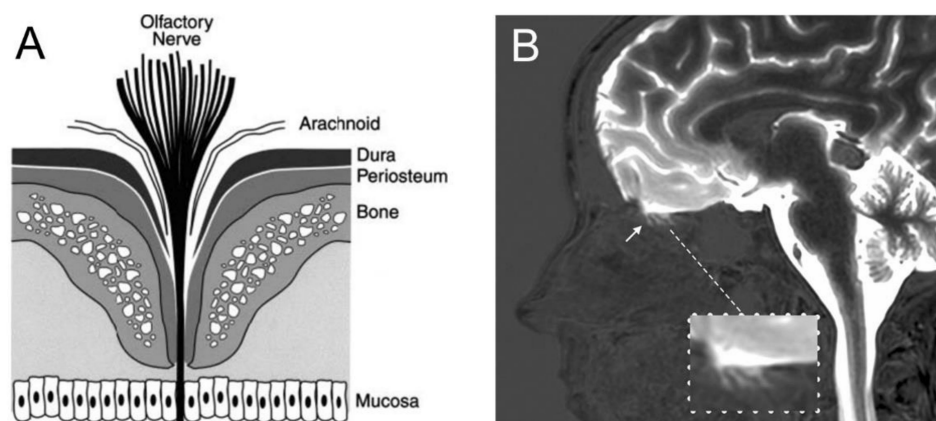


**Figure 7.** Anatomy of the cribriform plate separation of the cranial and nasal cavities. (A) The bipolar olfactory sensory neurons, which express the olfactory receptors, pass from the olfactory bulb to the nasal mucosa through the fenestrations of the cribriform plate. Reproduced with permission from [149], Copyright© 2003 JNS Publishing Group. (B) Magnetic resonance imaging (MRI) of the human head between 3–6 h following the injection into the lumbar CSF of gadobutrol, a macrocyclic gadolinium contrast agent. The gadolinium is visualized throughout the cerebral subarachnoid space within the convexities of the cerebrum, around the spinal cord, and is observed to penetrate into the superior regions of the fenestrations of the cribriform plate, which is magnified in the inset. No gadolinium passes into the inferior regions of the cribriform fenestrations, or into the nasal mucosa in humans (inset). Reproduced from [150], Copyright© 2020 licensed under Creative Commons Attribution License (CC-BY).

The evidence for the existence of a pathway of fluid flow from the CSF compartment of brain to the nose is less convincing for living humans. In 1937, Faber [151] observed in

rabbits the movement of radiographic contrast agent from the CSF of the cisterna magna to the nasal cavity. The mechanism of this transfer was clarified by the injection of radioiodinated albumin into the lateral ventricle of the rabbit [152]. A fraction of the radioactivity was recovered in the peripheral lymph, and this transfer to lymph was blocked by sealing the cribriform plate. Albumin, or at least the radioactivity, was demonstrated to pass from the CSF compartment of brain through the cribriform plate to the interstitial space of the olfactory submucosa or lamina propria [152]. The anatomical features enabling movement of olfactory CSF from above the cribriform plate to below the cribriform plate were examined at autopsy for the post-mortem human brain [149], as shown in Figure 7A. The olfactory CSF within the subarachnoid space of the olfactory bulb moves in parallel with the invaginations of the olfactory arachnoid membrane and dura around the olfactory nerves, which pass from the olfactory bulb to the nasal mucosa through the fenestrations of the neural foramina of the cribriform plate. The arachnoid membrane peels away from the olfactory nerve at 1–2 mm into these foramina, where the dura becomes continuous with the periosteum of the cribriform plate [149].

In the late embryonic rat, there are ‘olfactory bulb holes’, or disruptions of the arachnoid membrane at the cribriform fenestrations, which allow for drainage of olfactory CSF into the nasal mucosa [153]. However, the ultrastructural details of the junctions between the arachnoid, dura, and olfactory nerve at the proximal part of the cribriform fenestrations, and confirmation of holes in the olfactory arachnoid are not available for humans. The arachnoid membrane has high resistance tight junctions [149], similar to the endothelial junctions that form the BBB (Figure 4). The extent to which tight junctional complexes exist within the proximal part of the cribriform fenestrations is not known. An MRI study [150] in humans shows a gadolinium contrast agent that is injected into the CSF enters the proximal part of the cribriform fenestrations, but does not complete passage through these fenestrations, nor enter into the nasal submucosa (Figure 7B). This recent study in living humans does not confirm the hypothesis generated in animal investigations that CSF passes from the olfactory CSF into the nasal mucosa. Such passage of CSF from the olfactory region to the nasal submucosa would be a form of chronic subclinical CSF rhinorrhea, a condition associated in humans with local trauma to the cribriform plate [154].

### 3.2. Drug Delivery from Nose to Brain

Drug transport from nose to olfactory CSF involves drug transfer across 2 epithelial barriers, both of which are membrane barriers with tight junctions, and these barriers are the nasal epithelium and the arachnoid membrane. Therefore, drug delivery from nose to olfactory CSF is governed by the same principles that determine BBB transport. As discussed below in Section 6.1, lipid-soluble small molecules with a MW < 450 Da traverse these barriers by free diffusion. Any drug with a MW > 450 Da can only traverse the barrier by either (a) carrier- or receptor-mediated transport, or (b) membrane disruption, e.g., by local injury to the nasal mucosa. Similar to the BBB, the transport of small molecules from the nasal cavity to CSF is proportional to lipid solubility [155]. In 1982, progesterone was administered trans-nasally in primates, and the area under the concentration curve (AUC) in CSF was about twice as high as the AUC in CSF following IV administration [50]. These results were interpreted as evidence for a pathway of drug delivery from nose to CSF. However, the diluent injected in the nose in this study was 30% ethanol/30% propylene glycol [50], which may have had a solvent effect at the nasal mucosa. In a study in the rat, progesterone was administered via the nasal route in a saline diluent, and the AUC in CSF of progesterone was identical after IV or intra-nasal delivery [156]. Similarly, melatonin [157] and vitamin B12 [147] were administered via the intra-nasal and IV routes, and the AUC in CSF was identical for either form of delivery. If the drug passed directly from the nose to the olfactory CSF, then the AUC in the CSF should be higher after the nasal route as compared to the IV route. Conversely, the finding of a comparable AUC in CSF after either the IV or the nasal route indicates the drug passes across the nasal epithelium, enters blood, and then traverses the choroid plexus at the blood–CSF barrier, to enter the

CSF compartment. A 1990 study on the potential delivery of a novel cognitive enhancer for Alzheimer's disease (AD) via the trans-nasal route showed the brain AUC of the drug was the same following either IV or trans-nasal administration [158]. In 1991, the brain concentration of dextromethorphan was shown to be the same whether this drug was administered by the IV or the trans-nasal route [159]. In 2008, it was shown that the ratio of brain AUC/plasma AUC for diazepam was comparable following drug administration via either the IV or the trans-nasal routes [160].

Despite the early work showing the trans-nasal route conferred no selective delivery of drug to CSF, the number of investigations of the trans-nasal route grew exponentially, and 98% of the 1024 publications on trans-nasal brain drug delivery (Table 1) were published after 2000. Trans-nasal drug delivery to CSF succeeded once large volumes of drug were applied to the nasal cavity, particularly in rats and mice, where the olfactory region constitutes 50% of the nasal cavity surface area [146]. These large volumes induced local injury and disruption of the nasal barriers, similarly to the attempts to enhance brain drug delivery via BBB disruption as reviewed in Section 4. The instillation of drug volumes greater than 100  $\mu\text{L}$  per naris in humans causes local injury [147] and the preferred volume for nasal administration in humans is as low as 25  $\mu\text{L}$  per naris [161]. These volumes are <1% of the nasal cavity in humans. However, in studies in rats and mice the volume of drug introduced into the nose is typically 25–50  $\mu\text{L}$ , which is very large compared to the volume of the nasal cavity in the rat, 400  $\mu\text{L}$ , or the mouse, 30  $\mu\text{L}$  [148]. The introduction of large volumes into the naris can lead to drug loss into the oral cavity via drainage through the naso-palatine duct in rodents, although this duct is a vestigial organ in adult humans. Therefore, the naso-palatine duct was blocked prior to the nasal introduction of 50  $\mu\text{L}$  in the rat [162]. In this 1999 study, the intra-nasal administration of a volume of 50  $\mu\text{L}$  in the rat, which is 12% of the nasal cavity volume, produced a higher CSF concentration of 5-fluorouracil than the CSF drug concentration produced by IV administration [162].

The administration of 5  $\mu\text{L}$  in the naris of the mouse, which is a volume that is 15% of the nasal cavity in the mouse, resulted in the delivery of dopamine to the olfactory bulb of brain [163]. In a similar study, a 5  $\mu\text{L}$  volume of picolinic acid in the naris of the mouse resulted in drug delivery to the olfactory bulb [164]. Drug delivery to brain of either dopamine or picolinic acid was measured by film autoradiography, which showed the olfactory bulb was the only region of brain penetrated by the drug following the instillation of large volumes into the mouse nose [163,164]. In a recent study, insulin was injected into the naris of a mouse in a volume of 25  $\mu\text{L}$  [165], which is nearly equal to the entire nasal cavity in the mouse. Conversely, no delivery of IGF-1 to brain was produced following the intra-nasal administration of the peptide in a large volume, 35  $\mu\text{L}$ , in the mouse [166]. In addition to the introduction of large volumes into the nasal cavity, other means of membrane destabilization have been employed to enhance drug delivery across the nasal barriers. Carbamazepine was administered by either the IV or trans-nasal routes in the rat; for nasal administration the drug was co-administered in an unspecified volume with 50 mg of a gel composed of the Carbopol 974P bioadhesive [167]. Other nasal enhancers that have been employed include 0.5% peppermint oil [168] and 2% polysorbate-80 [169].

In keeping with the analogy of drug delivery across the nasal barrier and the BBB, a preferred approach is not membrane disruption, but rather modification of the drug so that the drug becomes a ligand for endocytosis. As discussed in Section 7, cationic agents may undergo endocytosis into the brain capillary endothelium via absorptive-mediated endocytosis. Lectins, such as wheat germ agglutinin (WGA), can also undergo absorptive-mediated endocytosis into the brain endothelium [170]. A conjugate of WGA and HRP, but not unconjugated HRP, distributes to the olfactory lobe in rats following the intranasal administration of 25–50  $\mu\text{L}$  into each naris of a 1% solution [171]. Cationization of a biologic also facilitates entry into CSF following intra-nasal administration. The lysosomal enzyme, iduronidase (IDUA), was cationized by conjugation of guanidinylated neomycin (Gneo) to the enzyme [172]. Guanidinylation of neomycin converts all 6 amino groups to positively charged guanidine moieties. Gneo is endocytosed by cells via absorptive-

mediated endocytosis, similar to other polycations, such as poly-arginine [173]. Gneo-IDUA was infused into the nose in a volume of 50  $\mu\text{L}$  in IDUA-null mice, and CSF enzyme activity was measured [172]. Gneo-IDUA entered the CSF, which peaked at 1 h and over 90% of the enzyme was cleared from CSF by 4 h after injection [172]. IDUA was also detected in the olfactory bulb, and the enzyme activity in this region of brain was >10-fold higher than any other region of brain [172].

Drug distribution following trans-nasal administration has been investigated by PET. The glucose analog, [ $^{18}\text{F}$ ]-fluorodeoxyglucose (FDG), was administered in the rat in volumes of 5  $\mu\text{L}$  [174]. FDG entered only the inferior part of the turbinates of the cribriform plate and did not reach the superior part of the turbinate, and did not enter into the olfactory bulb [174]. In another PET study in the rat, [ $^{11}\text{C}$ ]-orexin A, a 33-amino acid peptide that is a potential treatment of narcolepsy, was injected in the nose in an unspecified volume using a Precision Olfactory Delivery system [175]. PET imaging showed the only part of brain exposed to the peptide was the olfactory bulb ipsilateral to the injected naris [175].

In summary, when low volumes of drug are instilled into the nose, and local injury to the nasal mucosa is not produced, then there is little evidence for drug delivery to the olfactory CSF, much less the brain following trans-nasal drug delivery. Predictably, clinical trials in humans of trans-nasal drug delivery have failed to demonstrate selective drug distribution into CSF via the nasal route, as discussed in the next section.

### 3.3. Clinical Trials of Trans-Nasal Drug Delivery to Brain

The peptide, oxytocin, was administered by the nasal route in patients with autism, in a double-blind placebo-controlled randomized clinical trial (RCT), and this treatment showed no clinical efficacy in either autism [176] or early psychosis [177]. In a second autism trial of intra-nasal oxytocin, there was a significant effect on overt emotion salience, but the drug had no dose response effect on this symptom [178]. After these negative clinical trials, the distribution of oxytocin into the CSF of primates was measured, and identical distribution of peptide into CSF was observed with either the IV or trans-nasal route of administration [179]. A follow-up RCT of nasal oxytocin in autism showed no clinical benefit [180]. A RCT of trans-nasal delivery of insulin for AD showed no clinical benefit [181]. In this trial, the insulin was delivered as a nebulized stream through a nosepiece left in the nostril for 20 s, and 40 units of insulin was delivered daily for 12 months. Treatment caused no increase in CSF insulin [181]. To date, no RCT has shown a clinical benefit in a CNS disease using the trans-nasal route of brain drug delivery. A recent review of the literature shows the trans-nasal route results in no consistent increase in brain delivery of small molecules in animal models [182].

## 4. Brain Drug Delivery with Blood–Brain Barrier Disruption (BBBD)

### 4.1. BBBD Following Intra-Carotid Arterial Infusion

#### 4.1.1. BBBD with Intra-Arterial Hyper-Osmolar Solutions

The disruption of the BBB following the intra-arterial infusion of hypertonic solutions was first demonstrated by Broman in 1945 [183] and by Rapoport in 1970 [184]. In 1973, Brightman et al. [185] showed the disruption of the BBB following the intra-carotid arterial infusion of hypertonic urea caused the shrinkage of brain endothelial cells in association with opening of endothelial tight junctions. In 1979, three groups used hyperosmolar BBBD to enhance brain uptake of therapeutics such as methotrexate [49,186], or an enzyme [187], following the intra-arterial infusion of a poorly diffusible hypertonic monosaccharide, mannitol or arabinose. BBB delivery of a drug across the disrupted BBB was shown to be dependent on MW, which is consistent with a pore mechanism associated with opening of tight junctions [188]. Hypertonic BBBD caused an increase in brain ornithine decarboxylase (ODC) activity and increased brain polyamines, and the disruption of the BBB was blocked by an ODC inhibitor,  $\alpha$ -difluoromethylornithine (DFMO) [189]. BBBD mediated by arterial hyperosmolarity requires an intact BBB to establish the osmotic gradients across the endothelium. Consequently, the BBB in normal brain is disrupted to a

greater extent than in a brain tumor, where there may be a pre-existing disruption of the BBB [190]. This reduces the therapeutic index of the BBBD, as the toxic effect in normal brain is greater than the therapeutic effect in the brain tumor [190]. These findings in an experimental rat brain tumor model [190] were replicated in humans with a malignant glial tumor [191]. The BBB permeability–surface area (PS) product, also called the  $K_1$ , was measured for 82-rubidium with PET scans of the brain. Intra-carotid arterial infusion of 25% (1.4 M) mannitol was performed for 30 s at high flow rates (360–720 mL/min) under anesthesia and seizure prophylaxis with phenobarbital or phenytoin. The rubidium  $K_1$  increased 17-fold in normal brain, but was unchanged in the tumor brain. The  $T_{1/2}$  for return to normal BBB permeability was 8 min [191]. In contrast to hyper-osmolar BBBD, which preferentially effects normal brain, as compared to brain tumor, the intra-arterial infusion of vasoactive agents, such as bradykinin analogues, preferentially opens the BBB in tumor as compared to normal brain [192], as discussed in the next section.

Hyperosmolar BBBD, in combination with intra-arterial methotrexate, was demonstrated to enhance survival in patients with primary CNS lymphoma (PCNSL) [193]. At that time, PCNSL was known to be treatable with high dose methotrexate (HD-MTX) with leucovorin (folinic acid) rescue [194]. The efficacy of BBBD with hypertonic mannitol and intra-arterial methotrexate for PCNSL was confirmed in a larger cohort of patients [195], and is still in practice today [196]. There still is no FDA market approval for this approach, as a controlled clinical trial comparing intra-arterial mannitol/methotrexate vs. intra-arterial methotrexate has apparently not been performed in PCNSL.

Intra-carotid arterial hyperosmolar mannitol (ICAHM) administration is an aggressive intervention that is not without toxic sequelae. When the BBB is disrupted for the purpose of chemotherapeutic delivery to brain, virtually all substances in plasma, at least up to the size of the 420,000 Da fibrinogen, may also escape from blood to the brain ECS. Albumin is toxic to astrocytes, which can trigger a glial scar [197], and is pro-inflammatory [198]. Fibrinogen activates oligodendrocyte progenitor cells, which can lead to suppression of myelin production [199]. ICAHM induces a sterile inflammatory response (SIR) in brain, which is associated with activated astrocytes and microglia, an up-regulation of cytokines, chemokines, and trophic factors, and these changes are observed in the contralateral hemisphere, as well as the cerebral hemisphere ipsilateral to the infusion [200]. A similar SIR is observed with ultrasound-induced BBBD [201], as discussed below. Hyperosmolar BBBD causes vascular changes in brain [202], and chronic neuropathologic changes [203], owing to the brain uptake of plasma proteins that are normally excluded from brain by the BBB [204]. Peri-operative effects occur following ICAHM with a 13% incidence of seizures [205], despite pre-operative administration of anticonvulsants [206]. Electroencephalogram (EEG) abnormalities are used to monitor BBBD intra-operatively [207].

#### 4.1.2. BBBD with Intra-Arterial Bradykinin Analogs

The topical application of bradykinin (BK) to the pial surface of brain causes BBBD to small molecules such as fluorescein but not to large molecules such as albumin [208]. Since topical application of BK to the surface of the brain induces a pharmacologic effect, it is inferred that the BK receptor is expressed on the abluminal side of the BBB. It is not practical to use BK as an agent to induce BBBD as this peptide is rapidly degraded and has a plasma  $T_{1/2}$  of about 15 s, owing to first pass inactivation in the lung by angiotensin converting enzyme (ACE) [209]. A more metabolically stable analogue of BK was developed, RMP-7 [210], as an agent to induce biochemical BBBD, where RMP = receptor-mediated permeabilizer. Intra-carotid arterial administration of RMP-7 caused selective BBBD in an experimental brain tumor, as compared to normal brain [211]. This effect is opposite of hyperosmolar BBBD, which opens the BBB in normal brain to a much greater extent than in a brain tumor [191]. Capillaries perfusing the core of brain tumors are often leaky, which enables intra-arterial BK analogues to access the BK receptors on the abluminal side of the BBB in brain tumors. The carotid arterial infusion dose of RMP-7 was 0.1  $\mu\text{g}/\text{kg}$ , as higher doses, 1  $\mu\text{g}/\text{kg}$ , caused hypotension [211]. In humans with malignant glioma,



intra-arterial RMP-7, at a dose of 10–300 ng/kg, caused an increase in the PS product of [ $^{68}\text{Ga}$ ]-EDTA of  $46 \pm 42\%$  as determined by PET [212]. The cause of the wide variability in the opening of the blood–tumor barrier (BTB) is not clear, but may be related to differences in the degree of disruption of the BTB in brain tumors. Intra-arterial RMP-7 caused no BBBB in normal brain in humans [212], which is consistent with an abluminal expression of the BK receptor. Intravenous administration of RMP-7 caused no BBBB in dogs [213] or rats [214]. Intravenous RMP-7 did not increase the clinical efficacy of carboplatin in a RCT of malignant glioma [215]. The applications of RMP-7 proved to be limited to the intra-carotid arterial infusion route in conditions with a pre-existing BBBB, e.g., malignant gliomas. Given this limited scope of clinical applications, the drug development of RMP-7 was terminated in the 1990s.

#### 4.2. BBBB Following Intravenous Microbubble/Focused Ultrasound

Focused ultrasound (FUS) of the brain was described by Lynn et al. in 1942 in cats and dogs [216]. In 1960, Ballantine et al. [217] reviewed FUS of the brain and concluded that BBBB may be introduced without lesions of the surrounding parenchyma. However, high intensity FUS of brain was shown in 1968 to cause focal lesions in the CNS including vascular occlusion [218]. In 1995, attempts were made to modulate the sonication parameters so as to separate BBBB from parenchymal damage in brain [219]. FUS was combined with the IV administration of an ultrasonic contrast agent, which is composed of 2–4.5 micron microbubbles (MB) of Optison [66]. The Optison microbubble, as well as Definity microbubble, contains a gaseous interior of octafluoropropane. The FUS-MB treatment produced BBBB in rabbits [66]. The anatomical basis of the BBBB caused by microbubbles/FUS was shown by electron microscopy to be both opening of tight junctions and enhanced vesicular transport [220,221]. The BBBB caused by the FUS-MB method enabled brain penetration of 3 kDa and 70 kDa dextran, but not 2000 kDa dextran, and the brain penetration of 3 kDa dextran exceeded that for 70 kDa dextran [222]. The brain uptake of 3 kDa, 70 kDa, 500 kDa, and 2000 kDa dextran was measured following the administration of 3 different FUS-MB protocols that varied the acoustic power from 0.31 Mpa, 0.51 Mpa, and 0.84 Mpa, where Mpa = mega Pascals [223]. There was minimal entry of any dextran with an acoustic pressure of 0.31 mPa. At an acoustic pressure of 0.51 mPa, the 3 kDa dextran entered the brain to an extent greater than the 70 kDa dextran, and the 500 kDa and 2000 kDa dextrans did not enter brain. At the acoustic pressure of 0.84 Mpa, all dextrans entered the brain, although the entry of the 500 kDa and 2000 kDa dextrans was nearly background [223]. The gyration radii of 4 kDa, 70 kDa, 500 kDa, and 2000 kDa dextran are 2.2 nm, 9 nm, 10.5 nm, and 58 nm, respectively [224]. Therefore, the diameter of the pore created by FUS-MB treatment at an acoustic pressure of 0.51 Mpa is about 20 nm, which is of sufficient size for entry of plasma proteins and therapeutic antibodies, which have a diameter of 10–11 nm [225]. The opening of the BBB following FUS-MB is on the order of hours, and the BBBB is resolved by 6–24 h [226]. The extent to which the BBB is disrupted is a function of both the acoustic power applied to brain, and the injection dose (ID) of the microbubbles. The higher the acoustic power, and the higher the ID of the microbubble, the greater the disruption of the BBB [227]. If the acoustic power is increased from 0.53 Mpa to 0.64 Mpa, and the ID of the microbubbles is increased from 0.1 to 0.5 mL/kg, then even a 200 nm pegylated liposome enters the brain [227]. However, as the ID of the microbubble is increased from 0.15 mL/kg to 0.4 mL/kg, neuropathologic effects on brain are observed including neuronal apoptosis and intra-cerebral hemorrhage [228], and the neurotoxicity of FUS-MB treatment is discussed below.

The FUS-MB approach to BBBB has entered into phase 1–2 clinical trials. Patients with recurrent GBM were treated with a FUS dose escalation from 0.5 mPa to 1.1 Mpa, in conjunction with an ID of 0.1 mL/kg of SonoVue microbubbles, which contain a hexafluoride gas [229]. The FUS was administered by an ultrasonic transducer implanted in the skull. No clinical efficacy was evaluated in this trial as no therapeutic was co-administered with the BBBB. In a phase 1 trial of recurrent malignant glioma in 5 patients, the FUS-MB-

induced BBBB was performed in conjunction with doxorubicin/pegylated liposomes in 1 patient and temozolomide in 4 patients [230]. The ID of the Definity microbubble was up to 0.02 mL/kg. The FUS was administered by a helmet following shaving of the head and in the presence of stand-by anesthesia. The sonicated area was determined by contrast MRI of the head. The volume of the sonicated volume area of brain was about 0.5 mL, and a biopsy was performed of the sonicated and non-sonicated peri-tumor tissue. BBBB caused no increase in the brain concentration of either doxorubicin or temozolomide in this pilot study [230]. A phase 1 trial of FUS-MB treatment was performed in 6 subjects with recurrent glioblastoma [231]. In this acoustic power dose escalation study, the IV dose of microbubbles was 0.1 mL/kg. No drug was co-administered in this trial [231]. Clinical trials of the FUS-MB method of BBBB are being extended from life threatening focal disease of brain, such as malignant glioma, to chronic neurodegenerative disease of brain including Alzheimer's disease (AD) [232] and amyotrophic lateral sclerosis (ALS) [233]. In these phase 1 trials, no therapeutic was co-administered with the FUS-MB. To date, no clinical trial has demonstrated any clinical efficacy of the FUS-MB method of BBBB in human CNS disease.

The neuropathology of hyperosmolar BBBB is discussed in Section 4.1.1, and a similar profile of neuropathology is caused by the FUS-MB method of BBBB. In both cases, the brain parenchyma is exposed to serum protein, which enter brain following BBBB. The FUS-MB treatment causes cell uptake of albumin, which is associated with activation of astrocytes and microglia in brain [234]. Similar to the sterile inflammatory response (SIR) caused by hyperosmolar BBBB [200], the FUS-MB form of BBBB also causes an SIR in brain [201]. Albumin entry into the parenchyma of brain induces neuroinflammation triggered by the NF $\kappa$ B pathway [201]. This SIR response, which is similar to that observed in cerebral ischemia or traumatic brain injury [201], is associated with the up-regulation of >1000 genes within 6–24 h of the FUS-MB treatment [235]. A recent review [236] suggests that optimization of ultrasound parameters may allow for “safe” BBBB. However, the FUS-MB method of BBBB seems to be an example of a therapy with a therapeutic index of 1. If the BBB is disrupted, so as to allow the entry into brain of a therapeutic, the parallel entry of plasma proteins, which are toxic to brain, is inescapable.

#### 4.3. Miscellaneous Forms of BBBB

BBBB via intra-carotid arterial hyperosmolar mannitol (ICAHM), or via focused ultrasound-microbubbles (FUS-MB), are aggressive approaches to brain drug delivery that require treatment in the operating room either under anesthesia, in the case of ICAHM, or with standby anesthesia, in the case of FUS-MB. Attempts have been made to produce BBBB biochemically, which gave rise to the development of RMP-7. However, RMP-7 administration required an interventional radiologist for intra-carotid arterial administration, and only worked in conditions with a pre-existing BBBB such as advanced malignant gliomas [212]. A kind of ‘holy grail’ in brain pharmaceuticals is the development of a non-invasive form of BBBB following IV administration. The effort to disrupt the BBB as a therapeutic intervention is paradoxical, because the BBB “allows for maintenance of homeostasis of the CNS milieu” [237]. If this is true, then would not BBBB have serious toxicity in the brain? Indeed, the most developed forms of BBBB, ICAHM and FUS-MB, both cause a non-infectious inflammation in brain called a sterile inflammatory response (SIR) [200,201,235]. ICAHM was demonstrated over 30 years ago to cause vascular pathology in brain [202], and chronic neuropathologic effects in brain [203]. One of the earliest forms of BBBB described was the intra-carotid artery injection of micellar forming concentrations of common neuropsychiatric drugs, nortriptyline and chlorpromazine [238]. However, this arterial drug-induced BBBB was clearly a toxicologic effect of very high concentrations of these drugs. The miscellaneous forms of BBBB described below are also toxicologic, not therapeutic, approaches to brain drug delivery.

#### 4.3.1. BBBD with Tight Junction Modulators

Both ICAHM and FUS-MB disrupt the BBB by opening tight junctions [185,221]. Alternative approaches to opening tight junctions have been proposed, and these can be classified as to whether the agent is administered by the intravenous or the intra-arterial route. The Ser-His-Ala-Val-Ser (SHAVS) pentapeptide includes the HAV tripeptide sequence from the extracellular domain (ECD) of E-cadherin, a cell adhesion molecule involved in tight junction formation. A cyclic version of the pentapeptide was more stable in plasma [239]. The cyclic pentapeptide affected epithelial resistance in cell culture at high peptide concentration of 0.5–1 mM, and IV administration of the cyclic peptide in mice increased the brain uptake of gadolinium on MRI [239]. The co-administration of the linear form of the SHAVS peptide and peroxiredoxin-1, an anti-oxidant enzyme, reduced tumor growth in a mouse medulloblastoma tumor model [240]. The intra-arterial infusion of a high concentration, 1 mM, of the linear form of the SHAVS peptide increases mannitol uptake by brain [241].

A monoclonal antibody (MAb) against claudin-5 (CLDN5), a tight junction protein, caused BBBD in a cell culture model [242]. IV administration of this MAb in primates at an injection dose (ID) of 3 mg/kg caused increased uptake of fluorescein in the CSF. However, the MAb has a narrow therapeutic index, as a dose of 6 mg/kg of the CLDN5 MAb induced convulsions in monkeys [243].

Angubindin-1 is a 200-amino acid fragment derived from the *Clostridium perfringens* iota-toxin, and it binds tricellulin, a component of tricellular tight junctions [244]. Angubindin-1 was expressed as a glutathione S-transferase (GST) fusion protein, and was administered IV to mice at an ID of 10 mg/kg. This treatment increased the brain uptake of an antisense oligodeoxynucleotide [244].

The intra-carotid arterial infusion of membrane active agents can also induce BBBD by interference with tight junctions. Arterial infusion of 30 mM caproic acid, a 10-carbon monocarboxylic acid, for 30 s causes enhanced transport of mannitol across the BBB; however, 45–90 s infusions of caproic acid caused brain edema [245]. An emulsion of triolein, a neutral triglyceride, causes BBBD following a 3 min manual carotid arterial infusion over 60 s in the rat [246]. If BBBD enables the entry of plasma proteins into brain parenchyma, this produces, by definition, the vasogenic form of brain edema [247].

#### 4.3.2. BBBD with Adenosine Analogues

Regadenoson is an adenosine analogue that is FDA approved for cardiac stress tests, and is administered as an IV dose of ~5 µg/kg [248]. Regadenoson is an adenosine receptor (AR) agonist, and the IV injection of 1 µg/kg in rats produces only a marginal increase in the brain uptake of 10 kDa dextran [249]. This may be due to the very rapid plasma clearance of regadenoson, which has a plasma  $T_{1/2}$  of only 2–4 min [250]. The IV injection of 3 sequential doses of regadenoson enhances brain uptake of 10 kDa dextran [249]. It is not clear how regadenoson causes BBBD, since this drug, 5'-N-ethylcarboxamide adenosine (NECA), has a MW of 390 Da and forms 12 hydrogen bonds with water. As discussed in Section 6.1.2, small polar molecules with these properties do not cross the BBB. An adenosine transporter is expressed on the BBB, as discussed in Section 6.2.5, but it is not clear if NECA is a ligand for the adenosine transporter. Regadenoson, like RMP-7, may be effective in the treatment of brain tumors that have a pre-existing leakage of the BBB. Rats with an F344 experimental brain tumor were treated with oral temozolomide, 50 mg/kg, in conjunction with an IV dose of Regadenoson of 0.5 µg/kg, and the BBBD increased the tumor/plasma temozolomide ratio by 55% [250].

#### 4.3.3. BBBD with Anti-Bacteria Antibodies

A MAb, designated 13.6E1, against the filamentous hemagglutinin of *Bordetella pertussis* was injected intravenously in rabbits at a dose of 30 µg/kg, and this produced BBBD, as measured by the increased brain uptake of penicillin [251]. Immunohistochemistry showed the MAb bound to the vasculature of human and rabbit brain [251]. Complete

Freund's adjuvant (CFA), which is composed of inactivated mycobacteria, causes BBBB in mice, manifested by brain uptake of circulating IgG for 2–3 weeks, following a subcutaneous (SQ) injection of CFA [252]. The primary antigen of the mycobacterial cell wall is lipoarabinomannan, and an IgM anti-mannan MAb was generated [253]. Following the IV injection of 2 mg of the anti-mannan MAb in the rat, BBBB and vasogenic edema were observed, in parallel with global brain uptake of gadolinium by MRI [253]. The BBBB resolved within 24 h. BBBB is observed in experimental autoimmune encephalomyelitis (EAE), which is produced following the SQ injection of guinea pig brain extract mixed in complete Freund's adjuvant [254]. The BBBB in this model is nearly eliminated by either neuro-intermediate pituitary lobectomy or an arginine vasopressin (AVP) receptor blocker, conivaptan [254]. This study implicates the role of the V1a or V2 AVP receptors in the BBBB associated with EAE. Similarly, the vasogenic brain edema and BBBB that follows permanent occlusion of the middle cerebral artery in experimental stroke was reduced by conivaptan administration [255].

#### 4.3.4. BBBB with Intra-Arterial Polycations

The carotid arterial infusion of 50–500 µg/mL protamine sulfate for 1–2 min in the rat results in BBBB, associated with increase brain uptake of HRP in parallel with opening of brain endothelial tight junctions [256]. A similar finding was observed in rabbits following the carotid arterial infusion of protamine sulfate, and the BBBB to albumin caused by the arterial infusion of protamine was attenuated by the co-infusion of the anionic heparin, which neutralizes the cationic protamine [257]. No BBBB was induced by protamine if the polycationic agent was administered by the intravenous route. The arterial infusion of other polycationic agents, including poly-arginine, poly-lysine [258] or histone [259] similarly caused BBBB. The BBBB induced by the intra-arterial infusion of polycations is toxic, as the intra-arterial protamine infusion led to spongiotic shrunken nerve cells in brain [260].

#### 4.3.5. BBBB with Intra-Arterial Amphipathic Agents

Amphipathic agents form micelles at concentrations above the critical micellar concentration (CMC), and can disrupt the permeability of membranes [261], including the BBB [238]. The intra-carotid arterial infusion of dehydrocholate, an oxidized bile salt, causes BBBB to albumin [262]. Similar to hyperosmolar BBBB, which causes changes in the EEG [207], BBBB due to dehydrocholate administration also causes changes in the EEG [262]. The carotid arterial infusion of 20 µM oleic acid, an 18-carbon omega-9 free fatty acid (FFA), causes BBBB to albumin [263]. The BBBB caused by the administration of alkylglycerols was developed as a new brain drug delivery strategy [264]. However, alkylglycerols, such as 1-O-hexyldiglycerol or 1-O-heptyltriglycerol, cause BBBB only after carotid arterial infusion, and not after IV administration [265]. Only high 80 mM concentrations of alkylglycerols in the arterial infusate caused BBBB to small molecules. These concentrations exceed the CMC and cause the formation of vesicles, which appear to be the mechanism of increased BBB permeability [265]. Melittin, a 26 amino acid anti-microbial peptide from bee venom, has recently been suggested as a new brain drug delivery strategy, as intra-carotid arterial infusion of 3 µM melittin causes BBBB [266]. However, melittin is unlikely to have an acceptable safety profile, as this peptide is known to alter membrane permeability by inducing the formation of membrane holes [267]. These holes form when the concentration of the peptide reaches a threshold ratio of peptide to membrane lipid [267]. Other membrane active agents that have been proposed as new brain drug delivery strategies are L-borneol [268] and NEO100 [269], which have similar organic alcohol amphipathic structures. The oral administration of 1200 mg/kg of L-borneol causes BBBB to Evans blue/albumin [268]. However, this dose is near the 50% lethal dose (LD50) of L-borneol, which is 300–5800 mg/kg in rodents [270]. NEO100 is perillyl alcohol, and the intra-carotid arterial infusion of 20 mM NEO100 causes BBBB to albumin [269]. NEO100 produces no BBBB following IV administration [269], similar to the alkylglycerols [265].

#### 4.3.6. BBBD and Free Radicals

Methamphetamine causes BBBD in association with the formation of free radicals, and the effect on the BBB is attenuated by Trolox, an anti-oxidant water-soluble analogue of vitamin E [271]. The effect of methamphetamine on BBBD is not observed in the caveolin-1 knockout mouse [272]. Methamphetamine, a highly addictive drug of abuse, has been recently suggested as a new brain drug delivery strategy [272], which follows the original suggestion of this idea made by Kast in 2007 [273]. The methamphetamine-induced formation of reactive oxygen species in cultured endothelium is blocked by the anti-oxidant, N-tertbutyl- $\alpha$ -phenylnitron (PBN) [274]. PBN was originally tested in a failed phase 3 clinical trial in stroke [275], and the drug development of PBN for stroke was terminated [276]. PBN has a very low BBB PS product of only 0.1  $\mu\text{L}/\text{min}/\text{g}$  [277], which approximates the BBB PS produce for sucrose [278], which indicates there is minimal, if any, BBB transport of PBN. More recently, PBN, also called OKN-007, has been shown to cause BBBD to gadolinium in the rat following the IV administration of 18 mg/kg. BBBD peaked at 2 h and returned to baseline at 4 h [279].

#### 4.3.7. BBBD and Electromagnetic Radiation

The strength of an electric field can vary widely depending on the source, e.g., television, cell phone, microwave, or radar. Exposure of male rats to  $\sim 1$  GHz of radio-frequency radiation, which is comparable to the radiation emitted by a cell phone, causes BBBD [280]. The emission from a 5G cell phone is even higher [281]. Recently, the BBBD caused by exposure to pulsed electric fields (PEF) has been proposed as a new approach to brain drug delivery, which is considered to have advantages over FUS-MB, as no administration of microbubbles is required. BBBD in tumor-bearing rats was caused by repetitive electromagnetic pulses of 2.5 kV/m [282]. Focal BBBD was produced by the placement of an intra-cerebral probe that generated PEFs of  $\sim 1$  kV/m [283]. Presumably, the requisite preclinical toxicologic evaluations of The PEF technology will be performed prior to human clinical trials.

In conclusion, BBBD, by any means, is a drug delivery technology that likely has a therapeutic index of 1. If the BBB is disrupted, for the purpose of brain drug delivery, then BBB is also disrupted to plasma proteins, or other agents in blood, that induce neurotoxicity.

### 5. Cell-Mediated BBB Transport

#### 5.1. Stem Cells for Brain Drug Delivery

Mesenchymal stem cells (MSC), such as those derived from bone marrow, are said to cross the BBB and, therefore, to offer the potential as a conduit for brain drug delivery [284]. However, the studies cited [285,286] as evidence for BBB transport of MSCs do not support the hypothesis that stem cells cross the intact BBB. In one study of a spinal cord lesion model, the stem cells were injected directly into the spinal cord, thus bypassing the BBB [285]. In the other cited study, stem cells were injected intravenously at 1–6 weeks following a contusion spinal cord injury (SCI) model [286]. However, the blood-spinal cord barrier is disrupted for weeks in contusion SCI models [287]. These findings show there is no evidence that stem cells cross the BBB as discussed in a recent review [288]. Early work examined the distribution of stem cells in brain after IV injection, and observed that no stem cells were detected in brain parenchyma, although stem cells invade the meninges of brain [289], where there is no BBB. The delivery of stem cells for the treatment of recovery from cerebral ischemia requires BBBD with intra-arterial mannitol [290]. Stem cell transplant (SCT) with MSCs is a primary form of treatment of infants with MPSI or Hurler syndrome, which is caused by mutations in the IDUA gene [291]. SCT in MPSI reduces hydrocephalus [291], which is consistent with meningeal infiltration by the stem cells [289]. However, SCT in MPSI causes no reduction in CSF GAGs [292]. MSCs were permanently transfected with a cDNA encoding IDUA by lentiviral transfection, and injected in IDUA null MPSI mice [293]. The stem cells were transfected with lentivirus to a vector copy number (VCN) of 5–11. This VCN is considered high, whereas the FDA requires a VCN  $< 5$  for human

therapeutics, as the lentivirus is potentially mutagenic [294]. Despite the high VCN, the stem cell-lentiviral genome in brain was at the background level and log orders lower than in peripheral tissues [293]. Future forms of stem cell therapy will likely evolve toward the use of human-induced pluripotent stem cells (iPSC), which are reviewed in Section 11.7.2. However, at present, there is no evidence that iPSCs selectively cross the BBB relative to MSCs.

### 5.2. Exosomes for Brain Drug Delivery

The lack of success in brain drug delivery with stem cells has led to the development of exosomes as a brain drug delivery vehicle [295,296]. Exosomes are naturally occurring extracellular vesicles, which are released from the plasma membrane of cells, and may be taken up by neighboring cells. Exosomes are isolated from cultured cells. The cell debris is removed by centrifugation at  $12,000 \times g$ , and the exosomes are harvested at  $120,000 \times g$  [67]. For brain drug delivery, exosomes need a targeting mechanism so as to trigger receptor-mediated transcytosis (RMT) across the BBB. RMT is discussed below in Section 8.1. In the absence of a targeting mechanism built into the exosome, then BBB transport is minimal, unless the exosome naturally expresses a targeting ligand, as discussed below. In an early study on the brain drug delivery of short interfering RNA (siRNA), exosomes were prepared from bone marrow dendritic cells that had been permanently transfected with a cDNA encoding a fusion protein of lysosomal associated membrane protein 2b (Lamp2b) and a 29-amino acid peptide derived from the rabies virus glycoprotein (RVG). The RVG peptide is believed to trigger RMT across the BBB via the nicotinic acetylcholine receptor (nAChR) [297]. However, as discussed in Section 8.1.7, the IHC of brain shows no expression of the nAChR at the brain endothelium. The yield of exosomes from these transfected cells was 30  $\mu\text{g}$  protein from  $3 \times 10^6$  cells [67]. Since the protein content of  $10^6$  cells is 0.2 mg protein [298], the yield of exosomes from the cells was about 5%. The siRNA was encapsulated in the exosomes by electroporation [67]. The problem of encapsulating drugs into exosomes is the same as drug encapsulation in cells, and electroporation is required for a large molecule drug such as siRNA. The siRNA encapsulated in the RVG-targeted exosomes was injected into mice at a relatively large dose of siRNA of 6 mg/kg [67].

A limiting problem in exosome drug delivery is the encapsulation of the drug in the exosome. A hydrophobic small molecule can be passively encapsulated, but even a small molecule that is hydrophilic must be incorporated in the exosome by electroporation [299]. An alternative approach is to bind the drug to the surface of the exosome. This was performed for a siRNA therapeutic by engineering a fusion protein of the G58 domain of glyceraldehyde dehydrogenase, which binds the surface of exosomes and a RNA binding protein, trans-activation-responsive RNA-binding protein 2 (TARBP2), which binds double-stranded RNA, such as siRNA [300]. A three-way complex was then formed by mixing the exosomes derived from either mesenchymal stem cells or human embryonic kidney 293T cells, the G58-TARBP2 fusion protein, and the siRNA. IV administration in mice resulted in rapid clearance from the blood and a 10-fold higher uptake in peripheral organs as compared to brain [300]. The rapid clearance of exosomes from blood is the same pharmacokinetic (PK) problem that confounded early drug development of liposomes. After the IV administration of liposomes, the surface of the vesicles was coated by plasma proteins, which triggered uptake by cells lining the reticulo-endothelial system in liver and spleen. This problem of rapid clearance of liposomes was diminished by incorporation of polyethyleneglycol (PEG) in the surface of the liposome [301], which is discussed in Section 9. A post-insertion method for introducing PEG-lipids in pre-formed liposomes was developed [302], and presumably could be used with exosomes.

An alternative to the engineering of cell lines that produce targeting ligands on the exosome surface is the production of exosomes that naturally express a surface ligand that binds a receptor on the BBB. Exosomes derived from the SK-Mel-28 breast cancer cell line target the CD46 receptor [303]. CD46 is an inhibitory complement receptor that is expressed at the BBB and astrocyte foot processes [304]. Exosomes isolated from fresh mouse blood

express the transferrin receptor (TfR), and loading of brain endothelial cells in culture with transferrin triggered uptake of the Tf-coated exosomes [305]. Exosomes were isolated from bone marrow macrophages, and the therapeutic, the recombinant TPP1 proenzyme, a 70 kDa lysosomal enzyme, was incorporated into the exosomes by sonication [306]. With no exosome targeting ligand, it was necessary to bypass the BBB, and to administer these exosomes by intrathecal injection [306].

Exosomes have generated considerable enthusiasm as a brain drug delivery system, and multiple review articles have been published on exosomes and brain delivery in just the last 3–4 years. However, it is not clear how this technology can be translated to human therapeutics, nor is it clear how exosomes offer advantages over synthetic nanocontainers, such as targeted pegylated immunoliposomes discussed in Section 10.2. Translation of exosome brain drug delivery technology to human therapeutics will require solutions to multiple problems including:

- Low yield of exosomes from the starting cell line. These yields are generally not provided in exosome publications, but may be on the order of only 5%, as discussed above.
- Poor PK properties, and rapid exosome removal from blood, similar to non-pegylated liposomes [301].
- Drug encapsulation in the exosomes requires procedures such as electroporation [67] or sonication [306], which is difficult to scale up for manufacturing. Passive loading will work only for hydrophobic small molecules [299]. Many therapeutics may leak out of exosomes on storage, similar to the drug leakage from liposomes [307].
- Exosomes will generally require a targeting ligand on the surface of the vesicle, so as to promote RMT across the BBB. The incorporation of such ligands will require genetic modification of the cell line used to produce the exosomes.
- The stability of exosomes is unknown. A 2-year shelf life at 4 °C typically needs to be established for biologics, and it is not clear if exosomes, which are composed of multiple membrane elements, have any significant degree of stability on storage. To what extent exosomes can be lyophilized and then re-solubilized with both high drug retention and BBB transport is not known.

## 6. Brain Drug Delivery of Small Molecules

### 6.1. Lipid-Mediated Transport of Small Molecules

#### 6.1.1. Approved Small Molecule Drugs for the CNS

A review of the 200 most-prescribed drugs in the United States shows that CNS drugs comprise 19% of these pharmaceuticals [308]. Of these 38 most-prescribed CNS drugs, 66% are for psychiatric conditions, including depression, psychosis, anxiety, and hyperactivity, and 21% are for epilepsy. Therefore, 87% of the most-prescribed CNS drugs cover only two classes of CNS disorders, neuropsychiatric conditions and epilepsy. The MW of these CNS active drugs ranges from 135 Da to 448 Da, with a mean  $\pm$  SD of  $276 \pm 77$  Da. Only 2 of the 38 drugs have a MW between 400–450 Da. The number of hydrogen bonds formed by these 38 drugs ranges from 2–6, and only 2 drugs form 6 hydrogen bonds with water. CNS drug development in 2022 has not really advanced beyond the post-World War II era of the 1950s, when the prototypes of present-day CNS pharmaceuticals were developed, such as phenothiazines [40], tricyclic antidepressants [41], benzodiazepines [309], and phenytoin [310], i.e., treatments only for neuropsychiatric conditions and for epilepsy.

Only about 2% of small molecule drugs are active in the CNS [1]. This conclusion is drawn from the following reviews on small molecule CNS drugs. A survey of >6000 drugs in the Comprehensive Medicinal Chemistry database shows that only 6% of drugs are active in the CNS, and these drugs are generally confined to the treatment of psychiatric conditions and insomnia [311]. In another review of drugs, 12% were found to be active in the CNS, but if psychiatric disorders were excluded, only 1% of all drugs are active in the brain [312]. The 2% figure is a compromise between the fraction of all drugs active in the brain, 6–12%, and the fraction of drugs active in non-psychiatric conditions of brain, 1%. The reason that so few drugs are active in the CNS is that the type of small

molecule that crosses the BBB via free diffusion must exhibit two necessary properties: (a) a MW < 450 Da [313], and (b) a structure that forms less than eight hydrogen bonds [314]. The vast majority of small molecule drug candidates lack these molecular properties and cannot be developed for CNS conditions.

### 6.1.2. Mechanism of Small Molecule Diffusion through the BBB

The mechanism of small molecule diffusion through the BBB is the same as that which governs solute-free diffusion through biological membranes. For many years, it was believed that membrane permeability was proportional to lipid solubility, as reflected in the partition of the drug in a model solvent such as 1-octanol. Thus, measurement of the octanol partition coefficient (K) should predict membrane permeability as governed by the model of solute diffusion developed by Overton in 1901 [315]. The Overton model makes no allowance for solute size or MW. In 1980 Levin [316] observed that BBB permeability of drugs was proportional to lipid solubility providing the MW of the drug was <400 Da. This finding indicated that there was a threshold of MW governing BBB transport via free diffusion. The role of molecular size and MW in solute-free diffusion through lipid bilayers, as opposed to diffusion through a solvent, was formulated by Lieb and Stein [317]. The diffusion coefficient (D) of drug within a membrane was exponentially and inversely related to the size of the drug. The mechanism by which drug permeation through a biological membrane could be a function of solute size was put forward by Trauble in 1970 [318]. In this model, solutes penetrate a biological membrane by jumping through transitory holes in the membrane that are caused by the kinking of mobile fatty acyl side chains of membrane phospholipids, as depicted in Figure 8.

#### A Overton model of free diffusion of drugs through membranes (molecular size independent)

$$P = K \cdot D/d$$

*P* = membrane permeability (cm/sec)

*K* = organic phase partition coefficient

*D* = drug diffusion coefficient in organic phase (cm<sup>2</sup>/sec)

*d* = membrane thickness (cm)

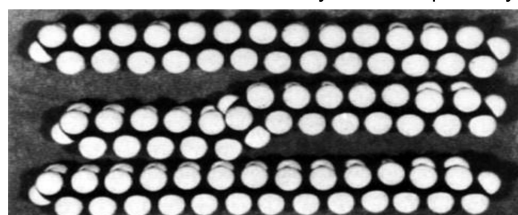
#### Stein model of free diffusion of drugs through membranes (molecular size dependent)

$$D \propto e^{-V_d/V_h}$$

transitory holes in lipid bilayer

*V<sub>d</sub>* = volume of drug

*V<sub>h</sub>* = volume of membrane  
hole



#### B

**Figure 8. Overton vs. Stein models of solute diffusion through membranes.** (A) Overton model of solute diffusion through biological membranes. Membrane permeability is independent of solute molecular size [315]. (B) Stein model of solute diffusion through membranes [317]. Membrane permeability is exponentially related to the molecular volume of the drug (*V<sub>d</sub>*) relative to the volume (*V<sub>h</sub>*) of transitory holes formed in the membrane. These membrane holes are formed by kinking of phospholipid fatty acyl side chains, as depicted in the model. Adapted from [15], Copyright© 2020 licensed under Creative Commons Attribution License (CC-BY).

Solutes are hypothesized to traverse a biological membrane through a process of molecular “hitch-hiking”, through neighboring holes within the phospholipid bilayer until



the solute traverses the membrane. The MW dependence of solute or drug free diffusion through a biological membrane is not predicted by the Overton model (Figure 8A), but is predicted by the Stein model (Figure 8B). If the MW or size of the drug is too large to fit into the membrane holes, then membrane permeation is decreased in proportion to molecular size. BBB permeability is decreased 100-fold when the cross-sectional area of the drug is increased from 52 Å<sup>2</sup> to a cross-sectional area of 105 Å<sup>2</sup> [319]. This exponential decrease in BBB permeation as the size of the drug increases comports with the models of Stein [317] and Trauble [318], as reviewed recently [320].

Apart from the molecular volume of the drug, as reflected in the MW, the other important factor limiting small molecule movement through membranes is polarity of the drug, as reflected in the number of hydrogen bonds formed between the drug and solvent water [317,321]. BBB permeation decreases by 1 log order for each pair of hydrogen bonds formed by functional groups on the drug as exemplified by either steroid hormones [322] or peptides [323]. The effect of hydrogen bonding on BBB transport is illustrated by the 1972 study of Oldendorf et al. [42]. The BBB transport of heroin, which is diacetylmorphine, is >10-fold faster than the BBB transport of morphine [42]. The acetylation of the 2 hydroxyl groups converts morphine to heroin, and removes a total of 4 hydrogen bonds from the parent drug.

In summary, the likelihood of BBB transport of a given small molecule can be estimated from the MW and structure of the drug. If the MW > 450 Da, and/or the structure of the drug includes polar functional groups that form >7 hydrogen bonds, then the BBB transport of the drug will be low, in the absence of carrier-mediated transport. Conversely, if the MW < 450 Da and the drug forms ≤7 hydrogen bonds with water, then the BBB transport of the drug may be significant, assuming the drug is not a substrate for an active efflux transporter, such as p-glycoprotein, as reviewed in Section 6.3.2.

### 6.1.3. Lipid-Soluble Pro-Drugs

The BBB transport of morphine is increased nearly 100-fold by acetylation of both hydroxyl groups on morphine to form heroin [42]. Heroin is a morphine prodrug. However, the development of CNS prodrugs has proven to be difficult, and there are few FDA-approved CNS drugs wherein medicinal chemistry was used to convert a hydrophilic CNS drug, that does not cross the BBB, to a lipid-soluble prodrug that does cross the BBB [324]. The ‘lipidization’ of the hydrophilic drug by blocking hydrogen bond forming functional groups can increase the BBB permeability–surface area (PS) product, assuming the MW of the prodrug is <450 Da. However, lipidization also increases drug uptake by peripheral tissues, which reduces the plasma AUC of the drug. The increase in PS product is offset by the reduced plasma AUC, which results in only minor changes in the brain uptake of the drug, or % injected dose (ID)/g brain. The relationships between brain drug uptake, BBB PS product, and plasma AUC are given by Equation (1),

$$\%ID/g = (\text{BBB PS product}) \times (\text{plasma AUC}) \quad (1)$$

Equation (1) is an approximation of Equation (7) in Section 11.4.4 (Methods), where the volume of distribution (VD) of the test drug is much greater than the brain plasma volume [1]. Equation (1) shows that drug lipidization that enhances BBB permeability, or PS product, does not translate to a parallel increase in brain uptake, or %ID/g, if there is a corresponding decrease in plasma AUC.

Xamoterol is a beta-1 adrenergic receptor agonist that is a potential treatment for AD [325]. Medicinal chemistry was used to replace a hydrogen bond forming amide functional group with a less polar ether group, and this xamoterol prodrug is designated STD-101-01 [325]. However, the oral bioavailability of the drug is low, which requires IV administration of the drug. The prodrug is rapidly removed from plasma, and the peak brain concentration of the prodrug in the rat is only 0.04%ID/g at 20 min after an IV injection of 10 mg/kg [325].

One of the few FDA-approved prodrugs for the CNS is dimethylfumarate for multiple sclerosis (MS) [326]. Monomethylfumarate activates the nuclear factor E2-related factor-2 pathway involved in oxidative stress [326]. Fumarate is a dicarboxylic acid, which does not cross the BBB [327]. Methyl esterification of both carboxyl groups reduces the hydrophilicity of the parent fumarate and enables BBB transfer. Other FDA-approved prodrugs, gabapentin enacarbil, and eslicarbazepine acetate [324], increase the oral bioavailability of drugs that already cross the BBB.

#### 6.1.4. Conjugation of Hydrophilic Drugs to Hydrophobic Carriers

A number of hydrophobic carriers have been used in an attempt to deliver hydrophilic drugs across the BBB. An early hydrophobic carrier was dihydropyridine (DHP) [328]. A hydrophilic drug, which did not cross the BBB, was conjugated to the DHP carrier. Once in brain, the DHP moiety was oxidized to a quaternary ammonium salt, which sequestered the conjugate in brain, since quaternary ammonium compounds do not cross the BBB. However, this approach does not block the hydrogen bond forming functional groups on the pharmaceutical agent, and BBB transport may not be enhanced by DHP conjugation [329]. The primary advantage of the DHP system is the sequestration in brain of a drug that is already hydrophobic such as estradiol (E2). The E2-DHP conjugate has a long residence time in brain compared to E2 alone [330]. However, the E2-DHP conjugate is highly hydrophobic and is administered IV in 100% dimethylsulfoxide (DMSO) [330]. The IV administration of 0.25 mL of 10–15% DMSO in the mouse causes BBBD to a 40 kDa protein, HRP [331]. Certain drug diluents, such as DMSO or sodium dodecylsulfate, may enable drug penetration through a BBB that is permeabilized by the detergent co-injected with the drug. Another problem with DHP conjugation is that the DHP modified drugs are labile, owing to oxidation [332].

Docosahexaenoic acid (DHA), a C22:6 essential free fatty acid (FFA), was proposed as a lipid carrier for brain drug delivery [57]. Interest in DHA as a lipid carrier was renewed by the finding that DHA is transported across the BBB via the major facilitator superfamily domain containing 2a (Mfsd2a) transporter [333], and DHA has been proposed as a ligand for the Mfsd2a-mediated transport of DHA-conjugated nanoparticles [334]. However, Mfsd2a does not transport unesterified DHA, but rather the lysolecithin form of esterified DHA [333]. Brain uptake of free DHA is not reduced in the Mfsd2a knockout mouse, and liver uptake of free DHA is 50-fold greater than the brain uptake of free DHA [333]. The brain uptake of DHA esterified as lysolecithin is nearly 10-fold greater than the unesterified form of DHA [333]. Nevertheless, the brain uptake of esterified DHA is still quite low,  $<<0.001\%$  ID/g [333]. A contributing factor to the poor BBB transport of DHA is the avid binding of this FFA to albumin [335]. Owing to the very low BBB transport of DHA, it was necessary to employ BBB disruption by focused ultrasound to produce a significant brain level of LDL nanoparticles conjugated with DHA [336].

Other FFAs, such as the C18 unsaturated stearic acid, have been proposed as lipid carriers, even for large proteins such as the 40 kDa HRP [337]. HRP was conjugated with stearate and radio-iodinated by chloramine T [337]. Conjugation of a FFA to a protein such as HRP would not be expected to mediate free diffusion through the BBB, owing to the 450 Da MW threshold discussed in Section 6.1.2. Stearate conjugation of HRP had no effect on the brain uptake of the protein, measured as %ID/g, over a 3 h period after IV administration [337].

In summary, neither the use of medicinal chemistry to block polar functional groups on hydrophilic drug candidates, nor the conjugation of hydrophilic drugs to lipid carriers, has led to a significant number of new drug candidates for CNS disease that cross the BBB and can enter CNS clinical trials. An alternative approach, discussed in Section 6.2, uses medicinal chemistry to target endogenous carrier-mediated transporters (CMT) expressed at the BBB.

## 6.2. Carrier-Mediated Transport of Small Molecules

BBB carrier-mediated transporters (CMT) are members of the Solute Carrier (SLC) gene superfamily, which is the second largest gene family of membrane proteins behind G protein-coupled receptors. There are >400 genes, and >60 families of the SLC transporter gene super-family, often with extensive redundancy [338]. For example, there are >10 GLUT glucose transporters. Owing to the presence of multiple transporters for any given class of nutrients, it is necessary to confirm that the substrate transporter profile (STP) that is observed *in vivo* at the BBB is the same as the STP that is observed following *in vitro* expression of the SLC transporter that is said to function at the BBB [339]. This correlation of the *in vivo*/*in vitro* STP is especially crucial if BBB-penetrating small molecule drugs are developed to traverse the BBB via a specific CMT member of the SLC gene superfamily.

### 6.2.1. GLUT1 Glucose Carrier

BBB glucose transport is stereospecific for D-glucose, and shows no affinity for L-glucose or fructose [48]. Multiple hexoses are transported via the BBB glucose transporter and the  $K_m$  values for 2-deoxyglucose, D-glucose, 3-O-methylglucose (3OMG), D-mannose, and D-galactose, are 6 mM, 9 mM, 10 mM, 22 mM, and 42 mM, respectively [340]. The  $V_{max}$  is constant for all hexoses, which means the  $K_m$  is a true affinity constant for hexose binding to the carrier, and the rate-limiting step is glucose mobility through the transporter cavity [340]. The BBB glucose transporter is sodium-independent and is inhibited by phloretin,  $K_i = 16 \mu\text{M}$ , and phlorizin,  $K_i = 400 \mu\text{M}$  [340]. There are at least 14 different sodium independent glucose transporter (GLUT) genes, and at least 5 GLUT genes are expressed in brain including GLUT1, GLUT3, GLUT6, GLUT8, and GLUT13 [341]. The GLUT1 transporter (SLC2A1) is responsible for >95% of BBB glucose transport. This was demonstrated by showing the concentration of immunoreactive GLUT1 in a bovine brain capillary plasma membrane fraction, quantified with purified human erythrocyte GLUT1 as an assay standard, was identical to the concentration of D-glucose displaceable cytochalasin B binding sites in the brain capillary membrane fraction [342]. The equivalence of total glucose transporter sites and total GLUT1 sites at the BBB was confirmed with intact microvessels isolated from 70-day-old rabbits [343]. The concentrations of total D-glucose displaceable cytochalasin B binding sites, and total immunoreactive GLUT1, were  $102 \pm 25 \text{ pmol/mg protein}$  and  $111 \pm 3 \text{ pmol/mg protein}$ , respectively [343]. Cytochalasin B binds to all GLUTs, so the equivalence of the total GLUT1 and total glucose transporter levels at the brain capillary excludes a significant role for GLUTs other than GLUT1 as a BBB glucose carrier [342]. The concentration of GLUT1 mRNA at the brain capillary is at least a log order higher than the concentration of GLUT1 mRNA in the parenchyma of bovine brain [344], a finding confirmed with qPCR for rat brain [345].

The crystal structure of the human GLUT1 glucose transporter has been determined by X-ray crystallography [346]. The formation of GLUT1 crystals was facilitated by two point mutations: N45T and E329Q. The N45T mutation removes the single N-linked glycosylation site, and the E329Q mutation locked the transporter in an inward facing orientation [346]. The three-dimensional structure of the GLUT1 transporter shows the transporter protein forms a trans-membrane cavity that can be alternately accessed by the substrate from either side of the plasma membrane. The transporter cavity may exist in either an inward closed conformation, to mediate transport of D-glucose from blood or brain ECS to the intra-endothelial compartment, or may exist in an outward closed conformation, to mediate sugar transport from the intra-endothelial compartment to the plasma or brain ECS [346]. The GLUT1 carrier is composed of 12 transmembrane regions (TMR), which form a carboxyl terminal domain and an amino terminal domain. TMRs 1–6 form the amino terminal domain, and TMRs 7–12 form the carboxyl terminal domain TMR. The outward open conformation is largely coordinated by Aas in the carboxyl terminal domain (C), whereas the inward open conformation is largely determined by AAs in the amino terminal domain (N) [346]. The carboxyl terminal and amino terminal domains are connected by a short intracellular (IC) helical bundle. The structure of the GLUT1

transporter was also visualized by a surface electrostatic model [346]. This model reveals the central transporter cavity through which D-glucose, but not L-glucose, and certain other hexoses move to traverse the endothelial membrane. This transporter cavity is small, with dimensions of  $0.8 \times 1.5$  nm [347], which is sufficiently large to accept D-glucose, which has a long axis of only 1 nm (10 angstroms). Therefore, as discussed below, it is dubious to expect that a conjugate of D-glucose and a drug, which does not cross the BBB, can be expected to move through the narrow, stereospecific gated cavity of the GLUT1 transporter. The TMR structure of the GLUT1 glucose transporter is shown in Figure 9A (left side), and the electrostatic model of the GLUT1 glucose transporter is shown in Figure 9A (right side).

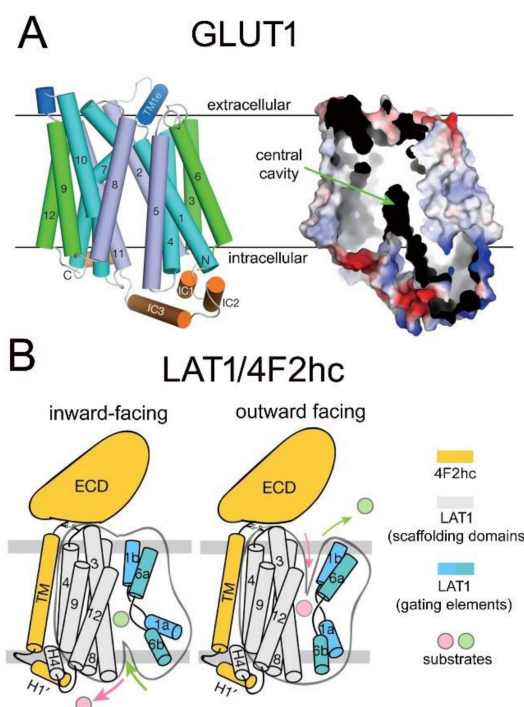


**Figure 9. Structure of GLUT1 and LAT1 carrier-mediated transporters.** (A) (Left) Model of crystal structure of human GLUT1 showing orientation of 12 transmembrane regions (TMR) in four 3-helical repeat domains composed of TMRs 1,4,7,10 (blue), TMRs 3,6,9,12 (green), and TMRs 2,5,8,11 (purple); the extracellular and intracellular helices are shown in dark blue and orange, respectively. (Right) Surface electrostatic potential model shows a central transporter cavity. Reproduced with permission from [346], Copyright© 2014 Springer-Nature. (B) Inward-facing and outward-facing models of the LAT1-4F2hc heteroduplex. LAT1 is composed of 12 TMRs, which form scaffolding and gating domains. The 4F2hc is formed by an extracellular domain (ECD), a transmembrane (TM) domain, which binds to TMR4 of LAT1, and an intracellular loop (H1'). Reproduced with permission from [348], Copyright© 2019 Springer-Nature.

Drugs that are designed to cross the BBB via the GLUT1 transporter, or for any BBB CMT system, fall into two categories: glucose-mimetic drugs or glucose-drug conjugates. A glucose-mimetic drug retains the basic structure of the D-glucose molecule, but certain substituents are added to the hexose that both (a) confer a pharmaceutical property on the glucose analogue, and (b) retain sufficient affinity for GLUT1 so that the glucose-mimetic drug traverses the BBB. Examples of glucose-mimetic drugs that are transported via GLUT1 include 2-deoxy [340] and 6-deoxy-6-chloro [349] analogues of D-glucose, both of which have a higher affinity for the BBB glucose carrier than D-glucose. The conjugation of a methylsulfonyl moiety to the 4-O and 6-O, but not the 3-O, hydroxyls was possible and a reasonable affinity of the glucose-mimetic for GLUT1 was retained [350].

The glucose-drug conjugate approach to brain drug delivery via GLUT1 involves the conjugation of a drug or peptide, which normally does not cross the BBB, to one of

the hydroxyl groups on D-glucose. Glucose conjugates have been prepared for peptides and small molecules. Glucose was conjugated to the serine hydroxyl group of enkephalin peptides, and brain delivery of the hexa- or heptapeptide glucose conjugate was hypothesized to be mediated via GLUT1 at the BBB [351], although subsequent carotid arterial perfusion studies showed the conjugate had no affinity for GLUT1 [352]. Venlafaxine, which is a hydrophobic small molecule that crosses the BBB, was conjugated to D-glucose via an extensive linker, and this construct produced a new agent four times the size of D-glucose [353]. Studies demonstrating affinity of the conjugate for GLUT1 were not performed. A carboranyl-methyl-glucose conjugate was synthesized to enable GLUT1 delivery of the boron agent for boron neutron capture therapy of cancer [354]. The borocaptate moiety conjugated to D-glucose was larger than the D-glucose molecule alone. Although the conjugate was taken up by a human cancer cell line in culture, no study showing this uptake was mediated via GLUT1 was performed [354].

### 6.2.2. LAT1 Large Neutral Amino Acid Carrier

Large neutral amino acids (LNAA) traverse the BBB via a saturable transporter [48] that is characterized by high affinity (low  $K_m$ ) for the LNAAs ranging from a  $K_m$  of 0.12 mM for L-phenylalanine to a  $K_m$  of 0.73 mM for L-threonine [355]. These  $K_m$  values approximate the LNAA plasma concentrations [356], which makes the brain selectively vulnerable to the high plasma concentrations of hyper-aminoacidemias, such as phenylketonuria, as discussed further in Section 11.4.1. The initial cloning of the major LNAA transporter, designated LAT1 (SLC7A5), from a C6 rat glioma line was enabled by the co-expression of 4F2hc (SLC3A2), which forms a hetero-duplex within the membrane with LAT1 [357]. The LNAA transporter at the BBB was cloned using frog oocyte expression of synthetic RNA produced from a bovine brain capillary cDNA library, and was shown to have an 89% amino acid identity with rat LAT1 [358]. Northern blotting showed the LAT1 mRNA was selectively expressed in brain capillary endothelial cells *in vivo*, and the LAT1 mRNA was at least 100-fold higher at the BBB as compared either to C6 rat glioma cells or to brain parenchyma [358]. The LAT1 mRNA was not detected in liver, heart, lung, or kidney [358]. Transport of tryptophan into oocytes expressing the cloned BBB LAT1 was characterized by high affinity with a  $K_m$  of 32  $\mu$ M [358], which correlates with the  $K_m$  of tryptophan transport across the BBB *in vivo* [355].

The 3D structure of the human LAT1/4F2hc hetero-duplex has been determined by cryo-electron microscopy [348], and is depicted in Figure 9B. The 4F2hc protein is composed of an extracellular domain (ECD), a transmembrane (TM) domain and an intracellular H1' loop (Figure 9B). The LAT1 protein is formed by 12 TMRs, and TMR4 of LAT1 has hydrophobic interactions with the TM domain of 4F2hc to stabilize the complex [348]. This interaction between LAT1 and 4F2hc occurs away from the transporter-gated cavity (Figure 9B). The narrow substrate cavity of LAT1 is adjacent to TMR1 and TMR6 (Figure 9B). BBB transport of LNAAs via LAT1 is sharply stereospecific for some amino acids [359]. The affinity of D-leucine is reduced about three-fold compared to L-leucine, but the affinity of D-tryptophan is >100-fold lower than the affinity of L-tryptophan, and the D-isomers of L-DOPA, isoleucine, valine, and threonine have no affinity for LAT1 [359]. The stereospecificity of BBB transport of LNAAs comports with the narrow-gated cavity through which amino acids traverse the membrane via LAT1 (Figure 9B).

There are major differences in the kinetics and transporter expression at the BBB for GLUT1 and LAT1 CMT systems. The  $K_m$  and  $V_{max}$  values for GLUT1 and LAT1 differ by more than two log orders of magnitude [339]. The brain capillary endothelial concentration ( $C_{cap}$ ) of a BBB CMT system was first determined for GLUT1 using quantitative Western blotting, and cytochalasin B Scatchard plots, which showed the  $C_{cap}$  of GLUT1 was 100–110 pmol/mg protein [343]. Subsequently, the  $C_{cap}$  of GLUT1 was determined by quantitative targeted absolute proteomics (QTAP). In this approach, isolated brain capillaries were combined with liquid chromatography/mass spectrometry (LC-MS), along with sequence specific peptide standards, to measure the mass of GLUT1 at

the brain capillary [360]. The concentration of GLUT1 in human brain capillaries (Ccap) is  $139 \pm 46$  pmol/mg protein [360], which correlates with the Ccap of immunoreactive GLUT1 [343]. The QTAP technology has produced measurements of the Ccap for many different CMT, RMT, and AET systems, as discussed below. The Ccap values for LAT1, the cationic amino acid transporter 1 (CAT1), and the monocarboxylic acid transporter 1 (MCT1) have been measured by QTAP, and the Ccap of LAT1, CAT1, and MCT1 is much lower than the Ccap of GLUT1. The lower Ccap values for LAT1, CAT1, and MCT1, as compared to GLUT1, parallels the Vmax values of substrate transport through these CMT systems at the BBB in vivo [361]. The Vmax/Ccap ratio provides a measure of the transporter turnover rate, or number of substrate molecules transported per second at maximal velocity. The Km, Vmax, Ccap, and transporter turnover rate for GLUT1, MCT1, LAT1, and CAT1 are shown in Table 2.

**Table 2.** Blood–brain barrier carrier-mediated transport system.

Carrier	SLC Gene	Substrate	Km ( $\mu$ M)	Vmax (nmol/min/g)	Ccap (pmol/mg <sub>p</sub> )	Molecules per S *
Hexose (GLUT1)	2A1	D-glucose	$11,000 \pm 1400$	$1420 \pm 140$	$139 \pm 46$	600
Monocarboxylates (MCT1)	16A1	L-lactate	$1800 \pm 600$	$91 \pm 35$	$2.3 \pm 0.8$	2300
Large neutral AAs (LAT1)	7A5	L-phenylalanine	$26 \pm 6$	$22 \pm 4$	$0.43 \pm 0.09$	3000
Cationic AAs (CAT1)	7A1	L-arginine	$40 \pm 24$	$5 \pm 3$	$1.1 \pm 0.2$	270

AA = amino acid; Km, Vmax and molecules/s from [361]; brain capillary transporter concentration (Ccap) from [360]; calculation of number of molecules transported per s derived from Vmax/Ccap ratio, assuming 0.14 mg capillary protein per gram brain, and that 50% of the capillary transporter is distributed to the luminal endothelial membrane [361]. \* Molecules/s is the number of substrate molecules that flux through the transporter per second at maximal velocity (Vmax).

The number of substrate molecules transported per second at maximal velocity, as determined from the Vmax/Ccap ratio [361], varies from 270–3000 substrates per second (Table 2). Thus, the transporter turnover rate can vary over a log order of magnitude, which explains why there is only an approximate correlation between the Vmax of the transporter in vivo, and the Ccap as measured by QTAP (Table 2).

There are a number of FDA-approved CNS drugs that penetrate the BBB via LAT1, although in all cases, this was a serendipitous finding. The first LAT1 drug developed was L-dihydroxyphenylalanine (L-DOPA) for PD, which was approved in 1970. L-DOPA crosses the BBB via LAT1 and is converted in brain to dopamine via the action of aromatic amino acid decarboxylase (AAAD). In 1959, Holtz [362] reviewed the conversion of L-DOPA into dopamine by AAAD. In 1963, Yoshida et al. [363] reported experiments showing the uptake of L-DOPA by brain slices was inhibited by LNAAAs, but not by a small neutral amino acid, alanine, or an acidic amino acid, glutamate. In 1966, Hornykiewicz [45] reviewed the low production of dopamine in the striatum of PD, and the ability of L-DOPA administration to increase brain dopamine, but did not mention either the BBB or how L-DOPA gains access to the CNS. In 1975, Wade and Katzman [45], using the Oldendorf BUI technique [46], demonstrated L-DOPA crosses the BBB on an amino acid transport system, and in 2000, Kageyama et al. [364] showed that L-DOPA is a substrate for LAT1. Phenylalanine mustard (melphalan), a chemotherapeutic alkylating agent, was shown to be therapeutic in mice with experimental brain cancer [365], and subsequent arterial infusion experiments demonstrated that melphalan crossed the BBB via the LNAA transporter [366]. Melphalan was subsequently shown to be a ligand for LAT1 [367]. Gabapentin, a  $\gamma$ -amino acid, was developed as a new anti-convulsant in the 1990s, and cerebral microdialysis showed gabapentin crossed the BBB, although no mention was made as to mechanism of transport [368]. Using the frog oocyte expression system, the LAT1-mediated uptake of [ $^{14}$ C]-phenylalanine was blocked by amino acid-like drugs, and the Ki for melphalan, L-DOPA, and gabapentin was 49  $\mu$ M, 67  $\mu$ M, and 340  $\mu$ M, respectively [367]. The transport

of gabapentin, a  $\gamma$ -amino acid, by LAT1 is unexpected, since LAT1 transports  $\alpha$ -amino acids, not  $\gamma$ -amino acids. However, gabapentin is a cyclic compound wherein the amino and carboxyl moieties sterically resemble an  $\alpha$ -amino acid. A perplexing example of a drug that is said to be transported by a LNAA transporter is paraquat, which is a quaternary ammonium salt, and such molecules do not cross the BBB. Paraquat is a widely used herbicide, and there is inconclusive evidence that paraquat neurotoxicity can be associated with PD [369]. Paraquat is structurally similar to the neurotoxin, 1-methyl-4-phenylpyridinium (MPP+), and MPP+ does not cross the BBB [370]. However, the SQ administration of 5–10 mg/kg paraquat results in drug distribution to brain via a process that is inhibited by a LNAA, L-valine, but not by a cationic amino acid, L-lysine [370]. Paraquat transport via LAT1 has not been tested. While the cyclic structure of gabapentin provides an explanation for gabapentin transport via LAT1, the structure of paraquat has no resemblance to an  $\alpha$ -amino acid, and paraquat transport at the BBB may be mediated by a transporter other than LAT1.

The development of drugs that mimic the structure of a LNAA, and which are transported via LAT1, is the most advanced area of CNS drug development that targets a BBB CMT system. This work has evolved in two parallel pathways. First, LAT1 structure-based ligand discovery was initiated following the stable transfection of HEK293 cells with the full length human LAT1 cDNA, followed by screening drugs that inhibit the uptake of [ $^3$ H]-gabapentin [371]. Subsequent to the elucidation of the 3D structure of the human LAT1/4F2hc heterocomplex [348,372], this structural information was used to assess the docking of LNAA-type drugs into the LAT1 transporter cavity [373]. To be effective in the CNS, a LNAA-type drug must not only bind to LAT1, but also undergo translocation through the membrane [373]. The second approach to the development of LNAA-type drugs that cross the BBB via LAT1 is executed without knowledge of the LAT1 binding site. Modifications to the LNAA structure are made and the affinity of the drug for LAT1 is then determined. An early example of the types of modifications to a neutral amino acid drug that can be made, and still retain LAT1 affinity, was the synthesis of 6-mercaptapurine-L-cysteine [374]. L-cysteine is a small neutral amino acid, which has a low affinity for the BBB LNAA transporter [48]. However, conversion of the free sulfhydryl group on L-cysteine to a disulfide linked therapeutic group converts L-cysteine to a LNAA, which has appreciable affinity for the BBB LNAA transporter *in vivo* [374]. An alternative approach to the use of medicinal chemistry to generate CNS drugs that penetrate the BBB via transport on LAT1 is the coupling of a pharmaceutical agent, ketoprofen, to the phenolic para-hydroxyl of L-tyrosine to form an ester compound [375]. The tyrosine-ketoprofen traversed the BBB *in vivo* via the LNAA transporter [375]. Subsequent work showed that higher affinity for LAT1 was achieved if the drug was linked to the meta position of the benzene ring of L-phenylalanine [376–378].

### 6.2.3. CAT1 Cationic Amino Acid Carrier

BBB transport of the cationic amino acids (arginine, lysine, ornithine) is mediated by a saturable carrier [48] with high affinity and  $K_m$  values ranging from 90  $\mu$ M to 230  $\mu$ M [355]. The original Rec-1 locus, which is a murine ecotropic retrovirus receptor, was shown to be a mammalian cationic amino acid transporter [379], now named CAT-1 (SLC7A1). The rat or mouse brain Rec-1 cDNA was cloned by reverse transcription of brain-derived RNA using oligodeoxynucleotides derived from the Rec-1 gene, and an RNase protection assay was used to demonstrate expression of the mRNA for CAT1 in isolated brain microvessels [380]. The crystal structure of mammalian CAT1 has not been reported, but hydropathy plots predict 14 transmembrane regions [381]. A novel use of medicinal chemistry to develop a BBB penetrating prodrug involved the conjugation of the carboxylic acid group of ketoprofen to the  $\epsilon$ -amino acid moiety of lysine [382]. This converted the lysine into a large neutral amino acid, and the ketoprofen-lysine conjugate was transported through the BBB by LAT1 [382].

#### 6.2.4. MCT1 Monocarboxylic Acid Carrier

Monocarboxylic acids (MCA), such as pyruvate, lactate, the ketone bodies ( $\beta$ -hydroxybutyrate and acetoacetate), are transported across the BBB by a specific MCA carrier [327,383]. The initial MCA carrier was cloned in 1994 and designated MCT1 (SLC16A1) [384]. The MCT1 mRNA was detected by PCR in rat brain microvessels [385], and MCT1 was localized to brain microvessels by immunohistochemistry [386]. MCT1 exists in the membrane as a hetero-duplex with the 60 kDa basigin protein (Bsg, CD147) [387], similar to the LAT1/4F2hc hetero-duplex (Figure 9B). The 3D structure of the MCT1-Bsg complex has recently been elucidated by cryoelectron microscopy [388]. The Bsg protein is formed by an ECD, which is composed of 2 immunoglobulin-like domains, a transmembrane (TM) domain, and a short intracellular loop. The MCT1 is composed of 12 transmembrane regions (TMR) with 6 TMRs forming the amino terminal domain (NTD) of MCT1, and 6 TMRs forming the carboxyl terminal domain (CTD) of MCT1 [388]. The TM domain of Bsg stabilizes the NTD of MCT1. Substrate translocation is proton dependent and rotation of the NTD and CTD expose the substrate binding site on each side of the membrane [388]. A prodrug transported by MCT1 was formed with an amide linkage between the ring nitrogen of 5-fluorouracil (5FU) and the carboxylic acid group of either adipic acid or suberic acid [389].

#### 6.2.5. CNT2 Purine Nucleoside Carrier and Adenine Carrier

Purine nucleosides (adenosine, guanosine), but not pyrimidine nucleosides (uridine, thymidine), traverse the BBB by a saturable carrier that is distinct from a nucleobase carrier [390]. BBB transport of adenosine is sodium-dependent and is not inhibited by nitrobenzylthioinosine (NBTI) [391]. The BBB adenosine carrier is characterized by a  $K_m$  of  $25 \pm 3 \mu\text{M}$  and a  $V_{max}$   $0.75 \pm 0.08 \text{ nmol/min/g}$  [361], which is 100-fold lower than the  $V_{max}$  of MCT1 (Table 2). The substrate transporter profile (STP) of the BBB adenosine transporter in vivo, e.g., lack of affinity for pyrimidine nucleosides and sodium-dependency, is consistent with the STP of the concentrative nucleoside transporter (CNT)2 or SLC28A1 [392]. The molecular identity of the BBB adenosine transporter has been ascribed to the equilibrative nucleoside transporter (ENT)2 or SLC29A2 [393], because the abundance of CNT2 is below the limit of quantitation (LOQ) using QTAP methodology and human CMEC/D3 cultured endothelium [394]. However, the abundance of LAT1 is also below the LOQ in this cell line [394]. A low abundance of the nucleoside transporter at the BBB is expected given the 100-fold lower  $V_{max}$  of the adenosine transporter compared to the MCT1 transporter [361]. Molecular cloning of the BBB adenosine transporter was performed with the frog oocyte system following oocyte injection of cloned RNA derived from a rat brain capillary cDNA library [395]. A clone was identified and DNA sequencing showed the BBB adenosine transporter was CNT2 [395]. The identification of the BBB adenosine transporter as CNT2 was consistent with the known properties of BBB adenosine transport, e.g., sodium dependency and NBTI insensitivity. The  $K_m$  of adenosine transport into the oocytes expressing CNT2,  $23 \pm 4 \mu\text{M}$  [395], is identical to the  $K_m$  of BBB transport of adenosine in vivo [361]. Adenosine transport into the oocytes was inhibited by adenosine, guanosine, and uridine, but not by cytidine or thymidine [361], and this STP of the cloned CNT2 parallels the STP of purine nucleoside transport across the BBB in vivo [390]. The sodium concentration required to produce maximal transport via the adenosine transporter expressed in frog oocytes, i.e., the  $K_{50}$ , is  $2.4 \pm 0.1 \text{ mM}$ , and the Hill coefficient is 1, indicating adenosine and sodium are co-transported in a 1:1 ratio via CNT2 [395].

The 3D structure of CNT2 has not yet been elucidated, but the structure of CNT3 has been reported using cryo-electron microscopy [396]. CNT3 has a high degree of sequence homology with CNT2 [396], although the sodium Hill coefficient for CNT2 is 2 [392]. CNT3 exists in the membrane as a homo-trimer [396]. If CNT2 also exists within the membrane as a homo-trimeric structure, this could explain the asymmetry of nucleoside transport via the BBB CNT2 expressed in frog oocytes [397]. Adenosine is transported via the BBB CNT2



on a high  $V_{max}$  site, whereas dideoxyinosine (DDI) and thymidine are transported on a second low  $V_{max}$  site on the CNT2 transporter [397].

The availability of the 3D structure of CNT3 enables the rational design of adenosine-based drugs that cross the BBB. One drug that may cross the BBB via CNT2 transport is cladribine, an immune-suppressive used in the treatment of multiple sclerosis [398]. Cladribine is a form of deoxy-chloro adenosine, and is transported by CNT2 [398].

An important consideration in the design of adenosine-based drugs that cross the BBB via CNT2 is the enzymatic barrier to adenosine. Although topical application of adenosine to pial vessels causes enhanced brain blood flow, the intra-arterial infusion of adenosine in dogs does not increase cerebral blood flow [399]. The lack of a pharmacologic effect of arterial administration of adenosine is due to an enzymatic BBB to adenosine transport. [ $^3\text{H}$ ]-adenosine was administered by internal carotid artery infusion for 15 s followed by microwave irradiation of the brain to cause immediate cessation of brain metabolism [391]. After 15 s of infusion, only  $10 \pm 3\%$  of brain radioactivity resided in the unmetabolized adenosine pool, with 34% of radioactivity in non-adenosine nucleosides (inosine, hypoxanthine), and 32% in various nucleotide pools [391]. Therefore, adenosine-based drugs that cross the BBB must be designed not only for CNT2 affinity, but also must be resistant to the enzymatic BBB to adenosine.

In addition to the CNT2 purine nucleoside transporter, purine bases, particularly adenine, traverse the BBB via a saturable carrier that is distinct from the adenosine carrier [390]. To date, no nucleobase transporter (NBT) has been identified at the BBB.

#### 6.2.6. CTL1 Choline Carrier

BBB transport of choline, a quaternary ammonium compound, was measured with the BUI method, and found to be saturable consistent with a carrier-mediated mechanism [400]. BBB transport is inhibited by hemicholinium (HC)-3, also a quaternary ammonium molecule, and by 2-(dimethylamino) ethanol (deanol), which is a tertiary amine compound [400]. The BBB choline carrier was subsequently examined with the internal carotid artery perfusion method, and these studies reported a choline transport  $K_m$  of  $40 \mu\text{M}$  and a  $V_{max}$  of  $2.7 \text{ nmol}/\text{min}/\text{g}$  [401]. The HC-3  $K_i$  was  $57 \pm 11 \mu\text{M}$  [401]. The BBB choline carrier tolerates a number of substitutions on the choline nucleus as N-n-octylcholine and N-n-octylnicotinium both inhibit choline transport, although no inhibition is observed for N-methylpyridinium [402]. One caveat is that a given molecule may inhibit a CMT transporter, but not actually be transported by the CMT system. The BBB choline carrier could be used as a brain drug delivery system [403], and early 3D-quantitative structure activity relationships (3D-QSAR) were initiated [404]. Different 3D-QSAR models were developed to predict drugs that cross the BBB on the choline carrier [405,406]. Such models would be aided by knowledge on the molecular properties of the BBB choline carrier. Choline transporters include the choline high affinity transporter (CHT)-1, which is a member of the sodium dependent glucose transporter gene family, and is designated SLC5A7. However, CHT1 can be excluded as the BBB choline transporter, as BBB choline transport in vivo is not high affinity [400,401]. Choline transporter-like (CTL) protein-1 (SLC44A1) and CTL2 (SLC44A2) exhibit transport properties consistent with BBB choline transport in vivo, e.g., choline  $K_m = 10\text{--}200 \mu\text{M}$ , HC-3  $K_i = 10\text{--}100 \mu\text{M}$  [407]. The mRNA encoding both CTL1 and CTL2 are detected in cultured human brain endothelium [408]. However, the abundance of both CTL1 and CTL2 is <LOQ in QTAP studies of rat brain capillaries [409], similar to other CMT systems at the BBB with a low  $V_{max}$ . More definitive evidence is needed that CTL1 or CTL2 mediates transport at the BBB of choline and choline-like drugs.

#### 6.2.7. Vitamin Carriers

The transport of the B vitamins across the BBB is carrier-mediated via members of the SLC transporter family. BBB transport of vitamin B1 (thiamine) is saturable [410], and the thiamine transporter (THTR)2 (SLC19A3) is expressed in brain [411]. Thiamine

deficiency leads to CNS morbidity [412]. Transport of vitamin B2 (riboflavin) is saturable at the BBB in vivo [413] and in cultured endothelium [414]. The riboflavin vitamin transporter (RFVT)2 is expressed in brain, and is SLC52A2. Mutations in either RFVT2 (SLC52A2) or RFVT3 (SLC52A3) lead to neurodegeneration [415]. Vitamin B3 (niacin, nicotinic acid) is a monocarboxylic acid transported by MCT1 [416]. However, niacin is amidated to form niacinamide, which is the major form of vitamin B3 in plasma, and niacinamide traverses the BBB by non-saturable free diffusion [417]. Vitamin B4 refers alternatively to choline, adenine, or carnitine, which are no longer considered vitamins, although adenine and choline are essential nutrients, and carnitine is a conditionally essential nutrient. Vitamin B5 (pantothenic acid) traverses the BBB via a saturable process with a  $K_m$  of 19  $\mu\text{M}$  [418]. Both pantothenic acid and biotin (vitamin B7 or B8) are monocarboxylic acids which are transported via the sodium dependent multivitamin transporter (SMVT, SLC5A6) [419], as listed in Table 3.

**Table 3.** Vitamin transporters at the blood–brain barrier.

Vitamin	MW	Polarity	Transporter	SLC
Thiamine (B1)	265	charged	THTR2	19A3
Riboflavin (B2)	376	hydrophilic	RFVT2	52A2
Niacin (B3)	123	carboxylate	MCT1	16A1
Pantothenic acid (B5)	219	carboxylate	SMVT	5A6
Pyridoxine (B6)	169	hydrophobic	THTR2	19A3
Biotin (B7, B8)	244	carboxylate	SMVT	5A6
Folic acid (B9, B11)	441	hydrophilic	FOLR1	receptor
Cobalamin (B12)	1355	hydrophilic	TCBLR	receptor

SMVT is expressed in brain capillary endothelium [420]. Brain biotin uptake is saturable [421], and the brain uptake of biotin in the rat is  $0.28 \pm 0.03\%ID/g$  [422]. Biotin may be transported either by MCT1 or SMVT [423]. Vitamin B6 (pyridoxine) is a small molecule with a MW of 169 Da which forms six hydrogen bonds with water, and should traverse the BBB via free diffusion. However, the brain uptake of pyridoxine is saturable [424], and transfection of cells encoding the THTR thiamine transporter (SLC19A3) leads to increased pyridoxine uptake [425]. Vitamin B9/B11 (folic acid) is transported by the folate receptor (FOLR)1, the reduced folate carrier (RFC, SLC19A1), and the intracellular proton-coupled folate transporter (PCFT, SLC46A1) [426]. The active metabolite of folic acid (FA) is 5'-methylenetetrahydrofolic acid (MTFA). The RFC has a higher affinity for MTFA than for FA, whereas the affinity of FOLR1 for MTFA and FA is comparable. The BBB transport of MTFA was equally inhibited by FA and MTFA, which suggests the major BBB folate transporter is FOLR1 [427]. Folate delivery to brain is suppressed in the FOLR1 knockout mouse [426]. However, the mRNA level of RFC exceeds the level for FOLR1 mRNA in isolated brain microvessels, which points to an important role for the RFC in BBB transport of folic acid [426]. Vitamin B10 is p-aminobenzoic acid, which is no longer considered a vitamin. Vitamin B12 (cobalamin) is transported in blood bound to the transcobalamin (TC) binding protein [428]. The B12/TC complex is endocytosed into cells via the TC receptor (TCbIR), also known as CD320, and the three-dimensional structure of the B12/TCbIR complex has been determined [428]. Knockout of the CD320 gene in the mouse is not lethal, although the brain concentration of B12 is >90% reduced, and metabolites associated with vitamin B12 deficiency are selectively increased in brain in the CD320 knockout mouse [429]. Expression of the TCbIR/CD320 at the BBB has been confirmed [430].

The vitamin transporters are potential conduits for drug delivery to brain. In an effort to deliver neuropeptide YY to brain, this peptide was conjugated to vitamin B12 [431]. An ampakine compound was conjugated to thiamine via a disulfide bridge, which resulted in increased brain uptake of the ampakine [432].

All of the SLC transporters for nutrients or vitamins described in Sections 6.2.1–6.2.7 are potential conduits to brain of drugs that mimic the structure of the nutrient or vitamin transported by the respective SLC transporter. These numerous SLC transporters recognize

a broad universe of molecular structures that can guide the medicinal chemist in creating nutrient-mimetic or vitamin-mimetic pharmaceuticals that cross the BBB via CMT.

#### 6.2.8. Thyroid Hormone Carriers

The saturable transport of the thyroid hormones, L-triiodothyronine (T3) and L-thyroxine (T4), across the BBB *in vivo* in the rat was demonstrated with the BUI method in 1979 [433]. The  $K_m$  of T3 transport was 1.1  $\mu\text{M}$  and the  $K_i$  of T4 inhibition of T3 transport was 2.6  $\mu\text{M}$ . T3 transport was not inhibited by high concentrations of LNAAs, leucine or tyrosine. The  $V_{\text{max}}$  of T3 transport was 0.2 nmol/min/g [433], which is 100-fold lower than the  $V_{\text{max}}$  of transport via LAT1 (Table 2). Subsequently, MCT8 (SLC16A2) was shown to transport both T3 and T4 to a comparable degree [434]. The low  $V_{\text{max}}$  of BBB T3 transport is consistent with the inability to detect MCT8 in brain endothelial cells by QTAP proteomics method [435], but immunohistochemistry with an antibody against MCT8 illuminated microvessels in human, rat, and mouse brain similarly to the immune staining obtained with an anti-Pgp antibody [436]. The knockout of the MCT8 gene in the mouse does not result in CNS impairment or CNS hypo-thyroidism [437], which suggests the mouse has an alternative pathway for thyroid hormone transport across the BBB, as discussed below. However, mutations in the MCT8 gene in humans causes impaired neurodevelopment, a condition known as the Allan–Herndon–Dudley syndrome [437], which indicates humans may not have an active alternative to the MCT8 pathway of thyroid hormone transport across the BBB, as discussed below.

A second thyroid hormone transporter is organic anion-transporting polypeptide (Oatp)1c1, also known as oatp14, and now designated Slco1c1. This gene was originally cloned as part of a BBB genomics investigation [438]. The new gene was named BBB-specific anion transporter 1 (BSAT1) because of a distant sequence homology with a liver specific anion transporter. The BSAT1 mRNA was not detected by Northern blotting in rat heart, lung, liver, kidney, or total brain, but was highly expressed in isolated rat brain capillaries [438]. The sequence of the full length 2736 nucleotide cDNA of rat BSAT1 was deposited in GenBank in 2001 (AF306546), and this sequence encoded for a 716-amino acid protein. Expression of the mouse oatp14 cDNA in HEK293 cells showed this transporter mediated uptake of the estradiol  $\beta$ -glucuronide ( $\text{E}_2\text{G}$ ) anion, but also mediated the uptake of T4 and T3 [439]. Expression of the rat BSAT1/oatp14/Slco1c1 in HEK293 cells showed the  $K_m$  of transport of T4 and  $\text{E}_2\text{G}$  via BSAT1 was  $0.72 \pm 0.10 \mu\text{M}$  and  $6.1 \pm 0.5 \mu\text{M}$ , respectively [440]. T3 inhibited the transport of T4 and  $\text{E}_2\text{G}$  with a  $K_i$  of  $50 \pm 17 \mu\text{M}$  and  $4.2 \pm 0.7 \mu\text{M}$ , respectively. Transport of T4, T3, and  $\text{E}_2\text{G}$  via BSAT1 (Slco1c1) was asymmetric and consistent with transport via two sites [440]. Site 1 transported T4, but not T3 or  $\text{E}_2\text{G}$ , and site 2 transported T4, T3, and  $\text{E}_2\text{G}$ . Using a prealbumin trap technique, the efflux of intracellular T4 was enhanced by the presence of  $\text{E}_2\text{G}$  in the extracellular compartment [440]. Prealbumin binds T4 with high affinity and prevented reuptake of T4 following efflux from the preloaded cell [440]. Immunohistochemistry with an antibody against Slco1c1 illuminated the microvessels in rat and mouse brain, but not in human brain [436]. The absence of expression of immunoreactive Slco1c1 in microvessels of human brain was confirmed by qPCR analysis measuring the Slco1c1 mRNA in total brain and brain microvessels. The Slco1c1 mRNA was highly enriched at the brain microvessel compared to total brain for rat and mouse, but there was no enrichment of the Slco1c1 mRNA in human microvessels [436]. Similarly, the Slco1c1 gene was repeatedly isolated in rat brain vascular genomic studies [438,441], but was not detected in a similar genomics investigation using microvessels isolated from fresh human brain obtained at neurosurgery [442]. These species difference in Slco1c1 expression at the BBB in rodents vs. humans suggest that Slco1c1 may not be a suitable target for brain drug delivery in humans. The high expression of Slco1c1 at the rodent BBB, but not the human BBB, explains why MCT8 mutations cause cerebral hypo-thyroidism in humans, but not in mice [437].

### 6.2.9. Organic Cation Carrier

Carnitine is essential to brain metabolism as a mediator of free fatty acid delivery to mitochondria [443]. Carnitine is an amino acid betaine with a quaternary ammonium terminus. Carnitine is transported via the organic cation (OCTN)2 transporter (SLC22A5) [443]. The transport of carnitine across the BBB in vivo is very low and comparable to sucrose [444], although OCTN2 mediates carnitine uptake in human brain endothelium in cell culture [445]. The SLC22 gene family includes both the organic cation transporter (OCT) and OCTN organic cation transporters as well as the organic anion transporters (OAT) [446]. A recent proteomics study of OCT expression at the human brain microvessel showed that OCT-3 (SLC22A3) is the most abundant OCT transporter at the human BBB, with an expression level of 0.15 pmol/mg capillary protein [447], a level that is about one-third the expression of LAT1 (Table 2). OCT-1 (SLC22A1) and OCT-2 (SLC22A2) were not detectable at the human BBB [447]. HEK293 cells transfected with human OCT-3 were used in a high throughput screen of over 2000 compounds that are potential OCT-3 substrates by measuring the inhibition of the cell uptake of a model OCT-3 fluorescent substrate, 4-(4-(dimethylamino)styryl)-N-methylpyridinium iodide (pinaflavol), which is a quaternary ammonium compound [447]. The investment of such a significant effort to find drugs that penetrate the BBB via transport on OCT-3 assumes that this transporter mediates the influx of drugs from blood to brain. This may not be the case as the striatal neurotoxin, MPP<sup>+</sup>, is transported via OCT-3 [448], but MPP<sup>+</sup> does not cross the BBB [370].

In summary, multiple CMT systems are expressed at the BBB that mediate the transport of nutrients, vitamins, thyroid hormones, and organic cations from blood to brain. The experiments demonstrating saturable BBB transport of nutrients were conducted largely in the 1970s using the BUI method [48,327,340,355,383,390,400,433]. Since then, BBB transporters are now classified on a molecular basis within the context of the SLC gene superfamily. The molecular biology of the BBB CMT systems is now complex as there are >400 members of the SLC transporter family. Therefore, it is crucial to show that the substrate transporter profile (STP) of the cloned SLC transporter mirrors the STP observed at the BBB with in vivo transport investigations. The expanded knowledge base of BBB transport via SLC carriers provides targets for solving current day brain drug delivery problems for small molecules. Solutions to the problem of BBB delivery of hydrophilic small molecules has, in the past, focused on the use of medicinal chemistry for the conversion of hydrophilic small molecules into lipid-soluble prodrugs. However, this had led to few FDA-approved drugs for the CNS, as reviewed above in Section 6.1. Instead, CNS drug developers can elucidate the STP of the individual BBB CMT systems both in vivo and with cloned transporters, and then use medicinal chemistry to convert hydrophilic small molecules into drugs that mimic the structure of endogenous ligands transported by the BBB CMT systems. Such work is ongoing in academic labs, particularly for LAT1, as reviewed above in Section 6.2.2. However, the pharmaceutical industry has yet to adopt this approach, as the industry continues to focus on the development of lipid-soluble small molecules that treat primarily only psychiatric disorders and epilepsy, as reviewed in Section 6.1.1

## 6.3. Active Efflux Transport of Small Molecules

### 6.3.1. Brain-to-Blood Efflux

The carrier-mediated SLC transporters reviewed in Section 6.2 enable the influx from blood to brain of specific classes of nutrients or vitamins. Brain-to-blood efflux across the BBB also takes place for excitatory neurotransmitters, such as the acidic amino acids, *L*-glutamate and *L*-aspartate, and for neurotransmitter metabolites, such as homovanillic acid (HVA), which is derived from catecholamine degradation. These molecules are polar and require access to specific efflux transporters in order to undergo exodus from brain-to-blood. Drugs may also be recognized by the endogenous BBB efflux transporters, which would adversely affect drug distribution to brain. An early study of drug efflux across the BBB was performed with the BUI technique, which showed the BBB permeability of valproic acid (VPA) in the brain-to-blood direction was several-fold greater than in the blood-to-brain

direction [449]. However, the saturability, or cross-competition of drug efflux, cannot be accessed with the BUI method. Terasaki and colleagues developed the Brain Efflux Index (BEI) method for the study of solute efflux from brain following the direct intra-cerebral injection under stereotaxic guidance [450]. While the BEI method is generally used to study the efflux of small molecules, this method can also be used to examine the brain-to-blood transport of large molecules, such as IgGs or transferrin [451,452]. The BEI method is particularly useful to assess the BBB efflux of drugs. The brain efflux of two drugs used for HIV infection, azidothymidine (AZT) and dideoxyinosine (DDI), was measured with the BEI method [453]. Both drugs effluxed from brain with a  $T_{1/2}$  of 22–28 min, and AZT and DDI efflux was inhibited by organic anions, probenecid and p-aminohippuric acid (PAH). Other organic anions, such as the bile salt, taurocholate (TC), were demonstrated to undergo efflux across the BBB, and the TC efflux was inhibited by cholic acid and probenecid, but not by PAH [454]. Acidic amino acids, glutamate and aspartate, have the lowest rate of influx from blood to brain of any of the amino acids [455]. The high rate of efflux of the acidic amino acid from brain to blood was demonstrated with the BEI method [456]. Similarly, the BEI method characterized the efflux from brain of endogenous organic anions, such as estrone 3-sulfate (E3S), as well as the neutral estrogen, estrone (E1). The  $T_{1/2}$  of efflux of either E3S or E1 from brain was about 10 min [457]. The efflux of E3S across the BBB via free diffusion is nil, owing to the highly polar sulfate group. Therefore, efflux of the E3S would require access to a transporter, and this was demonstrated by the inhibition of E3S efflux by another endogenous organic anion, dehydroepiandrosterone sulfate (DHEAS) [457]. E1 is a hydrophobic estrogen, and such unconjugated estrogens rapidly cross the BBB via free diffusion [322], but are reversibly sequestered in brain owing to binding to cytoplasmic proteins [458]. In the absence of this sequestration, E1 should efflux from brain with a  $T_{1/2}$  comparable to water, which is 1.1 min [450]. However, the cytoplasmic binding of E1 in brain results in the prolonged brain residence time [457], as discussed further in Section 11.5.2. The brain efflux and influx of DHEAS was assessed with the BEI and internal carotid artery perfusion (ICAP) methods, respectively [459]. The rate of efflux of DHEAS was more than 10-fold faster than the rate of influx. The influx from blood to brain was restricted by the polar sulfate moiety of DHEAS, as the sulfate group converted the DHEA steroid to an organic anion and a substrate for organic anion transporters. The carrier-mediated efflux of DHEAS from brain to blood was inhibited by other organic anions, TC and E3S [459]. An organic anion generated in the degradation of catecholamines is HVA, and HVA efflux from brain to blood is inhibited by other organic anions, probenecid and PAH [460]. Anticonvulsants may undergo active efflux from brain to blood, as demonstrated for phenytoin [461]. Frog oocyte expression studies implicated MCT8 as the principal efflux transporter at the BBB for phenytoin [461]. Active efflux transporters play an important role in the distribution to brain of anticonvulsants [462].

The assignment of nutrient or vitamin CMT systems to specific members of the SLC gene superfamily is discussed above in Section 6.2. The comparable assignment of the BBB efflux transporters to specific transporter genes is more difficult owing to the large number of transporter candidates. Active efflux transporters (AET) at the BBB may arise from either the ATP-binding cassette (ABC) gene superfamily or the SLC gene superfamily. The SLC gene family includes nearly 460 genes divided over 65 sub-families [463]. The ABC gene family is composed of nearly 50 genes divided over 7 sub-families [464,465].

### 6.3.2. ABC Efflux Transporters

ABCA1 and ABCG1 are cholesterol transporters, which mediate the efflux of cholesterol metabolites from brain to blood. Astrocytes and neurons synthesize cholesterol *de novo* [466]. Excess cholesterol is removed from brain by hydroxylation of cholesterol to form 24(S)hydroxycholesterol (24S-HC) [467], and 24S-HC is exported to blood via transport on ABCA1 and ABCG1 [466]. Brain capillary proteomics shows that ABCA1 is primarily expressed on the abluminal endothelial membrane [468]. The loss of ABCG1 leads to a toxic accumulation of 24S-HC and other oxysterols in brain [469]. All of chole-

terol in blood is bound to lipoproteins, and lipoprotein-bound cholesterol does not cross the BBB [466]. The BBB transport of free cholesterol in the blood-to-brain direction was measured with the internal carotid artery perfusion (ICAP) method. BBB transport of free cholesterol was rapid, and the BBB PS product was 0.64 mL/min/g in the wild-type mouse and 1.3 mL/min/g in the *abca1* knockout mouse [470]. However, these studies are difficult to interpret, because free cholesterol does not exist in plasma. The BUI of free [<sup>3</sup>H]-cholesterol following the carotid artery injection in either saline or serum is high  $63 \pm 8\%$  [471]. However, simply mixing cholesterol with serum does not lead to incorporation of cholesterol into lipoproteins, unless the serum is incubated overnight at 37C [471]. When this is performed, the BUI of [<sup>3</sup>H]-cholesterol in human serum is at the background level of brain uptake [471]. The absence of transport of lipoprotein bound cholesterol from blood to brain is consistent with the absence of expression of the low-density lipoprotein receptor (LDLR) at the BBB, as discussed below in Section 8.1.6.

ABCB1, also known as p-glycoprotein (Pgp), or the multi-drug resistance (MDR) gene product, was shown, in 1989, to be expressed at the BBB with immunohistochemistry of human brain and antibodies specific for human Pgp, although no PgG was detected at the epithelium of the choroid plexus [62]. A Pgp knockout mouse was developed in 1993 [472]. Quinidine is a lipid-soluble small molecule with a MW of 324 Da, and should cross the BBB. However, quinidine is a substrate of Pgp. The brain uptake of quinidine was increased nearly 30-fold in the Pgp knockout mouse [473]. Verapamil is a lipid-soluble small molecule that should cross the BBB, but is a substrate of Pgp. Brain uptake of [<sup>11</sup>C]-verapamil in the rat was measured by PET, and brain uptake was increased by the co-administration of cyclosporine A (CsA), a Pgp modulator [474]. CsA has a MW of 1203 Da, and has minimal BBB transport [475]. The effect of CsA on Pgp-mediated transport suggests the Pgp is expressed at the luminal membrane of the endothelium. Proteomics studies of brain capillaries show that Pgp is exclusively expressed at the luminal endothelial membrane [468].

A total of 42 small molecules were examined for Pgp regulated brain uptake [476]. This group was composed of both “CNS drugs”, which had a mean MW of 297 Da and a mean polar surface area of 48 Å<sup>2</sup>, and “non-CNS drugs”, which had a mean MW of 468 Da, and a mean polar surface area of 80 Å<sup>2</sup>. The brain:plasma ratio of Pgp ligands, such as metoclopramide and risperidone, in the Pgp knockout mouse relative to the brain:plasma ratio in the wild-type mouse, was 7–10-fold [476]. No change in the CSF:plasma ratio was observed [476], which is consistent with the lack of Pgp expression at the choroid plexus, as originally reported in 1989 [62]. A similar finding of lack of Pgp expression at the choroid plexus was made in the primate for the HIV protease inhibitor, nelfinavir, which is a substrate for Pgp. The co-administration of nelfinavir and a Pgp-inhibitor, zosuquidar, resulted in an increase in uptake of nelfinavir into brain, but not into CSF [477]. The absence of immunoreactive Pgp at the choroid plexus has been confirmed in the rat [478] and human [479]. Brain capillary proteomics shows the level of Pgp at the brain capillary is 6.7 pmol/mg protein, which is 45-fold higher than the Pgp level at the choroid plexus, 0.15 pmol/mg protein, which is near the limit of quantitation [480]. Pgp expression in brain is generally believed to be confined to the vasculature. However, immunoreactive Pgp is expressed on astrocyte foot processes in the brain of humans [481] and primates [482].

The multi-drug resistance-associated proteins (MRP)-1 to MRP-6 are encoded by the *ABCC1-ABCC6* genes. MRP1 is expressed at both the BBB and at the choroid plexus [478]. Confocal microscopy of brain shows MRP1 and MRP5 are primarily expressed at the abluminal endothelial membrane, whereas MRP4 is primarily expressed at the luminal membrane [345]. Of the MRPs, the mRNA encoding MRP6 is the most highly enriched at the microvasculature of human brain [483].

The breast cancer resistance protein (BCRP) is encoded by the *ABCG2* gene, and is an important efflux transporter at the BBB [484]. Confocal microscopy of human brain and glioma shows co-localization of BCRP with GLUT1 [485]. Brain vascular proteomics shows high expression of BCRP at the BBB across multiple species [360,435,480,486]. BCRP is

7-fold enriched at the luminal capillary endothelial membrane as compared to the abluminal membrane [468]. The BCRP mRNA is highly enriched at the human brain microvasculature, relative to total brain [483]. Ivermectin is not a substrate for BCRP as the brain uptake of ivermectin is not increased in the *bcrp* knockout mouse [487]. Ivermectin is a Pgp substrate, and brain ivermectin uptake is increased in the Pgp knockout mouse [472,487]. However, ivermectin is a highly polar drug macrocyclic lactone with a MW of 875 Da, which are not the molecular properties of a small molecule that penetrates the BBB via free diffusion, as reviewed in Section 6.1. The high brain uptake of ivermectin in the Pgp knockout mouse suggests ivermectin traverses the BBB via an unknown transport system.

### 6.3.3. SLC Efflux Transporters

SLC efflux systems at the BBB include transporters for both amino acids and organic anions. The acidic amino acids, glutamate and aspartate, are also excitatory amino acids [488], and CNS homeostasis is maintained by preventing changes in plasma concentrations of these amino acids causing similar changes in brain levels of the excitatory amino acids. A saturable carrier for *L*-glutamate and *L*-aspartate was identified at the BBB by the BUI method [455]. However, the rate of influx of glutamate or aspartate from blood to brain was lowest of any of the amino acids [455]. In parallel with this low rate of influx, the rate of efflux of the acidic amino acids from brain to blood was high [489]. These observations led to the hypothesis that the BBB acidic amino acid transporter was an active efflux system [490]. The active efflux of glutamate from brain to blood was confirmed with the BEI method [456]. The principle acidic amino acid transporters are the sodium-dependent excitatory amino acid transporter (EAAT)1 (SLC1A3), EAAT2 (SLC1A2), and EAAT3 (SLC1A1) [491], and these transporters are localized to the abluminal membrane of the BBB [492]. At the human brain capillary, the expression of EAAT1 is relatively high, 5.0 pmol/mg protein [409]. Small neutral amino acids may also play a role in neurotransmission. Serine is a neurotransmitter modulator, and alanine is a ligand for glycine neurotransmission [488]. Small neutral amino acids, such as alanine or serine are transported via the alanine (A)-system [493]. The A-system amino acid transporter was cloned, and this sodium dependent transporter was designated amino acid transporter 2 (ATA2, SLC38A2) [494]. ATA2 was subsequently localized to the BBB and identified as an active efflux system [495]. ATA2 is exclusively localized to the abluminal endothelial membrane [468,492].

Organic anion transporters also operate as BBB active efflux systems. The SLC22 gene family, which includes 28 transporters, comprises two parallel clades encoding for organic anion transporters (OAT) and organic cation transporters (OCT, OCTN) [446]. The mRNA encoding for OAT3 (SLC22A8) is highly expressed at the rat brain capillary [345]. Proteomics studies show species differences in the expression level of the OAT3 transporter protein as the level is 2.0 pmol/mg protein in mouse brain capillaries [435], but is less than the limit of quantitation (LOQ) for human or monkey brain microvessels [360,435]. The rodent organic anion transporting polypeptide (Oatp)1a4 is most homologous with the human OATP1A2 (SLCO1A2, previously named SLC21A3) and is expressed at the BBB [496], as well as retinal capillaries that form the blood–retinal barrier (BRB) [497]. Oatp1a4 is highly expressed at the rat arachnoid membrane [498], which is an important barrier system in brain that separates the CSF from the dura mater. Recent studies show that solute transport from CSF to the peripheral blood may take place via active transport across the arachnoid membrane. A fluorescent Oatp1a4 ligand, sulforhodamine (SR)-101, is actively transported out of CSF to blood at a rate much faster than inulin [498]. This efflux of SR-101 from CSF is blocked by taurocholate, which has broad specificity for the anion transporters, and by digoxin, which is specific for Oatp1a4 [498]. Oatp1a4 at the BBB is expressed on both luminal and abluminal endothelial membranes [499]. Unlike OAT3, which is highly expressed at the arachnoid membrane, OATP1A2 and OATP3A1 are not detectable at the arachnoid [500]. OATP1C1 (*Slco1c1*) is a BBB thyroid hormone transporter that can protect mouse brain deficient for MCT8 [437], although OATP1C1 expression at the human BBB is minimal [436], as discussed in Section 6.2.8. OATP3A1 is said to be another

alternative thyroid hormone transporter [501]. However, OATP3A1 protein expression is <LOQ at the primate BBB [486].

In summary of Section 6 on CNS drug development of small molecules, present day efforts in the pharmaceutical industry are still largely entrenched in a 20th century model that is restricted to the development of small molecules that cross the BBB via free diffusion. Only drugs with a MW < 400–450 Da that form <8 hydrogen bonds with water can cross the BBB by free diffusion, and such drugs invariably only treat psychiatric disorders or epilepsy. Future small molecule CNS drug developers should consider re-directing medicinal chemistry away from the production of lipid-soluble pro-drugs, and toward the synthesis of drugs that mimic the structure of nutrients or vitamins that are substrates for SLC transporters expressed at the BBB. The SLC transporter family is complex and is composed of >400 transporters among >60 families [338]. Only a small fraction of the SLC transporters is expressed at the BBB. Therefore, the selection of an SLC transporter to be targeted for small molecule CNS drug delivery should consider the following:

- The substrate transporter profile (STP) that characterizes BBB transport in vivo should be replicated by the STP of the cloned transporter that is expressed in vitro. STPs determined with in vitro BBB models should not be used as a primary method, owing to the marked alteration of gene expression within brain endothelial cells grown in cell culture, as discussed in Section 11.7.2. The STP should be determined in vivo with methods discussed in Section 11.4.
- Evidence should be available that the targeted SLC transporter is expressed on both luminal and abluminal endothelial membranes in the human brain. As discussed above, there are species differences in the expression of certain transporters at the human vs. the animal BBB. Some SLC transporters are only expressed on the abluminal endothelial membrane, and these abluminal transporters would not be available to transport drug from blood to brain.
- The BBB CMT systems form trans-membrane cavities, as illustrated for GLUT1 and LAT1 in Figure 9, and these cavities can be sharply stereospecific with low tolerance for bulky structural changes to the substrate. As an example, if the GLUT1 carrier is targeted for brain drug delivery, the drug should be modified, not by conjugation of the drug to D-glucose, but rather by alteration of the drug structure so as to mimic the structure of the endogenous substrate, D-glucose.
- If the lead CNS drug candidate is a ligand for Pgp, or one of the other active efflux transporters at the BBB, then a co-drug needs to be developed that inhibits the BBB efflux transporter.

## 7. Absorptive-Mediated Transport of Cationic Proteins or Lectins

### 7.1. Cationic Proteins

#### 7.1.1. Cationized Proteins

Cationization of proteins raises the isoelectric point (pI) to the alkaline range, and this modification enhances cell uptake of the protein via a charge or absorptive-mediated endocytosis. A protein can be cationized either by conjugation of a polycation, such as poly-L-lysine (PLL) [502], or diamino agents such as ethylenediamine [503] or hexamethylenediamine [504], to surface carboxyl groups using 1-ethyl-3-(3-dimethylamino-propyl) carbodiimide (EDAC). Conjugation of PLL to either albumin or HRP enhances protein uptake into cultured fibroblasts [502]. Cationization with amine reagents and EDAC is a pH-controlled reaction, and the lower the pH of the chemical conjugation, the higher the degree of cationization. Hexamethylenediamine was conjugated to bovine serum albumin with EDAC at a pH of either 7.8 or 6.8 to produce moderately cationized bovine serum albumin (cBSA) of pI of 8.5–9 and highly cationized cBSA with a pI > 10, respectively [54]. Highly cationized albumin or IgG, with a pI > 10, is nephrotoxic [503]. Moderately cBSA, pI = 8.5–9, was both bound, and endocytosed, by isolated bovine brain microvessels via a saturable process that was 50% inhibited at a cationized albumin concentration (ED50) of  $10.8 \pm 0.1 \mu\text{M}$  [54]. The binding of cBSA to brain capillaries was



competed by other polycations such as protamine or 70 kDa PLL. [ $^{125}$ I]-cBSA was infused in the carotid artery for 10 min and the brain was removed and sectioned on a cryostat for thaw-mount emulsion autoradiography [54]. This showed the cBSA was localized to the brain microvasculature with measurable distribution into the brain parenchyma. The first use of cationized albumin for brain drug delivery was tested with the opioid peptide,  $\beta$ -endorphin, which was conjugated to the cBSA [54]. There was minimal uptake of the unconjugated  $\beta$ -endorphin by brain microvessels, but the  $\beta$ -endorphin was both bound and endocytosed by brain microvessels following conjugation of the peptide to the cBSA delivery system [54]. These in vitro investigations were confirmed with in vivo studies measuring the brain distribution of a metabolically stable and peptidase-resistant opioid peptide, [D-Ala<sup>2</sup>]- $\beta$ -endorphin (DABE), which was conjugated to cBSA (pI = 8.5–9) with a disulfide cleavable linker using N-succinimidyl 3-(2-pyridyldithio(propionate)) [505]. The internal carotid artery perfusion (ICAP) method, coupled with the capillary depletion method [506], demonstrated transport of the DABE-cBSA conjugate through the BBB into brain parenchyma, whereas there was no BBB transport of the unconjugated DABE [505]. The DABE-cBSA conjugate was incubated with brain homogenate followed by gel filtration fast protein liquid chromatography (FPLC) to show cleavage in brain of the disulfide linker joining the DABE and the cBSA delivery vector [505]. This early study demonstrated that a pharmaceutical, such as an opioid peptide, could be chemically conjugated to a molecular Trojan horse, cBSA, for delivery across the BBB in vivo in confirmation of the earlier in vitro study [54].

Cationization of a protein enhances cell uptake, in general, including uptake into immune cells. Cationization of a heterologous protein enhances the immunogenicity and nephrotoxicity of the heterologous protein [503]. However, mild cationization of a homologous protein was shown to exert no toxicity in rats with chronic administration [507]. Rat serum albumin (RSA) was cationized at a pH of 7.8 to a pI of 8.5. The cationized RSA (cRSA) was bound and endocytosed by isolated rat brain microvessels with an ED<sub>50</sub> of  $2.5 \pm 1.1 \mu\text{M}$  [507]. The cRSA was cleared from plasma in rats with a  $T_{1/2}$  of  $2.5 \pm 0.4 \text{ h}$ , and the organ uptake in rats of the cRSA was compared to the organ uptake of native RSA (nRSA). The spectrum of organ uptake of the cRSA was kidney > brain > liver, with no enhanced uptake in heart or lung [507]. The cRSA was administered chronically to rats at a dose of 1 mg/kg subcutaneous (SQ) 5 days a week for 8 weeks. The treatment produced no changes in organ histology, body weight, or clinical chemistry, and produced a low titer anti-drug antibody (ADA) response [507].

Enhanced cell uptake of IgG is also enabled by protein cationization. Bovine IgG was cationized with hexamethylenediamine to a pI > 10 [508]. The cationized bovine IgG (cIgG) was both bound and endocytosed by isolated bovine brain capillaries. The ED<sub>50</sub> of binding was  $0.90 \pm 0.37 \mu\text{M}$ . The cIgG was radioiodinated and perfused via the internal carotid artery for 10 min followed by removal of brain, sectioning with a cryostat in the darkroom and emulsion autoradiography. The darkfield microscopy of the developed slides showed high sequestration of the cIgG around the brain microvessels, but also distribution into brain parenchyma. The [ $^{125}$ I]-cIgG sequestration at the brain microvessels and the transport into brain parenchyma was completely inhibited by the co-infusion 25 mg/mL cationized IgG [508].

Therapeutic antibodies do not cross the BBB, and an early approach to brain delivery of a therapeutic monoclonal antibody (MAb) employed cationization of the antibody [509]. The concern with cationization of a monoclonal antibody (MAb) is the loss of affinity of the MAb for the target antigen following cationization. Different antibodies are expected to have different degrees of loss of antigen affinity following cationization. In the case of a potential therapeutic MAb for the treatment of AIDS, a MAb directed against the *rev* protein of the human immunodeficiency virus-1 (HIV1) was developed and designated MAb111 [510]. However, the HIV virus invades the CNS to cause neuroAIDS, and an anti-*rev* MAb would not cross the BBB. In an effort to enhance brain delivery of the therapeutic antibody, the pI of the MAb111 was raised from 6.6 to 9.5 by cationization [509]. The

native MAb111 and the cationized MAb111 bound to the recombinant rev protein with comparable affinity. Incubation of [ $^{125}$ I]-native MAb111 and [ $^{125}$ I]-cationized MAb111 with human peripheral blood lymphocytes (PBLs) showed the native MAb111 did not enter the cells over the course of a 3 h incubation. However, the cationized MAb111 showed robust binding and endocytosis into the PBLs [509]. Incubation of PBLs with 25  $\mu$ g/mL concentrations of the cationized MAb111 had no effect on thymidine incorporation over a 24 h period [509]. A potential therapeutic MAb for Alzheimer's disease (AD) is an antibody against the amino terminal region of the Abeta peptide of AD, and one such antibody is the AMY33 antibody [511]. The pI of native AMY33 was 7.0, and this was raised to a pI of  $\sim$ 8 or a pI of  $\sim$ 9 by adjusting the molar ratios of hexamethylenediamine and EDAC, and the pH of the cationization reaction [512]. The binding of the native AMY33 and the cationized AMY33 to the A $\beta$ <sup>1–28</sup> amyloid peptide showed the dissociation constant (KD) of binding of the native and cationized antibodies was  $1.4 \pm 0.3$  nM and  $4.2 \pm 0.7$  nM, respectively. The cationized AMY33 also retained high affinity for binding Abeta amyloid in autopsy AD brain as shown by immunohistochemistry using either the native or cationized AMY33 antibody [512]. The use of cationized antibodies, and absorptive-mediated transcytosis for brain antibody delivery, have been reviewed [513,514]. Since these early studies on antibody cationization, a preferred method of therapeutic antibody transport into brain has emerged, which is the engineering of a bispecific antibody (BSA) that enters brain via receptor-mediated transport (RMT), as discussed in Section 8.3.4.

#### 7.1.2. Endogenous Cationic Proteins

Protamines are endogenous arginine-rich proteins with a MW of 4–7 kDa and a pI $\sim$ 10. Early studies showed the internal carotid artery infusion of 0.3–1.5 mg/kg of protamine over a 1–2 min period caused BBB disruption to HRP, and electron microscopy showed the BBB disruption was due to opening of tight junctions [256]. The administration of protamine via the IV route did not cause BBB disruption [257]. However, IV protamine can still enhance the delivery of macromolecules across the BBB by absorptive-mediated transport. Protamine binds anionic domains on the luminal surface of the brain endothelium. Electron microscopy shows the luminal membrane of the brain endothelium is rich in anionic sites composed of sialic acid residues on glycoproteins [515]. In parallel, protamine binds anionic domains on proteins such as albumin with a KD of 6–22  $\mu$ M [516]. Therefore, protamine can act as a molecular Trojan horse for albumin delivery to brain via the non-covalent electrostatic interactions between protamine and both albumin and the luminal membrane of the BBB. Protamine enhances the binding and endocytosis of native rat serum albumin (nRSA) by isolated bovine brain capillaries with an ED<sub>50</sub> of 70  $\mu$ M protamine, but has no effect on uptake of sucrose by the microvessels [516]. The co-injection of 1.5 mg/kg of histone free protamine base and nRSA IV in rats causes a 34-fold increase in RSA uptake by liver, an 11-fold increase in RSA uptake by lung, a 3-fold increase in RSA uptake by kidney, and a 2-fold increase in RSA uptake by brain and heart [516].

Histones are endogenous lysine/arginine-rich proteins with a MW of 11–15 kDa and a pI of  $\sim$ 10. Early work by Ryser [517] showed that polycationic substances such as protamine or histone can act as mediators for the cellular uptake of proteins. More recently, histones have been proposed as agents for drug delivery [518]. Similar to protamine, histones are endocytosed at the BBB *in vivo*, but also have toxic effects on the endothelial membrane [259]. Histone is bound and endocytosed by isolated brain microvessels with a KD of binding of  $15 \pm 3$   $\mu$ M, via a process that is inhibited by protamine and poly-L-lysine [259]. Following IV administration, histone is cleared rapidly from plasma with a T<sub>1/2</sub> of  $13 \pm 5$  sec, and is cleared primarily by kidney, lung, liver, and spleen. The volume of distribution (VD) of histone in brain is 10-fold greater than the VD for albumin at 60 min after IV injection in the rat [259]. Following 10 min of internal carotid artery perfusion in the rat, the brain VD of histone is 9-fold greater than the VD of albumin in the homogenate fraction of brain. However, capillary depletion analysis shows all of the histone taken up by brain is sequestered within the capillary endothelium without transcytosis into the

post-vascular compartment of brain. The internal carotid artery infusion of a low dose of histone cause leakiness of the BBB and a seven-fold increase in the brain VD of albumin, which should be confined to the brain blood volume [259]. The toxicity of polycations such as histone at the BBB is discussed below in Section 7.3.1.

### 7.1.3. Cell-Penetrating Peptides

The prototypic cell-penetrating peptide (CPP) is a portion of the *tat* protein of HIV1, which encompasses an 11-amino acid (AA) sequence enriched in arginine (Arg) and lysine (Lys) residues. In an early study, a 36-mer peptide derived from the HIV1 *tat* protein was conjugated to  $\beta$ -galactosidase, which resulted in increased cellular uptake of the  $\beta$ -galactosidase [55]. Following IV injection of the *tat*- $\beta$ -galactosidase conjugate, the enzyme uptake was enhanced for heart, liver, and spleen, and to a lesser extent for lung and skeletal muscle, but there was no enzyme uptake by brain mediated by the *tat* peptide [55]. Subsequently, a fusion protein was engineered that was composed of  $\beta$ -galactosidase and the *tat* peptide domain, (GGGG)<sub>4</sub>YGRKKRRQRRR, which included the 11-AA *tat* peptide sequence following the glycine (G)<sub>4</sub> linker [519]. At 4–8 h after IV administration, enzyme activity was visible histochemically in the brain parenchyma [519]. This delayed appearance of the *tat*-enzyme fusion protein in brain is difficult to resolve with other results showing complete inactivation of bacterial  $\beta$ -galactosidase enzyme in mouse brain by 4 h after IV injection of a TfRMAB- $\beta$ -galactosidase conjugate [520]. Subsequent studies failed to show any enhancement of protein uptake by brain using the *tat* peptide. A fusion protein of *tat* and lysosomal enzymes, beta-glucuronidase (GUSB) [521] or arylsulfatase A (ASA) [522], showed no enzyme uptake by brain *in vivo*. Brain uptake of the *tat* peptide alone could not be detected using radiolabeling methods including PET scanning in the mouse [523].

Another early CPP was the 16-AA highly cationic penetratin, which is derived from a *Drosophila* protein [524]. However, following radiolabeling of penetratin with 111-indium, the brain uptake of the peptide was very low, 0.1%ID/g, in the mouse [523]. The penetratin, and other CPPs, including *tat*, were conjugated with (1,4,7,10-tetraazacyclododecane-1,4,7,10-tetraacetic acid), also known as DOTA or tetraxetan, for chelation of the 111-indium. This is the preferred mode of radio-labeling of rapidly cleared peptides, as opposed to radio-iodination. The small molecular metabolites generated by peripheral degradation of peptides labeled with 111-indium are sequestered in peripheral tissues. In contrast, the radio-tyrosine generated by peripheral degradation of the iodinated peptide, can cross the BBB, and lead to artifactually high brain radioactivity [525], as discussed in Section 11.4.4.

SynB1 was an 18-AA highly cationic CPP that was taken up by brain following internal carotid artery perfusion via a saturable process with an ED<sub>50</sub> of 5.5  $\mu$ M [526–528]. The BBB transport after internal carotid artery perfusion was inhibited by another cationic peptide, poly-L-lysine [528]. However, the addition of serum to the perfusate suppressed brain uptake [527]. The brain uptake of SynB1, labeled with 111-indium, after IV administration is at the background level, 0.1%ID/g, similar to *tat* or penetratin [523]. The lack of significant BBB transport of the CPPs following IV administration necessitated the brain delivery of the CPP by ICV administration [529,530].

### 7.2. Lectins

Wheat germ agglutinin (WGA) is a 36 kDa glycoprotein that is a lectin, i.e., a sugar-binding protein, with affinity for N-acetyl D-glucosamine and sialic acid [531]. The luminal membrane of the BBB expresses sugar sites including sialic acid [515], and WGA binds the luminal membrane of the brain endothelium as demonstrated by lectin-gold electron microscopy [532]. A conjugate of WGA and HRP bound to cells, which triggered absorptive-mediated endocytosis [533]. Electron microscopic histochemistry of brain following the IV administration of 50 mg/kg of an HRP-WGA conjugate in the mouse demonstrated labeling of the luminal endothelial membrane as well as some endothelial vesicles. Vesicles within vascular pericytes were also labeled, which indicates the HRP-WGA conjugate

transcytosed through the endothelial barrier [170]. WGA has been used as a surface ligand on liposomes for brain delivery [534]. Apart from WGA, another lectin used for drug delivery is the ricinus communis agglutinin (RCA) [535]. RCA, which binds D-galactose groups on surface glycoproteins, avidly binds both the luminal and abluminal membranes of the brain capillary endothelium [532]. RCA is a product of *Ricinus communis* seeds, which also express a toxin, ricin. RCA and ricin are distinct proteins [536]. While there is evidence that RCA binds the BBB [532], there is no direct evidence to date that the ricin toxin binds the BBB. Ricin is composed of an A chain, which is the toxic domain, and an B chain, which binds cell surface carbohydrates to mediate endocytosis. Working on the assumption that the ricin B chain binds the luminal membrane of the brain endothelium to trigger transport into brain, ricin toxin B chain (RTB) fusion proteins were engineered for the treatment of the brain in lysosomal storage disease. A fusion protein of RTB and iduronidase (IDUA), the enzyme mutated in MPSI, or RTB and beta galactosidase 1 (GLB1), the enzyme mutated in GM1 gangliosidosis, were engineered and expressed in plants [537,538]. No evidence that the RTB fusion proteins cross the BBB in vivo was presented [537,538]. The RTB-IDUA fusion protein was administered to MPSI mice, which produce no IDUA [539]. However, brain IDUA enzyme activity was barely above background after the IV administration of 2 mg/kg of the RTB-IDUA fusion protein [539].

### 7.3. Toxicity of Cationic Proteins and Lectins

#### 7.3.1. Toxicity of Cationic Proteins

The intra-arterial infusion of protamine causes BBB disruption [258], owing to enhanced trans-endothelial vesicular transport [540]. This treatment produces toxic effects in brain including shrunken spongiotic neurons and reactive astrogliosis [260]. The IV administration of polycationic peptides can lead to death, which was demonstrated in the case of the K16ApoE peptide [541]. The K16ApoE peptide is a 36-mer composed of 16 lysine residues (Lys or K) followed by a 16-AA sequence derived from human ApoE [542]. Of the 36 AAs in this peptide, 24 are cationic amino acids (Lys, Arg). The Lys-rich domain of the peptide is intended to bind anionic domains of therapeutic proteins, which alone do not cross the BBB. The apoE peptide domain was intended to bind the ApoE receptor, to trigger receptor-mediated transcytosis through the BBB via the low-density lipoprotein receptor (LDLR). However, as discussed in Section 8.1.6, the LDLR is not expressed on the microvascular endothelium of brain. Given the highly cationic charge of the K16ApoE peptide, the likely mechanism of BBB transport is either AMT via a charge mechanism, or BBB disruption caused by the highly cationic peptide. Similar to other cationic import peptides, the K16ApoE peptide is rapidly removed from plasma in <5 min [543]. In an attempt to deliver the TPP1 enzyme to brain in TPP1 null mice, the enzyme was co-injected with the K16ApoE peptide at a dose of 40–120 nmol of the peptide. The 120 nmol dose of K16ApoE was lethal in all animals [541]. A dose of 40 nmol of the K16ApoE peptide increased brain uptake of Alexa Fluor 647-conjugated TPP1. However, fluorescent microscopy of brain revealed a highly punctate distribution of the enzyme in brain [541]. This punctate pattern was identical to that reported by Brightman in 1977 [544] following BBB disruption with intra-arterial hyperosmolar solutions. This suggests the K16ApoE peptide delivers enzyme to brain via BBB disruption, not RMT on a presumptive LDLR at the BBB. Neurotoxicity of CPPs may be a general property of these highly cationic agents. The intra-cerebral injection of 10 µg of penetratin in rat brain produces neurotoxic cell death and neuroinflammation [56]. Cellular toxicity has been reported for cells exposed to cationic CPPs [545,546].

#### 7.3.2. Toxicity of Lectins

WGA is toxic to Caco-2 epithelial cells in culture at concentrations of 0.25–2.5 µM [547,548]. Cell electrical resistance is diminished in parallel with increased permeability of the monolayer to mannitol and 3 kDa dextran. In another study, human peripheral blood mononuclear cells (PBMC) were treated with low concentrations, 14 nM, of WGA. The supernatants from these cells

were toxic to Caco-2 cell monolayers, resulting in increased permeability. The toxic effects of the WGA treated PBMC supernatant were reduced with interleukin blocking antibodies [549]. These findings corroborate early results from the 1970s that WGA at concentrations of 1–5  $\mu\text{g}/\text{mL}$  are toxic to cells [550]. Despite the toxicity of WGA, this molecule continues to be developed as a brain drug delivery vector [534].

In summary, delivery of drugs via absorptive-mediated transport (AMT) is problematic, particularly when compared to receptor-mediated transport (RMT) that is reviewed in the next section. First, ligands that traverse the BBB via AMT have dissociation constants (KD) of binding to the targets on the BBB in the  $\mu\text{M}$  range, which is up to 3 log orders of magnitude lower than the affinity of ligands that traverse the BBB via RMT. Second, ligands that cross the BBB via AMT are largely sequestered within the endothelium with minimal exocytosis into brain parenchyma. A polycationic protein, histone, was nearly completely sequestered within the vascular compartment [259]. Cationized albumin is largely sequestered in the vascular compartment of brain [54]. WGA is said to undergo transcytosis through the BBB [170], but inspection of the micrographs shows the lectin is largely sequestered within the endothelium. Third, polycationic proteins or lectins are toxic with narrow therapeutic indices. A dose of 40 nmol of the K16ApoE peptide was necessary to mediate brain uptake a K16ApoE/enzyme complex, but a dose of 120 nmol of K16ApoE peptide was lethal in all animals [541]. WGA is cytotoxic at concentrations of 1–5  $\mu\text{M}$  [548,550], and generates toxins in cells at concentrations as low as 14 nM [549]. The next section will review the delivery of biologics to brain via receptor-mediated transport (RMT).

## 8. Receptor-Mediated Transport of Peptides and Monoclonal Antibodies

### 8.1. Receptor-Mediated Transporters at the Blood–Brain Barrier

#### 8.1.1. Insulin Receptor

The insulin receptor (INSR or IR) is a hetero-tetrameric structure formed by two alpha chains, which bind insulin, and two beta chains, which are the tyrosine kinase domains, and the three-dimensional structure revealed by cryo-electron microscopy is shown in Figure 10A.

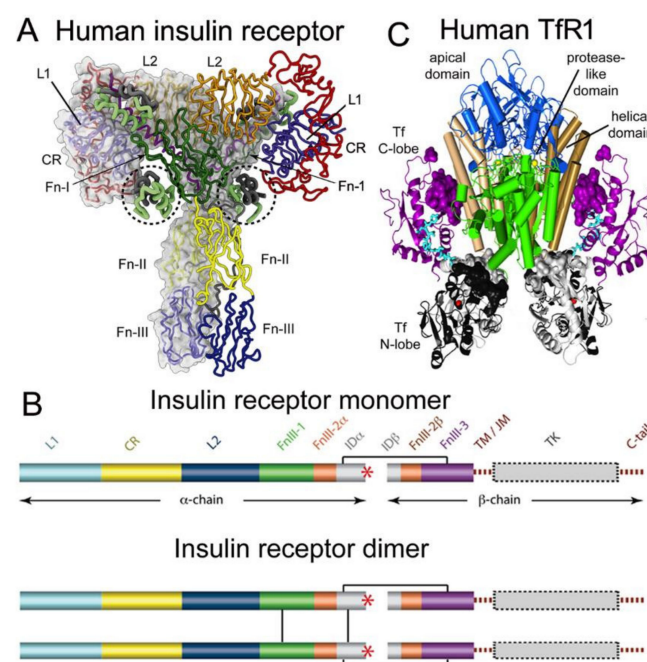


**Figure 10.** Structure of human insulin receptor and human transferrin receptor. (A) Complex of the IR tetramer and insulin is shown as determined by cryo-EM. The abbreviations of the domains are defined in the text. The structure shows a complex of 2 alpha chains, 2 beta chains, and 4 bound insulin molecules,

two of which are encircled. Reproduced with permission from [551], Copyright© 2021 Elsevier, as originally reported in [552]. (B) 2-dimensional structure of IR monomer and dimer. The inter-chain and intra-chain disulfides are shown. Carboxyl terminus of alpha chain shown by red asterisk. Reproduced from [553], Copyright© 2011 licensed under Creative Commons Attribution License (CC-BY). (C) The complex of human Tfr1 ECD and human holo-Tf is formed from 2 receptors and 2 holo-Tf molecules. The membrane surface is at the bottom and the apical domain (blue) is at the top. The regions shown in brown are the protease-like domains; the regions shown in brown/tan are the helical domains. The N-lobe and C-lobe of holo-Tf are shown in gray/black and purple, respectively. An Fe<sup>+3</sup> atom buried in each N-lobe is red, and the N-lobe and C-lobe linker is shown in cyan. Reproduced with permission [554].

The long form (B form) of the human IR (HIR) is translated as a 1382-AA polypeptide, which includes a 27-AA signal peptide [555]. The receptor is cleaved into separate alpha and beta chains at the furin cleavage site, RKRR, at AA 732–735 [556]. The domains of the alpha chain include the first leucine-rich domain (L1), the cysteine-rich (CR) domain, the second leucine-rich (L2) domain, the first fibronectin III domain (FnIII-1), the first part of the second FnIII domain (FnIII-2), and the first part of the insert domain (ID $\alpha$ ); the final 12 amino acids of the alpha chain form the  $\alpha$ CT domain, which is the high affinity insulin binding site. The beta chain is composed of the second part of the ID $\beta$  domain, the second part of the FnIII-2 domain, the third FnIII domain (FnIII-3), the transmembrane (TM) domain, the juxta-membrane (JM) domain, the tyrosine kinase (TK) domain and the carboxyl terminus (Figure 10B, top). The furin cleavage produces the ECD of the IR, which is about 900 AA in length [555]. The cryo-EM of the IR/insulin complex shows insulin binding at 2 sites: the L1/ $\alpha$ CT interface and the FnIII-1/FnIII-2 interface [552].

Insulin is synthesized as a 110-AA prepropeptide, which includes a 24-AA signal peptide and an 86-AA propeptide (AAW83741). The 35-AA C-peptide is formed by AA 31–66. Preproinsulin is cleaved internally to release the C-peptide, as well as a separate 30-AA B chain and a 21-AA A chain. Following cleavage, the A and B chains are joined by two disulfide bonds [551]. There are two tyrosine (Tyr) residues, which are sites of radio-iodination, in both the A chain and the B chain. The fasting plasma insulin concentration is ~0.3 nM in primates and humans [557,558], which is ~100-fold lower than the IR concentration at the brain capillary, 24 nM [559].

The characterization of insulin binding to the IR at the BBB was performed with radio-receptor assays and isolated brain microvessels, as first reported in 1981 for bovine brain capillaries [560], and in 1985 for human brain capillaries [561]. Insulin binding at the human brain capillary was saturable with a KD of the high affinity binding site of  $1.2 \pm 0.5$  nM. The saturable binding site for insulin at the human BBB was shown to be the IR, as affinity cross-linking of [<sup>125</sup>I]-insulin to the saturable binding site showed the MW of this site was 127 kDa, which is the size of the alpha subunit of the IR [561]. Insulin was rapidly endocytosed by the brain microvessels, and was metabolically stable over the course of a 60 min incubation at 37 °C [561]. The enrichment of the IR at the microvasculature of brain was demonstrated by immunohistochemistry for primate brain [61] and mouse brain [562]. The IR is also widely expressed in brain parenchyma, particularly in neurons [563].

Insulin is exocytosed into the brain post-vascular compartment following binding and endocytosis at the BBB. This was demonstrated with a 10 min carotid artery infusion of [<sup>125</sup>I]-insulin in the rabbit, followed by removal and freezing of the brain [564]. Thaw-mount autoradiography showed the distribution of insulin into brain parenchyma, and HPLC analysis of acid-ethanol extracts of brain showed the radioactivity in brain was unmetabolized insulin. The transcytosis of insulin across the BBB was completely suppressed by the co-infusion of high concentrations of unlabeled insulin [564]. Selective transport of insulin into brain, as compared to CSF, following IV administration was demonstrated in the rat using [<sup>125</sup>I-Tyr-A14]-insulin [565]. The latter is HPLC purified mono-iodinated insulin and is considered 'receptor grade' iodinated insulin [566]. [<sup>125</sup>I-Tyr-A14]-insulin was 95%

cleared from plasma within 5 min of IV injection [565], which indicates the  $T_{1/2}$  of plasma clearance of insulin is ~2 min. Following IV administration, [ $^{125}\text{I}$ -Tyr-A14]-insulin entered brain rapidly within 5 min. The brain uptake of insulin *in vivo*, as well as by cultured rat brain microvascular endothelial cells, was blocked by the IR antagonist, S961, which indicates that brain uptake of insulin is mediated by the BBB IR [565]. An alternative pathway of insulin transport into brain has been proposed based on studies with the EndoIRKO mouse [567], which has a targeted deletion of the IR in endothelial cells [568]. However, the study of [ $^{125}\text{I}$ ]-insulin transport in this mouse model was performed over a 20 min period after IV administration of radio-iodinated insulin [567]. The brain uptake of radioactivity is most likely artifact, because (a) the plasma  $T_{1/2}$  of insulin is only ~2 min [565], and (b) the insulin was labeled with 125-iodine and chloramine T, which is an oxidative reaction that iodates insulin at multiple tyrosine residues. This form of insulin is subject to rapid degradation *in vivo*, which produces free [ $^{125}\text{I}$ ]-tyrosine that may enter brain via transport on BBB LAT1. Artifacts in the brain uptake of radio-iodinated peptides following IV administration are discussed in Methods, Section 11.4.4. Insulin transport across the BBB has also been investigated with *in vitro* BBB models in cell culture. As discussed in Section 11.7.2, in Methods, *in vitro* BBB models should be used to support primary *in vivo* studies, as *in vitro* BBB models are leaky compared to the BBB *in vivo*, as recently reviewed [569]. In one *in vitro* BBB model, insulin transport is non-saturable and occurs through the leaky para-cellular route [570]. The same model also reports non-saturable transport of transferrin through the *in vitro* BBB [571]. In contrast, another *in vitro* BBB model using primary cultures of brain microvascular endothelial cells, and receptor-grade [ $^{125}\text{I}$ -Tyr-A14]-insulin, shows insulin transcytosis through the monolayer is mediated via the insulin receptor as transfer from the apical surface to the basolateral surface is blocked by the IR antagonist, S961 [572]. Heat-denatured labeled insulin was used as a control for a paracellular leak [572].

### 8.1.2. Transferrin Receptor

There are two human transferrin receptors (TfR), TfR1 and TfR2 [573], which have 39% AA identity [574]. The TfR isoform expressed at the BBB was identified with a BBB genomics investigation as TfR1 [438]. Northern blot studies with the cloned rat TfR1 cDNA showed a primary transcript of 5.0 kb encoding the TfR1 in both brain parenchyma, and at the BBB. In addition, a BBB-specific TfR1 transcript of 6.6 kb was detected by Northern blotting of brain capillary-derived RNA [438]. The three-dimensional structure of the complex of human holo-Tf and the human TfR1 ECD has been determined [554]. The tetrameric complex is formed by a dimer of TfR1s and two molecules of holo-Tf as shown in Figure 10C. The TfR1 is synthesized as a 760-AA protein that includes an intracellular domain, AA 1–67, the transmembrane domain, AA 68–88, the stalk domain, AA 89–120, which forms two disulfide inter-chain bonds, two protease-like domains, AA 121–188 and AA 384–606, an apical domain, AA 189–383, and a helical domain, AA 607–760 [554]. The ECD is formed by AA 121–760, which is a monomeric structure that lacks the stalk domain forming the inter-chain disulfide linked dimer. Transferrin (Tf) exists in plasma in three forms: about 40% is apo-Tf, which does not bind the TfR1 at physiologic pH, about 30% is monoferric holo-Tf, and about 30% is diferric holo-Tf [554]. The affinity of diferric holo-Tf for the TfR1 is 8- to 9-fold higher than the affinity of mono-ferric Tf for the receptor [575]. The Tf concentration in plasma is about 45,000 nM [576], and the concentration of holo-Tf is about 25,000 nM. This plasma concentration of holo-Tf is nearly 1000-fold greater than the TfR1 concentration at the brain microvasculature, which is 40 nM [559].

The high expression of the TfR at the brain microvasculature was shown in 1984 by immunohistochemistry of rat brain using the murine OX26 MAb against the rat TfR [577]. In 1987, the BBB TfR was shown to mediate the transcytosis of Tf [578], and the TfR at the human BBB was characterized by radio-receptor assays and isolated human brain microvessels [579]. Subsequent work questioned whether Tf underwent transcytosis through the BBB, as opposed to a model of endocytosis of holo-Tf into the brain endothelium fol-

lowed by retro-endocytosis of apo-Tf from the brain endothelium back to blood [580,581]. The evidence for this retro-endocytosis model was two-fold. First, the IV administration of dual labeled [ $^{59}\text{Fe}$ ,  $^{125}\text{I}$ ]-Tf in rats showed that the  $^{59}\text{Fe}$  radioactivity accumulated in brain to a greater extent than the  $^{125}\text{I}$  radioactivity [580]. However, this observation is also consistent with a model of Tf transcytosis into brain followed by uptake of holo-Tf by brain cells, release of iron and reverse transcytosis of apo-Tf to blood. Support for this reverse transcytosis model was produced with the BEI method, which showed that both apo-Tf and holo-Tf undergo reverse transcytosis from brain to blood in vivo [452]. In addition to reverse transcytosis of [ $^{125}\text{I}$ ]-apo-Tf, any  $^{125}\text{I}$ -iodide released from [ $^{125}\text{I}$ ]-Tf in brain is rapidly exported from brain to blood [582]. The second line of evidence used to support the reverse-endocytosis model was pre-embedding immune electron microscopy, which identified the TfR only on the luminal endothelial membrane, and not on the abluminal membrane [583]. However, abluminal receptors are not detected with pre-embedding methods, and post-embedding techniques are required to visualize abluminal receptors [515]. Confocal microscopy of unfixed rat brain capillaries identified the TfR on both luminal and abluminal brain capillary endothelial membranes [584]. The Tf transcytosis model was further supported by electron microscopy of rat brain following a 10 min carotid artery infusion of the OX26 MAb conjugated with 5 nm gold particles [585]. The gold-labeled antibody was observed bound to the luminal membrane, packaged within 100 nm intra-endothelial transcytotic vesicles, and exocytosed into the brain interstitial space [585]. The transcytosis model was also confirmed with the internal carotid artery infusion of [ $^{125}\text{I}$ ]-rat holo-Tf in rats, followed by removal of the brain for thaw-mount emulsion autoradiography. This worked showed that holo-Tf penetrates well into brain parenchyma within just 5 min of arterial infusion [586]. Holo-Tf distribution into the post-vascular brain was completely suppressed by infusion of the labeled Tf in 10% rat serum, which contains 2500 nM of holo-Tf [586].

The TfR is also highly expressed at the choroid plexus epithelium, which forms the blood–CSF barrier. Proteomics studies show the TfR1 is expression at the choroid plexus is 16-fold greater than the expression of the insulin receptor at the blood–CSF barrier [480]. The high expression of the TfR1 at the choroid plexus correlates with the high distribution of an MAb against the TfR1 into the CSF. A high affinity MAb against the human TfR1, which cross reacts with the TfR1 of Old World primates, distributes into CSF of Rhesus monkeys following IV administration with a 23 h CSF/serum ratio of 4.8% at an injection dose of 3 mg/kg [587]. The TfR1 is widely expressed in the brain parenchyma, as demonstrated by film autoradiography of rat brain with [ $^{125}\text{I}$ ]-ferrotransferrin [588].

### 8.1.3. IGF Receptor

The insulin-like growth factors (IGF)-1 and IGF-2 both bind with high affinity to the IGF1 receptor (IGFR), which is similar in structure to the IR [589]. IGF1 and IGF2 binding to the IGFR expressed at the human brain microvessel was reported in 1988 [590]. Both peptides are 7.5 kDa and both bind with high affinity to the BBB IGFR. The binding affinity for IGF2,  $\text{KD} = 1.1 \pm 0.1 \text{ nM}$ , is about twice the affinity for IGF1,  $\text{KD} = 2.1 \pm 0.4 \text{ nM}$ , and insulin is a very weak inhibitor of IGF1 or IGF2 binding to the human BBB IGFR [590]. The binding of either peptide to the BBB receptor is strongly inhibited by serum [590] which contains high affinity IGF binding proteins (IGFBP) [591]. Both peptides are endocytosed into the capillary endothelium [590]. Affinity cross-linking studies with either [ $^{125}\text{I}$ ]-IGF1 or [ $^{125}\text{I}$ ]-IGF2 show the MW of the saturable binding site of the human BBB IGFR is 141 kDa [590], which corresponds to the size of the alpha subunit of the IGFR [589]. Carotid arterial infusion of [ $^{125}\text{I}$ ]-IGF1 or [ $^{125}\text{I}$ ]-IGF2, in the absence of serum, shows that both peptides traverse the BBB and enter brain parenchyma via saturable process [592].

IGF-2 also binds with high affinity to the cation independent mannose 6-phosphate receptor (CI M6PR). However, the size of the CI M6PR is ~300 kDa, and the affinity cross-linking of IGF2 to the human brain microvessel shows no binding of IGF2 to a receptor larger than 141 kDa [590]. The absence of the CI M6PR on the BBB is the reason that



mannose 6-phosphorylated lysosomal enzymes do not cross the BBB, as discussed in Section 8.3.1. A fusion protein of IGF2 and NAGLU, a lysosomal enzyme, does not cross the BBB *in vivo*, and must be administered to brain by ICV injection [89]. Unlike insulin, IGF1 and IGF2 are avidly bound by IGFbps [591], and this is the presumptive reason for the lack of transport of an IGF2 fusion protein into brain via the BBB IGFR. The expression of the IGFR at the luminal membrane of the brain endothelium has been confirmed by pre-embedding electron microscopic histochemistry of rat brain [593]. As discussed above, detection of abluminal receptors at the brain endothelium requires a post-embedding labeling method [515]. The IGFR is also expressed in brain on both neurons and glial cells [594]. The gene expression of IGF-2, but not IGF-1, at the brain capillary endothelium was discovered with a rat brain capillary genomics program [438].

#### 8.1.4. Leptin Receptor

A high affinity binding site for leptin was identified with radio-receptor assays and isolated human brain microvessels [595]. The KD of leptin binding was  $5.1 \pm 2.8$  nM. Leptin binding was not inhibited by insulin or IGF-1, and leptin was endocytosed by the human brain microvessels. The Bmax of binding, in pmol/mg protein, was comparable to the Bmax of binding of insulin, Tf, or the IGFs to the human brain capillary [595]. PCR shows the predominant leptin receptor (LEPR) expressed at the BBB is the short form of the receptor [596], which has a truncated intracellular domain [597]. [<sup>125</sup>I]-leptin transport across the BBB *in vivo* in the rat has been confirmed with a carotid artery infusion method, and BBB leptin transport was saturable [598]. Leptin was also actively cleared by the choroid plexus, although there was a delay in leptin delivery into CSF [598]. Leptin distributes to CSF in humans and the CSF leptin parallels the plasma leptin concentration with a CSF/plasma ratio of 1.4–2.0% [599]. Leptin activation of cells leads to an increase in the STAT3 transcription factor, and leptin responsive cells were detected in brain in vascular endothelium, choroid plexus epithelium, and neurons [600]. Immunohistochemistry of rat or human brain showed the LEPR was highly expressed at the brain microvasculature [596], as shown in Figure 11A.

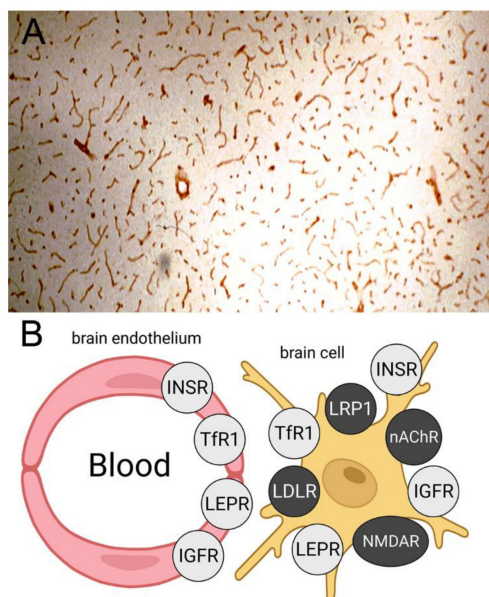


**Figure 11. Identification of BBB RMT targets by immunohistochemistry of brain.** (A) Immunohistochemistry of rat brain with an antibody to all isoforms LEPR. Reproduced with permission from [596], Copyright© 1998 John Wiley & Sons. (B) Expression of INSR, TfR1, IGFR, and LEPR on both the brain endothelium and on brain cells. In contrast, immunohistochemistry shows receptors such as LRP1, LDLR, NMDAR, and nAChR are expressed on brain cells but not endothelium. Reproduced from [525], Copyright© 2020 licensed under Creative Commons Attribution License (CC-BY).

The continuous immune staining of the microvasculature in brain in Figure 11A is evidence for an endothelial origin of the microvascular LEPR.

#### 8.1.5. LRP1 Receptor

The LDL receptor related protein 1 (LRP1) has been targeted for brain drug delivery with a number of peptide-based Trojan horses, as reviewed in Section 8.2.1. Targeting LRP1 for brain drug delivery assumes this receptor is expressed on the brain capillary endothelial membrane, including the luminal endothelial membrane. Early work used an *in vitro* BBB model to investigate LRP1-mediated transport [601,602]. As discussed in Section 11.7.2, *in vitro* models of the BBB should not be used as a primary line of investigation of BBB transport, owing to the loss of multiple BBB functions when brain endothelial cells are grown in cell culture. The *in vivo* evidence is that LRP1 is expressed in brain, but not at the microvascular endothelium. Early immunohistochemistry (IHC) of human brain found LRP1 expression in neurons and astrocytes, but not in endothelium [603]. *In situ* hybridization of rat brain shows LRP1 mRNA in neurons and astrocytes, but not in endothelium [604]. Endothelial LRP1 was originally suggested as the mechanism of clearance from brain of the Abeta amyloid peptide of AD [605]. The intra-cerebral injection of [<sup>125</sup>I]-Abeta in brain results in rapid decline of brain radioactivity, and this was attributed to LRP1-mediated efflux of the Abeta peptide across the BBB [605]. However, subsequent work showed that LRP1 ligands, such as  $\alpha_2$ -macroglobulin, do not efflux from brain following intra-cerebral injection [606]. When Abeta peptide content in brain was measured not by radioactivity, but by liquid chromatography mass spectrometry (LC-MS), the decline in brain Abeta after intra-cerebral injection was shown to be due to peptide metabolism in brain, not peptide efflux across the BBB [607]. It is not possible to quantify Abeta efflux from brain across the BBB using [<sup>125</sup>I]-Abeta and radioactivity measurements. The labeled peptide is rapidly degraded in brain to either [<sup>125</sup>I]-tyrosine, which can efflux to blood via transport on LAT1, or to [<sup>125</sup>I]-iodide, which is rapidly exported from brain to blood [582]. More recent work implicates the role of LRP1 on astrocytes [608] or pericytes [609]. In the schematic of receptor localization in brain, LRP1 is localized to brain cells, not the brain endothelium (Figure 11B). Expression of LRP1 at brain cells beyond the BBB explains the lack of brain uptake of a MAb against LRP1 following IV antibody administration [430].

#### 8.1.6. LDL Receptor

The low-density lipoprotein (LDL) receptor (LDLR) transports lipoprotein-bound cholesterol. Protein components of lipoproteins, such as apolipoprotein B-100 (ApoB), bind to the cell surface LDLR to trigger transport of lipoprotein-bound cholesterol into the cell. As discussed in Section 8.2.1, a number of peptide Trojan horses have been developed for brain targeting of the presumptive LDLR on the luminal surface of the BBB. Expression of the LDLR at the BBB was identified in an *in vitro* BBB model [610]. However, *in vitro* models may not predict BBB function *in vivo* as discussed in Section 11.7.2. IHC of brain does not detect the LDLR at the microvascular endothelium, although LDLR expression is observed in neurons [562]. In this same study, the insulin receptor is highly enriched at the brain microvasculature [562], which serves as a positive control for the IHC of the LDLR. Lack of expression of the LDLR, at least at the luminal membrane of the endothelium, is consistent with the lack of transport of LDL-bound cholesterol from blood to brain [611–613]. An early study shows that plasma cholesterol equilibrates with brain cholesterol over a time-frame of months [614]. In the adult brain, all cholesterol in brain is synthesized *de novo* [613].

#### 8.1.7. Nicotinic Acetylcholine Receptor

The rabies virus gains access to the CNS via the binding of a rabies virus glycoprotein (RVG) to the nicotinic acetylcholine receptor (nAChR) in skeletal muscle [615,616]. Working on the assumption that the nAChR was also expressed at the BBB, a truncated 29-AA peptide derived from the RVG was tested as a BBB Trojan horse [297]. However, the studies cited as evidence for expression of the nAChR at the brain microvascular endothelium

were only cell culture investigations [617]. IHC of brain with an antibody to the nAChR shows receptor expression in astrocytes and neurons, but not on endothelium [618–620]. IHC was performed on isolated rat brain microvessels with an antibody to the nAChR, but the immune staining was discontinuous suggesting the antibody was labeling abluminal elements such as remnants of astrocyte foot processes [621]. Abluminal immune staining of some microvessels was also observed in human cerebellum, and was attributed to perivascular astrocyte endfeet or nerve endings [622]. In contrast, there was robust expression of immunoreactive nAChR in brain parenchyma [622].

#### 8.1.8. Basigin/CD147

Basigin, also known as extracellular matrix metalloproteinase inducer, HT7, neurothelin, or CD147, is encoded by the BSG gene, and is a relatively small trans-membrane protein of 251 AA (BAC76828). A panel of MAbs against human CD147 has been produced as potential MAb BBB Trojan horses for brain drug delivery [623,624]. It is difficult to evaluate the utility of these BSG MAbs, because the only testing of BBB transport was performed with in vitro BBB models in cell culture [623,624]. As discussed in Sections 6.2.2 and 6.2.4, BSG forms a hetero-dimer with the MCT1 lactate transporter in a manner similar to the hetero-dimer formed between the 4F2hc (CD98hc) and the LAT1 large neutral amino acid transporter. BSG facilitates the insertion of the MCT1 transporter into the plasma membrane [625]. BSG is the receptor for the malaria parasite, *Plasmodium falciparum* [626]. However, BSG does not mediate the BBB transport of *P. falciparum* [627]. It is unclear how the intra-vascular parasite triggers the CNS manifestations of cerebral malaria [628]. BSG, like 4F2hc, participates in CMT transport at the BBB, not RMT. Nevertheless, antibodies against either Bsg [623,624] or 4F2hc [430] have been proposed as BBB molecular Trojan horses. A MAb against 4F2hc was developed as a RMT candidate and the activity was said to be greater than a TfRMAB [430], although this lead was not pursued. A cryo-electron microscopy study shows the three-dimensional structure of the LAT1/4F2hc hetero-dimer bound by a Fab directed against the 4F2hc subunit [372]. However, the MCT1 and LAT1 CMT systems are trans-membrane cavities that do not undergo endocytosis into the cell. Since neither the LAT1/4F2hc complex nor the MCT1/BSG complex undergoes endocytosis, it is not clear how developing a MAb against either 4F2hc or BSG can enable transcytosis across the endothelium. One caveat in developing BSG MAbs for RMT drug delivery to brain is the species differences in BSG expression at the BBB. Proteomics studies show high expression of BSG at the rat brain capillary, 30 pmol/mg protein [409]. In contrast, BSG at the human brain capillary is undetectable [360].

#### 8.1.9. Miscellaneous Receptors

The cross-reacting material (CRM)-197 is a 58 kDa mutated, non-toxic form of the diphtheria toxin (DT), which was proposed as a BBB Trojan horse [629]. The DT receptor (DTR) is the heparin binding epidermal growth factor (EGF)-like growth factor (HB-EGF). The use of CRM197 as a BBB Trojan horse assumes that the HB-EGF is expressed at the brain capillary endothelium. Early work on the IHC of brain shows expression of HB-EGF in neurons and glial cells with minimal, if any, expression in endothelium [630]. Liposomes were conjugated with CRM197, but this ligand provided no enhancement in the brain uptake of the liposomes in vivo in mice [631]. However, such in vivo studies with CRM197 should not be performed in mice, as the DTR in rats and mice is a variant. The rat DTR has low affinity for the DT or CRM197, and the mouse DTR has no affinity for DT or CRM197 [632]. Therefore, in vivo work with CRM197 must be performed in guinea pigs [629]. However, CRM197 is quite toxic in guinea pigs, as the IV administration of 50–500 µg/kg of CRM197 to guinea pigs causes BBBBD and neuropathological changes to brain endothelium [633].

Iron is sequestered in the intracellular compartment by binding to ferritin (Ft) and Ft is a 24 sub-unit hetero-polymer composed of heavy chains (HFt) and light chains (LFt). In rodents, HFt, but not LFt, is endocytosed by cells via the T cell immunoglobulin and mucin domain (Tim)-2 receptor [634]. However, Tim-2 is not expressed in humans [635], although

HFt binds the human Tim-1 receptor [635]. HFt also binds the human TfR1 at a site that is spatially removed from the binding site for holo-Tf [636–638]. Surface plasmon resonance (SPR) shows the KD of HFt binding to the human TfR1 is  $7.1 \pm 0.2$  nM [638]. Ft is present in plasma, although most of the circulating Ft is the light chain [639]. The use of HFt as a BBB Trojan horse was evaluated with the use of iron magnetic nanoparticles [640]. HFt or LFt shells were loaded with iron oxide at 65C to form the nanoparticles (NP). The HFt-NPs, relative to the LFt-NPs, were preferentially transported across a monolayer of cultured human hCMEC/D3 endothelial cells, and preferentially taken up by rat brain vivo based on external fluorescence imaging [640]. The extent to which the brain uptake of HFt is mediated by the BBB TfR1 or BBB Tim-2 receptor in rodents is not known. There is little evidence that Tim-2 is expressed at the rodent BBB. Fluorescent microscopy of mouse brain shows expression of Tim-2 in neurons and glial cells, but not at the microvasculature [641]. The IV administration of  $^{59}\text{Fe}$ -labeled HFt to rats resulted in very high uptake in liver and spleen, moderate uptake in kidney, heart, and lung, and very low uptake by brain [642]. The brain uptake of  $^{59}\text{Fe}$ -HFt was 100-fold lower than the uptake by liver or spleen [642].

The TCbIR (CD320) mediates brain uptake of the vitamin B12/cobalamin complex (Table 3 and Section 6.2.7). The mRNA encoding CD320 is enriched at the brain capillary [430]. However, a MAb against CD320 was not taken up by brain following IV administration [430]. It is possible other MAbs may undergo transport across the BBB via RMT on CD320, as not all receptor-specific antibodies are endocytosing antibodies. A panel of MAbs against human CD320 was prepared, and most antibodies did not inhibit cell uptake of the TCbIR [643], and would be potential candidates for RMT across the BBB via CD320. However, some anti-CD320 antibodies inhibit the endothelial transcytosis of the B12/TC complex [644], and would not be suitable candidates for RMT delivery.

## 8.2. Trojan Horse Delivery via Blood–Brain Barrier Receptor-Mediated Transport (RMT)

### 8.2.1. Peptide-Based RMT Trojan Horses

**Insulin receptor peptides.** Insulin was the first BBB Trojan horse developed. As described in a U.S. patent issued in 1989 [645], a neuropeptide, somatostatin, which does not cross the BBB, was covalently conjugated to insulin, a ligand for the BBB insulin receptor, which resulted in enhanced uptake of somatostatin by isolated brain capillaries. Insulin is composed of two disulfide linked chains, as discussed in Section 8.1.1. This dual chain structure is not amenable to fusion protein technology. The A and B chains of insulin were connected by a dodecapeptide linker, which converted insulin into a single chain [646]. The single chain form of insulin was genetically fused to albumin to form an insulin–albumin fusion protein, albondin. The insulin domain of albondin retained high affinity binding to the insulin receptor. The ED50 of binding to the HIR was 1.1 nM and 7.4 nM for insulin and albondin, respectively. This technology could be replicated for BBB delivery by fusion of the single chain form of insulin to another biologic that does not cross the BBB. A potential problem with such a fusion protein is that the insulin domain of the fusion protein would bind the insulin receptor in peripheral tissues, which may cause hypoglycemia.

**Transferrin receptor peptides.** Transferrin (Tf) has been used as a Trojan horse for nanoparticle delivery across the BBB, as discussed below in Section 9.5.3. The problem with using Tf as a Trojan horse is the exogenous Tf Trojan horse must compete with the endogenous holo-Tf in plasma for binding to the BBB TfR. The concentration of holo-Tf in plasma, 25,000, is nearly 1000-fold higher than the concentration of the TfR1 at the BBB [559]. Therefore, the BBB TfR1 is >99.9% saturated with endogenous holo-Tf [647]. Tf was conjugated to lysozyme in an effort to deliver this enzyme across the BBB, although no testing of the Tf-enzyme conjugate in vivo was reported [648]. Tf-mimetic peptides that bind the TfR at a site spatially removed from the Tf binding site have been developed [649]. One such peptide, designated 2DS25, bound to the human TfR1 ECD with a KD of 20 nM. However, the BBB transportability of the peptide was only tested in an in vitro model [649]. An alternative strategy to the development of Tf-mimetic peptides is the discovery of cysteine rich peptides (CDP) that have an affinity for the TfR [650]. Databases were searched

for peptides of 30–50 AAs in length with 6–10 cysteine residues. Lead candidates, of 6 kDa in size, and designated TfRB1G2 and TfRB1G3, had a KD of binding to the TfR1 of 8.7 and 0.22 nM, respectively. After IV injection in the mouse, the CDP was cleared by organs with liver > kidney > spleen >> brain. The brain uptake of the CDP was 100-fold lower than the liver uptake, and measurable uptake by brain was not observed with whole body autoradiography [650]. Nevertheless, the study concluded that the low brain uptake was pharmacologically significant, and a fusion protein of the 13-AA neuropeptide, neurotensin, and the CDP was observed to activate a cyclic AMP response element in brain following IV administration of 100 nmol/mouse [650]. This is a relatively large injection dose (ID), and is equal to an ID of 24 mg/kg of the 6 kDa CDP.

**LRP1 peptides.** LRP1 binds multiple peptides, at different domains of the receptor [651], and LRP1 ligands have been proposed as a peptide-based BBB Trojan horse [652,653]. Melanotransferrin (MTf) was said to cross the BBB via LRP1 based on an in vitro BBB model [601]. However, subsequent in vivo work showed that MTf does not cross the BBB [654,655]. Angiopep-2, a 19-AA cationic peptide, was said to cross the BBB via LRP1 based on an in vitro BBB model [602]. However, the angiopep-2 peptide has little to no affinity for LRP1. The ECD of LRP1 is composed of four domains, I, II, III, and IV. The KD of angiopep-2 binding to domains II or IV was >1000 nM [656]. In another study, binding of angiopep-2 to domains II or IV was not detectable [657]. Angiopep-2 failed to increase brain uptake of either a lysosomal enzyme [522] or liposomes [631]. Lactoferrin (Lf) was said to cross the BBB via transport on LRP1 based on a cell culture model of the BBB [658]. However, when Lf transport across the BBB was measured in vivo, the brain uptake of this protein is very low in the rat, 0.016%ID/g brain [659], which is a level of brain uptake expected for a protein trapped in the brain plasma volume. In contrast, the brain uptake of the OX26 TfRMAb in the rat after IV administration is  $0.44 \pm 0.02\%$ ID/g [660]. Another ligand of LRP1 is receptor associated protein (RAP), which was said to cross the BBB following IV administration of RAP labeled with  $^{125}\text{I}$  and chloramine T [654]. Based on the hypothesis that LRP1 was a RMT system expressed at the BBB, and that RAP was an endogenous ligand for this receptor, RAP-lysosomal enzyme fusion proteins were engineered for RMT delivery across the BBB [661]. The fusion proteins were only validated by cell culture models, and there was no subsequent development of the RAP-lysosomal enzyme fusion proteins. Another ligand of LRP1 is apolipoprotein E (ApoE), a 34 kDa protein associated with lipoproteins. In an effort to develop apoE peptidomimetics that are bound by LRP1, certain domains of apoE were synthesized as 15–20-AA peptides. Using an AA numbering system that does not include the signal peptide, ApoE(130–149) and ApoE(141–155) were synthesized [662]. ApoE(130–149) bound to domains II and IV of LRP1 with a KD of 51 and 129 nM, respectively; ApoE(141–155) bound to domains II and IV of LRP1 with a KD of 118 and 190 nM, respectively [662]. Both ApoE(130–149) and ApoE(141–155) are strongly cationic peptides and most likely enter cells via absorptive-mediated endocytosis, and not by RMT on LRP1. A peptide named COG-133 corresponds to ApoE(133–149) [631]. Liposomes were targeted with angiopep-2, COG-133, CRM197, and the RI7–217 TfRMAb, but only the TfRMAb Trojan horse mediated delivery to brain in vivo in the mouse [631]. The RI7-217 MAb is a rat antibody against the mouse TfR1, and is actively taken up by mouse brain in vivo [663]. The failure of the LRP1-targeted peptide Trojan horses to effectively deliver cargo to brain is consistent with the absence of expression of LRP1 on the endothelial luminal membrane (Figure 11B), as discussed in Section 8.1.5.

**LDLR peptides.** Apolipoprotein B100 (ApoB) binds the LDLR to trigger endocytosis of LDL into cells, and the LDLR is said to function at the BBB, based on cell culture studies [610]. To develop a peptide-based Trojan horse targeting the LDLR, a phage peptide library was screened for candidates [664], which led to the development of an 8-AA peptide, CMPRLRGC, designated VH434, that binds the LDLR with low affinity and a KD of 196 nM [665]. This peptide was fused to the carboxyl terminus of a human IgG1 Fc and the VH434-Fc injected intravenously at 8 mg/kg in either wild-type or *ldlr*<sup>-/-</sup> knockout mice [665]. The brain/plasma ratio at 24 h was 2.2% and 1.1% in the wild-type and *ldlr*<sup>-/-</sup> mice, respectively. However, the brain plasma volume is 10–30  $\mu\text{L/g}$  [666], which is 1–4% of the brain volume. Any Fc-peptide conjugate confined to the blood

volume of brain has not crossed the BBB. As discussed in BBB Methods (Section 11.4.4), it is important to correct brain uptake, especially for biologics, for the brain plasma volume. The primary lipoprotein that binds the LDLR is apolipoprotein B-100 (ApoB), which is a 500 kDa 4536-AA protein not counting the 27-AA signal peptide (NP\_000375). An LDLR binding domain lies at AA 3371–3409, and this sequence was fused to the carboxyl terminus of a lysosomal enzyme, and this fusion gene was incorporated in a lentivirus transfection vector [667]. Subsequently, this apoB-mimetic peptide was fused to the amino terminus of secretory neprilysin, an endopeptidase that degrades the Abeta amyloid peptide of AD, and this fusion protein is designated ASN12 [668]. The ASN12 fusion protein was injected intravenously at a dose of 1 mg/kg in the mouse and the brain fusion protein was measured by ELISA. The brain fusion protein concentration at 24 h was 210 ng/g [668], which is equal to a brain concentration of 0.3%ID/g. It is difficult to attribute this low level of brain uptake to RMT via the LDLR at the BBB, since IHC shows the LDLR is not expressed at the brain microvasculature in vivo [562]. The sequence of the apoB-mimetic peptide domain of the ASN12 fusion protein is SSVIDALQYKLEGTTTRLTRKRGLKLATALSLSNKFVEGS [669]. This is a highly cationic peptide with a pI of 10.2. It is likely that any BBB penetration that is achieved with this peptide is via absorptive-mediated endocytosis of a cationic peptide, as discussed in Section 7.1.

**Glutathione.** Glutathione (GSH) is a tripeptide that is said to cross the BBB to mediate the brain uptake of pegylated liposomes conjugated with GSH [670]. The basis for the use of GSH as a BBB Trojan horse is early work describing the enhanced uptake of GSH by frog oocytes injected with RNA isolated from SV40 transformed mouse brain endothelial cells in culture [671]. The presumptive sodium dependent GSH transporter was never identified. GSH is a low affinity ligand for the sodium dependent dicarboxylic acid transporter [672], but dicarboxylic acids do not cross the BBB [327]. GSH is a ligand for the N-methyl D-aspartate (NMDA) receptor (NMDAR) [673,674]. The NMDAR was localized to the brain microvasculature using a monoclonal antibody designated Glunomab [675]. This antibody was raised against synthetic peptides corresponding to the amino terminal domain of the GluN1 subunit of the NMDAR, which is a hetero-trimeric membrane protein. Fluorescent microscopy of the Glunomab immunoreactivity in brain microvessels is discontinuous [675], which is consistent with expression in either endothelium or astrocyte endfeet. The absence of the NMDAR at the brain endothelium is supported by several studies showing that brain endothelial cells lack a functional NMDAR [676]. Irrespective of what transporter or receptor GSH might access, early work on GSH transport at the BBB shows this tripeptide does not cross the BBB [677], as recently reviewed [678]. The lack of BBB transport of the GSH tripeptide is similar to the absence of BBB transport of another tripeptide, thyrotropin releasing hormone [677].

**Phage peptides.** In 1996, phage display libraries were first used to isolate peptides that bind the luminal membrane of the brain capillary endothelium [679]. Phage libraries encoding random CX<sub>7</sub>C octapeptide sequences were injected intravenously in mice and the brain harvested for phage recovery. After three rounds, a single phage was identified of known AA sequence. Subsequent use of the technology identified peptides that overlapped with domains of human Tf [680]. An f3 phage library with random 15-mer sequences were infused in the carotid artery of mice, which resulted in identification of a 15-AA peptide, designated the GLA peptide [681]. The GLA was conjugated to pegylated liposomes for delivery to cultured hCMEC/D3 endothelial cells, but uptake was low [682]. It was reasoned that the conformation of the 15-mer peptide differed from the conformation adopted by this sequence within the p3 phage coat protein. The 15-mer sequence was incorporated in a peptide encompassing 240 AA of the amino terminal domain of the p3 coat protein, and this new peptide was designated, p3-GLA [682]. Pegylated liposomes were targeted with either the GLA peptide or the p3-GLA peptide and incubated with cultured hCMEC/D3 endothelial cells followed by fluorescence-activated cell sorting. Liposomes targeted with the GLA peptide were not bound to the cells, whereas binding was detected with the p3-GLA peptide. It has been over 25 years since peptide phage

display methods have been used to identify peptides that target the BBB. The problems with this approach are (a) the receptor targeted by the peptide is generally not known, (b) the BBB binding site identified has to be a RMT system, (c) the synthetic peptide may not have the same binding activity as the peptide sequence presented as part of the phage coat protein, and (d) oligopeptides invariably have low affinity for the targeted receptor.

In summary, peptide-based RMT Trojan horses typically work well in vitro in cell culture models, but are difficult to translate to in vivo brain delivery. The peptide may have minimal activity in vivo owing to competition with the endogenous peptide ligand, or have a poor plasma pharmacokinetics profile owing to rapid clearance by peripheral tissues. Many RMT-based peptides used for brain drug delivery are highly cationic peptides. Cationic peptides are toxic with poor safety profiles, as reviewed in Section 7.3.1. In several instances, peptides that target a presumptive BBB RMT system, such as LRP1, LDLR, nAChR or NMDAR, are ligands for receptors that are not expressed on the brain endothelium, as depicted in Figure 11B.

### 8.2.2. Monoclonal Antibody-Based RMT Trojan Horses

Work in the early 1980s, using either isolated brain capillaries and radio-receptor assays [560], or immunohistochemistry [577], showed that the IR or TfR was highly expressed at the brain microvascular endothelium. By 1985, experiments with human brain capillaries showed the BBB IR mediated the endocytosis and exocytosis of insulin at the BBB [561]. This led to the chimeric peptide hypothesis, wherein a peptide drug, which normally does not cross the BBB, could be linked to a ligand that normally undergoes RMT across the BBB [58]. By 1987, the RMT of insulin and Tf across the BBB via the IR and TfR, respectively, was demonstrated in vivo [564,578]. In addition to endogenous ligands, early work with the LDLR showed that a monoclonal antibody (MAb) that bound an exofacial epitope on the receptor could also be endocytosed into the cell via receptor-mediated endocytosis [683]. Monoclonal antibodies (MAb) were then shown to undergo RMT across the BBB via binding to either the rat TfR [59,60] or primate IR [61]. The hypothesis that biologics could have pharmaceutical effects in the brain following linkage of the biologic to a BBB RMT ligand [58], was confirmed by in vivo pharmacologic studies using the OX26 TfRMAb [684,685]. In one model, vasoactive intestinal peptide (VIP) was conjugated to the OX26 TfRMAb with an avidin–biotin linker [684]. VIP is a potent cerebral vasodilator when applied topically to brain surface vessels. The carotid arterial infusion of VIP had no effect on cerebral blood flow (CBF) [684], because VIP does not cross the BBB. However, infusion of the OX26-VIP conjugate resulted in a 65% increase in CBF in the parenchyma of brain, whereas there was no change in CBF following the infusion of VIP alone or OX26 alone [684]. In another model, nerve growth factor (NGF) was chemically conjugated to the OX26 MAb and exerted trophic effects in an extra-cranial anterior eye transplant model [685]. The 83–14 MAb against the human insulin receptor (HIR) cross-reacted with the IR of Old World primates such as the Rhesus monkey, and was rapidly transported across the primate BBB in vivo as the brain uptake of the HIRMAb was 2.5–3.8%ID/brain [61]. The use of the HIRMAb as a BBB Trojan horse was initially tested in Rhesus monkeys with the goal of developing a BBB-penetrating peptide radiopharmaceutical for imaging the brain amyloid of AD. The  $A\beta^{1-40}$  amyloid peptide is a potential peptide radiopharmaceutical for imaging amyloid content in brain of AD [686], but the  $A\beta$  peptide does not cross the BBB [687]. [ $^{125}I$ ]-biotinyl  $A\beta^{1-40}$  was conjugated to the HIRMAb with a streptavidin linker [688]. Both the unconjugated [ $^{125}I$ ]-biotinyl  $A\beta^{1-40}$  and the HIRMAb conjugated [ $^{125}I$ ]-biotinyl  $A\beta^{1-40}$  avidly bound the amyloid plaques in autopsy AD brain [688]. Following IV injection of the unconjugated [ $^{125}I$ ]-biotinyl  $A\beta^{1-40}$  alone, no brain uptake could be detected by ex vivo brain imaging of the primate brain. In contrast, high resolution brain scans were observed following IV administration of the [ $^{125}I$ ]-biotinyl  $A\beta^{1-40}$  conjugated to the HIRMAb [688]. Brain radioactivity declined with a  $T_{1/2}$  of 16 h in the primate [688].

The OX26 TfRMAb is a species-specific antibody for the rat TfR and does not recognize the mouse TfR [663] or the human TfR [689]. The TfR in the mouse can be targeted with

the 8D3 antibody, which is a rat MAb against the mouse TfR [690], or the RI7-217 antibody, which is a rat MAb against the mouse TfR [691]. Both the 8D3 and the RI7-217 antibodies are taken up by brain at a level of 1.6–3.1%ID/g following IV administration in the mouse [663].

Biologics can be delivered to brain following the genetic fusion of the biologic and the MAb targeting an RMT system on the BBB. The engineering and expression of recombinant forms of the antibodies targeting the TfR or IR were enabled by the determination of the AA sequence of the variable region of the heavy chain (VH) and the variable region of the light chain (VL) for the OX26 TfRMAB [692], the 8D3 TfRMAB [693], and the 83-14 HIRMAb [694]. The availability of these sequences allows for the genetic engineering of TfRMAB or HIRMAb fusion protein, as reviewed in the next section.

**Valency of TfRMABs.** The valency of the TfRMAB domain of the fusion protein has been both bivalent and monovalent. The first monovalent TfRMAB engineered was part of a bispecific antibody (BSA) composed of one monovalent arm as the TfRMAB domain, and another monovalent arm targeting the beta secretase 1 as the therapeutic domain [695]. Engineering the TfRMAB domain in a monovalent form was obligatory since the BSA was engineered with a knob-in-hole technology [695]. In contrast, the first BBB-penetrating BSA engineered was a tetravalent BSA, where both the transporter domain targeting the HIR was bivalent, and the therapeutic domain targeting the Abeta amyloid of AD was bivalent [696]. The tetravalent BSA was engineered by fusion of a single chain form of the first antibody to the carboxyl terminus of each heavy chain of the second antibody [696]. Engineering a BSA where both the therapeutic antibody domain and the transporter antibody domain are bivalent allows for retention of high avidity binding of the BSA at both the BBB receptor and the therapeutic antibody target in brain. Conversely, in the monovalent BSA, the monovalent TfRMAB had the expected reduced binding affinity for the TfR as compared to the bivalent TfRMAB [695]. This reduced affinity was then considered advantageous and gave rise to the hypothesis that low affinity TfRMABs were preferred BBB Trojan horses. The basis for this hypothesis was the observation that the uptake of the low affinity TfRMAB by brain was higher following the IV administration of a very high injection dose (ID) of 20–50 mg/kg of the TfRMAB. This high ID selectively saturates binding of the high affinity TfRMAB at the BBB, while not affecting binding of the low affinity TfRMAB. In another monovalent format of the TfRMAB domain of a BSA, a single chain TfRMAB was fused to the carboxyl terminus of a bivalent anti-Abeta antibody using the knob-in-hole technology [697]. In this design of the BSA, the high-affinity bivalent structure of the therapeutic antibody is retained, whereas the transporter antibody is engineered as a moderate affinity monovalent antibody. The rationale for engineering the TfRMAB domain of the BSA in a monovalent format was that the bivalent TfRMAB would trigger dimerization of the TfR, which would redirect the receptor to the lysosome resulting in reduced expression of the TfR at the cell membrane [697]. This hypothesis is curious since the TfR1 normally exists as a dimer (Figure 10C). If chronic administration of a TfRMAB led to down-regulation of the BBB TfR, then the rate of brain clearance of the antibody, as reflected by the permeability–surface area (PS) product, would be decreased after chronic treatment. This is not observed. Mice were chronically treated for 12 weeks with 2 mg/kg IV twice weekly with a fusion protein of the chimeric form of the 8D3 TfRMAB and glial-derived neurotrophic factor (GDNF), designated cTfRMAB–GDNF [698]. The BBB PS product of the cTfRMAB–GDNF fusion protein was unchanged from the start of treatment to the end of 12 weeks of treatment [698]. In addition, the rate of plasma clearance of the fusion protein was unchanged with 12 weeks of treatment [698], which indicates the TfR is not down regulated in peripheral tissues. In yet another monovalent format of a TfRMAB, the CH3 region of the antibody heavy chain was engineered by mutagenesis of multiple amino acids to create a new TfR binding site in the CH3 region [699]. A lysosomal enzyme was fused to the amino terminus of a second antibody chain, and the two chains were combined by knob-in-hole technology [699]. The monovalent format of the TfRMAB was said to be advantageous so as to avoid intracellular clustering and degradation of the TfR, which is observed following exposure of cultured hematopoietic cells to a bivalent



TfRMAB [700,701]. However, these cell culture studies purporting to show intracellular clustering of a bivalent TfRMAB did not use a bivalent TfRMAB, per se, but rather a bivalent TfRMAB–avidin fusion protein. Such IgG–avidin fusion proteins form 400 kDa tetramers, owing to the dimerization of the avidin domain [700,702]. The apoptosis induced by the tetrameric TfRMAB–avidin fusion protein was not observed with the bivalent TfRMAB alone [700]. Chronic administration to mice with a high affinity bivalent TfRMAB causes no down-regulation of brain TfR or brain iron [703].

Apart from antibodies that target the TfR or IR, antibodies that target other BBB RMT systems, such as the LEPR or IGFR (Figure 11B), are also potential new BBB MAb-based Trojan horses. Recently, single domain VHH antibodies against the ECD of the human IGF1R were isolated following Llama immunization [704]. The VHH was fused to mouse Fc to generate either a monovalent or a bivalent format. Affinity for the human IGF1R was determined by SPR and the KD values ranged from 0.3 nM to 1.3 nM. BBB transcytosis was measured with an in vitro culture model as the primary model, although transcytosis was confirmed with carotid artery infusion and capillary depletion [704]. The IGF1R antibody cross reacted with the antibody in rats and mice and IV administration of the bivalent form of the antibody showed distribution into both CSF and post-vascular brain [704]. Leptin receptor (LEPR) antibodies are yet to be tested as BBB RMT agents. A panel of antibodies against the human LRPR ECD was isolated by panning a single chain Fv (ScFv) phage library with the human LEPR ECD [705]. For isolation of a LEPR antibody that does not inhibit leptin binding to the LEPR, panning of phage libraries can be performed with complexes of the LEPR ECD and leptin so as to eliminate capture of antibodies that bind the leptin binding site on the LEPR.

In summary, receptor-specific MAbs are more effective BBB RMT Trojan horses than are peptides. Virtually any research lab can custom order their own lot of recombinant 8D3 TfRMAB for brain delivery in mice, recombinant OX26 TfRMAB for brain delivery in rats, or recombinant 83-14 HIRMAb for brain delivery in Old World primates or human cells, because the sequences of the VH and VL for these antibodies have been published [692–694]. The production of recombinant antibodies based on these sequences has recently been described for a recombinant 8D3 TfRMAB [706] or recombinant 83-14 HIRMAb [707].

### 8.3. IgG Fusion Proteins for Blood–Brain Delivery of Biologics

All four classes of biologics have been reduced to practice as either TfRMAB and HIRMAb fusion proteins, including therapeutic antibodies, lysosomal enzymes, neurotrophins, and decoy receptors [708]. In the case of delivery of a therapeutic antibody to brain, the problem is engineering of a bispecific antibody (BSA), which includes a transporter antibody domain and a therapeutic antibody domain. There are multiple approaches to the genetic engineering of BBB-penetrating BSAs, as discussed in Section 8.3.4. In the case of brain delivery of a lysosomal enzyme, it is necessary to deliver the enzyme across both the BBB and the brain cell membrane, followed by triage of the IgG-lysosomal enzyme fusion protein to the lysosomal compartment [709]. A lysosomal enzyme can be delivered across both the BBB and the brain cell membrane (BCM) with an antibody targeting the IR, TfR, LEPR, or IGFR, as these receptors are expressed on both the BBB and the BCM, as depicted in Figure 11B. The engineering of bi-functional HIRMAb or TfRMAB lysosomal enzyme fusion proteins is discussed in Section 8.3.1. In the case of neurotrophin delivery to brain, the neurotrophin receptor (NTR) is generally expressed on the plasma membrane of brain cells, so the IgG–neurotrophin fusion protein need only traverse the BBB to access the target neurotrophin receptor in brain. The engineering of bi-functional HIRMAb or TfRMAB neurotrophin fusion proteins is discussed in Section 8.3.2. In the case of decoy receptor delivery to brain, the cytokine target of the decoy receptor is generally secreted to the extracellular space of brain, so the IgG–decoy receptor need only cross the BBB to come in contact with the target inflammatory cytokine. The engineering of bi-functional HIRMAb or TfRMAB decoy receptor fusion proteins is discussed in Section 8.3.3. The

delivery of therapeutic antibodies, lysosomal enzymes, neurotrophins, or decoy receptors to brain with an HIRMAb Trojan horse is depicted in Figure 12.

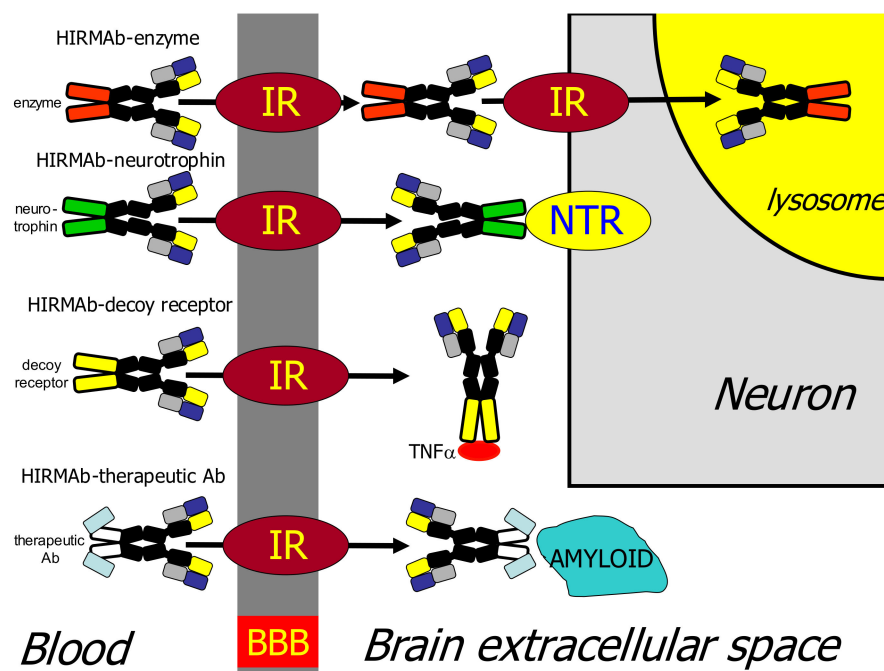


**Figure 12.** BBB receptor-mediated transport of IgG fusion proteins of lysosomal enzymes, neurotrophins, decoy receptors, and therapeutic antibodies. Model of RMT of 4 classes of biologics (lysosomal enzyme, neurotrophin, decoy receptor, or therapeutic antibody) across the BBB following fusion of the biologic to a BBB Trojan horse such as the HIRMAb. The IgG domain of the fusion protein targets the insulin receptor (IR) on the BBB and, if necessary, as in the case of lysosomal enzymes, on the brain cell membrane. In the examples depicted in this figure, the therapeutic domain is fused to the carboxyl terminus of each heavy chain of the HIRMAb. Reproduced with permission from [708], Copyright© 2015 John Wiley & Sons.

### 8.3.1. Lysosomal Enzymes

There are over 70 lysosomal storage diseases and over 50 of these affect the CNS [710,711]. The principal treatment for these conditions is Enzyme Replacement Therapy (ERT) with weekly IV infusions of the recombinant enzyme. However, ERT does not treat the brain because the enzymes do not cross the BBB, owing to the absence of the cation independent mannose-6 phosphate (M6P) receptor (M6PR) on the BBB [709]. Mucopolysaccharidosis (MPS) Type I (MPSI), also called Hurler syndrome, is caused by mutations in the gene encoding the lysosomal enzyme,  $\alpha$ -L-iduronidase (IDUA). The cDNA encoding human IDUA was cloned [712], and Chinese hamster ovary (CHO) lines expressing recombinant IDUA [713] were developed over 30 years ago. However, in 2022, the primary treatment of infants <16 months of age diagnosed with neuronopathic MPSI, also called Hurler syndrome, is stem cell transplant [291]. The problem with stem cell transplant as a treatment of the brain, as discussed in Section 5.1, is that stem cells do not cross the BBB.

In an effort to develop a treatment of the brain in MPSI, the IDUA lysosomal enzyme was re-engineered to enable BBB transport via RMT on the brain capillary insulin receptor. A fusion protein of human IDUA and the chimeric HIRMAb was engineered, wherein the IDUA enzyme, minus the enzyme signal peptide, was genetically fused to the carboxyl terminus of each heavy chain of the chimeric HIRMAb [714]. The structure of the HIRMAb-IDUA fusion protein, now named valanafusp alfa [715], is shown in Figure 12. The HIRMAb-IDUA fusion protein retained high affinity binding to the HIR and high IDUA enzyme activity [714]. The fusion protein was triaged to the lysosomal compartment of Hurler fibroblasts based on confocal microscopy and co-localization of the fusion protein

with lysosomal associated membrane protein-1, a lysosome marker [714]. Treatment of Hurler fibroblasts with the HIRMAb–IDUA fusion protein normalized intracellular IDUA enzyme activity, and caused a decrease in the intracellular content of sulfated glycoaminoglycans [714]. The impact on brain uptake of fusion of IDUA to the BBB-penetrating HIRMAb was examined in the adult Rhesus monkey. The recombinant IDUA (laronidase) and the HIRMAb–IDUA fusion protein (valanafusp alfa) were separately radio-iodinated with the [<sup>125</sup>I]-Bolton–Hunter reagent, and injected intravenously into separate Rhesus monkeys. The plasma concentration of each protein was determined over a 2 h period, followed by euthanasia of the primates, freezing, and determination of the organ distribution of each protein by whole body imaging of radioactivity using a phosphorimager. The brain was processed by sagittal sectioning. The impact of the IDUA fusion to the HIRMAb on the brain uptake of the lysosomal enzyme is shown in Figure 13A,B.

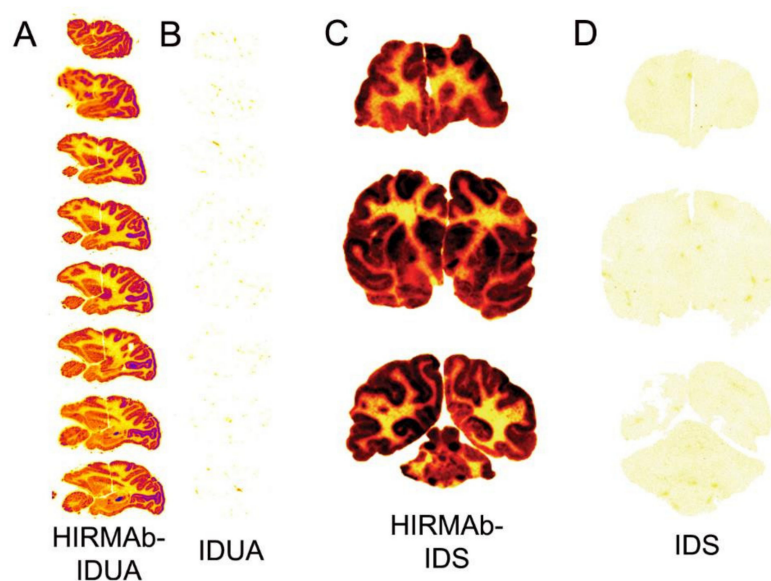


**Figure 13. Brain delivery in the primate of lysosomal enzymes fused to the HIRMAb.** Phosphorimager scans of sagittal sections of Rhesus monkey brain removed 2 h after the IV administration of [<sup>125</sup>I]-Bolton–Hunter labeled HIRMAb–IDUA fusion protein (A) or IDUA alone (B). Reproduced with permission from [716], Copyright© 2017 American Chemical Society. Film autoradiograms of coronal sections of Rhesus monkey brain removed 2 h after the IV administration of [<sup>125</sup>I]-Bolton–Hunter labeled HIRMAb-IDS fusion protein (C) or IDS alone (D). Reproduced with permission from [717], Copyright© 2013 American Chemical Society.

These ex vivo brain scans show (a) that IDUA does not cross the BBB (Figure 13B), and (b) that global distribution of IDUA to brain is possible after fusion of the enzyme to the HIRMAb BBB Trojan horse (Figure 13A). HIRMAb–IDUA and IDUA were radio-iodinated with the [<sup>125</sup>I]-Bolton–Hunter reagent [716]. This is the preferred method of radiolabeling biologics for the study of BBB transport in vivo, because Bolton–Hunter radiolabeled metabolites do not cross the BBB [717], as discussed in Methods, Section 11.4.4.

The pharmacologic efficacy of Trojan horse–IDUA fusion proteins was tested in the MPSI Hurler mouse. The HIRMAb cannot be tested in the mouse, because the HIRMAb does not recognize the murine insulin receptor [709]. Therefore, for treatment of the brain of the Hurler mouse, the murine IDUA was fused to the carboxyl terminus of each heavy chain of the recombinant 8D3 TfRMAb [718]. Aged MPSI mice were treated intravenously with 1 mg/kg of the TfRMAb–IDUA fusion protein weekly for 8 weeks. This treatment reduced lysosomal inclusion bodies in brain by 73% [718]. The safety pharmacology of chronic treatment with an IgG–IDUA fusion protein was evaluated in primates. Chronic treatment of Rhesus monkeys with weekly IV infusions of 3, 9, or 30 mg/kg of the HIRMAb–IDUA

fusion protein for 6 months showed the only adverse effect was hypoglycemia following rapid IV infusion of the high dose, 30 mg/kg, of the fusion protein in saline [709]. The hypoglycemia was eliminated by the addition of 5% dextrose to the infusion solution [709]. Chronic treatment of primates had no effect on glycemic control [709]. The HIRMAb-IDUA fusion protein was the first BBB Trojan horse pharmaceutical to enter human clinical trials, and a 1-year phase I-II trial was performed in children with MPSI [715]. Treatment stabilized the decline in cognitive impairment and cerebral atrophy. Over the course of 1 year, >500 IV infusions of the fusion protein were administered, and adverse events included a 1.7% incidence of infusion related reactions, treated with diphenhydramine, and a 2.1% incidence of mild hypoglycemia reversed with a snack [715]. The formation of anti-drug antibodies (ADA) against the valanafusp alfa was comparable to the ADA response to recombinant IDUA, laronidase [715].

In addition to IDUA, eight other lysosomal enzymes have been re-engineered for BBB transport by enzyme fusion to the HIRMAb or the TfRMAb, as recently reviewed [709], and these are listed in Table 4.

**Table 4.** IgG fusion proteins for blood–brain barrier delivery of biologics.

Class	Biologic	Disease	Reference
Lysosomal enzyme	IDUA	MPSI	[714,715]
	IDS	MPSII	[699,719–722]
	SGSH	MPSIIIA	[723,724]
	NAGLU	MPSIIIB	[725]
	ASA	MLD	[726]
	PPT1	CLN1	[727]
	ASM	NPDA	[727]
	HEXA	TSD	[727]
	GLB1	GM1 gangliosidosis	[727]
Neurotrophin	BDNF	Neurodegeneration	[728]
	GDNF	PD, stroke	[729–732]
	EPO	PD, AD	[733–735]
Decoy Receptor	TNFR2	PD, AD, stroke	[736–738]
Therapeutic antibody	Abeta amyloid MAb	AD	[696,697,739–741]
	BACE1 MAb	AD	[695,742,743]
	$\alpha$ -synuclein MAb	PD	[744]

In the case of the nine IgG-lysosomal enzyme fusion proteins listed in Table 4, high affinity binding of the fusion protein to the insulin or transferrin receptor and high lysosomal enzyme activity was retained.

MPSII, also known as Hunter syndrome, is caused by mutations in the gene encoding the lysosomal enzyme, iduronate 2-sulfatase (IDS). The cDNA encoding human IDS was cloned in 1990 [745], and recombinant IDS was produced in HT-1080 fibrosarcoma cells for clinical trials [746]. About two-thirds of MPSII subjects have CNS disease [747], and ERT with recombinant IDS does not treat the brain because the enzyme does not cross the BBB. Human IDS was re-engineered for BBB transport by fusion of the enzyme to the carboxyl terminus of each heavy chain of the HIRMAb [722] (Table 4). The HIRMAb-IDS fusion protein retained high affinity binding to the human insulin receptor and high IDS enzyme activity [722]. The impact of fusion of the IDS to the HIRMAb BBB delivery agent is demonstrated in Figure 13, which shows the film autoradiograms of coronal sections of Rhesus monkey brain removed 2 h after the IV injection of either the HIRMAb-IDS fusion protein (Figure 13C), or IDS alone (Figure 13D). The HIRMAb-IDS and IDS were radio-

iodinated with either the [<sup>125</sup>I]-Bolton–Hunter reagent or with 125-iodine and Iodogen for comparison of these different protein radio-labeling methods [717]. The data showed that low-MW metabolites formed by the degradation of the fusion protein in peripheral tissues, and released to blood, do not cross the BBB and enter brain when the protein is labeled with the [<sup>125</sup>I]-Bolton–Hunter reagent, whereas such metabolites do enter brain following Iodogen radiolabeling [717]. Labeling with the [<sup>125</sup>I]-Bolton–Hunter reagent is a non-oxidative process that conjugates the Bolton–Hunter reagent to ε-amino groups of surface lysine residues [748,749], and this modified lysine does not cross the BBB [717]. Labeling with 125-iodine and Iodogen is an oxidative process that places the iodine atom on tyrosine residues, and the iodo-tyrosine does cross the BBB [717]. To eliminate artifacts of brain uptake caused by peripheral metabolism, biologics should be iodinated with the Bolton–Hunter reagent or chelation of 111-indium, as discussed in Methods, Section 11.4.4. The safety pharmacology of chronic treatment with the HIRMAb–IDS fusion protein was evaluated in primates, and no adverse events were observed in a 6-month chronic GLP dosing study in 42 juvenile Rhesus monkeys [721].

The human IDS enzyme has also been fused to a TfRMAb that targets the human TfR1 [719]. This TfRMAb-IDS fusion protein, now designated pabinafusp alfa, has completed a successful phase 3 clinical trial [720]. As discussed in Section 13, pabinafusp alfa (IZCARGO<sup>®</sup>) is the first BBB Trojan horse fusion protein to receive market approval, as this TfRMAb–IDS fusion protein was approved in 2021 by the Ministry of Health, Labor, and Welfare (MHLW) in Japan for treatment of the brain in MPS-II.

### 8.3.2. Neurotrophins

Nerve growth factor (NGF) was discovered in 1951 [750]. Over the next 40 years, more than 30 neurotrophic factors were identified as potential new treatments of CNS disease [751], and in 1994, *Science* magazine hailed the entry of neurotrophic factors into clinical trials for CNS disorders, although the issue of how neurotrophins crossed the BBB was not discussed [752]. Nearly 30 years later, in 2022, and 70 years after the NGF discovery, there is not a single neurotrophin that is FDA approved for CNS disease. This lack of neurotrophin approval is not for the lack of trying. However, neurotrophin drug development for brain proceeded down a path that either ignored or avoided the BBB. The first neurotrophin clinical trials tested the effects of either brain-derived neurotrophic factor (BDNF) or ciliary neurotrophic factor (CNTF) for amyotrophic lateral sclerosis (ALS), wherein the neurotrophin was administered by subcutaneous (SQ) administration. The issue of BBB delivery of the neurotrophin was *in absentia*. Both trials failed, since neither neurotrophin reached the brain. In the report of the failed trial, the issue of BBB transport of the neurotrophin was not discussed for BDNF [753] or CNTF [754]. Having discovered that SQ administration of neurotrophins may not lead to clinical success in a CNS disease, the next neurotrophin to enter clinical trials, glial-derived neurotrophic factor (GDNF), was administered by ICV injection for the treatment of PD [107]. The ICV delivery route was used, even though the sponsor's own data demonstrated very limited penetration into brain following ICV administration [79], as shown in Figure 5C. For the reasons discussed in Section 2.1.4, the failure of the ICV trial of GDNF for PD was expected. Following the failure of the ICV delivery for PD, the next clinical trial for GDNF therapy of PD used convection-enhanced diffusion (CED) for brain drug delivery [130]. The limitations of CED for brain drug delivery are reviewed in Section 2.2.2. The CED clinical trial failed for GDNF in PD [130], and subsequent to the CED trial failure, a primate study showed that GDNF entry into brain tissue following CED was very limited [131], as shown in Figure 6A, and discussed in Section 2.2.2. Some 14 years after the failed CED trial of GDNF in PD, a panel discussed the future of GDNF therapy in PD [755]. Not much had changed in 30 years, as the role of the BBB in neurotrophin drug development for brain disorders was not mentioned in either 1994 [752] or in 2020 [755]. CNS drug developers are reluctant to discuss the BBB if they have no solution to the intractable problem of brain drug delivery.

Apart from chronic disease such as ALS or PD, neurotrophins could also be potent drugs for acute brain disease, such as acute stroke. Neurotrophins can rescue dying neurons if the neuroprotective agent is administered to the ischemic brain within 5 h after the stroke event [756,757]. Therefore, the neurotrophin stroke trials were designed to administer the neurotrophin by IV injection within 5 h of the stroke. The problem with this approach is that the BBB is intact in the early hours after acute cerebral ischemia in either experimental stroke [758,759] or human stroke [757,760]. Since no attempt was made to re-engineer the neurotrophin for BBB delivery, the trials met with the expected failed results for either the intravenous fibroblast growth factor (FGF)-2 stroke trial [761] or the intravenous erythropoietin (EPO) stroke trial [762]. The rationale for the EPO trial was that the IV administration of EPO results in EPO delivery to CSF, which was taken as evidence that EPO crosses the BBB [763]. However, EPO does not cross the BBB [733]. As discussed in Section 1.1, drug entry into CSF is evidence for drug transfer across the choroid plexus, which forms the blood–CSF barrier, but is not evidence for drug transfer across the brain endothelium, which forms the BBB (Figure 3). The use of biologic entry into CSF as confirmation of BBB transport, and as a rationale for a CNS clinical trial, leads predictably to clinical trial failure [762]. An approach to CNS drug development that relies on drug entry into CSF as a measure of BBB transport is reminiscent of concepts from over 100 years ago. As reviewed in Section 1.2, the prevailing view in 1913 was that CSF is an obligatory compartment between blood and brain [26].

Working on the hypothesis that neurotrophin drug development requires re-engineering of the neurotrophin for BBB transport, BDNF was conjugated to the OX26 TfRMAB. To optimize plasma pharmacokinetics, the cationic BDNF was pegylated on carboxyl groups [764]. The PEG-BDNF-TfRMAB conjugate was neuroprotective in both transient forebrain ischemia [765] and middle cerebral artery occlusion (MCAO) [766] following delayed IV administration. The reduction in stroke volume in the MCAO model correlated with a functional motor improvement using the rotarod test [767]. A BDNF-HIRMAb fusion protein was engineered, which retained high affinity binding to both the BDNF trkB receptor and the HIR [728]. A HIRMAb-GDNF fusion protein was engineered, which retained high affinity binding for the GDNF receptor and the HIR [730]. For preclinical studies in a mouse PD model, a TfRMAB-GDNF fusion protein was engineered [768], and this fusion protein was neuroprotective in both experimental PD [731], and experimental stroke following delayed IV administration in the mouse [732]. The HIRMAb-GDNF produced no adverse events in a GLP toxicology evaluation in 56 Rhesus monkeys that were administered up to 50 mg/kg of the fusion protein over 60 h [729].

A HIRMAb-EPO fusion protein was engineered that retained high affinity binding to both the HIR and the human EPO receptor (EPOR) [733]. The brain uptake and plasma pharmacokinetics of either EPO or the HIRMAb-EPO fusion protein was measured in the Rhesus monkey following radiolabeling of either EPO or the HIRMAb-EPO fusion protein with the [<sup>125</sup>I]-Bolton–Hunter reagent [733]. Fusion of the EPO to the HIRMAb had 2 beneficial effects. First, fusion to the HIRMAb enabled EPO to enter the primate brain with a brain uptake of  $2.1 \pm 0.1\%$ ID/brain. Conversely, the brain uptake of EPO alone was comparable to a brain plasma volume marker, an IgG1 isotype control antibody, which indicated EPO is retained in the brain plasma volume and does not cross the BBB [733]. Second, fusion of EPO to the HIRMAb resulted in a 13-fold reduction in the plasma AUC of EPO [733]. Since the hematopoietic effect of EPO is proportional to the plasma AUC [769], EPO fusion to the HIRMAb reduces the hematopoietic effect of the EPO domain by 13-fold. For preclinical studies in a mouse PD or AD model, EPO was fused to the 8D3-derived TfRMAB, and the TfRMAB-EPO fusion protein retained high affinity binding for the mouse EPOR and mouse TfR1 [770]. Chronic treatment of mice with experimental PD with the TfRMAB-EPO fusion protein was neuroprotective and had only a minor effect on hematocrit [734]. Sumbria and colleagues have demonstrated the therapeutic effects of chronic treatment of AD transgenic mice with the TfRMAB-EPO fusion protein [735].

### 8.3.3. Decoy Receptors

The leading decoy receptor pharmaceutical, etanercept, is a biologic formed by fusion of the ECD of human TNFR2 to the amino terminus of human IgG1 Fc, as originally described in 1991 [771]. Etanercept is a biologic tumor necrosis factor (TNF)- $\alpha$  inhibitor (TNFI). Other widely used biologic TNFIs are MAbs including adalimumab and rituximab. The global annual revenue for adalimumab in 2019 was USD 19 billion [772], and the combined revenues for etanercept and rituximab were comparable. The biologic TNFIs are only used for systemic disease of chronic inflammation, and none of these agents are FDA approved for treatment of CNS disease. The biologic TNFIs are not approved for the brain because these agents do not cross the BBB. This is an unfortunate situation, since TNF $\alpha$  plays a pro-inflammatory role in both acute brain disease, such as stroke [773,774], and chronic brain disease, such as AD [775] and PD [776,777]. In experimental models of brain disease, the intra-cerebral injection of the TNFR2 ECD is neuroprotective in experimental stroke [778]. The intra-cerebral, but not the intravenous, injection of etanercept is neuroprotective in traumatic brain injury (TBI) [779]. The use of the biologic TNFIs for brain disease will require re-engineering of these biologics as BBB-penetrating drugs. In the case of adalimumab and rituximab, these therapeutic antibodies can be fused to transporting antibodies for the engineering of new bi-specific antibodies (BSA) as discussed in the next section.

A BBB-penetrating form of etanercept was engineered by fusion of the human TNFR2 ECD to the carboxyl terminus of each heavy chain of the HIRMAb [736]. The IgG-decoy receptor orientation of this HIRMAb-TNFR fusion is opposite that of etanercept. With etanercept, the TNFR2 is fused to the *amino* terminus of the IgG Fc. In contrast, with the HIRMAb-TNFR fusion protein, the TNFR2 ECD is fused to the *carboxyl* terminus of the HIRMAb. This design of the fusion protein fixes the TNFR2 in a dimeric configuration (Figure 12), which enables high affinity binding for TNF $\alpha$  [780]. A dimeric configuration is the preferred orientation of the TNFR2, which crystallizes as a dimer [781]. The HIRMAb-TNFR fusion protein retained high affinity binding for both the HIR and TNF $\alpha$  [736,782]. The HIRMAb-TNFR fusion protein and etanercept were radiolabeled with the [<sup>125</sup>I]-Bolton-Hunter reagent and injected intravenously in the Rhesus monkey [782]. The brain uptake of etanercept was comparable to the IgG1 isotype control, which indicates etanercept is retained in the blood volume of brain without transport across the BBB. However, the HIRMAb-TNFR fusion protein rapidly crossed the BBB with a brain uptake of  $3.0 \pm 0.1\%$ ID/brain [782]. For treatment in preclinical models of stroke or PD in the mouse, an 8D3-derived TfRMAb-TNFR fusion protein was engineered and expressed, and this fusion protein retained high affinity binding to both the mouse TfR1 and TNF $\alpha$  [783]. The therapeutic effect of the TfRMAb-TNFR fusion protein was evaluated in experimental Parkinson's disease (PD) induced by the intra-cerebral injection of 6-hydroxydopamine [737]. PD mice were treated with saline, 1 mg/kg etanercept, or 1 mg/kg TfRMAb-TNFR fusion protein IV every other day for 3 weeks. Treatment with the TfRMAb-TNFR fusion protein resulted in an 83% reduction in apomorphine-induced rotation behavior, an 82% increase in vibrissae-elicited forelimb placing, and a 130% increase in striatal tyrosine hydroxylase enzyme activity. In contrast, neither saline nor etanercept treatment had any therapeutic effect in the PD mice [737]. Chronic treatment of mice with the fusion protein induced only a low titer ADA response [737]. The TfRMAb-TNFR fusion protein was also neuroprotective in experimental stroke, which was induced with a reversible middle cerebral artery occlusion (MCAO) method [738]. The mice were treated with delayed IV administration of either 1 mg/kg etanercept or 1 mg/kg TfRMAb-TNFR fusion protein. Neuroprotection was assessed at both 1 and 7 days after the 60 min MCAO. Treatment with the TfRMAb-TNFR fusion protein caused a 45%, 48%, 42%, and 54% reduction in hemispheric, cortical, and subcortical stroke volume, and neural deficit, respectively. Conversely, treatment with etanercept had no therapeutic effect [738]. The neuroprotective effects in the reversible MCAO model of combined treatment with the TfRMAb-GDNF and TfRMAb-TNFR fusion proteins were additive, illustrating the advantages of combination biologic therapy in a brain disease [732]. Similar to etanercept alone [738], GDNF alone

had no neuroprotective effect in experimental stroke [732]. IV etanercept or GDNF are not neuroprotective in experimental stroke because these biologics do not cross the BBB, and because the BBB is intact in the early hours after stroke [758,759], when neuroprotection in stroke is possible [756,757].

#### 8.3.4. Bispecific Antibodies

Biologic drugs, which are mainly monoclonal antibodies, are increasingly receiving FDA approval for non-CNS indications, and in 2019, biologics accounted for 43% of total prescription drug revenues [772]. The development of therapeutic antibodies, particularly for AD, has accounted for significant investment in clinical trials by the pharmaceutical industry. These trials involved the monthly IV infusion of anti-Aβ amyloid antibodies (AAA) on the assumption that a small amount of the antibody in blood would penetrate the BBB to enter brain tissue. It was, and is, commonly assumed that about 0.1–0.2% of the injected antibody reaches the brain [784,785]. This assumption is derived from the observation that the CSF concentration of IgG is about 0.1–0.2% of the plasma concentration [12]. However, as discussed in Section 1.1, it is expected that any antibody in plasma will enter into the CSF compartment owing to the leakiness of the choroid plexus, which forms the blood–CSF barrier, and that antibody penetration into CSF provides no information on BBB transport of the antibody. The important predictor of success in a CNS trial is not whether the biologic enters CSF, but whether the biologic crosses the BBB to enter brain, as demonstrated by *in vivo* methods reviewed in Section 11. When the brain uptake of a therapeutic antibody is measured *in vivo*, the brain/plasma ratio of a therapeutic antibody is <0.01%, not 0.1–0.2% [786].

The first AAA to fail in a large phase 3 trial in AD was bapineuzumab [787,788]. Bapineuzumab entered clinical trials even though the preclinical data showed the brain uptake of the antibody in the mouse was no higher than 0.07%ID/g [789], which indicates the antibody is confined to the blood volume of brain [739]. Following the failure of the bapineuzumab trial, another AAA, aducanumab, was developed [790]. Aducanumab was said to cross the BBB because the brain concentration increased as the injection dose (ID) was increased. However, this is expected for an antibody that is confined to the brain blood volume. The measurement of aducanumab in brain was determined after washout of the brain vasculature [790]. However, the brain/plasma ratio of aducanumab was 1 μL/g, which is 5–10% of the brain blood volume, and is indicative of incomplete washout of the brain [786]. Nevertheless, in clinical trials of AD subjects, the entry of aducanumab into the brain of these patients could be inferred, because antibody treatment reduced the amyloid plaque in brain [790]. The mechanism of aducanumab entry into the brain of AD subjects appears to be BBB disruption. A known side effect of AAA therapy in AD is amyloid related imaging abnormalities of edema (ARIA-E) as determined by MRI [790]. ARIA-E is a form of vasogenic edema that follows BBB disruption. In the aducanumab clinical trial, there is a direct relationship between the reduction in amyloid plaque and the ARIA-E, which suggests the aducanumab enters brain through a disrupted BBB [786]. The hypothesis that ARIA-E is required to cause a reduction in amyloid plaque is consistent with the clinical effects of another AAA, crenezumab, which does not cause ARIA-E [791] and does not reduce brain amyloid plaque [792]. Reduction in brain amyloid, as shown by PET, is a surrogate marker. The primary endpoint in the two large aducanumab phase 3 trials was the Clinical Dementia Rating-Sum of Boxes (CDR-SB) [793]. Although neither trial met the endpoint, a post hoc analysis showed a statistically significant improvement in CDR-SB in one of the trials [793]. On the basis of this post hoc analysis, the FDA-approved aducanumab in 2020 for treatment of patients with AD despite the near unanimous rejection of the aducanumab application by the FDA Advisory Committee [793]. Aducanumab was denied approval by the European Medicines Agency (EMA) in late 2021 and in early 2022 the Centers for Medicare and Medicaid Services (CMS) restricted aducanumab reimbursements only for patients in clinical trials. The road to FDA approval of the AAAs for AD proved to be as tortuous as the road to approval of neurotrophins, as reviewed in Section 8.3.2. Both



AAAs and neurotrophins, as well as lysosomal enzymes or decoy receptors, need to be re-engineered for BBB transport prior to entry into costly human clinical trials.

When the BBB Trojan horse is a MAb and the neurotherapeutic is a MAb, the re-engineering of the therapeutic antibody requires the production of a bi-specific antibody (BSA). The first BSA engineered for BBB transport was reported in 2007 and involved production of a tetravalent BSA [696]. An AAA was re-engineered as a single chain Fv (ScFv) antibody, and this ScFv was fused to the carboxyl terminus of each heavy chain of the HIRMAb. The HIRMAb-ScFv retained high affinity binding to both the HIR and to soluble  $A\beta^{1-40}$  as well as amyloid plaque in brain and amyloid fibrils [696]. The HIRMAb-ScFv fusion protein entered the brain of the Rhesus monkey following IV administration, whereas the AAA alone was confined to the brain blood volume [696]. To enable preclinical studies in AD transgenic mice, the anti-Abeta ScFv was fused to the carboxyl terminus of each heavy chain of the 8D3-derived TfrMAb, and this BSA retained high affinity binding to both the mouse Tfr and  $A\beta^{1-40}$  [794]. The brain uptake of the TfrMAb-ScFv BSA in the mouse was  $3.5 \pm 0.7\%$  ID/g following IV administration of [ $^{125}$ I]-Bolton-Hunter radio-labeled TfrMAb-ScFv fusion protein [794]. Double transgenic APP<sup>swe</sup>, PSEN1<sup>dE9</sup> mice at 12 months of age were treated for 12 weeks with daily SQ injections of saline or 5 mg/kg of the TfrMAb-ScFv BSA [739]. Abeta fibrils in brain were measured by immunohistochemistry with the 6E10 MAb and total amyloid plaque in brain was measured by thioflavin-S fluorescent microscopy. Treatment reduced total plaque in cortex and hippocampus by 49% and 43%, respectively, and reduced Abeta fibrils in cortex and hippocampus by 57% and 61%, respectively [739]. The ARIA-E in AD subjects treated with an AAA [790] is equivalent to the cerebral microhemorrhage in mice treated with an AAA [795]. Mice treated chronically with the TfrMAb-ScFv BSA did not develop cerebral microhemorrhage based on Prussian blue staining of brain, and developed only a low titer ADA response [739].

Subsequent to the description of the BBB-penetrating BSA derived from either with the HIRMAb [696] or the TfrMAb [794], a variety of BBB-penetrating BSAs were engineered that used a multitude of formats for BSA design. A BSA was engineered that targeted both the Tfr and BACE1 as a treatment for AD [695,742]. This BSA was engineered with the knob-in-hole technology which placed both the TfrMAb transporting antibody and the BACE1 therapeutic antibody each in a monovalent format. A BSA that targeted both the Tfr and the Abeta amyloid peptide was engineered with knob-in-hole technology by fusion of a single chain Fab form of the TfrMAb to the carboxyl terminus of one heavy chain (HC) of a hetero-tetrameric antibody against Abeta [697]. This design placed the TfrMAb in a monovalent form and the AAA in a bivalent format. In a modified tetravalent BSA format, the 8D3 TfrMAb was engineered as a ScFv, which was then fused to the carboxyl terminus of each light chain (LC) of the AAA, mAb158 [796], or an  $\alpha$ -synuclein MAb [744]. The mAb158 is the murine precursor to the BAN2401 AAA for AD [797]. Several therapeutic antibodies were re-engineered as a TfrMAb-based BSA using a dual variable domain format where the VH and VL for each antibody was placed in tandem at the amino terminus of each HC and LC [798]. Owing to steric hindrance by the outer domain antibody, the affinity of the inner domain antibody was reduced [798]. A similar tetravalent tandem BSA was engineered with a TfrMAb and an AAA that targeted the protofibrillar form of the Abeta peptide [740]. In another monovalent TfrMAb format, a BSA was engineered that targeted the Tfr as a monovalent antibody and BACE1 as a bivalent antibody using knob-in-hole technology [743]. The Tfr binding site was created in the CH3 region of one heavy chain by mutagenesis of multiple amino acids [743]. In yet another format for BSA engineering, a single domain shark variable domain of new antigen receptor antibody with high affinity binding to the Tfr was fused to the amino terminus of the heavy chain of the bapineuzumab antibody [741].

In summary, since the initial report of the engineering of a tetravalent BSA that targets either the insulin receptor [696] or transferrin receptor [794], at least eight different formats have been used for engineering a BBB-penetrating BSA [695,697,740–744,796,798]. The

antibodies range from monovalent for both arms of the BSA, to bivalent for both arms of the BSA, and to monovalent for one arm and bivalent for the other arm. The affinity of the BBB transporting arm of the BSA ranges from high affinity to moderate affinity to low affinity [559,647]. The final test of these BSAs is whether the BSA goes all the way to FDA approval for treatment of AD or another CNS disease. The one BBB-penetrating BSA that is currently in clinical trials is the Roche BSA [697], designated RO7126209, which is in a phase 2 clinical trial for AD [NCT04639050].

#### 8.4. Avidin-Biotin Technology

There are classes of biologics that cannot be delivered across the BBB with fusion protein technology, and these include small peptide drugs and nucleic acid pharmaceuticals. Oligopeptides may no longer bind the cognate receptor after fusion to a BBB Trojan horse even if a long linker is employed. Nucleic acid pharmaceuticals cannot be fused to a polypeptide. It is possible to deliver oligopeptides or antisense agents across the BBB with RMT technology that is combined with a linker system, such as avidin–biotin technology. In this approach, the pharmaceutical is formulated in two vials. The first vial contains the mono-biotinylated peptide or antisense agent. The second vial contains a fusion protein of avidin and the IgG RMT Trojan horse, which is generated by the genetic engineering of an IgG–avidin fusion protein. The use of RMT Trojan horse–avidin fusion proteins and peptide or antisense radiopharmaceuticals is particularly amenable to the development of neuro-diagnostics using positron emission tomography (PET) or single photon emission computed tomography external brain imaging.

##### 8.4.1. Peptide Radiopharmaceuticals for Brain Imaging

The first peptide radiopharmaceutical used as a diagnostic agent and external scanning was [<sup>111</sup>In]-octreotide, an 8-AA somatostatin (SST) analogue with a MW of 1395 Da, which enabled the external imaging of neuroendocrine tumors [799]. SST receptors (SSTR) are over-expressed in such tumors [800]. The SSTR is expressed in the CNS, as are receptors for >100 other neuropeptides [801]. However, since neuropeptides do not cross the BBB [802], the development of peptide radiopharmaceutical neuro-diagnostic agents is not possible in the absence of a BBB delivery technology. Epidermal growth factor (EGF) was used to develop a prototype of a BBB-penetrating peptide radiopharmaceutical. The EGF receptor (EGFR) is over-expressed in primary brain cancer [803]. The use of a targeted EGF peptide radiopharmaceutical as an imaging agent in experimental brain cancer was evaluated with an experimental intra-cranial U87 human glioma in nude rats [804].

The EGF was re-formulated for BBB delivery in a two-vial approach. Vial A contained EGF that was both radiolabeled and biotinylated. Vial B contained a conjugate of the OX26 TfRMAb specific for the rat TfR and streptavidin (SA). Prior to IV administration in EGFR expressing brain-tumor-bearing rats, the two vials were mixed. Owing to the very high affinity binding of biotin to SA, there was immediate formation of a complex of the EGF peptide radiopharmaceutical and the TfRMAb BBB Trojan horse [804]. The EGF was radiolabeled with 111-indium, which was chelated by a diethylenetriamine pentaacetate (DTPA) group attached to the peptide. In addition, the EGF was conjugated with 3400 Da polyethyleneglycol (PEG<sup>3400</sup>)-biotin. The placement of the PEG<sup>3400</sup> linker between the EGF and the biotin was necessary to eliminate steric hindrance on EGF binding to the EGFR caused by EGF capture by the OX26/SA conjugate [805]. When a 14-atom linker was placed between the EGF and the biotin, the high affinity binding of the 6 kDa biotinyl-EGF to the EGFR was sterically hindered by the 60 kDa SA [805]. The use of the PEG<sup>3400</sup> linker created a spacer >200 atoms in length between the EGF and the biotin/SA complex and this extended linker removed the steric hindrance of the SA complex on EGF binding to the EGFR on human glial tumor cells [805]. The [<sup>111</sup>In-DTPA, PEG<sup>3400</sup>-biotinyl]-EGF/SA-OX26 was injected intravenously in nude rats bearing an intracranial human U87 glioma, which over-expresses the EGFR [804]. As a control, the tumor-bearing rats were also injected with

the [ $^{111}\text{In}$ -DTPA, PEG<sup>3400</sup>-biotinyl]-EGF without attachment to the TfRMAb Trojan horse. The design of the BBB-penetrating EGF radiopharmaceutical is shown in Figure 14A.

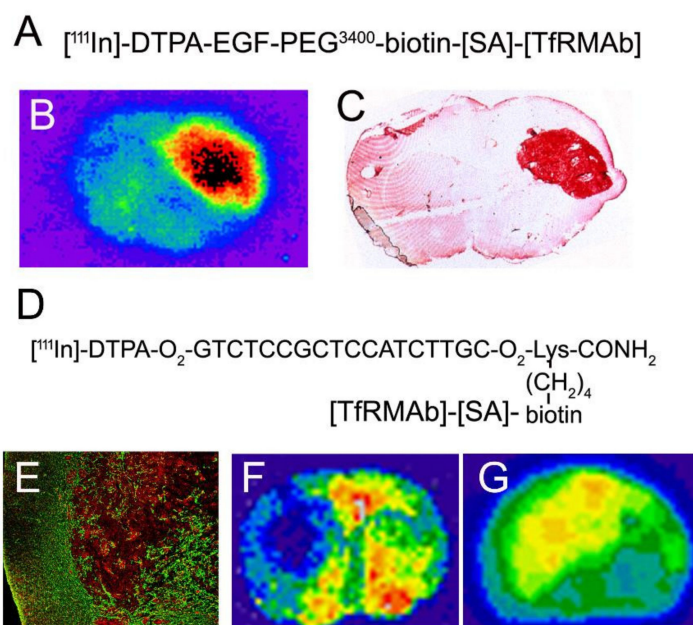


**Figure 14. Imaging brain cancer with peptide or antisense radiopharmaceuticals and BBB drug delivery technology.** (A) Structure of [ $^{111}\text{In}$ ]-DTPA-EGF-PEG<sup>3400</sup>-biotin bound to the OX26/SA conjugate. (B) Film autoradiogram of coronal section of nude rat brain bearing a U87 glioma removed 2 h after IV injection of the BBB-targeted EGF peptide radiopharmaceutical. (C) A section parallel to that shown in (B) was examined by immunohistochemistry using the 528 MAb against the human EGFR. Panels B and C reproduced with permission [804], Copyright© 1999 American Association Cancer Research. (D) Structure of [ $^{111}\text{In}$ ]-DTPA-O<sub>2</sub>-18-mer PNA antisense to nucleotides 20–37 of the rat GFAP mRNA. The carboxyl terminus of the PNA incorporates a lysine (Lys) residue and biotin is conjugated to the  $\epsilon$ -amino group of the Lys; O = 9-atom linker. The biotinyl PNA is bound by the OX26/SA conjugate. (E) Confocal microscopy of an intra-cranial RG-2 tumor in rats that is immune-stained with an antibody to caveolin-1 $\alpha$  (red) and an antibody to GFAP (green). (F) Film autoradiogram of coronal section of tumor-bearing rat brain removed 6 h after the IV injection of the biotinyl GFAP-PNA-OX26/SA conjugate. (G) Film autoradiogram of coronal section of tumor-bearing rat brain removed 6 h after the IV injection of the biotinyl CAV-PNA-OX26/SA conjugate. Panels (E–G) reproduced with permission [806], Copyright© 2004 SNMMI.

The BBB-targeted EGF peptide radiopharmaceutical shown in Figure 14A enabled brain imaging of an intra-cranial human glial tumor in the nude rats, as shown in Figure 14B. The over-expression of the tumor EGFR was confirmed by immunohistochemistry of the tumor at post-mortem (Figure 14C). No imaging of the tumor was possible following the IV injection of the [ $^{111}\text{In}$ -DTPA, PEG<sup>3400</sup>-biotinyl]-EGF not bound to the OX26 TfRMAb [804]. Recent reviews have discussed the use of peptide radiopharmaceuticals for either therapeutic [807] or diagnostic [808] agents for brain disease. Peptides have the potential for many medical applications in the CNS as there are >100 peptide systems in the brain [801,809]. Such therapeutic and diagnostic applications of peptide radiopharmaceuticals for the brain will require the re-engineering of the peptides with BBB peptide delivery technology.

#### 8.4.2. Antisense Radiopharmaceuticals for Brain Imaging

Over 20 years ago, there was promise for imaging CNS gene expression with sequence specific antisense radiopharmaceuticals [810,811]. Antisense agents are either phosphodiester antisense oligodeoxynucleotides (ASO), phosphorothioate ASOs, or peptide nucleic acids (PNA). Phosphodiester ASOs are not suitable agents for in vivo use, owing to the rapid degradation of phosphodiester ASOs by endo- and exo-nucleases in vivo. Phospho-

rothioate ASOs are more resistant to nucleases, but are not suitable imaging agents because binding of a phosphorothioate ASO to a target mRNA forms a DNA:RNA heteroduplex, which triggers mRNA degradation by RNase H [812]. PNAs are the preferred antisense imaging agents, as the PNA polypeptide backbone is not degraded by nucleases, and PNAs do not activate RNase H [813]. However, PNAs are highly polar molecules that do not cross the BBB [814]. PNAs can be re-formulated to cross the BBB and retain affinity for the target mRNA sequence using BBB RMT and avidin–biotin technology. An 18-mer PNA was synthesized with a nucleobase sequence that was antisense to either nucleotides (nt) 10–27 of the rat caveolin (CAV)-1 $\alpha$  mRNA (AF439778) or to nt 20–37 of the rat GFAP mRNA (NM\_017009) [806]. The sequence of the GFAP PNA is shown in Figure 14D. The amino terminus of the PNA was conjugated with DTPA, which chelates the 111-indium radiotracer. A double 9-atom linker (O) was placed at both the amino terminus between the DTPA and the PNA, and at the carboxyl terminus between the PNA and the terminal lysine (Lys) as shown in Figure 14D. The  $\epsilon$ -amino group of the Lys amino acid was biotinylated, which allowed binding of the biotinyl PNA to a conjugate of SA and the OX26 rat TfRMAb (Figure 14D). Northern blotting with synthetic GFAP or LAT1 mRNA, produced by *in vitro* transcription, showed the GFAP PNA bound to the GFAP mRNA, but not the LAT1 mRNA, despite being bound by the OX26/SA conjugate [806]. Fischer CD344 rats bearing an intra-cranial RG-2 tumor were studied for brain imaging with either the CAV PNA or the GFAP PNA. Confocal microscopy showed the experimental brain tumor over-expressed the CAV protein and under-expressed the GFAP protein (Figure 14E). Loss of GFAP expression is typical in high grade glial tumors [815]. GFAP mRNA in the RG-2 glioma cells in culture was not detectable by Northern blotting even after over-exposure of the film [806]. *In vivo* brain imaging of the RG-2 intra-cranial tumors with the CAV PNA or the GFAP PNA antisense radiopharmaceutical demonstrated the under-expression of the GFAP mRNA (Figure 14F) and the over-expression of CAV mRNA (Figure 14G) in the intra-cranial brain tumor, providing the PNA was conjugated to the TfRMAb Trojan horse [806]. Only blank brain scans were produced when the GFAP PNA alone or the CAV PNA alone were injected intravenously in the tumor-bearing rats [806]. Antisense agents had been proposed as new approaches to the *in vivo* imaging of gene expression in the brain [816]. This is still possible, providing the antisense agents are re-formulated with a BBB Trojan horse brain delivery technology [806].

#### 8.4.3. IgG–Avidin Fusion Proteins

TfRMAb–avidin fusion proteins were generated from the OX26 rat TfRMAb as either a ScFv–SA fusion protein produced in *E. coli* [692], or as a bivalent TfRMAb–avidin fusion protein produced in myeloma cells [817]. However, the problem with production of IgG–avidin fusion proteins in mammalian expression systems is the high concentration of biotin in tissue culture medium [818], coupled with the very slow dissociation of biotin from avidin. Biotin binding to avidin is characterized by a  $K_D$  of  $10^{-15}$  M, and a dissociation  $T_{1/2}$  of 3 months [819]. The IgG–avidin fusion protein produced with standard expression media is fully loaded with biotin [702], and only harsh denaturing conditions can separate the avidin and biotin [819]. An IgG–avidin fusion protein that is saturated with biotin has little utility for brain drug delivery of biotinylated agents. Therefore, it was necessary to develop culture conditions that produce a gradual depletion of medium biotin. In standard culture medium, the biotin concentration is 800 nM, which greatly exceeds the concentration of the avidin fusion protein. The CHO cells stably transfected with the HIRMAb–avidin fusion protein were re-suspended in custom biotin-free medium supplemented with 20 nM biotin. The medium biotin concentration was reduced to 10 nM, 3 nM, 1 nM, and 0.3 nM, at days 8, 14, 18, and 21 of growth in serum free medium [702]. The HIRMAb–AV fusion protein produced under these conditions retained 1 unoccupied biotin binding site per hetero-tetrameric IgG–avidin fusion proteins, which is composed of 2 avidin monomeric chains fused to the carboxyl terminus of each HIRMAb heavy chain [702].

An 8D3-derived TfRMAB–avidin fusion protein was produced in stably transfected CHO cells under conditions of biotin depletion, and the fusion protein retained high affinity binding for the mouse TfR and 1 biotin binding site per tetramer [820]. The biologic activity of the fusion protein was tested in vivo in mice with respect to brain delivery of [<sup>125</sup>I, biotinyl]-Aβ<sup>1–40</sup>, a potential peptide radiopharmaceutical for imaging the brain amyloid burden of AD [686,687]. Currently, the brain amyloid burden in AD is imaged with small molecules such as florbetapir [790], which has a brain uptake of 2–3%ID/g at 60 min after IV administration in the mouse [821]. However, lipid-soluble small molecules such as florbetapir are subject to rapid efflux from brain to blood [822], and a significant amount of florbetapir can efflux from brain during a 2 h scanning period. A peptide radiopharmaceutical, such as Aβ<sup>1–40</sup>, may be a preferred imaging agent owing to a longer brain residence time [688], should the peptide be made transportable through the BBB. Aβ<sup>1–40</sup> alone does not cross the BBB [687,820]. The delivery of N-biotinyl Aβ<sup>1–40</sup> to mouse brain was assessed following radio-iodination of the peptide with the [<sup>125</sup>I]-Bolton–Hunter reagent, and conjugation to the 8D3-derived TfRMAB–avidin fusion protein [820]. The brain uptake of [<sup>125</sup>I, biotinyl]-Aβ<sup>1–40</sup> conjugated to the TfRMAB–avidin fusion protein is 2.1 ± 0.2 %ID/g in the mouse following IV injection [820]. Therefore, the use of BBB RMT delivery technology increases the brain uptake of a large molecule peptide radiopharmaceutical to the same level of brain uptake observed with a lipid-soluble small molecule such as florbetapir [820].

## 9. Nanoparticles

### 9.1. Nanoparticle Formulations

There are three broad classes of nanoparticles (NP) [823]:

- **Polymer-based nanoparticles**, which include polymeric NPs (PNP), dendrimers, micelles, and protein nanoparticles, such as albumin nanoparticles;
- **Lipid-based nanoparticles**, which include liposomes, which have an aqueous interior, and solid lipid nanoparticles (SLN), which lack an aqueous interior; exosomes, which are reviewed in Section 5.2, can be considered natural liposomes;
- **Non-polymeric nanoparticles**, which include carbon nanotubes (CNT), graphene oxide (GO) fullerenes or quantum dots, and metallic nanoparticles produced from metals such as iron, gold, silver, or silica. Iron nanoparticles are magnetic.

Nanoparticles may be functionalized by conjugation of ligands on the surface of the nanoparticle, where such ligands are intended to mediate endocytosis of the nanoparticle following binding to either a carrier-mediated transporter (CMT) or a receptor-mediated transporter (RMT). Nanotechnology, which includes nanoparticles, liposomes, dendrimers, and exosomes, constitute 32% of all brain drug delivery research (Table 1). Despite the development of nanoparticles over the last 30 years, there have been few nanoparticle formulations to enter into CNS clinical drugs, and there have been no FDA approvals of nanoparticles for brain disease [824], as reviewed below. Nanoparticles are complex structures that can exert toxic effects in brain with neuropathologic changes, as discussed below. However, owing to the very few Investigational New Drug (IND) applications to the FDA for brain-targeted nanoparticles, these agents have not been subjected to the rigorous preclinical GLP safety pharmacology and toxicology studies in two species required for an IND. An IND application also requires a proven and scalable plan for manufacturing of the drug product under Good Manufacturing Practice (GMP). A PubMed search for ‘nanoparticle GMP manufacturing’ lists no entries (January 2022).

### 9.2. Polymer-Based Nanoparticles

#### 9.2.1. Polymeric Nanoparticles

The first use of polymeric nanoparticles (PNP) to deliver drug across the BBB was reported in 1995 [64]. The opioid hexapeptide, dalargin, was adsorbed to the surface of PNPs prepared from poly(butyl cyanoacrylate) or PBCA. The dalargin was added to the PBCA and the suspension was sonicated and either 0 or 1% polysorbate-80 (PS80, Tween-80), a non-ionic detergent, was added, and the suspension immediately injected

intravenously in mice. Analgesia was measured with the tail-flick method [64]. Analgesia was not induced by the peptide alone, the peptide adsorbed to the PNPs, or the peptide plus the PS80, but was induced by the combination of the peptide, the PNPs, and PS80 [64]. Subsequently, it was shown that plasma proteins are adsorbed to the surface of the PS80-coated PNPs, including apolipoprotein B (apoB) and apolipoprotein E (apoE), and it was hypothesized that apoB or apoE on the NP surface acted as ligands and attached the NP to the LDLR on the BBB to trigger transport of the PNP into brain [825]. However, as discussed in Section 8.1.6, the LDLR is not localized to the BBB by immunohistochemistry. The absence of the LDLR on the BBB is consistent with the lack of transport across the BBB of LDL cholesterol [611–613]. The model of BBB transport of the PNP was revised following the demonstration of binding of apoA-I to the surface of the nanoparticle, and it was then hypothesized that the apoA-I triggered transport not via the LDLR, but via the scavenger receptor (SR)-B [826], which is also known as CD36. CD36 is localized to the microvasculature in brain by immunohistochemistry [827]. The SR-B is a ligand for oxidized LDL, such as acetylated LDL [828]. Acetylated LDL is endocytosed, but not transcytosed, across the BBB in vivo as demonstrated by internal carotid artery infusion with capillary depletion [506]. Therefore, the BBB SR-B is only an endocytosis system, and does not mediate transcytosis through the BBB [506]. The microvascular SR-B/CD36 is believed to participate in phagocytosis at the neurovascular unit [829]. The presence of PS80, or other surfactants, in the PNP formulation is essential for BBB transport [830]. Given that the SR-B is only an endocytosis system at the BBB, the mechanism is unclear by which PS80 enables PBCA PNPs to cross the BBB in vivo. Toxic effects of the PS80-coated PBCA PNP at the BBB are discussed below in Section 9.7 on nanoparticle toxicity.

PNPs are also stabilized by the addition of a corona of polyethyleneglycol (PEG) on the surface of the nanoparticle [831]. PNPs were prepared from 45 kDa poly(lactic acid) (PLA) and PEG conjugated poly(lactic coglycolic acid) (PLGA). The size of the PEG varied from 2 to 20 kDa [831]. Pegylation of PNPs minimizes adsorption of plasma proteins to the surface of the PNP. In the absence of the PEG surface coating, this serum protein adsorption triggers rapid uptake by the reticulo-endothelial system in vivo and accounts for very rapid plasma clearance of the non-pegylated PNP [832].

### 9.2.2. Dendrimers

Dendrimers are tree-like branching structures that can vary in MW from ~1 kDa to ~1000 kDa, and can have a net neutral or cationic charge. A poly(amidoamine) (PAMAM) dendrimer was tritiated and injected intravenously in mice [65]. The cationic dendrimer had a higher organ uptake than the neutral dendrimer. The organ with the highest uptake was the lung and the organ with the lowest uptake was the brain. Dendrimers alone do not cross the intact BBB [833]. Therefore, dendrimers need to be targeted to brain. A PAMAM-PEG-Tf or PAMAM-PEG-Lf conjugate was prepared and injected intravenously in mice [834]. The organs with the highest uptake were liver, lung, spleen, and kidney and uptake by heart and brain was low. Exogenous Tf is not expected to act as a TfR-directed Trojan horse at the BBB in vivo, because the concentration of endogenous Tf fully saturates the BBB TfR [647], as discussed in Section 8.2.1. Lf, a ligand for LRP1, is not expected to act as a BBB Trojan horse, since the LRP1 is not expressed on the endothelium, as discussed in Section 8.2.1. The ultimate utility of amine-terminated dendrimers may be limited by the cytotoxicity of these agents and the aggregation of the cationic dendrimers when mixed with serum [834]. The serum aggregation of cationic dendrimers is similar to the saline-induced aggregation of cationic liposome/DNA complexes [835], which is discussed in Section 10.2.

### 9.2.3. Micelles

Amphiphilic sodium alginate cholesterol derivatives were synthesized and self-assembled into 200 nm micelles, which were loaded with a polar neuroprotective oxysteroid [836]. The micelles alone did not cross the BBB, so the micelles were targeted with lactoferrin (Lf). However, Lf

is not a useful ligand for brain targeting. Although Lf is a ligand for the LRP1, this receptor is not localized to the brain endothelium as discussed in Section 8.1.5. Additionally, Lf is not a ligand for the TfR [837]. The brain uptake of the Lf-targeted micelles was very low, 0.05%ID/g [836], which indicates the micelles are confined to the blood volume of brain. In another application, micelles were formed with distearoylphosphatidylethanolamine (DSPE)-PEG<sup>2000</sup>-CREKA, where CREKA is a pentapeptide that binds fibrin deposits at the tumor vasculature [838]. The micelles were formed at 80 °C, cooled and injected intravenously in mice. The micelles were primarily cleared by liver and kidney and demonstrated minimal, if any, transport across the BBB [838]. Micelles were formed by 24 h incubation in water of GM1 monosialogangliosides, which formed micelles with a mean diameter of 226 nm [839]. It was hypothesized that the GM1 gangliosides form a complex with serum albumin, which then mediates RMT across the BBB via the gp60 albumin receptor expressed in cultured endothelium [840]. However, the albumin receptor is not expressed on brain microvessels [841].

#### 9.2.4. Albumin Nanoparticles

Human serum albumin (HSA) is converted into nanoparticles by an ethanol desolvation/glutaraldehyde cross-linking method [842]. In an effort to deliver the HSA NPs across the BBB, apoE3 was chemically cross-linked to the HSA NPs [843]. As discussed in Section 9.2.1, PBCA NPs coated with PS80 were said to bind apoE to trigger RMT across the LDLR on the BBB [825]. However, the BBB transport of the apoE3-HSA NPs was only evaluated by electron microscopic identification of 200–250 nm electron dense particles in selected fields of mouse brain, and it is difficult to interpret this small sampling. Endocytosis was demonstrated by electron microscopy of bEND.3 brain endothelium in cell culture [843]. There is a rationale for endocytosis in the cultured endothelium, because cultured cells express the LDLR [610]. However, the LDLR is not expressed in brain *in vivo* at the brain microvasculature [562]. Lipid-free ApoE does bind the SR-B scavenger receptor [844], but this receptor at the BBB only mediates endocytosis, not transcytosis, across the BBB [506]. HSA NPs were produced by the ethanol desolvation/glutaraldehyde method as well as by an ethanol desolvation/thermal (90 °C) denaturation method. No coupling of lipoprotein or use of PS80 was used in this investigation [845]. BBB transport was estimated in rats by fluorescent microscopy following the IV injection of a large dose, 50 mg/kg, of the HSA NPs. On the basis of this qualitative microscopy method, the HSA NP was said to cross the BBB by a proposed mechanism of absorptive-mediated transport [845]. However, these HSA NPs were neither cationic or conjugated with lectins, which are the primary mechanisms of BBB absorptive-mediated transport (Section 7).

### 9.3. Lipid-Based Nanoparticles

#### 9.3.1. Liposomes

Liposomes are nanoparticles formed from lipids with an aqueous interior. In contrast, solid lipid nanoparticles (SLN) have a solid lipid interior. The first investigation of drug delivery to brain with liposomes was reported in 1990 [63]. Phosphatidylcholine/cholesterol liposomes were prepared and injected in the carotid artery of Fisher 344 rats with an intra-cranial 9 L glioma. The liposomes did not enter the hemisphere of brain contralateral to the tumor, which indicated liposomes do not cross the BBB in normal brain. There was uptake of the liposomes by the tumor and the brain adjacent tumor [63], because the blood–tumor barrier is leaky in the 9 L glioma model [846]. In this early study, the liposomes were infused into the carotid artery. It was not possible to use the IV route of administration, because liposomes are rapidly cleared from the blood similar to PNPs in the absence of a PEG corona [847]. Stealth liposomes have a PEG corona which produces a longer blood residence time, and Doxil<sup>®</sup> stealth liposomes were evaluated for brain uptake in 1995 [847]. Doxil is doxorubicin encapsulated in liposomes prepared from phosphatidylcholine/cholesterol/PEG<sup>1900</sup>, and was injected intravenously in rats with an intra-cranial glioma [847]. The Doxil liposomes were delivered to the experimental glioma, as this tumor was shown to have a leaky BBB, but the Doxil liposomes were not taken up

by the contralateral brain [847]. This study shows that pegylated liposomes do not cross the intact BBB, similar to the lack of BBB transport of pegylated HSA NPs [843].

### 9.3.2. Solid Lipid Nanoparticles

Solid lipid nanoparticles (SLN) have a solid lipid interior, as opposed to liposomes, which have an aqueous interior. The drug loading capacity of SLNs is not high, and the loading capacity is higher for nano-structured lipid carriers (NLC) [848]. Lipid nanoparticles (LNP) is a generic term that includes liposomes, SLNs, NLCs, and cationic lipoplexes [849]. The early work on SLNs for brain tested BBB transport only in cell culture models [848]. SLNs are particularly suited for drugs with low aqueous solubility. In one SLN application, a drug that is insoluble in water, camptothecin, was incorporated in cetyl palmitate SLNs with and without stabilization by PS80 [850]. The SLNs were formed by heating at 60 °C followed by homogenization and sonication. Brain uptake of the SLN/camptothecin was low unless the PS80 was added to the formulation. The explanation for the PS80 effect was taken from prior work with PBCA NPs [825,826], and it was assumed lipoproteins are bound to the PS80, which triggers uptake via the presumptive LDLR on the BBB. However, in this SLN study [851], as in the PBCA NP work [825,826], no evidence was provided that the LDLR is expressed at the BBB. SLNs require targeting agents to mediate delivery of the particles across the BBB [850], as reviewed below.

## 9.4. Non-Polymeric Nanoparticles

### 9.4.1. Carbon Nanotubes

Carbon nanotubes (CNT) are needle-like structures and may be single walled nanotubes (SWNT) or multi-walled nanotubes (MWNT), which have diameters of 0.4–2 nm and 10–100 nm, respectively, and can be 50 nm to >1000 nm in length [852]. CNTs are allotropes of carbon; CNTs have a tube structure, fullerenes have a cage structure, and graphene is flat. CNTs are produced by electric arc discharge and laser ablation or by passage of carbon-containing vapors in a furnace with a metal catalyst [852]. CNTs are insoluble in water and have to be functionalized by chemical modifications to the carbon lattice for biomedical applications. The ‘needle’ structure of CNTs is believed to facilitate the piercing of cell membranes so that CNTs may gain access to the intracellular compartment [852]. CNTs are toxic to cells [852,853]. SWNTs were loaded with acetylcholine by adsorption of the drug to the walls of the SWCNT and injected intravenously into mice at a dose of 20–50 mg/kg of SWNT, which corresponds to an acetylcholine dose of 4–10 mg/kg [853]. The SWCNTs were said to cross the BBB based on an improved performance by AD transgenic mice in a shuttle box test [853]. SWCNTs were said to cross the BBB based on experiments performed solely in cell culture [854]. MWCNTs were functionalized with surface cationic, anionic, or non-ionic groups and transport across the monolayer of cultured hCMEC/D3 endothelial cells was determined [855]. Cationic and non-ionic MWCNTs were largely confined to the cell glycocalyx. Anionic MWCNTs had the highest rate of transport in cell culture, and no *in vivo* studies of BBB transport of CNTs were performed [855]. Similar to PNPs and SLNs, CNTs must incorporate surface ligands to stimulate endocytosis without cell damage [856].

### 9.4.2. Graphene Oxide, Fullerenes, and Quantum Dots

Graphene is a two-dimensional carbon nanosheet, which is oxidized to form graphene oxide (GO), where the graphene surface is decorated with carboxyl or hydroxyl groups. Certain drugs, such as doxorubicin (Dox), were bonded non-covalently to the GO sheet by  $\pi$ - $\pi$  stacking [857]. The GO surface was also conjugated with PEG, and the Dox-GO-PEG, as well as free Dox, were injected intravenously in rats. Binding of the Dox to the GO-PEG had no effect on the brain uptake of the Dox [857]. The authors concluded that GO nanosheets need to be modified with receptor ligands to facilitate BBB transport, as discussed below.

Fullerenes are 60-carbon caged carbon structures, which are not water soluble. Chemical linking of water soluble groups such as tris-malonic acid produces a water soluble



fullerene designated C3, which is a superoxide dismutase (SOD)-mimetic [858]. The C3 fullerene was injected intravenously in mice, and the brain uptake of the fullerene appeared confined to the blood volume of the mouse, although no corrections for blood volume were performed [858].

Graphene oxide quantum dots are spherical structures with a diameter of about 10 nm [859]. GO carbon dots were conjugated to glucose to facilitate CMT across the BBB on the GLUT1 glucose carrier [860]. The carbon dot was also conjugated with fluorescein, and the glucose/GQD/fluorescein structure was designated GluCD-F. The complex was injected intravenously and BBB transport assessed qualitatively by fluorescent microscopy. It is difficult to confirm BBB transport of the GluCD-F in this small field sample. The GluCD-F dots had a mean diameter of 3.8 nm [860]. However, as shown in Figure 9A, the glucose cavity in the GLUT1 transporter is a highly confined space that has a diameter of only 1.2 nm [347]. Therefore, the GluCD-F structure has a diameter >3-fold greater than the diameter of the GLUT1 cavity, so it is difficult to see how this complex can traverse the BBB via GLUT1. The GLUT1 carrier can be expressed in transfected cells or frog oocytes for direct examination of whether the GluCD-F is transported via GLUT1, but this has not been performed.

#### 9.4.3. Metallic Nanoparticles

Nanoparticles have been produced from several metals including gold (Au), iron oxide (FeO), silver (Ag), and silica.

**Gold nanoparticles (AuNP).** AuNPs of 15 nm diameter were coated with albumin and poly(allylamine), a highly cationic polymer, and injected intravenously in mice [861]. The AuNPs were said to cross the BBB based on fluorescent microscopy, but the fluorescent signal may have been due to the aggregation of the AuNPs at the microvascular surface. In another study, AuNPs did not cross the BBB in the absence of BBB disruption caused by external laser irradiation of the brain [862]. Severe combined immune-deficient (Scid) mice with intra-cranial U87 human gliomas were treated with 13 nm AuNPs conjugated with siRNA, and the AuNPs were observed to cross the leaky blood–tumor barrier but not the BBB in normal brain [863]. A recent review of nearly 40 studies on the use of AuNPs for brain delivery showed an average brain uptake of 0.06%ID/g [864], which is very low and could be explained on the basis of AuNPs residing in the brain blood volume. AuNPs were hypothesized to cross the BBB via calcium or potassium channels [865]. Even very small AuNPs with a diameter of 2.5 nm are large compared to the diameter of the pore size of calcium or potassium channels, which is 0.9–1.5 nm [866–868]. Moreover, AuNPs conjugated with siRNA have a diameter of 19–34 nm [863].

**Silver nanoparticles (AgNP).** AgNPs were combined with PLGA polymeric nanoparticles (PNP), which produced AgPNPs of 191 nm in diameter [869]. The AgPNPs were conjugated with chlorotoxin, a 36-AA scorpion toxin that binds the matrix metalloproteinase 2 (MMP2) of glioma cells, and was sequestered in a flank glioma in mice after IV administration [869]. No studies of AgPNP transport across the intact BBB in brain were performed.

**Silica nanoparticles (SiNP).** SiNPs were prepared from tetraethylorthosilicate [870], which is  $(\text{CH}_3\text{CH}_2\text{O})_4\text{-Si}$ . The SiNPs were infused in the carotid artery of rats, and the brain was stained with a silica selective fluorescent compound used to detect silica in soils. Based on fluorescent microscopy [870], the SiNPs were said to cross the BBB, although the micrographs suggest the SiNPs are largely sequestered within the vasculature. In another study [871], SiNPs were produced from tetraethylorthosilicate and the surface was coated with PEG-poly(ethyleneimine), or PEI, which is a cationic polymer. The functionalized SiNPs were injected in the mouse and brain uptake visualized by two-photon microscopy through a cranial window. The SiNPs were said to cross the BBB [871], although inspection of the micrographs suggest the SiNPs are largely sequestered within the vasculature.

**Magnetic iron nanoparticles.** Iron NPs (FeNP) are magnetic and designated superparamagnetic iron oxide nanoparticles or SPION [872]. SPIONs were functionalized by

adsorption of PEG and PEI to the surface and stabilized by the addition of PS80. The SPIONs were injected intravenously in the rat, which was subjected to an external magnetic field (EMF) by fixation of a magnet over the skull. In the absence of either the EMF or the PS80, there was no brain uptake of the SPIONs; however, brain uptake of the PS80-stabilized SPIONs was observed in the rats subjected to an EMF [872]. This work was said to provide the basis for therapeutic applications of Tween-SPIONs under EMF [872]. Iron oxide NPs were mixed with a complex of PEI and DNA to form FeNPs. These were added to cultured cells for the assessment of gene expression, a process named magnetofection [873]. However, exposure of cultured cells to a magnet did not enhance gene expression with the FeNPs. The diameter of the FeNPs in water was ~150 nm. However, when the FeNPs were added to tissue culture medium, the FeNPs aggregated to a diameter >1 micron [873]. Such aggregation stimulates phagocytosis [874], which appears to be the principal mechanism for cell entry of the FeNPs coated with PEI/DNA.

In summary, despite the diversity of nanoparticle formulations that have evolved over the last 25 years, the data reviewed above show that nanoparticles do not cross an intact BBB. The one exception to this rule may be PBCA polymeric nanoparticles that are coated with the surfactant, PS80 [825,833]. An early study of PS80-coated PBCA nanoparticles and brain delivery showed pharmacologic effects could be attributed to the toxic effects of the PBCA polymer, which were augmented by the PS80 detergent [875], and the toxicity of PS80/PBCA PNPs is discussed further in Section 9.7. Given the lack of nanoparticle transport across the BBB, nanoparticles need to be re-formulated to access endogenous transport systems within the BBB, similar to classic small or large molecules discussed in Sections 6–8. As reviewed in Section 9.5, nanoparticles have been functionalized in a variety of ways so as to undergo transport through the BBB via CMT, AMT, or RMT mechanisms. In addition, nanoparticles have been delivered to brain with BBB avoidance strategies, such as BBBD with focused ultrasound, intra-cerebral delivery with convection-enhanced diffusion, or trans-nasal delivery.

### 9.5. Mediated Blood–Brain Barrier Delivery of Functionalized Nanoparticles

#### 9.5.1. Carrier-Mediated Transport of Nanoparticles

To facilitate nanoparticle transport across the BBB, micelles were produced with a PEG<sup>2000</sup>-poly( $\alpha,\beta$ -polyaspartic acid) co-block polymer, which included a terminal D-glucose moiety, so as to enable BBB passage via the GLUT1 glucose transporter [876]. Fluorescent microscopy showed the micelles were largely trapped in the intra-vascular compartment of brain and no quantitative measurement of brain uptake was reported. Pegylated PLGA nanoparticles were conjugated with ascorbic acid to facilitate transport of the PNPs across the BBB via the sodium dependent vitamin C (SVCT) carrier [877]. However, ascorbic acid does not cross the BBB; instead dehydroascorbate, the oxidized form of vitamin C, crosses the BBB via the GLUT1 transporter [878]. Similarly, dehydroascorbate, rather than ascorbate, is the form of vitamin C that crosses the blood–retinal barrier (BRB) on the GLUT1 carrier [879]. Transport of the ascorbate-targeted PEG-PLGA nanoparticles was demonstrated only in a cell culture model or with neurobehavior tests, without in vivo measurements of BBB transport [877]. AuNPs were targeted with L-DOPA to enable transport via the LAT1 large neutral amino acid carrier at the BBB, and BBB transport was only assessed with cell culture models [880]. Dendrimer-based micelles encapsulating doxorubicin (DOX) were conjugated with choline to enable transport on the BBB choline carrier, which is presumed to be CTL1, as discussed in Section 6.2.6. Whereas DOX uptake in a leaky experimental brain tumor was increased, the uptake of DOX across the intact BBB was negligible [881]. Pegylated liposomes were conjugated with the tripeptide, glutathione (GSH), on the assumption that a GSH transporter is expressed at the BBB [882]. However, as discussed in Section 8.2.1, GSH does not cross the BBB [677], and a GSH transporter at the BBB has not been identified [678].

The available data show that targeting CMT systems at the BBB for nanoparticle delivery is not advisable. Nutrients traverse the SLC CMT systems via narrow, stereospecific

cavities, as illustrated for the GLUT1 or LAT1 carriers in Figure 9. The width of these cavities is about 1 nm, as discussed in Section 6.2.1. There is no direct evidence that even small nanoparticles can fit through these CMT cavities. The SLC carriers do not mediate endocytosis, as is the case for the RMT systems, which means there is no plausible mechanism by which nanoparticles can be transported by the CMT systems. The counter argument is that certain viruses, which have a size comparable to a nanoparticle, enter cells by first binding a CMT system. As discussed in Section 6.2.3, the murine ecotropic retrovirus binds CAT1 [379], as does the bovine leukemia virus (BLV) [883]. The human T cell leukemia virus binds GLUT1 [884]. However, virus endocytosis into cells is a two-step process of binding to a cell membrane receptor, e.g., a CMT system, followed by membrane fusion, which then triggers endocytosis. This two-step process is illustrated with the Severe Acute Respiratory Syndrome Coronavirus 2 [885]. The S1 domain of the virus spike protein binds the cell membrane receptor, angiotensin converting enzyme 2 (ACE2). Binding to ACE2 alone does not trigger endocytosis of the virus. After ACE2 binding, the spike protein is cleaved by furin into the separate S1 and S2 subunits, and the cleaved S2 subunit fuses with the cell membrane to enable virus endocytosis [885]. Nanoparticles targeting a CMT system would need to be further functionalized with a membrane fusion domain.

#### 9.5.2. Absorptive-Mediated Transport of Nanoparticles

Nanoparticles have been modified by the addition of cationic agents, such as protamine or cationized albumin to facilitate BBB transfer via the AMT mechanism reviewed in Section 7. Cisplatin loaded PLGA PNPs were cationized by loading protamine to the surface of the nanoparticle [886]. However, BBB transfer was only evaluated in cell culture. Pegylated poly(lactic acid) (PLA) PNPs were prepared and surfaced conjugated with cationized bovine serum albumin (cBSA) with a thio-ether bond [887]. However, BBB transport was only assessed with an in vitro model, where transport of the cBSA-PNPs moved across the endothelial monolayer faster than PNPs conjugated with native bovine serum albumin [887]. Pegylated liposomes were covalently conjugated with cBSA, and brain uptake was assessed in vivo [888]. However, after IV injection in rats, the cBSA-liposomes were confined to the vascular wall without significant transport into brain parenchyma [888]. Cationized bovine serum albumin was conjugated to a PAMAM dendrimer, which was mixed with a DOX loaded PLGA PNP so as to enhance BBB transport of the DOX chemotherapeutic agent. However, BBB transport was only assessed in vitro [889]. As discussed in Section 7, AMT at the BBB can also be mediated by lectins such as WGA. This lectin was conjugated to PEG-PLA PNPs and cell uptake and toxicity was assessed in cell culture. The higher the WGA content of the nanoparticle, the higher the cell uptake, but the greater the cell toxicity [890]. The toxicity of the WGA nanoparticle is not unexpected given the known toxicity of this lectin as discussed in Section 7.3.2. In summary, the delivery of nanoparticles across the BBB via AMT pathways used by cationic proteins or lectins is not promising, owing to the sequestration of the complex in the endothelial compartment and to the toxicity of cationic proteins or lectins (Section 7.3).

#### 9.5.3. Receptor-Mediated Transport of Nanoparticles

The RMT delivery of nanoparticles across the BBB is similar to the delivery of large molecule biologics. Nanoparticles alone do not cross the non-disrupted BBB, as reviewed in Sections 9.2–9.4. Similar to biologics, the BBB transport of nanoparticles is not possible using CMT systems, as these transporters generally do not undergo endocytosis. Additionally, similar to biologics, the re-formulation of nanoparticles to access RMT systems within the BBB provides greater brain uptake as compared to nanoparticles that access AMT systems. As reviewed below, both peptides and receptor-specific MAb have been used as Trojan horses to enable RMT of nanoparticles across the BBB.

**Transferrin receptor antibody-targeted nanoparticles.** The first nanoparticle formulated for RMT across the BBB was reported in 1996 in the form of pegylated immunoliposomes [891], also called Trojan horse liposomes (THL). Pegylated liposomes were surface

conjugated with the mouse OX26 MAb against the rat TfR, and BBB transport was demonstrated *in vivo* in the rat [891]. The optimal use of THLs is the brain delivery of plasmid DNA for non-viral brain gene therapy, as discussed in Section 10.2. Subsequent to the description of BBB-penetrating pegylated immunoliposomes, pegylated PLA nanoparticles conjugated with the OX26 TfRMAb for brain delivery was described in 2002 [892]. The PNPs were produced from methoxy-PEG<sup>2600</sup>-PLA<sup>40000</sup> and maleimide-PEG<sup>3500</sup>-PLA<sup>40000</sup> with an emulsion/solvent evaporation method with 1% sodium cholate as a surfactant. The diameter of the pegylated PLA nanoparticles was  $121 \pm 5$  nm, based on dynamic light scattering. Transmission EM showed most of the PNPs had a diameter of  $\sim 100$  nm, although a few were 200–300 nm in size, as shown in Figure 15A.

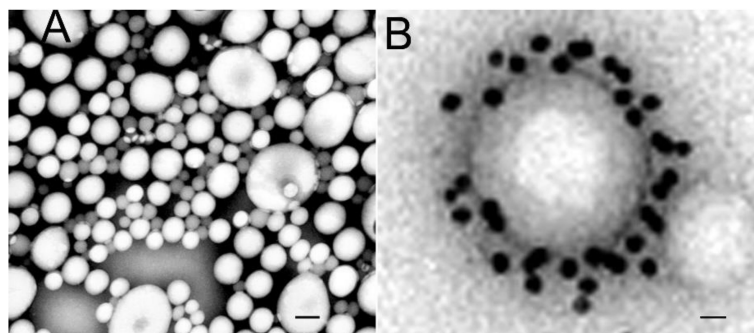


**Figure 15. Pegylated immuno-nanoparticles.** (A) Transmission EM of pegylated PLA nanoparticles counter-stained with phosphotungstic acid. Magnification bar = 100 nm. (B) Transmission EM of the complex of the OX26 antibody-pegylated immunonanoparticles bound by a 10 nm gold conjugated secondary antibody. Magnification bar = 15 nm. Reproduced with permission [892], Copyright© 2002 Springer-Nature.

The OX26 antibody was thiolated with 2-iminothiolane in parallel with production of the pegylated nanoparticles. The thiolated OX26 antibody was conjugated to the PEG-extended maleimide group on the surface of the nanoparticle to form a stable thio-ether linkage. The conjugation of the OX26 antibody to the surface of the pegylated nanoparticle is shown in Figure 15B. The relationship of the OX26 antibody and the nanoparticle surface was examined by binding a 10 nm gold conjugated secondary antibody to the pegylated immunonanoparticle, followed by washing and electron microscopy (Figure 15B). The number of OX26 antibodies conjugated per pegylated immunonanoparticle was  $67 \pm 4$  [892].

The OX26 TfRMAb is specific only for the rat TfR, and is not active in mice [663]. TfR antibodies that react with the mouse TfR that could be used for BBB delivery in the mouse were described in 2000, as it was shown the rat 8D3 MAb against the mouse TfR, or the rat RI7-217 MAb against the mouse TfR, penetrated the BBB in the mouse [663]. Just as the OX26 antibody is active in the rat, but not the mouse [663], the RI7-217 antibody is active in the mouse, but not in other species [691]. The species specificity of the TfRMAbs has not been considered in several studies of NP targeting to brain with a MAb against the TfR. For example, the BBB transport of OX26-targeted liposomes was evaluated in a human endothelial hCMEC/D3 culture model [893], but the OX26 TfRMAb does not recognize the human TfR [689]. If human cells are used as a model system, then a TfRMAb specific for the human TfR should be used, such as the 128.1 TfRMAb against the human TfR [894]. Pegylated chitosan nanoparticles were conjugated with the OX26 antibody [895]. However, these *in vivo* transport studies are difficult to interpret, since the studies were conducted in the mouse [895], and the OX26 antibody is not active in the mouse [663]. In another report confounded by species specificity of the TfRMAbs, pegylated PLA PNPs were conjugated with the OX26 antibody, and BBB transport was tested in cell culture with human cells, and *in vivo* in the mouse [896]. The OX26 antibody is not active in humans [689] or mice [663]. OX26-targeted pegylated immunoliposomes were prepared and the TfRMAb was bound to the surface of the liposome with a biotin-streptavidin bridge [893], as originally described by Huwyler and colleagues [897]. However, the BBB

transport of the OX26-targeted liposomes was then evaluated in the human CMEC/D3 endothelial line in cell culture [893], where the OX26 antibody does not react with the human TfR [894].

If the TfRMAb is matched to the correct species, then successful RMT delivery of NPs to brain is possible. PLGA PNPs encapsulating the opioid tetrapeptide, endomorphin, were conjugated with the OX26 antibody, and the effect on analgesia was tested in rats [898]. Pegylated PLA PNPs were conjugated with the OX26 antibody and BBB transport was demonstrated by cerebral microdialysis in rats [899]. Pegylated mesoporous silica nanoparticles were conjugated with the rat RI7-217 antibody against the mouse TfR, and BBB transport was demonstrated in cell culture using the mouse bEND5 cells and in vivo in the mouse using fluorescent microscopy [900]. BBB transport of nanoparticles in the mouse was investigated with AuNPs conjugated with the rat 8D3 antibody against the mouse TfR [901]. The AuNPs could be visualized by electron microscopy at the luminal endothelial membrane, within intra-endothelial vesicles, and at the abluminal endothelial membrane [901]. It was hypothesized that the 8D3 conjugated AuNPs were not released by the abluminal TfR into the brain parenchyma [901]. However, it is not expected that gold particles in the post-vascular brain could be visualized at the EM level, owing to the volumetrics of the brain. As discussed in an early 1994 study on the EM of rat brain following carotid arterial infusion of a 5 nm gold-OX26 conjugate [585], the volume of the brain extracellular space, 200  $\mu\text{L/g}$ , is 250-fold greater than the volume of the brain endothelial compartment, 0.8  $\mu\text{L/g}$ . Therefore, the gold particles undergo a 250-fold dilution subsequent to exocytosis at the abluminal membrane.

**Insulin receptor antibody-targeted nanoparticles.** THLs were targeted with a MAb against the human insulin receptor (HIR), which cross reacts with the insulin receptor of Old World monkeys, and the HIRMAb-targeted THLs were encapsulated with a  $\beta$ -galactosidase expression plasmid. IV administration of these THLs produced widespread expression of the transgene in Rhesus monkey brain [902], as discussed in Section 10.2. The same HIRMAb was conjugated to polymersomes produced from an amphiphilic diblock copolymer, and endocytosis of the nanoparticles was followed by fluorescent microscopy in human hCMEC/D3 endothelial cells [903]. Another antibody against the HIR, the 29B4 antibody, was incorporated in albumin nanoparticles, and the 29B4 conjugated nanoparticles produced analgesia following IV administration in mice [904]. These results are difficult to interpret, because the 29B4 antibody is directed against the tyrosine kinase (TK) domain of the beta subunit of the HIR [905], and this TK domain is localized within the intracellular region of the HIR (Figure 10B). An antibody in plasma cannot access the epitope on the receptor that is localized within the intracellular compartment. Antibodies used as BBB RMT Trojan horses bind exofacial epitopes on the extracellular domain of the receptor, which are accessible to the blood-born antibody. The extracellular domains of either the HIR or the human TfR1 are shown in Figure 10.

**Transferrin- and lactoferrin-targeted nanoparticles.** Nanoparticles have been conjugated with transferrin (Tf) for brain drug delivery [906–909]. The problem with using Tf as a Trojan horse is that the exogenous Tf, conjugated to the nanoparticle, must compete with the endogenous Tf in plasma. The concentration of holo-Tf in plasma, 25,000 nM, is nearly 1000-fold greater than the concentration, 40 nM, of the TfR1 at the BBB [559]. Therefore, the BBB TfR is >99.9% saturated with endogenous Tf. For this reason, a TfRMAb Trojan horse, which binds the apical region of the TfR (Figure 10C), a site spatially removed from the holo-Tf binding site, is the preferred type of TfR Trojan horse. The other factor to consider in the use of Tf as a Trojan horse is the iron content of the Tf. Apo-Tf does not bind the TfR at physiological pH, and mono-ferric Tf binds the TfR with an 8- to 9-fold lower affinity than the di-ferric form of Tf [575]. Iron loading of Tf to produce di-ferric Tf has been described [586]. Lactoferrin (Lf) has been conjugated to polymeric nanoparticles for brain drug delivery [908]. The problem with using Lf as a Trojan horse is that Lf is a ligand for LRP1, and LRP1 is not expressed at the luminal endothelial membrane, as discussed in Section 8.2.1.

**Folic acid-targeted nanoparticles.** Stearic acid SLNs were incorporated with a conjugate of stearic acid and folic acid [910]. The folate conjugated SLNs incorporated docetaxel and ketoconazole, both highly water insoluble chemotherapeutic agents, which are favored agents for SLN delivery. The use of folic acid as a BBB Trojan horse assumes the folate receptor (FOLR1, Table 3) is the principal folate transporter at the BBB. Folate is also transported by the reduced folate carrier (FRC). There is evidence for expression at the BBB of both the FOLR1 [427], which is an RMT system, and the FRC [426], which is a CMT system, as discussed in Section 6.2.7. If FOLR1 is the primary folate transporter at the BBB, then folate conjugated nanoparticles may undergo RMT across the BBB. However, the FRC is a CMT system, and if FRC is the primary BBB transporter for folic acid, then it is unlikely that folate conjugated nanoparticles may traverse the BBB via very narrow cavity of a CMT system, as discussed in Section 9.5.1.

**Dual receptor targeting of nanoparticles.** The dual receptor targeting of pegylated liposomes was reported in 2002 using both the 8D3 antibody, for targeting the mouse TfR, and the 83-14 antibody, for targeting the HIR in an experimental intra-cranial human glioma model in the mouse [911]. These dual targeted THLs are discussed further in Section 10.2. Subsequently, sphingomyelin/cholesterol liposomes were dual targeted with the RI7-217 rat antibody against the mouse TfR, and phosphatidic acid, which targets the Abeta amyloid peptide of AD [912]. However, BBB transport of the liposomes was evaluated in culture with human hCMEC/D3 endothelial cells, which express the human TfR, and the human TfR is not recognized by the RI7-217 antibody [691]. Pegylated liposomes were dual targeted with the OX26 antibody against the rat TfR and the 19B8 antibody against the Abeta amyloid peptide of AD [913]. One antibody was thiolated and conjugated to a PEG terminal maleimide moiety, and the other antibody was biotinylated and conjugated with a streptavidin bridge to a PEG terminal biotin group [913].

**Peptide targeting of nanoparticles.** The 29AA rabies virus glycoprotein (RVG) peptide was conjugated to PLGA nanoparticles [914], based on the assumption the RVG peptide targets the nAChR on the BBB as suggested by Kumar et al. [297]. However, CNS uptake of the PLGA nanoparticles was not enhanced by the RVG peptide [914], which is consistent with the lack of expression of the putative RVG receptor, the nAChR, at the brain endothelium as discussed in Section 8.1.7. Pegylated SLNs were targeted with the apoE141-150 peptide, which corresponds to AA 141-150 of the human apolipoprotein E (P02649), on the assumption this ligand would trigger RMT across the LDLR at the BBB [915]. However, fluorescent microscopy showed the apoE-targeted SLNs did not cross the BBB [915], which is consistent with the lack of expression of the LDLR at the BBB in vivo, as discussed in Section 8.1.6. The same apoE141-150 peptide was conjugated to PLGA nanoparticles, and brain uptake of the nanoparticles was monitored by fluorescent microscopy [916]. The sequence of the apoE141-150 peptide is LRKLRKRLLR, which has a pI of >10. To the extent this peptide mediates BBB transport, the mechanism is most likely not RMT via a LDLR, but rather AMT owing to the highly cationic charge of the peptide.

In summary, NP functionalization with ligands that trigger RMT across the BBB is necessary because NPs alone do not cross the BBB, as reviewed in Sections 9.2–9.4. The importance of functionalization of nanomedicines for transport across vascular barriers has been recently reviewed [917]. Functionalization with ligands that promote NP transport via CMT is not effective, as the NPs cannot fit within the narrow transport cavities of a CMT, as reviewed in Section 9.5.1. Delivery of NPs via AMT is not optimal, owing to the high degree of sequestration of the NP within the endothelial compartment of brain following endocytosis via an AMT process, as reviewed in Section 9.5.2. The optimal approach to NP functionalization for brain drug delivery is the incorporation on the NP surface of receptor-specific MABs that trigger RMT of the NP across the BBB. However, the TfR-specific MABs, e.g., the rat 8D3 MAB against the mouse TfR, the rat RI7-217 MAB against the mouse TfR, or the mouse OX26 MAB against the rat TfR, are species-specific. The OX26 TfRMAB does not recognize either the mouse TfR [663] or the human TfR [689]. The RI7-217 TfRMAB does not recognize the human TfR [691], and has not been shown

to bind with high affinity to the rat TfR. Therefore, it is important to match the species specificity of the TfRMAb with the species of the animal model or the species of origin of cells in culture.

#### 9.5.4. Brain Delivery of Nanoparticles with BBB Avoidance Strategies

Nanoparticles do not cross the BBB in the absence of a BBB delivery technology (Sections 9.2–9.4). In the absence of re-formulating the nanoparticles with a receptor-specific ligand to enable RMT at the BBB, one of the BBB avoidance strategies must be employed. These include convection-enhanced diffusion (CED) (Section 2.2.2), trans-nasal delivery (Section 3), and BBBD with focused ultrasound (Section 4.2). In an early study of CED and nanoparticles, camptothecin loaded PLGA PNPs were infused into the brain for 30 min by CED 7 days after implantation of a 9 L intra-cranial glioma in Fischer CD344 rats [918]. The infusion of a dose of 0.25 mg of the camptothecin had no effect on survival, although the infusion of a dose of 0.5 mg camptothecin in the PNPs increased median survival from 17 to 22 days. As reviewed in Section 2.2.2, clinical trials with the CED delivery system for brain conditions have failed. Therefore, in an effort to enhance drug distribution into the brain following CED, PLGA nanoparticles, with or without pegylation, were infused in the brain via CED in either isotonic (0.9%) or hypertonic (3%) saline [919]. The combination of pegylation of the PLGA PNPs, drug administration via CED, and the infusion of 3% hypertonic saline increased the distribution of the infusate in brain. This effect is presumed to be due to shrinkage of brain cells owing to osmotic fluid shifts in brain caused by the hypertonic saline infusion. Brain delivery of nanoparticles via the trans-nasal route was examined in mice following the nasal instillation of 5  $\mu$ L/nostril of a microemulsion of clobazam [920]. However, clobazam is a lipid-soluble small molecule with a MW of 301 Da and low hydrogen bonding, and is a benzodiazepine that crosses the BBB [921]. As reviewed in Section 3, such molecules may gain access to brain following nasal instillation by first passing from the nose to the blood compartment and then entry into brain across the BBB. In another study of nasal delivery of nanoparticles, paclitaxel was formulated in PLGA PNPs and infused into the nose in large volumes of 25  $\mu$ L in each nostril in the mouse with a pressurized olfactory device [922]. This volume of drug instilled is equal to the entire nasal volume in the mouse [148]. As reviewed in Section 3.2, this instillation of such a large volume causes local injury to the nasal mucosa. AuNPs were administered to mice in conjunction with BBBD induced by focused ultrasound (FUS) [923]. The size of the AuNPs varied from 3 nm to 15 nm to 120 nm. The dose of the microbubbles was  $8 \times 10^7$  per mouse IV, and the acoustic pressure used was 0.5–0.7 MPa. The highest distribution of AuNPs in brain was produced with the 15 nm AuNPs and an acoustic pressure of 0.7 MPa [923]. As discussed in Section 4.2, the FUS/microbubble form of BBBD creates pores at the BBB owing to opening of tight junctions. The 120 nm AuNPs may have a diameter that exceeds the transitory pores in the BBB caused by the FUS/microbubble procedure. BBBD caused by the FUS/microbubble treatment can lead to neuropathology (Section 4.2). As discussed below, nanoparticle administration is not without toxicity, as discussed below. Therefore, the NP toxicity would be additive with a toxicity profile of the BBB avoidance strategy, such as CED, nasal administration of large volumes, or FUS/microbubble BBB disruption.

#### 9.6. Nanoparticle Clinical Trials for the Brain

The NP-based pharmaceuticals that are FDA approved are nearly all liposomal formulations, and none are approved for the CNS [924]. FDA-approved formulations include:

- Pegylated and non-pegylated liposomes encapsulating cancer chemotherapeutic agents including doxorubicin, cytarabine/daunomycin, vincristine, irinotecan;
- Liposomes encapsulating amphotericin B for fungal infections;
- Liposomes encapsulating verteporfin for macular degeneration;
- Cremophor-free paclitaxel re-formulated as albumin nanoparticles for cancer;
- siRNA in cationic pegylated liposomes for hereditary transthyretin amyloidosis;

- Iron replacement therapies;
- Imaging agents.

Additional liposomal agents are in clinical trials as reviewed recently [924]. However, few of these clinical trials are designed for CNS indications, with some exceptions [925]:

- SGT-53 was developed as a treatment for brain cancer [926]. SGT-53 is a plasmid DNA encoding the p53 tumor suppressor gene that is adsorbed to cationic liposomes conjugated with a ScFv antibody against the human TfR [926]. This ScFv was derived from the 5E9 antibody [927], also known as the HB21 antibody [928]. The ScFv against the human TfR was chemically conjugated to the liposomal lipids with a thio-ether linkage. SGT-53 was administered to patients with recurrent glioblastoma multiforme (GBM) concurrent with temozolomide treatment (NCT02340156). Only one patient was enrolled and the trial was terminated. The SGT-53 formulation is a cationic lipoplex of DNA, and such agents demonstrate aggregation problems, as discussed in Section 10.2.
- MTX-110 is a complex of panobinostat, a histone decarboxylase inhibitor, and hydroxylpropyl  $\beta$ -cyclodextrin [929]. MTX-110 is a soluble form of panobinostat, which is poorly soluble in water. MTX-110 does not cross the BBB, and this formulation has been administered to rats by CED [929] and to primates by infusion in the fourth ventricle [930]. MTX-110 was administered to patients with a pontine glioma by CED; the phase 1 trial in 7 patients concluded in February 2022, with no advancement to phase 2 (NCT03566199).
- ARCT-810 is a mRNA encoding ornithine transcarbamylase (OTC) formulated in a LNP for the treatment of late onset OTC deficiency. This condition can lead to seizures, brain edema, and death [931]. The ARCT-810 clinical trial was initiated in 2020 and is ongoing (NCT04442347). The details of ARCT-810 manufacturing are not available, and it is not clear if this was formulated as a lipoplex/RNA mixture or if the mRNA was fully encapsulated in the LNPs.
- CNM-Au8 is a preparation of gold nanocrystals which are daily administered orally at a dose of 30 mg, and were tested in a phase 2 trial for ALS [932]. The trial was completed in 2022 and no results were yet reported (NCT04098406). It is not clear how such AuNPs, which are not functionalized, can cross the BBB in ALS. The BBB is intact in ALS [933].
- ABI-009 is a preparation of albumin NPs complexed with the macrolide antibiotic, rapamycin, an anti-tumor agent, which is administered to patients with newly diagnosed GBM (NCT03463265). The trial was first posted in 2018, and no results have been reported. Since the albumin NPs are not functionalized, no transport across the intact BBB is expected. The BBB may be leaky in the tumor area of GBM to small molecules [191]. However, much of the GBM tumor retains an intact BBB, and tumor eradication is not possible unless all cancer cells within the tumor are exposed to the therapeutic [934]. Therefore, new treatments for GBM need to be formulated or engineered to enable transport across an BBB.
- NU-0129 is an AuNP conjugated with siRNA and designated a spherical nucleic acid (SNA) [935]. The siRNA targets the Bcl1Like12 oncogene [935]. NU-0129 is said to be BBB-penetrating, but the AuNP is not functionalized. Only the gold part of this NU-0129 was tested for brain penetration, not the siRNA part. The siRNA was simply adsorbed to the surface of the AuNP, and there is immediate separation of the AuNP and the siRNA following IV administration [935]. The plasma  $T_{1/2}$  of the siRNA is  $5.4 \pm 5.1$  min, whereas the plasma  $T_{1/2}$  of the gold is  $17 \pm 6$  h [935]. A phase 1 trial in recurrent GBM was initiated for NU-0129 in 2017 with the last posting in 2020 and no study results are available (NCT03020017).

In summary, there are no nanoparticle formulations FDA approved for CNS diseases, and based on the ongoing clinical trials reviewed above, this situation is not likely to change in the near future. The challenge with nanoparticles for the brain is the same as that for biologics for the brain—FDA approval is unlikely unless the biologic, or the nanoparticle,



is re-engineered to enable transport across an intact BBB, preferably via an endogenous BBB RMT pathway.

### 9.7. Nanoparticle Neurotoxicology

There are several reviews on the neurotoxicology that follows from the accumulation of nanomaterials in the brain [936–940]. The greatest toxicity is observed with the chronic administration of either metallic NPs or CNTs/fullerenes. With respect to metallic NPs, toxicity is found after the administration of AuNPs [941–943], AgNPs [944,945], iron NPs [946], silica NPs [947], and titanium NPs [948]. Pregnant mice were fed AgNPs orally from the first to last day of gestation [944]. The silver content of brain increased 14-fold and 22-fold following the feeding of 30 nm and 10 nm AgNPs, respectively, which was associated with increased gene expression of inflammatory cytokines and impaired cognition [944]. Similar findings were made in rats fed AgNPs [945]. Silver ions may gain access to brain from blood similar to mechanisms that mediate the brain uptake of copper ions. Internal carotid perfusion studies show that copper gains access to brain via carrier mediated transport at the BBB of the free copper ion [949]. The SLC31 sub-family encodes for copper transporters (CTR) [950].

Pegylated graphene oxide (GO) nanosheets are toxic to cells following partial insertion in the cell membrane, which triggers an inflammatory response [951]. The intra-cerebral injection of C60 fullerenes into the hippocampus reduces neurotrophic factors and causes neuro-behavioral changes [952]. CNTs, including SWCNTs or MWCNTs, are particularly toxic to vascular cells both in brain and peripheral tissues [938]. Reduced graphene oxide NPs with an average diameter of 340 nm caused BBB disruption following an IV injection of 7 mg/kg in rats, and electron microscopy showed leaky tight junctions [953].

In addition to metallic NPs, and CNT/fullerene/GO nanoparticles, polymeric NPs may also cause toxicity in brain. PBCA NPs coated with polysorbate-80 (PS80) were the first NPs to be shown to cross the BBB [64], as reviewed in Section 9.2.1. The PBCA NPs were said to cross the BBB on the basis of analgesia induced by dalargin loaded nanoparticles [64]. Nanoparticle administration induced dalargin analgesia only if PS80 was added to the formulation. Subsequently, it was shown that the addition of PS80 causes rapid desorption of the opioid peptide from the PBCA NPs [875]. The impact of PS80-coated PBCA NPs on BBB integrity was examined with an in vitro BBB model [954]. The addition of PS80-coated PBCA NPs to the endothelium caused a dose-dependent disruption in the BBB, as measured by trans-endothelial electrical resistance (TEER). BBB disruption induced by the PS80-coated PBCA NPs caused enhanced flux across the endothelial monolayer of sucrose or albumin, which do not cross an intact BBB [954]. Significant toxicity was observed following the IV administration of PS80-coated chitosan NPs [955]. The PS80-coated chitosan NPs were demonstrated to cross the BBB by external fluorescent microscopy. Daily administration of 3–30 mg/kg of the NPs caused a dose-dependent decrease in body weight in rats [955]. A microscopic examination of the brain showed apoptotic and necrotic neurons and reduced GFAP reactive cerebellar astrocytes [955].

In summary, both polymeric and non-polymeric NPs may prove to have a significant toxicity profile with chronic administration. The toxicity of a pharmaceutical following long-term, e.g., 6 months, administration is generally not examined in detail until an Investigational New Drug (IND) application is submitted to the FDA to seek approval for a human phase 1 clinical trial [956]. The safety pharmacology and toxicology performed under Good Laboratory Practice (GLP) procedures in either a primate, or two lower species, is a required component of an IND. Only a few nanoparticle formulations for the brain have been tested in a clinical trial, as reviewed in Section 9.6. Therefore, few GLP safety pharmacology and toxicology evaluations of long-term nanoparticle administration have been performed.

An IND application also requires demonstration of a scalable manufacturing process under Good Manufacturing Practice (GMP) or ‘clean room’ conditions [957]. Few nanoparticle formulations for the brain have passed the rigors of a scalable GMP manufacturing

process, or the demonstration of long term, e.g., 2-year stability with storage. The challenges in scalability, process development, fill/finish, in-process testing, and release testing required for human pharmaceuticals will also have to be mastered for nanoparticle drugs for the brain, as recently reviewed [958]. A limiting problem for nanoparticles, which also limits development of liposomal formulations, is both (a) poor loading of the nanoparticle with drug, and (b) leakage of loaded drug from the nanoparticle on storage [959]. Doxorubicin is one of the few small molecules to be commercialized as a liposomal formulation, and a reason for this is that doxorubicin precipitates inside the liposome [960], which eliminates leakage on long term storage. Doxorubicin forms covalently bonded dimers in aqueous solution, which causes precipitation of the drug in the aqueous interior of the liposome [961].

## 10. Gene Therapy of the Brain

### 10.1. Viral Gene Therapy of Brain

#### 10.1.1. Lentiviral-Transfected Stem Cells

The lentivirus (LV) is a retrovirus, which permanently integrates into the host genome. Therefore, there is a risk of long-term cancer with this virus [962]. Following introduction of the expression cassette encoding the therapeutic gene into the LV genome, hematopoietic stem cells (HSC) are permanently transfected *ex vivo*, and this transfection is quantified by determination of the vector copy number (VCN), which is the number of LV genomes inserted into the HSC. So as to reduce the risks of insertional mutagenesis, the FDA requires a  $VCN < 5$  [294]. Mutations in the gene encoding the lysosomal enzyme, arylsulfatase A (ASA), causes metachromatic leukodystrophy (MLD), and nine MLD patients were treated with the LV-HSC-ASA gene therapy [963]. Long term follow-up showed normal ASA enzyme activity in peripheral blood lymphocytes and in CSF [964], as measured with an enzymatic fluorometric assay using 4-methylumbelliferyl sulfate (4-MUS) as the substrate [965]. These enzyme activity results are difficult to evaluate, because 4-MUS is hydrolyzed by arylsulfatase B and other O-sulfatases, and is not specific for ASA. A preferred surrogate marker would be immunoreactive ASA as determined by ELISA or similar methodology. The CSF data are difficult to assess, as any sulfatase in plasma would be expected to pass the blood–CSF barrier to enter CSF, as discussed in Section 2.1.2. The underlying difficulty with the HSC-LV approach is the lack of stem cell transport across the BBB, as discussed in Section 5.1.

#### 10.1.2. Adenovirus

Adenovirus (AV) is a common cold virus, and the majority of the human population has a pre-existing immunity to AV [966]. AV was evaluated as a vector for delivery of a transgene gene to the brain following intra-cerebral injection of the virus. In 1993, replication deficient AV encoding  $\beta$ -galactosidase was injected directly into rat brain, and gene expression was followed by  $\beta$ -galactosidase histochemistry [967]. The  $\beta$ -galactosidase transgene expression persisted for 45–60 days. However, by 1999, the AV virus was shown to produce an inflammatory reaction in brain, including microglial activation, astrogliosis, and demyelination in rats [968] and primates [969]. Additionally, in 1999, a patient with partial ornithine transcarbamylase (OTC) deficiency received a high intravenous dose,  $3.8 \times 10^{13}$  particles, of AV encoding the OTC gene, and this treatment proved to be fatal [970]. These events related to the toxicity of AV gene therapy suppressed the enthusiasm for the use of the AV vector in gene therapy.

#### 10.1.3. Herpes Simplex Virus

Herpes simplex virus type 1 (HSV1) is a common virus causing cold sores [971], and the majority of humans have a pre-existing immunity to the virus [972]. In 1989, a recombinant HSV-1 encoding the gene for human hypoxanthine-guanine phosphoribosyl transferase (HPRT) was injected into mouse brain, and this resulted in human HPRT expression in the brain [973]. However, by 1994, the toxicity of HSV1 administration to

brain was demonstrated, as the intra-cerebral injection of a replication deficient HSV1 amplicon in the rat caused a robust neuro-inflammatory reaction [974]. This was confirmed with intra-cerebral injections in either rats or mice of replication deficient HSV1, and the neuro-inflammation was associated with systemic illness and significant weight loss [975]. Subsequently, HSV1 was engineered as an oncolytic virus, which selectively replicated in tumor cells, but not normal cells, and this variant was designated the G207 HSV1 [976]. A phase 1b clinical trial for recurrent GBM tested the tumoricidal effects of the G207 variant, and in this application, the G207 virus carried no transgene [977]. A dose of  $10^8$  plaque forming units (pfu) of the virus was injected in a volume of 1 mL in the cavity of brain created by the tumor resection in patients with brain cancer [977]. The trial did not proceed further, but a genomic analysis of tumor biopsies was recently reported [978]. A potential problem with this approach is that the penetration of the virus into brain from the tumor cavity is limited by diffusion. GBM is notorious for microscopic spread into normal brain beyond the tumor cavity [979]. This microscopic extension to distant parts of brain, which cannot be visualized by imaging methods, is a major reason for the dismal prognosis of GBM.

#### 10.1.4. Adeno-Associated Virus

**Brain gene delivery via intra-cerebral injection.** Adeno-associated virus (AAV) expressing the lacZ  $\beta$ -galactosidase gene was injected directly into the brain of rats and expression persisted for about 4 months [980]. The problems pertaining to diffusion limitation with the intra-cerebral (IC) route for brain drug delivery are discussed in Section 2.2.1. The same problem pertains to brain gene delivery via intra-cerebral route, which is that the transgene is only expressed at the injection site [980,981]. In an attempt to increase transgene penetration into brain following intra-cerebral injection, the AAV was co-injected in 1.1 M mannitol [981], which causes osmotic shrinkage of brain cells. This potentially toxic formulation caused a modest improvement in the penetration of the transgene into brain from the injection site [981]. The futility of the IC route was manifest in the design of a 2010 clinical trial of CLN2 disease, where the AAV2 encoding the TPP1 enzyme was injected into 12 sites of the cerebrum through 6 burr holes [982]. This multiple IC-injection approach to brain gene delivery is reminiscent of the multiple catheter bundles proposed for either IC [126] or CED [140] drug delivery to brain, discussed in Sections 2.2.1 and 2.2.2, respectively.

**Brain gene delivery via intra-thecal injection.** In an attempt to achieve broader distribution of the transgene to brain, the intra-thecal injection into CSF was performed [983]. The CSF flow tracts in the brain are shown in Figure 16.

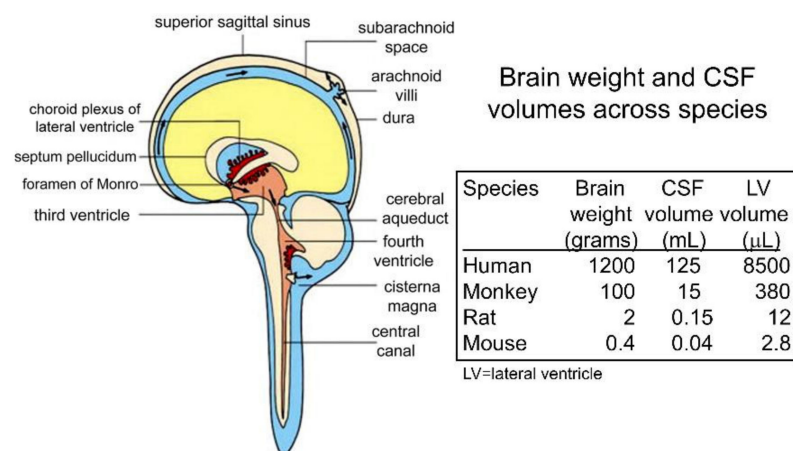


**Figure 16. CSF flow and volume in humans and animals. (Left)** CSF, shown in blue or brown, is produced at the choroid plexus lining the ventricles (red) and flows around the surface of the brain or spinal cord, and

is absorbed into the venous blood of the superior sagittal sinus at the arachnoid villi. The septum pellucidum separates the 2 lateral ventricles into separate compartments. The cisterna magna is at the base of the cerebellum next to the brain stem. Reproduced with permission from [984], Copyright© 2016, Elsevier. **(Right)** The brain weights, total CSF volume, and lateral ventricle (LV) volumes for humans, monkeys, rats, and mice are shown. CSF volumes are from [985], and the LV volumes are from [74], for the rat, from [986], for the mouse, from [987], for the monkey, and from [988], for humans.

AAV injection via the intrathecal route was proposed so as to “inject viral vectors directly into the cerebral lateral ventricles and allow the natural flow of the CSF to deliver the virus throughout the CNS” [983]. One could draw support from this hypothesis from the work of Mott 1913 [26], as the prevailing view over a 100 years ago was that nutrients in blood passed first into CSF from blood and then to brain, as discussed in Section 1.2. It is now known that drugs injected into the CSF do not flow throughout the CNS, as reviewed in Section 2.1.1 and illustrated in Figure 5. For ICV brain gene delivery, an AAV2 vector encoding GUSB was injected in a volume of 2  $\mu\text{L}$  in both lateral ventricles of mice on the day of birth [983]. The volume of the lateral ventricle of an adult mouse is 2.8  $\mu\text{L}$  [986], as shown in Figure 16. The brain weight of an adult mouse, 433 mg, is 6-fold greater than the brain weight of a newborn mouse, 73 mg [989]. A conservative estimate of the volume of the lateral ventricle in the newborn mouse is 0.6  $\mu\text{L}$ . Therefore, the injection of 2  $\mu\text{L}$  into each lateral ventricle of a newborn mouse is >300% of the ventricular volume. As discussed in Section 2.1.1, the injection of such large volumes of fluid in the lateral ventricle forces fluid into the brain via perivascular spaces, which is an artifact of the high injection volume.

Intrathecal (IT) delivery of viral gene therapy vectors can access the CSF via a lumbar injection, an ICV injection into a lateral ventricle, or injection into the cisterna magna (CM) at the base of the brain (Figure 16). MRI in primates shows an ICV injection preferentially delivers drug to the surface of the cerebrum with minimal distribution to the caudal portion of the spinal cord [990]. Injection into the lumbar CSF compartment results in distribution to the surface of the spinal cord with minimal distribution to the cerebrum [990]. Injection into the CM produces maximal distribution to the surface of both the cerebrum and the spinal cord [990]. However, an intra-cisternal injection in humans poses significant safety considerations, owing to the proximity of the CM to the vital structures of the brain stem (Figure 16). Another factor complicating the intra-cisternal route of brain gene delivery is that the volume of the CM in humans varies depending on individual neuroanatomy, and can range from near 0 to a maximal mean volume of 1.1 mL [991]. The CM volume in 60% of humans is only 0.35 mL [991].

Intra-thecal delivery of a AAV8 or AAV9 encoding IDUA was performed in primates via an intra-cisternal injection [992]. The injection volume, 0.5 mL, greatly exceeds the volume of the CM of the primate, which has a brain weight <10% of the human brain. As discussed in Section 2.2.1, drug injection into the CSF is akin to a slow IV infusion, and it is expected that AAV will rapidly move from the CSF compartment to the blood. The diameter of AAV is only 25 nm [993], and particles up to 7 microns pass the arachnoid villi to move from CSF to blood [68]. Injection of AAV into the CSF results in the formation of antibodies against both the AAV capsid protein, as well as to the protein product of the transgene. Intra-thecal delivery of AAV-IDUA in monkeys caused the formation of anti-IDUA antibodies that were found in both plasma and CSF [992]. The antibody formation in the periphery follows from movement of the AAV from CSF to blood. The peripheral anti-IDUA antibodies then move from plasma to CSF similar to any IgG in blood, as discussed in Section 8.3.4. The percent of cells transfected with the IDUA gene in brain varied from 1% to 30% depending on the region of brain [992]. Intra-thecal gene delivery is said to be advantageous over intravenous delivery of AAV9 to brain, as the injection dose of the AAV is lower with the intra-thecal route as compared to IV administration [992]. The ID of intravenous AAV9 for SMA is  $1.1 \times 10^{14}$  vg/kg in humans [994], and there is potential hepatotoxicity from such a high dose, as discussed below. The ID used in an ongoing clinical trial of MPS2 with intrathecal AAV-IDS is  $6.5 \times 10^{10}$  vg/g brain (NCT04571970).

Given a 20 kg child with a 1000 g brain, this ID is equivalent to  $3.3 \times 10^{12}$  vg/kg, which is more than a log order reduction in virus exposure to the patient, as compared to the IV route. However, the problem with the CSF route of AAV delivery to brain is the same as the CSF route for any pharmaceutical. The intrathecal route results in AAV delivery only to the CSF surface of the brain, as discussed in Section 2.1 (Figure 5), and results in AAV movement from CSF to the blood compartment, as discussed in Section 2.1.2.

**Brain gene delivery via intravenous injection.** In 2009, AAV9 was shown to penetrate the BBB following IV administration in the 1-day-old and 70-day-old mouse [995]. The form of AAV9 used in this study was the self-complementary AAV or scAAV. The ID in the newborn mouse, which weighs 1–2 g, was  $4 \times 10^{11}$  vg, which is equivalent to  $2.7 \times 10^{14}$  vg/kg. Although neurons were transduced in brain of the newborn, astrocytes were the principal site of transduction in the 70-day-old mouse [995]. These findings were replicated in the primate following the IV injection of  $1\text{--}3 \times 10^{14}$  vg/kg of a scAAV9 encoding green fluorescent protein (GFP) [996]. GFP expression was higher in grey matter as compared to white matter [996], which is consistent with the higher vascular density in gray matter as compared to white matter [997]. The survival motor neuron 1 (SMN1) gene is mutated in spinal muscular atrophy (SMA). An scAAV9 encoding SMN1, and designated Zolgensma<sup>®</sup>, or onasemnogene abeparvovec-xioi, was FDA approved in 2019 for treatment of SMA as a one-time IV administration of  $1.1 \times 10^{14}$  vg/kg of [994]. Zolgensma<sup>®</sup> is a scAAV as opposed to a single stranded AAV or ssAAV. The size of the expression cassette encoding the therapeutic gene, which includes the promoter, any 5'-untranslated region (UTR) and the 3'-UTR, is limited to <2.3 kb for scAAV, but is limited to <4.7 kb for ssAAV [998]. The scAAV is more effective as a brain delivery vector than the ssAAV [998]. An IV injection dose of  $4 \times 10^{13}$  vg/kg of scAAV or ssAAV transduces only 12% and 2% of neurons in brain, respectively [998]. These results indicate the transport of AAV9 across the BBB is not very efficient, which is why a high ID of Zolgensma,  $10^{14}$  vg/kg, is required for the IV treatment of SMA. New variants of AAV9 are being developed, which produce higher rates of transduction in brain following IV administration.

**New AAV variants.** AAV9 with mutated capsid protein, and designated ssAAV9-PHP.B, produce higher rates of neuronal expression of a GFP transgene, as compared to non-mutated ssAAV9 in the mouse [999]. The intravenous ID required for broad transgene expression in brain is still high, at  $4 \times 10^{13}$  vg/kg [999]. The new variants, PHP.B or PHP.eB, gain access to the mouse brain via a novel AAV receptor, lymphocyte antigen 6 family member a (Ly6a) [1000]. However, the injection dose of the new variants is still high at  $2 \times 10^{14}$  vg/kg [1000]. These new variants of AAV may be only effective in the mouse, as humans lack the Ly6a receptor [1001]. Recently, the Ly6a human homologue, Ly6e, has been proposed as a novel AAV9 receptor at the human BBB [1002], although this has yet to be experimentally confirmed.

**AAV immunogenicity.** AAV is a small 25 nm DNA parvovirus, which is non-pathogenic, but is infectious, and 60–70% of the human population has a pre-existing immunity to AAV [1003,1004]. The anti-AAV antibodies in humans include neutralizing antibodies (NAb), which can lead to rapid inactivation and clearance of the virus. A single injection of AAV in humans produces a high titer NAb response with long-lasting immunity [1004]. The immune response can cross react with the protein produced by the transgene inserted in the AAV backbone, and this immune response against the therapeutic protein is observed following intravenous or intrathecal administration of the AAV. Monkeys were injected intravenously with AAV9 encoding human NAGLU, and an immune response against the viral capsid protein developed over the ensuing weeks [1005]. A NAb response also developed against the endogenous NAGLU enzyme, which caused a >10-fold decrease in serum NAGLU enzyme activity in some animals [1005]. In another primate study, the AAV was administered by intrathecal injection in the cisterna magna. If the AAV encoded a foreign protein, then a severe immune response was generated, which resulted in ataxia and pathologic changes in the nearby cerebellum [1006], which is contiguous with the cisterna magna (Figure 16). Conversely, if a self-protein was encoded in the AAV, no immune response was observed [1006]. The AAV

capsid protein is effectively acting as an immune adjuvant for the transgene product. This could be a problem in the treatment of children with genetic disease secondary to nonsense mutations, wherein no endogenous protein is ever produced. The immune response against the AAV could trigger an immune response against the transgene product, which the immune system recognizes as a foreign protein. The intrathecal injection of AAV encoding human IDUA in monkeys produced an immune response against the IDUA enzyme, if the animals were not pre-tolerized by prior exposure of a liver directed AAV8-IDUA [992]. IDUA enzyme activity in CSF was reduced in the non-tolerized animals [992].

The issue of AAV immunity will become a primary concern when AAV-mediated gene expression terminates at some period following the initial single administration of the AAV. AAV exists within the cell as an episome, and while AAV gene expression may last for some years, it is expected that the patient will need subsequent courses of treatment in future years. Zolgensma<sup>®</sup> is approved only for a single use in the treatment of SMA. Significant questions remain in this area. When will a second and third dose be required? What type of immune response will the second or third doses generate? Will long last immunity against AAV result in prompt neutralization of future doses? Persistent T cell immunity against the NAGLU enzyme, which is mutated in MPSIIIB, has been confirmed in subjects treated with a single course of AAV-NAGLU by intra-cerebral injection [1007].

**AAV hepatotoxicity.** AAV is a hepatotropic virus [1008]. Patients treated with IV Zolgensma<sup>®</sup> develop abnormal liver function tests in 90% of subjects treated, and many require corticosteroid treatment [1009]. Zolgensma<sup>®</sup> is administered as a high injection dose of  $10^{14}$  vg/kg [994]. This dose,  $10^{14}$  vg/kg, when administered to newborn mice, produces hepatocellular carcinoma in about 70% of mice observed long term [1010]. These findings confirm an early study describing the generation of hepatocellular carcinoma in AAV-treated mice [1011].

**AAV neurotoxicity.** AAV induces an inflammatory response in the CNS as recently reviewed [1012]. The injection of AAV9-IDUA into the cisterna magna of primates produces a mononuclear pleocytosis in CSF and degenerative changes in the dorsal root ganglion [1013]. AAV8 was injected bilaterally in the thalamus in primates at a dose of  $10^{11}$ – $10^{12}$  vector genomes, and this produced severe white matter and gray matter necrosis along the injection track [1014]. In an important study pointing to the role of the inverted terminal repeats (ITRs) of the recombinant AAV, cerebellar neurotoxicity was observed in primates following AAV injection into this region of brain [1015]. This cerebellar toxicity was not observed in rodents [1015], which points to the importance of primate studies in the safety pharmacology and toxicology evaluation of new AAV gene products. The ITRs are 145 bp elements placed at both the 5'- and 3'-ends of the expression cassette [1016]. The ITRs can exert promoter activity on cross-packaged material present in the AAV formulation [1015,1016].

The use of AAV in brain gene therapy is a global enterprise with over 3000 citations in PubMed using the search term, 'adeno-associated virus and brain' (March 2022). The development of AAV serotypes that cross the BBB following IV administration is an advance over intrathecal or intra-cerebral routes of administration. Nevertheless, this is a field shadowed by potential long-term complications, including potential liver cancer, severe immune reactions from future repeat treatments, and neuropathologic side effects. Given these issues, it is important to develop, in parallel, non-viral plasmid DNA-based gene therapy of the brain.

## 10.2. Non-Viral Gene Therapy of Brain

### 10.2.1. Cationic Liposomes and Cationic Polyplexes

Lipofection is the process of delivery of plasmid DNA into cultured cells following the mixing of the anionic DNA with a cationic lipid, and this was first described in 1987 [1017]. The cationic liposomes were formed from a 1:1 mixture of a cationic lipid, N-[1-(2,3-dioleoyloxy)propyl]-N,N,N-trimethylammonium chloride, also known as DOTMA, and a helper lipid, dioleoyl phosphatidylethanolamine, also known as DOPE, and these agents,

or variants, are still used today, and widely known as Lipofectamine®. Lipofection is performed in many labs to produce transgene expression in cultured cells. However, the translation of *in vitro* lipofection to gene therapy *in vivo* proved to be difficult. Following IV administration of a reporter gene complexed with cationic liposomes, the transgene was effectively expressed only in the lung, as transgene expression in this organ was several log orders greater than transgene expression in liver or other organs [1018–1021]. Plasmid DNA lipoplexes are formulated in water, or saline-free buffered solutions of low tonicity, and have a diameter of ~100 nm. However, when DNA lipoplexes are transferred to physiologic saline, the structures aggregate into micron-sized particles, and precipitate overnight [835]. The saline-induced aggregation explains why lipofection is so successful in cultured cells, and why lipofection is unsuccessful *in vivo*. The saline induced aggregation triggers uptake by cultured cells via phagocytosis [1022]. Some cultured cell lines are difficult to lipofect if the cell line has a low level of phagocytosis [1023]. While this aggregation of DNA lipoplexes is useful for cell culture, the aggregation limits the utility of *in vivo* gene therapy with cationic liposomes. Following the *in vivo* injection of the DNA lipoplexes, these aggregate immediately and embolize in the first vascular bed encountered after an IV administration, which is the pulmonary circulation [1018–1021]. A histological exam of lung shows the transgene is only expressed in the pulmonary endothelium [1018]. The IV administration of DNA lipoplexes produces an inflammatory response and elevated cytokines [1024], which is due largely to the DNA component [1025]. Cationic liposomes do not cross the BBB [1026], and must be injected directly into the brain to produce transfection of brain cells [1027].

The cationic lipid can be substituted with cationic polymers, such as polyethylenimine (PEI) [1028]. PEI DNA polyplexes have the same properties as lipid DNA polyplexes, and transfect essentially only the lung after IV administration, where gene expression is 2–3 log orders higher than in liver [1028]. In cell culture PEI-mediated transfection correlates with the size of the aggregates formed when PEI/DNA complexes are added to physiologic saline [874]. Aggregate size is larger if linear PEI is used as compared to branched PEI [874].

The first example of receptor-targeting of a DNA polyplex described the complexation of a chloramphenicol acetyltransferase expression plasmid DNA to a polycationic polymer, poly-L-lysine (PLL), which was conjugated to asialoorosomuroid (ASOR), a ligand for the liver asialoglycoprotein receptor [1029]. A large dose of plasmid DNA, 5 mg/kg, complexed to the PLL-ASOR was injected intravenously in rats, and chloramphenicol acetyltransferase gene expression in liver was observed. However, as with all cationic polyplex/DNA complexes, the PLL/DNA complex aggregated in physiologic saline [1030], which aborted further development of this form of non-viral gene therapy for humans.

#### 10.2.2. Pegylated Liposomes

A detergent dialysis method was used to encapsulate plasmid DNA in the interior of pegylated liposomes, also called stabilized plasmid–lipid particles, or SPLP [1031]. The SPLPs do not aggregate *in vivo*, and do not target the lung [1032]. However, SPLPs lack any targeting ligand, and do not produce efficient gene expression *in vivo*. A luciferase expression plasmid DNA was encapsulated in SPLPs and injected in mice bearing a Neuro-2a flank tumor. Luciferase gene expression in the flank tumor was 2 log orders of magnitude higher than in liver, spleen, or lung [1032], which is consistent with the known accumulation of pegylated liposomes in mouse flank tumors. These tumors have a leaky vasculature with open endothelial clefts and discontinuous basement membrane [1033]. Luciferase gene expression in the flank tumor was 100 pg/g [1032], which is equivalent to 1 pg/mg protein, given 100 mg protein per gram tissue [1034]. Luciferase gene expression in mouse organs (lung, spleen, liver) was very low,  $\leq 0.01$  pg/mg protein. In contrast, as discussed in the next section, Trojan horse liposomes (THLs), which are receptor-targeted pegylated liposomes, produce much higher levels of transgene expression *in vivo* following IV administration. A THL, also called a pegylated immunoliposome, is a pegylated liposome, where the tips of some of the polyethyleneglycol (PEG) strands are conjugated with a receptor-specific MAb.

THLs targeted with a MAb against the human insulin receptor (HIR), and encapsulating a luciferase expression plasmid, produced levels of luciferase enzyme activity in the liver, brain, spleen, and lung of 16, 9, 3, and 2 pg/mg protein, respectively, in the Rhesus monkey [902].

### 10.2.3. Trojan Horse Liposomes

The *in vivo* delivery and brain expression of a plasmid DNA was reported in 2000 using pegylated immunoliposomes, also called Trojan horse liposomes (THLs) [1035]. In this approach, a plasmid DNA is encapsulated in the interior of a pegylated liposome, and the tips of some of the PEG strands on the surface of the liposome are conjugated with a MAb that targets a RMT system at the BBB such as the TfR or insulin receptor. The incorporation of the receptor targeting ligand or MAb on the surface of the liposome is essential for delivery into brain *in vivo* following IV administration, as non-functionalized pegylated liposomes do not cross the BBB [891,1035].

Despite the requirement for a receptor targeting ligand on the surface of pegylated liposomes for plasmid DNA delivery [1036], the field of liposome-mediated delivery of nucleic acid therapeutics has evolved without a major emphasis on the incorporation of a targeting ligand in the liposome. A recent review of nucleic acid delivery with lipid nanoparticles (LNP), which is a generic term for pegylated liposomes, makes no reference to the need for functionalization of the LNP with a targeting ligand to enable receptor-mediated uptake into cells, apart from the presumed coating of the surface of the LNP with apoE in plasma [1037]. The incorporation of short chain pegylated lipids on the surface of the LNP is advocated, so as to facilitate rapid dissociation of this PEG-lipid *in vivo* in plasma [1037]. The dissociation of the pegylated lipid from the surface of the liposome is said to enable fusion of the liposome with the plasma membrane, which then initiates endocytosis of the nucleic acid encapsulated in the liposome into the cell [1037]. This approach of deploying short chain pegylated lipids, so as to enhance dissociation of the PEG lipid *in vivo*, is opposite of the design of THLs, where long chain pegylated lipids are incorporated on the surface of the liposome for conjugation of the targeting MAb at the tip of the pegylated lipid [1036]. Early dissociation of the lipid-PEG-MAb from the surface of the THL would eliminate RMT of the THL across the BBB. The incorporation of the receptor targeting ligand or MAb on the surface of the liposome is essential for delivery into brain *in vivo* following IV administration, as non-functionalized pegylated liposomes do not cross the BBB [891,1035].

A THL is a 100–150 nm pegylated liposome that encapsulates a single plasmid DNA, and is functionalized for RMT delivery to brain by conjugation of a receptor-specific MAb on the surface PEG strands of the liposome (Figure 17A).

THLs are formed by first encapsulating the plasmid DNA in the interior of pegylated liposomes, followed by conjugation of the targeting MAb to the surface of the liposome. THLs were initially produced from 96% 1-palmitoyl-2-oleoyl-glycero-3-phosphocholine (POPC), 3% 1,2-distearoyl-sn-glycero-3-phosphoethanolamine (DSPE)-polyethyleneglycol (PEG) 2000 Da (DSPE-PEG<sup>2000</sup>), 1% dimethyldioctadecylammonium (DDAB), and 0.15% DSPE-PEG<sup>2000</sup>-maleimide [1035]. The DDAB has a cationic charge, but the DSPE-PEG<sup>2000</sup> has an anionic charge, so the THL has a net negative charge. In parallel, the targeting MAb is thiolated with a reagent such as 2-iminothiolane. The thiolated receptor-specific MAb is conjugated to the maleimide group of the PEG<sup>2000</sup> on the liposome surface to form a stable thio-ether bond. Typically, each THL incorporates ~50 MAb molecules per liposome, and each THL encapsulates a single double stranded plasmid DNA in the interior of the liposome, such that the DNA is protected from nucleases. For dual receptor targeting, two MAb molecules of different receptor specificity may be conjugated to the THL surface so as to engage two different cell membrane receptors, as discussed below. Binding of the MAb domain of the THL to the cell membrane receptor triggers receptor-mediated transcytosis of the THL across the BBB, followed by receptor-mediated endocytosis into brain cells. As



discussed in Section 8.1, certain receptors, such as the insulin or transferrin receptors, are expressed at both the BBB and the brain cell membrane (Figure 11B).

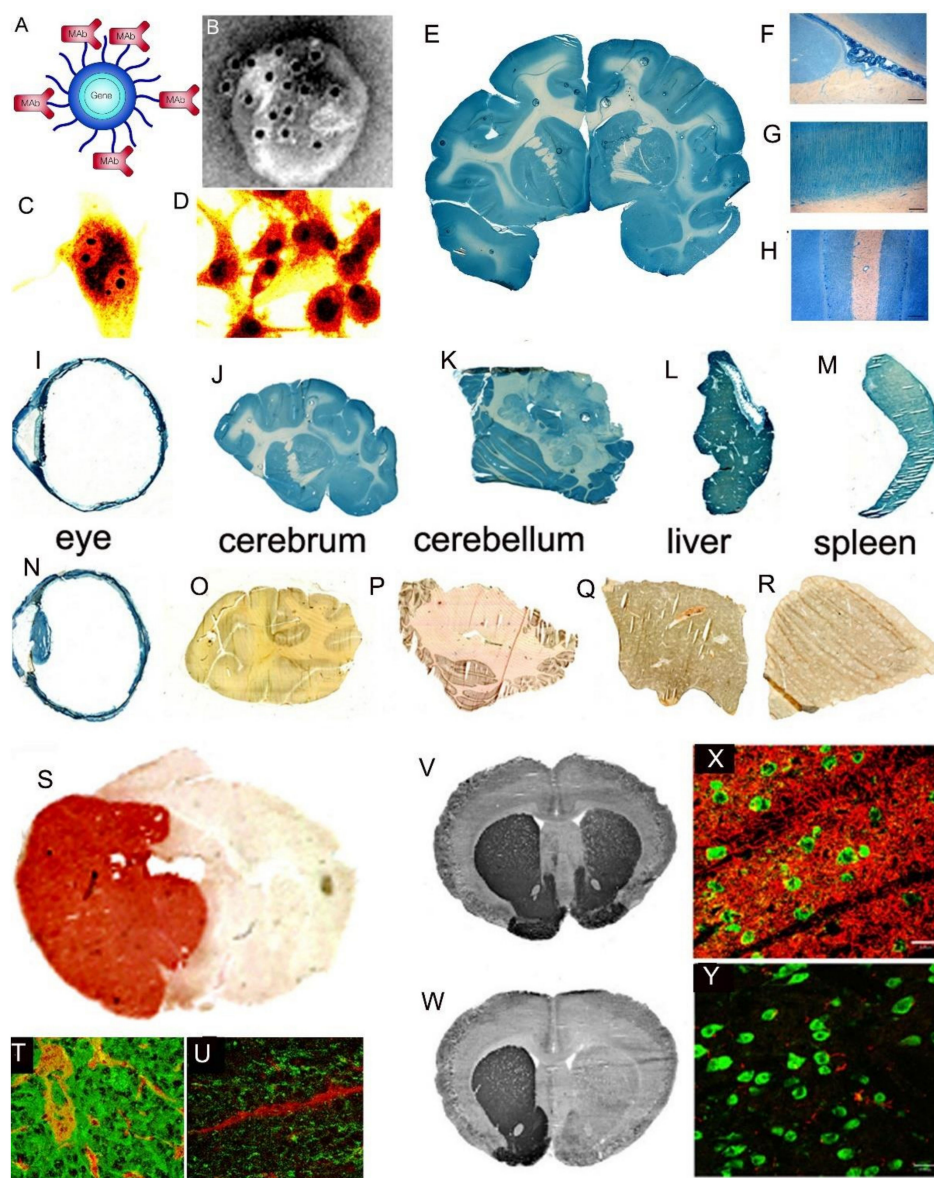


**Figure 17. Trojan horse liposomes and non-viral gene therapy of the brain.** (A) Model of a THL showing single plasmid DNA encapsulated in interior of pegylated liposome, where the tips of a small fraction of the surface PEG strands are conjugated with a receptor-specific MAb. Reproduced with permission from [1038], Copyright© 2002 Springer-Nature. (B) Electron micrograph of a THL co-incubated with secondary antibody conjugated with 10 nm gold particles. Reproduced from [1039]. (C,D) Confocal microscopy of U87 human glioma cells after 6 h (C) or 24 h (D) incubation with HIRMAb-targeted THLs encapsulating fluorescein conjugated plasmid DNA. Reproduced with permission from [1040], Copyright© 2002 John Wiley & Sons. (E) Beta galactosidase histochemistry of coronal section of brain from Rhesus monkey removed 48 h after the IV administration of 12 ug/kg of pSV-lacZ expression plasmid DNA encapsulated in HIRMAb-THLs. (F–H) Beta galactosidase histochemistry of choroid plexus (F), occipital lobe (G), and cerebellum (H) of brain shown in (E). (I–R) Beta galactosidase histochemistry of Rhesus monkey eye (I), cerebrum (J), cerebellum (K), liver (L), and spleen (M) at 48 h after the IV administration of HIRMAb-targeted THLs encapsulating a lacZ expression plasmid DNA under the influence of the widely expressed SV40 promoter, and of Rhesus monkey eye (N), cerebrum (O), cerebellum (P), liver (Q),

and spleen (R) at 48 h after the IV administration of HIRMAb-targeted THLs encapsulating a lacZ expression plasmid DNA under the influence of the eye-specific opsin promoter. (E–M) reproduced from [902], Copyright© 2003 licensed under Creative Commons Attribution License (CC-BY-NC-ND 4.0); (I,N,O,Q,R) reproduced from [1041], Copyright© 2003 licensed under Creative Commons Attribution License (CC-BY-NC-ND 3.0); (P) reproduced with permission from [1042], Copyright© 2007 Elsevier. (S) Intracranial U87 human glioma in the brain of a severe combined immunodeficient (scid) mouse removed at autopsy and stained immunohistochemically with an anti-EGFR antibody. Reproduced from [911], Copyright© 2002 licensed under Creative Commons Attribution License (CC-BY-NC-ND 4.0). (T,U) Confocal microscopy of scid mouse intra-cranial U87 human glioma at autopsy stained with antibodies against the mouse TfR (red) and the human EGFR (green); the mice in (T) were treated with saline and the mice in (U) were treated with doubly targeted HIRMAb/8D3-TfRMAb THLs encapsulating a plasmid DNA encoding a short hairpin RNA (shRNA) directed against nucleotides 2525–2557 of the human EGFR mRNA. (T,U) reproduced from [1043]. (V,W) Coronal sections of rat brain stained immunohistochemically with an antibody to tyrosine hydroxylase. Brains removed 3 days after a single IV injection of THLs encapsulating a plasmid DNA encoding rat tyrosine hydroxylase under the influence of a brain specific glial fibrillary acidic protein promoter and conjugated with either the OX26-TfRMAb (V) or a mouse IgG2a isotype control (W). The THLs were administered 7 days after the intra-cerebral injection of a neurotoxin, 6-hydroxydopamine, in the right median forebrain bundle. (V,W) from [1044]. (X,Y) Confocal microscopy of striatum ipsilateral to toxin lesion and double immune stained with antibodies against tyrosine hydroxylase (red) and neuronal neuN (green). Confocal micrograph in (X) corresponds to histochemistry in (V), and confocal micrograph in (Y) corresponds to histochemistry in (W). (X,Y) from [1044].

The PEG linked MAb extended from the surface of the THL is shown with electron microscopy (EM) in Figure 17B. In this study a 10 nm gold conjugated secondary antibody was mixed with the THL prior to EM. The size of the 10 nm gold is about the same size as the MAb, and the micrograph shows there are multiple MAb molecules conjugated to the surface of the THL [1039].

**THLs target plasmid DNA to the nuclear compartment of cells.** Lipofection of cells with plasmid DNA bound to cationic liposomes is an inefficient process, as the majority of the DNA that enters the cell is retained in the cytoplasm aggregated within pre-lysosomal vesicles [1045]. However, in the case of THLs, the majority of the endocytosed plasmid DNA is incorporated in the nuclear compartment. This was demonstrated with the confocal micrographs shown in Figure 17C,D. In this study, a plasmid DNA encoding an antisense RNA against the human epidermal growth factor receptor (EGFR) was labeled with fluorescein by nick translation and fluorescein-12-2'-deoxyuridine-5'-triphosphate [1040], and incorporated in THLs targeted with a MAb against the human insulin receptor, and designated the HIRMAb. The HIRMAb-THLs were incubated with human U87 glioma cells in culture and confocal microscopy was performed at 6 h (Figure 17C), and 24 h (Figure 17D). By 6 h, the majority of the DNA is in the cytosolic compartment, although transgene is visible in the nucleolus of the nucleus at 6 h. By 24 h, virtually all of the cellular transgene is localized to the nuclear compartment (Figure 17D). The insulin receptor is expressed on both the BBB and the brain cell membrane as discussed in Section 8.1.1. Following RMT of the THL across the BBB, and following insulin receptor-mediated endocytosis of the THL into brain cells, the liposome cargo must then be delivered to the nuclear compartment for gene expression. A MAb targeting the insulin receptor may be particularly suited to nuclear delivery of plasmid DNA, because the insulin receptor normally serves to deliver insulin to the nuclear compartment [1046,1047].

**THL brain delivery of reporter genes.** Plasmid DNAs encoding reporter genes such as the lacZ and luciferase genes have been encapsulated in HIRMAb-THLs for gene expression in the primate [902], in OX26 TfRMAb-THLs for gene expression in the rat [1035,1048], and in 8D3 TfRMAb-THLs for gene expression in the mouse [1049]. The global expression of the lacZ transgene in the Rhesus monkey brain following IV administration of HIRMAb-THLs was confirmed by X-Gal histochemistry. Histochemistry of un-injected primate brain showed no

reaction [1050]. However, global expression of the lacZ transgene was observed in the primate brain at 48 h after the IV administration of the HIRMAb-targeted THLs encapsulating the lacZ expression plasmid DNA as shown in Figure 17E. The injection dose (ID) of lacZ plasmid DNA in this primate study, 12 µg/kg, is more than 2 log orders of magnitude lower than the ID, 5 mg/kg, of CAT plasmid DNA required for gene delivery to liver in the rat with the PLL-ASOR conjugate [1029], or luciferase gene delivery in the mouse with SPLPs [1032]. In a primate study with a luciferase reporter gene, the expression plasmid DNA was encapsulated in HIRMAb-THLs for IV administration in the Rhesus monkey and the injection dose of the luciferase plasmid DNA was also 12 µg/kg [902]. The brain luciferase gene expression at 48 h was 9–10 pg/mg protein [902], and qPCR analysis showed the luciferase plasmid DNA content in primate brain declined with a  $T_{1/2}$  of  $1.3 \pm 0.3$  days, which correlated with the  $T_{1/2}$  of decline of brain luciferase enzyme activity of  $2.1 \pm 0.1$  days [1051]. The qPCR quantitation of luciferase plasmid DNA content in brain at 2 days following the IV administration of the HIRMAb-THLs indicated that ~3 plasmid DNA molecules was delivered to every cell in brain [1051]. This finding on the global delivery to brain of a luciferase expression plasmid DNA correlates with the global expression of the lacZ transgene expression in the primate brain (Figure 17E). Light microscopy of regions of primate brain from the lacZ study showed transgene expression in the choroid plexus epithelium and the capillary endothelium of white matter (Figure 17F), in the cortical columns of the occipital cortex (Figure 17G), and in the molecular and granular layers and the intermediate Purkinje cells of the cerebellum (Figure 17H). Similar findings of global expression in brain of the lacZ gene were made in the mouse and rat following the IV administration of 8D3-THLs and OX26 TfRMAb-THLs, respectively [1048,1049]. Significant levels of lacZ gene expression were visible by histochemistry at 6 days following IV administration of THLs in the rat [1048]. The average number of HIRMAb, OX26 TfRMAb, or 8D3 TfRMAb antibodies conjugated per THL can be computed [891], and in the primate, rat, and mouse studies was 35–50 [902,1048,1049]. In both the rat and mouse study, no lacZ expression was detected in brain following the IV administration of THLs conjugated with the isotype control antibody, which is mouse IgG2a for OX26, and rat IgG for 8D3 [1048,1049]. The absence of gene expression with THLs targeted with the isotype control IgG shows that gene expression is determined by the receptor specificity of the MAb domain of the THL.

#### **Tissue-specific promoters and encapsulation of large sized plasmid DNA in THLs.**

The lacZ gene encapsulated in the HIRMAb-THLs used for the primate study shown in Figure 17E–H was under the influence of the widely expressed SV40 promoter [902]. HIRMAb-THLs encapsulated with the SV40-lacZ produced transgene expression in the eye, the cerebrum and the cerebellum of the primate (Figure 17I–K), but also produced lacZ expression in peripheral organs such as liver (Figure 17L) and spleen (Figure 17M) in the primate [902,1041]. A lacZ expression plasmid under the influence of 2 kb of the 5'-flanking sequence (FS) of the bovine opsin gene, and designated pLacF [1052], was encapsulated in HIRMAb-THLs and injected intravenously in the Rhesus monkey. This resulted in lacZ expression in the eye (Figure 17N), but no lacZ gene expression in the cerebrum, cerebellum, liver or spleen (Figure 17O–R). IV administration of a lacZ plasmid encapsulated in HIRMAb-THLs produced global expression of the transgene in all layers of the retina (Figure 17L,N). There is greater expression of a lacZ transgene in the multiple layers of the primate retina following IV administration of HIRMAb-THLs [1041], as compared to lacZ expression in the layers of the retina of the mouse following IV administration of 8D3 TfRMAb-THLs [1053], and this is attributed to the widespread expression of the insulin receptor in human ocular tissues [1054].

An expression plasmid encoding the rat tyrosine hydroxylase (TH) cDNA under the influence of the SV40 promoter was encapsulated in OX26 TfRMAb-THLs and injected intravenously in the rat. This treatment produced off-target TH expression in the liver [1044]. The SV40 promoter was replaced with a GFAP promoter [1044], which was taken from the 2 kb of the 5'-FS of the human GFAP gene [1055]. IV administration of the GFAP-TH plasmid encapsulated in OX26 TfRMAb-THLs in the rat produced no TH transgene expres-

sion in the liver [1044], which is consistent with the lack of expression in liver of GFAP, a brain-specific gene.

The 1.5 kb 5'-FS of the human platelet-derived growth factor B (PDGFB) gene is a neuron specific promoter [1056]. An expression plasmid composed of the 4 kb cDNA encoding for the human Niemann Pick disease type 1 (NPC1) cholesterol transporter, and under the influence of the 1.5 kb human PDGF-B promoter, was engineered and this 8 kb plasmid was encapsulated in 8D3 TfrMAb-THLs for treatment of the NPC1 mouse [773], as described below.

Tissue-specific gene expression can be enabled by the administration of chromosomal-derived transgenes, as compared to cDNA-derived transgenes. The largest size plasmid DNA encapsulated in THLs is a 21 kb plasmid encoding the entire 18 kb rat TH gene, which is composed of 8.4 kb 5'-FS, 7.3 kb coding region with 13 exons and 12 introns, and 1.9 kb of 3'-FS [1057]. Following encapsulation of this 21 kb plasmid DNA in OX26 TfrMAb-THLs, the THLs were injected intravenously in the rat with experimental PD, and this treatment produced a >10-fold increase in striatal TH enzyme activity [1057]. TH gene therapy in PD only replaces the TH deficiency, but does nothing to abort the neurodegeneration of the nigral-striatal tract in PD. GDNF is a potent nigral-striatal neurotrophin [1058]. So as to restrict GDNF gene expression in the brain to the nigral-striatal tract, the cDNA encoding human prepro GDNF was placed under the influence of the 8.4 kb 5'-FS of the rat TH gene, and the size of the expression plasmid was 13 kb [1059]. This plasmid was encapsulated in OX26 TfrMAb THLs for treatment of the rat with experimental PD [1059], as described below. The expression in brain of the TH gene is restricted primarily to the nigral-striatal tract that degenerates in PD, so the TH promoter allows for region-specific GDNF gene expression in this region of brain.

In summary, tissue-specific gene expression following IV administration of plasmid DNA is possible with the combined use of tissue-specific gene promoters and THL plasmid DNA delivery technology. Some tissue-specific promoters are large, e.g., the 8.4 kb TH promoter used to restrict GDNF expression to the nigral-striatal tract of brain [1059]. In addition to the use of tissue-specific promoters, another goal in gene therapy is production of high levels of expression of the transgene. Gene expression can be enhanced by insertion of 5'-untranslated region (UTR) and 3'-UTR elements flanking the open reading frame of the transgene. The interaction of the 5'-UTR and 3'-UTR elements can have synergistic effects on gene expression. When a 171 nt 5'-UTR or a 200 nt 3'-UTR from the GLUT1 mRNA was inserted 5' and 3' in a luciferase expression cassette, transgene expression was increased 10-fold and 6-fold, respectively [1060]. However, when the luciferase expression cassette contained both GLUT1 mRNA 5'-UTR and 3'-UTR elements, transgene expression was increased 59-fold [1060]. The more the therapeutic gene expression cassette is modified with tissue-specific promoters or 5'-UTR or 3'-UTR elements, the greater the size of the expression cassette. The construction of advanced expression cassettes of larger size is not possible with AAV gene therapy, given the limited size of the expression cassette that can be inserted in the AAV backbone, e.g., <4.7 kb for incorporation in ssAAV, and <2.1 kb for incorporation in scAAV [998], as discussed in Section 10.1.4. In contrast, plasmid DNA up to 21 kb in size is expressed in vivo in brain following encapsulation and brain delivery with THLs [1057].

**THL brain delivery of therapeutic genes for brain cancer.** Human glial tumors over-express the EGFR gene, which plays an oncogenic role in these tumors [1061]. Treatment of glial tumors aim to suppress the expression of the tumor EGFR. To determine the effect of EGFR suppression, a human intracranial experimental glioma was produced by implantation of human U87 glioma cells in the caudate nucleus of scid mice [911]. The size of the tumor at autopsy is shown by the EGFR immunohistochemistry (Figure 17S). A plasmid DNA encoding an antisense RNA corresponding to nucleotides (nt) 2317–3006 of the human EGFR mRNA was inserted in a 11 kb plasmid under the influence of the SV40 promoter, and encapsulated in THLs [911]. These THLs were dual conjugated with both the HIRMAb, to target the HIR on the human glial cells, and the 8D3 TfrMAb, to target the

mouse TfR on the tumor vascular endothelium, which originates from mouse brain. These antibodies are species specific, and the HIRMAB does not recognize the mouse insulin receptor on the tumor vascular endothelium, which originates from mouse brain, and the 8D3 TfRMAB does not recognize the tumor cell human TfR [911,1043]. Prior to treatment of the tumor-bearing mice, the dual Mab-targeted THLs were produced that encapsulated a luciferase expression plasmid DNA, which was injected intravenously in the mice with the U87 gliomas. The luciferase enzyme activity in the human tumor, targeted by the HIRMAB, was >10-fold higher than in normal mouse brain, targeted by the TfRMAB [911]. This greater degree of gene expression using the HIRMAB as compared to the TfRMAB was also observed with comparison of luciferase gene expression in the primate, targeted with the HIRMAB, as compared to luciferase gene expression in the rat, targeted with the TfRMAB [902]. The higher gene expression with the HIRMAB is attributed to the selective triage of the insulin receptor to the nucleus [1046,1047]. At 5 days following implantation of 500,000 U87 glioma cells in the caudate-putamen, mice were treated weekly by IV administration of (a) saline, (b) HIRMAB/TfRMAB-THLs encapsulating the luciferase expression plasmid, or (c) HIRMAB/TfRMAB-THLs encapsulating the EGFR antisense RNA expression plasmid. The time of 50% mortality, ED50, was 18 days for either the saline treated mice or the mice treated with THLs encapsulated with the luciferase plasmid DNA. However, the survival ED50 was increased 100% to 36 days for the mice treated with the THLs encapsulated with the plasmid DNA encoding the EGFR antisense RNA [911].

RNA interference (RNAi) therapeutics can be either short interfering RNA (siRNA) or short hairpin RNA (shRNA). The siRNA is administered as a short RNA duplex, and the shRNA is produced in target cells following the delivery of an shRNA expression plasmid DNA under the influence of a U6 promoter. Biotinylated siRNA is delivered to brain with a MAb Trojan horse coupled with avidin–biotin technology [1062]. For shRNA therapy, an expression plasmid was engineered that encoded a shRNA targeting nt 2529–2557 of the human EGFR under the influence of the U6 promoter [1043]. The intracranial tumor model used for the RNAi treatment was the U87/scid mouse model (Figure 17S) applied previously for testing the therapeutic effects of THL-mediated antisense gene therapy [911]. Treatment of U87 cells in culture with the HIRMAB-THLs encapsulating the shRNA expression plasmid produced a >90% suppression of EGF-mediated intracellular calcium flux [1043]. At 5 days following implantation of 500,000 U87 human glioma cells in the caudate-putamen, mice were treated weekly by IV administration of (a) saline or (b) 5 µg DNA per mouse of HIRMAB/TfRMAB-THLs encapsulating the anti-EGFR shRNA expression plasmid. The time of 50% mortality, ED50, was 17 days for the saline treated mice, and the ED50 was increased 88% to 32 days for the mice treated with THLs encapsulating the plasmid DNA encoding the shRNA [1043]. Confocal microscopy of the tumor at autopsy for the saline treated mouse and the THL/RNAi treated mice is shown in Figure 17T and 17U, respectively, where the immunoreactive human EGFR is shown in green and the immunoreactive mouse TfR is shown in red [1043]. This study shows RNAi treatment against the EGFR caused a knockdown in both the level of immunoreactive EGFR in the human tumor and the vascular density of the tumor, as shown by the level of immunoreactive mouse TfR at the vasculature. The capillary density, as assessed by immunohistochemistry of vascular TfR, was  $35 \pm 1$  capillaries/mm<sup>2</sup> in either the saline or the RNAi treated mice in the non-tumor mouse brain. However, the capillary density was reduced to  $15 \pm 2$  and  $3 \pm 0$  capillaries/mm<sup>2</sup> in the center of the tumor in the saline and RNAi treated mice, respectively. The capillary density was  $29 \pm 4$  and  $9 \pm 1$  capillaries/mm<sup>2</sup> in the periphery of the tumor in the saline and RNAi treated mice, respectively [1043]. The EGFR has a pro-angiogenic effect in brain tumors [1063]. Therefore, the knockdown of the tumor EGFR by the THL-mediated RNAi therapy caused a suppression of the vascular density of the tumor. Since the RNAi therapeutic is delivered to the brain tumor via the tumor vasculature, the knockdown of tumor EGFR has a self-limiting effect on the ultimate survival outcome. THL delivery of plasmid DNA encoding either antisense RNA [911] or shRNA [1043] directed against the EGFR has a therapeutic effect in brain cancer, but needs to be combined with

other therapies that halt tumor progression before the sharp decline in tumor vasculature that occurs in the terminal stages of the tumor growth.

**THL brain delivery of therapeutic genes for Parkinson's disease.** Parkinson's disease (PD) is caused by degeneration of the nigral-striatal tract, resulting in reduced TH enzyme activity and dopamine production in the striatum. In an effort to develop a non-viral gene therapy of PD, an expression plasmid encoding the rat TH cDNA was engineered under the influence of either the widely expressed SV40 promoter [1039] or the brain-specific GFAP promoter [1044]. Experimental PD was induced by the intra-cerebral injection of 6-hydroxydopamine in the median forebrain bundle of one side of the brain in rats. At 1 week after toxin injection, rats were treated with a single dose of OX26 TfrMAB-THLs encapsulating 10  $\mu\text{g}$ /rat of either the SV40-TH plasmid or the GFAP-TH plasmid. As a control, THLs were targeted with the mouse IgG2a isotype control antibody instead of the OX26 TfrMAB. PD rats were treated with 1  $\mu\text{g}$ , 5  $\mu\text{g}$ , or 10  $\mu\text{g}$  of SV40-TH plasmid DNA encapsulated in the TfrMAB-THLs. Treatment at the 1  $\mu\text{g}$  DNA/rat dose had no therapeutic effect; treatment at the 5  $\mu\text{g}$  DNA/rat dose caused a partial restoration of striatal TH enzyme activity, while treatment at the 10  $\mu\text{g}$  DNA/rat dose caused a complete normalization of the striatal TH enzyme activity. The therapeutic effect of the THLs was due singularly to the TfrMAB targeting, as THLs targeted with the mouse IgG2a isotype control antibody had no therapeutic effect [1039]. The striatal TH enzyme activity produced with the single THL treatment of 10  $\mu\text{g}$  DNA/rat dose declined with a  $T_{1/2}$  of 6 days [1039]. The normalization of striatal TH enzyme activity was correlated with an improvement in motor function measured by the number of 360° rotations/min (RPM) induced by apomorphine treatment. In the study with the SV40-TH treatment, the apomorphine RPM was reduced from  $20 \pm 5$  to  $6 \pm 2$  [1039], and in the study with the GFAP-TH treatment, the apomorphine RPM was reduced from  $22 \pm 3$  to  $4 \pm 3$  [1044]. The increase in striatal TH enzyme activity caused by THL treatment correlated with the immunoreactive TH in the striatum. The treatment with the GFAP-TH plasmid encapsulated in OX26 TfrMAB-THLs normalized the immunoreactive TH in striatum of the PD rats (Figure 17V,X), whereas there was no therapeutic effect in PD rats treated with the GFAP-TH plasmid encapsulated in IgG<sub>2a</sub>-THLs (Figure 17W,Y).

The therapeutic effect of THL-mediated TH enzyme replacement in experimental PD lasts only 1 week [1039], owing to degradation of the plasmid DNA in brain [1051]. Therefore, treatment of brain with THL gene therapy requires chronic repeat administration. However, TH replacement gene therapy of PD does not address the underlying problem in PD, which is degeneration of the nigral-striatal tract. What is needed for PD is neurotrophin gene therapy that reverses the degeneration of the nigral-striatal region of brain, and GDNF is a potent neurotrophin for this region of brain. A human prepro GDNF expression plasmid DNA under the influence of the 8 kb rat TH promoter was engineered [1059], and encapsulated in OX26 TfrMAB-THLs and injected into PD rats at 1, 2, and 3 weeks after toxin administration at a dose of 10  $\mu\text{g}$  DNA/rat per injection [1064]. The rats were then tested at 6 weeks after toxin administration, which was 3 weeks after the third and final dose of THLs, for apomorphine-induced rotation, for amphetamine-induced rotation, and for striatal TH enzyme activity. By 6 weeks after toxin administration, apomorphine-induced 360° rotation was increased to  $25 \pm 2$  RPM in the saline treated PD rats, but was reduced 87% to  $3 \pm 1$  RPM in the THL treated rats. Amphetamine-induced 360° rotation at 6 weeks after toxin injection was  $11 \pm 1$  RPM in saline treated rats, and this was reduced 90% to  $1.1 \pm 0.2$  RPM in the THL treated PD rats. The striatal TH enzyme activity was reduced 99% at 6 weeks after toxin injection in the saline treated rats, but was reduced only 23% at 6 weeks after toxin injection in the THL treated rats [1064]. These results indicate a more durable therapeutic effect in experimental PD is achieved with GDNF gene therapy as compared to TH gene therapy. Placement of the GDNF transgene under the influence of the TH promoter restricts GDNF expression only to sites where the TH gene is transcriptionally active [1059].

**THL brain delivery of a therapeutic gene for Niemann-Pick C1 disease.** Niemann-Pick C1 (NPC1) disease is an inherited disorder caused by mutations in the NPC1 gene, which encodes an intracellular membrane transporter of non-esterified cholesterol [1065]. The NPC1 cholesterol transporter is a large protein with an open reading frame of 3.9 kb. Therefore, the NPC1 cDNA can only be inserted in a ssAAV and with a small promoter and 3'-UTR, so that the expression cassette is <4.7 kb. It would be desirable to place the NPC1 gene under a neuron-specific promoter, such as the 1.5 kb human PDGF-B promoter [1056]. However, such a construct would be too large to insert into an AAV vector. An 8 kb expression plasmid was engineered, designated pPDGFB-NPC1, which placed the 3.9 kb NPC1 open reading frame under the influence of the 1.5 kb PDGFB promoter and a bovine growth hormone poly A sequence [706]. NPC1 mice replicate the neuropathology of human NPC1 [1066,1067]. Owing to the severe neuropathology, NPC1 mice die young at about 10 weeks with reduced body weight [706]. So as to encapsulate the pPDGFB-NPC1 plasmid in THLs active in the mouse, the recombinant 8D3 TfrMab was expressed [706], based on the previously reported amino acid sequence for the heavy and light chains of this antibody [693]. THLs were produced from the recombinant 8D3 TfrMab and encapsulated the pPDGFB-NPC1 plasmid DNA. Weekly intravenous THL treatment of NPC1 mice began at the age of 6–7 weeks. After euthanasia, the mass of the pPDGFB-NPC1 plasmid DNA was measured by qPCR in brain, liver, and spleen removed at 4 days following the last dose of THLs. The plasmid concentration in brain, liver, and spleen was  $10.1 \pm 3.1$ ,  $107 \pm 9$ , and  $40 \pm 8$  pg plasmid DNA per mg wet tissue [706]. High plasmid DNA content in spleen is attributed to the high expression of the Tfr1 in spleen in the mouse [1068]. Based on the number of brain cells per mg wet brain, these qPCR studies indicate ~4 plasmid DNA molecules are delivered to each cell in brain [706]. The expression of the NPC1 mRNA in brain, spleen, and liver, relative to the mRNA of glyceraldehyde 3'-phosphate dehydrogenase (GAPDH), was measured by reverse transcriptase PCR [706]. The  $\Delta Cq$  parameter is the difference in qPCR Cq value for NPC1 and GAPDH for brain, spleen, or liver. The  $\Delta\Delta Cq$  is the difference in  $\Delta Cq$  for the vehicle treated mouse and the THL treated mouse. The change in NPC1 mRNA abundance in the organs of the THL treated mouse was computed from the base 2 antilog of the  $\Delta\Delta Cq$  [706]. The  $\Delta\Delta Cq$  values between THL and vehicle treatment groups showed the NPC1 mRNA, relative to the GAPDH mRNA, was increased 338-fold, 8192-fold, and 238-fold in brain, spleen, and liver, respectively [706], which indicates THL treatment resulted in a significant increase in NPC1 transcript in brain in the NPC1 null mice. THL treatment caused a reduction in cholesterol inclusion bodies in brain, and peripheral organs, but did not increase lifespan in these mice [706]. The lack of effect on lifespan was attributed to the delay in initiation of treatment until 6–7 weeks of age. By this time, the NPC1 mice already have developed pathologic changes in brain including autophagic lysosomal inclusion bodies, astrogliosis, microglia activation, and suppressed myelin production [1069–1072]. Future treatment of the NPC1 mouse should initiate THL gene therapy at birth.

**Safety pharmacology of chronic THL administration.** The safety of chronic administration of THLs was tested by treating rats with THLs encapsulated with a 7 kb TH expression plasmid under the influence of the SV40 promoter and conjugated with either the OX26 TfrMab or its isotype mouse IgG<sub>2a</sub> control [1073]. A dose of 20  $\mu$ g/kg of THL encapsulated DNA was administered by weekly IV injections for 6 consecutive weeks. A third group of rats were treated with weekly saline and served as a control. Delivery of the TH expression plasmid to brain was confirmed by Southern blot. There was no change in body weight, 14 serum chemistries or histology of brain and peripheral organs (liver, spleen, heart, lung, kidney) following chronic THL administration. Immunohistochemistry of brain using primary antibodies against multiple markers of inflammation showed no inflammatory reaction in brain.

**THL manufacturing.** THLs described above were produced at scale of 1–5 mL using sonication, extrusion, and purification by gel filtration chromatography [1036]. These procedures are not scalable for commercial manufacturing. A scalable manufacturing process

for pegylated liposomes, which can be adapted to THLs, uses an ethanol dilution method, which eliminates sonication, extrusion, and gel filtration [1074]. This scalable manufacturing approach, as recently reviewed [1037], adapts previously developed methods of liposome production by an ethanol injection method [1075], and use of a T-shaped device for rapid mixing of lipids and aqueous plasmid DNA [1076]. Ethanol dilution has two favorable effects on the encapsulation of plasmid DNA in pegylated liposomes. First, the ethanol dilution causes condensation of the plasmid DNA [1077], which is necessary to enable encapsulation of the plasmid DNA within the 100–150 nm vesicles. The gyration radius of 10 kb supercoiled plasmid DNA is 460 nm [1078], which greatly exceeds the radius of the small vesicles. Second, ethanol dilution induces the conversion of large multivesicular vesicles into small 100–150 nm vesicles [1079]. THL manufacturing at a 10 L level has been outlined using ethanol dilution and tangential flow filtration [525]. A relatively small volume of THL manufacturing of 15 L could provide an amount sufficient to treat an orphan disease with 50% market penetration for a year at a weekly IV infusion dose of 10 µg/kg of THL encapsulated plasmid DNA [525]. The primary problem in the manufacturing of THLs is product formulation to ensure a shelf life of 1–2 years, and this is possible with THL lyophilization. Recent work shows that THLs fully conjugated with MAb and encapsulating plasmid DNA can be lyophilized, stored, and re-hydrated providing the proper lyoprotectant is used [707]. Lyophilized and re-hydrated THLs passed manufacturing specifications when hydroxypropyl- $\gamma$ -cyclodextrin is used as the lyoprotectant [707]. The lyophilized, re-hydrated HIRMAb-THLs encapsulating a 5 kb plasmid DNA was injected intravenously in Rhesus monkeys at injection doses of 12 and 58 µg/kg of THL encapsulated plasmid DNA. The pharmacokinetics (PK) of plasma clearance of the plasmid DNA was determined by qPCR [707], and these PK parameters were comparable to those reported previously for HIRMAb plasma clearance in the primate [61]. IV administration of the lyophilized, hydrated THLs to Rhesus monkeys produced no adverse clinical events and no change in 25 serum chemistries [707].

**Variety of THL formulations.** Polymeric NPs (PNPs) were prepared with 45 kDa PLA and PLA-PEG-maleimide [1080], similar to the PLA NPs shown in Figure 15. The PNPs were mixed with an expression plasmid encoding TNF related apoptosis-inducing ligand (TRAIL), which is cytotoxic in tumors. The PLA-PEG, PLA-PEG-maleimide, and plasmid DNA were mixed and PNPs produced with an emulsion/solvent evaporation. The primary and secondary emulsions were produced by sonication [1080]. There is concern about the integrity of the DNA using such a procedure, since sonication can nick super-coiled plasmid DNA [1081,1082], which would reduce or eliminate gene expression. The Trojan horse used in these THLs was cationized bovine serum albumin (cBSA) and the thiolated cBSA was conjugated to the PEG extended maleimide [1080]. The Trojan horse PNPs were tested *in vivo* with a rat C6 intra-cranial glioma implanted in the striatum of BALB/c mice. Mice were treated at 7 days following implantation of the rat glioma cells, and were treated every 2–3 days for 2 weeks with a large dose, 100 µg/kg, of PNP encapsulated plasmid DNA. This treatment extended the median survival from 20 days to 42 days [1080]. In another study, OX26 TfRMAb THLs encapsulated a LacZ expression plasmid under the influence of either a cytomegalovirus or GFAP promoter, were injected intravenously in rats, and THL-mediated transgene expression in brain was confirmed [1083]. THLs were prepared by double conjugation with the OX26 TfRMAb, for delivery of liposomes across the rat BBB, and with chlorotoxin (CTX), a 4 kDa peptide from scorpion venom, which binds glioma cells [1084]. The plasmid DNA, pC27, encodes a 27 kDa carboxyl terminal peptide of human telomerase reverse transcriptase, which suppresses glioma growth. For production of THLs, the lipids, which included a PEG-maleimide, and plasmid DNA were initially sonicated prior to liposome formation by extrusion. The thiolated OX26 and thiolated CTX were then conjugated at the maleimide group on the THLs. Since sonication can damage super-coiled DNA [1081,1082], it is not advisable to sonicate after addition of DNA to the preparation. When DNA is exposed to sonication, the retention of the super-coiled conformation of the plasmid DNA should be confirmed by agarose gel electrophoresis, which typically elutes as



multiple bands [707]. The therapeutic effects of the double conjugated THLs encapsulating the pC27 plasmid DNA were tested with a C6 intra-cranial glioma model in rats. The THLs conjugated only with the OX26 TfRMAb extended median survival of the tumor-bearing rats from 13 days to 29 days, and THLs double conjugated with the OX26 TfRMAb and CTX extended median survival of the rats to 46 days [1084]. In another approach, THLs were conjugated with an antibody against the IGF2 receptor (IGF2R), and encapsulated a plasmid DNA encoding p11, a 10–12 kDa protein implicated in depression [1085]. The results of these studies are difficult to interpret, since no information on the IGF2R MAb is provided. There are two types of IGF2R, and only one of these is expressed at the BBB. The IGF1R, which has high affinity for both IGF1 and IGF2, is expressed at the BBB, as discussed in Section 8.1.3. IGF2 also binds the 300 kDa cation independent M6PR, but this receptor is not expressed at the BBB, as discussed in Section 8.1.3, and recently reviewed [709]. Glutathione (GSH) has been conjugated to pegylated liposomes to trigger transport across the BBB by a putative GSH transporter at the brain endothelium (672). A pharmacokinetic analysis of brain transport of the GSH-pegylated liposome concluded the data did not support a model of transcytosis through the brain endothelium [1086]. This finding is expected for GSH conjugated THLs, since there is no known receptor for GSH at the BBB, and GSH does not cross the BBB, as discussed in Section 8.2.1.

**THL diffusion in brain.** Pegylated immunoliposomes were conjugated with the rat RI7-217 MAb against the mouse TfR [1087], as this 'RI7' TfRMAb undergoes RMT across the mouse BBB in vivo [663]. The transport of the RI7 TfRMAb-THLs across pial microvessels in mouse brain was investigated with two-photon microscopy through a cranial window [1087]. The findings led to the conclusion that while receptor-mediated endocytosis of the TfRMAb-THLs was an active process at the brain capillary, the exocytosis of the THL from the capillary endothelium into brain ECS was limited, as compared to a much higher rate of exocytosis into the brain ECS at post-capillary venules [1087]. The differential transport of THLs across the endothelium of the capillary vs. the post-capillary venule was said to be due to the lack of a peri-vascular space (PVS) at the capillary, and the presence of a PVS at the post-capillary venule [1087]. The hypothesis of an absent capillary PVS is derived from the assumption that the brain capillary is >90% invested by astrocyte foot processes. Electron microscopy of rat brain removed following aldehyde perfusion fixation shows an essentially complete ensheathment of the abluminal surface of the brain capillary by astrocyte foot processes [1088]. Owing to this complete investment of the capillary by astrocyte foot processes, it is assumed there is a fusion of the capillary basement membrane and the separate basement membrane lining the glial limitans or astrocyte foot processes, thus eliminating any PVS at the brain capillary [1089]. Conversely, at the post-capillary venule, it is said there is a separation of the capillary basement membrane and the glial limitans basement membrane, which creates a PVS at the post-capillary venule [1089]. The problem with this theory of complete investment of the capillary by the astrocyte endfeet, thus obliterating a PVS at the capillary, is that the theory is based on an artifact derived from electron microscopy of chemically fixed brain. A different picture of the brain PVS and astrocyte endfeet emerges with cryo-fixation of brain, as shown in Figure 18 and discussed below.

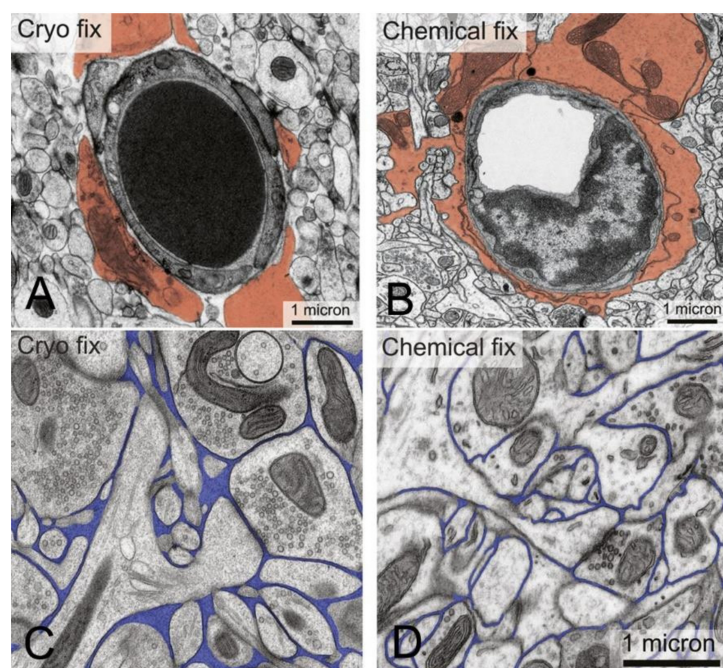


**Figure 18. Astrocyte endfeet and brain extracellular space in cryo-fixed and chemical-fixed brain.** (A,B) Brain capillary ultrastructure after cryo-fixation (A) and chemical fixation (B). The astrocyte endfeet are pseudo-colored in orange. An erythrocyte is present within the capillary lumen in (A). (C,D). Brain extracellular space after cryo-fixation (C) and chemical fixation (D). The extracellular space is pseudo-colored in blue. Reproduced from [22], Copyright© 2015 licensed under Creative Commons Attribution License (CC-BY).

Electron microscopy of chemically fixed brain performed in the 1950s found a very small ECS in brain of only 3%, which did not comport with physiologic measurements of a brain ECS of ~25% of brain, as reviewed by Van Harreveld and colleagues in 1965 [1090]. A brain ECS volume of 24% was estimated by electron microscopy following cryo-fixation of brain [1090]. More recently, the investment of the capillary by astrocyte endfeet has been examined with electron microscopy following cryo-fixation of brain in comparison with chemical fixation of brain [22]. Chemical fixation causes astrocyte swelling and ECS shrinkage, which leads to an over-estimation of the capillary endothelial coverage by astrocyte foot processes [22]. Following cryo-fixation, only 63% of the capillary abluminal surface is invested by astrocyte foot process [22], whereas 94% coverage of the abluminal surface of the brain capillary by astrocyte endfeet is found with chemical fixation of brain [22]. The ECS volume of brain is estimated to be 15% following cryo-fixation, but only 2.5% following chemical fixation [22]. The brain capillary ultrastructure and brain ECS revealed by electron microscopy and cryofixation, which demonstrates the incomplete investment of the brain capillary by astrocyte endfeet, and the expanded brain ECS, is reproduced in Figure 18.

Following exocytosis at the abluminal membrane of the endothelium, the THL must diffuse 5–20 microns through the brain ECS to the neighboring neuron or glial cell body. The extent to which nanoparticles with a diameter of 100–150 nm can diffuse through the porous structure of the brain ECS was examined in living mouse brain with fluorescent microscopy through a cranial window following the intra-cerebral injection of pegylated polystyrene nanoparticles [1091]. Diffusion of pegylated nanoparticles was also measured with slices of fresh human brain removed at neurosurgery [1091]. Surface pegylation of the nanoparticle enhanced nanoparticle diffusion through the brain ECS [1091]. Functional pores in the ECS of human brain as large as 200 nm were observed, and 25% of human ECS pores had a diameter  $\geq 100$  nm [1091]. A definitive proof that THLs transcytose through the BBB, diffuse through brain ECS, and are taken up by brain cells is the histochemistry

of brain showing global expression of a transgene in brain following IV administration of THLs encapsulating the plasmid DNA, as illustrated in Figure 17E–H for primate brain. Similar studies show global expression in brain of the transgene following THL delivery in the rat [1048] and mouse [1049].

### 11. Blood–Brain Barrier Transport Methodology

**Log BB.** The BBB is the limiting factor in the development of small molecule drugs for the CNS. In an effort to predict which small molecule drugs cross the BBB, the log BB parameter has been used for decades [1092], where BB is the brain/blood ratio of total drug in each compartment. A linear correlation between log BB and log P, where P = the drug partition coefficient in 1-octanol and water, was observed [1092]. The log BB is still used today [1093], despite the fact that the limitations of this parameter have been known for many years [1094]. The BB parameter, or brain/blood ratio, is a measure of the brain volume of distribution (VD), which is driven largely by brain tissue binding of drug. Thus, two drugs could have comparable rates of BBB transport, but widely disparate BB values, because one of the two drugs was avidly bound by brain tissue binding proteins, which increase the brain VD or BB ratio. The log BB parameter is being replaced by a new parameter,  $K_{p,uu}$  [1095], which is the concentration of *unbound* drug in brain, designated here as  $L_M$ , divided by the *unbound* drug in plasma, designated here as  $L_F$ . The problem with the  $K_{p,uu}$  parameter, i.e., the  $L_M/L_F$  ratio, relates to how one experimentally measures the concentration of unbound drug in brain and the concentration of unbound drug in plasma, and whether the *in vitro* methods used to compute  $K_{p,uu}$  are reliable indices of the  $L_M/L_F$  ratio in brain *in vivo*. An understanding of the factors controlling  $L_M$  and  $L_F$  in brain *in vivo* can be aided with a physiologic-based mathematical model of free drug in brain and plasma *in vivo*.

#### 11.1. Physiologic Model of Free Drug in Brain and Plasma

A physiologic partly flow/partly compartmental mathematical model of brain transport of circulating drugs or hormones was developed to understand the relationship between the free drug in brain *in vivo* and the free drug in the brain capillary plasma compartment *in vivo* [1096], and this model is shown in Figure 19A.

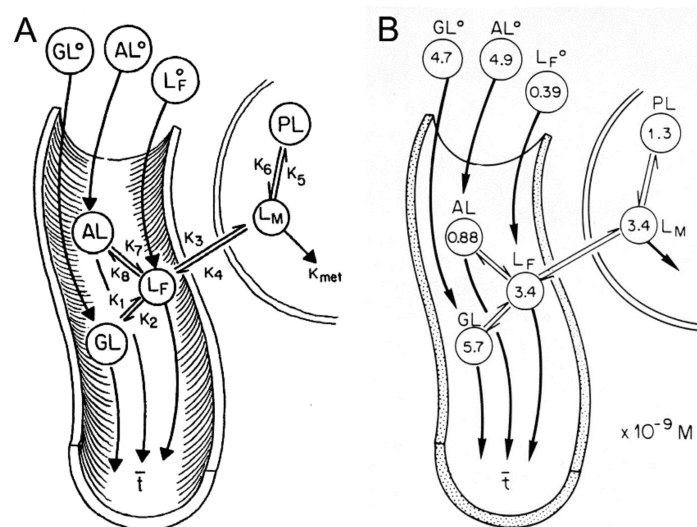


**Figure 19.** Partly flow-partly compartmental model of drug influx and efflux at the BBB and drug binding to plasma proteins and brain tissue proteins. (A) Drug in plasma may be bound to a plasma globulin, such as  $\alpha_1$ -acid glycoprotein (AAG), which is  $GL^\circ$  and GL in the arterial and capillary compartments, respectively, or bound to albumin, which is  $AL^\circ$  and AL, or may be free, which is  $LF^\circ$  or  $LF$ , in the arterial and capillary compartments, respectively. The free drug in brain is  $L_M$ , and the tissue bound drug in brain is PL. The rate constant of drug metabolism is  $K_{met}$ . The rate constants of drug dissociation with AAG, albumin, and the tissue binding protein are  $K_1$ ,  $K_7$ , and  $K_6$ ,

respectively. The products of the rate constants of drug association and the concentration of the respective protein are given by  $K_2$ ,  $K_8$ , and  $K_5$ , respectively, for AAG, albumin, and the tissue binding protein. The rate constants of drug influx and efflux across the BBB are  $K_3$  and  $K_4$ , respectively. The brain capillary transit time is denoted as  $\bar{t}$ . (B) Model predictions for testosterone concentrations in plasma and brain pools shown in (A). Model simulation is based on plasma sex hormone binding globulin and albumin concentrations of 28 nM and 640  $\mu\text{M}$ , respectively. Reproduced with permission from [1096], Copyright© 1985 American Physiological Society.

The mathematical model of Figure 19A was solved analytically, and yielded the relationship for the ratio of free drug in brain ( $L_M$ ) and free drug in plasma ( $L_F$ ) given in Equation (2),

$$\frac{L_M}{L_F} = (K_3 \cdot V_p) / [(K_4 + K_{\text{met}}) VT] \quad (2)$$

where  $V_p$  is the plasma volume of brain, 10  $\mu\text{L/g}$ ,  $VT$  is tissue volume of brain, 700  $\mu\text{L/g}$ ,  $K_3$  is the rate constant of drug influx from blood to brain across the BBB,  $K_4$  is the rate constant of drug efflux from brain to blood across the BBB, and  $K_{\text{met}}$  is the rate constant of drug metabolism in brain. Drug metabolism in brain may also take place within the endothelial compartment, owing to an enzymatic BBB, such as in the case for adenosine [391]. Since  $K_3 \cdot V_p$  is equivalent to the permeability–surface area (PS) product of influx,  $PS^{\text{influx}}$ , from plasma to brain across the BBB, and  $K_4 \cdot VT$  is equivalent to the PS product of efflux,  $PS^{\text{efflux}}$ , from brain to plasma across the BBB, then in the absence of significant drug metabolism in brain, where  $K_{\text{met}} = 0$ , then Equation (2) reduces to,

$$K_{p,uu} = \frac{L_M}{L_F} = \frac{PS^{\text{influx}}}{PS^{\text{efflux}}} \text{ or, } L_M = \left[ \frac{PS^{\text{influx}}}{PS^{\text{efflux}}} \right] \cdot L_F \quad (3)$$

The approximation of  $K_{p,uu}$  by the  $PS^{\text{influx}}/PS^{\text{efflux}}$  ratio, given in Equation (3), has been recently proposed by Huttenen and colleagues [1097]. A  $PS^{\text{influx}}/PS^{\text{efflux}}$  ratio  $< 1$  is indicative of active efflux transport at the BBB. A  $PS^{\text{influx}}/PS^{\text{efflux}}$  ratio  $= 1$  is indicative of symmetric BBB transport, e.g., for a lipid-soluble drug that traverses the BBB via free diffusion.

The complexity of the factors controlling  $L_M$  and  $L_F$  in brain in vivo arises from the fact that many CNS drugs are bound by proteins in both plasma and in brain [1098]. Drug binding plasma proteins include albumin and globulins. The major drug binding globulin is  $\alpha_1$ -acid glycoprotein (AAG) also called orosomucoid. The physiologic model in Figure 19A accounts for the kinetics of drug binding to albumin and globulin plasma proteins, drug binding to brain tissue proteins, drug influx and efflux across the BBB, and drug metabolism in brain [1096].

The model in Figure 19A treats the brain interstitial and intracellular spaces as a single extravascular pool, owing to a much greater brain cell membrane surface area as compared to the surface area of the BBB, which is 120  $\text{cm}^2/\text{g}$  [11]. There are approximately 200 billion neuronal and non-neuronal cells in the 1000 g human brain [1099]. Modeling each cell as a 10-micron cuboidal structure yields a total brain cellular surface area of 1200  $\text{cm}^2/\text{g}$ , which is 10-fold greater than the surface area of the BBB.

The model in Figure 19A was evaluated for testosterone transport from blood to brain, and the results of the model simulation for testosterone are shown in Figure 19B, which gives the testosterone concentrations in the various pools of plasma and brain, as reported previously [1096]. As discussed in the next section, there is enhanced dissociation of testosterone from albumin within the brain capillary compartment in vivo [1100]. This enhanced dissociation produces a 9-fold elevation in the concentration of free (bioavailable) testosterone in the brain capillary in vivo ( $L_F$ ), 3.4 nM, relative to the concentration of free (dialyzable) drug in vitro, 0.39 nM, which is represented by the drug concentration in the arterial compartment ( $L_F^\circ$ ) in Figure 19. The concentration of free drug in brain,  $L_M$ , is identical to the bioavailable drug in the brain capillary compartment,  $L_F$  (Figure 19B). This

identity between  $L_M$  and  $L_F$  is predicted by Equation (3) when drug transport across the BBB is symmetrical, i.e.,  $PS^{influx} = PS^{efflux}$ , and the drug is not metabolized in brain [1096].

The sections below review the methods available for determination of the 4 principal factors controlling in vivo  $K_{p,uu}$ , which are the free (bioavailable) drug in plasma ( $L_F$ ), the free drug in brain ( $L_M$ ),  $PS^{influx}$ , and  $PS^{efflux}$ , with the assumption that drug metabolism in brain is nil, i.e.,  $K_{met} = 0$ .

### 11.2. Free Drug in Plasma In Vivo and Role of Plasma Protein Binding

The major drug binding plasma proteins are albumin and  $\alpha_1$ -acid glycoprotein (AAG), also called orosomucoid. AAG is a 42 kDa heavily glycosylated plasma protein and the 3D structure of human AAG has been determined [1101]. AAG binds many drugs, and together with albumin, plays a major role in plasma protein binding of drugs [1101]. AAG is an acute-phase reactant, and the plasma AAG concentration can vary over 7-fold depending on the clinical condition [1102]. The concentration of AAG in plasma, about 0.1 g/dL, is 50-fold lower than the plasma albumin concentration [1102]. However, the affinity of AAG for many drugs can be 100-fold higher than the affinity of the drug for albumin binding. Therefore, many CNS drugs are bound by both albumin and by AAG in plasma.

The number of drugs that are highly bound by plasma proteins, e.g., >95% bound, is increasing. Before 2003, only about 30% of FDA-approved small molecules were classified as highly bound, but this number has increased to 45% of all drugs by 2019 [1103]. Therefore, it is important to develop a model of how plasma protein binding impacts the brain uptake of small molecule CNS drugs. The free drug hypothesis posits that the fraction of drug in plasma that is bioavailable for transport across the BBB, i.e., pool  $L_F$  in Figure 19 and Equation (3), is the same fraction that is free in plasma in vitro, as determined by a variety of methods, one of which is equilibrium dialysis [1104]. The free drug hypothesis is equivalent to the assertion that the dissociation constant,  $K_D$ , governing the binding of drug to the plasma protein that is measured in vitro, or  $K_D^{in vitro}$ , is identical to the  $K_D$  of drug binding to the plasma protein at the brain endothelial interface in vivo, or  $K_D^{in vivo}$ . If the guiding principle is, "to measure is to know" [1105], then this assumption of the free hormone hypothesis should be subjected to direct empiric testing in vivo. That is, the  $K_D$  of the drug–plasma protein binding should be measured in vivo. If the drug–plasma protein  $K_D^{in vivo}$  is  $\gg$  than the  $K_D^{in vitro}$ , then enhanced ligand dissociation from the plasma protein occurs in vivo within the brain capillary compartment, relative to the dissociation rates observed in vitro. Conversely, if the  $K_D^{in vivo} = K_D^{in vitro}$ , then the precepts of the free drug hypothesis are upheld with in vivo testing of the hypothesis.

Enhanced drug dissociation from plasma proteins such as albumin or AAG would be caused by conformational changes about the drug binding site on the plasma protein that takes place in vivo at the brain endothelial surface. Surface-mediated conformational changes have been documented for both albumin and AAG [1106,1107]. As plasma courses through the cerebral microcirculation, plasma proteins such as albumin or AAG transiently and reversibly bind the endothelial luminal glycocalyx [1108]. The brain endothelial glycocalyx is shown in Figure 20.

The glycocalyx covers 40% of the luminal surface of the brain capillary endothelium [20]. The thickness of the glycocalyx of the brain endothelial luminal membrane is up to 400 nm based on two-photon microscopy [19], and this finding on the thickness of the brain endothelial glycocalyx is confirmed by the electron micrograph in Figure 20. Therefore, the thickness of the endothelial glycocalyx is actually greater than the thickness of the brain capillary endothelium, 300 nm [17], as illustrated in Figure 20. Albumin binds reversibly to the glycocalyx surface of both the endothelium [1109] and the hepatocyte [1110]. The glycocalyx is composed of glycosaminoglycans (GAGs), which bind plasma proteins, including albumin and AAG [1108].

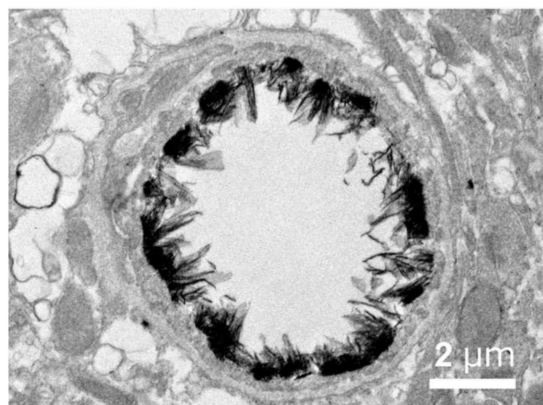


**Figure 20. Glycocalyx at the blood–brain barrier.** Brain capillary endothelial glycocalyx is visualized with lanthanum nitrate staining in the mouse. Reproduced from [20], Copyright© 2018 licensed under Creative Commons Attribution License (CC-BY).

Albumin conformational changes have been observed following albumin binding either to GAGs [1107] or to the liver cell surface [1110]. The binding of AAG to GAGs [1111], or to biomembranes [1112], triggers conformational changes within the AAG protein that results in enhanced dissociation of drugs bound to AAG [1112]. If enhanced dissociation does occur at the brain endothelial interface, then the plasma protein-bound drug is operationally available for transport into brain, although there is no egress of the plasma protein, per se, from the plasma compartment of brain.

The  $KD^{in vivo}$  of drug binding to AAG, human serum albumin, or bovine serum albumin within the brain capillary has been measured using the Brain Uptake Index (BUI) carotid artery injection technique [1100], described below in Section 11.4.1. The  $KD^{in vivo}$  in brain, and the  $KD^{in vitro}$ , as measured by equilibrium dialysis, is shown in Table 5 for multiple drugs and hormones.

**Table 5.** Drug binding to plasma proteins in vitro and in vivo within the brain capillary.

Drug	Plasma Protein	$KD^{in vitro}$ ( $\mu M$ )	$KD^{in vivo}$ ( $\mu M$ )	Reference
propranolol	bovine albumin	$299 \pm 25$	$220 \pm 40$	[1102]
	AAG	$3.3 \pm 0.1$	$19 \pm 4$	
bupivacaine	bovine albumin	$141 \pm 10$	$211 \pm 107$	[1113]
	AAG	$6.5 \pm 0.5$	$17 \pm 4$	
piroxicam	human albumin	$10.9 \pm 0.1$	$910 \pm 105$	[1114]
	AAG	$29 \pm 1$	$35 \pm 3$	
diazepam	bovine albumin	2	13,900	[1115]
	human albumin	$6.3 \pm 0.1$	$156 \pm 35$	
devazepide	human albumin	$8.2 \pm 0.8$	$266 \pm 38$	[1116]
imipramine	AAG	$4.9 \pm 0.3$	$90 \pm 9$	[1117]
	human albumin	$62 \pm 8$	$221 \pm 7$	
isradipine	AAG	$6.9 \pm 0.9$	$35 \pm 2$	[1118]
	human albumin	$94 \pm 5$	$203 \pm 14$	
darodipine	AAG	$2.5 \pm 0.5$	$55 \pm 7$	[1115]
	bovine albumin	35	$36 \pm 4$	
L-tryptophan	bovine albumin	$130 \pm 30$	$1700 \pm 100$	[1119]
L-T3	bovine albumin	$4.7 \pm 0.1$	$46 \pm 4$	[1100]
testosterone	bovine albumin	$53 \pm 1$	$2520 \pm 710$	[1100]

AAG = human  $\alpha_1$ -acid glycoprotein; assumes 1 drug binding site on each plasma protein.

The  $KD^{in vivo}$  was measured with the Kety–Renkin–Crone equation of capillary physiology, as described in Equation (4).

$$E = 1 - e^{-f \cdot \frac{PS}{F}}, \text{ where } f = \left( \frac{KD^{in vivo}}{n} \right) / \left( A + \frac{KD^{in vivo}}{n} \right) \quad (4)$$

The extraction (E) of unidirectional influx of drug across the BBB following the carotid injection of the radiolabeled drug in the presence of different concentrations of the plasma protein is fit to Equation (4), where  $F$  = cerebral blood flow,  $f$  = the fraction of bioavailable drug in vivo in the brain capillary,  $A$  = the plasma protein concentration in the carotid artery injection solution, and  $n$  = the number of binding sites on the plasma protein [1100]. Curve fits are performed with non-linear regression analysis to estimate two parameters: the PS/F ratio and the  $KD^{in vivo}/n$ . The 'A' parameter is technically the concentration of unbound plasma protein ( $A_F$ ). However, the concentration of total albumin or total AAG in the carotid artery injection solution is >10-fold greater than the drug concentration. Therefore, the unoccupied plasma protein concentration is approximated by the total plasma protein concentration in the carotid arterial injection solution. The extraction  $E$  of the drug by brain is plotted on the  $y$ -axis, vs. the protein concentration ( $A$ ) on the  $x$ -axis, and non-linear regression analysis allows for computation of the PS/F ratio and the  $KD^{in vivo}/n$ , as described by Equation (4) [1100]. In parallel, the  $KD^{in vitro}$  is determined by equilibrium dialysis.

The  $KD^{in vivo}$  at the brain capillary, as measured with the BUI technique, and the  $KD^{in vitro}$ , as measured by equilibrium dialysis, have been determined in several studies on the binding of CNS drugs to AAG and to albumin, and these are summarized in Table 5. The experimental findings show that several albumin-bound drugs do not undergo enhanced dissociation at the brain capillary in vivo, and that the  $KD^{in vivo}$  is equal to the  $KD^{in vitro}$ , e.g., propranolol, bupivacaine, and domitroban [1098]. However, drugs such as piroxicam, diazepam, devazepide, isradipine, darodipine, the amino acid, L-tryptophan, L-triiodothyronine, and a steroid hormone such as testosterone, do undergo enhanced rates of ligand dissociation from albumin in vivo within the brain capillary, which is indicated by the finding of  $KD^{in vivo} \gg KD^{in vitro}$  (Table 5). With respect to drugs that bind AAG, propranolol, bupivacaine, imipramine, isradipine, and darodipine undergo enhanced dissociation within the brain capillary in vivo, whereas the binding of piroxicam to AAG in vivo within the brain capillary conforms to the binding of this drug to AAG in vitro [1098]. The measurement of the  $KD^{in vivo}$  with the BUI method can confirm the predictions of the free drug hypothesis, i.e.,  $KD^{in vivo} = KD^{in vitro}$ . However, in many instances, the free drug hypothesis is not confirmed in vivo, and the  $KD^{in vivo}$  is  $\gg KD^{in vitro}$ .

The finding of  $KD^{in vivo} \gg KD^{in vitro}$  is evidence for enhanced dissociation of ligand from the plasma protein binding site in vivo within the brain capillary, which nullifies the key assumption of the free drug hypothesis. The only way to reconcile the in vivo brain drug uptake results with a hypothesis that asserts the  $KD^{in vivo} = KD^{in vitro}$  is a dissociation-limited model [1098]. The dissociation-limited model must posit that *both* drug re-association with the plasma protein in vivo *and* drug dissociation from the plasma protein in vivo are very slow compared to membrane permeation. Using the parameters in Figure 19A, the dissociation-limited model assumes both  $K_7 \ll K_3$  and  $K_8A_F \ll K_3$ . Given the parameters of drug binding to the plasma protein, membrane permeation ( $K_3$ ) would have to be more than 2–3 log orders greater than the transit time of plasma through the brain capillary [1098], which would be equivalent to a BBB PS product that is 2–3 log orders higher than the rate of cerebral blood flow ( $F$ ). The PS/F ratios for the drugs studied in the reports cited in Table 5 ranged from 0.14–1.35 with a mean of 0.88. These PS/F ratios are far too low to allow for a dissociation-limited mechanism of plasma protein-bound drugs across the BBB in vivo.

The discordance between drug binding to a plasma protein in vitro vs. drug binding in vivo within the capillary extends to organs other than brain. As an example, warfarin is bound by albumin, and albumin-bound warfarin, similar to some other albumin-bound drugs (Table 5), does not undergo enhanced dissociation at the BBB in vivo [1120]. However, warfarin undergoes enhanced dissociation from albumin in the microcirculation of liver, where the  $KD^{in vivo}$  of albumin binding of warfarin is 403  $\mu$ M as compared to the  $KD^{in vitro}$  of albumin binding of warfarin, 20  $\mu$ M [1121]. Therefore, warfarin undergoes a 20-fold enhanced dissociation from albumin at the liver microcirculation [1121], but

there is no enhanced dissociation at the warfarin binding site on albumin at the brain microcirculation [1120].

Albumin bound steroid hormones, e.g., testosterone, albumin bound thyroid hormones, e.g., L-triiodothyronine (T3), and albumin bound L-tryptophan are available for transport across the BBB [322,433,1122], as exemplified by the high  $KD^{in vivo}$  relative to the  $KD^{in vitro}$  (Table 5). Conversely, globulin-bound steroid and thyroid hormones are generally not available for transport into brain, but are available for transport into liver in vivo [322,1098,1122,1123]. The plasma protein, per se, does not undergo transport into brain or liver. The plasma protein-bound drug or hormone is said to undergo transport into the organ in vivo, because the fraction of drug or hormone that is free (bioavailable) in the organ capillary in vivo is much greater than the free fraction of drug or hormone measured in vitro, e.g., with equilibrium dialysis. The enhanced dissociation of drug or hormone from albumin and/or globulin binding sites in vivo within the brain capillary compartment increases the free drug in the brain capillary plasma compartment,  $L_F$ , relative to the free drug measured in vitro,  $L_F^\circ$  (Figure 19B). The fact that the  $KD^{in vivo}$  is often many-fold higher than the  $KD^{in vitro}$ , as shown in Table 5, means the use of in vitro measurements of free drug in plasma, e.g., with equilibrium dialysis, may not provide an accurate representation of the drug–plasma protein binding interactions that take place in vivo at the brain endothelial surface. Under these conditions, the free drug in plasma in vivo within the brain capillary compartment,  $L_F$ , is much greater than the free drug in plasma in vitro in a test tube.

### 11.3. Measurement of Free Drug in Brain

#### 11.3.1. CSF as a Measure of Free Drug in Brain

CSF is frequently used as a surrogate measure of drug transfer across the BBB, particularly in humans. This is based on ideas from the first half of the 20th century that CSF represents brain interstitial fluid (ISF) [26,32]. However, early dialysis fiber experiments showed that atenolol did not appear in the intra-cerebral micro-dialysate following ICV injection [88], and subsequent reviews commented on the lack of suitability of use of CSF drug penetration as an index of BBB transport [1124,1125]. In addition to the lack of equilibrium between CSF and ISF, the CSF and ISF compartments are separated from blood by different membrane systems. The ISF is separated from the blood by the BBB and the CSF is separated from the blood by the choroid plexus. These anatomically distinct barriers are also functionally distinct and transporters that exist at the BBB may not exist at the choroid plexus and vice versa. As reviewed in Section 6.3.2, P-glycoprotein (Pgp) is expressed at the BBB [62], but is not expressed at the choroid plexus [62,478,479]. Co-administration of a Pgp inhibitor, zosuquidar, with nelfinavir, a Pgp substrate, produced an increase in brain distribution into brain, but not into CSF [477]. While the use of CSF as a surrogate for BBB transport has declined over the years for small molecule CNS drugs, developers of biologic drugs for the CNS still use CSF as a surrogate measure of BBB penetration, as discussed in Section 8.3.4. The CSF concentration of a therapeutic antibody is 0.1–0.2% of the plasma concentration, and this is said to indicate a small, but significant passage of the antibody across the BBB [784,785]. What is overlooked is that all IgG in plasma penetrates into CSF via passage across a leaky choroid plexus, and that the ratio of any IgG in CSF/plasma is normally 0.1–0.2% [12], which exists in the absence of any IgG transport across the BBB.

#### 11.3.2. Free Drug in Brain with Cerebral Microdialysis

Brain ISF is a protein-free compartment, so drug concentration in brain ISF is considered a measure of the free drug concentration in brain. Brain ISF is experimentally accessible with the implantation of an intra-cerebral dialysis probe [1126]. The experimental limitations of cerebral microdialysis were recognized early [88], and they include the lack of correlation of drug recovery across the dialysis membrane in vivo vs. in vitro, role of infusate temperature, and changes in the local brain environment triggered by what is effectively a stab wound of brain. The neuropathologic changes that are induced



by insertion of a dialysis probe into brain was shown by an early study, which detected BBB disruption to circulating albumin by immunohistochemistry of brain following probe insertion [1127]. The entry of albumin into brain triggers an astrogliosis and microglia reaction in brain following insertion of the fiber [1128]. Placement of the microdialysis fiber in brain induces BBB disruption to small molecules as well as to albumin [1129,1130]. Film autoradiography was used to follow the BBB disruption to sucrose following insertion of the dialysis fiber. BBB permeability to sucrose was increased in a biphasic manner, and was increased 19-fold immediately after fiber insertion, and then 17-fold at 2 days after fiber insertion. BBB disruption persisted for at least 28 days after fiber implantation [1129].

#### 11.3.3. Free Drug in Brain In Vitro with Brain Slices or Homogenates

An alternative to cerebral microdialysis was developed using brain slices or homogenates. Drug is mixed with either the brain slice or brain homogenate and the volume of distribution of drug is measured from the ratio of drug concentration in the slice or homogenate relative to the medium drug concentration [1095,1131]. Drugs may be avidly bound by brain proteins, and this sequestration by brain can be examined with either brain homogenate or brain slice preparations. However, many CNS drugs are lipophilic amines, which are sequestered within the acidic intracellular lysosomal compartment, which can have a pH of 4.5–5.5. This acidity will trap a drug with a high pKa, where pKa is the pH at which 50% of the drug is ionized. The brain slice method is superior to the homogenate method as intracellular organelles, as well as brain cell membrane transporters, are intact in the brain slice preparation [1131]. The data provided with the brain slice or brain homogenate method is very useful in understanding the mechanisms by which drugs are bound and sequestered in brain. The problem with this in vitro methodology is that the free drug that is measured with a brain slice or homogenate in vitro, which is dominated by brain binding/sequestration mechanisms, is said to represent the free drug in brain in vivo [1095,1131]. However, the concentration of free drug in brain in vivo, which is shown as  $L_M$  in Figure 19A, is fully independent of brain binding/sequestration [1096]. As shown in Equation (2), the concentration of unbound drug in brain,  $L_M$ , is a function of the  $PS^{influx}$ ,  $PS^{efflux}$ ,  $K_{met}$ , and the bioavailable drug in plasma ( $L_F$ ), and is independent of tissue binding [1096]. The continuous flow of bioavailable drug in plasma,  $L_F$ , acts as a forcing function in vivo [1132], and this forcing function of the continuous flow of plasma is non-existent with in vitro preparations of brain. The tissue bound drug in brain in vivo ( $PL$ , Figure 19) contributes to the total brain drug concentration, and determines the brain VD or brain/blood ratio or the log BB. However, the free drug in brain in vivo is independent of tissue binding, and is controlled by bi-directional BBB transport ( $PS^{influx}$  and  $PS^{efflux}$ ), the plasma bioavailable drug ( $L_F$ ), and brain drug metabolism,  $K_{met}$ , as shown by Equation (2).

### 11.4. In Vivo Measurement of $PS^{influx}$

#### 11.4.1. Brain Uptake Index Method

The BBB permeability–surface area (PS) product of influx from blood to brain can be measured with the Brain Uptake Index (BUI) method of Oldendorf [46]. An ~0.2 mL buffered solution of a [ $^{14}C$ ]-test molecule, and a [ $^3H$ ]-water reference is rapidly injected into the common carotid artery of an anesthetized rat through a 27-gauge needle, followed by decapitation at 15 s. The BUI is the ratio of extraction of the unidirectional influx of the test molecule ( $E_{test}$ ), divided by the extraction of the water reference ( $E_{ref}$ ), and is computed from the ratio of  $^{14}C$ -DPM/ $^3H$ -DPM in brain divided by the same ratio in the injection solution. Since the BUI is a ratio of ratios, no measurements of brain weight or volume of injection solution are required. Since the test solution is injected into the common carotid artery, most of the injection solution is dispersed to organs other than brain via the external carotid artery [46]. However, this does not impact the measurement of  $E_{test}$ , because an identical fraction of the test and reference molecules are distributed to brain. The  $E_{test} = (BUI) \cdot (E_{ref})$ , and the PS product can be computed from  $E_{test}$  using Equation (4), which is the Kety–Renkin–Crone equation, where  $f = 1$

when there is no plasma protein binding. If the test molecule is [<sup>3</sup>H]-labeled, then a [<sup>14</sup>C]-butanol reference can be used [1133]. Alternatively, three isotopes (<sup>3</sup>H, <sup>14</sup>C, <sup>125</sup>I) can be injected followed by triple isotope liquid scintillation counting [1133]. BUIs may be performed in conscious rats by placement of a PE-10 catheter into the external carotid artery a day before the study [1133]. The co-injection of [<sup>3</sup>H]-water, [<sup>14</sup>C]-butanol, and [<sup>125</sup>I]-N-isopropyl-p-iodoamphetamine allows for computation of the E<sub>ref</sub> for either the [<sup>3</sup>H]-water or [<sup>14</sup>C]-butanol reference, which is 0.55 ± 0.01 and 0.87 ± 0.01, respectively, in the conscious rat [1133]. The cerebral blood flow (F) in the conscious, ketamine-anesthetized, and pentobarbital anesthetized rat is 1.64 ± 0.11, 0.93 ± 0.03, and 0.81 ± 0.09 mL/min/g, respectively [1133]. With the E<sub>ref</sub> value, the BUI is converted to E<sub>test</sub>, and, the PS<sup>influx</sup> is computed from the E<sub>test</sub> and F with the Kety–Renkin–Crone equation (4). The unidirectional clearance (CL) from blood to brain is defined as CL = E<sub>test</sub>·F, or CL = (BUI)·E<sub>ref</sub>·F. When cerebral blood flow (F) is greater than the PS<sup>influx</sup>, then the Kety–Renkin–Crone equation, given in Equation (4) where f = 1.0, is approximated by E = PS<sup>influx</sup>/F, and unidirectional CL ≈ PS<sup>influx</sup> [490].

**Carrier-mediated transport.** The Michaelis–Menten kinetics of carrier-mediated transport across the BBB in vivo can be determined with the BUI method, and Km and Vmax values for representative substrates of CMT systems are listed in Table 2. The relationship between PS, Km, Vmax, and K<sub>NS</sub>, where K<sub>NS</sub> is the constant of non-saturable transport (μL/min/g), is defined in Equation (5),

$$PS = [Vmax / (Km + S)] + K_{NS} \quad (5)$$

where Vmax is the maximal transport velocity (nmol/min/g), and Km (nmol/mL) is the absolute Km, which is the concentration (μM) of substrate (S) that causes 50% inhibition of transport. The Vmax, Km, and K<sub>NS</sub> are determined by non-linear regression analysis, where the substrate clearance (CL) is plotted on the y-axis and the substrate concentration in the injection solution (S) is plotted on the x-axis, and CL = (BUI)·(E<sub>ref</sub>)·(F).

In the case of a CMT system that transports multiple competing substrates, e.g., LAT1 or CAT1, then the Km is an apparent Km, or Km<sup>app</sup>, which is defined by Equation (6),

$$Km^{app} = Km \cdot \left[ 1 + \sum \left( \frac{S_i}{K_i} \right) \right] \quad (6)$$

The Km<sup>app</sup> is derived from the absolute Km of the substrate, which is determined in the absence of competing inhibitors, the absolute Km for each inhibitor (K<sub>i</sub>), and the concentration of competing inhibitor, S<sub>i</sub>, as shown in Equation (6) [1134]. The affinity of the CMT system is defined by the relationship between the absolute Km and the substrate concentration (S) in plasma. If the plasma S approximates Km, then the CMT system is high affinity, and Km<sup>app</sup> > Km, which indicates substrate competition effects take place in vivo. If the plasma S ≪ Km, then the CMT system is low affinity, and Km<sup>app</sup> = Km, which indicates there are no competition effects in vivo. The transport of LNAAs across the BBB via LAT1 is the classic high affinity system, as the plasma concentrations of LNAAs approximate the absolute Km values for the individual LNAAs [355]. The high affinity (low Km) of the BBB LAT1 system, and the approximation of LAT1 Km values by the concentrations of the individual LNAAs in plasma, is the physical basis of the selective vulnerability of the CNS to hyperaminoacidemias [356]. The hyperphenylalaninemia of phenylketonuria (PKU) saturates the BBB LAT1 system with phenylalanine, and this saturation inhibits the brain uptake of other LNAAs, which are needed in brain to sustain cerebral protein synthesis. Conversely, LNAA transport in peripheral tissues is mediated by low affinity transporters with high Km values, and peripheral tissues are not exposed to LNAA starvation in the case of a hyperaminoacidemia such as PKU. Any drug, e.g., L-DOPA or gabapentin, that crosses the BBB via transport on LAT1 is subject to competition effects for BBB transport by the LNAAs in plasma.

In summary, the BUI technique is a versatile methodology that allows for quantitation of the kinetics of substrate influx from blood to brain via a CMT system, as defined by Equation (5). The BUI method also allows for the determination of the KD of binding of drugs or hormones to plasma proteins *in vivo* within the brain microcirculation, as defined by Equation (4). This is possible because the injection solution traverses the brain microcirculation as a first pass bolus with only ~5% mixing with rat plasma [1134].

#### 11.4.2. Internal Carotid Artery Perfusion Method

The BUI method is less sensitive when the  $E^{\text{test}} < 3\text{--}5\%$ . In this case, BBB  $PS^{\text{influx}}$  can be determined with an internal carotid artery perfusion (ICAP) method [1135]. A PE-10 or PE-50 catheter is inserted in the external carotid artery, and the common carotid and pterygopalatine arteries are closed by ligation. Buffered fluid is perfused at rates of 1.2–5 mL/min for up to 5 min. At the end of the perfusion, the brain is removed for determination of brain radioactivity. A brain volume of distribution of the test molecule ( $VD^{\text{test}}$ ) is computed from the ratio of (DPM/g)/(DPM/ $\mu\text{L}$  perfusate). The perfusate also contains a second radiolabeled plasma volume (pv) marker, such as sucrose, and the VD of the plasma volume,  $VD^{\text{pv}}$ , is also determined [1135]. The  $PS^{\text{influx}} = (VD^{\text{test}} - VD^{\text{pv}})/T$ , where T = the length of the perfusion. The ICAP method is more labor-intensive than the BUI method.

#### 11.4.3. Capillary Depletion Method

The ICAP method was modified to allow for study of the kinetics of AMT or RMT of biologic large molecules [506]. In this approach, the perfusion rate was 1.0–1.2 mL/min and the perfusion time was extended up to 10 min. For perfusion times  $>2.5$  min, the rat blood volume was maintained constant by withdrawal of blood from a femoral artery catheter at the same rate as the infusion [506]. In the case of AMT or RMT of large molecules, it is important to separate endocytosis at the endothelium from transcytosis through the endothelial barrier, and this was performed with the capillary depletion method [506]. At the end of the perfusion, the brain is homogenized in cold 13% 60 kDa dextran, followed by centrifugation at 4 °C for 15 min at  $5400 \times g$  in a swinging bucket rotor, and the post-vascular supernatant is carefully separated from the vascular pellet. Radioactivity is measured in each of the three fractions: total homogenate, post-vascular supernatant, and vascular pellet. Measurement of the activity of vascular specific enzymes,  $\gamma$ -glutamyl transpeptidase ( $\gamma\text{GTP}$ ) and alkaline phosphatase, showed the post-vascular supernatant was 94–95% depleted of brain vasculature [506]. Therefore, test molecules that distributed to the post-vascular supernatant had undergone transcytosis through the BBB during the perfusion period. The capillary depletion method was validated by the perfusion of acetylated LDL, a molecule that is only endocytosed into the capillary endothelium, and not transcytosed, as discussed in Section 9.2.1. Acetylated LDL was recovered only in the vascular compartment and not in the post-vascular supernatant [506]. During the homogenization of brain, the acetylated LDL was retained in the vascular pellet owing to the high affinity binding of this ligand to the scavenger receptor, which has a binding  $KD = 3$  nM [1136]. Owing to this high affinity binding of acetylated LDL to the scavenger receptor, and also to the performance of the capillary depletion method at 4 °C at all steps, the acetylated LDL stays retained in the vascular compartment despite the homogenization of brain. Since the description of the capillary depletion method in 1990 [506], the method has been described in  $>300$  publications in PubMed. In several of these studies, the capillary depletion method has not been used as originated, because the method has been applied to ligands with low affinity binding to the putative receptor at the BBB. Such low affinity ligands have rapid dissociation rates, and will most likely dissociate from the brain vasculature and appear in the supernatant during the homogenization process. This ligand dissociation from the BBB receptor during the homogenization will produce an artifact of ligand distribution to the post-vascular supernatant, and this artifact will be ascribed to BBB transcytosis. The capillary depletion method was developed only for ligands that bind to the target receptor

on the BBB with high affinity, such that there is no dissociation from the capillary receptor during the homogenization process.

#### 11.4.4. Intravenous Injection Methods

The  $PS^{\text{influx}}$  can be determined following the IV co-injection of the labeled test molecule and a radiolabeled plasma volume marker, such as albumin. The drug concentration in brain (nmol/g), divided by the drug concentration in plasma (nmol/uL), is the brain VD ( $\mu\text{L/g}$ ) of the test molecule,  $VD^{\text{test}}$ . The brain VD of the plasma volume marker,  $VD^{\text{PV}}$ , also with units of  $\mu\text{L/g}$ , is measured in parallel. The terminal plasma concentration,  $C_p(T)$ , (nmol/ $\mu\text{L}$ ), and the plasma area under the curve concentration (pAUC) (nmol·min/uL) during the time period (min) between IV injection and removal of brain, are also measured, as shown by Equation (7). The  $PS^{\text{influx}}$  is computed as follows [1094],

$$PS^{\text{influx}} = \frac{[(VD^{\text{test}} - VD^{\text{PV}}) \cdot C_p(T)]}{pAUC} \quad (7)$$

There are several caveats associated with determination of the  $PS^{\text{influx}}$  by IV injection methods, and these include (a) limitation of the time period of the influx measurement so that there is minimal efflux from brain back to blood; (b) measurement of the brain plasma volume ( $VD^{\text{PV}}$ ); (c) elimination of artifacts of brain uptake caused by peripheral degradation of the radiolabeled test molecule, and (d) determination of the plasma AUC or pAUC.

**Brain plasma volume.** The brain plasma volume is visualized by the histochemistry of mouse brain removed after the IV administration of HRP, as shown in Figure 21.

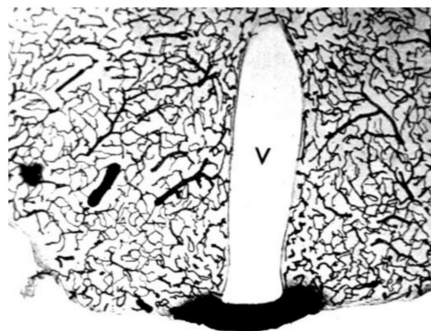


**Figure 21. Brain plasma volume.** Histochemistry of mouse brain following the IV administration of horseradish peroxidase (HRP), a 40 kDa enzyme. The enzyme is retained in the plasma volume of brain, except for the median eminence at the base of the third ventricle (V). Image provided as a gift from Dr. Milton W. Brightman. Reproduced from [709], Copyright© 2022 licensed under Creative Commons Attribution License (CC-BY).

It may seem paradoxical that a CNS drug, particularly a biologic drug, such as a therapeutic antibody, could be measurable in a homogenate of brain following IV administration, yet have not crossed the BBB. This paradox is visualized by the HRP histochemistry in Figure 21. The histochemistry shows the HRP in brain is confined to the brain plasma volume, except for the median eminence at the base of the third ventricle. The median eminence is a circumventricular organ (CVO), which are four tiny regions of brain that have no BBB [1137]. If the brain shown in Figure 21 was homogenized and HRP enzyme activity was measured, one might conclude that HRP crosses the BBB, when, in fact, the HRP does not cross the BBB, but is confined to the plasma volume of brain.

It is necessary to determine *both* the  $VD^{\text{test}}$  of the test molecule and the brain plasma volume ( $VD^{\text{PV}}$ ), which is explicitly included in Equation (7), as an experimental variable in the measurement of drug uptake by brain. The brain plasma volume is determined with either albumin or a non-specific IgG, neither of which cross the BBB. If the brain uptake of the test molecule is low, and  $VD^{\text{test}}$  approximates  $VD^{\text{PV}}$ , then  $(VD^{\text{test}} - VD^{\text{PV}}) = 0$ , and

there is no BBB transport of the test molecule, as described in Equation (7). When there is no difference between  $VD^{\text{test}}$  and  $VD^{\text{PV}}$ , then the BBB  $PS^{\text{influx}} = 0$ . In this setting, the test molecule is solely retained in brain within the plasma volume, as illustrated in Figure 21. The measurement of drug distribution in the brain plasma volume is particularly germane to the determination of the brain uptake of biologics following IV administration. As discussed in Section 8.3.4 for therapeutic antibodies for brain, antibodies have been injected intravenously and antibody was detected in homogenates of brain. If the injection dose of the antibody was increased, then a higher amount of antibody was detected in brain homogenate, because the antibody in plasma is increased at the higher injection dose. However, if no correction for brain plasma volume is made, then the higher antibody concentration in brain homogenate at the higher injection dose will be erroneously interpreted as evidence that the therapeutic antibody crossed the BBB [786].

**Artifacts caused by metabolism.** The second confounding variable in the measurement of the  $PS^{\text{influx}}$  using an IV injection technique is metabolism of the radiolabeled test molecule following uptake by peripheral tissues. The metabolic degradation of the  $[^{125}\text{I}]$ -labeled test molecule leads to the release into the plasma of low molecular  $[^{125}\text{I}]$ -metabolites that can cross the BBB. This brain uptake of metabolites produces radioactivity in brain that is not representative of the brain uptake of the test molecule. Instead, the brain uptake of the radioactivity is an artifact of metabolism of the test molecule. Such artifacts are exemplified in the case of the brain uptake of radioactivity following the IV injection of  $[^{125}\text{I}]$ -EGF or  $[^{125}\text{I}]$ -BDNF. The standard method of radio-iodination of a biologic is an oxidative reaction with 125-iodine and either chloramine T or Iodogen. This reaction places the  $^{125}\text{I}$  radiolabel on the aromatic ring of tyrosine residues on the protein or peptide. Following uptake and metabolism of the  $[^{125}\text{I}]$ -peptide by peripheral tissues, there is a gradual increase in the plasma concentration of TCA-soluble radiolabeled metabolites, such as  $[^{125}\text{I}]$ -tyrosine [1138]. The  $[^{125}\text{I}]$ -tyrosine then enters the brain via CMT on BBB LAT1 to give an artifactual picture of brain uptake of the original radio-iodinated biologic, such as the  $[^{125}\text{I}]$ -EGF (Figure 22A,B).

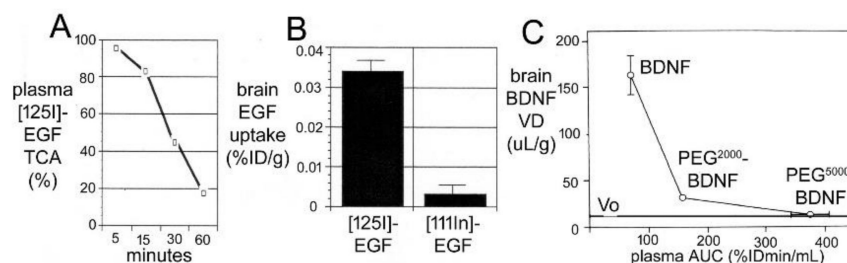


**Figure 22. Peptide metabolism and artifacts of brain uptake of radiolabeled peptide.** (A) Rapid a of trichloroacetic acid (TCA)-precipitable plasma radioactivity following the IV injection of  $[^{125}\text{I}]$ -EGF in the rat. (B) Brain uptake of radioactivity is increased >10-fold following the IV injection of  $[^{125}\text{I}]$ -EGF as compared to brain uptake after the IV injection of  $[^{111}\text{In}]$ -EGF. (A,B) drawn from data reported in [805]. (C) The brain/plasma ratio of radioactivity is equal to the brain volume of distribution (VD), and this is plotted against the plasma AUC for 3 forms of radio-iodinated BDNF:  $[^{125}\text{I}]$ -BDNF,  $[^{125}\text{I}]$ -PEG<sup>2000</sup>-BDNF, and  $[^{125}\text{I}]$ -PEG<sup>5000</sup>-BDNF. The progressive pegylation of BDNF with PEG<sup>2000</sup> and then PEG<sup>5000</sup> blocks the peripheral metabolism of BDNF, as reflected in the increasing plasma AUC. As the BDNF metabolism is progressively inhibited, the brain VD of BDNF decreases. The  $V_0$ ,  $13 \pm 1 \mu\text{L/g}$ , shown by the horizontal bar is the brain plasma volume measured with  $[^{14}\text{C}]$ -rat albumin. The brain VD of BDNF following pegylation with PEG<sup>5000</sup> completely suppresses peripheral metabolism of the BDNF and the brain  $VD = V_0$ , which shows that BDNF does not cross the BBB. Reproduced with permission from [1139], Copyright© 1997 Springer-Nature.

Conversely, when the EGF is conjugated with DTPA and chelated with 111-indium, the amount of radioactivity that enters the brain is decreased >10-fold (Figure 22B). The  $[^{111}\text{In}]$ -EGF is taken up and metabolized by peripheral tissues to the same extent as the  $[^{125}\text{I}]$ -EGF, but the  $^{111}\text{In}$  radioactivity is sequestered in the intracellular compartment of peripheral

tissues and is not released to plasma [1138]. In another example of brain uptake artifact caused by peripheral metabolism of chloramine T/Iodogen labeled peptides, TCA-soluble metabolites appear in plasma soon after the IV injection of [ $^{125}$ I]-BDNF radio-iodinated with chloramine T, and this produces a high brain uptake of radioactivity (Figure 22C). However, the peripheral degradation of [ $^{125}$ I]-BDNF is progressively blocked by pegylation with either PEG<sup>2000</sup> or PEG<sup>5000</sup>, as demonstrated by comparison of the plasma AUC for [ $^{125}$ I]-BDNF, [ $^{125}$ I]-PEG<sup>2000</sup>-BDNF, and [ $^{125}$ I]-PEG<sup>5000</sup>-BDNF shown in Figure 22C. The pegylation of BDNF reduced the amount of TCA-soluble radiolabeled metabolites in plasma and reduced the brain uptake of radioactivity to the extent that the radioactivity was confined solely to the brain plasma volume following injection of [ $^{125}$ I]-PEG<sup>5000</sup>-BDNF (Figure 22C). The data in Figure 22B shows that the preferred form of radio-labeling of a biologic is chelation of 111-indium. Alternatively, biologics can be radio-iodinated with the [ $^{125}$ I]-Bolton–Hunter reagent, which conjugates the radiolabeled reagent to surface lysine residues in a non-oxidative reaction. Lysine conjugated with the [ $^{125}$ I]-Bolton–Hunter reagent that is released to plasma does not cross the BBB [717].

**Plasma AUC.** The third caveat in the quantitation of  $PS^{\text{influx}}$  with IV injection methods is the need to determine the plasma AUC, pAUC, which is explicitly included in Equation (7) as an experimental variable. The measurement of pAUC can be performed with standard pharmacokinetic methods when the experimental study period is long, e.g., >30 min between IV injection and harvesting of brain, which is typically the case for biologics. If brain uptake is measured during short experimental time periods between IV injection and organ harvesting, which is the case for small molecules, then the plasma AUC can be measured with an external organ method. In this approach, a femoral artery is catheterized and blood is withdrawn with a syringe pump during the experimental period [1140]. The plasma AUC (nmol·min/mL) is the drug concentration in the syringe (nmol/mL) multiplied by the experimental time period (minutes).

### 11.5. Measurement of $PS^{\text{efflux}}$

The  $PS^{\text{efflux}}$  is the product of  $K_4$  VT, where  $K_4$  is the rate constant of drug efflux from brain to blood across the BBB, as illustrated in Figure 19 and Equation (2), and VT is the brain water space, 700  $\mu\text{L/g}$  [1096]. The measurement of  $PS^{\text{efflux}}$  is more challenging than the estimation of  $PS^{\text{influx}}$ , because a number of variables contribute to the rate of efflux of test molecules across the BBB from brain to blood. These variables include brain metabolism of the test molecule, brain binding of the test molecule, or active uptake of the test molecule by brain cells. Both the Brain Uptake Index (BUI) and Brain Efflux Index (BEI) methods can be used to measure the rate constant ( $K_4$ , Figure 19) of test molecule efflux across the BBB.

#### 11.5.1. Brain Uptake Index Method

The Brain Uptake Index (BUI) method was first used to estimate solute efflux from brain to blood in 1975 [340,1141]. To use the BUI method to measure efflux, the time between carotid arterial injection and decapitation is prolonged from the usual 0.25 min to 1, 2, and 4 min. The brain is pulsed with solute within 5 s of the arterial injection, and efflux from brain to blood may then be monitored over the time period up to 4 min. Beyond 4 min, there is a loss of linearity of the efflux from brain owing to recirculation [1141]. Any metabolism of the test molecule during the 4 min will prevent reliable estimates of efflux, so studies are generally restricted to solutes not metabolized within 4 min of administration. Both the influx and the efflux of the non-metabolizable glucose analogue, 3-O-methyl D-glucose (3OMG), were measured with the BUI technique [340]. The  $PS^{\text{influx}}$  and  $PS^{\text{efflux}}$  were not significantly different, which indicated the BBB glucose carrier was a symmetrical transporter [340], as originally suggested by Crone [1142]. The kinetic analysis of 3OMG efflux from brain was based on the earlier theoretical analyses of solute efflux from skeletal muscle [1143].

### 11.5.2. Brain Efflux Index Method

The Brain Efflux Index (BEI) method has advantages over the BUI method for the study of solute efflux from brain to blood. First, efflux of solute that has a low rate of influx from blood to brain can be measured with the BEI method. The study of efflux with the BUI method requires a significant influx of the test solute into brain from blood so that efflux from brain can be measured. In the BEI method, the radiolabeled test solute is injected directly into brain under stereotaxic guidance [450]. The second advantage of the BEI method is that the effects of cross-competition between substrates or drugs and the radiolabeled test solute can be measured, as reviewed in Section 6.3.1. Solute or drug efflux from brain is typically measured over time periods of 20–60 min with the BEI method. Under these conditions, it is important to confirm there is no metabolism of the test solute during the experimental period. If the test molecule was metabolized in brain, then efflux of the radiolabeled metabolite would produce an artifact, and lead to erroneous conclusions about solute efflux from brain. The classic example of artifacts of solute efflux caused by brain metabolism is the case of the Abeta amyloid peptide, as discussed in Section 8.1.5. In the original study [1144], [ $^{125}\text{I}$ ]- $\text{A}\beta^{1-40/42}$  was injected into brain, and efflux of radioactivity from brain to blood was observed, and ascribed to LRP1-mediated efflux of the  $\text{A}\beta^{1-40}$  peptide from brain to blood. This model had important implications for the understanding of the formation of  $\text{A}\beta$  amyloid plaques in AD, and the extent to which receptor-mediated efflux of  $\text{A}\beta$  peptides from brain to blood had on this process. However, the efflux of radioactivity from brain was shown to be an artifact caused by rapid degradation of [ $^{125}\text{I}$ ]- $\text{A}\beta^{1-40/42}$  in brain following intra-cerebral injection of the amyloid peptide [607]. The suppression of degradation of [ $^{125}\text{I}$ ]- $\text{A}\beta^{1-40}$  in brain eliminates the efflux of radioactivity [607], which indicates the  $\text{A}\beta$  amyloid peptide of AD does not efflux from brain across the BBB.

In addition to metabolism, interpretation of BEI data is also confounded by brain tissue binding/sequestration of the ligand. The rate constant of efflux ( $K_{\text{eff}}$ ) of estrone, a highly lipid-soluble sex steroid that freely crosses the BBB [322], is only  $0.069 \text{ min}^{-1}$  as measured with the BEI method [457]. This  $K_{\text{eff}}$  for estrone is not a measure of BBB permeability on the brain side of the barrier, i.e., the  $K_4$  parameter in Figure 19A. The  $K_{\text{eff}}$  measured with the BEI method is much less than the  $K_4$  of estrone efflux from brain to blood across the BBB, owing to sequestration by brain tissue binding proteins of sex steroids such as estrone. A mathematical model, similar to that developed for analysis of efflux across the BBB and brain tissue binding *in vivo*, for either steroid hormones [458] or drugs [1145], must be developed to discern how both efflux across the BBB and brain tissue binding/sequestration influences the  $K_{\text{eff}}$  determined with the BEI method.

### 11.6. Measurement of Drug Sequestration in Brain *In Vivo*

The ratio of propranolol concentration in brain (B), relative to plasma (P), in humans is high, e.g., the BP ratio is 17 [1145]. A BB or BP ratio greater than 1 is indicative of either active transport of drug into brain, or more likely sequestration of the drug in brain, e.g., by brain tissue binding. The BUI method was used to compute the rate constants of binding of drugs, such as propranolol or lidocaine [1145], to brain tissue *in vivo*, as shown in Figure 23 for propranolol.

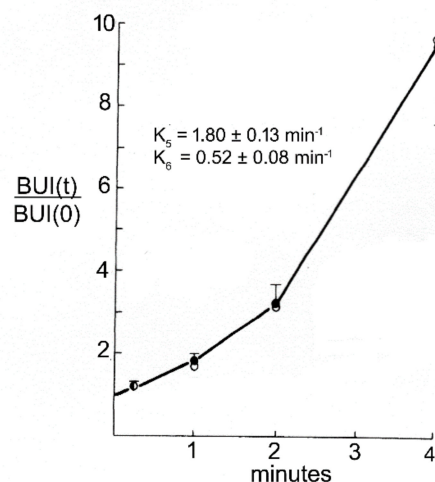


**Figure 23.** Propranolol binding to brain tissue proteins. The BUI at 1, 2, or 4 min after injection,  $BUI(t)$ , relative to the BUI at  $T = 0$ , is plotted against the time after carotid artery injection. The data were fit to a compartmental model of efflux and tissue binding similar to that shown in Figure 19, which allowed for determination of the rate constant of drug association ( $K_5$ ) and the rate constant of drug dissociation ( $K_6$ ) from tissue binding proteins. The closed circles are the experimentally determined BUI values, and the open circles are the BUI values predicted from fitting these data to the model of drug efflux and binding in brain. Reproduced in part with permission from [1145], Copyright© 1984 American Physiological Society.

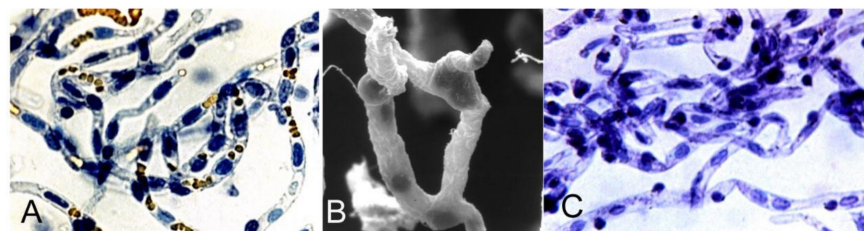
Fitting BUI data to a mathematical model allowed for estimation of the rate constants of drug association ( $K_5$ ) and dissociation ( $K_6$ ) of binding to brain tissue in vivo, where these rate constants are defined in Figure 19A. The BUI of [ $^3\text{H}$ ]-propranolol, relative to [ $^{14}\text{C}$ ]-butanol, was measured for up to 4 min after common carotid artery injection (Figure 23). Thin layer chromatography of brain showed there was no metabolism of the [ $^3\text{H}$ ]-propranolol during the 4 min experimental period [1145]. The differential equations and analytic solutions of the mathematical model used to derive from BUI data the  $K_5$  and  $K_6$  parameters of propranolol binding in brain in vivo have been reported previously [458,1145]. The increase in the BUI with time after carotid arterial injection shown in Figure 23 is due to (a) binding/sequestration of [ $^3\text{H}$ ]-propranolol by brain, and (b) the rapid efflux from brain of the freely diffusible [ $^{14}\text{C}$ ]-butanol reference, which is not sequestered by brain. Similar to propranolol, sex steroid hormones are also avidly sequestered by brain [458]. Unlike the sex steroid hormones, the corticosteroid, corticosterone, is not sequestered in brain in vivo [458]. The selective sequestration of sex steroids, but not corticosteroids, by brain in vivo explains the high brain VD, i.e., high BB ratios, of the sex steroids relative to a much lower BB ratio for the corticosteroids [458]. Developmental regulation of brain sequestration of sex steroid hormones is observed, as no brain tissue binding is found in newborn rabbits [458]. The selectivity of the brain binding of sex steroid hormones, but not corticosteroids, and the developmental regulation of this process for steroid hormones, suggests that specific binding proteins are responsible for the sequestration in brain of hormones and drugs. However, mechanisms other than tissue binding may account for a high BB or BP ratio, particularly for lipophilic amine drugs such as propranolol or lidocaine, which may exist in protonated forms. The effect of plasma pH on BBB transport of propranolol or lidocaine in vivo was investigated with the BUI method [1145]. Influx of either drug across the BBB in vivo was inhibited 40–50% when the pH of the injection solution was lowered from 7.5 to 5.5. The lower transport of the protonated form of the drug was attributed to preferential transport of the unprotonated drug across the BBB in vivo. Similarly, CNS drugs with a high  $pK_a$  may be protonated in the acidic compartment of the lysosome, which would contribute to the sequestration of the drug by brain, as demonstrated with the brain slice preparation [1131] discussed in Section 11.3.3.



### 11.7. In Vitro Models of BBB Transport

#### 11.7.1. Isolated Brain Microvessels

Brain microvessels were first isolated in 1969 from bovine and human brain [1146], and subsequently from rat brain [1147,1148]. The microvessels are isolated free of adjoining brain tissue as shown in Figure 24.



#### Isolated Brain Microvessels: Applications

- RMT: Peptide receptor ligand binding by radio-receptor assay
- CMT: Ex vivo transporter kinetics
- RNA isolation-BBB genomics, cDNA library, gene cloning
- BBB proteomics
- Human vascular pathology in brain disease

**Figure 24. Isolated brain microvessels.** (A) Trypan blue stain of freshly isolated bovine brain microvessels. (B) Scanning electron micrograph of bovine brain capillaries with attached nerve endings. (C) Trypan blue stain of microvessels isolated from human autopsy brain. Reproduced from [569], Copyright© 2020 licensed under Creative Commons Attribution License (CC-BY).

Isolated brain microvessels were originally proposed as models for the investigation of brain endothelial metabolism [1148,1149]. The original methods for isolation of brain microvessels used a mechanical homogenization technique. Subsequently, microvessels were isolated with an enzymatic homogenization method, and it was said that brain capillaries isolated with the enzymatic method excluded trypan blue, whereas capillaries isolated with the mechanical homogenization method failed to exclude trypan blue [1150]. Microvessels stained with trypan blue are shown in Figure 24A,C for bovine brain or human brain, respectively. The failure of cells to exclude trypan blue is an index of cellular metabolic dysfunction. The cellular ATP levels of brain microvessels isolated with either a mechanical or enzymatic homogenization procedure have ATP concentrations <10% of normal [1151]. The cause of the metabolic dysfunction, and severe loss of cellular ATP, in microvessels freshly isolated from brain has not been elucidated. Despite the metabolic impairment of isolated brain microvessels, these structures have proven over the last 50 years to be a versatile in vitro model for the study of the cellular and molecular biology of the BBB and neurovascular unit [569], and the major areas of study include (a) radio-receptor assays for characterization of BBB receptor-mediated transport (RMT) systems; (b) ex vivo kinetic studies of the uptake of nutrients and vitamins via BBB carrier-mediated transport (CMT) systems; (c) isolation of brain microvessel RNA, which allows for BBB genomics and an analysis of the brain microvascular transcriptome; (d) quantitative absolute targeted proteomics (QTAP) determinations of brain microvessel concentration of RMT and CMT systems; (e) vascular pathology in human brain disease, as outlined in Figure 24.

**Radio-receptor assays, isolated brain capillaries, and BBB RMT systems.** Several of the RMT systems at the BBB discussed in Section 8.1 were identified with radio-receptor assays and microvessels isolated from human autopsy brain, including the human BBB insulin receptor [561], the human BBB transferrin receptor [579], the human IGF receptor [590], and the human leptin receptor [595].

**Ex vivo kinetics of BBB CMT systems.** Ex vivo kinetics of transport of nutrients via BBB CMT systems, discussed in Section 6.2, have been determined with isolated brain

capillaries. The isolated human brain capillary preparation was used in 1985 to describe the kinetics of BBB transport of [<sup>3</sup>H]-phenylalanine, and the selective inhibition of phenylalanine transport by other LNAAs [1152]. The use of isolated brain capillaries to characterize multiple BBB CMT and AET transporters has been recently reviewed [569], as have methods for experimental design of ex vivo transport with isolated brain capillaries [1153]. The isolation of plasma membranes from brain capillaries was first reported in 1980 [1154], and in 1992, these membrane vesicles were used to characterize luminal and abluminal amino acid transport at the BBB [1155].

**BBB genomics.** The field of BBB genomics was first described in 2001 using RNA purified from capillaries isolated from fresh rat brain [438] and in 2002 using RNA purified from capillaries isolated from fresh human brain removed at neurosurgery [442]. The microvessel-derived RNA was used to produce cDNA libraries, which facilitated the molecular cloning of multiple BBB transporters, including GLUT1 [1156], LAT1 [358], CNT2 [395], and BSAT1/Slco1c1 [440]. The BBB transcriptome has been characterized with multiple experimental approaches [1157–1160], as recently reviewed [569].

**BBB proteomics.** The combined use of the isolated brain capillary preparation and liquid chromatography-mass spectrometry (LC-MS) allowed for quantitative targeted absolute proteomics (QTAP), which was first described in 2011 for the human brain capillary [360]. The QTAP methodology subsequently was described for the hCMEC/D3 human cultured endothelium [394], the rat brain capillary [409], the monkey brain capillary [435,486], the choroid plexus [480], the arachnoid membrane [500], and isolated luminal and abluminal capillary membranes [468]. The QTAP programs allowed for quantitation of the multiple CMT and RMT systems at the BBB discussed in Sections 6.2 and 8.1.

**Vascular pathology in human neural disease.** The brain microvasculature plays a primary role in the pathogenesis of AD, as all extracellular amyloid plaques arise from the peri-vascular surface [1161]. Cortical microvessels were first isolated from AD cortical brain in 1987, which allowed for the purification and AA sequencing of the microvascular A $\beta$  amyloid peptide of AD [1162]. These studies confirmed earlier results on the sequence of the A $\beta$  amyloid peptide isolated from meningeal vessels of AD brain [1163]. Microvessels have since been isolated from AD autopsy brain for a variety of experimental applications [1164–1167]. One of the earliest lesions in brain in multiple sclerosis (MS) is a peri-vascular cuffing of lymphocytes [1168]. Microvessels were first isolated from human MS brain in 1989, which showed selective expression of the class II histocompatibility DR antigen in microvascular pericytes in MS brain [1169], a finding subsequently confirmed [1170]. Capillaries can be isolated from frozen human autopsy brain stored in brain banks [1171]. The brain microvasculature plays a primary role in multiple neural diseases, apart from AD or MS. The molecular analysis of capillaries isolated from brain bank specimens of human neural disease represents a unique, yet currently under-developed, area of the neurosciences. Caution should be used for any study that generates RNA from capillaries isolated from brain bank specimens, as the time period between death, autopsy, and freezing of the brain specimen is generally not known, and degradation of capillary RNA may take place. For RNA work, it is preferable to isolate microvessels from fresh human brain. Methods for isolation of microvessels from fresh human brain have been recently reviewed [1172].

#### 11.7.2. In Vitro Models of BBB Transport in Cell Culture

**History of in vitro BBB model development.** The development of an in vitro model of the BBB that was suitable for high throughput screening of multiple compounds for BBB permeability has been long sought by the pharmaceutical industry, and the development of such in vitro BBB models have a history covering the last 40 years. In 1983, bovine brain microvessel endothelial cells were grown in tissue culture as “a model for the study of blood-brain barrier permeability” [1173]. However, in vivo/in vitro BBB permeability comparisons showed the in vitro BBB model was leaky and over-estimated BBB permeability for small molecules that crossed the BBB by free diffusion, and under-estimated BBB permeability for small molecules that crossed the BBB by CMT [1174]. No specific CMT transport of L-DOPA across the in vitro BBB could be measured [1174], which was due to the marked

down-regulation of LAT1 gene expression when brain endothelial cells are grown in cell culture. Detection of the LAT1 transcript by Northern blot using 2 µg polyA + RNA purified from either isolated brain capillaries or cultured brain endothelial cells required development of the film autoradiogram for 2 h vs. 7 days, respectively [358,1175], which indicates LAT1 gene expression is down-regulated ~100-fold when brain endothelial cells are grown in culture. A similar level of down-regulation of GLUT1 gene expression was observed when brain endothelial cells were grown in cell culture [1156]. Early studies showed down-regulation of a BBB-specific enzyme,  $\gamma$ GTP, in cell culture, and the partial up-regulation of  $\gamma$ GTP expression by co-culture of endothelial cells with astrocytes [1176]. In 1990, the transwell model was developed, where primary cultures of bovine brain endothelial cells were grown on one side of a transwell, and primary cultures of newborn rat brain astrocytes were grown on the other side of Millicell-CM filter with a pore size of 0.4 microns [1177]. The transwell model lacks the shear stress caused by capillary blood flow. The shear stress on brain endothelial cells in vivo is 5–20 dyne/cm<sup>2</sup> [1178]. This flow-related shear stress was produced with an in vitro BBB model by co-culture of bovine aortic endothelial cells and rat C6 glioma cells in a hollow fiber cartridge; fluid flow through the cartridge at 4 mL/min produced a shear stress of 4 dyne/cm<sup>2</sup> [1179]. This dynamic in vitro BBB model was a precursor to a microfluidic ‘BBB on a chip’ models where a silicone chip was fabricated to allow for fluid flow through an outer endothelial chamber with astrocytes cultured in an inner chamber [1180]. The BBB-on-a-chip model was first described in 2005, although this model had no fluid flow component [1181]. It is not clear that in vitro BBB models require continuous flow of culture medium. The hypothesis that fluid flow induces BBB properties in brain endothelial cells is at odds with the lack of barrier properties in endothelia of non-brain organs, which are also exposed to flow induced shear stress [569]. In 2012, human-induced pluripotent stem cells (iPSC) were used to produce an in vitro BBB model [1182], and expression of tight junction proteins in the iPSC in vitro models was enhanced by the addition of 5 µM retinoic acid to the medium [1183]. Retinoic acid increases tight junctions via the Wnt signaling pathway [1184], which plays a special role in the differentiation of brain endothelium [1185]. The in vitro BBB model has undergone significant improvements over the last 40 years [1186]. However, the central issue is the extent to which even modern in vitro BBB models replicate the properties of the BBB in vivo. The in vitro/in vivo comparisons address the trans-endothelial electrical resistance (TEER), the permeability coefficient (Pe, cm/s) of sucrose, and the tissue-specific gene expression at the BBB in vitro and in vivo.

**Trans-endothelial electrical resistance.** The TEER has been measured for pial vessels on the surface of the brain and is 1600 ohm·cm<sup>2</sup> [7], which is high compared to the TEER across the choroid plexus, 26 ohm·cm<sup>2</sup> [6]. However, pial vessels are not representative of intra-parenchymal vessels in brain, as pial vessels lack an astrocyte ensheathment found in parenchymal vessels [8]. The TEER across intra-parenchymal vessels has been estimated at 8000 ohm·cm<sup>2</sup> [10]. The TEER is very low, <50 ohm·cm<sup>2</sup>, with a human vitro BBB model using the hCMEC/D3 line [1187]. The TEER in the transwell co-culture model increases to 600–800 ohm·cm<sup>2</sup> [1177,1188]. The TEER is 1700–3000 ohm·cm<sup>2</sup> in cultures derived from iPSCs exposed to 5 µM retinoic acid [1183]. TEER values approximate 8000 ohm·cm<sup>2</sup> when iPSC-derived endothelial cells are grown on transwells opposite co-cultures with pericytes followed by neurons/astrocytes [1189]. Although TEER values in these advanced co-culture models are approximating the TEER at intra-parenchymal vessels in brain in vivo, the in vitro models are still leaky compared to the BBB in vivo, when Pe values for sucrose are measured.

**Sucrose permeability in the in vitro BBB models.** The high and low ranges of BBB permeability coefficients (Pe, cm/s) may be defined by diazepam and sucrose. Based on the in vivo PS product for diazepam [1115], a brain capillary endothelial surface area in vivo of 120 cm<sup>2</sup>/g [11], the in vivo diazepam Pe =  $1.8 \times 10^{-4}$  cm/s [569]. The in vivo PS product for [<sup>13</sup>C]-sucrose is 0.04 uL/min/g [1190,1191], which corresponds to a sucrose Pe of  $5.5 \times 10^{-9}$  cm/s, a value 5 log orders lower than the in vivo Pe for diazepam. The

sucrose Pe value is  $5 \times 10^{-6}$  cm/s in either a flow-based dynamic in vitro BBB model [1179] or a transwell co-culture model [1188], which is 1000-fold higher than the sucrose Pe value in vivo. The sucrose Pe,  $5 \times 10^{-7}$  cm/s, in a retinoic acid differentiated iPSC in vitro model that produces a TEER up to 3000 ohm·cm<sup>2</sup> [1183], is still 100-fold higher than the sucrose Pe value in vivo [1190,1191].

**BBB-specific gene expression in in vitro BBB models.** BBB-specific gene expression is down-regulated when brain capillary endothelial cells are grown in cell culture [1192]. The mRNA encoding BBB-specific transporters such as GLUT1 or LAT1 was decreased at least 100-fold when transporter mRNA levels in freshly isolated brain capillaries was compared to cultured endothelium [358,1156,1175]. Gene expression in freshly isolated rat brain microvessels was up to 3 log orders of magnitude higher than expression of the same BBB-related genes in primary cultures of rat brain endothelium [1193]. Gene expression in primary cultures of human brain endothelium was down-regulated up to 6 log orders of magnitude [1194], when compared to BBB gene expression in vivo [1158]. The cause of the down-regulation of BBB specific gene expression in cell culture is not known, but may be related to the breakdown of the neuro-vascular unit in cell culture. There is a close apposition of astrocyte foot processes and the brain microvascular endothelium in vivo as these cellular structures are separated by a distance of only 20 nm [1088]. Given this close proximity of endothelial cells, astrocyte foot processes, and pericytes, which share the same basement membrane with the endothelium, it may be that current co-culture models do not replicate the proximity between these cells that exist in vivo.

**Cellular proximity with the in vitro BBB model.** Early work showed that the induction of BBB properties in cultured endothelium was observed only in mixed cultures, not co-cultures of endothelium and astrocytes [1195]. BBB properties could be induced by co-cultures of endothelium and astrocytes if the pore size of the transwell was 3.0 microns, but not if the pore size was 0.45 microns [1196]. Similarly, if the channel size is only 0.4 microns in a BBB-on-a-chip model, there is no spread of astrocyte processes into the endothelial chamber [1181]. The larger pore size of 3 microns enabled astrocyte cellular processes to extend through the pore to come in contact with the endothelium [1196]. The pore size of standard in vitro BBB co-cultures is 0.4 microns [1177,1179,1197], which prevents cell-to-cell contact between endothelium and the cells on the other side of the filter. The close proximity of neurovascular unit cells is produced in spheroid mixed cultures [1198], but transport through such cultures cannot be measured. In a more recent BBB-on-a-chip model, the size of the channels connecting the inner and outer chambers is 3 microns [1199]. However, these channels are long, 100 microns, as compared to the thickness of transwell chambers, 10 microns. Astrocyte processes do not extend over a distance of 100 microns in the in vitro BBB-on-a-chip model [1199].

In summary of cell culture models of BBB transport, considerable progress has been made in the development of in vitro BBB models since these were first introduced 40 years ago. However, these models have not been fully validated with in vivo/in vitro comparisons of solute and drug permeability via either lipid-mediated free diffusion, carrier-mediated transport, or receptor-mediated transport. Therefore, in vitro models should not be used as a primary method of determining drug transport across the BBB. In vitro models need to be validated and confirmed with in vivo measurements of BBB permeability. It may be that the real value of in vitro BBB models is not for the screening of drug transport across the BBB, but rather as a model that elucidates the mechanisms responsible for the induction of tissue-specific gene expression at the brain capillary endothelium, and the neuro-vascular unit.

### 11.8. BBB Transport Methods from Perspective of Pharmaceutical Industry

The methods reviewed above for the determination of the PS product of drug transport across the BBB in vivo, in either the blood-to-brain or brain-to-blood direction, are not widely employed within the pharmaceutical industry. Instead, industry seeks a unified parameter of drug distribution into brain, such as the CSF concentration, for biologics, or

the log BB for small molecules. The 'BB' parameter, which is the ratio of total drug in brain divided by the total drug in blood (or plasma), has given way to the  $K_{p,uu}$  [1200], which is the ratio of *free* drug in brain divided by the *free* drug in blood (or plasma), as defined in Equation (3). Underlying the use of the  $K_{p,uu}$  is the likely supposition that the concentration of drug in brain that drives receptor occupancy is the free drug in brain, not the tissue-bound drug in brain. The problem with the interpretation of data on the  $K_{p,uu}$  parameter relates to how the 'free drug in plasma', and the 'free drug in brain', are experimentally determined. The 'free drug' methods advocated by industry allow for the measurement of the free drug in plasma and brain with in vitro methods, such as equilibrium dialysis of an aliquot of plasma in parallel with an aliquot of brain homogenate [1200].

**Free drug in plasma.** The measurement of free drug in plasma in vitro with equilibrium dialysis assumes the KD governing the binding of the drug to the plasma protein in vitro in a test tube is the same as the KD of binding of the drug to the plasma protein in vivo at the glycocalyx surface of the brain capillary endothelium. If this assumption is never subjected to direct empiric testing in vivo, then there is no adherence to the principle of "to measure is to know" [1105]. The  $KD^{in\ vivo}$  can be measured with in vivo BBB methods as described in Section 11.2. In many, although not all, instances the  $KD^{in\ vivo} \gg KD^{in\ vitro}$  (Table 5). In this case, the measurement of free drug in vitro with equilibrium dialysis significantly underestimates the fraction of drug in plasma that is bioavailable for transport into brain. The lack of a reliable measure of the bioavailable drug in plasma, or  $L_F$ , impacts on estimates of the free drug in brain in vivo, or  $L_M$ , as the latter is directly related to the former, as shown by Equation (3). The measurement of free drug in plasma in vitro with a method such as equilibrium dialysis is a useful screen of the extent to which a given drug is plasma protein bound. However, if the bioavailable drug in brain in vivo is not measured, and in vitro free drug is extrapolated to the in vivo condition, then only confirmation bias is supporting the free drug hypothesis.

**Free drug in brain.** The measurement of free drug in brain in vitro with equilibrium dialysis of a homogenate of brain is useful in predicting the brain volume of distribution, or total drug BB ratio. However, the use of in vitro equilibrium dialysis of brain homogenate does not yield reliable estimates of the free drug in brain in vivo, because this in vitro homogenate approach measures free drug in brain in the absence of the continuous flow in vivo of bioavailable drug in plasma. The in vivo bioavailable drug in plasma, the  $L_F$  parameter in Figure 19, acts as a forcing function controlling the free drug in brain ( $L_M$ ), along with  $PS^{influx}$  and  $PS^{efflux}$ , as described in Equation (3). The concentration of free drug in brain, which determines metabolic clearance and receptor occupancy in brain, is independent of brain tissue binding [1096]. This is a re-statement of pharmacokinetic principles, developed over 40 years ago, that tissue binding of drug affects tissue volume of distribution, e.g., the BB ratio, but has no effect on the tissue concentration of free drug [1201].

## 12. Summary

This review has covered the diverse array of brain drug delivery technologies that have emerged over the last three decades, and which are outlined in Figure 2, and these are highlighted below:

### ICV drug delivery to brain:

- Drug injected into the CSF enters brain by diffusion, and diffusion decreases exponentially with the diffusion distance. Consequently, following ICV delivery, drug traverses a distance of only 1–2 mm from the CSF surface of the brain (Figure 5), as reviewed in Section 2.1.1.
- An intrathecal injection of drug is akin to a slow intravenous infusion of drug, as noted by Fishman and Christy in 1965 [83]. Therefore, the control group in a clinical trial of a drug administered by ICV injection, e.g., with an Ommaya reservoir, should be a cohort of patients administered the same drug by IV infusion, as suggested by Aird in 1984 [85], and reviewed in Section 2.1.4.

**Intra-cerebral implants:**

- Drug enters brain from an intra-cerebral implant by diffusion, which decreases exponentially with the distance from the implant. The maximal distance from the implant covered by the drug is 0.2–2 mm [118].
- To overcome the limitations of diffusion, viral vectors have been delivered to brain via multiple Burr holes drilled in the skull [982]. However, the virus penetration into the brain is limited to the area around the tip of the injection needle [980,981].

**Convection-enhanced diffusion:**

- Convection-enhanced diffusion (CED) attempts to overcome the limitations of diffusion in brain. A catheter inserted in the brain is connected to a pump [53]. A clinical trial of GDNF delivery to brain with bilateral CED failed in PD [130]. A primate study demonstrated the GDNF concentration in brain decreases exponentially with each mm of distance from the catheter [131], as illustrated in Figure 6A. Such an exponential decay in drug distribution in brain is indicative of diffusion, not convection.
- The maximum volume covered by CED in the cat brain was 100 mm<sup>3</sup> [53], or 300 mm<sup>3</sup> in the primate brain [120], which is only a fraction of the volume of the putamen in the human brain, 6000 mm<sup>3</sup>, on each side of the brain [127].

**Trans-nasal drug delivery to brain:**

- There are >1000 publications in PubMed on trans-nasal delivery to brain (Table 1). However, all clinical trials of drug delivery to brain via the nose have failed, as reviewed in Section 3.3.
- The olfactory region covers 50% of the nasal mucosa in the rat, but only 3% in humans [146].
- Drug delivery to olfactory CSF following nasal administration in preclinical studies is generally performed in rodents wherein large volumes are instilled in the nose, and these large volumes cause local injury to the nasal mucosa. The volume of the nasal mucosa in humans and mice is 20 mL and 0.03 mL, respectively [148]. Instillation of a volume >100 µL in the human naris causes local injury [147,148].

**Blood–brain barrier disruption (BBBD):**

- BBBD has been induced by intra-carotid artery hyperosmolar mannitol (ICAHM), by focused ultrasound with IV microbubbles (FUS-MB), and by a variety of methods such as opening tight junctions with an anti-claudin-5 antibody, or even electromagnetic radiation, as reviewed in Section 4.
- Disruption of the BBB to drugs also opens the BBB to plasma proteins, which are toxic to brain [197,198].
- BBBD with either ICAHM or FUS-MB causes a sterile inflammatory response in brain [200,201], vasculopathy [202], and chronic neuropathologic changes in the brain [203,228].

**Stem cell delivery to brain:**

- Stem cells do not cross the BBB [288], nor enter brain parenchyma [289] as reviewed in Section 5.1.
- Stem cells do invade the meninges of brain [289], where there is no BBB.
- Stem cells were permanently transfected with lentivirus (LV) and injected into mice, but the LV genome in brain was near the background of the method and log orders lower than in peripheral tissues [293].

**Exosome delivery to brain:**

- Exosomes are liposome-like membrane vesicles derived from cultured cells, as reviewed in Section 5.2.
- Similar to liposomes, exosomes do not cross the BBB in the absence of a surface ligand that triggers RMT across the BBB.
- The future translation of exosomes to human neurotherapeutics is limited by low encapsulation of drug in exosomes, drug efflux from exosomes on storage, the lack of

stability of exosomes on long-term storage required for commercialization, the low yield of exosomes from cultured cells, and the unfavorable pharmacokinetic profiles of exosomes following IV administration.

#### **Small molecule delivery to brain via free diffusion:**

- All CNS drugs on the market have a MW < 450 Da and form <8 hydrogen bonds with solvent water. Only about 2% of all small molecules have these molecular properties of MW and hydrogen bonding, and these drugs typically treat only neuropsychiatric conditions or epilepsy, as reviewed in Section 6.1.1.
- The model of MW dependence of small molecule diffusion through biological membranes was developed by Stein decades ago [317], and is reviewed in Section 6.1.2, and in Figure 8.
- Water-soluble drugs have been conjugated to lipid-soluble carriers, including dihydroxydipyrindine, free fatty acid, or docosahexaenoic acid (DHA), but with little success as reviewed in Section 6.1.4.
- The 20th century model of CNS drug development of lipid-soluble small molecules needs to be expanded to include drugs that cross the BBB via carrier-mediated transport.

#### **Small molecule delivery to brain via BBB carrier-mediated transport:**

- Several carrier-mediated transporters (CMT) are expressed at the BBB for transport of nutrients, including GLUT1, LAT1, CAT1, MCT1, CTL1, and CNT2.
- The genes encoding these CMT systems are members of the Solute Carrier (SLC) superfamily, which includes >400 transporters and >60 families [338].
- There are >10 glucose transporters (GLUT) genes in the SLC superfamily. Therefore, if a given CMT system is being targeted as a conduit for brain drug delivery, it is important to first confirm the Substrate Transporter Profile (STP) of the CMT system that exists in vivo at the BBB correlates with the STP of the cloned transporter expressed in vitro.
- In addition to the CMT systems for nutrients, there are also several SLC transporters that mediate vitamin transport across the BBB, as reviewed in Section 6.2.7 and Table 3.
- The 3D structure of some CMT systems have been elucidated, as shown in Figure 9 for GLUT1 and LAT1. The dimensions of the transporter cavity are only 0.8–1.5 nm [347]. Therefore, drugs, which do not cross the BBB, should not be conjugated to an endogenous CMT substrate, as the transporter cavity will most likely reject the conjugate.
- Medicinal chemistry can be used to create a dual-purpose pharmaceutical that has affinity for both the CMT cavity as well as for the drug receptor in brain.

#### **Small molecule transport via active efflux transporters:**

- Active efflux transporters (AET) mediate the transport of molecules in the brain-to-blood direction and include members of both the SLC and the ATP-binding cassette (ABC) gene families. There are ~50 genes and 7 families in the ATP superfamily, and many of these AET systems are expressed at the BBB, as reviewed in Section 6.3.
- The model AET system is P-glycoprotein (ABCB1), but there are multiple other ABC transporters expressed at the BBB.
- Drug efflux via either ABC or SLC transporters can be assessed with the Brain Efflux Index (BEI) method, as reviewed in Section 11.5.2.

#### **Absorptive-mediated transport:**

- Cationic proteins or lectins traverse the BBB via absorptive-mediated transport (AMT), as reviewed in Section 7.
- Cationic proteins include cationized proteins, endogenous cationic proteins, e.g., protamine or histone, and cell-penetrating peptides (CPP), such as the tat or penetratin peptides. Wheat germ agglutinin (WGA) is the model lectin that undergoes AMT at the BBB.
- AMT ligands are not preferred delivery systems, as these tend to have low affinity for BBB binding sites, are largely sequestered within the brain endothelium, and have unacceptable toxicity profiles.

**Receptor-mediated transport:**

- Receptor-mediated transporters at the BBB include the endogenous receptors for insulin, transferrin, leptin, and the IGFs, as reviewed in Section 8.1.
- Localization of a putative BBB RMT system should be confirmed by brain immunohistochemistry (IHC), as exemplified by Figure 11A. Brain IHC for several receptors targeted for RMT shows these receptors are localized at brain cells, not at the capillary endothelium, including LRP1, LDLR, nAChR, and the NMDAR (Figure 11B).
- Receptor-specific MABs act as molecular Trojan horses to ferry across the BBB a biologic drug that is genetically fused to the MAB. IgG fusion proteins for biologics drug delivery to brain have been engineered and validated in vivo for lysosomal enzymes, neurotrophins, decoy receptors, and therapeutic antibodies (Figure 12, Table 4).
- Avidin-biotin technology, and the engineering of IgG–avidin fusion proteins, allows for the BBB delivery of peptide or antisense radiopharmaceuticals for neuro-imaging as shown in Figure 14.

**Nanoparticles:**

- Nanoparticles (NP) are reviewed in Section 9, and they include polymer-based nanoparticles (polymeric NPs, dendrimers, micelles, and protein NPs, such as albumin NPs), lipid NPs (solid lipid NPs, liposomes), and non-polymeric NPs (magnetic NPs, carbon nanotubes).
- NPs do not cross the BBB without surface functionalization of the NP with a ligand that triggers RMT across the BBB.
- NPs have been functionalized with ligands that target CMT systems, but the narrow cavities of the CMT systems do not allow for transport of the 100 nm NP, as reviewed in Section 9.5.1.
- Apart from vaccines, NP have been slow to enter clinical trials, and no successful CNS clinical trials have been performed to date with NP formulations, as reviewed in Section 9.6.
- NPs have significant toxicity profiles, particularly for magnetic NPs, carbon nanotubes, and PBCA polymeric NPs, as reviewed in Section 9.7. Detailed safety pharmacology and toxicology studies of the effects of long-term NP administration are lacking. Such 6-month GLP toxicology studies are required for an IND application, but few IND applications have been submitted for CNS clinical trials with NPs.

**Gene therapy of the brain:**

- Viral gene therapy and non-viral gene therapy of the brain are reviewed in Sections 10.1 and 10.2, respectively.
- Zolgensma<sup>®</sup> is an intravenous AAV gene therapeutic, and was FDA approved in 2019 as a single-dose treatment for spinal muscular atrophy (SMA) at an IV dose of  $1.1 \times 10^{14}$  vg/kg [994]. Zolgensma is a self-complementary (sc) form of adeno-associated virus (AAV)-9, which undergoes BBB transport following IV administration [995].
- AAV is a hepatotropic virus [1008], and Zolgensma treatment causes abnormal liver function tests in 90% of subjects [1009]. The IV injection of  $10^{14}$  vg/kg of AAV to newborn mice induces hepatocellular cancer in 70% of mice observed long-term [1010].
- AAV treatment induces a strong immune response against both the viral capsid protein, as well as the protein product of the therapeutic gene [992,1005]. Long term T cell immunity against the NAGLU lysosomal enzyme was observed in subjects receiving an intra-cerebral injection of AAV-NAGLU [1007].
- Non-viral gene therapy of brain is possible with Trojan horse liposomes (THLs) as described in Figure 17. THLs are produced by conjugation of a receptor-specific MAB to the tips of polyethyleneglycol strands on the surface of 100–150 nm pegylated liposomes. Both reporter genes and therapeutic genes have been delivered to mice, rats, and monkeys with antibodies that target either the insulin receptor or the transferrin receptor at the BBB.



### 13. Perspective

Brain drug delivery science is important to the overall mission of CNS drug development because ~100% of biologics do not cross the BBB, and ~98% of small molecules do not cross the BBB. The absence of drug transport across the BBB is the singular reason that CNS drug development is so difficult. Yet, CNS drug developers practice their craft by adhering to two conflicting beliefs: (a) drugs for CNS disease can be developed, and (b) CNS drug development can take place in the absence of any consideration of the blood–brain barrier. These contradictory beliefs are illustrated by recent reviews of drug development for AD [1202–1205], PD [755,1206], stroke [1207], brain cancer [1208], Huntington’s disease [1209], ALS [1210], ataxia [1211], spinal cord injury [1212], traumatic brain injury [1213], or addiction [1214]. In none of these reviews on drug development for specific brain diseases was the BBB even mentioned, so the crucial issue of brain drug delivery was uniformly *in absentia* in the CNS drug development process. If the drug does not cross the BBB, and delivery to the target in brain is not possible, then drug development will lead to clinical trial failure.

The futility of CNS drug development in the absence of BBB delivery technology over the course of the last 25 years is illustrated by a review of failed clinical trials of biologics for CNS disease. New drug approvals are increasingly biologics, and by 2019, 43% of all prescription revenues were generated by biologics [772]. The earliest biologics to enter CNS clinical trials were recombinant human BDNF or CNTF, which were developed as new treatments for neuro-degeneration, such as AD, PD, or ALS. The initial neurodegenerative condition targeted for clinical testing with neurotrophic factors was ALS. Both BDNF and CNTF were administered by SQ injection to patients with ALS in large phase 3 clinical trials [753,754]. Neither BDNF nor CNTF cross the BBB, and cannot reach the therapeutic targets within the brain following SQ administration of the neurotrophin. Both the BDNF and the CNTF clinical trials for ALS ended in failure [753,754], and are depicted in Figure 25 as the beginning of 25 years of CNS biologics drug development.

#### 25 years of biologic drug development for CNS disease

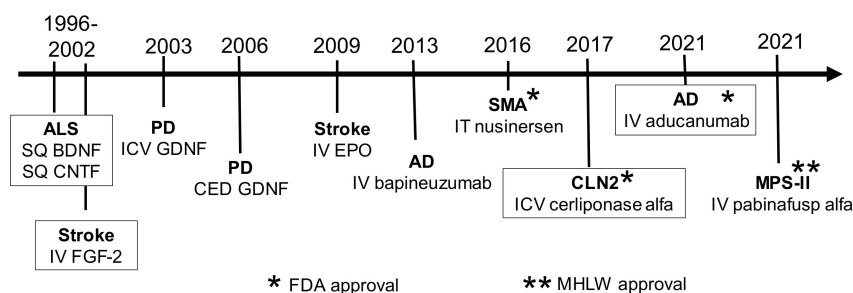


**Figure 25.** Biologics drug development for the CNS over the last 25 years. See Abbreviations section.

In neither the report of the failed BDNF clinical trial [753] nor the report of the failed CNTF clinical trial [754] was the issue of BBB delivery discussed. Another neurotrophin, GDNF, was developed as a new treatment for PD. Since GDNF does not cross the BBB, the neurotrophin was administered in one phase 3 trial for PD by ICV injection, and in another phase 3 trial for PD by CED. These BBB avoidance strategies do not result in adequate drug delivery to brain, as reviewed in Sections 2.1.4 and 2.2.2, respectively, and both phase 3 trials ended in failure [107,130]. Neurotrophins were also developed as new treatments of acute stroke, and FGF-2 and EPO were administered as IV infusions within the first 5 h of the stroke. These neurotrophins do not cross the BBB, and the BBB is intact in the early hours after stroke when neuroprotection is still possible, as reviewed in Section 8.3.2. Both phase 3 clinical trials for neurotrophin treatment of acute stroke ended in failure [761,762]. Anti-Abeta amyloid antibodies (AAA) were developed as new treatments for AD, and the first AAA developed for AD, bapineuzumab, was followed by over a half dozen AAAs

that entered clinical trials for AD. Bapineuzumab does not cross the BBB, as reviewed in Section 8.3.4, yet bapineuzumab was administered by IV infusion to AD patients. Since the BBB is intact in AD [786], the therapeutic antibody could not reach the amyloid targets in brain, and the bapineuzumab phase 3 trial ended in failure [787,788]. Aducanumab, another AAA for AD, also does not cross the intact BBB [786]. However, aducanumab reduces brain amyloid in AD [790]. The mechanism for aducanumab entry into brain of AD subjects appears to be BBB disruption, since there is a linear correlation between plaque reduction and ARIA-E [786], as discussed in Section 8.3.4. Aducanumab was approved in 2021 for AD amid controversy [793], and its use has been rejected by the health care community [1215]. Aducanumab is most likely a superior form of treatment for AD, should the antibody be enabled to enter the brain without BBB disruption. Aducanumab, and other AAAs, can be re-engineered with BBB Trojan horse technology to enable RMT across the BBB, as reviewed in Section 8.3.4. Nusinersen, a phosphorothioate-ASO, was approved for treatment of SMA by injection into the lumbar CSF [95]. As reviewed in Section 2.1.3, SMA is amenable to lumbar intrathecal delivery, because the drug targets, spinal cord motor neurons, lie near the surface of the spinal cord contiguous with the intra-lumbar injection. Despite the unique spatial relationship of motor neurons in the lumbar spinal cord to a lumbar CSF injection, attempts were made to replicate the nusinersen/SMA model for brain diseases of the parenchyma of brain or spinal cord. Tominersen is a phosphorothioate-ASO for Huntington's disease (HD), and tofersen is a phosphorothioate-ASO for ALS, and both drugs entered phase 3 trials where the phosphorothioate-ASO was administered by monthly intrathecal injection in the lumbar CSF. As discussed in Section 2.1, this route of brain drug delivery is not expected to deliver drug to the parenchyma of brain. The phase 3 trials for tominersen for HD and tofersen for ALS were terminated in 2021 [1216,1217]. Recombinant TPP1 (cerliponase alfa) was approved for treatment of the brain in CLN2 disease, an inherited lysosomal storage disorder, and the enzyme was infused into one lateral ventricle bimonthly via an Ommaya reservoir [110]. The control group in the pivotal clinical trial was historical controls, perhaps from a natural reluctance to subject young patients to a chronically implanted Ommaya reservoir for the purpose of placebo infusion. However, as emphasized over 40 years ago by Aird [85], the proper control group for an ICV drug trial is IV administration of the study drug. This is because drug injected into the CSF is rapidly exported to blood as noted by Fishman and Christy over 50 years ago [83]. Therefore, the study drug may exert therapeutic effects owing to drug action in peripheral organs, which are falsely attributed to a drug effect on the CNS, as discussed in Section 2.1.4.

In all of the clinical trials outlined in Figure 25, and discussed thus far, the CNS drug development program either was silent on the issue of BBB delivery, or employed a BBB avoidance strategy. The first drug to be re-engineered with a BBB drug delivery technology and receive market approval following a phase 3 clinical trial is the IgG-iduronate 2-sulfatase fusion protein, pabinafusp alfa (IZCARGO<sup>®</sup>) [720], which received MHLW approval in Japan in 2021 for treatment of the brain with MPSII (Figure 25). The IgG domain of this fusion protein is a TfRMAb, which enables RMT of the IgG-lysosomal enzyme fusion protein across the BBB in vivo, followed by receptor-mediated endocytosis into brain cells, as discussed in Section 8.3.1. This model of re-engineering biologics with BBB Trojan horse antibodies for RMT across the BBB can be replicated for all classes of biologics, including enzymes, neurotrophins, decoy receptors, and therapeutic antibodies. However, the CNS drug developer must first engineer a BBB drug delivery technology.

The re-engineering of the biologic for BBB delivery must take place in the earliest phases of preclinical drug development, and well before entry into clinical trials for brain disease. Should the CNS drug developer choose to go forward with a drug for brain that is not a lipid-soluble small molecule, and without BBB drug delivery technology, then the clinical trial failures of the past 25 years will only be replicated. Such a decision would be reminiscent of the choice of Fitzgerald's Gatsby, "so we beat on, boats against the current, borne back ceaselessly into the past".

**Funding:** This research received no external funding.

**Institutional Review Board Statement:** Not applicable.

**Informed Consent Statement:** Not applicable.

**Data Availability Statement:** Data sharing not applicable.

**Conflicts of Interest:** W.M.P. is an inventor of patents on the delivery of biologics to brain.

## Abbreviations

AA, amino acid; AAA, anti-amyloid antibody; AAAD, aromatic amino acid decarboxylase; AAG,  $\alpha_1$ -acid glycoprotein; AAV, adeno-associated virus; ABC, ATP binding cassette; ACE, angiotensin converting enzyme; AD, Alzheimer's disease; ADA, anti-drug antibody; AET, active efflux transport; AIDS, acquired immune deficiency syndrome; ALS, amyotrophic lateral sclerosis; AMT, absorptive-mediated transcytosis; ARIA-E, amyloid-related imaging abnormalities of edema; ASA, arylsulfatase A; ASM, acid sphingomyelinase; ASO, antisense oligodeoxynucleotide; ASOR, asialoorosomucoid; AUC, area under the concentration curve; AVP, arginine vasopressin; AZT, azidothymidine; BACE, beta secretase; BB, brain: blood ratio; BP, brain: plasma ratio; BBB, blood-brain barrier; BBBD, BBB disruption; BCM, brain cell membrane; BCNU, 1,3-bis(2-chloroethyl)-1-nitroso urea; BCRP, breast cancer resistance protein; BDNF, brain-derived neurotrophic factor; BEI, brain efflux index; bFGF, basic fibroblast growth factor; BK, bradykinin; BSA, bispecific antibody; BSAT, BBB-specific anion transporter; BSG, basigin; BTB, blood-tumor barrier; BUI, brain uptake index; CAT, cationic amino acid transporter; CAV, caveolin; cBSA, cationized bovine serum albumin; Ccap, capillary transporter concentration; CCK, cholecystokinin; CDP, cystine-dense peptide; CDR-SB, Clinical Dementia Rating-Sum of Boxes; CED, convection-enhanced diffusion; CFA, complete Freund's adjuvant; CHO, Chinese hamster ovary; CI, cation independent; CL, clearance; CLDN, claudin; CM, cisterna magna; CMC, critical micellar concentration; CMT, carrier-mediated transport; CNT, carbon nanotube; CNT2, concentrative nucleoside transporter 2; CPP, cell-penetrating peptide; CRM, cross reacting material; cRSA, cationized rat serum albumin; CsA, cyclosporine A; CSF, cerebrospinal fluid; CTD, carboxyl terminal domain; CTL, choline transporter-like protein; CTX, chlorotoxin; Da, Dalton; DABE, [D-Ala<sup>2</sup>]-b-endorphin; DDI, dideoxyinosine; DHA, docosahexaenoic acid; DHEAS, dehydroepiandrosterone sulfate; DHP, dihydropyridine; DMSO, dimethylsulfoxide; Dox, doxorubicin; DSPE, distearoylphosphatidylethanolamine; DTPA, diethylenetriamine pentaacetate; E2, estradiol; E2G, estradiol glucuronide; E3S, estrone-3 sulfate; EAAT, excitatory amino acid transporter; ECD, extracellular domain; ECS, extracellular space; EDAC, 1-ethyl-3-(3-dimethylamino-propyl) carbodiimide; EEG, electroencephalogram; EGF, epidermal growth factor; EGFR, EGF receptor; EM, electron microscopy; EMF, external magnetic field; EPO, erythropoietin; EPOR, EPO receptor; ERT, enzyme replacement therapy; F, cerebral blood flow; FA, folic acid; FDA, Food and Drug Administration; FDG, fluorodeoxyglucose; FFA, free fatty acid; FOLR, folic acid receptor; FRC, reduced folate carrier; FS, flanking sequence; FUS, focused ultrasound; GABA, gamma aminobutyric acid; GAG, glycosaminoglycan; GAPDH, glyceraldehyde 3'-phosphate dehydrogenase; GBM, glioblastoma multiforme; GDNF, glial cell derived neurotrophic factor; GFAP, glial fibrillary acidic protein; GFP, green fluorescent protein; GLB, beta galactosidase; GLP, Good Laboratory Practice; GLUT, glucose transporter; GMP, Good Manufacturing Practice; GO, graphene oxide; GSH, glutathione; GST, glutathione S-transferase; GTP, glutamyl transpeptidase; HB-EGF, heparin binding EGF-like growth factor; HC, hemicholinium; HD, Huntington's disease; HFt, ferritin heavy chain; HIR, human IR; HIV, human immunodeficiency virus; HPRT, hypoxanthine-guanine phosphoribosyl transferase; HRP, horseradish peroxidase; HSC, hematopoietic stem cells; HSV, herpes simplex virus; IC, intra-cerebral; ICAHM, intra-carotid arterial hyperosmolar mannitol; ICAP, internal carotid artery perfusion; ICV, intra-cerebroventricular; ID, injection dose; IDS, iduronate 2-sulfatase; IDUA,  $\alpha$ -L-iduronidase; IGF, insulin-like growth factor; IGFBP, IGF binding protein; IGFR, IGF receptor; IHC, immunohistochemistry; IND, Investigational New Drug; INSR, insulin

receptor; iPSC, induced pluripotent stem cells; IR, insulin receptor; ISF, interstitial fluid; IT, intrathecal; ITR, inverted terminal repeat; IV, intravenous; KD, dissociation constant; lacZ, bacterial  $\beta$ -galactosidase; LAT, large neutral amino acid transporter; LC-MS, liquid chromatography mass spectrometry; LDL, low-density lipoprotein; LDLR, LDL receptor; LEPR, leptin receptor; Lf, lactoferrin; LFt, ferritin light chain; LNAA, large neutral amino acid; LNP, lipid NP; LOQ, limit of quantitation; LRP, LDL related protein receptor; LV, lentivirus; M6P, mono-6-phosphate; M6PR, M6P receptor; MAb, monoclonal antibody; MB, microbubble; MCAO, middle cerebral artery occlusion; MCT, monocarboxylic acid transporter; MHLW, Ministry of Health, Labor and Welfare; MDR, multidrug resistance; MPP, 1-methyl-4-phenylpyridinium; MPS, mucopolysaccharidosis; MRI, magnetic resonance imaging; MRP, multi-drug resistance protein; MS, multiple sclerosis; MSC, mesenchymal stem cell; MTf, melanotransferrin; MTFA, 5'-metylenetetrahydrofolic acid; MUS, methylumbelliferone sulfate; MW, molecular weight; MWCNT, multi-walled CNT; NAb, neutralizing antibody; nAChR, nicotinic acetylcholine receptor; NAGLU, N-acetyl- $\alpha$ -glucosaminidase; NBT, nucleobase transporter; NLC, nano-structured lipid carriers; NMDAR, N-methyl D-aspartate receptor; NP, nanoparticle; NPC, Niemann Pick disease, type C; nt, nucleotide; NTD, amino terminal domain; NTR, neurotrophin receptor; OAT, organic anion transporter; OCT, organic cation transporter; OCTN, organic cation/carnitine transporter; ODC, ornithine decarboxylase; OR, olfactory receptor; OTC, ornithine transcarbamylase; PAMAM, poly(amidoamine); PBCA, poly(butyl cyanoacrylate); PBL, peripheral blood lymphocyte; PBN, N-tertbutyl- $\alpha$ -phenylnitron; PCNSL, primary CNS lymphoma; PD, Parkinson's disease; PDGF, platelet-derived growth factor; Pe, permeability coefficient; PEF, pulsed electric field; PEG, polyethyleneglycol; PEI, poly(ethyleneimine); PET, positron emission tomography; Pgp, P-glycoprotein; pI, isoelectric point; PK, pharmacokinetics; PLA, poly(lactic acid); PLGA, poly(lactic coglycolic acid); PLL, poly-L-lysine; PNA, peptide nucleic acid; PNP, polymeric NP; PPT, palmitoyl protein thioesterase; PS, permeability–surface area; PVS, peri-vascular space; QSAR, quantitative structure activity relationship; RAP, receptor associated protein; RCA, ricinus communis agglutinin; RCT, randomized controlled clinical trial; RFVT, riboflavin vitamin transporter; RMP, receptor-mediated permeabilizer; RMT, receptor-mediated transport; RPM, revolutions per minute; RTB, ricin toxin B chain; RVG, rabies virus glycoprotein; SA, streptavidin; scAAV, self-complementary AAV; ScFv, single chain Fv; SCI, spinal cord injury; scid, severe combined immunodeficient; SGSH, N-sulfoglucosamine sulfohydrolase; shRNA, short hairpin RNA; siNP, silica NP; SIR, sterile inflammatory response; siRNA, short interfering RNA; SLC, solute carrier; SLN, solid lipid NP; SMA, spinal muscular atrophy; SMVT; sodium dependent multivitamin transporter; SOD, superoxide dismutase; SPION, superparamagnetic iron oxide nanoparticles; SPLP, stabilized plasmid–lipid particles; SQ, subcutaneous; SR, scavenger receptor; ssAAV, single stranded AAV; SST, somatostatin; SSTR, SST receptor; STP, substrate transporter profile; SWCNT, single-walled CNT; TARBP, trans-activation-responsive RNA-binding protein; T3, triiodothyronine; TBI, traumatic brain injury; TC, transcobalamin; TcBLR, transcobalamin receptor; TEER, trans-endothelial electrical resistance; Tf, transferrin; TfR, Tf receptor; TH, tyrosine hydroxylase; THL, Trojan horse liposome; THTR, thiamine transporter; TK, tyrosine kinase; TM, transmembrane; TMR, transmembrane region; TNF, tumor necrosis factor; TNFI, TNF inhibitor; TNFR, TNF receptor; TPP, tripeptidyl tripeptidase; UPDRS, Unified Parkinson Disease Rating Scale; VCN, vector copy number; VD, volume of distribution; VIP, vasoactive intestinal peptide; VPA, valproic acid; Vp, brain plasma volume; VT, brain water volume; WGA, wheat germ agglutinin.

## References

1. Pardridge, W.M. The blood-brain barrier: Bottleneck in brain drug development. *NeuroRX* **2005**, *2*, 3–14. [CrossRef] [PubMed]
2. Pardridge, W.M.; Oldendorf, W.H.; Cancilla, P.; Frank, H.J. Blood-brain barrier: Interface between internal medicine and the brain. *Ann. Intern. Med.* **1986**, *105*, 82–95. [CrossRef] [PubMed]
3. Brightman, M.W.; Reese, T.S. Junctions between intimately apposed cell membranes in the vertebrate brain. *J. Cell Biol.* **1969**, *40*, 648–677. [CrossRef] [PubMed]

4. Reese, T.S.; Karnovsky, M.J. Fine structural localization of a blood-brain barrier to exogenous peroxidase. *J. Cell Biol.* **1967**, *34*, 207–217. [CrossRef]
5. Maxwell, D.S.; Pease, D.C. The electron microscopy of the choroid plexus. *J. Cell Biol.* **1956**, *2*, 467–474. [CrossRef]
6. Zeuthen, T.; Wright, E.M. Epithelial potassium transport: Tracer and electrophysiological studies in choroid plexus. *J. Membr. Biol.* **1981**, *60*, 105–128. [CrossRef]
7. Butt, A.M.; Jones, H.C.; Abbott, N.J. Electrical resistance across the blood-brain barrier in anaesthetized rats: A developmental study. *J. Physiol.* **1990**, *429*, 47–62. [CrossRef]
8. Allt, G.; Lawrenson, J.G. Is the pial microvessel a good model for blood-brain barrier studies? *Brain Res. Rev.* **1997**, *24*, 67–76. [CrossRef]
9. Mastorakos, P.; McGavern, D. The anatomy and immunology of vasculature in the central nervous system. *Sci. Immunol.* **2019**, *4*, eaav0492. [CrossRef]
10. Smith, Q.R.; Rapoport, S.I. Cerebrovascular permeability coefficients to sodium, potassium, and chloride. *J. Neurochem.* **1986**, *46*, 1732–1742. [CrossRef]
11. Pardridge, W.M. CSF, blood-brain barrier, and brain drug delivery. *Expert Opin. Drug Deliv.* **2016**, *13*, 963–975. [CrossRef]
12. Reiber, H. Proteins in cerebrospinal fluid and blood: Barriers, CSF flow rate and source-related dynamics. *Restor. Neurol. Neurosci.* **2003**, *21*, 79–96.
13. Yadav, D.B.; Maloney, J.A.; Wildsmith, K.R.; Fuji, R.N.; Meilandt, W.J.; Solanoy, H.; Lu, Y.; Peng, K.; Wilson, B.; Chan, P.; et al. Widespread brain distribution and activity following i.c.v. infusion of anti-beta-secretase (BACE1) in nonhuman primates. *Br. J. Pharmacol.* **2017**, *174*, 4173–4185. [CrossRef]
14. Duvernoy, H.M.; Delon, S.; Vannson, J.L. Cortical blood vessels of the human brain. *Brain Res. Bull.* **1981**, *7*, 519–579. [CrossRef]
15. Pardridge, W.M. Treatment of Alzheimer’s Disease and Blood-Brain Barrier Drug Delivery. *Pharmaceutics* **2020**, *13*, 394. [CrossRef]
16. Kutuzov, N.; Flyvbjerg, H.; Lauritzen, M. Contributions of the glycocalyx, endothelium, and extravascular compartment to the blood-brain barrier. *Proc. Natl. Acad. Sci. USA* **2018**, *115*, E9429–E9438. [CrossRef]
17. Cornford, E.M.; Hyman, S.; Cornford, M.E.; Landaw, E.M.; Delgado-Escueta, A.V. Interictal seizure resections show two configurations of endothelial Glut1 glucose transporter in the human blood-brain barrier. *J. Cereb. Blood Flow Metab.* **1998**, *18*, 26–42. [CrossRef]
18. Vogel, J.; Sperandio, M.; Pries, A.R.; Linderkamp, O.; Gaehtgens, P.; Kuschinsky, W. Influence of the endothelial glycocalyx on cerebral blood flow in mice. *J. Cereb. Blood Flow Metab.* **2000**, *20*, 1571–1578. [CrossRef]
19. Yoon, J.H.; Lee, E.S.; Jeong, Y. In vivo Imaging of the Cerebral Endothelial Glycocalyx in Mice. *J. Vasc. Res.* **2017**, *54*, 59–67. [CrossRef]
20. Ando, Y.; Okada, H.; Takemura, G.; Suzuki, K.; Takada, C.; Tomita, H.; Zaikokuji, R.; Hotta, Y.; Miyazaki, N.; Yano, H.; et al. Brain-Specific Ultrastructure of Capillary Endothelial Glycocalyx and Its Possible Contribution for Blood Brain Barrier. *Sci. Rep.* **2018**, *8*, 17523. [CrossRef]
21. Thomsen, M.S.; Routhe, L.J.; Moos, T. The vascular basement membrane in the healthy and pathological brain. *J. Cereb. Blood Flow Metab.* **2017**, *37*, 3300–3317. [CrossRef]
22. Korogod, N.; Petersen, C.C.; Knott, G.W. Ultrastructural analysis of adult mouse neocortex comparing aldehyde perfusion with cryo fixation. *Elife* **2015**, *4*, e05793. [CrossRef]
23. Liddelw, S.A. Fluids and barriers of the CNS: A historical viewpoint. *Fluids Barriers CNS* **2011**, *8*, 2. [CrossRef]
24. Thakur, J.D.; Sonig, A.; Chittiboina, P.; Khan, I.S.; Wadhwa, R.; Nanda, A. Humphrey Ridley (1653–1708): 17th century evolution in neuroanatomy and selective cerebrovascular injections for cadaver dissection. *Neurosurg. Focus* **2012**, *33*, E3. [CrossRef]
25. Marcinowski, F. Max Lewandowsky (1876–1918). *J. Neurol.* **2020**, *267*, 1223–1224. [CrossRef]
26. Mott, F.W. The Late Professor Edwin Goldmann’s Investigations on the Central Nervous System by Vital Staining. *Br. Med. J.* **1913**, *2*, 871–873.
27. McIntosh, J.; Fildes, P. The factors which govern the penetration of arsenic (salvarsan) and aniline dyes into the brain and their bearing upon the treatment of cerebral syphilis. *Brain* **1916**, *39*, 478–483. [CrossRef]
28. Vein, A.A. Science and fate: Lina Stern (1878–1968), a neurophysiologist and biochemist. *J. Hist. Neurosci.* **2008**, *17*, 195–206. [CrossRef] [PubMed]
29. Broman, T. The possibilities of the passage of substances from the blood to the central nervous system. *Acta Psychiatr. Scand.* **1941**, *16*, 1–25. [CrossRef]
30. Friedemann, U. Blood-brain barrier. *Physiol. Rev.* **1942**, *22*, 125–142. [CrossRef]
31. Krough, A. The active and passive exchange of inorganic ions through the surface of living cells and through living membranes generally. *Proc. R. Soc. London Ser. B* **1946**, *133*, 140–200. [CrossRef]
32. Hassin, G.B. Cerebrospinal fluid, its origin, nature and function. *J. Neuropathol. Exp. Neurol.* **1948**, *7*, 172–181. [CrossRef]
33. Dobbing, J. The blood-brain barrier. *Physiol. Rev.* **1961**, *41*, 130–188. [CrossRef]
34. Zheng, W.; Ghersi-Egea, J.F. Brain Barrier Systems Play No Small Roles in Toxicant-induced Brain Disorders. *Toxicol. Sci.* **2020**, *175*, 147–148. [CrossRef]
35. Ehrlich, P. Address in Pathology, on Chemiotherapy: Delivered before the Seventeenth International Congress of Medicine. *Br. Med. J.* **1913**, *2*, 353–359. [CrossRef]

36. Lloyd, N.C.; Morgan, H.W.; Nicholson, B.K.; Ronimus, R.S. The composition of Ehrlich's salvarsan: Resolution of a century-old debate. *Angew. Chem. Int. Ed. Engl.* **2005**, *44*, 941–944. [CrossRef]
37. Bosch, F.; Rosich, L. The contributions of Paul Ehrlich to pharmacology: A tribute on the occasion of the centenary of his Nobel Prize. *Pharmacology* **2008**, *82*, 171–179. [CrossRef]
38. Wile, U.J. Experimental Syphilis in the Rabbit Produced by the Brain Substance of the Living Paretic. *J. Exp. Med.* **1916**, *23*, 199–202. [CrossRef]
39. McIntosh, J.; Fildes, P. The fixation of arsenic by the brain after intravenous injection of salvarsan. *Proc. R. Soc. London Ser. B* **1914**, *88*, 320–326. [CrossRef]
40. Winkelman, N.W., Jr. Chlorpromazine in the treatment of neuropsychiatric disorders. *J. Am. Med. Assoc.* **1954**, *155*, 18–21. [CrossRef]
41. Barsa, J.A. Combination drug therapy in psychiatry. *Am. J. Psychiatry* **1960**, *117*, 448–449. [CrossRef] [PubMed]
42. Oldendorf, W.H.; Hyman, S.; Braun, L.; Oldendorf, S.Z. Blood-brain barrier: Penetration of morphine, codeine, heroin, and methadone after carotid injection. *Science* **1972**, *178*, 984–986. [CrossRef] [PubMed]
43. Shanbrom, E.; Miller, S.; Fairbanks, V.F. Intrathecal administration of amethopterin in leukemic encephalopathy of young adults. *N. Engl. J. Med.* **1961**, *265*, 169–171. [CrossRef] [PubMed]
44. Ommaya, A.K. Subcutaneous reservoir and pump for sterile access to ventricular cerebrospinal fluid. *Lancet* **1963**, *2*, 983–984. [CrossRef]
45. Hornykiewicz, O. Dopamine (3-hydroxytyramine) and brain function. *Pharmacol. Rev.* **1966**, *18*, 925–964. [PubMed]
46. Wade, L.A.; Katzman, R. Synthetic amino acids and the nature of L-DOPA transport at the blood-brain barrier. *J. Neurochem.* **1975**, *25*, 837–842. [CrossRef]
47. Oldendorf, W.H. Measurement of brain uptake of radiolabeled substances using a tritiated water internal standard. *Brain Res.* **1970**, *24*, 372–376. [CrossRef]
48. Oldendorf, W.H. Brain uptake of radiolabeled amino acids, amines, and hexoses after arterial injection. *Am. J. Physiol.* **1971**, *221*, 1629–1639. [CrossRef]
49. Neuwelt, E.A.; Maravilla, K.R.; Frenkel, E.P.; Rapaport, S.I.; Hill, S.A.; Barnett, P.A. Osmotic blood-brain barrier disruption. Computerized tomographic monitoring of chemotherapeutic agent delivery. *J. Clin. Investig.* **1979**, *64*, 684–688. [CrossRef]
50. Anand Kumar, T.C.; David, G.F.; Sankaranarayanan, A.; Puri, V.; Sundram, K.R. Pharmacokinetics of progesterone after its administration to ovariectomized rhesus monkeys by injection, infusion, or nasal spraying. *Proc. Natl. Acad. Sci. USA* **1982**, *79*, 4185–4189. [CrossRef]
51. Brem, H.; Tamargo, R.J.; Olivi, A.; Pinn, M.; Weingart, J.D.; Wharam, M.; Epstein, J.I. Biodegradable polymers for controlled delivery of chemotherapy with and without radiation therapy in the monkey brain. *J. Neurosurg.* **1994**, *80*, 283–290. [CrossRef]
52. Frim, D.M.; Uhler, T.A.; Galpern, W.R.; Beal, M.F.; Breakefield, X.O.; Isacson, O. Implanted fibroblasts genetically engineered to produce brain-derived neurotrophic factor prevent 1-methyl-4-phenylpyridinium toxicity to dopaminergic neurons in the rat. *Proc. Natl. Acad. Sci. USA* **1994**, *91*, 5104–5108. [CrossRef]
53. Morrison, P.F.; Laske, D.W.; Bobo, H.; Oldfield, E.H.; Dedrick, R.L. High-flow microinfusion: Tissue penetration and pharmacodynamics. *Am. J. Physiol.* **1994**, *266*, R292–R305. [CrossRef]
54. Kumagai, A.K.; Eisenberg, J.B.; Pardridge, W.M. Absorptive-mediated endocytosis of cationized albumin and a beta-endorphin-cationized albumin chimeric peptide by isolated brain capillaries. Model system of blood-brain barrier transport. *J. Biol. Chem.* **1987**, *262*, 15214–15219. [CrossRef]
55. Fawell, S.; Seery, J.; Daikh, Y.; Moore, C.; Chen, L.L.; Pepinsky, B.; Barsoum, J. Tat-mediated delivery of heterologous proteins into cells. *Proc. Natl. Acad. Sci. USA* **1994**, *91*, 664–668. [CrossRef]
56. Bolton, S.J.; Jones, D.N.; Darker, J.G.; Eggleston, D.S.; Hunter, A.J.; Walsh, F.S. Cellular uptake and spread of the cell-permeable peptide penetratin in adult rat brain. *Eur. J. Neurosci.* **2000**, *12*, 2847–2855. [CrossRef]
57. Shashoua, V.E.; Hesse, G.W. N-docosahexaenoyl, 3 hydroxytyramine: A dopaminergic compound that penetrates the blood-brain barrier and suppresses appetite. *Life Sci.* **1996**, *58*, 1347–1357. [CrossRef]
58. Pardridge, W.M. Receptor-mediated peptide transport through the blood-brain barrier. *Endocr. Rev.* **1986**, *7*, 314–330. [CrossRef]
59. Pardridge, W.M.; Buciak, J.L.; Friden, P.M. Selective transport of an anti-transferrin receptor antibody through the blood-brain barrier in vivo. *J. Pharmacol. Exp. Ther.* **1991**, *259*, 66–70.
60. Friden, P.M.; Walus, L.R.; Musso, G.F.; Taylor, M.A.; Malfroy, B.; Starzyk, R.M. Anti-transferrin receptor antibody and antibody-drug conjugates cross the blood-brain barrier. *Proc. Natl. Acad. Sci. USA* **1991**, *88*, 4771–4775. [CrossRef]
61. Pardridge, W.M.; Kang, Y.S.; Buciak, J.L.; Yang, J. Human insulin receptor monoclonal antibody undergoes high affinity binding to human brain capillaries in vitro and rapid transcytosis through the blood-brain barrier in vivo in the primate. *Pharm. Res.* **1995**, *12*, 807–816. [CrossRef] [PubMed]
62. Cordon-Cardo, C.; O'Brien, J.P.; Casals, D.; Rittman-Grauer, L.; Biedler, J.L.; Melamed, M.R.; Bertino, J.R. Multidrug-resistance gene (P-glycoprotein) is expressed by endothelial cells at blood-brain barrier sites. *Proc. Natl. Acad. Sci. USA* **1989**, *86*, 695–698. [CrossRef] [PubMed]
63. Shibata, S.; Ochi, A.; Mori, K. Liposomes as carriers of cisplatin into the central nervous system—experiments with 9L gliomas in rats. *Neurol. Med.-Chir.* **1990**, *30*, 242–245. [CrossRef] [PubMed]

64. Kreuter, J.; Alyautdin, R.N.; Kharkevich, D.A.; Ivanov, A.A. Passage of peptides through the blood-brain barrier with colloidal polymer particles (nanoparticles). *Brain Res.* **1995**, *674*, 171–174. [CrossRef]
65. Nigavekar, S.S.; Sung, L.Y.; Llanes, M.; El-Jawahri, A.; Lawrence, T.S.; Becker, C.W.; Balogh, L.; Khan, M.K. 3H dendrimer nanoparticle organ/tumor distribution. *Pharm. Res.* **2004**, *21*, 476–483. [CrossRef]
66. Hynynen, K.; McDannold, N.; Vykhodtseva, N.; Jolesz, F.A. Noninvasive MR imaging-guided focal opening of the blood-brain barrier in rabbits. *Radiology* **2001**, *220*, 640–646. [CrossRef]
67. Alvarez-Erviti, L.; Seow, Y.; Yin, H.; Betts, C.; Lakhali, S.; Wood, M.J. Delivery of siRNA to the mouse brain by systemic injection of targeted exosomes. *Nat. Biotechnol.* **2011**, *29*, 341–345. [CrossRef]
68. Davson, H. Review lecture. The blood-brain barrier. *J. Physiol.* **1976**, *255*, 1–28. [CrossRef]
69. Chodobski, A.; Szmydynger-Chodobska, J.; Johanson, C.E. Vasopressin mediates the inhibitory effect of central angiotensin II on cerebrospinal fluid formation. *Eur. J. Pharmacol.* **1998**, *347*, 205–209. [CrossRef]
70. Brinker, T.; Stopa, E.; Morrison, J.; Klinge, P. A new look at cerebrospinal fluid circulation. *Fluids Barriers CNS* **2014**, *11*, 10. [CrossRef]
71. Cserr, H.F.; Cooper, D.N.; Suri, P.K.; Patlak, C.S. Efflux of radiolabeled polyethylene glycols and albumin from rat brain. *Am. J. Physiol.* **1981**, *240*, F319–F328. [CrossRef]
72. Wagner, H.J.; Pilgrim, C.; Brandl, J. Penetration and removal of horseradish peroxidase injected into the cerebrospinal fluid: Role of cerebral perivascular spaces, endothelium and microglia. *Acta Neuropathol.* **1974**, *27*, 299–315. [CrossRef]
73. Rennels, M.L.; Gregory, T.F.; Blaumanis, O.R.; Fujimoto, K.; Grady, P.A. Evidence for a ‘paravascular’ fluid circulation in the mammalian central nervous system, provided by the rapid distribution of tracer protein throughout the brain from the subarachnoid space. *Brain Res.* **1985**, *326*, 47–63. [CrossRef]
74. Hamezah, H.S.; Durani, L.W.; Ibrahim, N.F.; Yanagisawa, D.; Kato, T.; Shiino, A.; Tanaka, S.; Damanhuri, H.A.; Ngah, W.Z.W.; Tooyama, I. Volumetric changes in the aging rat brain and its impact on cognitive and locomotor functions. *Exp. Gerontol.* **2017**, *99*, 69–79. [CrossRef]
75. Przyborowska, P.; Adamiak, Z.; Zhalniarovich, Y. Quantification of cerebral lateral ventricular volume in cats by low- and high-field MRI. *J. Feline Med. Surg.* **2017**, *19*, 1080–1086. [CrossRef]
76. Hladky, S.B.; Barrand, M.A. The glymphatic hypothesis: The theory and the evidence. *Fluids Barriers CNS* **2022**, *19*, 9. [CrossRef]
77. Wolak, D.J.; Pizzo, M.E.; Thorne, R.G. Probing the extracellular diffusion of antibodies in brain using in vivo integrative optical imaging and ex vivo fluorescence imaging. *J. Control. Release* **2015**, *197*, 78–86. [CrossRef]
78. Blasberg, R.G.; Patlak, C.; Fenstermacher, J.D. Intrathecal chemotherapy: Brain tissue profiles after ventriculocisternal perfusion. *J. Pharmacol. Exp. Ther.* **1975**, *195*, 73–83.
79. Yan, Q.; Matheson, C.; Sun, J.; Radeke, M.J.; Feinstein, S.C.; Miller, J.A. Distribution of intracerebral ventricularly administered neurotrophins in rat brain and its correlation with trk receptor expression. *Exp. Neurol.* **1994**, *127*, 23–36. [CrossRef]
80. Levin, V.A.; Fenstermacher, J.D.; Patlak, C.S. Sucrose and inulin space measurements of cerebral cortex in four mammalian species. *Am. J. Physiol.* **1970**, *219*, 1528–1533. [CrossRef]
81. Stadlbauer, A.; Salomonowitz, E.; van der Riet, W.; Buchfelder, M.; Ganslandt, O. Insight into the patterns of cerebrospinal fluid flow in the human ventricular system using MR velocity mapping. *Neuroimage* **2010**, *51*, 42–52. [CrossRef]
82. Nagaraja, T.N.; Patel, P.; Gorski, M.; Gorevic, P.D.; Patlak, C.S.; Fenstermacher, J.D. In normal rat, intraventricularly administered insulin-like growth factor-1 is rapidly cleared from CSF with limited distribution into brain. *Cerebrospinal Fluid Res.* **2005**, *2*, 5. [CrossRef]
83. Fishman, R.A.; Christy, N.P. Fate of Adrenal Cortical Steroids Following Intrathecal Injection. *Neurology* **1965**, *15*, 1. [CrossRef] [PubMed]
84. Reed, D.J.; Woodbury, D.M. Kinetics of Movement of Iodide, Sucrose, Inulin and Radio-Iodinated Serum Albumin in the Central Nervous System and Cerebrospinal Fluid of the Rat. *J. Physiol.* **1963**, *169*, 816–850. [CrossRef]
85. Aird, R.B. A study of intrathecal, cerebrospinal fluid-to-brain exchange. *Exp. Neurol.* **1984**, *86*, 342–358. [CrossRef]
86. Billiau, A.; Heremans, H.; Ververken, D.; van Damme, J.; Carton, H.; de Somer, P. Tissue distribution of human interferons after exogenous administration in rabbits, monkeys, and mice. *Arch. Virol.* **1981**, *68*, 19–25. [CrossRef]
87. Crawley, J.N.; Fiske, S.M.; Durieux, C.; Derrien, M.; Roques, B.P. Centrally administered cholecystokinin suppresses feeding through a peripheral-type receptor mechanism. *J. Pharmacol. Exp. Ther.* **1991**, *257*, 1076–1080.
88. De Lange, E.C.; Danhof, M.; de Boer, A.G.; Breimer, D.D. Critical factors of intracerebral microdialysis as a technique to determine the pharmacokinetics of drugs in rat brain. *Brain Res.* **1994**, *666*, 1–8. [CrossRef]
89. Kan, S.H.; Aoyagi-Scharber, M.; Le, S.Q.; Vincelette, J.; Ohmi, K.; Bullens, S.; Wendt, D.J.; Christianson, T.M.; Tiger, P.M.; Brown, J.R.; et al. Delivery of an enzyme-IGFII fusion protein to the mouse brain is therapeutic for mucopolysaccharidosis type IIIB. *Proc. Natl. Acad. Sci. USA* **2014**, *111*, 14870–14875. [CrossRef]
90. Larson, S.M.; Carrasquillo, J.A.; Cheung, N.K.; Press, O.W. Radioimmunotherapy of human tumours. *Nat. Rev. Cancer* **2015**, *15*, 347–360. [CrossRef]
91. Onofrio, B.M.; Yaksh, T.L. Long-term pain relief produced by intrathecal morphine infusion in 53 patients. *J. Neurosurg.* **1990**, *72*, 200–209. [CrossRef] [PubMed]
92. Wang, D.; Tawfik, V.L.; Corder, G.; Low, S.A.; Francois, A.; Basbaum, A.I.; Scherrer, G. Functional Divergence of Delta and Mu Opioid Receptor Organization in CNS Pain Circuits. *Neuron* **2018**, *98*, 90–108.e5. [CrossRef] [PubMed]

93. Jacobs, N.W.; Maas, E.M.; Brusse-Keizer, M.; Rietman, H.J.S. Effectiveness and safety of cervical catheter tip placement in intrathecal baclofen treatment of spasticity: A systematic review. *J. Rehabil. Med.* **2021**, *53*, jrm00215. [CrossRef] [PubMed]
94. Fukuhara, K.; Katafuchi, T.; Yoshimura, M. Effects of baclofen on mechanical noxious and innocuous transmission in the spinal dorsal horn of the adult rat: In vivo patch-clamp analysis. *Eur. J. Neurosci.* **2013**, *38*, 3398–3407. [CrossRef]
95. Aartsma-Rus, A. FDA Approval of Nusinersen for Spinal Muscular Atrophy Makes 2016 the Year of Splice Modulating Oligonucleotides. *Nucleic Acid. Ther.* **2017**, *27*, 67–69. [CrossRef]
96. Rigo, F.; Chun, S.J.; Norris, D.A.; Hung, G.; Lee, S.; Matson, J.; Fey, R.A.; Gaus, H.; Hua, Y.; Grundy, J.S.; et al. Pharmacology of a central nervous system delivered 2'-O-methoxyethyl-modified survival of motor neuron splicing oligonucleotide in mice and nonhuman primates. *J. Pharmacol. Exp. Ther.* **2014**, *350*, 46–55. [CrossRef]
97. Shababi, M.; Lorson, C.L.; Rudnik-Schoneborn, S.S. Spinal muscular atrophy: A motor neuron disorder or a multi-organ disease? *J. Anat.* **2014**, *224*, 15–28. [CrossRef]
98. Kulkarni, J.A.; Witzigmann, D.; Thomson, S.B.; Chen, S.; Leavitt, B.R.; Cullis, P.R.; van der Meel, R. The current landscape of nucleic acid therapeutics. *Nat. Nanotechnol.* **2021**, *16*, 630–643. [CrossRef]
99. Muenzer, J.; Hendriks, C.J.; Fan, Z.; Vijayaraghavan, S.; Perry, V.; Santra, S.; Solanki, G.A.; Mascelli, M.A.; Pan, L.; Wang, N.; et al. A phase I/II study of intrathecal idursulfase-IT in children with severe mucopolysaccharidosis II. *Genet. Med.* **2016**, *18*, 73–81. [CrossRef]
100. Jones, S.A.; Breen, C.; Heap, F.; Rust, S.; de Ruijter, J.; Tump, E.; Marchal, J.P.; Pan, L.; Qiu, Y.; Chung, J.K.; et al. A phase 1/2 study of intrathecal heparan-N-sulfatase in patients with mucopolysaccharidosis IIIA. *Mol. Genet. Metab.* **2016**, *118*, 198–205. [CrossRef]
101. Wijburg, F.A.; Whitley, C.B.; Muenzer, J.; Gasperini, S.; Del Toro, M.; Muschol, N.; Cleary, M.; Sevin, C.; Shapiro, E.; Alexanderian, D. A multicenter open-label extension study of intrathecal heparan-N-sulfatase in patients with Sanfilippo syndrome type A. *Mol. Genet. Metab.* **2021**, *134*, 175–181. [CrossRef]
102. Shapiro, W.R.; Young, D.F.; Mehta, B.M. Methotrexate: Distribution in cerebrospinal fluid after intravenous, ventricular and lumbar injections. *N. Engl. J. Med.* **1975**, *293*, 161–166. [CrossRef]
103. Rieselbach, R.E.; Di Chiro, G.; Freireich, E.J.; Rall, D.P. Subarachnoid distribution of drugs after lumbar injection. *N. Engl. J. Med.* **1962**, *267*, 1273–1278. [CrossRef]
104. Peyrl, A.; Chocholous, M.; Azizi, A.A.; Czech, T.; Dorfer, C.; Mitteregger, D.; Gojo, J.; Minichmayr, E.; Slavc, I. Safety of Ommaya reservoirs in children with brain tumors: A 20-year experience with 5472 intraventricular drug administrations in 98 patients. *J. Neuro-Oncol.* **2014**, *120*, 139–145. [CrossRef]
105. Gerber, N.U.; Muller, A.; Bellut, D.; Bozinov, O.; Berger, C.; Grotzer, M.A. Ventricular Catheter Systems with Subcutaneous Reservoirs (Ommaya Reservoirs) in Pediatric Patients with Brain Tumors: Infections and Other Complications. *Neuropediatrics* **2015**, *46*, 401–409. [CrossRef]
106. Hall, C.D.; Dafni, U.; Simpson, D.; Clifford, D.; Wetherill, P.E.; Cohen, B.; McArthur, J.; Hollander, H.; Yainnoutsos, C.; Major, E.; et al. Failure of cytarabine in progressive multifocal leukoencephalopathy associated with human immunodeficiency virus infection. AIDS Clinical Trials Group 243 Team. *N. Engl. J. Med.* **1998**, *338*, 1345–1351. [CrossRef]
107. Nutt, J.G.; Burchiel, K.J.; Comella, C.L.; Jankovic, J.; Lang, A.E.; Laws, E.R., Jr.; Lozano, A.M.; Penn, R.D.; Simpson, R.K., Jr.; Stacy, M.; et al. Randomized, double-blind trial of glial cell line-derived neurotrophic factor (GDNF) in PD. *Neurology* **2003**, *60*, 69–73. [CrossRef]
108. Yamada, K.; Kinoshita, A.; Kohmura, E.; Sakaguchi, T.; Taguchi, J.; Kataoka, K.; Hayakawa, T. Basic fibroblast growth factor prevents thalamic degeneration after cortical infarction. *J. Cereb. Blood Flow Metab.* **1991**, *11*, 472–478. [CrossRef]
109. Day-Lollini, P.A.; Stewart, G.R.; Taylor, M.J.; Johnson, R.M.; Chellman, G.J. Hyperplastic changes within the leptomeninges of the rat and monkey in response to chronic intracerebroventricular infusion of nerve growth factor. *Exp. Neurol.* **1997**, *145*, 24–37. [CrossRef]
110. Schulz, A.; Ajayi, T.; Specchio, N.; de Los Reyes, E.; Gissen, P.; Ballon, D.; Dyke, J.P.; Cahan, H.; Slasor, P.; Jacoby, D.; et al. Study of Intraventricular Cerliponase Alfa for CLN2 Disease. *N. Engl. J. Med.* **2018**, *378*, 1898–1907. [CrossRef]
111. Williams, R.E.; Adams, H.R.; Blohm, M.; Cohen-Pfeffer, J.L.; de Los Reyes, E.; Denecke, J.; Drago, K.; Fairhurst, C.; Frazier, M.; Guelbert, N.; et al. Management Strategies for CLN2 Disease. *Pediatr. Neurol.* **2017**, *69*, 102–112. [CrossRef]
112. Lin, L.; Lobel, P. Production and characterization of recombinant human CLN2 protein for enzyme-replacement therapy in late infantile neuronal ceroid lipofuscinosis. *Biochem. J.* **2001**, *357*, 49–55. [CrossRef]
113. Meng, Y.; Sohar, I.; Wang, L.; Sleat, D.E.; Lobel, P. Systemic administration of tripeptidyl peptidase I in a mouse model of late infantile neuronal ceroid lipofuscinosis: Effect of glycan modification. *PLoS ONE* **2012**, *7*, e40509. [CrossRef]
114. Vuilleminot, B.R.; Kennedy, D.; Reed, R.P.; Boyd, R.B.; Butt, M.T.; Musson, D.G.; Keve, S.; Cahayag, R.; Tsuruda, L.S.; O'Neill, C.A. Recombinant human tripeptidyl peptidase-1 infusion to the monkey CNS: Safety, pharmacokinetics, and distribution. *Toxicol. Appl. Pharmacol.* **2014**, *277*, 49–57. [CrossRef]
115. Martin-Kleiner, I.; Gall Troselj, K. Mannose-6-phosphate/insulin-like growth factor 2 receptor (M6P/IGF2R) in carcinogenesis. *Cancer Lett.* **2010**, *289*, 11–22. [CrossRef]
116. Anderson, G.W.; Goebel, H.H.; Simonati, A. Human pathology in NCL. *Biochim. Biophys. Acta* **2013**, *1832*, 1807–1826. [CrossRef]
117. Naseri Kouzehgarani, G.; Feldsien, T.; Engelhard, H.H.; Mirakhor, K.K.; Phipps, C.; Nimmrich, V.; Clausznitzer, D.; Lefebvre, D.R. Harnessing cerebrospinal fluid circulation for drug delivery to brain tissues. *Adv. Drug Deliv. Rev.* **2021**, *173*, 20–59. [CrossRef]



118. Mak, M.; Fung, L.; Strasser, J.F.; Saltzman, W.M. Distribution of drugs following controlled delivery to the brain interstitium. *J. Neuro-Oncol.* **1995**, *26*, 91–102. [CrossRef]
119. Grossman, S.A.; Reinhard, C.; Colvin, O.M.; Chasin, M.; Brundrett, R.; Tamargo, R.J.; Brem, H. The intracerebral distribution of BCNU delivered by surgically implanted biodegradable polymers. *J. Neurosurg.* **1992**, *76*, 640–647. [CrossRef]
120. Brem, H.; Piantadosi, S.; Burger, P.C.; Walker, M.; Selker, R.; Vick, N.A.; Black, K.; Sisti, M.; Brem, S.; Mohr, G.; et al. Placebo-controlled trial of safety and efficacy of intraoperative controlled delivery by biodegradable polymers of chemotherapy for recurrent gliomas. The Polymer-brain Tumor Treatment Group. *Lancet* **1995**, *345*, 1008–1012. [CrossRef]
121. Valtonen, S.; Timonen, U.; Toivanen, P.; Kalimo, H.; Kivipelto, L.; Heiskanen, O.; Unsgaard, G.; Kuurne, T. Interstitial chemotherapy with carmustine-loaded polymers for high-grade gliomas: A randomized double-blind study. *Neurosurgery* **1997**, *41*, 44–48, discussion 48–49. [CrossRef]
122. Westphal, M.; Hilt, D.C.; Bortey, E.; Delavault, P.; Olivares, R.; Warnke, P.C.; Whittle, I.R.; Jaaskelainen, J.; Ram, Z. A phase 3 trial of local chemotherapy with biodegradable carmustine (BCNU) wafers (Gliadel wafers) in patients with primary malignant glioma. *Neuro-Oncology* **2003**, *5*, 79–88. [CrossRef] [PubMed]
123. Hart, M.G.; Grant, R.; Garside, R.; Rogers, G.; Somerville, M.; Stein, K. Chemotherapy wafers for high grade glioma. *Cochrane Database Syst. Rev.* **2011**, *2011*, CD007294. [CrossRef] [PubMed]
124. Bensadoun, J.C.; Pereira de Almeida, L.; Fine, E.G.; Tseng, J.L.; Deglon, N.; Aebischer, P. Comparative study of GDNF delivery systems for the CNS: Polymer rods, encapsulated cells, and lentiviral vectors. *J. Control. Release* **2003**, *87*, 107–115. [CrossRef]
125. Batrakova, E.V.; Gendelman, H.E.; Kabanov, A.V. Cell-mediated drug delivery. *Expert Opin. Drug Deliv.* **2011**, *8*, 415–433. [CrossRef]
126. Bouvier, G.; Penn, R.D.; Kroin, J.S.; Beique, R.A.; Guerard, M.J.; Lesage, J. Intratumoral chemotherapy with multiple sources. *Ann. N. Y. Acad. Sci.* **1988**, *531*, 213–214. [CrossRef]
127. Yin, D.; Valles, F.E.; Fiandaca, M.S.; Forsayeth, J.; Larson, P.; Starr, P.; Bankiewicz, K.S. Striatal volume differences between non-human and human primates. *J. Neurosci. Methods* **2009**, *176*, 200–205. [CrossRef]
128. Voges, J.; Reszka, R.; Gossmann, A.; Dittmar, C.; Richter, R.; Garlip, G.; Kracht, L.; Coenen, H.H.; Sturm, V.; Wienhard, K.; et al. Imaging-guided convection-enhanced delivery and gene therapy of glioblastoma. *Ann. Neurol.* **2003**, *54*, 479–487. [CrossRef]
129. Stine, C.A.; Munson, J.M. Convection-Enhanced Delivery: Connection to and Impact of Interstitial Fluid Flow. *Front. Oncol.* **2019**, *9*, 966. [CrossRef]
130. Lang, A.E.; Gill, S.; Patel, N.K.; Lozano, A.; Nutt, J.G.; Penn, R.; Brooks, D.J.; Hotton, G.; Moro, E.; Heywood, P.; et al. Randomized controlled trial of intraputamenal glial cell line-derived neurotrophic factor infusion in Parkinson disease. *Ann. Neurol.* **2006**, *59*, 459–466. [CrossRef]
131. Salvatore, M.F.; Ai, Y.; Fischer, B.; Zhang, A.M.; Grondin, R.C.; Zhang, Z.; Gerhardt, G.A.; Gash, D.M. Point source concentration of GDNF may explain failure of phase II clinical trial. *Exp. Neurol.* **2006**, *202*, 497–505. [CrossRef]
132. Pardridge, W.M. Biopharmaceutical drug targeting to the brain. *J. Drug Target.* **2010**, *18*, 157–167. [CrossRef]
133. Dunlop, D.S.; Yang, X.R.; Lajtha, A. The effect of elevated plasma phenylalanine levels on protein synthesis rates in adult rat brain. *Biochem. J.* **1994**, *302 Pt 2*, 601–610. [CrossRef]
134. Ai, Y.; Markesbery, W.; Zhang, Z.; Grondin, R.; Elseberry, D.; Gerhardt, G.A.; Gash, D.M. Intraputamenal infusion of GDNF in aged rhesus monkeys: Distribution and dopaminergic effects. *J. Comp. Neurol.* **2003**, *461*, 250–261. [CrossRef]
135. Eslamboli, A.; Georgievska, B.; Ridley, R.M.; Baker, H.F.; Muzyczka, N.; Burger, C.; Mandel, R.J.; Annett, L.; Kirik, D. Continuous low-level glial cell line-derived neurotrophic factor delivery using recombinant adeno-associated viral vectors provides neuroprotection and induces behavioral recovery in a primate model of Parkinson’s disease. *J. Neurosci.* **2005**, *25*, 769–777. [CrossRef]
136. Sampson, J.H.; Archer, G.; Pedain, C.; Wembacher-Schroder, E.; Westphal, M.; Kunwar, S.; Vogelbaum, M.A.; Coan, A.; Herndon, J.E.; Raghavan, R.; et al. Poor drug distribution as a possible explanation for the results of the PRECISE trial. *J. Neurosurg.* **2010**, *113*, 301–309. [CrossRef]
137. Mehta, A.I.; Choi, B.D.; Raghavan, R.; Brady, M.; Friedman, A.H.; Bigner, D.D.; Pastan, I.; Sampson, J.H. Imaging of convection enhanced delivery of toxins in humans. *Toxins* **2011**, *3*, 201–206. [CrossRef]
138. Lewis, G.K., Jr.; Schulz, Z.R.; Pannullo, S.C.; Southard, T.L.; Olbricht, W.L. Ultrasound-assisted convection-enhanced delivery to the brain in vivo with a novel transducer cannula assembly: Laboratory investigation. *J. Neurosurg.* **2012**, *117*, 1128–1140. [CrossRef]
139. Brady, M.L.; Raghavan, R.; Mata, J.; Wilson, M.; Wilson, S.; Odland, R.M.; Broaddus, W.C. Large-Volume Infusions into the Brain: A Comparative Study of Catheter Designs. *Ster. Funct. Neurosurg.* **2018**, *96*, 135–141. [CrossRef]
140. Vogelbaum, M.A.; Brewer, C.; Barnett, G.H.; Mohammadi, A.M.; Peereboom, D.M.; Ahluwalia, M.S.; Gao, S. First-in-human evaluation of the Cleveland Multiport Catheter for convection-enhanced delivery of topotecan in recurrent high-grade glioma: Results of pilot trial 1. *J. Neurosurg.* **2018**, *130*, 476–485. [CrossRef]
141. Faraji, A.H.; Jaquins-Gerstl, A.S.; Valenta, A.C.; Ou, Y.; Weber, S.G. Electrokinetic Convection-Enhanced Delivery of Solutes to the Brain. *ACS Chem. Neurosci.* **2020**, *11*, 2085–2093. [CrossRef]
142. Valles, F.; Fiandaca, M.S.; Bringas, J.; Dickinson, P.; LeCouteur, R.; Higgins, R.; Berger, M.; Forsayeth, J.; Bankiewicz, K.S. Anatomic compression caused by high-volume convection-enhanced delivery to the brain. *Neurosurgery* **2009**, *65*, 579–585, discussion 576–585. [CrossRef]

143. Selvaraj, K.; Gowthamarajan, K.; Karri, V. Nose to brain transport pathways an overview: Potential of nanostructured lipid carriers in nose to brain targeting. *Artif. Cells Nanomed. Biotechnol.* **2018**, *46*, 2088–2095. [CrossRef]
144. Niimura, Y. Olfactory receptor multigene family in vertebrates: From the viewpoint of evolutionary genomics. *Curr. Genom.* **2012**, *13*, 103–114. [CrossRef]
145. Quignon, P.; Giraud, M.; Rimbault, M.; Lavigne, P.; Tacher, S.; Morin, E.; Retout, E.; Valin, A.S.; Lindblad-Toh, K.; Nicolas, J.; et al. The dog and rat olfactory receptor repertoires. *Genome Biol.* **2005**, *6*, R83. [CrossRef]
146. Harkema, J.R.; Carey, S.A.; Wagner, J.G. The nose revisited: A brief review of the comparative structure, function, and toxicologic pathology of the nasal epithelium. *Toxicol. Pathol.* **2006**, *34*, 252–269. [CrossRef]
147. Merkus, P.; Guchelaar, H.J.; Bosch, D.A.; Merkus, F.W. Direct access of drugs to the human brain after intranasal drug administration? *Neurology* **2003**, *60*, 1669–1671. [CrossRef]
148. Erdo, F.; Bors, L.A.; Farkas, D.; Bajza, A.; Gizurarson, S. Evaluation of intranasal delivery route of drug administration for brain targeting. *Brain Res. Bull.* **2018**, *143*, 155–170. [CrossRef]
149. Dare, A.O.; Balos, L.L.; Grand, W. Neural-dural transition at the medial anterior cranial base: An anatomical and histological study with clinical applications. *J. Neurosurg.* **2003**, *99*, 362–365. [CrossRef]
150. Melin, E.; Eide, P.K.; Ringstad, G. In vivo assessment of cerebrospinal fluid efflux to nasal mucosa in humans. *Sci. Rep.* **2020**, *10*, 14974. [CrossRef]
151. Faber, W.M. The nasal mucosa and the subarachnoid space. *Am. J. Anat.* **1937**, *62*, 121–148. [CrossRef]
152. Bradbury, M.W.; Westrop, R.J. Factors influencing exit of substances from cerebrospinal fluid into deep cervical lymph of the rabbit. *J. Physiol.* **1983**, *339*, 519–534. [CrossRef] [PubMed]
153. Weller, R.O.; Sharp, M.M.; Christodoulides, M.; Carare, R.O.; Mollgard, K. The meninges as barriers and facilitators for the movement of fluid, cells and pathogens related to the rodent and human CNS. *Acta Neuropathol.* **2018**, *135*, 363–385. [CrossRef] [PubMed]
154. Schuknecht, B.; Simmen, D.; Briner, H.R.; Holzmann, D. Nontraumatic skull base defects with spontaneous CSF rhinorrhea and arachnoid herniation: Imaging findings and correlation with endoscopic sinus surgery in 27 patients. *AJNR Am. J. Neuroradiol.* **2008**, *29*, 542–549. [CrossRef]
155. Sakane, T.; Akizuki, M.; Yamashita, S.; Nadai, T.; Hashida, M.; Sezaki, H. The transport of a drug to the cerebrospinal fluid directly from the nasal cavity: The relation to the lipophilicity of the drug. *Chem. Pharm. Bull.* **1991**, *39*, 2456–2458. [CrossRef]
156. Van den Berg, M.P.; Verhoef, J.C.; Romeijn, S.G.; Merkus, F.W. Uptake of estradiol or progesterone into the CSF following intranasal and intravenous delivery in rats. *Eur. J. Pharm. Biopharm.* **2004**, *58*, 131–135. [CrossRef]
157. Van den Berg, M.P.; Merkus, P.; Romeijn, S.G.; Verhoef, J.C.; Merkus, F.W. Uptake of melatonin into the cerebrospinal fluid after nasal and intravenous delivery: Studies in rats and comparison with a human study. *Pharm. Res.* **2004**, *21*, 799–802. [CrossRef]
158. Hussain, M.A.; Rakestraw, D.; Rowe, S.; Aungst, B.J. Nasal administration of a cognition enhancer provides improved bioavailability but not enhanced brain delivery. *J. Pharm. Sci.* **1990**, *79*, 771–772. [CrossRef]
159. Char, H.; Kumar, S.; Patel, S.; Piemontese, D.; Iqbal, K.; Malick, A.W.; Salvador, R.A.; Behl, C.R. Nasal delivery of [<sup>14</sup>C]dextromethorphan hydrochloride in rats: Levels in plasma and brain. *J. Pharm. Sci.* **1992**, *81*, 750–752. [CrossRef]
160. Kaur, P.; Kim, K. Pharmacokinetics and brain uptake of diazepam after intravenous and intranasal administration in rats and rabbits. *Int. J. Pharm.* **2008**, *364*, 27–35. [CrossRef]
161. Wu, H.; Hu, K.; Jiang, X. From nose to brain: Understanding transport capacity and transport rate of drugs. *Expert Opin. Drug Deliv.* **2008**, *5*, 1159–1168. [CrossRef]
162. Sakane, T.; Yamashita, S.; Yata, N.; Sezaki, H. Transnasal delivery of 5-fluorouracil to the brain in the rat. *J. Drug Target.* **1999**, *7*, 233–240. [CrossRef]
163. Dahlin, M.; Bergman, U.; Jansson, B.; Bjork, E.; Brittebo, E. Transfer of dopamine in the olfactory pathway following nasal administration in mice. *Pharm. Res.* **2000**, *17*, 737–742. [CrossRef]
164. Bergstrom, U.; Franzen, A.; Eriksson, C.; Lindh, C.; Brittebo, E.B. Drug targeting to the brain: Transfer of picolinic acid along the olfactory pathways. *J. Drug Target.* **2002**, *10*, 469–478. [CrossRef]
165. Fukuda, M.; Kanazawa, T.; Iioka, S.; Oguma, T.; Iwasa, R.; Masuoka, S.; Suzuki, N.; Kosuge, Y.; Suzuki, T. Quantitative analysis of inulin distribution in the brain focused on nose-to-brain route via olfactory epithelium by reverse esophageal cannulation. *J. Control. Release* **2021**, *332*, 493–501. [CrossRef]
166. Lopes, C.; Ribeiro, M.; Duarte, A.I.; Humbert, S.; Saudou, F.; Pereira de Almeida, L.; Hayden, M.; Rego, A.C. IGF-1 intranasal administration rescues Huntington's disease phenotypes in YAC128 mice. *Mol. Neurobiol.* **2014**, *49*, 1126–1142. [CrossRef]
167. Barakat, N.S.; Omar, S.A.; Ahmed, A.A. Carbamazepine uptake into rat brain following intra-olfactory transport. *J. Pharm. Pharmacol.* **2006**, *58*, 63–72. [CrossRef]
168. Vaka, S.R.; Murthy, S.N. Enhancement of nose-brain delivery of therapeutic agents for treating neurodegenerative diseases using peppermint oil. *Pharmazie* **2010**, *65*, 690–692.
169. Gao, M.; Mei, D.; Huo, Y.; Mao, S. Effect of polysorbate 80 on the intranasal absorption and brain distribution of tetramethylpyrazine phosphate in rats. *Drug Deliv. Transl. Res.* **2019**, *9*, 311–318. [CrossRef]
170. Broadwell, R.D.; Balin, B.J.; Salzman, M. Transcytotic pathway for blood-borne protein through the blood-brain barrier. *Proc. Natl. Acad. Sci. USA* **1988**, *85*, 632–636. [CrossRef]

171. Thorne, R.G.; Emory, C.R.; Ala, T.A.; Frey, W.H., 2nd. Quantitative analysis of the olfactory pathway for drug delivery to the brain. *Brain Res.* **1995**, *692*, 278–282. [CrossRef]
172. Tong, W.; Dwyer, C.A.; Thacker, B.E.; Glass, C.A.; Brown, J.R.; Hamill, K.; Moremen, K.W.; Sarrazin, S.; Gordts, P.; Dozier, L.E.; et al. Guanidinylated Neomycin Conjugation Enhances Intranasal Enzyme Replacement in the Brain. *Mol. Ther.* **2017**, *25*, 2743–2752. [CrossRef]
173. Luedtke, N.W.; Carmichael, P.; Tor, Y. Cellular uptake of aminoglycosides, guanidinoglycosides, and poly-arginine. *J. Am. Chem. Soc.* **2003**, *125*, 12374–12375. [CrossRef]
174. Shingaki, T.; Katayama, Y.; Nakaoka, T.; Irie, S.; Onoe, K.; Okauchi, T.; Hayashinaka, E.; Yamaguchi, M.; Tanki, N.; Ose, T.; et al. Visualization of drug translocation in the nasal cavity and pharmacokinetic analysis on nasal drug absorption using positron emission tomography in the rat. *Eur. J. Pharm. Biopharm.* **2016**, *99*, 45–53. [CrossRef]
175. Van de Bittner, G.C.; Van de Bittner, K.C.; Wey, H.Y.; Rowe, W.; Dharanipragada, R.; Ying, X.; Hurst, W.; Giovanni, A.; Alving, K.; Gupta, A.; et al. Positron Emission Tomography Assessment of the Intranasal Delivery Route for Orexin A. *ACS Chem. Neurosci.* **2018**, *9*, 358–368. [CrossRef]
176. Guastella, A.J.; Gray, K.M.; Rinehart, N.J.; Alvares, G.A.; Tonge, B.J.; Hickie, I.B.; Keating, C.M.; Cacciotti-Saija, C.; Einfeld, S.L. The effects of a course of intranasal oxytocin on social behaviors in youth diagnosed with autism spectrum disorders: A randomized controlled trial. *J. Child Psychol. Psychiatry* **2015**, *56*, 444–452. [CrossRef]
177. Cacciotti-Saija, C.; Langdon, R.; Ward, P.B.; Hickie, I.B.; Scott, E.M.; Naismith, S.L.; Moore, L.; Alvares, G.A.; Redoblado Hodge, M.A.; Guastella, A.J. A double-blind randomized controlled trial of oxytocin nasal spray and social cognition training for young people with early psychosis. *Schizophr. Bull.* **2015**, *41*, 483–493. [CrossRef]
178. Quintana, D.S.; Westlye, L.T.; Hope, S.; Naerland, T.; Elvsashagen, T.; Dorum, E.; Rustan, O.; Valstad, M.; Rezvaya, L.; Lishaugen, H.; et al. Dose-dependent social-cognitive effects of intranasal oxytocin delivered with novel Breath Powered device in adults with autism spectrum disorder: A randomized placebo-controlled double-blind crossover trial. *Transl. Psychiatry* **2017**, *7*, e1136. [CrossRef]
179. Lee, M.R.; Scheidweiler, K.B.; Diao, X.X.; Akhlaghi, F.; Cummins, A.; Huestis, M.A.; Leggio, L.; Averbeck, B.B. Oxytocin by intranasal and intravenous routes reaches the cerebrospinal fluid in rhesus macaques: Determination using a novel oxytocin assay. *Mol. Psychiatry* **2018**, *23*, 115–122. [CrossRef]
180. Mayer, A.V.; Wermter, A.K.; Stroth, S.; Alter, P.; Haberhausen, M.; Stehr, T.; Paulus, F.M.; Krach, S.; Kamp-Becker, I. Randomized clinical trial shows no substantial modulation of empathy-related neural activation by intranasal oxytocin in autism. *Sci. Rep.* **2021**, *11*, 15056. [CrossRef]
181. Craft, S.; Raman, R.; Chow, T.W.; Rafii, M.S.; Sun, C.K.; Rissman, R.A.; Donohue, M.C.; Brewer, J.B.; Jenkins, C.; Harless, K.; et al. Safety, Efficacy, and Feasibility of Intranasal Insulin for the Treatment of Mild Cognitive Impairment and Alzheimer Disease Dementia: A Randomized Clinical Trial. *JAMA Neurol.* **2020**, *77*, 1099–1109. [CrossRef] [PubMed]
182. Dhuyvetter, D.; Tekle, F.; Nazarov, M.; Vreeken, R.J.; Borghys, H.; Rombouts, F.; Lenaerts, I.; Bottelbergs, A. Direct nose to brain delivery of small molecules: Critical analysis of data from a standardized in vivo screening model in rats. *Drug Deliv.* **2020**, *27*, 1597–1607. [CrossRef] [PubMed]
183. Broman, T.; Lindberg-Broman, A.M. An experimental study of disorders in the permeability of the cerebral vessels (“the Blood-Brain Barrier”) produced by chemical and physico-chemical agents. *Acta Physiol. Scand.* **1945**, *10*, 102–125. [CrossRef]
184. Rapoport, S.I. Effect of concentrated solutions on blood-brain barrier. *Am. J. Physiol.* **1970**, *219*, 270–274. [CrossRef]
185. Brightman, M.W.; Hori, M.; Rapoport, S.I.; Reese, T.S.; Westergaard, E. Osmotic opening of tight junctions in cerebral endothelium. *J. Comp. Neurol.* **1973**, *152*, 317–325. [CrossRef]
186. Hasegawa, H.; Allen, J.C.; Mehta, B.M.; Shapiro, W.R.; Posner, J.B. Enhancement of CNS penetration of methotrexate by hyperosmolar intracarotid mannitol or carcinomatous meningitis. *Neurology* **1979**, *29*, 1280–1286. [CrossRef]
187. Barranger, J.A.; Rapoport, S.I.; Fredericks, W.R.; Pentchev, P.G.; MacDermot, K.D.; Steusing, J.K.; Brady, R.O. Modification of the blood-brain barrier: Increased concentration and fate of enzymes entering the brain. *Proc. Natl. Acad. Sci. USA* **1979**, *76*, 481–485. [CrossRef]
188. Mayhan, W.G.; Heistad, D.D. Permeability of blood-brain barrier to various sized molecules. *Am. J. Physiol.* **1985**, *248*, H712–H718. [CrossRef]
189. Koenig, H.; Goldstone, A.D.; Lu, C.Y. Polyamines mediate the reversible opening of the blood-brain barrier by the intracarotid infusion of hyperosmolar mannitol. *Brain Res.* **1989**, *483*, 110–116. [CrossRef]
190. Shapiro, W.R.; Voorhies, R.M.; Hiesiger, E.M.; Sher, P.B.; Basler, G.A.; Lipschutz, L.E. Pharmacokinetics of tumor cell exposure to [<sup>14</sup>C]methotrexate after intracarotid administration without and with hyperosmotic opening of the blood-brain and blood-tumor barriers in rat brain tumors: A quantitative autoradiographic study. *Cancer Res.* **1988**, *48*, 694–701.
191. Zunkeler, B.; Carson, R.E.; Olson, J.; Blasberg, R.G.; DeVroom, H.; Lutz, R.J.; Saris, S.C.; Wright, D.C.; Kammerer, W.; Patronas, N.J.; et al. Quantification and pharmacokinetics of blood-brain barrier disruption in humans. *J. Neurosurg.* **1996**, *85*, 1056–1065. [CrossRef]
192. Black, K.L.; Ningaraj, N.S. Modulation of brain tumor capillaries for enhanced drug delivery selectively to brain tumor. *Cancer Control* **2004**, *11*, 165–173. [CrossRef]
193. Neuwelt, E.A.; Balaban, E.; Diehl, J.; Hill, S.; Frenkel, E. Successful treatment of primary central nervous system lymphomas with chemotherapy after osmotic blood-brain barrier opening. *Neurosurgery* **1983**, *12*, 662–671. [CrossRef]

194. Pitman, S.W.; Frei, E., 3rd. Weekly methotrexate-calcium leucovorin rescue: Effect of alkalinization on nephrotoxicity; pharmacokinetics in the CNS; and use in CNS non-Hodgkin's lymphoma. *Cancer Treat. Rep.* **1977**, *61*, 695–701.
195. Angelov, L.; Doolittle, N.D.; Kraemer, D.F.; Siegal, T.; Barnett, G.H.; Peereboom, D.M.; Stevens, G.; McGregor, J.; Jahnke, K.; Lacy, C.A.; et al. Blood-brain barrier disruption and intra-arterial methotrexate-based therapy for newly diagnosed primary CNS lymphoma: A multi-institutional experience. *J. Clin. Oncol.* **2009**, *27*, 3503–3509. [CrossRef]
196. Iorio-Morin, C.; Gahide, G.; Morin, C.; Vanderweyen, D.; Roy, M.A.; St-Pierre, I.; Massicotte-Tisluck, K.; Fortin, D. Management of Primary Central Nervous System Lymphoma Using Intra-Arterial Chemotherapy With Osmotic Blood-Brain Barrier Disruption: Retrospective Analysis of the Sherbrooke Cohort. *Front. Oncol.* **2020**, *10*, 543648. [CrossRef]
197. Nadal, A.; Fuentes, E.; Pastor, J.; McNaughton, P.A. Plasma albumin is a potent trigger of calcium signals and DNA synthesis in astrocytes. *Proc. Natl. Acad. Sci. USA* **1995**, *92*, 1426–1430. [CrossRef]
198. LeVine, S.M. Albumin and multiple sclerosis. *BMC Neurol.* **2016**, *16*, 47. [CrossRef]
199. Petersen, M.A.; Ryu, J.K.; Chang, K.J.; Etxeberria, A.; Bardehle, S.; Mendiola, A.S.; Kamau-Devers, W.; Fancy, S.P.J.; Thor, A.; Bushong, E.A.; et al. Fibrinogen Activates BMP Signaling in Oligodendrocyte Progenitor Cells and Inhibits Remyelination after Vascular Damage. *Neuron* **2017**, *96*, 1003–1012. [CrossRef]
200. Burks, S.R.; Kersch, C.N.; Witko, J.A.; Pagel, M.A.; Sundby, M.; Muldoon, L.L.; Neuwelt, E.A.; Frank, J.A. Blood-brain barrier opening by intracarotid artery hyperosmolar mannitol induces sterile inflammatory and innate immune responses. *Proc. Natl. Acad. Sci. USA* **2021**, *118*, e2021915118. [CrossRef]
201. Kovacs, Z.I.; Kim, S.; Jikaria, N.; Qureshi, F.; Milo, B.; Lewis, B.K.; Bresler, M.; Burks, S.R.; Frank, J.A. Disrupting the blood-brain barrier by focused ultrasound induces sterile inflammation. *Proc. Natl. Acad. Sci. USA* **2017**, *114*, E75–E84. [CrossRef]
202. Lossinsky, A.S.; Vorbrod, A.W.; Wisniewski, H.M. Scanning and transmission electron microscopic studies of microvascular pathology in the osmotically impaired blood-brain barrier. *J. Neurocytol.* **1995**, *24*, 795–806. [CrossRef]
203. Salahuddin, T.S.; Johansson, B.B.; Kalimo, H.; Olsson, Y. Structural changes in the rat brain after carotid infusions of hyperosmolar solutions. An electron microscopic study. *Acta Neuropathol.* **1988**, *77*, 5–13. [CrossRef]
204. Salahuddin, T.S.; Kalimo, H.; Johansson, B.B.; Olsson, Y. Observations on exudation of fibronectin, fibrinogen and albumin in the brain after carotid infusion of hyperosmolar solutions. An immunohistochemical study in the rat indicating longlasting changes in the brain microenvironment and multifocal nerve cell injuries. *Acta Neuropathol.* **1988**, *76*, 1–10. [CrossRef]
205. Elkassabany, N.M.; Bhatia, J.; Deogaonkar, A.; Barnett, G.H.; Lotto, M.; Maurtua, M.; Ebrahim, Z.; Schubert, A.; Ference, S.; Farag, E. Perioperative complications of blood brain barrier disruption under general anesthesia: A retrospective review. *J. Neurosurg. Anesthesiol.* **2008**, *20*, 45–48. [CrossRef]
206. Doolittle, N.D.; Petrillo, A.; Bell, S.; Cummings, P.; Eriksen, S. Blood-brain barrier disruption for the treatment of malignant brain tumors: The National Program. *J. Neurosci. Nurs.* **1998**, *30*, 81–90. [CrossRef]
207. Kiviniemi, V.; Korhonen, V.; Kortelainen, J.; Rytty, S.; Keinanen, T.; Tuovinen, T.; Isokangas, M.; Sonkajarvi, E.; Siniluoto, T.; Nikkinen, J.; et al. Real-time monitoring of human blood-brain barrier disruption. *PLoS ONE* **2017**, *12*, e0174072. [CrossRef]
208. Unterberg, A.; Wahl, M.; Baethmann, A. Effects of bradykinin on permeability and diameter of pial vessels in vivo. *J. Cereb. Blood Flow Metab.* **1984**, *4*, 574–585. [CrossRef]
209. Witherow, F.N.; Helmy, A.; Webb, D.J.; Fox, K.A.; Newby, D.E. Bradykinin contributes to the vasodilator effects of chronic angiotensin-converting enzyme inhibition in patients with heart failure. *Circulation* **2001**, *104*, 2177–2181. [CrossRef]
210. Doctrow, S.R.; Abelleira, S.M.; Curry, L.A.; Heller-Harrison, R.; Kozarich, J.W.; Malfroy, B.; McCarroll, L.A.; Morgan, K.G.; Morrow, A.R.; Musso, G.F.; et al. The bradykinin analog RMP-7 increases intracellular free calcium levels in rat brain microvascular endothelial cells. *J. Pharmacol. Exp. Ther.* **1994**, *271*, 229–237.
211. Inamura, T.; Nomura, T.; Bartus, R.T.; Black, K.L. Intracarotid infusion of RMP-7, a bradykinin analog: A method for selective drug delivery to brain tumors. *J. Neurosurg.* **1994**, *81*, 752–758. [CrossRef] [PubMed]
212. Black, K.L.; Cloughesy, T.; Huang, S.C.; Gobin, Y.P.; Zhou, Y.; Grous, J.; Nelson, G.; Farahani, K.; Hoh, C.K.; Phelps, M. Intracarotid infusion of RMP-7, a bradykinin analog, and transport of gallium-68 ethylenediamine tetraacetic acid into human gliomas. *J. Neurosurg.* **1997**, *86*, 603–609. [CrossRef] [PubMed]
213. Fike, J.R.; Gobbel, G.T.; Mesiwala, A.H.; Shin, H.J.; Nakagawa, M.; Lamborn, K.R.; Seilhan, T.M.; Elliott, P.J. Cerebrovascular effects of the bradykinin analog RMP-7 in normal and irradiated dog brain. *J. Neuro-Oncol.* **1998**, *37*, 199–215. [CrossRef] [PubMed]
214. Barth, R.F.; Yang, W.; Bartus, R.T.; Moeschberger, M.L.; Goodman, J.H. Enhanced delivery of boronophenylalanine for neutron capture therapy of brain tumors using the bradykinin analog Cereport (Receptor-Mediated Permeabilizer-7). *Neurosurgery* **1999**, *44*, 351–359, discussion 359–360. [CrossRef]
215. Prados, M.D.; Schold, S.C., Jr.; Fine, H.A.; Jaeckle, K.; Hochberg, F.; Mechtler, L.; Fetell, M.R.; Phuphanich, S.; Feun, L.; Janus, T.J.; et al. A randomized, double-blind, placebo-controlled, phase 2 study of RMP-7 in combination with carboplatin administered intravenously for the treatment of recurrent malignant glioma. *Neuro-Oncology* **2003**, *5*, 96–103. [CrossRef]
216. Lynn, J.G.; Zwemer, R.L.; Chick, A.J.; Miller, A.E. A New Method for the Generation and Use of Focused Ultrasound in Experimental Biology. *J. Gen. Physiol.* **1942**, *26*, 179–193. [CrossRef]
217. Ballantine, H.T., Jr.; Bell, E.; Manlapaz, J. Progress and problems in the neurological applications of focused ultrasound. *J. Neurosurg.* **1960**, *17*, 858–876. [CrossRef]

218. Warwick, R.; Pond, J. Trackless lesions in nervous tissues produced by high intensity focused ultrasound (high-frequency mechanical waves). *J. Anat.* **1968**, *102*, 387–405.
219. Vykholdtseva, N.I.; Hynynen, K.; Damianou, C. Histologic effects of high intensity pulsed ultrasound exposure with subharmonic emission in rabbit brain in vivo. *Ultrasound Med. Biol.* **1995**, *21*, 969–979. [CrossRef]
220. Sheikov, N.; McDannold, N.; Vykholdtseva, N.; Jolesz, F.; Hynynen, K. Cellular mechanisms of the blood-brain barrier opening induced by ultrasound in presence of microbubbles. *Ultrasound Med. Biol.* **2004**, *30*, 979–989. [CrossRef]
221. Sheikov, N.; McDannold, N.; Sharma, S.; Hynynen, K. Effect of focused ultrasound applied with an ultrasound contrast agent on the tight junctional integrity of the brain microvascular endothelium. *Ultrasound Med. Biol.* **2008**, *34*, 1093–1104. [CrossRef]
222. Choi, J.J.; Wang, S.; Tung, Y.S.; Morrison, B., 3rd; Konofagou, E.E. Molecules of various pharmacologically-relevant sizes can cross the ultrasound-induced blood-brain barrier opening in vivo. *Ultrasound Med. Biol.* **2010**, *36*, 58–67. [CrossRef]
223. Chen, H.; Konofagou, E.E. The size of blood-brain barrier opening induced by focused ultrasound is dictated by the acoustic pressure. *J. Cereb. Blood Flow Metab.* **2014**, *34*, 1197–1204. [CrossRef]
224. Armstrong, J.K.; Wenby, R.B.; Meiselman, H.J.; Fisher, T.C. The hydrodynamic radii of macromolecules and their effect on red blood cell aggregation. *Biophys. J.* **2004**, *87*, 4259–4270. [CrossRef]
225. Lawrence, J.R.; Swerhone, G.D.; Kuhlicke, U.; Neu, T.R. In situ evidence for metabolic and chemical microdomains in the structured polymer matrix of bacterial microcolonies. *FEMS Microbiol. Ecol.* **2016**, *92*, fiw183. [CrossRef]
226. O'Reilly, M.A.; Hough, O.; Hynynen, K. Blood-Brain Barrier Closure Time After Controlled Ultrasound-Induced Opening Is Independent of Opening Volume. *J. Ultrasound Med.* **2017**, *36*, 475–483. [CrossRef]
227. Shen, Y.; Guo, J.; Chen, G.; Chin, C.T.; Chen, X.; Chen, J.; Wang, F.; Chen, S.; Dan, G. Delivery of Liposomes with Different Sizes to Mice Brain after Sonication by Focused Ultrasound in the Presence of Microbubbles. *Ultrasound Med. Biol.* **2016**, *42*, 1499–1511. [CrossRef]
228. Tsai, H.C.; Tsai, C.H.; Chen, W.S.; Inserra, C.; Wei, K.C.; Liu, H.L. Safety evaluation of frequent application of microbubble-enhanced focused ultrasound blood-brain-barrier opening. *Sci. Rep.* **2018**, *8*, 17720. [CrossRef]
229. Carpentier, A.; Canney, M.; Vignot, A.; Reina, V.; Beccaria, K.; Horodyckid, C.; Karachi, C.; Leclercq, D.; Lafon, C.; Chapelon, J.Y.; et al. Clinical trial of blood-brain barrier disruption by pulsed ultrasound. *Sci. Transl. Med.* **2016**, *8*, 343re342. [CrossRef]
230. Mainprize, T.; Lipsman, N.; Huang, Y.; Meng, Y.; Bethune, A.; Ironside, S.; Heyn, C.; Alkins, R.; Trudeau, M.; Sahgal, A.; et al. Blood-Brain Barrier Opening in Primary Brain Tumors with Non-invasive MR-Guided Focused Ultrasound: A Clinical Safety and Feasibility Study. *Sci. Rep.* **2019**, *9*, 321. [CrossRef]
231. Chen, K.T.; Lin, Y.J.; Chai, W.Y.; Lin, C.J.; Chen, P.Y.; Huang, C.Y.; Kuo, J.S.; Liu, H.L.; Wei, K.C. Neuronavigation-guided focused ultrasound (NaviFUS) for transcranial blood-brain barrier opening in recurrent glioblastoma patients: Clinical trial protocol. *Ann. Transl. Med.* **2020**, *8*, 673. [CrossRef] [PubMed]
232. Lipsman, N.; Meng, Y.; Bethune, A.J.; Huang, Y.; Lam, B.; Masellis, M.; Herrmann, N.; Heyn, C.; Aubert, I.; Boutet, A.; et al. Blood-brain barrier opening in Alzheimer's disease using MR-guided focused ultrasound. *Nat. Commun.* **2018**, *9*, 2336. [CrossRef] [PubMed]
233. Abrahao, A.; Meng, Y.; Llinas, M.; Huang, Y.; Hamani, C.; Mainprize, T.; Aubert, I.; Heyn, C.; Black, S.E.; Hynynen, K.; et al. First-in-human trial of blood-brain barrier opening in amyotrophic lateral sclerosis using MR-guided focused ultrasound. *Nat. Commun.* **2019**, *10*, 4373. [CrossRef] [PubMed]
234. Alonso, A.; Reinze, E.; Fatar, M.; Hennerici, M.G.; Meairs, S. Clearance of albumin following ultrasound-induced blood-brain barrier opening is mediated by glial but not neuronal cells. *Brain Res.* **2011**, *1411*, 9–16. [CrossRef]
235. Mathew, A.S.; Gorick, C.M.; Price, R.J. Multiple regression analysis of a comprehensive transcriptomic data assembly elucidates mechanically- and biochemically-driven responses to focused ultrasound blood-brain barrier disruption. *Theranostics* **2021**, *11*, 9847–9858. [CrossRef]
236. Beccaria, K.; Sabbagh, A.; de Groot, J.; Canney, M.; Carpentier, A.; Heimberger, A.B. Blood-brain barrier opening with low intensity pulsed ultrasound for immune modulation and immune therapeutic delivery to CNS tumors. *J. Neuro-Oncol.* **2021**, *151*, 65–73. [CrossRef]
237. Bynoe, M.S.; Viret, C.; Yan, A.; Kim, D.G. Adenosine receptor signaling: A key to opening the blood-brain door. *Fluids Barriers CNS* **2015**, *12*, 20. [CrossRef]
238. Pardridge, W.M.; Crawford, I.L.; Connor, J.D. Permeability changes in the blood-brain barrier induced by nortriptyline and chlorpromazine. *Toxicol. Appl. Pharmacol.* **1973**, *26*, 49–57. [CrossRef]
239. Alaofi, A.; On, N.; Kiptoo, P.; Williams, T.D.; Miller, D.W.; Siahaan, T.J. Comparison of Linear and Cyclic His-Ala-Val Peptides in Modulating the Blood-Brain Barrier Permeability: Impact on Delivery of Molecules to the Brain. *J. Pharm. Sci.* **2016**, *105*, 797–807. [CrossRef]
240. Sajesh, B.V.; On, N.H.; Omar, R.; Alrushaid, S.; Kopec, B.M.; Wang, W.G.; Sun, H.D.; Lillico, R.; Lakowski, T.M.; Siahaan, T.J.; et al. Validation of Cadherin HAV6 Peptide in the Transient Modulation of the Blood-Brain Barrier for the Treatment of Brain Tumors. *Pharmaceutics* **2019**, *11*, 481. [CrossRef]
241. Kiptoo, P.; Sinaga, E.; Calcagno, A.M.; Zhao, H.; Kobayashi, N.; Tambunan, U.S.; Siahaan, T.J. Enhancement of drug absorption through the blood-brain barrier and inhibition of intercellular tight junction resealing by E-cadherin peptides. *Mol. Pharm.* **2011**, *8*, 239–249. [CrossRef]

242. Hashimoto, Y.; Shirakura, K.; Okada, Y.; Takeda, H.; Endo, K.; Tamura, M.; Watari, A.; Sadamura, Y.; Sawasaki, T.; Doi, T.; et al. Claudin-5-Binders Enhance Permeation of Solutes across the Blood-Brain Barrier in a Mammalian Model. *J. Pharmacol. Exp. Ther.* **2017**, *363*, 275–283. [CrossRef]
243. Tachibana, K.; Hashimoto, Y.; Shirakura, K.; Okada, Y.; Hirayama, R.; Iwashita, Y.; Nishino, I.; Ago, Y.; Takeda, H.; Kuniyasu, H.; et al. Safety and efficacy of an anti-claudin-5 monoclonal antibody to increase blood-brain barrier permeability for drug delivery to the brain in a non-human primate. *J. Control. Release* **2021**, *336*, 105–111. [CrossRef]
244. Zeniya, S.; Kuwahara, H.; Daizo, K.; Watari, A.; Kondoh, M.; Yoshida-Tanaka, K.; Kaburagi, H.; Asada, K.; Nagata, T.; Nagahama, M.; et al. Angubindin-1 opens the blood-brain barrier in vivo for delivery of antisense oligonucleotide to the central nervous system. *J. Control. Release* **2018**, *283*, 126–134. [CrossRef]
245. Preston, E.; Slinn, J.; Vinokourov, I.; Stanimirovic, D. Graded reversible opening of the rat blood-brain barrier by intracarotid infusion of sodium caprate. *J. Neurosci. Methods* **2008**, *168*, 443–449. [CrossRef]
246. Sol, Y.; Choi, S.H.; Kim, H.J.; Kim, Y.W.; Cho, B.M.; Han, H.S.; Choi, K.J. Morphologic mechanisms of increased vascular permeability of triolein emulsion to the blood-brain barrier. *Microscopy* **2017**, *66*, 366–370. [CrossRef]
247. Michinaga, S.; Koyama, Y. Pathogenesis of brain edema and investigation into anti-edema drugs. *Int. J. Mol. Sci.* **2015**, *16*, 9949–9975. [CrossRef]
248. Townsend, R.; Desai, A.; Rammelsberg, D.; Kowalski, D.; Simmons, N.; Kitt, T.M. Safety and tolerability of intravenous regadenoson in healthy subjects: A randomized, repeat-dose, placebo-controlled study. *J. Nucl. Cardiol.* **2017**, *24*, 57–65. [CrossRef]
249. Carman, A.J.; Mills, J.H.; Krenz, A.; Kim, D.G.; Bynoe, M.S. Adenosine receptor signaling modulates permeability of the blood-brain barrier. *J. Neurosci.* **2011**, *31*, 13272–13280. [CrossRef]
250. Vezina, A.; Manglani, M.; Morris, D.; Foster, B.; McCord, M.; Song, H.; Zhang, M.; Davis, D.; Zhang, W.; Bills, J.; et al. Adenosine A2A Receptor Activation Enhances Blood-Tumor Barrier Permeability in a Rodent Glioma Model. *Mol. Cancer Res.* **2021**, *19*, 2081–2095. [CrossRef]
251. Tuomanen, E.I.; Prasad, S.M.; George, J.S.; Hoepelman, A.I.; Ibsen, P.; Heron, I.; Starzyk, R.M. Reversible opening of the blood-brain barrier by anti-bacterial antibodies. *Proc. Natl. Acad. Sci. USA* **1993**, *90*, 7824–7828. [CrossRef] [PubMed]
252. Rabchevsky, A.G.; Degos, J.D.; Dreyfus, P.A. Peripheral injections of Freund's adjuvant in mice provoke leakage of serum proteins through the blood-brain barrier without inducing reactive gliosis. *Brain Res.* **1999**, *832*, 84–96. [CrossRef]
253. Namer, I.J.; Steibel, J. Antibody directed against mannan of the Mycobacterium tuberculosis cell envelope provokes blood-brain barrier breakdown. *J. Neuroimmunol.* **2000**, *103*, 63–68. [CrossRef]
254. Vinuela-Berni, V.; Gomez-Gonzalez, B.; Quintanar-Stephano, A. Blockade of Arginine Vasopressin receptors prevents blood-brain barrier breakdown in Experimental Autoimmune Encephalomyelitis. *Sci. Rep.* **2020**, *10*, 467. [CrossRef] [PubMed]
255. Zeynalov, E.; Jones, S.M.; Seo, J.W.; Snell, L.D.; Elliott, J.P. Arginine-Vasopressin Receptor Blocker Conivaptan Reduces Brain Edema and Blood-Brain Barrier Disruption after Experimental Stroke in Mice. *PLoS ONE* **2015**, *10*, e0136121. [CrossRef]
256. Nagy, Z.; Peters, H.; Huttner, I. Charge-related alterations of the cerebral endothelium. *Lab. Investig.* **1983**, *49*, 662–671.
257. Strausbaugh, L.J. Intracarotid infusions of protamine sulfate disrupt the blood-brain barrier of rabbits. *Brain Res.* **1987**, *409*, 221–226. [CrossRef]
258. Westergren, I.; Johansson, B.B. Altering the blood-brain barrier in the rat by intracarotid infusion of polycations: A comparison between protamine, poly-L-lysine and poly-L-arginine. *Acta Physiol. Scand.* **1993**, *149*, 99–104. [CrossRef]
259. Pardridge, W.M.; Triguero, D.; Buciak, J. Transport of histone through the blood-brain barrier. *J. Pharmacol. Exp. Ther.* **1989**, *251*, 821–826.
260. Westergren, I.; Nordborg, C.; Johansson, B.B. Glutamate enhances brain damage and albumin content in cerebrospinal fluid after intracarotid protamine infusion. *Acta Neuropathol.* **1993**, *85*, 285–290. [CrossRef]
261. Heerklotz, H.; Seelig, J. Correlation of membrane/water partition coefficients of detergents with the critical micelle concentration. *Biophys. J.* **2000**, *78*, 2435–2440. [CrossRef]
262. Zappulla, R.A.; Spigelman, M.K.; Omsberg, E.; Rosen, J.J.; Malis, L.I.; Holland, J.F. Electroencephalographic consequences of sodium dehydrocholate-induced blood-brain barrier disruption: Part 1. Acute and chronic effects of intracarotid sodium dehydrocholate. *Neurosurgery* **1985**, *16*, 630–638. [CrossRef]
263. Sztriha, L.; Betz, A.L. Oleic acid reversibly opens the blood-brain barrier. *Brain Res.* **1991**, *550*, 257–262. [CrossRef]
264. Erdlenbruch, B.; Jendrossek, V.; Eibl, H.; Lakomek, M. Transient and controllable opening of the blood-brain barrier to cytostatic and antibiotic agents by alkylglycerols in rats. *Exp. Brain Res.* **2000**, *135*, 417–422. [CrossRef]
265. Lee, H.J.; Zhang, Y.; Pardridge, W.M. Blood-brain barrier disruption following the internal carotid arterial perfusion of alkyl glycerols. *J. Drug Target.* **2002**, *10*, 463–467. [CrossRef]
266. Linville, R.M.; Komin, A.; Lan, X.; DeStefano, J.G.; Chu, C.; Liu, G.; Walczak, P.; Hristova, K.; Searson, P.C. Reversible blood-brain barrier opening utilizing the membrane active peptide melittin in vitro and in vivo. *Biomaterials* **2021**, *275*, 120942. [CrossRef]
267. Lee, M.T.; Sun, T.L.; Hung, W.C.; Huang, H.W. Process of inducing pores in membranes by melittin. *Proc. Natl. Acad. Sci. USA* **2013**, *110*, 14243–14248. [CrossRef]
268. Yin, Y.; Cao, L.; Ge, H.; Duanmu, W.; Tan, L.; Yuan, J.; Tunan, C.; Li, F.; Hu, R.; Gao, F.; et al. L-Borneol induces transient opening of the blood-brain barrier and enhances the therapeutic effect of cisplatin. *Neuroreport* **2017**, *28*, 506–513. [CrossRef]

269. Wang, W.; Marin-Ramos, N.I.; He, H.; Zeng, S.; Cho, H.Y.; Swenson, S.D.; Zheng, L.; Epstein, A.L.; Schonthal, A.H.; Hofman, F.M.; et al. NEO100 enables brain delivery of blood-brain barrier impermeable therapeutics. *Neuro-Oncology* **2021**, *23*, 63–75. [CrossRef]
270. Zhang, Q.L.; Fu, B.M.; Zhang, Z.J. Borneol, a novel agent that improves central nervous system drug delivery by enhancing blood-brain barrier permeability. *Drug Deliv.* **2017**, *24*, 1037–1044. [CrossRef]
271. Ramirez, S.H.; Potula, R.; Fan, S.; Eidem, T.; Papugani, A.; Reichenbach, N.; Dykstra, H.; Weksler, B.B.; Romero, I.A.; Couraud, P.O.; et al. Methamphetamine disrupts blood-brain barrier function by induction of oxidative stress in brain endothelial cells. *J. Cereb. Blood Flow Metab.* **2009**, *29*, 1933–1945. [CrossRef]
272. Chang, J.H.; Greene, C.; Frudd, K.; Araujo Dos Santos, L.; Futter, C.; Nichols, B.J.; Campbell, M.; Turowski, P. Methamphetamine enhances caveolar transport of therapeutic agents across the rodent blood-brain barrier. *Cell Rep. Med.* **2022**, *3*, 100497. [CrossRef]
273. Kast, R.E. Using blood brain barrier disruption by methamphetamine for drug delivery. *J. Neuro-Oncol.* **2007**, *85*, 109–110. [CrossRef]
274. Hwang, J.S.; Cha, E.H.; Park, B.; Ha, E.; Seo, J.H. PBN inhibits a detrimental effect of methamphetamine on brain endothelial cells by alleviating the generation of reactive oxygen species. *Arch. Pharm. Res.* **2020**, *43*, 1347–1355. [CrossRef]
275. Lees, K.R.; Zivin, J.A.; Ashwood, T.; Davalos, A.; Davis, S.M.; Diener, H.C.; Grotta, J.; Lyden, P.; Shuaib, A.; Hardemark, H.G.; et al. NXY-059 for acute ischemic stroke. *N. Engl. J. Med.* **2006**, *354*, 588–600. [CrossRef]
276. Antonic, A.; Dottori, M.; Macleod, M.R.; Donnan, G.A.; Howells, D.W. NXY-059, a Failed Stroke Neuroprotectant, Offers No Protection to Stem Cell-Derived Human Neurons. *J. Stroke Cerebrovasc. Dis.* **2018**, *27*, 2158–2165. [CrossRef]
277. Kuroda, S.; Tsuchidate, R.; Smith, M.L.; Maples, K.R.; Siesjo, B.K. Neuroprotective effects of a novel nitrone, NXY-059, after transient focal cerebral ischemia in the rat. *J. Cereb. Blood Flow Metab.* **1999**, *19*, 778–787. [CrossRef]
278. Samii, A.; Bickel, U.; Stroth, U.; Pardridge, W.M. Blood-brain barrier transport of neuropeptides: Analysis with a metabolically stable dermorphin analogue. *Am. J. Physiol.* **1994**, *267*, E124–E131. [CrossRef]
279. Towner, R.A.; Saunders, D.; Lerner, M.; Silasi Mansat, R.; Yuan, T.; Barber, D.; Faakye, J.; Nyul-Toth, A.; Csiszar, A.; Greenwood-Van Meerveld, B.; et al. Temporary opening of the blood-brain barrier with the nitrone compound OKN-007. *Am. J. Nucl. Med. Mol. Imaging* **2021**, *11*, 363–373.
280. Sirav, B.; Seyhan, N. Blood-brain barrier disruption by continuous-wave radio frequency radiation. *Electromagn. Biol. Med.* **2009**, *28*, 215–222. [CrossRef]
281. Selmaoui, B.; Mazet, P.; Petit, P.B.; Kim, K.; Choi, D.; de Seze, R. Exposure of South Korean Population to 5G Mobile Phone Networks (3.4–3.8 GHz). *Bioelectromagnetics* **2021**, *42*, 407–414. [CrossRef] [PubMed]
282. Li, K.; Zhang, K.; Xu, S.; Wang, X.; Zhou, Y.; Zhou, Y.; Gao, P.; Lin, J.; Ding, G.; Guo, G. EMP-induced BBB-disruption enhances drug delivery to glioma and increases treatment efficacy in rats. *Bioelectromagnetics* **2018**, *39*, 60–67. [CrossRef] [PubMed]
283. Lorenzo, M.F.; Campelo, S.N.; Arroyo, J.P.; Aycocock, K.N.; Hinckley, J.; Arena, C.B.; Rossmesl, J.H., Jr.; Davalos, R.V. An Investigation for Large Volume, Focal Blood-Brain Barrier Disruption with High-Frequency Pulsed Electric Fields. *Pharmaceutics* **2021**, *14*, 1333. [CrossRef] [PubMed]
284. Aleynik, A.; Gernavage, K.M.; Mourad, Y.; Sherman, L.S.; Liu, K.; Gubenko, Y.A.; Rameshwar, P. Stem cell delivery of therapies for brain disorders. *Clin. Transl. Med.* **2014**, *3*, 24. [CrossRef]
285. Akiyama, Y.; Radtke, C.; Kocsis, J.D. Remyelination of the rat spinal cord by transplantation of identified bone marrow stromal cells. *J. Neurosci.* **2002**, *22*, 6623–6630. [CrossRef]
286. Osaka, M.; Honmou, O.; Murakami, T.; Nonaka, T.; Houkin, K.; Hamada, H.; Kocsis, J.D. Intravenous administration of mesenchymal stem cells derived from bone marrow after contusive spinal cord injury improves functional outcome. *Brain Res.* **2010**, *1343*, 226–235. [CrossRef]
287. Popovich, P.G.; Horner, P.J.; Mullin, B.B.; Stokes, B.T. A quantitative spatial analysis of the blood-spinal cord barrier. I. Permeability changes after experimental spinal contusion injury. *Exp. Neurol.* **1996**, *142*, 258–275. [CrossRef]
288. Chia, Y.C.; Anjum, C.E.; Yee, H.R.; Kenisi, Y.; Chan, M.K.S.; Wong, M.B.F.; Pan, S.Y. Stem Cell Therapy for Neurodegenerative Diseases: How Do Stem Cells Bypass the Blood-Brain Barrier and Home to the Brain? *Stem Cells Int.* **2020**, *2020*, 8889061. [CrossRef]
289. Soper, B.W.; Duffy, T.M.; Lessard, M.D.; Jude, C.D.; Schuldt, A.J.; Vogler, C.A.; Levy, B.; Barker, J.E. Transplanted ER-MP12hi20-58med/hi myeloid progenitors produce resident macrophages from marrow that are therapeutic for lysosomal storage disease. *Blood Cells Mol. Dis.* **2004**, *32*, 199–213. [CrossRef]
290. Choi, C.; Kim, H.M.; Shon, J.; Park, J.; Kim, H.T.; Kang, S.H.; Oh, S.H.; Kim, N.K.; Kim, O.J. The combination of mannitol and temozolomide increases the effectiveness of stem cell treatment in a chronic stroke model. *Cytotherapy* **2018**, *20*, 820–829. [CrossRef]
291. Aldenhoven, M.; Wynn, R.F.; Orchard, P.J.; O’Meara, A.; Veys, P.; Fischer, A.; Valayannopoulos, V.; Neven, B.; Rovelli, A.; Prasad, V.K.; et al. Long-term outcome of Hurler syndrome patients after hematopoietic cell transplantation: An international multicenter study. *Blood* **2015**, *125*, 2164–2172. [CrossRef]
292. Zhang, H.; Young, S.P.; Auray-Blais, C.; Orchard, P.J.; Tolar, J.; Millington, D.S. Analysis of glycosaminoglycans in cerebrospinal fluid from patients with mucopolysaccharidoses by isotope-dilution ultra-performance liquid chromatography-tandem mass spectrometry. *Clin. Chem.* **2011**, *57*, 1005–1012. [CrossRef]

293. Visigalli, I.; Delai, S.; Ferro, F.; Cecere, F.; Vezzoli, M.; Sanvito, F.; Chanut, F.; Benedicenti, F.; Spinozzi, G.; Wynn, R.; et al. Preclinical Testing of the Safety and Tolerability of Lentiviral Vector-Mediated Above-Normal Alpha-L-Iduronidase Expression in Murine and Human Hematopoietic Cells Using Toxicology and Biodistribution Good Laboratory Practice Studies. *Hum. Gene Ther.* **2016**, *27*, 813–829. [CrossRef]
294. Zhao, Y.; Stepto, H.; Schneider, C.K. Development of the First World Health Organization Lentiviral Vector Standard: Toward the Production Control and Standardization of Lentivirus-Based Gene Therapy Products. *Hum. Gene Ther. Methods* **2017**, *28*, 205–214. [CrossRef]
295. Heidarzadeh, M.; Gursoy-Ozdemir, Y.; Kaya, M.; Eslami Abriz, A.; Zarebkohan, A.; Rahbarghazi, R.; Sokullu, E. Exosomal delivery of therapeutic modulators through the blood-brain barrier; promise and pitfalls. *Cell Biosci.* **2021**, *11*, 142. [CrossRef]
296. Morad, G.; Carman, C.V.; Hagedorn, E.J.; Perlin, J.R.; Zon, L.I.; Mustafaoglu, N.; Park, T.E.; Ingber, D.E.; Daisy, C.C.; Moses, M.A. Tumor-Derived Extracellular Vesicles Breach the Intact Blood-Brain Barrier via Transcytosis. *ACS Nano* **2019**, *13*, 13853–13865. [CrossRef]
297. Kumar, P.; Wu, H.; McBride, J.L.; Jung, K.E.; Kim, M.H.; Davidson, B.L.; Lee, S.K.; Shankar, P.; Manjunath, N. Transvascular delivery of small interfering RNA to the central nervous system. *Nature* **2007**, *448*, 39–43. [CrossRef]
298. Wisniewski, J.R.; Hein, M.Y.; Cox, J.; Mann, M. A “proteomic ruler” for protein copy number and concentration estimation without spike-in standards. *Mol. Cell Proteom.* **2014**, *13*, 3497–3506. [CrossRef]
299. Fuhrmann, G.; Serio, A.; Mazo, M.; Nair, R.; Stevens, M.M. Active loading into extracellular vesicles significantly improves the cellular uptake and photodynamic effect of porphyrins. *J. Control. Release* **2015**, *205*, 35–44. [CrossRef]
300. Dar, G.H.; Mendes, C.C.; Kuan, W.L.; Speciale, A.A.; Conceicao, M.; Gorgens, A.; Uliyakina, I.; Lobo, M.J.; Lim, W.F.; El Andaloussi, S.; et al. GAPDH controls extracellular vesicle biogenesis and enhances the therapeutic potential of EV mediated siRNA delivery to the brain. *Nat. Commun.* **2021**, *12*, 6666. [CrossRef]
301. Allen, T.M.; Hansen, C. Pharmacokinetics of stealth versus conventional liposomes: Effect of dose. *Biochim. Biophys. Acta* **1991**, *1068*, 133–141. [CrossRef]
302. Iden, D.L.; Allen, T.M. In vitro and in vivo comparison of immunoliposomes made by conventional coupling techniques with those made by a new post-insertion approach. *Biochim. Biophys. Acta* **2001**, *1513*, 207–216. [CrossRef]
303. Kuroda, H.; Tachikawa, M.; Yagi, Y.; Umetsu, M.; Nurdin, A.; Miyauchi, E.; Watanabe, M.; Uchida, Y.; Terasaki, T. Cluster of Differentiation 46 Is the Major Receptor in Human Blood-Brain Barrier Endothelial Cells for Uptake of Exosomes Derived from Brain-Metastatic Melanoma Cells (SK-Mel-28). *Mol. Pharm.* **2019**, *16*, 292–304. [CrossRef]
304. Shusta, E.V.; Zhu, C.; Boado, R.J.; Pardridge, W.M. Subtractive expression cloning reveals high expression of CD46 at the blood-brain barrier. *J. Neuropathol. Exp. Neurol.* **2002**, *61*, 597–604. [CrossRef]
305. Qu, M.; Lin, Q.; Huang, L.; Fu, Y.; Wang, L.; He, S.; Fu, Y.; Yang, S.; Zhang, Z.; Zhang, L.; et al. Dopamine-loaded blood exosomes targeted to brain for better treatment of Parkinson’s disease. *J. Control. Release* **2018**, *287*, 156–166. [CrossRef]
306. Haney, M.J.; Zhao, Y.; Jin, Y.S.; Batrakova, E.V. Extracellular Vesicles as Drug Carriers for Enzyme Replacement Therapy to Treat CLN2 Batten Disease: Optimization of Drug Administration Routes. *Cells* **2020**, *9*, 1273. [CrossRef] [PubMed]
307. Sercombe, L.; Veerati, T.; Moheimani, F.; Wu, S.Y.; Sood, A.K.; Hua, S. Advances and Challenges of Liposome Assisted Drug Delivery. *Front. Pharmacol.* **2015**, *6*, 286. [CrossRef] [PubMed]
308. Fuentes, A.V.; Pineda, M.D.; Venkata, K.C.N. Comprehension of Top 200 Prescribed Drugs in the US as a Resource for Pharmacy Teaching, Training and Practice. *Pharmacy* **2018**, *6*, 43. [CrossRef] [PubMed]
309. Kerry, R.J.; Jenner, F.A. A double blind crossover comparison of diazepam (Valium, Ro5-2807) with chlordiazepoxide (Librium) in the treatment of neurotic anxiety. *Psychopharmacologia* **1962**, *3*, 302–306. [CrossRef] [PubMed]
310. Swinyard, E.A.; Toman, J.E. A comparison of the anticonvulsant actions of some phenylhydantoins and their corresponding phenylacetylureas. *J. Pharmacol. Exp. Ther.* **1950**, *100*, 151–157. [PubMed]
311. Ghose, A.K.; Viswanadhan, V.N.; Wendoloski, J.J. A knowledge-based approach in designing combinatorial or medicinal chemistry libraries for drug discovery. 1. A qualitative and quantitative characterization of known drug databases. *J. Comb. Chem.* **1999**, *1*, 55–68. [CrossRef]
312. Lipinski, C.A. Drug-like properties and the causes of poor solubility and poor permeability. *J. Pharmacol. Toxicol. Methods* **2000**, *44*, 235–249. [CrossRef]
313. Van de Waterbeemd, H.; Camenisch, G.; Folkers, G.; Chretien, J.R.; Raevsky, O.A. Estimation of blood-brain barrier crossing of drugs using molecular size and shape, and H-bonding descriptors. *J. Drug Target.* **1998**, *6*, 151–165. [CrossRef]
314. Ajay; Bemis, G.W.; Murcko, M.A. Designing libraries with CNS activity. *J. Med. Chem.* **1999**, *42*, 4942–4951. [CrossRef]
315. Missner, A.; Pohl, P. 110 years of the Meyer-Overton rule: Predicting membrane permeability of gases and other small compounds. *Chemphyschem* **2009**, *10*, 1405–1414. [CrossRef]
316. Levin, V.A. Relationship of octanol/water partition coefficient and molecular weight to rat brain capillary permeability. *J. Med. Chem.* **1980**, *23*, 682–684. [CrossRef]
317. Lieb, W.R.; Stein, W.D. Non-Stokesian nature of transverse diffusion within human red cell membranes. *J. Membr. Biol.* **1986**, *92*, 111–119. [CrossRef]
318. Trauble, H. The movement of molecules across lipid membranes: A molecular theory. *J. Membr. Biol.* **1971**, *4*, 193–208. [CrossRef]
319. Fischer, H.; Gottschlich, R.; Seelig, A. Blood-brain barrier permeation: Molecular parameters governing passive diffusion. *J. Membr. Biol.* **1998**, *165*, 201–211. [CrossRef]



320. Disalvo, E.A.; Pinto, O.A.; Martini, M.F.; Bouchet, A.M.; Hollmann, A.; Frias, M.A. Functional role of water in membranes updated: A tribute to Trauble. *Biochim. Biophys. Acta* **2015**, *1848*, 1552–1562. [CrossRef]
321. Diamond, J.M.; Wright, E.M. Molecular forces governing non-electrolyte permeation through cell membranes. *Proc. R. Soc. Lond. Ser. B Biol. Sci.* **1969**, *171*, 273–316. [CrossRef]
322. Pardridge, W.M.; Mietus, L.J. Transport of steroid hormones through the rat blood-brain barrier. Primary role of albumin-bound hormone. *J. Clin. Investig.* **1979**, *64*, 145–154. [CrossRef]
323. Chikhale, E.G.; Ng, K.Y.; Burton, P.S.; Borchardt, R.T. Hydrogen bonding potential as a determinant of the in vitro and in situ blood-brain barrier permeability of peptides. *Pharm. Res.* **1994**, *11*, 412–419. [CrossRef]
324. Najjar, A.; Karaman, R. The prodrug approach in the era of drug design. *Expert Opin. Drug Deliv.* **2019**, *16*, 1–5. [CrossRef]
325. Yi, B.; Jahangir, A.; Evans, A.K.; Briggs, D.; Ravina, K.; Ernest, J.; Farimani, A.B.; Sun, W.; Rajadas, J.; Green, M.; et al. Discovery of novel brain permeable and G protein-biased beta-1 adrenergic receptor partial agonists for the treatment of neurocognitive disorders. *PLoS ONE* **2017**, *12*, e0180319. [CrossRef] [PubMed]
326. Kappos, L.; Gold, R.; Miller, D.H.; Macmanus, D.G.; Havrdova, E.; Limmroth, V.; Polman, C.H.; Schmierer, K.; Yousry, T.A.; Yang, M.; et al. Efficacy and safety of oral fumarate in patients with relapsing-remitting multiple sclerosis: A multicentre, randomised, double-blind, placebo-controlled phase IIIb study. *Lancet* **2008**, *372*, 1463–1472. [CrossRef]
327. Oldendorf, W.H. Carrier-mediated blood-brain barrier transport of short-chain monocarboxylic organic acids. *Am. J. Physiol.* **1973**, *224*, 1450–1453. [CrossRef] [PubMed]
328. Bodor, N.; Shek, E.; Higuchi, T. Delivery of a quaternary pyridinium salt across the blood-brain barrier by its dihydropyridine derivative. *Science* **1975**, *190*, 155–156. [CrossRef]
329. Torrence, P.F.; Kinjo, J.; Khamnei, S.; Greig, N.H. Synthesis and pharmacokinetics of a dihydropyridine chemical delivery system for the antiimmunodeficiency virus agent dideoxycytidine. *J. Med. Chem.* **1993**, *36*, 529–537. [CrossRef]
330. Simpkins, J.W.; McCornack, J.; Estes, K.S.; Brewster, M.E.; Shek, E.; Bodor, N. Sustained brain-specific delivery of estradiol causes long-term suppression of luteinizing hormone secretion. *J. Med. Chem.* **1986**, *29*, 1809–1812. [CrossRef]
331. Broadwell, R.D.; Salzman, M.; Kaplan, R.S. Morphologic effect of dimethyl sulfoxide on the blood-brain barrier. *Science* **1982**, *217*, 164–166. [CrossRef]
332. Yoshikawa, T.; Sakaeda, T.; Sugawara, T.; Hirano, K.; Stella, V.J. A novel chemical delivery system for brain targeting. *Adv. Drug Deliv. Rev.* **1999**, *36*, 255–275. [CrossRef]
333. Nguyen, L.N.; Ma, D.; Shui, G.; Wong, P.; Cazenave-Gassiot, A.; Zhang, X.; Wenk, M.R.; Goh, E.L.; Silver, D.L. Mfsd2a is a transporter for the essential omega-3 fatty acid docosahexaenoic acid. *Nature* **2014**, *509*, 503–506. [CrossRef]
334. Guo, P.; Si, M.; Wu, D.; Xue, H.Y.; Hu, W.; Wong, H.L. Incorporation of docosahexaenoic acid (DHA) enhances nanodelivery of antiretroviral across the blood-brain barrier for treatment of HIV reservoir in brain. *J. Control. Release* **2020**, *328*, 696–709. [CrossRef]
335. Anel, A.; Calvo, M.; Naval, J.; Iturralde, M.; Alava, M.A.; Pineiro, A. Interaction of rat alpha-fetoprotein and albumin with polyunsaturated and other fatty acids: Determination of apparent association constants. *FEBS Lett.* **1989**, *250*, 22–24. [CrossRef]
336. Mulik, R.S.; Bing, C.; Ladouceur-Wodzak, M.; Munaweera, I.; Chopra, R.; Corbin, I.R. Localized delivery of low-density lipoprotein docosahexaenoic acid nanoparticles to the rat brain using focused ultrasound. *Biomaterials* **2016**, *83*, 257–268. [CrossRef]
337. Batrakova, E.V.; Vinogradov, S.V.; Robinson, S.M.; Niehoff, M.L.; Banks, W.A.; Kabanov, A.V. Polypeptide point modifications with fatty acid and amphiphilic block copolymers for enhanced brain delivery. *Bioconjug. Chem.* **2005**, *16*, 793–802. [CrossRef]
338. Schumann, T.; Konig, J.; Henke, C.; Willmes, D.M.; Bornstein, S.R.; Jordan, J.; Fromm, M.F.; Birkenfeld, A.L. Solute Carrier Transporters as Potential Targets for the Treatment of Metabolic Disease. *Pharmacol. Rev.* **2020**, *72*, 343–379. [CrossRef]
339. Pardridge, W.M. Blood-brain barrier endogenous transporters as therapeutic targets: A new model for small molecule CNS drug discovery. *Expert Opin. Ther. Targets* **2015**, *19*, 1059–1072. [CrossRef]
340. Pardridge, W.M.; Oldendorf, W.H. Kinetics of blood-brain transport of hexoses. *Biochim. Biophys. Acta* **1975**, *382*, 377–392. [CrossRef]
341. Long, W.; Cheeseman, C.I. Structure of, and functional insight into the GLUT family of membrane transporters. *Cell Health Cytoskel.* **2015**, *7*, 167–183. [CrossRef]
342. Pardridge, W.M.; Boado, R.J.; Farrell, C.R. Brain-type glucose transporter (GLUT-1) is selectively localized to the blood-brain barrier. Studies with quantitative western blotting and in situ hybridization. *J. Biol. Chem.* **1990**, *265*, 18035–18040. [CrossRef]
343. Dwyer, K.J.; Pardridge, W.M. Developmental modulation of blood-brain barrier and choroid plexus GLUT1 glucose transporter messenger ribonucleic acid and immunoreactive protein in rabbits. *Endocrinology* **1993**, *132*, 558–565. [CrossRef]
344. Boado, R.J.; Pardridge, W.M. The brain-type glucose transporter mRNA is specifically expressed at the blood-brain barrier. *Biochem. Biophys. Res. Commun.* **1990**, *166*, 174–179. [CrossRef]
345. Roberts, L.M.; Black, D.S.; Raman, C.; Woodford, K.; Zhou, M.; Haggerty, J.E.; Yan, A.T.; Cwirla, S.E.; Grindstaff, K.K. Subcellular localization of transporters along the rat blood-brain barrier and blood-cerebral-spinal fluid barrier by in vivo biotinylation. *Neuroscience* **2008**, *155*, 423–438. [CrossRef]
346. Deng, D.; Xu, C.; Sun, P.; Wu, J.; Yan, C.; Hu, M.; Yan, N. Crystal structure of the human glucose transporter GLUT1. *Nature* **2014**, *510*, 121–125. [CrossRef]

347. Salas-Burgos, A.; Iserovich, P.; Zuniga, F.; Vera, J.C.; Fischbarg, J. Predicting the three-dimensional structure of the human facilitative glucose transporter glut1 by a novel evolutionary homology strategy: Insights on the molecular mechanism of substrate migration, and binding sites for glucose and inhibitory molecules. *Biophys. J.* **2004**, *87*, 2990–2999. [CrossRef]
348. Yan, R.; Zhao, X.; Lei, J.; Zhou, Q. Structure of the human LAT1-4F2hc heteromeric amino acid transporter complex. *Nature* **2019**, *568*, 127–130. [CrossRef] [PubMed]
349. Cremer, J.E.; Cunningham, V.J. Effects of some chlorinated sugar derivatives on the hexose transport system of the blood/brain barrier. *Biochem. J.* **1979**, *180*, 677–679. [CrossRef]
350. Halmos, T.; Santarromana, M.; Antonakis, K.; Scherman, D. Synthesis of O-methylsulfonyl derivatives of D-glucose as potential alkylating agents for targeted drug delivery to the brain. Evaluation of their interaction with the human erythrocyte GLUT1 hexose transporter. *Carbohydr. Res.* **1997**, *299*, 15–21. [CrossRef]
351. Polt, R.; Porreca, F.; Szabo, L.Z.; Bilsky, E.J.; Davis, P.; Abbruscato, T.J.; Davis, T.P.; Harvath, R.; Yamamura, H.I.; Hruby, V.J. Glycopeptide enkephalin analogues produce analgesia in mice: Evidence for penetration of the blood-brain barrier. *Proc. Natl. Acad. Sci. USA* **1994**, *91*, 7114–7118. [CrossRef] [PubMed]
352. Egleton, R.D.; Mitchell, S.A.; Huber, J.D.; Janders, J.; Stropova, D.; Polt, R.; Yamamura, H.I.; Hruby, V.J.; Davis, T.P. Improved bioavailability to the brain of glycosylated Met-enkephalin analogs. *Brain Res.* **2000**, *881*, 37–46. [CrossRef]
353. Zhao, Y.; Zhang, L.; Peng, Y.; Yue, Q.; Hai, L.; Guo, L.; Wang, Q.; Wu, Y. GLUT1-mediated venlafaxine-thiamine disulfide system-glucose conjugates with “lock-in” function for central nervous system delivery. *Chem. Biol. Drug Des* **2018**, *91*, 707–716. [CrossRef] [PubMed]
354. Matovic, J.; Jarvinen, J.; Sokka, I.K.; Imlimthan, S.; Raitanen, J.E.; Montaser, A.; Maaheimo, H.; Huttunen, K.M.; Peraniemi, S.; Airaksinen, A.J.; et al. Exploring the Biochemical Foundations of a Successful GLUT1-Targeting Strategy to BNCT: Chemical Synthesis and In Vitro Evaluation of the Entire Positional Isomer Library of ortho-Carboranyl-methyl-Bearing Glucoconjugates. *Mol. Pharm.* **2021**, *18*, 285–304. [CrossRef]
355. Pardridge, W.M.; Oldendorf, W.H. Kinetic analysis of blood-brain barrier transport of amino acids. *Biochim. Biophys. Acta* **1975**, *401*, 128–136. [CrossRef]
356. Pardridge, W.M. Kinetics of competitive inhibition of neutral amino acid transport across the blood-brain barrier. *J. Neurochem.* **1977**, *28*, 103–108. [CrossRef]
357. Kanai, Y.; Segawa, H.; Miyamoto, K.; Uchino, H.; Takeda, E.; Endou, H. Expression cloning and characterization of a transporter for large neutral amino acids activated by the heavy chain of 4F2 antigen (CD98). *J. Biol. Chem.* **1998**, *273*, 23629–23632. [CrossRef]
358. Boado, R.J.; Li, J.Y.; Nagaya, M.; Zhang, C.; Pardridge, W.M. Selective expression of the large neutral amino acid transporter at the blood-brain barrier. *Proc. Natl. Acad. Sci. USA* **1999**, *96*, 12079–12084. [CrossRef]
359. Oldendorf, W.H. Stereospecificity of blood-brain barrier permeability to amino acids. *Am. J. Physiol.* **1973**, *224*, 967–969. [CrossRef]
360. Uchida, Y.; Ohtsuki, S.; Katsukura, Y.; Ikeda, C.; Suzuki, T.; Kamiie, J.; Terasaki, T. Quantitative targeted absolute proteomics of human blood-brain barrier transporters and receptors. *J. Neurochem.* **2011**, *117*, 333–345. [CrossRef]
361. Pardridge, W.M. Drug transport across the blood-brain barrier. *J. Cereb. Blood Flow Metab.* **2012**, *32*, 1959–1972. [CrossRef]
362. Holtz, P. Role of L-DOPA decarboxylase in the biosynthesis of catecholamines in nervous tissue and the adrenal medulla. *Pharmacol. Rev.* **1959**, *11*, 317–329.
363. Yoshida, H.; Kanike, K.; Namba, J. Properties of a carrier system to transport L-dopa into brain slices. *Nature* **1963**, *198*, 191–192. [CrossRef]
364. Kageyama, T.; Nakamura, M.; Matsuo, A.; Yamasaki, Y.; Takakura, Y.; Hashida, M.; Kanai, Y.; Naito, M.; Tsuruo, T.; Minato, N.; et al. The 4F2hc/LAT1 complex transports L-DOPA across the blood-brain barrier. *Brain Res.* **2000**, *879*, 115–121. [CrossRef]
365. Friedman, H.S.; Colvin, O.M.; Ludeman, S.M.; Schold, S.C., Jr.; Boyd, V.L.; Mulhbaier, L.H.; Bigner, D.D. Experimental chemotherapy of human medulloblastoma with classical alkylators. *Cancer Res.* **1986**, *46*, 2827–2833.
366. Greig, N.H.; Momma, S.; Sweeney, D.J.; Smith, Q.R.; Rapoport, S.I. Facilitated transport of melphalan at the rat blood-brain barrier by the large neutral amino acid carrier system. *Cancer Res.* **1987**, *47*, 1571–1576.
367. Uchino, H.; Kanai, Y.; Kim, D.K.; Wempe, M.F.; Chairoungdua, A.; Morimoto, E.; Anders, M.W.; Endou, H. Transport of amino acid-related compounds mediated by L-type amino acid transporter 1 (LAT1): Insights into the mechanisms of substrate recognition. *Mol. Pharmacol.* **2002**, *61*, 729–737. [CrossRef]
368. Wang, Y.; Welty, D.F. The simultaneous estimation of the influx and efflux blood-brain barrier permeabilities of gabapentin using a microdialysis-pharmacokinetic approach. *Pharm. Res.* **1996**, *13*, 398–403. [CrossRef]
369. Weed, D.L. Does paraquat cause Parkinson’s disease? A review of reviews. *Neurotoxicology* **2021**, *86*, 180–184. [CrossRef]
370. Shimizu, K.; Ohtaki, K.; Matsubara, K.; Aoyama, K.; Uezono, T.; Saito, O.; Suno, M.; Ogawa, K.; Hayase, N.; Kimura, K.; et al. Carrier-mediated processes in blood-brain barrier penetration and neural uptake of paraquat. *Brain Res.* **2001**, *906*, 135–142. [CrossRef]
371. Geier, E.G.; Schlessinger, A.; Fan, H.; Gable, J.E.; Irwin, J.J.; Sali, A.; Giacomini, K.M. Structure-based ligand discovery for the Large-neutral Amino Acid Transporter 1, LAT-1. *Proc. Natl. Acad. Sci. USA* **2013**, *110*, 5480–5485. [CrossRef]
372. Lee, Y.; Wiriyasermkul, P.; Jin, C.; Quan, L.; Ohgaki, R.; Okuda, S.; Kusakizako, T.; Nishizawa, T.; Oda, K.; Ishitani, R.; et al. Cryo-EM structure of the human L-type amino acid transporter 1 in complex with glycoprotein CD98hc. *Nat. Struct. Mol. Biol.* **2019**, *26*, 510–517. [CrossRef]

373. Karkkainen, J.; Laitinen, T.; Markowicz-Piasecka, M.; Montaser, A.; Lehtonen, M.; Rautio, J.; Gynther, M.; Poso, A.; Huttunen, K.M. Molecular characteristics supporting l-Type amino acid transporter 1 (LAT1)-mediated translocation. *Bioorg. Chem.* **2021**, *112*, 104921. [CrossRef]
374. Killian, D.M.; Hermeling, S.; Chikhale, P.J. Targeting the cerebrovascular large neutral amino acid transporter (LAT1) isoform using a novel disulfide-based brain drug delivery system. *Drug Deliv.* **2007**, *14*, 25–31. [CrossRef]
375. Gynther, M.; Laine, K.; Ropponen, J.; Leppanen, J.; Mannila, A.; Nevalainen, T.; Savolainen, J.; Jarvinen, T.; Rautio, J. Large neutral amino acid transporter enables brain drug delivery via prodrugs. *J. Med. Chem.* **2008**, *51*, 932–936. [CrossRef]
376. Karkkainen, J.; Gynther, M.; Kokkola, T.; Petsalo, A.; Auriola, S.; Lahtela-Kakkonen, M.; Laine, K.; Rautio, J.; Huttunen, K.M. Structural properties for selective and efficient l-type amino acid transporter 1 (LAT1) mediated cellular uptake. *Int. J. Pharm.* **2018**, *544*, 91–99. [CrossRef]
377. Huttunen, J.; Peltokangas, S.; Gynther, M.; Natunen, T.; Hiltunen, M.; Auriola, S.; Ruponen, M.; Vellonen, K.S.; Huttunen, K.M. L-Type Amino Acid Transporter 1 (LAT1/Lat1)-Utilizing Prodrugs Can Improve the Delivery of Drugs into Neurons, Astrocytes and Microglia. *Sci. Rep.* **2019**, *9*, 12860. [CrossRef]
378. Huttunen, J.; Agami, M.; Tampio, J.; Montaser, A.B.; Huttunen, K.M. Comparison of Experimental Strategies to Study l-Type Amino Acid Transporter 1 (LAT1) Utilization by Ligands. *Molecules* **2021**, *27*, 37. [CrossRef]
379. Albritton, L.M.; Bowcock, A.M.; Eddy, R.L.; Morton, C.C.; Tseng, L.; Farrer, L.A.; Cavalli-Sforza, L.L.; Shows, T.B.; Cunningham, J.M. The human cationic amino acid transporter (ATRC1): Physical and genetic mapping to 13q12-q14. *Genomics* **1992**, *12*, 430–434. [CrossRef]
380. Stoll, J.; Wadhvani, K.C.; Smith, Q.R. Identification of the cationic amino acid transporter (System y<sup>+</sup>) of the rat blood-brain barrier. *J. Neurochem.* **1993**, *60*, 1956–1959. [CrossRef]
381. Closs, E.I.; Boissel, J.P.; Habermeier, A.; Rotmann, A. Structure and function of cationic amino acid transporters (CATs). *J. Membr. Biol.* **2006**, *213*, 67–77. [CrossRef] [PubMed]
382. Gynther, M.; Jalkanen, A.; Lehtonen, M.; Forsberg, M.; Laine, K.; Ropponen, J.; Leppanen, J.; Knuuti, J.; Rautio, J. Brain uptake of ketoprofen-lysine prodrug in rats. *Int. J. Pharm.* **2010**, *399*, 121–128. [CrossRef] [PubMed]
383. Cremer, J.E.; Cunningham, V.J.; Pardridge, W.M.; Braun, L.D.; Oldendorf, W.H. Kinetics of blood-brain barrier transport of pyruvate, lactate and glucose in suckling, weanling and adult rats. *J. Neurochem.* **1979**, *33*, 439–445. [CrossRef] [PubMed]
384. Garcia, C.K.; Goldstein, J.L.; Pathak, R.K.; Anderson, R.G.; Brown, M.S. Molecular characterization of a membrane transporter for lactate, pyruvate, and other monocarboxylates: Implications for the Cori cycle. *Cell* **1994**, *76*, 865–873. [CrossRef]
385. Takanaga, H.; Tamai, I.; Inaba, S.; Sai, Y.; Higashida, H.; Yamamoto, H.; Tsuji, A. cDNA cloning and functional characterization of rat intestinal monocarboxylate transporter. *Biochem. Biophys. Res. Commun.* **1995**, *217*, 370–377. [CrossRef]
386. Gerhart, D.Z.; Enerson, B.E.; Zhdankina, O.Y.; Leino, R.L.; Drewes, L.R. Expression of monocarboxylate transporter MCT1 by brain endothelium and glia in adult and suckling rats. *Am. J. Physiol.* **1997**, *273*, E207–E213. [CrossRef]
387. Poole, R.C.; Halestrap, A.P. Interaction of the erythrocyte lactate transporter (monocarboxylate transporter 1) with an integral 70-kDa membrane glycoprotein of the immunoglobulin superfamily. *J. Biol. Chem.* **1997**, *272*, 14624–14628. [CrossRef]
388. Wang, N.; Jiang, X.; Zhang, S.; Zhu, A.; Yuan, Y.; Xu, H.; Lei, J.; Yan, C. Structural basis of human monocarboxylate transporter 1 inhibition by anti-cancer drug candidates. *Cell* **2021**, *184*, 370–383.e13. [CrossRef]
389. Sun, Y.; Zhao, D.; Wang, G.; Jiang, Q.; Guo, M.; Kan, Q.; He, Z.; Sun, J. A novel oral prodrug-targeting transporter MCT 1: 5-fluorouracil-dicarboxylate monoester conjugates. *Asian J. Pharm. Sci.* **2019**, *14*, 631–639. [CrossRef]
390. Cornford, E.M.; Oldendorf, W.H. Independent blood-brain barrier transport systems for nucleic acid precursors. *Biochim. Biophys. Acta* **1975**, *394*, 211–219. [CrossRef]
391. Pardridge, W.M.; Yoshikawa, T.; Kang, Y.S.; Miller, L.P. Blood-brain barrier transport and brain metabolism of adenosine and adenosine analogs. *J. Pharmacol. Exp. Ther.* **1994**, *268*, 14–18.
392. Young, J.D. The SLC28 (CNT) and SLC29 (ENT) nucleoside transporter families: A 30-year collaborative odyssey. *Biochem. Soc. Trans.* **2016**, *44*, 869–876. [CrossRef]
393. Morris, M.E.; Rodriguez-Cruz, V.; Felmlee, M.A. SLC and ABC Transporters: Expression, Localization, and Species Differences at the Blood-Brain and the Blood-Cerebrospinal Fluid Barriers. *AAPS J.* **2017**, *19*, 1317–1331. [CrossRef]
394. Ohtsuki, S.; Ikeda, C.; Uchida, Y.; Sakamoto, Y.; Miller, F.; Glacial, F.; Decleves, X.; Scherrmann, J.M.; Couraud, P.O.; Kubo, Y.; et al. Quantitative targeted absolute proteomic analysis of transporters, receptors and junction proteins for validation of human cerebral microvascular endothelial cell line hCMEC/D3 as a human blood-brain barrier model. *Mol. Pharm.* **2013**, *10*, 289–296. [CrossRef]
395. Li, J.Y.; Boado, R.J.; Pardridge, W.M. Cloned blood-brain barrier adenosine transporter is identical to the rat concentrative Na<sup>+</sup> nucleoside cotransporter CNT2. *J. Cereb. Blood Flow Metab.* **2001**, *21*, 929–936. [CrossRef]
396. Zhou, Y.; Liao, L.; Wang, C.; Li, J.; Chi, P.; Xiao, Q.; Liu, Q.; Guo, L.; Sun, L.; Deng, D. Cryo-EM structure of the human concentrative nucleoside transporter CNT3. *PLoS Biol.* **2020**, *18*, e3000790. [CrossRef]
397. Li, J.Y.; Boado, R.J.; Pardridge, W.M. Differential kinetics of transport of 2',3'-dideoxyinosine and adenosine via concentrative Na<sup>+</sup> nucleoside transporter CNT2 cloned from rat blood-brain barrier. *J. Pharmacol. Exp. Ther.* **2001**, *299*, 735–740.
398. Hermann, R.; Krajcsi, P.; Fluck, M.; Seithel-Keuth, A.; Bytyqi, A.; Galazka, A.; Munafo, A. Cladribine as a Potential Object of Nucleoside Transporter-Based Drug Interactions. *Clin. Pharmacokinet.* **2022**, *61*, 167–187. [CrossRef]

399. Boarini, D.J.; Kassell, N.F.; Sprowell, J.A.; Olin, J. Intravertebral artery adenosine fails to alter cerebral blood flow in the dog. *Stroke* **1984**, *15*, 1057–1060. [CrossRef]
400. Cornford, E.M.; Braun, L.D.; Oldendorf, W.H. Carrier mediated blood-brain barrier transport of choline and certain choline analogs. *J. Neurochem.* **1978**, *30*, 299–308. [CrossRef]
401. Allen, D.D.; Smith, Q.R. Characterization of the blood-brain barrier choline transporter using the in situ rat brain perfusion technique. *J. Neurochem.* **2001**, *76*, 1032–1041. [CrossRef]
402. Allen, D.D.; Lockman, P.R.; Roder, K.E.; Dwoskin, L.P.; Crooks, P.A. Active Transport of High-Affinity Choline and Nicotine Analogs into the Central Nervous System by the Blood-Brain Barrier Choline Transporter. *J. Pharmacol. Exp. Ther.* **2002**, *304*, 1268–1274. [CrossRef]
403. Allen, D.D.; Lockman, P.R. The blood-brain barrier choline transporter as a brain drug delivery vector. *Life Sci.* **2003**, *73*, 1609–1615. [CrossRef]
404. Geldenhuys, W.J.; Lockman, P.R.; McAfee, J.H.; Fitzpatrick, K.T.; Van der Schyf, C.J.; Allen, D.D. Molecular modeling studies on the active binding site of the blood-brain barrier choline transporter. *Bioorg. Med. Chem. Lett.* **2004**, *14*, 3085–3092. [CrossRef]
405. Geldenhuys, W.J.; Manda, V.K.; Mittapalli, R.K.; Van der Schyf, C.J.; Crooks, P.A.; Dwoskin, L.P.; Allen, D.D.; Lockman, P.R. Predictive screening model for potential vector-mediated transport of cationic substrates at the blood-brain barrier choline transporter. *Bioorg. Med. Chem. Lett.* **2010**, *20*, 870–877. [CrossRef]
406. Shityakov, S.; Forster, C. In silico predictive model to determine vector-mediated transport properties for the blood-brain barrier choline transporter. *Adv. Appl. Bioinform. Chem.* **2014**, *7*, 23–36. [CrossRef]
407. Inazu, M. Functional Expression of Choline Transporters in the Blood-Brain Barrier. *Nutrients* **2019**, *11*, 2265. [CrossRef]
408. Iwao, B.; Yara, M.; Hara, N.; Kawai, Y.; Yamanaka, T.; Nishihara, H.; Inoue, T.; Inazu, M. Functional expression of choline transporter like-protein 1 (CTL1) and CTL2 in human brain microvascular endothelial cells. *Neurochem. Int.* **2016**, *93*, 40–50. [CrossRef]
409. Uchida, Y.; Zhang, Z.; Tachikawa, M.; Terasaki, T. Quantitative targeted absolute proteomics of rat blood-cerebrospinal fluid barrier transporters: Comparison with a human specimen. *J. Neurochem.* **2015**, *134*, 1104–1115. [CrossRef]
410. Spector, R. Thiamine transport in the central nervous system. *Am. J. Physiol.* **1976**, *230*, 1101–1107. [CrossRef]
411. Mir, A.; Almudhry, M.; Alghamdi, F.; Albaradie, R.; Ibrahim, M.; Aldurayhim, F.; Alhedaihy, A.; Alamr, M.; Bawazir, M.; Mohammad, S.; et al. SLC gene mutations and pediatric neurological disorders: Diverse clinical phenotypes in a Saudi Arabian population. *Hum. Genet.* **2022**, *141*, 81–99. [CrossRef] [PubMed]
412. Dhir, S.; Tarasenko, M.; Napoli, E.; Giulivi, C. Neurological, Psychiatric, and Biochemical Aspects of Thiamine Deficiency in Children and Adults. *Front. Psychiatry* **2019**, *10*, 207. [CrossRef] [PubMed]
413. Spector, R. Riboflavin homeostasis in the central nervous system. *J. Neurochem.* **1980**, *35*, 202–209. [CrossRef] [PubMed]
414. Patel, M.; Vadlapatla, R.K.; Pal, D.; Mitra, A.K. Molecular and functional characterization of riboflavin specific transport system in rat brain capillary endothelial cells. *Brain Res.* **2012**, *1468*, 1–10. [CrossRef] [PubMed]
415. Jaeger, B.; Bosch, A.M. Clinical presentation and outcome of riboflavin transporter deficiency: Mini review after five years of experience. *J. Inher. Metab. Dis.* **2016**, *39*, 559–564. [CrossRef] [PubMed]
416. Tamai, I.; Takanaga, H.; Maeda, H.; Sai, Y.; Ogiwara, T.; Higashida, H.; Tsuji, A. Participation of a proton-cotransporter, MCT1, in the intestinal transport of monocarboxylic acids. *Biochem. Biophys. Res. Commun.* **1995**, *214*, 482–489. [CrossRef] [PubMed]
417. Spector, R. Niacinamide transport through the blood-brain barrier. *Neurochem. Res.* **1987**, *12*, 27–31. [CrossRef]
418. Spector, R.; Sivesind, C.; Kinzenbaw, D. Pantothenic acid transport through the blood-brain barrier. *J. Neurochem.* **1986**, *47*, 966–971. [CrossRef]
419. Park, S.; Sinko, P.J. The blood-brain barrier sodium-dependent multivitamin transporter: A molecular functional in vitro-in situ correlation. *Drug Metab. Dispos.* **2005**, *33*, 1547–1554. [CrossRef]
420. Uchida, Y.; Ito, K.; Ohtsuki, S.; Kubo, Y.; Suzuki, T.; Terasaki, T. Major involvement of Na<sup>+</sup>-dependent multivitamin transporter (SLC5A6/SMVT) in uptake of biotin and pantothenic acid by human brain capillary endothelial cells. *J. Neurochem.* **2015**, *134*, 97–112. [CrossRef]
421. Spector, R.; Mock, D. Biotin transport through the blood-brain barrier. *J. Neurochem.* **1987**, *48*, 400–404. [CrossRef] [PubMed]
422. Kang, Y.S.; Saito, Y.; Pardridge, W.M. Pharmacokinetics of [<sup>3</sup>H]biotin bound to different avidin analogues. *J. Drug Target.* **1995**, *3*, 159–165. [CrossRef] [PubMed]
423. Azhar, A.; Booker, G.W.; Polyak, S.W. Mechanisms of biotin transport. *Biochem. Anal. Biochem.* **2015**, *4*, 1–8. [CrossRef]
424. Spector, R. Vitamin B6 transport in the central nervous system: In vivo studies. *J. Neurochem.* **1978**, *30*, 881–887. [CrossRef] [PubMed]
425. Yamashiro, T.; Yasujima, T.; Said, H.M.; Yuasa, H. pH-dependent pyridoxine transport by SLC19A2 and SLC19A3: Implications for absorption in acidic microclimates. *J. Biol. Chem.* **2020**, *295*, 16998–17008. [CrossRef] [PubMed]
426. Alam, C.; Aufreiter, S.; Georgiou, C.J.; Hoque, M.T.; Finnell, R.H.; O'Connor, D.L.; Goldman, I.D.; Bendayan, R. Upregulation of reduced folate carrier by vitamin D enhances brain folate uptake in mice lacking folate receptor alpha. *Proc. Natl. Acad. Sci. USA* **2019**, *116*, 17531–17540. [CrossRef]
427. Wu, D.; Pardridge, W.M. Blood-brain barrier transport of reduced folic acid. *Pharm. Res.* **1999**, *16*, 415–419. [CrossRef]
428. Alam, A.; Woo, J.S.; Schmitz, J.; Prinz, B.; Root, K.; Chen, F.; Bloch, J.S.; Zenobi, R.; Locher, K.P. Structural basis of transcobalamin recognition by human CD320 receptor. *Nat. Commun.* **2016**, *7*, 12100. [CrossRef]

429. Lai, S.C.; Nakayama, Y.; Sequeira, J.M.; Wlodarczyk, B.J.; Cabrera, R.M.; Finnell, R.H.; Bottiglieri, T.; Quadros, E.V. The transcobalamin receptor knockout mouse: A model for vitamin B12 deficiency in the central nervous system. *FASEB J.* **2013**, *27*, 2468–2475. [CrossRef]
430. Zuchero, Y.J.; Chen, X.; Bien-Ly, N.; Bumbaca, D.; Tong, R.K.; Gao, X.; Zhang, S.; Hoyte, K.; Luk, W.; Huntley, M.A.; et al. Discovery of Novel Blood-Brain Barrier Targets to Enhance Brain Uptake of Therapeutic Antibodies. *Neuron* **2016**, *89*, 70–82. [CrossRef]
431. Henry, K.E.; Elfers, C.T.; Burke, R.M.; Chepurny, O.G.; Holz, G.G.; Blevins, J.E.; Roth, C.L.; Doyle, R.P. Vitamin B12 conjugation of peptide-YY(3-36) decreases food intake compared to native peptide-YY(3-36) upon subcutaneous administration in male rats. *Endocrinology* **2015**, *156*, 1739–1749. [CrossRef] [PubMed]
432. Xiao, D.; Meng, F.H.; Dai, W.; Yong, Z.; Liu, J.Q.; Zhou, X.B.; Li, S. Design, Synthesis and Biological Evaluation of Brain-Targeted Thiamine Disulfide Prodrugs of Ampakine Compound LCX001. *Molecules* **2016**, *21*, 488. [CrossRef]
433. Pardridge, W.M. Carrier-mediated transport of thyroid hormones through the rat blood-brain barrier: Primary role of albumin-bound hormone. *Endocrinology* **1979**, *105*, 605–612. [CrossRef] [PubMed]
434. Friesema, E.C.; Ganguly, S.; Abdalla, A.; Manning Fox, J.E.; Halestrap, A.P.; Visser, T.J. Identification of monocarboxylate transporter 8 as a specific thyroid hormone transporter. *J. Biol. Chem.* **2003**, *278*, 40128–40135. [CrossRef] [PubMed]
435. Ito, K.; Uchida, Y.; Ohtsuki, S.; Aizawa, S.; Kawakami, H.; Katsukura, Y.; Kamiie, J.; Terasaki, T. Quantitative membrane protein expression at the blood-brain barrier of adult and younger cynomolgus monkeys. *J. Pharm. Sci.* **2011**, *100*, 3939–3950. [CrossRef]
436. Roberts, L.M.; Woodford, K.; Zhou, M.; Black, D.S.; Haggerty, J.E.; Tate, E.H.; Grindstaff, K.K.; Mengesha, W.; Raman, C.; Zerangue, N. Expression of the thyroid hormone transporters monocarboxylate transporter-8 (SLC16A2) and organic ion transporter-14 (SLCO1C1) at the blood-brain barrier. *Endocrinology* **2008**, *149*, 6251–6261. [CrossRef]
437. Morte, B.; Gil-Ibanez, P.; Heuer, H.; Bernal, J. Brain Gene Expression in Systemic Hypothyroidism and Mouse Models of MCT8 Deficiency: The Mct8-Oatp1c1-Dio2 Triad. *Thyroid* **2021**, *31*, 985–993. [CrossRef]
438. Li, J.Y.; Boado, R.J.; Pardridge, W.M. Blood-brain barrier genomics. *J. Cereb. Blood Flow Metab.* **2001**, *21*, 61–68. [CrossRef]
439. Tohyama, K.; Kusuhara, H.; Sugiyama, Y. Involvement of multispecific organic anion transporter, Oatp14 (Slc21a14), in the transport of thyroxine across the blood-brain barrier. *Endocrinology* **2004**, *145*, 4384–4391. [CrossRef]
440. Chu, C.; Li, J.Y.; Boado, R.J.; Pardridge, W.M. Blood-brain barrier genomics and cloning of a novel organic anion transporter. *J. Cereb. Blood Flow Metab.* **2008**, *28*, 291–301. [CrossRef]
441. Li, J.Y.; Boado, R.J.; Pardridge, W.M. Rat blood-brain barrier genomics. II. *J. Cereb. Blood Flow Metab.* **2002**, *22*, 1319–1326. [CrossRef]
442. Shusta, E.V.; Boado, R.J.; Mathern, G.W.; Pardridge, W.M. Vascular genomics of the human brain. *J. Cereb. Blood Flow Metab.* **2002**, *22*, 245–252. [CrossRef]
443. Kou, L.; Sun, R.; Ganapathy, V.; Yao, Q.; Chen, R. Recent advances in drug delivery via the organic cation/carnitine transporter 2 (OCTN2/SLC22A5). *Expert Opin. Ther. Targets* **2018**, *22*, 715–726. [CrossRef]
444. Kido, Y.; Tamai, I.; Ohnari, A.; Sai, Y.; Kagami, T.; Nezu, J.; Nikaido, H.; Hashimoto, N.; Asano, M.; Tsuji, A. Functional relevance of carnitine transporter OCTN2 to brain distribution of L-carnitine and acetyl-L-carnitine across the blood-brain barrier. *J. Neurochem.* **2001**, *79*, 959–969. [CrossRef]
445. Okura, T.; Kato, S.; Deguchi, Y. Functional expression of organic cation/carnitine transporter 2 (OCTN2/SLC22A5) in human brain capillary endothelial cell line hCMEC/D3, a human blood-brain barrier model. *Drug Metab. Pharmacokinet.* **2014**, *29*, 69–74. [CrossRef]
446. Nigam, S.K. The SLC22 Transporter Family: A Paradigm for the Impact of Drug Transporters on Metabolic Pathways, Signaling, and Disease. *Annu. Rev. Pharmacol. Toxicol.* **2018**, *58*, 663–687. [CrossRef]
447. Chen, E.C.; Matsson, P.; Azimi, M.; Zhou, X.; Handin, N.; Yee, S.W.; Artursson, P.; Giacomini, K.M. High Throughput Screening of a Prescription Drug Library for Inhibitors of Organic Cation Transporter 3, OCT3. *Pharm. Res.* **2022**, 1–15. [CrossRef]
448. Shang, T.; Uihlein, A.V.; Van Asten, J.; Kalyanaraman, B.; Hillard, C.J. 1-Methyl-4-phenylpyridinium accumulates in cerebellar granule neurons via organic cation transporter 3. *J. Neurochem.* **2003**, *85*, 358–367. [CrossRef]
449. Cornford, E.M.; Diep, C.P.; Pardridge, W.M. Blood-brain barrier transport of valproic acid. *J. Neurochem.* **1985**, *44*, 1541–1550. [CrossRef]
450. Kakee, A.; Terasaki, T.; Sugiyama, Y. Brain efflux index as a novel method of analyzing efflux transport at the blood-brain barrier. *J. Pharmacol. Exp. Ther.* **1996**, *277*, 1550–1559.
451. Zhang, Y.; Pardridge, W.M. Mediated efflux of IgG molecules from brain to blood across the blood-brain barrier. *J. Neuroimmunol.* **2001**, *114*, 168–172. [CrossRef]
452. Zhang, Y.; Pardridge, W.M. Rapid transferrin efflux from brain to blood across the blood-brain barrier. *J. Neurochem.* **2001**, *76*, 1597–1600. [CrossRef]
453. Takasawa, K.; Terasaki, T.; Suzuki, H.; Sugiyama, Y. In vivo evidence for carrier-mediated efflux transport of 3'-azido-3'-deoxythymidine and 2',3'-dideoxyinosine across the blood-brain barrier via a probenecid-sensitive transport system. *J. Pharmacol. Exp. Ther.* **1997**, *281*, 369–375.
454. Kitazawa, T.; Terasaki, T.; Suzuki, H.; Kakee, A.; Sugiyama, Y. Efflux of taurocholic acid across the blood-brain barrier: Interaction with cyclic peptides. *J. Pharmacol. Exp. Ther.* **1998**, *286*, 890–895.

455. Oldendorf, W.H.; Szabo, J. Amino acid assignment to one of three blood-brain barrier amino acid carriers. *Am. J. Physiol.* **1976**, *230*, 94–98. [CrossRef]
456. Hosoya, K.; Sugawara, M.; Asaba, H.; Terasaki, T. Blood-brain barrier produces significant efflux of L-aspartic acid but not D-aspartic acid: In vivo evidence using the brain efflux index method. *J. Neurochem.* **1999**, *73*, 1206–1211. [CrossRef]
457. Hosoya, K.; Asaba, H.; Terasaki, T. Brain-to-blood efflux transport of estrone-3-sulfate at the blood-brain barrier in rats. *Life Sci.* **2000**, *67*, 2699–2711. [CrossRef]
458. Pardridge, W.M.; Moeller, T.L.; Mietus, L.J.; Oldendorf, W.H. Blood-brain barrier transport and brain sequestration of steroid hormones. *Am. J. Physiol.* **1980**, *239*, E96–E102. [CrossRef]
459. Asaba, H.; Hosoya, K.; Takanaga, H.; Ohtsuki, S.; Tamura, E.; Takizawa, T.; Terasaki, T. Blood-brain barrier is involved in the efflux transport of a neuroactive steroid, dehydroepiandrosterone sulfate, via organic anion transporting polypeptide 2. *J. Neurochem.* **2000**, *75*, 1907–1916. [CrossRef]
460. Mori, S.; Takanaga, H.; Ohtsuki, S.; Deguchi, T.; Kang, Y.S.; Hosoya, K.; Terasaki, T. Rat organic anion transporter 3 (rOAT3) is responsible for brain-to-blood efflux of homovanillic acid at the abluminal membrane of brain capillary endothelial cells. *J. Cereb. Blood Flow Metab.* **2003**, *23*, 432–440. [CrossRef]
461. Jomura, R.; Akanuma, S.I.; Bauer, B.; Yoshida, Y.; Kubo, Y.; Hosoya, K.I. Participation of Monocarboxylate Transporter 8, But Not P-Glycoprotein, in Carrier-Mediated Cerebral Elimination of Phenytoin across the Blood-Brain Barrier. *Pharm. Res.* **2021**, *38*, 113–125. [CrossRef]
462. Potschka, H. Role of CNS efflux drug transporters in antiepileptic drug delivery: Overcoming CNS efflux drug transport. *Adv. Drug Deliv. Rev.* **2012**, *64*, 943–952. [CrossRef]
463. Pizzagalli, M.D.; Bensimon, A.; Superti-Furga, G. A guide to plasma membrane solute carrier proteins. *FEBS J.* **2021**, *288*, 2784–2835. [CrossRef]
464. Qiu, Y.; Li, H.; Xie, J.; Qiao, X.; Wu, J. Identification of ABCC5 Among ATP-Binding Cassette Transporter Family as a New Biomarker for Hepatocellular Carcinoma Based on Bioinformatics Analysis. *Int. J. Gen. Med.* **2021**, *14*, 7235–7246. [CrossRef]
465. Kerr, I.D.; Hutchison, E.; Gerard, L.; Aleidi, S.M.; Gelissen, I.C. Mammalian ABCG-transporters, sterols and lipids: To bind perchance to transport? *Biochim. Biophys. Acta Mol. Cell Biol. Lipids* **2021**, *1866*, 158860. [CrossRef]
466. Chen, J.; Zhang, X.; Kusumo, H.; Costa, L.G.; Guizzetti, M. Cholesterol efflux is differentially regulated in neurons and astrocytes: Implications for brain cholesterol homeostasis. *Biochim. Biophys. Acta* **2013**, *1831*, 263–275. [CrossRef]
467. Saint-Pol, J.; Vandenhoute, E.; Boucau, M.C.; Candela, P.; Dehouck, L.; Cecchelli, R.; Dehouck, M.P.; Fenart, L.; Gosselet, F. Brain pericytes ABCA1 expression mediates cholesterol efflux but not cellular amyloid-beta peptide accumulation. *J. Alzheimer's Dis.* **2012**, *30*, 489–503. [CrossRef]
468. Kubo, Y.; Ohtsuki, S.; Uchida, Y.; Terasaki, T. Quantitative Determination of Luminal and Abluminal Membrane Distributions of Transporters in Porcine Brain Capillaries by Plasma Membrane Fractionation and Quantitative Targeted Proteomics. *J. Pharm. Sci.* **2015**, *104*, 3060–3068. [CrossRef]
469. Kober, A.C.; Manavalan, A.P.C.; Tam-Amersdorfer, C.; Holmer, A.; Saeed, A.; Fanaee-Danesh, E.; Zandl, M.; Albrecher, N.M.; Bjorkhem, I.; Kostner, G.M.; et al. Implications of cerebrovascular ATP-binding cassette transporter G1 (ABCG1) and apolipoprotein M in cholesterol transport at the blood-brain barrier. *Biochim. Biophys. Acta Mol. Cell Biol. Lipids* **2017**, *1862*, 573–588. [CrossRef]
470. Do, T.M.; Ouellet, M.; Calon, F.; Chimini, G.; Chacun, H.; Farinotti, R.; Bourasset, F. Direct evidence of abca1-mediated efflux of cholesterol at the mouse blood-brain barrier. *Mol. Cell Biochem.* **2011**, *357*, 397–404. [CrossRef]
471. Pardridge, W.M.; Mietus, L.J. Palmitate and cholesterol transport through the blood-brain barrier. *J. Neurochem.* **1980**, *34*, 463–466. [CrossRef] [PubMed]
472. Schinkel, A.H.; Smit, J.J.; van Tellingen, O.; Beijnen, J.H.; Wagenaar, E.; van Deemter, L.; Mol, C.A.; van der Valk, M.A.; Robanus-Maandag, E.C.; te Riele, H.P.; et al. Disruption of the mouse *mdr1a* P-glycoprotein gene leads to a deficiency in the blood-brain barrier and to increased sensitivity to drugs. *Cell* **1994**, *77*, 491–502. [CrossRef]
473. Kusuhara, H.; Suzuki, H.; Terasaki, T.; Kakee, A.; Lemaire, M.; Sugiyama, Y. P-Glycoprotein mediates the efflux of quinidine across the blood-brain barrier. *J. Pharmacol. Exp. Ther.* **1997**, *283*, 574–580. [PubMed]
474. Bart, J.; Willemsen, A.T.; Groen, H.J.; van der Graaf, W.T.; Wegman, T.D.; Vaalburg, W.; de Vries, E.G.; Hendrikse, N.H. Quantitative assessment of P-glycoprotein function in the rat blood-brain barrier by distribution volume of [<sup>11</sup>C]verapamil measured with PET. *Neuroimage* **2003**, *20*, 1775–1782. [CrossRef]
475. Cefalu, W.T.; Pardridge, W.M. Restrictive transport of a lipid-soluble peptide (cyclosporin) through the blood-brain barrier. *J. Neurochem.* **1985**, *45*, 1954–1956. [CrossRef]
476. Doran, A.; Obach, R.S.; Smith, B.J.; Hosea, N.A.; Becker, S.; Callegari, E.; Chen, C.; Chen, X.; Choo, E.; Cianfrogna, J.; et al. The impact of P-glycoprotein on the disposition of drugs targeted for indications of the central nervous system: Evaluation using the MDR1A/1B knockout mouse model. *Drug Metab. Dispos.* **2005**, *33*, 165–174. [CrossRef]
477. Kaddoumi, A.; Choi, S.U.; Kinman, L.; Whittington, D.; Tsai, C.C.; Ho, R.J.; Anderson, B.D.; Unadkat, J.D. Inhibition of P-glycoprotein activity at the primate blood-brain barrier increases the distribution of nelfinavir into the brain but not into the cerebrospinal fluid. *Drug Metab. Dispos.* **2007**, *35*, 1459–1462. [CrossRef]
478. Mercier, C.; Masseguin, C.; Roux, F.; Gabrion, J.; Scherrmann, J.M. Expression of P-glycoprotein (ABCB1) and Mrp1 (ABCC1) in adult rat brain: Focus on astrocytes. *Brain Res.* **2004**, *1021*, 32–40. [CrossRef]

479. Matsumoto, K.; Chiba, Y.; Fujihara, R.; Kubo, H.; Sakamoto, H.; Ueno, M. Immunohistochemical analysis of transporters related to clearance of amyloid-beta peptides through blood-cerebrospinal fluid barrier in human brain. *Histochem. Cell Biol.* **2015**, *144*, 597–611. [CrossRef]
480. Braun, C.; Sakamoto, A.; Fuchs, H.; Ishiguro, N.; Suzuki, S.; Cui, Y.; Klinder, K.; Watanabe, M.; Terasaki, T.; Sauer, A. Quantification of Transporter and Receptor Proteins in Dog Brain Capillaries and Choroid Plexus: Relevance for the Distribution in Brain and CSF of Selected BCRP and P-gp Substrates. *Mol. Pharm.* **2017**, *14*, 3436–3447. [CrossRef]
481. Golden, P.L.; Pardridge, W.M. P-Glycoprotein on astrocyte foot processes of unfixed isolated human brain capillaries. *Brain Res.* **1999**, *819*, 143–146. [CrossRef]
482. Schlachetzki, F.; Pardridge, W.M. P-glycoprotein and caveolin-1alpha in endothelium and astrocytes of primate brain. *Neuroreport* **2003**, *14*, 2041–2046. [CrossRef]
483. Warren, M.S.; Zerangue, N.; Woodford, K.; Roberts, L.M.; Tate, E.H.; Feng, B.; Li, C.; Feuerstein, T.J.; Gibbs, J.; Smith, B.; et al. Comparative gene expression profiles of ABC transporters in brain microvessel endothelial cells and brain in five species including human. *Pharmacol. Res.* **2009**, *59*, 404–413. [CrossRef]
484. Miller, D.S. Regulation of ABC transporters blood-brain barrier: The good, the bad, and the ugly. *Adv. Cancer Res.* **2015**, *125*, 43–70. [CrossRef]
485. Cooray, H.C.; Blackmore, C.G.; Maskell, L.; Barrand, M.A. Localisation of breast cancer resistance protein in microvessel endothelium of human brain. *Neuroreport* **2002**, *13*, 2059–2063. [CrossRef]
486. Hoshi, Y.; Uchida, Y.; Tachikawa, M.; Inoue, T.; Ohtsuki, S.; Terasaki, T. Quantitative atlas of blood-brain barrier transporters, receptors, and tight junction proteins in rats and common marmoset. *J. Pharm. Sci.* **2013**, *102*, 3343–3355. [CrossRef]
487. Geyer, J.; Gavrilova, O.; Petzinger, E. Brain penetration of ivermectin and selamectin in *mdr1a,b* P-glycoprotein- and *bcrp*-deficient knockout mice. *J. Vet. Pharmacol. Ther.* **2009**, *32*, 87–96. [CrossRef]
488. Dalangin, R.; Kim, A.; Campbell, R.E. The Role of Amino Acids in Neurotransmission and Fluorescent Tools for Their Detection. *Int. J. Mol. Sci.* **2020**, *21*, 6197. [CrossRef]
489. Drewes, L.R.; Conway, W.P.; Gilboe, D.D. Net amino acid transport between plasma and erythrocytes and perfused dog brain. *Am. J. Physiol.* **1977**, *233*, E320–E325. [CrossRef]
490. Pardridge, W.M. Brain metabolism: A perspective from the blood-brain barrier. *Physiol. Rev.* **1983**, *63*, 1481–1535. [CrossRef]
491. Helms, H.C.C.; Nielsen, C.U.; Waagepetersen, H.S.; Brodin, B. Glutamate Transporters in the Blood-Brain Barrier. *Adv. Neurobiol.* **2017**, *16*, 297–314. [CrossRef]
492. Hawkins, R.A.; Vina, J.R. How Glutamate Is Managed by the Blood-Brain Barrier. *Biology* **2016**, *5*, 37. [CrossRef]
493. Christensen, H.N. Distinguishing amino acid transport systems of a given cell or tissue. *Methods Enzymol.* **1989**, *173*, 576–616. [CrossRef]
494. Sugawara, M.; Nakanishi, T.; Fei, Y.J.; Huang, W.; Ganapathy, M.E.; Leibach, F.H.; Ganapathy, V. Cloning of an amino acid transporter with functional characteristics and tissue expression pattern identical to that of system A. *J. Biol. Chem.* **2000**, *275*, 16473–16477. [CrossRef]
495. Takanaga, H.; Tokuda, N.; Ohtsuki, S.; Hosoya, K.; Terasaki, T. ATA2 is predominantly expressed as system A at the blood-brain barrier and acts as brain-to-blood efflux transport for L-proline. *Mol. Pharmacol.* **2002**, *61*, 1289–1296. [CrossRef]
496. Thompson, B.J.; Sanchez-Covarrubias, L.; Slosky, L.M.; Zhang, Y.; Laracuenta, M.L.; Ronaldson, P.T. Hypoxia/reoxygenation stress signals an increase in organic anion transporting polypeptide 1a4 (*Oatp1a4*) at the blood-brain barrier: Relevance to CNS drug delivery. *J. Cereb. Blood Flow Metab.* **2014**, *34*, 699–707. [CrossRef]
497. Akanuma, S.; Hirose, S.; Tachikawa, M.; Hosoya, K. Localization of organic anion transporting polypeptide (*Oatp*) 1a4 and *Oatp1c1* at the rat blood-retinal barrier. *Fluids Barriers CNS* **2013**, *10*, 29. [CrossRef]
498. Yaguchi, Y.; Tachikawa, M.; Zhang, Z.; Terasaki, T. Organic Anion-Transporting Polypeptide 1a4 (*Oatp1a4*/*Slco1a4*) at the Blood-Arachnoid Barrier is the Major Pathway of Sulforhodamine-101 Clearance from Cerebrospinal Fluid of Rats. *Mol. Pharm.* **2019**, *16*, 2021–2027. [CrossRef]
499. Abdullahi, W.; Davis, T.P.; Ronaldson, P.T. Functional Expression of P-glycoprotein and Organic Anion Transporting Polypeptides at the Blood-Brain Barrier: Understanding Transport Mechanisms for Improved CNS Drug Delivery? *AAPS J.* **2017**, *19*, 931–939. [CrossRef]
500. Uchida, Y.; Goto, R.; Takeuchi, H.; Luczak, M.; Usui, T.; Tachikawa, M.; Terasaki, T. Abundant Expression of OCT2, MATE1, OAT1, OAT3, PEPT2, BCRP, MDR1, and xCT Transporters in Blood-Arachnoid Barrier of Pig and Polarized Localizations at CSF- and Blood-Facing Plasma Membranes. *Drug Metab. Dispos.* **2020**, *48*, 135–145. [CrossRef]
501. Ferrara, A.M.; Liao, X.H.; Gil-Ibanez, P.; Marcinkowski, T.; Bernal, J.; Weiss, R.E.; Dumitrescu, A.M.; Refetoff, S. Changes in thyroid status during perinatal development of MCT8-deficient male mice. *Endocrinology* **2013**, *154*, 2533–2541. [CrossRef] [PubMed]
502. Shen, W.C.; Ryser, H.J. Conjugation of poly-L-lysine to albumin and horseradish peroxidase: A novel method of enhancing the cellular uptake of proteins. *Proc. Natl. Acad. Sci. USA* **1978**, *75*, 1872–1876. [CrossRef] [PubMed]
503. Gauthier, V.J.; Mannik, M.; Striker, G.E. Effect of cationized antibodies in performed immune complexes on deposition and persistence in renal glomeruli. *J. Exp. Med.* **1982**, *156*, 766–777. [CrossRef] [PubMed]
504. Bergmann, P.; Kacenenbogen, R.; Vizet, A. Plasma clearance, tissue distribution and catabolism of cationized albumins with increasing isoelectric points in the rat. *Clin. Sci.* **1984**, *67*, 35–43. [CrossRef]

505. Pardridge, W.M.; Triguero, D.; Buciak, J.L. Beta-endorphin chimeric peptides: Transport through the blood-brain barrier in vivo and cleavage of disulfide linkage by brain. *Endocrinology* **1990**, *126*, 977–984. [CrossRef]
506. Triguero, D.; Buciak, J.; Pardridge, W.M. Capillary depletion method for quantification of blood-brain barrier transport of circulating peptides and plasma proteins. *J. Neurochem.* **1990**, *54*, 1882–1888. [CrossRef]
507. Pardridge, W.M.; Triguero, D.; Buciak, J.; Yang, J. Evaluation of cationized rat albumin as a potential blood-brain barrier drug transport vector. *J. Pharmacol. Exp. Ther.* **1990**, *255*, 893–899.
508. Triguero, D.; Buciak, J.B.; Yang, J.; Pardridge, W.M. Blood-brain barrier transport of cationized immunoglobulin G: Enhanced delivery compared to native protein. *Proc. Natl. Acad. Sci. USA* **1989**, *86*, 4761–4765. [CrossRef]
509. Pardridge, W.M.; Bickel, U.; Buciak, J.; Yang, J.; Diagne, A.; Aepinus, C. Cationization of a monoclonal antibody to the human immunodeficiency virus REV protein enhances cellular uptake but does not impair antigen binding of the antibody. *Immunol. Lett.* **1994**, *42*, 191–195. [CrossRef]
510. Voll, R.; Aepinus, C.; Krapf, F.; Herrmann, M.; Kalden, J.R.; Fleckenstein, B. Monoclonal antibodies directed against the rev protein of human immunodeficiency virus type 1. *Mol. Cell Probes* **1990**, *4*, 63–72. [CrossRef]
511. Stern, R.A.; Otvos, L., Jr.; Trojanowski, J.Q.; Lee, V.M. Monoclonal antibodies to a synthetic peptide homologous with the first 28 amino acids of Alzheimer's disease beta-protein recognize amyloid and diverse glial and neuronal cell types in the central nervous system. *Am. J. Pathol.* **1989**, *134*, 973–978.
512. Bickel, U.; Lee, V.M.; Trojanowski, J.Q.; Pardridge, W.M. Development and in vitro characterization of a cationized monoclonal antibody against beta A4 protein: A potential probe for Alzheimer's disease. *Bioconjug. Chem.* **1994**, *5*, 119–125. [CrossRef]
513. Vaisitti, T.; Deaglio, S.; Malavasi, F. Cationization of monoclonal antibodies: Another step towards the "magic bullet"? *J. Biol. Regul. Homeost. Agents* **2005**, *19*, 105–112.
514. Herve, F.; Ghinea, N.; Scherrmann, J.M. CNS delivery via adsorptive transcytosis. *AAPS J.* **2008**, *10*, 455–472. [CrossRef]
515. Vorbrodtt, A.W. Ultracytochemical characterization of anionic sites in the wall of brain capillaries. *J. Neurocytol.* **1989**, *18*, 359–368. [CrossRef]
516. Pardridge, W.M.; Buciak, J.L.; Kang, Y.S.; Boado, R.J. Protamine-mediated transport of albumin into brain and other organs of the rat. Binding and endocytosis of protamine-albumin complex by microvascular endothelium. *J. Clin. Investig.* **1993**, *92*, 2224–2229. [CrossRef]
517. Ryser, H.J. Uptake of protein by mammalian cells: An underdeveloped area. The penetration of foreign proteins into mammalian cells can be measured and their functions explored. *Science* **1968**, *159*, 390–396. [CrossRef]
518. Goryukhina, O.A.; Martyushin, S.V.; Pinaev, G.P. On the possible use of exogenous histones in cell technology. *Cell Biol. Int.* **2011**, *35*, 1189–1193. [CrossRef]
519. Schwarze, S.R.; Ho, A.; Vocero-Akbani, A.; Dowdy, S.F. In vivo protein transduction: Delivery of a biologically active protein into the mouse. *Science* **1999**, *285*, 1569–1572. [CrossRef]
520. Zhang, Y.; Pardridge, W.M. Delivery of beta-galactosidase to mouse brain via the blood-brain barrier transferrin receptor. *J. Pharmacol. Exp. Ther.* **2005**, *313*, 1075–1081. [CrossRef]
521. Orii, K.O.; Grubb, J.H.; Vogler, C.; Levy, B.; Tan, Y.; Markova, K.; Davidson, B.L.; Mao, Q.; Orii, T.; Kondo, N.; et al. Defining the pathway for Tat-mediated delivery of beta-glucuronidase in cultured cells and MPS VII mice. *Mol. Ther.* **2005**, *12*, 345–352. [CrossRef]
522. Bockenhoff, A.; Cramer, S.; Wolte, P.; Knieling, S.; Wohlenberg, C.; Gieselmann, V.; Galla, H.J.; Matzner, U. Comparison of five peptide vectors for improved brain delivery of the lysosomal enzyme arylsulfatase A. *J. Neurosci.* **2014**, *34*, 3122–3129. [CrossRef]
523. Sarko, D.; Beijer, B.; Garcia Boy, R.; Nothelfer, E.M.; Leotta, K.; Eisenhut, M.; Altmann, A.; Haberkorn, U.; Mier, W. The pharmacokinetics of cell-penetrating peptides. *Mol. Pharm.* **2010**, *7*, 2224–2231. [CrossRef]
524. Gallo, M.; Defaus, S.; Andreu, D. 1988–2018: Thirty years of drug smuggling at the nano scale. Challenges and opportunities of cell-penetrating peptides in biomedical research. *Arch. Biochem. Biophys.* **2019**, *661*, 74–86. [CrossRef]
525. Pardridge, W.M. Brain Delivery of Nanomedicines: Trojan Horse Liposomes for Plasmid DNA Gene Therapy of the Brain. *Front. Med. Technol.* **2020**, *2*, 602236. [CrossRef]
526. Adenot, M.; Merida, P.; Lahana, R. Applications of a blood-brain barrier technology platform to predict CNS penetration of various chemotherapeutic agents. 2. Cationic peptide vectors for brain delivery. *Chemotherapy* **2007**, *53*, 73–76. [CrossRef]
527. Rousselle, C.; Clair, P.; Lefauconnier, J.M.; Kaczorek, M.; Scherrmann, J.M.; Tamsamani, J. New advances in the transport of doxorubicin through the blood-brain barrier by a peptide vector-mediated strategy. *Mol. Pharmacol.* **2000**, *57*, 679–686. [CrossRef]
528. Rousselle, C.; Smirnova, M.; Clair, P.; Lefauconnier, J.M.; Chavanieu, A.; Calas, B.; Scherrmann, J.M.; Tamsamani, J. Enhanced delivery of doxorubicin into the brain via a peptide-vector-mediated strategy: Saturation kinetics and specificity. *J. Pharmacol. Exp. Ther.* **2001**, *296*, 124–131. [PubMed]
529. Bersani, M.; Rizzuti, M.; Pagliari, E.; Garbellini, M.; Saccomanno, D.; Moulton, H.M.; Bresolin, N.; Comi, G.P.; Corti, S.; Nizzardo, M. Cell-penetrating peptide-conjugated Morpholino rescues SMA in a symptomatic preclinical model. *Mol. Ther.* **2022**, *30*, 1288–1299. [CrossRef] [PubMed]
530. Kizil, C.; Iltzsche, A.; Thomas, A.K.; Bhattarai, P.; Zhang, Y.; Brand, M. Efficient Cargo Delivery into Adult Brain Tissue Using Short Cell-Penetrating Peptides. *PLoS ONE* **2015**, *10*, e0124073. [CrossRef] [PubMed]
531. Ryva, B.; Zhang, K.; Asthana, A.; Wong, D.; Vicioso, Y.; Parameswaran, R. Wheat Germ Agglutinin as a Potential Therapeutic Agent for Leukemia. *Front. Oncol.* **2019**, *9*, 100. [CrossRef]



532. Vorbrodt, A.W.; Dobrogowska, D.H.; Lossinsky, A.S.; Wisniewski, H.M. Ultrastructural localization of lectin receptors on the luminal and abluminal aspects of brain micro-blood vessels. *J. Histochem. Cytochem* **1986**, *34*, 251–261. [CrossRef]
533. Harper, C.G.; Gonatas, J.O.; Stieber, A.; Gonatas, N.K. In vivo uptake of wheat germ agglutinin-horseradish peroxidase conjugates into neuronal GERL and lysosomes. *Brain Res.* **1980**, *188*, 465–472. [CrossRef]
534. Kuo, Y.C.; Lin, C.Y.; Li, J.S.; Lou, Y.I. Wheat germ agglutinin-conjugated liposomes incorporated with cardiolipin to improve neuronal survival in Alzheimer's disease treatment. *Int. J. Nanomed.* **2017**, *12*, 1757–1774. [CrossRef]
535. Bies, C.; Lehr, C.M.; Woodley, J.F. Lectin-mediated drug targeting: History and applications. *Adv. Drug Deliv. Rev.* **2004**, *56*, 425–435. [CrossRef]
536. Worbs, S.; Skiba, M.; Soderstrom, M.; Rapinoja, M.L.; Zeleny, R.; Russmann, H.; Schimmel, H.; Vanninen, P.; Fredriksson, S.A.; Dorner, B.G. Characterization of Ricin and R. communis Agglutinin Reference Materials. *Toxins* **2015**, *7*, 4906–4934. [CrossRef]
537. Acosta, W.; Ayala, J.; Dolan, M.C.; Cramer, C.L. RTB Lectin: A novel receptor-independent delivery system for lysosomal enzyme replacement therapies. *Sci. Rep.* **2015**, *5*, 14144. [CrossRef]
538. Condori, J.; Acosta, W.; Ayala, J.; Katta, V.; Flory, A.; Martin, R.; Radin, J.; Cramer, C.L.; Radin, D.N. Enzyme replacement for GM1-gangliosidosis: Uptake, lysosomal activation, and cellular disease correction using a novel beta-galactosidase:RTB lectin fusion. *Mol. Genet. Metab.* **2016**, *117*, 199–209. [CrossRef]
539. Ou, L.; Przybilla, M.J.; Koniar, B.; Whitley, C.B. RTB lectin-mediated delivery of lysosomal alpha-l-iduronidase mitigates disease manifestations systemically including the central nervous system. *Mol. Genet. Metab.* **2018**, *123*, 105–111. [CrossRef]
540. Vorbrodt, A.W.; Dobrogowska, D.H.; Ueno, M.; Lossinsky, A.S. Immunocytochemical studies of protamine-induced blood-brain barrier opening to endogenous albumin. *Acta Neuropathol.* **1995**, *89*, 491–499. [CrossRef]
541. Meng, Y.; Wiseman, J.A.; Nemtsova, Y.; Moore, D.F.; Guevarra, J.; Reuhl, K.; Banks, W.A.; Daneman, R.; Sleat, D.E.; Lobel, P. A Basic ApoE-Based Peptide Mediator to Deliver Proteins across the Blood-Brain Barrier: Long-Term Efficacy, Toxicity, and Mechanism. *Mol. Ther.* **2017**, *25*, 1531–1543. [CrossRef] [PubMed]
542. Sarkar, G.; Curran, G.L.; Mahlum, E.; Decklever, T.; Wengenack, T.M.; Blahnik, A.; Hoesley, B.; Lowe, V.J.; Poduslo, J.F.; Jenkins, R.B. A carrier for non-covalent delivery of functional beta-galactosidase and antibodies against amyloid plaques and IgM to the brain. *PLoS ONE* **2011**, *6*, e28881. [CrossRef]
543. Aasen, S.N.; Espedal, H.; Holte, C.F.; Keunen, O.; Karlsen, T.V.; Tenstad, O.; Maheraly, Z.; Miletic, H.; Hoang, T.; Eikeland, A.V.; et al. Improved Drug Delivery to Brain Metastases by Peptide-Mediated Permeabilization of the Blood-Brain Barrier. *Mol. Cancer Ther.* **2019**, *18*, 2171–2181. [CrossRef] [PubMed]
544. Brightman, M.W. Morphology of blood-brain interfaces. *Exp. Eye Res.* **1977**, *25* (Suppl. S1), 1–25. [CrossRef]
545. Saar, K.; Lindgren, M.; Hansen, M.; Eiriksdottir, E.; Jiang, Y.; Rosenthal-Aizman, K.; Sassian, M.; Langel, U. Cell-penetrating peptides: A comparative membrane toxicity study. *Anal. Biochem.* **2005**, *345*, 55–65. [CrossRef] [PubMed]
546. Kanekura, K.; Harada, Y.; Fujimoto, M.; Yagi, T.; Hayamizu, Y.; Nagaoka, K.; Kuroda, M. Characterization of membrane penetration and cytotoxicity of C9orf72-encoding arginine-rich dipeptides. *Sci. Rep.* **2018**, *8*, 12740. [CrossRef] [PubMed]
547. Schwarz, R.E.; Wojciechowicz, D.C.; Picon, A.I.; Schwarz, M.A.; Paty, P.B. Wheatgerm agglutinin-mediated toxicity in pancreatic cancer cells. *Br. J. Cancer* **1999**, *80*, 1754–1762. [CrossRef]
548. Dalla Pellegrina, C.; Rizzi, C.; Mosconi, S.; Zoccatelli, G.; Peruffo, A.; Chignola, R. Plant lectins as carriers for oral drugs: Is wheat germ agglutinin a suitable candidate? *Toxicol. Appl. Pharmacol.* **2005**, *207*, 170–178. [CrossRef]
549. Dalla Pellegrina, C.; Perbellini, O.; Scupoli, M.T.; Tomelleri, C.; Zanetti, C.; Zoccatelli, G.; Fusi, M.; Peruffo, A.; Rizzi, C.; Chignola, R. Effects of wheat germ agglutinin on human gastrointestinal epithelium: Insights from an experimental model of immune/epithelial cell interaction. *Toxicol. Appl. Pharmacol.* **2009**, *237*, 146–153. [CrossRef]
550. Li, E.; Kronfeld, S. Effects of wheat germ agglutinin on membrane transport. *Biochim. Biophys. Acta* **1977**, *469*, 202–210. [CrossRef]
551. Lawrence, M.C. Understanding insulin and its receptor from their three-dimensional structures. *Mol. Metab.* **2021**, *52*, 101255. [CrossRef]
552. Gutmann, T.; Schafer, I.B.; Poojari, C.; Brankatschk, B.; Vattulainen, I.; Strauss, M.; Coskun, U. Cryo-EM structure of the complete and ligand-saturated insulin receptor ectodomain. *J. Cell Biol.* **2020**, *219*, e201907210. [CrossRef]
553. Ward, C.W.; Lawrence, M.C. Landmarks in insulin research. *Front. Endocrinol.* **2011**, *2*, 76. [CrossRef]
554. Eckenroth, B.E.; Steere, A.N.; Chasteen, N.D.; Everse, S.J.; Mason, A.B. How the binding of human transferrin primes the transferrin receptor potentiating iron release at endosomal pH. *Proc. Natl. Acad. Sci. USA* **2011**, *108*, 13089–13094. [CrossRef]
555. Menting, J.G.; Whittaker, J.; Margetts, M.B.; Whittaker, L.J.; Kong, G.K.; Smith, B.J.; Watson, C.J.; Zakova, L.; Kletvikova, E.; Jiracek, J.; et al. How insulin engages its primary binding site on the insulin receptor. *Nature* **2013**, *493*, 241–245. [CrossRef]
556. Bravo, D.A.; Gleason, J.B.; Sanchez, R.I.; Roth, R.A.; Fuller, R.S. Accurate and efficient cleavage of the human insulin proreceptor by the human proprotein-processing protease furin. Characterization and kinetic parameters using the purified, secreted soluble protease expressed by a recombinant baculovirus. *J. Biol. Chem.* **1994**, *269*, 25830–25837. [CrossRef]
557. Bar, R.S.; Gorden, P.; Roth, J.; Kahn, C.R.; De Meyts, P. Fluctuations in the affinity and concentration of insulin receptors on circulating monocytes of obese patients: Effects of starvation, refeeding, and dieting. *J. Clin. Investig.* **1976**, *58*, 1123–1135. [CrossRef]
558. Bremer, A.A.; Stanhope, K.L.; Graham, J.L.; Cummings, B.P.; Wang, W.; Saville, B.R.; Havel, P.J. Fructose-fed rhesus monkeys: A nonhuman primate model of insulin resistance, metabolic syndrome, and type 2 diabetes. *Clin. Transl. Sci.* **2011**, *4*, 243–252. [CrossRef]

559. Pardridge, W.M.; Chou, T. Mathematical Models of Blood-Brain Barrier Transport of Monoclonal Antibodies Targeting the Transferrin Receptor and the Insulin Receptor. *Pharmaceutics* **2021**, *14*, 535. [CrossRef]
560. Frank, H.J.; Pardridge, W.M. A direct in vitro demonstration of insulin binding to isolated brain microvessels. *Diabetes* **1981**, *30*, 757–761. [CrossRef]
561. Pardridge, W.M.; Eisenberg, J.; Yang, J. Human blood-brain barrier insulin receptor. *J. Neurochem.* **1985**, *44*, 1771–1778. [CrossRef]
562. Kurata, T.; Miyazaki, K.; Morimoto, N.; Kawai, H.; Ohta, Y.; Ikeda, Y.; Abe, K. Atorvastatin and pitavastatin reduce oxidative stress and improve IR/LDL-R signals in Alzheimer's disease. *Neurol. Res.* **2013**, *35*, 193–205. [CrossRef]
563. Unger, J.; McNeill, T.H.; Moxley, R.T., 3rd; White, M.; Moss, A.; Livingston, J.N. Distribution of insulin receptor-like immunoreactivity in the rat forebrain. *Neuroscience* **1989**, *31*, 143–157. [CrossRef]
564. Duffy, K.R.; Pardridge, W.M. Blood-brain barrier transcytosis of insulin in developing rabbits. *Brain Res.* **1987**, *420*, 32–38. [CrossRef]
565. Meijer, R.I.; Gray, S.M.; Aylor, K.W.; Barrett, E.J. Pathways for insulin access to the brain: The role of the microvascular endothelial cell. *Am. J. Physiol. Heart Circ. Physiol.* **2016**, *311*, H1132–H1138. [CrossRef] [PubMed]
566. Drejer, K.; Kruse, V.; Larsen, U.D.; Hougaard, P.; Bjorn, S.; Gammeltoft, S. Receptor binding and tyrosine kinase activation by insulin analogues with extreme affinities studied in human hepatoma HepG2 cells. *Diabetes* **1991**, *40*, 1488–1495. [CrossRef] [PubMed]
567. Rhea, E.M.; Rask-Madsen, C.; Banks, W.A. Insulin transport across the blood-brain barrier can occur independently of the insulin receptor. *J. Physiol.* **2018**, *596*, 4753–4765. [CrossRef]
568. Konishi, M.; Sakaguchi, M.; Lockhart, S.M.; Cai, W.; Li, M.E.; Homan, E.P.; Rask-Madsen, C.; Kahn, C.R. Endothelial insulin receptors differentially control insulin signaling kinetics in peripheral tissues and brain of mice. *Proc. Natl. Acad. Sci. USA* **2017**, *114*, E8478–E8487. [CrossRef]
569. Pardridge, W.M. The Isolated Brain Microvessel: A Versatile Experimental Model of the Blood-Brain Barrier. *Front. Physiol.* **2020**, *11*, 398. [CrossRef]
570. Hersom, M.; Helms, H.C.; Schmalz, C.; Pedersen, T.A.; Buckley, S.T.; Brodin, B. The insulin receptor is expressed and functional in cultured blood-brain barrier endothelial cells but does not mediate insulin entry from blood to brain. *Am. J. Physiol. Endocrinol. Metab.* **2018**, *315*, E531–E542. [CrossRef]
571. Hersom, M.; Helms, H.C.; Pretzer, N.; Goldman, C.; Jensen, A.I.; Severin, G.; Nielsen, M.S.; Holm, R.; Brodin, B. Transferrin receptor expression and role in transendothelial transport of transferrin in cultured brain endothelial monolayers. *Mol. Cell Neurosci.* **2016**, *76*, 59–67. [CrossRef]
572. Gray, S.M.; Aylor, K.W.; Barrett, E.J. Unravelling the regulation of insulin transport across the brain endothelial cell. *Diabetologia* **2017**, *60*, 1512–1521. [CrossRef]
573. Kawabata, H.; Yang, R.; Hiramata, T.; Vuong, P.T.; Kawano, S.; Gombart, A.F.; Koeffler, H.P. Molecular cloning of transferrin receptor 2. A new member of the transferrin receptor-like family. *J. Biol. Chem.* **1999**, *274*, 20826–20832. [CrossRef]
574. Fleming, R.E.; Migas, M.C.; Holden, C.C.; Waheed, A.; Britton, R.S.; Tomatsu, S.; Bacon, B.R.; Sly, W.S. Transferrin receptor 2: Continued expression in mouse liver in the face of iron overload and in hereditary hemochromatosis. *Proc. Natl. Acad. Sci. USA* **2000**, *97*, 2214–2219. [CrossRef]
575. Mason, A.B.; Byrne, S.L.; Everse, S.J.; Roberts, S.E.; Chasteen, N.D.; Smith, V.C.; MacGillivray, R.T.; Kandemir, B.; Bou-Abdallah, F. A loop in the N-lobe of human serum transferrin is critical for binding to the transferrin receptor as revealed by mutagenesis, isothermal titration calorimetry, and epitope mapping. *J. Mol. Recognit.* **2009**, *22*, 521–529. [CrossRef]
576. Schmaier, A.H. Transferrin: A blood coagulation modifier. *Cell Res.* **2020**, *30*, 101–102. [CrossRef]
577. Jefferies, W.A.; Brandon, M.R.; Hunt, S.V.; Williams, A.F.; Gatter, K.C.; Mason, D.Y. Transferrin receptor on endothelium of brain capillaries. *Nature* **1984**, *312*, 162–163. [CrossRef]
578. Fishman, J.B.; Rubin, J.B.; Handrahan, J.V.; Connor, J.R.; Fine, R.E. Receptor-mediated transcytosis of transferrin across the blood-brain barrier. *J. Neurosci. Res.* **1987**, *18*, 299–304. [CrossRef]
579. Pardridge, W.M.; Eisenberg, J.; Yang, J. Human blood-brain barrier transferrin receptor. *Metabolism* **1987**, *36*, 892–895. [CrossRef]
580. Taylor, E.M.; Crowe, A.; Morgan, E.H. Transferrin and iron uptake by the brain: Effects of altered iron status. *J. Neurochem.* **1991**, *57*, 1584–1592. [CrossRef]
581. Moos, T.; Morgan, E.H. Transferrin and transferrin receptor function in brain barrier systems. *Cell. Mol. Neurobiol.* **2000**, *20*, 77–95. [CrossRef]
582. Okamura, T.; Igarashi, J.; Kikuchi, T.; Fukushi, K.; Arano, Y.; Irie, T. A radiotracer method to study efflux transport of iodide liberated from thyroid hormones via deiodination metabolism in the brain. *Life Sci.* **2009**, *84*, 791–795. [CrossRef]
583. Roberts, R.L.; Fine, R.E.; Sandra, A. Receptor-mediated endocytosis of transferrin at the blood-brain barrier. *J. Cell Sci.* **1993**, *104 Pt 2*, 521–532. [CrossRef]
584. Huwyler, J.; Pardridge, W.M. Examination of blood-brain barrier transferrin receptor by confocal fluorescent microscopy of unfixed isolated rat brain capillaries. *J. Neurochem.* **1998**, *70*, 883–886. [CrossRef]
585. Bickel, U.; Kang, Y.S.; Yoshikawa, T.; Pardridge, W.M. In vivo demonstration of subcellular localization of anti-transferrin receptor monoclonal antibody-colloidal gold conjugate in brain capillary endothelium. *J. Histochem. Cytochem* **1994**, *42*, 1493–1497. [CrossRef]

586. Skarlatos, S.; Yoshikawa, T.; Pardridge, W.M. Transport of [<sup>125</sup>I]transferrin through the rat blood-brain barrier. *Brain Res.* **1995**, *683*, 164–171. [CrossRef]
587. Pardridge, W.M.; Boado, R.J.; Patrick, D.J.; Ka-Wai Hui, E.; Lu, J.Z. Blood-Brain Barrier Transport, Plasma Pharmacokinetics, and Neuropathology Following Chronic Treatment of the Rhesus Monkey with a Brain Penetrating Humanized Monoclonal Antibody Against the Human Transferrin Receptor. *Mol. Pharm.* **2018**, *15*, 5207–5216. [CrossRef] [PubMed]
588. Mash, D.C.; Pablo, J.; Flynn, D.D.; Efange, S.M.; Weiner, W.J. Characterization and distribution of transferrin receptors in the rat brain. *J. Neurochem.* **1990**, *55*, 1972–1979. [CrossRef]
589. Whitten, A.E.; Smith, B.J.; Menting, J.G.; Margetts, M.B.; McKern, N.M.; Lovrecz, G.O.; Adams, T.E.; Richards, K.; Bentley, J.D.; Trehwella, J.; et al. Solution structure of ectodomains of the insulin receptor family: The ectodomain of the type 1 insulin-like growth factor receptor displays asymmetry of ligand binding accompanied by limited conformational change. *J. Mol. Biol.* **2009**, *394*, 878–892. [CrossRef]
590. Duffy, K.R.; Pardridge, W.M.; Rosenfeld, R.G. Human blood-brain barrier insulin-like growth factor receptor. *Metabolism* **1988**, *37*, 136–140. [CrossRef]
591. Clemmons, D.R. Role of IGF-binding proteins in regulating IGF responses to changes in metabolism. *J. Mol. Endocrinol.* **2018**, *61*, T139–T169. [CrossRef] [PubMed]
592. Reinhardt, R.R.; Bondy, C.A. Insulin-like growth factors cross the blood-brain barrier. *Endocrinology* **1994**, *135*, 1753–1761. [CrossRef] [PubMed]
593. Garcia-Segura, L.M.; Rodriguez, J.R.; Torres-Aleman, I. Localization of the insulin-like growth factor I receptor in the cerebellum and hypothalamus of adult rats: An electron microscopic study. *J. Neurocytol.* **1997**, *26*, 479–490. [CrossRef] [PubMed]
594. Madathil, S.K.; Evans, H.N.; Saatman, K.E. Temporal and regional changes in IGF-1/IGF-1R signaling in the mouse brain after traumatic brain injury. *J. Neurotrauma* **2010**, *27*, 95–107. [CrossRef]
595. Golden, P.L.; Maccagnan, T.J.; Pardridge, W.M. Human blood-brain barrier leptin receptor. Binding and endocytosis in isolated human brain microvessels. *J. Clin. Investig.* **1997**, *99*, 14–18. [CrossRef]
596. Boado, R.J.; Golden, P.L.; Levin, N.; Pardridge, W.M. Up-regulation of blood-brain barrier short-form leptin receptor gene products in rats fed a high fat diet. *J. Neurochem.* **1998**, *71*, 1761–1764. [CrossRef]
597. Hileman, S.M.; Tornoe, J.; Flier, J.S.; Bjorbaek, C. Transcellular transport of leptin by the short leptin receptor isoform ObRa in Madin-Darby Canine Kidney cells. *Endocrinology* **2000**, *141*, 1955–1961. [CrossRef]
598. Kurrimbux, D.; Gaffen, Z.; Farrell, C.L.; Martin, D.; Thomas, S.A. The involvement of the blood-brain and the blood-cerebrospinal fluid barriers in the distribution of leptin into and out of the rat brain. *Neuroscience* **2004**, *123*, 527–536. [CrossRef]
599. Schwartz, M.W.; Peskind, E.; Raskind, M.; Boyko, E.J.; Porte, D., Jr. Cerebrospinal fluid leptin levels: Relationship to plasma levels and to adiposity in humans. *Nat. Med.* **1996**, *2*, 589–593. [CrossRef]
600. Mutze, J.; Roth, J.; Gerstberger, R.; Matsumura, K.; Hubschle, T. Immunohistochemical evidence of functional leptin receptor expression in neuronal and endothelial cells of the rat brain. *Neurosci. Lett.* **2006**, *394*, 105–110. [CrossRef]
601. Demeule, M.; Poirier, J.; Jodoin, J.; Bertrand, Y.; Desrosiers, R.R.; Dagenais, C.; Nguyen, T.; Lanthier, J.; Gabathuler, R.; Kennard, M.; et al. High transcytosis of melanotransferrin (P97) across the blood-brain barrier. *J. Neurochem.* **2002**, *83*, 924–933. [CrossRef]
602. Demeule, M.; Currie, J.C.; Bertrand, Y.; Che, C.; Nguyen, T.; Regina, A.; Gabathuler, R.; Castaigne, J.P.; Beliveau, R. Involvement of the low-density lipoprotein receptor-related protein in the transcytosis of the brain delivery vector angiopep-2. *J. Neurochem.* **2008**, *106*, 1534–1544. [CrossRef]
603. Moestrup, S.K.; Gliemann, J.; Pallesen, G. Distribution of the alpha 2-macroglobulin receptor/low density lipoprotein receptor-related protein in human tissues. *Cell Tissue Res.* **1992**, *269*, 375–382. [CrossRef]
604. Bu, G.; Maksymovitch, E.A.; Nerbonne, J.M.; Schwartz, A.L. Expression and function of the low density lipoprotein receptor-related protein (LRP) in mammalian central neurons. *J. Biol. Chem.* **1994**, *269*, 18521–18528. [CrossRef]
605. Deane, R.; Wu, Z.; Sagare, A.; Davis, J.; Du Yan, S.; Hamm, K.; Xu, F.; Parisi, M.; LaRue, B.; Hu, H.W.; et al. LRP/amyloid beta-peptide interaction mediates differential brain efflux of Abeta isoforms. *Neuron* **2004**, *43*, 333–344. [CrossRef]
606. Ito, S.; Ueno, T.; Ohtsuki, S.; Terasaki, T. Lack of brain-to-blood efflux transport activity of low-density lipoprotein receptor-related protein-1 (LRP-1) for amyloid-beta peptide(1-40) in mouse: Involvement of an LRP-1-independent pathway. *J. Neurochem.* **2010**, *113*, 1356–1363. [CrossRef]
607. Ito, S.; Matsumiya, K.; Ohtsuki, S.; Kamiie, J.; Terasaki, T. Contributions of degradation and brain-to-blood elimination across the blood-brain barrier to cerebral clearance of human amyloid-beta peptide(1-40) in mouse brain. *J. Cereb. Blood Flow Metab.* **2013**, *33*, 1770–1777. [CrossRef]
608. Liu, C.C.; Hu, J.; Zhao, N.; Wang, J.; Wang, N.; Cirrito, J.R.; Kanekiyo, T.; Holtzman, D.M.; Bu, G. Astrocytic LRP1 Mediates Brain Aβ Clearance and Impacts Amyloid Deposition. *J. Neurosci.* **2017**, *37*, 4023–4031. [CrossRef]
609. Ma, Q.; Zhao, Z.; Sagare, A.P.; Wu, Y.; Wang, M.; Owens, N.C.; Verghese, P.B.; Herz, J.; Holtzman, D.M.; Zlokovic, B.V. Blood-brain barrier-associated pericytes internalize and clear aggregated amyloid-β42 by LRP1-dependent apolipoprotein E isoform-specific mechanism. *Mol. Neurodegener.* **2018**, *13*, 57. [CrossRef]
610. Dehouck, B.; Fenart, L.; Dehouck, M.P.; Pierce, A.; Torpier, G.; Cecchelli, R. A new function for the LDL receptor: Transcytosis of LDL across the blood-brain barrier. *J. Cell Biol.* **1997**, *138*, 877–889. [CrossRef]
611. Turley, S.D.; Burns, D.K.; Rosenfeld, C.R.; Dietschy, J.M. Brain does not utilize low density lipoprotein-cholesterol during fetal and neonatal development in the sheep. *J. Lipid Res.* **1996**, *37*, 1953–1961. [CrossRef]

612. Bjorkhem, I.; Meaney, S. Brain cholesterol: Long secret life behind a barrier. *Arter. Thromb. Vasc. Biol.* **2004**, *24*, 806–815. [CrossRef]
613. Martin, M.G.; Pfrieger, F.; Dotti, C.G. Cholesterol in brain disease: Sometimes determinant and frequently implicated. *EMBO Rep.* **2014**, *15*, 1036–1052. [CrossRef]
614. Serougne, C.; Lefevre, C.; Chevallier, F. Cholesterol transfer between brain and plasma in the rat: A model for the turnover of cerebral cholesterol. *Exp. Neurol.* **1976**, *51*, 229–240. [CrossRef]
615. Lafon, M. Rabies virus receptors. *J. Neurovirol.* **2005**, *11*, 82–87. [CrossRef]
616. Gastka, M.; Horvath, J.; Lentz, T.L. Rabies virus binding to the nicotinic acetylcholine receptor alpha subunit demonstrated by virus overlay protein binding assay. *J. Gen. Virol.* **1996**, *77 Pt 10*, 2437–2440. [CrossRef]
617. Abbruscato, T.J.; Lopez, S.P.; Mark, K.S.; Hawkins, B.T.; Davis, T.P. Nicotine and cotinine modulate cerebral microvascular permeability and protein expression of ZO-1 through nicotinic acetylcholine receptors expressed on brain endothelial cells. *J. Pharm. Sci.* **2002**, *91*, 2525–2538. [CrossRef]
618. Deutch, A.Y.; Holliday, J.; Roth, R.H.; Chun, L.L.; Hawrot, E. Immunohistochemical localization of a neuronal nicotinic acetylcholine receptor in mammalian brain. *Proc. Natl. Acad. Sci. USA* **1987**, *84*, 8697–8701. [CrossRef]
619. Gahring, L.C.; Persiyarov, K.; Rogers, S.W. Neuronal and astrocyte expression of nicotinic receptor subunit beta4 in the adult mouse brain. *J. Comp. Neurol.* **2004**, *468*, 322–333. [CrossRef] [PubMed]
620. Lykhus, O.; Voytenko, L.P.; Lips, K.S.; Bergen, I.; Krasteva-Christ, G.; Vetter, D.E.; Kummer, W.; Skok, M. Nicotinic Acetylcholine Receptor alpha9 and alpha10 Subunits Are Expressed in the Brain of Mice. *Front. Cell Neurosci.* **2017**, *11*, 282. [CrossRef]
621. Hawkins, B.T.; Egleton, R.D.; Davis, T.P. Modulation of cerebral microvascular permeability by endothelial nicotinic acetylcholine receptors. *Am. J. Physiol. Heart Circ. Physiol.* **2005**, *289*, H212–H219. [CrossRef] [PubMed]
622. Graham, A.; Court, J.A.; Martin-Ruiz, C.M.; Jaros, E.; Perry, R.; Volsen, S.G.; Bose, S.; Evans, N.; Ince, P.; Kuryatov, A.; et al. Immunohistochemical localisation of nicotinic acetylcholine receptor subunits in human cerebellum. *Neuroscience* **2002**, *113*, 493–507. [CrossRef]
623. Christensen, S.C.; Krogh, B.O.; Jensen, A.; Andersen, C.B.F.; Christensen, S.; Nielsen, M.S. Characterization of basigin monoclonal antibodies for receptor-mediated drug delivery to the brain. *Sci. Rep.* **2020**, *10*, 14582. [CrossRef] [PubMed]
624. Christensen, S.C.; Hudecz, D.; Jensen, A.; Christensen, S.; Nielsen, M.S. Basigin Antibodies with Capacity for Drug Delivery Across Brain Endothelial Cells. *Mol. Neurobiol.* **2021**, *58*, 4392–4403. [CrossRef]
625. Kirk, P.; Wilson, M.C.; Heddle, C.; Brown, M.H.; Barclay, A.N.; Halestrap, A.P. CD147 is tightly associated with lactate transporters MCT1 and MCT4 and facilitates their cell surface expression. *EMBO J.* **2000**, *19*, 3896–3904. [CrossRef]
626. Crosnier, C.; Bustamante, L.Y.; Bartholdson, S.J.; Bei, A.K.; Theron, M.; Uchikawa, M.; Mboup, S.; Ndir, O.; Kwiatkowski, D.P.; Duraisingh, M.T.; et al. Basigin is a receptor essential for erythrocyte invasion by Plasmodium falciparum. *Nature* **2011**, *480*, 534–537. [CrossRef]
627. Renia, L.; Howland, S.W.; Claser, C.; Charlotte Gruner, A.; Suwanarusk, R.; Hui Teo, T.; Russell, B.; Ng, L.F. Cerebral malaria: Mysteries at the blood-brain barrier. *Virulence* **2012**, *3*, 193–201. [CrossRef]
628. Idro, R.; Marsh, K.; John, C.C.; Newton, C.R. Cerebral malaria: Mechanisms of brain injury and strategies for improved neurocognitive outcome. *Pediatr. Res.* **2010**, *68*, 267–274. [CrossRef]
629. Gaillard, P.J.; de Boer, A.G. A novel opportunity for targeted drug delivery to the brain. *J. Control. Release* **2006**, *116*, e60–e62. [CrossRef]
630. Hayase, Y.; Higashiyama, S.; Sasahara, M.; Amano, S.; Nakagawa, T.; Taniguchi, N.; Hazama, F. Expression of heparin-binding epidermal growth factor-like growth factor in rat brain. *Brain Res.* **1998**, *784*, 163–178. [CrossRef]
631. Van Rooy, I.; Mastrobattista, E.; Storm, G.; Hennink, W.E.; Schifflers, R.M. Comparison of five different targeting ligands to enhance accumulation of liposomes into the brain. *J. Control. Release* **2011**, *150*, 30–36. [CrossRef]
632. Saito, M.; Iwawaki, T.; Taya, C.; Yonekawa, H.; Noda, M.; Inui, Y.; Mekada, E.; Kimata, Y.; Tsuru, A.; Kohno, K. Diphtheria toxin receptor-mediated conditional and targeted cell ablation in transgenic mice. *Nat. Biotechnol.* **2001**, *19*, 746–750. [CrossRef]
633. Wang, P.; Liu, Y.; Shang, X.; Xue, Y. CRM197-induced blood-brain barrier permeability increase is mediated by upregulation of caveolin-1 protein. *J. Mol. Neurosci.* **2011**, *43*, 485–492. [CrossRef]
634. Han, J.; Seaman, W.E.; Di, X.; Wang, W.; Willingham, M.; Torti, F.M.; Torti, S.V. Iron uptake mediated by binding of H-ferritin to the TIM-2 receptor in mouse cells. *PLoS ONE* **2011**, *6*, e23800. [CrossRef]
635. Chiou, B.; Neal, E.H.; Bowman, A.B.; Lippmann, E.S.; Simpson, I.A.; Connor, J.R. Endothelial cells are critical regulators of iron transport in a model of the human blood-brain barrier. *J. Cereb. Blood Flow Metab.* **2019**, *39*, 2117–2131. [CrossRef]
636. Li, L.; Fang, C.J.; Ryan, J.C.; Niemi, E.C.; Lebron, J.A.; Bjorkman, P.J.; Arase, H.; Torti, F.M.; Torti, S.V.; Nakamura, M.C.; et al. Binding and uptake of H-ferritin are mediated by human transferrin receptor-1. *Proc. Natl. Acad. Sci. USA* **2010**, *107*, 3505–3510. [CrossRef]
637. Sakamoto, S.; Kawabata, H.; Masuda, T.; Uchiyama, T.; Mizumoto, C.; Ohmori, K.; Koeffler, H.P.; Kadowaki, N.; Takaori-Kondo, A. H-Ferritin Is Preferentially Incorporated by Human Erythroid Cells through Transferrin Receptor 1 in a Threshold-Dependent Manner. *PLoS ONE* **2015**, *10*, e0139915. [CrossRef]
638. Montemiglio, L.C.; Testi, C.; Ceci, P.; Falvo, E.; Pitea, M.; Savino, C.; Arcovito, A.; Peruzzi, G.; Baiocco, P.; Mancina, F.; et al. Cryo-EM structure of the human ferritin-transferrin receptor 1 complex. *Nat. Commun.* **2019**, *10*, 1121. [CrossRef]
639. Cullis, J.O.; Fitzsimons, E.J.; Griffiths, W.J.; Tsochatzis, E.; Thomas, D.W.; The British Society for Haematology. Investigation and management of a raised serum ferritin. *Br. J. Haematol.* **2018**, *181*, 331–340. [CrossRef]

640. Fan, K.; Jia, X.; Zhou, M.; Wang, K.; Conde, J.; He, J.; Tian, J.; Yan, X. Ferritin Nanocarrier Traverses the Blood Brain Barrier and Kills Glioma. *ACS Nano* **2018**, *12*, 4105–4115. [CrossRef]
641. Todorich, B.; Zhang, X.; Slagle-Webb, B.; Seaman, W.E.; Connor, J.R. Tim-2 is the receptor for H-ferritin on oligodendrocytes. *J. Neurochem.* **2008**, *107*, 1495–1505. [CrossRef]
642. Fisher, J.; Devraj, K.; Ingram, J.; Slagle-Webb, B.; Madhankumar, A.B.; Liu, X.; Klinger, M.; Simpson, I.A.; Connor, J.R. Ferritin: A novel mechanism for delivery of iron to the brain and other organs. *Am. J. Physiol. Cell Physiol.* **2007**, *293*, C641–C649. [CrossRef]
643. Jiang, W.; Nakayama, Y.; Sequeira, J.M.; Quadros, E.V. Characterizing monoclonal antibodies to antigenic domains of TCbIR/CD320, the receptor for cellular uptake of transcobalamin-bound cobalamin. *Drug Deliv.* **2011**, *18*, 74–78. [CrossRef]
644. Hannibal, L.; Bolisetty, K.; Axhemi, A.; DiBello, P.M.; Quadros, E.V.; Fedosov, S.; Jacobsen, D.W. Transcellular transport of cobalamin in aortic endothelial cells. *FASEB J.* **2018**, *32*, 5506–5519. [CrossRef]
645. Pardridge, W.M. Chimeric Peptides for Neuropeptide Delivery through the Blood-Brain Barrier. US Patent 4,801,575, 31 January 1989.
646. Duttaroy, A.; Kanakaraj, P.; Osborn, B.L.; Schneider, H.; Pickeral, O.K.; Chen, C.; Zhang, G.; Kaithamana, S.; Singh, M.; Schulingkamp, R.; et al. Development of a long-acting insulin analog using albumin fusion technology. *Diabetes* **2005**, *54*, 251–258. [CrossRef]
647. Pardridge, W.M. Kinetics of Blood-Brain Barrier Transport of Monoclonal Antibodies Targeting the Insulin Receptor and the Transferrin Receptor. *Pharmaceutics* **2021**, *15*, 3. [CrossRef]
648. Nguyen, S.N.; Bobst, C.E.; Kaltashov, I.A. Mass spectrometry-guided optimization and characterization of a biologically active transferrin-lysozyme model drug conjugate. *Mol. Pharm.* **2013**, *10*, 1998–2007. [CrossRef] [PubMed]
649. Sahtoe, D.D.; Coscia, A.; Mustafaoglu, N.; Miller, L.M.; Olal, D.; Vulovic, I.; Yu, T.Y.; Goreshnik, I.; Lin, Y.R.; Clark, L.; et al. Transferrin receptor targeting by de novo sheet extension. *Proc. Natl. Acad. Sci. USA* **2021**, *118*, e2021569118. [CrossRef] [PubMed]
650. Crook, Z.R.; Girard, E.; Sevilla, G.P.; Merrill, M.; Friend, D.; Rupert, P.B.; Pakiam, F.; Nguyen, E.; Yin, C.; Ruff, R.O.; et al. A TfR-Binding Cystine-Dense Peptide Promotes Blood-Brain Barrier Penetration of Bioactive Molecules. *J. Mol. Biol.* **2020**, *432*, 3989–4009. [CrossRef] [PubMed]
651. Potere, N.; Del Buono, M.G.; Mauro, A.G.; Abbate, A.; Toldo, S. Low Density Lipoprotein Receptor-Related Protein-1 in Cardiac Inflammation and Infarct Healing. *Front. Cardiovasc. Med.* **2019**, *6*, 51. [CrossRef] [PubMed]
652. Pulgar, V.M. Transcytosis to Cross the Blood Brain Barrier, New Advancements and Challenges. *Front. Neurosci.* **2018**, *12*, 1019. [CrossRef]
653. Guo, Q.; Zhu, Q.; Miao, T.; Tao, J.; Ju, X.; Sun, Z.; Li, H.; Xu, G.; Chen, H.; Han, L. LRP1-upregulated nanoparticles for efficiently conquering the blood-brain barrier and targetedly suppressing multifocal and infiltrative brain metastases. *J. Control. Release* **2019**, *303*, 117–129. [CrossRef]
654. Pan, W.; Kastin, A.J.; Zankel, T.C.; van Kerkhof, P.; Terasaki, T.; Bu, G. Efficient transfer of receptor-associated protein (RAP) across the blood-brain barrier. *J. Cell Sci.* **2004**, *117*, 5071–5078. [CrossRef]
655. Richardson, D.R.; Morgan, E.H. The transferrin homologue, melanotransferrin (p97), is rapidly catabolized by the liver of the rat and does not effectively donate iron to the brain. *Biochim. Biophys. Acta* **2004**, *1690*, 124–133. [CrossRef]
656. Regina, A.; Demeule, M.; Tripathy, S.; Lord-Dufour, S.; Currie, J.C.; Iddir, M.; Annabi, B.; Castaigne, J.P.; Lachowicz, J.E. ANG4043, a novel brain-penetrant peptide-mAb conjugate, is efficacious against HER2-positive intracranial tumors in mice. *Mol. Cancer Ther.* **2015**, *14*, 129–140. [CrossRef]
657. Sakamoto, K.; Shinohara, T.; Adachi, Y.; Asami, T.; Ohtaki, T. A novel LRP1-binding peptide L57 that crosses the blood brain barrier. *Biochem. Biophys. Rep.* **2017**, *12*, 135–139. [CrossRef]
658. Fillebeen, C.; Descamps, L.; Dehouck, M.P.; Fenart, L.; Benaissa, M.; Spik, G.; Cecchelli, R.; Pierce, A. Receptor-mediated transcytosis of lactoferrin through the blood-brain barrier. *J. Biol. Chem.* **1999**, *274*, 7011–7017. [CrossRef]
659. Ji, B.; Maeda, J.; Higuchi, M.; Inoue, K.; Akita, H.; Harashima, H.; Suhara, T. Pharmacokinetics and brain uptake of lactoferrin in rats. *Life Sci.* **2006**, *78*, 851–855. [CrossRef]
660. Pardridge, W.M. Vector mediated peptide drug delivery to the brain. *Adv. Drug Del Rev* **1995**, *15*, 109–146. [CrossRef]
661. Prince, W.S.; McCormick, L.M.; Wendt, D.J.; Fitzpatrick, P.A.; Schwartz, K.L.; Aguilera, A.I.; Koppaka, V.; Christianson, T.M.; Vellard, M.C.; Pavloff, N.; et al. Lipoprotein receptor binding, cellular uptake, and lysosomal delivery of fusions between the receptor-associated protein (RAP) and alpha-L-iduronidase or acid alpha-glucosidase. *J. Biol. Chem.* **2004**, *279*, 35037–35046. [CrossRef]
662. Croy, J.E.; Brandon, T.; Komives, E.A. Two apolipoprotein E mimetic peptides, ApoE(130-149) and ApoE(141-155)<sub>2</sub>, bind to LRP1. *Biochemistry* **2004**, *43*, 7328–7335. [CrossRef] [PubMed]
663. Lee, H.J.; Engelhardt, B.; Lesley, J.; Bickel, U.; Pardridge, W.M. Targeting rat anti-mouse transferrin receptor monoclonal antibodies through blood-brain barrier in mouse. *J. Pharmacol. Exp. Ther.* **2000**, *292*, 1048–1052.
664. Malcor, J.D.; Payrot, N.; David, M.; Faucon, A.; Abouzid, K.; Jacquot, G.; Floquet, N.; Debarbieux, F.; Rougon, G.; Martinez, J.; et al. Chemical optimization of new ligands of the low-density lipoprotein receptor as potential vectors for central nervous system targeting. *J. Med. Chem.* **2012**, *55*, 2227–2241. [CrossRef]
665. Molino, Y.; David, M.; Varini, K.; Jabes, F.; Gaudin, N.; Fortoul, A.; Bakloul, K.; Masse, M.; Bernard, A.; Drobecq, L.; et al. Use of LDL receptor-targeting peptide vectors for in vitro and in vivo cargo transport across the blood-brain barrier. *FASEB J.* **2017**, *31*, 1807–1827. [CrossRef]

666. Boswell, C.A.; Mundo, E.E.; Ulufatu, S.; Bumbaca, D.; Cahaya, H.S.; Majidy, N.; Van Hoy, M.; Schweiger, M.G.; Fielder, P.J.; Prabhu, S.; et al. Comparative physiology of mice and rats: Radiometric measurement of vascular parameters in rodent tissues. *Mol. Pharm.* **2014**, *11*, 1591–1598. [CrossRef]
667. Spencer, B.J.; Verma, I.M. Targeted delivery of proteins across the blood-brain barrier. *Proc. Natl. Acad. Sci. USA* **2007**, *104*, 7594–7599. [CrossRef]
668. Spencer, B.; Verma, I.; Desplats, P.; Morvinski, D.; Rockenstein, E.; Adame, A.; Masliah, E. A neuroprotective brain-penetrating endopeptidase fusion protein ameliorates Alzheimer disease pathology and restores neurogenesis. *J. Biol. Chem.* **2014**, *289*, 17917–17931. [CrossRef]
669. Masliah, E.; Spencer, B. Applications of ApoB LDLR-Binding Domain Approach for the Development of CNS-Penetrating Peptides for Alzheimer's Disease. *Methods Mol. Biol.* **2015**, *1324*, 331–337. [CrossRef]
670. Gaillard, P.J.; Appeldoorn, C.C.; Rip, J.; Dorland, R.; van der Pol, S.M.; Kooij, G.; de Vries, H.E.; Reijkerkerk, A. Enhanced brain delivery of liposomal methylprednisolone improved therapeutic efficacy in a model of neuroinflammation. *J. Control. Release* **2012**, *164*, 364–369. [CrossRef]
671. Kannan, R.; Kuhlenkamp, J.F.; Ookhtens, M.; Kaplowitz, N. Transport of glutathione at blood-brain barrier of the rat: Inhibition by glutathione analogs and age-dependence. *J. Pharmacol. Exp. Ther.* **1992**, *263*, 964–970.
672. Schorbach, L.; Krick, W.; Burckhardt, G.; Burckhardt, B.C. Glutathione is a low-affinity substrate of the human sodium-dependent dicarboxylate transporter. *Nephron Physiol.* **2013**, *124*, 1–5. [CrossRef] [PubMed]
673. Varga, V.; Jenei, Z.; Janaky, R.; Saransaari, P.; Oja, S.S. Glutathione is an endogenous ligand of rat brain N-methyl-D-aspartate (NMDA) and 2-amino-3-hydroxy-5-methyl-4-isoxazolepropionate (AMPA) receptors. *Neurochem. Res.* **1997**, *22*, 1165–1171. [CrossRef] [PubMed]
674. Fatima, S.; Mohammad, T.; Jairajpuri, D.S.; Rehman, M.T.; Hussain, A.; Samim, M.; Ahmad, F.J.; Alajmi, M.F.; Hassan, M.I. Identification and evaluation of glutathione conjugate gamma-l-glutamyl-l-cysteine for improved drug delivery to the brain. *J. Biomol. Struct. Dyn.* **2020**, *38*, 3610–3620. [CrossRef]
675. Macrez, R.; Ortega, M.C.; Bardou, I.; Mehra, A.; Fournier, A.; Van der Pol, S.M.; Haelewyn, B.; Maubert, E.; Lesept, F.; Chevilly, A.; et al. Neuroendothelial NMDA receptors as therapeutic targets in experimental autoimmune encephalomyelitis. *Brain* **2016**, *139*, 2406–2419. [CrossRef]
676. Mapelli, L.; Gagliano, G.; Soda, T.; Laforenza, U.; Moccia, F.; D'Angelo, E.U. Granular Layer Neurons Control Cerebellar Neurovascular Coupling Through an NMDA Receptor/NO-Dependent System. *J. Neurosci.* **2017**, *37*, 1340–1351. [CrossRef]
677. Cornford, E.M.; Braun, L.D.; Crane, P.D.; Oldendorf, W.H. Blood-brain barrier restriction of peptides and the low uptake of enkephalins. *Endocrinology* **1978**, *103*, 1297–1303. [CrossRef]
678. Aoyama, K. Glutathione in the Brain. *Int. J. Mol. Sci.* **2021**, *22*, 5010. [CrossRef]
679. Pasqualini, R.; Ruoslahti, E. Organ targeting in vivo using phage display peptide libraries. *Nature* **1996**, *380*, 364–366. [CrossRef]
680. Staquicini, F.I.; Ozawa, M.G.; Moya, C.A.; Driessen, W.H.; Barbu, E.M.; Nishimori, H.; Soghomonyan, S.; Flores, L.G., 2nd; Liang, X.; Paolillo, V.; et al. Systemic combinatorial peptide selection yields a non-canonical iron-mimicry mechanism for targeting tumors in a mouse model of human glioblastoma. *J. Clin. Investig.* **2011**, *121*, 161–173. [CrossRef]
681. Van Rooy, I.; Cakir-Tascioglu, S.; Couraud, P.O.; Romero, I.A.; Weksler, B.; Storm, G.; Hennink, W.E.; Schifflers, R.M.; Mastrobattista, E. Identification of peptide ligands for targeting to the blood-brain barrier. *Pharm. Res.* **2010**, *27*, 673–682. [CrossRef]
682. Van Rooy, I.; Hennink, W.E.; Storm, G.; Schifflers, R.M.; Mastrobattista, E. Attaching the phage display-selected GLA peptide to liposomes: Factors influencing target binding. *Eur. J. Pharm. Sci.* **2012**, *45*, 330–335. [CrossRef] [PubMed]
683. Beisiegel, U.; Schneider, W.J.; Goldstein, J.L.; Anderson, R.G.; Brown, M.S. Monoclonal antibodies to the low density lipoprotein receptor as probes for study of receptor-mediated endocytosis and the genetics of familial hypercholesterolemia. *J. Biol. Chem.* **1981**, *256*, 11923–11931. [CrossRef]
684. Bickel, U.; Yoshikawa, T.; Landaw, E.M.; Faull, K.F.; Pardridge, W.M. Pharmacologic effects in vivo in brain by vector-mediated peptide drug delivery. *Proc. Natl. Acad. Sci. USA* **1993**, *90*, 2618–2622. [CrossRef]
685. Friden, P.M.; Walus, L.R.; Watson, P.; Doctrow, S.R.; Kozarich, J.W.; Backman, C.; Bergman, H.; Hoffer, B.; Bloom, F.; Granholm, A.C. Blood-brain barrier penetration and in vivo activity of an NGF conjugate. *Science* **1993**, *259*, 373–377. [CrossRef]
686. Maggio, J.E.; Stimson, E.R.; Ghilardi, J.R.; Allen, C.J.; Dahl, C.E.; Whitcomb, D.C.; Vigna, S.R.; Vinters, H.V.; Labenski, M.E.; Mantyh, P.W. Reversible in vitro growth of Alzheimer disease beta-amyloid plaques by deposition of labeled amyloid peptide. *Proc. Natl. Acad. Sci. USA* **1992**, *89*, 5462–5466. [CrossRef]
687. Saito, Y.; Buciak, J.; Yang, J.; Pardridge, W.M. Vector-mediated delivery of 125I-labeled beta-amyloid peptide A beta 1-40 through the blood-brain barrier and binding to Alzheimer disease amyloid of the A beta 1-40/vector complex. *Proc. Natl. Acad. Sci. USA* **1995**, *92*, 10227–10231. [CrossRef]
688. Wu, D.; Yang, J.; Pardridge, W.M. Drug targeting of a peptide radiopharmaceutical through the primate blood-brain barrier in vivo with a monoclonal antibody to the human insulin receptor. *J. Clin. Investig.* **1997**, *100*, 1804–1812. [CrossRef]
689. Jefferies, W.A.; Brandon, M.R.; Williams, A.F.; Hunt, S.V. Analysis of lymphopoietic stem cells with a monoclonal antibody to the rat transferrin receptor. *Immunology* **1985**, *54*, 333–341.
690. Kissel, K.; Hamm, S.; Schulz, M.; Vecchi, A.; Garlanda, C.; Engelhardt, B. Immunohistochemical localization of the murine transferrin receptor (TfR) on blood-tissue barriers using a novel anti-TfR monoclonal antibody. *Histochem. Cell Biol.* **1998**, *110*, 63–72. [CrossRef]

691. Lesley, J.; Domingo, D.L.; Schulte, R.; Trowbridge, I.S. Effect of an anti-murine transferrin receptor-ricin A conjugate on bone marrow stem and progenitor cells treated in vitro. *Exp. Cell Res.* **1984**, *150*, 400–407. [CrossRef]
692. Li, J.Y.; Sugimura, K.; Boado, R.J.; Lee, H.J.; Zhang, C.; Duebel, S.; Pardridge, W.M. Genetically engineered brain drug delivery vectors: Cloning, expression and in vivo application of an anti-transferrin receptor single chain antibody-streptavidin fusion gene and protein. *Protein Eng.* **1999**, *12*, 787–796. [CrossRef]
693. Boado, R.J.; Zhang, Y.; Wang, Y.; Pardridge, W.M. Engineering and expression of a chimeric transferrin receptor monoclonal antibody for blood-brain barrier delivery in the mouse. *Biotechnol. Bioeng.* **2009**, *102*, 1251–1258. [CrossRef]
694. Boado, R.J.; Zhang, Y.; Zhang, Y.; Pardridge, W.M. Humanization of anti-human insulin receptor antibody for drug targeting across the human blood-brain barrier. *Biotechnol. Bioeng.* **2007**, *96*, 381–391. [CrossRef]
695. Yu, Y.J.; Zhang, Y.; Kenrick, M.; Hoyte, K.; Luk, W.; Lu, Y.; Atwal, J.; Elliott, J.M.; Prabhu, S.; Watts, R.J.; et al. Boosting brain uptake of a therapeutic antibody by reducing its affinity for a transcytosis target. *Sci. Transl. Med.* **2011**, *3*, 84ra44. [CrossRef] [PubMed]
696. Boado, R.J.; Zhang, Y.; Zhang, Y.; Xia, C.F.; Pardridge, W.M. Fusion antibody for Alzheimer's disease with bidirectional transport across the blood-brain barrier and abeta fibril disaggregation. *Bioconjug. Chem.* **2007**, *18*, 447–455. [CrossRef] [PubMed]
697. Niewoehner, J.; Bohrmann, B.; Collin, L.; Urich, E.; Sade, H.; Maier, P.; Rueger, P.; Stracke, J.O.; Lau, W.; Tissot, A.C.; et al. Increased brain penetration and potency of a therapeutic antibody using a monovalent molecular shuttle. *Neuron* **2014**, *81*, 49–60. [CrossRef] [PubMed]
698. Zhou, Q.H.; Boado, R.J.; Hui, E.K.; Lu, J.Z.; Pardridge, W.M. Chronic dosing of mice with a transferrin receptor monoclonal antibody-glia-derived neurotrophic factor fusion protein. *Drug Metab. Dispos.* **2011**, *39*, 1149–1154. [CrossRef]
699. Ullman, J.C.; Arguello, A.; Getz, J.A.; Bhalla, A.; Mahon, C.S.; Wang, J.; Giese, T.; Bedard, C.; Kim, D.J.; Blumenfeld, J.R.; et al. Brain delivery and activity of a lysosomal enzyme using a blood-brain barrier transport vehicle in mice. *Sci. Transl. Med.* **2020**, *12*, eaay1163. [CrossRef]
700. Ng, P.P.; Dela Cruz, J.S.; Sorour, D.N.; Stinebaugh, J.M.; Shin, S.U.; Shin, D.S.; Morrison, S.L.; Penichet, M.L. An anti-transferrin receptor-avidin fusion protein exhibits both strong proapoptotic activity and the ability to deliver various molecules into cancer cells. *Proc. Natl. Acad. Sci. USA* **2002**, *99*, 10706–10711. [CrossRef]
701. Ng, P.P.; Helguera, G.; Daniels, T.R.; Lomas, S.Z.; Rodriguez, J.A.; Schiller, G.; Bonavida, B.; Morrison, S.L.; Penichet, M.L. Molecular events contributing to cell death in malignant human hematopoietic cells elicited by an IgG3-avidin fusion protein targeting the transferrin receptor. *Blood* **2006**, *108*, 2745–2754. [CrossRef]
702. Boado, R.J.; Zhang, Y.; Zhang, Y.; Xia, C.F.; Wang, Y.; Pardridge, W.M. Genetic engineering, expression, and activity of a chimeric monoclonal antibody-avidin fusion protein for receptor-mediated delivery of biotinylated drugs in humans. *Bioconjug. Chem.* **2008**, *19*, 731–739. [CrossRef]
703. Castellanos, D.M.; Sun, J.; Yang, J.; Ou, W.; Zambon, A.C.; Pardridge, W.M.; Sumbria, R.K. Acute and Chronic Dosing of a High-Affinity Rat/Mouse Chimeric Transferrin Receptor Antibody in Mice. *Pharmaceutics* **2020**, *12*, 852. [CrossRef]
704. Alata, W.; Yogi, A.; Brunette, E.; Delaney, C.E.; van Faassen, H.; Hussack, G.; Iqbal, U.; Kemmerich, K.; Haqqani, A.S.; Moreno, M.J.; et al. Targeting insulin-like growth factor-1 receptor (IGF1R) for brain delivery of biologics. *FASEB J.* **2022**, *36*, e22208. [CrossRef]
705. Tao, P.; Kuang, Y.; Li, Y.; Li, W.; Gao, Z.; Liu, L.; Qiang, M.; Zha, Z.; Fan, K.; Ma, P.; et al. Selection of a Full Agonist Combinatorial Antibody that Rescues Leptin Deficiency In Vivo. *Adv. Sci.* **2020**, *7*, 2000818. [CrossRef]
706. Jiang, D.; Lee, H.; Pardridge, W.M. Plasmid DNA gene therapy of the Niemann-Pick C1 mouse with transferrin receptor-targeted Trojan horse liposomes. *Sci. Rep.* **2020**, *10*, 13334. [CrossRef]
707. Lee, H.; Jiang, D.; Pardridge, W.M. Lyoprotectant Optimization for the Freeze-Drying of Receptor-Targeted Trojan Horse Liposomes for Plasmid DNA Delivery. *Mol. Pharm.* **2020**, *17*, 2165–2174. [CrossRef]
708. Pardridge, W.M. Targeted delivery of protein and gene medicines through the blood-brain barrier. *Clin. Pharmacol. Ther.* **2015**, *97*, 347–361. [CrossRef]
709. Pardridge, W.M. Blood-brain barrier delivery for lysosomal storage disorders with IgG-lysosomal enzyme fusion proteins. *Adv. Drug Deliv. Rev.* **2022**, *184*, 114234. [CrossRef]
710. Giugliani, R.; Vairo, F.; Kubaski, F.; Poswar, F.; Riegel, M.; Baldo, G.; Saute, J.A. Neurological manifestations of lysosomal disorders and emerging therapies targeting the CNS. *Lancet Child Adolesc. Health* **2018**, *2*, 56–68. [CrossRef]
711. Muro, S. Strategies for delivery of therapeutics into the central nervous system for treatment of lysosomal storage disorders. *Drug Deliv. Transl. Res.* **2012**, *2*, 169–186. [CrossRef]
712. Scott, H.S.; Anson, D.S.; Orsborn, A.M.; Nelson, P.V.; Clements, P.R.; Morris, C.P.; Hopwood, J.J. Human alpha-L-iduronidase: cDNA isolation and expression. *Proc. Natl. Acad. Sci. USA* **1991**, *88*, 9695–9699. [CrossRef] [PubMed]
713. Kakkis, E.D.; Matynia, A.; Jonas, A.J.; Neufeld, E.F. Overexpression of the human lysosomal enzyme alpha-L-iduronidase in Chinese hamster ovary cells. *Protein Expr. Purif.* **1994**, *5*, 225–232. [CrossRef] [PubMed]
714. Boado, R.J.; Zhang, Y.; Zhang, Y.; Xia, C.F.; Wang, Y.; Pardridge, W.M. Genetic engineering of a lysosomal enzyme fusion protein for targeted delivery across the human blood-brain barrier. *Biotechnol. Bioeng.* **2008**, *99*, 475–484. [CrossRef] [PubMed]

715. Giugliani, R.; Giugliani, L.; de Oliveira Poswar, F.; Donis, K.C.; Corte, A.D.; Schmidt, M.; Boado, R.J.; Nestrasil, I.; Nguyen, C.; Chen, S.; et al. Neurocognitive and somatic stabilization in pediatric patients with severe Mucopolysaccharidosis Type I after 52 weeks of intravenous brain-penetrating insulin receptor antibody-iduronidase fusion protein (valanafusp alpha): An open label phase 1-2 trial. *Orphanet J. Rare Dis.* **2018**, *13*, 110. [CrossRef] [PubMed]
716. Boado, R.J.; Pardridge, W.M. Brain and Organ Uptake in the Rhesus Monkey in Vivo of Recombinant Iduronidase Compared to an Insulin Receptor Antibody-Iduronidase Fusion Protein. *Mol. Pharm.* **2017**, *14*, 1271–1277. [CrossRef]
717. Boado, R.J.; Hui, E.K.; Lu, J.Z.; Sumbria, R.K.; Pardridge, W.M. Blood-brain barrier molecular trojan horse enables imaging of brain uptake of radioiodinated recombinant protein in the rhesus monkey. *Bioconjug. Chem.* **2013**, *24*, 1741–1749. [CrossRef]
718. Boado, R.J.; Hui, E.K.; Lu, J.Z.; Zhou, Q.H.; Pardridge, W.M. Reversal of lysosomal storage in brain of adult MPS-I mice with intravenous Trojan horse-iduronidase fusion protein. *Mol. Pharm.* **2011**, *8*, 1342–1350. [CrossRef]
719. Sonoda, H.; Morimoto, H.; Yoden, E.; Koshimura, Y.; Kinoshita, M.; Golovina, G.; Takagi, H.; Yamamoto, R.; Minami, K.; Mizoguchi, A.; et al. A Blood-Brain-Barrier-Penetrating Anti-human Transferrin Receptor Antibody Fusion Protein for Neuro-nathic Mucopolysaccharidosis II. *Mol. Ther.* **2018**, *26*, 1366–1374. [CrossRef]
720. Okuyama, T.; Eto, Y.; Sakai, N.; Nakamura, K.; Yamamoto, T.; Yamaoka, M.; Ikeda, T.; So, S.; Tanizawa, K.; Sonoda, H.; et al. A Phase 2/3 Trial of Pabinafusp Alfa, IDS Fused with Anti-Human Transferrin Receptor Antibody, Targeting Neurodegeneration in MPS-II. *Mol. Ther.* **2021**, *29*, 671–679. [CrossRef]
721. Boado, R.J.; Ka-Wai Hui, E.; Zhiqiang Lu, J.; Pardridge, W.M. Insulin receptor antibody-iduronate 2-sulfatase fusion protein: Pharmacokinetics, anti-drug antibody, and safety pharmacology in Rhesus monkeys. *Biotechnol. Bioeng.* **2014**, *111*, 2317–2325. [CrossRef]
722. Lu, J.Z.; Hui, E.K.; Boado, R.J.; Pardridge, W.M. Genetic engineering of a bifunctional IgG fusion protein with iduronate-2-sulfatase. *Bioconjug. Chem.* **2010**, *21*, 151–156. [CrossRef]
723. Boado, R.J.; Lu, J.Z.; Hui, E.K.; Pardridge, W.M. Insulin receptor antibody-sulfamidase fusion protein penetrates the primate blood-brain barrier and reduces glycosaminoglycans in Sanfilippo type A cells. *Mol. Pharm.* **2014**, *11*, 2928–2934. [CrossRef]
724. Boado, R.J.; Lu, J.Z.; Hui, E.K.; Pardridge, W.M. Reduction in Brain Heparan Sulfate with Systemic Administration of an IgG Trojan Horse-Sulfamidase Fusion Protein in the Mucopolysaccharidosis Type IIIA Mouse. *Mol. Pharm.* **2018**, *15*, 602–608. [CrossRef]
725. Boado, R.J.; Lu, J.Z.; Hui, E.K.; Lin, H.; Pardridge, W.M. Insulin Receptor Antibody-alpha-N-Acetylglucosaminidase Fusion Protein Penetrates the Primate Blood-Brain Barrier and Reduces Glycosaminoglycans in Sanfilippo Type B Fibroblasts. *Mol. Pharm.* **2016**, *13*, 1385–1392. [CrossRef]
726. Boado, R.J.; Lu, J.Z.; Hui, E.K.; Sumbria, R.K.; Pardridge, W.M. Pharmacokinetics and brain uptake in the rhesus monkey of a fusion protein of arylsulfatase a and a monoclonal antibody against the human insulin receptor. *Biotechnol. Bioeng.* **2013**, *110*, 1456–1465. [CrossRef]
727. Boado, R.J.; Lu, J.Z.; Hui, E.K.; Lin, H.; Pardridge, W.M. Bi-functional IgG-lysosomal enzyme fusion proteins for brain drug delivery. *Sci. Rep.* **2019**, *9*, 18632. [CrossRef]
728. Boado, R.J.; Zhang, Y.; Zhang, Y.; Pardridge, W.M. Genetic engineering, expression, and activity of a fusion protein of a human neurotrophin and a molecular Trojan horse for delivery across the human blood-brain barrier. *Biotechnol. Bioeng.* **2007**, *97*, 1376–1386. [CrossRef]
729. Pardridge, W.M.; Boado, R.J. Pharmacokinetics and safety in rhesus monkeys of a monoclonal antibody-GDNF fusion protein for targeted blood-brain barrier delivery. *Pharm. Res.* **2009**, *26*, 2227–2236. [CrossRef]
730. Boado, R.J.; Zhang, Y.; Zhang, Y.; Wang, Y.; Pardridge, W.M. GDNF fusion protein for targeted-drug delivery across the human blood-brain barrier. *Biotechnol. Bioeng.* **2008**, *100*, 387–396. [CrossRef]
731. Fu, A.; Zhou, Q.H.; Hui, E.K.; Lu, J.Z.; Boado, R.J.; Pardridge, W.M. Intravenous treatment of experimental Parkinson's disease in the mouse with an IgG-GDNF fusion protein that penetrates the blood-brain barrier. *Brain Res.* **2010**, *1352*, 208–213. [CrossRef]
732. Sumbria, R.K.; Boado, R.J.; Pardridge, W.M. Combination stroke therapy in the mouse with blood-brain barrier penetrating IgG-GDNF and IgG-TNF decoy receptor fusion proteins. *Brain Res.* **2013**, *1507*, 91–96. [CrossRef]
733. Boado, R.J.; Hui, E.K.; Lu, J.Z.; Pardridge, W.M. Drug targeting of erythropoietin across the primate blood-brain barrier with an IgG molecular Trojan horse. *J. Pharmacol. Exp. Ther.* **2010**, *333*, 961–969. [CrossRef]
734. Zhou, Q.H.; Hui, E.K.; Lu, J.Z.; Boado, R.J.; Pardridge, W.M. Brain penetrating IgG-erythropoietin fusion protein is neuroprotective following intravenous treatment in Parkinson's disease in the mouse. *Brain Res.* **2011**, *1382*, 315–320. [CrossRef]
735. Sun, J.; Yang, J.; Whitman, K.; Zhu, C.; Cribbs, D.H.; Boado, R.J.; Pardridge, W.M.; Sumbria, R.K. Hematologic safety of chronic brain-penetrating erythropoietin dosing in APP/PS1 mice. *Alzheimer's Dement.* **2019**, *5*, 627–636. [CrossRef] [PubMed]
736. Hui, E.K.; Boado, R.J.; Pardridge, W.M. Tumor necrosis factor receptor-IgG fusion protein for targeted drug delivery across the human blood-brain barrier. *Mol. Pharm.* **2009**, *6*, 1536–1543. [CrossRef] [PubMed]
737. Zhou, Q.H.; Sumbria, R.; Hui, E.K.; Lu, J.Z.; Boado, R.J.; Pardridge, W.M. Neuroprotection with a brain-penetrating biologic tumor necrosis factor inhibitor. *J. Pharmacol. Exp. Ther.* **2011**, *339*, 618–623. [CrossRef] [PubMed]
738. Sumbria, R.K.; Boado, R.J.; Pardridge, W.M. Brain protection from stroke with intravenous TNFalpha decoy receptor-Trojan horse fusion protein. *J. Cereb. Blood Flow Metab.* **2012**, *32*, 1933–1938. [CrossRef]
739. Sumbria, R.K.; Hui, E.K.; Lu, J.Z.; Boado, R.J.; Pardridge, W.M. Disaggregation of amyloid plaque in brain of Alzheimer's disease transgenic mice with daily subcutaneous administration of a tetravalent bispecific antibody that targets the transferrin receptor and the Abeta amyloid peptide. *Mol. Pharm.* **2013**, *10*, 3507–3513. [CrossRef]



740. Do, T.M.; Capdevila, C.; Pradier, L.; Blanchard, V.; Lopez-Grancha, M.; Schussler, N.; Steinmetz, A.; Beninga, J.; Boulay, D.; Dugay, P.; et al. Tetravalent Bispecific Tandem Antibodies Improve Brain Exposure and Efficacy in an Amyloid Transgenic Mouse Model. *Mol. Ther. Methods Clin. Dev.* **2020**, *19*, 58–77. [CrossRef]
741. Sehlin, D.; Stocki, P.; Gustavsson, T.; Hultqvist, G.; Walsh, F.S.; Rutkowski, J.L.; Syvanen, S. Brain delivery of biologics using a cross-species reactive transferrin receptor 1 VNAR shuttle. *FASEB J.* **2020**, *34*, 13272–13283. [CrossRef]
742. Yu, Y.J.; Atwal, J.K.; Zhang, Y.; Tong, R.K.; Wildsmith, K.R.; Tan, C.; Bien-Ly, N.; Hersom, M.; Maloney, J.A.; Meilandt, W.J.; et al. Therapeutic bispecific antibodies cross the blood-brain barrier in nonhuman primates. *Sci. Transl. Med.* **2014**, *6*, 261ra154. [CrossRef]
743. Kariolis, M.S.; Wells, R.C.; Getz, J.A.; Kwan, W.; Mahon, C.S.; Tong, R.; Kim, D.J.; Srivastava, A.; Bedard, C.; Henne, K.R.; et al. Brain delivery of therapeutic proteins using an Fc fragment blood-brain barrier transport vehicle in mice and monkeys. *Sci. Transl. Med.* **2020**, *12*, eaay1359. [CrossRef]
744. Roshanbin, S.; Xiong, M.; Hultqvist, G.; Soderberg, L.; Zachrisson, O.; Meier, S.; Ekmark-Lewen, S.; Bergstrom, J.; Ingelsson, M.; Sehlin, D.; et al. In vivo imaging of alpha-synuclein with antibody-based PET. *Neuropharmacology* **2022**, *208*, 108985. [CrossRef]
745. Wilson, P.J.; Morris, C.P.; Anson, D.S.; Occhiodoro, T.; Bielicki, J.; Clements, P.R.; Hopwood, J.J. Hunter syndrome: Isolation of an iduronate-2-sulfatase cDNA clone and analysis of patient DNA. *Proc. Natl. Acad. Sci. USA* **1990**, *87*, 8531–8535. [CrossRef]
746. Muenzer, J.; Wraith, J.E.; Beck, M.; Giugliani, R.; Harmatz, P.; Eng, C.M.; Vellodi, A.; Martin, R.; Ramaswami, U.; Gucevas-Calikoglu, M.; et al. A phase II/III clinical study of enzyme replacement therapy with idursulfase in mucopolysaccharidosis II (Hunter syndrome). *Genet. Med.* **2006**, *8*, 465–473. [CrossRef]
747. Muenzer, J.; Jones, S.A.; Tylki-Szymanska, A.; Harmatz, P.; Mendelsohn, N.J.; Guffon, N.; Giugliani, R.; Burton, B.K.; Scarpa, M.; Beck, M.; et al. Ten years of the Hunter Outcome Survey (HOS): Insights, achievements, and lessons learned from a global patient registry. *Orphanet J. Rare Dis.* **2017**, *12*, 82. [CrossRef]
748. Bolton, A.E.; Hunter, W.M. The labelling of proteins to high specific radioactivities by conjugation to a 125I-containing acylating agent. *Biochem. J.* **1973**, *133*, 529–539. [CrossRef]
749. Gaudriault, G.; Vincent, J.P. Selective labeling of alpha- or epsilon-amino groups in peptides by the Bolton-Hunter reagent. *Peptides* **1992**, *13*, 1187–1192. [CrossRef]
750. Levi-Montalcini, R.; Hamburger, V. Selective growth stimulating effects of mouse sarcoma on the sensory and sympathetic nervous system of the chick embryo. *J. Exp. Zool.* **1951**, *116*, 321–361. [CrossRef]
751. Hefti, F. Pharmacology of neurotrophic factors. *Annu. Rev. Pharmacol. Toxicol.* **1997**, *37*, 239–267. [CrossRef]
752. Barinaga, M. Neurotrophic factors enter the clinic. *Science* **1994**, *264*, 772–774. [CrossRef]
753. The BDNF Study Group (Phase III). A controlled trial of recombinant methionyl human BDNF in ALS. *Neurology* **1999**, *52*, 1427–1433. [CrossRef]
754. Miller, R.G.; Petajan, J.H.; Bryan, W.W.; Armon, C.; Barohn, R.J.; Goodpasture, J.C.; Hoagland, R.J.; Parry, G.J.; Ross, M.A.; Stromatt, S.C. A placebo-controlled trial of recombinant human ciliary neurotrophic (rhCNTF) factor in amyotrophic lateral sclerosis. rhCNTF ALS Study Group. *Ann. Neurol.* **1996**, *39*, 256–260. [CrossRef]
755. Manfredsson, F.P.; Polinski, N.K.; Subramanian, T.; Boulis, N.; Wakeman, D.R.; Mandel, R.J. The Future of GDNF in Parkinson's Disease. *Front. Aging Neurosci.* **2020**, *12*, 593572. [CrossRef]
756. Zivin, J.A. Factors determining the therapeutic window for stroke. *Neurology* **1998**, *50*, 599–603. [CrossRef]
757. Del Zoppo, G.J.; Sharp, F.R.; Heiss, W.D.; Albers, G.W. Heterogeneity in the penumbra. *J. Cereb. Blood Flow Metab.* **2011**, *31*, 1836–1851. [CrossRef]
758. Menzies, S.A.; Betz, A.L.; Hoff, J.T. Contributions of ions and albumin to the formation and resolution of ischemic brain edema. *J. Neurosurg.* **1993**, *78*, 257–266. [CrossRef]
759. Belayev, L.; Busto, R.; Zhao, W.; Ginsberg, M.D. Quantitative evaluation of blood-brain barrier permeability following middle cerebral artery occlusion in rats. *Brain Res.* **1996**, *739*, 88–96. [CrossRef]
760. Latour, L.L.; Kang, D.W.; Ezzeddine, M.A.; Chalela, J.A.; Warach, S. Early blood-brain barrier disruption in human focal brain ischemia. *Ann. Neurol.* **2004**, *56*, 468–477. [CrossRef]
761. Bogousslavsky, J.; Victor, S.J.; Salinas, E.O.; Pallay, A.; Donnan, G.A.; Fieschi, C.; Kaste, M.; Orgogozo, J.M.; Chamorro, A.; Desmet, A.; et al. Fiblast (trafermin) in acute stroke: Results of the European-Australian phase II/III safety and efficacy trial. *Cerebrovasc. Dis.* **2002**, *14*, 239–251. [CrossRef] [PubMed]
762. Ehrenreich, H.; Weissenborn, K.; Prange, H.; Schneider, D.; Weimar, C.; Wartenberg, K.; Schellinger, P.D.; Bohn, M.; Becker, H.; Wegrzyn, M.; et al. Recombinant human erythropoietin in the treatment of acute ischemic stroke. *Stroke* **2009**, *40*, e647–e656. [CrossRef] [PubMed]
763. Ehrenreich, H.; Hasselblatt, M.; Dembowski, C.; Cepek, L.; Lewczuk, P.; Stiefel, M.; Rustenbeck, H.H.; Breiter, N.; Jacob, S.; Knerlich, F.; et al. Erythropoietin therapy for acute stroke is both safe and beneficial. *Mol. Med.* **2002**, *8*, 495–505. [CrossRef]
764. Pardridge, W.M.; Wu, D.; Sakane, T. Combined use of carboxyl-directed protein pegylation and vector-mediated blood-brain barrier drug delivery system optimizes brain uptake of brain-derived neurotrophic factor following intravenous administration. *Pharm. Res.* **1998**, *15*, 576–582. [CrossRef] [PubMed]
765. Wu, D.; Pardridge, W.M. Neuroprotection with noninvasive neurotrophin delivery to the brain. *Proc. Natl. Acad. Sci. USA* **1999**, *96*, 254–259. [CrossRef]

766. Zhang, Y.; Pardridge, W.M. Neuroprotection in transient focal brain ischemia after delayed intravenous administration of brain-derived neurotrophic factor conjugated to a blood-brain barrier drug targeting system. *Stroke* **2001**, *32*, 1378–1384. [CrossRef]
767. Zhang, Y.; Pardridge, W.M. Blood-brain barrier targeting of BDNF improves motor function in rats with middle cerebral artery occlusion. *Brain Res.* **2006**, *1111*, 227–229. [CrossRef]
768. Zhou, Q.H.; Boado, R.J.; Lu, J.Z.; Hui, E.K.; Pardridge, W.M. Monoclonal antibody-glial-derived neurotrophic factor fusion protein penetrates the blood-brain barrier in the mouse. *Drug Metab. Dispos.* **2010**, *38*, 566–572. [CrossRef]
769. Elliott, S.; Pham, E.; Macdougall, I.C. Erythropoietins: A common mechanism of action. *Exp. Hematol* **2008**, *36*, 1573–1584. [CrossRef]
770. Zhou, Q.H.; Boado, R.J.; Lu, J.Z.; Hui, E.K.; Pardridge, W.M. Re-engineering erythropoietin as an IgG fusion protein that penetrates the blood-brain barrier in the mouse. *Mol. Pharm.* **2010**, *7*, 2148–2155. [CrossRef]
771. Peppel, K.; Crawford, D.; Beutler, B. A tumor necrosis factor (TNF) receptor-IgG heavy chain chimeric protein as a bivalent antagonist of TNF activity. *J. Exp. Med.* **1991**, *174*, 1483–1489. [CrossRef]
772. Lee, C.C.; Najafzadeh, M.; Kesselheim, A.S.; Sarpatwari, A. Cost to Medicare of Delayed Adalimumab Biosimilar Availability. *Clin. Pharmacol. Ther.* **2021**, *110*, 1050–1056. [CrossRef]
773. Bonetti, N.R.; Diaz-Canestro, C.; Liberale, L.; Crucet, M.; Akhmedov, A.; Merlini, M.; Reiner, M.F.; Gobbato, S.; Stivala, S.; Kollias, G.; et al. Tumour Necrosis Factor-alpha Inhibition Improves Stroke Outcome in a Mouse Model of Rheumatoid Arthritis. *Sci. Rep.* **2019**, *9*, 2173. [CrossRef]
774. Xue, Y.; Zeng, X.; Tu, W.J.; Zhao, J. Tumor Necrosis Factor-alpha: The Next Marker of Stroke. *Dis. Markers* **2022**, *2022*, 2395269. [CrossRef]
775. Chang, R.; Knox, J.; Chang, J.; Derbedrossian, A.; Vasilevko, V.; Cribbs, D.; Boado, R.J.; Pardridge, W.M.; Sumbria, R.K. Blood-Brain Barrier Penetrating Biologic TNF-alpha Inhibitor for Alzheimer's Disease. *Mol. Pharm.* **2017**, *14*, 2340–2349. [CrossRef]
776. Wang, Q.; Liu, Y.; Zhou, J. Neuroinflammation in Parkinson's disease and its potential as therapeutic target. *Transl. Neurodegener.* **2015**, *4*, 19. [CrossRef] [PubMed]
777. Pajares, M.; Rojo, A.I.; Manda, G.; Boscá, L.; Cuadrado, A. Inflammation in Parkinson's Disease: Mechanisms and Therapeutic Implications. *Cells* **2020**, *9*, 1687. [CrossRef] [PubMed]
778. Nawashiro, H.; Martin, D.; Hallenbeck, J.M. Neuroprotective effects of TNF binding protein in focal cerebral ischemia. *Brain Res.* **1997**, *778*, 265–271. [CrossRef]
779. Knoblach, S.M.; Fan, L.; Faden, A.I. Early neuronal expression of tumor necrosis factor-alpha after experimental brain injury contributes to neurological impairment. *J. Neuroimmunol.* **1999**, *95*, 115–125. [CrossRef]
780. Shoji-Hosaka, E.; Kobayashi, Y.; Wakitani, M.; Uchida, K.; Niwa, R.; Nakamura, K.; Shitara, K. Enhanced Fc-dependent cellular cytotoxicity of Fc fusion proteins derived from TNF receptor II and LFA-3 by fucose removal from Asn-linked oligosaccharides. *J. Biochem.* **2006**, *140*, 777–783. [CrossRef]
781. Chan, K.F.; Siegel, M.R.; Lenardo, J.M. Signaling by the TNF receptor superfamily and T cell homeostasis. *Immunity* **2000**, *13*, 419–422. [CrossRef]
782. Boado, R.J.; Hui, E.K.; Lu, J.Z.; Zhou, Q.H.; Pardridge, W.M. Selective targeting of a TNFR decoy receptor pharmaceutical to the primate brain as a receptor-specific IgG fusion protein. *J. Biotechnol.* **2010**, *146*, 84–91. [CrossRef]
783. Zhou, Q.H.; Boado, R.J.; Hui, E.K.; Lu, J.Z.; Pardridge, W.M. Brain-penetrating tumor necrosis factor decoy receptor in the mouse. *Drug Metab. Dispos.* **2011**, *39*, 71–76. [CrossRef]
784. Atwal, J.K.; Chen, Y.; Chiu, C.; Mortensen, D.L.; Meilandt, W.J.; Liu, Y.; Heise, C.E.; Hoyte, K.; Luk, W.; Lu, Y.; et al. A therapeutic antibody targeting BACE1 inhibits amyloid-beta production in vivo. *Sci. Transl. Med.* **2011**, *3*, 84ra43. [CrossRef]
785. Bohrmann, B.; Baumann, K.; Benz, J.; Gerber, F.; Huber, W.; Knoflach, F.; Messer, J.; Oroszlan, K.; Rauchenberger, R.; Richter, W.F.; et al. Gantenerumab: A novel human anti-Abeta antibody demonstrates sustained cerebral amyloid-beta binding and elicits cell-mediated removal of human amyloid-beta. *J. Alzheimer's Dis.* **2012**, *28*, 49–69. [CrossRef]
786. Pardridge, W.M. Alzheimer's disease: Future drug development and the blood-brain barrier. *Expert Opin. Investig. Drugs* **2019**, *28*, 569–572. [CrossRef]
787. Vellas, B.; Carrillo, M.C.; Sampaio, C.; Brashear, H.R.; Siemers, E.; Hampel, H.; Schneider, L.S.; Weiner, M.; Doody, R.; Khachaturian, Z.; et al. Designing drug trials for Alzheimer's disease: What we have learned from the release of the phase III antibody trials: A report from the EU/US/CTAD Task Force. *Alzheimer's Dement.* **2013**, *9*, 438–444. [CrossRef]
788. Laske, C.; De La Torre, J.C.; Doody, R.S.; Farlow, M.; Aisen, P.S.; Alzheimer's Disease Cooperative Study Data Analysis and Publication Committee; Salloway, S.; Sperling, R.; Brashear, H.R. Phase 3 trials of solanezumab and bapineuzumab for Alzheimer's disease. *N. Engl. J. Med.* **2014**, *370*, 1460. [CrossRef]
789. Bard, F.; Fox, M.; Friedrich, S.; Seubert, P.; Schenk, D.; Kinney, G.G.; Yednock, T. Sustained levels of antibodies against Aβeta in amyloid-rich regions of the CNS following intravenous dosing in human APP transgenic mice. *Exp. Neurol.* **2012**, *238*, 38–43. [CrossRef]
790. Sevigny, J.; Chiao, P.; Bussiere, T.; Weinreb, P.H.; Williams, L.; Maier, M.; Dunstan, R.; Salloway, S.; Chen, T.; Ling, Y.; et al. The antibody aducanumab reduces Aβeta plaques in Alzheimer's disease. *Nature* **2016**, *537*, 50–56. [CrossRef]
791. Cummings, J.L.; Cohen, S.; van Dyck, C.H.; Brody, M.; Curtis, C.; Cho, W.; Ward, M.; Friesenhahn, M.; Rabe, C.; Brunstein, F.; et al. ABBY: A phase 2 randomized trial of crenezumab in mild to moderate Alzheimer disease. *Neurology* **2018**, *90*, e1889–e1897. [CrossRef]

792. Salloway, S.; Honigberg, L.A.; Cho, W.; Ward, M.; Friesenhahn, M.; Brunstein, F.; Quartino, A.; Clayton, D.; Mortensen, D.; Bittner, T.; et al. Amyloid positron emission tomography and cerebrospinal fluid results from a crenezumab anti-amyloid-beta antibody double-blind, placebo-controlled, randomized phase II study in mild-to-moderate Alzheimer's disease (BLAZE). *Alzheimer's Res. Ther.* **2018**, *10*, 96. [CrossRef]
793. Liu, K.Y.; Howard, R. Can we learn lessons from the FDA's approval of aducanumab? *Nat. Rev. Neurol.* **2021**, *17*, 715–722. [CrossRef]
794. Boado, R.J.; Zhou, Q.H.; Lu, J.Z.; Hui, E.K.; Pardridge, W.M. Pharmacokinetics and brain uptake of a genetically engineered bifunctional fusion antibody targeting the mouse transferrin receptor. *Mol. Pharm.* **2010**, *7*, 237–244. [CrossRef]
795. Wilcock, D.M.; Rojiani, A.; Rosenthal, A.; Levkowitz, G.; Subbarao, S.; Alamed, J.; Wilson, D.; Wilson, N.; Freeman, M.J.; Gordon, M.N.; et al. Passive amyloid immunotherapy clears amyloid and transiently activates microglia in a transgenic mouse model of amyloid deposition. *J. Neurosci.* **2004**, *24*, 6144–6151. [CrossRef]
796. Hultqvist, G.; Syvanen, S.; Fang, X.T.; Lannfelt, L.; Sehlin, D. Bivalent Brain Shuttle Increases Antibody Uptake by Monovalent Binding to the Transferrin Receptor. *Theranostics* **2017**, *7*, 308–318. [CrossRef]
797. Logovinsky, V.; Satlin, A.; Lai, R.; Swanson, C.; Kaplow, J.; Osswald, G.; Basun, H.; Lannfelt, L. Safety and tolerability of BAN2401—A clinical study in Alzheimer's disease with a protofibril selective Abeta antibody. *Alzheimer's Res. Ther.* **2016**, *8*, 14. [CrossRef]
798. Karaoglu Hanzatian, D.; Schwartz, A.; Gizatullin, F.; Erickson, J.; Deng, K.; Villanueva, R.; Stedman, C.; Harris, C.; Ghayur, T.; Goodearl, A. Brain uptake of multivalent and multi-specific DVD-Ig proteins after systemic administration. *mAbs* **2018**, *10*, 765–777. [CrossRef] [PubMed]
799. O'Byrne, K.J.; Goggins, M.G.; McDonald, G.S.; Daly, P.A.; Kelleher, D.P.; Weir, D.G. A metastatic neuroendocrine anaplastic small cell tumor in a patient with multiple endocrine neoplasia type 1 syndrome. Assessment of disease status and response to doxorubicin, cyclophosphamide, etoposide chemotherapy through scintigraphic imaging with <sup>111</sup>In-pentetreotide. *Cancer* **1994**, *74*, 2374–2378. [CrossRef] [PubMed]
800. Vesterinen, T.; Leijon, H.; Mustonen, H.; Remes, S.; Knuutila, A.; Salmenkivi, K.; Vainio, P.; Arola, J.; Haglund, C. Somatostatin Receptor Expression Is Associated With Metastasis and Patient Outcome in Pulmonary Carcinoid Tumors. *J. Clin. Endocrinol. Metab.* **2019**, *104*, 2083–2093. [CrossRef] [PubMed]
801. Russo, A.F. Overview of Neuropeptides: Awakening the Senses? *Headache* **2017**, *57* (Suppl. S2), 37–46. [CrossRef] [PubMed]
802. Pardridge, W.M. Neuropeptides and the blood-brain barrier. *Annu. Rev. Physiol.* **1983**, *45*, 73–82. [CrossRef]
803. Xu, H.; Zong, H.; Ma, C.; Ming, X.; Shang, M.; Li, K.; He, X.; Du, H.; Cao, L. Epidermal growth factor receptor in glioblastoma. *Oncol. Lett.* **2017**, *14*, 512–516. [CrossRef]
804. Kurihara, A.; Pardridge, W.M. Imaging brain tumors by targeting peptide radiopharmaceuticals through the blood-brain barrier. *Cancer Res.* **1999**, *59*, 6159–6163.
805. Kurihara, A.; Deguchi, Y.; Pardridge, W.M. Epidermal growth factor radiopharmaceuticals: <sup>111</sup>In chelation, conjugation to a blood-brain barrier delivery vector via a biotin-polyethylene linker, pharmacokinetics, and in vivo imaging of experimental brain tumors. *Bioconjug. Chem.* **1999**, *10*, 502–511. [CrossRef]
806. Suzuki, T.; Wu, D.; Schlachetzki, F.; Li, J.Y.; Boado, R.J.; Pardridge, W.M. Imaging endogenous gene expression in brain cancer in vivo with <sup>111</sup>In-peptide nucleic acid antisense radiopharmaceuticals and brain drug-targeting technology. *J. Nucl. Med.* **2004**, *45*, 1766–1775.
807. Cimini, A.; Ricci, M.; Russo, F.; Egidi, M.; Calabria, F.; Bagnato, A.; Schillaci, O.; Chiaravalloti, A. Peptide Receptor Radionuclide Therapy and Primary Brain Tumors: An Overview. *Pharmaceutics* **2021**, *14*, 872. [CrossRef]
808. Hall, A.J.; Haskali, M.B. Radiolabeled peptides: Optimal candidates for theranostic application in oncology. *Aust. J. Chem.* **2022**, *75*, 34–54. [CrossRef]
809. Catalani, E.; De Palma, C.; Perrotta, C.; Cervia, D. Current Evidence for a Role of Neuropeptides in the Regulation of Autophagy. *BioMed. Res. Int.* **2017**, *2017*, 5856071. [CrossRef]
810. Hnatowich, D.J. Antisense and nuclear medicine. *J. Nucl. Med.* **1999**, *40*, 693–703.
811. Heckl, S.; Pipkorn, R.; Nagele, T.; Vogel, U.; Kuker, W.; Voight, K. Molecular imaging: Bridging the gap between neuroradiology and neurohistology. *Histol. Histopathol.* **2004**, *19*, 651–668. [CrossRef]
812. Agrawal, S. The Evolution of Antisense Oligonucleotide Chemistry—A Personal Journey. *Biomedicines* **2021**, *9*, 503. [CrossRef] [PubMed]
813. Knudsen, H.; Nielsen, P.E. Antisense properties of duplex- and triplex-forming PNAs. *Nucleic Acids Res.* **1996**, *24*, 494–500. [CrossRef] [PubMed]
814. Pardridge, W.M.; Boado, R.J.; Kang, Y.S. Vector-mediated delivery of a polyamide (“peptide”) nucleic acid analogue through the blood-brain barrier in vivo. *Proc. Natl. Acad. Sci. USA* **1995**, *92*, 5592–5596. [CrossRef] [PubMed]
815. Wilhelmsson, U.; Eliasson, C.; Bjerkvig, R.; Pekny, M. Loss of GFAP expression in high-grade astrocytomas does not contribute to tumor development or progression. *Oncogene* **2003**, *22*, 3407–3411. [CrossRef] [PubMed]
816. Tavittian, B. In vivo imaging with oligonucleotides for diagnosis and drug development. *Gut* **2003**, *52* (Suppl. S4), iv40–iv47. [CrossRef] [PubMed]

817. Penichet, M.L.; Kang, Y.S.; Pardridge, W.M.; Morrison, S.L.; Shin, S.U. An antibody-avidin fusion protein specific for the transferrin receptor serves as a delivery vehicle for effective brain targeting: Initial applications in anti-HIV antisense drug delivery to the brain. *J. Immunol.* **1999**, *163*, 4421–4426. [PubMed]
818. Manthey, K.C.; Griffin, J.B.; Zempleni, J. Biotin supply affects expression of biotin transporters, biotinylation of carboxylases and metabolism of interleukin-2 in Jurkat cells. *J. Nutr.* **2002**, *132*, 887–892. [CrossRef]
819. Green, N.M. Avidin. *Adv. Protein Chem.* **1975**, *29*, 85–133. [CrossRef]
820. Zhou, Q.H.; Lu, J.Z.; Hui, E.K.; Boado, R.J.; Pardridge, W.M. Delivery of a peptide radiopharmaceutical to brain with an IgG-avidin fusion protein. *Bioconj. Chem.* **2011**, *22*, 1611–1618. [CrossRef]
821. Ono, M.; Cheng, Y.; Kimura, H.; Cui, M.; Kagawa, S.; Nishii, R.; Saji, H. Novel 18F-labeled benzofuran derivatives with improved properties for positron emission tomography (PET) imaging of beta-amyloid plaques in Alzheimer's brains. *J. Med. Chem.* **2011**, *54*, 2971–2979. [CrossRef]
822. Arakawa, Y.; Nai, Y.; Shidahara, M.; Furumoto, S.; Seki, C.; Okamura, N.; Tashiro, M.; Kudo, Y.; Yanai, K.; Gonda, K.; et al. Prediction of the Clinical SUV Ratio in Amyloid PET Imaging Using a Biomathematic Modeling Approach Toward the Efficient Development of a Radioligand. *J. Nucl. Med.* **2017**, *58*, 1285–1292. [CrossRef]
823. Yetisgin, A.A.; Cetinel, S.; Zuvin, M.; Kosar, A.; Kutlu, O. Therapeutic Nanoparticles and Their Targeted Delivery Applications. *Molecules* **2020**, *25*, 2193. [CrossRef]
824. Mitchell, M.J.; Billingsley, M.M.; Haley, R.M.; Wechsler, M.E.; Peppas, N.A.; Langer, R. Engineering precision nanoparticles for drug delivery. *Nat. Rev. Drug Discov.* **2021**, *20*, 101–124. [CrossRef]
825. Kreuter, J.; Shamenkov, D.; Petrov, V.; Ramge, P.; Cychutek, K.; Koch-Brandt, C.; Alyautdin, R. Apolipoprotein-mediated transport of nanoparticle-bound drugs across the blood-brain barrier. *J. Drug Target.* **2002**, *10*, 317–325. [CrossRef]
826. Petri, B.; Bootz, A.; Khalansky, A.; Hekmatara, T.; Muller, R.; Uhl, R.; Kreuter, J.; Gelperina, S. Chemotherapy of brain tumour using doxorubicin bound to surfactant-coated poly(butyl cyanoacrylate) nanoparticles: Revisiting the role of surfactants. *J. Control. Release* **2007**, *117*, 51–58. [CrossRef]
827. Ueno, M.; Nakagawa, T.; Nagai, Y.; Nishi, N.; Kusaka, T.; Kanenishi, K.; Onodera, M.; Hosomi, N.; Huang, C.; Yokomise, H.; et al. The expression of CD36 in vessels with blood-brain barrier impairment in a stroke-prone hypertensive model. *Neuropathol. Appl. Neurobiol.* **2011**, *37*, 727–737. [CrossRef]
828. Gillotte-Taylor, K.; Boullier, A.; Witztum, J.L.; Steinberg, D.; Quehenberger, O. Scavenger receptor class B type I as a receptor for oxidized low density lipoprotein. *J. Lipid Res.* **2001**, *42*, 1474–1482. [CrossRef]
829. Ioghen, O.; Chitoiu, L.; Gherghiceanu, M.; Ceafalan, L.C.; Hinescu, M.E. CD36—A novel molecular target in the neurovascular unit. *Eur. J. Neurosci.* **2021**, *53*, 2500–2510. [CrossRef]
830. Voigt, N.; Henrich-Noack, P.; Kockentiedt, S.; Hintz, W.; Tomas, J.; Sabel, B.A. Surfactants, not size or zeta-potential influence blood-brain barrier passage of polymeric nanoparticles. *Eur. J. Pharm. Biopharm.* **2014**, *87*, 19–29. [CrossRef]
831. Gref, R.; Luck, M.; Quellec, P.; Marchand, M.; Dellacherie, E.; Harnisch, S.; Blunk, T.; Muller, R.H. 'Stealth' corona-core nanoparticles surface modified by polyethylene glycol (PEG): Influences of the corona (PEG chain length and surface density) and of the core composition on phagocytic uptake and plasma protein adsorption. *Colloids Surf. B Biointerfaces* **2000**, *18*, 301–313. [CrossRef]
832. Gref, R.; Domb, A.; Quellec, P.; Blunk, T.; Muller, R.H.; Verbavatz, J.M.; Langer, R. The controlled intravenous delivery of drugs using PEG-coated sterically stabilized nanospheres. *Adv. Drug Deliv. Rev.* **1995**, *16*, 215–233. [CrossRef]
833. Kannan, S.; Dai, H.; Navath, R.S.; Balakrishnan, B.; Jyoti, A.; Janisse, J.; Romero, R.; Kannan, R.M. Dendrimer-based postnatal therapy for neuroinflammation and cerebral palsy in a rabbit model. *Sci. Transl. Med.* **2012**, *4*, 130ra146. [CrossRef]
834. Kurokawa, Y.; Sone, H.; Win-Shwe, T.T.; Zeng, Y.; Kimura, H.; Koyama, Y.; Yagi, Y.; Matsui, Y.; Yamazaki, M.; Hirano, S. Aggregation is a critical cause of poor transfer into the brain tissue of intravenously administered cationic PAMAM dendrimer nanoparticles. *Int. J. Nanomed.* **2017**, *12*, 3967–3975. [CrossRef]
835. Plank, C.; Tang, M.X.; Wolfe, A.R.; Szoka, F.C., Jr. Branched cationic peptides for gene delivery: Role of type and number of cationic residues in formation and in vitro activity of DNA polyplexes. *Hum. Gene Ther.* **1999**, *10*, 319–332. [CrossRef]
836. Zheng, S.; Xie, Y.; Li, Y.; Li, L.; Tian, N.; Zhu, W.; Yan, G.; Wu, C.; Hu, H. Development of high drug-loading nanomicelles targeting steroids to the brain. *Int. J. Nanomed.* **2014**, *9*, 55–66. [CrossRef]
837. Olakanmi, O.; Rasmussen, G.T.; Lewis, T.S.; Stokes, J.B.; Kemp, J.D.; Britigan, B.E. Multivalent metal-induced iron acquisition from transferrin and lactoferrin by myeloid cells. *J. Immunol.* **2002**, *169*, 2076–2084. [CrossRef]
838. Chung, E.J.; Cheng, Y.; Morshed, R.; Nord, K.; Han, Y.; Wegscheid, M.L.; Auffinger, B.; Wainwright, D.A.; Lesniak, M.S.; Tirrell, M.V. Fibrin-binding, peptide amphiphile micelles for targeting glioblastoma. *Biomaterials* **2014**, *35*, 1249–1256. [CrossRef]
839. Zou, D.; Wang, W.; Lei, D.; Yin, Y.; Ren, P.; Chen, J.; Yin, T.; Wang, B.; Wang, G.; Wang, Y. Penetration of blood-brain barrier and antitumor activity and nerve repair in glioma by doxorubicin-loaded monosialoganglioside micelles system. *Int. J. Nanomed.* **2017**, *12*, 4879–4889. [CrossRef] [PubMed]
840. Schnitzer, J.E.; Oh, P. Albondin-mediated capillary permeability to albumin. Differential role of receptors in endothelial transcytosis and endocytosis of native and modified albumins. *J. Biol. Chem.* **1994**, *269*, 6072–6082. [CrossRef]
841. Pardridge, W.M.; Eisenberg, J.; Cefalu, W.T. Absence of albumin receptor on brain capillaries in vivo or in vitro. *Am. J. Physiol.* **1985**, *249*, E264–E267. [CrossRef] [PubMed]

842. Weber, C.; Kreuter, J.; Langer, K. Desolvation process and surface characteristics of HSA-nanoparticles. *Int. J. Pharm.* **2000**, *196*, 197–200. [CrossRef]
843. Zensi, A.; Begley, D.; Pontikis, C.; Legros, C.; Mihoreanu, L.; Wagner, S.; Buchel, C.; von Briesen, H.; Kreuter, J. Albumin nanoparticles targeted with Apo E enter the CNS by transcytosis and are delivered to neurones. *J. Control. Release* **2009**, *137*, 78–86. [CrossRef]
844. Bultel-Brienne, S.; Lestavel, S.; Pilon, A.; Laffont, I.; Tailleux, A.; Fruchart, J.C.; Siest, G.; Clavey, V. Lipid free apolipoprotein E binds to the class B Type I scavenger receptor I (SR-BI) and enhances cholesteryl ester uptake from lipoproteins. *J. Biol. Chem.* **2002**, *277*, 36092–36099. [CrossRef]
845. Bergonzi, M.C.; Guccione, C.; Grossi, C.; Piazzini, V.; Torracchi, A.; Luccarini, I.; Casamenti, F.; Bilia, A.R. Albumin Nanoparticles for Brain Delivery: A Comparison of Chemical versus Thermal Methods and in vivo Behavior. *ChemMedChem*. **2016**, *11*, 1840–1849. [CrossRef]
846. Ozawa, T.; Britz, G.W.; Kinder, D.H.; Spence, A.M.; VandenBerg, S.; Lamborn, K.R.; Deen, D.F.; Berger, M.S. Bromophenol blue staining of tumors in a rat glioma model. *Neurosurgery* **2005**, *57*, 1041–1047. [CrossRef]
847. Siegal, T.; Horowitz, A.; Gabizon, A. Doxorubicin encapsulated in sterically stabilized liposomes for the treatment of a brain tumor model: Biodistribution and therapeutic efficacy. *J. Neurosurg.* **1995**, *83*, 1029–1037. [CrossRef]
848. Bondi, M.L.; Di Gesu, R.; Craparo, E.F. Lipid nanoparticles for drug targeting to the brain. *Methods Enzymol.* **2012**, *508*, 229–251. [CrossRef]
849. Tenchov, R.; Bird, R.; Curtze, A.E.; Zhou, Q. Lipid Nanoparticles-From Liposomes to mRNA Vaccine Delivery, a Landscape of Research Diversity and Advancement. *ACS Nano* **2021**, *15*, 16982–17015. [CrossRef]
850. Gastaldi, L.; Battaglia, L.; Peira, E.; Chirio, D.; Muntoni, E.; Solazzi, I.; Gallarate, M.; Dosio, F. Solid lipid nanoparticles as vehicles of drugs to the brain: Current state of the art. *Eur. J. Pharm. Biopharm.* **2014**, *87*, 433–444. [CrossRef]
851. Martins, S.M.; Sarmiento, B.; Nunes, C.; Lucio, M.; Reis, S.; Ferreira, D.C. Brain targeting effect of camptothecin-loaded solid lipid nanoparticles in rat after intravenous administration. *Eur. J. Pharm. Biopharm.* **2013**, *85*, 488–502. [CrossRef]
852. Costa, P.M.; Bourgoignon, M.; Wang, J.T.; Al-Jamal, K.T. Functionalised carbon nanotubes: From intracellular uptake and cell-related toxicity to systemic brain delivery. *J. Control. Release* **2016**, *241*, 200–219. [CrossRef]
853. Yang, Z.; Zhang, Y.; Yang, Y.; Sun, L.; Han, D.; Li, H.; Wang, C. Pharmacological and toxicological target organelles and safe use of single-walled carbon nanotubes as drug carriers in treating Alzheimer disease. *Nanomedicine* **2010**, *6*, 427–441. [CrossRef]
854. Shityakov, S.; Salvador, E.; Pastorin, G.; Forster, C. Blood-brain barrier transport studies, aggregation, and molecular dynamics simulation of multiwalled carbon nanotube functionalized with fluorescein isothiocyanate. *Int. J. Nanomed.* **2015**, *10*, 1703–1713. [CrossRef]
855. Gonzalez-Carter, D.; Goode, A.E.; Kiryushko, D.; Masuda, S.; Hu, S.; Lopes-Rodrigues, R.; Dexter, D.T.; Shaffer, M.S.P.; Porter, A.E. Quantification of blood-brain barrier transport and neuronal toxicity of unlabelled multiwalled carbon nanotubes as a function of surface charge. *Nanoscale* **2019**, *11*, 22054–22069. [CrossRef] [PubMed]
856. Wong, B.S.; Yoong, S.L.; Jagusiak, A.; Panczyk, T.; Ho, H.K.; Ang, W.H.; Pastorin, G. Carbon nanotubes for delivery of small molecule drugs. *Adv. Drug Deliv. Rev.* **2013**, *65*, 1964–2015. [CrossRef]
857. Liu, G.; Shen, H.; Mao, J.; Zhang, L.; Jiang, Z.; Sun, T.; Lan, Q.; Zhang, Z. Transferrin modified graphene oxide for glioma-targeted drug delivery: In vitro and in vivo evaluations. *ACS Appl. Mater. Interfaces* **2013**, *5*, 6909–6914. [CrossRef]
858. Hardt, J.I.; Perlmutter, J.S.; Smith, C.J.; Quick, K.L.; Wei, L.; Chakraborty, S.K.; Dugan, L.L. Pharmacokinetics and Toxicology of the Neuroprotective e,e,e-Methanofullerene(60)-63-tris Malonic Acid [C<sub>3</sub>] in Mice and Primates. *Eur. J. Drug Metab. Pharmacokinet.* **2018**, *43*, 543–554. [CrossRef]
859. Ahn, M.; Song, J.; Hong, B.H. Facile Synthesis of N-Doped Graphene Quantum Dots as Novel Transfection Agents for mRNA and pDNA. *Nanomaterials* **2021**, *11*, 2816. [CrossRef]
860. Seven, E.S.; Seven, Y.B.; Zhou, Y.; Poudel-Sharma, S.; Diaz-Rucco, J.J.; Kirbas Cilingir, E.; Mitchell, G.S.; Van Dyken, J.D.; Leblanc, R.M. Crossing the blood-brain barrier with carbon dots: Uptake mechanism and in vivo cargo delivery. *Nanoscale Adv.* **2021**, *3*, 3942–3953. [CrossRef]
861. Sousa, F.; Mandal, S.; Garrovo, C.; Astolfo, A.; Bonifacio, A.; Latawiec, D.; Menk, R.H.; Arfelli, F.; Huewel, S.; Legname, G.; et al. Functionalized gold nanoparticles: A detailed in vivo multimodal microscopic brain distribution study. *Nanoscale* **2010**, *2*, 2826–2834. [CrossRef]
862. Li, X.; Vemireddy, V.; Cai, Q.; Xiong, H.; Kang, P.; Li, X.; Giannotta, M.; Hayenga, H.N.; Pan, E.; Sirsi, S.R.; et al. Reversibly Modulating the Blood-Brain Barrier by Laser Stimulation of Molecular-Targeted Nanoparticles. *Nano Lett* **2021**, *21*, 9805–9815. [CrossRef] [PubMed]
863. Jensen, S.A.; Day, E.S.; Ko, C.H.; Hurley, L.A.; Luciano, J.P.; Kouri, F.M.; Merkel, T.J.; Luthi, A.J.; Patel, P.C.; Cutler, J.I.; et al. Spherical nucleic acid nanoparticle conjugates as an RNAi-based therapy for glioblastoma. *Sci. Transl. Med.* **2013**, *5*, 209ra152. [CrossRef] [PubMed]
864. Behroozi, Z.; Rahimi, B.; Kookli, K.; Safari, M.S.; Hamblin, M.R.; Razmgir, M.; Janzadeh, A.; Ramezani, F. Distribution of gold nanoparticles into the brain: A systematic review and meta-analysis. *Nanotoxicology* **2021**, *15*, 1059–1072. [CrossRef] [PubMed]
865. Sela, H.; Cohen, H.; Elia, P.; Zach, R.; Karpas, Z.; Zeiri, Y. Spontaneous penetration of gold nanoparticles through the blood brain barrier (BBB). *J. Nanobiotechnol.* **2015**, *13*, 71. [CrossRef]

866. Koch, S.E.; Bodi, I.; Schwartz, A.; Varadi, G. Architecture of Ca<sup>2+</sup> channel pore-lining segments revealed by covalent modification of substituted cysteines. *J. Biol. Chem.* **2000**, *275*, 34493–34500. [CrossRef]
867. Hou, X.; Pedi, L.; Diver, M.M.; Long, S.B. Crystal structure of the calcium release-activated calcium channel Orai. *Science* **2012**, *338*, 1308–1313. [CrossRef]
868. Naranjo, D.; Moldenhauer, H.; Pincuntureo, M.; Diaz-Franulic, I. Pore size matters for potassium channel conductance. *J. Gen. Physiol.* **2016**, *148*, 277–291. [CrossRef]
869. Locatelli, E.; Naddaka, M.; Uboldi, C.; Loudos, G.; Fragogeorgi, E.; Molinari, V.; Pucci, A.; Tsoதாகos, T.; Psimadas, D.; Ponti, J.; et al. Targeted delivery of silver nanoparticles and alisertib: In vitro and in vivo synergistic effect against glioblastoma. *Nanomedicine* **2014**, *9*, 839–849. [CrossRef]
870. Jampilek, J.; Zaruba, K.; Oravec, M.; Kunes, M.; Babula, P.; Ulbrich, P.; Brezaniova, I.; Opatrilova, R.; Triska, J.; Suchy, P. Preparation of silica nanoparticles loaded with nootropics and their in vivo permeation through blood-brain barrier. *BioMed. Res. Int.* **2015**, *2015*, 812673. [CrossRef]
871. Baghirov, H.; Karaman, D.; Viitala, T.; Duchanoy, A.; Lou, Y.R.; Mamaeva, V.; Pryazhnikov, E.; Khiroug, L.; de Lange Davies, C.; Sahlgren, C.; et al. Feasibility Study of the Permeability and Uptake of Mesoporous Silica Nanoparticles across the Blood-Brain Barrier. *PLoS ONE* **2016**, *11*, e0160705. [CrossRef]
872. Huang, Y.; Zhang, B.; Xie, S.; Yang, B.; Xu, Q.; Tan, J. Superparamagnetic Iron Oxide Nanoparticles Modified with Tween 80 Pass through the Intact Blood-Brain Barrier in Rats under Magnetic Field. *ACS Appl. Mater. Interfaces* **2016**, *8*, 11336–11341. [CrossRef]
873. Rohiwal, S.S.; Dvorakova, N.; Klima, J.; Vaskovicova, M.; Senigl, F.; Slouf, M.; Pavlova, E.; Stepanek, P.; Babuka, D.; Benes, H.; et al. Polyethylenimine based magnetic nanoparticles mediated non-viral CRISPR/Cas9 system for genome editing. *Sci. Rep.* **2020**, *10*, 4619. [CrossRef]
874. Pezzoli, D.; Giupponi, E.; Mantovani, D.; Candiani, G. Size matters for in vitro gene delivery: Investigating the relationships among complexation protocol, transfection medium, size and sedimentation. *Sci. Rep.* **2017**, *7*, 44134. [CrossRef]
875. Olivier, J.C.; Fenart, L.; Chauvet, R.; Pariat, C.; Cecchelli, R.; Couet, W. Indirect evidence that drug brain targeting using polysorbate 80-coated polybutylcyanoacrylate nanoparticles is related to toxicity. *Pharm. Res.* **1999**, *16*, 1836–1842. [CrossRef]
876. Anraku, Y.; Kuwahara, H.; Fukusato, Y.; Mizoguchi, A.; Ishii, T.; Nitta, K.; Matsumoto, Y.; Toh, K.; Miyata, K.; Uchida, S.; et al. Glycaemic control boosts glucosylated nanocarrier crossing the BBB into the brain. *Nat. Commun.* **2017**, *8*, 1001. [CrossRef]
877. Gajbhiye, K.R.; Gajbhiye, V.; Siddiqui, I.A.; Pilla, S.; Soni, V. Ascorbic acid tethered polymeric nanoparticles enable efficient brain delivery of galantamine: An in vitro-in vivo study. *Sci. Rep.* **2017**, *7*, 11086. [CrossRef]
878. Agus, D.B.; Gambhir, S.S.; Pardridge, W.M.; Spielholz, C.; Baselga, J.; Vera, J.C.; Golde, D.W. Vitamin C crosses the blood-brain barrier in the oxidized form through the glucose transporters. *J. Clin. Investig.* **1997**, *100*, 2842–2848. [CrossRef]
879. Hosoya, K.; Minamizono, A.; Katayama, K.; Terasaki, T.; Tomi, M. Vitamin C transport in oxidized form across the rat blood-retinal barrier. *Investig. Ophthalmol. Vis. Sci.* **2004**, *45*, 1232–1239. [CrossRef]
880. Gonzalez-Carter, D.A.; Ong, Z.Y.; McGilvery, C.M.; Dunlop, I.E.; Dexter, D.T.; Porter, A.E. L-DOPA functionalized, multi-branched gold nanoparticles as brain-targeted nano-vehicles. *Nanomedicine* **2019**, *15*, 1–11. [CrossRef]
881. Li, J.; Yang, H.; Zhang, Y.; Jiang, X.; Guo, Y.; An, S.; Ma, H.; He, X.; Jiang, C. Choline Derivate-Modified Doxorubicin Loaded Micelle for Glioma Therapy. *ACS Appl. Mater. Interfaces* **2015**, *7*, 21589–21601. [CrossRef]
882. Reginald-Opara, J.N.; Svirskis, D.; O’Carroll, S.J.; Sreebhavan, S.; Dean, J.M.; Wu, Z. Optimisation of glutathione conjugation to liposomes quantified with a validated HPLC assay. *Int. J. Pharm.* **2019**, *567*, 118451. [CrossRef]
883. Bai, L.; Sato, H.; Kubo, Y.; Wada, S.; Aida, Y. CAT1/SLC7A1 acts as a cellular receptor for bovine leukemia virus infection. *FASEB J.* **2019**, *33*, 14516–14527. [CrossRef]
884. Manel, N.; Kim, F.J.; Kinet, S.; Taylor, N.; Sitbon, M.; Battini, J.L. The ubiquitous glucose transporter GLUT-1 is a receptor for HTLV. *Cell* **2003**, *115*, 449–459. [CrossRef]
885. Xia, X. Domains and Functions of Spike Protein in Sars-Cov-2 in the Context of Vaccine Design. *Viruses* **2021**, *13*, 109. [CrossRef]
886. Dhami, N.K.; Pandey, R.S.; Jain, U.K.; Chandra, R.; Madan, J. Non-aggregated protamine-coated poly(lactide-co-glycolide) nanoparticles of cisplatin crossed blood-brain barrier, enhanced drug delivery and improved therapeutic index in glioblastoma cells: In vitro studies. *J. Microencapsul.* **2014**, *31*, 685–693. [CrossRef]
887. Lu, W.; Tan, Y.Z.; Hu, K.L.; Jiang, X.G. Cationic albumin conjugated pegylated nanoparticle with its transcytosis ability and little toxicity against blood-brain barrier. *Int. J. Pharm.* **2005**, *295*, 247–260. [CrossRef]
888. Helm, F.; Fricker, G. Liposomal conjugates for drug delivery to the central nervous system. *Pharmaceutics* **2015**, *7*, 27–42. [CrossRef]
889. Muniswamy, V.J.; Raval, N.; Gondaliya, P.; Tambe, V.; Kalia, K.; Tekade, R.K. ‘Dendrimer-Cationized-Albumin’ encrusted polymeric nanoparticle improves BBB penetration and anticancer activity of doxorubicin. *Int. J. Pharm.* **2019**, *555*, 77–99. [CrossRef]
890. Shen, Y.; Chen, J.; Liu, Q.; Feng, C.; Gao, X.; Wang, L.; Zhang, Q.; Jiang, X. Effect of wheat germ agglutinin density on cellular uptake and toxicity of wheat germ agglutinin conjugated PEG-PLA nanoparticles in Calu-3 cells. *Int. J. Pharm.* **2011**, *413*, 184–193. [CrossRef] [PubMed]
891. Huwyler, J.; Wu, D.; Pardridge, W.M. Brain drug delivery of small molecules using immunoliposomes. *Proc. Natl. Acad. Sci. USA* **1996**, *93*, 14164–14169. [CrossRef]
892. Olivier, J.C.; Huertas, R.; Lee, H.J.; Calon, F.; Pardridge, W.M. Synthesis of pegylated immunonanoparticles. *Pharm. Res.* **2002**, *19*, 1137–1143. [CrossRef] [PubMed]

893. Markoutsas, E.; Pampalakis, G.; Niarakis, A.; Romero, I.A.; Weksler, B.; Couraud, P.O.; Antimisiaris, S.G. Uptake and permeability studies of BBB-targeting immunoliposomes using the hCMEC/D3 cell line. *Eur. J. Pharm. Biopharm.* **2011**, *77*, 265–274. [CrossRef] [PubMed]
894. White, S.; Taetle, R.; Seligman, P.A.; Rutherford, M.; Trowbridge, I.S. Combinations of anti-transferrin receptor monoclonal antibodies inhibit human tumor cell growth in vitro and in vivo: Evidence for synergistic antiproliferative effects. *Cancer Res.* **1990**, *50*, 6295–6301. [PubMed]
895. Monsalve, Y.; Tosi, G.; Ruozi, B.; Belletti, D.; Vilella, A.; Zoli, M.; Vandelli, M.A.; Forni, F.; Lopez, B.L.; Sierra, L. PEG-g-chitosan nanoparticles functionalized with the monoclonal antibody OX26 for brain drug targeting. *Nanomedicine* **2015**, *10*, 1735–1750. [CrossRef]
896. Tang, X.; Liang, Y.; Zhu, Y.; Xie, C.; Yao, A.; Chen, L.; Jiang, Q.; Liu, T.; Wang, X.; Qian, Y.; et al. Anti-transferrin receptor-modified amphotericin B-loaded PLA-PEG nanoparticles cure Candidal meningitis and reduce drug toxicity. *Int. J. Nanomed.* **2015**, *10*, 6227–6241. [CrossRef]
897. Schnyder, A.; Krahenbuhl, S.; Drewe, J.; Huwyler, J. Targeting of daunomycin using biotinylated immunoliposomes: Pharmacokinetics, tissue distribution and in vitro pharmacological effects. *J. Drug Target.* **2005**, *13*, 325–335. [CrossRef]
898. Bao, H.; Jin, X.; Li, L.; Lv, F.; Liu, T. OX26 modified hyperbranched polyglycerol-conjugated poly(lactic-co-glycolic acid) nanoparticles: Synthesis, characterization and evaluation of its brain delivery ability. *J. Mater. Sci. Mater. Med.* **2012**, *23*, 1891–1901. [CrossRef]
899. Bommana, M.M.; Kirthivasan, B.; Squillante, E. In vivo brain microdialysis to evaluate FITC-dextran encapsulated immunopeglylated nanoparticles. *Drug Deliv.* **2012**, *19*, 298–306. [CrossRef]
900. Bouchoucha, M.; Beliveau, E.; Kleitz, F.; Calon, F.; Fortin, M.A. Antibody-conjugated mesoporous silica nanoparticles for brain microvessel endothelial cell targeting. *J. Mater. Chem. B* **2017**, *5*, 7721–7735. [CrossRef]
901. Cabezon, I.; Manich, G.; Martin-Venegas, R.; Camins, A.; Pelegri, C.; Vilaplana, J. Trafficking of Gold Nanoparticles Coated with the 8D3 Anti-Transferrin Receptor Antibody at the Mouse Blood-Brain Barrier. *Mol. Pharm.* **2015**, *12*, 4137–4145. [CrossRef]
902. Zhang, Y.; Schlachetzki, F.; Pardridge, W.M. Global non-viral gene transfer to the primate brain following intravenous administration. *Mol. Ther.* **2003**, *7*, 11–18. [CrossRef]
903. Dieu, L.H.; Wu, D.; Palivan, C.G.; Balasubramanian, V.; Huwyler, J. Polymersomes conjugated to 83-14 monoclonal antibodies: In vitro targeting of brain capillary endothelial cells. *Eur. J. Pharm. Biopharm.* **2014**, *88*, 316–324. [CrossRef]
904. Ulbrich, K.; Knobloch, T.; Kreuter, J. Targeting the insulin receptor: Nanoparticles for drug delivery across the blood-brain barrier (BBB). *J. Drug Target.* **2011**, *19*, 125–132. [CrossRef]
905. Morgan, D.O.; Ho, L.; Korn, L.J.; Roth, R.A. Insulin action is blocked by a monoclonal antibody that inhibits the insulin receptor kinase. *Proc. Natl. Acad. Sci. USA* **1986**, *83*, 328–332. [CrossRef]
906. Chen, Z.L.; Huang, M.; Wang, X.R.; Fu, J.; Han, M.; Shen, Y.Q.; Xia, Z.; Gao, J.Q. Transferrin-modified liposome promotes alpha-mangostin to penetrate the blood-brain barrier. *Nanomedicine* **2016**, *12*, 421–430. [CrossRef]
907. Ghadiri, M.; Vasheghani-Farahani, E.; Atyabi, F.; Kobarfard, F.; Mohamadyar-Toupkanlou, F.; Hosseinkhani, H. Transferrin-conjugated magnetic dextran-spermine nanoparticles for targeted drug transport across blood-brain barrier. *J. BioMed. Mater. Res. A* **2017**, *105*, 2851–2864. [CrossRef]
908. Lu, Q.; Cai, X.; Zhang, X.; Li, S.; Song, Y.; Du, D.; Dutta, P.; Lin, Y. Synthetic Polymer Nanoparticles Functionalized with Different Ligands for Receptor-mediated Transcytosis across Blood-Brain Barrier. *ACS Appl. Bio Mater.* **2018**, *1*, 1687–1694. [CrossRef]
909. Xiao, W.; Wang, Y.; Zhang, H.; Liu, Y.; Xie, R.; He, X.; Zhou, Y.; Liang, L.; Gao, H. The protein corona hampers the transcytosis of transferrin-modified nanoparticles through blood-brain barrier and attenuates their targeting ability to brain tumor. *Biomaterials* **2021**, *274*, 120888. [CrossRef]
910. Venishetty, V.K.; Komuravelli, R.; Kuncha, M.; Sistla, R.; Diwan, P.V. Increased brain uptake of docetaxel and ketoconazole loaded folate-grafted solid lipid nanoparticles. *Nanomedicine* **2013**, *9*, 111–121. [CrossRef]
911. Zhang, Y.; Zhu, C.; Pardridge, W.M. Antisense gene therapy of brain cancer with an artificial virus gene delivery system. *Mol. Ther.* **2002**, *6*, 67–72. [CrossRef]
912. Salvati, E.; Re, F.; Sesana, S.; Cambianica, I.; Sancini, G.; Masserini, M.; Gregori, M. Liposomes functionalized to overcome the blood-brain barrier and to target amyloid-beta peptide: The chemical design affects the permeability across an in vitro model. *Int. J. Nanomed.* **2013**, *8*, 1749–1758. [CrossRef]
913. Loureiro, J.A.; Gomes, B.; Fricker, G.; Cardoso, I.; Ribeiro, C.A.; Gaiteiro, C.; Coelho, M.A.; Pereira Mdo, C.; Rocha, S. Dual ligand immunoliposomes for drug delivery to the brain. *Colloids Surf. B Biointerfaces* **2015**, *134*, 213–219. [CrossRef]
914. Cook, R.L.; Householder, K.T.; Chung, E.P.; Prakapenka, A.V.; DiPerna, D.M.; Sirianni, R.W. A critical evaluation of drug delivery from ligand modified nanoparticles: Confounding small molecule distribution and efficacy in the central nervous system. *J. Control. Release* **2015**, *220*, 89–97. [CrossRef]
915. Dal Magro, R.; Ornaghi, F.; Cambianica, I.; Beretta, S.; Re, F.; Musicanti, C.; Rigolio, R.; Donzelli, E.; Canta, A.; Ballarini, E.; et al. ApoE-modified solid lipid nanoparticles: A feasible strategy to cross the blood-brain barrier. *J. Control. Release* **2017**, *249*, 103–110. [CrossRef]
916. Portioli, C.; Bovi, M.; Benati, D.; Donini, M.; Perduca, M.; Romeo, A.; Dusi, S.; Monaco, H.L.; Bentivoglio, M. Novel functionalization strategies of polymeric nanoparticles as carriers for brain medications. *J. BioMed. Mater. Res. A* **2017**, *105*, 847–858. [CrossRef]

917. Li, J.; Kataoka, K. Chemo-physical Strategies to Advance the in Vivo Functionality of Targeted Nanomedicine: The Next Generation. *J. Am. Chem. Soc.* **2021**, *143*, 538–559. [CrossRef]
918. Sawyer, A.J.; Saucier-Sawyer, J.K.; Booth, C.J.; Liu, J.; Patel, T.; Piepmeier, J.M.; Saltzman, W.M. Convection-enhanced delivery of camptothecin-loaded polymer nanoparticles for treatment of intracranial tumors. *Drug Deliv. Transl. Res.* **2011**, *1*, 34–42. [CrossRef]
919. Zhang, C.; Mastorakos, P.; Sobral, M.; Berry, S.; Song, E.; Nance, E.; Eberhart, C.G.; Hanes, J.; Suk, J.S. Strategies to enhance the distribution of nanotherapeutics in the brain. *J. Control. Release* **2017**, *267*, 232–239. [CrossRef]
920. Florence, K.; Manisha, L.; Kumar, B.A.; Ankur, K.; Kumar, M.A.; Ambikanandan, M. Intranasal clobazam delivery in the treatment of status epilepticus. *J. Pharm. Sci.* **2011**, *100*, 692–703. [CrossRef]
921. Arendt, R.M.; Greenblatt, D.J.; Liebisch, D.C.; Luu, M.D.; Paul, S.M. Determinants of benzodiazepine brain uptake: Lipophilicity versus binding affinity. *Psychopharmacology* **1987**, *93*, 72–76. [CrossRef]
922. Ullah, I.; Chung, K.; Bae, S.; Li, Y.; Kim, C.; Choi, B.; Nam, H.Y.; Kim, S.H.; Yun, C.O.; Lee, K.Y.; et al. Nose-to-Brain Delivery of Cancer-Targeting Paclitaxel-Loaded Nanoparticles Potentiates Antitumor Effects in Malignant Glioblastoma. *Mol. Pharm.* **2020**, *17*, 1193–1204. [CrossRef] [PubMed]
923. Ohta, S.; Kikuchi, E.; Ishijima, A.; Azuma, T.; Sakuma, I.; Ito, T. Investigating the optimum size of nanoparticles for their delivery into the brain assisted by focused ultrasound-induced blood-brain barrier opening. *Sci. Rep.* **2020**, *10*, 18220. [CrossRef] [PubMed]
924. Anselmo, A.C.; Mitragotri, S. Nanoparticles in the clinic: An update. *Bioeng. Transl. Med.* **2019**, *4*, e10143. [CrossRef] [PubMed]
925. Jena, L.; McErlean, E.; McCarthy, H. Delivery across the blood-brain barrier: Nanomedicine for glioblastoma multiforme. *Drug Deliv. Transl. Res.* **2020**, *10*, 304–318. [CrossRef]
926. Kim, S.S.; Harford, J.B.; Moghe, M.; Slaughter, T.; Doherty, C.; Chang, E.H. A tumor-targeting nanomedicine carrying the p53 gene crosses the blood-brain barrier and enhances anti-PD-1 immunotherapy in mouse models of glioblastoma. *Int. J. Cancer* **2019**, *145*, 2535–2546. [CrossRef]
927. Xu, L.; Tang, W.H.; Huang, C.C.; Alexander, W.; Xiang, L.M.; Pirollo, K.F.; Rait, A.; Chang, E.H. Systemic p53 gene therapy of cancer with immunolipoplexes targeted by anti-transferrin receptor scFv. *Mol. Med.* **2001**, *7*, 723–734. [CrossRef]
928. Daniels, T.R.; Bernabeu, E.; Rodriguez, J.A.; Patel, S.; Kozman, M.; Chiappetta, D.A.; Holler, E.; Ljubimova, J.Y.; Helguera, G.; Penichet, M.L. The transferrin receptor and the targeted delivery of therapeutic agents against cancer. *Biochim. Biophys. Acta* **2012**, *1820*, 291–317. [CrossRef]
929. Singleton, W.G.B.; Bienemann, A.S.; Woolley, M.; Johnson, D.; Lewis, O.; Wyatt, M.J.; Damment, S.J.P.; Boulter, L.J.; Kilkick-Cole, C.L.; Asby, D.J.; et al. The distribution, clearance, and brainstem toxicity of panobinostat administered by convection-enhanced delivery. *J. Neurosurg. Pediatr.* **2018**, *22*, 288–296. [CrossRef]
930. Sandberg, D.I.; Kharas, N.; Yu, B.; Janssen, C.F.; Trimble, A.; Ballester, L.Y.; Patel, R.; Mohammad, A.S.; Elmquist, W.F.; Sirianni, R.W. High-dose MTX110 (soluble panobinostat) safely administered into the fourth ventricle in a nonhuman primate model. *J. Neurosurg. Pediatr.* **2020**, *26*, 127–135. [CrossRef]
931. Lu, D.; Han, F.; Qiu, W.; Zhang, H.; Ye, J.; Liang, L.; Wang, Y.; Ji, W.; Zhan, X.; Gu, X.; et al. Clinical and molecular characteristics of 69 Chinese patients with ornithine transcarbamylase deficiency. *Orphanet J. Rare Dis.* **2020**, *15*, 340. [CrossRef]
932. Vucic, S.; Kiernan, M.C.; Menon, P.; Huynh, W.; Rynders, A.; Ho, K.S.; Glanzman, R.; Hotchkiss, M.T. Study protocol of RESCUE-ALS: A Phase 2, randomised, double-blind, placebo-controlled study in early symptomatic amyotrophic lateral sclerosis patients to assess bioenergetic catalysis with CNM-Au8 as a mechanism to slow disease progression. *BMJ Open* **2021**, *11*, e041479. [CrossRef]
933. Garbuzova-Davis, S.; Haller, E.; Saporta, S.; Kolomey, I.; Nicosia, S.V.; Sanberg, P.R. Ultrastructure of blood-brain barrier and blood-spinal cord barrier in SOD1 mice modeling ALS. *Brain Res.* **2007**, *1157*, 126–137. [CrossRef]
934. Sarkaria, J.N.; Hu, L.S.; Parney, I.F.; Pafundi, D.H.; Brinkmann, D.H.; Laack, N.N.; Giannini, C.; Burns, T.C.; Kizilbash, S.H.; Laramy, J.K.; et al. Is the blood-brain barrier really disrupted in all glioblastomas? A critical assessment of existing clinical data. *Neuro-Oncology* **2018**, *20*, 184–191. [CrossRef]
935. Kumthekar, P.; Ko, C.H.; Paunesku, T.; Dixit, K.; Sonabend, A.M.; Bloch, O.; Tate, M.; Schwartz, M.; Zuckerman, L.; Lezon, R.; et al. A first-in-human phase 0 clinical study of RNA interference-based spherical nucleic acids in patients with recurrent glioblastoma. *Sci. Transl. Med.* **2021**, *13*, eabb3945. [CrossRef]
936. Cupaioli, F.A.; Zucca, F.A.; Boraschi, D.; Zecca, L. Engineered nanoparticles. How brain friendly is this new guest? *Prog. Neurobiol.* **2014**, *119–120*, 20–38. [CrossRef]
937. Catalan-Figueroa, J.; Palma-Florez, S.; Alvarez, G.; Fritz, H.F.; Jara, M.O.; Morales, J.O. Nanomedicine and nanotoxicology: The pros and cons for neurodegeneration and brain cancer. *Nanomedicine* **2016**, *11*, 171–187. [CrossRef]
938. Cao, Y.; Luo, Y. Pharmacological and toxicological aspects of carbon nanotubes (CNTs) to vascular system: A review. *Toxicol. Appl. Pharmacol.* **2019**, *385*, 114801. [CrossRef]
939. Boyes, W.K.; van Thriel, C. Neurotoxicology of Nanomaterials. *Chem. Res. Toxicol.* **2020**, *33*, 1121–1144. [CrossRef]
940. Christop, V.V.; Prilepskii, A.Y.; Nikonorova, V.G.; Mironov, V.A. Nanosafety vs. nanotoxicology: Adequate animal models for testing in vivo toxicity of nanoparticles. *Toxicology* **2021**, *462*, 152952. [CrossRef]
941. Jung, S.; Bang, M.; Kim, B.S.; Lee, S.; Kotov, N.A.; Kim, B.; Jeon, D. Intracellular gold nanoparticles increase neuronal excitability and aggravate seizure activity in the mouse brain. *PLoS ONE* **2014**, *9*, e91360. [CrossRef]



942. Li, C.H.; Shyu, M.K.; Jhan, C.; Cheng, Y.W.; Tsai, C.H.; Liu, C.W.; Lee, C.C.; Chen, R.M.; Kang, J.J. Gold Nanoparticles Increase Endothelial Paracellular Permeability by Altering Components of Endothelial Tight Junctions, and Increase Blood-Brain Barrier Permeability in Mice. *Toxicol. Sci.* **2015**, *148*, 192–203. [CrossRef]
943. Lira-Diaz, E.; Gonzalez-Pedroza, M.G.; Vasquez, C.; Morales-Luckie, R.A.; Gonzalez-Perez, O. Gold nanoparticles produce transient reactive gliosis in the adult brain. *Neurosci. Res.* **2021**, *170*, 76–86. [CrossRef]
944. Amiri, S.; Yousefi-Ahmadipour, A.; Hosseini, M.J.; Haj-Mirzaian, A.; Momeny, M.; Hosseini-Chegeni, H.; Mokhtari, T.; Kharrazi, S.; Hassanzadeh, G.; Amini, S.M.; et al. Maternal exposure to silver nanoparticles are associated with behavioral abnormalities in adulthood: Role of mitochondria and innate immunity in developmental toxicity. *Neurotoxicology* **2018**, *66*, 66–77. [CrossRef]
945. Opris, R.V.; Toma, V.; Baci, A.M.; Moldovan, R.; Dume, B.; Berghian-Sevastre, A.; Moldovan, B.; Clichici, S.; David, L.; Filip, G.A.; et al. Neurobehavioral and Ultrastructural Changes Induced by Phytosynthesized Silver-Nanoparticle Toxicity in an In Vivo Rat Model. *Nanomaterials* **2021**, *12*, 58. [CrossRef]
946. D'Agata, F.; Ruffinatti, F.A.; Boschi, S.; Stura, I.; Rainero, I.; Abollino, O.; Cavalli, R.; Guiot, C. Magnetic Nanoparticles in the Central Nervous System: Targeting Principles, Applications and Safety Issues. *Molecules* **2017**, *23*, 9. [CrossRef]
947. Murugadoss, S.; Lison, D.; Godderis, L.; Van Den Brule, S.; Mast, J.; Brassinne, F.; Sebaihi, N.; Hoet, P.H. Toxicology of silica nanoparticles: An update. *Arch. Toxicol.* **2017**, *91*, 2967–3010. [CrossRef]
948. Song, B.; Liu, J.; Feng, X.; Wei, L.; Shao, L. A review on potential neurotoxicity of titanium dioxide nanoparticles. *Nanoscale Res. Lett.* **2015**, *10*, 1042. [CrossRef]
949. Choi, B.S.; Zheng, W. Copper transport to the brain by the blood-brain barrier and blood-CSF barrier. *Brain Res.* **2009**, *1248*, 14–21. [CrossRef]
950. Kim, H.; Wu, X.; Lee, J. SLC31 (CTR) family of copper transporters in health and disease. *Mol. Asp. Med.* **2013**, *34*, 561–570. [CrossRef]
951. Luo, N.; Weber, J.K.; Wang, S.; Luan, B.; Yue, H.; Xi, X.; Du, J.; Yang, Z.; Wei, W.; Zhou, R.; et al. PEGylated graphene oxide elicits strong immunological responses despite surface passivation. *Nat. Commun.* **2017**, *8*, 14537. [CrossRef]
952. Kraemer, A.B.; Parfitt, G.M.; Acosta, D.D.S.; Bruch, G.E.; Cordeiro, M.F.; Marins, L.F.; Ventura-Lima, J.; Monserrat, J.M.; Barros, D.M. Fullerene (C60) particle size implications in neurotoxicity following infusion into the hippocampi of Wistar rats. *Toxicol. Appl. Pharmacol.* **2018**, *338*, 197–203. [CrossRef] [PubMed]
953. Mendonca, M.C.; Soares, E.S.; de Jesus, M.B.; Ceragioli, H.J.; Ferreira, M.S.; Catharino, R.R.; da Cruz-Hofling, M.A. Reduced graphene oxide induces transient blood-brain barrier opening: An in vivo study. *J. Nanobiotechnol.* **2015**, *13*, 78. [CrossRef] [PubMed]
954. Rempe, R.; Cramer, S.; Huwel, S.; Galla, H.J. Transport of Poly(n-butylcyano-acrylate) nanoparticles across the blood-brain barrier in vitro and their influence on barrier integrity. *Biochem. Biophys. Res. Commun.* **2011**, *406*, 64–69. [CrossRef] [PubMed]
955. Yuan, Z.Y.; Hu, Y.L.; Gao, J.Q. Brain Localization and Neurotoxicity Evaluation of Polysorbate 80-Modified Chitosan Nanoparticles in Rats. *PLoS ONE* **2015**, *10*, e0134722. [CrossRef]
956. Baldrick, P. Successful regulatory agency interaction—A nonclinical regulatory strategist's perspective. *Regul. Toxicol. Pharmacol.* **2022**, *130*, 105130. [CrossRef]
957. Webb, C.; Forbes, N.; Roces, C.B.; Anderluzzi, G.; Lou, G.; Abraham, S.; Ingalls, L.; Marshall, K.; Leaver, T.J.; Watts, J.A.; et al. Using microfluidics for scalable manufacturing of nanomedicines from bench to GMP: A case study using protein-loaded liposomes. *Int. J. Pharm.* **2020**, *582*, 119266. [CrossRef]
958. Zhi, K.; Raji, B.; Nookala, A.R.; Khan, M.M.; Nguyen, X.H.; Sakshi, S.; Pourmotabbed, T.; Yallapu, M.M.; Kochat, H.; Tadrous, E.; et al. PLGA Nanoparticle-Based Formulations to Cross the Blood-Brain Barrier for Drug Delivery: From R&D to cGMP. *Pharmaceutics* **2021**, *13*, 500. [CrossRef]
959. Wen, M.M.; El-Salamouni, N.S.; El-Refaie, W.M.; Hazzah, H.A.; Ali, M.M.; Tosi, G.; Farid, R.M.; Blanco-Prieto, M.J.; Billa, N.; Hanafy, A.S. Nanotechnology-based drug delivery systems for Alzheimer's disease management: Technical, industrial, and clinical challenges. *J. Control. Release* **2017**, *245*, 95–107. [CrossRef]
960. Lasic, D.D.; Ceh, B.; Stuart, M.C.; Guo, L.; Frederik, P.M.; Barenholz, Y. Transmembrane gradient driven phase transitions within vesicles: Lessons for drug delivery. *Biochim. Biophys. Acta* **1995**, *1239*, 145–156. [CrossRef]
961. Yamada, Y. Dimerization of Doxorubicin Causes Its Precipitation. *ACS Omega* **2020**, *5*, 33235–33241. [CrossRef]
962. Romano, G. Development of safer gene delivery systems to minimize the risk of insertional mutagenesis-related malignancies: A critical issue for the field of gene therapy. *ISRN Oncol.* **2012**, *2012*, 616310. [CrossRef]
963. Sessa, M.; Lorioli, L.; Fumagalli, F.; Acquati, S.; Redaelli, D.; Baldoli, C.; Canale, S.; Lopez, I.D.; Morena, F.; Calabria, A.; et al. Lentiviral haemopoietic stem-cell gene therapy in early-onset metachromatic leukodystrophy: An ad-hoc analysis of a non-randomised, open-label, phase 1/2 trial. *Lancet* **2016**, *388*, 476–487. [CrossRef]
964. Fumagalli, F.; Calbi, V.; Natali Sora, M.G.; Sessa, M.; Baldoli, C.; Rancoita, P.M.V.; Ciotti, F.; Sarzana, M.; Fraschini, M.; Zambon, A.A.; et al. Lentiviral haematopoietic stem-cell gene therapy for early-onset metachromatic leukodystrophy: Long-term results from a non-randomised, open-label, phase 1/2 trial and expanded access. *Lancet* **2022**, *399*, 372–383. [CrossRef]
965. Hultberg, B. Fluorometric assay of the arylsulphatases in human urine. *J. Clin. Chem. Clin. Biochem.* **1979**, *17*, 795–797. [CrossRef]
966. Pandey, A.; Singh, N.; Vemula, S.V.; Couetil, L.; Katz, J.M.; Donis, R.; Sambhara, S.; Mittal, S.K. Impact of preexisting adenovirus vector immunity on immunogenicity and protection conferred with an adenovirus-based H5N1 influenza vaccine. *PLoS ONE* **2012**, *7*, e33428. [CrossRef]

967. Akli, S.; Caillaud, C.; Vigne, E.; Stratford-Perricaudet, L.D.; Poenaru, L.; Perricaudet, M.; Kahn, A.; Peschanski, M.R. Transfer of a foreign gene into the brain using adenovirus vectors. *Nat. Genet.* **1993**, *3*, 224–228. [CrossRef]
968. Byrnes, A.P.; Rusby, J.E.; Wood, M.J.; Charlton, H.M. Adenovirus gene transfer causes inflammation in the brain. *Neuroscience* **1995**, *66*, 1015–1024. [CrossRef]
969. Lawrence, M.S.; Foellmer, H.G.; Elsworth, J.D.; Kim, J.H.; Leranath, C.; Kozlowski, D.A.; Bothwell, A.L.; Davidson, B.L.; Bohn, M.C.; Redmond, D.E., Jr. Inflammatory responses and their impact on beta-galactosidase transgene expression following adenovirus vector delivery to the primate caudate nucleus. *Gene Ther.* **1999**, *6*, 1368–1379. [CrossRef]
970. Lehrman, S. Virus treatment questioned after gene therapy death. *Nature* **1999**, *401*, 517–518. [CrossRef]
971. Mody, P.H.; Pathak, S.; Hanson, L.K.; Spencer, J.V. Herpes Simplex Virus: A Versatile Tool for Insights Into Evolution, Gene Delivery, and Tumor Immunotherapy. *Virology* **2020**, *11*, 1178122X20913274. [CrossRef]
972. Herrlinger, U.; Kramm, C.M.; Aboody-Guterman, K.S.; Silver, J.S.; Ikeda, K.; Johnston, K.M.; Pechan, P.A.; Barth, R.F.; Finkelstein, D.; Chiocca, E.A.; et al. Pre-existing herpes simplex virus 1 (HSV-1) immunity decreases, but does not abolish, gene transfer to experimental brain tumors by a HSV-1 vector. *Gene Ther.* **1998**, *5*, 809–819. [CrossRef]
973. Palella, T.D.; Hidaka, Y.; Silverman, L.J.; Levine, M.; Glorioso, J.; Kelley, W.N. Expression of human HPRT mRNA in brains of mice infected with a recombinant herpes simplex virus-1 vector. *Gene* **1989**, *80*, 137–144. [CrossRef]
974. Wood, M.J.; Byrnes, A.P.; Pfaff, D.W.; Rabkin, S.D.; Charlton, H.M. Inflammatory effects of gene transfer into the CNS with defective HSV-1 vectors. *Gene Ther.* **1994**, *1*, 283–291. [PubMed]
975. McMenamin, M.M.; Byrnes, A.P.; Charlton, H.M.; Coffin, R.S.; Latchman, D.S.; Wood, M.J. A gamma34.5 mutant of herpes simplex 1 causes severe inflammation in the brain. *Neuroscience* **1998**, *83*, 1225–1237. [CrossRef]
976. Cinatl, J., Jr.; Michaelis, M.; Driever, P.H.; Cinatl, J.; Hrabeta, J.; Suhan, T.; Doerr, H.W.; Vogel, J.U. Multimutated herpes simplex virus g207 is a potent inhibitor of angiogenesis. *Neoplasia* **2004**, *6*, 725–735. [CrossRef] [PubMed]
977. Markert, J.M.; Liechty, P.G.; Wang, W.; Gaston, S.; Braz, E.; Karrasch, M.; Nabors, L.B.; Markiewicz, M.; Lakeman, A.D.; Palmer, C.A.; et al. Phase Ib trial of mutant herpes simplex virus G207 inoculated pre-and post-tumor resection for recurrent GBM. *Mol. Ther.* **2009**, *17*, 199–207. [CrossRef]
978. Miller, K.E.; Cassady, K.A.; Roth, J.C.; Clements, J.; Schieffer, K.M.; Leraas, K.; Miller, A.R.; Prasad, N.; Leavenworth, J.W.; Aban, I.B.; et al. Immune Activity and Response Differences of Oncolytic Viral Therapy in Recurrent Glioblastoma: Gene Expression Analyses of a Phase IB Study. *Clin. Cancer Res.* **2022**, *28*, 498–506. [CrossRef]
979. Huang, R.; Harmsen, S.; Samii, J.M.; Karabeber, H.; Pitter, K.L.; Holland, E.C.; Kircher, M.F. High Precision Imaging of Microscopic Spread of Glioblastoma with a Targeted Ultrasensitive SERRS Molecular Imaging Probe. *Theranostics* **2016**, *6*, 1075–1084. [CrossRef]
980. Kaplitt, M.G.; Leone, P.; Samulski, R.J.; Xiao, X.; Pfaff, D.W.; O'Malley, K.L.; During, M.J. Long-term gene expression and phenotypic correction using adeno-associated virus vectors in the mammalian brain. *Nat. Genet.* **1994**, *8*, 148–154. [CrossRef]
981. Mastakov, M.Y.; Baer, K.; Xu, R.; Fitzsimons, H.; During, M.J. Combined injection of rAAV with mannitol enhances gene expression in the rat brain. *Mol. Ther.* **2001**, *3*, 225–232. [CrossRef]
982. Souweidane, M.M.; Fraser, J.F.; Arkin, L.M.; Sondhi, D.; Hackett, N.R.; Kaminsky, S.M.; Heier, L.; Kosofsky, B.E.; Worgall, S.; Crystal, R.G.; et al. Gene therapy for late infantile neuronal ceroid lipofuscinosis: Neurosurgical considerations. *J. Neurosurg. Pediatr.* **2010**, *6*, 115–122. [CrossRef]
983. Passini, M.A.; Wolfe, J.H. Widespread gene delivery and structure-specific patterns of expression in the brain after intraventricular injections of neonatal mice with an adeno-associated virus vector. *J. Virol.* **2001**, *75*, 12382–12392. [CrossRef]
984. LeRhun, E.; Taillibert, S.; Chamberlain, M.C. Neuroradiology of leptomeningeal metastases. In *Handbook of Neuro-Oncology Neuroimaging*; Newton, H., Ed.; Elsevier: London, UK, 2016; pp. 705–711. [CrossRef]
985. Vuilleminot, B.R.; Korte, S.; Wright, T.L.; Adams, E.L.; Boyd, R.B.; Butt, M.T. Safety Evaluation of CNS Administered Biologics—Study Design, Data Interpretation, and Translation to the Clinic. *Toxicol. Sci.* **2016**, *152*, 3–9. [CrossRef]
986. Lee, M.J.; Chang, C.P.; Lee, Y.H.; Wu, Y.C.; Tseng, H.W.; Tung, Y.Y.; Wu, M.T.; Chen, Y.H.; Kuo, L.T.; Stephenson, D.; et al. Longitudinal evaluation of an N-ethyl-N-nitrosourea-created murine model with normal pressure hydrocephalus. *PLoS ONE* **2009**, *4*, e7868. [CrossRef]
987. Lasky, R.E.; Luck, M.L.; Parikh, N.A.; Laughlin, N.K. The effects of early lead exposure on the brains of adult rhesus monkeys: A volumetric MRI study. *Toxicol. Sci.* **2005**, *85*, 963–975. [CrossRef]
988. Stratchko, L.; Filatova, I.; Agarwal, A.; Kanekar, S. The Ventricular System of the Brain: Anatomy and Normal Variations. *Semin. Ultrasound CT MRI* **2016**, *37*, 72–83. [CrossRef]
989. Orr, M.E.; Garbarino, V.R.; Salinas, A.; Buffenstein, R. Extended Postnatal Brain Development in the Longest-Lived Rodent: Prolonged Maintenance of Neotenic Traits in the Naked Mole-Rat Brain. *Front. Neurosci.* **2016**, *10*, 504. [CrossRef]
990. Ohno, K.; Samaranch, L.; Hadaczek, P.; Bringas, J.R.; Allen, P.C.; Sudhakar, V.; Stockinger, D.E.; Snieckus, C.; Campagna, M.V.; San Sebastian, W.; et al. Kinetics and MR-Based Monitoring of AAV9 Vector Delivery into Cerebrospinal Fluid of Nonhuman Primates. *Mol. Ther. Methods Clin. Dev.* **2019**, *13*, 47–54. [CrossRef]
991. Whitney, N.; Sun, H.; Pollock, J.M.; Ross, D.A. The human foramen magnum—normal anatomy of the cisterna magna in adults. *Neuroradiology* **2013**, *55*, 1333–1339. [CrossRef]
992. Hordeaux, J.; Hinderer, C.; Buza, E.L.; Louboutin, J.P.; Jahan, T.; Bell, P.; Chichester, J.A.; Tarantal, A.F.; Wilson, J.M. Safe and Sustained Expression of Human Iduronidase After Intrathecal Administration of Adeno-Associated Virus Serotype 9 in Infant Rhesus Monkeys. *Hum. Gene Ther.* **2019**, *30*, 957–966. [CrossRef]

993. Horowitz, E.D.; Rahman, K.S.; Bower, B.D.; Dismuke, D.J.; Falvo, M.R.; Griffith, J.D.; Harvey, S.C.; Asokan, A. Biophysical and ultrastructural characterization of adeno-associated virus capsid uncoating and genome release. *J. Virol.* **2013**, *87*, 2994–3002. [CrossRef]
994. Mendell, J.R.; Al-Zaidy, S.; Shell, R.; Arnold, W.D.; Rodino-Klapac, L.R.; Prior, T.W.; Lowes, L.; Alfano, L.; Berry, K.; Church, K.; et al. Single-Dose Gene-Replacement Therapy for Spinal Muscular Atrophy. *N. Engl. J. Med.* **2017**, *377*, 1713–1722. [CrossRef]
995. Foust, K.D.; Nurre, E.; Montgomery, C.L.; Hernandez, A.; Chan, C.M.; Kaspar, B.K. Intravascular AAV9 preferentially targets neonatal neurons and adult astrocytes. *Nat. Biotechnol.* **2009**, *27*, 59–65. [CrossRef] [PubMed]
996. Bevan, A.K.; Duque, S.; Foust, K.D.; Morales, P.R.; Braun, L.; Schmelzer, L.; Chan, C.M.; McCrate, M.; Chicoine, L.G.; Coley, B.D.; et al. Systemic gene delivery in large species for targeting spinal cord, brain, and peripheral tissues for pediatric disorders. *Mol. Ther.* **2011**, *19*, 1971–1980. [CrossRef]
997. Schnieder, T.P.; Zhou Qin, I.D.; Trencavska-Ivanovska, I.; Rosoklija, G.; Stankov, A.; Pavlovski, G.; Mann, J.J.; Dwork, A.J. Blood Vessels and Perivascular Phagocytes of Prefrontal White and Gray Matter in Suicide. *J. Neuropathol. Exp. Neurol.* **2019**, *78*, 15–30. [CrossRef] [PubMed]
998. Hudry, E.; Andres-Mateos, E.; Lerner, E.P.; Volak, A.; Cohen, O.; Hyman, B.T.; Maguire, C.A.; Vandenberghe, L.H. Efficient Gene Transfer to the Central Nervous System by Single-Stranded Anc80L65. *Mol. Ther. Methods Clin. Dev.* **2018**, *10*, 197–209. [CrossRef] [PubMed]
999. Deverman, B.E.; Pravdo, P.L.; Simpson, B.P.; Kumar, S.R.; Chan, K.Y.; Banerjee, A.; Wu, W.L.; Yang, B.; Huber, N.; Pasca, S.P.; et al. Cre-dependent selection yields AAV variants for widespread gene transfer to the adult brain. *Nat. Biotechnol.* **2016**, *34*, 204–209. [CrossRef] [PubMed]
1000. Finneran, D.J.; Njoku, I.P.; Flores-Pazarin, D.; Ranabothu, M.R.; Nash, K.R.; Morgan, D.; Gordon, M.N. Toward Development of Neuron Specific Transduction After Systemic Delivery of Viral Vectors. *Front. Neurol.* **2021**, *12*, 685802. [CrossRef]
1001. Huang, L.; Wan, J.; Wu, Y.; Tian, Y.; Yao, Y.; Yao, S.; Ji, X.; Wang, S.; Su, Z.; Xu, H. Challenges in adeno-associated virus-based treatment of central nervous system diseases through systemic injection. *Life Sci.* **2021**, *270*, 119142. [CrossRef]
1002. Ille, A.M.; Kishel, E.; Bodea, R.; Ille, A.; Lamont, H.; Amico-Ruvio, S. Protein LY6E as a candidate for mediating transport of adeno-associated virus across the human blood-brain barrier. *J. Neurovirol.* **2020**, *26*, 769–778. [CrossRef]
1003. Mingozi, F.; High, K.A. Immune responses to AAV vectors: Overcoming barriers to successful gene therapy. *Blood* **2013**, *122*, 23–36. [CrossRef]
1004. Fitzpatrick, Z.; Leborgne, C.; Barbon, E.; Masat, E.; Ronzitti, G.; van Wittenberghe, L.; Vignaud, A.; Collaud, F.; Charles, S.; Simon Sola, M.; et al. Influence of Pre-existing Anti-capsid Neutralizing and Binding Antibodies on AAV Vector Transduction. *Mol. Ther. Methods Clin. Dev.* **2018**, *9*, 119–129. [CrossRef]
1005. Murrey, D.A.; Naughton, B.J.; Duncan, F.J.; Meadows, A.S.; Ware, T.A.; Campbell, K.J.; Bremer, W.G.; Walker, C.M.; Goodchild, L.; Bolon, B.; et al. Feasibility and safety of systemic rAAV9-hNAGLU delivery for treating mucopolysaccharidosis IIIB: Toxicology, biodistribution, and immunological assessments in primates. *Hum. Gene Ther. Clin. Dev.* **2014**, *25*, 72–84. [CrossRef]
1006. Samaranch, L.; Sebastian, W.S.; Kells, A.P.; Salegio, E.A.; Heller, G.; Bringas, J.R.; Pivrotto, P.; DeArmond, S.; Forsayeth, J.; Bankiewicz, K.S. AAV9-mediated expression of a non-self protein in nonhuman primate central nervous system triggers widespread neuroinflammation driven by antigen-presenting cell transduction. *Mol. Ther.* **2014**, *22*, 329–337. [CrossRef]
1007. Gougeon, M.L.; Poirier-Beaudouin, B.; Ausseil, J.; Zerach, M.; Artaud, C.; Heard, J.M.; Deiva, K.; Tardieu, M. Cell-Mediated Immunity to NAGLU Transgene Following Intracerebral Gene Therapy in Children With Mucopolysaccharidosis Type IIIB Syndrome. *Front. Immunol.* **2021**, *12*, 655478. [CrossRef]
1008. Murphy, S.L.; Bhagwat, A.; Edmonson, S.; Zhou, S.; High, K.A. High-throughput screening and biophysical interrogation of hepatotropic AAV. *Mol. Ther.* **2008**, *16*, 1960–1967. [CrossRef]
1009. Chand, D.; Mohr, F.; McMillan, H.; Tukov, F.F.; Montgomery, K.; Kleyn, A.; Sun, R.; Tauscher-Wisniewski, S.; Kaufmann, P.; Kullak-Ublick, G. Hepatotoxicity following administration of onasemnogene abeparvovec (AVXS-101) for the treatment of spinal muscular atrophy. *J. Hepatol.* **2021**, *74*, 560–566. [CrossRef]
1010. Chandler, R.J.; LaFave, M.C.; Varshney, G.K.; Trivedi, N.S.; Carrillo-Carrasco, N.; Senac, J.S.; Wu, W.; Hoffmann, V.; Elkahloun, A.G.; Burgess, S.M.; et al. Vector design influences hepatic genotoxicity after adeno-associated virus gene therapy. *J. Clin. Investig.* **2015**, *125*, 870–880. [CrossRef]
1011. Donsante, A.; Vogler, C.; Muzyczka, N.; Crawford, J.M.; Barker, J.; Flotte, T.; Campbell-Thompson, M.; Daly, T.; Sands, M.S. Observed incidence of tumorigenesis in long-term rodent studies of rAAV vectors. *Gene Ther.* **2001**, *8*, 1343–1346. [CrossRef]
1012. Perez, B.A.; Shutterly, A.; Chan, Y.K.; Byrne, B.J.; Corti, M. Management of Neuroinflammatory Responses to AAV-Mediated Gene Therapies for Neurodegenerative Diseases. *Brain Sci.* **2020**, *10*, 119. [CrossRef]
1013. Hordeaux, J.; Hinderer, C.; Goode, T.; Katz, N.; Buza, E.L.; Bell, P.; Calcedo, R.; Richman, L.K.; Wilson, J.M. Toxicology Study of Intra-Cisterna Magna Adeno-Associated Virus 9 Expressing Human Alpha-L-Iduronidase in Rhesus Macaques. *Mol. Ther. Methods Clin. Dev.* **2018**, *10*, 79–88. [CrossRef] [PubMed]
1014. Golebiowski, D.; van der Bom, I.M.J.; Kwon, C.S.; Miller, A.D.; Petrosky, K.; Bradbury, A.M.; Maitland, S.; Kuhn, A.L.; Bishop, N.; Curran, E.; et al. Direct Intracranial Injection of AAVrh8 Encoding Monkey beta-N-Acetylhexosaminidase Causes Neurotoxicity in the Primate Brain. *Hum. Gene Ther.* **2017**, *28*, 510–522. [CrossRef] [PubMed]

1015. Keiser, M.S.; Ranum, P.T.; Yrigollen, C.M.; Carrell, E.M.; Smith, G.R.; Muehlmann, A.L.; Chen, Y.H.; Stein, J.M.; Wolf, R.L.; Radaelli, E.; et al. Toxicity after AAV delivery of RNAi expression constructs into nonhuman primate brain. *Nat. Med.* **2021**, *27*, 1982–1989. [CrossRef] [PubMed]
1016. Earley, L.F.; Conatser, L.M.; Lue, V.M.; Dobbins, A.L.; Li, C.; Hirsch, M.L.; Samulski, R.J. Adeno-Associated Virus Serotype-Specific Inverted Terminal Repeat Sequence Role in Vector Transgene Expression. *Hum. Gene Ther.* **2020**, *31*, 151–162. [CrossRef] [PubMed]
1017. Felgner, P.L.; Gadek, T.R.; Holm, M.; Roman, R.; Chan, H.W.; Wenz, M.; Northrop, J.P.; Ringold, G.M.; Danielsen, M. Lipofection: A highly efficient, lipid-mediated DNA-transfection procedure. *Proc. Natl. Acad. Sci. USA* **1987**, *84*, 7413–7417. [CrossRef] [PubMed]
1018. Hofland, H.E.; Nagy, D.; Liu, J.J.; Spratt, K.; Lee, Y.L.; Danos, O.; Sullivan, S.M. In vivo gene transfer by intravenous administration of stable cationic lipid/DNA complex. *Pharm. Res.* **1997**, *14*, 742–749. [CrossRef]
1019. Hong, K.; Zheng, W.; Baker, A.; Papahadjopoulos, D. Stabilization of cationic liposome-plasmid DNA complexes by polyamines and poly(ethylene glycol)-phospholipid conjugates for efficient in vivo gene delivery. *FEBS Lett.* **1997**, *400*, 233–237. [CrossRef]
1020. Barron, L.G.; Uyechi, L.S.; Szoka, F.C., Jr. Cationic lipids are essential for gene delivery mediated by intravenous administration of lipoplexes. *Gene Ther.* **1999**, *6*, 1179–1183. [CrossRef]
1021. Simberg, D.; Weisman, S.; Talmon, Y.; Faerman, A.; Shoshani, T.; Barenholz, Y. The role of organ vascularization and lipoplex-serum initial contact in intravenous murine lipofection. *J. Biol. Chem.* **2003**, *278*, 39858–39865. [CrossRef]
1022. Niidome, T.; Ohmori, N.; Ichinose, A.; Wada, A.; Mihara, H.; Hirayama, T.; Aoyagi, H. Binding of cationic alpha-helical peptides to plasmid DNA and their gene transfer abilities into cells. *J. Biol. Chem.* **1997**, *272*, 15307–15312. [CrossRef]
1023. Matsui, H.; Johnson, L.G.; Randell, S.H.; Boucher, R.C. Loss of binding and entry of liposome-DNA complexes decreases transfection efficiency in differentiated airway epithelial cells. *J. Biol. Chem.* **1997**, *272*, 1117–1126. [CrossRef]
1024. Tan, Y.; Liu, F.; Li, Z.; Li, S.; Huang, L. Sequential injection of cationic liposome and plasmid DNA effectively transfects the lung with minimal inflammatory toxicity. *Mol. Ther.* **2001**, *3*, 673–682. [CrossRef]
1025. Ito, Y.; Kawakami, S.; Charoensit, P.; Higuchi, Y.; Hashida, M. Evaluation of proinflammatory cytokine production and liver injury induced by plasmid DNA/cationic liposome complexes with various mixing ratios in mice. *Eur. J. Pharm. Biopharm.* **2009**, *71*, 303–309. [CrossRef]
1026. Osaka, G.; Carey, K.; Cuthbertson, A.; Godowski, P.; Patapoff, T.; Ryan, A.; Gadek, T.; Mordenti, J. Pharmacokinetics, tissue distribution, and expression efficiency of plasmid [<sup>33</sup>P]DNA following intravenous administration of DNA/cationic lipid complexes in mice: Use of a novel radionuclide approach. *J. Pharm. Sci.* **1996**, *85*, 612–618. [CrossRef]
1027. Al Qtaish, N.; Gallego, I.; Villate-Beitia, I.; Sainz-Ramos, M.; Martinez-Navarrete, G.; Soto-Sanchez, C.; Fernandez, E.; Galvez-Martin, P.; Lopez-Mendez, T.B.; Puras, G.; et al. Sphingolipid extracts enhance gene delivery of cationic lipid vesicles into retina and brain. *Eur. J. Pharm. Biopharm.* **2021**, *169*, 103–112. [CrossRef]
1028. Zou, S.M.; Erbacher, P.; Remy, J.S.; Behr, J.P. Systemic linear polyethylenimine (L-PEI)-mediated gene delivery in the mouse. *J. Gene Med.* **2000**, *2*, 128–134. [CrossRef]
1029. Wu, G.Y.; Wu, C.H. Receptor-mediated gene delivery and expression in vivo. *J. Biol. Chem.* **1988**, *263*, 14621–14624. [CrossRef]
1030. Kwok, D.Y.; Coffin, C.C.; Lollo, C.P.; Jovenal, J.; Banaszczyk, M.G.; Mullen, P.; Phillips, A.; Amini, A.; Fabrycki, J.; Bartholomew, R.M.; et al. Stabilization of poly-L-lysine/DNA polyplexes for in vivo gene delivery to the liver. *Biochim. Biophys. Acta* **1999**, *1444*, 171–190. [CrossRef]
1031. Mok, K.W.; Lam, A.M.; Cullis, P.R. Stabilized plasmid-lipid particles: Factors influencing plasmid entrapment and transfection properties. *Biochim. Biophys. Acta* **1999**, *1419*, 137–150. [CrossRef]
1032. Ambegia, E.; Ansell, S.; Cullis, P.; Heyes, J.; Palmer, L.; MacLachlan, I. Stabilized plasmid-lipid particles containing PEG-diacylglycerols exhibit extended circulation lifetimes and tumor selective gene expression. *Biochim. Biophys. Acta* **2005**, *1669*, 155–163. [CrossRef]
1033. Yuan, F.; Leunig, M.; Huang, S.K.; Berk, D.A.; Papahadjopoulos, D.; Jain, R.K. Microvascular permeability and interstitial penetration of sterically stabilized (stealth) liposomes in a human tumor xenograft. *Cancer Res.* **1994**, *54*, 3352–3356.
1034. Sohlenius-Sternbeck, A.K. Determination of the hepatocellularity number for human, dog, rabbit, rat and mouse livers from protein concentration measurements. *Toxicol. Vitro* **2006**, *20*, 1582–1586. [CrossRef] [PubMed]
1035. Shi, N.; Pardridge, W.M. Noninvasive gene targeting to the brain. *Proc. Natl. Acad. Sci. USA* **2000**, *97*, 7567–7572. [CrossRef]
1036. Pardridge, W.M. Gene targeting in vivo with pegylated immunoliposomes. *Methods Enzymol.* **2003**, *373*, 507–528. [CrossRef]
1037. Kulkarni, J.A.; Cullis, P.R.; van der Meel, R. Lipid Nanoparticles Enabling Gene Therapies: From Concepts to Clinical Utility. *Nucleic Acid. Ther.* **2018**, *28*, 146–157. [CrossRef]
1038. Pardridge, W.M. Drug and gene targeting to the brain with molecular Trojan horses. *Nat. Rev. Drug Discov.* **2002**, *1*, 131–139. [CrossRef]
1039. Zhang, Y.; Calon, F.; Zhu, C.; Boado, R.J.; Pardridge, W.M. Intravenous nonviral gene therapy causes normalization of striatal tyrosine hydroxylase and reversal of motor impairment in experimental parkinsonism. *Hum. Gene Ther.* **2003**, *14*, 1–12. [CrossRef]
1040. Zhang, Y.; Jeong Lee, H.; Boado, R.J.; Pardridge, W.M. Receptor-mediated delivery of an antisense gene to human brain cancer cells. *J. Gene Med.* **2002**, *4*, 183–194. [CrossRef]
1041. Zhang, Y.; Schlachetzki, F.; Li, J.Y.; Boado, R.J.; Pardridge, W.M. Organ-specific gene expression in the rhesus monkey eye following intravenous non-viral gene transfer. *Mol. Vis.* **2003**, *9*, 465–472.

1042. Pardridge, W.M. Brain drug development and brain drug targeting. *Pharm. Res.* **2007**, *24*, 1729–1732. [CrossRef]
1043. Zhang, Y.; Zhang, Y.F.; Bryant, J.; Charles, A.; Boado, R.J.; Pardridge, W.M. Intravenous RNA interference gene therapy targeting the human epidermal growth factor receptor prolongs survival in intracranial brain cancer. *Clin. Cancer Res.* **2004**, *10*, 3667–3677. [CrossRef] [PubMed]
1044. Zhang, Y.; Schlachetzki, F.; Zhang, Y.F.; Boado, R.J.; Pardridge, W.M. Normalization of striatal tyrosine hydroxylase and reversal of motor impairment in experimental parkinsonism with intravenous nonviral gene therapy and a brain-specific promoter. *Hum. Gene Ther.* **2004**, *15*, 339–350. [CrossRef] [PubMed]
1045. Zabner, J.; Fasbender, A.J.; Moninger, T.; Poellinger, K.A.; Welsh, M.J. Cellular and molecular barriers to gene transfer by a cationic lipid. *J. Biol. Chem.* **1995**, *270*, 18997–19007. [CrossRef] [PubMed]
1046. Podlecki, D.A.; Smith, R.M.; Kao, M.; Tsai, P.; Huecksteadt, T.; Brandenburg, D.; Lasher, R.S.; Jarett, L.; Olefsky, J.M. Nuclear translocation of the insulin receptor. A possible mediator of insulin's long term effects. *J. Biol. Chem.* **1987**, *262*, 3362–3368. [CrossRef]
1047. Amaya, M.J.; Oliveira, A.G.; Guimaraes, E.S.; Casteluber, M.C.; Carvalho, S.M.; Andrade, L.M.; Pinto, M.C.; Mennone, A.; Oliveira, C.A.; Resende, R.R.; et al. The insulin receptor translocates to the nucleus to regulate cell proliferation in liver. *Hepatology* **2014**, *59*, 274–283. [CrossRef]
1048. Shi, N.; Boado, R.J.; Pardridge, W.M. Receptor-mediated gene targeting to tissues in vivo following intravenous administration of pegylated immunoliposomes. *Pharm. Res.* **2001**, *18*, 1091–1095. [CrossRef]
1049. Shi, N.; Zhang, Y.; Zhu, C.; Boado, R.J.; Pardridge, W.M. Brain-specific expression of an exogenous gene after i.v. administration. *Proc. Natl. Acad. Sci. USA* **2001**, *98*, 12754–12759. [CrossRef]
1050. Schlachetzki, F.; Zhang, Y.; Boado, R.J.; Pardridge, W.M. Gene therapy of the brain: The trans-vascular approach. *Neurology* **2004**, *62*, 1275–1281. [CrossRef]
1051. Chu, C.; Zhang, Y.; Boado, R.J.; Pardridge, W.M. Decline in exogenous gene expression in primate brain following intravenous administration is due to plasmid degradation. *Pharm. Res.* **2006**, *23*, 1586–1590. [CrossRef]
1052. Zack, D.J.; Bennett, J.; Wang, Y.; Davenport, C.; Klaunberg, B.; Gearhart, J.; Nathans, J. Unusual topography of bovine rhodopsin promoter-lacZ fusion gene expression in transgenic mouse retinas. *Neuron* **1991**, *6*, 187–199. [CrossRef]
1053. Zhu, C.; Zhang, Y.; Pardridge, W.M. Widespread expression of an exogenous gene in the eye after intravenous administration. *Invest. Ophthalmol. Vis. Sci.* **2002**, *43*, 3075–3080.
1054. Naeser, P. Insulin receptors in human ocular tissues. Immunohistochemical demonstration in normal and diabetic eyes. *Uppsala J. Med. Sci.* **1997**, *102*, 35–40. [CrossRef]
1055. Segovia, J.; Vergara, P.; Brenner, M. Differentiation-dependent expression of transgenes in engineered astrocyte cell lines. *Neurosci. Lett.* **1998**, *242*, 172–176. [CrossRef]
1056. Sasahara, M.; Fries, J.W.; Raines, E.W.; Gown, A.M.; Westrum, L.E.; Frosch, M.P.; Bonthron, D.T.; Ross, R.; Collins, T. PDGF B-chain in neurons of the central nervous system, posterior pituitary, and in a transgenic model. *Cell* **1991**, *64*, 217–227. [CrossRef]
1057. Xia, C.F.; Chu, C.; Li, J.; Wang, Y.; Zhang, Y.; Boado, R.J.; Pardridge, W.M. Comparison of cDNA and genomic forms of tyrosine hydroxylase gene therapy of the brain with Trojan horse liposomes. *J. Gene Med.* **2007**, *9*, 605–612. [CrossRef]
1058. Hoffer, B.J.; Hoffman, A.; Bowenkamp, K.; Huettl, P.; Hudson, J.; Martin, D.; Lin, L.F.; Gerhardt, G.A. Glial cell line-derived neurotrophic factor reverses toxin-induced injury to midbrain dopaminergic neurons in vivo. *Neurosci. Lett.* **1994**, *182*, 107–111. [CrossRef]
1059. Xia, C.F.; Boado, R.J.; Zhang, Y.; Chu, C.; Pardridge, W.M. Intravenous glial-derived neurotrophic factor gene therapy of experimental Parkinson's disease with Trojan horse liposomes and a tyrosine hydroxylase promoter. *J. Gene Med.* **2008**, *10*, 306–315. [CrossRef]
1060. Boado, R.J.; Pardridge, W.M. Amplification of gene expression using both 5'- and 3'-untranslated regions of GLUT1 glucose transporter mRNA. *Brain Res. Mol. Brain Res.* **1999**, *63*, 371–374. [CrossRef]
1061. Hatanpaa, K.J.; Burma, S.; Zhao, D.; Habib, A.A. Epidermal growth factor receptor in glioma: Signal transduction, neuropathology, imaging, and radioresistance. *Neoplasia* **2010**, *12*, 675–684. [CrossRef]
1062. Xia, C.F.; Zhang, Y.; Zhang, Y.; Boado, R.J.; Pardridge, W.M. Intravenous siRNA of brain cancer with receptor targeting and avidin-biotin technology. *Pharm. Res.* **2007**, *24*, 2309–2316. [CrossRef]
1063. Abe, T.; Terada, K.; Wakimoto, H.; Inoue, R.; Tyminski, E.; Bookstein, R.; Basilion, J.P.; Chiocca, E.A. PTEN decreases in vivo vascularization of experimental gliomas in spite of proangiogenic stimuli. *Cancer Res.* **2003**, *63*, 2300–2305.
1064. Zhang, Y.; Pardridge, W.M. Near complete rescue of experimental Parkinson's disease with intravenous, non-viral GDNF gene therapy. *Pharm. Res.* **2009**, *26*, 1059–1063. [CrossRef]
1065. Burlina, A. Niemann-Pick disease type C: Introduction and main clinical features. *J. Neurol.* **2014**, *261* (Suppl. S2), S525–S527. [CrossRef]
1066. Pentchev, P.G.; Gal, A.E.; Booth, A.D.; Omodeo-Sale, F.; Fouks, J.; Neumeyer, B.A.; Quirk, J.M.; Dawson, G.; Brady, R.O. A lysosomal storage disorder in mice characterized by a dual deficiency of sphingomyelinase and glucocerebrosidase. *Biochim. Biophys. Acta* **1980**, *619*, 669–679. [CrossRef]
1067. Loftus, S.K.; Morris, J.A.; Carstea, E.D.; Gu, J.Z.; Cummings, C.; Brown, A.; Ellison, J.; Ohno, K.; Rosenfeld, M.A.; Tagle, D.A.; et al. Murine model of Niemann-Pick C disease: Mutation in a cholesterol homeostasis gene. *Science* **1997**, *277*, 232–235. [CrossRef]

1068. Chua, A.C.; Delima, R.D.; Morgan, E.H.; Herbison, C.E.; Tirnitz-Parker, J.E.; Graham, R.M.; Fleming, R.E.; Britton, R.S.; Bacon, B.R.; Olynyk, J.K.; et al. Iron uptake from plasma transferrin by a transferrin receptor 2 mutant mouse model of haemochromatosis. *J. Hepatol.* **2010**, *52*, 425–431. [CrossRef]
1069. Baudry, M.; Yao, Y.; Simmons, D.; Liu, J.; Bi, X. Postnatal development of inflammation in a murine model of Niemann-Pick type C disease: Immunohistochemical observations of microglia and astroglia. *Exp. Neurol.* **2003**, *184*, 887–903. [CrossRef]
1070. Liao, G.; Yao, Y.; Liu, J.; Yu, Z.; Cheung, S.; Xie, A.; Liang, X.; Bi, X. Cholesterol accumulation is associated with lysosomal dysfunction and autophagic stress in *Npc1*<sup>-/-</sup> mouse brain. *Am. J. Pathol.* **2007**, *171*, 962–975. [CrossRef] [PubMed]
1071. Qiao, L.; Yang, E.; Luo, J.; Lin, J.; Yan, X. Altered myelination in the Niemann-Pick type C1 mutant mouse. *Histol. Histopathol.* **2018**, *33*, 1311–1321. [CrossRef] [PubMed]
1072. Santiago-Mujica, E.; Flunkert, S.; Rabl, R.; Neddens, J.; Loeffler, T.; Hutter-Paier, B. Hepatic and neuronal phenotype of NPC1<sup>-/-</sup> mice. *Heliyon* **2019**, *5*, e01293. [CrossRef] [PubMed]
1073. Zhang, Y.F.; Boado, R.J.; Pardridge, W.M. Absence of toxicity of chronic weekly intravenous gene therapy with pegylated immunoliposomes. *Pharm. Res.* **2003**, *20*, 1779–1785. [CrossRef]
1074. Jeffs, L.B.; Palmer, L.R.; Ambegia, E.G.; Giesbrecht, C.; Ewanick, S.; MacLachlan, I. A scalable, extrusion-free method for efficient liposomal encapsulation of plasmid DNA. *Pharm. Res.* **2005**, *22*, 362–372. [CrossRef]
1075. Batzri, S.; Korn, E.D. Single bilayer liposomes prepared without sonication. *Biochim. Biophys. Acta* **1973**, *298*, 1015–1019. [CrossRef]
1076. Hirota, S.; de Ilarduya, C.T.; Barron, L.G.; Szoka, F.C., Jr. Simple mixing device to reproducibly prepare cationic lipid-DNA complexes (lipoplexes). *Biotechniques* **1999**, *27*, 286–290. [CrossRef]
1077. Wang, Y.; Ran, S.; Man, B.; Yang, G. Ethanol induces condensation of single DNA molecules. *Soft Matter* **2011**, *7*, 4425–4434. [CrossRef]
1078. Latulippe, D.R.; Zydney, A.L. Radius of gyration of plasmid DNA isoforms from static light scattering. *Biotechnol. Bioeng.* **2010**, *107*, 134–142. [CrossRef]
1079. Stano, P.; Bufali, S.; Pisano, C.; Bucci, F.; Barbarino, M.; Santaniello, M.; Carminati, P.; Luisi, P.L. Novel camptothecin analogue (gimatecan)-containing liposomes prepared by the ethanol injection method. *J. Liposome Res.* **2004**, *14*, 87–109. [CrossRef]
1080. Lu, W.; Sun, Q.; Wan, J.; She, Z.; Jiang, X.G. Cationic albumin-conjugated pegylated nanoparticles allow gene delivery into brain tumors via intravenous administration. *Cancer Res.* **2006**, *66*, 11878–11887. [CrossRef]
1081. Thompson, M.; Aukema, K.; O'Bryan, D.; Rader, S.; Murray, B. Plasmid sonication improves sequencing efficiency and quality in the Beckman Coulter CEQ system. *Biotechniques* **2008**, *45*, 327–329. [CrossRef]
1082. Catanese, D.J., Jr.; Fogg, J.M.; Schrock, D.E., 2nd; Gilbert, B.E.; Zechiedrich, L. Supercoiled Minivector DNA resists shear forces associated with gene therapy delivery. *Gene Ther.* **2012**, *19*, 94–100. [CrossRef]
1083. Zhao, H.; Li, G.L.; Wang, R.Z.; Li, S.F.; Wei, J.J.; Feng, M.; Zhao, Y.J.; Ma, W.B.; Yang, Y.; Li, Y.N.; et al. A comparative study of transfection efficiency between liposomes, immunoliposomes and brain-specific immunoliposomes. *J. Int. Med. Res.* **2010**, *38*, 957–966. [CrossRef]
1084. Yue, P.J.; He, L.; Qiu, S.W.; Li, Y.; Liao, Y.J.; Li, X.P.; Xie, D.; Peng, Y. OX26/CTX-conjugated PEGylated liposome as a dual-targeting gene delivery system for brain glioma. *Mol. Cancer* **2014**, *13*, 191. [CrossRef] [PubMed]
1085. Gandhi, M.; Bhatt, P.; Chauhan, G.; Gupta, S.; Misra, A.; Mashru, R. IGF-II-Conjugated Nanocarrier for Brain-Targeted Delivery of p11 Gene for Depression. *AAPS PharmSciTech* **2019**, *20*, 50. [CrossRef] [PubMed]
1086. Lindqvist, A.; Friden, M.; Hammarlund-Udenaes, M. Pharmacokinetic considerations of nanodelivery to the brain: Using modeling and simulations to predict the outcome of liposomal formulations. *Eur. J. Pharm. Sci.* **2016**, *92*, 173–182. [CrossRef]
1087. Kucharz, K.; Kristensen, K.; Johnsen, K.B.; Lund, M.A.; Lonstrup, M.; Moos, T.; Andresen, T.L.; Lauritzen, M.J. Post-capillary venules are the key locus for transcytosis-mediated brain delivery of therapeutic nanoparticles. *Nat. Commun.* **2021**, *12*, 4121. [CrossRef]
1088. Mathiisen, T.M.; Lehre, K.P.; Danbolt, N.C.; Ottersen, O.P. The perivascular astroglial sheath provides a complete covering of the brain microvessels: An electron microscopic 3D reconstruction. *Glia* **2010**, *58*, 1094–1103. [CrossRef]
1089. Engelhardt, B.; Vajkoczy, P.; Weller, R.O. The movers and shapers in immune privilege of the CNS. *Nat. Immunol.* **2017**, *18*, 123–131. [CrossRef]
1090. Vanharreveld, A.; Crowell, J.; Malhotra, S.K. A Study of Extracellular Space in Central Nervous Tissue by Freeze-Substitution. *J. Cell Biol.* **1965**, *25*, 117–137. [CrossRef]
1091. Nance, E.A.; Woodworth, G.F.; Sailor, K.A.; Shih, T.Y.; Xu, Q.; Swaminathan, G.; Xiang, D.; Eberhart, C.; Hanes, J. A dense poly(ethylene glycol) coating improves penetration of large polymeric nanoparticles within brain tissue. *Sci. Transl. Med.* **2012**, *4*, 149ra119. [CrossRef] [PubMed]
1092. Young, R.C.; Mitchell, R.C.; Brown, T.H.; Ganellin, C.R.; Griffiths, R.; Jones, M.; Rana, K.K.; Saunders, D.; Smith, I.R.; Sore, N.E.; et al. Development of a new physicochemical model for brain penetration and its application to the design of centrally acting H2 receptor histamine antagonists. *J. Med. Chem.* **1988**, *31*, 656–671. [CrossRef]
1093. Grumetto, L.; Russo, G. cDeltalog kw (IAM): Can we afford estimation of small molecules' blood-brain barrier passage based upon in silico phospholipophilicity? *ADMET DMPK* **2021**, *9*, 267–281. [CrossRef]
1094. Bickel, U. How to measure drug transport across the blood-brain barrier. *NeuroRX* **2005**, *2*, 15–26. [CrossRef]

1095. Hammarlund-Udenaes, M.; Friden, M.; Syvanen, S.; Gupta, A. On the rate and extent of drug delivery to the brain. *Pharm. Res.* **2008**, *25*, 1737–1750. [CrossRef]
1096. Pardridge, W.M.; Landaw, E.M. Testosterone transport in brain: Primary role of plasma protein-bound hormone. *Am. J. Physiol.* **1985**, *249*, E534–E542. [CrossRef]
1097. Huttunen, K.M.; Terasaki, T.; Urtti, A.; Montaser, A.B.; Uchida, Y. Pharmacoproteomics of Brain Barrier Transporters and Substrate Design for the Brain Targeted Drug Delivery. *Pharm. Res.* **2022**, 1–30. [CrossRef]
1098. Pardridge, W.M. Targeted delivery of hormones to tissues by plasma proteins. In *Handbook of Physiology, The Endocrine System, Cellular Endocrinology*; Conn, P.M., Goodman, H.M., Kostyo, J.L., Eds.; Oxford University Press: New York, NY, USA, 1998; Section 7; Volume 1, Chapter 14; pp. 335–382. [CrossRef]
1099. Herculano-Houzel, S. The remarkable, yet not extraordinary, human brain as a scaled-up primate brain and its associated cost. *Proc. Natl. Acad. Sci. USA* **2012**, *109* (Suppl. S1), 10661–10668. [CrossRef]
1100. Pardridge, W.M.; Landaw, E.M. Tracer kinetic model of blood-brain barrier transport of plasma protein-bound ligands. Empiric testing of the free hormone hypothesis. *J. Clin. Investig.* **1984**, *74*, 745–752. [CrossRef]
1101. Schonfeld, D.L.; Ravelli, R.B.; Mueller, U.; Skerra, A. The 1.8-Å crystal structure of alpha1-acid glycoprotein (Orosomuroid) solved by UV RIP reveals the broad drug-binding activity of this human plasma lipocalin. *J. Mol. Biol.* **2008**, *384*, 393–405. [CrossRef]
1102. Pardridge, W.M.; Sakiyama, R.; Fierer, G. Transport of propranolol and lidocaine through the rat blood-brain barrier. Primary role of globulin-bound drug. *J. Clin. Investig.* **1983**, *71*, 900–908. [CrossRef]
1103. Smith, S.A.; Waters, N.J. Pharmacokinetic and Pharmacodynamic Considerations for Drugs Binding to Alpha-1-Acid Glycoprotein. *Pharm. Res.* **2018**, *36*, 30. [CrossRef]
1104. Bohnert, T.; Gan, L.S. Plasma protein binding: From discovery to development. *J. Pharm. Sci.* **2013**, *102*, 2953–2994. [CrossRef] [PubMed]
1105. Griffith, J.I.; Elmquist, W.F. To Measure is to Know: A Perspective on the Work of Dr. Margareta Hammarlund-Udenaes. *Pharm. Res.* **2022**, 1–15. [CrossRef] [PubMed]
1106. Roach, P.; Farrar, D.; Perry, C.C. Interpretation of protein adsorption: Surface-induced conformational changes. *J. Am. Chem. Soc.* **2005**, *127*, 8168–8173. [CrossRef]
1107. Rees, S.G.; Wassell, D.T.; Shellis, R.P.; Embery, G. Effect of serum albumin on glycosaminoglycan inhibition of hydroxyapatite formation. *Biomaterials* **2004**, *25*, 971–977. [CrossRef]
1108. Reitsma, S.; Slaaf, D.W.; Vink, H.; van Zandvoort, M.A.; oude Egbrink, M.G. The endothelial glycocalyx: Composition, functions, and visualization. *Pflug. Arch.* **2007**, *454*, 345–359. [CrossRef]
1109. Osterloh, K.; Ewert, U.; Pries, A.R. Interaction of albumin with the endothelial cell surface. *Am. J. Physiol. Heart Circ. Physiol.* **2002**, *283*, H398–H405. [CrossRef]
1110. Horie, T.; Mizuma, T.; Kasai, S.; Awazu, S. Conformational change in plasma albumin due to interaction with isolated rat hepatocyte. *Am. J. Physiol.* **1988**, *254*, G465–G470. [CrossRef]
1111. Sobczak, A.I.S.; Pitt, S.J.; Stewart, A.J. Glycosaminoglycan Neutralization in Coagulation Control. *Arter. Thromb. Vasc. Biol.* **2018**, *38*, 1258–1270. [CrossRef]
1112. Matsuo, K.; Namatame, H.; Taniguchi, M.; Gekko, K. Membrane-induced conformational change of alpha1-acid glycoprotein characterized by vacuum-ultraviolet circular dichroism spectroscopy. *Biochemistry* **2009**, *48*, 9103–9111. [CrossRef]
1113. Terasaki, T.; Pardridge, W.M.; Denson, D.D. Differential effect of plasma protein binding of bupivacaine on its in vivo transfer into the brain and salivary gland of rats. *J. Pharmacol. Exp. Ther.* **1986**, *239*, 724–729.
1114. Jolliet, P.; Simon, N.; Bree, F.; Urien, S.; Pagliara, A.; Carrupt, P.A.; Testa, B.; Tillement, J.P. Blood-to-brain transfer of various oxycams: Effects of plasma binding on their brain delivery. *Pharm. Res.* **1997**, *14*, 650–656. [CrossRef]
1115. Tanaka, H.; Mizojiri, K. Drug-protein binding and blood-brain barrier permeability. *J. Pharmacol. Exp. Ther.* **1999**, *288*, 912–918.
1116. Lin, T.H.; Lin, J.H. Effects of protein binding and experimental disease states on brain uptake of benzodiazepines in rats. *J. Pharmacol. Exp. Ther.* **1990**, *253*, 45–50.
1117. Riant, P.; Urien, S.; Albengres, E.; Renouard, A.; Tillement, J.P. Effects of the binding of imipramine to erythrocytes and plasma proteins on its transport through the rat blood-brain barrier. *J. Neurochem.* **1988**, *51*, 421–425. [CrossRef]
1118. Urien, S.; Pinquier, J.L.; Paquette, B.; Chaumet-Riffaud, P.; Kiechel, J.R.; Tillement, J.P. Effect of the binding of isradipine and darodipine to different plasma proteins on their transfer through the rat blood-brain barrier. Drug binding to lipoproteins does not limit the transfer of drug. *J. Pharmacol. Exp. Ther.* **1987**, *242*, 349–353.
1119. Pardridge, W.M.; Fierer, G. Transport of tryptophan into brain from the circulating, albumin-bound pool in rats and in rabbits. *J. Neurochem.* **1990**, *54*, 971–976. [CrossRef]
1120. Mandula, H.; Parepally, J.M.; Feng, R.; Smith, Q.R. Role of site-specific binding to plasma albumin in drug availability to brain. *J. Pharmacol. Exp. Ther.* **2006**, *317*, 667–675. [CrossRef]
1121. Tsao, S.C.; Sugiyama, Y.; Sawada, Y.; Iga, T.; Hanano, M. Kinetic analysis of albumin-mediated uptake of warfarin by perfused rat liver. *J. Pharmacokinetic. Biopharm.* **1988**, *16*, 165–181. [CrossRef]
1122. Pardridge, W.M. Selective delivery of sex steroid hormones to tissues by albumin and by sex hormone-binding globulin. *Oxf. Rev. Reprod. Biol.* **1988**, *10*, 237–292. [CrossRef]

1123. Pardridge, W.M.; Mietus, L.J. Influx of thyroid hormones into rat liver in vivo. Differential availability of thyroxine and triiodothyronine bound by plasma proteins. *J. Clin. Investig.* **1980**, *66*, 367–374. [CrossRef]
1124. De Lange, E.C.; Danhof, M. Considerations in the use of cerebrospinal fluid pharmacokinetics to predict brain target concentrations in the clinical setting: Implications of the barriers between blood and brain. *Clin. Pharmacokinet.* **2002**, *41*, 691–703. [CrossRef]
1125. Shen, D.D.; Artru, A.A.; Adkison, K.K. Principles and applicability of CSF sampling for the assessment of CNS drug delivery and pharmacodynamics. *Adv. Drug Deliv. Rev.* **2004**, *56*, 1825–1857. [CrossRef]
1126. Ballarin, M.; Herrera-Marschitz, M.; Casas, M.; Ungerstedt, U. Striatal adenosine levels measured ‘in vivo’ by microdialysis in rats with unilateral dopamine denervation. *Neurosci. Lett.* **1987**, *83*, 338–344. [CrossRef]
1127. Westergren, I.; Nystrom, B.; Hamberger, A.; Johansson, B.B. Intracerebral dialysis and the blood-brain barrier. *J. Neurochem.* **1995**, *64*, 229–234. [CrossRef]
1128. Hascup, E.R.; af Bjerken, S.; Hascup, K.N.; Pomerleau, F.; Huettl, P.; Stromberg, I.; Gerhardt, G.A. Histological studies of the effects of chronic implantation of ceramic-based microelectrode arrays and microdialysis probes in rat prefrontal cortex. *Brain Res.* **2009**, *1291*, 12–20. [CrossRef]
1129. Groothuis, D.R.; Ward, S.; Schlageter, K.E.; Itskovich, A.C.; Schwerin, S.C.; Allen, C.V.; Dills, C.; Levy, R.M. Changes in blood-brain barrier permeability associated with insertion of brain cannulas and microdialysis probes. *Brain Res.* **1998**, *803*, 218–230. [CrossRef]
1130. Morgan, M.E.; Singhal, D.; Anderson, B.D. Quantitative assessment of blood-brain barrier damage during microdialysis. *J. Pharmacol. Exp. Ther.* **1996**, *277*, 1167–1176.
1131. Friden, M.; Bergstrom, F.; Wan, H.; Rehngren, M.; Ahlin, G.; Hammarlund-Udenaes, M.; Bredberg, U. Measurement of unbound drug exposure in brain: Modeling of pH partitioning explains diverging results between the brain slice and brain homogenate methods. *Drug Metab. Dispos.* **2011**, *39*, 353–362. [CrossRef] [PubMed]
1132. Gallo, J.M.; Vicini, P.; Orlansky, A.; Li, S.; Zhou, F.; Ma, J.; Pulfer, S.; Bookman, M.A.; Guo, P. Pharmacokinetic model-predicted anticancer drug concentrations in human tumors. *Clin. Cancer Res.* **2004**, *10*, 8048–8058. [CrossRef] [PubMed]
1133. Pardridge, W.M.; Fierer, G. Blood-brain barrier transport of butanol and water relative to N-isopropyl-p-iodoamphetamine as the internal reference. *J. Cereb. Blood Flow Metab.* **1985**, *5*, 275–281. [CrossRef] [PubMed]
1134. Pardridge, W.M.; Landaw, E.M.; Miller, L.P.; Braun, L.D.; Oldendorf, W.H. Carotid artery injection technique: Bounds for bolus mixing by plasma and by brain. *J. Cereb. Blood Flow Metab.* **1985**, *5*, 576–583. [CrossRef]
1135. Takasato, Y.; Rapoport, S.I.; Smith, Q.R. An in situ brain perfusion technique to study cerebrovascular transport in the rat. *Am. J. Physiol.* **1984**, *247*, H484–H493. [CrossRef]
1136. De Rijke, Y.B.; Biessen, E.A.; Vogelesang, C.J.; van Berkel, T.J. Binding characteristics of scavenger receptors on liver endothelial and Kupffer cells for modified low-density lipoproteins. *Biochem. J.* **1994**, *304 Pt 1*, 69–73. [CrossRef]
1137. Miyata, S. New aspects in fenestrated capillary and tissue dynamics in the sensory circumventricular organs of adult brains. *Front. Neurosci.* **2015**, *9*, 390. [CrossRef]
1138. Press, O.W.; Shan, D.; Howell-Clark, J.; Eary, J.; Appelbaum, F.R.; Matthews, D.; King, D.J.; Haines, A.M.; Hamann, P.; Hinman, L.; et al. Comparative metabolism and retention of iodine-125, yttrium-90, and indium-111 radioimmunoconjugates by cancer cells. *Cancer Res.* **1996**, *56*, 2123–2129.
1139. Sakane, T.; Pardridge, W.M. Carboxyl-directed pegylation of brain-derived neurotrophic factor markedly reduces systemic clearance with minimal loss of biologic activity. *Pharm. Res.* **1997**, *14*, 1085–1091. [CrossRef]
1140. Wu, D.; Clement, J.G.; Pardridge, W.M. Low blood-brain barrier permeability to azidothymidine (AZT), 3TC, and thymidine in the rat. *Brain Res.* **1998**, *791*, 313–316. [CrossRef]
1141. Bradbury, M.W.; Patlak, C.S.; Oldendorf, W.H. Analysis of brain uptake and loss of radiotracers after intracarotid injection. *Am. J. Physiol.* **1975**, *229*, 1110–1115. [CrossRef]
1142. Crone, C. Facilitated transfer of glucose from blood into brain tissue. *J. Physiol.* **1965**, *181*, 103–113. [CrossRef]
1143. Lassen, N.A.; Trap-Jensen, J. Theoretical considerations on measurement of capillary diffusion capacity in skeletal muscle by the local clearance method. *Scand. J. Clin. Lab. Investig.* **1968**, *21*, 108–115. [CrossRef]
1144. Bell, R.D.; Sagare, A.P.; Friedman, A.E.; Bedi, G.S.; Holtzman, D.M.; Deane, R.; Zlokovic, B.V. Transport pathways for clearance of human Alzheimer’s amyloid beta-peptide and apolipoproteins E and J in the mouse central nervous system. *J. Cereb. Blood Flow Metab.* **2007**, *27*, 909–918. [CrossRef]
1145. Pardridge, W.M.; Sakiyama, R.; Fierer, G. Blood-brain barrier transport and brain sequestration of propranolol and lidocaine. *Am. J. Physiol.* **1984**, *247*, R582–R588. [CrossRef]
1146. Siakotos, A.N.; Rouser, G. Isolation of highly purified human and bovine brain endothelial cells and nuclei and their phospholipid composition. *Lipids* **1969**, *4*, 234–239. [CrossRef]
1147. Joo, F.; Karnushina, I. A procedure for the isolation of capillaries from rat brain. *Cytobios* **1973**, *8*, 41–48.
1148. Goldstein, G.W.; Wolinsky, J.S.; Csejtey, J.; Diamond, I. Isolation of metabolically active capillaries from rat brain. *J. Neurochem.* **1975**, *25*, 715–717. [CrossRef]
1149. Brendel, K.; Meezan, E.; Carlson, E.C. Isolated brain microvessels: A purified, metabolically active preparation from bovine cerebral cortex. *Science* **1974**, *185*, 953–955. [CrossRef]



1150. Williams, S.K.; Gillis, J.F.; Matthews, M.A.; Wagner, R.C.; Bitensky, M.W. Isolation and characterization of brain endothelial cells: Morphology and enzyme activity. *J. Neurochem.* **1980**, *35*, 374–381. [CrossRef] [PubMed]
1151. Lasbennes, F.; Gayet, J. Capacity for energy metabolism in microvessels isolated from rat brain. *Neurochem. Res.* **1984**, *9*, 1–10. [CrossRef] [PubMed]
1152. Choi, T.B.; Pardridge, W.M. Phenylalanine transport at the human blood-brain barrier. Studies with isolated human brain capillaries. *J. Biol. Chem.* **1986**, *261*, 6536–6541. [CrossRef]
1153. Chan, G.N.Y.; Cannon, R.E. Assessment of Ex Vivo Transport Function in Isolated Rodent Brain Capillaries. *Curr. Protoc Pharmacol.* **2017**, *76*, 7.16.1–7.16.16. [CrossRef] [PubMed]
1154. Betz, A.L.; Firth, J.A.; Goldstein, G.W. Polarity of the blood-brain barrier: Distribution of enzymes between the luminal and antiluminal membranes of brain capillary endothelial cells. *Brain Res.* **1980**, *192*, 17–28. [CrossRef]
1155. Sanchez del Pino, M.M.; Hawkins, R.A.; Peterson, D.R. Neutral amino acid transport by the blood-brain barrier. Membrane vesicle studies. *J. Biol. Chem.* **1992**, *267*, 25951–25957. [CrossRef]
1156. Boado, R.J.; Pardridge, W.M. Molecular cloning of the bovine blood-brain barrier glucose transporter cDNA and demonstration of phylogenetic conservation of the 5'-untranslated region. *Mol. Cell Neurosci.* **1990**, *1*, 224–232. [CrossRef]
1157. Enerson, B.E.; Drewes, L.R. The rat blood-brain barrier transcriptome. *J. Cereb. Blood Flow Metab.* **2006**, *26*, 959–973. [CrossRef]
1158. Daneman, R.; Zhou, L.; Agalliu, D.; Cahoy, J.D.; Kaushal, A.; Barres, B.A. The mouse blood-brain barrier transcriptome: A new resource for understanding the development and function of brain endothelial cells. *PLoS ONE* **2010**, *5*, e13741. [CrossRef]
1159. Chasseigneaux, S.; Moraca, Y.; Cochois-Guegan, V.; Boulay, A.C.; Gilbert, A.; Le Crom, S.; Blugeon, C.; Firmo, C.; Cisternino, S.; Laplanche, J.L.; et al. Isolation and differential transcriptome of vascular smooth muscle cells and mid-capillary pericytes from the rat brain. *Sci. Rep.* **2018**, *8*, 12272. [CrossRef]
1160. Munji, R.N.; Soung, A.L.; Weiner, G.A.; Sohet, F.; Semple, B.D.; Trivedi, A.; Gimlin, K.; Kotoda, M.; Korai, M.; Aydin, S.; et al. Profiling the mouse brain endothelial transcriptome in health and disease models reveals a core blood-brain barrier dysfunction module. *Nat. Neurosci.* **2019**, *22*, 1892–1902. [CrossRef]
1161. Miyakawa, T. Vascular pathology in Alzheimer's disease. *Psychogeriatrics* **2010**, *10*, 39–44. [CrossRef]
1162. Pardridge, W.M.; Vinters, H.V.; Yang, J.; Eisenberg, J.; Choi, T.B.; Tourtellotte, W.W.; Huebner, V.; Shively, J.E. Amyloid angiopathy of Alzheimer's disease: Amino acid composition and partial sequence of a 4,200-dalton peptide isolated from cortical microvessels. *J. Neurochem.* **1987**, *49*, 1394–1401. [CrossRef]
1163. Glenner, G.G.; Wong, C.W. Alzheimer's disease: Initial report of the purification and characterization of a novel cerebrovascular amyloid protein. *Biochem. Biophys. Res. Commun.* **1984**, *120*, 885–890. [CrossRef]
1164. Grammas, P.; Ovase, R. Inflammatory factors are elevated in brain microvessels in Alzheimer's disease. *Neurobiol. Aging* **2001**, *22*, 837–842. [CrossRef]
1165. Luo, J.; Grammas, P. Endothelin-1 is elevated in Alzheimer's disease brain microvessels and is neuroprotective. *J. Alzheimer's Dis.* **2010**, *21*, 887–896. [CrossRef]
1166. Wang, S.; Qaisar, U.; Yin, X.; Grammas, P. Gene expression profiling in Alzheimer's disease brain microvessels. *J. Alzheimer's Dis.* **2012**, *31*, 193–205. [CrossRef]
1167. Kirabali, T.; Rigotti, S.; Siccoli, A.; Liebsch, F.; Shobo, A.; Hock, C.; Nitsch, R.M.; Multhaup, G.; Kulic, L. The amyloid-beta degradation intermediate Abeta34 is pericyte-associated and reduced in brain capillaries of patients with Alzheimer's disease. *Acta Neuropathol. Commun.* **2019**, *7*, 194. [CrossRef]
1168. Wu, G.F.; Alvarez, E. The immunopathophysiology of multiple sclerosis. *Neurol. Clin.* **2011**, *29*, 257–278. [CrossRef]
1169. Pardridge, W.M.; Yang, J.; Buciac, J.; Tourtellotte, W.W. Human brain microvascular DR-antigen. *J. Neurosci. Res.* **1989**, *23*, 337–341. [CrossRef]
1170. Washington, R.; Burton, J.; Todd, R.F., 3rd; Newman, W.; Dragovic, L.; Dore-Duffy, P. Expression of immunologically relevant endothelial cell activation antigens on isolated central nervous system microvessels from patients with multiple sclerosis. *Ann. Neurol.* **1994**, *35*, 89–97. [CrossRef] [PubMed]
1171. Pardridge, W.M.; Yang, J.; Eisenberg, J.; Tourtellotte, W.W. Isolation of intact capillaries and capillary plasma membranes from frozen human brain. *J. Neurosci. Res.* **1987**, *18*, 352–357. [CrossRef] [PubMed]
1172. Hartz, A.M.S.; Schulz, J.A.; Sokola, B.S.; Edelmann, S.E.; Shen, A.N.; Rempe, R.G.; Zhong, Y.; Seblani, N.E.; Bauer, B. Isolation of Cerebral Capillaries from Fresh Human Brain Tissue. *J. Vis. Exp.* **2018**, e57346. [CrossRef]
1173. Bowman, P.D.; Ennis, S.R.; Rarey, K.E.; Betz, A.L.; Goldstein, G.W. Brain microvessel endothelial cells in tissue culture: A model for study of blood-brain barrier permeability. *Ann. Neurol.* **1983**, *14*, 396–402. [CrossRef] [PubMed]
1174. Pardridge, W.M.; Triguero, D.; Yang, J.; Cancilla, P.A. Comparison of in vitro and in vivo models of drug transcytosis through the blood-brain barrier. *J. Pharmacol. Exp. Ther.* **1990**, *253*, 884–891.
1175. Boado, R.J.; Li, J.Y.; Tsukamoto, H.; Pardridge, W.M. Hypoxia induces de-stabilization of the LAT1 large neutral amino acid transporter mRNA in brain capillary endothelial cells. *J. Neurochem.* **2003**, *85*, 1037–1042. [CrossRef]
1176. DeBault, L.E.; Cancilla, P.A. gamma-Glutamyl transpeptidase in isolated brain endothelial cells: Induction by glial cells in vitro. *Science* **1980**, *207*, 653–655. [CrossRef]
1177. Dehouck, M.P.; Meresse, S.; Delorme, P.; Fruchart, J.C.; Cecchelli, R. An easier, reproducible, and mass-production method to study the blood-brain barrier in vitro. *J. Neurochem.* **1990**, *54*, 1798–1801. [CrossRef]

1178. Mairey, E.; Genovesio, A.; Donnadiou, E.; Bernard, C.; Jaubert, F.; Pinaud, E.; Seylaz, J.; Olivo-Marin, J.C.; Nassif, X.; Dumenil, G. Cerebral microcirculation shear stress levels determine *Neisseria meningitidis* attachment sites along the blood-brain barrier. *J. Exp. Med.* **2006**, *203*, 1939–1950. [CrossRef]
1179. Santaguida, S.; Janigro, D.; Hossain, M.; Oby, E.; Rapp, E.; Cucullo, L. Side by side comparison between dynamic versus static models of blood-brain barrier in vitro: A permeability study. *Brain Res.* **2006**, *1109*, 1–13. [CrossRef]
1180. Brown, T.D.; Nowak, M.; Bayles, A.V.; Prabhakarandian, B.; Karande, P.; Lahann, J.; Helgeson, M.E.; Mitragotri, S. A microfluidic model of human brain (muHuB) for assessment of blood brain barrier. *Bioeng. Transl. Med.* **2019**, *4*, e10126. [CrossRef]
1181. Ma, S.H.; Lepak, L.A.; Hussain, R.J.; Shain, W.; Shuler, M.L. An endothelial and astrocyte co-culture model of the blood-brain barrier utilizing an ultra-thin, nanofabricated silicon nitride membrane. *Lab Chip* **2005**, *5*, 74–85. [CrossRef]
1182. Lippmann, E.S.; Azarin, S.M.; Kay, J.E.; Nessler, R.A.; Wilson, H.K.; Al-Ahmad, A.; Palecek, S.P.; Shusta, E.V. Derivation of blood-brain barrier endothelial cells from human pluripotent stem cells. *Nat. Biotechnol.* **2012**, *30*, 783–791. [CrossRef]
1183. Lippmann, E.S.; Al-Ahmad, A.; Azarin, S.M.; Palecek, S.P.; Shusta, E.V. A retinoic acid-enhanced, multicellular human blood-brain barrier model derived from stem cell sources. *Sci. Rep.* **2014**, *4*, 4160. [CrossRef]
1184. Mizee, M.R.; Wooldrik, D.; Lakeman, K.A.; van het Hof, B.; Drexhage, J.A.; Geerts, D.; Bugiani, M.; Aronica, E.; Mebius, R.E.; Prat, A.; et al. Retinoic acid induces blood-brain barrier development. *J. Neurosci.* **2013**, *33*, 1660–1671. [CrossRef]
1185. Daneman, R.; Agalliu, D.; Zhou, L.; Kuhnert, F.; Kuo, C.J.; Barres, B.A. Wnt/beta-catenin signaling is required for CNS, but not non-CNS, angiogenesis. *Proc. Natl. Acad. Sci. USA* **2009**, *106*, 641–646. [CrossRef]
1186. Katt, M.E.; Shusta, E.V. In vitro Models of the Blood-Brain Barrier: Building in physiological complexity. *Curr. Opin. Chem. Eng.* **2020**, *30*, 42–52. [CrossRef] [PubMed]
1187. Al-Ahmad, A.J. Comparative study of expression and activity of glucose transporters between stem cell-derived brain microvascular endothelial cells and hCMEC/D3 cells. *Am. J. Physiol. Cell Physiol.* **2017**, *313*, C421–C429. [CrossRef] [PubMed]
1188. Coisne, C.; Dehouck, L.; Faveeuw, C.; Delplace, Y.; Miller, F.; Landry, C.; Morissette, C.; Fenart, L.; Cecchelli, R.; Tremblay, P.; et al. Mouse syngenic in vitro blood-brain barrier model: A new tool to examine inflammatory events in cerebral endothelium. *Lab. Invest.* **2005**, *85*, 734–746. [CrossRef] [PubMed]
1189. Canfield, S.G.; Stebbins, M.J.; Faubion, M.G.; Gastfriend, B.D.; Palecek, S.P.; Shusta, E.V. An isogenic neurovascular unit model comprised of human induced pluripotent stem cell-derived brain microvascular endothelial cells, pericytes, astrocytes, and neurons. *Fluids Barriers CNS* **2019**, *16*, 25. [CrossRef]
1190. Miah, M.K.; Bickel, U.; Mehvar, R. Effects of hepatic ischemia-reperfusion injury on the blood-brain barrier permeability to [<sup>14</sup>C] and [<sup>13</sup>C]sucrose. *Metab. Brain Dis.* **2017**, *32*, 1903–1912. [CrossRef]
1191. Miah, M.K.; Chowdhury, E.A.; Bickel, U.; Mehvar, R. Evaluation of [<sup>14</sup>C] and [<sup>13</sup>C]Sucrose as Blood-Brain Barrier Permeability Markers. *J. Pharm. Sci.* **2017**, *106*, 1659–1669. [CrossRef]
1192. Sabbagh, M.F.; Nathans, J. A genome-wide view of the de-differentiation of central nervous system endothelial cells in culture. *Elife* **2020**, *9*, e51276. [CrossRef]
1193. Calabria, A.R.; Shusta, E.V. A genomic comparison of in vivo and in vitro brain microvascular endothelial cells. *J. Cereb. Blood Flow Metab.* **2008**, *28*, 135–148. [CrossRef]
1194. Urich, E.; Lazic, S.E.; Molnos, J.; Wells, I.; Freskgard, P.O. Transcriptional profiling of human brain endothelial cells reveals key properties crucial for predictive in vitro blood-brain barrier models. *PLoS ONE* **2012**, *7*, e38149. [CrossRef] [PubMed]
1195. Meyer, J.; Rauh, J.; Galla, H.J. The susceptibility of cerebral endothelial cells to astroglial induction of blood-brain barrier enzymes depends on their proliferative state. *J. Neurochem.* **1991**, *57*, 1971–1977. [CrossRef] [PubMed]
1196. Hurwitz, A.A.; Berman, J.W.; Rashbaum, W.K.; Lyman, W.D. Human fetal astrocytes induce the expression of blood-brain barrier specific proteins by autologous endothelial cells. *Brain Res.* **1993**, *625*, 238–243. [CrossRef]
1197. Canfield, S.G.; Stebbins, M.J.; Morales, B.S.; Asai, S.W.; Vatine, G.D.; Svendsen, C.N.; Palecek, S.P.; Shusta, E.V. An isogenic blood-brain barrier model comprising brain endothelial cells, astrocytes, and neurons derived from human induced pluripotent stem cells. *J. Neurochem.* **2017**, *140*, 874–888. [CrossRef]
1198. Cho, C.F.; Wolfe, J.M.; Fadzen, C.M.; Calligaris, D.; Hornburg, K.; Chiocca, E.A.; Agar, N.Y.R.; Pentelute, B.L.; Lawler, S.E. Blood-brain-barrier spheroids as an in vitro screening platform for brain-penetrating agents. *Nat. Commun.* **2017**, *8*, 15623. [CrossRef]
1199. Deosarkar, S.P.; Prabhakarandian, B.; Wang, B.; Sheffield, J.B.; Krynska, B.; Kiani, M.F. A Novel Dynamic Neonatal Blood-Brain Barrier on a Chip. *PLoS ONE* **2015**, *10*, e0142725. [CrossRef]
1200. Loryan, I.; Reichel, A.; Feng, B.; Bundgaard, C.; Shaffer, C.; Kalvass, C.; Bednarczyk, D.; Morrison, D.; Lesuisse, D.; Hoppe, E.; et al. Unbound Brain-to-Plasma Partition Coefficient,  $K_{p,uu,brain}$ —A Game Changing Parameter for CNS Drug Discovery and Development. *Pharm. Res.* **2022**, 1–21. [CrossRef]
1201. Gibaldi, M.; Koup, J.R. Pharmacokinetic concepts? Drug binding, apparent volume of distribution and clearance. *Eur. J. Clin. Pharmacol.* **1981**, *20*, 299–305. [CrossRef]
1202. Panza, F.; Lozupone, M.; Dibello, V.; Greco, A.; Daniele, A.; Seripa, D.; Logroscino, G.; Imbimbo, B.P. Are antibodies directed against amyloid-beta (Aβ) oligomers the last call for the Aβ hypothesis of Alzheimer’s disease? *Immunotherapy* **2019**, *11*, 3–6. [CrossRef]
1203. Cummings, J.; Lee, G.; Ritter, A.; Sabbagh, M.; Zhong, K. Alzheimer’s disease drug development pipeline: 2019. *Alzheimer’s Dement.* **2019**, *5*, 272–293. [CrossRef]

1204. Gauthier, S.; Aisen, P.S.; Cummings, J.; Detke, M.J.; Longo, F.M.; Raman, R.; Sabbagh, M.; Schneider, L.; Tanzi, R.; Tariot, P.; et al. Non-Amyloid Approaches to Disease Modification for Alzheimer's Disease: An EU/US CTAD Task Force Report. *J. Prev. Alzheimer's Dis.* **2020**, *7*, 152–157. [CrossRef]
1205. Sun, A.; Benet, L.Z. Late-Stage Failures of Monoclonal Antibody Drugs: A Retrospective Case Study Analysis. *Pharmacology* **2020**, *105*, 145–163. [CrossRef]
1206. Prasad, E.M.; Hung, S.Y. Current Therapies in Clinical Trials of Parkinson's Disease: A 2021 Update. *Pharmaceutics* **2021**, *14*, 717. [CrossRef]
1207. Macrae, I.M.; Allan, S.M. Stroke: The past, present and future. *Brain Neurosci. Adv.* **2018**, *2*, 2398212818810689. [CrossRef]
1208. Sokolov, A.V.; Dostdar, S.A.; Attwood, M.M.; Krasilnikova, A.A.; Ilina, A.A.; Nabieva, A.S.; Lisitsyna, A.A.; Chubarev, V.N.; Tarasov, V.V.; Schioth, H.B. Brain Cancer Drug Discovery: Clinical Trials, Drug Classes, Targets, and Combinatorial Therapies. *Pharmacol. Rev.* **2021**, *73*, 1172–1203. [CrossRef]
1209. Bard, J.; Wall, M.D.; Lazari, O.; Arjomand, J.; Munoz-Sanjuan, I. Advances in huntington disease drug discovery: Novel approaches to model disease phenotypes. *J. Biomol. Screen.* **2014**, *19*, 191–204. [CrossRef]
1210. DeLoach, A.; Cozart, M.; Kiaei, A.; Kiaei, M. A retrospective review of the progress in amyotrophic lateral sclerosis drug discovery over the last decade and a look at the latest strategies. *Expert Opin. Drug Discov.* **2015**, *10*, 1099–1118. [CrossRef]
1211. Perlman, S.L. Update on the Treatment of Ataxia: Medication and Emerging Therapies. *Neurotherapeutics* **2020**, *17*, 1660–1664. [CrossRef]
1212. Shah, M.; Peterson, C.; Yilmaz, E.; Halalmeh, D.R.; Moisi, M. Current advancements in the management of spinal cord injury: A comprehensive review of literature. *Surg. Neurol. Int.* **2020**, *11*, 2. [CrossRef]
1213. Mondello, S.; Hasan, A.; Shear, D.A. Editorial: Developing Successful Neuroprotective Treatments for TBI: Translational Approaches, Novel Directions, Opportunities and Challenges. *Front. Neurol.* **2019**, *10*, 1326. [CrossRef]
1214. Xu, B.; LaBar, K.S. Advances in understanding addiction treatment and recovery. *Sci. Adv.* **2019**, *5*, eaaz6596. [CrossRef]
1215. Bauchner, H.; Alexander, G.C. Rejection of Aducanumab (Aduhelm) by the Health Care Community: Lessons Learned and the Path Ahead. *Med. Care* **2022**, *60*, 392–393. [CrossRef]
1216. Kwon, D. Failure of genetic therapies for Huntington's devastates community. *Nature* **2021**, *593*, 180. [CrossRef]
1217. Mullard, A. ALS antisense drug falters in phase III. *Nat. Rev. Drug Discov.* **2021**, *20*, 883–885. [CrossRef]

Review

# IgG Fusion Proteins for Brain Delivery of Biologics via Blood–Brain Barrier Receptor-Mediated Transport

Ruben J. Boado

Department of Medicine, University of California, Los Angeles (UCLA), Los Angeles, CA 90095, USA; boado@ucla.edu

**Abstract:** The treatment of neurological disorders with large-molecule biotherapeutics requires that the therapeutic drug be transported across the blood–brain barrier (BBB). However, recombinant biotherapeutics, such as neurotrophins, enzymes, decoy receptors, and monoclonal antibodies (MAb), do not cross the BBB. These biotherapeutics can be re-engineered as brain-penetrating bifunctional IgG fusion proteins. These recombinant proteins comprise two domains, the transport domain and the therapeutic domain, respectively. The transport domain is an MAb that acts as a molecular Trojan horse by targeting a BBB-specific endogenous receptor that induces receptor-mediated transcytosis into the brain, such as the human insulin receptor (HIR) or the transferrin receptor (TfR). The therapeutic domain of the IgG fusion protein exerts its pharmacological effect in the brain once across the BBB. A generation of bifunctional IgG fusion proteins has been engineered using genetically engineered MAbs directed to either the BBB HIR or TfR as the transport domain. These IgG fusion proteins were validated in animal models of lysosomal storage disorders; acute brain conditions, such as stroke; or chronic neurodegeneration, such as Parkinson’s disease and Alzheimer’s disease. Human phase I–III clinical trials were also completed for Hurler MPSI and Hunter MPSII using brain-penetrating IgG-iduronidase and -iduronate-2-sulfatase fusion protein, respectively.

**Keywords:** blood–brain barrier; protein-based therapy; monoclonal antibody; insulin receptor; transferrin receptor; lysosomal storage disorders; fusion proteins; Parkinson’s disease; Alzheimer’s disease; neurotrophic factors; decoy receptors

**Citation:** Boado, R.J. IgG Fusion Proteins for Brain Delivery of Biologics via Blood–Brain Barrier Receptor-Mediated Transport. *Pharmaceutics* **2022**, *14*, 1476. <https://doi.org/10.3390/pharmaceutics14071476>

Academic Editor: Ken-ichi Hosoya

Received: 15 June 2022

Accepted: 12 July 2022

Published: 15 July 2022

**Publisher’s Note:** MDPI stays neutral with regard to jurisdictional claims in published maps and institutional affiliations.



**Copyright:** © 2022 by the author. Licensee MDPI, Basel, Switzerland. This article is an open access article distributed under the terms and conditions of the Creative Commons Attribution (CC BY) license (<https://creativecommons.org/licenses/by/4.0/>).

## 1. Introduction

The hematoencephalic or blood–brain barrier (BBB) is the anatomical and molecular barrier that separates in vivo the brain from the blood. This barrier evolved to prevent the transport to the brain of peripheral neurotransmitters, cytokines, and microorganisms, which may produce deleterious, if not lethal, effects in the central nervous system (CNS). The characteristics of this barrier have been extensively reviewed, and it is basically only permeable to lipophilic molecules of <400 Da [1–4]. Thus, histamine, a small polar molecule of 110 Da does not cross the BBB [2]. Hydrophobic nutrients of low molecular weight gain access to the brain through the BBB via facilitated transporters, as in the case of GLUT1 for glucose and LAT1 for large neutral amino acids [5,6]. Proteins, in general, do not cross the BBB; however, there are a few exceptions where proteins produced in peripheral organs gain access to the brain via receptor-mediated transcytosis, as in the case of insulin, transferrin, leptin, and insulin-like growth factor [7–10]. Targeting these BBB endogenous transporters with monoclonal antibodies gained attention in the early 1990s, and an in vivo demonstration of the efficacy of a brain-penetrating construct was published using vasopressin intestinal peptide (VIP) conjugated to the OX26 monoclonal antibody to the rat transferrin receptor using the avidin–biotin technology [11]. The administration of the OX26-avidin-biotinylated-VIP produced a marked increase in the brain blood flow. On the contrary, the biotinylated-VIP had no effect in the brain, as it does not cross the BBB [11]. The construction and efficacy of chemical conjugates targeting either the transferrin or the insulin receptor in rodents and non-human primates have been reported [12–15].

With the cloning of monoclonal antibodies to the mouse transferrin (TfRMAB) and human insulin (HIRMAB) BBB receptors, respectively [16,17], the engineering of bifunctional IgG fusion proteins was possible [18–20]. These fusion proteins comprise a transport domain, i.e., TfRMAB or HIRMAb, and a therapeutic domain fused to the C-terminus of either the heavy or light chain of the transporting MAb. Thus, any potential protein therapeutic can be transported through the BBB into the brain in the form of a fusion protein targeting a BBB-receptor-mediated transport (Figure 1). In this schematic representation, a protein therapeutic is fused to the C-terminus of the transporting MAb, which binds to a BBB receptor, inducing the transport of the fusion protein through the BBB. The binding of the MAb fusion protein to its BBB receptor does not interfere with the binding of its endogenous ligand, so both the ligand and the MAb fusion are transported through the BBB and released into the brain interstitial fluid. Depending on the characteristics of the therapeutic domain, the fusion protein can (i) target a receptor on the surface of brain cells, as in the case of neurotrophic factors; (ii) bind and inactivate a target molecule, as in the case of decoy receptors and bispecific MAbs; and (iii) be internalized in brain cells via receptor-mediated endocytosis through the same transport systems used to cross the BBB, as in the case of enzymes for the treatment of lysosomal storage disorders (LSD) and/or bispecific MAbs. A detailed mathematical model of receptor-mediated transport across the BBB was recently published [21]. A generation of IgG fusion proteins targeting both the human and mouse BBB transport systems has been engineered (Tables 1 and 2). The aim of this article is to review this generation of IgG fusion proteins.

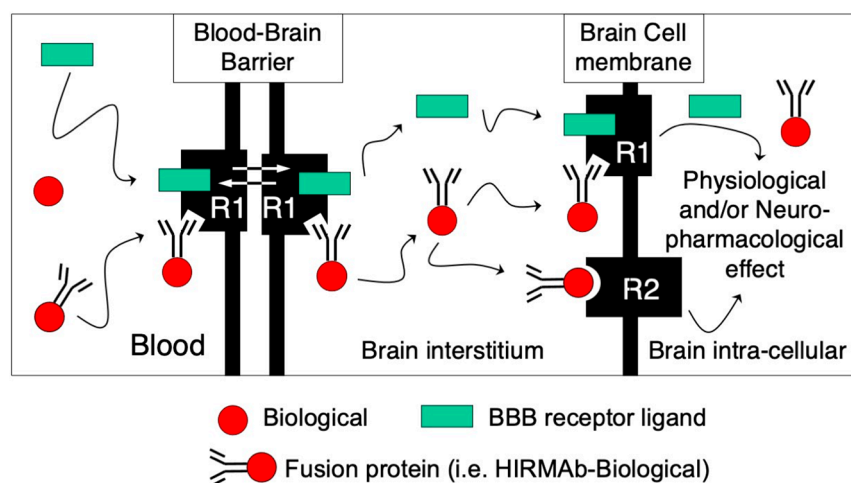


**Figure 1.** Receptor-mediated transport of IgG fusion proteins across the BBB. Biologicals (red circle) do not cross the BBB and stay in circulation following IV administration, as in the case of enzymes, MAbs, decoy receptors, and/or neurotrophic factors. These potential therapeutic agents for the CNS can be re-engineered as fusion proteins with an MAb targeting a BBB receptor that induces receptor-mediated transcytosis (R1), such as the human BBB insulin receptor (HIR) or the transferrin receptor (TfR). The transport domain of the IgG fusion protein targets the BBB R1 endogenous receptor to gain access to the brain. The transport MAb binds to an exofacial epitope of the receptor without interfering with the normal transport of its endogenous ligand (green rectangle) to gain access to the brain. Depending on the therapeutic domain of the IgG fusion protein, it can (i) bind to its ligand in the brain interstitial compartment, as in the case of bispecific MAbs or decoy receptors; (ii) target a brain cell membrane receptor (R2), such as neurotrophic factors; or (iii) be endocytosed via the same targeted R1 receptor in brain cells as lysosomal enzymes to produce physiological and/or neuropharmacological effect.

**Table 1.** Brain-penetrating human IgG fusion proteins.

IgG Fusion Protein <sup>1</sup>	Therapeutic Domain	Indication	Reference
HIRMAB-IDUA (valanafusp alpha)	Iduronidase (IDUA)	Hurler syndrome (MPS I)	[22]
HIRMAB-IDS	Iduronate-2-sulfatase (IDS)	Hunter syndrome (MPS II)	[23]
TfRMAB-IDS (pabinafusp alfa)	Iduronate-2-sulfatase (IDS)	Hunter syndrome (MPS II)	[24]
HIRMAB-ASA	Arylsulfatase A (ASA)	Metachromatic leukodystrophy *	[25]
HIRMAB-SGSH	Sulfamidase (SGSH)	Sanfilippo A (MPSIIIA) *	[26]
HIRMAB-NAGLU	N-acetyl-alpha-D-glucosaminidase (NAGLU)	Sanfilippo B (MPSIIIB) *	[27]
HIRMAB-ASM	Acid shingomyelinase (ASM)	Niemann–Pick A/B *	[28]
HIRMAB-HEXA	Hexoaminidase A (HEXA)	Tay–Sachs *	[28]
HIRMAB-PPT1	Palmitoyl-protein thioesterase (PPT1)	Batten Type 1 *	[28]
HIRMAB-GLB1	$\beta$ -galactosidase (GLB1)	GM1-gangliosidosis *	[28]
HIRMAB-A $\beta$ bispecific antibody	Anti-A $\beta$ amyloid single-chain Fv antibody (scFv)	Alzheimer's *	[29]
HIRMAB-TNFR	Tumor necrosis factor decoy receptor (TNFR)	Parkinson's, ALS, Alzheimer's, and/or stroke *	[30]
HIRMAB-EPO	Erythropoietin (EPO)	Parkinson's, Alzheimer's, and/or Friedreich ataxia *	[31]
HIRMAB-GDNF	Glial-cell-derived neurotrophic factor (GDNF)	Parkinson's, stroke, and/or drug/EtOH addiction *	[32]
HIRMAB-BDNF	Brain-derived neurotrophic factor (BDNF)	Stroke, neural repair *	[33]
HIRMAB-Avidin	Any mono-biotinylated therapeutic	Various	[34]

<sup>1</sup> The transport domain of these human fusion proteins is a monoclonal antibody directed to the human BBB insulin receptor (HIRMAB) or the transferrin receptor (TfRMAB). The therapeutic domain of the fusion protein and its application are listed for the corresponding IgG fusion protein. \* Indication has a primary CNS disease burden.

**Table 2.** Brain-penetrating mouse IgG fusion proteins.

IgG Fusion Protein <sup>1</sup>	Therapeutic Domain	Indication	Reference
TfRMAB-IDUA	Iduronidase (IDUA)	Hurler syndrome (MPS I)	[35]
TfRMAB-IDS	Iduronate-2-sulfatase (IDS)	Hunter syndrome (MPS II)	[36]
TfRMAB-SGSH	Sulfamidase (SGSH)	Sanfilippo A (MPSIIIA) *	[37]
TfRMAB-A $\beta$ bispecific antibody	Anti-A $\beta$ amyloid single-chain Fv antibody (scFv)	Alzheimer's *	[38]
TfRMAB-TNFR	Tumor necrosis factor decoy receptor (TNFR)	Parkinson's, Alzheimer's, and/or stroke *	[39]
TfRMAB-EPO	Erythropoietin (EPO)	Parkinson's, Alzheimer's, and/or stroke *	[40]
TfRMAB-GDNF	Glial-cell-derived neurotrophic factor (GDNF)	Parkinson's, and/or stroke *	[41]
TfRMAB-Avidin	Any mono-biotinylated therapeutic	Various	[42]

<sup>1</sup> The transport domain of these mouse fusion proteins is a monoclonal antibody directed to the mouse BBB-transferrin receptor (TfRMAB). The therapeutic domain of the fusion protein and its experimental application are listed for the corresponding IgG fusion protein. \* Indication has a primary CNS disease burden.

## 2. Genetic Engineering of IgG Fusion Proteins

The genetic engineering of IgG fusion proteins has been performed using either individual expression vectors for light- and heavy-chain expression genes or tandem vectors carrying both light- and heavy-chain expression genes [22–42]. The cDNA corresponding to the mature therapeutic domain (without the signal peptide) is ligated into the C-terminus of the appropriate expression gene via designed restriction endonuclease sites, which provides a short linker composed of 2–4 serine residues. The therapeutic gene can be inserted in either the heavy or light chain of the transport MAb, and a few examples are shown in Figure 2. In particular cases, the short linker approach produces suboptimal levels of enzyme activity and/or production, which may be restored by the introduction of a long

31-amino-acid linker corresponding to the IgG3 hinge region [27,28]. The engineering of IgG fusion proteins may be performed by fusing the therapeutic domain on the N-terminus of the transport MAb, i.e., the heavy chain of the MAb. However, it was demonstrated using a glucuronidase (GUSB) fusion protein that this construct had a marked reduction in the affinity for the target receptor, to levels that would abolish its transport through the BBB [43]. For studies in rodents, the engineering of IgG fusion proteins has been performed targeting the mouse or rat transferrin receptor [17,19,20,44]. For studies in humans and non-human primates, the IgG fusion proteins were initially produced with an MAb directed to the human insulin receptor, and lately the MABs have been directed to the human transferrin receptor as well [16,24]. The anti-human insulin receptor MAb cross-reacts with the BBB insulin receptor of old-world primates, such as the rhesus monkey [45]. Targeting the rodent transferrin receptor or the human insulin or transferrin receptors at the BBB resulted in a comparable brain uptake of 1–3% of the injected dose. This relates to the abundance of these receptors at the BBB, which is comparable in humans [46]. However, the abundance of the mouse BBB transferrin receptor is approximately 7-fold higher than that of the mouse BBB insulin receptor [46,47]. Therefore, targeting the mouse BBB insulin receptor would produce lower levels of brain uptake. The manufacturing of IgG fusion proteins presents advantages compared to chemical conjugation, including simplified downstream purification due to protein-A capture [48]. IgG fusion proteins were engineered targeting both transferrin and insulin BBB receptors with high affinities in the low nM range (Tables 1 and 2). The extensive number of peer-reviewed publications discussed below validated the high-affinity approach for the transport across the BBB, targeting either the insulin or the transferrin receptor.

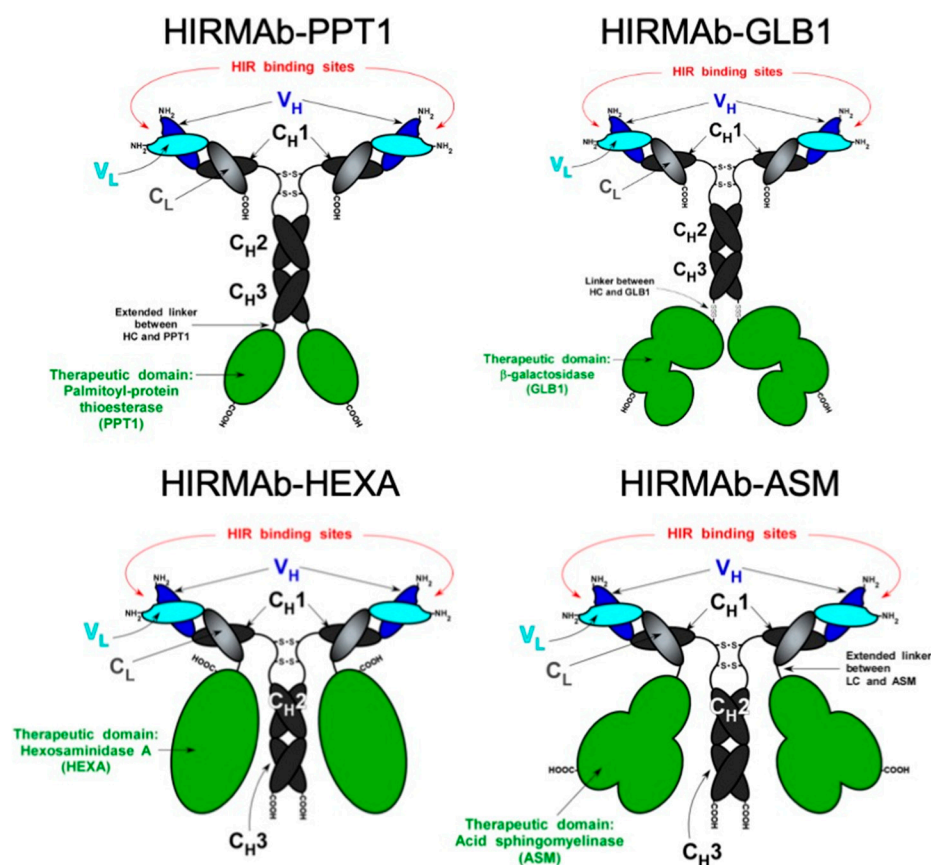


**Figure 2.** Genetic engineering of IgG fusion proteins. The therapeutic domain of the IgG bifunctional fusion protein can be fused to the C-terminus of either the heavy or light chain of the transport

monoclonal antibody (MAb), in this case targeting the BBB human insulin receptor (HIR). The indication for these IgG fusion proteins is: HIRMAB-PPT1, Batten disease type 1; HIRMAB-GLB1, GM1-gangliosidosis; HIRMAB-HEXA, Tay–Sachs disease; and HIRMAB-ASM, Niemann–Pick disease types A and B. From reference [28].

There are, however, few publications postulating that a low-affinity monovalent MAb directed to the BBB TfR transport system may result in improved brain uptake [49,50]. This is based on the hypothesis that bivalent TfRMABs cause TfR clustering and selective triage of the antibody-TfR complex to the lysosome and degradation of TfR on the cell membrane, whereas this is avoided with monovalent TfRMABs [49,50]. However, this was based on tissue culture experiments with TfRMAB-avidin fusion proteins, which are known to form tetrameric structures from the association of avidin monomers [51,52]. No toxic effects of other high-affinity TfRMAB fusion proteins were reported in *in vitro* or *in vivo* studies. Chronic treatment with intravenous (IV) 2 mg/kg BW TfRMAB-GDNF twice weekly for 12 weeks produced no downregulation of the BBB TfR, as the terminal pharmacokinetics and brain uptake were comparable to those obtained prior to the chronic treatment [53]. Moreover, no evidence of BBB TfR downregulation was reported in a chronic study performed in the cynomolgus monkey with pabinafusp alfa, the high-affinity human TfRMAB-IDS fusion protein, with doses up to 30 mg/kg/week for 26 weeks [54]. Kinetics modeling of the receptor-mediated transport across the BBB showed that the optimal receptor-binding properties would be an MAb with a KD of 0.5–5 nM and an association rate constant ( $k_{on}$ ) of  $10^5$ – $10^6$  M<sup>-1</sup> s<sup>-1</sup>, which would produce a dissociation T<sub>1/2</sub> of ~10–120 min [55]. Targeting MABs, i.e., TfRMAB and/or HIRMAB, with these kinetic properties produced therapeutic brain delivery at a low injection dose of 1–3 mg/kg BW in the various CNS models discussed below, including clinical trials in LSD.

The brain uptake via a BBB receptor-mediated transport is a function of the antibody affinity for the receptor, the injection dose, and the plasma area under the curve (AUC), which may be affected by the therapeutic domain of the fusion protein, as in the case of LSD enzymes targeting peripheral M6P receptors. For example, the fusion of IDUA to the transport MAb reduces the brain AUC of the fusion protein compared to the MAb alone [56]. Kinetics modeling showed that the lower the affinity of the antibody for the TfR, the greater the ID required to maintain a given brain AUC [55]. For example, the brain AUC of a TfRMAB-IDUA fusion protein with a moderate affinity for the TfR, KD = 36 nM, would require an injected dose of 30 mg/kg BW to produce a brain AUC comparable to the one of a TfRMAB-IDUA fusion protein with high affinity (KD = 0.36–3.6 nM) at a 10-fold lower injected dose of 3 mg/kg BW [55]. A lower therapeutic dose is also preferred to reduce potential adverse effects, as in the case of IgG-neurotrophic factor fusion proteins [31,57].

### 3. Enzyme-IgG Fusion Proteins

Most of the lysosomal storage disorders (LSD) affect the CNS, causing neurologic manifestations such as mental retardation and neurodegeneration [58,59]. The treatment of LSD is possible with enzyme replacement therapy (ERT). However, ERT is unable to treat the brain, as these large proteins do not cross the BBB [60,61]. The re-engineering of these enzymes as brain-penetrating IgG fusion proteins represents a potential solution for the treatment of LSD. Today, the genetic engineering of several IgG-enzyme fusion proteins has been reported (Tables 1 and 2). These fusion proteins were designed for the treatment of a variety of LSDs, and their corresponding bifunctionality was validated biochemically and in experimental animals as well as in clinical trials. This technology was also validated for other potential therapeutics for the CNS, including decoy receptors, bispecific MABs, and neurotrophins (Tables 1 and 2).

#### 3.1. HIRMAB-Iduronidase (HIRMAB-IDUA)

A brain-penetrating iduronidase (IDUA), an enzyme that is mutated in Hurler’s MPSI syndrome [58], was completed by the insertion of the cDNA of the mature human IDUA (GenBank NP\_00194), minus the 26-amino-acid signal peptide at the C-terminus of the



heavy chain of the HIRMAb via a short Ser-Ser linker (Table 1) [22]. The HIRMAb-IDUA fusion protein maintained the affinity for the targeting insulin receptor in the low nM range, and the IDUA enzyme activity was comparable to the specific activity of the recombinant IDUA [22]. The fusion protein targeted the lysosomal compartment in Hurler fibroblasts and markedly reduced the accumulation of glycosaminoglycans (GAG) in these cells [22]. The biodistribution of the HIRMAb-IDUA was investigated in the rhesus monkey using radio-iodinated material and compared to that of the recombinant human IDUA (Aldurazyme) [62]. The quantitative whole-body autoradiography confirmed the transport of the fusion protein across the BBB, showing a global biodistribution of the HIRMAb-IDUA throughout the brain (Figure 3). On the contrary, recombinant IDUA did not penetrate the brain through the BBB, showing background activity in the primate brain (Figure 3). The levels of brain uptake of the HIRMAb-IDUA approximated 1% of injected dose (ID) [22,62]. The biodistribution of the HIRMAb-IDUA fusion protein in the peripheral tissues was comparable to that of the recombinant IDUA, as both were taken up in the peripheral organs through the mannose-6-phosphate (M6P) receptor [62]. In addition, a significant increase in the uptake of the HIRMAb-IDUA fusion protein was observed in the vertebral bodies and joints [62]. Taking into consideration that the normal enzyme activity of IDUA in a human brain ranges from 0.5 to 1.5 units/mg of protein [63], it may be possible to normalize the brain IDUA in a Hurler individual with the administration of 1 mg/kg BW of the fusion protein, which may result in a brain concentration of 3.0 ng/mg of brain protein or 1.1 units of IDUA enzyme activity per mg of brain protein [22].



**Figure 3.** Autoradiography through eight parallel sagittal sections of the cerebral hemisphere of the rhesus monkey obtained 2 h after the IV administration of either the [ $^{125}$ I]-HIRMAb-IDUA fusion protein (**bottom**) or [ $^{125}$ I]-IDUA (**top**). The section on the left-hand side is the most lateral part of brain, and the section on the right-hand side is the most medial part of brain. The cerebellum is visible in the more medial sections of the brain. The BBB-penetrating HIRMAb-IDUA gained access to the brain, producing a global distribution throughout this organ. On the contrary, IDUA does not cross the BBB, showing just background activity in the primate brain. From [62] with permission.

The efficacy of the IgG-IDUA fusion protein was investigated in a mouse model of MPSI using a surrogate fusion protein that comprised the mouse TfrMAb fused to the mouse IDUA (Table 2) [35]. Six-month-old MPSI mice were treated with 1 mg/kg BW TfrMAb-IDUA IV twice weekly for 8 weeks. Electron microscopy showed a marked reduction in lysosomal inclusion bodies in animals treated with brain-penetrating IDUA fusion protein compared with saline (Figure 4) [35]. The administration of the TfrMAb-IDUA produced a marked reduction in GAG in the peripheral organs that was comparable to that reported for the recombinant IDUA [35].

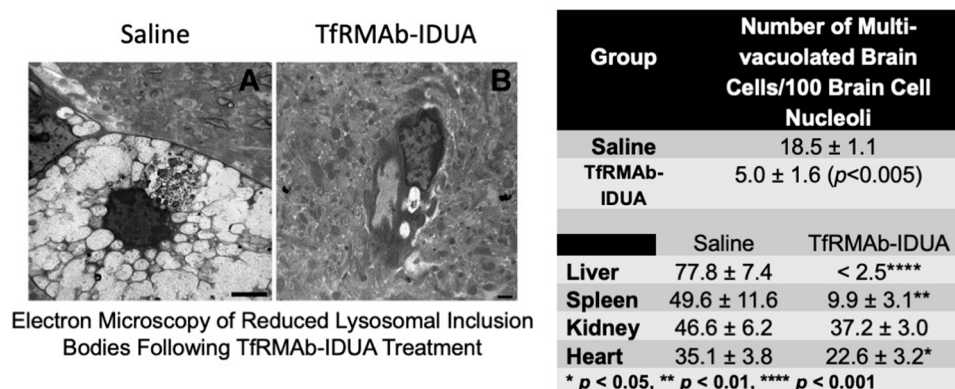


**Figure 4.** Reversal of lysosomal storage in brain of adult MPSI mice with IV injections of mouse TfrMab-IDUA fusion protein. Six-month-old MPSI mice were treated with 1 mg/kg BW TfrMab-IDUA IV twice weekly for 8 weeks. Electron microscopy showed a marked reduction in lysosomal inclusion bodies in animals treated with brain-penetrating IDUA fusion protein (**B**) compared with saline (**A**), resulting in a 73% reduction in brain lysosomal inclusion bodies (**right top**). The administration of the TfrMab-IDUA produced a marked reduction in glycosaminoglycans (GAG) in the peripheral organs (**right bottom**) that was comparable to that reported for the recombinant IDUA. The data (means ± SE) are terminal organ assays at the end of the 8-week study of MPSI mice treated with either saline or 1 mg/kg BW of the TfrMab-IDUA fusion protein. From [35] with permission.

The HIRMAb-IDUA (valanafusp alpha) was the first brain-penetrating IgG fusion protein that completed a phase I/II clinical trial in Hurler MPSI [64,65]. Pediatric MPSI patients treated with laronidase were switched to valanafusp alpha and treated with weekly IV infusions of 1, 3, or 6 mg/kg for 6 months. Patients completing the study remained in the extension arm for another 6 months [65]. A dramatic improvement in somatic parameters was described in the valanafusp-alpha-treated patients for 52 weeks, including 23% and 26% reductions in liver and spleen volumes, respectively, compared with the baseline levels [65]. The improvement in the somatic parameters was attributed to the dual targeting of valanafusp alpha in the peripheral organs via both the insulin and M6P receptor [65]. In addition, there was a significant increase in shoulder flexion (10.9°) and extension (9.5°) following treatment with valanafusp alpha for 26 weeks [65], which may be related to the preferential targeting of the HIRMAb-IDUA in the vertebral bodies and joints that was observed in primates [62]. The treatment of severe and attenuated MPSI patients with valanafusp alpha resulted in a mean improvement across all cognitive domains [65].

### 3.2. HIRMAb-Iduronate 2-Sulfatase (HIRMAb-IDS)

Iduronate 2-sulfatase (IDS) is the lysosomal storage enzyme that is mutated in Hunter's MPSII syndrome [66]. A brain-penetrating form of IDS was engineered as HIRMAb-IDS fusion protein using a similar strategy as the one used in the production of HIRMAb-IDUA described above in Section 3.1 (Table 1) [23]. The cDNA of the mature human IDS (GenBank NP\_000193), minus the 25-amino-acid signal peptide, was fused at the C-terminus of the heavy chain of the HIRMAb via a short Ser-Ser linker. The HIRMAb-IDS fusion protein, expressed in either COS or CHO cells, maintained the affinity for the targeting insulin receptor in the low nM range, and the IDS enzyme activity was comparable to the specific activity of the recombinant IDS, Elapraxe [23]. The HIRMAb-IDS fusion protein targeted the lysosomal compartment in Hunter MPSII fibroblasts, and it was able to reduce the accumulation of GAG [23,67]. The biodistributions of both the HIRMAb-IDS fusion protein and Elapraxe were investigated in the rhesus monkey using Bolton-Hunter-iodinated material [68]. The film autoradiography of the primate brain confirmed a global distribution of the fusion protein, whereas the non-brain-penetrating Elapraxe showed background activity (Figure 5) [68]. The brain uptake of the HIRMAb-IDS fusion protein approximated 1% ID/primate brain [68]. The organ uptake ratio of HIRMAb-IDS:Elapraxe

was 38-fold higher in the brain, as IDS does not cross the BBB, whereas in the peripheral tissues, this ratio was near 1, as both proteins are taken up via the M6P receptor [68]. The brain uptake estimate following the administration of 1 mg/kg BW in humans was projected to be 0.34 U/mg protein, which may produce a therapeutic effect in the brains of MPSII patients [67,68]. The safety and dose ranging study for the HIRMAb-IDS fusion protein was completed in patients with Hunter syndrome; however, the results have not yet been published (NCT02262338). A mouse surrogate molecule with the anti-mouse TfR as the transport domain and human IDS as the therapeutic domain was also produced and validated in mice, wherein the brain uptake was high and comparable to the human fusion protein at 1.3% ID/mouse brain [36].

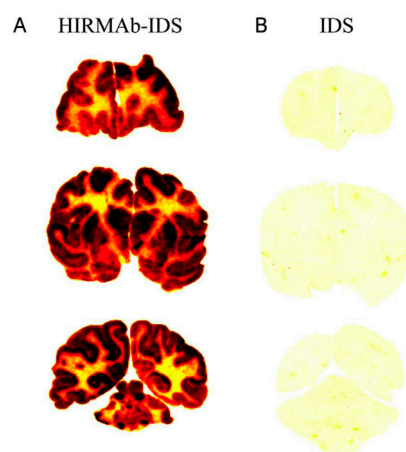


**Figure 5.** Film autoradiogram (20 µm sections) of rhesus monkey brain removed 2 h after IV injection of the HIRMAb-IDS fusion protein (A) or IDS (B). Scans were produced after labeling of the HIRMAb-IDS fusion protein or IDS with [<sup>125</sup>I]-Bolton–Hunter reagent. The forebrain section is on the top, the midbrain section is in the middle, and the hindbrain section with cerebellum is on the bottom. From reference [68] with permission.

The production of another brain-penetrating IgG-IDS fusion protein was also reported [24]. This fusion protein is similar to the HIRMAb-IDS described above but is directed to the human TfR. The TfRMAb-IDS, later designated pabinafusp alfa, was used to complete phase I/II clinical trials in Hunter MPSII patients in Japan and Brazil [69,70] and a phase II/III trial in Japan [71]. It was reported that the pabinafusp alfa, dosed at 2 mg/kg BW for 52 weeks in MPSII subjects, produced a significant reduction in the levels of heparan sulfate (HS) in the cerebrospinal fluid (CSF), which was used as the primary efficacy endpoint [71]. Evaluations of neurocognitive developments, used as the secondary end point, showed positive changes in the age-equivalent score in subjects with attenuated MPSII and in the initial phase of the severe subtype but not in severe MPSIII patients in the middle and late stages of the disease [71]. The positive effect of the fusion protein in the peripheral end points, i.e., serum HS and liver and spleen volumes, was comparable to that of the IDS enzyme replacement therapy [71]. Based on this trial, pabinafusp alfa was approved by the Ministry of Health, Labour and Welfare (MHLW) in Japan for the treatment of Hunter MPSII syndrome [72].

### 3.3. HIRMAb-Arylsulfatase A (HIRMAb-ASA)

A mutation of the Arylsulfatase A (ASA) gene causes the lysosomal storage disorder metachromatic leukodystrophy (MLD) [73]. Since ASA does not cross the BBB, it may be possible to treat the brain in MLD with a brain-penetrating IgG-ASA fusion protein. The genetic engineering of the HIRMAb-ASA fusion protein was performed using the standard recombinant technology strategy, wherein cDNA of the mature human ASA (GenBank NP\_000478), minus the signal peptide, was fused at the C-terminus of the heavy chain of the HIRMAb via a short Ser-Ser linker (Table 1) [25]. The HIRMAb-ASA fusion protein

maintained a high affinity for the targeting insulin receptor in the low nM range and high ASA enzyme activity [25]. Confocal microscopy showed that the ASA fusion protein is triaged to the lysosomal compartment. The biodistribution of the HIRMAb-ASA fusion protein in the rhesus monkey showed a global distribution in brain, with a brain uptake of 1.1% ID/primate brain [25]. Based on this finding, the brain levels of HIRMAb-ASA were predicted to be 14 ng/mg protein following the administration of 2.5 mg/kg in humans [25]. This represents 14% of the levels of ASA in the normal human brain [74], and it may be sufficient to treat this lysosomal storage disorder, as the replacement of just 1–2% of the normal enzyme activity is expected to be therapeutic [75]. This is also supported by the fact that 5–20% of the population has ASA pseudo-deficiency, with just 3–8% of the normal levels of ASA enzyme activity in brain and no MLD symptoms [76].

### 3.4. HIRMAb-N-Sulfoglucosamine Sulfohydrolase (HIRMAb-SGSH)

The Sanfilippo type A syndrome or MPSIIIA is caused by a mutation of the N-sulfoglucosamine sulfohydrolase (SGSH) gene [77]. It is possible to treat the brain in MPSIIIA with a brain-penetrating IgG-SGSH fusion protein, as SGSH does cross the BBB. The genetic engineering of the HIRMAb-SGSH fusion protein was completed as described above for other enzymes, wherein cDNA of the mature human SGSH (GenBank NP\_000190), minus the signal peptide, was fused at the C-terminus of the heavy chain of the HIRMAb via a short Ser-Ser-Ser-Ser linker (Table 1) [26]. The HIRMAb-SGSH fusion protein maintained a high affinity for the targeting insulin receptor and SGSH enzyme activity near 100% of the one of the recombinant SGSHs [26]. The brain uptake in the rhesus monkey approximated 1% ID/primate brain [26]. The brain level of SGSH enzyme activity was predicted to be 0.25 U/g of brain following the administration of 3 mg/kg HIRMAb-SGSH [26]. This is comparable to the normal endogenous levels of SGSH in the brain [78], suggesting that it is possible to achieve therapeutic levels of SGSH in the MPSIIIA brain following the administration of the HIRMAb-SGSH fusion protein. The efficacy of the IgG-SGSH fusion protein was investigated in a mouse model of MPSIIIA using a subrogate fusion protein comprising the mouse TfRMAb fused to the human SGSH (Table 2) [37]. Two-week-old MPSIIIA mice were treated three times per week for 6 weeks with intraperitoneal (IP) 5 mg/kg of the TfRMAb-SGSH fusion protein or the isotype control. Studies in mice demonstrated that the administration 5 mg/kg BW IgG fusion protein IP is equivalent to the IV injection of 1 mg/kg BW [79]. High plasma levels of HIRMAb were also reported in the rhesus monkey following subcutaneous (SC) administration [80]. Mice were euthanized 1 week after the last dose of either the control or the test article [37]. HS was measured in the brain and liver by LC-MS following enzymatic digestion into disaccharides using HS disaccharide standards [37]. MPSIIIA animals treated with saline showed 30- and 36-fold elevations in HS in the brain and liver, respectively, compared to the wild-type animals (Figure 6). Treatment with the TfRMAb-SGSH reduced the levels of HS by 70% in the brain and by 85% in the liver, whereas the isotype control had no effect [37]. The data confirmed that the administration of brain-penetrating IgG-SGSH fusion protein is able to reduce the accumulation of HS in the MPSIIIA brain and a peripheral organ.

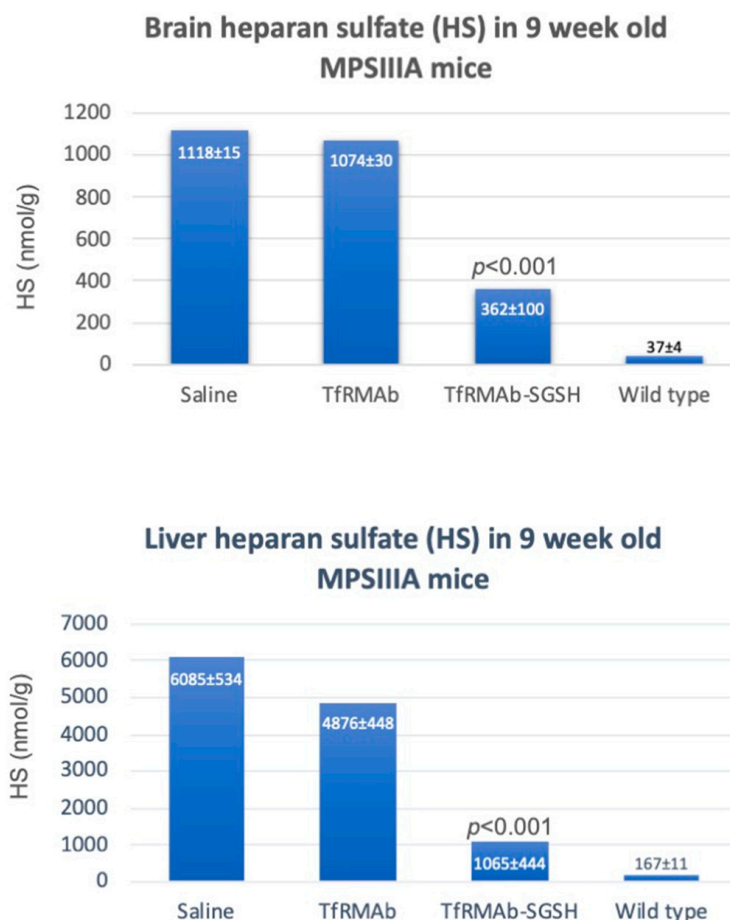


**Figure 6.** Reduction in brain heparan sulfate (HS) in the MPSIIIA mouse with systemic administration of a mouse TfrMAb-SGSH fusion protein. Two-week-old MPSIIIA mice (JAX) were treated three times per week for 6 weeks with IP 5 mg/kg of the TfrMAb-SGSH fusion protein or the isotype control (TfrMAb). The mice were euthanized 1 week after the last dose. HS was measured in brain and liver by LC-MS following enzymatic digestion into disaccharides using HS disaccharide standards. The 30-fold elevation in HS in the brain was reduced 70% by the chronic treatment with the IgG fusion protein (**top**). HS was also elevated in liver, and treatment with the mouse TfrMAb-SGSH reduced hepatic HS by 85% (**bottom**). Data are expressed as means  $\pm$  SD ( $n = 8$  mice/group). From [37] with permission.

### 3.5. HIRMAb- $\alpha$ -N-Acetylglucosaminidase (HIRMAb-NAGLU)

The Sanfilippo type B syndrome or MPSIIIB is caused by a mutation of the  $\alpha$ -N-acetylglucosaminidase (NAGLU) gene [81]. Since NAGLU does cross the BBB, it is possible to treat the brain in MPSIIIB with a brain-penetrating IgG-NAGLU fusion protein. The genetic engineering of the HIRMAb-NAGLU fusion protein was constructed as described above for other enzymes, wherein cDNA of the mature human NAGLU (GenBank NP\_000263), minus the signal peptide, was fused at the C-terminus of the heavy chain of the HIRMAb via a short Ser-Ser-Ser-Ser linker (Table 1) [27]. However, this fusion protein showed poor levels of expression in COS cells [27]. This problem was solved by the introduction of a 31-amino-acid extended linker, corresponding to the hinge region of IgG3 [27]. The HIRMAb-NAGLU fusion protein with the extended linker was produced in CHO cells and showed a high affinity for the targeting insulin receptor. The NAGLU enzyme activity was comparable to that of the recombinant NAGLU [27]. The biochemical properties of the HIRMAb-NAGLU fusion protein were confirmed by SDS-PAGE, human IgG and NAGLU Western blot analysis, the uptake in MPSIIIB fibroblasts, and the reduction in GAG in MPSIIIB fibroblasts [27]. The brain uptake in the rhesus monkey was 1%

ID/primate brain [27]. The brain level of NAGLU enzyme activity was predicted to be 0.36 U/mg of brain protein following the administration of 1 mg/kg HIRMAb-NAGLU, which is comparable to the NAGLU enzyme activity in the normal brain [82]. The data suggest that it is possible to achieve therapeutic levels of NAGLU in the MLDIIIIB brain following the administration of the HIRMAb-NAGLU fusion protein.

### 3.6. HIRMAb-Acid Sphingomyelinase (HIRMAb-ASM)

A mutation of the acid sphingomyelinase (ASM) gene causes Niemann–Pick disease type A (NPDA) [83]. Since ASM does cross the BBB, it is possible to treat the brain in NPDA with a brain-penetrating IgG-ASM fusion protein. The genetic engineering of the HIRMAb-ASM fusion protein was designed as described above for other enzymes, with the exception that the ASM gene was fused to the light chain of HIRMAb in lieu of the heavy chain (Figure 2) (Table 1) [28]. The C-terminus of the enzyme genes to the C-terminus of the heavy chain of an MAb places the enzyme in a dimeric configuration, as opposed to the monomeric configuration obtained by fusion to the light chain of an MAb. ASM forms a heterodimer with saposin C [84], so it was fused to the C-terminus of the light chain to provide a more flexible configuration (Figure 2) [28]. The cDNA of the mature human ASM (GenBank NP\_000534), minus the signal peptide, was fused at the C-terminus of the light chain of HIRMAb via the 31-amino-acid extended linker corresponding to the hinge region of IgG3 [28]. The HIRMAb-ASM fusion protein was produced in COS or CHO cells and showed a high affinity for the targeting insulin receptor and high ASM enzyme activity [28]. Assuming a brain uptake of 1% ID for the HIRMAb-ASM, the administration of 3 mg/kg BW of the fusion protein produces a brain concentration of 1.5 mg/brain, which represents a therapeutic enzyme level in the brain of an NPDA mouse [85].

### 3.7. HIRMAb-Hexoaminidase A (HIRMAb-HEXA)

A mutation of the Hexoaminidase A (HEXA) gene produces Tay–Sachs disease (TSD) [86]. It is possible to treat the brain in TSD with a brain-penetrating IgG-HEXA fusion protein, as the recombinant HEXA does not cross the BBB. The genetic engineering of the HIRMAb-HEXA fusion protein was designed as described above for ASM [28]. The HEXA gene was fused to the light chain of HIRMAb to place this enzyme in a monomeric configuration (Figure 2) (Table 1) [28] and was able to form a heterodimer complex with the GM2 activator protein [87]. The cDNA of the mature human HEXA (GenBank NP\_000511), minus the signal peptide, was fused at the C-terminus of the light chain of the HIRMAb via the 31-amino-acid extended linker [28]. The HIRMAb-HEXA fusion protein was produced in COS or CHO cells and showed a high affinity for the targeting insulin receptor and a high HEXA enzyme activity comparable to the recombinant HEXA protein [28]. Assuming a brain uptake of 1% ID for the HIRMAb-HEXA, the administration of 3 mg/kg BW of the fusion protein may produce a brain concentration of 2.5 U/brain, which represents a therapeutic enzyme level in the TSD brain [88].

### 3.8. HIRMAb-Palmitoyl-Protein Thioesterase (HIRMAb-PPT1)

Batten type 1 disease, or neuronal ceroid pilofuscinosis type 1 (CLN1) disease, is produced by a mutation of the palmitoyl-protein thioesterase (PPT1) [89]. In order to produce a brain-penetrating IgG-PPT1 fusion protein, the cDNA of the mature human PPT1 (GenBank NP\_000301), minus the signal peptide, was fused at the C-terminus of the heavy chain of the HIRMAb, as described above for other fusion proteins, using the short Ser-Ser-Ser linker (Table 1) (Figure 2) [28]. This construct places the therapeutic domain in a dimeric configuration, as in the native PPT1 (Figure 2). However, the production of the HIRMAb-PPT1 with the short Ser linker generated a fusion protein with suboptimal enzyme activity [28]. This problem was solved by the introduction of the flexible 31-amino-acid extended linker, which allowed the production of a fusion protein with a high PPT1 enzyme activity, maintaining its affinity for the insulin receptor in the low nM range [28]. Assuming a brain uptake of 1% ID for the HIRMAb-PPT1, the administration of 3 mg/kg BW of the

fusion protein may produce a brain concentration of 2.6 U/brain, which represents 2.2% of the normal endogenous PPT1 activity; however, it would be therapeutic, as just 0.5% of the endogenous PPT1 activity is needed to reverse the neuropathology of CLN1 [90].

### 3.9. HIRMAb- $\beta$ -Galactosidase (GLB1) (HIRMAb-GLB1)

The gene mutated in GM1-gangliosidosis is  $\beta$ -galactosidase (GLB1) [91]. In order to reformulate GLB1 into a brain-penetrating IgG fusion protein, the cDNA of the mature human GLB1 (GenBank NP\_000395), minus the signal peptide, was fused at the C-terminus of the heavy chain of the HIRMAb, as described above for other fusion proteins, using the short Ser-Ser-Ser linker (Table 1) (Figure 2) [28]. This construct places the therapeutic domain in dimeric configuration, as in the native GLB1 (Figure 2). However, as described above for the HIRMAb-PPT1, the production of the HIRMAb-GLB1 with the short Ser linker produced a fusion protein with a marked decrease in its specific enzyme activity [28]. The GLB1 enzyme activity of the HIRMAb-GLB1 fusion protein was restored by the introduction of the flexible 31-amino-acid extended linker (Table 1) [28]. This fusion protein also maintained its affinity for the insulin receptor in the low nM range [28]. Assuming a brain uptake of 1% ID for the HIRMAb-GLB1, the administration of 3 mg/kg BW of the fusion protein may produce a brain concentration of 256 U/g brain, which may represent a therapeutic GLB1 enzyme level in the brain [92]. In an attempt to validate the efficacy of the IgG-GLB1 fusion protein, a surrogate fusion protein comprising the mouse TfRMAb fused to the human GLB1 was produced and tested in a mouse model of GM1-gangliosidosis [93]. The TfRMAb-GLB1 fusion protein was able to increase the GLB1 enzyme activity in the liver by 20%; however, it failed to increase the GLB1 activity in the brain or reduce the ganglioside content [93]. Since this surrogate fusion protein was engineered with a short Ser linker [93] that is known to produce suboptimal levels of GLB1 [28], a negative conclusion on brain effects is premature at the present time. Further studies with a surrogate mouse GLB1 construct with optimal GLB1 enzyme activity, i.e., engineered with an extended linker [28], may be needed to clarify this matter.

## 4. Bispecific Therapeutic Antibodies

Monoclonal antibodies (MAbs) are potential therapies for the CNS, i.e., in Alzheimer's disease (AD), if they are re-engineered to cross the BBB. Novel strategies for the immune therapy of AD have been proposed with the design of bispecific MAbs [29,94]. Some designs propose the use of low-affinity MAbs for the transport domain of the fusion MAb due to limitations in the technology that is used, i.e., knobs-into-holes, which produces monovalent antibodies composed of two heterologous half-antibody molecules for either the transport or the therapeutic domain [50]. However, as discussed above in Section 2, a low-affinity transport domain presents no advantages over the high-affinity targeting MAb. Other designs maintain the bivalency of both domains, resulting in a tetravalent bispecific MAb fusion protein with a high affinity for both the transport and therapeutic domain (Figure 7) [29,94].

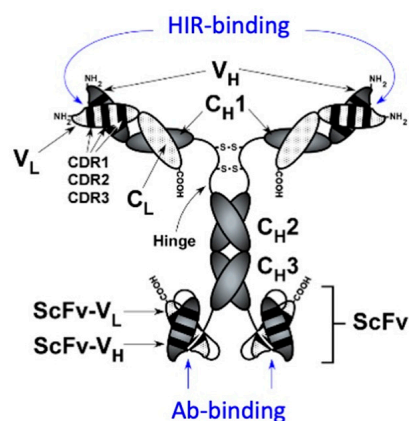


**Figure 7.** Schematic representation of a tetraivalent bispecific MAb. In this construct, the transport domain of the fusion protein targets the BBB human insulin receptor (HIR), and the therapeutic domain is a single-chain anti-A $\beta$  antibody monomer (ScFv) fused to the carboxyl terminus of the heavy chain of the HIRMAb. This tetraivalent bispecific Mab maintains a high affinity for both A $\beta$  and the BBB insulin receptor [29].

For example, an anti-A $\beta$  MAb was re-engineered to cross the BBB in both directions for the immune therapy of AD [29]. This process involves three-steps: (i) the transport of the anti-A $\beta$  antibody from the blood to the brain across the BBB; (ii) the binding to and disaggregation of A $\beta$  fibrils in the brain; and (iii) the efflux of the anti-A $\beta$  antibody from the brain back into the blood. This trifunctional molecule, designated HIRMAb-A $\beta$ -ScFv, comprises (i) the transport domain, i.e., the HIRMAb; (ii) the therapeutic domain, i.e., a single-chain anti-A $\beta$  antibody monomer (ScFv) fused to the carboxyl terminus of the heavy chain of the HIRMAb; and (iii) the binding site for the neonatal Fc receptor or FcRn, located at the CH2-CH3 interface of the human IgG constant region (Figure 7), which mediates the brain efflux of the HIRMAb-A $\beta$ -ScFv [29]. The HIRMAb-A $\beta$ -ScFv fusion bifunctional antibody was engineered by the insertion of an scFv directed to the A $\beta$ <sup>1-28</sup> peptide at the C-terminus of the heavy chain of HIRMAb via a short Ser-Ser linker (Table 1) [29]. The tetraivalent bifunctional Mab maintained a high affinity for both A $\beta$  and the BBB insulin receptor [29]. The pharmacokinetics and biodistribution of the HIRMAb-A $\beta$ -ScFv fusion Mab were investigated in a rhesus monkey using an [<sup>125</sup>I]-labeled test article and compared with a control article that comprised the [<sup>3</sup>H]-labeled original murine MAb directed to A $\beta$  (Mab-A $\beta$ ) (Figure 8) [29]. Following administration, there was no measurable decrease in the blood concentration of the control MAb-A $\beta$ , as MAbs do not target any organ remaining in the blood compartment (Figure 8). On the contrary, there was a rapid clearance of the [<sup>125</sup>I]-HIRMAb-A $\beta$ -ScFv fusion antibody from blood (Figure 8), as this fusion protein targets the brain and peripheral organs expressing the insulin receptor [29]. Thus, there was a global distribution of the fusion Mab in the brain with a preferential uptake in the gray matter relative to the white matter. The capillary depletion technique showed a high brain volume of distribution (VD) of the bifunctional fusion Mab, demonstrating that the HIRMAb-A $\beta$ -ScFv was transcytosed across the BBB into the postcapillary brain compartment (Figure 8) [29]. On the other hand, the control mouse MAb-A $\beta$  had a brain VD of 10  $\mu$ L/g of brain, which approximates the arterial blood volume of the brain, confirming that the control MAb-A $\beta$  does not cross the BBB, remaining in the primate blood compartment (Figure 8) [29].



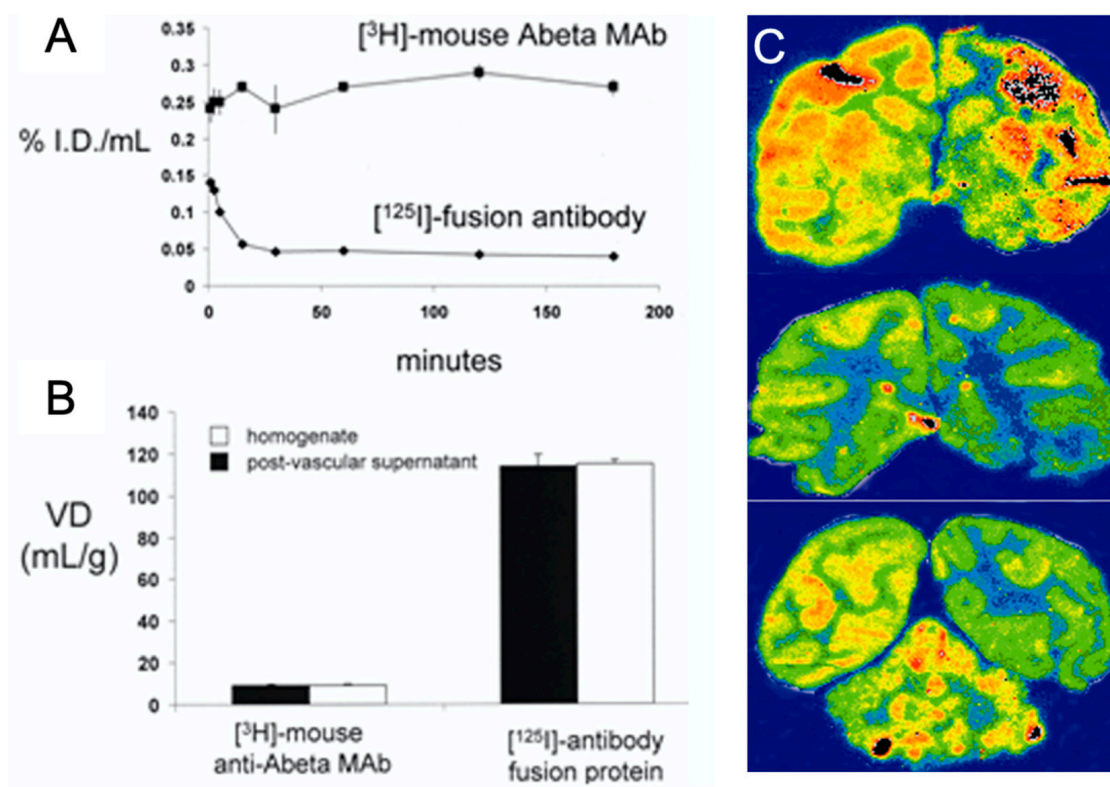


**Figure 8.** Pharmacokinetics and brain uptake of a tetraivalent bispecific MAb fusion protein in the rhesus monkey. The structure of the tetraivalent bispecific MAb fusion protein is shown in Figure 7. This fusion protein, designated  $[^{125}\text{I}]$ -fusion antibody in this figure, comprises the transport domain, which targets the BBB human insulin receptor, and the therapeutic domain, which is a single-chain anti- $\text{A}\beta$  antibody monomer (ScFv). (A) Plasma pharmacokinetics analysis showing no measurable clearance from the blood of the control  $[^3\text{H}]$ -mouse Abeta MAB, whereas the  $[^{125}\text{I}]$ -fusion antibody is rapidly cleared from blood due to uptake via the insulin receptor. (B) Brain VD for the  $[^{125}\text{I}]$ -fusion antibody is  $>100$   $\mu\text{L/g}$  in both the brain homogenate and the post-vascular supernatant, which indicates the  $[^{125}\text{I}]$ -fusion antibody is transported across the BBB. The VD for the  $[^3\text{H}]$ -mouse Abeta MAB, 10  $\mu\text{L/g}$ , is equal to the brain arterial blood volume, which indicates this antibody is not transported across the primate BBB in vivo. (C) Global distribution of fusion antibody to primate brain. Brain scans of adult rhesus monkey at 3 h after the intravenous administration of the  $[^{125}\text{I}]$ -fusion antibody demonstrates the widespread distribution of the fusion antibody into the primate brain in vivo. The top scan is the most frontal part of brain, and the bottom scan is the most caudal part of brain and includes the cerebellum. From [29] with permission.

In order to validate the bifunctional HIRMAb- $\text{A}\beta$ -ScFv in a mouse model of AD, a surrogate molecule targeting the mouse TfR was engineered (Table 2) [38]. This molecule was similar to the one shown in Figure 7, with an identical therapeutic domain that comprised the ScFv to the  $\text{A}\beta^{1-28}$  peptide but with an anti-mouse TfR as the transport domain [38]. This fusion protein maintained a high affinity for both  $\text{A}\beta$  and the mouse TfR and produced a brain uptake of 3.5% [38]. The administration of 1 mg/kg BW TfRMAb- $\text{A}\beta$ -ScFv IV three times per week or 5 mg/kg BW SC daily for 12 weeks to B6C3-Tg(APP<sup>swe</sup>, PSEN1dE9)85 Dbo/J (PSAPP) double transgenic mice produced a 40–61% reduction in the brain concentration of  $\text{A}\beta^{1-42}$  [95,96] without brain microhemorrhage [97], a common adverse side effect seen in the immune therapy of AD. A reverse construct wherein the transport domain is a form of an ScFv fused to the C-terminus of the light chain of a therapeutic MAb has also been reported [98]. These constructs present the advantage of re-engineering any therapeutic MAb into a brain-penetrating tetraivalent bispecific MAb targeting either the BBB-TfR [98] or the BBB-HIR [99].

## 5. Decoy Receptor–IgG Fusion Proteins

Other potential new therapeutics for brain disorders are decoy receptors. A decoy receptor is formed by the extracellular domain (ECD) of the molecule of interest to be inactivated fused to the amino terminus of the Fc region of human IgG1 for stability and to facilitate downstream protein production and purification. A good example is the ECD of the tumor necrosis factor (TNF) receptor (TNFR) type II:Fc fusion protein, etanercept [100]. The TNFR decoy receptor is used to suppress inflammatory reactions in non-brain tissues [101]. TNF $\alpha$  has also been involved in disorders of the CNS, including stroke [102], traumatic brain and spinal cord injury [103,104], neurodegeneration [105], and depression [106]. Therefore, the production of a brain-penetrating TNFR decoy receptor may provide a treatment for these pathologies of the CNS. A model of such a protein was engineered by the insertion of the cDNA encoding the human TNFR ECD to the C-terminus of the heavy chain of the HIRMAb via a Ser-Ser linker (Table 1) [30], as described above in Section 4 for the tetravalent bispecific MAb. This construct produced in CHO cells maintained a high affinity for the BBB insulin receptor and TNF $\alpha$  [30]. The brain uptake of the HIRMAb-TNFR was investigated in the rhesus monkey and compared with that of the TNFR:Fc. The HIRMAb-TNFR fusion protein was transported across the BBB, producing a brain uptake of 3% ID [30]. On the other hand, the non-brain-penetrating TNFR:Fc produced a brain uptake comparable to that of IgG1, which is confined to the blood compartment in the brain (Figure 9). The ratio for the organ permeability–surface area (PS) of the HIRMAb-TNFR relative to the organ PS for the TNFR:Fc in the rhesus monkey is shown in Figure 9 (bottom). This ratio demonstrates that both HIRMAb-TNFR and TNFR:Fc are transported into peripheral organs, as the PS ratio approximates 1 (Figure 9). The PS ratio was >30 in the brain, as just the HIRMAb-TNFR is transported into the primate brain (Figure 9) [30].

A surrogate molecule was engineered to validate this construct in experimental mouse models of stroke, Parkinson's disease (PD), and AD. This construct was produced by the insertion of the human TNFR into the C-terminus of the heavy chain of an MAb directed to the mouse BBB TfR (Table 2) [39]. The bifunctional construct maintained a high affinity for TNF $\alpha$ , which was comparable to that of etanercept, as well as a high binding affinity for the mouse TfR [39]. In a 6-hydroxydopamine model of PD, the mouse TfRMAb-TNFR was neuroprotective, reducing both the apomorphine- and amphetamine-induced rotation and increasing the vibrissae-elicited forelimb placing and the striatal tyrosine hydroxylase (TH) enzyme activity [39]. On the contrary, etanercept had no effect on striatal TH enzyme activity or neurobehavior, as it is not transported through the BBB [39]. In a reversible middle cerebral artery occlusion mouse stroke model, the TfRMAb-TNFR also produced neuroprotection, causing a significant reduction in the hemispheric, cortical, and subcortical stroke volumes and neuronal deficit, whereas etanercept had no effect [107]. In a mouse model of AD, chronic treatment with TfRMAb-TNFR, but not with either saline or etanercept, produced a marked reduction in neuroinflammation and in both A $\beta$  peptide and plaque load and improved recognition memory [108]. As observed with the TfRMAb-A $\beta$ -ScFv [38], no sign of microhemorrhage was seen with the chronic treatment of TfRMAb-TNFR [108].

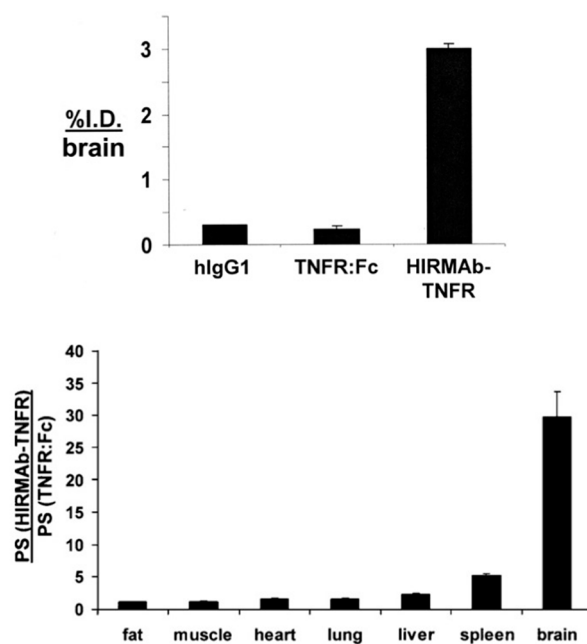


**Figure 9.** Selective targeting of a TNFR decoy receptor pharmaceutical to the primate brain as a receptor-specific IgG fusion protein. This fusion protein, HIRMAb-TNFR comprises a transport domain targeting the BBB human insulin receptor and the TNFR ECD as therapeutic domain. The brain uptake and peripheral biodistribution of the HIRMAb-TNFR were investigated in the rhesus monkey and compared with those of the control TNFR:Fc, etanercept, with [ $^{125}$ I]-Bolton–Hunter reagent-labeled articles. The HIRMAb-TNFR fusion protein was transported across the BBB, producing a brain uptake of 3% ID. On the other hand, the non-brain-penetrating TNFR:Fc produced a brain uptake comparable to IgG1, which is confined to the blood compartment in the brain (top). The ratio for the organ permeability–surface area (PS) of the HIRMAb-TNFR relative to the organ PS for the TNFR:Fc in the rhesus monkey approximates 1 (bottom), as both molecules are transported into the peripheral organs. The PS ratio was >30 in the brain, as just the HIRMAb-TNFR is transported across the BBB and into the primate brain. From [30] with permission.

## 6. Neurotrophic Factor-IgG Fusion Proteins

Neurotrophic factors could potentially be developed as new treatments of brain disorders, as in the case of stroke, traumatic brain injury, or chronic neurodegeneration, such as Parkinson’s disease (PD) [109–118]. However, as discussed above for other protein-based therapeutics for the CNS, the drug development of neurotrophic factors is limited by the lack of transport of across the BBB. The engineering of brain-penetrating neurotrophic factors has been reported for erythropoietin (EPO), glial-derived neurotrophic factor (GDNF), and brain-derived neurotrophic factor (BDNF), and details are discussed below.

### 6.1. HIRMAb-Erythropoietin (EPO) (HIRMAb-EPO)

The engineering of the brain-penetrating EPO was completed by the insertion of the cDNA of the mature human EPO (GenBank NP\_000790) at the C-terminus of the heavy chain of the HIRMAb using the short Ser-Ser-Ser linker (Table 1) in a tandem vector carrying both the light and heavy chain of HIRMAb [31]. The design of this fusion protein placed the EPO in dimeric configuration, as shown in Figure 2 for HIRMAb-PPT1 or HIRMAb-GLB1. The HIRMAb-EPO fusion protein expressed in COS cells demonstrated a high affinity for both the BBB insulin receptor and the EPO receptor (EPOR). The biodistribution of both EPO and HIRMAb-EPO was investigated in the rhesus monkey. The brain uptake of HIRMAb-EPO was high at 2% ID/monkey brain [31]. On the contrary, EPO, which does not cross the BBB, had a brain uptake comparable to human IgG1, which is confined to the blood compartment of the primate [31]. The mouse TfRMAb-EPO surrogate fusion protein (Table 2) was constructed to investigate the efficacy of the brain-penetrating EPO in an

experimental model of stroke and PD [40]. The TfRMAB-EPO traversed the mouse BBB and had an uptake of 2% ID/mouse brain, which is similar to that of the HIRMAb-EPO in the rhesus monkey, and maintained a high affinity for the mouse BBB TfR and EPOR [40]. The mouse TfRMAB-EPO fusion protein was neuroprotective in a reversible middle cerebral artery occlusion (MACO) stroke model, dosed at 1 mg/kg BW IV following MACO. There was a significant reduction in the hemispheric stroke volume as well as in the neuronal deficit, whereas EPO had no effect [119,120]. The mouse TfRMAB-EPO fusion protein was also neuroprotective in a 6-hydroxydopamine model of PD [121]. The IV administration of 1 mg/kg BW of the fusion protein given 1 h after the toxin and every other day for 3 weeks was neuroprotective, reducing both the apomorphine- and amphetamine-induced rotation and increasing the vibrissae-elicited forelimb placing and the striatal TH enzyme activity [121]. In a model of experimental AD, this fusion protein presented therapeutic benefits on A $\beta$  load, synaptic loss, and microglial activation as well as improved spatial memory and did not show evidence of microhemorrhage [122].

## 6.2. HIRMAb-Glial-Cell-Derived Neurotrophic Factor (GDNF) (HIRMAb-GDNF)

The production of a brain-penetrating IgG-GDNF fusion protein was also reported targeting either the human IR or the mouse TfR, respectively (Tables 1 and 2) [32,41]. The mature human GDNF cDNA corresponding to amino acids Ser<sup>78</sup>-Ile<sup>211</sup> (GenBank P39905) was fused to the C-terminus of the heavy chain of the HIRMAb of the TfRMAB using the short Ser-Ser linker [32,41]. As mentioned above, this construct placed the GDNF in a dimeric configuration, as shown in Figure 2 for HIRMAb-PPT1 or HIRMAb-GLB1. These fusion proteins, expressed in either COS or CHO cells, demonstrated a high affinity for both the corresponding target receptor and the GDNF receptor (GFR $\alpha$ 1). The administration of [<sup>125</sup>I]-HIRMAb-GDNF in a rhesus monkey showed a global distribution of the fusion protein throughout the brain, with a brain clearance (CL) of 0.8  $\mu$ L/min/g [123]. Conversely, [<sup>125</sup>I]-labeled GDNF, which is not transported across the BBB, produced a brain CL comparable to human IgG1, as both molecules remain in the blood compartment [123]. The brain uptake of the mouse fusion protein was high at 3% ID/mouse brain [41]. The mouse IgG-GDNF surrogate was neuroprotective in a 6-hydroxydopamine model of PD [124]. The IV administration of 1 mg/kg BW of the fusion protein given 1 h after the toxin and every other day for 3 weeks was neuroprotective, reducing both the apomorphine- and amphetamine-induced rotation and increasing the vibrissae-elicited forelimb placing and the striatal TH enzyme activity [124]. The mouse TfRMAB-GDNF fusion protein was also neuroprotective in the MACO stroke model. The administration of 1 mg/kg BW IV fusion protein following MACO produced a 30% reduction in cortical stroke volume, whereas GDNF alone had no effect on stroke volume (Figure 10) [125]. Furthermore, cotreatment with TfRMAB-GDNF and TfRMAB-TNFR following MCAO enhanced neuroprotection, reducing the cortical stroke volume to 69% [125]. A study of an MAb-GDNF fusion protein targeting the human insulin receptor failed to produce neuroprotection in an MPTP (1-methyl-4-phenyl-1,2,3,6-tetrahydropyridine) model of PD in primates [126]. Animals were treated a week after the neurotoxin with 1 or 5 mg/kg BW IV twice weekly for 22 doses, and no improvements in parkinsonian motor symptoms were reported in either dose [126]. Since a BBB-penetrating GDNF was neuroprotective in the 6-hydroxydopamine mouse model of PD at the low dose of 1 mg/kg BW, it is unclear why negative results were observed in the MPTP primate model. Besides the obvious difference in animal models, additional time course and dose-finding studies in the MPTP model may be needed to clarify this matter.

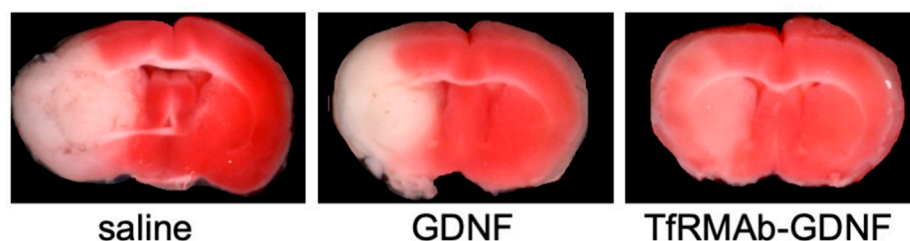


**Figure 10.** Neuroprotection of the mouse TfRMAB-GDNF fusion protein in a reversible middle cerebral artery occlusion (MCAO) stroke model. Brain coronal sections were obtained 24 h after MCAO and stained with 2,3,5-triphenyltetrazolium chloride (TTC), and representative brains are shown in the figure. Saline, 1 mg/kg BW mouse TfRMAB-GDNF fusion protein, and an equimolar dose of GDNF (0.17 mg/kg BW), were injected IV 45 min after MCAO. The mouse TfRMAB-GDNF fusion protein produced a 30% reduction in cortical stroke volume (**right**) compared with the control treated with saline (**left**), whereas GDNF alone had no effect on stroke volume (**center**). From [125] with permission.

### 6.3. HIRMAb-Brain-Derived Neurotrophic Factor (BDNF) (HIRMAb-BDNF)

Another neurotrophic factor that was re-engineered to cross the BBB was BDNF (Table 1) [33]. The genetic engineering was performed as described above for EPO and GDNF, by insertion of the mature cDNA of BDNF coding for amino acids His<sup>1</sup>-Arg<sup>117</sup> into C-terminus of the HIRMAb heavy chain via a short Ser-Ser-Met linker [33]. The expression of the HIRMAb-BDNF fusion protein was performed in either COS or CHO cells using a TV coding for both the light and heavy chain of the HIRMAb-BDNF [33]. The fusion protein maintained a high affinity for both the human BBB insulin receptor and the human trkB receptor for BDNF [33]. Studies in the rhesus monkey showed that the brain VD for the [<sup>3</sup>H]-labeled HIRMAb-BDNF fusion protein was constant in the post-vascular supernatant measured with the capillary depletion method, demonstrating that the HIRMAb-BDNF fusion protein is transcytosed through the BBB and into brain parenchyma. Based on the specific activity of the labeled fusion protein, the brain VD was 24 ± 1 ng/g of HIRMAb-BDNF fusion protein at 3 h after injection [33]. This value is >10-fold higher than the endogenous concentration of BDNF in the adult primate brain [127], suggesting that it may be possible to reach therapeutic levels of this neurotrophic factor in brain following the administration of the BBB-penetrating HIRMAb-BDNF fusion protein.

### 7. Avidin-IgG Fusion Protein

The genetic engineering, expression, and validation of an HIRMAb-avidin (AV) fusion protein and its mouse TfRMAB-AV surrogate molecule were reported (Tables 1 and 2) [34,42]. These avidin fusion proteins were aimed to develop a universal brain delivery system that can be adapted to a variety of mono-biotinylated drugs, including siRNA [15,34,42]. A potential concern with avidin fusion proteins is the possible immunogenicity of the chicken avidin in humans and the induction of a human anti-avidin response. However, avidin has been administered to humans in 5–10 mg doses intravenously without immunologic reactions [128,129]. These fusion proteins were generated by the insertion of the AV cDNA corresponding to amino acids Ala<sup>1</sup>-Glu<sup>128</sup> of the mature chicken avidin protein (GenBank X05343) at the C-terminus of the heavy chain of both HIRMAb and mouse TfRMAB with a short Ser-Ser-Ser linker [34,42]. This configuration places the avidin moiety in a parallel dimer conformation (as in the case of the neurotrophic factors discussed above in Section 6), which replicates the parallel association of two avidin monomers to form a dimer [130]. The binding activity of the AV-fusion proteins for the corresponding target BBB receptor was comparable to the appropriate Mab control. The mouse AV-fusion protein showed a high brain uptake of 2% ID/mouse brain. The therapeutic efficacy of the fusion protein was demonstrated in human U87 cancer cells with a knockdown of luciferase gene expression by mono-biotinylated siRNA [15]. The potential application of brain-penetrating AV-fusion proteins as peptide radiopharmaceuticals for AD was also reported [34,131].

## 8. Safety

As valanafusp alpha (HIRMAB-IDUA) and HIRMAB-IDS entered phase I/II clinical trials in Hurler MPSI and Hunter MPSII, respectively, these fusion proteins were subjected to extensive safety evaluations. Tissue cross-reactivity studies were performed under Good Laboratory Practice (GLP) and showed comparable binding of HIRMAB fusion proteins to human and rhesus monkey organs [56,132], validating further the toxicological studies in these animals. A 6-month GLP toxicological study was conducted with HIRMAB-IDUA in 40 juvenile primates that were dosed weekly with IV infusions of up to 30 mg/kg BW for 6 months [56]. The sole adverse event was hypoglycemia at a high dose of 30 mg/kg BW [133]. This was due to a secondary pharmacologic effect related to an allosteric agonistic effect of insulin and was fully preventable by performing the infusion of the drug in dextrose-saline [133]. No evidence of chronic toxicity was observed in any primate during the 6-month treatment study, including animals euthanized after a 1-month recovery period. No significant changes were reported in physical exam, food intake, EKG, ophthalmoscopic exam, body weights, or organ weights in any of the treatment groups relative to controls [56]. The pharmacokinetics was predictable over the entire dose range. As expected, anti-drug antibodies (ADA) were generated in response to the human fusion protein in primates; however, those were not neutralizing as the end-of-study pharmacokinetics shows no change in either clearance from plasma or in plasma enzyme activity [56]. Similar GLP chronic toxicological studies were performed with the HIRMAB-IDS in rhesus monkey, with exception that the infusion of the fusion protein was conducted in dextrose-saline to prevent any potential hypoglycemic event [132]. No adverse effect or chronic toxicity were reported; thus, the no-adverse-event level (NOAEL) for the HIRMAB-IDS was set at 30 mg/kg BW [132]. The generation of ADA in HIRMAB-IDS-treated rhesus monkeys was similar to that described in the HIRMAB-IDUA toxicological study [56], with the majority of ADAs against this fusion protein directed to the HIRMAB alone [132]. Valanafusp alpha was produced under Good Manufacturing Practice and passed the safety and potency testing set up by regulatory agencies, i.e., the U.S. Food and Drug Administration and the Brazilian Health Regulatory Agency (Anvisa) [65]. In the phase I/II clinical trial with valanafusp alpha in pediatric MPS I patients, the test article was administered by infusion in 5% dextrose-saline at 1, 3, or 6 mg/kg for 6 months, followed by an extension of another 6 months. The IDUA fusion protein was well-tolerated in more than 570 infusions. There was a hypoglycemic drug-related adverse effect with an incidence of 5.9%, which was transient and resolved within 10–20 min following a snack or glucose sachet. It must be noticed that 62% of all episodes were at the high dose of 6 mg/kg, so the hypoglycemic incidence at the therapeutic dose of 1–3 mg/kg BW was just 2.8% [65]. The mean glucose was reported to be normal at  $101 \pm 20$  mg/dL over the course of the 52 trial weeks and >3000 glycemia measurements [65]. There were 10 infusion-related reactions (IRRs) reported in this clinical trial, which represent an incidence of just 1.7%, and 60% of the IRRs were observed in a single patient that was not previously on enzyme replacement therapy and in whom tolerance to the drug developed by the 10th week [65]. There was a poor correlation between IRRs and the ADA titer [65]. The relatively low rate in IRR may be due to the presence of Tregitopes in the constant region of human IgG, which may induce immunotolerance [134]. The pharmacology and safety were also reported for the acute administration HIRMAB-GDNF in the rhesus monkey [135]. The GLP toxicological study aimed for an acute treatment of stroke was completed with IV doses of up to 50 mg/kg BW of fusion protein over a 60 h period to 56 primates [135]. No adverse events were reported in the 2-week terminal toxicology study, and no neuropathologic changes were observed either [135]. Thus, a no-observable-adverse-effect level was established in the rhesus monkey for the acute administration of the HIRMAB-GDNF fusion protein [135]. A publication claimed that the treatment with HIRMAB-GDNF caused proliferative lesions in the pancreas of four of seven animals at the low dose of 1 mg/kg but not at the high dose of 5 mg/kg in an MPTP-PD model in the rhesus monkey [126]. This observation is difficult to interpret, as there was no dose-dependent effect reported, as the high dose of

the fusion protein had no adverse effect. The lesions observed in the primate pancreas are detected in 30% of all human autopsies, and they are not pre-malignant [136]. Furthermore, no pancreatic lesions were reported following 6 months of treatment with either HIRMAb-IDUA or -IDS fusion protein at doses as high as 30 mg/kg BW/week [56,132]. Another study reported no toxic effect of the surrogate mouse TfRMAb-GDNF fusion protein in IV-dosed mice at 2 mg/kg BW twice weekly for 12 weeks [53]. The chronic treatment with the mouse fusion protein caused no histologic changes in the brain and cerebellum, kidney, liver, spleen, heart, or pancreas; no change in body weight; and no change in 23 serum chemistry measurements [53]. A low-titer immune response against the fusion protein was reported, which was directed against the variable region of the antibody part of the fusion protein, with no immune response directed against either the constant region of the antibody or against GDNF. As shown for HIRMAb fusion proteins, these antibodies were not neutralizing, as no changes were reported in the pharmacokinetics and brain uptake at the end of the 12 weeks of treatment [53].

The safety for the TfR pathway has raised some concerns. A decrease in circulating reticulocytes was reported after an acute dosing of a low-affinity TfRMAb [137]. A mutation of the Fc effector function seemed to rescue the reduction in reticulocytes [137]. However, several chronic studies using high-affinity TfRMAb did not report changes in circulating reticulocytes [35,37,39,53,95,96,107,108,119–122]. Moreover, the elimination of the effector function in the TfRMAb-EPO fusion protein by the substitution of the Asn residue at position 292 of the mouse IgG1 constant region in the TfRMAb with Gly produced a mutant fusion protein with a marked increase in clearance, resulting in a several-fold reduction in C<sub>max</sub> following IV or SC administration compared to the wild-type molecule [57]. The data suggest that the acute effect of TfRMABs on reticulocytes is transient and reversed by chronic treatments, and that the potential benefit of the elimination of the effector function may be offset by its rapid pharmacokinetic clearance. In addition, a chronic study with the mouse TfRMAb-EPO fusion protein in the PSAPP mouse model of AD demonstrated improved hematology safety as well as better behavioral and therapeutic indices compared with recombinant EPO alone [138]. Another study in rhesus monkeys reported toxicity associated with the chronic administration of a humanized TfRMAb [139]. Treatment with 30 mg/kg BW of this MAb caused anemia associated with suppressed blood reticulocytes. The immunohistochemistry of terminal brain tissue showed microglia activation in conjunction with astrogliosis. A moderate axonal/myelin degeneration was also reported in the sciatic nerve, suggesting that this vector may have a narrow therapeutic index [139]. Nevertheless, the authors speculated that further studies may be needed to determine if this neuropathology is induced by the antibody effector function or if it is an intrinsic property of targeting the TfR in the brain [139]. On the contrary, another chronic study performed in the cynomolgus monkey with pabinafusp alfa (human TfRMAb-IDS fusion protein) reported no effector function and no significant toxicological changes at doses up to 30 mg/kg/week for 26 weeks [54]. It is possible that discrepancies in toxic effects targeting the BBB TfR are related to the intrinsic nature of the different TfRMABs, most likely involving the target epitope. TfRMABs were reported to have different properties, including the inhibition of cell growth [140,141]. In a phase II-III clinical trial with pabinafusp alfa in Hunter MPSII patients, 14 of 28 subjects presented IRR that were transient and clinically manageable without the cessation of the administration of the test article. Another 14 patients developed anti-pabinafusp alfa antibodies but had no IRR. Serious adverse events in five patients were reported to be unrelated to the test drug. These included one death due to respiratory failure and resultant hypoxic encephalopathy, conditions that are associated with MPSII [71].

The production of IgG fusion proteins for the GLP toxicological studies was conducted in 50 L Wave bioreactors in perfusion mode in serum-free culture medium and with stably transfected CHO cell lines [48,56,132,133,135,139,142]. Two bioreactor volumes of the conditioned medium were collected per day over a 3–4-week period. The downstream purification process involved protein A affinity chromatography, acid hold for

viral inactivation, cation and anion exchange chromatography, nanofiltration, and diafiltration [48,56,132,133,135]. The safety of the production process was validated by GLP viral clearance validation studies and by parameters set up by the FDA, including CHO host protein and DNA, residual protein A, endotoxin, and sterility [48,56,132,133,135]. IgG fusion proteins were reported to be stable in a liquid formulation at 2–8 °C for more than 2 years [48,56,132,133,135]. The process was successfully transferred to a contract manufacturing organization and scaled up 10-fold for the GMP production used in clinical trials [143].

## 9. Overview and Future Perspectives

Based on the data discussed in this review, it is possible to reformulate virtually any protein-based therapeutic into a brain-penetrating IgG fusion protein therapeutic. These IgG fusion proteins comprise a transport domain that targets BBB endogenous transporters that induce receptor-mediated transport into the brain and a therapeutic domain, which exerts its pharmacological effect in the brain following transport through the BBB (Figure 1). This technology has been reduced to practice in a broad range of potential protein-based brain treatments with MABs directed to both the BBB insulin and transferrin receptors, respectively (Tables 1 and 2). In the majority of these constructs, the therapeutic domain is fused to the C-terminus of the heavy chain of the transport MAB domain (Figure 2), which places the therapeutic domain of the fusion protein in a dimeric configuration and mimics the mature native structure of enzymes, neurotrophic factors, decoy receptors, and bispecific MABs. In other examples, a more flexible configuration is preferred, wherein the therapeutic domain is inserted at the C-terminus of the light chain, as in the case of HIRMAB-HEXA and HIRMAB-ASM (Figure 2), which both form heterodimer complexes with other proteins, i.e., the GM2 activator protein and saposin C, respectively (Sections 3.6 and 3.7). Bispecific MABs have also been engineered by the fusion of the therapeutic domain in the form of ScFv at the C-terminus of the heavy chain of the transport MAB (Figure 7). In addition, the reverse configuration of bispecific MABs was also reported, wherein the therapeutic MAB is in a full antibody form and the transport MAB is an ScFv configuration fused to the C-terminus of the light chain of the therapeutic MAB (Section 4). The reverse configuration presents the advantage of converting any MAB into a brain-penetrating tetravalent bispecific MAB. The IgG fusion proteins are, in general, engineered with short linkers, i.e., 2–4 Ser residues, separating the transport and therapeutic domains of the fusion protein. In some examples, the short linker produced suboptimal levels of quality attributes of the fusion protein, i.e., enzyme activity, expression, and/or stability. In such a case, these attributes were restored by the introduction of a flexible 31-amino-acid extended linker corresponding to the hinge region of IgG3, as in the case of HIRMAB-NAGLU, -HEXA, -ASM, -PPT1, and -GLB1 (Section 3).

The pharmacokinetics and biodistribution of both human and mouse surrogate IgG fusion proteins were reported in rhesus primates and mice, respectively. The pharmacokinetics of the IgG fusion proteins resemble those of small molecules with rapid clearance, as these proteins target the BBB as well as peripheral organs expressing the target receptor. The latter represents an advantage for the treatment of CNS disorders also affecting peripheral organs, such as LSD. The rapid turnover rate is also advantageous, as it reduces potential adverse side effects, as in the case of EPO. The brain uptake of human and mouse IgG fusion proteins ranged from 1 to 3 % ID/brain (Sections 3–7). These levels of brain uptake are comparable to those of small molecules that cross the BBB, i.e., morphine and diazepam, which produce known pharmacological effects in the brain [144,145]. Based on the brain uptake data, the brain levels of IgG fusion proteins were calculated following therapeutic doses of 1–3 mg/kg BW. These estimates were shown to produce brain levels of lysosomal enzymes that were able to normalize their CNS levels in LSD, as in the case of Hurler MPSI, Hunter MPSII, MLD, Sanfilippo MPSIIIA and MPSIIIB, Niemann–Pick A, Tay–Sachs, Batten Type 1, and GM1-gangliosidosis (Section 3). Furthermore, IgG-LSD enzyme fusion proteins were validated in experimental models of Hurler MPSI, Hunter MPSII, and Sanfilippo



MPSIIIA (Section 3). In addition, a model of a BBB-penetrating tetravalent bispecific MAb directed to Ab was validated in experimental AD in mice (Section 4). IgG fusion proteins with TNFR and EPO were also effective in a mouse model of AD (Sections 5 and 6). Finally, brain-penetrating TNFR and neurotrophic factors were neuroprotective in mouse models of PD and stroke (Sections 5 and 6).

BBB-penetrating IgG fusion proteins have shown excellent safety profiles in mice, non-human primates, and humans, in general (Section 8). Anti-drug antibodies were reported; however, those were not neutralizing, as no pharmacokinetic changes were seen at the end of chronic treatments compared with the basal parameters. Minor infusion-related immune reactions were also reported in humans, and those were similar to those seen in standard ERT. Transient hypoglycemia was reported following the administration of IgG-LSD enzymes targeting the BBB insulin receptor, an effect that was prevented by infusing the fusion protein in dextrose-saline.

In conclusion, a broad range of brain-penetrating IgG fusion proteins have been engineered and validated in various animal models of CNS disorders. The development of IgG fusion proteins is well-advanced for the treatment of Hurler MPSI and Hunter MPSII, which culminated in positive phase I-III clinical trials and the approval of the latter by the regulatory agency in Japan. Pending further drug development, other members of the brain-penetrating IgG fusion protein family discussed here are positioned to become a new generation of pharmaceutical drugs for the treatment of human CNS disorders.

**Funding:** This review received no external funding.

**Conflicts of Interest:** The author is the co-inventor of patents on the delivery of biological drugs to the brain.

## References

1. Pardridge, W.M.; Boado, R.J.; Black, K.L.; Cancilla, P.A. Blood-brain barrier and new approaches to brain drug delivery. *West. J. Med.* **1992**, *156*, 281–286. [PubMed]
2. Pardridge, W.M. The blood-brain barrier: Bottleneck in brain drug development. *NeuroRx* **2005**, *2*, 3–14. [CrossRef] [PubMed]
3. Abbott, N.J.; Patabendige, A.A.K.; Dolman, D.E.M.; Yusof, S.R.; Begley, D.J. Structure and function of the blood-brain barrier. *Neurobiol. Dis.* **2010**, *37*, 13–25. [CrossRef]
4. Pardridge, W.M. CSF, blood-brain barrier, and brain drug delivery. *Expert Opin. Drug Deliv.* **2016**, *13*, 963–975. [CrossRef] [PubMed]
5. Boado, R.J.; Pardridge, W.M. Molecular cloning of the bovine blood-brain barrier glucose transporter cDNA and demonstration of phylogenetic conservation of the 5'-untranslated region. *Mol. Cell. Neurosci.* **1990**, *1*, 224–232. [CrossRef]
6. Boado, R.J.; Li, J.Y.; Nagaya, M.; Zhang, C.; Pardridge, W.M. Selective expression of the large neutral amino acid transporter at the blood-brain barrier. *Proc. Natl. Acad. Sci. USA* **1999**, *96*, 12079–12084. [CrossRef]
7. Pardridge, W.M.; Eisenberg, J.; Yang, Y. Human blood-brain barrier insulin receptor. *J. Neurochem.* **1985**, *44*, 1771–1778. [CrossRef]
8. Fishman, J.B.; Rubin, J.B.; Handrahan, J.V.; Connor, J.R.; Fine, R.E. Receptor-mediated transcytosis of transferrin across the blood-brain barrier. *J. Neurosci. Res.* **1987**, *18*, 299–304. [CrossRef]
9. Boado, R.J.; Golden, P.L.; Levin, N.; Pardridge, W. Up-Regulation of Blood-Brain Barrier Short-Form Leptin Receptor Gene Products in Rats Fed a High Fat Diet. *J. Neurochem.* **2002**, *71*, 1761–1764. [CrossRef]
10. Duffy, K.R.; Pardridge, W.M.; Rosenfeld, R.G. Human blood-brain barrier insulin-like growth factor receptor. *Metabolism* **1988**, *37*, 136–140. [CrossRef]
11. Bickel, U.; Yoshikawa, T.; Landaw, E.M.; Faull, K.F.; Pardridge, W.M. Pharmacologic effects in vivo in brain by vector-mediated peptide drug delivery. *Proc. Natl. Acad. Sci. USA* **1993**, *90*, 2618–2622. [CrossRef] [PubMed]
12. Kang, Y.S.; Bickel, U.; Pardridge, W.M. Pharmacokinetics and saturable blood-brain barrier transport of biotin bound to a conjugate of avidin and a monoclonal antibody to the transferrin receptor. *Drug Metab. Dispos.* **1994**, *22*, 99–105. [PubMed]
13. Wu, D.; Boado, R.J.; Pardridge, W.M. Pharmacokinetics and blood-brain barrier transport of [3H]-biotinylated phos-phorothioate oligodeoxynucleotide conjugated to a vector-mediated drug delivery system. *J. Pharmacol. Exp. Ther.* **1996**, *276*, 206–211. [PubMed]
14. Wu, D.; Yang, J.; Pardridge, W.M. Drug targeting of a peptide radiopharmaceutical through the primate blood-brain barrier in vivo with a monoclonal antibody to the human insulin receptor. *J. Clin. Investig.* **1997**, *100*, 1804–1812. [CrossRef] [PubMed]
15. Xia, C.-F.; Zhang, Y.; Zhang, Y.; Boado, R.J.; Pardridge, W.M. Intravenous siRNA of Brain Cancer with Receptor Targeting and Avidin-Biotin Technology. *Pharm. Res.* **2007**, *24*, 2309–2316. [CrossRef] [PubMed]

16. Coloma, M.J.; Lee, H.J.; Kurihara, A.; Landaw, E.M.; Boado, R.J.; Morrison, S.L.; Pardridge, W.M. Transport across the primate blood-brain barrier of a genetically engineered chimeric monoclonal antibody to the human insulin receptor. *Pharm. Res.* **2000**, *17*, 266–274. [CrossRef] [PubMed]
17. Boado, R.J.; Zhang, Y.; Wang, Y.; Pardridge, W.M. Engineering and expression of a chimeric transferrin receptor mono-clonal antibody for blood-brain barrier delivery in the mouse. *Biotechnol. Bioeng.* **2009**, *102*, 1251–1258. [CrossRef]
18. Boado, R.J. A new generation of neurobiological drugs engineered to overcome the challenges of brain drug delivery. *Drug News Perspect.* **2008**, *21*, 489–503. [CrossRef]
19. Pardridge, W.M. Re-Engineering Biopharmaceuticals for Delivery to Brain with Molecular Trojan Horses. *Bioconjug. Chem.* **2008**, *19*, 1327–1338. [CrossRef]
20. Pardridge, W.M.; Boado, R.J. Reengineering Biopharmaceuticals for Targeted Delivery Across the Blood–Brain Barrier. *Methods Enzymol.* **2012**, *503*, 269–292. [CrossRef]
21. Pardridge, W.; Chou, T. Mathematical Models of Blood-Brain Barrier Transport of Monoclonal Antibodies Targeting the Transferrin Receptor and the Insulin Receptor. *Pharmaceutics* **2021**, *14*, 535. [CrossRef] [PubMed]
22. Boado, R.J.; Zhang, Y.; Zhang, Y.; Xia, C.-F.; Wang, Y.; Pardridge, W.M. Genetic engineering of a lysosomal enzyme fusion protein for targeted delivery across the human blood-brain barrier. *Biotechnol. Bioeng.* **2007**, *99*, 475–484. [CrossRef] [PubMed]
23. Lu, J.Z.; Boado, R.J.; Hui, E.K.; Zhou, Q.H.; Pardridge, W.M. Expression in CHO cells and pharmacokinetics and brain uptake in the Rhesus monkey of an IgG-iduronate-2-sulfatase fusion protein. *Biotechnol. Bioeng.* **2011**, *108*, 1954–1964. [CrossRef] [PubMed]
24. Sonoda, H.; Morimoto, H.; Yoden, E.; Koshimura, Y.; Kinoshita, M.; Golovina, G.; Takagi, H.; Yamamoto, R.; Minami, K.; Mizoguchi, A.; et al. A Blood-Brain-Barrier-Penetrating Anti-human Transferrin Receptor Antibody Fusion Protein for Neuro-nopathic Mucopolysaccharidosis II. *Mol. Ther.* **2018**, *26*, 1366–1374. [CrossRef] [PubMed]
25. Boado, R.J.; Lu, J.Z.; Hui, E.K.-W.; Sumbria, R.K.; Pardridge, W.M. Pharmacokinetics and brain uptake in the rhesus monkey of a fusion protein of arylsulfatase a and a monoclonal antibody against the human insulin receptor. *Biotechnol. Bioeng.* **2012**, *110*, 1456–1465. [CrossRef] [PubMed]
26. Boado, R.J.; Lu, J.Z.; Hui, E.K.-W.; Pardridge, W.M. Insulin Receptor Antibody—Sulfamidase Fusion Protein Penetrates the Primate Blood–Brain Barrier and Reduces Glycosoaminoglycans in Sanfilippo Type A Cells. *Mol. Pharm.* **2014**, *11*, 2928–2934. [CrossRef] [PubMed]
27. Boado, R.J.; Lu, J.Z.; Hui, E.K.-W.; Lin, H.; Pardridge, W.M. Insulin Receptor Antibody— $\alpha$ -N-Acetylglucosaminidase Fusion Protein Penetrates the Primate Blood–Brain Barrier and Reduces Glycosoaminoglycans in Sanfilippo Type B Fibroblasts. *Mol. Pharm.* **2016**, *13*, 1385–1392. [CrossRef]
28. Boado, R.J.; Lu, J.Z.; Hui, E.K.; Lin, H.; Pardridge, W.M. Bi-functional IgG-lysosomal enzyme fusion proteins for brain drug delivery. *Sci. Rep.* **2019**, *9*, 18632. [CrossRef]
29. Boado, R.J.; Zhang, Y.; Zhang, Y.; Xia, C.F.; Pardridge, W.M. Fusion antibody for Alzheimer’s disease with bidirectional transport across the blood-brain barrier and A $\beta$  fibril disaggregation. *Bioconjug. Chem.* **2007**, *18*, 447–455. [CrossRef]
30. Boado, R.J.; Hui, E.K.-W.; Lu, J.Z.; Zhou, Q.-H.; Pardridge, W.M. Selective targeting of a TNFR decoy receptor pharmaceutical to the primate brain as a receptor-specific IgG fusion protein. *J. Biotechnol.* **2010**, *146*, 84–91. [CrossRef]
31. Boado, R.J.; Hui, E.K.-W.; Lu, J.Z.; Pardridge, W.M. Drug Targeting of Erythropoietin Across the Primate Blood-Brain Barrier with an IgG Molecular Trojan Horse. *J. Pharmacol. Exp. Ther.* **2010**, *333*, 961–969. [CrossRef]
32. Boado, R.J.; Zhang, Y.; Zhang, Y.; Wang, Y.; Pardridge, W.M. GDNF fusion protein for targeted-drug delivery across the human blood–brain barrier. *Biotechnol. Bioeng.* **2007**, *100*, 387–396. [CrossRef]
33. Boado, R.J.; Zhang, Y.; Zhang, Y.; Pardridge, W.M. Genetic engineering, expression, and activity of a fusion protein of a human neurotrophin and a molecular Trojan horse for delivery across the human blood-brain barrier. *Biotechnol. Bioeng.* **2007**, *97*, 1376–1386. [CrossRef]
34. Boado, R.J.; Zhang, Y.; Zhang, Y.; Xia, C.F.; Wang, Y.; Pardridge, W.M. Genetic engineering, expression, and activity of a chimeric monoclonal antibody-avidin fusion protein for receptor-mediated delivery of biotinylated drugs in humans. *Bioconjug. Chem.* **2008**, *19*, 731–739. [CrossRef] [PubMed]
35. Boado, R.J.; Hui, E.K.-W.; Lu, J.Z.; Zhou, Q.-H.; Pardridge, W.M. Reversal of Lysosomal Storage in Brain of Adult MPS-I Mice with Intravenous Trojan Horse-Iduronidase Fusion Protein. *Mol. Pharm.* **2011**, *8*, 1342–1350. [CrossRef] [PubMed]
36. Zhou, Q.H.; Boado, R.J.; Lu, J.Z.; Hui, E.K.; Pardridge, W.M. Brain-penetrating IgG-iduronate 2-sulfatase fusion protein for the mouse. *Drug Metab. Dispos.* **2012**, *40*, 329–335. [CrossRef] [PubMed]
37. Boado, R.J.; Lu, J.Z.; Hui, E.K.-W.; Pardridge, W.M. Reduction in Brain Heparan Sulfate with Systemic Administration of an IgG Trojan Horse–Sulfamidase Fusion Protein in the Mucopolysaccharidosis Type IIIA Mouse. *Mol. Pharm.* **2017**, *15*, 602–608. [CrossRef]
38. Boado, R.J.; Zhou, Q.H.; Lu, J.Z.; Hui, E.K.; Pardridge, W.M. Pharmacokinetics and brain uptake of a genetically engineered bifunctional fusion antibody targeting the mouse transferrin receptor. *Mol. Pharm.* **2010**, *7*, 237–244. [CrossRef]
39. Zhou, Q.H.; Sumbria, R.; Hui, E.K.; Lu, J.Z.; Boado, R.J.; Pardridge, W.M. Neuroprotection with a brain-penetrating bio-logic tumor necrosis factor inhibitor. *J. Pharmacol. Exp. Ther.* **2011**, *339*, 618–623. [CrossRef]
40. Zhou, Q.-H.; Boado, R.J.; Lu, J.Z.; Hui, E.K.-W.; Pardridge, W.M. Re-Engineering Erythropoietin as an IgG Fusion Protein That Penetrates the Blood–Brain Barrier in the Mouse. *Mol. Pharm.* **2010**, *7*, 2148–2155. [CrossRef]

41. Zhou, Q.-H.; Boado, R.J.; Lu, J.Z.; Hui, E.K.-W.; Pardridge, W.M. Monoclonal Antibody-Glial-Derived Neurotrophic Factor Fusion Protein Penetrates the Blood-Brain Barrier in the Mouse. *Drug Metab. Dispos.* **2010**, *38*, 566–572. [CrossRef] [PubMed]
42. Zhou, Q.H.; Lu, J.Z.; Hui, E.K.; Boado, R.J.; Pardridge, W.M. Delivery of a peptide radiopharmaceutical to brain with an IgG-avidin fusion protein. *Bioconjug. Chem.* **2011**, *22*, 611–618. [CrossRef]
43. Boado, R.J.; Pardridge, W.M. Genetic engineering of IgG-glucuronidase fusion proteins. *J. Drug Target.* **2010**, *18*, 205–211. [CrossRef] [PubMed]
44. Li, J.Y.; Sugimura, K.; Boado, R.J.; Lee, H.J.; Zhang, C.; Duebel, S.; Pardridge, W.M. Genetically engineered brain drug delivery vectors: Cloning, expression and in vivo application of an anti-transferrin receptor single chain anti-body-streptavidin fusion gene and protein. *Protein Eng.* **1999**, *12*, 787–796. [CrossRef] [PubMed]
45. Pardridge, W.M.; Kang, Y.-S.; Buciak, J.L.; Yang, J. Human insulin receptor monoclonal antibody undergoes high affinity binding to human brain capillaries in vitro and rapid transcytosis through the blood-brain barrier in vivo in the primate. *Pharm. Res.* **1995**, *12*, 807–816. [CrossRef]
46. Uchida, Y.; Ohtsuki, S.; Katsukura, Y.; Ikeda, C.; Suzuki, T.; Kamiie, J.; Terasaki, T. Quantitative targeted absolute proteomics of human blood-brain barrier transporters and receptors. *J. Neurochem.* **2011**, *117*, 333–345. [CrossRef]
47. Hoshi, Y.; Uchida, Y.; Tachikawa, M.; Inoue, T.; Ohtsuki, S.; Terasaki, T. Quantitative atlas of blood-brain barrier transporters, receptors, and tight junction proteins in rats and common marmoset. *J. Pharm. Sci.* **2013**, *102*, 3343–3355. [CrossRef]
48. Boado, R.J.; Hui, E.K.-W.; Lu, J.Z.; Pardridge, W.M. AGT-181: Expression in CHO cells and pharmacokinetics, safety, and plasma iduronidase enzyme activity in Rhesus monkeys. *J. Biotechnol.* **2009**, *144*, 135–141. [CrossRef]
49. Ullman, J.C.; Arguello, A.; Getz, J.A.; Bhalla, A.; Mahon, C.S.; Wang, J.; Giese, T.; Bedard, C.; Kim, D.J.; Blumenfeld, J.R.; et al. Brain delivery and activity of a lysosomal enzyme using a blood-brain barrier transport vehicle in mice. *Sci. Transl. Med.* **2020**, *12*, 1163. [CrossRef]
50. Niewoehner, J.; Bohrmann, B.; Collin, L.; Urich, E.; Sade, H.; Maier, P.; Rueger, P.; Stracke, J.O.; Lau, W.; Tissot, A.C.; et al. Increased Brain Penetration and Potency of a Therapeutic Antibody Using a Monovalent Molecular Shuttle. *Neuron* **2014**, *81*, 49–60. [CrossRef]
51. Ng, P.P.; Dela Cruz, J.S.; Sorour, D.N.; Stinebaugh, J.M.; Shin, S.U.; Shin, D.S.; Morrison, S.L.; Penichet, M.L. An anti-transferrin receptor-avidin fusion protein exhibits both strong proapoptotic activity and the ability to deliver various molecules into cancer cells. *Proc. Natl. Acad. Sci. USA* **2002**, *99*, 10706–10711. [CrossRef] [PubMed]
52. Ng, P.P.; Helguera, G.; Daniels, T.R.; Lomas, S.Z.; Rodriguez, J.A.; Schiller, G.; Bonavida, B.; Morrison, S.L.; Penichet, M.L. Molecular events contributing to cell death in malignant human hematopoietic cells elicited by an IgG3-avidin fusion protein targeting the transferrin receptor. *Blood* **2006**, *108*, 2745–2754. [CrossRef] [PubMed]
53. Zhou, Q.-H.; Boado, R.J.; Hui, E.K.-W.; Lu, J.Z.; Pardridge, W.M. Chronic Dosing of Mice with a Transferrin Receptor Monoclonal Antibody-Glial-Derived Neurotrophic Factor Fusion Protein. *Drug Metab. Dispos.* **2011**, *39*, 1149–1154. [CrossRef]
54. Yamamoto, R.; Yoden, E.; Tanaka, N.; Kinoshita, M.; Imakiire, A.; Hirato, T.; Minami, K. Nonclinical safety evaluation of pabinafusp alfa, an anti-human transferrin receptor antibody and iduronate-2-sulfatase fusion protein, for the treatment of neuronopathic mucopolysaccharidosis type II. *Mol. Genet. Metab. Rep.* **2021**, *27*, 100758. [CrossRef] [PubMed]
55. Pardridge, W.M. Kinetics of Blood-Brain Barrier Transport of Monoclonal Antibodies Targeting the Insulin Receptor and the Transferrin Receptor. *Pharmaceutics* **2021**, *15*, 3. [CrossRef]
56. Boado, R.J.; Hui, E.K.; Lu, J.Z.; Pardridge, W.M. IgG-enzyme fusion protein: Pharmacokinetics and anti-drug antibody response in Rhesus monkeys. *Bioconjug. Chem.* **2013**, *24*, 97–104. [CrossRef]
57. Sun, J.; Boado, R.J.; Pardridge, W.M.; Sumbria, R.K. Plasma pharmacokinetics of high-affinity transferrin receptor anti-body-erythropoietin fusion protein is a function of effector attenuation in mice. *Mol. Pharm.* **2019**, *16*, 3534–3543. [CrossRef]
58. Neufeld, E.F. Lysosomal storage diseases. *Annu. Rev. Biochem.* **1991**, *60*, 257–280. [CrossRef]
59. Cheng, S.H.; Smith, A.E. Gene therapy progress and prospects: Gene therapy of lysosomal storage disorders. *Gene Ther.* **2003**, *10*, 1275–1281. [CrossRef]
60. Brady, R.O.; Schiffmann, R. Enzyme-replacement therapy for metabolic storage disorders. *Lancet Neurol.* **2004**, *3*, 752–756. [CrossRef]
61. Wraith, J.E. Enzyme replacement therapy in mucopolysaccharidosis type I: Progress and emerging difficulties. *J. Inherit. Metab. Dis.* **2001**, *24*, 245–250. [CrossRef] [PubMed]
62. Boado, R.J.; Pardridge, W.M. Brain and Organ Uptake in the Rhesus Monkey in Vivo of Recombinant Iduronidase Compared to an Insulin Receptor Antibody-Iduronidase Fusion Protein. *Mol. Pharm.* **2017**, *14*, 1271–1277. [CrossRef] [PubMed]
63. Crow, J.; A Gibbs, D.; Cozens, W.; Spellacy, E.; Watts, R.W. Biochemical and histopathological studies on patients with mucopolysaccharidoses, two of whom had been treated by fibroblast transplantation. *J. Clin. Pathol.* **1983**, *36*, 415–430. [CrossRef] [PubMed]
64. Pardridge, W.M.; Boado, R.J.; Giugliani, R.; Schmidt, M. Plasma Pharmacokinetics of Valanafusp Alpha, a Human Insulin Receptor Antibody-Iduronidase Fusion Protein, in Patients with Mucopolysaccharidosis Type I. *BioDrugs* **2018**, *32*, 169–176. [CrossRef] [PubMed]

65. Giugliani, R.; Giugliani, L.; de Oliveira Poswar, F.; Donis, K.C.; Corte, A.D.; Schmidt, M.; Boado, R.J.; Nestrasil, I.; Nguyen, C.; Chen, S.; et al. Neurocognitive and somatic stabilization in pediatric patients with severe Mucopolysaccharidosis Type I after 52 weeks of intravenous brain-penetrating insulin receptor antibody-iduronidase fusion protein (valanafusp alpha): An open label phase 1–2 trial. *Orphanet. J. Rare Dis.* **2018**, *13*, 110. [CrossRef] [PubMed]
66. Wilson, P.J.; Morris, C.P.; Anson, D.S.; Occhiodoro, T.; Bielicki, J.; Clements, P.R.; Hopwood, J.J. Hunter syndrome: Isolation of an iduronate-2-sulfatase cDNA clone and analysis of patient DNA. *Proc. Natl. Acad. Sci. USA* **1990**, *87*, 8531–8535. [CrossRef]
67. Lu, J.Z.; Hui, E.K.; Boado, R.J.; Pardridge, W.M. Genetic Engineering of a Bifunctional IgG Fusion Protein with Iduronate-2-Sulfatase. *Bioconjug. Chem.* **2010**, *21*, 151–156. [CrossRef]
68. Boado, R.J.; Hui, E.K.-W.; Lu, J.Z.; Sumbria, R.K.; Pardridge, W.M. Blood-Brain Barrier Molecular Trojan Horse Enables Imaging of Brain Uptake of Radioiodinated Recombinant Protein in the Rhesus Monkey. *Bioconjug. Chem.* **2013**, *24*, 1741–1749. [CrossRef]
69. Okuyama, T.; Eto, Y.; Sakai, N.; Minami, K.; Yamamoto, T.; Sonoda, H.; Yamaoka, M.; Tachibana, K.; Hirato, T.; Sato, Y. Iduronate-2-sulfatase with anti-human transferrin receptor antibody for neuropathic mucopolysaccharidosis II: A Phase 1/2 Trial. *Mol. Ther.* **2019**, *27*, 456–464. [CrossRef]
70. Giugliani, R.; Martins, A.M.; So, S.; Yamamoto, T.; Yamaoka, M.; Ikeda, T.; Tanizawa, K.; Sonoda, H.; Schmidt, M.; Sato, Y. Iduronate-2-sulfatase fused with anti-hTfR antibody, pabinafusp alfa, for MPS-II: A phase 2 trial in Brazil. *Mol. Ther.* **2021**, *29*, 2378–2386. [CrossRef]
71. Okuyama, T.; Eto, Y.; Sakai, N.; Nakamura, K.; Yamamoto, T.; Yamaoka, M.; Ikeda, T.; So, S.; Tanizawa, K.; Sonoda, H.; et al. A Phase 2/3 Trial of Pabinafusp Alfa, IDS Fused with Anti-Human Transferrin Receptor Antibody, Targeting Neurodegeneration in MPS-II. *Mol. Ther.* **2021**, *29*, 671–679. [CrossRef] [PubMed]
72. Yamamoto, R.; Kawashima, S. Pharmacological property, mechanism of action and clinical study results of Pabinafusp Alfa (Genetical Recombination) (IZCARGO® I.V. Infusion 10 mg) as the therapeutic for Mucopolysaccharidosis type-II (Hunter syndrome). *Nihon Yakurigaku Zasshi* **2022**, *157*, 62–75. [CrossRef] [PubMed]
73. Molander-Melin, M.; Pernber, Z.; Franken, S.; Gieselmann, V.; Månsson, J.E.; Fredman, P. Accumulation of sulfatide in neuronal and glial cells of arylsulfatase A deficient mice. *J. Neurocytol.* **2004**, *33*, 417–427. [CrossRef] [PubMed]
74. Sevin, C.; Benraiss, A.; Van Dam, D.; Bonnin, D.; Nagels, G.; Verot, L.; Laurendeau, I.; Vidaud, M.; Gieselmann, V.; Vanier, M.; et al. Intracerebral adeno-associated virus-mediated gene transfer in rapidly progressive forms of metachromatic leukodystrophy. *Hum. Mol. Genet.* **2006**, *15*, 53–64. [CrossRef]
75. Muenzer, J.; Fisher, A. Advances in the Treatment of Mucopolysaccharidosis Type I. *N. Engl. J. Med.* **2004**, *350*, 1932–1934. [CrossRef]
76. Penzien, J.M.; Kappler, J.; Herschkowitz, N.; Schuknecht, B.; Leinekugel, P.; Propping, P.; Tønnesen, T.; Lou, H.; Moser, H.; Zierz, S. Compound heterozygosity for metachromatic leukodystrophy and arylsulfatase A pseudodeficiency alleles is not associated with progressive neurological disease. *Am. J. Hum. Genet.* **1993**, *52*, 557–564.
77. Valstar, M.J.; Ruijter, G.J.G.; van Diggelen, O.P.; Poorthuis, B.J.; Wijburg, F.A. Sanfilippo syndrome: A mini-review. *J. Inherit. Metab. Dis.* **2008**, *31*, 240–252. [CrossRef]
78. Tomatsu, S.; Vogler, C.; Montaña, A.M.; Gutierrez, M.; Oikawa, H.; Dung, V.C.; Orii, T.; Noguchi, A.; Sly, W.S. Murine model (Galns(tm(C76S)slu)) of MPS IVA with missense mutation at the active site cysteine conserved among sulfatase proteins. *Mol. Genet. Metab.* **2007**, *91*, 251–258. [CrossRef]
79. Sumbria, R.K.; Zhou, Q.H.; Hui, E.K.; Lu, J.Z.; Boado, R.J.; Pardridge, W.M. Pharmacokinetics and brain uptake of an IgG-TNF decoy receptor fusion protein following intravenous, intraperitoneal, and subcutaneous administration in mice. *Mol. Pharm.* **2013**, *10*, 1425–1431. [CrossRef]
80. Boado, R.J.; Hui, E.K.-W.; Lu, J.Z.; Pardridge, W.M. Very High Plasma Concentrations of a Monoclonal Antibody against the Human Insulin Receptor Are Produced by Subcutaneous Injection in the Rhesus Monkey. *Mol. Pharm.* **2016**, *13*, 3241–3246. [CrossRef]
81. Zhao, H.G.; Li, H.H.; Bach, G.; Schmidtchen, A.; Neufeld, E.F. The molecular basis of Sanfilippo syndrome type B. *Proc. Natl. Acad. Sci. USA* **1996**, *93*, 6101–6105. [CrossRef]
82. Murrey, D.A.; Naughton, B.J.; Duncan, F.J.; Meadows, A.S.; Ware, T.A.; Campbell, K.J.; Bremer, W.G.; Walker, C.M.; Goodchild, L.; Bolon, B.; et al. Feasibility and safety of systemic rAAV9-hNAGLU delivery for treating mucopolysaccharidosis IIIB: Toxicology, biodistribution, and immunological assessments in primates. *Hum. Gene Ther. Clin. Dev.* **2014**, *25*, 72–84. [CrossRef] [PubMed]
83. Quintern, L.E.; Schuchman, E.H.; Levran, O.; Suchi, M.; Ferlinz, K.; Reinke, H.; Sandhoff, K.; Desnick, R.J. Isolation of cDNA clones encoding human acid sphingomyelinase: Occurrence of alternatively processed transcripts. *EMBO J.* **1989**, *8*, 2469–2473. [CrossRef] [PubMed]
84. Linke, T.; Wilkening, G.; Lansmann, S.; Moczall, H.; Bartelsen, O.; Weisgerber, J.; Sandhoff, K. Stimulation of Acid Sphingomyelinase Activity by Lysosomal Lipids and Sphingolipid Activator Proteins. *Biol. Chem.* **2001**, *382*, 283–290. [CrossRef] [PubMed]
85. Bu, J.; Ashe, K.M.; Bringas, J.; Marshall, J.; Dodge, J.C.; Cabrera-Salazar, M.A.; Forsayeth, J.; Schuchman, E.H.; Bankie-wicz, K.S.; Cheng, S.H.; et al. Merits of combination cortical, subcortical, and cerebellar injections for the treatment of Niemann-Pick disease type A. *Mol. Ther.* **2012**, *20*, 1893–1901. [CrossRef]
86. Myerowitz, R.; Piekarz, R.; Neufeld, E.F.; Shows, T.B.; Suzuki, K. Human beta-hexosaminidase alpha chain: Coding sequence and homology with the beta chain. *Proc. Natl. Acad. Sci. USA* **1985**, *82*, 7830–7834. [CrossRef]

87. Tropak, M.B.; Yonekawa, S.; Karumuthil-Melethil, S.; Thompson, P.; Wakarchuk, W.; Gray, S.J.; Walia, J.S.; Mark, B.L.; Mahuran, D. Construction of a hybrid  $\beta$ -hexosaminidase subunit capable of forming stable homodimers that hydrolyze GM2 ganglioside in vivo. *Mol. Ther. Methods Clin. Dev.* **2016**, *3*, 15057. [CrossRef]
88. Bradbury, A.M.; Morrison, N.E.; Hwang, M.; Cox, N.R.; Baker, H.J.; Martin, D.R. Neurodegenerative lysosomal storage disease in European Burmese cats with hexosaminidase beta-subunit deficiency. *Mol. Genet. Metab.* **2009**, *97*, 53–59. [CrossRef]
89. Camp, L.A.; Verkruyse, L.A.; Afendis, S.J.; Slaughter, C.A.; Hofmann, S.L. Molecular cloning and expression of palmitoyl-protein thioesterase. *J. Biol. Chem.* **1994**, *269*, 23212–23219. [CrossRef]
90. Hobert, J.A.; Dawson, G. Neuronal ceroid lipofuscinoses therapeutic strategies: Past, present and future. *Biochim. Biophys. Acta.* **2006**, *1762*, 945–953. [CrossRef]
91. Oshima, A.; Tsuji, A.; Nagao, Y.; Sakuraba, H.; Suzuki, Y. Cloning, sequencing, and expression of cDNA for human  $\beta$ -galactosidase. *Biochem. Biophys. Res. Commun.* **1988**, *157*, 238–244. [CrossRef]
92. Weismann, C.M.; Ferreira, J.; Keeler, A.M.; Su, Q.; Qui, L.; Shaffer, S.A.; Xu, Z.; Gao, G.; Sena-Esteves, M. Systemic AAV9 gene transfer in adult GM1 gangliosidosis mice reduces lysosomal storage in CNS and extends lifespan. *Hum. Mol. Genet.* **2015**, *24*, 4353–4364. [CrossRef] [PubMed]
93. Przybilla, M.J.; Stewart, C.; Carlson, T.W.; Ou, L.; Koniar, B.L.; Sidhu, R.; Kell, P.J.; Jiang, X.; James, J.R.; O’Sullivan, M.G.; et al. Examination of a blood-brain barrier targeting  $\beta$ -galactosidase-monoclonal antibody fusion protein in a murine model of GM1-gangliosidosis. *Mol. Genet. Metab. Rep.* **2021**, *27*, 100748. [CrossRef] [PubMed]
94. Boado, R.J.; Lu, J.Z.; Hui, E.K.; Pardridge, W.M. IgG-single chain Fv fusion protein therapeutic for Alzheimer’s disease: Expression in CHO cells and pharmacokinetics and brain delivery in the Rhesus monkey. *Biotechnol. Bioeng.* **2010**, *105*, 627–635. [CrossRef]
95. Zhou, Q.-H.; Fu, A.; Boado, R.J.; Hui, E.K.-W.; Lu, J.Z.; Pardridge, W.M. Receptor-Mediated Abeta Amyloid Antibody Targeting to Alzheimer’s Disease Mouse Brain. *Mol. Pharm.* **2010**, *8*, 280–285. [CrossRef]
96. Sumbria, R.K.; Hui, E.K.-W.; Lu, J.Z.; Boado, R.J.; Pardridge, W.M. Disaggregation of Amyloid Plaque in Brain of Alzheimer’s Disease Transgenic Mice with Daily Subcutaneous Administration of a Tetravalent Bispecific Antibody That Targets the Transferrin Receptor and the Abeta Amyloid Peptide. *Mol. Pharm.* **2013**, *10*, 3507–3513. [CrossRef]
97. Wilcock, D.M.; Colton, C.A. Immunotherapy, vascular pathology, and microhemorrhages in transgenic mice. *CNS Neurol. Disord. Drug Targets* **2009**, *8*, 50–64. [CrossRef]
98. Faresjö, R.; Lindberg, H.; Ståhl, S.; Löfblom, J.; Syvänen, S.; Sehlin, D. Transferrin Receptor Binding BBB-Shuttle Facilitates Brain Delivery of Anti-A $\beta$ -Affibodies. *Pharm. Res.* **2022**, *39*, 1509–1521. [CrossRef]
99. Boado, R.J.; (UCLA, Los Angeles, CA, USA); Pardridge, W.M.; (UCLA, Los Angeles, CA, USA). Unpublished work.
100. Poppel, K.; Crawford, D.; Beutler, B. A tumor necrosis factor (TNF) receptor-IgG heavy chain chimeric protein as a bivalent antagonist of TNF activity. *J. Exp. Med.* **1991**, *174*, 1483–1489. [CrossRef]
101. Valesini, G.; Iannuccelli, C.; Marocchi, E.; Pascoli, L.; Scalzi, V.; Di Franco, M. Biological and clinical effects of anti-TNF alpha treatment. *Autoimmun. Rev.* **2007**, *7*, 35–41. [CrossRef]
102. Nawashiro, H.; Martin, D.; Hallenbeck, J.M. Neuroprotective effects of TNF binding protein in focal cerebral ischemia. *Brain Res.* **1997**, *778*, 265–271. [CrossRef]
103. Knoblach, S.M.; Fan, L.; Faden, A.I. Early neuronal expression of tumor necrosis factor- $\alpha$  after experimental brain injury contributes to neurological impairment. *J. Neuroimmunol.* **1999**, *95*, 115–125. [CrossRef]
104. Marchand, F.; Tsantoulas, C.; Singh, D.; Grist, J.; Clark, A.; Bradbury, E.; McMahon, S.B. Effects of Etanercept and Minocycline in a rat model of spinal cord injury. *Eur. J. Pain* **2009**, *13*, 673–681. [CrossRef] [PubMed]
105. Tweedie, D.; Sambamurti, K.; Greig, N.H. TNF- $\alpha$  Inhibition as a Treatment Strategy for Neurodegenerative Disorders: New Drug Candidates and Targets. *Curr. Alzheimer Res.* **2007**, *4*, 378–385. [CrossRef] [PubMed]
106. Himmerich, H.; Fulda, S.; Linseisen, J.; Seiler, H.; Wolfram, G.; Himmerich, S.; Gedrich, K.; Kloiber, S.; Lucae, S.; Ising, M.; et al. Depression, comorbidities and the TNF-alpha system. *Eur. Psychiatry* **2008**, *23*, 421–429. [CrossRef] [PubMed]
107. Sumbria, R.K.; Boado, R.J.; Pardridge, W.M. Brain Protection from Stroke with Intravenous TNF  $\alpha$  Decoy Receptor-Trojan Horse Fusion Protein. *J. Cereb. Blood Flow Metab.* **2012**, *32*, 1933–1938. [CrossRef]
108. Chang, R.; Knox, J.; Chang, J.; Derbedrossian, A.; Vasilevko, V.; Cribbs, D.; Boado, R.J.; Pardridge, W.M.; Sumbria, R.K. Blood-brain barrier penetrating biologic TNF- $\alpha$  inhibitor for Alzheimer’s Disease. *Mol. Pharm.* **2017**, *14*, 2340–2349. [CrossRef]
109. Lin, L.-F.H.; Doherty, D.H.; Lile, J.D.; Bektesh, S.; Collins, F. GDNF: A Glial Cell Line-Derived Neurotrophic Factor for Midbrain Dopaminergic Neurons. *Science* **1993**, *260*, 1130–1132. [CrossRef]
110. Lapchak, P.; Miller, P.; Collins, F.; Jiao, S. Glial cell line-derived neurotrophic factor attenuates behavioural deficits and regulates nigrostriatal dopaminergic and peptidergic markers in 6-hydroxydopamine-lesioned adult rats: Comparison of intraventricular and intranigral delivery. *Neuroscience* **1997**, *78*, 61–72. [CrossRef]
111. Hefti, F. Pharmacology of neurotrophic factors. *Annu. Rev. Pharmacol. Toxicol.* **1997**, *37*, 239–267. [CrossRef]
112. Sakanaka, M.; Wen, T.-C.; Matsuda, S.; Morishita, E.; Nagao, M.; Sasaki, R. In vivo evidence that erythropoietin protects neurons from ischemic damage. *Proc. Natl. Acad. Sci. USA* **1998**, *95*, 4635–4640. [CrossRef] [PubMed]
113. Bohn, M.C. Motoneurons crave glial cell line-derived neurotrophic factor. *Exp. Neurol.* **2004**, *190*, 263–275. [CrossRef] [PubMed]
114. Jin, K.; LaFevre-Bernt, M.; Sun, Y.; Chen, S.; Gafni, J.; Crippen, D.; Logvinova, A.; Ross, C.A.; Greenberg, D.A.; Ellerby, L.M. FGF-2 promotes neurogenesis and neuroprotection and prolongs survival in a transgenic mouse model of Hunting-ton’s disease. *Proc. Natl. Acad. Sci. USA* **2005**, *102*, 18189–18194. [CrossRef] [PubMed]

115. Rossi, C.; Angelucci, A.; Costantin, L.; Braschi, C.; Mazzantini, M.; Babbini, F.; Fabbri, M.E.; Tessarollo, L.; Maffei, L.; Berardi, N.; et al. Brain-derived neurotrophic factor (BDNF) is required for the enhancement of hippocampal neurogenesis following environmental enrichment. *Eur. J. Neurosci.* **2006**, *24*, 1850–1856. [CrossRef]
116. Kobayashi, T.; Ahlenius, H.; Thored, P.; Kobayashi, R.; Kokaia, Z.; Lindvall, O. Intracerebral Infusion of Glial Cell Line-Derived Neurotrophic Factor Promotes Striatal Neurogenesis After Stroke in Adult Rats. *Stroke* **2006**, *37*, 2361–2367. [CrossRef] [PubMed]
117. Grasso, G.; Sfacteria, A.; Meli, F.; Fodale, V.; Buemi, M.; Iacopino, D.G. Neuroprotection by erythropoietin administration after experimental traumatic brain injury. *Brain Res.* **2007**, *1182*, 99–105. [CrossRef]
118. Xue, Y.-Q.; Zhao, L.-R.; Guo, W.-P.; Duan, W.-M. Intrastriatal administration of erythropoietin protects dopaminergic neurons and improves neurobehavioral outcome in a rat model of Parkinson's disease. *Neuroscience* **2007**, *146*, 1245–1258. [CrossRef]
119. Fu, A.; Hui, E.K.; Lu, J.Z.; Boado, R.J.; Pardridge, W.M. Neuroprotection in experimental stroke in the rat with an IgG-erythropoietin fusion protein. *Brain Res.* **2010**, *1360*, 193–197. [CrossRef]
120. Fu, A.; Hui, E.K.; Lu, J.Z.; Boado, R.J.; Pardridge, W.M. Neuroprotection in stroke in the mouse with intravenous erythropoietin-Trojan horse fusion protein. *Brain Res.* **2011**, *1369*, 203–207. [CrossRef]
121. Zhou, Q.H.; Hui, E.K.; Lu, J.Z.; Boado, R.J.; Pardridge, W.M. Brain penetrating IgG-erythropoietin fusion protein is neuroprotective following intravenous treatment in Parkinson's disease in the mouse. *Brain Res.* **2011**, *1382*, 315–320. [CrossRef]
122. Chang, R.; Al Maghribi, A.; Vanderpoel, V.; Vasilevko, V.; Cribbs, D.H.; Boado, R.; Pardridge, W.M.; Sumbria, R.K. Brain Penetrating Bifunctional Erythropoietin-Transferrin Receptor Antibody Fusion Protein for Alzheimer's Disease. *Mol. Pharm.* **2018**, *15*, 4963–4973. [CrossRef] [PubMed]
123. Boado, R.J.; Pardridge, W.M. Comparison of blood-brain barrier transport of glial-derived neurotrophic factor (GDNF) and an IgG-GDNF fusion protein in the Rhesus monkey. *Drug Metab. Dispos.* **2009**, *37*, 2299–2304. [CrossRef] [PubMed]
124. Fu, A.; Zhou, Q.H.; Hui, E.K.; Lu, J.Z.; Boado, R.J.; Pardridge, W.M. Intravenous treatment of experimental Parkinson's disease in the mouse with an IgG-GDNF fusion protein that penetrates the blood-brain barrier. *Brain Res.* **2010**, *1352*, 208–213. [CrossRef]
125. Sumbria, R.K.; Boado, R.J.; Pardridge, W.M. Combination stroke therapy in the mouse with blood-brain barrier penetrating IgG-GDNF and IgG-TNF decoy receptor fusion proteins. *Brain Res.* **2013**, *1507*, 91–96. [CrossRef] [PubMed]
126. Ohshima-Hosoyama, S.; Simmons, H.A.; Goecks, N.; Joers, V.; Swanson, C.R.; Bondarenko, V.; Velotta, R.; Brunner, K.; Wood, L.D.; Hruban, R.H.; et al. A monoclonal antibody-GDNF fusion protein is not neuroprotective and is associated with proliferative pancreatic lesions in parkinsonian monkeys. *PLoS ONE* **2012**, *7*, 39036. [CrossRef]
127. Mori, T.; Shimizu, K.; Hayashi, M. Differential expression patterns of TrkB ligands in the macaque monkey brain. *NeuroReport* **2004**, *15*, 2507–2511. [CrossRef]
128. Magnani, P.; Paganelli, G.; Songini, C.; Samuel, A.; Sudati, F.; Siccardi, A.; Fazio, F. Pretargeted immunoscintigraphy in patients with medullary thyroid carcinoma. *Br. J. Cancer* **1996**, *74*, 825–831. [CrossRef]
129. Samuel, A.; Paganelli, G.; Chiesa, R.; Sudati, F.; Calvitto, M.; Melissano, G.; Grossi, A.; Fazio, F. Detection of prosthetic vascular graft infection using avidin/indium-111-biotin scintigraphy. *J. Nucl. Med.* **1996**, *37*, 55–61.
130. Hendrickson, W.A.; Pähler, A.; Smith, J.L.; Satow, Y.; Merritt, E.A.; Phizackerley, R.P. Crystal structure of core streptavidin determined from multiwavelength anomalous diffraction of synchrotron radiation. *Proc. Natl. Acad. Sci. USA* **1989**, *86*, 2190–2194. [CrossRef]
131. Sumbria, R.K.; Boado, R.J.; Pardridge, W.M. Imaging amyloid plaque in Alzheimer's disease brain with a biotinylated A $\beta$  peptide radiopharmaceutical conjugated to an IgG-avidin fusion protein. *Bioconjug. Chem.* **2012**, *23*, 1318–1321. [CrossRef]
132. Boado, R.J.; Hui, E.K.; Lu, J.Z.; Pardridge, W.M. Insulin receptor antibody-iduronate 2-sulfatase fusion protein: Pharmacokinetics, anti-drug antibody, and safety pharmacology in Rhesus monkeys. *Biotechnol. Bioeng.* **2014**, *111*, 2317–2325. [CrossRef] [PubMed]
133. Boado, R.J.; Hui, E.K.-W.; Lu, J.Z.; Pardridge, W.M. Glycemic Control and Chronic Dosing of Rhesus Monkeys with a Fusion Protein of Iduronidase and a Monoclonal Antibody Against the Human Insulin Receptor. *Drug Metab. Dispos.* **2012**, *40*, 2021–2025. [CrossRef] [PubMed]
134. De Groot, A.S.; Moise, L.; McMurry, J.A.; Wambre, E.; Van Overtvelt, L.; Moingeon, P.; Scott, D.W.; Martin, W. Activation of natural regulatory T cells by IgG Fc-derived peptide "Tregitopes". *Blood* **2008**, *112*, 3303–3311. [CrossRef] [PubMed]
135. Pardridge, W.M.; Boado, R.J. Pharmacokinetics and Safety in Rhesus Monkeys of a Monoclonal Antibody-GDNF Fusion Protein for Targeted Blood-Brain Barrier Delivery. *Pharm. Res.* **2009**, *26*, 2227–2236. [CrossRef] [PubMed]
136. Kozuka, S.; Sassa, R.; Taki, T.; Masamoto, K.; Nagasawa, S.; Saga, S.; Hasegawa, K.; Takeuchi, M. Relation of pancreatic duct hyperplasia to carcinoma. *Cancer* **1979**, *43*, 1418–1428. [CrossRef]
137. Couch, J.A.; Yu, Y.J.; Zhang, Y.; Tarrant, J.M.; Fuji, R.N.; Meilandt, W.J.; Solanoy, H.; Tong, R.K.; Hoyte, K.; Luk, W.; et al. Addressing Safety Liabilities of TfR Bispecific Antibodies That Cross the Blood-Brain Barrier. *Sci. Transl. Med.* **2013**, *5*, 183ra57. [CrossRef]
138. Sun, J.; Yang, J.; Whitman, K.; Zhu, C.; Cribbs, D.H.; Boado, R.J.; Pardridge, W.M.; Sumbria, R.K. Hematologic safety of chronic brain-penetrating erythropoietin dosing in APP/PS1 mice. *Alzheimer's Dement. Transl. Res. Clin. Interv.* **2019**, *5*, 627–636. [CrossRef]
139. Pardridge, W.M.; Boado, R.J.; Patrick, D.J.; Hui, E.K.-W.; Lu, J.Z. Blood-Brain Barrier Transport, Plasma Pharmacokinetics, and Neuropathology Following Chronic Treatment of the Rhesus Monkey with a Brain Penetrating Humanized Monoclonal Antibody Against the Human Transferrin Receptor. *Mol. Pharm.* **2018**, *15*, 5207–5216. [CrossRef]

140. White, S.; Taetle, R.; A Seligman, P.; Rutherford, M.; Trowbridge, I.S. Combinations of anti-transferrin receptor monoclonal antibodies inhibit human tumor cell growth in vitro and in vivo: Evidence for synergistic antiproliferative effects. *Cancer Res.* **1990**, *50*, 6295–6301.
141. Trowbridge, I.S. Transferrin Receptor as a Potential Therapeutic Target. *Prog. Allergy* **1988**, *45*, 121–146. [CrossRef]
142. Walsh, K.; Hui, E.; Lu, J.; Boado, R.; Kaisermayer, C. Using Pre-Sterilized External Filters in Long-Term Perfusion Cell Culture Applications. *Bioprocess. J.* **2011**, *10*, 21–26. [CrossRef]
143. Boado, R.J. (UCLA, Los Angeles, CA, USA). Unpublished work.
144. Wu, D.; Kang, Y.S.; Bickel, U.; Pardridge, W.M. Blood-brain barrier permeability to morphine-6-glucuronide is markedly reduced compared with morphine. *Drug Metab. Dispos.* **1997**, *25*, 768–771. [PubMed]
145. Greenblatt, D.J.; Sethy, V.H. Benzodiazepine concentrations in brain directly reflect receptor occupancy: Studies of diazepam, lorazepam, and oxazepam. *Psychopharmacology* **1990**, *1*, 373–378. [CrossRef] [PubMed]

Review

# Treatment of Neuronopathic Mucopolysaccharidoses with Blood–Brain Barrier-Crossing Enzymes: Clinical Application of Receptor-Mediated Transcytosis

Hiroyuki Sonoda, Kenichi Takahashi, Kohtaro Minami, Toru Hirato, Tatsuyoshi Yamamoto, Sairei So, Kazunori Tanizawa, Mathias Schmidt and Yuji Sato \* 

JCR Pharmaceuticals, Ashiya 659-0021, Hyogo, Japan; sonoda-h@jp.jcrpharm.com (H.S.); takahasi@jp.jcrpharm.com (K.T.); minami-k@jp.jcrpharm.com (K.M.); hirato-t@jp.jcrpharm.com (T.H.); t-yamamoto@jp.jcrpharm.com (T.Y.); sou-s@jp.jcrpharm.com (S.S.); tanizawa-k@jp.jcrpharm.com (K.T.); mschmidt@us.jcrpharm.com (M.S.)

\* Correspondence: sato-yuji@jp.jcrpharm.com; Tel.: +81-797-32-8591

**Abstract:** Enzyme replacement therapy (ERT) has paved the way for treating the somatic symptoms of lysosomal storage diseases (LSDs), but the inability of intravenously administered enzymes to cross the blood–brain barrier (BBB) has left the central nervous system (CNS)-related symptoms of LSDs largely impervious to the therapeutic benefits of ERT, although ERT via intrathecal and intracerebroventricular routes can be used for some neuronopathic LSDs (in particular, mucopolysaccharidoses). However, the considerable practical issues involved make these routes unsuitable for long-term treatment. Efforts have been made to modify enzymes (e.g., by fusing them with antibodies against innate receptors on the cerebrovascular endothelium) so that they can cross the BBB via receptor-mediated transcytosis (RMT) and address neuronopathy in the CNS. This review summarizes the various scientific and technological challenges of applying RMT to the development of safe and effective enzyme therapeutics for neuronopathic mucopolysaccharidoses; it then discusses the translational and methodological issues surrounding preclinical and clinical evaluation to establish RMT-applied ERT.

**Keywords:** lysosomal storage disease; neuronopathic mucopolysaccharidosis; blood–brain barrier; neurodegeneration; enzyme replacement therapy; receptor-mediated transcytosis; transferrin receptor; insulin receptor

**Citation:** Sonoda, H.; Takahashi, K.; Minami, K.; Hirato, T.; Yamamoto, T.; So, S.; Tanizawa, K.; Schmidt, M.; Sato, Y. Treatment of Neuronopathic Mucopolysaccharidoses with Blood–Brain Barrier-Crossing Enzymes: Clinical Application of Receptor-Mediated Transcytosis. *Pharmaceutics* **2022**, *14*, 1240. <https://doi.org/10.3390/pharmaceutics14061240>

Academic Editor: William M. Pardridge

Received: 19 May 2022

Accepted: 10 June 2022

Published: 11 June 2022

**Publisher's Note:** MDPI stays neutral with regard to jurisdictional claims in published maps and institutional affiliations.



**Copyright:** © 2022 by the authors. Licensee MDPI, Basel, Switzerland. This article is an open access article distributed under the terms and conditions of the Creative Commons Attribution (CC BY) license (<https://creativecommons.org/licenses/by/4.0/>).

## 1. Introduction

Delivery of therapeutics to the brain has always been hampered by the blood–brain barrier (BBB), which protects the brain from external macromolecules, such as pathogenic and toxic substances [1]. Indeed, the brain has been touted as a ‘sanctuary’ against chemotherapy, because extravasating malignant cells escape from anti-cancer drugs in the peripheral blood stream, lurk in the brain, and eventually cause fatal metastases therein [2]. Various efforts have been made, therefore, to deliver therapeutics for brain diseases by circumventing the BBB, including temporary mechanical disruption of the BBB by hyperthermia [3] and ultrasound [4,5], and drug administration into the cerebrospinal fluid (CSF) by intrathecal [6,7] and intracerebroventricular (ICV) [8] routes, whereby the drugs are expected to diffuse through the CSF and become immersed in the brain parenchyma.

In contrast to the traditional view of the BBB as being made up primarily of restrictive endothelial tight junctions that sequester the systemic/peripheral blood flow and the brain, recent advances in BBB research have revealed that the BBB works more as a dynamic neurovascular unit that regulates the transport of substances [9]. Transcytosis is one such innate transport mechanism by the neurovascular unit, in particular, the vascular endothelial cells. Receptor-mediated transcytosis (RMT), as opposed to non-selective



adsorptive transcytosis, has received attention as a promising pathway through which to traffic large molecules such as enzymes and biologics across the BBB [10].

Lysosomal storage diseases (LSDs) are a group of some 70 genetic metabolic disorders in which enzyme deficiencies in lysosomes cause systemic pathological accumulation of uncatabolized substrates, resulting in multisystemic progressive damage that manifests in a broad spectrum of debilitating symptoms, including coarse facies, hepatosplenomegaly, upper airway obstruction, cardiac dysfunction, and neurocognitive impairments [11], some of which are life-limiting. Successful development of recombinant enzyme therapeutics has enabled restoration of enzyme activities in some LSDs [12–14], and the advent of enzyme replacement therapy (ERT) has since led to significant improvements in somatic/peripheral symptoms and proximal outcomes in some LSDs [15]. However, as the BBB impedes the delivery of the therapeutic enzymes into the brain, conventional ERT cannot alleviate substance accumulation in the central nervous system (CNS), so progressive neurodegeneration in the CNS remains unbridled and culminates in neurocognitive deterioration [16]. Since most LSDs involve such unassailable CNS pathology, they are also known as neuronopathic LSDs, and to this day, the means to deliver enzyme therapeutics to the brain remains a critical unmet medical need [17,18].

For intra-CSF administration of therapeutic enzymes, the ICV route has proved viable, as exemplified by cerliponase alfa for the treatment of neuronal ceroid lipofuscinosis type 2 [19,20] and idursulfase beta for mucopolysaccharidosis II (MPS II, Hunter syndrome) [21]. However, even after successful drug distribution to the brain parenchyma following intra-CSF administration, significant drug efficacy is not yet fully guaranteed [22], because the CSF remains problematic as a vehicle for drug delivery [23]. Moreover, concomitant peripheral administration of enzyme therapeutics to deal with substance accumulations in the periphery is necessary, which imposes further burdens on pediatric patients and is inimical to lifelong treatment for these chronic ailments.

Consequently, an enzyme therapeutic designed to address both the peripheral/somatic and CNS manifestations will be the most suitable means of overcoming these difficulties and providing an improved form of ERT for neuronopathic LSDs. Several attempts have been made to realize these objectives by equipping enzyme therapeutics with the capacity to undergo RMT. This review summarizes the hitherto known applications of RMT for drug delivery to treat neuronopathic MPSs, in particular, illustrates the pitfalls and challenges of engineering enzyme therapeutics to harness effective RMT, highlights translational issues in establishing RMT-applied ERT by preclinical and clinical evaluations, and, finally, delineates the remaining issues surrounding drug delivery to the brain in general.

## **2. Transcytosis through the BBB: A Breakthrough for Brain Drug Delivery**

### *2.1. Application of Receptor-Mediated Transcytosis for Brain Drug Delivery*

Transcytosis is a mechanism of transcellular transport of molecules via vesicles [9,24] and contributes to the physiological function of the BBB in regulating substance transport from the systemic circulation to the CNS. When activated in cerebrovascular endothelial cells, this mechanism can also serve as a potential conduit for ferrying large molecules into the brain parenchyma. It has, therefore, kindled various research projects to apply it to brain drug delivery by what is known as the Trojan horse method [25], whereby a drug normally nontransferable across the BBB is, by chimeric peptide technology, conjugated or fused to a BBB transport vector, the vector being an endogenous peptide or anti-receptor monoclonal antibody that undergoes RMT without competing with endogenous ligands. RMT has been actively utilized in modifying enzyme therapeutics for ERT for neuronopathic LSDs [26,27]. This application has become possible thanks to the evolving understanding of intracellular trafficking, receptor binding, and protein engineering [28]. RMT is considered very suitable for application to pharmacotherapy [29] due to the innate physiological mechanism of the BBB that makes abundant receptors available, in addition to which, the very small inter-capillary distances in the brain allow each neuron to be perfused by the blood vessels surrounding it, making it ready to receive the trafficked substance [30]. Moreover, RMT

allows highly specific trafficking of the targeted substance to which specific antibodies are fused. Therefore, RMT enables more stable and repeatable substance trafficking than modification of BBB permeability, which can be transient and perturb the normal function and structure of the BBB [29].

The main receptors studied for RMT so far are insulin [31–33] and transferrin receptors (TfRs) [34–38], although others (e.g., low-density lipoprotein receptor [39,40], neurotropic virulence factor receptors [41,42], CD98 heavy chain [43], and GLUT1 [44,45]) have also been suggested as potentially useful for brain drug delivery.

Figure 1 illustrates the mechanism of transcytosis mediated by TfRs [46]. Transferrin binds to the TfRs located on the luminal side of the microvascular endothelial cells in the brain and is absorbed into the endothelial cells (endocytosis), in which it is then transported towards the abluminal side of the cells facing the brain, and subsequently released from the receptors to reach the brain parenchyma (exocytosis). Likewise, enzymes fused with anti-TfR antibodies bind to the TfRs, are then internalized into and trafficked across the endothelial cells, and are finally unleashed into the abluminal side of the endothelium so that they can reach the brain parenchyma to exert drug efficacy in the targeted sites of action (i.e., neurons and glial cells).

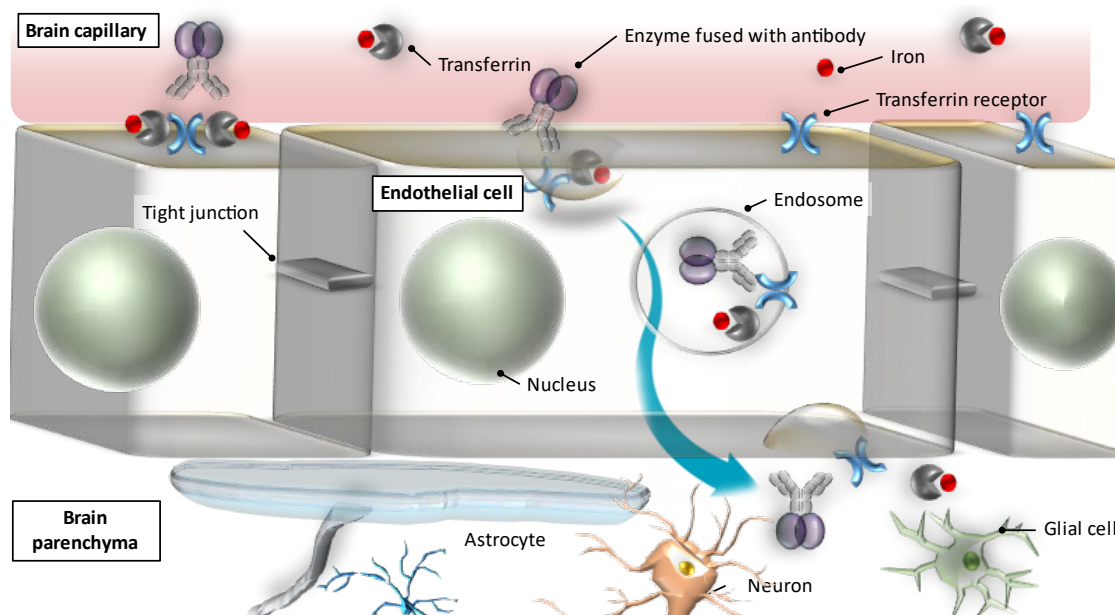


**Figure 1.** A schematic representation of transferrin receptor-mediated transcytosis in the blood–brain barrier (Revised from Yamamoto and Kawashima [46]).

## 2.2. Optimizing RMT for ERT

Successful application of RMT for ERT can be realized, first, when attachment of the enzyme to the ‘Trojan horse’ (i.e., a molecular cargo on which to load the drug for delivery across the BBB) is achieved through high-standard genetic engineering [25], and, secondly, when critical factors affecting RMT [47] are modulated so as to enable the most efficient and stable trafficking of the drug. The former requires optimal molecular architecture of the enzyme therapeutic as a whole [48] with the help of precise protein and antibody engineering [24], whilst the latter requires elucidation of the mechanism of antibody passage across the BBB [29], which involves many hitherto unanswered questions.

### 2.2.1. Antibody Engineering for RMT

In order to design and generate ideal antibodies for specific RMT, several serious limitations that have long compromised biotherapeutic engineering need to be overcome; these include poor pharmacokinetic parameters, non-optimal distribution, inhibition of their binding with Fc receptors, toxicity [49], and untoward influence on the original receptor

functions. Furthermore, the immunogenicity inherent in biotherapeutics that is associated with risks of decreased tolerance and efficacy must be controlled if a therapeutic is to be utilized for long-term treatment, as is the case with ERT for neuronopathic MPS. Therefore, production of biotherapeutics requires continual optimization processes to maximize their therapeutic potential, on the one hand, and to ensure an acceptable safety profile on the other [50]. The optimization processes must also aim to achieve the most favorable pharmacodynamic response and pharmacokinetic parameters as possible. Furthermore, when a suitable antibody is tailored as a biotherapeutic for RMT-applied ERT targeting a specific neuronopathic MPS, the bioengineering processes may very well have to be revamped when a different enzyme needs to be fused with an antibody for separate ERT for a different LSD, even when the same previously established RMT mechanism is utilized. In other words, successful realization of RMT-applied ERT for a neuronopathic LSD depends heavily on whether specifically optimized design and production of an antibody-fused therapeutic can be achieved in the time and with the resources and bioengineering prowess available.

Goulatis [51] pointed out that antibody-antigen receptor interaction plays a pivotal role in optimizing substance trafficking across the BBB, which is deeply affected by binding affinity, avidity, and pH sensitivity. Ongoing controversies surround the optimal combination of antibody affinity towards the antigen receptor and the brain's uptake of antibody-fused therapeutics. Whereas moderate-affinity monovalent anti-TfR antibodies fused with an enzyme therapeutic have been reported to traverse the BBB more efficiently than high-affinity bivalent antibodies fused with a comparable enzyme [48], antibodies with relatively high affinity have been shown to achieve efficient transport across a wide range of injection doses, as opposed to antibodies with low affinity transported only at high doses [52].

Most of the enzymes that are deficient in LSDs incorporate modified mannose-6-phosphatase (M6P) and undergo hepatic and other clearance dependent on M6P receptors (M6PRs), which accounts for their limited plasma retention time. This negatively affects their binding to the TfRs on cerebrovascular endothelial cells. In order to ensure sufficient binding to the TfRs, enzyme therapeutics need to have binding affinity higher than is generally seen in biologics with good plasma retention. However, when enzymes are released from endothelial cells into the brain parenchyma, high binding affinity invariably leads to reduced dissociation of the enzymes from the TfRs, thereby diminishing the number of molecules that reach the brain. Taken together, it seems sensible to strike a balance between the binding efficiency of enzyme therapeutics to the apical side of endothelial cells and their efficient dissociation on the vasolateral side at the same time to achieve the most suitable avidity for drug delivery across the BBB. Furthermore, accumulated clinical data from mid- to long-term ERT are needed to determine the optimal dosage and actual clinical efficacy of the therapeutics for neuronopathic LSDs, because such matters cannot be resolved by preclinical and theoretical discussions alone.

After appropriate bioengineering methods for creating a biotherapeutic for RMT-applied ERT are duly established, sufficient quantities have to be manufactured for the drug to be tested in preclinical and clinical studies. This invariably involves timely scaling-up of drug production, with an eye to further augmentation to supply a wider patient population after the drug is approved. Unlike the preclinical and clinical studies of the therapeutic, the ingenious and painstaking efforts devoted to the bioengineering and manufacturing of the drug usually remain unpublished, because these endeavors involve essential information pertaining to intellectual property. Thus, discussion of these critical processes is inevitably restricted to mere general descriptions of the major issues without any quantitative or qualitative details. It would actually be very helpful if detailed descriptions of the caveats and other issues were published to avoid unnecessary repetition of mistakes, underestimation of critical points, and unguided guesswork in this uncharted field. Figure 2 summarizes the complex processes of selecting, optimizing, and manufacturing enzyme therapeutics for RMT-applied ERT for neuronopathic LSDs.

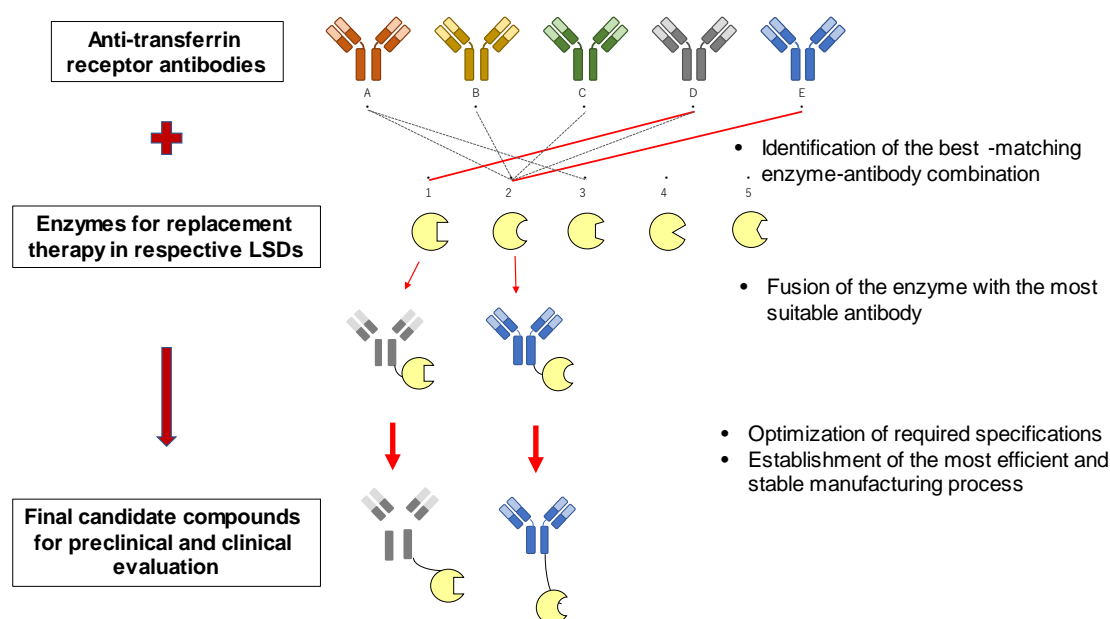


**Figure 2.** Schematic flow of optimization process of biotherapeutic for RMT-applied ERT.

### 2.2.2. Other Known Factors Regulating Transcytosis

Numerous factors are known to affect the transcytosis mechanism [47], with physiochemical factors playing an indispensable role, as seen in TfR-mediated transcytosis, which depends on the pH and polarity of proteins [53]. Temperature [54] and oxygen levels have also been suggested to influence transcytosis, the latter being observed, for instance, in BBB permeability affected by hypoxia [55]. Furthermore, several cytokines have been identified as related to transcytosis via cellular signaling amongst endothelial cells, pericytes, and astrocytes [56]. Muldoon et al. [57] postulated a physiological barrier at the basal lamina of the brain microvasculature distal to the anatomic BBB (tight junction), which limits the distribution of proteins and viral particles with large molecular weights after transvascular delivery to the brain. Although the roles of these factors in relation to transcytosis are far from being fully understood, their potential implications may require attention in optimizing RMT for ERT.

## 3. Preclinical Evaluation of RMT-Applied ERT

A PubMed literature search using enzyme replacement therapy and transcytosis as keywords produced only 10 hits for the past 10 years up to April 2022. Given this limited number of references, this section looks mainly at the preclinical and clinical studies of pabinafusp alfa (JR-141), a recently developed drug for RMT-applied ERT. Pabinafusp alfa is a genetically engineered fusion protein developed by JCR Pharmaceuticals for intravenous ERT for neuronopathic MPS II. It consists of an anti-human TfR (hTfR) antibody and human iduronate-2-sulfatase (IDS) fused to the C terminus of the immunoglobulin G (IgG) heavy chain. Robust preclinical [37,58–61] and clinical [62–65] evidence shows that it exhibits unequivocal dual efficacy against peripheral/somatic and CNS manifestations in patients with genetic IDS deficiency by delivering the enzyme therapeutic via TfR-mediated transcytosis across the BBB (a proprietary technology named J-Brain Cargo<sup>®</sup>). It received regulatory approval in Japan in 2021, spearheading other RMT-applied enzyme therapeutics in development worldwide.

### 3.1. Preclinical Efficacy Evaluation

Preclinical proof of concept of pabinafusp alfa in terms of its dual efficacy was examined stepwise [37]. First, human TfR-mediated cellular incorporation of the drug was shown in cultured human fibroblasts as *in vitro* evidence of its intracellular uptake via TfR-mediated endocytosis. Pabinafusp alfa was then administered intravenously to hTfR

knock-in mice (an animal model of MPS II). While pabinafusp alfa was detected in the brain, naked hIDS was not, thereby providing *in vivo* evidence of delivery of the drug to the brain through the BBB. Finally, to underpin its dual efficacy, the enzyme activity of pabinafusp alfa was substantiated by observed reductions in the accumulation of substrates (i.e., glycosaminoglycans [GAGs]) in both the peripheral tissues and the brains of hTfR-knockin/Ids-knockout mice following intravenous administration of the drug.

Measurement of intracerebral GAG accumulations is the most direct indicator of enzyme activity in the brain, but because such measurement is inimical to clinical drug evaluation in patients, a surrogate efficacy endpoint had to be sought instead that could be used in both the preclinical and clinical investigations [58]. GAG concentrations (particularly those of heparan sulfate [HS]) in the CSF were found to correlate well with intracerebral GAG accumulations in the hTfR-knockin/Ids-knockout mice. An assay method to quantify HS concentrations by liquid chromatography-tandem mass spectrometry was established, which reliably measured HS accumulations in the CSF of the mice and demonstrated correlations between the intracerebral and intra-CSF HS levels. Furthermore, reductions in intracerebral and intra-CSF HS levels following intravenous administration of pabinafusp alfa, which had been observed previously in mouse brains, were replicated by this method in the hTfR-knockin/Ids-knockout mice, constituting preclinical proof of concept of the drug.

To further validate the efficacy of pabinafusp alfa against neurodegeneration, Morimoto et al. [59] demonstrated that the clearance of intracerebral HS accumulations induced by intravenous administration of pabinafusp alfa prevents neurodegeneration and resultant neurocognitive dysfunctions in MPS II mice. The drug reduced HS levels and attenuated histopathological changes in both the brain and peripheral tissues. Moreover, the loss of spatial learning abilities, a manifestation of neurocognitive impairment in MPS II mice, was completely suppressed by pabinafusp alfa, but not by idursulfase, indicating an association between HS deposition in the brain, neurodegeneration, and CNS manifestations. Furthermore, HS concentrations in the brain and their pabinafusp alfa-induced reduction correlated with those in the CSF. Dose-dependent relationships between long-term intravenous treatment with pabinafusp alfa and its effects on the CNS (reductions in HS levels in the brain and CSF, prevention of neuronal damage, and improved neurobehavioural performance) in the model mice [61] corroborates a quantitative dose-dependent relationship between HS reduction in the CNS and neurocognitive improvements in MPS II mice. Taken together, these preclinical findings establish the central efficacy of the drug in both stabilizing and preventing neuronopathy in MPS II.

Arguello et al. [48] have also reported positive results with an IDS transport vehicle (DNL 310) utilizing transferrin receptor-mediated transcytosis in MPS II mice: reduced levels of peripheral and CNS GAGs were noted along with improvements in auricular, skeletal, and neurobehavioural abnormalities, although the dose-response relationship between these effects and DNL 310 have apparently not yet been examined.

These preclinical evaluations have revealed a number of challenges that may be informative for similar future endeavors to establish RMT-applied ERT for neuronopathic LSDs at large. First, in contrast to the ostensibly straightforward pathophysiology common in LSDs (i.e., genetic enzyme deficiency causing accumulation of uncatabolized substrates that leads to systemic dysfunction), the exact neuropathogenesis is complex and remains to be elucidated [26]. Moreover, there is no established optimal method for evaluating novel therapeutics with new mechanisms of action against this complex and severe progressive disease. At the very least, the items listed below should be conceptualized, examined in practice, validated, and included in the evaluation process of novel therapeutics for neuronopathic LSDs. These items also need to be shared and discussed with regulatory agencies to confirm their scientific, medical, and regulatory acceptability and ensure timely regulatory approval.

- Key pathognomonic signs and symptoms to be selected and focused on;
- Clinical efficacy endpoints that correlate well with these signs and symptoms and are considered most likely to respond to treatment;
- Surrogate endpoints that can represent and correlate with these clinical endpoints, and that are also measurable in animal models of the disease;
- Quantitative and qualitative methods to evaluate these endpoints: these methods also need to be conducive to both preclinical and clinical studies.

### 3.2. Preclinical Safety Evaluation

Antibody-based drugs generally have high target specificity [66], as seen in the complement-dependent cytotoxicity (CDC) and antibody-dependent cellular cytotoxicity (ADCC) of biotherapeutics for cancer [67,68]. However, in therapeutic areas outside oncology, cytotoxicity mediated by the antibody would merely compromise the safety of the biotherapeutic and be counterproductive to its expected efficacy. On the other hand, whether the physiological functions of the innate receptors specifically utilized in RMT can be affected by their utilization needs to be evaluated, particularly when the drug is used long-term. Iron and glucose metabolism, for instance, should be examined for its potential untoward influence on ERT via the transferrin and insulin receptors, respectively.

#### 3.2.1. Evaluation of Antibody-Derived Cytotoxicity

A four-week repeat-dose toxicity study of pabinafusp alfa at dosages of up to 30 mg/kg/week was conducted in sexually mature and juvenile monkeys, along with a 26-week repeat-dose study in 2- to 4-year-old monkeys [60]. CDC (an effector function of IgG and IgM) is a cytolytic cascade triggered by binding of the complement C1q to the constant region of cell-bound antibodies, followed by activation of a series of complement proteins [69,70]. CDC was elicited by the anti-hTfR monoclonal antibodies (mAb) used in pabinafusp alfa, but not by the fusion protein as a whole. This is probably because the fusion of the enzyme to the mAb interferes with the access of complement proteins to the antibody moiety via steric hindrance, hence the loss of CDC activity of pabinafusp alfa. ADCC (another effector function of IgG) is involved in the cytotoxicity towards opsonized cells (cells coated with antibodies) of such effector cells in the immune system as natural killer cells [ibid]. Thus, ADCC requires an interaction between the antibody CDR domains and antigens on the target cells (i.e., endothelial cells) along with binding of the antibody Fc domains to the Fc $\gamma$  receptors on the effector cells. Neither the humanized anti-hTfR mAb nor pabinafusp alfa caused ADCC in this toxicology study [60]. The carbohydrate structure of the Fc region is known to be critical for the binding of antibodies to the Fc $\gamma$  receptors of the effector cells [ibid]. As the structure of the anti-TfR mAb moiety in pabinafusp alfa is similar to that of natural IgG1, the binding ability of pabinafusp alfa to the Fc $\gamma$  receptors may be retained at least to some degree. Therefore, the bridge formation between the effector cells and the endothelial cells, an essential step in initiating ADCC, is lacking, thus precluding safety concerns regarding ADCC.

#### 3.2.2. Potential Influence of RMT on the Original Receptor Functions

The receptor-binding property of an antibody-fused therapeutic for RMT-applied ERT may raise concerns about its influence through the antibody-receptor interaction on the original physiological functions of the receptors. Indeed, a clinical trial of AGT-181 (valanafusp alfa),  $\alpha$ -L-iduronidase fused with anti-insulin receptor antibody, found drug-related transient hypoglycemia in 6.4% of the patients with MPS I [71]. However, this finding can be attributed to the insulin agonist activity of the anti-insulin receptor antibody that constitutes AGT-181 [72], and is not necessarily related to the transcytotic effect per se of the compound. In a clinical trial of DNL-310, an enzyme fusion protein that contains a low-affinity transferrin-binding peptide, anemia was detected in two of the five patients with MPS II given DNL-310, although this was not considered to be related to the drug [73].

However, the potential association of DNL-310 with anemia in relation to the transferrin receptors, also expressed in high amounts on erythroblasts, may require further evaluation.

In contrast, preclinical studies of pabinafusp alfa show no interference with the binding of transferrin to its receptors [60]. We consider this to be because the TfR epitope recognized by the anti-TfR antibody in pabinafusp alfa is distinct from the transferrin binding site of the TfR. More importantly, cynomolgus monkeys treated with pabinafusp alfa showed no abnormalities in such iron-related parameters as serum iron, unsaturated iron binding capacity, ferritin, haptoglobin, and total iron binding capacity [ibid]. Thus, pabinafusp alfa has minimal potential to produce any toxicity related to perturbation of the iron metabolism. The clinical trials of pabinafusp alfa so far conducted, as detailed below, have elicited no adverse events associated with the iron metabolism [62–65].

Overall, the likelihood of potential interactions between the antibody in the RMT-applied therapeutic and the targeted receptor seems to differ from one therapeutic to another, and is, perhaps, not dependent on the kind of receptor that mediates transcytosis. Furthermore, preclinically identified interactions may not directly translate into relevant or clinically significant adverse events, while preclinically undetected interactions may very well lead to receptor-associated adverse events. Translating preclinical toxicological findings into clinically meaningful safety endpoints is never easy, but given the debilitating nature of progressive neurodegeneration in neuronopathic LSDs, for which no ERT is available, the potential risks of these events are almost certainly outweighed by the clinical benefits of RMT-applied ERT, provided that adverse events related to RMT, if any, are clinically manageable and do not offset the overall benefits of the treatment.

### 3.2.3. Anti-Drug Antibodies and Resultant Infusion-Associated Reactions

As detailed in Section 4.3.3, repeated enzyme replacement is known to generate anti-drug antibodies that can lead to infusion-associated reactions (IARs) that are detrimental to safety and efficacy. Furthermore, cross-reactive immunological material (CRIM)-negative LSD patients with complete absence of enzyme activity are known to frequently exhibit IARs caused by neutralizing antibodies in particular. While the anti-drug antibodies and enzyme therapeutics can be trafficked together to intracellular lysosomes in which the enzyme can function once the antibody degrades, the neutralizing antibodies inhibit the M6PR-dependent intracellular uptake of the enzyme, significantly reducing drug efficacy. However, this is not the case with fusion proteins such as pabinafusp alfa, which is expected to allow TfR-dependent cellular uptake, as long as no neutralizing antibodies against the antibody CDR domain are generated, even if anti-drug antibodies against the enzyme or neutralizing antibodies against M6PRs are present. Such a mechanism of action involving both TfRs and M6PRs is, therefore, expected to contribute to reducing the risk of neutralizing antibody generation and ensuring better safety and efficacy in long-term ERT.

## 4. Translation and Clinical Establishment of RMT-Applied ERT

### 4.1. RMT-Applied ERT

Table 1 summarizes the clinical development of five therapeutics to which RMT has been applied in order to establish ERT for neuronopathic MPS. AGT-181 and AGT-182 utilize the insulin receptor, while the other three harness RMT via the TfR.

### 4.2. Issues with Extrapolating Preclinical Findings to Humans

The antibodies utilized for enzyme therapeutics in RMT-applied ERT are designed to bind to the innate human receptors on the cerebrovascular endothelial cells. However, preclinical efficacy and safety evaluations of the therapeutics have to be conducted in animal models (mice, rats, and monkeys). Although inter-species differences in the amino acid sequence of the TfR may be relatively small, subtle differences in the epitope of the TfR can have a significant influence on the antibody affinity of the biotherapeutic. Therefore, hTfR-knockin/Ids-knockout mice were required, as they enable comparable and extrapolatable efficacy evaluation. However, as genetic induction in rats and monkeys is

prohibitively difficult, the extrapolability of the preclinical data on these animals depends on the extent to which the antibody affinity of the biotherapeutics to their respective TfRs is reasonably comparable to that in humans. This general issue of scientific appropriateness and regulatory acceptability of extrapolated preclinical data is of particular importance for RMT-applied ERT in terms of pharmacokinetics and pharmacodynamics, as detailed below.

**Table 1.** Clinical trials of the new therapeutics for neuronopathic MPS that utilize receptor-mediated transcytosis.

Disease	Compound	Clinical Phase/Status	Targeted Receptors	Sponsor	Publication	Identifier
MPS I	AGT-181 (valanafusp alpha)	Phase I (completed)	Insulin receptors	ArmaGen	Giugliani et al. [70]	NCT02262338
	JR-171 (lepunafusp alfa)	Phase I (completed)	Transferrin receptors	JCR Pharmaceuticals	Not available	NCT04227600
MPS II	AGT-182	Phase I/II (completed)	Insulin receptors	ArmaGen	Not available	NCT03053089
	Pabinafusp alfa (JR-141)	Phase III (completed) Approved in Japan in 2021	Transferrin receptors	JCR Pharmaceuticals	Okuyama et al. [62,63] Giugliani et al. [65]	NCT03568175
		Phase II/III (completed) Filed for regulatory approval in Brazil in 2021			Giugliani et al. [64]	NCT03359213
		Phase III (recruiting in the US, EU, UK and Brazil)			Not available	NCT04573023
DNL-310	Phase I/II (recruiting)	Transferrin receptors	Denali Therapeutics	Not available	NCT04251026	

#### 4.2.1. Pharmacodynamic Issues

Higher brain functions (e.g., memory, consciousness, emotion, and cognition) and their disorders are notoriously difficult to evaluate in animal experiments and, even if it is possible, further difficulties arise in extrapolating the preclinical data to humans, hence the low clinical success rate for drugs that show tremendous promise in animal experiments intended to model psychiatric pathophysiology [74,75]. As it is all but impossible to comprehensively capture the multifaceted manifestations of neuronopathic LSDs either preclinically or clinically [26], some key features must be selected, taking account of their clinical significance, quantifiability, correlation with treatment response, operational feasibility, and regulatory acceptability. For this purpose, a two-pronged approach to pharmacodynamic evaluation has been taken: (1) measuring GAG levels (in particular HS levels) in the CSF as a representative etiological factor for the subsequent neuropathological cascade of events, and (2) conducting evaluation and analysis of neurocognitive development as one of the most notable clinical correlates in the final stage of the cascade. The latter was done preclinically by using the Morris water maze test for spatial learning assessment [59], and clinically by employing reliable and validated neurodevelopmental batteries for neurocognitive assessment [63–65], in addition to other quantitative and qualitative measures, such as histopathological assessment of the brain for preclinical evaluation, and magnetic resonance imaging of the brain in MPS II patients. These pharmacodynamic evaluations may be applicable to other types of neuronopathic MPS, but they probably need to be modified or supplanted with other disease-specific assessments for individual neuronopathic LSDs, given the marked heterogeneity in their manifestations, clinical courses, outcomes, and severity [11].

In our preclinical studies with mouse disease models, we have often observed markedly aggressive behavior (e.g., fighting) in caged animals (unpublished). Such behavioral findings may be of translational importance, because they may correspond to neurocognitive impairments and associated behavioral features that have been well documented in MPS II patients. Indeed, throughout our clinical trials in Japan and Brazil, many patients exhib-



ited anxiety, excitability, and hyperactivity that often rendered even sitting at a table for meals difficult and family outings impossible. As the trials continued, narrative reports from physicians, caregivers, and family members described markedly improved mood, emotional stability, comprehension, and responsiveness in the patients, some of whom then even managed to stay calm during mealtimes in and outside their homes [62–65,76]. These positive behavioral changes often seem to be preceded by subtle yet important non-verbal aspects such as smiling, which, as an attachment behavior, is regarded as a critical developmental milestone in child development [77]. These behavioral changes may be taken as early favorable signs that foreshadow later, more recognizable CNS function-related responses to treatment. In turn, the aforementioned specific behavioral characteristics observed in the mouse models may be worth further attention, as they might potentially serve as preclinical endpoints for capturing early treatment response.

#### 4.2.2. Pharmacokinetic Issues

In intrathecal and intracerebroventricular administration of enzyme therapeutics for delivery to the brain, the CSF in the subarachnoid space and the ventricles assumes an essential pharmacokinetic role as a medium for drug administration, distribution, and elimination. In allowing the substrate concentrations therein to serve as a critical surrogate efficacy endpoint, as described above, the CSF is also of pharmacodynamic importance. However, RMT-applied ERT differs from ERT via intra-CSF drug administration in terms of the role of the CSF. In the former, the drug is distributed through the systemic blood circulation; RMT then occurs, followed by drug diffusion towards the brain parenchyma. In this process, the CSF works more or less as a reservoir into which a very limited portion of the drug is excreted after being consumed, making the intra-CSF drug concentrations negligibly small. In contrast, drug concentrations in the CSF are naturally very high after intra-CSF drug administration, although smaller quantities of the drugs actually reach the brain parenchyma than in RMT-applied ERT. This is because drugs administered via the CSF must be distributed in retrograde (i.e., cephalad or headward) diffusion against the normal CSF flow to reach the brain parenchyma, so drug penetration from the CSF can be minimal [1,78]. Thus, interpretation of the CSF-related pharmacokinetic parameters must take account of the unique characteristics of the CSF circulation in relation to drug delivery. Here again, the extrapolability of the CSF findings and related pharmacokinetic parameters in experimental animals needs further attention [79].

### 4.3. Clinical Investigation with RMT-Applied ERT for Neuronopathic LSDs

#### 4.3.1. Overall Challenges

The general challenges for clinical trials involving rare diseases include paucity of patients available for trials, limited enrollment capacity/efficiency at investigational sites, limited numbers of investigators/specialists globally, and operational hurdles to conducting multinational multi-site trials. It follows that the oft-employed strategy of increasing the number of participating sites to compensate for the limited number of patients at each one is not as helpful when it comes to clinical trials involving rare diseases as it is in other therapeutic areas. Neuronopathic LSDs present further problems related mostly to their complex and progressive pathology, which renders efficacy evaluation and subsequent determination of therapeutic effects difficult and time-consuming. One counterintuitive challenge is that even though neuronopathic LSDs are rare, they exhibit enormous phenotypic heterogeneity, which partly accounts for their frequently delayed diagnosis and treatment initiation. These factors only further complicate the constraints involved in designing and conducting clinical trials, making the gold standard of clinical trials—A sufficiently powered comparative randomized controlled trial—enormously challenging to conduct in a timely and operationally realistic fashion. Furthermore, when there is no established standard treatment at all for the disease, an untreated comparator arm is not ethically acceptable. In such cases, one sensible option for making informative efficacy comparisons is to compare the treatment group with what is known as a historical control,

which means using clinical data on previous patients with the same disease. It is necessary to ensure, of course, that both datasets are collected using the same, or at least comparable, assessment methods to allow meaningful efficacy analysis [80].

#### 4.3.2. Clinical Efficacy Evaluation

Treatment for neuronopathic LSDs must address both the peripheral/somatic and CNS manifestations, so both of these efficacy endpoints need to be captured quantitatively and qualitatively.

Peripheral efficacy endpoints focus on major somatic signs and symptoms (urinary and plasma concentrations of substrates, hepatosplenomegaly, cardiac and pulmonary functions, 6-minute walk test, and joint motion), while central efficacy evaluation needs to examine some major aspects of the neuronopathy that affect the manifold functions and structures of the CNS. The trials described above (completed or ongoing) have commonly examined substrate levels in the CSF, along with various neuropsychological functions via such established test batteries as the Bayley Scales of Infant and Toddler Development, the Kaufman Assessment Battery for Children, and the Vineland Adaptive Behavior Scales [63–65]. Neuroimaging is also necessary to identify cerebral atrophy, ventricular enlargement, and other discernible structural changes of the brain, and to assess visual and auditory functions.

One fundamental difficulty inherent in neurodevelopmental assessment is that while normal development always takes years, in patients with neuronopathic LSDs, it can proceed without marked disturbance from birth, reach a plateau in early childhood, and then deteriorate afterwards, albeit with marked variability [81]. Therefore, evaluations of the potential effects of RMT-applied ERT on developmental trajectories in patients with notable interindividual differences will invariably require observations over several years. This seriously compromises the mission to develop novel therapeutics expeditiously for patients with deteriorating neuronopathy, although it should also be noted that with short-term observation there is a risk of overlooking treatment efficacy that might have been noted with sufficiently long observation. A sensible compromise between the scientific requirement to establish long-term efficacy and the critical clinical need to expedite the introduction of novel treatments would be to use neurodevelopmental batteries for several years to evaluate neurocognitive efficacy along with surrogate endpoints to buttress positive CNS efficacy signals, and then to seek conditional regulatory approval with the data obtained, which should later be corroborated by long-term developmental and other CNS-related data collected in post-marketing surveys.

#### 4.3.3. Clinical Safety Evaluation

For RMT-applied ERT, two groups of safety endpoints require particular attention: adverse events related to the infusion of biotherapeutics (i.e., IARs) [82], and adverse events related to the effects of the test drugs on the specific innate receptors utilized for RMT. IARs are a set of common adverse drug reactions to monoclonal antibodies, and they involve various symptoms ranging from discomfort, skin and/or mucosal tissue manifestations (e.g., generalized hives, pruritis, and flushing), and gastrointestinal symptoms (nausea and vomiting), to more severe symptoms, such as respiratory compromise (dyspnea, wheezing, and hypoxemia) and hypotension. Serious manifestations, such as anaphylaxis and cytokine release syndrome, are sometimes reported, and these can be fatal if not properly managed. IRAs generally occur on the first day of drug administration, often starting within seconds or minutes of the first exposure. Premedication with antihistamines or corticosteroids, for example, is sometimes given to prevent or ease their occurrence, and slowing the infusion rate can also be effective. However, immunogenicity is a concern in enzyme replacement therapy [83], and various measures have been proposed to mitigate the long-term risk of immunogenicity and to ensure the therapeutic benefit of ERT for patients with LSDs (e.g., prophylactic immune tolerance induction). Such measures are necessary, because IARs affect not only the long-term tolerability and safety profile of the

drug, but also the efficacy of the drug itself, which is why concurrent immunomodulation is sometimes recommended to maximize the efficacy of ERT [84].

The potential adverse events related to the specific receptors utilized for RMT-applied ERT are discussed in Section 3.2.2.

#### 4.3.4. Post-Approval Evaluations

Regulatory approval of RMT-applied ERT for neuronopathic LSDs on the basis of relatively limited efficacy data is necessary to meet the urgent medical needs of affected patients, but this means that long-term efficacy data are of particular importance to consolidate the effects of the drug on the CNS and ensure that the regulatory conditions for its approval are fully met. Furthermore, because neuronopathic LSDs are rare yet heterogeneous as a nosological entity, much about them remains to be elucidated. It is very likely, therefore, that clinical data and observations from both pre- and post-approval studies will shed new light on the pathogenesis, clinical course, and prognosis of the disease by, for instance, differentiating patients with the same diagnosis according to their treatment response, thereby revealing hitherto unknown characteristics of the disease. Information thus obtained will facilitate accurate and timely diagnosis of the disease, which will, in turn, enable early initiation of the most appropriate treatment. The intertwined yet reciprocal relationship between diagnosis and treatment seen in LSDs, whereby a novel treatment helps refine diagnosis and vice versa, is reminiscent of the ancient clinical approach known as *diagnosis ex juvantibus* (attempting to diagnose a disease by treating it) [85].

## 5. Conclusions

This review summarizes some of the trailblazing efforts made to apply RMT to ERT for the treatment of neuronopathic MPSs. After more than 25 years and umpteen attempts to develop biotherapeutics for brain diseases, the possibility of using transcytotic mechanisms to reengineer biologics has been greeted with great excitement [86]. However, as the targeted disease itself and the application of RMT both involve innumerable unclarified issues, these efforts have confronted formidable obstacles. To overcome these, a relentless process of trial and error leading to ingenious ideas for improvement and serendipitous discoveries was required, and the true innovative originality of many of these advances remains unacknowledged. Indeed, some of the preclinical and clinical findings gained in establishing RMT-applied ERT [1] may, when put in a wider context, clear up many of the historical misconceptions about the CSF, the BBB, and the delivery of drugs to the brain [30].

Nevertheless, the efficacy of RMT-applied ERT against CNS symptoms requires long-term evaluation. Furthermore, in addition to its inability to treat neuronopathy, conventional ERT suffers from other notable limitations, such as lack of effect on the cardiac valves, trachea and bronchi, ears, and eyes, due to its limited ability to penetrate these tissues [87]. Notably, respiratory failure, which is the most common cause of death in patients with MPS II [88], is associated with obstructions caused by GAG deposits in the respiratory tract, which neither conventional ERT nor RMT-applied ERT can address sufficiently. Therefore, further research and improvement of ERT is called for. Firstly, it needs to be fortified so that the substance accumulations outside the reach of current ERT can be addressed in order to improve survival outcomes. Secondly, the effects of RMT-applied ERT on neuronopathy in MPS I and II need to be corroborated and established, beyond which it must then be applied to other neuronopathic LSDs. Last, but not least, complex development and provision of RMT-applied ERT can lead to considerable socioeconomic burden on healthcare at large. Hopefully, RMT will enable brain delivery of a wider range of therapeutics for other neurodegenerative diseases, many of which still defy treatment, in a sustainable and approachable manner to the patients and their caregivers.

**Author Contributions:** Conceptualization and methodology: H.S., K.T. (Kenichi Takahashi) and K.T. (Kazunori Tanizawa); investigation and data curation: K.M. and T.Y.; writing (original draft preparation): Y.S.; writing (review and editing): K.M., T.H., S.S. and K.T. (Kenichi Takahashi), T.Y.;

supervision: M.S.; project administration: S.S. All authors have read and agreed to the published version of the manuscript.

**Funding:** This review article received no external funding.

**Institutional Review Board Statement:** This article contains no original data from studies with human participants or animals performed by any of the authors, apart from the data already published and described herein.

**Informed Consent Statement:** Not applicable.

**Data Availability Statement:** Not applicable.

**Acknowledgments:** The contributions of Ryuji Yamamoto, Satoshi Kawashima, Minako Kobayashi, and Haru Ikeda of JCR Pharmaceuticals in preparing the manuscript are duly appreciated. The authors are also grateful to Timothy Minton, Keio University, Tokyo, for his immense editorial help.

**Conflicts of Interest:** All authors are employees of JCR Pharmaceuticals, the patent holder of pabina-fusp alfa and MAA holder of IZCARGO® in Japan.

## References

- Sato, Y.; Minami, K.; Hirato, T.; Tanizawa, K.; Sonoda, H.; Schmidt, M. Drug delivery for neuronopathic lysosomal storage diseases: Evolving roles of the blood brain barrier and cerebrospinal fluid. *Metab. Brain Dis.* **2022**. [CrossRef]
- Wilhelm, I.; Fazakas, C.; Molnar, K.; Vegh, A.G.; Hasko, J.; Krizbai, I.A. Foe or friend? Janus-faces of the neurovascular unit in the formation of brain metastases. *J. Cereb. Blood Flow Metab.* **2018**, *38*, 563–587. [CrossRef]
- Leuthardt, E.C.; Duan, C.; Kim, M.J.; Campian, J.L.; Kim, A.H.; Miller-Thomas, M.M.; Shimony, J.S.; Tran, D.D. Hyperthermic Laser Ablation of Recurrent Glioblastoma Leads to Temporary Disruption of the Peritumoral Blood Brain Barrier. *PLoS ONE* **2016**, *11*, e0148613. [CrossRef]
- Lipsman, N.; Meng, Y.; Bethune, A.J.; Huang, Y.; Lam, B.; Masellis, M.; Herrmann, N.; Heyn, C.; Aubert, I.; Boutet, A.; et al. Blood-brain barrier opening in Alzheimer's disease using MR-guided focused ultrasound. *Nat. Commun.* **2018**, *9*, 2336. [CrossRef]
- Abrahamo, A.; Meng, Y.; Llinas, M.; Huang, Y.; Hamani, C.; Mainprize, T.; Aubert, I.; Heyn, C.; Black, S.E.; Hynynen, K.; et al. First-in-human trial of blood-brain barrier opening in amyotrophic lateral sclerosis using MR-guided focused ultrasound. *Nat. Commun.* **2019**, *10*, 4373. [CrossRef]
- Muenzer, J.; Hendriks, C.J.; Fan, Z.; Vijayaraghavan, S.; Perry, V.; Santra, S.; Solanki, G.A.; Mascelli, M.A.; Pan, L.; Wang, N.; et al. A phase I/II study of intrathecal idursulfase-IT in children with severe mucopolysaccharidosis II. *Genet. Med.* **2016**, *18*, 73–81. [CrossRef]
- Jones, S.A.; Breen, C.; Heap, F.; Rust, S.; de Ruijter, J.; Tump, E.; Marchal, J.P.; Pan, L.; Qiu, Y.; Chung, J.K.; et al. A phase 1/2 study of intrathecal heparan-N-sulfatase in patients with mucopolysaccharidosis IIIA. *Mol. Genet. Metab.* **2016**, *118*, 198–205. [CrossRef]
- Matsuoka, K.; Tamura, T.; Tsuji, D.; Dohzono, Y.; Kitakaze, K.; Ohno, K.; Saito, S.; Sakuraba, H.; Itoh, K. Therapeutic potential of intracerebroventricular replacement of modified human beta-hexosaminidase B for GM2 gangliosidosis. *Mol. Ther.* **2011**, *19*, 1017–1024. [CrossRef]
- Ayloo, S.; Gu, C. Transcytosis at the blood-brain barrier. *Curr. Opin. Neurobiol.* **2019**, *57*, 32–38. [CrossRef]
- Banks, W.A. From blood-brain barrier to blood-brain interface: New opportunities for CNS drug delivery. *Nat. Rev. Drug Discov.* **2016**, *15*, 275–292. [CrossRef]
- Mehta, A.; Winchester, B. *Lysosomal Storage Disorders: A Practical Guide*; Wiley-Blackwell: Chichester, UK, 2012.
- Platt, F.M. Emptying the stores: Lysosomal diseases and therapeutic strategies. *Nat. Rev. Drug Discov.* **2018**, *17*, 133–150. [CrossRef] [PubMed]
- Kelly, J.M.; Bradbury, A.; Martin, D.R.; Byrne, M.E. Emerging therapies for neuropathic lysosomal storage disorders. *Prog. Neurobiol.* **2017**, *152*, 166–180. [CrossRef] [PubMed]
- Solomon, M.; Muro, S. Lysosomal enzyme replacement therapies: Historical development, clinical outcomes, and future perspectives. *Adv. Drug Deliv. Rev.* **2017**, *118*, 109–134. [CrossRef] [PubMed]
- Beck, M. Treatment strategies for lysosomal storage disorders. *Dev. Med. Child Neurol.* **2018**, *60*, 13–18. [CrossRef]
- Giugliani, R.; Vairo, F.; Kubaski, F.; Poswar, F.; Riegel, M.; Baldo, G.; Saute, J.A. Neurological manifestations of lysosomal disorders and emerging therapies targeting the CNS. *Lancet Child Adolesc. Health* **2018**, *2*, 56–68. [CrossRef]
- Begley, D.; Scarpa, M. Central Nervous System Aspects, Neurodegeneration and the Blood-Brain Barrier. In *Lysosomal Storage Disorders: A Practical Guide*; Mehta, A., Winchester, B., Eds.; Wiley-Blackwell: Chichester, UK, 2012; pp. 166–173.
- Scarpa, M.; Orchard, P.J.; Schulz, A.; Dickson, P.I.; Haskins, M.E.; Escolar, M.L.; Giugliani, R. Treatment of brain disease in the mucopolysaccharidoses. *Mol. Genet. Metab.* **2017**, *122S*, 25–34. [CrossRef]
- Schulz, A.; Ajayi, T.; Specchio, N.; de Los Reyes, E.; Gissen, P.; Ballon, D.; Dyke, J.P.; Cahan, H.; Slasor, P.; Jacoby, D.; et al. Study of Intraventricular Cerliponase Alfa for CLN2 Disease. *N. Engl. J. Med.* **2018**, *378*, 1898–1907. [CrossRef]



20. De Los Reyes, E.; Lehwald, L.; Augustine, E.F.; Berry-Kravis, E.; Butler, K.; Cormier, N.; Demarest, S.; Lu, S.; Madden, J.; Olaya, J.; et al. Intracerebroventricular Cerliponase Alfa for Neuronal Ceroid Lipofuscinosis Type 2 Disease: Clinical Practice Considerations From US Clinics. *Pediatr. Neurol.* **2020**, *110*, 64–70. [CrossRef]
21. Seo, J.H.; Kosuga, M.; Hamazaki, T.; Shintaku, H.; Okuyama, T. Impact of intracerebroventricular enzyme replacement therapy in patients with neuronopathic mucopolysaccharidosis type II. *Mol. Ther. Methods Clin. Dev.* **2021**, *21*, 67–75. [CrossRef]
22. Naseri Kouzehgarani, G.; Feldsien, T.; Engelhard, H.H.; Mirakhor, K.K.; Phipps, C.; Nimmrich, V.; Clausznitzer, D.; Lefebvre, D.R. Harnessing cerebrospinal fluid circulation for drug delivery to brain tissues. *Adv. Drug Deliv. Rev.* **2021**, *173*, 20–59. [CrossRef]
23. Abbott, N.J.; Pizzo, M.E.; Preston, J.E.; Janigro, D.; Thorne, R.G. The role of brain barriers in fluid movement in the CNS: Is there a ‘glymphatic’ system? *Acta Neuropathol.* **2018**, *135*, 387–407. [CrossRef]
24. Abdul Razzak, R.; Florence, G.J.; Gunn-Moore, F.J. Approaches to CNS Drug Delivery with a Focus on Transporter-Mediated Transcytosis. *Int. J. Mol. Sci.* **2019**, *20*, 3108. [CrossRef]
25. Pardridge, W.M. Drug and gene targeting to the brain with molecular Trojan horses. *Nat. Rev. Drug Discov.* **2002**, *1*, 131–139. [CrossRef]
26. Sato, Y.; Okuyama, T. Novel Enzyme Replacement Therapies for Neuronopathic Mucopolysaccharidoses. *Int. J. Mol. Sci.* **2020**, *21*, 400. [CrossRef]
27. Terstappen, G.C.; Meyer, A.H.; Bell, R.D.; Zhang, W. Strategies for delivering therapeutics across the blood-brain barrier. *Nat. Rev. Drug Discov.* **2021**, *20*, 362–383. [CrossRef]
28. Pulgar, V.M. Transcytosis to Cross the Blood Brain Barrier, New Advancements and Challenges. *Front. Neurosci.* **2018**, *12*, 1019. [CrossRef]
29. Kouhi, A.; Pachipulusu, V.; Kapenstein, T.; Hu, P.; Epstein, A.L.; Khawli, L.A. Brain Disposition of Antibody-Based Therapeutics: Dogma, Approaches and Perspectives. *Int. J. Mol. Sci.* **2021**, *22*, 6442. [CrossRef]
30. Pardridge, W.M. CSF, blood-brain barrier, and brain drug delivery. *Expert Opin. Drug Deliv.* **2016**, *13*, 963–975. [CrossRef]
31. Boado, R.J.; Zhang, Y.; Zhang, Y.; Pardridge, W.M. Humanization of anti-human insulin receptor antibody for drug targeting across the human blood-brain barrier. *Biotechnol. Bioeng.* **2007**, *96*, 381–391. [CrossRef]
32. Boado, R.J.; Hui, E.K.; Lu, J.Z.; Pardridge, W.M. Drug targeting of erythropoietin across the primate blood-brain barrier with an IgG molecular Trojan horse. *J. Pharmacol. Exp. Ther.* **2010**, *333*, 961–969. [CrossRef]
33. Boado, R.J.; Ka-Wai Hui, E.; Zhiqiang Lu, J.; Pardridge, W.M. Insulin receptor antibody-iduronate 2-sulfatase fusion protein: Pharmacokinetics, anti-drug antibody, and safety pharmacology in Rhesus monkeys. *Biotechnol. Bioeng.* **2014**, *111*, 2317–2325. [CrossRef]
34. Friden, P.M.; Walus, L.R.; Musso, G.F.; Taylor, M.A.; Malfroy, B.; Starzyk, R.M. Anti-transferrin receptor antibody and antibody-drug conjugates cross the blood-brain barrier. *Proc. Natl. Acad. Sci. USA* **1991**, *88*, 4771–4775. [CrossRef]
35. Fu, A.; Hui, E.K.; Lu, J.Z.; Boado, R.J.; Pardridge, W.M. Neuroprotection in stroke in the mouse with intravenous erythropoietin-Trojan horse fusion protein. *Brain Res.* **2011**, *1369*, 203–207. [CrossRef]
36. Bien-Ly, N.; Yu, Y.J.; Bumbaca, D.; Elstrott, J.; Boswell, C.A.; Zhang, Y.; Luk, W.; Lu, Y.; Dennis, M.S.; Weimer, R.M.; et al. Transferrin receptor (TfR) trafficking determines brain uptake of TfR antibody affinity variants. *J. Exp. Med.* **2014**, *211*, 233–244. [CrossRef]
37. Sonoda, H.; Morimoto, H.; Yoden, E.; Koshimura, Y.; Kinoshita, M.; Golovina, G.; Takagi, H.; Yamamoto, R.; Minami, K.; Mizoguchi, A.; et al. A Blood-Brain-Barrier-Penetrating Anti-human Transferrin Receptor Antibody Fusion Protein for Neuronopathic Mucopolysaccharidosis II. *Mol. Ther.* **2018**, *26*, 1366–1374. [CrossRef]
38. Ullman, J.C.; Arguello, A.; Getz, J.A.; Bhalla, A.; Mahon, C.S.; Wang, J.; Giese, T.; Bedard, C.; Kim, D.J.; Blumenfeld, J.R.; et al. Brain delivery and activity of a lysosomal enzyme using a blood-brain barrier transport vehicle in mice. *Sci. Transl. Med.* **2020**, *12*, eaay1163. [CrossRef]
39. May, P.; Woldt, E.; Matz, R.L.; Boucher, P. The LDL receptor-related protein (LRP) family: An old family of proteins with new physiological functions. *Ann. Med.* **2007**, *39*, 219–228. [CrossRef]
40. Demeule, M.; Currie, J.C.; Bertrand, Y.; Che, C.; Nguyen, T.; Regina, A.; Gabathuler, R.; Castaigne, J.P.; Beliveau, R. Involvement of the low-density lipoprotein receptor-related protein in the transcytosis of the brain delivery vector angiopep-2. *J. Neurochem.* **2008**, *106*, 1534–1544. [CrossRef]
41. Kumar, P.; Wu, H.; McBride, J.L.; Jung, K.E.; Kim, M.H.; Davidson, B.L.; Lee, S.K.; Shankar, P.; Manjunath, N. Transvascular delivery of small interfering RNA to the central nervous system. *Nature* **2007**, *448*, 39–43. [CrossRef]
42. Huey, R.; Hawthorne, S.; McCarron, P. The potential use of rabies virus glycoprotein-derived peptides to facilitate drug delivery into the central nervous system: A mini review. *J. Drug Target.* **2017**, *25*, 379–385. [CrossRef]
43. Zuchero, Y.J.; Chen, X.; Bien-Ly, N.; Bumbaca, D.; Tong, R.K.; Gao, X.; Zhang, S.; Hoyte, K.; Luk, W.; Huntley, M.A.; et al. Discovery of Novel Blood-Brain Barrier Targets to Enhance Brain Uptake of Therapeutic Antibodies. *Neuron* **2016**, *89*, 70–82. [CrossRef]
44. Anraku, Y.; Kuwahara, H.; Fukusato, Y.; Mizoguchi, A.; Ishii, T.; Nitta, K.; Matsumoto, Y.; Toh, K.; Miyata, K.; Uchida, S.; et al. Glycaemic control boosts glucosylated nanocarrier crossing the BBB into the brain. *Nat. Commun.* **2017**, *8*, 1001. [CrossRef]
45. Xie, J.; Gonzalez-Carter, D.; Tockary, T.A.; Nakamura, N.; Xue, Y.; Nakakido, M.; Akiba, H.; Dirisala, A.; Liu, X.; Toh, K.; et al. Dual-Sensitive Nanomicelles Enhancing Systemic Delivery of Therapeutically Active Antibodies Specifically into the Brain. *ACS Nano* **2020**, *14*, 6729–6742. [CrossRef]

46. Yamamoto, R.; Kawashima, S. [Pharmacological property, mechanism of action and clinical study results of Pabinafusp Alfa (Genetical Recombination) (IZCARGO((R)) I.V. Infusion 10 mg) as the therapeutic for Mucopolysaccharidosis type-II (Hunter syndrome)]. *Nihon Yakurigaku Zasshi* **2022**, *157*, 62–75. [CrossRef]
47. Tjakra, M.; Wang, Y.; Vania, V.; Hou, Z.; Durkan, C.; Wang, N.; Wang, G. Overview of Crosstalk Between Multiple Factor of Transcytosis in Blood Brain Barrier. *Front. Neurosci.* **2019**, *13*, 1436. [CrossRef]
48. Arguello, A.; Mahon, C.S.; Calvert, M.E.K.; Chan, D.; Dugas, J.C.; Pizzo, M.E.; Thomsen, E.R.; Chau, R.; Damo, L.A.; Duque, J.; et al. Molecular architecture determines brain delivery of a transferrin receptor-targeted lysosomal enzyme. *J. Exp. Med.* **2022**, *219*, e20211057. [CrossRef]
49. Zvonova, E.; Tyurin, A.; Soloviev, A. Strategies for Modulation of Pharmacokinetics of Recombinant Therapeutic Proteins. *Biol. Bull. Rev.* **2018**, *8*, 124–141. [CrossRef]
50. Kuramochi, T.; Igawa, T.; Tsunoda, H.; Hattori, K. Humanization and simultaneous optimization of monoclonal antibody. *Methods Mol. Biol.* **2014**, *1060*, 123–137.
51. Goulatis, L.I.; Shusta, E.V. Protein engineering approaches for regulating blood-brain barrier transcytosis. *Curr. Opin. Struct. Biol.* **2017**, *45*, 109–115. [CrossRef]
52. Pardridge, W.M.; Chou, T. Mathematical Models of Blood-Brain Barrier Transport of Monoclonal Antibodies Targeting the Transferrin Receptor and the Insulin Receptor. *Pharmaceutics* **2021**, *14*, 535. [CrossRef]
53. Sade, H.; Baumgartner, C.; Hugematter, A.; Moessner, E.; Freskgard, P.O.; Niewoehner, J. A human blood-brain barrier transcytosis assay reveals antibody transcytosis influenced by pH-dependent receptor binding. *PLoS ONE* **2014**, *9*, e96340. [CrossRef]
54. Delvendahl, I.; Vyleta, N.P.; von Gersdorff, H.; Hallermann, S. Fast, Temperature-Sensitive and Clathrin-Independent Endocytosis at Central Synapses. *Neuron* **2016**, *90*, 492–498. [CrossRef]
55. Bailey, D.M.; Bain, A.R.; Hoiland, R.L.; Barak, O.F.; Drvis, I.; Hirtz, C.; Lehmann, S.; Marchi, N.; Janigro, D.; MacLeod, D.B.; et al. Hypoxemia increases blood-brain barrier permeability during extreme apnea in humans. *J. Cereb. Blood Flow Metab.* **2022**, *42*, 1120–1135. [CrossRef]
56. Dohgu, S.; Banks, W.A. Brain pericytes increase the lipopolysaccharide-enhanced transcytosis of HIV-1 free virus across the in vitro blood-brain barrier: Evidence for cytokine-mediated pericyte-endothelial cell crosstalk. *Fluids Barriers CNS* **2013**, *10*, 23. [CrossRef]
57. Muldoon, L.L.; Pagel, M.A.; Kroll, R.A.; Roman-Goldstein, S.; Jones, R.S.; Neuwelt, E.A. A physiological barrier distal to the anatomic blood-brain barrier in a model of transvascular delivery. *AJNR Am. J. Neuroradiol.* **1999**, *20*, 217–222.
58. Tanaka, N.; Kida, S.; Kinoshita, M.; Morimoto, H.; Shibasaki, T.; Tachibana, K.; Yamamoto, R. Evaluation of cerebrospinal fluid heparan sulfate as a biomarker of neuropathology in a murine model of mucopolysaccharidosis type II using high-sensitivity LC/MS/MS. *Mol. Genet. Metab.* **2018**, *125*, 53–58. [CrossRef]
59. Morimoto, H.; Kida, S.; Yoden, E.; Kinoshita, M.; Tanaka, N.; Yamamoto, R.; Koshimura, Y.; Takagi, H.; Takahashi, K.; Hirato, T.; et al. Clearance of heparan sulfate in the brain prevents neurodegeneration and neurocognitive impairment in MPS II mice. *Mol. Ther.* **2021**, *29*, 1853–1861. [CrossRef]
60. Yamamoto, R.; Yoden, E.; Tanaka, N.; Kinoshita, M.; Imakiire, A.; Hirato, T.; Minami, K. Nonclinical safety evaluation of pabinafusp alfa, an anti-human transferrin receptor antibody and iduronate-2-sulfatase fusion protein, for the treatment of neuronopathic mucopolysaccharidosis type II. *Mol. Genet. Metab. Rep.* **2021**, *27*, 100758. [CrossRef]
61. Morimoto, H.; Imakiire, A.M.H.; Yamamoto, R.; Hirato, T.; Sonoda, H.; Minami, K. Dose-dependent effects of a brain-penetrating iduronate-2-sulfatase on neurobehavioral impairments in mucopolysaccharidosis II mice. *Mol. Ther.* **2022**, *25*, 534–544. [CrossRef]
62. Okuyama, T.; Eto, Y.; Sakai, N.; Minami, K.; Yamamoto, T.; Sonoda, H.; Yamaoka, M.; Tachibana, K.; Hirato, T.; Sato, Y. Iduronate-2-Sulfatase with Anti-human Transferrin Receptor Antibody for Neuropathic Mucopolysaccharidosis II: A Phase 1/2 Trial. *Mol. Ther.* **2019**, *27*, 456–464. [CrossRef]
63. Okuyama, T.; Eto, Y.; Sakai, N.; Nakamura, K.; Yamamoto, T.; Yamaoka, M.; Ikeda, T.; So, S.; Tanizawa, K.; Sonoda, H.; et al. A Phase 2/3 Trial of Pabinafusp Alfa, IDS Fused with Anti-Human Transferrin Receptor Antibody, Targeting Neurodegeneration in MPS-II. *Mol. Ther.* **2021**, *29*, 671–679. [CrossRef]
64. Giugliani, R.; Martins, A.M.; So, S.; Yamamoto, T.; Yamaoka, M.; Ikeda, T.; Tanizawa, K.; Sonoda, H.; Schmidt, M.; Sato, Y. Iduronate-2-sulfatase fused with anti-hTfR antibody, pabinafusp alfa, for MPS-II: A phase 2 trial in Brazil. *Mol. Ther.* **2021**, *29*, 2378–2386. [CrossRef]
65. Giugliani, R.; Martins, A.M.; Okuyama, T.; Eto, Y.; Sakai, N.; Nakamura, K.; Morimoto, H.; Minami, K.; Yamamoto, T.; Yamaoka, M.; et al. Enzyme Replacement Therapy with Pabinafusp Alfa for Neuronopathic Mucopolysaccharidosis II: An Integrated Analysis of Preclinical and Clinical Data. *Int. J. Mol. Sci.* **2021**, *22*, 10938. [CrossRef]
66. Kesik-Brodacka, M. Progress in biopharmaceutical development. *Biotechnol. Appl. Biochem.* **2018**, *65*, 306–322. [CrossRef]
67. Luria-Perez, R.; Helguera, G.; Rodriguez, J.A. Antibody-mediated targeting of the transferrin receptor in cancer cells. *Bol. Med. Hosp. Infant. Mex.* **2016**, *73*, 372–379.
68. Leoh, L.S.; Daniels-Wells, T.R.; Martinez-Maza, O.; Penichet, M.L. Insights into the effector functions of human IgG3 in the context of an antibody targeting transferrin receptor 1. *Mol. Immunol.* **2015**, *67 Pt B*, 407–415. [CrossRef]
69. Liu, R.; Oldham, R.J.; Teal, E.; Beers, S.A.; Cragg, M.S. Fc-Engineering for Modulated Effector Functions-Improving Antibodies for Cancer Treatment. *Antibodies* **2020**, *9*, 64. [CrossRef]

70. Van der Horst, H.J.; Nijhof, I.S.; Mutis, T.; Chamuleau, M.E.D. Fc-Engineered Antibodies with Enhanced Fc-Effector Function for the Treatment of B-Cell Malignancies. *Cancers* **2020**, *12*, 3041. [CrossRef]
71. Giugliani, R.; Giugliani, L.; de Oliveira Poswar, F.; Donis, K.C.; Corte, A.D.; Schmidt, M.; Boado, R.J.; Nestrasil, I.; Nguyen, C.; Chen, S.; et al. Neurocognitive and somatic stabilization in pediatric patients with severe Mucopolysaccharidosis Type I after 52 weeks of intravenous brain-penetrating insulin receptor antibody-iduronidase fusion protein (valanafusp alpha): An open label phase 1–2 trial. *Orphanet J. Rare Dis.* **2018**, *13*, 110. [CrossRef]
72. Boado, R.J.; Hui, E.K.; Lu, J.Z.; Pardridge, W.M. Glycemic control and chronic dosing of rhesus monkeys with a fusion protein of iduronidase and a monoclonal antibody against the human insulin receptor. *Drug Metab. Dispos.* **2012**, *40*, 2021–2025. [CrossRef]
73. Watts, R.; Ho, C. Interim Data from DNL310 Phase 1/2 Hunter Syndrome Patient Study. Available online: <https://www.denalitherapeutics.com/sites/default/files/2021-09/iMPS%20DNL310%20Webinar%20Final.pdf> (accessed on 15 April 2022).
74. Kaffman, A.; White, J.D.; Wei, L.; Johnson, F.K.; Krystal, J.H. Enhancing the Utility of Preclinical Research in Neuropsychiatry Drug Development. *Methods Mol. Biol.* **2019**, *2011*, 3–22.
75. Schulz, P. Opportunities and challenges in psychopharmacology. *Dialogues Clin. Neurosci.* **2019**, *21*, 119–130. [CrossRef] [PubMed]
76. Daher, A.S.; Martins, A.M. New hope for an old battle: Fighting Hunter disease. *J. Paediatr. Child Health* **2022**, *58*, 360. [CrossRef]
77. Bowlby, J. *Attachment*, 2nd ed.; Basic Books: New York, NY, USA, 1969.
78. Pardridge, W.M. Drug transport in brain via the cerebrospinal fluid. *Fluids Barriers CNS* **2011**, *8*, 7. [CrossRef] [PubMed]
79. Chang, H.Y.; Wu, S.; Chowdhury, E.A.; Shah, D.K. Towards a translational physiologically-based pharmacokinetic (PBPK) model for receptor-mediated transcytosis of anti-transferrin receptor monoclonal antibodies in the central nervous system. *J. Pharmacokinet. Pharmacodyn.* **2022**, *49*, 337–362. [CrossRef] [PubMed]
80. Ghadessi, M.; Tang, R.; Zhou, J.; Liu, R.; Wang, C.; Toyozumi, K.; Mei, C.; Zhang, L.; Deng, C.Q.; Beckman, R.A. A roadmap to using historical controls in clinical trials—by Drug Information Association Adaptive Design Scientific Working Group (DIA-ADSWG). *Orphanet J. Rare Dis.* **2020**, *15*, 69. [CrossRef]
81. Shapiro, E.G.; Eisengart, J.B. The natural history of neurocognition in MPS disorders: A review. *Mol. Genet. Metab.* **2021**, *133*, 8–34. [CrossRef]
82. Doessegger, L.; Banholzer, M.L. Clinical development methodology for infusion-related reactions with monoclonal antibodies. *Clin. Transl. Immunol.* **2015**, *4*, e39. [CrossRef]
83. Kishnani, P.S.; Dickson, P.I.; Muldowney, L.; Lee, J.J.; Rosenberg, A.; Abichandani, R.; Bluestone, J.A.; Burton, B.K.; Dewey, M.; Freitas, A.; et al. Immune response to enzyme replacement therapies in lysosomal storage diseases and the role of immune tolerance induction. *Mol. Genet. Metab.* **2016**, *117*, 66–83. [CrossRef]
84. Broomfield, A.; Jones, S.A.; Hughes, S.M.; Bigger, B.W. The impact of the immune system on the safety and efficiency of enzyme replacement therapy in lysosomal storage disorders. *J. Inherit. Metab. Dis.* **2016**, *39*, 499–512. [CrossRef]
85. Laragh, J.H.; Lampion, B.; Sealey, J.; Alderman, M.H. Diagnosis ex juvantibus. Individual response patterns to drugs reveal hypertension mechanisms and simplify treatment. *Hypertension* **1988**, *12*, 223–226. [CrossRef] [PubMed]
86. Pardridge, W.M. Delivery of Biologics Across the Blood-Brain Barrier with Molecular Trojan Horse Technology. *Biodrugs* **2017**, *31*, 503–519. [CrossRef] [PubMed]
87. Parini, R.; Deodato, F. Intravenous Enzyme Replacement Therapy in Mucopolysaccharidoses: Clinical Effectiveness and Limitations. *Int. J. Mol. Sci.* **2020**, *21*, 2975. [CrossRef] [PubMed]
88. Burton, B.K.; Jegu, V.; Mikl, J.; Jones, S.A. Survival in idursulfase-treated and untreated patients with mucopolysaccharidosis type II: Data from the Hunter Outcome Survey (HOS). *J. Inherit. Metab. Dis.* **2017**, *40*, 867–874. [CrossRef] [PubMed]

## Article

# Efficacy and Safety of a Brain-Penetrant Biologic TNF- $\alpha$ Inhibitor in Aged APP/PS1 Mice

Weijun Ou <sup>1</sup>, Yuu Ohno <sup>2</sup>, Joshua Yang <sup>1,2</sup>, Devaraj V. Chandrashekar <sup>1</sup>, Tamara Abdullah <sup>1</sup>, Jiahong Sun <sup>1</sup>, Riley Murphy <sup>3</sup>, Chuli Roules <sup>1</sup>, Nataraj Jagadeesan <sup>1</sup> , David H. Cribbs <sup>4</sup> and Rachita K. Sumbria <sup>1,5,\*</sup> 

<sup>1</sup> Department of Biomedical and Pharmaceutical Sciences, School of Pharmacy, Chapman University, Irvine, CA 92618, USA

<sup>2</sup> Henry E. Riggs School of Applied Life Sciences, Keck Graduate Institute, 535 Watson Dr, Claremont, CA 91711, USA

<sup>3</sup> Crean College of Health and Behavioral Sciences, Chapman University, Irvine, CA 92618, USA

<sup>4</sup> MIND Institute, University of California, Irvine, CA 92697, USA

<sup>5</sup> Department of Neurology, University of California, Irvine, CA 92868, USA

\* Correspondence: sumbria@chapman.edu

**Abstract:** Tumor necrosis factor alpha (TNF- $\alpha$ ) plays a vital role in Alzheimer's disease (AD) pathology, and TNF- $\alpha$  inhibitors (TNFIs) modulate AD pathology. We fused the TNF- $\alpha$  receptor (TNFR), a biologic TNFI that sequesters TNF- $\alpha$ , to a transferrin receptor antibody (TfRMAB) to deliver the TNFI into the brain across the blood–brain barrier (BBB). TfRMAB-TNFR was protective in 6-month-old transgenic APP/PS1 mice in our previous work. However, the effects and safety following delayed chronic TfRMAB-TNFR treatment are unknown. Herein, we initiated the treatment when the male APP/PS1 mice were 10.7 months old (delayed treatment). Mice were injected intraperitoneally with saline, TfRMAB-TNFR, etanercept (non-BBB-penetrating TNFI), or TfRMAB for ten weeks. Biologic TNFIs did not alter hematology indices or tissue iron homeostasis; however, TfRMAB altered hematology indices, increased splenic iron transporter expression, and increased spleen and liver iron. TfRMAB-TNFR and etanercept reduced brain insoluble-amyloid beta (A $\beta$ ) 1-42, soluble-oligomeric A $\beta$ , and microgliosis; however, only TfRMAB-TNFR reduced A $\beta$  peptides, Thioflavin-S-positive A $\beta$  plaques, and insoluble-oligomeric A $\beta$  and increased plaque-associated phagocytic microglia. Accordingly, TfRMAB-TNFR improved spatial reference memory and increased BBB-tight junction protein expression, whereas etanercept did not. Overall, despite delayed treatment, TfRMAB-TNFR resulted in a better therapeutic response than etanercept without any TfRMAB-related hematology- or iron-dysregulation in aged APP/PS1 mice.

**Keywords:** Alzheimer's disease; transferrin receptor; TNF- $\alpha$  inhibitor; blood–brain barrier; molecular Trojan horse

**Citation:** Ou, W.; Ohno, Y.; Yang, J.; Chandrashekar, D.V.; Abdullah, T.; Sun, J.; Murphy, R.; Roules, C.; Jagadeesan, N.; Cribbs, D.H.; et al. Efficacy and Safety of a Brain-Penetrant Biologic TNF- $\alpha$  Inhibitor in Aged APP/PS1 Mice. *Pharmaceutics* **2022**, *14*, 2200. <https://doi.org/10.3390/pharmaceutics14102200>

Academic Editors: Paul Chi Lui Ho and Salvatore Cisternino

Received: 22 June 2022

Accepted: 10 October 2022

Published: 16 October 2022

**Publisher's Note:** MDPI stays neutral with regard to jurisdictional claims in published maps and institutional affiliations.



**Copyright:** © 2022 by the authors. Licensee MDPI, Basel, Switzerland. This article is an open access article distributed under the terms and conditions of the Creative Commons Attribution (CC BY) license (<https://creativecommons.org/licenses/by/4.0/>).

## 1. Introduction

Alzheimer's disease (AD) is a chronic and progressive neurodegenerative disease characterized by extracellular amyloid-beta (A $\beta$ ) plaques and intraneuronal neurofibrillary tangles [1]. Besides A $\beta$  and tau tangles, mounting evidence suggests a central role of neuroinflammation in AD pathogenesis [2]. Neuroinflammation is an inflammatory response to a pathological stimulus in the brain orchestrated by the cerebral immune cells, primarily the microglia [2]. In the AD brain, A $\beta$  aggregates trigger microglial activation, which results in the release of pro-inflammatory cytokines, including tumor necrosis factor alpha (TNF- $\alpha$ ) [2,3]. Accordingly, elevated serum levels of TNF- $\alpha$  in AD patients correlate with increased physical and cognitive impairment [4,5], and TNF- $\alpha$  is widely studied as a target for AD treatment [6]. Further, a genome-wide association study demonstrated that TNF- $\alpha$  polymorphisms that are associated with inflammatory diseases and elevated TNF- $\alpha$  levels are linked with late-onset AD [7].



Several biologic TNF- $\alpha$  inhibitors have been approved for autoimmune conditions and have been tested on AD rodent models and in humans. To achieve TNF- $\alpha$  inhibition within the AD brain, biologic TNF- $\alpha$  inhibitors are administered via different routes or at high doses to bypass the blood–brain barrier (BBB) due to their limited BBB penetration [6]. For example, infliximab, a bivalent IgG monoclonal antibody acting as a competitive inhibitor to TNF- $\alpha$ , reduced A $\beta$  and tau pathology [8] and improved visual recognition memory [9] upon intracerebroventricular injection in transgenic mouse models of AD. A woman AD patient experienced rapid cognitive improvement upon intrathecal administration of infliximab [10]. Similarly, etanercept, a fusion protein consisting of the fragment crystallizable (Fc) region of human IgG1 and the extracellular ligand-binding domain of the type-II human TNF- $\alpha$  receptor (TNFR2), improved clinical measures in AD patients when given by the perispinal route [11]. High-dose (30 mg/kg) peripheral (subcutaneous) etanercept administration reduced A $\beta$ -associated pathology in a non-transgenic mouse model of A $\beta$ -induced cognitive deficit [12]. However, a double-blinded phase 2 trial showed no clinical benefit of peripheral (subcutaneous) etanercept administration in AD patients [13].

To bypass the BBB and enter the brain parenchyma, the biologic TNF- $\alpha$  inhibitor of choice can be fused to a monoclonal antibody against the mouse transferrin receptor (TfRMAb); the latter undergoes receptor-mediated transcytosis from the blood into the brain across the BBB [14]. A fusion protein of TfRMAb and the extracellular domain of human TNFR2 (TNFR), a TNF- $\alpha$  inhibitor, was engineered [14]. The TfRMAb-TNFR fusion protein enters the mouse brain following intravenous, subcutaneous, and intraperitoneal administration owing to the TfRMAb domain, and the TNFR domain of the fusion protein binds to TNF- $\alpha$  to block downstream TNF- $\alpha$  signaling [15]. The TfRMAb-TNFR fusion protein enters the brain with an uptake of ~3% injected dose/gram brain post intravenous injection; in contrast, the brain uptake of the OX26 monoclonal antibody that does not recognize the mouse TfR is negligible in mice [16]. TfRMAb-TNFR is, therefore, a brain-penetrant biologic TNF- $\alpha$  inhibitor that rapidly enters the brain via the transvascular route without the need for invasive administration or high doses [14,15].

Our previous work with the TfRMAb-TNFR in six-month-old mutant APP/PS1 male mice showed better therapeutic indices for the TfRMAb-TNFR fusion protein in comparison to the non-BBB penetrating etanercept [17]. There was a significant reduction in brain A $\beta$  burden, intercellular adhesion molecule-1 (neuroinflammatory marker), brain parenchymal IgG (BBB damage marker), and recognition memory deficits in the adult APP/PS1 mice treated with the TfRMAb-TNFR [17]. Further, TfRMAb-TNFR fusion protein treatment resulted in low antidrug-antibody formation, which was comparable to etanercept after twelve weeks of chronic dosing, with no signs of an immune response or cerebral microhemorrhage development [17]. Furthermore, the antidrug-antibodies formed against TfRMAb-TNFR are expected to be non-neutralizing as no changes in TfRMAb-TNFR plasma concentrations or clearance were observed following chronic dosing [18]. However, the effect of initiating TfRMAb-TNFR treatment in older APP/PS1 mice when the AD pathology is full-blown, and its safety profile following chronic administration in comparison to TfRMAb alone, have not been studied and were the focus of the current investigation. The former is important given that AD is a progressive neurodegenerative disease that advances with age [1], and the latter is crucial due to the reported hematology- and iron-related dysregulation with chronic TfRMAb dosing [19] and because TfRMAb-based fusion proteins have now advanced to humans [20]. Therefore, in the current study, we used older 10.7-month-old APP/PS1 male mice (instead of the 6-month-old male APP/PS1 mice used in our prior work [17]) to mimic a delayed-treatment regimen and evaluated the effect of the TfRMAb-TNFR on spatial reference memory, A $\beta$  load, and microgliosis following ten weeks of treatment. Further, the effect of chronic TfRMAb-TNFR dosing on hematology indices, iron transporter expression, and tissue iron levels was studied in comparison with TfRMAb.

## 2. Materials and Methods

### 2.1. Fusion Protein

Recombinant TfRMAB-TNFR was produced via transient expression in Chinese hamster ovary (CHO)-K1 cells, sequentially purified by protein A and size exclusion chromatography (WuXi Biologics, Cranbury, NJ, USA), and verified by immunoblot as described previously [17,18]. The affinity of TfRMAB-TNFR to the mouse TfR and human TNF- $\alpha$  was confirmed by enzyme-linked immunoassays (ELISAs) [18]. Both the TfRMAB-TNFR fusion protein and etanercept (International Laboratory USA, San Francisco, CA, USA) were formulated in 100 mM glycine, 150 mM NaCl, 28 mM Tris, and 0.01% Polysorbate 80, pH = 6.4, sterile filtered, and stored at  $-80^{\circ}\text{C}$  until use. The chimeric TfRMAB (Genscript, Piscataway, NJ, USA) was produced via transient expression in ExpiCHO cells, sequentially purified by a protein G column and size exclusion chromatography, and verified by immunoblot, high performance liquid chromatography, and for endotoxin [19]. TfRMAB was formulated in 10 mM sodium acetate, 150 mM NaCl, and 0.01% polysorbate 80, pH = 6, sterile filtered, and stored at  $-80^{\circ}\text{C}$  until use, as previously described [19].

### 2.2. Chronic Dosing in a Mouse Model of Human Amyloidosis

Animal studies were performed on the 10.7-months-old hemizygous (APP<sup>swe</sup>, PSEN1<sup>dE9</sup>) APP/PS1 male mice (Jackson Laboratories, Bar Harbor, ME, USA) in compliance with University Laboratory Animal Resources under protocols approved by the University of California, Irvine, Institutional Animal Care, and Use Committee. All the mice were housed in standard cages under 12 h light/12 h dark cycles, with constant free access to food and water, and divided into the following four groups: APP/PS1-Saline (treated with saline;  $n = 20$ ), APP/PS1-TfRMAB-TNFR (treated with 3 mg/kg TfRMAB-TNFR;  $n = 10$ ), APP/PS1-Etanercept (treated with 1.5 mg/kg etanercept;  $n = 10$ ) and APP/PS1-TfRMAB (treated with 2.25 mg/kg TfRMAB;  $n = 5$ ). The doses were based on the amino acid sequence of TfRMAB-TNFR, which is 25% TNFR and 75% TfRMAB [14,16]. Etanercept is 50% TNFR based on its amino acid sequence [21]. Mice were injected intraperitoneally (IP) with the respective agents three days per week for ten weeks. All injected mice were carefully observed to check for any abnormal response to the treatment (general appearance, spontaneous locomotion, posture, and breathing) after each injection, and their body weights were monitored weekly [19]. After ten weeks of treatment, locomotion and spatial reference memory were assessed using the open-field and Y-maze tests, respectively. Terminal blood was collected at 11 weeks, and a subset of blood samples per group was shipped out on ice for a complete blood count (Molecular Diagnostic Services, Inc., San Diego, CA, USA), after which mice were euthanized with Euthasol (150 mg/kg, IP) and perfused with cold phosphate-buffered saline (PBS). After mice were sacrificed (the age of mice at sacrifice was 13 months), brains were excised, the right hemi-brains were immediately fixed in 4% paraformaldehyde for immunostaining, and the left hemi-brains were frozen in dry ice for ELISA and Western blotting.

### 2.3. Open-Field Testing

The open-field test was performed after ten weeks of treatment, as described previously, using a square-shaped white open-field box (72 cm  $\times$  72 cm with 36 cm walls) with a center square (36 cm  $\times$  36 cm) to measure locomotion and exploration [18]. Briefly, each mouse was gently placed in the white open-field box, and their movements were recorded for 5 min. Resting time, mean speed, and distance traveled were measured by the SMART Video Tracking Software (Panlab, Harvard Apparatus, Holliston, MA, USA) [18].

### 2.4. Modified Y-Maze

The modified Y-maze was used to evaluate the spatial reference memory in aged APP/PS1 mice [18]. The Y-maze apparatus consisting of three radial 30 cm arms (start arm, novel arm, and familiar arm), was placed at the ground level. During the training phase, mice were placed in the start arm to face the center of the maze and allowed to locate and

explore only the start and familiar arms for 8 min, while a removable door blocked the novel arm. After a 30 min interval, the door blocking the novel arm was removed, and the mice were placed into the start arm again and allowed to explore the three arms for an additional 8 min during the testing phase. Mice that did not explore the familiar arm during the training phase or did not leave the start arm during the training or testing phase were excluded from the analysis. Time and distance in the novel arm, latency to the novel arm, and percentage of mice selecting the novel arm as the first arm choice were measured using the SMART Video Tracking Software (Panlab, Harvard Apparatus, Holliston, MA, USA).

### 2.5. Brain Tissue Cryosection

The right hemi-brain of each mouse was fixed with 4% paraformaldehyde in PBS for 24 h, then serially cryoprotected in 10%, 20%, and 30% sucrose solution at 4 °C for 24 h each, followed by freezing at −80 °C. The frozen hemi-brains were mounted using the Tissue-Tek optimal-cutting temperature compound (Fisher Scientific, Waltham, MA, USA) and cut into 20 µm sagittal sections using a freezing cryostat (Micron Instruments, Simi Valley, CA, USA). Three sections (600 µm apart) per mouse were used for immunostaining as described below.

### 2.6. A $\beta$ Detection

Alexa Fluor 488-conjugated 6E10 monoclonal antibody (BioLegend, San Diego, CA, USA) and Thioflavin-S (Thio-S) (Sigma-Aldrich, St. Louis, MO, USA) staining were used to stain A $\beta$  peptides and senile plaques, respectively, as described previously [17]. For A $\beta$  immunofluorescence, free-floating brain sections were washed in PBS for 5 min and blocked with 0.5% bovine serum albumin (BSA) in PBS containing 0.3% TritonX-100 for 1 h at room temperature (RT), then stained for A $\beta$  peptides with 1 µg/mL of Alexa Fluor 488-conjugated 6E10 monoclonal antibody overnight at 4 °C after epitope exposure using 70% formic acid for 10 min at RT. Thio-S staining was performed with 1% Thio-S solution in 80% ethanol for 15 min on mounted sections which had been sequentially washed with 70% and 80% ethanol for 1 min thrice. Slides were then sealed with the Vectamount aqueous mounting media (Vector Laboratories, Newark, CA, USA) and stored at 4 °C until imaging. The Thio-S- or 6E10-stained brain tissue sections were imaged using a BZ-X710 Keyence fluorescence microscope (Keyence, Itasca, IL, USA) under a 2 × objective to capture the entire brain tissue section in one image, and digitized images were analyzed using the NIH ImageJ software (version 1.53e), National Institutes of Health, Bethesda, MD, USA (<https://imagej.nih.gov/ij>) as published previously [22].

### 2.7. Microglial Immunostaining

Free-floating sagittal brain sections from each mouse were washed three times in PBS for 5 min, followed by antigen retrieval in 10 mM sodium citrate buffer (10 mM sodium citrate, 0.05% Tween 20, pH 6.0) at 90 °C for 15 min. Brain sections were washed twice in distilled water for 5 min and blocked with 0.5% BSA in PBS containing 0.3% Triton X-100 for 60 min at RT. The tissue sections were incubated with a primary antibody solution consisting of both 15 µg/mL anti-mouse A $\alpha$ 1 polyclonal goat antibody (R&D system, Minneapolis, MN, USA) and 0.5 µg/mL anti-ionized calcium binding adaptor molecule 1 (Iba1) polyclonal rabbit antibody (Wako, Richmond, VA, USA) in PBS containing 0.3% Triton X-100 and 0.5% BSA overnight at 4 °C. The tissue sections were washed three times in PBS for 5 min and incubated in the dark with a secondary antibody solution consisting of both 0.2% Alexa fluor 594 donkey anti-goat IgG (Thermo Fisher Scientific, Waltham, MA, USA) and 0.1% Alexa fluor 488 donkey anti-rabbit IgG (BioLegend; San Diego, CA, USA) in PBS containing 0.3% Triton X-100 and 0.5% BSA for 2 h at RT. The sections were then washed three times in PBS for 10 min and rinsed in distilled water. The sections were mounted onto glass slides, coverslipped with Vectamount aqueous mounting media (Vector Laboratories, Newark, CA, USA), and sealed with nail polish. Slides were stored at 4 °C until imaging.

### 2.8. *Axl* and *Iba1* Quantification

Microgliosis was assessed using the *Iba1* immunostaining, and phagocytic microglia were identified by immunostaining for *Axl*, a phagocytic receptor expressed on microglial cells [23,24]. For *Axl* and *Iba1* double-label immunostaining, three distinct brain sections were selected for analysis for each mouse from the experimental groups except for the saline-treated APP/PS1 mice, from which a random subset of saline mice was used for the analysis. For each brain section, two regions in the cerebral cortex and one region in the hippocampus were imaged using a Nikon Ti-E Confocal Microscope (Nikon Instruments Inc., Melville, NY, USA) at a 40× magnification. Mature A $\beta$  plaques were detected by the autofluorescence generated by the  $\beta$ -sheet-rich structures in A $\beta$  plaques under ultraviolet (UV) light (405 nm) [25]. *Iba1* was visualized using the blue laser (green), *Axl* was visualized using the green laser (red), and the A $\beta$  plaques were visualized under UV light (blue). The digitized images were analyzed using NIH ImageJ (version 1.53e, Bethesda, MD, USA) using a threshold setting to calculate tissue area positive for *Axl*, *Iba1*, or A $\beta$  plaques [18]. For microgliosis, total and plaque-associated microglia were quantified. To determine plaque-associated microgliosis, only microglia associated with plaques were outlined and included in the analysis. For this, immunofluorescent images were converted to the RGB format, and the threshold values of images were manually calibrated to eliminate background noise [18]. After adjusting the threshold, the “analyze” function was used to report the tissue area positive for *Axl*, *Iba1*, or A $\beta$  plaques. To determine the microglial association with A $\beta$  plaques, the plaque-associated *Iba1*-positive area was normalized to the plaque area and total *Iba1* area to yield the plaque-associated microglia ratio. Similarly, to determine the phagocytic phenotype of the microglia associated with the A $\beta$  plaques, the area of the *Axl*-positive microglia was normalized to the plaque area and the *Iba1* area to yield the plaque-associated *Axl* ratio. Three investigators blinded to the experimental groups performed all the ImageJ analyses.

### 2.9. Quantification of A $\beta$ (1-42) and Oligomeric A $\beta$ by ELISA

The left hemi-brain cerebrum (without the cerebellum) was used for the A $\beta$  (1-42) and high-molecular-weight oligomeric A $\beta$  ELISA. Briefly, pulverized cerebrums were homogenized in 10 volumes of homogenization buffer (50 mM Tris-HCl, pH 7.6, 150 mM NaCl, 1 tablet/10 mL of Roche complete ethylenediaminetetraacetic acid (EDTA)-free Mini protease inhibitor, 5 mM EDTA, 2 mM 1,10-phenanthroline; tris-buffered saline (TBS) buffer) and centrifuged at 100,000× *g* for 1 h at 4 °C. The supernatant (TBS-soluble fraction) was used to measure soluble high-molecular-weight oligomeric A $\beta$  (>30 kDa). The pellet was further homogenized in 10 volumes of homogenization buffer (5 M guanidine HCl (Gu-HCl), 0.05 M Tris, pH = 8.0) and rotated for 3 h at RT. The homogenate was centrifuged at 20,800× *g* for 15 min at RT, and the supernatant (Gu-HCl-soluble fraction) was used to measure insoluble A $\beta$  (1-42) and insoluble high-molecular-weight oligomeric A $\beta$  (>30 kDa) species. Protein assay was performed by bicinchoninic acid kit (Pierce Chemical Co., Rockford, IL, USA), and immunoreactive human A $\beta$  (1-42) and oligomeric A $\beta$  were measured using the A $\beta$  (1-42) human ELISA Kit (Thermo Fisher Scientific, Waltham, MA, USA) and the high-molecular-weight oligomeric A $\beta$  ELISA kit (Wako, Richmond, VA, USA), respectively.

### 2.10. Western Blot Analysis

Protein was extracted from the brain, spleen, and liver using the Radio-Immunoprecipitation Assay (RIPA) buffer or TBS with Pierce Protease Inhibitor (Thermo Fisher Scientific, Waltham, MA, USA) as previously described [19]. Briefly, a subset of the pulverized brains was homogenized in 10 volumes of RIPA (25 mM Tris-HCl, pH 7.6, 150 mM NaCl, 1% NP-40, 1% sodium deoxycholate, 0.1% SDS with 5 mM EDTA) or TBS and centrifuged at 20,800× *g* for 20 min at 4 °C. The supernatants were processed with 4× Laemmli buffer (Bio-Rad, Hercules, CA, USA) with 10% beta-mercaptoethanol by boiling for 10 min. Protein samples (30–50  $\mu$ g) were separated on 4–20% sodium dodecyl sulfate (SDS) ready precast

gels (Bio-Rad, Hercules, CA, USA) and transferred to Polyvinylidene fluoride (PVDF) membranes (Bio-Rad, Hercules, CA, USA). Membranes were probed at 4 °C overnight with anti-mouse zonula occludens-1 (ZO-1) rabbit polyclonal antibody (1:1000 in 3% milk, Thermo Fisher Scientific, Waltham, MA, USA), anti-human amyloid precursor protein (APP) mouse monoclonal antibody (1:1000 in 3% milk, BioLegend, San Diego, CA, USA), anti-claudin-5 mouse monoclonal antibody (1:1000 in 3% milk, Santa Cruz Biotechnology, Dallas, TX, USA), anti- $\beta$ -site APP cleaving enzyme 1 (BACE1) rabbit polyclonal antibody (1:1000 in 3% milk, Thermo Fisher Scientific, Waltham, MA, USA), anti-I $\kappa$ B $\alpha$  mouse monoclonal antibody (1:1000 in 3% milk, Cell Signaling Technology, Danvers, MA, USA), anti-TfR-1 mouse monoclonal antibody (1:1000 in 3% milk, Thermo Fisher Scientific, Waltham, MA, USA), anti-TfR-2 mouse monoclonal antibody (1:1000 in 3% milk, Thermo Fisher Scientific, Waltham, MA, USA) and anti-ferroportin rabbit polyclonal antibody (1:1000 in 3% milk, Novus Biologicals, Centennial, CO, USA). Membranes were probed with anti-mouse IgG kappa, horseradish peroxidase (HRP)-linked antibody (Santa Cruz Biotechnology, Dallas, TX, USA) or anti-rabbit IgG, HRP-linked antibody (Cell Signaling Technology, Danvers, MA, USA) for 1 h at RT. Finally, membranes were probed with an anti- $\beta$ -actin antibody (Santa Cruz Biotechnology, Dallas, TX, USA) as a loading control. Chemiluminescence was detected using the Azure C500 gel imager (Azure Biosystems, Dublin, CA, USA), and NIH ImageJ (version 1.53e, Bethesda, MD, USA) was used to quantify the intensity of Western blot bands. All the values were normalized to APP/PS1-Saline mice.

#### 2.11. Tissue Iron Measurements

For all the mice, a part of the left hemi-brain, spleen, and liver was processed to determine tissue iron levels using the Agilent 8900 triple quadrupole Inductively Coupled Plasma Mass Spectrometer (ICP-MS; Agilent, Lomita, CA, USA), as described previously, at the Pomona College Environmental Analysis Laboratories [19]. Briefly, tissue samples were digested in 67% nitric acid overnight at RT, followed by digestion using 30% hydrogen peroxide for 1 h at 90 °C before running the samples using the ICP-MS.

#### 2.12. Statistical Analysis

Data are represented as mean  $\pm$  standard deviation (SD), and all statistical analysis was performed using GraphPad Prism 9 (GraphPad Software Inc., San Diego, CA, USA). Outliers were identified using the Grubb's test, and the normality of numerical variables was assessed using the Kolmogorov–Smirnov test. One-way analysis of variance (ANOVA) with Holm Sidak's post hoc test was used to compare normal numerical data. The % of mice selecting the novel arm (nominal data) was analyzed using the Fisher's exact test, and the Pearson correlation was used for correlation analysis. A two-tailed  $p < 0.05$  was considered statistically significant.

### 3. Results

#### 3.1. Chronic TfRMAb-TNFR Dosing Reduced A $\beta$ Load in Aged APP/PS1 Mice

Chronic TfRMAb-TNFR treatment significantly reduced cortical 6E10-positive A $\beta$  area ( $p < 0.05$ ; Figure 1a,e) and 6E10-positive puncta number ( $p < 0.05$ ; Figure 1b,e) compared to the saline-treated mice. TfRMAb-TNFR treatment also significantly reduced hippocampal 6E10-positive A $\beta$  area ( $p < 0.01$ ; Figure 1c,e) and 6E10-positive puncta number ( $p < 0.01$ ; Figure 1d,e) compared to the saline-treated mice. Etanercept or TfRMAb treatment did not reduce the 6E10-positive A $\beta$  load in the aged APP/PS1 mice compared to the saline-treated mice. Etanercept-treated mice had significantly higher cortical 6E10-positive A $\beta$  area ( $p < 0.01$ ; Figure 1a,e) and 6E10-positive puncta number ( $p < 0.05$ ; Figure 1b,e) compared to the TfRMAb-TNFR-treated mice. The hippocampal 6E10-positive puncta number ( $p < 0.05$ ; Figure 1d,e) was significantly higher in the etanercept-treated mice compared to the TfRMAb-TNFR-treated mice and a similar trend was observed for the hippocampal 6E10-positive area ( $p = 0.054$ ; Figure 1c,e).

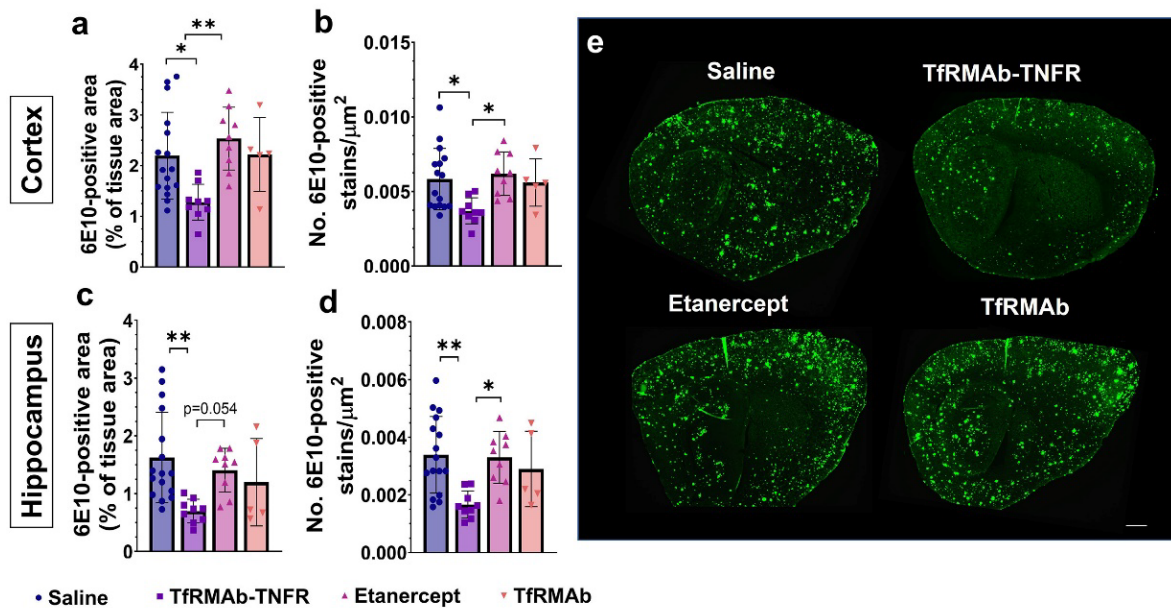


**Figure 1.** Effect of TfrMab-TNFR dosing on 6E10-positive A $\beta$  load. Cortical 6E10-positive A $\beta$  area (a) and puncta number (b) were significantly lower in the TfrMab-TNFR-treated mice compared to the saline-treated mice. There was a significant reduction in the hippocampal 6E10-positive A $\beta$  area (c) and puncta number (d) in the TfrMab-TNFR-treated mice compared to the saline-treated mice. Etanercept-treated mice had a higher 6E10-positive area and puncta number in the cortex and a higher puncta number in the hippocampus compared to the TfrMab-TNFR-treated mice. 6E10-positive A $\beta$  stains are shown in the representative sagittal brain section images in (e). Scale bar = 200  $\mu\text{m}$ . Data are presented as mean  $\pm$  SD of  $n = 5$ –16 per treatment group, and data were analyzed using the one-way ANOVA with the Holm Sidak's post hoc test. \*  $p < 0.05$ , \*\*  $p < 0.01$  for the indicated comparisons.

With respect to the cerebrum A $\beta$  ELISAs, both TfrMab-TNFR and etanercept reduced insoluble (Gu-HCl-soluble) A $\beta$  (1-42) ( $p < 0.001$ ; Figure 2a) and soluble (TBS-soluble) high-molecular-weight A $\beta$  oligomers ( $p < 0.001$ ; Figure 2b) compared with the saline-treated mice. However, only TfrMab-TNFR significantly reduced the insoluble (Gu-HCl-soluble) high-molecular-weight A $\beta$  species ( $p < 0.05$ ; Figure 2c) and the cortical Thio-S-positive mature A $\beta$  plaque numbers ( $p < 0.05$ ; Figure 2d,f). A similar trend of reduced hippocampal Thio-S-positive mature A $\beta$  plaque numbers ( $p = 0.07$ ; Figure 2e,f) was observed for the TfrMab-TNFR-treated mice. Like the 6E10-positive A $\beta$  load, etanercept-treated mice had a significantly higher cortical Thio-S-positive mature A $\beta$  plaque number compared with the TfrMab-TNFR-treated mice ( $p < 0.01$ ; Figure 2d,f) and a similar trend was observed in the hippocampus ( $p = 0.06$ ; Figure 2e,f). TfrMab alone did not affect A $\beta$  (1-42) or oligomeric A $\beta$ .

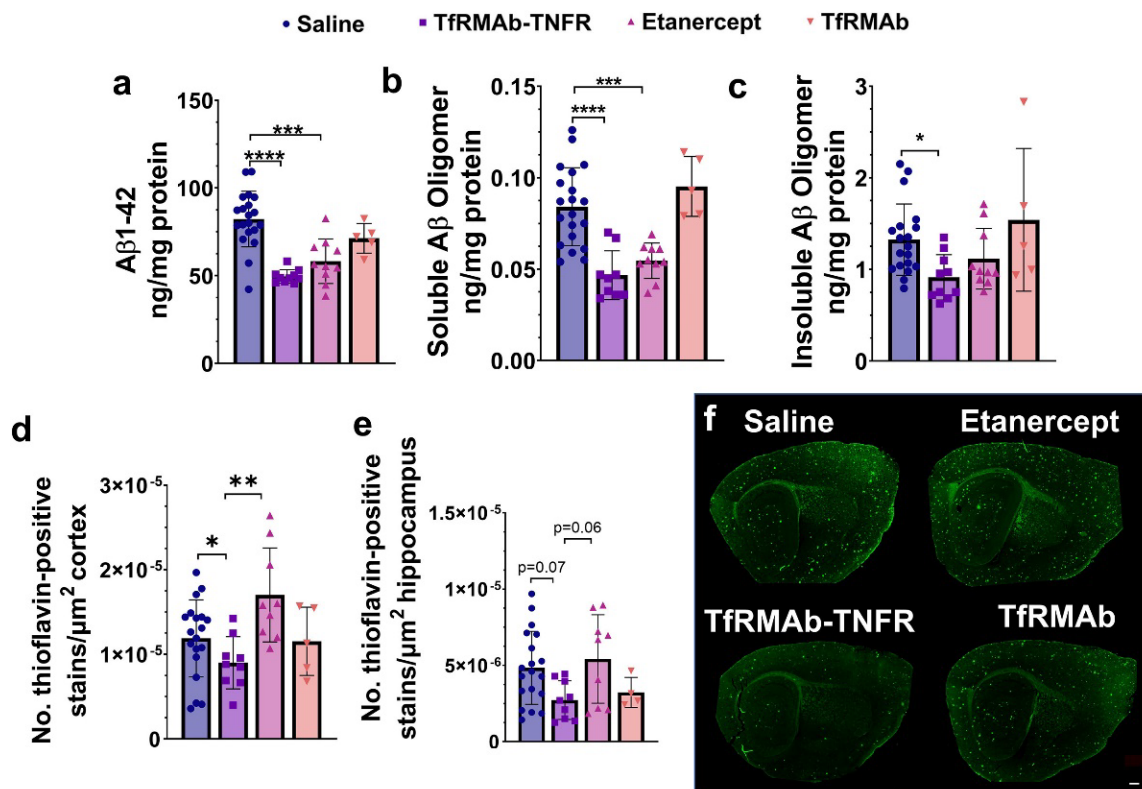


**Figure 2.** Effect of TfrMAb-TNFR on insoluble A $\beta$  (1-42) and high-molecular-weight A $\beta$  assemblies. TfrMAb-TNFR and etanercept reduced insoluble (Gu-HCl-soluble) A $\beta$  (1-42) (a) and soluble (TBS-soluble) high-molecular-weight oligomeric A $\beta$  (b) in cerebrum homogenates compared to the saline-treated mice. TfrMAb-TNFR, but not etanercept, significantly reduced insoluble (Gu-HCl-soluble) oligomeric A $\beta$  in the cerebrum homogenates (c). TfrMAb-TNFR-treated mice also had a lower number of Thio-S-positive A $\beta$  plaques compared to the saline-treated mice (d), and a similar trend was observed in the hippocampus (e). Representative sagittal brain section images of Thio-S-stained mature A $\beta$  plaques (f). Scale bar = 200  $\mu\text{m}$ . Data are presented as mean  $\pm$  SD of  $n = 4$ –20 per treatment group, and data were analyzed using the one-way ANOVA with the Holm Sidak's post hoc test. \*  $p < 0.05$ , \*\*  $p < 0.01$ , \*\*\*  $p < 0.001$ , \*\*\*\*  $p < 0.0001$  for the indicated comparisons.

### 3.2. Chronic TfrMAb-TNFR Improved Spatial Reference Memory in Aged APP/PS1 Mice

TfrMAb-TNFR-treated mice spent more time ( $p < 0.01$ ; Figure 3a,e) and traveled more distance ( $p < 0.01$ ; Figure 3b,e) in the novel arm compared to the saline-treated mice. TfrMAb-TNFR-treated mice had a reduced latency to enter the novel arm ( $p < 0.05$ , Figure 3c), and the percentage of mice selecting the novel arm as their first arm choice was significantly higher for the TfrMAb-TNFR-treated mice compared to the saline-treated mice ( $p < 0.0001$ , Figure 3d). The percentage of mice selecting the novel arm was significantly lower for the TfrMAb-treated mice than for the saline-treated mice ( $p < 0.01$ , Figure 3d). However, due to the small sample size of the TfrMAb group, these results should be interpreted with caution. To rule out the impact of locomotion on the Y-maze outcome, we performed the open-field test to assess the exploration and locomotion of the APP/PS1 mice. As shown in Figure 4a–d, all three locomotion parameters: resting time (Figure 4a), mean speed (Figure 4b), and distance traveled (Figure 4c), did not differ significantly between any experimental group.

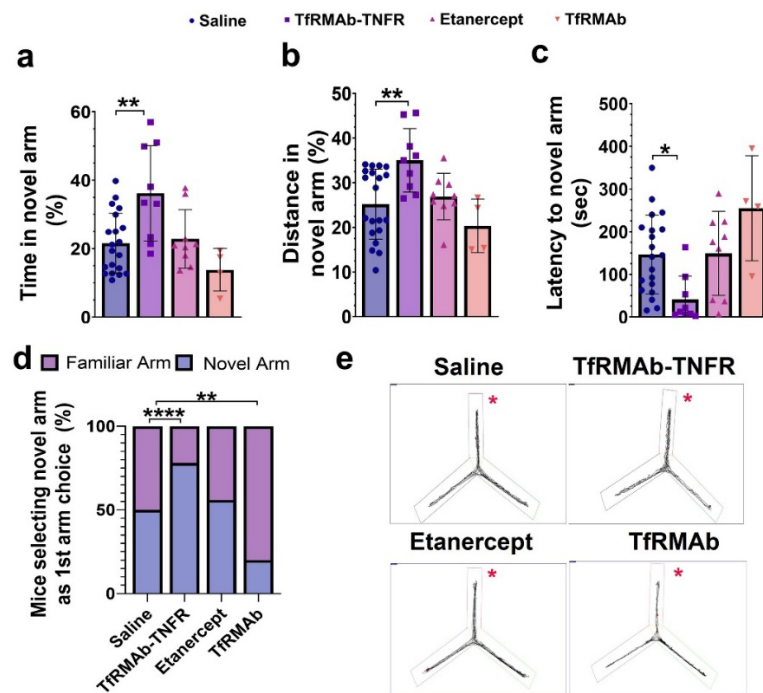


**Figure 3.** Effect of chronic TfrMAB-TNFR dosing on spatial reference memory using the Y-maze test. TfrMAB-TNFR treatment increased the time spent (a) and distance traveled (b) in the novel arm and reduced the latency to the novel arm (c) compared to the saline-treated mice. More TfrMAB-TNFR-treated mice selected the novel arm as their first choice compared to the saline-treated mice (d). Representative trajectory maps of mice in the Y-maze (e). The novel arm is shown by the red asterisk. Data are presented as mean  $\pm$  SD of  $n = 4$ –20 per treatment group, numerical data were analyzed using the one-way ANOVA with the Holm Sidak’s post hoc test, and nominal data were analyzed using the Fisher’s exact test. \*  $p < 0.05$ , \*\*  $p < 0.01$ , \*\*\*\*  $p < 0.0001$  for the indicated comparisons.

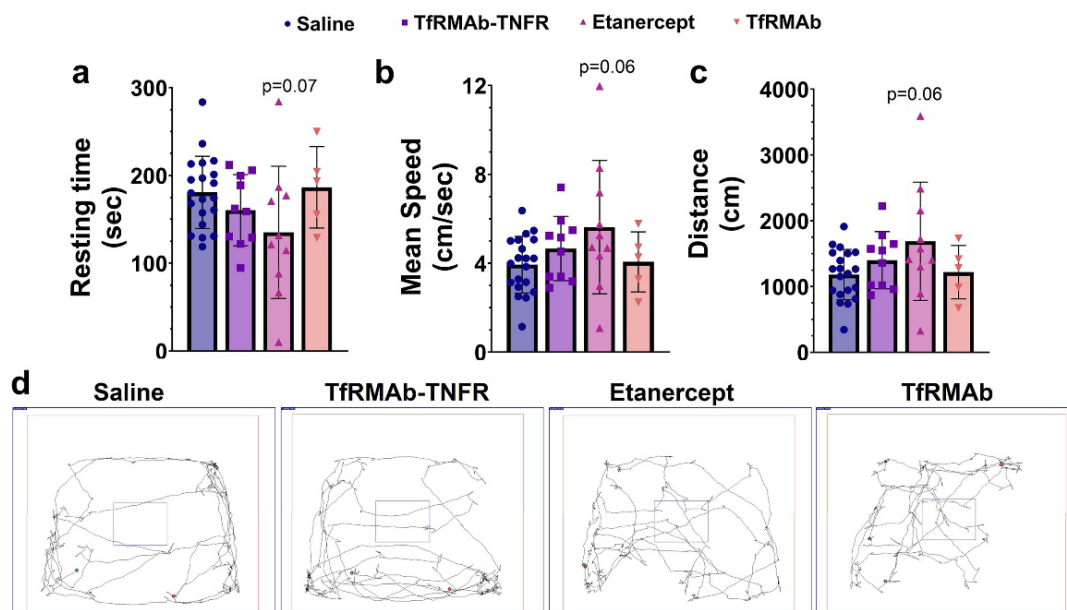


**Figure 4.** Effect of chronic TfrMAB-TNFR dosing on locomotion and exploration. The resting time (a), mean speed (b), and distance traveled (c) did not differ between any experimental group. The representative trajectory maps show mouse movement in the different groups (d). Data are presented as mean  $\pm$  SD of  $n = 5$ –20 per treatment group, and data were analyzed using the one-way ANOVA with the Holm Sidak’s post hoc test.



### 3.3. Chronic TfrMAB-TNFR Dosing Did Not Alter APP and BACE-1 Levels but Reduced Microgliosis and Increased Plaque-Associated Phagocytic Microglia

The protein levels of APP and BACE-1 were determined in the cerebrum homogenates and are shown in Figure 5a,b. No differences in APP (Figure 5a) and BACE-1 (Figure 5b) protein levels were found between the experimental groups. Chronic TfrMAB-TNFR or etanercept treatment reduced the Iba1-positive area (microgliosis) in the cortex ( $p < 0.05$  for TfrMAB-TNFR and  $p < 0.01$  for etanercept; Figure 5c) and the hippocampus ( $p < 0.05$  for TfrMAB-TNFR and etanercept; Figure 5d). Chronic TfrMAB dosing did not alter microgliosis in the aged APP/PS1 mice.

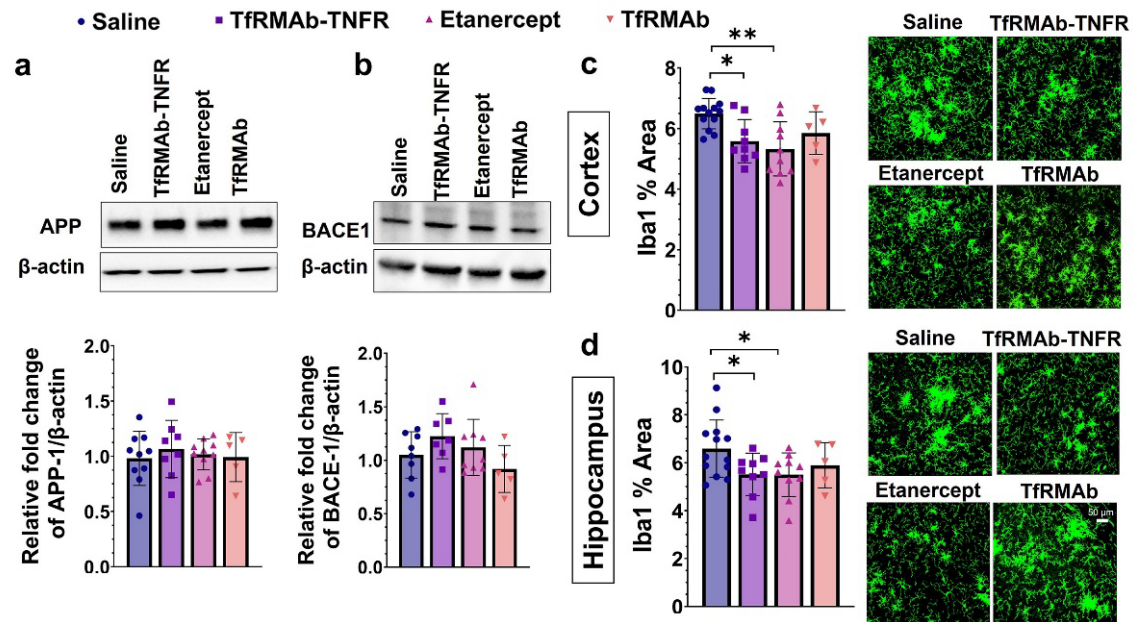


**Figure 5.** Effect of TfrMAB-TNFR on amyloid precursor protein (APP) and the  $\beta$ -site APP cleaving enzyme (BACE-1) levels, and microgliosis. There was no change in the protein levels of APP (a) or BACE-1 (b) between experimental groups by Western blotting of the cerebrum homogenates. TfrMAB-TNFR and etanercept reduced cortical (c) and hippocampal (d) Iba1-positive area. TfrMAB-treated mice showed no change in the Iba1-positive area. Scale bar = 50  $\mu$ m. Data are presented as mean  $\pm$  SD of  $n = 5$ –13 per treatment group, and data were analyzed using the one-way ANOVA with the Holm Sidak's post hoc test. \*  $p < 0.05$ , \*\*  $p < 0.01$  for the indicated comparisons.

To study the association between mature A $\beta$  plaques and microglia, we measured the plaque-associated microglia ratio, which measures the area occupied by the microglia associated with the plaque normalized to the A $\beta$  plaque area. As shown in Figure 6, the plaque-associated microglia ratio was significantly higher in the cortex ( $p < 0.05$ ; Figure 6a,c) and hippocampus ( $p < 0.01$ ; Figure 6d,f) of the TfrMAB-TNFR-treated mice compared to the etanercept-treated mice. The hippocampal plaque-associated microglia were also significantly higher in the TfrMAB-TNFR-treated mice compared to the saline-treated mice ( $p < 0.05$ ; Figure 6d). Interestingly, the plaque-associated Axl ratio, which represents the immunoreactivity of Axl, a phagocytic marker [23], in the plaque-associated microglia, was significantly higher in the cortex ( $p < 0.05$  compared to saline and etanercept; Figure 6b,c) and the hippocampus ( $p < 0.05$  compared to saline and  $p < 0.01$  compared to etanercept; Figure 6e,f) of the TfrMAB-TNFR-treated mice compared to the saline- and etanercept-treated mice. The measured autofluorescent A $\beta$  plaque area was not negatively correlated with the plaque-associated microglia ratio or the plaque-associated Axl ratio suggesting that the higher plaque-associated microglia or Axl ratio in the TfrMAB-TNFR-treated mice and the lower plaque-associated microglia or Axl ratio in the etanercept-treated mice are

not driven by the lower and higher autofluorescent A $\beta$  plaque area in the TfrMab-TNFR and etanercept groups, respectively (Supplementary Materials Figure S1).

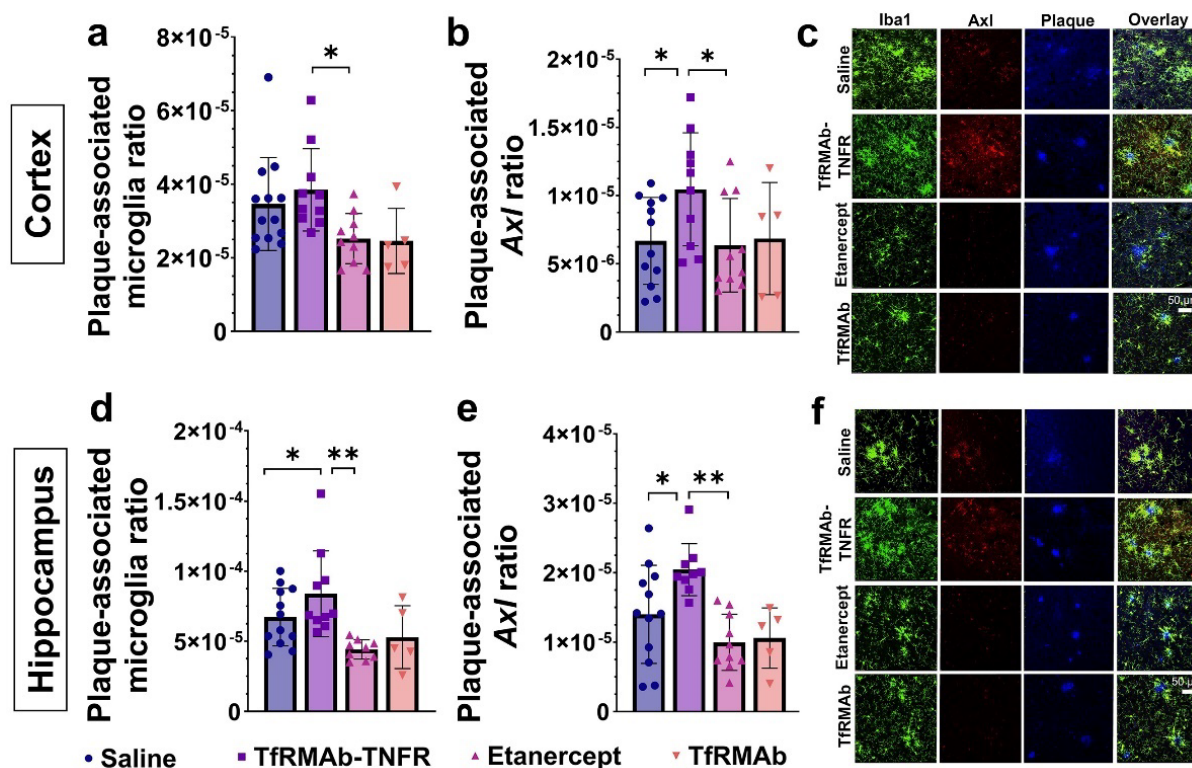


**Figure 6.** Effect of TfrMab-TNFR on plaque-associated phagocytic microglia. Cortical plaque-associated microglia (a) and plaque-associated Axl-positive phagocytic microglia (b) were significantly higher in the TfrMab-TNFR-treated mice compared with the etanercept-treated mice. Similarly, hippocampal plaque-associated microglia (d) and plaque-associated Axl-positive phagocytic microglia (e) were significantly higher in the TfrMab-TNFR-treated mice than in the saline- and etanercept-treated mice. Representative 40 $\times$  confocal images showing Iba1 (green), Axl (red), and autofluorescent mature A $\beta$  plaques (blue) in the cortex (c) and hippocampus (f). Scale bar = 50  $\mu$ m. Data are presented as mean  $\pm$  SD of  $n = 5$ –13 per treatment group, and data were analyzed using the one-way ANOVA with the Holm Sidak's post hoc test. \*  $p < 0.05$ , \*\*  $p < 0.01$  for the indicated comparisons.

### 3.4. TfrMab-TNFR Treatment Increased BBB Tight-Junction Proteins and Reduced Neuroinflammation

Chronic TfrMab-TNFR dosing significantly increased the BBB tight-junction proteins, ZO-1 ( $p < 0.05$ ; Figure 7a) and claudin-5 ( $p < 0.05$ ; Figure 7b), in the cerebrum homogenates of the aged APP/PS1 mice compared with the saline-treated mice. Etanercept or TfrMab did not alter BBB tight-junction protein expression levels in the aged APP/PS1 mice. Both TfrMab-TNFR ( $p < 0.05$ ; Figure 7c) and etanercept ( $p < 0.01$ ; Figure 7c) increased I $\kappa$ B $\alpha$ , a marker of attenuation of TNF- $\alpha$  signaling, in the cerebrum homogenates of the aged APP/PS1 mice. TfrMab did not alter brain I $\kappa$ B $\alpha$  protein expression in the aged APP/PS1 mice.

### 3.5. Chronic TfrMab but Not TfrMab-TNFR Dosing Altered Hematologic Indices in Aged APP/PS1 Mice

TfrMab dosing of 10.7-month-old APP/PS1 mice for ten weeks reduced hematocrit ( $p < 0.0001$ ; Figure 8a), hemoglobin ( $p < 0.0001$ ; Figure 8b), and mean corpuscular volume (MCV,  $p < 0.01$ ; Figure 8c), and increased white blood cell count (WBC,  $p < 0.01$ ; Figure 8d) compared to the saline-treated mice. No change in reticulocytes (Figure 8e), red blood

cells (RBC) (Figure 8f), and platelets (Figure 8g) was observed between any treatment group compared to the saline-treated mice. TfrMab-TNFR or etanercept treatment did not alter any hematology indices following a ten-week treatment compared to the saline-treated mice.

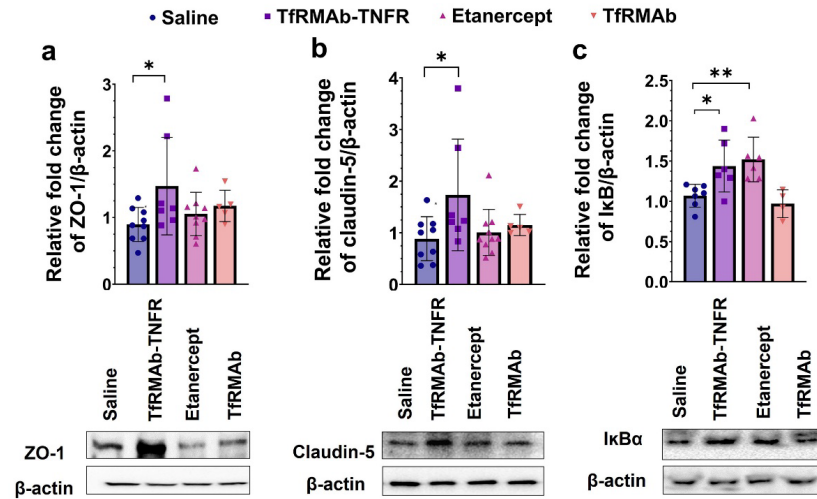


**Figure 7.** Effect of TfrMab-TNFR on BBB tight-junction proteins and brain inflammation. Chronic TfrMab-TNFR dosing in aged APP/PS1 mice significantly increased ZO-1 (a) and claudin-5 (b) compared to the saline-treated mice measured using Western blotting of the cerebrum homogenates. Both TfrMab-TNFR and etanercept increased IκBα in the cerebrum homogenates compared to the saline-treated mice (c). Data are presented as mean ± SD of  $n = 4-9$  per treatment group, and data were analyzed using the one-way ANOVA with the Holm Sidak's post hoc test. \*  $p < 0.05$  and \*\*  $p < 0.01$  for the indicated comparisons.

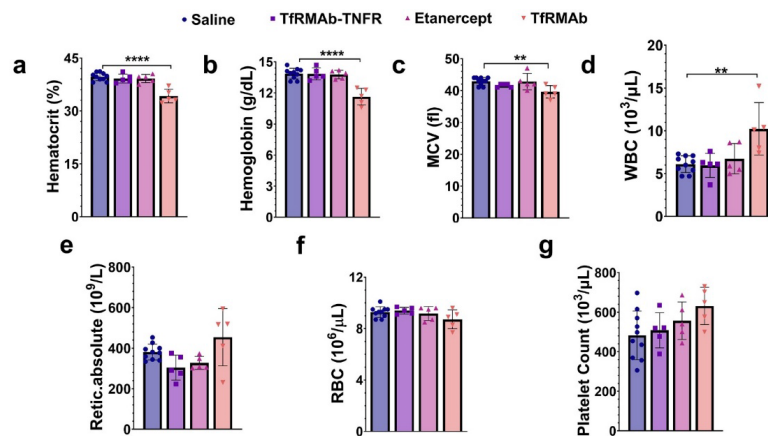


**Figure 8.** Effect of chronic TfrMab-TNFR dosing on hematologic parameters. Long-term (ten-week) treatment with TfrMab alone, but not TfrMab-TNFR, decreased hematocrit (a), hemoglobin (b), and mean corpuscular volume (MCV; (c)), and elevated white blood cell (WBC; (d)) count compared to the saline-treated mice. No change in reticulocytes (e), red blood cells (RBC) (f), and platelets (g) was observed. Etanercept did not alter any hematology parameter. Data are presented as mean ± SD of  $n = 5-10$  per treatment group, and data were analyzed using the one-way ANOVA with the Holm Sidak's post hoc test. \*\*  $p < 0.01$  and \*\*\*\*  $p < 0.0001$  for the indicated comparisons.

### 3.6. Chronic TfrMab but Not TfrMab-TNFR Dosing Increased Splenic Iron Transporters and Iron Levels

The protein levels of TfR (TfR1 in the brain and spleen, and TfR2 in the liver), the principal iron importer, and ferroportin, the major iron exporter, in the brain, spleen, and liver are shown in Figure 9. Brain levels of TfR1 (Figure 9a,g) and ferroportin (Figure 9d,g) did

not differ between experimental groups. Similarly, the liver expression of TfR2 (Figure 9c,i) and ferroportin (Figure 9f,i) did not differ between experimental groups. However, chronic TfRMAB dosing significantly increased splenic TfR1 ( $p < 0.05$ ; Figure 9b,h) and ferroportin ( $p < 0.01$ ; Figure 9e,h) levels compared to the saline-treated mice. Chronic TfRMAB dosing also increased splenic ( $p < 0.05$ ; Figure 9j) and liver ( $p < 0.0001$ ; Figure 9k) iron in the aged APP/PS1 mice. TfRMAB-TNFR or etanercept dosing did not alter splenic or liver iron in the aged APP/PS1 mice.

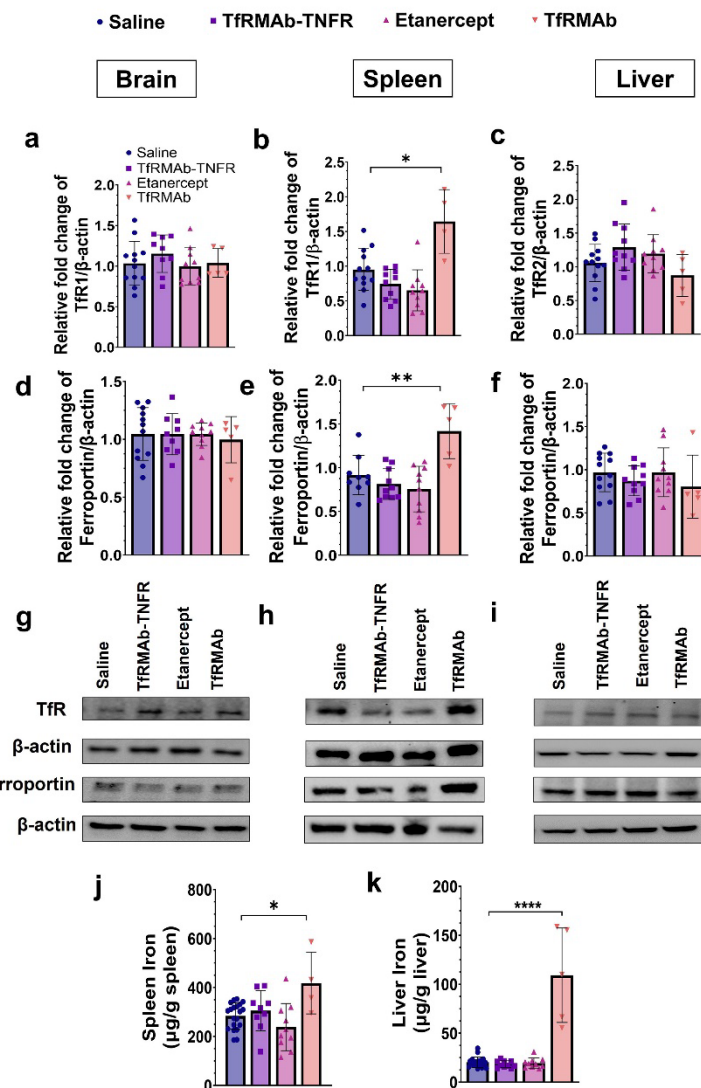


**Figure 9.** Effect of chronic TfRMAB-TNFR dosing on the expression of iron transporters and tissue iron levels. The protein levels of TfR (TfR1 in the brain and spleen, and TfR2 in the liver) in the brain (a), spleen (b), and liver (c). No significant difference in the brain and liver TfR expression between experimental groups. However, TfRMAB treatment significantly elevated splenic TfR levels compared to the saline-treated mice (b). The protein levels of ferroportin in the brain (d), spleen (e), and liver (f). No significant difference in the brain and liver ferroportin expression between experimental groups. However, TfRMAB treatment significantly elevated splenic ferroportin levels compared to the saline-treated mice (e). Representative western blot images showing TfR and ferroportin expression in the brain (g), spleen (h) and liver (i). Chronic TfRMAB dosing significantly increased spleen (j) and liver (k) iron levels. Data are presented as mean  $\pm$  SD of  $n = 4$ –20 per treatment group, and data were analyzed using the one-way ANOVA with the Holm Sidak’s post hoc test. \*  $p < 0.05$ , \*\*  $p < 0.01$ , and \*\*\*\*  $p < 0.0001$  for the indicated comparisons.

#### 4. Discussion

TfRMAB-TNFR is a brain-penetrant biologic TNF- $\alpha$  inhibitor that can sequester both peripheral and brain TNF- $\alpha$  to attenuate or prevent downstream TNF- $\alpha$  signaling [14]. The role of TNF- $\alpha$  in AD pathogenesis has been well studied [6], and our previous work highlighted the protective effects of the brain-penetrant TfRMAB-TNFR in 6-month-old APP/PS1 male mice compared to etanercept, a biologic TNF- $\alpha$  inhibitor with limited brain uptake [17,26]. In the aforementioned proof-of-concept study, we showed that TfRMAB-TNFR reduced A $\beta$  load, which is regarded as the primary initiator of AD [27]. Notably, A $\beta$  deposition in the AD brain is a function of time and progresses with age [27], therefore, an ideal therapeutic for AD may be one that reduces A $\beta$  pathology at both early and late stages of the disease when the A $\beta$  load is full-blown. The advantages of developing such a therapeutic are twofold: first, it will provide an A $\beta$  lowering agent that works at early and late stages of the disease, and second, such investigations will elucidate if A $\beta$  lowering effects at late stages of the disease or following delayed treatment are coincident with cognitive benefits. Therefore, in pursuit of such a therapeutic, in the current study, we initiated TfRMAB-TNFR treatment in older 10.7-month-old APP/PS1 mice, as opposed to treatment initiation in younger 6-month-old mice [17], and continued the treatment till the mice were 13 months old, a stage at which we expect the A $\beta$  pathology to plateau in this mouse model to mimic late stages of AD [28]. Despite the advanced age of the APP/PS1 mice, delayed treatment with TfRMAB-TNFR resulted in an impressive ~50–56% reduction in the 6E10-positive total A $\beta$  load, which is consistent with the reduction seen in the younger 6-month-old APP/PS1 mice [17]. However, chronic equimolar dosing of etanercept did not reduce the 6E10-positive A $\beta$  load, which is consistent with our previous work in the APP/PS1 mice [28] and work of others using the triple transgenic (3xTg) mice showing that peripheral TNF- $\alpha$  inhibitors do not reduce 6E10-positive A $\beta$  load [29].

Amyloidogenic A $\beta$  is formed through the sequential cleavage of the transmembrane APP by  $\beta$ - and  $\gamma$ -secretases resulting in the formation of A $\beta$  monomers [30]. The primary A $\beta$  isoforms associated with AD include A $\beta$  (1-40) and A $\beta$  (1-42) [31], of which, A $\beta$  (1-40) is more abundant while A $\beta$  (1-42) is more prone to aggregation and induces toxicity [32,33]. Monomeric amyloidogenic A $\beta$  isoforms are hydrophobic and self-assemble to form high-molecular-weight oligomers and  $\beta$ -sheet-rich fibrils that form the core of A $\beta$  plaques [34]. The original amyloid cascade hypothesis puts A $\beta$  plaques at the center of AD-neurotoxicity and cognitive decline [35]; however, over the last two decades, there has been a paradigm shift towards the central role of A $\beta$  oligomers in AD pathogenesis and cognitive decline [36]. Therefore, to understand if the A $\beta$ -lowering effects of TfRMAB-TNFR were directed towards a specific A $\beta$  specie, and since the 6E10 antibody detects all A $\beta$  isoforms [37], we measured the levels of different A $\beta$  species: A $\beta$  (1-42), high-molecular-weight A $\beta$  oligomers, and Thio-S-positive  $\beta$ -sheet rich A $\beta$  plaques. Both TfRMAB-TNFR and etanercept reduced insoluble A $\beta$  (1-42) and soluble high-molecular-weight A $\beta$  oligomers. TfRMAB-TNFR treatment significantly reduced insoluble high-molecular-weight A $\beta$  oligomers, and a similar trend was seen with etanercept, but these values did not reach statistical significance. Similarly, TfRMAB-TNFR, but not etanercept, significantly reduced the Thio-S-positive mature A $\beta$  plaques compared to the saline-treated mice and the Thio-S-positive A $\beta$  plaques were lower by almost 50% in the TfRMAB-TNFR-treated mice compared with the etanercept-treated mice. These data collectively show that TfRMAB-TNFR, but not etanercept, results in a significant reduction in total A $\beta$  peptide and mature A $\beta$  plaque load in the aged APP/PS1 mice.

While A $\beta$  accumulation in the brain represents one of the major pathological hallmarks of AD, cognitive impairment represents the main clinical feature of AD [1]. In the APP/PS1 used in the current study, cognitive function is an inverse correlate of A $\beta$  accumulation [38]. Accordingly, TfRMAB-TNFR, which reduced the total A $\beta$  peptide load and A $\beta$  plaque load by half compared to the etanercept treated mice, resulted in a significant improvement in spatial reference memory, implying that the cognitive improvement in the aged APP/PS1 mice may be driven by the lowering of total A $\beta$  peptide and/or A $\beta$  plaque load with

TfRMAB-TNFR. Further, increased A $\beta$  load in the brain can be driven by BBB impairment and breakdown, which is an early biomarker of cognitive dysfunction in AD [39,40]. In the current study, apart from reducing A $\beta$  load, TfRMAB-TNFR significantly increased the expression of BBB tight-junction proteins, claudin-5 and ZO-1, while etanercept treatment did not. This increase in BBB tight-junction protein expression concomitant with a reduction in A $\beta$  peptide and/or A $\beta$  plaque load in the TfRMAB-TNFR-treated mice may underlie the improvement in memory of the TfRMAB-TNFR-treated but not of etanercept-treated aged APP/PS1 mice.

Excessive extracellular A $\beta$  deposition in the AD brain is hypothesized to result from an imbalance between A $\beta$  production and A $\beta$  clearance, and TNF- $\alpha$  is implicated in both these processes. Studies show that genetic deletion of TNF- $\alpha$  in 5xFAD mice or its receptor in the APP23 mice reduced A $\beta$  plaque by lowering the levels and activity of the APP cleaving enzymes [41,42]. Further, TNF- $\alpha$  increased the expression of BACE-1 and enhanced APP processing in astrocytes in vitro [43]. In the current study, TfRMAB-TNFR treatment did not alter APP or BACE-1 levels in the cerebrum homogenates, suggesting that the A $\beta$ -lowering effects of TfRMAB-TNFR are not mediated by attenuation of APP processing or A $\beta$  production. However, it must be noted that we did not measure the activity of BACE-1 or the levels of BACE-1 cleavage products in the current study. Given that blockade of TNF- $\alpha$  signaling can reduce BACE-1 activity [41,42], the contribution of lowered BACE-1 activity to A $\beta$  reduction by TfRMAB-TNFR cannot be ruled out.

Microglia are the innate immune cells of the brain, and their primary function is to survey the CNS and respond to pathological stimuli, including A $\beta$  deposits [44,45]. In the AD brain, microglia are found in close proximity to A $\beta$  plaques, become activated in response to the A $\beta$  plaques, and secrete pro-inflammatory cytokines, including TNF- $\alpha$  [44,45]. The secreted pro-inflammatory cytokines can stimulate a self-perpetuating cycle of microglial activation and cytokine release resulting in sustained neuroinflammation [44,45]. In the current study, microgliosis was assessed by Iba1 immunostaining, and chronic treatment with TfRMAB-TNFR reduced the Iba1-positive area in the brains of the aged APP/PS1 mice. A similar reduction in microgliosis was observed in the etanercept-treated mice suggesting that peripheral TNF- $\alpha$  can modulate microglial activation in the CNS. This is consistent with our previous work in the PS19 mouse model of tauopathy and other studies reporting a reduction in microglial activation with attenuation or blockage of peripheral TNF- $\alpha$  signaling [18,41,42] and an increase in microglial activation with increased peripheral TNF- $\alpha$  signaling [46] in AD mouse models.

Besides mounting an inflammatory response to A $\beta$  deposits, microglia surrounding the A $\beta$  plaques can form a protective barrier to reduce neurite dystrophy and perform phagocytic clearance of A $\beta$  plaques [45]. However, despite significant microglial recruitment, there is increased A $\beta$  accumulation in the AD brain, suggesting that microglia cannot effectively clear A $\beta$  deposits in AD [45]. One mechanism resulting in reduced phagocytic activity of microglia is excessive secretion of A $\beta$ -induced pro-inflammatory cytokines [47]. To determine the role of microglia in TfRMAB-TNFR mediated A $\beta$  lowering, we first studied the association of microglia with A $\beta$  plaques in the brains of the aged APP/PS1 mice. Interestingly, despite a reduction in microgliosis, more microglia were associated with A $\beta$  plaques in the TfRMAB-TNFR-treated mice compared to the saline- and etanercept-treated mice. The plaque-associated microglia in the TfRMAB-TNFR-treated mice also had a higher expression of Axl, a phagocytic receptor involved in A $\beta$  plaque phagocytosis [24], compared to the saline- and etanercept-treated mice. These results are consistent with previous findings showing that cytokine suppression can increase microglia-mediated A $\beta$  plaque phagocytosis [47] and that increased expression of Axl on microglial cells is associated with increased A $\beta$  plaque clearance [24]. Therefore, the differential effects of TfRMAB-TNFR and etanercept on lowering A $\beta$  load may be attributed to enhanced plaque-associated phagocytic microglia in the TfRMAB-TNFR-treated mice.

The TfRMAB used in the current study is a high-affinity bivalent antibody [16], and our previous work revealed some alterations in hematology indices and splenic iron with

TfRMAB dosing in mice [19]. A single (acute) dose of TfRMAB in mice resulted in severe reticulocyte (immature RBCs) suppression that was not observed with chronic TfRMAB dosing [19]. Reticulocyte suppression with TfRMABs has been reported for different TfRMAB variants and is suggested to be an immunologic effector function response and related to TfR expression on reticulocytes [19,48]. However, this reticulocyte suppression is short-lived and was not observed with long-term TfRMAB dosing [19], and this was confirmed in the current study, wherein ten-week chronic dosing of TfRMAB was not associated with reticulocyte suppression. However, we did observe a modest but significant decline in other RBC parameters, including hematocrit, hemoglobin, and MCV, following ten weeks of TfRMAB dosing. This contrasts with our results obtained during the 4-week TfRMAB dosing study [19]. RBCs have a life-span of about 40–50 days in a mouse [49,50], and therefore the acute suppression of reticulocytes seen with a single TfRMAB injection will translate into reduced RBC indices around 6–7 weeks after treatment initiation, and a reduction in RBC indices is not likely to appear within four weeks of TfRMAB dosing. This may explain why no changes in RBC indices were seen in the previous four-week TfRMAB dosing study but appeared in the current ten-week dosing study. Longer studies will be needed to determine if this modest reduction in RBC indices with TfRMAB dosing are normalized. Interestingly, these alterations in the hematology indices were TfRMAB specific, and chronic TfRMAB-TNFR dosing did not alter any hematology parameter. This suggests that the fusion of the therapeutic partner alters the safety profile of the TfRMAB, and is consistent with our previous work showing no changes in hematology parameters with chronic eight-week TfRMAB-erythropoietin (EPO) dosing [51]. Similar findings were reported for a humanized TfRMAB chronically dosed in cynomolgus monkeys, wherein humanized TfRMAB-induced effector function was eliminated in monkeys dosed with the humanized TfRMAB fused to a therapeutic enzyme [52]. Stearic hindrance due to the fusion of the therapeutic moiety to the TfRMAB was suggested to interfere with the access of the TfRMAB to the complement proteins that trigger effector function [52]. Chronic etanercept dosing also did not impact the hematology profile of aged APP/PS1 mice.

The TfRMAB is directed towards the mouse TfR1 [16], the principal iron import receptor highly enriched at the BBB and spleen [16,53]. The levels of TfR1 in the liver are low, and the primary hepatic TfR isoform is TfR2 and was measured in the current study [53]. Prior work showed no change in the brain TfR1 expression with chronic four-week TfRMAB dosing in mice [19], and the results from the current investigation are consistent with this. Chronic ten-week TfRMAB or TfRMAB-TNFR dosing did not alter brain TfR1 levels. Additionally, the brain levels of the iron exporter, ferroportin, remained unaltered with chronic TfRMAB or TfRMAB-TNFR dosing. Chronic ten-week TfRMAB dosing, however, elevated TfR1 expression in the spleen of aged APP/PS1 mice, consistent with an increase in splenic TfR1 in young wild-type C57 mice following four-week dosing [19]. This increase in splenic TfR1 correlated with an elevation in the protein level of ferroportin and iron level in the spleen, indicative of altered iron homeostasis in the spleen with chronic TfRMAB dosing. We also studied the impact of chronic TfRMAB dosing on liver TfR2 and ferroportin and did not observe an increase in hepatic TfR2 or ferroportin levels. Interestingly, no correlation between hepatic TfR2 and iron levels was observed, and despite no change in hepatic TfR2 levels, we saw a significant increase in hepatic iron levels with chronic TfRMAB dosing. The reason for this discrepancy is unclear but may be explained by the limited role of hepatic TfR2 in iron uptake [53]. Interestingly, chronic TfRMAB-TNFR dosing did not dysregulate iron transporters or tissue iron levels post ten-week dosing. These findings are intriguing because both TfRMAB and TfRMAB-TNFR are directed towards TfR1, which is highly enriched in the spleen [53]. Accordingly, biodistribution studies following a single injection show enhanced accumulation of TfRMAB-targeted therapeutics, including TfRMAB-TNFR [15], in the spleen [54–56]. However, despite the known increased splenic-accumulation of both TfRMAB and TfRMAB-TNFR, only the TfRMAB resulted in iron dysregulation in our hands. Therefore, the effects of TfRMAB on splenic iron and transporters do not appear to be driven by its biodistribution in vivo.

These findings highlight the positive impact of the fusion partner in normalizing the TfrMAB-associated altered iron homeostasis, and the mechanism underlying these effects of TfrMAB needs to be further investigated. The positive effect of fusing TfrMAB with a therapeutic partner has been previously observed. While chronic TfrMAB dosing increased its plasma clearance, chronic TfrMAB-TNFR dosing was not associated with altered plasma pharmacokinetics [18,19]. Similarly, TfrMAB-induced effector function was eliminated in the presence of a therapeutic fusion partner, as discussed above [52].

The study has some limitations. First, only aged male APP/PS1 mice were used in the current investigation to compare with prior results obtained from younger 6-month-old male APP/PS1 mice [17]. Therefore, sex differences in the therapeutic effects of TfrMAB-TNFR in APP/PS1 mice were not studied. Second, the sample size for the TfrMAB group is much smaller than the remaining experimental groups. The TfrMAB group was powered for safety studies based on our previous work [19] since the main intent of including the TfrMAB group was to determine if the TfrMAB-related adverse events are also seen with TfrMAB-TNFR. Therefore, the effect of TfrMAB on efficacy endpoints needs to be interpreted with caution. Third, the plaque-associated microglial studies were based on the autofluorescence microscopy of A $\beta$  plaques and did not use classical methods for A $\beta$  plaque detection (6E10 immunostaining and Thio-S). Notably, the use of autofluorescence microscopy to detect A $\beta$  plaques in mouse and human tissue is shown to be a reliable and sensitive method for plaque detection [57,58]. This method provides a chemical- and label-free method for A $\beta$  plaque detection that can be easily combined with Iba1 immunostaining and was therefore used in the current study. Finally, the A $\beta$  oligomer ELISA kit used in the study uses the same detector and capture antibody, which enables the quantification of A $\beta$  dimers and larger A $\beta$  assemblies, thus excluding A $\beta$  monomers [36]. However, it is possible that the A $\beta$  oligomers detected in the Gu-HCl fraction represent undissociated A $\beta$  plaques or larger A $\beta$  assemblies, and the possibility of an overlap between A $\beta$  plaque measurements and insoluble A $\beta$  oligomer measurements cannot be ruled out.

## 5. Conclusions

In conclusion, the results from the current study show that the brain-penetrant TNF- $\alpha$  inhibitor, TfrMAB-TNFR, offers greater therapeutic benefit than its non-brain-penetrant analog, etanercept, even in aged APP/PS1 mice. The superior A $\beta$ -lowering effects of TfrMAB-TNFR were associated with an increase in BBB-tight-junction proteins, plaque-associated phagocytic microglia, and significant memory improvement, effects that were not observed with etanercept. Finally, despite hematology and iron dysregulation with chronic TfrMAB dosing, TfrMAB-TNFR resulted in a stable hematology profile and iron transporter and tissue iron levels. With its stable safety and strong therapeutic profile, TfrMAB-TNFR is a potential therapeutic agent for both the early and late stages of AD.

**Supplementary Materials:** The following supporting information can be downloaded at: <https://www.mdpi.com/article/10.3390/pharmaceutics14102200/s1>, Figure S1: Scatter plots show no significant correlation between autofluorescent A $\beta$  plaque area and the plaque-associated microglia ratio in the cortex (a) and hippocampus (b) and plaque-associated Axl ratio in the cortex (c) and the hippocampus (d) for the biologic TNFI treated groups. Pearson correlation  $r$  was used for the analysis.

**Author Contributions:** Conceptualization, R.K.S.; Data curation, R.K.S.; Formal analysis, W.O., Y.O., J.Y., D.V.C., J.S. and R.K.S.; Funding acquisition, R.K.S.; Investigation, W.O., Y.O., J.Y. and R.K.S.; Methodology, W.O., D.H.C. and R.K.S.; Project administration, R.K.S.; Supervision, R.K.S.; Validation, W.O., Y.O., J.Y., D.V.C., T.A., J.S., R.M. and N.J.; Visualization, W.O., Y.O., J.Y., D.V.C. and J.S.; Writing—original draft, W.O., Y.O. and R.K.S.; Writing—review and editing, W.O., Y.O., J.Y., D.V.C., T.A., J.S., R.M., C.R., N.J., D.H.C. and R.K.S. All authors have read and agreed to the published version of the manuscript.



**Funding:** Research reported in this publication was supported by the National Institute of Aging of the National Institutes of Health under award numbers R01AG062840 and R01AG072896 to R.K.S. Approximately USD 250k of federal funds supported the effort (100%) on this project. The content is solely the responsibility of the authors and does not necessarily represent the official views of the National Institutes of Health. The article processing fee was funded by R01AG062840.

**Institutional Review Board Statement:** The animal study protocol was approved by the Institutional Animal Care and Use Committee of the University of California, Irvine (AUP-18-047 approved on 6/14/18).

**Informed Consent Statement:** Not applicable.

**Data Availability Statement:** All relevant data are within the paper and its supporting files.

**Conflicts of Interest:** The authors declare no conflict of interest. The funders had no role in the design of the study; in the collection, analyses, or interpretation of data; in the writing of the manuscript, or in the decision to publish the results.

## References

- 2021 Alzheimer's disease facts and figures. *Alzheimer's Dement.* **2021**, *17*, 327–406. [CrossRef] [PubMed]
- Calsolaro, V.; Edison, P. Neuroinflammation in Alzheimer's disease: Current evidence and future directions. *Alzheimer's Dement.* **2016**, *12*, 719–732. [CrossRef] [PubMed]
- Varnum, M.M.; Ikezu, T. The Classification of Microglial Activation Phenotypes on Neurodegeneration and Regeneration in Alzheimer's Disease Brain. *Arch. Immunol. Et Ther. Exp.* **2012**, *60*, 251–266. [CrossRef] [PubMed]
- Álvarez, A.; Cacabelos, R.; Sanpedro, C.; García-Fantini, M.; Aleixandre, M. Serum TNF-alpha levels are increased and correlate negatively with free IGF-I in Alzheimer disease. *Neurobiol. Aging* **2007**, *28*, 533–536. [CrossRef]
- Paganelli, R.; Di Iorio, A.; Patricelli, L.; Ripani, F.; Sparvieri, E.; Faricelli, R.; Iarlori, C.; Porreca, E.; Gioacchino, M.D.; Abate, G. Proinflammatory cytokines in sera of elderly patients with dementia: Levels in vascular injury are higher than those of mild-moderate Alzheimer's disease patients. *Exp. Gerontol.* **2002**, *37*, 257–263. [CrossRef]
- Chang, R.; Yee, K.L.; Sumbria, R.K. Tumor necrosis factor alpha Inhibition for Alzheimer's Disease. *J. Cent. Nerv. Syst. Dis.* **2017**, *9*, 1179573517709278. [CrossRef]
- Collins, J.S.; Perry, R.T.; Watson, B.; Harrell, L.E.; Acton, R.T.; Blacker, D.; Albert, M.S.; Tanzi, R.E.; Bassett, S.S.; McInnis, M.G.; et al. Association of a haplotype for tumor necrosis factor in siblings with late-onset Alzheimer disease: The NIMH Alzheimer disease genetics initiative. *Am. J. Med. Genet.* **2000**, *96*, 823–830. [CrossRef]
- Shi, J.-Q.; Shen, W.; Chen, J.; Wang, B.-R.; Zhong, L.-L.; Zhu, Y.-W.; Zhu, H.-Q.; Zhang, Q.-Q.; Zhang, Y.-D.; Xu, J. Anti-TNF- $\alpha$  reduces amyloid plaques and tau phosphorylation and induces CD11c-positive dendritic-like cell in the APP/PS1 transgenic mouse brains. *Brain Res.* **2011**, *1368*, 239–247. [CrossRef]
- Kim, D.H.; Choi, S.M.; Jho, J.; Park, M.S.; Kang, J.; Park, S.J.; Ryu, J.H.; Jo, J.; Kim, H.H.; Kim, B.C. aduximab ameliorates AD-associated object recognition memory impairment. *Behav. Brain Res.* **2016**, *311*, 384–391. [CrossRef] [PubMed]
- Shi, J.Q.; Wang, B.R.; Jiang, W.W.; Chen, J.; Zhu, Y.W.; Zhong, L.L.; Zhang, Y.-D.; Xu, J. Cognitive improvement with intrathecal administration of infliximab in a woman with Alzheimer's disease. *J. Am. Geriatr. Soc.* **2011**, *59*, 1142–1144. [CrossRef] [PubMed]
- Tobinick, E.; Gross, H.; Weinberger, A.; Cohen, H. TNF-alpha modulation for treatment of Alzheimer's disease: A 6-month pilot study. *Med. Gen. Med.* **2006**, *8*, 25.
- Detrait, E.; Danis, B.; Lamberty, Y.; Foerch, P. Peripheral administration of an anti-TNF-alpha receptor fusion protein counteracts the amyloid induced elevation of hippocampal TNF-alpha levels and memory deficits in mice. *Neurochem. Int.* **2014**, *72*, 10–13. [CrossRef] [PubMed]
- Butchart, J.; Brook, L.; Hopkins, V.; Teeling, J.; Puntener, U.; Culliford, D.; Sharples, R.; Sharif, S.; McFarlane, B.; Raybould, R.; et al. Etanercept in Alzheimer disease: A randomized, placebo-controlled, double-blind, phase 2 trial. *Neurology* **2015**, *84*, 2161–2168. [CrossRef]
- Zhou, Q.-H.; Boado, R.J.; Hui, E.K.-W.; Lu, J.Z.; Pardridge, W.M. Brain-Penetrating Tumor Necrosis Factor Decoy Receptor in the Mouse. *Drug Metab. Dispos.* **2010**, *39*, 71–76. [CrossRef] [PubMed]
- Sumbria, R.K.; Zhou, Q.H.; Hui, E.K.; Lu, J.Z.; Boado, R.J.; Pardridge, W.M. Pharmacokinetics and brain uptake of an IgG-TNF decoy receptor fusion protein following intravenous, intraperitoneal, and subcutaneous administration in mice. *Mol. Pharm.* **2013**, *10*, 1425–1431. [CrossRef] [PubMed]
- Boado, R.J.; Zhang, Y.; Wang, Y.; Pardridge, W.M. Engineering and expression of a chimeric transferrin receptor monoclonal antibody for blood-brain barrier delivery in the mouse. *Biotechnol. Bioeng.* **2008**, *102*, 1251–1258. [CrossRef] [PubMed]
- Chang, R.; Knox, J.; Chang, J.; DerBedrossian, A.; Vasilevko, V.; Cribbs, D.; Boado, R.J.; Pardridge, W.M.; Sumbria, R.K. Blood-Brain Barrier Penetrating Biologic TNF- $\alpha$  Inhibitor for Alzheimer's Disease. *Mol. Pharm.* **2017**, *14*, 2340–2349. [CrossRef]
- Ou, W.; Yang, J.; Simanauskaite, J.; Choi, M.; Castellanos, D.M.; Chang, R.; Sun, J.; Jagadeesan, N.; Parfitt, K.D.; Cribbs, D.H.; et al. Biologic TNF- $\alpha$  inhibitors reduce microgliosis, neuronal loss, and tau phosphorylation in a transgenic mouse model of tauopathy. *J. Neuroinflammation* **2021**, *18*, 1–19. [CrossRef] [PubMed]

19. Castellanos, D.M.; Sun, J.; Yang, J.; Ou, W.; Zambon, A.; Pardridge, W.M.; Sumbria, R.K. Acute and Chronic Dosing of a High-Affinity Rat/Mouse Chimeric Transferrin Receptor Antibody in Mice. *Pharmaceutics* **2020**, *12*, 852. [CrossRef]
20. Okuyama, T.; Eto, Y.; Sakai, N.; Nakamura, K.; Yamamoto, T.; Yamaoka, M.; Ikeda, T.; So, S.; Tanizawa, K.; Sonoda, H.; et al. A Phase 2/3 Trial of Pabinafusp Alfa, IDS Fused with Anti-Human Transferrin Receptor Antibody, Targeting Neurodegeneration in MPS-II. *Mol. Ther.* **2021**, *29*, 671–679. [CrossRef]
21. Hassett, B.; McMillen, S.; Fitzpatrick, B. Characterization and comparison of commercially available TNF receptor 2-Fc fusion protein products: Letter to the editor. *mAbs* **2013**, *5*, 624–625. [CrossRef]
22. Ohno, Y.; Murphy, R.; Choi, M.; Ou, W.; Sumbria, R.K. Full- versus Sub-Regional Quantification of Amyloid-Beta Load on Mouse Brain Sections. *J. Vis. Exp.* **2022**, *183*, e63669. [CrossRef] [PubMed]
23. Huang, Y.; Happonen, K.E.; Burrola, P.G.; O'Connor, C.; Hah, N.; Huang, L.; Nimmerjahn, A.; Lemke, G. Microglia use TAM receptors to detect and engulf amyloid beta plaques. *Nat. Immunol.* **2021**, *22*, 586–594. [CrossRef]
24. Savage, J.C.; Jay, T.; Goduni, E.; Quigley, C.; Mariani, M.M.; Malm, T.; Ransohoff, R.M.; Lamb, B.T.; Landreth, G.E. Nuclear receptors license phagocytosis by trem2<sup>+</sup> myeloid cells in mouse models of Alzheimer's disease. *J. Neurosci.* **2015**, *35*, 6532–6543. [CrossRef] [PubMed]
25. Thal, D.R.; Ghebremedhin, E.; Haass, C.; Schultz, C. UV light-induced autofluorescence of full-length Abeta-protein deposits in the human brain. *Clin. Neuropathol.* **2002**, *21*, 35–40. [PubMed]
26. Boado, R.J.; Hui, E.K.-W.; Lu, J.Z.; Zhou, Q.-H.; Pardridge, W.M. Selective targeting of a TNFR decoy receptor pharmaceutical to the primate brain as a receptor-specific IgG fusion protein. *J. Biotechnol.* **2010**, *146*, 84–91. [CrossRef] [PubMed]
27. Selkoe, D.J.; Hardy, J. The amyloid hypothesis of Alzheimer's disease at 25 years. *EMBO Mol. Med.* **2016**, *8*, 595–608. [CrossRef] [PubMed]
28. Finnie, G.S.; Gunnarsson, R.; Manavis, J.; Blumbergs, P.C.; Mander, K.A.; Edwards, S.; den Heuvel, C.V.; Finnie, J.W. Characterization of an 'Amyloid Only' Transgenic (B6C3-Tg(APPswe,PSEN1dE9)85Dbo/Mmjax) Mouse Model of Alzheimer's Disease. *J. Comp. Pathol.* **2017**, *156*, 389–399. [CrossRef] [PubMed]
29. Gabbita, S.P.; Johnson, M.F.; Kobritz, N.; Eslami, P.; Poteshkina, A.; Varadarajan, S.; Turman, J.; Zemlan, F.; Harris-White, M.E. Oral TNFalpha Modulation Alters Neutrophil Infiltration, Improves Cognition and Diminishes Tau and Amyloid Pathology in the 3xTgAD Mouse Model. *PLoS ONE* **2015**, *10*, e0137305. [CrossRef] [PubMed]
30. De Strooper, B.; Annaert, W. Proteolytic processing and cell biological functions of the amyloid precursor protein. *J. Cell Sci.* **2000**, *113*, 1857–1870. [CrossRef] [PubMed]
31. Wang, R.; Sweeney, D.; Gandy, S.E.; Sisodia, S.S. The profile of soluble amyloid beta protein in cultured cell media. Detection and quantification of amyloid beta protein and variants by immunoprecipitation-mass spectrometry. *J. Biol. Chem.* **1996**, *271*, 31894–31902. [CrossRef] [PubMed]
32. Fraser, P.E.; Nguyen, J.T.; Surewicz, W.K.; Kirschner, D.A. pH-dependent structural transitions of Alzheimer amyloid peptides. *Biophys. J.* **1991**, *60*, 1190–1201. [CrossRef]
33. Pike, C.; Burdick, D.; Walencewicz, A.J.; Glabe, C.G.; Cotman, C.W. Neurodegeneration induced by beta-amyloid peptides in vitro: The role of peptide assembly state. *J. Neurosci.* **1993**, *13*, 1676–1687. [CrossRef] [PubMed]
34. Knowles, T.P.; Vendruscolo, M.; Dobson, C.M. The amyloid state and its association with protein misfolding diseases. *Nat. Rev. Mol. Cell Biol.* **2014**, *15*, 384–396. [CrossRef] [PubMed]
35. Hensley, K.; Carney, J.M.; Mattson, M.P.; Aksenova, M.; Harris, M.; Wu, J.F.; Floyd, R.A.; Butterfield, D.A. A model for beta-amyloid aggregation and neurotoxicity based on free radical generation by the peptide: Relevance to Alzheimer disease. *Proc. Natl. Acad. Sci. USA* **1994**, *91*, 3270–3274. [CrossRef]
36. Hayden, E.Y.; Teplow, D.B. Amyloid beta-protein oligomers and Alzheimer's disease. *Alzheimer's Res. Ther.* **2013**, *5*, 60. [CrossRef] [PubMed]
37. Grant, M.K.O.; Handoko, M.; Rozga, M.; Brinkmalm, G.; Portelius, E.; Blennow, K.; Ashe, K.H.; Zahs, K.R.; Liu, P. Human cerebrospinal fluid 6E10-immunoreactive protein species contain amyloid precursor protein fragments. *PLoS ONE* **2019**, *14*, e0212815. [CrossRef] [PubMed]
38. Janus, C.; Flores, A.Y.; Xu, G.; Borchelt, D.R. Behavioral abnormalities in APPSwe/PS1dE9 mouse model of AD-like pathology: Comparative analysis across multiple behavioral domains. *Neurobiol. Aging* **2015**, *36*, 2519–2532. [CrossRef] [PubMed]
39. Nation, D.A.; Sweeney, M.D.; Montagne, A.; Sagare, A.P.; D'Orazio, L.M.; Pachicano, M.; Sepehrband, F.; Nelson, A.R.; Buennagel, D.P.; Harrington, M.G.; et al. Blood-brain barrier breakdown is an early biomarker of human cognitive dysfunction. *Nat. Med.* **2019**, *25*, 270–276. [CrossRef] [PubMed]
40. Hussain, B.; Fang, C.; Chang, J. Blood-Brain Barrier Breakdown: An Emerging Biomarker of Cognitive Impairment in Normal Aging and Dementia. *Front. Neurosci.* **2021**, *15*, 688090. [CrossRef]
41. He, P.; Zhong, Z.; Lindholm, K.; Berning, L.; Lee, W.; Lemere, C.; Staufenbiel, M.; Li, R.; Shen, Y. Deletion of tumor necrosis factor death receptor inhibits amyloid beta generation and prevents learning and memory deficits in Alzheimer's mice. *J. Cell Biol.* **2007**, *178*, 829–841. [CrossRef] [PubMed]
42. Paouri, E.; Tzara, O.; Zenelak, S.; Georgopoulos, S. Genetic Deletion of Tumor Necrosis Factor-alpha Attenuates Amyloid-beta Production and Decreases Amyloid Plaque Formation and Glial Response in the 5XFAD Model of Alzheimer's Disease. *J. Alzheimer's Dis.* **2017**, *60*, 165–181. [CrossRef] [PubMed]

43. Yamamoto, M.; Kiyota, T.; Horiba, M.; Buescher, J.L.; Walsh, S.M.; Gendelman, H.E.; Ikezu, T. Interferon-gamma and tumor necrosis factor-alpha regulate amyloid-beta plaque deposition and beta-secretase expression in Swedish mutant APP transgenic mice. *Am. J. Pathol.* **2007**, *170*, 680–692. [CrossRef] [PubMed]
44. Leng, F.; Edison, P. Neuroinflammation and microglial activation in Alzheimer disease: Where do we go from here? *Nat. Rev. Neurol.* **2021**, *17*, 157–172. [CrossRef] [PubMed]
45. Brown, M.R.; Radford, S.E.; Hewitt, E.W. Modulation of beta-Amyloid Fibril Formation in Alzheimer's Disease by Microglia and Infection. *Front. Mol. Neurosci.* **2020**, *13*, 609073. [CrossRef]
46. Kalovyra, N.; Apokotou, O.; Boulekou, S.; Paouri, E.; Boutou, A.; Georgopoulos, S. A 3'UTR modification of the TNF-alpha mouse gene increases peripheral TNF-alpha and modulates the Alzheimer-like phenotype in 5XFAD mice. *Sci. Rep.* **2020**, *10*, 1–15. [CrossRef]
47. Koenigsnecht-Talboo, J.; Landreth, G.E. Microglial phagocytosis induced by fibrillar beta-amyloid and IgGs are differentially regulated by proinflammatory cytokines. *J. Neurosci.* **2005**, *25*, 8240–8249. [CrossRef]
48. Couch, J.A.; Yu, Y.J.; Zhang, Y.; Tarrant, J.M.; Fuji, R.N.; Meilandt, W.J.; Solanoy, H.; Tong, R.K.; Hoyte, K.; Luk, W.; et al. Addressing Safety Liabilities of TfR Bispecific Antibodies That Cross the Blood-Brain Barrier. *Sci. Transl. Med.* **2013**, *5*, 183ra57. [CrossRef]
49. Van Putten, L.M. The life span of red cells in the rat and the mouse as determined by labeling with DFP32 in vivo. *Blood* **1958**, *13*, 789–794. [CrossRef]
50. Goodman, J.W.; Smith, L.H. Erythrocyte life span in normal mice and in radiation bone marrow chimeras. *Am. J. Physiol. Content* **1961**, *200*, 764–770. [CrossRef]
51. Sun, J.; Yang, J.; Whitman, K.; Zhu, C.; Cribbs, D.H.; Boado, R.J.; Pardridge, W.M.; Sumbria, R.K. Hematologic safety of chronic brain-penetrating erythropoietin dosing in APP/PS1 mice. *Alzheimer's Dement.* **2019**, *5*, 627–636. [CrossRef] [PubMed]
52. Yamamoto, R.; Yoden, E.; Tanaka, N.; Kinoshita, M.; Imakiire, A.; Hirato, T.; Minami, K. Nonclinical safety evaluation of pabinafusp alfa, an anti-human transferrin receptor antibody and iduronate-2-sulfatase fusion protein, for the treatment of neuronopathic mucopolysaccharidosis type II. *Mol. Genet. Metab. Rep.* **2021**, *27*, 100758. [CrossRef]
53. Kawabata, H.; Germain, R.S.; Ikezoe, T.; Tong, X.; Green, E.M.; Gombart, A.F.; Koefler, H.P. Regulation of expression of murine transferrin receptor 2. *Blood* **2001**, *98*, 1949–1954. [CrossRef] [PubMed]
54. Johnsen, K.B.; Bak, M.; Melander, F.; Thomsen, M.S.; Burkhart, A.; Kempen, P.J.; Andresen, T.L.; Moos, T. Modulating the antibody density changes the uptake and transport at the blood-brain barrier of both transferrin receptor-targeted gold nanoparticles and liposomal cargo. *J. Control. Release* **2019**, *295*, 237–249. [CrossRef] [PubMed]
55. Johnsen, K.B.; Burkhart, A.; Melander, F.; Kempen, P.J.; Vejlebo, J.B.; Siupka, P.; Nielsen, M.S.; Andresen, T.L.; Moos, T. Targeting transferrin receptors at the blood-brain barrier improves the uptake of immunoliposomes and subsequent cargo transport into the brain parenchyma. *Sci. Rep.* **2017**, *7*, 1–13.
56. Boado, R.J.; Zhou, Q.-H.; Lu, J.Z.; Hui, E.K.-W.; Pardridge, W.M. Pharmacokinetics and Brain Uptake of a Genetically Engineered Bifunctional Fusion Antibody Targeting the Mouse Transferrin Receptor. *Mol. Pharm.* **2009**, *7*, 237–244. [CrossRef]
57. Lochocki, B.; Boon, B.D.C.; Verheul, S.R.; Zada, L.; Hoozemans, J.J.M.; Ariese, F.; de Boer, J.F. Multimodal, label-free fluorescence and Raman imaging of amyloid deposits in snap-frozen Alzheimer's disease human brain tissue. *Commun. Biol.* **2021**, *4*, 474. [CrossRef]
58. Gao, Y.; Liu, Q.; Xu, L.; Zheng, N.; He, X.; Xu, F. Imaging and Spectral Characteristics of Amyloid Plaque Autofluorescence in Brain Slices from the APP/PS1 Mouse Model of Alzheimer's Disease. *Neurosci. Bull.* **2019**, *35*, 1126–1137. [CrossRef]

## Article

# Reduction of $\alpha$ SYN Pathology in a Mouse Model of PD Using a Brain-Penetrating Bispecific Antibody

Sahar Roshanbin <sup>1,\*</sup>, Ulrika Julku <sup>1</sup>, Mengfei Xiong <sup>1</sup>, Jonas Eriksson <sup>2,3</sup>, Eliezer Masliah <sup>4</sup>, Greta Hultqvist <sup>5</sup>, Joakim Bergström <sup>1</sup>, Martin Ingelsson <sup>1,6,7</sup>, Stina Syvänen <sup>1</sup> and Dag Sehlin <sup>1,\*</sup>

<sup>1</sup> Department of Public Health and Caring Sciences, Uppsala University, 751 85 Uppsala, Sweden; ulrika.julku@pubcare.uu.se (U.J.); mengfei.xiong@pubcare.uu.se (M.X.); joakim.bergstrom@pubcare.uu.se (J.B.); martin.ingelsson@pubcare.uu.se (M.I.); stina.syvanen@pubcare.uu.se (S.S.)

<sup>2</sup> Department of Medicinal Chemistry, Uppsala University, 751 23 Uppsala, Sweden; jonas.p.eriksson@akademiska.se

<sup>3</sup> PET Centre, Uppsala University Hospital, 751 85 Uppsala, Sweden

<sup>4</sup> Division of Neuroscience and Laboratory of Neurogenetics, NIA-NIH, Bethesda, MD 20814, USA; eliezer.masliah@nih.gov

<sup>5</sup> Department of Pharmacy, Uppsala University, 752 37 Uppsala, Sweden; greta.hultqvist@farmaci.uu.se

<sup>6</sup> Krembil Brain Institute, University Health Network, Toronto, ON M5T 1M8, Canada

<sup>7</sup> Department of Medicine and Tanz Centre for Research in Neurodegenerative Diseases, University of Toronto, Toronto, ON M5T 1M8, Canada

\* Correspondence: sahar.roshanbin@pubcare.uu.se (S.R.); dag.sehlin@pubcare.uu.se (D.S.)

**Citation:** Roshanbin, S.; Julku, U.; Xiong, M.; Eriksson, J.; Masliah, E.; Hultqvist, G.; Bergström, J.; Ingelsson, M.; Syvänen, S.; Sehlin, D. Reduction of  $\alpha$ SYN Pathology in a Mouse Model of PD Using a Brain-Penetrating Bispecific Antibody. *Pharmaceutics* **2022**, *14*, 1412. <https://doi.org/10.3390/pharmaceutics14071412>

Academic Editors: William M. Pardridge and Patrick T. Ronaldson

Received: 25 May 2022

Accepted: 1 July 2022

Published: 5 July 2022

**Publisher's Note:** MDPI stays neutral with regard to jurisdictional claims in published maps and institutional affiliations.



**Copyright:** © 2022 by the authors. Licensee MDPI, Basel, Switzerland. This article is an open access article distributed under the terms and conditions of the Creative Commons Attribution (CC BY) license (<https://creativecommons.org/licenses/by/4.0/>).

**Abstract:** Immunotherapy targeting aggregated alpha-synuclein ( $\alpha$ SYN) is a promising approach for the treatment of Parkinson's disease. However, brain penetration of antibodies is hampered by their large size. Here, RmAbSynO2-scFv8D3, a modified bispecific antibody that targets aggregated  $\alpha$ SYN and binds to the transferrin receptor for facilitated brain uptake, was investigated to treat  $\alpha$ SYN pathology in transgenic mice. Ex vivo analyses of the blood and brain distribution of RmAbSynO2-scFv8D3 and the unmodified variant RmAbSynO2, as well as in vivo analyses with microdialysis and PET, confirmed fast and efficient brain uptake of the bispecific format. In addition, intravenous administration was shown to be superior to intraperitoneal injections in terms of brain uptake and distribution. Next, aged female  $\alpha$ SYN transgenic mice (L61) were administered either RmAbSynO2-scFv8D3, RmAbSynO2, or PBS intravenously three times over five days. Levels of TBS-T soluble aggregated  $\alpha$ SYN in the brain following treatment with RmAbSynO2-scFv8D3 were decreased in the cortex and midbrain compared to RmAbSynO2 or PBS controls. Taken together, our results indicate that facilitated brain uptake of  $\alpha$ SYN antibodies can improve treatment of  $\alpha$ SYN pathology.

**Keywords:** bispecific antibody; blood-brain barrier (BBB); alpha-synuclein ( $\alpha$ SYN); Parkinson's disease (PD); immunotherapy; monoclonal antibody; transferrin receptor (TfR); receptor-mediated transcytosis (RMT)

## 1. Introduction

The number of patients suffering from neurodegenerative diseases will increase due to an aging population in combination with a lack of efficient disease-modifying treatments available for brain disorders. Immunotherapy directed against intrabrain targets remains both a promising and challenging approach to treating neurodegeneration. Parkinson's disease (PD) is a progressive, degenerative neurological disorder characterized by the presence of pathological, aggregated forms of the protein alpha-synuclein ( $\alpha$ SYN), eventually depositing as insoluble, intracellular Lewy bodies (LB), and ultimately, neuronal death. Since the discovery of PD-causing point mutations in the SNCA gene encoding  $\alpha$ SYN [1,2] in combination with  $\alpha$ SYN being identified as one of the main components of LBs [3], a large body of evidence points toward  $\alpha$ SYN as a key target for therapeutic interventions.

However, current treatment options for PD are limited to symptomatic treatment, such as restoration and correction of dopaminergic and cholinergic deficits [4,5]. A number of preclinical studies have demonstrated the effectiveness of both active and passive immunotherapy aimed at the pathological forms of  $\alpha$ SYN for halting the disease progression [6–9]. Despite the development of clinical therapeutic antibodies targeting  $\alpha$ SYN thus far showing good safety and tolerability [10,11], the efficacy of immunotherapies in meeting their clinical endpoints has been limited. The underlying reasons behind these results are, in all probability, multifactorial. One important aspect to consider is the form of  $\alpha$ SYN to target. Aggregated  $\alpha$ SYN has been shown to exhibit acquired toxicity as well as to cause a potential loss of function of normal  $\alpha$ SYN [12,13] by altering neurophysiological functions, including impairment of macroautophagy [14] and dysfunction of mitochondria and endoplasmic reticulum [15–18]. Therefore, conformation selective antibodies that preferentially bind to pathological  $\alpha$ SYN over the monomeric, physiologically relevant form are probably necessary for successful  $\alpha$ SYN immunotherapy. We have previously demonstrated the reduction of  $\alpha$ SYN aggregates in the central nervous system (CNS) of (Thy-1)-h[A30P] transgenic mice following systemic treatment with the murine aggregate-selective antibody mAb47 [7]. In addition, as monomeric  $\alpha$ SYN is abundant in blood, it is likely that therapeutic antibodies that bind  $\alpha$ SYN monomers will be sequestered in blood and thereby be prevented from engaging with pathological protein forms in the brain. Another major obstacle is the access of the antibody to the pathological, intrabrain  $\alpha$ SYN. Monoclonal antibodies are large molecules with restricted brain distribution. One of the main challenges lies within the physical, biochemical, and immune barriers of the CNS comprised of the blood-brain barrier (BBB). The architecture of the BBB is highly dynamic and complex, consisting of specialized brain microvascular endothelial cells (BMECs). The BMECs form tight junctions that regulate paracellular transport, whereas transcellular transport is tightly regulated by transport systems consisting of active transporters, pumps, and receptors [19–21]. Restricted direct access to pathology as a major obstacle to treatment efficacy in brain disorders is further strengthened by the fact that many peripheral diseases have been subject to successful immunotherapy [22,23].

Despite the restrictive nature of the BBB, it is the largest brain-blood interface and thus a highly relevant transport route for drug delivery as it allows access to the entire brain volume, which is advantageous when targeting whole-brain disorders such as PD. As the main purpose of the BBB is to maintain the microenvironment in the brain, a non-invasive approach to circumvent the BBB is preferred. One such approach is represented by receptor-mediated transport (RMT). Earlier studies with  $\alpha$ SYN targeting single-chain antibodies fused with an LDL receptor-binding domain for increased brain penetration have shown reduced  $\alpha$ SYN pathology and amelioration of functional deficits in the Line D and L61  $\alpha$ SYN pathology models [24,25]. The most studied transporter for this purpose is the transferrin receptor (TfR) which is highly expressed in the endothelial cells of the BBB and is involved in the transport of transferrin-bound iron into the brain [26–28]. Antibodies can be engineered into bispecific formats, with an additional binding moiety targeting the TfR to enable RMT. Active transport across the BBB will enhance both the amount and the spatial distribution of antibodies, likely expanding the therapeutic potential of brain immunotherapy [29–31]. Therefore, active transport is of particular importance when targeting intrabrain  $\alpha$ SYN, where the pool of accessible pathology is scarcer in comparison with other proteinopathies such as Alzheimer's disease (AD).

We have previously expressed several  $\alpha$ SYN antibodies in a bispecific format with a single chain variable fragment of the TfR1 antibody 8D3 [32] targeting the TfR as well as aggregated forms of  $\alpha$ SYN, resulting in a dramatically increased brain uptake for in vivo  $\alpha$ SYN detection in  $\alpha$ SYN deposition model mice [33]. Here, we have used one of these antibodies, RmAbSynO2-scFv8D3, for targeting the extracellular pool of aggregated  $\alpha$ SYN in a short-term treatment study in the L61  $\alpha$ SYN mouse model, following the characterization of biochemical and pharmacokinetic properties of the antibody.

## 2. Materials and Methods

### 2.1. Animals

Transgenic L61 mice, overexpressing wild-type (WT) human  $\alpha$ SYN under the Thy-1 promoter [34–36], were bred in-house by crossing B6D2F1 (C57Bl6/DBA2) with heterozygous L61 females on a B6D2F1 background. L61 mice display an age-dependent increase in  $\alpha$ SYN pathology, with high levels of oligomeric, aggregated  $\alpha$ SYN detected already at 3 months of age [37]. Due to random X-inactivation, insertion of the transgene on the X-chromosome manifests as notable differences in pathology levels and phenotype between males and females. For the pharmacokinetic and microdialysis studies of intravenous (i.v.) and intraperitoneal (i.p.) injections, as well as in the positron emission tomography (PET) study, female WT B6D2F1 mice were used,  $n = 4$  for each time point and antibody ( $n = 2$  for each administration route),  $n = 2$  for PET. For the immunotherapy study, female L61 mice were used, with  $n = 8$  for each treatment group. All mice were 14–16 months of age and randomized across treatments by litter and date of birth. Animals were housed in groups of a maximum of five mice in open cages on a 12:12 h constant light cycle in a temperature- and humidity-controlled room and were given food and water ad libitum. All experiments were approved by the Uppsala Animal Ethics Committee (approval 5.8.18-13350/2017, 5.8.18-12230/2019, and 5.8.18-20401/2020) and the use of mice was conducted in accordance with the EU directive 2010/63/EU for animal experiments.

### 2.2. Antibody Design and Expression

The antibodies were based on RmAbSynO2 [38], with a high affinity for large  $\alpha$ SYN oligomers and fibrils. RmAbSynO2-scFv8D3 targeting  $\alpha$ SYN and mTfR was generated by the fusion of a single-chain variable fragment of the mTfR binding antibody 8D3 [32] to the C-terminal end of the IgG light chain with a short linker as previously described [33,39]. An IgG2C backbone was chosen to stimulate interaction with microglia. In short, the bispecific antibody was recombinantly generated in-house according to a previously published protocol [33] by transient transfection of Expi293 cells with pcDNA3.4 vectors carrying the sequence of either the heavy or the light chain of the antibody with polyethyleneimine as the transfection reagent and valproic acid as the cell cycle inhibitor. The unmodified RmAbSynO2 IgG was generated in a similar way for comparison. For further details on the antibody binding characteristics, see supplementary information.

### 2.3. Radiolabeling

The antibodies were labeled with iodine-125 ( $^{125}\text{I}$ ) for ex vivo measurement of the brain and blood distribution in the pharmacokinetics, microdialysis, and treatment studies. Labeling was performed using direct iodination with Chloramine-T [40], as previously described [33]. Molar activity after labeling was  $14.6 \pm 2.8$  MBq/nmol for [ $^{125}\text{I}$ ]RmAbSynO2-scFv8D3 and  $12.9 \pm 2.1$  MBq/nmol for [ $^{125}\text{I}$ ]RmAbSynO2. The radiolabeling was always performed less than 2 h before the experiments. For PET imaging of brain distribution, antibodies were labeled with fluorine-18 ( $^{18}\text{F}$ ), using the inverse electron demand Diels-Alder (IEDDA) click reaction, as previously described [41]. In short, antibodies were chemically functionalized with transcyclooctene (TCO) and then reacted with an  $^{18}\text{F}$ -labeled tetrazine in PBS. Molar activity after labeling was 116 MBq/nmol for [ $^{18}\text{F}$ ]RmAbSynO2-scFv8D3 and 96 MBq/nmol for [ $^{18}\text{F}$ ]RmAbSynO2. As a quality control, radiolabeled antibodies were analyzed for binding to  $\alpha$ SYN and TfR with ELISA in comparison with non-labeled antibodies, as previously described [33].

### 2.4. In Vivo Experiments and Ex Vivo Measurements

For the pharmacokinetic studies, mice were injected with [ $^{125}\text{I}$ ]RmAbSynO2-scFv8D3 (1 mg/kg,  $0.35 \pm 0.08$  MBq) or [ $^{125}\text{I}$ ]RmAbSynO2 (1 mg/kg,  $0.39 \pm 0.09$  MBq), either i.p. ( $n = 2$ /time point) or i.v. ( $n = 2$ /time point) and sacrificed at 30 min, 2 h, 4 h, or 24 h post-injection. Tail-vein blood samples (8  $\mu\text{L}$ ) were obtained at 30 min and 1 h post-injection from the 2 h and 4 h animals, with an additional sample at 2 h from the 4 h animals. From

the 24 h animals, blood samples were obtained 1 h, 4 h, and 6 h post-injection. All mice were subject to a terminal blood sample at the time of euthanasia prior to transcardial perfusion with 0.9% NaCl, followed by isolation, subdissection, and flash-freezing of the brain on dry ice. Radioactivity in the brain and blood were measured using a  $\gamma$ -counter (1480 Wizard<sup>TM</sup>; Wallac Oy, Turku, Finland) and expressed as a percentage injected dose/g brain tissue normalized to body weight (%ID/g brain/BW and %ID/g blood/BW). Antibody exposure in blood was expressed area under the curve (AUC<sub>blood</sub>).

For the treatment study, L61 mice were i.v. injected with three doses of 10 mg/kg of either RmAbSynO2-scFv8D3 or RmAbSynO2 ( $n = 8$ /group). Each dose was supplemented with the radiolabeled antibody of the same type, corresponding to 0.05 mg/kg, to be able to follow the treatment dose pharmacokinetics throughout the study,  $0.24 \pm 0.09$  MBq and  $0.29 \pm 0.065$  MBq of [<sup>125</sup>I]RmAbSynO2-scFv8D3 and [<sup>125</sup>I]RmAbSynO2 respectively. Antibody injections were performed on day 1, 2, and 4, followed by euthanasia by transcardial perfusion with 0.9% NaCl on day 5, 24 h after the last injection. Tail-vein blood samples (8  $\mu$ L) were obtained 1 h, 4 h, and 24 h after each injection, and a terminal blood sample was collected prior to euthanasia. Brain isolation and radioactivity measurements were performed as above.

### 2.5. Ex Vivo Autoradiography

Frozen 20  $\mu$ m sagittal sections were prepared with a cryostat (CM1850, Leica Biosystems, Mölndal, Sweden) and mounted on Superfrost Plus glass slides (Menzel Gläser, Braunschweig, Germany). Dried sections were exposed to a phosphor screen (MS, Multi-Sensitive, PerkinElmer, Downers Grove, IL, USA) for seven days and scanned with Typhoon PhosphorImager (GE Healthcare). The radioactive signal was converted to a false-color scale (Royal) in ImageJ (NIH, Bethesda, MD, USA).

### 2.6. Microdialysis

A guide cannula (AT12.8.iC, AgnTho's, Lidingö, Sweden) was inserted into the left striatum (coordinates A/P + 0.6, M/L + 1.8 from bregma, and D/V – 2.7 from dura) under isoflurane anesthesia (induction 4% and maintenance 2%; Isofluran Baxter, Baxter S.A., Lessines, Belgium) with stereotaxic surgery. The cannula was attached to the skull with two anchor screws (1  $\times$  2 mm, AgnTho's) and dental cement (Dentalon plus, Heraeus Kulzer GmbH, Hanau, Germany). Buprenorphine (Bupaq vet, Richter Pharma AG, Wels, Austria) and carprofen (Norocarp vet 50 mg/mL, Norbrook Laboratories Ltd., Newry, UK) were administered subcutaneously for post-operative pain and lidocaine (Xylocaine, Aspen Pharma Trading Ltd., Dublin, Ireland) were used as a local anesthetic. Mice were allowed to recover for 24–48 h before the microdialysis.

Prior to the microdialysis, fluorinated ethylene propylene inlet tubing (FEP PTFE tubing, ID 0.12 mm, AgnTho's), outlet tubing (Tygon LMT-55, ID 0.13 mm, Ismatec, Cole-Parmer GmbH, Wertheim, Germany), and the probe (AT12.8.1, 1 mm PE membrane, 3 MDa cut-off, AgnTho's) were coated with 5% polyethyleneimine (PEI MW ~2000, Sigma Aldrich, Saint Louis, MO, USA) 0.5  $\mu$ L/min for 16 h, and then washed with water 10  $\mu$ L/min for 10 min following 1  $\mu$ L/min for 8 h to prevent binding of the radiolabeled antibody in the tubing and probe and to improve probe recovery during the microdialysis as described in [42].

The probe was connected to a push-and-pull microdialysis system containing a CMA 402 Microdialysis syringe pump (CMA Microdialysis AB) and a Reglo ICC Digital Peristaltic pump (CMA Microdialysis AB) and perfused at 0.5  $\mu$ L/min with Ringer solution containing 0.15% BSA. The mice were quickly anesthetized with isoflurane and injected i.p. or i.v. with [<sup>125</sup>I]RmAbSynO2-scFv8D3 (1 mg/kg;  $4.97 \pm 0.61$  MBq). The probe was inserted into the brain right after the antibody injection. Mice were kept under isoflurane anesthesia (1.2–2%) on a heating pad during the microdialysis. The dialysate was collected 8  $\times$  30 min post-injection. One mouse from each group died after 2–2.5 h after starting the microdialysis; thus, samples were collected only until the time of death from these two mice. The volume

of the dialysate was measured by weighing the dialysate, and the peristaltic pump flow rate was adjusted if needed to reach fluid recovery of 97–103%, as described in [43]. Mice were perfused transcardially with saline after the microdialysis and the brain was dissected for the biodistribution measurement. Radioactivity in the dialysate was measured using a  $\gamma$ -counter (1480 Wizard<sup>TM</sup>; Wallac Oy).

### 2.7. PET Imaging

For PET imaging, 14-month-old WT mice ( $n = 2$ ) were anesthetized with sevoflurane, placed in a preheated bed in the PET scanner (Mediso nanoScan system) and injected with a bolus i.v. injection of 5.8 MBq [<sup>18</sup>F]RmAbSynO2-scFv8D3 or 5.9 MBq [<sup>18</sup>F]RmAbSynO2 at the start of PET acquisition. Mice were kept under mild anesthesia and scanned for 120 min with a field of view of 9.8 cm, followed by a CT examination for 5 min. Dynamic PET data were obtained by reconstruction with a Tera-Tomo 3-dimensional algorithm (Mediso) with 4 iterations and 6 subsets. CT raw files were reconstructed using filtered back projection (FBP). All subsequent processing of the PET and CT images was performed with imaging software Amide 1.0.4 [44].

### 2.8. $\alpha$ SYN Extraction

Sequential extraction of  $\alpha$ SYN from brain tissue was performed as previously described [37]. In short, flash-frozen brain tissue samples were homogenized with a PreCellys Evolution (VWR, Stockholm, Sweden) in ice-cold Tris-buffered saline (TBS) supplemented with cComplete protease inhibitor (Roche, Mannheim, Germany) and PhosStop phosphatase inhibitor (Sigma, Gillingham, UK) at a 1:10 *w/v* ratio. Next,  $\alpha$ SYN species of decreasing solubility were extracted with TBS with 0.5% Triton X-100 (TBS-T) at 16,000 $\times$  *g* and 70% formic acid (FA) at 100,000 $\times$  *g*.

### 2.9. ELISA

Levels of different  $\alpha$ SYN species and soluble TREM2 (sTREM2) were measured as previously described [37,45] with sandwich enzyme-linked immunosorbent assay (ELISA), using antibodies and enzyme conjugates as summarized in Table 1. For all  $\alpha$ SYN ELISAs, half-area 96-well plates were coated overnight with coating antibody at 4 °C. The following day, plates were decanted and blocked for 2 h with 1% BSA at room temperature (RT) and then incubated with brain extracts diluted in 0.1% BSA/0.05 Tween-20 overnight at 4 °C. Plates were incubated with the detection antibody for 1 h, followed by the secondary antibody for 1 h. The sTREM2 ELISA was performed in a similar manner as described above, except that the incubation time for blocking and detecting antibodies was 2 h at RT. For all ELISAs, signals were developed with K-blue Aqueous TMS substrate (Neogen Corporation, Lansing, MI, USA), neutralized with 1 M sulfuric acid, and read at 450 nm on Tecan Infinite Pro (Tecan Group Ltd., Männedorf, Switzerland).

**Table 1.** The concentration of antibodies and enzyme conjugates used in sandwich ELISAs.

Assay	Oligomeric $\alpha$ SYN	Total $\alpha$ SYN	sTREM2
Coat	MJFR-14-6-4-2 (Abcam, ab209538) 1 $\mu$ g/mL	MJFR1 (Abcam, ab138501) 0.25 $\mu$ g/mL	AF1729 (R&D, AF1729), 0.5 $\mu$ g/mL
	MJFR-14-6-4-2 biotinylated (Abcam, ab209538) 1 $\mu$ g/mL	Syn-1 (BD Biosciences, 610787) 0.35 $\mu$ g/mL	BAF1729 (R&D, BAF1729), 0.5 $\mu$ g/mL
Detection	SA-HRP (Mabtech AB, 3310-9-1000) 1:2000	anti-mouse IgG F (ab') <sub>2</sub> (Jackson Immuno Research, 115-036-006) 0.4 $\mu$ g/mL	SA-HRP (Mabtech AB, 3310-9-1000) 1:2000



### 2.10. Immunohistochemistry

Immunohistochemistry was performed as previously described [37], with the exception that fresh-frozen cryosections were used. In short, 20  $\mu\text{m}$  sections were fixed with 4% formaldehyde, followed by heat-induced antigen retrieval in 25 mM citrate buffer (pH 6.0) prior to permeabilization with 0.4% PBS-Triton X-100 for 20 min and blocking in 5% normal goat serum for 1 h in RT. Next, sections were incubated overnight at 4 °C with anti- $\alpha$ -syn phospho-Ser129 EP1536Y (pSer129, 1:250, Abcam, Cambridge, UK, ab51253) for detection of pathological  $\alpha$ SYN phosphorylated on serine 129 and inflammation markers anti-Iba1 (1:500, WAKO Chemicals, Richmond, VA, USA, 019-19,741) or anti-TREM2 (1:50, R&D Systems, AF1729). The next day, sections were incubated with biotinylated goat anti-rabbit IgG (H + L, 1:250, Vector) for detection of pSer129 and Iba1 or biotinylated goat anti-sheep IgG (H + L, 1:250, Vector) for 30 min, followed by a 30 min incubation with horseradish peroxidase-conjugated streptavidin (1:500, Mabtech AB, Stockholm, Sweden, 3310-9-1000). Sections were developed with NovaRED Chromogen Peroxidase Substrate kit (Vector, SK-4800) according to the manufacturer's instructions and counterstained with hematoxylin. Lastly, stained sections were washed thoroughly in dH<sub>2</sub>O, dehydrated and fixed in an ethanol gradient (70–100%) and xylene, mounted with Pertex (Histolab, Gothenburg, Sweden), and left to dry overnight. Sections were washed with PBS between each step except for between blocking and incubation in the primary antibody.

Images were acquired at 4 $\times$  and 60 $\times$  magnification with Nikon Eclipse 80i microscope and NIS-Elements BR 4. 20.00 software.

### 2.11. Statistical Analyses

All statistical calculations and analyses were made in Prism 8 (GraphPad Software, Inc. La Jolla, CA, USA). Results are presented as mean  $\pm$  standard deviation (SD) unless otherwise stated. The levels of [<sup>125</sup>I]RmAbSynO2-scFv8D3 in interstitial fluid (ISF) dialysate were analyzed with the mixed-effects model (REML) for repeated measurements. Brain levels of antibodies upon the termination of the therapy study were analyzed by an unpaired t-test. Brain levels of  $\alpha$ SYN and TREM2 were analyzed with a one-way analysis of variance (ANOVA) followed by Sidak's multiple comparison test.

## 3. Results

### 3.1. Increased Brain Uptake following Intravenous Injections of RmAbSynO2-scFv8D3

To investigate the binding properties of the recombinantly expressed RmAbSynO2-scFv8D3 and RmAbSynO2 (Figure 1A), an inhibition ELISA was performed, indicating a high selectivity for  $\alpha$ SYN aggregates (oligomers and fibrils) over monomers and a high degree of similarity between the two antibody formats (Figure S1A). In addition, the affinity to  $\alpha$ SYN oligomers and mTfR was not altered after radiolabeling, as validated with ELISA (Figure S1B). Antibody administration can be performed through different routes. While intraperitoneal (i.p.) administration is easier to perform, intravenous (i.v.) injections may result in better bioavailability. To investigate the optimal delivery route for a treatment study, the brain and blood pharmacokinetics of [<sup>125</sup>I]RmAbSynO2-scFv8D3 and [<sup>125</sup>I]RmAbSynO2 were evaluated after 1 mg/kg i.v. and i.p. injections in WT mice.

The blood pharmacokinetic profiles of the bispecific and the unmodified antibody displayed similar differences between administration routes. While i.v. administration was characterized by high antibody blood concentration immediately after injection, followed by a gradual decline, i.p. administration was initially low with the highest antibody concentration 4–6 h after injection, followed by a gradual decline. As expected, due to its interaction with peripheral TfR, the overall exposure for RmAbSynO2-scFv8D3 (Figure 1B) was lower compared to RmAbSynO2 (Figure 1C). The AUC<sub>blood</sub> of RmAbSynO2-scFv8D3 was 3393 and 3036 for i.v. and i.p., respectively, while the AUC<sub>blood</sub> of RmAbSynO2 was 13,823 and 10,840 for i.v. and i.p. administration, respectively. When comparing brain concentrations following i.v. and i.p. administration of the two antibodies, it was evident that i.p. administration reduced brain concentrations compared to i.v. injections at early

time points, i.e., at 30 min, 2 h, and 4 h post-injection (Figure 1D,E). Thus, i.v. injection resulted in substantially higher total brain exposure. At the late time point, 24 h post-injection, brain concentrations were similar after i.p. and i.v. administration. At all studied time points, levels of RmAbSynO2-scFv8D3 in the brain, including brain vasculature, were much higher than for RmAbSynO2. The difference between the mono- and bispecific antibody in total brain concentrations after i.v. administration was 50-fold at the 2 h time point. For both antibodies, the total brain uptake for each administration route was similar across different brain regions (Figure S2).

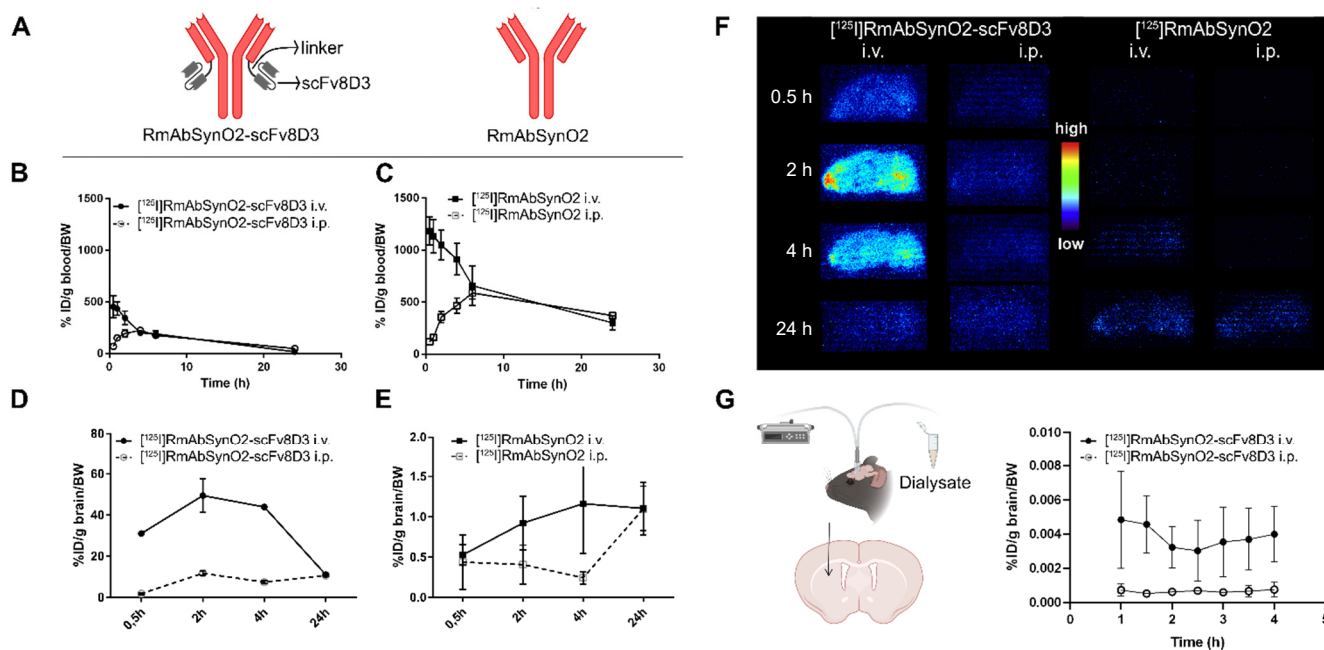


**Figure 1.** (A) Design of the bispecific RmAbSynO2-scFv8D3 with a single chain variable fragment of the mTfR binding antibody 8D3 fused to the C-terminus of the light chain with a short linker and the unmodified RmAbSynO2. (B) Blood exposure of  $[^{125}\text{I}]\text{RmAbSynO2-scFv8D3}$  and (C)  $[^{125}\text{I}]\text{RmAbSynO2}$  following intravenous (i.v.) and intraperitoneal (i.p.) injections. Blood exposure of both antibody formats was higher after i.v. compared to i.p. administration, with  $[^{125}\text{I}]\text{RmAbSynO2-scFv8D3}$  displaying lower total exposure. (D) Total brain concentrations of  $[^{125}\text{I}]\text{RmAbSynO2-scFv8D3}$  and (E)  $[^{125}\text{I}]\text{RmAbSynO2}$  were both higher after i.v. injections in comparison with i.p., with  $[^{125}\text{I}]\text{RmAbSynO2-scFv8D3}$  concentrations peaking 2–4 h post-injection and substantially higher than  $[^{125}\text{I}]\text{RmAbSynO2}$  at all points (NB different y-axis scale). (F) Radioactive signal in 20  $\mu\text{m}$  sagittal brain cryosections from WT mice in (D,E), demonstrating that mice i.v. injected with  $[^{125}\text{I}]\text{RmAbSynO2-scFv8D3}$  showed the highest signals at all time points. (G) Levels of  $[^{125}\text{I}]\text{RmAbSynO2-scFv8D3}$  were higher in interstitial fluid (ISF) dialysate measured by microdialysis in the striatum after i.v. injections compared to after i.p. injections (mean  $\pm$  SEM,  $p = 0.0313$ ,  $n = 4$ /administration route). All blood and brain concentrations are expressed as % injected dose per gram tissue, normalized to bodyweight (%ID/g tissue/BW).

Ex vivo autoradiography on tissue sections prepared from brains isolated at different time points post-injection confirmed the impact of the administration route on brain delivery with higher signals on sections obtained from i.v. injected animals (Figure 1F). Ex vivo measurements and autoradiography give information on the total concentration of antibodies associated with the brain tissue, including vasculature. To obtain further information about the concentration of free antibodies in the extracellular space of the brain, interstitial fluid (ISF) levels of antibodies were measured by microdialysis over a period of 4 h (Figure 1G). This analysis demonstrated that RmAbSynO2-scFv8D3 ISF concentration in the striatum was significantly higher following i.v. injections in comparison with i.p.

( $p = 0.0313$ ). Overall, the i.v. route was determined to be most efficient for brain delivery of RmAbSynO2-scFv8D3 and was therefore used in the subsequent experiments.

For further *in vivo* evaluation of whole-brain uptake and distribution of the two different antibody formats after i.v. administration, RmAbSynO2-scFv8D3 and RmAbSynO2 were  $^{18}\text{F}$ -labeled and visualized with PET imaging in WT mice. During the first 5 min after administration, both antibodies were present at relatively low concentrations in the brain, as compared to surrounding tissues. At 90–120 min post-injection, brain concentration of [ $^{18}\text{F}$ ]RmAbSynO2-scFv8D3 had increased, while [ $^{18}\text{F}$ ]RmAbSynO2 brain concentration had decreased (Figure 2A), seemingly at a similar rate as the concentration in blood indicated that the signal in the brain region largely originated from the blood volume in the brain rather than from the actual brain tissue (Figure 2B). Similar to its faster elimination from blood, [ $^{18}\text{F}$ ]RmAbSynO2-scFv8D3 was low in surrounding tissue.

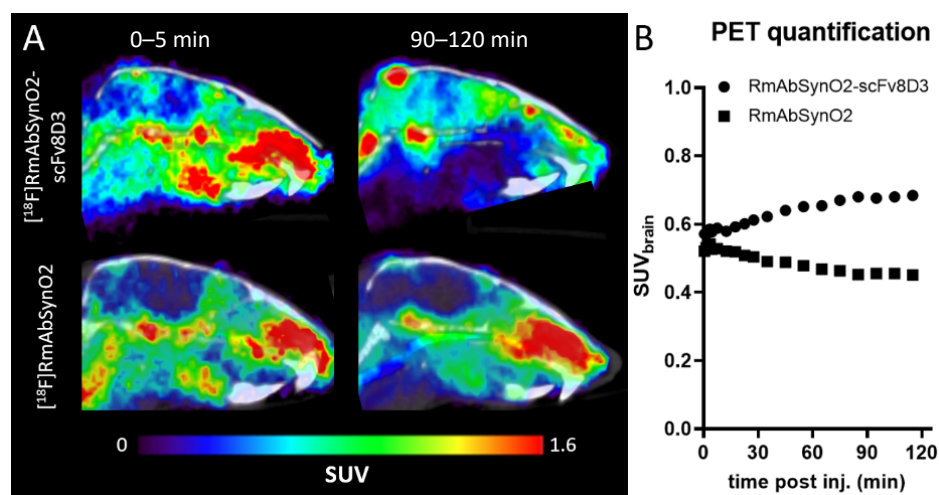


**Figure 2.** (A) Sagittal PET images of WT mice injected with [ $^{18}\text{F}$ ]RmAbSynO2-scFv8D3 (upper;  $n = 1$ ) or [ $^{18}\text{F}$ ]RmAbSynO2 (lower;  $n = 1$ ) at 0–5 min and 90–120 min post-injection. (B) Quantification of brain (whole brain except cerebellum) activity concentration (SUV) from 0–120 min after antibody injection in same animals as (A).

### 3.2. Increased Treatment Efficacy of RmAbSynO2-scFv8D3 Compared to Its Unmodified Variant RmAbSynO2

In a short-term treatment study in female L61 mice, aged mice received three i.v. injections of 10 mg/kg RmAbSynO2-scFv8D3 or RmAbSynO2 or PBS as a control during one week (Figure 3A). This dosing regime was based on the outcome of the brain and blood pharmacokinetics of RmAbSynO2-scFv8D3 and RmAbSynO2. The blood pharmacokinetics, tracked by trace amounts of  $^{125}\text{I}$ -labeled antibody mixed in with each treatment dose, showed similar concentrations in blood following the three injections at 1 h, 4 h, and 24 h post-injection (Figure 3B). Despite the low concentration of [ $^{125}\text{I}$ ]RmAbSynO2-scFv8D3 in the blood, antibody measurements in the brain at study termination showed significantly higher brain tissue concentration of the bispecific antibody compared to the unmodified antibody (Figure 3C) as well as a significantly higher brain-to-blood ratio (Figure 3D) 24 h after the final dose. In accordance with its low blood concentrations, [ $^{125}\text{I}$ ]RmAbSynO2-scFv8D3 was lower than [ $^{125}\text{I}$ ]RmAbSynO2 in all peripheral organs except bone, probably due to interaction with TfR in the bone marrow (Figure S3A). Taken together, this indicates that [ $^{125}\text{I}$ ]RmAbSynO2-scFv8D3 was more efficiently transported into the brain compared to the unmodified format also after repeated injections.

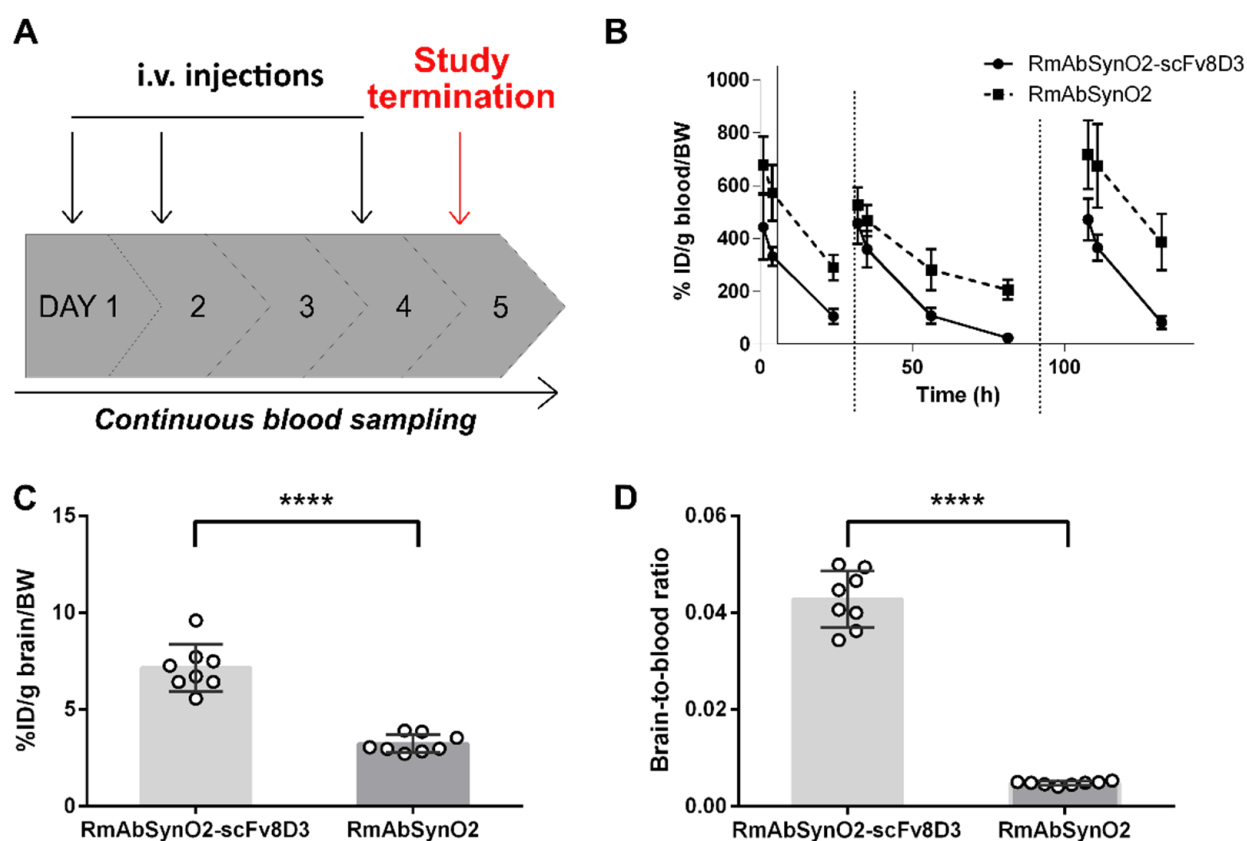


**Figure 3.** (A) Study design of a short-term treatment study in female L61  $\alpha$ SYN mice between 14–16 months of age. Mice were treated with i.v. injections 10 mg/kg RmAbSynO2-scFv8D3 or RmAbSynO2 or PBS ( $n = 8$  per treatment group) on day 1, 3 and 4, with study termination on day 5. (B) Lower blood exposure of [ $^{125}$ I]RmAbSynO2-scFv8D3 compared with [ $^{125}$ I]RmAbSynO2 at 1 h, 4 h and 24 h after each injection. (C) Higher concentration of [ $^{125}$ I]RmAbSynO2-scFv8D3 in the brain compared to [ $^{125}$ I]RmAbSynO2 ( $7.1 \pm 0.43$  and  $3.2 \pm 0.16\%$  ID/g brain/bw, respectively) upon study termination. (D) Higher brain-to-blood ratio of [ $^{125}$ I]RmAbSynO2-scFv8D3 ( $0.043 \pm 0.0021$ ) in comparison with [ $^{125}$ I]RmAbSynO2 ( $0.0048 \pm 0.00013$ ). All values are presented as means  $\pm$  SD and analyzed with an unpaired  $t$ -test. \*\*\*\*  $p < 0.0001$ .

Next, we quantified  $\alpha$ SYN levels in brain homogenates from different regions with two separate sandwich ELISAs, measuring the amount of total  $\alpha$ SYN and oligomeric  $\alpha$ SYN, respectively. While total  $\alpha$ SYN levels in TBS soluble brain extracts did not differ between the treatment groups, RmAbSynO2-scFv8D3 treated mice displayed decreased total  $\alpha$ SYN in cortical TBS-T extract in comparison with the PBS treated group (Figure 4A).

Measurement of  $\alpha$ SYN oligomers, the target of the treatment antibody, indicated increased levels of oligomeric  $\alpha$ SYN in TBS extracts from both cortex and midbrain of RmAbSynO2-scFv8D3 treated animals when compared to PBS treated controls. In contrast,  $\alpha$ SYN oligomer levels in the TBS-T soluble fraction were decreased in RmAbSynO2-scFv8D3 treated mice, in both cortex and midbrain, compared to the PBS group (Figure 4B). No differences in total  $\alpha$ SYN levels were observed in the FA fraction, which represents insoluble  $\alpha$ SYN aggregates (Figure S3B). Likewise, immunohistochemical staining of pSer129, as a measure of pathological  $\alpha$ SYN in different brain regions, did not reveal any differences between the different treatments in comparison with the control group (Figure 4C).

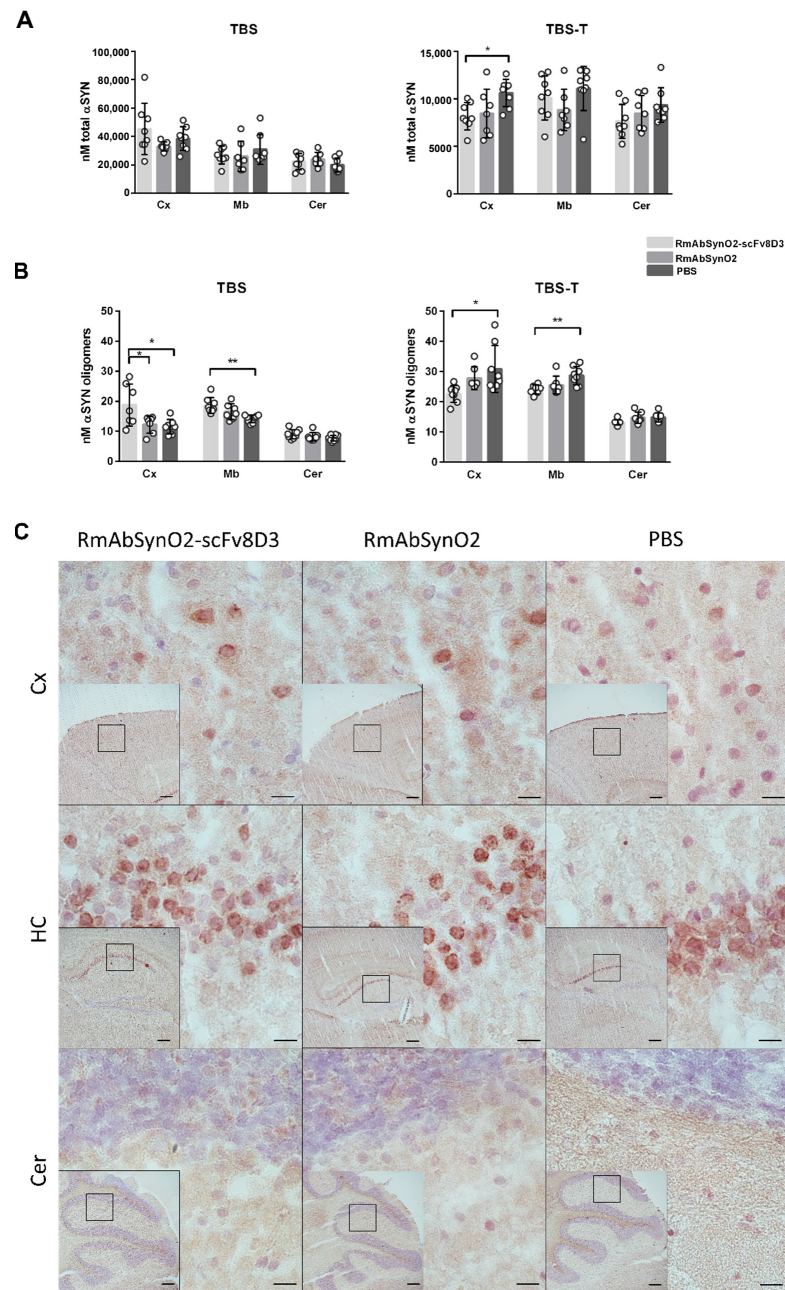


**Figure 4.** (A) Levels of total  $\alpha$ SYN in TBS and TBS-T brain extracts measured with MJFR1/Syn-1 enzyme-linked immunosorbent assay (ELISA) measuring all forms of  $\alpha$ SYN. No differences in total  $\alpha$ SYN in the cortex (Cx), midbrain (Mb), and cerebellum (Cer). Reduced total  $\alpha$ SYN in Cx in the TBS-T fraction in mice treated with RmAbSynO2-scFv8D3 in comparison with the PBS group. (B) Oligomeric  $\alpha$ SYN levels in TBS and TBS-T extracts measured with a homogenous MJFR-14-6-4-2 ELISA. Oligomeric  $\alpha$ SYN in the TBS fraction was increased in Cx in the RmAbSynO2-scFv8D3 group in comparison with both the RmAbSynO2- and the PBS control groups and in Mb compared to the PBS group. Oligomeric  $\alpha$ SYN levels in the TBS-T fraction were instead decreased in Cx and Mb in the RmAbSynO2-scFv8D3 group compared to PBS controls, while Cer  $\alpha$ SYN levels were unchanged. (C) Representative images of 20  $\mu$ m cryosections stained for Iba1 in Cx, hippocampus (HC), and Cer at 60 $\times$  magnification, with 4 $\times$  magnifications embedded with squares representing the magnified area. No differences in immunoreactivity were noted between the treatment groups. All values are presented as means  $\pm$  SD, with a one-way analysis of variance followed by Sidak’s multiple comparison test. \*  $p < 0.05$ , \*\*  $p < 0.005$ . Scale bars: 200  $\mu$ m in embedded images, 10  $\mu$ m in magnified images.

### 3.3. Increased Microglial Response following Antibody Treatment Independent of Format

To investigate the microglial response to treatment with RmAbSynO2-scFv8D3 and RmAbSynO2, levels of soluble TREM2 (sTREM2), a microglial marker, were measured in brain homogenates from treated mice. Compared to PBS injected control mice, levels of sTREM2 were increased after antibody treatment in the TBS fraction of all examined brain regions, independent of the antibody format (Figure 5A). Increased sTREM2 levels were also observed in the TBS-T fraction in the cortex and cerebellum for both antibody formats and in the midbrain for RmAbSynO2-scFv8D3 compared to the PBS-treated animals. Furthermore, increased microglial immunostaining in treated animals was noted on brain sections stained for Iba1, a marker for activated microglia (Figure 5B), as well as for TREM2 (Figure S4). Taken together, this data indicates an increased microglial response to antibody treatment, regardless of the format of the treatment antibody.

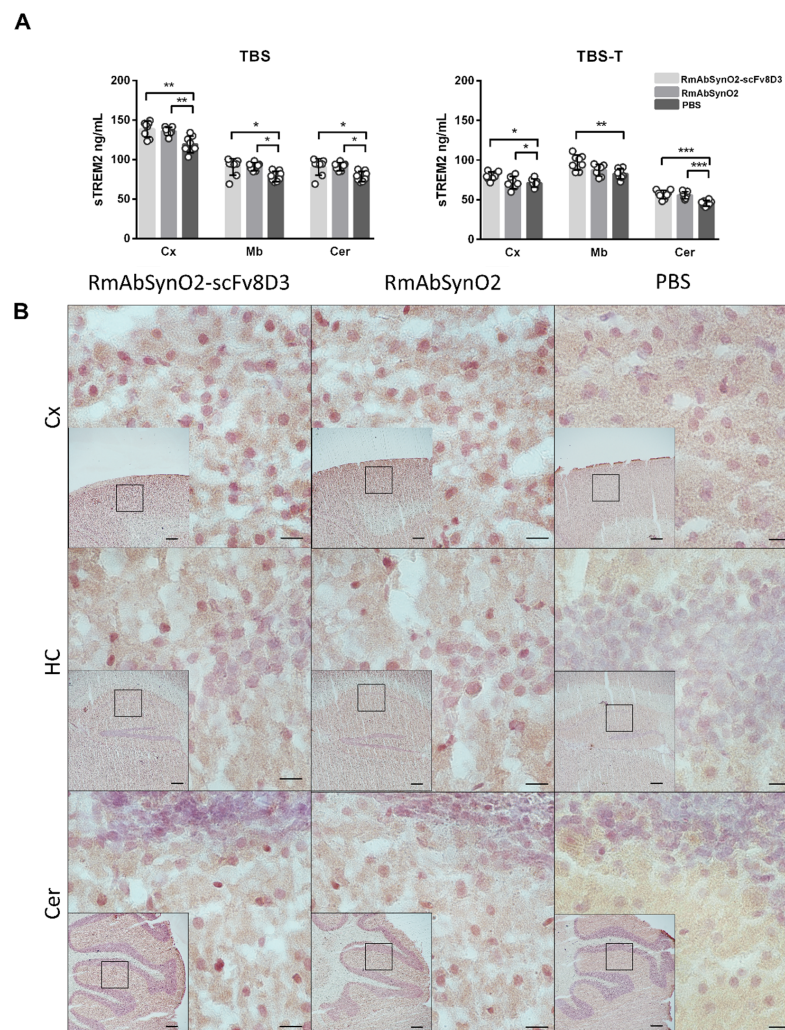


**Figure 5.** (A) ELISA quantification of sTREM2 levels in TBS and TBS-T extracts from the cortex (Cx), midbrain (Mb), and cerebellum (Cer), following treatment with RmAbSynO2-scFv8D3 or RmAbSynO2 in comparison with PBS. Both antibody treatment groups displayed increased sTREM2 levels in both TBS and TBS-T extract of most examined regions. (B) Representative images of 20 µm cryosections stained for Iba1 in Cx, hippocampus (HC), and Cer at 60× magnification, with 4× magnifications embedded with squares representing the magnified area, showing increased immunoreactivity on sections from mice treated with both antibody formats. All values are presented as means ± SD, with a one-way analysis of variance followed by Sidak's multiple comparison test. \*  $p < 0.05$ , \*\*  $p < 0.005$ , \*\*\*  $p < 0.001$ . Scale bars: 200 µm in embedded images, 10 µm in magnified images.

#### 4. Discussion

Passive immunotherapy by targeting  $\alpha$ SYN remains one of the most promising strategies in halting the underlying neuropathological processes in synucleinopathies. Here, we have investigated the brain distribution and therapeutic effects of a brain-penetrating, a bispecific variant of RmAbSynO2, a conformation selective monoclonal antibody targeting aggregated forms of  $\alpha$ SYN [38,46]. Several lines of evidence point toward secreted extracellular  $\alpha$ SYN as the cause of the spreading of pathology in synucleinopathy brains [47–50] by seeding the aggregation of endogenous  $\alpha$ SYN in recipient cells. However, accessibility to parenchymal pathology of conventional antibodies is severely limited by their restricted passage across the BBB.

We have previously demonstrated that a bispecific form of RmAbSynO2, which in addition to  $\alpha$ SYN, also targets the mTfR, is actively transported through the BBB of the entire brain capillary network [33]. As confirmed in the present study, this format dramatically increases antibody brain concentration and mediates its distribution into the whole volume of the brain. We further show that PET scanning can dynamically visualize this process *in vivo*, showing a rapid and gradual increase in whole-brain uptake of [ $^{18}$ F]RmAbSynO2-scFv8D3. Importantly, in parallel with PET, antibody entry into the brain ISF was verified with microdialysis. A high ISF concentration of therapeutic antibody is particularly important for the treatment of synucleinopathies, where the protein pathology is mainly intracellular and only low amounts of extracellular pathological  $\alpha$ SYN are accessible to be targeted by therapeutic antibodies. Conventional antibodies have been hypothesized to enter the brain via perivascular routes, resulting in slow transport and a low degree of diffusion into the brain parenchyma [51], which could explain why  $\alpha$ SYN-directed treatment, in particular, has so far shown a low rate of success. Although antibody brain entry is also limited in AD immunotherapy, A $\beta$  deposits are extracellular and abundant and can therefore be accessed by low antibody concentrations resulting from a slow, gradual leakage into the brain. Indeed, although the clinical outcome is debated, A $\beta$  immunotherapy has demonstrated a robust reduction in plaque load by amyloid PET [52].

Additionally, we demonstrate that the administration route greatly affects brain distribution, especially for the bispecific antibody. RmAbSynO2-scFv8D3 administered *i.v.* results in more than double the brain concentrations at early time points compared to the *i.p.* route. This was also seen with *ex vivo* autoradiography, with a higher radioactive signal in the brain following *i.v.* injections of RmAbSynO2-scFv8D3. The large differences between administration routes were also evident in ISF concentration of RmAbSynO2-scFv8D3 when measured with microdialysis in the striatum of WT mice, confirming that not only association with brain vasculature but also parenchymal entry is affected. The peritoneal cavity is vast with a large blood supply, in addition to being associated with low impact of stress and thus more suitable for repeated dosing. However, the limited bioavailability offered by this route in comparison with the *i.v.* route suggests that a high initial systemic concentration is required for optimal TfR-mediated brain delivery.

Here we aimed to study the levels of soluble, membrane-associated and insoluble  $\alpha$ SYN following short-term treatment with three *i.v.* injections of RmAbSynO2-scFv8D3 during five days, in comparison with the unmodified RmAbSynO2 and PBS controls in aged female L61 mice. Monitoring the antibody blood pharmacokinetics following each injection throughout the study revealed similar blood pharmacokinetics and presumably similar brain uptake of the antibodies after each dose. Upon study termination, the levels of RmAbSynO2-scFv8D3 in the brain were higher in comparison with RmAbSynO2, as well as higher in the brain relative to the concentrations in blood. This suggests that repeated dosing is feasible for TfR-mediated brain delivery. In addition, it may indicate target engagement of RmAbSynO2-scFv8D3 with intrabrain  $\alpha$ SYN. The difference in brain concentrations between the antibodies was also reflected in the therapeutic effect, where only the bispecific antibody variant significantly altered  $\alpha$ SYN levels in the brain. Interestingly, the levels of oligomeric, TBS soluble  $\alpha$ SYN were increased in the cortex and midbrain after RmAbSynO2-scFv8D3 treatment. In contrast, RmAbSynO2-scFv8D3 treatment reduced

$\alpha$ SYN oligomers in the membrane-associated fraction of the same regions. Aggregated  $\alpha$ SYN is proposed to exert cellular toxicity by aberrant interactions with biological membranes [53–55]. Our findings point toward a shift in the solubility of the oligomeric  $\alpha$ SYN toward a more soluble form, likely induced by engagement of the therapeutic antibody with aggregated  $\alpha$ SYN associated with membranes. It is important to bear in mind that this is an acute study conducted over a short period of time, with analysis of tissue only 24 h after the last dose. The observed shift in solubility likely reflects a dynamic transition of  $\alpha$ SYN through different states of solubility, where a subsequent clearance of the solubilized  $\alpha$ SYN may occur later in the process. In a chronic treatment setting, this could eventually also lead to the removal of less soluble forms of  $\alpha$ SYN aggregates, which was not observed here. Still, although antibody treatment did not alter levels of total  $\alpha$ SYN in the most soluble brain extracts, levels of membrane-associated total  $\alpha$ SYN were lowered in the cortex of RmAbSynO2-scFv8D3 treated mice. However, formic acid-soluble  $\alpha$ SYN, as well as immunoreactivity of pSer129  $\alpha$ SYN, used as a proxy for pathological  $\alpha$ SYN (i.e., less soluble  $\alpha$ SYN aggregates) did not readily mirror changes in  $\alpha$ SYN load between the different treatments.

Further, we investigated the microglial response in treated mice, as there is a clear link between released, extracellular pathogenic  $\alpha$ SYN and positive microglial inflammatory response [56–58]. In addition, microglia-mediated phagocytosis of antibody-target complexes is usually suggested as a plausible mechanism for clearance in CNS immunotherapy. The transition to a pro-inflammatory phenotype is key in the promotion of microglial phagocytosis of pathogenic  $\alpha$ SYN and it has been suggested that TREM2, which is highly expressed on the surface of microglia in the CNS, participates in this process [59]. In addition, mutations in TREM2 have been identified as risk factors for several neurodegenerative diseases, including PD [60]. Here, sTREM2 levels were significantly increased in all brain regions following both the RmAbSynO2-scFv8D3 as well as RmAbSynO2 treatment as compared with PBS controls. The impact of antibody treatment, regardless of format and brain concentrations, on the TREM2 levels indicates that a common mechanism is at play. Increased immunoreactivity of Iba1, a marker for activated microglia, in addition to TREM2, was also observed on brain sections from both antibody treatment groups, further verifying that treatment induced an increased microglial response. However, to fully understand the impact of the antibody treatment on microglial response, an isotype-matched, non- $\alpha$ SYN-targeting control antibody should be studied in parallel.

## 5. Conclusions

Taken together, this study demonstrates that RMT greatly enhances the brain distribution of a therapeutic antibody that specifically targets toxic  $\alpha$ SYN aggregates in a mouse model of  $\alpha$ SYN pathology. The rapid and widespread distribution of the antibody into the brain at high concentrations facilitates the clearance of  $\alpha$ SYN oligomers.

**Supplementary Materials:** The following supporting information can be downloaded at: <https://www.mdpi.com/article/10.3390/pharmaceutics14071412/s1>.

**Author Contributions:** S.R.: Conceptualization, Methodology, Formal analysis, Investigation, Data curation, Writing—original draft, Supervision, Visualization, Funding acquisition. U.J.: Conceptualization, Methodology, Formal analysis, Investigation, Data curation, Writing—review & editing. M.X.: Methodology, Investigation, Writing—review & editing. J.E.: Methodology, Investigation, Writing—review & editing. E.M.: Methodology, Writing—review & editing. G.H.: Methodology, Writing—review & editing. J.B.: Methodology, Writing—review & editing. M.I.: Conceptualization, Writing—review & editing, Funding acquisition. S.S.: Conceptualization, Methodology, Formal analysis, Investigation, Writing—original draft, Supervision, Project administration, Funding acquisition. D.S.: Conceptualization, Methodology, Formal analysis, Investigation, Writing—original draft, Supervision, Project administration, Funding acquisition. All authors have read and agreed to the published version of the manuscript.



**Funding:** This work was supported by grants from the Swedish Research Council (2017-02413, 2018-02715, 2021-03524 and 2021-01083), the Swedish Innovation Agency (2016-04050, 2019-00106), Hjärnfonden, Torsten Söderbergs stiftelse, Åke Wibergs stiftelse, Hedlunds stiftelse, Åhlénstiftelsen, Parkinsonfonden, Magnus Bergvalls stiftelse, Stiftelsen för gamla tjänarinnor, Stohnes stiftelse, Neurofonden, Demensfonden, Syskonen Inger och Sixten Norheds stiftelse and Konung Gustaf V:s och Drottning Victorias frimuaerstiftelse. The funding organizations did not take part in the study design, analysis or interpretation of the results.

**Institutional Review Board Statement:** All experiments were approved by the Uppsala Animal Ethics Committee (approval 5.8.18-13350/2017, approved 22 September 2017, 5.8.18-12230/2019, approved 27 September 2019 and 5.8.18-20401/2020, approved 26 February 2021) and the use of mice was conducted in accordance with the EU directive 2010/63/EU for animal experiments.

**Informed Consent Statement:** Not applicable.

**Data Availability Statement:** Imaging data is available in Dicom or text format and can be transferred per request by the corresponding author. Processed data, i.e., %ID/g/BW,  $\alpha$ SYN concentrations, are available in table format in GraphPad Prism files.

**Acknowledgments:** We would like to acknowledge Omar El-Agnaf and Nishant Vaikath, who developed and characterized the SynO2 antibody. The molecular imaging work in this study was performed at the SciLifeLab Pilot Facility for Preclinical PET-MRI, a Swedish nationally available imaging platform at Uppsala University, Sweden, financed by the Knut and Alice Wallenberg Foundation.

**Conflicts of Interest:** The authors declare no conflict of interest.

## References

1. Polymeropoulos, M.H.; Lavedan, C.; Leroy, E.; Ide, S.E.; Dehejia, A.; Dutra, A.; Pike, B.; Root, H.; Rubenstein, J.; Boyer, R.; et al. Mutation in the alpha-synuclein gene identified in families with Parkinson's disease. *Science* **1997**, *276*, 2045–2047. [CrossRef] [PubMed]
2. Krüger, R.; Kuhn, W.; Müller, T.; Woitalla, D.; Graeber, M.; Kösel, S.; Przuntek, H.; Epplen, J.T.; Schöls, L.; Riess, O. Ala30Pro mutation in the gene encoding alpha-synuclein in Parkinson's disease. *Nat. Genet.* **1998**, *18*, 106–108. [CrossRef] [PubMed]
3. Spillantini, M.G.; Schmidt, M.L.; Lee, V.M.; Trojanowski, J.Q.; Jakes, R.; Goedert, M. Alpha-synuclein in Lewy bodies. *Nature* **1997**, *388*, 839–840. [CrossRef] [PubMed]
4. Bohnen, N.I.; Albin, R.L. The cholinergic system and Parkinson disease. *Behav. Brain Res.* **2011**, *221*, 564–573. [CrossRef]
5. Schapira, A.H.; Emre, M.; Jenner, P.; Poewe, W. Levodopa in the treatment of Parkinson's disease. *Eur. J. Neurol.* **2009**, *16*, 982–989. [CrossRef]
6. Masliah, E.; Rockenstein, E.; Adame, A.; Alford, M.; Crews, L.; Hashimoto, M.; Seubert, P.; Lee, M.; Goldstein, J.; Chilcote, T.; et al. Effects of alpha-synuclein immunization in a mouse model of Parkinson's disease. *Neuron* **2005**, *46*, 857–868. [CrossRef]
7. Lindström, V.; Fagerqvist, T.; Nordström, E.; Eriksson, F.; Lord, A.; Tucker, S.; Andersson, J.; Johannesson, M.; Schell, H.; Kahle, P.J.; et al. Immunotherapy targeting  $\alpha$ -synuclein protofibrils reduced pathology in (Thy-1)-h[A30P]  $\alpha$ -synuclein mice. *Neurobiol. Dis.* **2014**, *69*, 134–143. [CrossRef]
8. Weihofen, A.; Liu, Y.; Arndt, J.W.; Huy, C.; Quan, C.; Smith, B.A.; Baeriswyl, J.L.; Cavegn, N.; Senn, L.; Su, L.; et al. Development of an aggregate-selective, human-derived  $\alpha$ -synuclein antibody BIIB054 that ameliorates disease phenotypes in Parkinson's disease models. *Neurobiol. Dis.* **2019**, *124*, 276–288. [CrossRef]
9. Masliah, E.; Rockenstein, E.; Mante, M.; Crews, L.; Spencer, B.; Adame, A.; Patrick, C.; Trejo, M.; Ubhi, K.; Rohn, T.T.; et al. Passive immunization reduces behavioral and neuropathological deficits in an alpha-synuclein transgenic model of Lewy body disease. *PLoS ONE* **2011**, *6*, e19338. [CrossRef]
10. Jankovic, J.; Goodman, I.; Safirstein, B.; Marmon, T.K.; Schenk, D.B.; Koller, M.; Zago, W.; Ness, D.K.; Griffith, S.G.; Grundman, M.; et al. Safety and Tolerability of Multiple Ascending Doses of PRX002/RG7935, an Anti- $\alpha$ -Synuclein Monoclonal Antibody, in Patients With Parkinson Disease: A Randomized Clinical Trial. *JAMA Neurol.* **2018**, *75*, 1206–1214. [CrossRef]
11. Schenk, D.B.; Koller, M.; Ness, D.K.; Griffith, S.G.; Grundman, M.; Zago, W.; Soto, J.; Atiee, G.; Ostrowitzki, S.; Kinney, G.G. First-in-human assessment of PRX002, an anti- $\alpha$ -synuclein monoclonal antibody, in healthy volunteers. *Mov. Disord.* **2017**, *32*, 211–218. [CrossRef]
12. Abeliovich, A.; Schmitz, Y.; Fariñas, I.; Choi-Lundberg, D.; Ho, W.H.; Castillo, P.E.; Shinsky, N.; Verdugo, J.M.; Armanini, M.; Ryan, A.; et al. Mice lacking alpha-synuclein display functional deficits in the nigrostriatal dopamine system. *Neuron* **2000**, *25*, 239–252. [CrossRef]
13. Volpicelli-Daley, L.A.; Luk, K.C.; Patel, T.P.; Tanik, S.A.; Riddle, D.M.; Stieber, A.; Meaney, D.F.; Trojanowski, J.Q.; Lee, V.M. Exogenous  $\alpha$ -synuclein fibrils induce Lewy body pathology leading to synaptic dysfunction and neuron death. *Neuron* **2011**, *72*, 57–71. [CrossRef]

14. Tanik, S.A.; Schultheiss, C.E.; Volpicelli-Daley, L.A.; Brunden, K.R.; Lee, V.M. Lewy body-like  $\alpha$ -synuclein aggregates resist degradation and impair macroautophagy. *J. Biol. Chem.* **2013**, *288*, 15194–15210. [CrossRef]
15. Colla, E.; Jensen, P.H.; Pletrnikova, O.; Troncoso, J.C.; Glabe, C.; Lee, M.K. Accumulation of toxic  $\alpha$ -synuclein oligomer within endoplasmic reticulum occurs in  $\alpha$ -synucleinopathy in vivo. *J. Neurosci.* **2012**, *32*, 3301–3305. [CrossRef]
16. Kim, I.; Xu, W.; Reed, J.C. Cell death and endoplasmic reticulum stress: Disease relevance and therapeutic opportunities. *Nat. Rev. Drug Discov.* **2008**, *7*, 1013–1030. [CrossRef]
17. Cole, N.B.; Dieuiliis, D.; Leo, P.; Mitchell, D.C.; Nussbaum, R.L. Mitochondrial translocation of alpha-synuclein is promoted by intracellular acidification. *Exp. Cell Res.* **2008**, *314*, 2076–2089. [CrossRef]
18. Chen, H.; Chan, D.C. Mitochondrial dynamics—fusion, fission, movement, and mitophagy—in neurodegenerative diseases. *Hum. Mol. Genet.* **2009**, *18*, R169–R176. [CrossRef]
19. Abbott, N.J.; Rönnebeck, L.; Hansson, E. Astrocyte-endothelial interactions at the blood-brain barrier. *Nat. Rev. Neurosci.* **2006**, *7*, 41–53. [CrossRef]
20. Abbott, N.J.; Patabendige, A.A.; Dolman, D.E.; Yusof, S.R.; Begley, D.J. Structure and function of the blood-brain barrier. *Neurobiol. Dis.* **2010**, *37*, 13–25. [CrossRef]
21. Hawkins, B.T.; Davis, T.P. The blood-brain barrier/neurovascular unit in health and disease. *Pharmacol. Rev.* **2005**, *57*, 173–185. [CrossRef]
22. Dalakas, M.C. Intravenous immunoglobulin in autoimmune neuromuscular diseases. *JAMA* **2004**, *291*, 2367–2375. [CrossRef]
23. Vaitla, P.M.; McDermott, E.M. The role of high-dose intravenous immunoglobulin in rheumatology. *Rheumatology* **2010**, *49*, 1040–1048. [CrossRef]
24. Spencer, B.; Emadi, S.; Desplats, P.; Eleuteri, S.; Michael, S.; Kosberg, K.; Shen, J.; Rockenstein, E.; Patrick, C.; Adame, A.; et al. ESCRT-mediated uptake and degradation of brain-targeted  $\alpha$ -synuclein single chain antibody attenuates neuronal degeneration in vivo. *Mol. Ther.* **2014**, *22*, 1753–1767. [CrossRef]
25. Spencer, B.; Williams, S.; Rockenstein, E.; Valera, E.; Xin, W.; Mante, M.; Florio, J.; Adame, A.; Masliah, E.; Sierks, M.R.  $\alpha$ -synuclein conformational antibodies fused to penetratin are effective in models of Lewy body disease. *Ann. Clin. Transl. Neurol.* **2016**, *3*, 588–606. [CrossRef] [PubMed]
26. Johnsen, K.B.; Moos, T. Revisiting nanoparticle technology for blood-brain barrier transport: Unfolding at the endothelial gate improves the fate of transferrin receptor-targeted liposomes. *J. Control. Release* **2016**, *222*, 32–46. [CrossRef] [PubMed]
27. Leitner, D.F.; Connor, J.R. Functional roles of transferrin in the brain. *Biochim. Biophys. Acta* **2012**, *1820*, 393–402. [CrossRef]
28. Jefferies, W.A.; Brandon, M.R.; Hunt, S.V.; Williams, A.F.; Gatter, K.C.; Mason, D.Y. Transferrin receptor on endothelium of brain capillaries. *Nature* **1984**, *312*, 162–163. [CrossRef] [PubMed]
29. Gustavsson, T.; Syvänen, S.; O’Callaghan, P.; Sehlin, D. SPECT imaging of distribution and retention of a brain-penetrating bispecific amyloid- $\beta$  antibody in a mouse model of Alzheimer’s disease. *Transl. Neurodegener.* **2020**, *9*, 37. [CrossRef] [PubMed]
30. Syvänen, S.; Hultqvist, G.; Gustavsson, T.; Gumucio, A.; Laudon, H.; Söderberg, L.; Ingelsson, M.; Lannfelt, L.; Sehlin, D. Efficient clearance of A $\beta$  protofibrils in A $\beta$ PP-transgenic mice treated with a brain-penetrating bifunctional antibody. *Alzheimers Res. Ther.* **2018**, *10*, 49. [CrossRef] [PubMed]
31. Faresjö, R.; Bonvicini, G.; Fang, X.T.; Aguilar, X.; Sehlin, D.; Syvänen, S. Brain pharmacokinetics of two BBB penetrating bispecific antibodies of different size. *Fluids Barriers CNS* **2021**, *18*, 26. [CrossRef]
32. Kissel, K.; Hamm, S.; Schulz, M.; Vecchi, A.; Garlanda, C.; Engelhardt, B. Immunohistochemical localization of the murine transferrin receptor (TfR) on blood-tissue barriers using a novel anti-TfR monoclonal antibody. *Histochem. Cell Biol.* **1998**, *110*, 63–72. [CrossRef]
33. Roshanbin, S.; Xiong, M.; Hultqvist, G.; Söderberg, L.; Zachrisson, O.; Meier, S.; Ekmark-Lewén, S.; Bergström, J.; Ingelsson, M.; Sehlin, D.; et al. In vivo imaging of alpha-synuclein with antibody-based PET. *Neuropharmacology* **2022**, *208*, 108985. [CrossRef]
34. Kim, C.; Spencer, B.; Rockenstein, E.; Yamakado, H.; Mante, M.; Adame, A.; Fields, J.A.; Masliah, D.; Iba, M.; Lee, H.J.; et al. Immunotherapy targeting toll-like receptor 2 alleviates neurodegeneration in models of synucleinopathy by modulating  $\alpha$ -synuclein transmission and neuroinflammation. *Mol. Neurodegener* **2018**, *13*, 43. [CrossRef]
35. Chesselet, M.F.; Richter, F.; Zhu, C.; Magen, I.; Watson, M.B.; Subramaniam, S.R. A progressive mouse model of Parkinson’s disease: The Thy1-aSyn (“Line 61”) mice. *Neurotherapeutics* **2012**, *9*, 297–314. [CrossRef]
36. Rockenstein, E.; Mallory, M.; Hashimoto, M.; Song, D.; Shults, C.W.; Lang, I.; Masliah, E. Differential neuropathological alterations in transgenic mice expressing alpha-synuclein from the platelet-derived growth factor and Thy-1 promoters. *J. Neurosci. Res.* **2002**, *68*, 568–578. [CrossRef]
37. Roshanbin, S.; Aniszewska, A.; Gumucio, A.; Masliah, E.; Erlandsson, A.; Bergström, J.; Ingelsson, M.; Ekmark-Lewén, S. Age-related increase of alpha-synuclein oligomers is associated with motor disturbances in L61 transgenic mice. *Neurobiol. Aging* **2021**, *101*, 207–220. [CrossRef]
38. Vaikath, N.N.; Majbour, N.K.; Paleologou, K.E.; Ardah, M.T.; van Dam, E.; van de Berg, W.D.; Forrest, S.L.; Parkkinen, L.; Gai, W.P.; Hattori, N.; et al. Generation and characterization of novel conformation-specific monoclonal antibodies for  $\alpha$ -synuclein pathology. *Neurobiol. Dis.* **2015**, *79*, 81–99. [CrossRef]
39. Hultqvist, G.; Syvänen, S.; Fang, X.T.; Lannfelt, L.; Sehlin, D. Bivalent Brain Shuttle Increases Antibody Uptake by Monovalent Binding to the Transferrin Receptor. *Theranostics* **2017**, *7*, 308–318. [CrossRef]

40. Greenwood, F.C.; Hunter, W.M.; Glover, J.S. The preparation of I-131-labelled human growth hormone of high specific radioactivity. *Biochem. J.* **1963**, *89*, 114–123. [CrossRef]
41. Syvänen, S.; Fang, X.T.; Faresjö, R.; Rokka, J.; Lannfelt, L.; Olberg, D.E.; Eriksson, J.; Sehlin, D. Fluorine-18-Labeled Antibody Ligands for PET Imaging of Amyloid- $\beta$  in Brain. *ACS Chem. Neurosci.* **2020**, *11*, 4460–4468. [CrossRef] [PubMed]
42. Zhou, Y.; Wong, J.M.; Mabrouk, O.S.; Kennedy, R.T. Reducing adsorption to improve recovery and in vivo detection of neuropeptides by microdialysis with LC-MS. *Anal. Chem.* **2015**, *87*, 9802–9809. [CrossRef] [PubMed]
43. Chang, H.Y.; Morrow, K.; Bonacquisti, E.; Zhang, W.; Shah, D.K. Antibody pharmacokinetics in rat brain determined using microdialysis. *MAbs* **2018**, *10*, 843–853. [CrossRef] [PubMed]
44. Loening, A.M.; Gambhir, S.S. AMIDE: A free software tool for multimodality medical image analysis. *Mol. Imaging* **2003**, *2*, 131–137. [CrossRef]
45. Meier, S.R.; Sehlin, D.; Hultqvist, G.; Syvänen, S. Pinpointing Brain TREM2 Levels in Two Mouse Models of Alzheimer’s Disease. *Mol. Imaging Biol.* **2021**, *23*, 665–675. [CrossRef]
46. Kumar, S.T.; Jagannath, S.; Francois, C.; Vanderstichele, H.; Stoops, E.; Lashuel, H.A. How specific are the conformation-specific  $\alpha$ -synuclein antibodies? Characterization and validation of 16  $\alpha$ -synuclein conformation-specific antibodies using well-characterized preparations of  $\alpha$ -synuclein monomers, fibrils and oligomers with distinct structures and morphology. *Neurobiol. Dis.* **2020**, *146*, 105086. [CrossRef]
47. Steiner, J.A.; Quansah, E.; Brundin, P. The concept of alpha-synuclein as a prion-like protein: Ten years after. *Cell Tissue Res.* **2018**, *373*, 161–173. [CrossRef]
48. Kordower, J.H.; Chu, Y.; Hauser, R.A.; Freeman, T.B.; Olanow, C.W. Lewy body-like pathology in long-term embryonic nigral transplants in Parkinson’s disease. *Nat. Med.* **2008**, *14*, 504–506. [CrossRef]
49. Danzer, K.M.; Kranich, L.R.; Ruf, W.P.; Cagsal-Getkin, O.; Winslow, A.R.; Zhu, L.; Vanderburg, C.R.; McLean, P.J. Exosomal cell-to-cell transmission of alpha synuclein oligomers. *Mol. Neurodegener.* **2012**, *7*, 42. [CrossRef]
50. Emmanouilidou, E.; Melachroinou, K.; Roumeliotis, T.; Garbis, S.D.; Ntzouni, M.; Margaritis, L.H.; Stefanis, L.; Vekrellis, K. Cell-produced alpha-synuclein is secreted in a calcium-dependent manner by exosomes and impacts neuronal survival. *J. Neurosci.* **2010**, *30*, 6838–6851. [CrossRef]
51. Pizzo, M.E.; Wolak, D.J.; Kumar, N.N.; Brunette, E.; Brunquell, C.L.; Hannocks, M.J.; Abbott, N.J.; Meyerand, M.E.; Sorokin, L.; Stanimirovic, D.B.; et al. Intrathecal antibody distribution in the rat brain: Surface diffusion, perivascular transport and osmotic enhancement of delivery. *J. Physiol.* **2018**, *596*, 445–475. [CrossRef]
52. Sevigny, J.; Chiao, P.; Bussi ere, T.; Weinreb, P.H.; Williams, L.; Maier, M.; Dunstan, R.; Salloway, S.; Chen, T.; Ling, Y.; et al. The antibody aducanumab reduces A $\beta$  plaques in Alzheimer’s disease. *Nature* **2016**, *537*, 50–56. [CrossRef]
53. Auluck, P.K.; Caraveo, G.; Lindquist, S.  $\alpha$ -Synuclein: Membrane interactions and toxicity in Parkinson’s disease. *Annu. Rev. Cell Dev. Biol.* **2010**, *26*, 211–233. [CrossRef]
54. Winner, B.; Jappelli, R.; Maji, S.K.; Desplats, P.A.; Boyer, L.; Aigner, S.; Hetzer, C.; Loher, T.; Vilar, M.; Campioni, S.; et al. In vivo demonstration that alpha-synuclein oligomers are toxic. *Proc. Natl. Acad. Sci. USA* **2011**, *108*, 4194–4199. [CrossRef]
55. Danzer, K.M.; Haasen, D.; Karow, A.R.; Moussaud, S.; Habeck, M.; Giese, A.; Kretschmar, H.; Hengerer, B.; Kostka, M. Different species of alpha-synuclein oligomers induce calcium influx and seeding. *J. Neurosci.* **2007**, *27*, 9220–9232. [CrossRef]
56. Su, X.; Maguire-Zeiss, K.A.; Giuliano, R.; Prifti, L.; Venkatesh, K.; Federoff, H.J. Synuclein activates microglia in a model of Parkinson’s disease. *Neurobiol. Aging* **2008**, *29*, 1690–1701. [CrossRef]
57. Austin, S.A.; Floden, A.M.; Murphy, E.J.; Combs, C.K. Alpha-synuclein expression modulates microglial activation phenotype. *J. Neurosci.* **2006**, *26*, 10558–10563. [CrossRef]
58. Grozdanov, V.; Bousset, L.; Hoffmeister, M.; Bliederhaeuser, C.; Meier, C.; Madiona, K.; Pieri, L.; Kiechle, M.; McLean, P.J.; Kassubek, J.; et al. Increased Immune Activation by Pathologic  $\alpha$ -Synuclein in Parkinson’s Disease. *Ann. Neurol.* **2019**, *86*, 593–606. [CrossRef]
59. Mecca, C.; Giambanco, I.; Donato, R.; Arcuri, C. Microglia and Aging: The Role of the TREM2-DAP12 and CX3CL1-CX3CR1 Axes. *Int. J. Mol. Sci.* **2018**, *19*, 318. [CrossRef]
60. Rayaprolu, S.; Mullen, B.; Baker, M.; Lynch, T.; Finger, E.; Seeley, W.W.; Hatanpaa, K.J.; Lomen-Hoerth, C.; Kertesz, A.; Bigio, E.H.; et al. TREM2 in neurodegeneration: Evidence for association of the p.R47H variant with frontotemporal dementia and Parkinson’s disease. *Mol. Neurodegener.* **2013**, *8*, 19. [CrossRef]

## Article

# A Single Domain Shark Antibody Targeting the Transferrin Receptor 1 Delivers a TrkB Agonist Antibody to the Brain and Provides Full Neuroprotection in a Mouse Model of Parkinson's Disease

Emily Clarke <sup>1</sup>, Pawel Stocki <sup>2</sup>, Elizabeth H. Sinclair <sup>2</sup>, Aziz Gauhar <sup>2</sup>, Edward J. R. Fletcher <sup>1</sup>, Alicja Krawczun-Rygmaczewska <sup>1</sup>, Susan Duty <sup>1</sup>, Frank S. Walsh <sup>2</sup>, Patrick Doherty <sup>1</sup> and Julia Lynn Rutkowski <sup>2,\*</sup>

<sup>1</sup> King's College London, Institute of Psychiatry, Psychology and Neuroscience, Wolfson Centre for Age-Related Disease, Guy's Campus, London SE1 1UL, UK; emily.clarke@kcl.ac.uk (E.C.); edward.fletcher@ucl.ac.uk (E.J.R.F.); alicja.krawczun-rygmaczewska@kcl.ac.uk (A.K.-R.); susan.duty@kcl.ac.uk (S.D.); patrick.doherty@kcl.ac.uk (P.D.)

<sup>2</sup> Ossianix, Inc., Gunnels Wood Rd., Stevenage SG1 2FX, UK; pawel@ossianix.com (P.S.); liz@ossianix.com (E.H.S.); aziz@ossianix.com (A.G.); walsh@ossianix.com (F.S.W.)

\* Correspondence: rutkowski@ossianix.com; Tel.: +1-(610)-291-1724

**Citation:** Clarke, E.; Stocki, P.; Sinclair, E.H.; Gauhar, A.; Fletcher, E.J.R.; Krawczun-Rygmaczewska, A.; Duty, S.; Walsh, F.S.; Doherty, P.; Rutkowski, J.L. A Single Domain Shark Antibody Targeting the Transferrin Receptor 1 Delivers a TrkB Agonist Antibody to the Brain and Provides Full Neuroprotection in a Mouse Model of Parkinson's Disease. *Pharmaceutics* **2022**, *14*, 1335. <https://doi.org/10.3390/pharmaceutics14071335>

Academic Editor: William M. Pardridge

Received: 30 May 2022

Accepted: 22 June 2022

Published: 24 June 2022

**Publisher's Note:** MDPI stays neutral with regard to jurisdictional claims in published maps and institutional affiliations.



**Copyright:** © 2022 by the authors. Licensee MDPI, Basel, Switzerland. This article is an open access article distributed under the terms and conditions of the Creative Commons Attribution (CC BY) license (<https://creativecommons.org/licenses/by/4.0/>).

**Abstract:** Single domain shark antibodies that bind to the transferrin receptor 1 (TfR1) on brain endothelial cells have been used to shuttle antibodies and other cargos across the blood brain barrier (BBB) to the brain. For these studies the TXB4 brain shuttle was fused to a TrkB neurotrophin receptor agonist antibody. The TXB4-TrkB fusion retained potent agonist activity at its cognate receptor and after systemic administration showed a 12-fold increase in brain levels over the unmodified antibody. Only the TXB4-TrkB antibody fusion was detected within the brain and localized to TrkB positive cells in the cortex and tyrosine hydroxylase (TH) positive dopaminergic neurons in the substantia nigra pars compacta (SNc), where it was associated with activated ERK1/2 signaling. When tested in the 6-hydroxydopamine (6-OHDA) mouse model of Parkinson's disease (PD), TXB4-TrkB, but not the unmodified antibody, completely prevented the 6-OHDA induced death of TH positive neurons in the SNc. In conclusion, the fusion of the TXB4 brain shuttle allows a TrkB agonist antibody to reach neuroprotective concentrations in the brain parenchyma following systemic administration.

**Keywords:** TrkB; agonist antibody; variable new antigen receptor (VNAR); neuroprotection; transferrin receptor 1 (TfR1); blood-brain barrier (BBB); 6-OHDA; Parkinson's disease

## 1. Introduction

The interaction of neurotrophins (NGF, BDNF, NT3 and NT4) with their cognate Trk receptors (TrkA, TrkB and TrkC, respectively) protects neurons from naturally occurring cell death during development [1,2]. Their ability to nurture developing neurons spawned numerous studies to determine if they can promote the survival of adult neurons, particularly in the context of neurodegenerative disease or acute brain injury [3,4]. In this context, promising results have been found with BDNF which, by activating the TrkB receptor, can protect neurons from death in, for example, preclinical models of PD [5], Alzheimer's disease (AD) [6,7], and ischemic lesions [8–11]. In addition, BDNF can promote functional recovery of injured neurons following spinal cord injury [12–14] and stimulate the production of new neurons in the adult brain [15,16]. The loss of BDNF has also been suggested as a contributory factor to the progression of PD [17–19], AD [20] and Huntington's disease [21–23], as well as to conditions such as depression [24,25].

However, the therapeutic potential of BDNF in neurodegenerative diseases, acute brain injury and other neurological conditions has not been realized in the clinical setting due in part to a short plasma half-life in vivo [26], exclusion from the brain parenchyma

following systemic administration, and poor diffusion throughout the parenchyma due to a high isoelectric point [27]. Agonist antibodies that directly bind the TrkB receptor and mimic the neurotrophic activity of BDNF provides a long in vivo half-life, but the challenge of poor blood brain barrier (BBB) penetration remains. This has generally limited the systemic delivery of TrkB antibody to peripheral disorders such as obesity [28,29] and peripheral neuropathy [30]. Nonetheless, when delivered directly across the BBB by intracerebroventricular injection prior to an ischemic injury, the 29D7 TrkB agonist antibody enhances neuronal survival and promotes functional recovery [31–34].

There is considerable interest in the possibility of utilizing the receptor-mediated transcytosis pathways that exist on brain endothelial cells that form the BBB to carry biotherapeutics from the blood to the brain parenchyma with the transferrin receptor 1 (TfR1) being the most widely studied [35]. TXB4 is a single domain shark variable new antigen receptor (VNAR) antibody specific to TfR1 with enhanced brain penetration which was derived from the previously reported TXB2 VNAR [36] by restricted randomization of the CDR3 domain [37]. We hypothesized that if the TXB4 module was fused to the 29D7 TrkB agonist antibody it would accumulate in the brain following systemic administration to provide neuroprotection following disease or injury. In the present study we produced a bivalent, bispecific TrkB antibody by cloning the variable regions of the 29D7 agonist antibody into human IgG1 and genetically fusing it to the TXB4 brain shuttle.

Our results show that, unlike the unmodified TrkB agonist antibody, the TXB4-TrkB fusion rapidly accumulated in the brain following a single IV injection. We also found that TXB4-TrkB associates with and activates ERK1/2 signaling in TrkB positive cells in the cortex and tyrosine hydroxylase (TH) positive dopaminergic neurons in the substantia nigra compacta (SNc). When tested in the mouse 6-OHDA model of PD, the TXB4-TrkB antibody completely prevented the loss of TH positive neurons throughout the SNc. In conclusion, fusion with the TXB4 module allows the TrkB agonist antibody to reach neuroprotective concentrations in the brain parenchyma following systemic administration, generating a new class of biologic with therapeutic potential in a wide range of neurodegenerative diseases, acute brain injury situations and possibly depression.

## 2. Materials and Methods

**Production of bivalent VNAR-agonist antibody fusions.** The VH and VL domain sequences from the mouse anti-TrkB 29D7 or anti-TrkC agonist antibody 6.4.1 [33,38] were cloned into the constant regions of the human heavy chain IgG1 and human light chain kappa, respectively. The human Fc domain of both antibodies contained the LALA double mutation (Leu234Ala and Leu235Ala) to attenuate effector function [39]. The original TXB2 BBB shuttle [36] was subjected to restricted CDR3 mutagenesis and the TXB4 variant, which showed enhanced brain penetration [37], was used to generate bivalent VNAR-antibody fusions. TXB4 was fused to either the N-terminus of the heavy chain VH domain via a 3xG4S linker (HC2N format) or between the CH1 and CH2 domain via a 3xG4S and a 1xG4S linker (HV2N format), respectively. The TrkC-TXB4 antibody fusion was produced in the HC2N format and used as a control.

All antibodies were expressed in CHO cells by transient transfection. Supernatants were collected and filtered through 0.22  $\mu$ m membranes and loaded onto HiTrap MabSelect SuRe Protein A columns (GE Healthcare, Chicago, IL, USA) pre-equilibrated with phosphate-buffered saline (PBS, pH 7.4). Antibodies were eluted with 0.1 M glycine, pH 3.5 into neutralizing buffer (1 M Tris-HCl, pH 9.0) and the buffer exchanged to PBS using HiPrep 26/10 Desalting columns (GE Healthcare). Antibody purity was determined by analytical size exclusion chromatography (SEC) using a Superdex200 column.

**Target binding assays.** For ELISAs, Nunc MaxiSorp plates (Thermo Fisher, Waltham, MA, USA) were coated with 100  $\mu$ L of 1  $\mu$ g/mL of human TrkB (Sino Biological, 10047H80M, Beijing, China) mouse or human TfR1 (mTfR1 and hTfR1 ectodomains produced internally) and incubated at 4  $^{\circ}$ C overnight. Plates were incubated with a blocking buffer (2.5% non-fat dry milk in PBS with 0.1% Tween20, PBST) for 1 h at RT. Purified proteins

were mixed with non-fat dry milk in PBST to a final concentration of 2.5% and incubated for 30 min. The blocked protein solutions (100  $\mu$ L) were transferred to the blocked plates and incubated for 1 h. The plates were washed with PBST and incubated with a goat anti-human Fc–peroxidase antibody diluted 1:5000 (Sigma) in blocking buffer for 30 min. The plates were washed and developed with SureBlue (VWR). The reaction was measured at 370 nm in real time for Vmax analysis and EC50 values were calculated using 4-parametric non-linear regression (Prism). Receptor binding kinetics were measured by surface plasmon resonance (SPR) using a Biacore T200 (GE Healthcare) as described [36]. In brief, a Fc-capture kit (GE Healthcare) was used to immobilize ligand in 0.1% BSA in HBS-EP+ buffer (GE Healthcare). Analyte binding was measured using the single cycle kinetic SPR method in HBS-EP+ at a flow rate 30  $\mu$ L/min. A flow cell without ligand captured served as a reference. Sensorgrams were fitted using a 1:1 binding model and kinetic constants were determined using Biacore T200 Evaluation software.

**Trk receptor reporter assay.** TrkB- and TrkC- $\beta$ -lactamase reporter cell lines (CellSensor NFAT-bla CHO-K1, Invitrogen) were passaged twice weekly in DMEM-GlutaMAX medium (Gibco) supplemented with 10% dialyzed fetal bovine serum (dFBS), 100 U/mL penicillin, 100  $\mu$ g/mL streptomycin, 5  $\mu$ g/mL blasticidin, 200  $\mu$ g/mL zeocin, 0.1 mM non-essential amino acid solution (NEAA), and 25 mM HEPES buffer (all from Sigma). For the assay,  $2 \times 10^4$  cells were seeded per well of black-wall clear-bottom 96-well plates (Corning, Corning, NY, USA) in 100 mL of the same medium but with 0.5% dFBS and incubated overnight at 37 °C in 5% CO<sub>2</sub>. Antibodies were diluted in assay media and 50  $\mu$ L was added per well to achieve a final concentration range as indicated in the results. Cells were incubated with the antibodies for 4 h at 37 °C, 5% CO<sub>2</sub> before the addition of 30  $\mu$ L of the fluorescence resonance energy transfer (FRET) substrate CCF2-AM (ThermoFisher, Waltham, MA, USA). After incubation at room temperature for 90 min protected from light, conversion to CCF2 was measured by a shift in FRET emission. The excitation filter was set at 405 nm, and the emission filters at 460 and 530 nm (FlexStation, Molecular Devices, San Jose, CA, USA) and the ratio of the emission wavelengths ( $\lambda_1/\lambda_2$ ) was calculated as a measure of  $\beta$ -lactamase activity driven by TrkB or TrkC receptor activation.

**Animal studies.** All in vivo studies were performed in accordance with UK Animals Scientific Procedures Act (1986) and were approved by King's College London Animal Welfare and Ethical Review Body. A total of 65 adult BalbC mice (8–12 weeks old, Envigo) were used: 45 for the brain accumulation study, three for the brain localization studies and 17 for the 6-OHDA neuroprotection study. All animals were maintained on a 12:12 h light/dark cycle with food and water available *ad libitum*.

**Brain accumulation of injected antibodies by ELISA.** Female BalbC mice were injected IV with molar equivalent doses of either unmodified antibodies (3.6 mg/kg = 25 nmol/kg) or bivalent TXB4-antibody fusions (4.3 mg/kg = 25 nmol/kg). Animals were euthanized at 30 min, 1, 2, 4 or 18 h post injection by phenobarbital overdose (1 mL of 200 mg/mL Euthatal) before intracardiac perfusion with PBS. Brains were dissected into left and right hemispheres and stored at –80 °C. Tissue samples were homogenized in 3:1 (*v/w*) of PBS containing 1% Triton X-100 supplemented with protease inhibitors (cComplete™, Sigma) using the TissueRuptor (Qiagen, Hilden, Germany) at medium speed for 10 s and then incubated for 30 min on ice. Lysates were centrifuged at 17,000  $\times g$  for 20 min, and the supernatant was blocked overnight at 4 °C in 2.5% milk in PBS with 0.1% Tween 20. MaxiSorp plates (ThermoFisher) were coated with 100  $\mu$ L of goat anti-human Fc antibody (Sigma) diluted 1:500 in PBS overnight at 4 °C. The plates were washed and incubated with blocking buffer for 1 h at room temperature. Blocked brain lysates (100  $\mu$ L) were added to the blocked plates and incubated for 1 h at room temperature. After washing, plates were incubated with goat anti-human Fc-HRP conjugated antibody (Sigma) diluted 1:5000 for 1 h. Plates were then washed and developed with tetramethylbenzidine and the reaction was stopped with 1% HCl. Absorbance was measured at 450 nm and antibody concentrations were determined using standard curves prepared separately for each antibody.

**Brain localization of injected antibodies by immunohistochemistry.** All antibodies were injected at 10 mg/kg SC into male BalbC mice. The animals were euthanized after 18 h by phenobarbital overdose before being intracardially perfused with PBS followed by 10% neutral buffered formalin (Sigma, St. Louis, MO, USA). Brains were removed and submerged in 10% neutral buffered formalin for 24 h and embedded in paraffin wax. Serial 7  $\mu$ m sagittal sections were dewaxed (2  $\times$  5 min in xylene, 4  $\times$  2 min 100% IMS) and endogenous peroxidases quenched by immersion in 3% H<sub>2</sub>O<sub>2</sub> for 10 min. Antigen retrieval was performed by boiling sections in 1 mM citric acid at a pH of 6.0 for 10 min. A blocking solution containing 3% porcine serum albumin in 0.05 M tris buffered saline (TBS, pH 7.6) was applied for 90 min before sections were incubated with primary antibodies at 4 °C overnight in a humidified chamber. IV-injected antibodies were detected in the brain with a biotinylated goat anti-human IgG (Vector Laboratories, BA-3000, diluted 1:500, Newark, CA, USA). Marker proteins were detected with chicken anti-TH (Abcam ab76442, diluted 1:1500, Cambridge, UK), rabbit anti-pErk1/2 (Cell Signaling Technology 9101, diluted 1:250, Danvers, MA, USA), and rabbit anti-TrkB (Abcam ab18987). Sections were washed for 2  $\times$  5 min in 0.025% Triton-X100 in TBS before incubation with fluorescent-tagged secondaries (all from ThermoFisher, diluted 1:500, Waltham, MA, USA) for 90 min at room temperature. Biotinylated anti-human IgG was detected with streptavidin-Alexa Fluor 647 and the following were used to detect marker proteins: goat anti-chicken-Alexa Fluor 488; donkey anti rabbit-Alexa Fluor 488; and donkey anti-rabbit Alexa Fluor 647. After secondary incubations, sections were washed for 2  $\times$  5 min in 0.025% Triton-X100 in TBS before incubation with 0.1% Sudan Black B in 70% ethanol for 20 min at room temperature to quench autofluorescence. Slides were washed under running water, dried, and coverslips mounted in Vectashield with DAPI (Vector Laboratories, H-1800). Fluorescence images were acquired using a Zeiss 710 confocal microscope and Axiovision image analysis software.

**6-OHDA unilateral lesion model of Parkinson's disease.** A single SC injection of either 5 mg/kg of the TrkB antibody, TXB4-TrkB antibody fusion or TXB4-TrkC fusion or 5 mL/kg of PBS was given to male BalbC mice 24 h prior to lesioning. A second 2.5 mg/kg dose of each antibody or PBS was administered at post-lesion day seven. For 6-OHDA lesioning, anesthesia was induced with 5% isoflurane/oxygen and animals were placed in a stereotaxic frame with blunt ear bars. Anesthesia was maintained at 3% isoflurane/oxygen and body temperature was maintained at 37 °C. The surgical site was sterilized with 0.4% chlorhexidine before making an antero-proximal incision along the scalp. Fine-bore holes ( $\varnothing$  0.5 mm) were made in the skull at coordinates AP: +0.5 mm and ML: +2.2 mm (relative to bregma and skull surface) through which a blunt-ended 30-gauge needle was inserted to DV: -3.5 mm. 6-OHDA.HBr (4  $\mu$ g in 3  $\mu$ L 0.02% ascorbate/saline) was infused unilaterally into the striatum (0.5  $\mu$ L/min) and the needle withdrawn 5 min later. This dose was predicted to produce a partial lesion over a two-week period [40]. Animals received a single dose of buprenorphine (Vetergesic; 0.1 mg/kg, SC) after suturing and 1 mL of rehydrating Hartmann's solution was administered SC daily for 5 days. One animal in the TrkB antibody group failed to recover adequately from surgery and was excluded from the study.

**Immunohistochemical assessment of TH+ cell bodies in the SNc.** On post-lesion day 14, animals were euthanized by phenobarbital overdose before intracardiac perfusion with PBS followed by 10% neutral buffered formalin (Sigma). Brains were removed and submerged in 10% neutral buffered formalin for 24 h before being embedded in paraffin wax. Serial 7  $\mu$ m coronal sections encompassing the rostral, medial, and caudal SNc were obtained and processed for TH staining. Sections were dewaxed (2  $\times$  5 min in xylene, 4  $\times$  2 min in industrial methylated spirits) and endogenous peroxidases quenched by immersion in 3% H<sub>2</sub>O<sub>2</sub> for 10 min. Antigen was retrieved by boiling sections in 1 mM citric acid with a pH of 6.0 for 10 min. Blocking solution containing 1% bovine serum albumin in TBS was applied for 10 min before sections were incubated with primary polyclonal rabbit anti-TH antibody (Millipore ab152, diluted 1:500) at room temperature overnight in

a humidified chamber. Sections were washed for 5 min in TBS before incubation with biotinylated goat anti-rabbit secondary antibody (Vector Laboratories BA1000, diluted 1:500) at room temperature for 1 h. Sections were washed for 5 min in TBS before detection with Vectastain Elite ABC Kit (Vector Laboratories, PK6100) followed by the DAB substrate Kit (Vector Laboratories, SK4100). Sections were rinsed in distilled H<sub>2</sub>O for 10 min, dehydrated in 100% IMS (4 × 2 min), cleared in xylene (2 × 5 min) and then mounted with coverslips using the solvent based plastic DPX (Sigma). Photomicrographs of TH-stained SNc sections (3–6 sections per mouse at each of the caudal [AP: −3.52 mm], medial [AP: −3.16 mm] and rostral [AP: −2.92 mm] levels relative to bregma) were acquired at 20X magnification using a Zeiss Apotome microscope and Axiovision software (Carl Zeiss Ltd., Tokyo, Japan). Image J software was used to manually count viable (intact round cells with a clear nucleus and cytoplasm) TH-positive A9 dopaminergic cells of the SNc in both the lesioned and intact hemispheres. SNc cell number in the lesion hemisphere was calculated as a percentage of that lost in the intact hemisphere (n = 3–5 per group). Data were combined across all three rostro-caudal levels to generate a single average value for each animal and the mean calculated per treatment group.

**Statistical analysis.** All statistical analysis was performed using Graphpad Prism 8 software. The concentration response curve of antibodies in the NFAT reporter assay was analyzed by non-linear regression to give EC<sub>50</sub> values (n = 3–5 independent experiments per concentration per treatment). Percentage TH+ cell loss in the lesioned relative to the intact SNc in the 6-OHDA PD mouse model was tested for Gaussian distribution by Shapiro-Wilk and parametric statistics applied accordingly. The percentage TH+ cell loss of the lesioned relative to intact SNc was compared across treatment groups by one-way ANOVA followed by Tukey's HSD, \*  $p \leq 0.05$ .

### 3. Results

**In vitro activity of TXB4-TrkB agonist antibody fusions.** The TXB4 module was fused to the TrkB antibody in two different formats and binding to TfR1 and TrkB was evaluated (Figure 1A). The TfR1 ELISA binding curve for the HC2N format overlapped with that of the TXB4-human Fc fusion control, whereas the binding curve for the HV2N format was shifted to the right for both species of TfR1 (Figure 1B,C). The calculated ELISA EC<sub>50</sub> values for HV2N and HC2N formats were all within a similar range (2.3 nM vs 0.7 nM for mTfR1; 3.2 nM vs 1 nM for hTfR1, respectively). The TrkB ELISA binding curves for the unmodified TrkB antibody and both TXB4-TrkB antibody formats closely overlapped with calculated EC<sub>50</sub>s of 0.5–0.6 nM (Figure 1D). The binding kinetics to the TrkB receptor of the TXB4-TrkB HV2N format were virtually identical to that of the unmodified TrkB antibody as determined by SPR with KDs of 1.30–1.37 nM (Table 2). However, the dissociation rate was slower for the HC2N format, resulting in a lower KD of 0.4 nM.

The relative agonist activity of the various antibodies was evaluated in the TrkB-NFAT-bla CHO-K1 cell line. While all three antibodies achieved the full agonist activity of BDNF, the dose-response curves were shifted to the right (Figure 1E). The calculated EC<sub>50</sub> for the unmodified TrkB agonist antibody was 0.34 nM and was relatively close to 0.11 nM for the BDNF. Fusing the TXB4 module in either format reduced the potency relative to the unmodified antibody. The EC<sub>50</sub> for the HC2N format was 6.9 nM (20-fold reduction), while that for the HV2N format was 0.9 nM (3-fold reduction) and this format was selected for further animal studies (Table 1). The control TXB4-TrkC antibody fusion in the HC2N format retained was a full agonist in the TrkC-NFAT-bla CHO-K1 assay and had an EC<sub>50</sub> of 3.1 nM (data not shown).

**Brain accumulation of the unmodified TrkB antibody versus the TXB4-TrkB fusion.** Mice were injected IV with 25 nmol/kg of either the TrkB antibody or TXB4-TrkB fusion (HV2N format), and antibody concentrations in brain and plasma were determined by ELISA at the indicated timepoints (Figure 2A). Brain levels of the TrkB antibody remained low (0.13–0.39 nM) throughout the study, whereas the TXB4-TrkB fusion antibody steadily accumulated over the study period reached 4.7 nM, which represents a 12-fold increase



over the unmodified antibody at the 18 h timepoint (Figure 2B). The plasma concentration between the TrkB antibody (218 nM) and the TXB4 fusion (187 nM) were not significantly different (Figure 2C). For the control TXB4-TrkB antibody, the brain concentration averaged 6.5 nM at 18 h after IV in injection with 25 nmol/kg compared to 0.3 nM for the unmodified TrkB agonist antibody.

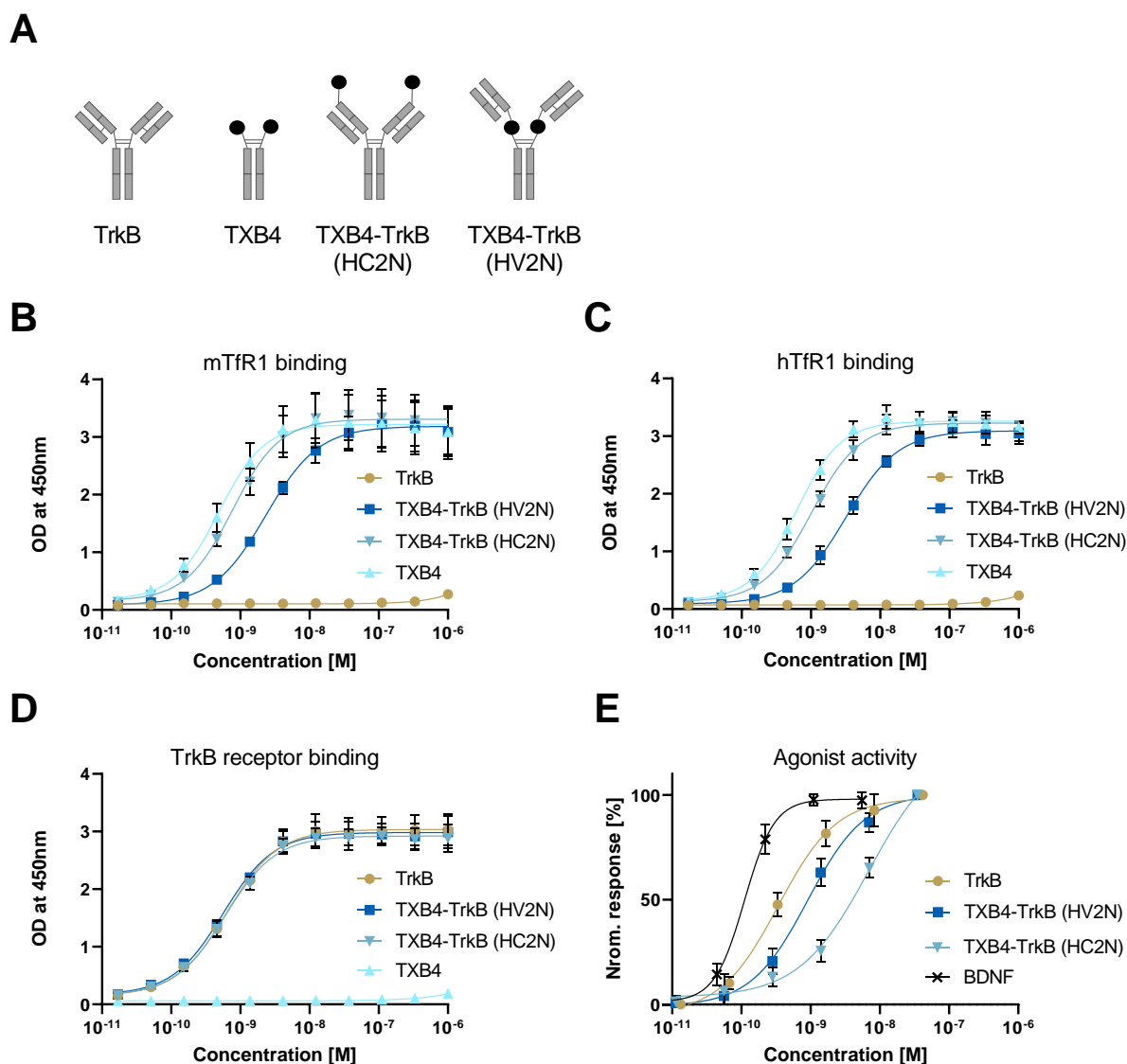


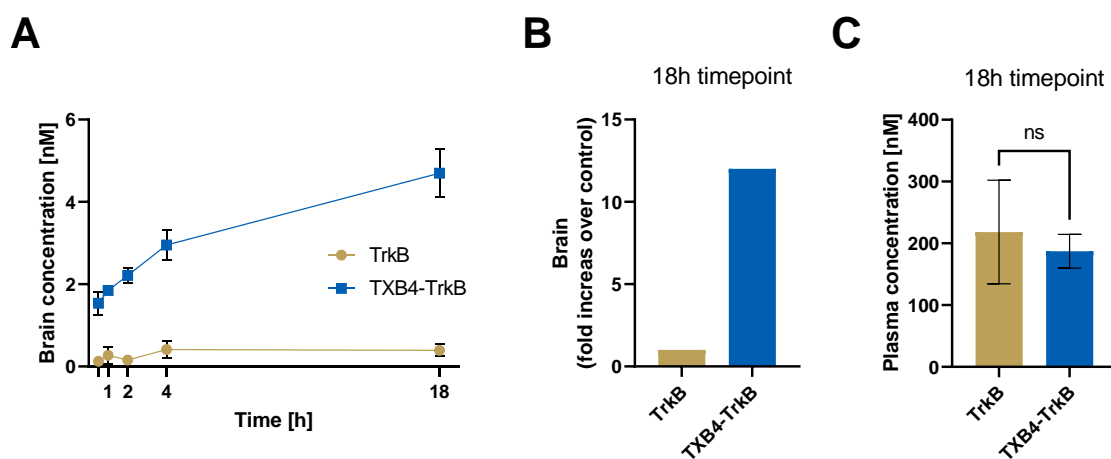
**Figure 1.** Binding and agonist activity of TrkB antibody and TXB4—TrkB fusions. (A) Diagram of various antibody formats with the TXB4 VNAR module represented by black-filled circles. The binding of TXB4-TrkB antibody fusion to mTfR1 and (B) hTfR1. (C) was measured by ELISA compared to the unmodified TXB4 VNAR-hFc and TXB4 module as references. (D) Binding to TrkB was measured by ELISA compared to the unmodified TXB4 VNAR-hFc and TXB4 as references compared to the same as references. OD values were used for 4-parametric non-linear regression model to calculate EC50s ( $\pm$ SD,  $n = 3$ ). (E) TrkB and TXB4-TrkB fusion protein were tested for agonist activity using the TrkB-NFAT-bla CHO-K1 reporter cell line assay. Data were normalized and 4-parametric non-linear regression model was used to calculate EC50 values ( $\pm$ SD,  $n = 3$ –5) (see Table 1).

**Table 1.** Agonist activity using the TrkB-NFAT-bla CHO-K1 reporter cell line assay. A 4-parametric non-linear regression model was used to calculate EC50 values (n = 3–5) (see Figure 1E).

Agonist Activity EC50 [M]				
TrkB Antibody	TXB4-TrkB (HV2N)	TXB4-TrkB (HC2N)	TXB4	BDNF
$3.4 \times 10^{-10}$	$9.1 \times 10^{-10}$	$6.9 \times 10^{-9}$	NA	$1.1 \times 10^{-10}$

**Table 2.** Binding kinetics of the TrkB antibody and bivalent TXB4-antibody fusions to the TrkB receptor determined by SPR.

	TrkB Receptor		
	ka 1/[Ms]	kd [1/s]	KD [M]
TrkB antibody	$2.18 \times 10^5$	$3 \times 10^{-4}$	$1.37 \times 10^{-9}$
TXB4-TrkB (HV2N)	$2.32 \times 10^5$	$3.02 \times 10^{-4}$	$1.3 \times 10^{-9}$
TXB4-TrkB (HC2N)	$2.20 \times 10^5$	$9.77 \times 10^{-5}$	$4.44 \times 10^{-10}$

**Figure 2.** Brain uptake of TrkB antibody and TXB4-TrkB antibody fusion. Equimolar doses of the TrkB antibody (3.6 mg/kg) or TXB4-TrkB fusion in the HV2N format (4.3 mg/kg) were administered by single IV injection. Brains were perfused and harvested, and antibody concentrations were determined at the given timepoints. The brain concentration of the TXB4-TrkB fusion rapidly increases after injection (A) with brain levels reaching 12-fold over the control by 18 h (B), whereas the difference in plasma levels was not significant (ns) as determined by two-tailed, unpaired t-test (C). Data are presented as the mean  $\pm$ SD, n = 3.

**Brain Localization of the TXB4-TrkB antibody fusion after peripheral administration.** The unmodified TrkB antibody or TXB4-TrkB antibody fusion (HV2N) was administered by a single SC injection (10 mg/kg). Perfused brains were harvested 18 h later and stained by immunohistochemistry using an anti-human IgG to detect the injected antibodies. At lower magnification, no TrkB agonist antibody staining was seen anywhere in the brain (Figure 3A). In stark contrast, the TXB4-TrkB antibody fusion was readily detected within endothelial cells that line capillaries throughout the brain (Figure 3B). If the TrkB or TXB4-TrkB antibodies engage TrkB receptors on the cell surface, internalization into those cells would be expected [41]. The most conspicuous staining for the TrkB receptor was the intracellular staining of large neurons in the cortex (inserts in Figure 3C,D). The TXB4-TrkB antibody fusion was also readily seen in these cells (Figure 3C), but the unmodified TrkB antibody was not detected (Figure 3D). Activation of the ERK1/2 signaling pathway is a canonical feature of neurotrophin receptor activation, which can be detected by antibodies that recognize the phosphorylated form of ERK1/2 [2]. Activated ERK1/2 was not detected by this method in the brains of animals treated with the TrkB agonist antibody (Figure 3E);

however, it was readily detected in the brain following treatment with TXB4-TrkB antibody fusion and this was most obvious in the cortex (Figure 3F).

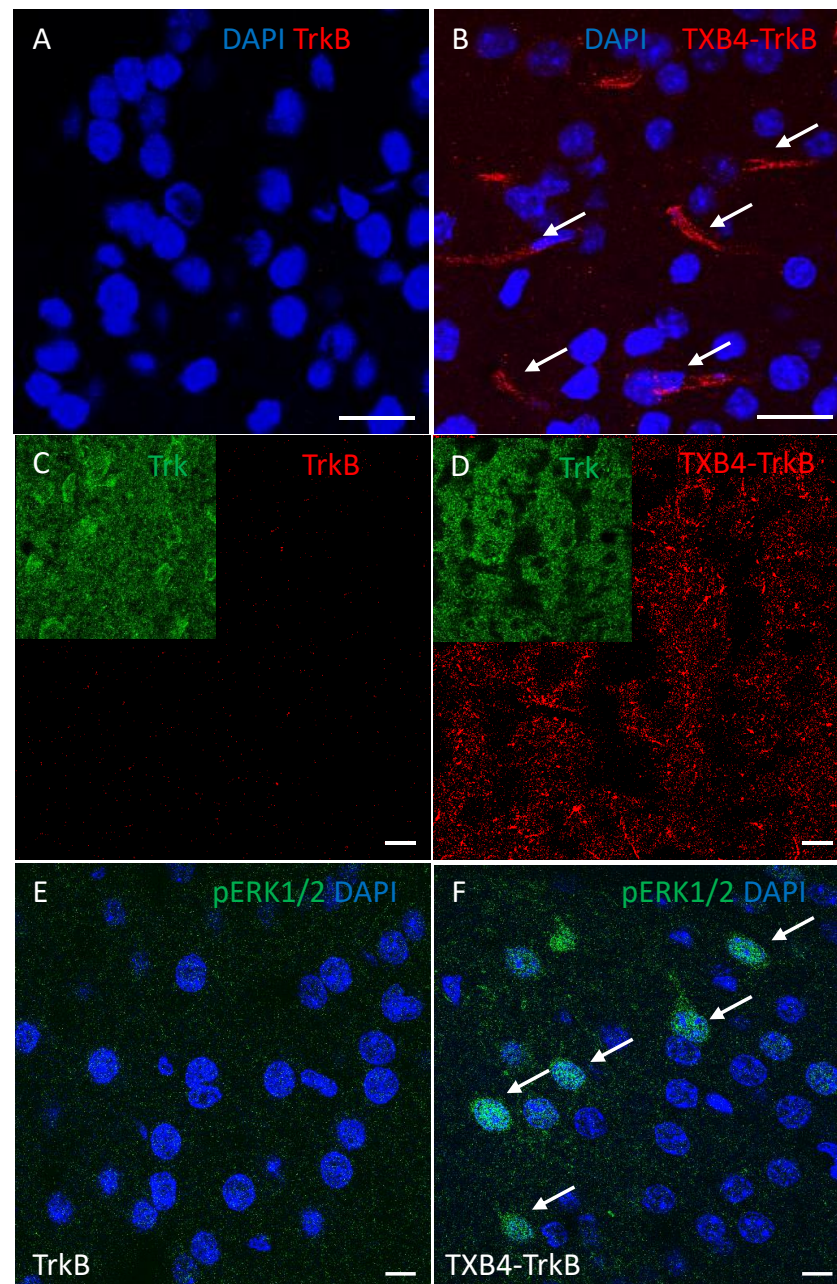


**Figure 3. Brain localization of the TXB4-TrkB antibody fusion with ERK1/2 activation after peripheral administration.** Perfused brains were harvested 18 h after administration of the TrkB or TXB4-TrkB antibody fusion (10 mg/kg, SC). Human IgG was not detected immunohistochemistry (40 $\times$ ) following TrkB antibody administration (A) but was readily seen in endothelial cells (arrows) following TXB4-TrkB administration (B). At higher magnification (63 $\times$ ) human IgG was not detected in the cortex following TrkB antibody administration (C) but was readily seen in a punctate intracellular pattern in large neurons following TXB4-TrkB administration (D). Inserts show the expression of the TrkB receptor in the same field. The same cortical regions as in C and D were also stained with an antibody that recognizes pERK1/2, which was not detected at high magnification (63 $\times$ ) following TrkB agonist antibody administration (E) but was readily detected in cells and nuclei (arrows) following TXB4-TrkB administration (F). Nuclei were labeled with DAPI in A, B, E and F. Scale bars = 10  $\mu$ m.

**Target engagement in the 6-OHDA model of PD.** When delivered locally, BDNF limits the death of TH+ dopaminergic neurons in the SNc that normally accompanies the injection of 6-OHDA into the striatum [42–45]; to this end we have tested if the systemic administration of TXB4-TrkB is neuroprotective in this model of PD. We first wanted to determine if the systemically administered TXB4-TrkB antibody fusion localizes to the SNc in a healthy animal. Using tissue from the brain localization studies in Figure 3, the presence of the TrkB agonist antibody was not within the vicinity of TH+ cells in the SNc 18 h after SC delivery as expected (Figure 4A). In contrast, TXB4-TrkB was readily seen in this brain region 18 h after SC administration (Figure 4B). Moreover, while ERK1/2 is not activated in TH+ neurons following TrkB agonist antibody administration (Figure 4C), it is clearly activated in TH+ neurons following TXB4-TrkB administration (Figure 4D). In contrast, the TXB4-TrkC antibody fusion was not detected in the SNc at the same dose and timepoint, nor was pERK1/2 detected in TH+ cells (data not shown).

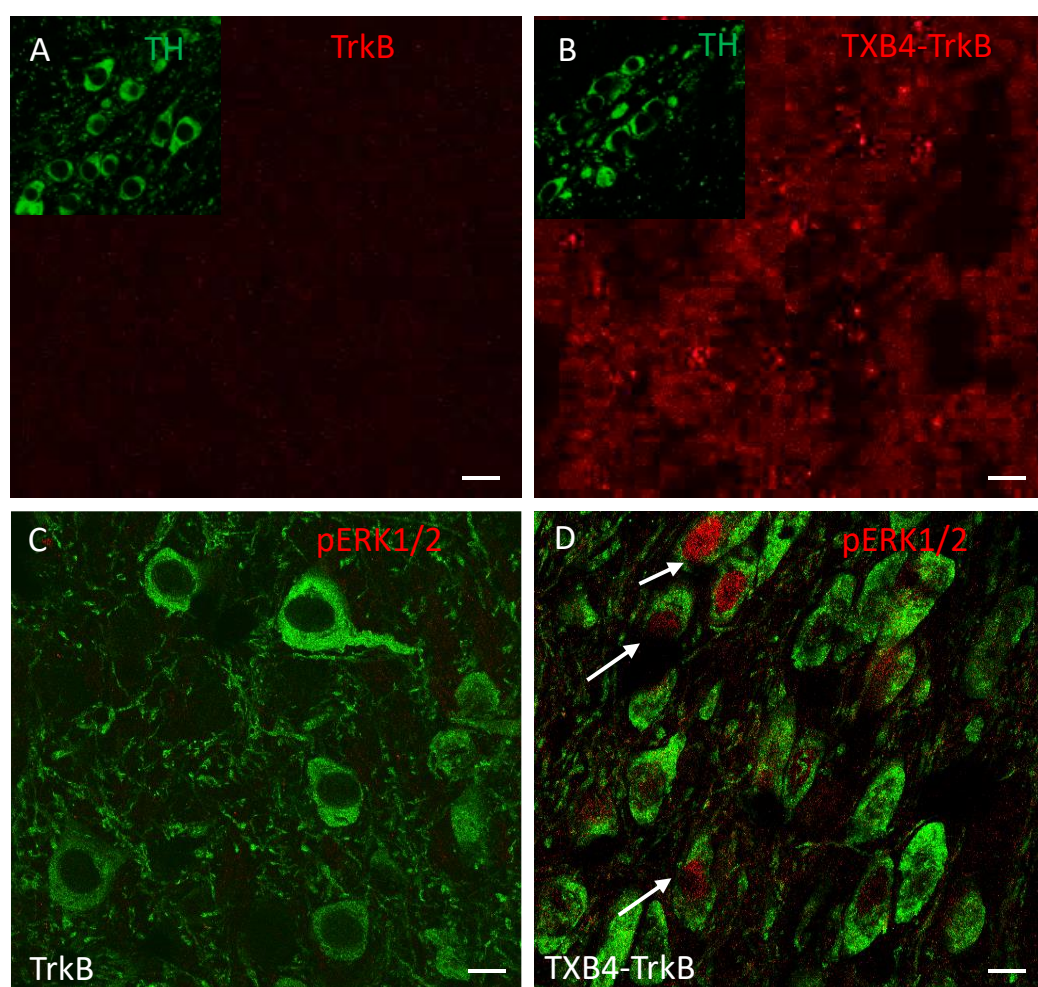


**Figure 4.** Localization of human IgG, TH and pERK1/2 in the SNc of animals treated with TrkB agonist antibody or TXB4-TrkB. TrkB agonist antibody or TXB4-TrkB were administered SC to mice (10 mg/kg) and brains harvested after 18 h and stained (see methods for details). Within the SNc human IgG (red) was not detected after TrkB agonist antibody administration (A) but diffuse and punctate staining was seen following TXB4-TrkB administration (B). The inserts in both show dopaminergic neurons within the same field revealed by co-staining for TH. The same regions as in A and B were also co-stained for TH and pERK1/2. pERK1/2 was not detected at high magnification (63×) following TrkB agonist antibody administration (C) but was readily detected in some cell nuclei (as indicated by arrows) following TXB4-TrkB administration (D). Scale bars = 10 μm.

**Neuroprotection in the 6-OHDA model of PD.** To test for neuroprotection, mice were treated with either PBS (control), TrkB agonist antibody, the TXB4-TrkC or the TXB4-TrkB antibody fusions (5 mg/kg) 24 h before inducing a partial 6-OHDA lesion and again at day seven (with reduced antibody dose of 2.5 mg/kg). Fourteen days after injection of 6-OHDA, brains were isolated and processed for TH immunoreactivity in the rostral, medial, and caudal SNc. As expected, there was a clear reduction ( $27.30 \pm 7.31\%$ ) in the number of TH+ cells as a percentage of the intact hemisphere following 6-OHDA treatment in the PBS control (Figure 5). In contrast there was essentially no cell loss in mice treated with the TXB4-TrkB antibody fusion ( $3.18 \pm 2.6\%$ ) relative to the PBS control (One-way ANOVA, Tukey's HSD,  $* p = 0.035$ ). Neuronal loss was still apparent with either the TrkB agonist antibody ( $12.47 \pm 2.97\%$ ) or TXB4-TrkC antibody fusion control ( $20.74 \pm 4.11\%$ ) treatment and not significantly different from the PBS control (Figure 5).

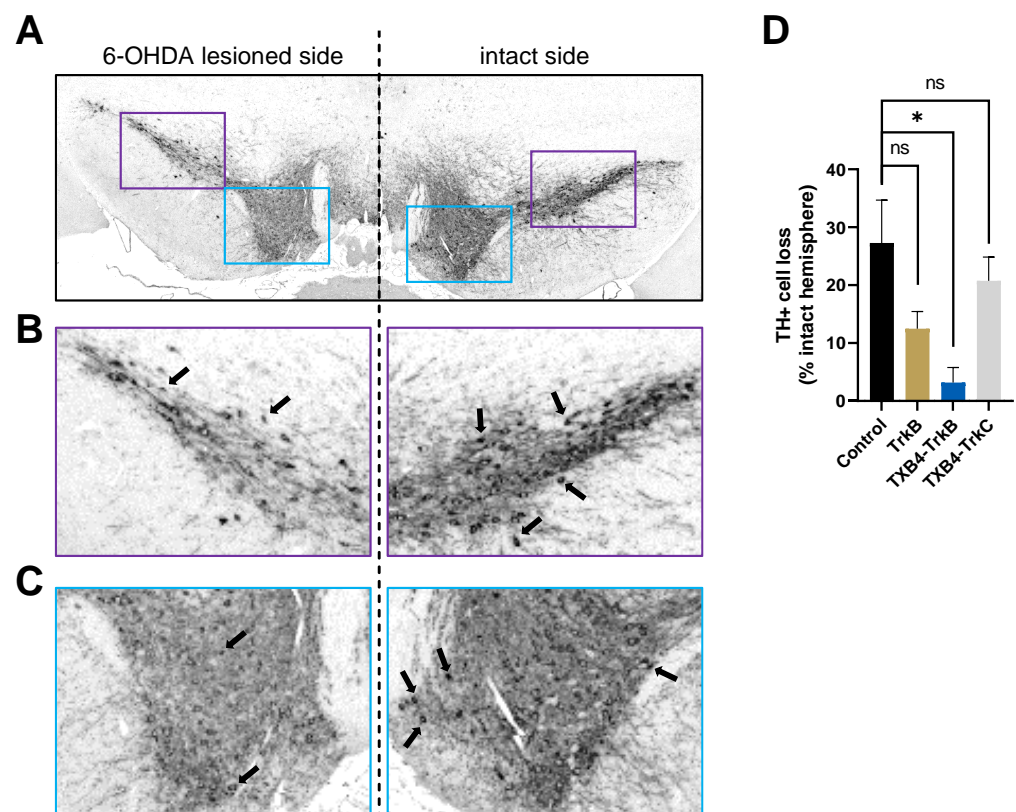


**Figure 5.** TXB4-TrkB protects dopaminergic cell bodies in the substantia nigra (SNc) against neuronal loss in the 6-OHDA model of PD. Representative section of TH+ dopaminergic SNc cells within the 6-OHDA lesioned (left) and intact (right) sides of PBS control (A) at  $20\times$  magnification. Enlargements of the boxed areas of lateral (B) and medial regions (C) show examples of the TH+ cell bodies (arrows) counted per section. Cell loss within the 6-OHDA lesioned side relative to the control side is shown (D) for groups treated with PBS, TrkB agonist antibody, TXB4-TrkB or TXB4-TrkC fusion antibodies. Data represented as mean  $\pm$  SEM % TH+ cell loss relative to intact hemisphere  $\pm$  SEM. One-way ANOVA, Tukey's HSD,  $* p = 0.035$ ,  $n = 3\text{--}5$  mice per group, ns = not significant.

#### 4. Discussion

The BDNF-TrkB signaling pathway is considered a drug target for a wide range of neurological diseases and depression. However, a short half-life of approximately 10 min in plasma [26] and 1 h in CSF [46], and a high isoelectric point ( $pI \sim 10$ ) that limits its diffusion in tissues [27] have in part hampered clinical development. BDNF can also bind to the p75 neurotrophin receptor (p75NTR) and in some instances activation of this receptor can induce apoptosis [47]. p75NTR is also an integral component of a receptor complex that inhibits axonal growth and the interaction of BDNF with this complex might detract

from its regenerative function [48]. The BDNF/p75NTR interaction might also limit the therapeutic potential of BDNF.

TrkB antibodies do not bind p75NTR, in general have a plasma half-life of several days, and are effective if directly delivered to the site of neural injury. The intravitreal delivery of the 29D7 TrkB agonist antibody delays retinal ganglion cell death in models of acute and chronic retinal injury [49,50], whilst intracerebroventricular administration prior to initiation of a neonatal hypoxic-ischemic brain injury in rats significantly increased neuronal survival and behavioral recovery [31]. Intrathecal application of 29D7 improves motor neuron survival and regeneration in models of spinal cord injury and motor neuron degeneration [14]. It follows that there might be opportunities in the development of a version of 29D7 or other TrkB agonist antibodies if they could readily cross the BBB following systemic administration.

Using TfR1 receptor antibodies to deliver cargos across the BBB is not novel [51–53]. However, obstacles have been encountered with particular antibodies including the retention of TfR1 antibodies within brain capillaries [54,55], the lysis of TfR1-expressing reticulocytes [56], competition with transferrin for binding to the TfR1 and/or antibody induced targeting of TfR1 to lysosomes [57–60]. Moreover, the ubiquitous expression of the receptor in peripheral tissues [61] likely contributes to the short plasma half-life reported for TfR1 antibodies [62–64]. Various strategies have been employed to overcome these obstacles, including a reduction in binding affinity, valency, and bispecific antibody formatting. Interestingly, high-affinity single domain VNAR antibodies to TfR1 do not share these problems. The small VNAR domain (12–15 kDa) with an extended CDR3 loop can engage cryptic epitopes inaccessible to standard immunoglobulins [65], which may enable the selective tissue binding, and consequently a longer plasma half-life observed with TXB2 shuttle [66]. TXB4 was derived from TXB2 shuttle by CDR3 mutagenesis and was selected for these studies for its improved physicochemical properties and enhanced brain penetration [37,67].

A brain penetrant TrkB agonist antibody was configured with the TXB4 shuttle in two different formats. In one version, the VNAR domain was fused to the N-terminus of the HC (HC2N), while in the other, it was positioned between the CH1 and CH2 domains above the hinge region (HV2N) to avoid possible steric hinderance of the TrkB paratope. Placing the TXB4 module in the HC2N format had virtually no effect on TfR1 binding and while the ELISA binding curve of the HV2N format was right shifted, the binding EC50 for TfR1 was still in the low nM range. Neither format adversely affected the TrkB binding kinetics of the antibody and while both bispecific formats were full agonists in a TrkB reporter cell assay, the HV2N format was approximately seven-fold more potent. Overall, the N-terminal placement better preserved TfR1 binding, but interference with the TrkB binding paratope resulted in reduced activity. Consequently, the HV2N format was selected for in vivo studies.

After peripheral administration of TXB4-TrkB in the HV2N format (4.3 mg/kg, IV), mouse brain concentrations reached the predicted  $C_{max}$  at approximately 18-h post injection [36,68]. The achieved 5 nM brain level was expected to trigger robust activation of endogenous TrkB receptors. Target engagement and activation would be manifested by the uptake of TXB4-TrkB into TrkB expressing cells and the activation of canonical signaling pathways such as the ERK1/2 cascade [69]. Indeed, following a single dose (10 mg/kg, SC) in a healthy animal, we could readily detect TXB4-TrkB within the large TrkB positive neurons in the cortex and also found activation of the ERK1/2 cascade throughout the cortex. Likewise, TXB4-TrkB was found in the SNc and ERK1/2 was clearly activated in the TH+ dopaminergic neurons in the SNc in the same animals. As a control, antibody accumulation and ERK1/2 activation were not seen in the SNc following systemic administration of the unmodified TrkB agonist antibody.

When injected into the striatum, 6-OHDA is taken up into dopaminergic neurons via the high-affinity dopamine transporter. It is then oxidized, and the toxicity of the released reactive oxygen species is reflected in a loss of dopaminergic tracts and terminals

in the striatum and cell bodies in the SNc [70]. This is a well-established preclinical model of PD [71], but it is noteworthy that toxicity due to generation of reactive oxygen species might be causative of neuronal loss in a wide range of other neurodegenerative diseases. In this study the unilateral administration of 6-OHDA was associated with the loss of 20%–30% of the neurons throughout the SNc. Remarkably, there was no significant neuronal loss throughout the SNc in animals treated with TXB4-TrkB. Control construct TXB4-TrkC also accumulated in the brain but did not localize to or activate ERK1/2 in the TH+ dopaminergic neurons nor offer any neuroprotection against the 6-OHDA lesion. Future studies will be required to determine the impact of TXB4-TrkB on the development of the motor deficits that are a well-studied trait in this model.

Antibodies can show efficacy in neurodegenerative models when administered without a shuttle due to passive transfer and/or uptake through a disease related or injury induced “leaky” BBB. Indeed, there is evidence suggesting that the BBB is damaged to some extent for a limited period in 6-OHDA models [72]. In this study the unmodified TrkB agonist antibody showed a trend towards limited neuroprotection in the SNc, although it did not reach statistical significance, despite a 3-fold greater potency relative to TXB4-TrkB. While there might have been partial neuroprotection due to some leakage of the TrkB agonist antibody, TXB4-TrkB was by far the more effective treatment. Nonetheless, Han et al., has demonstrated the therapeutic potential of IV administered TrkB agonist antibody Ab4B19 for ischemic brain injury based on leakage across the compromised BBB at the site of injury [73]. While many neurodegenerative diseases are associated with a compromised BBB related to neuroinflammatory processes [74,75], one needs to consider the likely beneficial effects of using a shuttle to deliver a therapeutic antibody to the brain. The most obvious is that the therapeutic antibody can be delivered to regions of the brain where the BBB has yet to be compromised or indeed has recovered from damage. Likewise, the use of a brain shuttle is always likely to result in more antibody reaching the parenchyma, increasing the probability of a therapeutic response. Finally, getting more antibody from the serum to the brain will obviously affect the systemic dose required for a therapeutic effect and minimize the risk of adverse effects.

## 5. Conclusions

In summary, this paper shows that the VNAR TXB4 shuttle targeting the TfR1 can be fused to an agonist antibody to allow for the efficient transport across the BBB and access to the brain parenchyma at physiologically relevant concentrations. The TXB4-TrkB fusion antibody crossed the BBB, accumulated in the brain, and triggered neurotrophin signaling in target cells susceptible to loss in AD (cortical neurons) and PD (dopaminergic neurons in the SNc). Furthermore, systemic treatment with TXB4-TrkB prevented the neuronal loss normally seen in a partial lesion mouse model of PD. As such, TXB4-TrkB can be considered as the first in a new generation of brain penetrant agonist antibodies with therapeutic potential in a wide range of neurodegenerative diseases, acute brain and spinal cord injury, and possibly depression.

## 6. Patents

Stocki, P., Wicher, K.B., Szary, J.M. and Rutkowski, J.L., inventors. Ossianix, Inc., assignee. Improved TfR-selective binding peptides capable of crossing the blood brain barrier International Publication No. WO2019089395A1, published 9 May 2019.

Rutkowski, J.L., Walsh, F., Sinclair, E.H. and Stocki, P., inventors. Ossianix, Inc., assignee. BBB-shuttling VNARs conjugated to neurotrophic agonist antibodies to treat neurodegenerative diseases and conditions. International Publication No. WO2021102276 A1, published 27 May 2021.

**Author Contributions:** P.D., F.S.W. and J.L.R. developed the hypothesis. P.S., E.H.S. and A.G. designed, produced, and analyzed the VNAR—TrkB constructs. E.C. and A.K.-R. performed animal experiment and analyzed data. P.D., E.J.R.F., S.D. and J.L.R. supervised research and assisted in data analysis. E.C. and P.D. co-wrote the first draft of the manuscript. All authors have read and agreed to the published version of the manuscript.

**Funding:** This research received no external funding.

**Institutional Review Board Statement:** The study was conducted in accordance with UK Animals Scientific Procedures Act (1986) and were approved by King’s College London Animal Welfare and Ethical Review Body.

**Informed Consent Statement:** Not applicable.

**Data Availability Statement:** Data is contained within the article.

**Conflicts of Interest:** E.H.S., P.S., A.G., F.S.W. and J.L.R. were employees of Ossianix, Inc. Ossianix, Inc. filled patents on the subject matter of this manuscript.

## References

- Huang, E.J.; Reichardt, L.F. Neurotrophins: Roles in neuronal development and function. *Annu. Rev. Neurosci.* **2001**, *24*, 677–736. [CrossRef] [PubMed]
- Reichardt, L.F. Neurotrophin-regulated signalling pathways. *Philos. Trans. R. Soc. Lond. Ser. B Biol. Sci.* **2006**, *361*, 1545–1564. [CrossRef] [PubMed]
- Houlton, J.; Abumaria, N.; Hinkley, S.F.R.; Clarkson, A.N. Therapeutic Potential of Neurotrophins for Repair After Brain Injury: A Helping Hand From Biomaterials. *Front. Neurosci.* **2019**, *13*, 790. [CrossRef] [PubMed]
- Simmons, D.A. Modulating Neurotrophin Receptor Signaling as a Therapeutic Strategy for Huntington’s Disease. *J. Huntingt. Dis.* **2017**, *6*, 303–325. [CrossRef]
- Ding, Y.X.; Xia, Y.; Jiao, X.Y.; Duan, L.; Yu, J.; Wang, X.; Chen, L.W. The TrkB-positive dopaminergic neurons are less sensitive to MPTP insult in the substantia nigra of adult C57/BL mice. *Neurochem. Res.* **2011**, *36*, 1759–1766. [CrossRef]
- Nagahara, A.H.; Mateling, M.; Kovacs, I.; Wang, L.; Eggert, S.; Rockenstein, E.; Koo, E.H.; Masliah, E.; Tuszynski, M.H. Early BDNF treatment ameliorates cell loss in the entorhinal cortex of APP transgenic mice. *J. Neurosci. Off. J. Soc. Neurosci.* **2013**, *33*, 15596–15602. [CrossRef]
- Nagahara, A.H.; Merrill, D.A.; Coppola, G.; Tsukada, S.; Schroeder, B.E.; Shaked, G.M.; Wang, L.; Blesch, A.; Kim, A.; Conner, J.M.; et al. Neuroprotective effects of brain-derived neurotrophic factor in rodent and primate models of Alzheimer’s disease. *Nat. Med.* **2009**, *15*, 331–337. [CrossRef]
- Zhang, J.; Yu, Z.; Yu, Z.; Yang, Z.; Zhao, H.; Liu, L.; Zhao, J. rAAV-mediated delivery of brain-derived neurotrophic factor promotes neurite outgrowth and protects neurodegeneration in focal ischemic model. *Int. J. Clin. Exp. Pathol.* **2011**, *4*, 496–504.
- Takeshima, Y.; Nakamura, M.; Miyake, H.; Tamaki, R.; Inui, T.; Horiuchi, K.; Wajima, D.; Nakase, H. Neuroprotection with intraventricular brain-derived neurotrophic factor in rat venous occlusion model. *Neurosurgery* **2011**, *68*, 1334–1341. [CrossRef]
- Kiprianova, I.; Freiman, T.M.; Desiderato, S.; Schwab, S.; Galmbacher, R.; Gillardon, F.; Spranger, M. Brain-derived neurotrophic factor prevents neuronal death and glial activation after global ischemia in the rat. *J. Neurosci. Res.* **1999**, *56*, 21–27. [CrossRef]
- Bejot, Y.; Mossiat, C.; Giroud, M.; Prigent-Tessier, A.; Marie, C. Circulating and brain BDNF levels in stroke rats. Relevance to clinical studies. *PLoS ONE* **2011**, *6*, e29405. [CrossRef]
- Kobayashi, N.R.; Fan, D.P.; Giehl, K.M.; Bedard, A.M.; Wiegand, S.J.; Tetzlaff, W. BDNF and NT-4/5 prevent atrophy of rat rubrospinal neurons after cervical axotomy, stimulate GAP-43 and Talpha1-tubulin mRNA expression, and promote axonal regeneration. *J. Neurosci.* **1997**, *17*, 9583–9595. [CrossRef]
- Tuinstra, H.M.; Aviles, M.O.; Shin, S.; Holland, S.J.; Zelivyanskaya, M.L.; Fast, A.G.; Ko, S.Y.; Margul, D.J.; Bartels, A.K.; Boehler, R.M.; et al. Multifunctional, multichannel bridges that deliver neurotrophin encoding lentivirus for regeneration following spinal cord injury. *Biomaterials* **2012**, *33*, 1618–1626. [CrossRef] [PubMed]
- Fouad, K.; Vavrek, R.; Cho, S. A TrkB antibody agonist promotes plasticity following cervical spinal cord injury in adult rats. *J. Neurotrauma* **2021**, *38*, 1338–1348. [CrossRef]
- Vilar, M.; Mira, H. Regulation of Neurogenesis by Neurotrophins during Adulthood: Expected and Unexpected Roles. *Front. Neurosci.* **2016**, *10*, 26. [CrossRef]
- Numakawa, T.; Odaka, H.; Adachi, N. Actions of Brain-Derived Neurotrophin Factor in the Neurogenesis and Neuronal Function, and Its Involvement in the Pathophysiology of Brain Diseases. *Int. J. Mol. Sci.* **2018**, *19*, 3650. [CrossRef]
- Mogi, M.; Togari, A.; Kondo, T.; Mizuno, Y.; Komure, O.; Kuno, S.; Ichinose, H.; Nagatsu, T. Brain-derived growth factor and nerve growth factor concentrations are decreased in the substantia nigra in Parkinson’s disease. *Neurosci. Lett.* **1999**, *270*, 45–48. [CrossRef]
- Huang, Y.; Huang, C.; Yun, W. Peripheral BDNF/TrkB protein expression is decreased in Parkinson’s disease but not in Essential tremor. *J. Clin. Neurosci.* **2019**, *63*, 176–181. [CrossRef]



19. Huang, Y.; Yun, W.; Zhang, M.; Luo, W.; Zhou, X. Serum concentration and clinical significance of brain-derived neurotrophic factor in patients with Parkinson's disease or essential tremor. *J. Int. Med. Res.* **2018**, *46*, 1477–1485. [CrossRef]
20. Tanila, H. The role of BDNF in Alzheimer's disease. *Neurobiol. Dis.* **2017**, *97*, 114–118. [CrossRef]
21. Park, H. Cortical Axonal Secretion of BDNF in the Striatum Is Disrupted in the Mutant-huntingtin Knock-in Mouse Model of Huntington's Disease. *Exp. Neurobiol.* **2018**, *27*, 217–225. [CrossRef] [PubMed]
22. Nguyen, K.Q.; Rymar, V.V.; Sadikot, A.F. Impaired TrkB Signaling Underlies Reduced BDNF-Mediated Trophic Support of Striatal Neurons in the R6/2 Mouse Model of Huntington's Disease. *Front. Cell. Neurosci.* **2016**, *10*, 37. [CrossRef] [PubMed]
23. Ma, Q.; Yang, J.; Li, T.; Milner, T.A.; Hempstead, B.L. Selective reduction of striatal mature BDNF without induction of proBDNF in the zQ175 mouse model of Huntington's disease. *Neurobiol. Dis.* **2015**, *82*, 466–477. [CrossRef] [PubMed]
24. Phillips, C. Brain-Derived Neurotrophic Factor, Depression, and Physical Activity: Making the Neuroplastic Connection. *Neural Plast.* **2017**, *2017*, 7260130. [CrossRef]
25. Rantamaki, T. TrkB neurotrophin receptor at the core of antidepressant effects, but how? *Cell Tissue Res.* **2019**, *377*, 115–124. [CrossRef]
26. Sakane, T.; Pardridge, W.M. Carboxyl-directed pegylation of brain-derived neurotrophic factor markedly reduces systemic clearance with minimal loss of biologic activity. *Pharm. Res.* **1997**, *14*, 1085–1091. [CrossRef]
27. Croll, S.D.; Chesnutt, C.R.; Rudge, J.S.; Acheson, A.; Ryan, T.E.; Siuciak, J.A.; DiStefano, P.S.; Wiegand, S.J.; Lindsay, R.M. Co-infusion with a TrkB-Fc receptor body carrier enhances BDNF distribution in the adult rat brain. *Exp. Neurol.* **1998**, *152*, 20–33. [CrossRef]
28. Perreault, M.; Feng, G.; Will, S.; Gareski, T.; Kubasiak, D.; Marquette, K.; Vugmeyster, Y.; Unger, T.J.; Jones, J.; Qadri, A.; et al. Activation of TrkB with TAM-163 results in opposite effects on body weight in rodents and non-human primates. *PLoS ONE* **2013**, *8*, e62616. [CrossRef]
29. Xu, L.; Zhang, Y.; Cohen, S.B.; DiPetrillo, K. TrkB agonist antibody dose-dependently raises blood pressure in mice with diet-induced obesity. *Am. J. Hypertens.* **2010**, *23*, 732–736. [CrossRef]
30. Sahenk, Z.; Galloway, G.; Edwards, C.; Malik, V.; Kaspar, B.K.; Eagle, A.; Yetter, B.; Forgie, A.; Tsao, D.; Lin, J.C. TrkB and TrkC agonist antibodies improve function, electrophysiologic and pathologic features in Trembler J mice. *Exp. Neurol.* **2010**, *224*, 495–506. [CrossRef]
31. Kim, G.S.; Cho, S.; Nelson, J.W.; Zipfel, G.J.; Han, B.H. TrkB agonist antibody pretreatment enhances neuronal survival and long-term sensory motor function following hypoxic ischemic injury in neonatal rats. *PLoS ONE* **2014**, *9*, e88962. [CrossRef] [PubMed]
32. Todd, D.; Gowers, I.; Dowler, S.J.; Wall, M.D.; McAllister, G.; Fischer, D.F.; Dijkstra, S.; Fratantoni, S.A.; van de Bospoort, R.; Veenman-Koepke, J.; et al. A monoclonal antibody TrkB receptor agonist as a potential therapeutic for Huntington's disease. *PLoS ONE* **2014**, *9*, e87923. [CrossRef] [PubMed]
33. Qian, M.D.; Zhang, J.; Tan, X.Y.; Wood, A.; Gill, D.; Cho, S. Novel agonist monoclonal antibodies activate TrkB receptors and demonstrate potent neurotrophic activities. *J. Neurosci.* **2006**, *26*, 9394–9403. [CrossRef] [PubMed]
34. Merkouris, S.; Barde, Y.A.; Binley, K.E.; Allen, N.D.; Stepanov, A.V.; Wu, N.C.; Grande, G.; Lin, C.W.; Li, M.; Nan, X.; et al. Fully human agonist antibodies to TrkB using autocrine cell-based selection from a combinatorial antibody library. *Proc. Natl. Acad. Sci. USA* **2018**, *115*, E7023–E7032. [CrossRef] [PubMed]
35. Pardridge, W.M. Blood-brain barrier drug delivery of IgG fusion proteins with a transferrin receptor monoclonal antibody. *Expert. Opin. Drug. Deliv.* **2015**, *12*, 207–222. [CrossRef] [PubMed]
36. Stocki, P.; Szary, J.; Rasmussen, C.L.M.; Demydchuk, M.; Northall, L.; Logan, D.B.; Gauhar, A.; Thei, L.; Moos, T.; Walsh, F.S.; et al. Blood-brain barrier transport using a high affinity, brain-selective VNAR antibody targeting transferrin receptor 1. *FASEB J.* **2021**, *35*, e21172. [CrossRef] [PubMed]
37. Stocki, P.; Wicher, K.B.; Szary, J.; Rutkowski, J.L. Improved TfR-Selective Binding Peptides Capable of Crossing the Blood Brain Barrier. U.S. Patent WO2019089395A1, 9 May 2019.
38. Devaux, B.; Hongo, J.A.; Presta, L.G.; Shelton, D.L. Methods for Treating Neuropathy by Agonist Anti-Trk-C Monoclonal Antibodies. US7615383B2, 10 November 2009.
39. Strohl, W.R. Optimization of Fc-mediated effector functions of monoclonal antibodies. *Curr. Opin. Biotechnol.* **2009**, *20*, 685–691. [CrossRef]
40. Fletcher, E.J.R.; Moon, L.D.F.; Duty, S. Chondroitinase ABC reduces dopaminergic nigral cell death and striatal terminal loss in a 6-hydroxydopamine partial lesion mouse model of Parkinson's disease. *BMC Neurosci.* **2019**, *20*, 61. [CrossRef]
41. Sommerfeld, M.T.; Schweigreiter, R.; Barde, Y.A.; Hoppe, E. Down-regulation of the neurotrophin receptor TrkB following ligand binding. Evidence for an involvement of the proteasome and differential regulation of TrkA and TrkB. *J. Biol. Chem.* **2000**, *275*, 8982–8990. [CrossRef]
42. Nie, S.; Xu, Y.; Chen, G.; Ma, K.; Han, C.; Guo, Z.; Zhang, Z.; Ye, K.; Cao, X. Small molecule TrkB agonist deoxygedunin protects nigrostriatal dopaminergic neurons from 6-OHDA and MPTP induced neurotoxicity in rodents. *Neuropharmacology* **2015**, *99*, 448–458. [CrossRef]
43. Altar, C.A.; Boylan, C.B.; Jackson, C.; Hershenson, S.; Miller, J.; Wiegand, S.J.; Lindsay, R.M.; Hyman, C. Brain-derived neurotrophic factor augments rotational behavior and nigrostriatal dopamine turnover in vivo. *Proc. Natl. Acad. Sci. USA* **1992**, *89*, 11347–11351. [CrossRef]

44. Klein, R.L.; Lewis, M.H.; Muzyczka, N.; Meyer, E.M. Prevention of 6-hydroxydopamine-induced rotational behavior by BDNF somatic gene transfer. *Brain Res.* **1999**, *847*, 314–320. [CrossRef]
45. Somoza, R.; Juri, C.; Baes, M.; Wyneken, U.; Rubio, F.J. Intranigral transplantation of epigenetically induced BDNF-secreting human mesenchymal stem cells: Implications for cell-based therapies in Parkinson's disease. *Biol. Blood Marrow Transplant. J. Am. Soc. Blood Marrow Transplant.* **2010**, *16*, 1530–1540. [CrossRef] [PubMed]
46. Soderquist, R.G.; Milligan, E.D.; Sloane, E.M.; Harrison, J.A.; Douvas, K.K.; Potter, J.M.; Hughes, T.S.; Chavez, R.A.; Johnson, K.; Watkins, L.R.; et al. PEGylation of brain-derived neurotrophic factor for preserved biological activity and enhanced spinal cord distribution. *J. Biomed. Mater. Res. Part A* **2009**, *91*, 719–729. [CrossRef] [PubMed]
47. Barker, P.A. p75NTR is positively promiscuous: Novel partners and new insights. *Neuron* **2004**, *42*, 529–533. [CrossRef] [PubMed]
48. Williams, G.; Williams, E.J.; Maison, P.; Pangalos, M.N.; Walsh, F.S.; Doherty, P. Overcoming the inhibitors of myelin with a novel neurotrophin strategy. *J. Biol. Chem.* **2005**, *280*, 5862–5869. [CrossRef]
49. Bai, Y.; Xu, J.; Brahim, F.; Zhuo, Y.; Sarunic, M.V.; Saragovi, H.U. An agonistic TrkB mAb causes sustained TrkB activation, delays RGC death, and protects the retinal structure in optic nerve axotomy and in glaucoma. *Investig. Ophthalmol. Vis. Sci.* **2010**, *51*, 4722–4731. [CrossRef]
50. Hu, Y.; Cho, S.; Goldberg, J.L. Neurotrophic effect of a novel TrkB agonist on retinal ganglion cells. *Investig. Ophthalmol. Vis. Sci.* **2010**, *51*, 1747–1754. [CrossRef]
51. Friden, P.M.; Walus, L.R.; Musso, G.F.; Taylor, M.A.; Malfroy, B.; Starzyk, R.M. Anti-transferrin receptor antibody and antibody-drug conjugates cross the blood-brain barrier. *Proc. Natl. Acad. Sci. USA* **1991**, *88*, 4771–4775. [CrossRef]
52. Pardridge, W.M.; Buciak, J.L.; Friden, P.M. Selective transport of an anti-transferrin receptor antibody through the blood-brain barrier in vivo. *J. Pharmacol. Exp. Ther.* **1991**, *259*, 66–70.
53. Kordower, J.H.; Charles, V.; Bayer, R.; Bartus, R.T.; Putney, S.; Walus, L.R.; Friden, P.M. Intravenous administration of a transferrin receptor antibody-nerve growth factor conjugate prevents the degeneration of cholinergic striatal neurons in a model of Huntington disease. *Proc. Natl. Acad. Sci. USA* **1994**, *91*, 9077–9080. [CrossRef] [PubMed]
54. Moos, T.; Morgan, E.H. Restricted transport of anti-transferrin receptor antibody (OX26) through the blood-brain barrier in the rat. *J. Neurochem.* **2001**, *79*, 119–129. [CrossRef] [PubMed]
55. Manich, G.; Cabezón, I.; del Valle, J.; Duran-Vilaregut, J.; Camins, A.; Pallas, M.; Pelegri, C.; Vilaplana, J. Study of the transcytosis of an anti-transferrin receptor antibody with a Fab' cargo across the blood-brain barrier in mice. *Eur. J. Pharm. Sci.* **2013**, *49*, 556–564. [CrossRef]
56. Lesley, J.; Schulte, R.; Woods, J. Modulation of transferrin receptor expression and function by anti-transferrin receptor antibodies and antibody fragments. *Exp. Cell Res.* **1989**, *182*, 215–233. [CrossRef]
57. Pardridge, W.M.; Boado, R.J.; Patrick, D.J.; Ka-Wai Hui, E.; Lu, J.Z. Blood-Brain Barrier Transport, Plasma Pharmacokinetics, and Neuropathology Following Chronic Treatment of the Rhesus Monkey with a Brain Penetrating Humanized Monoclonal Antibody Against the Human Transferrin Receptor. *Mol. Pharm.* **2018**, *15*, 5207–5216. [CrossRef]
58. Couch, J.A.; Yu, Y.J.; Zhang, Y.; Tarrant, J.M.; Fuji, R.N.; Meilandt, W.J.; Solanoy, H.; Tong, R.K.; Hoyte, K.; Luk, W.; et al. Addressing safety liabilities of TFR bispecific antibodies that cross the blood-brain barrier. *Sci. Transl. Med.* **2013**, *5*, 183ra157. [CrossRef]
59. Daniels, T.R.; Delgado, T.; Rodriguez, J.A.; Helguera, G.; Penichet, M.L. The transferrin receptor part I: Biology and targeting with cytotoxic antibodies for the treatment of cancer. *Clin. Immunol.* **2006**, *121*, 144–158. [CrossRef]
60. Niewoehner, J.; Bohrmann, B.; Collin, L.; Ulrich, E.; Sade, H.; Maier, P.; Rueger, P.; Stracke, J.O.; Lau, W.; Tissot, A.C.; et al. Increased brain penetration and potency of a therapeutic antibody using a monovalent molecular shuttle. *Neuron* **2014**, *81*, 49–60. [CrossRef]
61. The Human Protein Atlas. Available online: <http://www.proteinatlas.org/ENSG00000072274-TFRC/tissue> (accessed on 20 April 2022).
62. Yu, Y.J.; Zhang, Y.; Kenrick, M.; Hoyte, K.; Luk, W.; Lu, Y.; Atwal, J.; Elliott, J.M.; Prabhu, S.; Watts, R.J.; et al. Boosting brain uptake of a therapeutic antibody by reducing its affinity for a transcytosis target. *Sci. Transl. Med.* **2011**, *3*, 84ra44. [CrossRef]
63. Webster, C.I.; Hatcher, J.; Burrell, M.; Thom, G.; Thornton, P.; Gurrell, I.; Chessell, I. Enhanced delivery of IL-1 receptor antagonist to the central nervous system as a novel anti-transferrin receptor-IL-1RA fusion reverses neuropathic mechanical hypersensitivity. *Pain* **2017**, *158*, 660–668. [CrossRef]
64. Thom, G.; Burrell, M.; Haqqani, A.S.; Yogi, A.; Lessard, E.; Brunette, E.; Delaney, C.; Baumann, E.; Callaghan, D.; Rodrigo, N.; et al. Enhanced Delivery of Galanin Conjugates to the Brain through Bioengineering of the Anti-Transferrin Receptor Antibody OX26. *Mol. Pharm.* **2018**, *15*, 1420–1431. [CrossRef] [PubMed]
65. Wesolowski, J.; Alzogaray, V.; Reyelt, J.; Unger, M.; Juarez, K.; Urrutia, M.; Cauerhff, A.; Danquah, W.; Rissiek, B.; Scheuplein, F.; et al. Single domain antibodies: Promising experimental and therapeutic tools in infection and immunity. *Med. Microbiol. Immunol.* **2009**, *198*, 157–174. [CrossRef] [PubMed]
66. Panaccio, M.; Zalcberg, J.R.; Thompson, C.H.; Leyden, M.J.; Sullivan, J.R.; Lichtenstein, M.; McKenzie, I.F. Heterogeneity of the human transferrin receptor and use of anti-transferrin receptor antibodies to detect tumours in vivo. *Immunol. Cell Biol.* **1987**, *65 Pt 6*, 461–472. [CrossRef]
67. Rutkowski, J.L.; Walsh, F.S.; Sinclair, E.H.; Stocki, P. BBB-Shuttling-VNARs Conjugated to Neurotrophic Agonist Antibodies to Treat Neurodegenerative Diseases and Conditions. WO2021102276A1, 27 May 2021.

68. Sehlin, D.; Stocki, P.; Gustavsson, T.; Hultqvist, G.; Walsh, F.S.; Rutkowski, J.L.; Syvanen, S. Brain delivery of biologics using a cross-species reactive transferrin receptor 1 VNAR shuttle. *FASEB J.* **2020**, *34*, 13272–13283. [CrossRef] [PubMed]
69. Guo, W.; Nagappan, G.; Lu, B. Differential effects of transient and sustained activation of BDNF-TrkB signaling. *Dev. Neurobiol.* **2018**, *78*, 647–659. [CrossRef]
70. Glinka, Y.; Gassen, M.; Youdim, M.B. Mechanism of 6-hydroxydopamine neurotoxicity. *J. Neural Transmission. Suppl.* **1997**, *50*, 55–66. [CrossRef]
71. Duty, S.; Jenner, P. Animal models of Parkinson's disease: A source of novel treatments and clues to the cause of the disease. *Br. J. Pharmacol.* **2011**, *164*, 1357–1391. [CrossRef]
72. Olmedo-Diaz, S.; Estevez-Silva, H.; Oradd, G.; Af Bjerken, S.; Marcellino, D.; Virel, A. An altered blood-brain barrier contributes to brain iron accumulation and neuroinflammation in the 6-OHDA rat model of Parkinson's disease. *Neuroscience* **2017**, *362*, 141–151. [CrossRef]
73. Han, F.; Guan, X.; Guo, W.; Lu, B. Therapeutic potential of a TrkB agonistic antibody for ischemic brain injury. *Neurobiol. Dis.* **2019**, *127*, 570–581. [CrossRef]
74. Desai, B.S.; Monahan, A.J.; Carvey, P.M.; Hendey, B. Blood-brain barrier pathology in Alzheimer's and Parkinson's disease: Implications for drug therapy. *Cell Transplant.* **2007**, *16*, 285–299. [CrossRef]
75. Sweeney, M.D.; Sagare, A.P.; Zlokovic, B.V. Blood-brain barrier breakdown in Alzheimer disease and other neurodegenerative disorders. *Nat. Rev. Neurol.* **2018**, *14*, 133–150. [CrossRef] [PubMed]

## Article

# Brain Delivery of IGF1R5, a Single-Domain Antibody Targeting Insulin-like Growth Factor-1 Receptor

Alvaro Yogi, Greg Hussack , Henk van Faassen, Arsalan S. Haqqani, Christie E. Delaney, Eric Brunette, Jagdeep K. Sandhu , Melissa Hewitt, Traian Sulea , Kristin Kemmerich and Danica B. Stanimirovic \*

Human Health Therapeutics Research Centre, National Research Council Canada, Ottawa, ON K1A 0R6, Canada; alvaro.yogi@nrc-cnrc.gc.ca (A.Y.); greg.hussack@nrc-cnrc.gc.ca (G.H.); henk.vanfaassen@nrc-cnrc.gc.ca (H.v.F.); arsalan.haqqani@nrc-cnrc.gc.ca (A.S.H.); christie.delaney@nrc-cnrc.gc.ca (C.E.D.); eric.brunette@nrc-cnrc.gc.ca (E.B.); jagdeep.sandhu@nrc-cnrc.gc.ca (J.K.S.); melissa.hewitt@nrc-cnrc.gc.ca (M.H.); traian.sulea@nrc-cnrc.gc.ca (T.S.); kristin.kemmerich@nrc-cnrc.gc.ca (K.K.)

\* Correspondence: danica.stanimirovic@nrc-cnrc.gc.ca

**Abstract:** The ability of drugs and therapeutic antibodies to reach central nervous system (CNS) targets is greatly diminished by the blood–brain barrier (BBB). Receptor-mediated transcytosis (RMT), which is responsible for the transport of natural protein ligands across the BBB, was identified as a way to increase drug delivery to the brain. In this study, we characterized IGF1R5, which is a single-domain antibody (sdAb) that binds to insulin-like growth factor-1 receptor (IGF1R) at the BBB, as a ligand that triggers RMT and could deliver cargo molecules that otherwise do not cross the BBB. Surface plasmon resonance binding analyses demonstrated the species cross-reactivity of IGF1R5 toward IGF1R from multiple species. To overcome the short serum half-life of sdAbs, we fused IGF1R5 to the human (hFc) or mouse Fc domain (mFc). IGF1R5 in both N- and C-terminal mFc fusion showed enhanced transmigration across a rat BBB model (SV-ARBE) in vitro. Increased levels of hFc-IGF1R5 in the cerebrospinal fluid and vessel-depleted brain parenchyma fractions further confirmed the ability of IGF1R5 to cross the BBB in vivo. We next tested whether this carrier was able to ferry a pharmacologically active payload across the BBB by measuring the hypothermic and analgesic properties of neurotensin and galanin, respectively. The fusion of IGF1R5-hFc to neurotensin induced a dose-dependent reduction in the core temperature. The reversal of hyperalgesia by galanin that was chemically linked to IGF1R5-mFc was demonstrated using the Hargreaves model of inflammatory pain. Taken together, our results provided a proof of concept that appropriate antibodies, such as IGF1R5 against IGF1R, are suitable as RMT carriers for the delivery of therapeutic cargos for CNS applications.

**Keywords:** blood–brain barrier; receptor-mediated transcytosis; single domains antibody; IGF1R; neurotensin

**Citation:** Yogi, A.; Hussack, G.; van Faassen, H.; Haqqani, A.S.; Delaney, C.E.; Brunette, E.; Sandhu, J.K.; Hewitt, M.; Sulea, T.; Kemmerich, K.; et al. Brain Delivery of IGF1R5, a Single-Domain Antibody Targeting Insulin-like Growth Factor-1 Receptor. *Pharmaceutics* **2022**, *14*, 1452. <https://doi.org/10.3390/pharmaceutics14071452>

Academic Editor: William M. Partridge

Received: 15 June 2022

Accepted: 8 July 2022

Published: 12 July 2022

**Publisher's Note:** MDPI stays neutral with regard to jurisdictional claims in published maps and institutional affiliations.



**Copyright:** © 2022 by the authors. Licensee MDPI, Basel, Switzerland. This article is an open access article distributed under the terms and conditions of the Creative Commons Attribution (CC BY) license (<https://creativecommons.org/licenses/by/4.0/>).

## 1. Introduction

The development of therapies for central nervous system (CNS) indications is hampered by several factors, including poor delivery due to the blood–brain barrier (BBB). Tight junctions between the endothelial cells forming the BBB prevent the paracellular transport of most synthetic drugs and large molecules, such as biologics [1]. The brain delivery of essential macromolecules and nutrients can be achieved via receptor-mediated transcytosis (RMT)-dependent and RMT-independent mechanisms [2–4]. RMT is initiated by ligand binding to a receptor on the luminal surface of brain endothelial cells (BECs). The ligand–receptor complex undergoes trafficking through multiple intracellular endosomal compartments where the cargo is detached from the receptor and then released on the abluminal side of the barrier. Meanwhile, the receptor recycles ‘back’ to accept additional cargo molecules. Targeting this endogenous mechanism of transcytosis is an attractive approach to delivering therapeutic cargos, especially macromolecules, across the BBB [5–7].

Currently, the main RMT receptors that have been studied are the transferrin receptor (TfR) and insulin receptor (IR), and ligands against these receptors were shown to deliver different therapeutic cargos into the brain [8–10]. Additional targets shown to mediate RMT include insulin-like growth factor receptors (IGF1R) and transmembrane protein 30A (TMEM30A/CDC50A). It should be noted that several other targets, including low-density lipoprotein receptor (LDLR), low-density lipoprotein-related protein 1 (LRP-1), CD98hc, LRP8 and others, were implicated in BBB transcytosis, although the exact mechanisms of their BBB crossing remain unclear [11–19].

We previously developed camelid single-domain antibodies (sdAbs,  $V_{HH}$ s) against some of these target receptors (TMEM30A/CDC50A, IGF1R) and demonstrated the feasibility of antibody-mediated drug delivery via the RMT pathway [11–13]. In addition, it was shown that drug cargos can be incorporated into liposomes or nanoparticles decorated with the RMT-targeting ligand to boost brain delivery [17,20]. However, when compared with conventional antibodies and nanotechnologies, camelid sdAbs present numerous advantages for this application, including their small size, ease of engineering, optimization and humanization, strong biophysical properties and low immunogenicity.

Insulin-like growth factor-1 receptor (IGF1R) was identified as a potential RMT candidate based on the observation that its ligand IGF-1 was transported across the BBB and its elevated expression in BECs relative to peripheral tissue [21]. SdAbs targeting the ectodomain of IGF1R were isolated via llama immunization, and their transmigration was demonstrated in rat and human BBB models *in vitro* [22,23]. We further confirmed these findings *in vivo* by showing that three of the sdAbs isolated from the initial panning displayed increased accumulation in the brains of rats and mice [11]. By isolating brain microvessel and parenchymal fractions followed by mass spectroscopy quantification of antibodies, we were able to quantify the IGF1R4 sdAb that was shuttled into the brain parenchyma versus the fraction bound or accumulated inside the endothelial cells [11].

One of the potential side effects associated with RMT targets is interfering with their normal physiological functions. To mitigate this possibility, we recently mapped the binding epitope of one of the BBB-crossing sdAbs, namely, IGF1R5, on IGF1R in relation to IGF-1 using differential hydrogen–deuterium exchange mass spectrometry and nuclear magnetic resonance spectroscopy [24]. Furthermore, we demonstrated that this IGF1R sdAb has no detectable impact on the functional activation of IGF1R. Whether this sdAb variant is able to effectively deliver a pharmacologically active payload across the BBB remains to be determined. The ability of mFc and hFc fusions in variable C- or N-terminus linkages of IGF1R5 to cross the BBB, as well as their ability to shuttle a pharmacologically active payload across the BBB, was confirmed in this study by analyzing the hypothermic properties of neurotensin when fused to IGF1R5hFc constructs. Furthermore, we demonstrated that IGF1R5 humanization by modifications in the backbone structure of IGF1R5 did not affect its BBB permeability. The present study provided a proof of concept and validated IGF1R5 as an RMT receptor ligand that is suitable for the delivery of therapeutic cargos for CNS applications.

## 2. Materials and Methods

### 2.1. $V_{HH}$ Isolation

Llama single-domain antibodies ( $V_{HH}$ s) against IGF1R were isolated and produced as described previously [23]. Briefly, one male llama (*Lama glama*) was immunized with the extracellular domain of human IGF1R consisting of 933 amino acids. The antigen-specific immune response was monitored at different time points post-immunization, and on day 84, peripheral blood mononuclear cells (PBMCs) were collected for sdAb phage display library construction and panning. IGF1R5 sdAb isolated through library panning were subcloned and expressed in TG1 *Escherichia coli* cells and purified using HiTrap Chelating HP columns (GE Healthcare, North Richland Hills, TX, USA).

## 2.2. Humanization

The camelid IGF1R5 sdAb sequence was humanized following a CDR grafting protocol [25]. Briefly, a human VH3 germline was used as a framework (FR) template. The complementarity-determining region (CDR) was defined according to the Kabat definition and sequence numbering. Back-mutations were selected to arrive at several humanized variants based on multiple criteria, among which proximity to CDR required 3D structural homology modeling of the camelid V<sub>H</sub>H. In the case of the H2 humanized variant, camelizing back-mutations in the FR2 were not introduced. Instead, only 4 back-mutations were considered for this variant, all of which were in the Vernier zone supporting the CDR loops. Additionally, the CDR2 point mutation A57T was introduced to enable scalable purification using Protein A affinity chromatography [26] if required for future large-scale biomanufacturing. The mutations introduced in the humanized IGF1R5-H2 relative to the camelid IGF1R5 sdAbs are highlighted in Supplementary Figure S1A. The humanized IGF1R5-H2 sdAb was produced and purified as described for the llama sdAbs.

## 2.3. Surface Plasmon Resonance (SPR) Binding of IGF1R5 and IGF1R5-H2 V<sub>H</sub>Hs to IGF1R

The affinities of wild-type IGF1R5 and humanized IGF1R5-H2 V<sub>H</sub>Hs for several IGF1R ectodomain orthologues (human, rhesus, mouse and rat) were determined using SPR. Immediately prior to SPR, V<sub>H</sub>Hs were purified using preparative size exclusion chromatography (SEC) to isolate pure monomeric V<sub>H</sub>H fractions. SEC was performed by injecting 250–300 µg of each V<sub>H</sub>H over a Superdex S75 Increase 10/300 GL column (Cytiva, Marlborough, MA, USA) controlled by an ÄKTA FPLC Purifier (Cytiva) at a flow rate of 0.8 mL/min in HBS-EP buffer (10 mM HEPES, pH 7.4, containing 150 mM NaCl, 3 mM EDTA and 0.005% *v/v* surfactant P20 (polyoxyethylene 20 sorbitan monolaurate); Cytiva). All SPR experiments were performed on a Biacore 3000 and a Biacore T200 (Cytiva) at 25 °C in an HBS-EP buffer. Ectodomains of human IGF1R (R&D Systems, Cat#391-GR-050), rhesus IGF1R (NRC Montreal, aa31-932), rat IGF1R (NRC Montreal, aa31-936) and mouse IGF1R (R&D Systems, Cat#6630-GR/CF-025) were amine coupled on CM5 sensor chips (Cytiva) at 10 µg/mL in 10 mM acetate pH 4.0 using an amine-coupling kit (Cytiva), resulting in approximately 1500–2000 response units (RUs) of each IGF1R ectodomain immobilized. The remaining active sites were blocked with 1 M ethanolamine at pH 8.5. An ethanolamine-blocked empty flow cell served as a reference surface. On the Biacore 3000, using multi-cycle kinetics (MCK), V<sub>H</sub>Hs at various concentration ranges were injected over the IGF1R ectodomains and reference surface at a flow rate of 20 µL/min for 300 s followed by 300 s of dissociation. On the Biacore T200, using single-cycle kinetics (SCK), V<sub>H</sub>Hs were injected at 40 µL/min for 180 s followed by 600 sec of dissociation. The V<sub>H</sub>H concentration ranges were 0.25–10 nM (IGF1R5) and 1–25 nM (IGF1R5-H2). Surfaces were regenerated with a 24 s pulse of 10 mM glycine, pH 2.0, at a flow rate of 100 µL/min. Reference subtracted sensorgrams were analyzed and fit to a 1:1 binding model with BIAevaluation 4.1 software (Biacore 3000) or BIAevaluation 3.2 software (Biacore T200; Cytiva, Marlborough, MA, USA). IGF1R5 and IGF1R5-H2 affinities for human and mouse IGF1R were also determined at pH 5.6 using an HBS-EP MES buffer (10 mM HEPES, 10 mM MES, 150 mM NaCl, 3 mM EDTA, 0.005% P20, pH 5.6) at 37 °C. Prior to injection, V<sub>H</sub>Hs were buffer exchanged using Amicon ultra-centrifugal filters (0.5 mL, 3K MWCO). IGF1R5 flowed at 0.25–10 nM and IGF1R5-H2 flowed at 1–50 nM with similar contact times, dissociation times, regeneration conditions and fitting as those described above.

## 2.4. Rat and Human BBB Models In Vitro

Simian virus 40-immortalized adult rat brain endothelial cells (SV-ARBECS) were seeded at 80,000 cells/membrane on rat-tail-collagen-coated 0.83 cm<sup>2</sup> Falcon cell inserts (1 µm pore size) in 1 mL SV-ARBEC culture medium without phenol red. The inserts were placed in the wells of a 12-well tissue culture plate containing 1 mL of SV-ARBEC medium without phenol red and 1 mL rat astrocyte-conditioned medium to generate an in vitro model of the BBB as described previously [11,12,27]. Permeability was monitored and

the cultures were used only when  $P_e$  [sucrose] was between 0.4 and 0.6 ( $\times 10^{-3}$ ) cm/min. Transport experiments were performed by adding an equimolar mixture of antibodies to the top chamber and collecting a 100  $\mu$ L aliquot from the bottom chamber at 15, 30, 60 and 90 min for simultaneous quantification of the antibodies using the SRM method. Control antibodies of the same were added to each transport well to determine the background transport resulting from paracellular/nonspecific flux. The apparent permeability coefficient  $P_{app}$  was calculated using  $P_{app} = \Delta Q / \Delta t \times 1 / AC_0$ , where  $\Delta Q / \Delta t$  is the steady-state flux (mol/min),  $A$  is the surface area of the filter ( $\text{cm}^2$ ) and  $C_0$  is the initial concentration in the top chamber.

Human-amniotic-fluid-derived induced pluripotent stem cells (AF-iPSCs) were generated from human amniotic fluid (AF) cells and differentiated into iBECs as previously described [22]. Briefly, AF-iPSCs were seeded at a density of  $8 \times 10^3$  cells/ $\text{cm}^2$  in DMEM/F12 medium (Thermo Fisher Scientific, Waltham, MA, USA) supplemented with 20% KnockOut Serum Replacement, 1  $\times$  Glutamax, 1  $\times$  Non-Essential Amino Acids and 0.1 mM  $\beta$ -mercaptoethanol (all from Life Technologies, Carlsbad, CA, USA) for 6 days. The medium was changed to EM medium (human Endothelial Serum-Free medium, Life Technologies) supplemented with 20 ng/mL basic fibroblast growth factor (bFGF, Life Technologies), 10  $\mu$ M retinoic acid (RA, Sigma Aldrich, Oakville, ON, Canada) and 1% fetal bovine serum (FBS, Hyclone Laboratories, Logan, UT, USA) for an additional 2 days. To establish the in vitro transwell BBB model, iBECs were dissociated with Accutase (Stem Cell Technologies, Vancouver, BC, Canada) and seeded at a density of  $2.5 \times 10^5$  cells per 24 well transwell insert (3  $\mu$ m pore size, 0.33  $\text{cm}^2$  surface area; BD, Mississauga, ON, Canada) pre-coated with collagen type-IV (80  $\mu$ g/mL, Sigma) and fibronectin (20  $\mu$ g/mL, Sigma) in complete EM medium with 10  $\mu$ M Y27362 (ROCK Inhibitor, Stem Cell Technologies). iBEC transwells were incubated overnight at 37  $^\circ\text{C}$  in 5%  $\text{CO}_2$  and the next day, the medium was changed to an EM medium without bFGF and RA for an additional 24 h in the luminal chamber. Antibody transport experiments and apparent permeability coefficient calculations were performed as described above.

### 2.5. NanoLC-SRM Mass Spectrometry Analyses

The nanoflow ultrahigh performance liquid chromatography-coupled selected-reaction monitoring (nanoLC-SRM) mass spectrometry method was used to quantify absolute or relative levels of proteins in a BBB model, serum, cerebrospinal fluid and vessel-depleted brain parenchyma fractions. All protein extracts were reduced, alkylated and trypsin-digested using a previously described protocol [28]. Mass spectrometry analyses were carried out on a NanoAcquity UPLC (Waters, Milford, MA, USA) containing a C18 PepMap<sup>TM</sup> 100 trap (ThermoFisher, Waltham, MA, USA) followed by a nanoLC BEH130C18 column (Waters) coupled with ESI-LTQ-XL-ETD or ESI-TSQ-Quantiva mass spectrometers (ThermoFisher). Peptide signatures of various antibodies and vessel/parenchymal markers were identified by analyzing the respective samples with tandem mass spectrometry (nanoLC-MS/MS) using data-dependent acquisition on ESI-LTQ-XL-ETD44. For the absolute quantification of antibodies, at least 9 standards consisting of calibration and QC standards between 0.05 and 16 fmol range were created by spiking antibodies in their respective control matrices. Each sample was analyzed using nanoLC-SRM and data was extracted from raw files and analyzed using Skyline 64-bit 20.2.0.286 software (MacCoss Lab Software, University of Washington, Seattle, WA, USA) available as open source software from <https://skyline.ms> (last accessed on 11 July 2022).

### 2.6. Animals

Male Wistar rats (weight range, 150–200 g) and CD-1 mice (22–30 g) were purchased from Charles River Laboratories, Inc. (Montreal, QC, Canada). Animals were housed in groups of 3 in a 12 h light–dark cycle at a temperature of 24  $^\circ\text{C}$ , relative humidity of  $50 \pm 5\%$  and were allowed free access to food and water. All animal procedures were approved by

the NRC's Animal Care Committee and were in compliance with the Canadian Council of Animal Care guidelines.

### 2.7. Serum, Cerebrospinal Fluid and Brain Exposure

All compounds were administered to rats via the tail vein. Twenty-four hours post-injection, rats were anesthetized with 3% isoflurane and CSF was collected from a direct puncture to the cisterna magna. Blood samples were taken from the tail vein following CSF collection and samples were centrifuged (15 min at 15,000 rpm; room temperature). Samples were stored at  $-80^{\circ}\text{C}$  until analysis.

Following blood collection, rats were thoroughly perfused with 10 mL of heparinized (100 U/mL) saline at a rate of 1 mL/min via the left common carotid artery to facilitate specific perfusion of the brain. Brains were then removed and homogenized in an ice-cold homogenization buffer containing 50 mM Tris-HCl pH 8, 150 mM NaCl, and a protease inhibitor cocktail (Sigma-Aldrich, Oakville, ON, Canada) using a Dounce homogenizer (10–12 strokes at  $4^{\circ}\text{C}$ ). Brain homogenates were depleted of vessels using a sequential filtration through 100 and 20  $\mu\text{m}$  nylon Nitex mesh filters (pluriSelect, Leipzig, Germany). Successful vascular depletion of parenchymal fractions was confirmed using the enrichment of a parenchymal marker (Slc1a3) with the concomitant absence of a specific vascular marker (Slc2a1) as previously observed [11]. The concentration of injected antibodies was determined in vessel-depleted parenchymal fraction using SRM as described above.

### 2.8. Immunofluorescence

Brains were removed from the skull and drop fixed in 4% paraformaldehyde for 24 h at room temperature, followed by cryoprotection in 30% sucrose solution for 48 h at  $4^{\circ}\text{C}$ . Brains were then embedded in an Optimal Cutting Temperature compound (OCT), frozen over dry ice and stored at  $-80^{\circ}\text{C}$  until sectioning. Coronal sections were cut at 15  $\mu\text{m}$ , mounted on Superfrost plus slides (Thermo Fisher Scientific, Waltham, MA, USA) and subjected to immunofluorescent staining. Sections were incubated with DAKO serum-free protein block (DAKO Diagnostics, Burlington, Canada) containing 0.25% Tween-20 for 40 min at room temperature, followed by overnight incubation at  $4^{\circ}\text{C}$ . The following antibodies were used: goat anti-mouse-IgG Fc $\gamma$ -cy3 (1:200, Cat#115-165-071, Jackson ImmunoResearch, West Grove, PA, USA), mouse-anti-NueN (1:100, Cat# ab13938, Abcam, UK) and RCAI (1:500, Cat# FL-1081, Vector Laboratories, Newark, NJ, USA). Following overnight incubation, sections were washed 3 $\times$  with Tris-buffered saline (TBS, DAKO) and the conjugate was detected via incubation for 45 min at room temperature with 1:300 goat anti-mouse Alexa 647 (A21235, Invitrogen, Waltham, MA, USA) or 1:500 goat anti-rabbit Alexa 647 (A21244, Invitrogen, Waltham, MA, USA). After washing 3 $\times$  with TBS, sections were mounted in DAKO fluorescent mounting medium and spiked with Hoechst (2  $\mu\text{g}/\text{mL}$ , Cat#H3570, Invitrogen, Waltham, MA, USA). Images were captured with an Olympus 1  $\times$  81 Fluorescent Microscope using 10 $\times$  and 60 $\times$  objectives and following the manufacturer's instructions for excitation and emission channels.

### 2.9. Expression and Purification of IGF1R5 Fusions with Fc Domain and Neurotensin

DNA encoding hFc-IGF1R5, IGF1R5-mFc, mFc-IGF1R5 and IGF1R5-hFc-neurotensin was synthesized using Genescript. A schematic showing different constructs/fusion proteins used in this study is presented in Figure 1. The sequences for IGF1R5, mouse IgG Fc2b and human IgG Fc fragment were as previously described [12,23]. The IGF1R5-hFc-neurotensin sequence includes a linker (amino acid sequence GGGSGGGGS). Constructs were expressed in transiently transfected Chinese hamster ovary cells (CHO-3E7). The culture medium was harvested 7 days post-transfection via centrifugation and clarified using 0.2  $\mu\text{m}$  filter bottles (Millipore Stericup, MilliporeSigma, Burlington, VT, USA). Clarified medium was applied on a column packed with 5 mL (volume of columns used depended on protein titer and volume of culture) protein-A MabSelect SuRe resin (GE Healthcare, Mississauga, ON, Canada). After loading, the column was washed with 5–10 volumes



of phosphate-buffered saline pH 7.1 (PBS) and the constructs were eluted with 100 mM sodium citrate buffer pH 3.0 to 3.6. Then, a buffer exchange was performed by loading on a desalting NAP-25 column (GE Healthcare, Mississauga, ON, Canada) equilibrated in PBS. Desalted constructs were then sterile-filtered by passing through a Millex GP (Millipore-Sigma, Burlington, VT, USA) filter unit (0.22 μm) and aliquoted. The purity of the protein was verified using SDS-PAGE and they were stored at −80 °C.

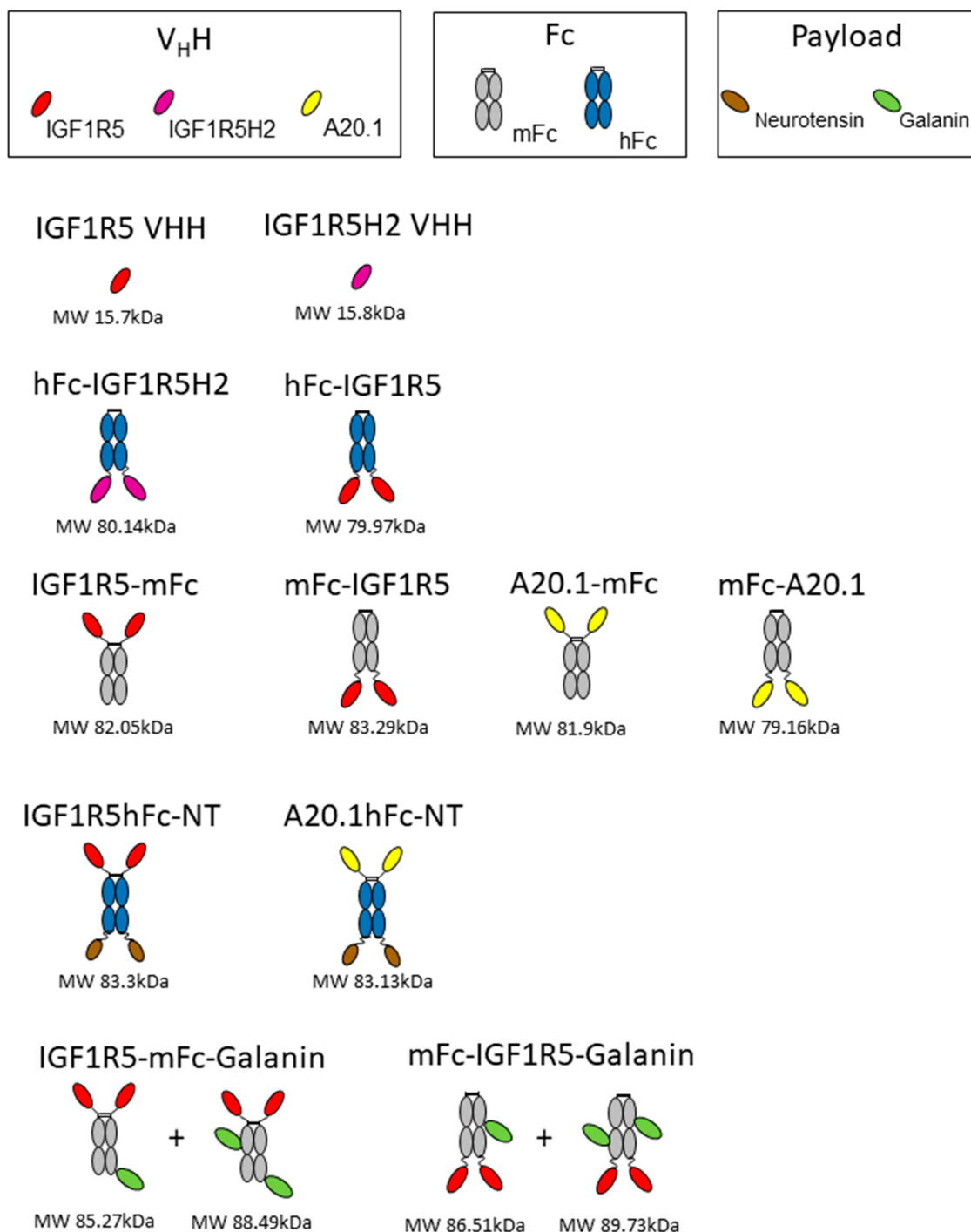


**Figure 1.** A schematic figure depicting the different constructs used in this study. Three different V<sub>H</sub>Hs, Fc regions with human and mouse origins, and two neuropeptides (neurotensin and galanin) were used to generate the antibodies. The predicted molecular weight (MW) for each construct is also shown.

### 2.10. Cell-Based Neurotensin Receptor 1 Activation

A receptor functional assay was carried out using the PathHunter eXpress NTR1 kit (DiscoverX, Fremont, CA, USA). Briefly, engineered HEK293 cells expressing a (Pro-Link or PK)-tagged NTR1 and an enzyme acceptor (EA)-tagged SH2 domain were used. Upon receptor activation, EA-SH2 binds to the phosphorylated NTR1 and reconstitutes an active  $\beta$ -galactosidase enzyme, which hydrolyzes the substrate to generate a chemiluminescent readout. Cells were thawed and plated in a 384-well white-wall clear-bottom plate (Greiner, Monroe, LA, USA) at 20,000 cells/well for 24 h at 37 °C in 5% CO<sub>2</sub> following the manufacturer's instructions. Cells were then treated with neurotensin (Sigma-Aldrich, Oakville, ON, Canada) or IGF1R5-hFc-neurotensin. The chemiluminescent substrate was added and cells were incubated at RT for 60 min. The resulting luminescence was measured using the CLARIOstar plate reader (BMG LABTECH, Ortenberg, Germany) and concentration–response curves were generated using nonlinear regression analysis (GraphPad Prism Software, San Diego, CA, USA).

### 2.11. IGF1R5-hFc-Neurotensin-Induced Hypothermia in Rats and Mice

Wistar rats and CD-1 mice were used. Before surgery, animals were injected with sustained-release buprenorphine (1.2 mg/kg) subcutaneously for analgesia. Temperature data loggers were implanted in the peritoneal cavity of rats (DST micro-T, Star-Oddi, Gardabaer, Iceland) and mice (DST nano-T, Star-Oddi, Gardabaer, Iceland) under isoflurane anesthesia. Animals were allowed to recover from surgery for 1 week prior to the injection of the test compound.

Data recording on temperature loggers was initiated 48 h prior to injection for calculations of baseline values. Intravenous injection of the test compound was performed between 7:00 AM and 9:00 AM by experienced personnel to avoid stress-induced hyperthermia. The data loggers measured the core body temperature of animals at a time interval of 1 min to an accuracy of 0.1 °C for up to 6 h post-injection.

Core temperature baseline values were taken in undisturbed animals 24 h or 48 h prior to the test compound injection. To avoid variability due to regular changes in temperature during the circadian cycle, the start point and time frame of baseline values matched that of test compound injection. The average baseline value (T<sub>b</sub>) and standard deviation (SD) of baseline values were used to calculate the duration of response. Hypothermia duration was defined as the time in which T<sub>c</sub> < T<sub>b</sub>–2SD during the interval from dosing up to 240 min in rats and 360 min in mice. The maximum change in core body temperature was expressed as the difference measured at the minimum temperature observed after the test compound injection compared with the baseline core body temperature measured as described above. The area under the curve (AUC) was calculated using the trapezoidal rule from 0 to 240 min and 360 min in rats and mice, respectively. The AUC calculation was performed using GraphPad Prism.

### 2.12. IGF1R5mFc-Galanin and mFcIGF1R5-Galanin-Induced Analgesia in Rats

To further demonstrate whether IGF1R5 constructs in C- and N-terminal fusion to mFc can cross the BBB *in vivo* and deliver a molecule that cannot cross the BBB on its own, the neuropeptide galanin was chemically conjugated to IGF1R5 and administered systemically as previously described [29]. Galanin is a neuroactive peptide that produces analgesia by binding GalR1 and GalR2 expressed in brain tissue. When given peripherally, galanin has no analgesic effects because it cannot cross the BBB on its own.

IGF1R5-mFc and mFc-IGF1R5 were conjugated to a rat galanin fragment with a cysteamide-modified C-terminus (Biomatik, Cambridge, ON, Canada) (GWTLSAGYLLGPHAIDNHRFSFSDKHGLT-cysteamide) as previously described [29]. Briefly, 2 mg of each IGF1R5 was placed in 4 separate 1.5 mL micro-centrifuge tubes and diluted to 2 mg/mL with PBS. Sulfo-SMCC was added in a 6.5x excess molar ratio; specifically, 29.5  $\mu$ L of the 2.5 mg/mL Sulfo-SMCC was added to each micro-centrifuge tube. The micro-centrifuge tubes containing the mixture were incubated for 30 min at room

temperature (RT) with short vortexing every 10 min. Once the reaction was done, the unreacted Sulfo-SMCC was removed from the maleimide-activated IGF1R5 using a 10 mL 7K Zeba column (Pierce). Prior to sample loading, the column was washed 3 times with 5 mL PBS and spun at  $1000\times g$  for 2 min. The 4 separate reactions were combined and loaded on the column. The column was spun for 2 min at  $1000\times g$ .

Separately and concurrently, a 1 mg/mL stock of galanin-cysteamide was prepared in Milli-Q H<sub>2</sub>O. The purified maleimide-activated IGF1R5 constructs were mixed with galanin-cysteamide, sealed and incubated overnight at 4 °C or 1 h at RT. The unreacted galanin-cysteamide was removed using Amicon-15 30K column (MilliporeSigma, Oakville, ON, Canada). The samples were added to the column, and the volume was filled to 15 mL with PBS and spun at  $4000\times g$  for 7 min until the volume was reduced to 2 mL. The conjugated sample was then added to a 5 mL 7K Zeba column (ThermoFisher Scientific, Waltham, MA, USA) prepared as described above (wash was done with 2.5 mL PBS), and then spun for 2 min at  $1000\times g$ . The collected sample comprised the IGF1R5-mFc-galanin and mFc-IGF1R5-galanin conjugation product. The protein concentration was determined by measuring the absorbance at A280 on a NanoDrop. The reaction was titrated to achieve about 1 to 2 galanin molecules per construct. A reaction was confirmed by loading and silver staining conjugated IGF1R5-mFc-Gal and mFc-IGF1R5-Gal samples on a 10% SDS-PAGE to confirm a shift in molecular weight size after conjugation.

The Hargreaves model of hyperalgesia was used to evaluate the efficacy of IGF1R5 to deliver galanin into the brain and induce antinociceptive effects, as previously demonstrated [11,12,29]. Chronic inflammatory hyperalgesia was induced in one of the paws of Wistar rats by injecting 100 µL of complete Freund's adjuvant (CFA; heat-killed *Mycobacterium tuberculosis*; Sigma-Aldrich, Oakville, ON, Canada) suspended in an oil:saline (1:1) emulsion. Then, the plantar surface of both the right and left paw was exposed to a radiant stimulus and the paw withdrawal latency (PWL) of each paw was measured using the plantar Analgesia Meter equipment for paw stimulation (IITC Life Science, Woodland Hills, CA, USA). The time spent between starting the radiant exposure and clicking or flicking the paw was interpreted as a positive nociceptive response. A cut-off of 20 s was established to avoid tissue damage. Three days post-CFA injection, inflammatory hyperalgesia was confirmed by measuring the baseline PWL of the right and left paws. Test compounds were then administered intravenously through the tail vein and a time-course of the antinociceptive response was determined. The experimenter performing pain experiments was blinded to the contents of the injectable compounds. The area under the curve (AUC) was calculated by the trapezoidal method to derive the percentage of maximal possible effect (%MPE) using the formula  $\%MPE = [(AUC_{molecule} - AUC_{inflamed\ paw}) / (AUC_{normal\ paw} - AUC_{inflamed\ paw})] \times 100$ , where  $AUC_{inflamed\ paw}$  and  $AUC_{normal\ paw}$  are the values obtained from the group injected with the vehicle (PBS).

### 2.13. Statistical Analysis

The results are expressed as the mean  $\pm$  SEM or SD as indicated. Where applicable, a paired *t*-test was used. One-way ANOVA followed by Newman-Keuls' post-test was used to compare multiple groups. A *p*-value of less than 0.05 was considered statistically significant.

## 3. Results

### 3.1. Surface Plasmon Resonance (SPR) Binding of IGF1R5 and IGF1R5-H2 V<sub>H</sub>Hs to IGF1R

SPR was used to determine the affinities of the V<sub>H</sub>Hs for various IGF1R ectodomain orthologues (Table 1, Figure 2). IGF1R5 bound to IGF1R from all species tested, with affinities of  $K_D = 0.6$  nM, 0.4 nM, 1.1 nM and 1.1 nM for human, rhesus, mouse and rat IGF1R, respectively. To avoid potential immunogenicity of llama-derived IGF1R5 when applied as a BBB carrier for therapeutics, this V<sub>H</sub>H was humanized using mutations of defined 'camelid' residues in the parental molecule. In the case of the IGF1R5-H2 variant, four back-mutations in the Vernier zone supporting the CDR loops were introduced. This humanized version showed similar cross-reactivity, albeit with slightly weaker binding

affinities of  $K_D = 7.6$  nM, 17 nM, 9.1 nM and 11 nM for human, rhesus, mouse and rat IGF1R.  $V_{HH}$  affinities for human and mouse IGF1R were also determined at pH 5.6 (37 °C). IGF1R5 was bound with comparable affinities to that observed at neutral pH, whereas IGF1R5-H2 possessed weaker binding affinity at acidic pH ( $K_D = 150$ – $160$  nM), with a faster off-rate ( $k_d$ ), which is a desirable characteristic for BBB crossing since the low pH present in endosomal trafficking would facilitate the sorting process, releasing the carrier from its receptor and sorting the membrane proteins and the carrier into different domains.

**Table 1.** SPR-derived kinetics and equilibrium dissociation constants for  $V_{HH}$ -IGF1R interactions. <sup>1</sup> Determined at pH 7.4, 25 °C; <sup>2</sup> determined at pH 5.6, 37 °C.

IGF1R Ectodomain	pH	IGF1R5			IGF1R5-H2		
		$k_a$ ( $M^{-1}s^{-1}$ )	$k_d$ ( $s^{-1}$ )	$K_D$ (M)	$k_a$ ( $M^{-1}s^{-1}$ )	$k_d$ ( $s^{-1}$ )	$K_D$ (M)
Human <sup>1</sup>	7.4	$5.3 \times 10^5$	$3.4 \times 10^{-4}$	$6.4 \times 10^{-10}$	$3.8 \times 10^5$	$2.9 \times 10^{-3}$	$7.6 \times 10^{-9}$
Rhesus <sup>1</sup>	7.4	$1.5 \times 10^6$	$5.9 \times 10^{-4}$	$4.0 \times 10^{-10}$	$2.3 \times 10^5$	$3.8 \times 10^{-3}$	$1.7 \times 10^{-8}$
Mouse <sup>1</sup>	7.4	$2.6 \times 10^5$	$3.0 \times 10^{-4}$	$1.1 \times 10^{-9}$	$2.3 \times 10^5$	$2.1 \times 10^{-3}$	$9.1 \times 10^{-9}$
Rat <sup>1</sup>	7.4	$3.4 \times 10^5$	$3.8 \times 10^{-4}$	$1.1 \times 10^{-9}$	$2.3 \times 10^5$	$2.6 \times 10^{-3}$	$1.1 \times 10^{-8}$
Human <sup>2</sup>	5.6	$6.9 \times 10^5$	$2.8 \times 10^{-3}$	$4.0 \times 10^{-9}$	$2.1 \times 10^5$	$3.4 \times 10^{-2}$	$1.6 \times 10^{-7}$
Mouse <sup>2</sup>	5.6	$5.9 \times 10^5$	$2.8 \times 10^{-3}$	$4.8 \times 10^{-9}$	$2.9 \times 10^5$	$4.3 \times 10^{-2}$	$1.5 \times 10^{-7}$

### 3.2. In Vitro and In Vivo BBB Transport of IGF1R5

The BBB permeability of IGF1R5 in the  $V_{HH}$  format, the humanized H2 variant of IGF1R5 and the hFc-IGF1R5H2, along with their respective negative controls, were assessed in rat (SV-ARBEC) and human (iBEC) BBB models in vitro. Negative controls were A20.1 sdAbs generated against *C. difficile* toxin A, which has no recognizable mammalian target that does not cross the intact BBB. Figure 3A demonstrates that all formats were transported across both BBB models. Interestingly, whereas the humanized variant of IGF1R5 displayed increased Papp values in the rat model, its Papp value was similar to the other constructs in the human model. Next, the rat BBB model in vitro was used to determine the rate of transport of IGF1R5 and a negative control, namely, A20.1 with either C- or N-terminus mFc fusion. The molecules were co-applied to the upper chamber and quantified using targeted proteomics (SRM) in the bottom compartment. The Papp value for each antibody was calculated over 90 min. Figure 3B demonstrates that IGF1R5 constructs fused with mFc in both C- and N-terminus displayed enhanced transcytosis when compared with their counterpart negative controls. Although slightly higher, the Papp value for the IGF1R5–N-terminus mFc fusion (mFc-IGF1R5) was not significantly different from the IGF1R5–C-terminus mFc fusion (IGF1R-mFc). This is an important property of IGF1R5 not typically observed with other sdAbs since it allows for a ‘platform’ use of IGF1R5 in different types of fusion proteins where the specific orientation of the therapeutic cargo is important for its activity, most notably, therapeutic antibodies, where the addition of the BBB carrier to the C-terminus allows for the unimpeded activity of its target-binding Fab portion.

We next investigated the ability of IGF1R5 constructs to transport across the BBB in vivo by injecting hFc-IGF1R5 intravenously into rats (15 mg/kg) and measuring their CSF and capillary-depleted brain parenchyma levels 24 h post-injection. Figure 3C indicates that no difference in serum concentration was observed between hFc-IGF1R5 and the negative control used, namely, A20.1-mFc. On the other hand, both the CSF and brain levels of hFc-IGF1R5 were significantly increased when compared with A20.1-mFc, further highlighting the capacity of IGF1R5 constructs to be transported across the BBB. We also performed immunofluorescence staining to determine the localization of IGF1R5-mFc and A20.1-mFc in brain tissue following a single intravenous injection (15 mg/kg). Whereas a co-localization of IGF1R-mFc with RCA-1 (Figure 3E) suggested the presence in brain

vasculature, there was also some co-localization with neurons (NeuN stain, Figure 3F), further supporting our observation that IGF1R5-mFc was able to cross the BBB and reach the brain parenchyma. As expected, A20.1-mFc staining was not observed in either brain vasculature (or was occasionally seen due to perfusion artifact) or in neurons (Figure 3G,H).

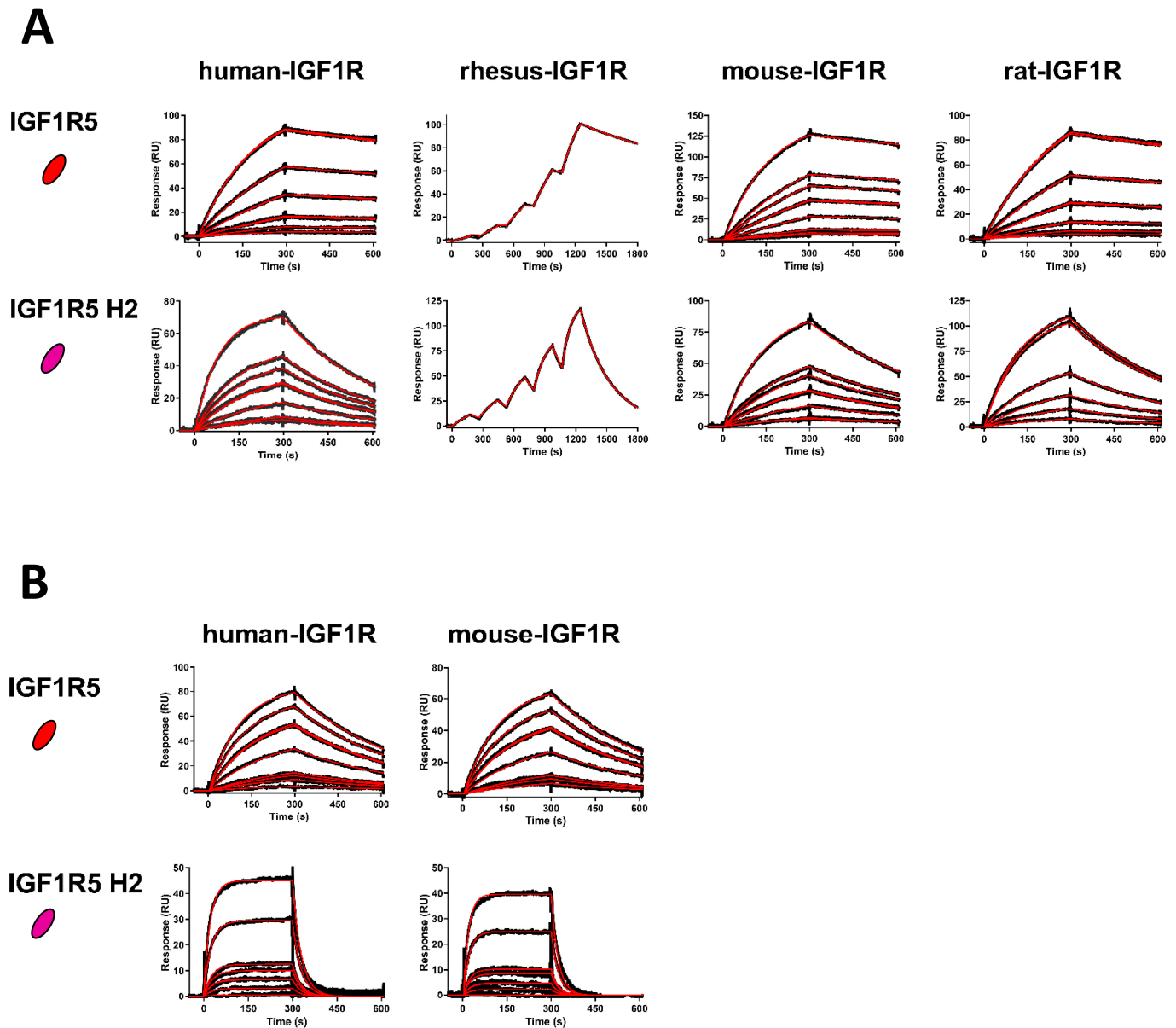


**Figure 2.** High-affinity binding of IGF1R5  $V_H$ Hs to IGF1R ectodomains. **(A)** SPR sensorgrams demonstrating wild-type IGF1R5 and humanized IGF1R5-H2  $V_H$ Hs binding to surface-immobilized human, rhesus, mouse and rat IGF1R (pH 7.4, 25 °C).  $V_H$ H concentrations in flow ranged from 0.25 to 10 nM (IGF1R5) and from 1 to 25 nM (IGF1R5-H2). Kinetics and affinities were determined using multi-cycle kinetics (human, mouse, rat IGF1R) or single-cycle kinetics (rhesus IGF1R) analyses. **(B)** Sensorgrams demonstrating the binding of  $V_H$ Hs to human and mouse IGF1R at acidic pH (pH 5.6, 37 °C).  $V_H$ H concentrations in flow ranged from 0.25 to 10 nM (IGF1R5) and from 1 to 50 nM (IGF1R5-H2). Black lines: raw data; red lines: 1:1 binding model fitting.

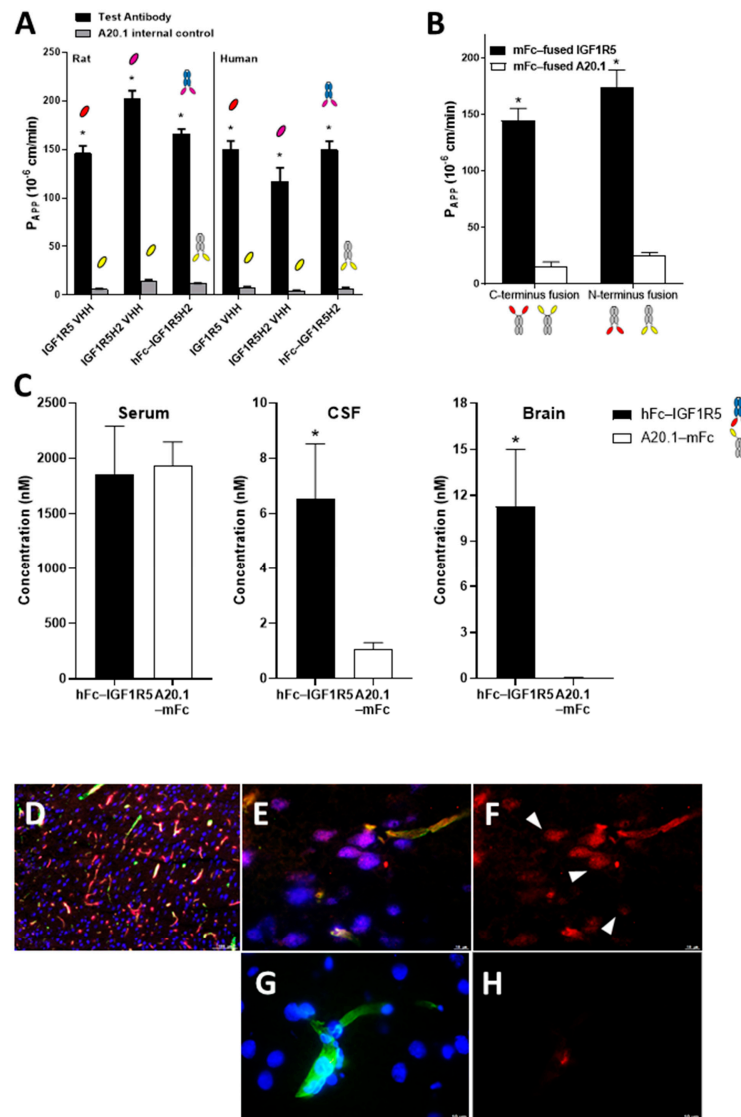


**Figure 3.** In vitro and in vivo BBB transport of IGF1R5 in the V<sub>H</sub>H format or in hFc or mFc fusions. (A) Transport of IGF1R5 in the V<sub>H</sub>H format, and humanized (H2) and hFc fused variants of IGF1R5 across a rat (SV-ARBE) and human (iBEC) in vitro BBB model. Antibodies were applied in the upper compartment of the BBB insert and then quantified over time in the bottom chamber using SRM to determine Papp values. Papp values (cm/min) of antibodies are shown as means ± sd derived from 6 separate transwell inserts. \* *p* < 0.05 vs. respective negative control. (B) Transport of mFc-IGF1R5 and IGF1R5-mFc across a rat BBB model in vitro. Antibodies were paired with corresponding controls in the upper compartment of the BBB insert and then quantified over time in the bottom chamber using SRM to determine the Papp values. Papp values (cm/min) of antibodies are shown as means ± sd derived from 6 separate transwell inserts. \* *p* < 0.05 vs. respective negative control. (C) Concentrations of hFc-IGF1R5 or A20.1-mFc in serum, CSF or capillary-depleted brain of rats at 24 h following a bolus i.v. injection of 15 mg/kg of each antibody. The concentrations were measured using SRM analysis in at least 3 animals and the bars represent mean and SD. \* *p* < 0.01 vs. A20.1-mFc. (D–G) Immunofluorescence staining of the rat frontal cortex 48 h after intravenous injection of 15 mg/kg of IGF1R5-mFc (D–F) or an equimolar dose of A20.1-mFc (G,H). Brain vessels were detected using RCA-1 (green); neurons were detected using antibodies against NeuN (blue); IGF1R5-mFc (red). Images were observed at 10x objective (D) and 60x (E–H). Scale bars, 100 μm and 10 μm.

In addition to hFc fusions, we further increased the molecular weight of the constructs by generating and injecting animals with Ig fusions of IGF1R5 (Supplementary Figure S3A). We observed that the IgG-IGF1R5 concentrations in CSF and brain but not serum were significantly increased when compared with Ig alone 24 h post-injection. Interestingly, although the serum levels of both Fc- and Ig- fusions were similar, CSF and brain levels were slightly higher in hFc-IGF1R5 versus IgG-IGF1R5 ( $6.52 \pm 2.00$  vs.  $5.11 \pm 0.11$ ;  $11.27 \pm 3.7$  vs.  $5.36 \pm 0.58$ , respectively), suggesting that the molecular weight of the cargo may have an impact on its BBB permeability, although other causes, such as steric hindrance, should not be discarded. To confirm this observation, we generated multiple IGF1R5 constructs with molecular weights ranging from 80 kDa to 300 kDa and measured their transport across the in vitro BBB model (Supplementary Figure S3B). An inverse correlation was observed between Papp values and the MW of different IGF1R5 constructs, further supporting our in vivo observations. No change in BBB transport was observed for the A20.1 constructs with different sizes.

### 3.3. Hypothermic Properties of IGF1R5-hFc-Neurotensin in Rats and Mice

Next, we determined whether IGF1R5 is capable of delivering a pharmacologically active payload into the brain. Neurotensin and its receptors are highly expressed in the brain [30]. It was shown that neurotensin elicits hypothermia in rodents through neurotensin receptor type 1 (NTR1) located within the central nervous system [31]. Here, we first demonstrated that fusion constructs of IGF1R5-hFc-neurotensin were able to activate NTR1 in a cell-based assay (Figure 4A). Although a slight shift to the right was observed in the concentration–response curve when compared with the 13 amino-acid neuropeptide alone, this difference was not significant.

Intravenous injection of IGF1R5-hFc-neurotensin in rats and mice induced a dose-dependent drop in core body temperature (Figure 4B,F, respectively). We also observed that no change in core body temperature was observed when animals were injected with A20.1-hFc-neurotensin (Supplementary Figure S4), which is consistent with its inability to cross the BBB. To further characterize the hypothermic effect of the IGF1R5-hFc-neurotensin constructs, three parameters were extrapolated from the dose–response curves; maximum response (Figure 4C,G), duration of response (Figure 4D,H) and area under the curve (Figure 4E,I). Quantification and statistical analysis of these parameters further demonstrated the hypothermic properties of IGF1R5-hFc-neurotensin, thus demonstrating that not only IGF1R5 constructs are able to cross the BBB but they are also able to deliver a pharmacologically active payload to target neurons.

### 3.4. Analgesic Properties of IGF1R5-mFc-Galanin and mFc-IGF1R5-Galanin in Rats

We further tested the ability of IGF1R5 to deliver a pharmacologically active payload by chemically conjugating galanin, which is a 29-amino-acid peptide that also does not cross the BBB, to its Fc fusion variants. Galanin was shown to reduce pain when directly injected into the brain [32]. We also demonstrated the analgesic properties of galanin when conjugated to single-domain antibodies that cross the BBB by RMT using the Hargreaves model of hyperalgesia [11,29]. In this model, paw inflammation was induced via subcutaneous injection of CFA in the hindpaw and reversal of hyperalgesia was observed via an increase in the latency of paw withdrawal from a thermal stimulus. Here, we demonstrated a dose-dependent analgesic response of galanin when conjugated to both mFc-IGF1R5 and IGF1R5-mFc (Supplementary Figure S5). Interestingly, when the reversal of hyperalgesia of mFc-IGF1R5-galanin and IGF1R5-mFc-galanin were compared at equimolar doses (4.96 mg/kg and 5.00 mg/kg, respectively), we noted that the analgesic effect was slightly higher in mFc-IGF1R5-galanin when compared with IGF1R5-mFc-galanin. This result is in accordance with what was observed in the BBB permeability assay in vitro, where the Papp values of IGF1R5 with mFc fusion in its C- or N-terminus were compared (Figure 3B).

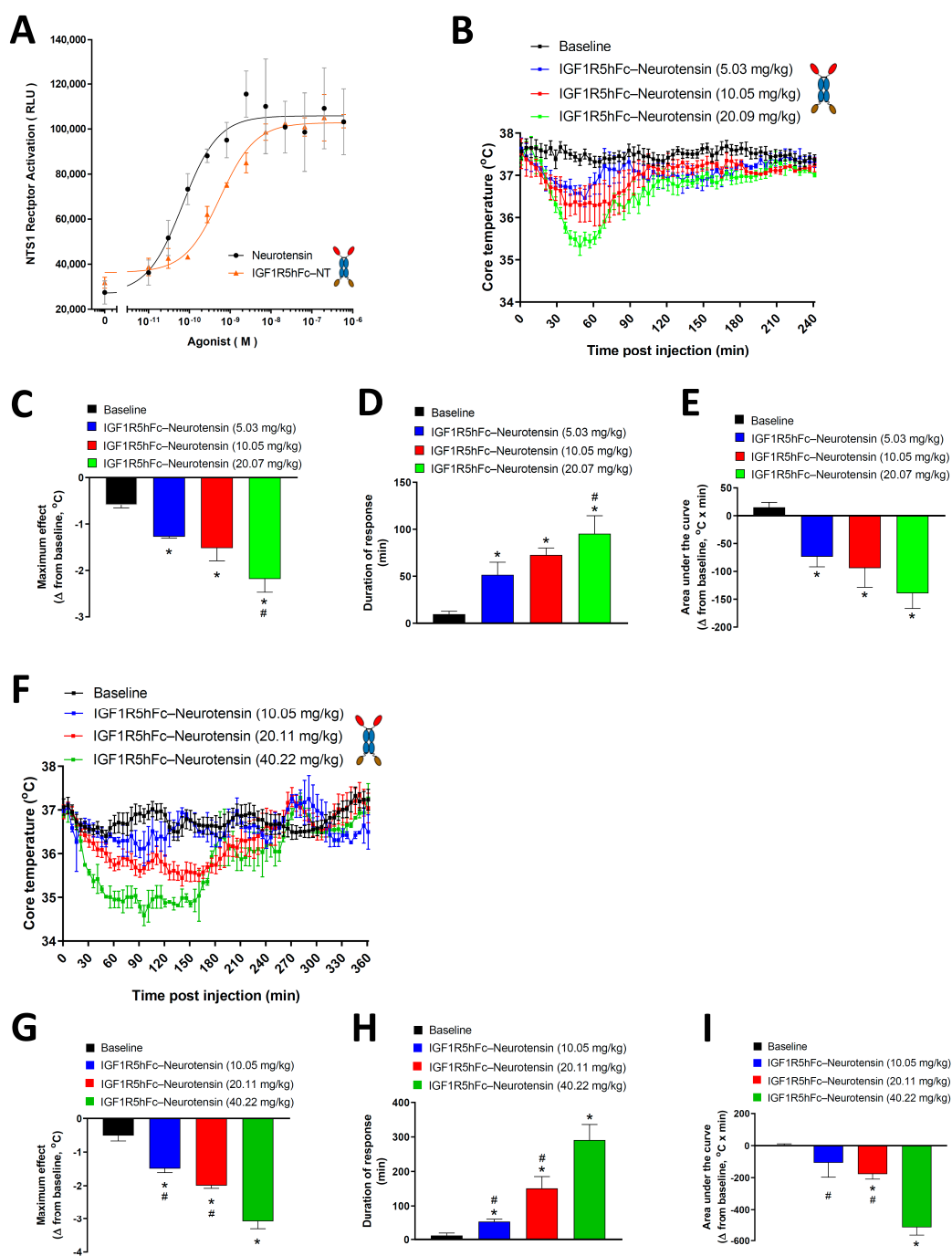


**Figure 4.** NTR1 activation and IGF1R5-hFc-neurotensin-induced hypothermia in rats and mice. (A) Concentration–response curve of neurotensin and IGF1R5-hFc-NT-induced activation of NTR1 in a cell-based assay. (B) Dose–response curve of the hypothermic effects of IGF1R5-hFc-neurotensin in rats (5.03 mg/kg, *n* = 3; 10.05 mg/kg, *n* = 6; 20.07 mg/kg, *n* = 4). Core body temperature was monitored using telemetry up to 4 h post intravenous injection of test compounds and the maximum response (C), duration of response (D) and area under the curve (E) were obtained. (F) Dose–response curve of the hypothermic effects of IGF1R5-hFc-neurotensin in mice (10.05 mg/kg, *n* = 2; 20.11 mg/kg, *n* = 7, 40.22 mg/kg, *n* = 2). Core body temperature was monitored using telemetry up to 6 h post-intravenous injection of test compounds and maximum response (G), duration of response (H) and area under the curve (I) were obtained. Results are mean ± SEM of 2–8 animals in each group. \* *p* < 0.05 vs. baseline; # *p* < 0.05 vs. highest dose injected (20.06 mg/kg in rats and 40.22 mg/kg in mice).



#### 4. Discussion

Despite growing knowledge and understanding of the pathophysiology of neurodegenerative and other brain diseases, the development of CNS drug candidates is severely hampered by poor tissue distribution due to the blood–brain barrier (BBB).

The BBB is responsible for protecting the brain from exposure to circulating toxins and pathogens. However, this protective function also presents a key challenge to the development of drugs targeting the CNS, in particular, biologics [1]. It was proposed that drug candidates could be delivered across the BBB via a process known as receptor-mediated transcytosis (RMT) [2], whereby ligands to receptors that transport large molecules across the BBB to supply the brain with nutrients needed for physiological homeostasis, such as transferrin receptor (TfR) or insulin receptor (IR), could be used to ‘shuttle’ attached therapeutic cargo molecules across the BBB. We previously generated single-domain antibodies (sdAbs) against different targets present in brain endothelial cells (BECs) that undergo RMT, including TMEM30A and IGF1R, and demonstrated their ability to cross the BBB in both *in vitro* and *in vivo* models [5,11–13].

In the present study, we demonstrated that IGF1R5, which is a camelid single-domain antibody (V<sub>H</sub>H) that targets IGF1R, transmigrated across the BBB and delivered diverse pharmacologically active payloads into the brain. IGF1R5 was humanized and may be considered a strong candidate for development as a BBB-delivery platform due to its stability, pH sensitivity and tolerance of different fusion formats.

One of the main advantages of targeting IGF1R for brain delivery of therapeutics is its enrichment in brain endothelial cells/brain microvessels when compared with peripheral tissue [33]. Furthermore, we recently showed that IGF1R transcript levels were twofold more abundant than another known RMT target, namely, TfR, in mouse BBB [33]. In our recent study [11], we demonstrated BBB crossing of a panel of IGF1R V<sub>H</sub>Hs in mice using an *in situ* brain perfusion technique, confirming that this BBB receptor could facilitate RMT of binding ligands, including antibodies.

Camelid V<sub>H</sub>Hs possess numerous desirable properties as BBB carriers, including high thermostability, resistance to proteases [34] and ease of optimization and engineering into various protein fusion formats. Llama V<sub>H</sub>H IGF1R5 demonstrated a high-affinity (sub-nanomolar) binding to IGF1R with a broad species cross-reactivity against human, rhesus, mouse and rat receptors. The linear epitope in the IGF1R structure recognized by the IGF1R5 that triggers structural re-arrangement of the receptor (and subsequent transcytosis) was mapped and shown to involve a single  $\alpha$ -CT helix without activating any downstream signaling events [24].

Antibody humanization is a critical approach to eliminating or reducing the immunogenicity and improving the clinical translation of camelid antibodies; in contrast to shark-derived sdAbs (VNARs), which are difficult to humanize, humanization of camelid V<sub>H</sub>Hs has been routinely achieved. The main challenge in the humanization process is to maintain the full biological function while reducing the risk of adverse side effects [35]. Through CDR grafting and resurfacing methods, we successfully generated a series of humanized variants of IGF1R5. One of these variants, namely, IGF1R5-H2, acquired a target-binding profile that was characterized by slightly weaker binding affinities and accelerated ‘off-rates’ compared with the parent camelid variant, which is a feature that is considered advantageous for RMT carriers where fast endosomal dissociation from the target receptor may facilitate its abluminal release. This humanized variant also displayed weaker binding affinity at acidic pH, which is another desirable characteristic previously demonstrated to facilitate the abluminal release of TfR-binding antibodies [36]. In our subsequent studies, the IGF1R5-H2 sdAb variant demonstrated improved transcytosis compared to the parent IGF1R5 sdAb in the rat BBB model *in vitro*, while in the human BBB model, both variants had similar Papp values. Further studies employing the pulse–chase method or dynamic analyses of trafficking through intracellular endosomal compartments of these two variants will be necessary to dissect the potential benefits to transcytosis

efficiency imparted by different levels of affinity and pH sensitivity of their binding to the target receptor.

Due to their size (~15 kD), sdAbs have a short plasma half-life and are rapidly cleared from the circulation by glomerular filtration in the kidney, thus limiting their use as systemic therapeutics. Numerous strategies are available to improve the pharmacokinetic profiles of sdAbs, including their fusion to the Fc region of IgG. The tolerance of BBB carrier sdAbs to fusion at both N- and C-terminus is advantageous, as it creates a platform that can be used for different types of therapeutic payloads. For example, for monoclonal antibodies, it is preferable to fuse BBB carriers to their C-terminus, as it would not affect the antibody target binding. Our data indicated that IGF1R5 BBB permeability was not affected in fusions through either its N- or C-terminus.

We next examined the serum, CSF and brain levels of hFc-IGF1R5 24 h after its systemic administrations. As expected, a significant amount of hFc-IGF1R5 was still present in the serum samples, suggesting that the hFc fusion greatly increased the half-life of IGF1R5. This was not surprising since, unlike high-affinity TfR antibodies that were shown to have accelerated systemic clearance due to peripheral target-mediated clearance [37], we showed that IGF1R constructs have pharmacokinetic profiles that are comparable to control monoclonal antibodies [23]. hFc-IGF1R5 levels were significantly increased in both CSF and capillary-depleted brain fractions. Similar to Fc fusions, IgG-IGF1R5 bi-specific antibodies demonstrated considerable accumulation in CSF and brain tissue. Interestingly, we noted that levels in brain fractions were slightly reduced for IgG fusions when compared with the Fc format, suggesting that the size of the molecule may have an impact on BBB permeability.

For drug development purposes, it is necessary to demonstrate that sdAbs are capable of transporting a pharmacologically active payload into the CNS following RMT in pre-clinical models using rodents and non-human primates. SPR data acquired in our study demonstrated the binding cross-reactivity of IGF1R5 across different species, providing great versatility in the choice of preclinical models. This is an important departure from the preclinical studies involving TfR that required the use of transgenic animals expressing human TfR since those antibodies showed no species cross-reactivity [38]. We fused the neuropeptide neurotensin to the C-terminus of IGF1R5-hFc and measured its pharmacological effect. Neurotensin (NT) is a 13-amino-acid neuropeptide that is widely distributed in the CNS that mediates its effects, mainly through neurotensin receptor type 1 (NTR1), a G-protein-coupled receptor [31]. It was shown that central injection of NT leads to a sustained decrease in core body temperature [39]. This effect was also determined to be mediated by NTR1 since, in NTR1 knockout mice, NT administration failed to induce changes in body temperature [40]. Additionally, analogs that are selective for other subtypes of NT receptors did not induce hypothermia, further supporting the involvement of the NTR1 receptor subtype in mediating this effect [41]. In the present study, we demonstrated that IGF1R5-hFc-neurotensin constructs induced a dose-dependent hypothermic response in both mice and rats. Interestingly, although the levels of IGF1R5 constructs are elevated even 24 h post-injection, the effects of IGF1R5-hFc-neurotensin lasted a maximum of 290 and 95 min in mice and rats, respectively, at the highest dose studied. We speculate that feedback mechanisms, including thyroid activity and brown adipose tissue stimulation, play a role in normalizing the core temperature to baseline levels.

We also measured the analgesic properties of galanin when conjugated to IGF1R5. Galanin is a neuropeptide of 29 amino acids (30 in humans) that was originally isolated from a porcine intestine [42]. Galanin effects are mediated by three subtypes of galanin receptors (Gal R1, Gal R2 and Gal R3) that belong to the family of G-protein coupled receptors [43]. The analgesic properties of galanin were further demonstrated by studies showing that direct injection of galanin into the central nervous system has antinociceptive effects in different experimental models of pain [32,44]. Here, we showed that IGF1R5 sdAb Fc fusion constructs conjugated with galanin were capable of reversing hyperalgesia of rats in the Hargreaves model. Interestingly, in accordance with what we observed in the BBB model *in vitro*, mFc-IGF1R5-galanin constructs performed slightly better than

IGF1R5-mFc-galanin. Different efficacy of these constructs could be the result of attenuation/modification of either IGF1R5 or galanin functionality or both.

The hypothermic and analgesic effects of neurotensin and galanin, respectively, when conjugated to IGF1R5 further confirmed the delivery of pharmacologically active amounts of payloads to the site of actions in the CNS. Taken together, we demonstrated the feasibility of delivering cargos into the brain with single-domain antibodies against IGF1R, notably IGF1R5, which permeated the BBB through RMT, highlighting its potential use for the development of drugs targeting the central nervous system.

## 5. Conclusions

In conclusion, we demonstrated that IGF1R5, which is a sdAb targeting IGF1R in the BBB, is a promising carrier for delivering drugs targeting the central nervous system. This antibody can be presented in different formats and fused to payloads of variable sizes, further highlighting its clinical potential, especially considering that poor brain distribution is one of the major limitations of drugs developed for CNS applications.

**Supplementary Materials:** The following supporting information can be downloaded at <https://www.mdpi.com/article/10.3390/pharmaceutics14071452/s1>. Figure S1: Sequence alignment between the camelid IGF1R5 sdAb and the humanized variant IGF1R5-H2. Figure S2: Representative SDS-PAGE images of IGF1R5 constructs. Figure S3: In vitro BBB transport of IgG-fused IGF1R5 and molecular weight/transmigration value of various IGF1R5 constructs. Figure S4: A20.1hFc-neurotensin injection in rats and mice. Figure S5: Reversal of thermal hyperalgesia induced by IGF1R5-mFc-galanin and mFc-IGF1R5-galanin in the Hargreaves model of inflammatory pain.

**Author Contributions:** Conceptualization, D.B.S. and K.K.; methodology, A.Y., H.v.F., A.S.H., C.E.D., E.B., J.K.S., M.H. and T.S.; software, A.S.H., G.H. and T.S.; validation, A.Y., A.S.H., G.H. and J.K.S.; formal analysis, A.Y., G.H., A.S.H. and E.B.; investigation, A.Y., E.B. and K.K.; resources, D.B.S.; data curation, A.Y., G.H., A.S.H., J.K.S., T.S., H.v.F., C.E.D. and M.H.; writing—original draft preparation, A.Y.; writing—review and editing, D.B.S., T.S., J.K.S. and G.H.; visualization, D.B.S.; supervision, G.H., A.S.H., K.K., T.S. and J.K.S.; project administration, K.K. and D.B.S.; funding acquisition, D.B.S. All authors have read and agreed to the published version of the manuscript.

**Funding:** This research received no external funding.

**Institutional Review Board Statement:** The animal study protocols were approved by the Animal Care Committee of the National Research Council Canada. CSF and Brain exposure (protocol code AUP2018.04, date of approval 16 May 2018), neurotensin studies (protocol code AUP2015.07, date of approval 15 October 2015), galanin studies (protocol code AUP2018.05, date of approval 16 May 2018).

**Informed Consent Statement:** All studies with human cells and tissues were approved by the Ottawa Hospital and the National Research Council of Canada's Research Ethics Boards. Informed written consent was obtained to use the amniotic fluid for research purposes and all the methods were carried out in accordance with the relevant guidelines and regulations as approved by the Ottawa Hospital Research Ethics Board.

**Data Availability Statement:** Not applicable.

**Acknowledgments:** We would like to thank Alex Pelletier and Yves Durocher for the production and purification of the neurotensin-fused constructs. We would like to thank Wen Ding, Alex Star, Xigeng Zhao, Ken Chan and Luc Tessier for technical assistance with sample prep and MS running.

**Conflicts of Interest:** The authors declare no conflict of interest.

## References




1. Pardridge, W.M. The blood-brain barrier: Bottleneck in brain drug development. *NeuroRx* **2005**, *2*, 3–14. [CrossRef] [PubMed]
2. Wang, Y.Y.; Lui, P.C.; Li, J.Y. Receptor-mediated therapeutic transport across the blood-brain barrier. *Immunotherapy* **2009**, *1*, 983–993. [CrossRef] [PubMed]
3. Fishman, J.B.; Rubin, J.B.; Handrahan, J.V.; Connor, J.R.; Fine, R.E. Receptor-mediated transcytosis of transferrin across the blood-brain barrier. *J. Neurosci. Res.* **1987**, *18*, 299–304. [CrossRef] [PubMed]

4. Ju, X.; Miao, T.; Chen, H.; Ni, J.; Han, L. Overcoming Mfsd2a-mediated low transcytosis to boost nanoparticle delivery to brain for chemotherapy of brain metastases. *Adv. Healthc. Mater.* **2021**, *10*, e2001997. [CrossRef]
5. Haqqani, A.S.; Delaney, C.E.; Brunette, E.; Baumann, E.; Farrington, G.K.; Sisk, W.; Eldredge, J.; Ding, W.; Tremblay, T.L.; Stanimirovic, D.B. Endosomal trafficking regulates receptor-mediated transcytosis of antibodies across the blood brain barrier. *J. Cereb. Blood Flow. Metab.* **2018**, *38*, 727–740. [CrossRef]
6. Pardridge, W.M. Delivery of biologics across the blood-brain barrier with molecular trojan horse technology. *BioDrugs* **2017**, *31*, 503–519. [CrossRef]
7. Jones, A.R.; Shusta, E.V. Blood-brain barrier transport of therapeutics via receptor-mediation. *Pharm. Res.* **2007**, *24*, 1759–1771. [CrossRef]
8. Giugliani, R.; Giugliani, L.; de Oliveira Poswar, F.; Donis, K.C.; Corte, A.D.; Schmidt, M.; Boado, R.J.; Nestrasil, I.; Nguyen, C.; Chen, S.; et al. Neurocognitive and somatic stabilization in pediatric patients with severe Mucopolysaccharidosis Type I after 52 weeks of intravenous brain-penetrating insulin receptor antibody-iduronidase fusion protein (valanafusp alpha): An open label phase 1–2 trial. *Orphanet J. Rare Dis.* **2018**, *13*, 110. [CrossRef]
9. Yu, Y.J.; Zhang, Y.; Kenrick, M.; Hoyte, K.; Luk, W.; Lu, Y.; Atwal, J.; Elliott, J.M.; Prabhu, S.; Watts, R.J.; et al. Boosting brain uptake of a therapeutic antibody by reducing its affinity for a transcytosis target. *Sci. Transl. Med.* **2011**, *3*, 84ra44. [CrossRef]
10. Coloma, M.J.; Lee, H.J.; Kurihara, A.; Landaw, E.M.; Boado, R.J.; Morrison, S.L.; Pardridge, W.M. Transport across the primate blood-brain barrier of a genetically engineered chimeric monoclonal antibody to the human insulin receptor. *Pharm. Res.* **2000**, *17*, 266–274. [CrossRef]
11. Alata, W.; Yogi, A.; Brunette, E.; Delaney, C.E.; van Faassen, H.; Hussack, G.; Iqbal, U.; Kemmerich, K.; Haqqani, A.S.; Moreno, M.J.; et al. Targeting insulin-like growth factor-1 receptor (IGF1R) for brain delivery of biologics. *FASEB J.* **2022**, *36*, e22208. [CrossRef] [PubMed]
12. Farrington, G.K.; Caram-Salas, N.; Haqqani, A.S.; Brunette, E.; Eldredge, J.; Pepinsky, B.; Antognetti, G.; Baumann, E.; Ding, W.; Garber, E.; et al. A novel platform for engineering blood-brain barrier-crossing bispecific biologics. *FASEB J.* **2014**, *28*, 4764–4778. [CrossRef] [PubMed]
13. Muruganandam, A.; Tanha, J.; Narang, S.; Stanimirovic, D. Selection of phage-displayed llama single-domain antibodies that transigrate across human blood-brain barrier endothelium. *FASEB J.* **2002**, *16*, 240–242. [CrossRef]
14. Molino, Y.; David, M.; Varini, K.; Jabès, F.; Gaudin, N.; Fortoul, A.; Bakloul, K.; Masse, M.; Bernard, A.; Drobecq, L.; et al. Use of LDL receptor-targeting peptide vectors for in vitro and in vivo cargo transport across the blood-brain barrier. *FASEB J.* **2017**, *31*, 1807–1827. [CrossRef] [PubMed]
15. Jacquot, G.; Lécorché, P.; Malcor, J.D.; Laurencin, M.; Smirnova, M.; Varini, K.; Malicet, C.; Gassiot, F.; Abouzid, K.; Faucon, A.; et al. Optimization and in vivo validation of peptide vectors targeting the LDL receptor. *Mol. Pharm.* **2016**, *13*, 4094–4105. [CrossRef] [PubMed]
16. Masliah, E.; Spencer, B. Applications of ApoB LDLR-binding domain approach for the development of CNS-penetrating peptides for alzheimer's Disease. *Methods Mol. Biol.* **2015**, *1324*, 331–337. [PubMed]
17. Guo, Q.; Zhu, Q.; Miao, T.; Tao, J.; Ju, X.; Sun, Z.; Li, H.; Xu, G.; Chen, H.; Han, L. LRP1-upregulated nanoparticles for efficiently conquering the blood-brain barrier and targetedly suppressing multifocal and infiltrative brain metastases. *J. Control. Release* **2019**, *303*, 117–129. [CrossRef] [PubMed]
18. Zuchero, Y.J.; Chen, X.; Bien-Ly, N.; Bumbaca, D.; Tong, R.K.; Gao, X.; Zhang, S.; Hoyte, K.; Luk, W.; Huntley, M.A.; et al. Discovery of novel blood-brain barrier targets to enhance brain uptake of therapeutic antibodies. *Neuron* **2016**, *89*, 70–82. [CrossRef]
19. Chen, H.; Zhou, M.; Zeng, Y.; Miao, T.; Luo, H.; Tong, Y.; Zhao, M.; Mu, R.; Gu, J.; Yang, S.; et al. Biomimetic lipopolysaccharide-free bacterial outer membrane-functionalized nanoparticles for brain-targeted drug delivery. *Adv. Sci.* **2022**, *9*, e2105854. [CrossRef]
20. Wiley, D.T.; Webster, P.; Gale, A.; Davis, M.E. Transcytosis and brain uptake of transferrin-containing nanoparticles by tuning avidity to transferrin receptor. *Proc. Natl. Acad. Sci. USA* **2013**, *110*, 8662–8667. [CrossRef]
21. Werner, H.; LeRoith, D. Insulin and insulin-like growth factor receptors in the brain: Physiological and pathological aspects. *Eur. Neuropsychopharmacol.* **2014**, *24*, 1947–1953. [CrossRef] [PubMed]
22. Ribocco-Lutkiewicz, M.; Sodja, C.; Haukenfrers, J.; Haqqani, A.S.; Ly, D.; Zachar, P.; Baumann, E.; Ball, M.; Huang, J.; Rukhlova, M.; et al. A novel human induced pluripotent stem cell blood-brain barrier model: Applicability to study antibody-triggered receptor-mediated transcytosis. *Sci. Rep.* **2018**, *8*, 1873. [CrossRef] [PubMed]
23. Stanimirovic, D.; Kemmerich, K.; Haqqani, A.S.; Sulea, T.; Arbabi-Ghahroudi, M.; Massie, B.; Gilbert, R. Insulin-Like Growth Factor 1 Receptor-Specific Antibodies and Uses Thereof. WO2015131256A1, 11 September 2015.
24. Sheff, J.; Wang, P.; Xu, P.; Arbour, M.; Masson, L.; van Faassen, H.; Hussack, G.; Kemmerich, K.; Brunette, E.; Stanimirovic, D.; et al. Defining the epitope of a blood-brain barrier crossing single domain antibody specific for the type 1 insulin-like growth factor receptor. *Sci. Rep.* **2021**, *11*, 4284. [CrossRef] [PubMed]
25. Sulea, T. Humanization of camelid single-domain antibodies. *Methods Mol. Biol.* **2022**, *2446*, 299–312.
26. Henry, K.A.; Sulea, T.; van Faassen, H.; Hussack, G.; Purisima, E.O.; MacKenzie, C.R.; Arbabi-Ghahroudi, M. A rational engineering strategy for designing protein a-binding camelid single-domain antibodies. *PLoS ONE* **2016**, *11*, e0163113.

27. Webster, C.I.; Caram-Salas, N.; Haqqani, A.S.; Thom, G.; Brown, L.; Rennie, K.; Yogi, A.; Costain, W.; Brunette, E.; Stanimirovic, D.B. Brain penetration, target engagement, and disposition of the blood-brain barrier-crossing bispecific antibody antagonist of metabotropic glutamate receptor type 1. *FASEB J.* **2016**, *30*, 1927–1940. [CrossRef]
28. Haqqani, A.S.; Kelly, J.F.; Stanimirovic, D.B. Quantitative protein profiling by mass spectrometry using label-free proteomics. *Methods Mol. Biol.* **2008**, *439*, 241–256.
29. Thom, G.; Burrell, M.; Haqqani, A.S.; Yogi, A.; Lessard, E.; Brunette, E.; Delaney, C.; Baumann, E.; Callaghan, D.; Rodrigo, N.; et al. Enhanced delivery of galanin conjugates to the brain through bioengineering of the anti-transferrin receptor antibody OX26. *Mol. Pharm.* **2018**, *15*, 1420–1431. [CrossRef]
30. Boules, M.; Li, Z.; Smith, K.; Fredrickson, P.; Richelson, E. Diverse roles of neurotensin agonists in the central nervous system. *Front. Endocrinol.* **2013**, *4*, 36. [CrossRef]
31. Besserer-Offroy, É.; Brouillette, R.L.; Lavenus, S.; Froehlich, U.; Brumwell, A.; Murza, A.; Longpré, J.; Marsault, É.; Grandbois, M.; Sarret, P.; et al. The signaling signature of the neurotensin type 1 receptor with endogenous ligands. *Eur. J. Pharmacol.* **2017**, *805*, 1–13. [CrossRef]
32. Wang, D.; Lundeberg, T.; Yu, L.C. Antinociceptive role of galanin in periaqueductal grey of rats with experimentally induced mononeuropathy. *Neuroscience* **2000**, *96*, 767–771. [CrossRef]
33. Zhang, W.; Liu, Q.Y.; Haqqani, A.S.; Leclerc, S.; Liu, Z.; Fauteux, F.; Baumann, E.; Delaney, C.E.; Ly, D.; Star, A.T.; et al. Differential expression of receptors mediating receptor-mediated transcytosis (RMT) in brain microvessels, brain parenchyma and peripheral tissues of the mouse and the human. *Fluids Barriers CNS* **2020**, *17*, 47. [CrossRef] [PubMed]
34. Kunz, P.; Flock, T.; Soler, N.; Zaiss, M.; Vincke, C.; Sterckx, Y.; Kastelic, D.; Muyldermans, S.; Hoheisel, J.D. Exploiting sequence and stability information for directing nanobody stability engineering. *Biochim. Biophys. Acta Gen. Subj.* **2017**, *1861*, 2196–2205. [CrossRef] [PubMed]
35. Rossotti, M.A.; Bélanger, K.; Henry, K.A.; Tanha, J. Immunogenicity and humanization of single-domain antibodies. *FEBS J.* **2021**. [CrossRef]
36. Sade, H.; Baumgartner, C.; Hugenmatter, A.; Moessner, E.; Freskgård, P.O.; Niewoehner, J. A human blood-brain barrier transcytosis assay reveals antibody transcytosis influenced by pH-dependent receptor binding. *PLoS ONE* **2014**, *9*, e96340.
37. Gadkar, K.; Yadav, D.B.; Zuchero, J.Y.; Couch, J.A.; Kanodia, J.; Kenrick, M.K.; Atwal, J.K.; Dennis, M.S.; Prabhu, S.; Watts, R.J.; et al. Mathematical PKPD and safety model of bispecific Tfr/BACE1 antibodies for the optimization of antibody uptake in brain. *Eur. J. Pharm. Biopharm.* **2016**, *101*, 53–61. [CrossRef]
38. Ullman, J.C.; Arguello, A.; Getz, J.A.; Bhalla, A.; Mahon, C.S.; Wang, J.; Giese, T.; Bedard, C.; Kim, D.J.; Blumenfeld, J.R.; et al. Brain delivery and activity of a lysosomal enzyme using a blood-brain barrier transport vehicle in mice. *Sci. Transl. Med.* **2020**, *12*, eaay1163. [CrossRef]
39. Bisette, G.; Nemeroff, C.B.; Loosen, P.T.; Prange, A.J.; Lipton, M.A. Hypothermia and intolerance to cold induced by intracisternal administration of the hypothalamic peptide neurotensin. *Nature* **1976**, *262*, 607–609. [CrossRef]
40. Remaury, A.; Vita, N.; Gendreau, S.; Jung, M.; Arnone, M.; Poncelet, M.; Culouscou, J.M.; Le Fur, G.; Soubrié, P.; Caput, D.; et al. Targeted inactivation of the neurotensin type 1 receptor reveals its role in body temperature control and feeding behavior but not in analgesia. *Brain Res.* **2002**, *953*, 63–72. [CrossRef]
41. Boules, M.; Liang, Y.; Briody, S.; Miura, T.; Fauq, I.; Oliveros, A.; Wilson, M.; Khaniev, S.; Williams, K.; Li, Z.; et al. NT79: A novel neurotensin analog with selective behavioral effects. *Brain Res.* **2010**, *1308*, 35–46. [CrossRef]
42. Tatemoto, K.; Rökaeus, A.; Jörnvall, H.; McDonald, T.J.; Mutt, V. Galanin—A novel biologically active peptide from porcine intestine. *FEBS Lett.* **1983**, *164*, 124–128. [CrossRef]
43. Lang, R.; Gundlach, A.L.; Kofler, B. The galanin peptide family: Receptor pharmacology, pleiotropic biological actions, and implications in health and disease. *Pharmacol. Ther.* **2007**, *115*, 177–207. [CrossRef] [PubMed]
44. Yang, Y.; Zhang, Y.; Li, X.H.; Li, Y.; Qian, R.; Li, J.; Xu, S.L. Involvements of galanin and its receptors in antinociception in nucleus accumbens of rats with inflammatory pain. *Neurosci. Res.* **2015**, *97*, 20–25. [CrossRef] [PubMed]

## Article

# The 46.1 Antibody Mediates Neurotensin Uptake into the CNS and the Effects Depend on the Route of Intravenous Administration

Julia V. Georgieva<sup>1</sup>, Moriah Katt<sup>1,†</sup>, Zhou Ye<sup>1,†</sup>, Benjamin J. Umlauf<sup>1</sup>, Cody J. Wenthur<sup>2</sup>  
and Eric V. Shusta<sup>1,3,\*</sup>

<sup>1</sup> Department of Chemical and Biological Engineering, University of Wisconsin-Madison, Madison, WI 53706, USA

<sup>2</sup> Divisions of Pharmaceutical Sciences and Pharmacy Practice, School of Pharmacy, University of Wisconsin-Madison, Madison, WI 53705, USA

<sup>3</sup> Department of Neurological Surgery, University of Wisconsin-Madison, Madison, WI 53792, USA

\* Correspondence: [eshusta@wisc.edu](mailto:eshusta@wisc.edu)

† These authors contributed equally to this work.

**Abstract:** Central nervous system (CNS) exposure to blood-borne biotherapeutics is limited by the restrictive nature of the brain vasculature. In particular, tightly sealed endothelial cells of the blood–brain barrier (BBB) prevent the uptake of protein and gene medicines. An approach to increase the bioavailability of such therapeutics is harnessing the BBB endothelial cells’ own receptor-mediated transcytosis (RMT) mechanisms. Key to this process is a targeting ligand that can engage a BBB-resident RMT receptor. We recently identified an antibody, named 46.1, that accumulates in the mouse brain after intravenous injection. To further characterize the brain targeting and penetrating properties of clone 46.1, we conjugated neurotensin (NT) to an scFv-Fc form of the antibody (46.1-scFv-Fc-LongLinker-NT). While centrally administered NT decreases the core body temperature and locomotor activity, effects attributed to two spatially segregated brain areas, systemically administered NT has limited effects. Hence, NT can be used as a model therapeutic payload to evaluate the brain penetration of BBB-targeting antibodies and their capability to accumulate in discrete brain areas. We demonstrate that intravenously administered 46.1-scFv-Fc-LL-NT can elicit transient hypothermia and reduce drug-induced hyperlocomotion, confirming that 46.1 can deliver drug cargo to the CNS at pharmacologically relevant doses. Interestingly, when two intravenous administration routes in mice, retro-orbital and tail vein, were compared, only retro-orbital administration led to transient hypothermia. We further explored the retro-orbital route and demonstrated that the 46.1-scFv-Fc-LL-NT could enter the brain arterial blood supply directly from the retro-orbital/cavernous sinus. Taken together, the 46.1 antibody is capable of transporting drug cargo into the CNS, and at least of a portion of its CNS accumulation occurs via the cavernous sinus–arterial route.

**Keywords:** blood-brain barrier; brain drug delivery; receptor-mediated transcytosis; antibody; cavernous sinus

**Citation:** Georgieva, J.V.; Katt, M.; Ye, Z.; Umlauf, B.J.; Wenthur, C.J.; Shusta, E.V. The 46.1 Antibody Mediates Neurotensin Uptake into the CNS and the Effects Depend on the Route of Intravenous Administration. *Pharmaceutics* **2022**, *14*, 1706. <https://doi.org/10.3390/pharmaceutics14081706>

Academic Editor: William M. Pardridge

Received: 1 July 2022

Accepted: 11 August 2022

Published: 16 August 2022

**Publisher’s Note:** MDPI stays neutral with regard to jurisdictional claims in published maps and institutional affiliations.



**Copyright:** © 2022 by the authors. Licensee MDPI, Basel, Switzerland. This article is an open access article distributed under the terms and conditions of the Creative Commons Attribution (CC BY) license (<https://creativecommons.org/licenses/by/4.0/>).

## 1. Introduction

Drug delivery into the brain remains the rate limiting step in the development of new therapies whose targets lie within the central nervous system (CNS). In particular, the passage of newer biologic therapeutics (antibodies, peptides, nucleic acids, etc.) from the systemic circulation into the brain is substantially restricted by the blood–brain barrier (BBB) [1]. As a result, various technologies are being developed to increase the brain bioavailability. Despite known limitations [2], those that co-opt endogenous receptor-mediated transcytosis (RMT) systems in BBB endothelial cells hold particular promise [3–8]. The transport of a drug payload from the blood into the brain tissue by RMT is mediated by a BBB-targeting motif that recognizes a cognate receptor on the blood-side endothelial membrane and initiates transcytosis. In preceding work, we identified antibodies capable

of BBB transcytosis using a phenotypic transcytosis screen of a large phage displayed human single-chain antibody (scFv) library [9]. The lead molecule, scFv 46.1, bound mouse and human BBB in tissue sections and accumulated in the mouse brain parenchyma after intravenous administration.

A key step in the preclinical evaluation of BBB-targeting motifs is demonstrable transport of a drug payload into the brain. Advanced disease models in translational research such as those examining  $\beta$ -amyloid clearance have been used to demonstrate the uptake of pharmacologically relevant doses of the therapeutic using RMT-directed brain drug delivery approaches [7]. Other strategies that are more focused on validating the RMT-targeted antibody as capable of mediating drug uptake into the CNS, rather than a therapeutic outcome, have also been used to validate RMT-targeting antibodies [10]. One such approach employs the conjugation of the RMT-targeting antibody to neurotensin (NT), a 13 amino acid peptide with a myriad of physiological functions. If administered peripherally, NT has a very low BBB permeability [11] and does not elicit profound effects in the CNS. However, if NT is introduced into the CNS, it can interact with NT receptors expressed on brain cells (NTSR1 and NTSR2) in different brain regions. For example, NT and its analogs inhibit food intake in arcuate nucleus [12], modulate pain response [13], and mitigate addiction behavior in nucleus accumbens [14–16]. In addition, NT integrates with dopamine neurotransmission, acting as an endogenous neuroleptic, leading to decreased drug-induced hyper- and spontaneous locomotor activity [17,18]. Upon release in the median preoptic nucleus (MnPO), NT activates its cognate receptors NTSR1 and NTSR2, which results in decreased core body temperature [19]. Since the CNS effects of NT are limited to central local release or central administration, fusion of NT to BBB-targeting antibodies can be used to test the BBB-permeation of the complex [8,10,11]. Notably, given the anatomically distinct effects of NT, it can also be used as a proxy for verifying brain uptake in different brain regions. For instance, in this study, we measured the effects of 46.1-NT fusions on the body temperature in mice (i.e., NT response from the MnPO), and additionally measured their drug-induced locomotor activity (i.e., response from the striatum) to demonstrate that 46.1 could mediate the uptake of pharmacologically relevant levels of NT in the CNS.

It has been shown that the pharmacokinetic profile of intravenous therapeutic antibodies can be independent of the route of intravenous administration [20]. Nevertheless, viral particles with CNS tropism seem to distribute differently upon tail vein, facial vein, or retro-orbital vein injection [21–23], a phenomenon speculated to arise in the cavernous sinus (Sin. Cavern.). The cavernous sinus consists of trabeculated cavities formed by splitting of the layers of the dura mater that are covered by endothelial cells. Located in the base of the skull, right below the hypophyseal gland, the cavernous sinus collects venous blood from the retro-orbital sinus, ophthalmic veins, superficial, and interior cerebral veins. The internal carotid artery spans the Sin. Cavern. before branching and entering the brain in a segment known as the cavernous portion of the internal carotid artery [24]. Thus, in the Sin. Cavern., venous blood is separated from the arterial blood by the wall of the internal carotid artery, a multilayered structure with an innermost endothelial cell layer, covered by internal elastic lamina, smooth muscle cell layer, and adventitia [25,26]. In this study, we additionally examined the effects of the route of intravenous administration (retro-orbital versus tail vein) on the hypothermic response in mice and demonstrated that the 46.1-NT fusion could enter the internal carotid artery directly from the retro-orbital/cavernous sinus and be transported throughout the brain via the microvasculature.

## 2. Materials and Methods

### 2.1. Construction of Neurotensin–Antibody Fusion Proteins

A previously described pIRES vector with the test and control scFvs fused to the rabbit Fc region was used to generate the neurotensin fusion construct [9]. Long linker (G<sub>4</sub>S)<sub>2</sub> and mouse neurotensin sequences (NM\_024435) were subcloned at the C-terminal of the rabbit Fc region between the custom inserted BamHI and NotI restriction sites. The following

oligonucleotide was used: 5'-GGATCCGGTGGTGGCGGCTCTGGTGGCGGTGGCAGCCA GCTGTATGAAAATAAACCCAGAGGCCCTACATTCTCTGAGCGGCCGC-3'. The oligonucleotide duplex was inserted with standard restriction cloning. The sequence identity was verified at the UW-Madison sequencing facility and had the final annotation Clone ID-scFv-Fc-LL-NT. Fused proteins were produced and purified exactly as previously described [9]. The functional activity of neurotensin was monitored for each batch with the Path-Hunter<sup>®</sup> eXpress NTSR1 CHO-K1  $\beta$ -Arrestin GPCR assay (Eurofins/DiscoverX, #93-0280E2CP0L, Fremont, CA, USA), according to the manufacturer's protocol.

## 2.2. Microvascular Endothelial Cell Immunocytochemistry

IPSC-derived brain microvascular endothelial cells (iPSC-BMEC-like cells) were purified on Lab Tek II chamber slides (Nunc #154917, Thermo Fisher Scientific, Madison, WI, USA) (Figure 1C) or on 0.4  $\mu$ m Transwell filters (Figure A2), as described previously [27,28]. Cells grown on chamber slides were washed once and the media exchanged with prewarmed PBS<sup>++</sup> (PBS supplemented with Ca<sup>2+</sup> and Mg<sup>2+</sup>). Antibody 46.1-scFv-Fc-LL-NT was added to the PBS<sup>++</sup> to a final concentration of 5  $\mu$ g/mL. Cells were kept at 37 °C for 45 min to allow for antibody binding and internalization. Afterward, cells were washed with ice cold PBS<sup>++</sup> and media exchanged with ice cold PBS<sup>++</sup> plus 10% goat serum (PBSG). Secondary anti-rabbit AlexaFluor555 (Invitrogen #A21428, Thermo Fisher Scientific, Madison, WI, USA)-conjugated antibody of a final dilution 1:1000 was added to the live cells to label the membrane bound fraction. After an additional 20 min on ice, the cells were washed three times with cold PBS<sup>++</sup>, fixed with ice cold 4% paraformaldehyde (PFA) for 15 min, permeabilized with 0.2% Triton X for 2 min, and washed with PBS<sup>++</sup>. Anti-rabbit AlexaFluor488 (Invitrogen #A11008, Thermo Fisher Scientific, Madison, WI, USA) diluted 1:1000 in PBSG was added to the chamber slides to label the internalized fraction and incubated at RT for an additional 20 min. The iPSC-BMECs were washed and mounted with ProLong Gold anti-fade reagent with DAPI (Invitrogen, P36935, Thermo Fisher Scientific, Madison, WI, USA). Images were acquired on a Zeiss Axio Imager Z2 Upright microscope (Carl Zeiss Microscopy, LLC, White Plains, NY, USA) and processed with ImageJ (Version 1.53e, Wayne Rasband and contributors, NIH, USA, <http://imagej.nih.gov/ij>).

The TEER value of iPSC-BMECs, grown on Transwell filters (n = 3) was measured and on the day of the experiment averaged  $\sim$ 1600  $\Omega$ /cm<sup>2</sup>. Cells were washed and media exchanged with prewarmed PBS<sup>++</sup>. Antibody 46.1-scFv-Fc-LL-NT was added to the basolateral compartment to a final concentration of 5  $\mu$ g/mL. The iPSC-BMEC-like cells were kept at 37 °C for 45 min. After a brief washing step with ice cold PBS<sup>++</sup> and PBSG, the apical and the basolateral compartment solution was exchanged with ice cold PBSG containing secondary anti-rabbit antibodies in a 1:1000 dilution, AlexaFluor647 (Invitrogen #A-21235, Thermo Fisher Scientific, Madison, WI, USA) in the apical compartment to label the apical membrane associated 46.1-scFv-Fc-LL-NT and AlexaFluor555 (Invitrogen #A21428, Thermo Fisher Scientific, Madison, WI, USA) in the basolateral compartment to label the basolateral membrane bound 46.1-scFv-Fc-LL-NT. The live, not-permeabilized cells were kept on ice for 20 min. The filter was washed quickly 3x with cold PBS<sup>++</sup>. Cells were fixed with ice cold 4% PFA for 15 min and permeabilized with 0.2% Triton X for 2 min, applied on both sides of the filter. Anti-rabbit AlexaFluor488 (Invitrogen #A11008, Thermo Fisher Scientific, Madison, WI, USA) in 1:1000 dilution was added to both sides of the filter to label the internalized 46.1-scFv-Fc-LL-NT and incubated at RT for an additional 20 min. Cells were washed and mounted with the ProLong Gold mounting media. Images were acquired on a Zeiss Axio Imager Z2 upright microscope and processed with ImageJ.



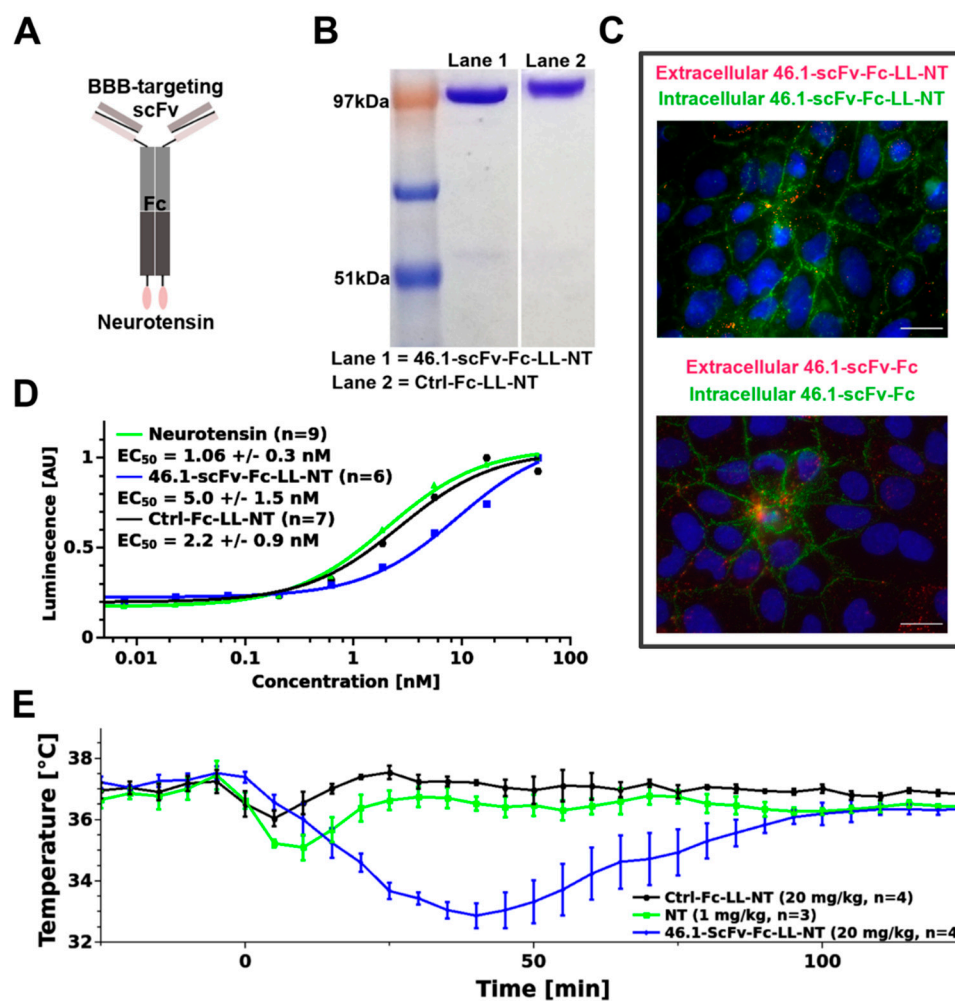


**Figure 1.** ScFv 46.1 transports neurotensin into the MnPO. (A) Cartoon of the antibody-NT construct. (B) Purified fusion constructs resolved with SDS-PAGE and Coomassie staining. (C) Conjugation of neurotensin to the parent antibody (lower image) has no influence on the binding- and internalization activity of 46.1-scFv-Fc-LL-NT (upper image) in iPSC-BMEC-like cells, as evident from both antibodies having a characteristic punctate appearance on the plasma membrane (pseudocolored in red) and localization to the internal cell-cell contacts (pseudocolored in green). Scale bar, 20  $\mu$ m. (D) NT alone or antibody-NT-fusions (control and 46.1 antibody) were added in serial dilutions to NTSR1 (G-protein coupled receptor (GPCR)) expressing CHO-cells. The activation of NTSR1 was measured as a chemiluminescent light, produced by active  $\beta$ -galactosidase, which formed upon the recruitment of  $\beta$ -arrestin to the NTSR1 construct. The inset provides the fitted EC<sub>50</sub> values (mean  $\pm$  s.e.m.). The curves represent one biological replicate and n is listed in the inset. One-way ANOVA was used to analyze the data. The EC<sub>50</sub> value for 46.1 fusion differs significantly from the EC<sub>50</sub> of neurotensin with a Holm corrected *p*-value = 0.009 (Table A1). (E) Mice were injected at time 0 via the retro-orbital sinus with the control and 46.1 fusions or free neurotensin and the temperature recorded with an intraperitoneally-implanted probe, as described in the Materials and Methods Section. Mixed ANOVA was used to model the data (mean  $\pm$  s.e.m.). The Holm-Bonferroni post hoc multiple comparisons test revealed a statistically significant difference between the 46.1-scFv-Fc-LL-NT group vs. the control (*p* = 0.001) and NT (*p* < 0.05) (Table A2).

### 2.3. Animal Experiments

Animal studies were approved by the Institutional Animal Care and Use Committee (IACUC) at the University of Wisconsin-Madison and performed in compliance with the National Institutes of Health Guide for the Care and Use of Laboratory Animals. Mice were

group housed in an AAALAC accredited vivarium on a standardized light cycle (lights on: 8 a.m.–8 p.m.) with ad libitum access to food and water.

#### 2.4. Logger Implantation and Temperature Measurement

Mice C57BL6 (Harlan Laboratories, Inc., Envigo Bioproducts, Inc., Madison, WI, USA), male, ~18 g were anesthetized with 100/10 mg/kg ketamine/xylazine (Vetaket C-III (N), Akorn, Inc., #2010020, Lake Forest, IL, USA). Under aseptic conditions, an incision was made in the peritoneal cavity and a sterile temperature recording logger was inserted (DST nano-T, StarOddi, Garðabær, Iceland). The incision was sutured with a vicryl suture (Ethicon, #J422H, Bridgewater NJ, USA) and the skin glued with the tissue adhesive Vetbond (3M, #70200742529, Maplewood, MN, USA). Twenty minutes prior to recovery from anesthesia, mice received s.c. 1 mg/kg Buprenorphine SR Lab 0.5 mg/mL (ZooPharm, Laramie, WY, USA). Mice were allowed to fully recover after surgery before being transferred to their home cages. On day 6 after logger implantation, the mice were injected via the retro-orbital sinus (under brief isoflurane anesthesia, <2 min) or tail vein with 20 mg/kg control and test antibody, and 1 mg/kg neurotensin dissolved in PBS (Sigma-Aldrich, #N6383, Burlington, MA, USA). For the duration of the temperature recordings, mice were returned to their home cages.

#### 2.5. Locomotor Activity Measurement

Mice C57BL6 (Harlan Laboratories, Inc., Envigo Bioproducts, Inc, Madison, WI, USA), male, ~18 g were housed under normal conditions for 5 days. On the sixth day, each mouse was transferred to a clean plastic open field apparatus (25 cm W × 40 cm D × 20 cm H) in the recording room. Light intensity was adjusted to ~55 lux. Mice were habituated to the apparatus for 60 min prior to treatment. Animals received, via tail vein, 20 mg/kg test antibody, 1 mg/kg PD149163 (Sigma-Aldrich, #PZ0175), 1 mg/kg neurotensin, or saline. All animals also received 3 mg/kg phencyclidine (Sigma-Aldrich, #P3029) s.c. Ten minutes later, mice were returned in the same, freshly ethanol wiped apparatus and their activity was recorded for an additional 90 min. Data were collected and the distance traveled measured with ANY-maze software (Stoelting Co., Wood Dale, IL, USA). The number of animals per group is specified in the figure legends.

#### 2.6. Surgery and Cavernous Sinus Immunohistochemistry

Mice C57BL6 (Harlan Laboratories, Inc., Envigo Bioproducts, Inc, Madison, WI, USA), male, ~20 g were anesthetized with 100/10 mg/kg ketamine/xylazine and fully prepped for whole body cardiac perfusion. Test or control antibody (20 mg/kg) was injected in the retro-orbital sinus. The perfusion pump was switched on immediately and the right atrium perforated right after. To keep the tissue metabolically active, the perfusion buffer was artificial cerebrospinal fluid (119 mM NaCl, 26.2 mM NaHCO<sub>3</sub>, 2.5 mM KCl, 1 mM NaH<sub>2</sub>PO<sub>4</sub>, 1.3 mM MgCl<sub>2</sub>, 10 mM glucose, 2.5 mM CaCl<sub>2</sub>) kept at 37 °C for the 15 min duration of the perfusion at 1.7 mL/min. Afterward, the perfusion buffer was exchanged with ice-cold 4% PFA in PBS for an additional 5 min at rate 5 mL/min. Animals were decapitated, the skull skinned, and placed in ice-cold 12% EDTA, pH = 7. The decalcification of the skull continued for 7 days by refreshing the 12% EDTA solution every other day. The skulls were washed once with PBS, dried on a tissue paper, and snap frozen in liquid nitrogen. Consecutive coronal sections (30 µm) spanning the cavernous sinus were made on a Thermo Scientific Microm HM 525 (Thermo Fisher Scientific, Waltham, MA, USA). Sections were air dried for 1 h, permeabilized with 0.05% saponin for 30 min, and blocked with 10% goat serum in PBS for 30 min at RT. To visualize the endothelial cells and blood vessels, the sections were incubated for 2 h at RT with rat anti-mouse CD31 (Biolegend, #102501, San Diego, CA, USA) diluted 1:50 in dilution buffer (10% goat serum with 0.05% saponin in PBS). Sections were then washed 5 × with 0.05% saponin in PBS and incubated for 2 h at RT with the goat anti-mouse AlexaFluor488-conjugated secondary antibody (Invitrogen, #A-11029) 1:1000 in dilution buffer. They were washed 5 × more

and incubated with the goat anti-rabbit AlexaFluor555-conjugated secondary antibody (Invitrogen, #A21428) that recognizes the rabbit Fc region of the control and test antibodies, diluted 1:1000, overnight at 4 °C. After 5 × more washing steps, sections were mounted with ProLong Gold antifade reagent with DAPI (Invitrogen, P36935) and imaged on a Zeiss Axio Imager Z2 Upright microscope or Nikon A1R HD Upright Multi-Photon (Nikon USA, Melville, NY, USA), and processed with ImageJ.

### 2.7. Statistical Analysis

Two-way repeated measures (mixed) ANOVA and Bayesian (mixed) ANOVA with treatment as the between subjects factor and time as the within subjects factor were used to model the hyperlocomotor data, which were grouped into 5 min blocks across the entire trial period. Average baseline locomotion for each individual subject was calculated across all 5 min blocks from 0 to 60 min. Hyperlocomotion data were transformed to a percent of the average baseline locomotion for each independent animal to correct for underlying individual variance in locomotor behavior. The *p* values by the multiple comparisons post hoc test were corrected with Holm–Bonferroni. Statistical analysis was performed with Jamovi (The Jamovi project, 2020, version 1.6, retrieved from <https://www.jamovi.org>, accessed on 2 March 2021). *p* values < 0.05 were considered as statistically significant. The posterior odds and Bayes factors were calculated with JASP software (JASP Team 2020, version 0.14.1, retrieved from <https://www.jasp-stats.org>, accessed on 3 March 2021). The posterior odds were corrected for multiple testing by fixing to 0.5 the prior probability that the null hypothesis holds across all comparisons [29]. Individual comparisons were based on the default *t*-test with a Cauchy (0,  $r = 1/\sqrt{2}$ ) prior. The “U” in the Bayes factor denotes that it is uncorrected.

## 3. Results

### 3.1. ScFv 46.1 Mediates the Transport of Neurotensin across the Blood Brain Barrier and Its Accumulation in the Median Preoptic Nucleus

Intracisternal administration of NT results in a decrease in the core body temperature through interactions with neurotensin receptors in the MnPO [30]; and thus, a decrease in body temperature can be used as a readout of the brain penetrating properties of RMT targeting reagents. Hence, we constructed an scFv-NT fusion protein. Neurotensin (NT) was linked via the (Gly<sub>4</sub>Ser)<sub>2</sub> linker (LL) to the C-terminus of scFv-Fc fusions with 46.1 scFv or a control binding domain, a variable lymphocyte receptor that binds to human H antigen trisaccharide [31], to create 46.1-scFv-Fc-LL-NT and Ctrl-Fc-LL-NT fusions, respectively (Figure 1A). The fusions were produced and purified (Figure 1B), and the activity of the binding and NT moieties were confirmed. The 46.1-scFv-Fc-LL-NT fusion bound and internalized into induced pluripotent stem cell-derived BMEC-like cells (iPSC BMEC-like cells), the original cell type that was used to identify 46.1, similar to that of the parent 46.1-scFv-Fc format (Figure 1C). In particular, scFv 46.1 drives the trafficking and internalization of the parent and the NT-fused antibody in iPSC-BMEC-like cells to the intracellular cell–cell junctions as previously described (Figure 1C, green) [9]. The activity of NT in the fusion protein was measured using the PathHunter® eXpress NTSR1 CHO-K1 β-Arrestin GPCR assay. Figure 1D depicts the EC<sub>50</sub> values indicating a slightly diminished activity of NT when fused to the 46.1-antibody, but potency remains in the nanomolar range. Next, the Control-, scFv-46.1- fusions (20 mg/kg, ~194 nmol/kg), and NT alone (1 mg/kg, 598 nmol/kg NT) were administered via the retro-orbital sinus in C57BL6 mice. 46.1-scFv-Fc-LL-NT caused a significant transient reduction in the body temperature compared to Ctrl-Fc-LL-NT or free NT (Figure 1E) (mixed model ANOVA,  $F_{\text{Treatment}}(2, 8) = 17.6, p = 0.001$ ), providing evidence for the scFv 46.1 mediated delivery of NT to postvascular cells in the MnPO.

### 3.2. ScFv 46.1 Mediates the Delivery of Neurotensin to the Striatum

NT is a well-known modulator of dopaminergic neurotransmission. Notably, spontaneous locomotor activity can be decreased by NT through interactions with dopaminergic neurons in the nucleus accumbens either by directly expressing NTSR1 or by communicating with NTSR1-responsive neurons or by receiving inhibitory signals from the ventral tegmental area [17,18]. Inspired by previous studies with BBB-permeable brain-penetrating NT analogs [32,33] that demonstrated the reversal of phencyclidine (PCP)-induced hyperlocomotor activity, and in analogy to other psychostimulants [34,35] pointing toward the activation of striatal NTSR1 in the nucleus accumbens [36] and caudate-putamen [37] as a mechanism for this effect, we explored whether scFv 46.1-mediated NT delivery would have an effect on PCP-induced changes in locomotion (Figure 2).

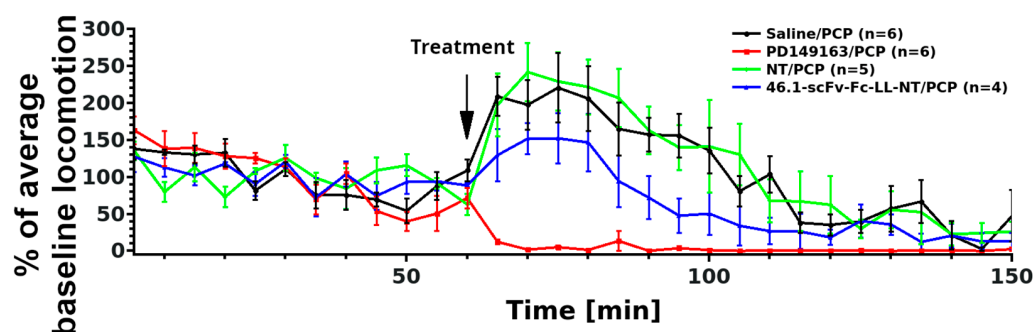


**Figure 2.** ScFv 46.1 affects NT impact on PCP-induced hyperactivity in mice. Animals were habituated in the recording setting for 1 h (0–60). The recording was stopped and saline, PD149163 (1 mg/kg), NT (1 mg/kg), or 46.1-scFv-Fc-LL-NT (20 mg/kg) were injected via the tail vein. Ten minutes later, this was followed by subcutaneous injection of PCP (3 mg/kg) to induce hyperactivity and the recording was resumed (arrow). The distance traveled is presented as a percent of the average baseline for each animal (mean  $\pm$  s.e.m.). Frequentist mixed ANOVA and Bayesian mixed model ANOVA were used to analyze the data. Detailed statistical parameters can be found in Tables 1 and 2.

To avoid any interference of isoflurane anesthesia (necessary for retro-orbital sinus injection) on the effects of PCP administration, all substances were administered via tail vein injection in unanesthetized mice. The distance traveled was used as a readout of mouse locomotor activity. PCP (3 mg/kg, s.c.) was introduced 10 min after prophylactic treatment with 46.1-scFv-Fc-LL-NT or controls. The BBB permeable NT analog, PD149163, was used as a positive control, and saline and NT alone were used as the negative controls. Mixed ANOVA of the baseline-normalized, PCP-induced hyperlocomotor effects from 0–90 min identified a significant treatment effect ( $F_{\text{Treatment}}(3, 17) = 13, p < 0.001$ ). Subsequent post hoc testing could not discriminate the 46.1-scFv-Fc-LL-NT treatment group from the other groups at a significance level of  $\alpha = 0.05$ . The associated adjusted and non-adjusted  $p$  values are shown in Table 1.

**Table 1.** The statistical parameters for mixed ANOVA analysis of PCP-induced hyperlocomotion.

Comparison		Mean Difference	SE	df	t	p	$P_{\text{Holm}}$
Saline	46.1-scFv-Fc-LL-NT (20 mg/kg)	47.46	22.3	17.0	2.128	0.048	0.096
	Neurotensin (1 mg/kg)	−7.76	20.9	17.0	−0.371	0.715	0.715
	PD149163 (1 mg/kg)	105.2	19.9	17.0	5.275	<0.001	<0.001
46.1-scFv-Fc-LL-NT (20 mg/kg)	Neurotensin (1 mg/kg)	−55.22	23.2	17.0	−2.383	0.029	0.087
	PD149163 (1 mg/kg)	57.74	22.3	17.0	2.589	0.019	0.076
Neurotensin (1 mg/kg)	PD149163 (1 mg/kg)	112.96	20.9	17.0	5.400	<0.001	<0.001

We additionally used Bayesian mixed ANOVA to assign the probability of differentiating between the experimental groups. Table 2 reports the posterior odds and the Bayes factors ( $BF_{10}$ ) in multiple comparison tests. The Bayes factors ( $BF_{10}$ ) calculated for the positive control PD149163 (vs. saline:  $BF_{10} = 2.64 \times 10^{20}$ , vs. NT:  $BF_{10} = 2.5 \times 10^{19}$ , vs. 46.1-scFv-Fc-LL-NT:  $BF_{10} = 1.36 \times 10^{13}$ ) indicate extreme evidence in favor of the alternative hypothesis (i.e., PD149163 reverts the hyperlocomotion of PCP compared to any other group). The Bayes factors ( $BF_{10}$ ) for the experimental treatment 46.1-scFv-Fc-LL-NT compared to saline or NT indicate very strong ( $BF_{10} = 70.34$ ) and extreme ( $BF_{10} = 147.72$ ) evidence for accepting the alternative hypothesis, respectively (i.e., 46.1-scFv-Fc-LL-NT reverts the hyperlocomotion of PCP compared with saline or NT groups). The interpretation of the Bayes factors as very strong or extreme follows that in [38]. Thus, 46.1-scFv-Fc-LL-NT has a distinguishable effect on the PCP-induced hyperactivity that can be assigned to its own experimental group, indicating that 46.1 can mediate transport of the NT cargo into the striatum. The effect is moderate compared to the BBB permeable PD149163, which is perhaps not surprising given that the brain bioavailability of NT in the form of 46.1-scFv-Fc-LL-NT also depends on the transcytosis of the construct across the BBB.

**Table 2.** The statistical parameters for the Bayesian mixed ANOVA analysis of PCP-induced hyperlocomotion.

Comparison					
Treatment	Treatment	Prior Odds	Posterior Odds	$BF_{10, U}$	Error (%)
Saline	46.1-scFv-Fc-LL-NT (20 mg/kg)	0.414	29.136	70.34	$2.603 \times 10^{-8}$
	Neurotensin (1 mg/kg)	0.414	0.074	0.178	$4.210 \times 10^{-6}$
	PD149163 (1 mg/kg)	0.414	$1.093 \times 10^{20}$	$2.638 \times 10^{20}$	$3.010 \times 10^{-27}$
46.1-scFv-Fc-LL-NT (20 mg/kg)	Neurotensin (1 mg/kg)	0.414	61.063	147.42	$1.607 \times 10^{-9}$
	PD149163 (1 mg/kg)	0.414	$5.637 \times 10^{12}$	$1.361 \times 10^{13}$	$2.716 \times 10^{-17}$
Neurotensin (1 mg/kg)	PD149163 (1 mg/kg)	0.414	$1.033 \times 10^{19}$	$2.493 \times 10^{19}$	$2.053 \times 10^{-26}$

Note. The posterior odds were corrected for multiple testing by fixing to 0.5 the prior probability that the null hypothesis holds across all comparisons [29]. Individual comparisons were based on the default *t*-test with a Cauchy (0,  $r = 1/\sqrt{2}$ ) prior. The “U” in the Bayes factor denotes that it is uncorrected.

### 3.3. Transient Hypothermia Response Depends on the Route of Delivery

For the body temperature measurements in Figure 1, we administered the 46.1-scFv-Fc-LL-NT via retro-orbital sinus injection. We also observed that 46.1-scFv-Fc-LL-NT had a modest effect on PCP-induced hyperlocomotion when administered via the tail vein, and wondered whether the route of administration could affect the responses observed. Retro-orbital injection was not compatible with the PCP hyperlocomotion experiment as it requires brief isoflurane anesthesia prior to PCP administration. Thus, we instead explored whether or not the transient hypothermia response would be altered by tail vein administration versus retro-orbital administration. Mice received the same doses of 46.1-scFv-Fc-LL-NT and the control (20 mg/kg antibody-NT fusion or 1 mg/kg NT), as described in Figure 1 with the tail vein administration being the only difference. Unexpectedly, no discernible changes in the core body temperature were observed between the groups (Figure 3), despite the potency of PD149163 to induce hypothermia after tail vein injection (Figure A3). As detailed in the discussion below, it may be possible that there is a dilution or loss of 46.1-scFv-Fc-LL-NT as it travels from the tail vein to the heart. Alternatively, there may be a unique attribute of the retro-orbital administration paradigm with respect to the 46.1 scFv targeting system that could lead to enhanced effects in the CNS.

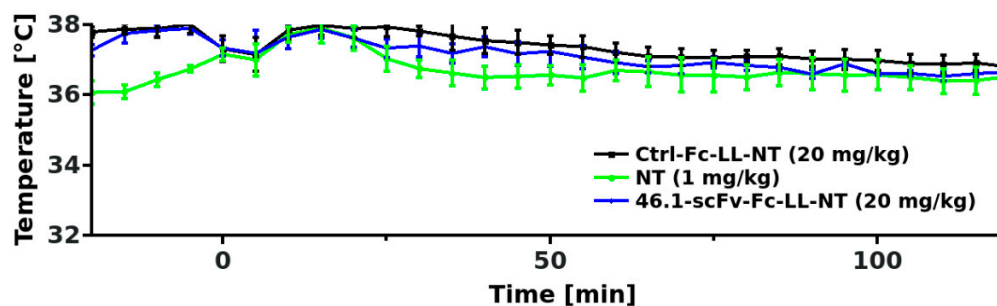


**Figure 3.** Tail vein administration abolishes the temperature response to NT. Mice ( $n = 4$ ) were injected at time 0 via the tail vein with the control and 46.1 fusions or free neurotensin, and the temperature recorded with an intraperitoneally-implanted probe as described in the Materials and Methods Section. Mixed ANOVA was used to model the data (mean  $\pm$  s.e.m.),  $F_{\text{Treatment}(2, 9)} = 1.01$ ,  $p = 0.401$ .

#### 3.4. Trans-Carotid Transport of ScFv 46.1 at the Cavernous Sinus Allows for Enhanced Accumulation of the Antibody-NT Construct in the Brain after Retro-Orbital Sinus Administration

The retro-orbital sinus has direct access to the cavernous sinus. Substances introduced into the retro-orbital sinus will follow the venous blood flow to the cavernous sinus and drain through the jugular veins into the systemic venous blood, eventually reaching the heart through the superior caval vein. Likewise, substances injected into the tail vein will flow in the venous blood into the heart through the inferior caval vein. After a round of circulation through the lungs, substances, originally administered via both iv routes, will flow with the arterial blood through the carotid arteries into the brain. Unless there is a differential loss or dilution of injected material as it travels from the lateral tail vein to the heart, both intravenous routes should deliver material into the brain circulation at a comparable concentration. While not excluding the potential loss of 46.1-scFv-Fc-LL-NT after tail vein injection, we examined whether the 46.1 scFv could mediate a direct alternative uptake pathway into the brain circulation after introduction into the retro-orbital/cavernous sinuses that could possibly explain the differences observed in the body temperature responses to 46.1-scFv-Fc-LL-NT administration. In a bit more detail, before branching to enter the brain, the internal carotid arteries (left and right) span the cavernous sinus, where the outer arterial wall bathes in venous blood flowing from the retro-orbital sinus (Figure 4A). If a substance in the venous blood of the cavernous sinus can penetrate the wall of the internal carotid artery, it would directly enter the arterial flow and the brain. Figure 4A shows the experimental scheme designed to decouple antibody entry into the brain after return to the heart from a direct trans-arterial entry mechanism.

Under deep anesthesia, mice were prepared for whole body perfusion. Ctrl-Fc-LL-NT (20 mg/kg) or 46.1-scFv-Fc-LL-NT (20 mg/kg) was injected into the retro-orbital sinus, and heart perfusion through the left ventricle began immediately after injection to assure unidirectional flow of fluid from the heart to brain, and the incision in the right atrium was made to prevent the antibody from the injection site from entering the heart. In this way, only local transport of retro-orbitally injected antibody from the venous into the arterial blood can act as an entry point to the brain circulation. To keep the tissue metabolically active, artificial cerebrospinal fluid at 37 °C was used as a perfusion buffer over the 15 min perfusion timeframe. The whole skull was processed for immunohistochemistry according to a standard procedure of bone decalcification that preserves the brain and underlying structures of the head during sectioning (Figure 4B). In the cavernous sinus at the site of the injection (ipsilateral), multiple structures were positive for 46.1-scFv-Fc-LL-NT (Figure 4B(i), yellow arrow—N. trigeminus). The outer wall of the internal carotid artery (Figure 4B(i), white arrow) showed very strong immunoreactivity for 46.1-scFv-Fc-LL-NT. In contrast, the corresponding structures on the contralateral side (Figures 4B(iv) and A1A) were negative for 46.1-scFv-Fc-LL-NT. Despite being cut off from any transport mediated by the arterial blood supply from the heart, 46.1-scFv-Fc-LL-NT reached and accumulated in brain capillar-

ies in the ipsilateral hemisphere (Figure 4B(ii), thalamus and Figure A1B(ii), hypothalamus) but not in the contralateral hemisphere (Figure 4B(v)) other than the region, directly adjacent to the third ventricle (Figure A1B(iv)). The internal carotid artery also provides arterial blood supply for the hypophyseal gland and the median eminence (ME). We observed the accumulation of 46.1-scFv-Fc-LL-NT in both of these structures (Figure A1A), albeit only in the surrounding vessels of the hypophyseal gland. The antibody was confined within the floor of the median eminence, and multiple cell bodies and projections throughout the median eminence were also positive (Figure A1B(i)). 46.1-scFv-Fc-LL-NT also showed a very strong immunoreactivity for a subset of cells on the border of ME and the arcuate nucleus, which based on their location, were presumed to be tanycytes. Additionally, non-vascular cells in the hypothalamus, in the ipsilateral, and the contralateral hemisphere, respectively, were positive for 46.1-scFv-Fc-LL-NT (Figure A1B(iii,iv)). In comparison, Ctrl-Fc-LL-NT was not detected in the ipsilateral or contralateral cavernous sinus or in the brain (Figures 4B(iii,vi) and A1C). Taken together, the data provide evidence for a first pass effect on the accumulation of 46.1-scFv-Fc-LL-NT in the CNS. After initial administration in the retro-orbital sinus, the 46.1-scFv-Fc-LL-NT is transported from the venous into the arterial blood in the cavernous sinus. Diluted in the perfusate, 46.1-scFv-Fc-LL-NT followed the natural arterial blood flow to the ME, brain capillaries, and because of its BBB-penetrating capacity, the parenchymal brain cells.

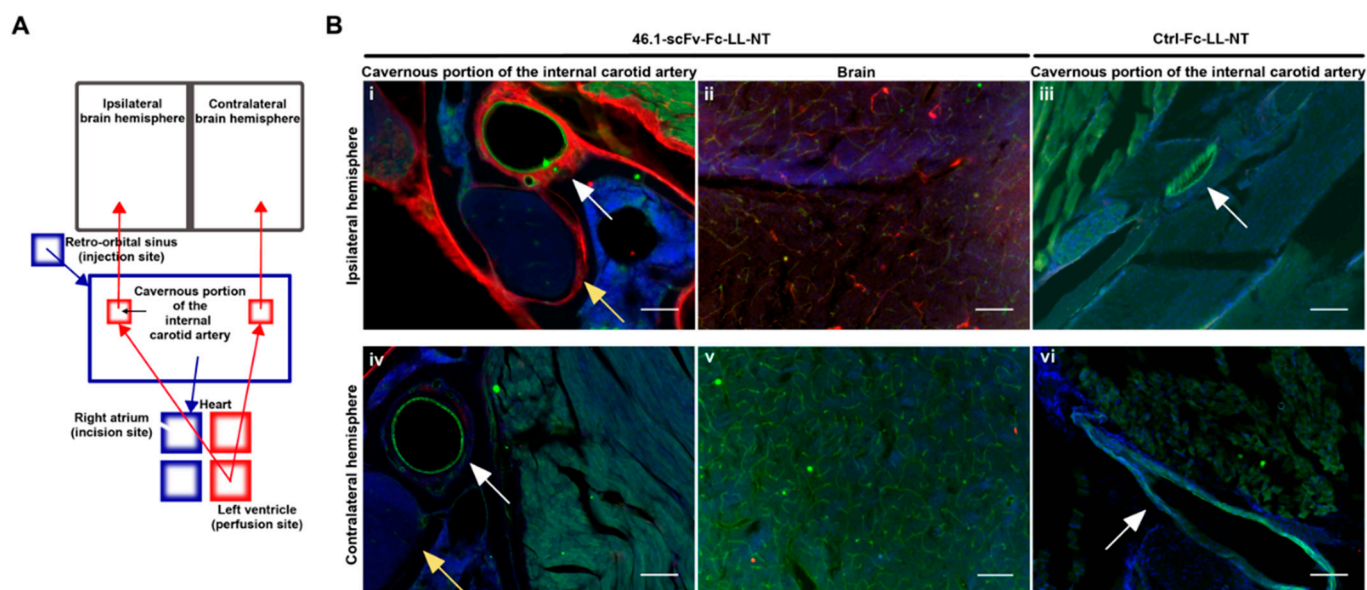


**Figure 4.** 46.1-scFv-Fc-LL-NT accumulates in the cavernous sinus and brain after retro-orbital injection. (A) Compartmental scheme of the surgery procedure and fluid flows. Blue arrows represent the venous blood flow, red arrows the arterial flow, the black arrow represents the putative reverse transcytosis. Mice were injected with 46.1-scFv-Fc-LL-NT or Ctrl-Fc-LL-NT (20 mg/kg) in the retro-orbital sinus and immediately whole body perfused as an incision was made in the right atrium to disconnect the lung circulation. (B) Coronal sections of the skull at the level of the cavernous sinus were labeled for the fusion proteins with fluorescent anti-rabbit Fc AlexaFluor555 antibody (red), internal carotid artery endothelial cells (green, white arrows), and blood vessels in brain were visualized with CD31 and secondary AlexaFluor488-conjugated antibody (green). N. trigeminus (yellow arrows), nuclei (blue). Scale bar, 100  $\mu$ m.

Concentration gradients between venous blood in the cavernous sinus and arterial blood in the internal carotid artery have been hypothesized to be a driving force of transport for small molecules from venous to arterial blood [39]. However, 46.1-scFv-Fc-LL-NT is a macromolecule with an approx. size of 103 kDa and gradient triggered diffusion across the endothelial wall of the carotid artery is unlikely to occur for molecules of this size.

From the outer to inner, the layers of the internal carotid artery are strongly positive for 46.1-scFv-Fc-LL-NT (Figure 4B(i)), suggesting that the innermost layer of endothelial cells is the limiting transport barrier. In a previous work [9], we demonstrated the apical to basolateral receptor-mediated transcytosis of the scFv clone 46.1 across the brain endothelial cells *in vivo*. Here, the reverse process would be required to move 46.1-scFv-Fc-LL-NT from the basolateral side of the carotid endothelial cells to the apical side in order to enter the brain circulation. Thus, using the iPSC BMEC-like cell the *in vitro* Transwell system, we tested whether the 46.1-scFv-Fc-LL-NT could undergo such “reverse” transcytosis. After pulsing the 46.1-scFv-Fc-LL-NT into the basolateral compartment, it could be found bound, internalized, and trafficked to the apical side, indicating that the transport process triggered by 46.1 scFv is reversible (Figure A2). In summary, it is possible that 46.1 scFv co-opts a reverse transcytosis mechanism for rapid first pass transport from the cavernous sinus to the brain arterial blood supply.

#### 4. Discussion and Conclusions

The results presented in this study are consistent with the following conclusions. First, scFv 46.1 can accumulate in the postvascular brain after intravenous administration. In particular, scFv 46.1 mediates the accumulation of NT into the MnPO and into the striatum in the form of 46.1-scFv-Fc-LL-NT fusion. Next, the route of intravenous administration affected the accumulation of 46.1-scFv-Fc-LL-NT, with the retro-orbital route leading to transient hypothermia, while 46.1-scFv-Fc-LL-NT administered via the tail vein route showed no effect. Further examination of the retro-orbital route of delivery supports a mechanism for first pass cavernous sinus to the carotid artery transport of 46.1-scFv-Fc-LL-NT, which can lead to widespread vascular distribution of fusion throughout the brain, and could be at least partially responsible for the differential effects of the administration route observed with transient hypothermia experiments.

While we have previously demonstrated the capability of the scFv 46.1 to cross the BBB and enter the brain [9], the decrease in the core body temperature evoked by 46.1-scFv-Fc-LL-NT further demonstrates that scFv 46.1 is also capable of transporting the model drug cargo, NT, across the BBB. This effect was very clear upon retro-orbital injection of the fusion protein, but we did not observe a temperature reduction when 46.1-scFv-Fc-LL-NT was administered at the same 20 mg/kg dose via the tail vein. Clearly, the bioavailability of 46.1-scFv-Fc-LL-NT in the brain capillaries of MnPO is dependent on the route of intravenous administration. While we demonstrated the local transport of the antibody from the venous and cavernous sinus to the carotid artery as one potential factor for these differences, it is also possible that loss or dilution of the antibody while it transits in venous blood from the tail vein to the heart impacts its potency once it reaches the brain circulation. Studies with contrast agents can be used to compare both routes of delivery: injected contrast media in the retro-orbital sinus flows through the superficial temporal vein, the inferior palpebral vein, and the ocular angle vein to the external jugular vein, which drains into the subclavian vein that forms the left and right superior caval veins, respectively. Injected contrast media in the lateral tail vein flows into the middle caudal vein, which merges with the left and right external iliac veins to form the inferior caval vein. Content from the superior caval veins and the inferior caval vein flows into the right atrium of the heart [40]. Thus, both administration routes merge anatomically in the right atrium of the heart for the first pass through the lungs. As scFv 46.1 also binds to the lung endothelium [9], the concentration of antibodies in the arterial blood flushing the brain may be reduced, but should be reduced to the same extent independent of the administration route. Hence, the determining factor is likely to be the concentration of antibodies reaching the right atrium, which could be a function of blood volumes, dilution differences, or antibody loss from venous blood traveling to the heart from the tail vein versus that coming from the cavernous sinus. While beyond the scope of the current study, a dose escalation study with tail vein injection could help inform as to whether the lack of response was due to antibody-NT fusion concentration differences.



While 46.1-scFv-Fc-LL-NT did not elicit transient hypothermia after tail vein administration at 20 mg/kg, it did have an effect on PCP-induced hyperactivity. The positive control small molecule, PD149163, is brain-permeable with a  $K_i = 159$  nM (vs. 3H-NT) for NTSR1 [41] and produced almost complete immobility in the PCP-treated mice. In contrast, 46.1-scFv-Fc-LL-NT had a more modest, but statistically distinguishable effect. While tail vein administered 46.1-scFv-Fc-LL-NT decreased PCP-induced hyperactivity in the striatum, it had no effect on transient hypothermia in the MnPO. Given the differences in these anatomically distinct brain regions and the differences in the physiologic responses, it is perhaps not unreasonable to expect differential effects. For example, a recent study suggested that the activation of the high affinity NTSR1 ( $K_d = 0.5$  nM) on neurons is modulated by the activation of low affinity NTSR2 ( $K_d = 3\text{--}5$  nM) on astrocytes in the median preoptic nucleus (MnPO) [19], whereas the activation of NTSR1 on neurons in the striatum is involved in the depression of PCP-induced hyperactivity. Thus, a higher concentration of NT in the MnPO would be necessary to reduce the core body temperature than in the striatum to activate NTSR1 and downstream control of locomotion, as indeed previously demonstrated [42].

Given the differences in transient hypothermia outcomes based on the route of administration and since previous studies have reported differences in the observed transduction efficiency of brain cells with the rAAV9 vector, possibly due to alternative intravenous routes of delivery [21,22], we decided to explore the potential that the 46.1 scFv could be transported in a unique way. We therefore blocked the heart circulation of retro-orbitally administered test- and control antibodies and replaced the arterial blood flow and brain circulation with a perfusion solution. With this approach, we questioned the plausibility that antibody fusions could directly access the brain circulation. Indeed, 46.1-scFv-Fc-LL-NT was readily detectable in the brain microvasculature and post-vascular brain cells. The distribution of 46.1-scFv-Fc-LL-NT in the skull and brain followed the arterial blood flow, and was largely found in the ipsilateral hemisphere consistent with a successful elimination of heart circulation of the injected antibody fusions. While such counter current transfer from the cavernous sinus to the arterial blood flow has been described for small molecules [43–45], likely due to purely diffusive phenomena, this would be inefficient for large protein fusions (e.g., no Ctrl-Fc-LL-NT was detected in any brain region or in the underlying cavernous sinus using this approach). Thus, after the fusion protein diffuses through the supportive layers of the internal carotid artery, we believe that the fusion protein enters the arterial blood supply through an active transport process whereby the 46.1 scFv engages its cognate RMT receptor at the carotid artery endothelial cell and transcytoses from the cavernous sinus into the arterial blood supply. Of note, in our previous study, we measured the  $K_d = \sim 150$  nM of 46.1-scFv-Fc fusion and its brain concentration was  $\sim 8$  nM at 1 h post retro-orbital administration (same dosage as in Figure 1). Thus, while the high concentration of antibodies in the cavernous sinus after injection favors basolateral to apical transcytosis, the concentration in the brain parenchyma is likely to be insufficient to drive significant basolateral to apical elimination of 46.1-scFv-Fc-LL-NT after brain uptake.

Once in the brain circulation, we found the 46.1-scFv-Fc-LL-NT associated with the microvasculature throughout the ipsilateral cortex. This included immunoreactivity within and outside of vessels in the hypothalamus, with postvascular cells staining positive, potentially explaining how the transient hypothermia effects are elicited within the MnPO portion of the hypothalamus. An additional interesting localization of the 46.1-scFv-Fc-LL-NT was identified in the median eminence, which is a circumventricular organ that is perfused by capillaries lacking BBB properties. Here, we observed accumulation of the fusion protein within the median eminence with high immunoreactivity at the putative tanycytes that surround the median eminence. While plausible, paracellular diffusion of 46.1-scFv-Fc-LL-NT from the median eminence as a gateway to the brain parenchyma and NTSR-neurons in the MnPO and the striatum is unlikely given that the diffusion of antibodies within the extracellular brain space is spatially limited [46].

In humans, the cavernous sinus is readily accessible via the transvenous route for routine therapeutic and diagnostic interventions [47,48]. While it would be a surgical intervention, one-time catheterization of the cavernous sinus would allow for multiple, consequent dosing, and essentially provides a new intravenous administration route compared to other invasive techniques [49]. As an alternative to the retro-orbital sinus in mice, the supratrochlear (frontal) vein of the face through the nasofrontal and superior ophthalmic vein additionally gives intravenous access to the cavernous sinus in human neonates/infants [50] and adults [51]. To our knowledge, the administration of therapeutics into the cavernous sinus has not been described thus far. However, an AAV vector with a similar administration route-dependent CNS exposure [21] is already in clinical use [52], and warrants the continued discussion of how the administration route could impact the CNS delivery, particularly with a targeting motif like scFv 46.1.

**Author Contributions:** Conceptualization, J.V.G., C.J.W. and E.V.S.; Data curation, J.V.G.; Formal analysis, J.V.G., C.J.W. and E.V.S.; Funding acquisition, E.V.S.; Investigation, J.V.G., M.K. and Z.Y.; Methodology, B.J.U.; Writing—original draft, J.V.G.; Writing—review & editing, J.V.G., C.J.W. and E.V.S. All authors have read and agreed to the published version of the manuscript.

**Funding:** This work was supported in part by the National Institutes of Health grants (NS071513 and NS118028) and a Defense Threat Reduction Agency grant (HDTRA1-15-1-0012).

**Institutional Review Board Statement:** The animal study protocol was approved by the Institutional Animal Care and Use Committee at the University of Wisconsin-Madison (M005138 approved on 5/28/2021).

**Informed Consent Statement:** Not applicable.

**Data Availability Statement:** The data presented in this study are available in the figures and tables of the main text and Appendix A.

**Acknowledgments:** We thank the Research Animal Resources Center Comparative Pathology Laboratory of University of Wisconsin—Madison for the help with the localization of the hypophyseal gland in rodents and Benjamin D. Gastfriend for kindly providing the iPSC BMEC-like cells.

**Conflicts of Interest:** J.V.G. and E.V.S. are inventors on a United States Patent application.

## Appendix A

**Table A1.** The statistical parameters for the NT activity assay.

Comparison		Mean Difference	SE	df	t	P <sub>Holm</sub>
Treatment	Treatment					
46.1-scFv-Fc-LL-NT (20 mg/kg)	Ctrl-Fc-LL-NT (20 mg/kg)	2.8	1.22	19.0	2.3	0.066
	Neurotensin (1 mg/kg)	3.95	1.16	19.0	3.41	0.009
Ctrl-Fc-LL-NT (20 mg/kg)	Neurotensin (1 mg/kg)	1.14	1.11	19.0	1.03	0.314

**Table A2.** The statistical parameters for the mixed ANOVA analysis of transient hypothermia.

Comparison		Mean Difference	SE	df	t	P <sub>Holm</sub>
Treatment	Treatment					
46.1-scFv-Fc-LL-NT (20 mg/kg)	Ctrl-Fc-LL-NT (20 mg/kg)	−1.888	0.323	8.0	−5.84	0.001
	Neurotensin (1 mg/kg)	−1.281	0.349	8.0	−3.67	0.013
Ctrl-Fc-LL-NT (20 mg/kg)	Neurotensin (1 mg/kg)	−55.22	0.349	8.0	1.74	0.12

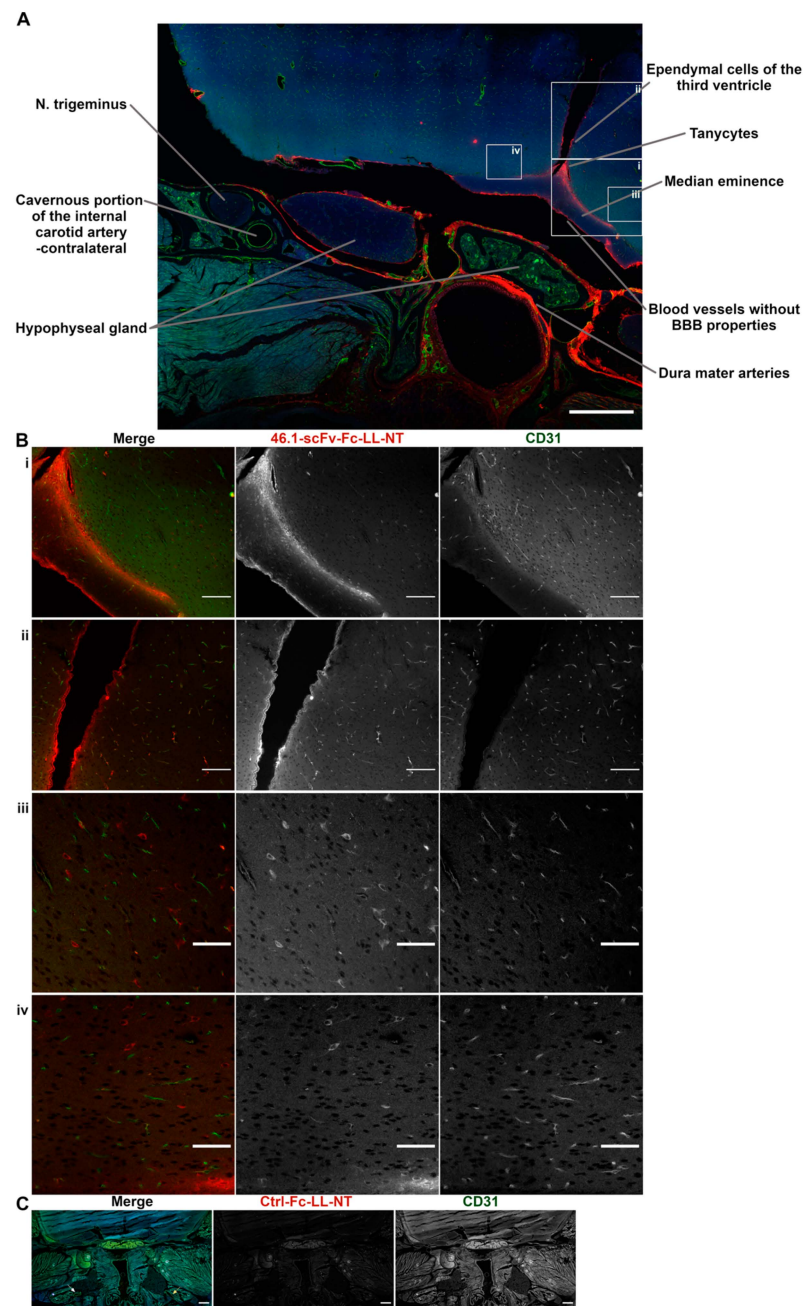


**Figure A1.** Detailed localization of 46.1-scFv-Fc-LL-NT in the cavernous sinus and brain. (A) Overview at low magnification of the distribution of 46.1-scFv-Fc-LL-NT (red) and CD31 (green) in the head and brain, as described in Figure 4. Scale bar, 500  $\mu$ m. (B) Boxed areas from (A) (i) 46.1-scFv-Fc-LL-NT (red) is localized at the floor of the median eminence, tanycytes, cell bodies, and emanating projections of ME parenchymal cells. Scale bar, 100  $\mu$ m. (ii) Hypothalamic microvasculature and ependymal cells of the third ventricle show immunoreactivity for 46.1-scFv-Fc-LL-NT. Scale bar, 100  $\mu$ m. (iii,iv) Ipsilateral and contralateral hypothalamic non-vascular cells are labeled for 46.1-scFv-Fc-LL-NT. Scale bar, 50  $\mu$ m. (C) Control antibody (red) is not detected in the head and brain. White and yellow arrows represent the cavernous portion of the internal carotid artery, contralateral, and ipsilateral, respectively. Scale bar, 500  $\mu$ m.

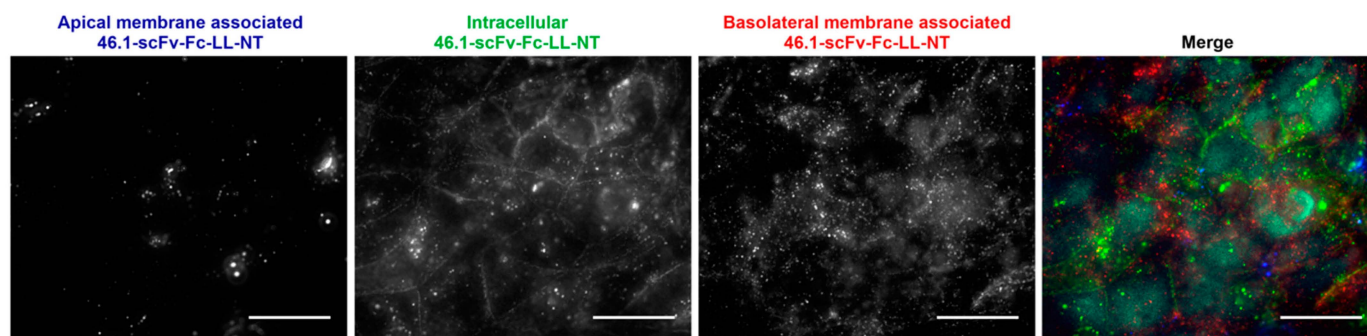


**Figure A2.** Basolateral to apical transport of 46.1-scFv-Fc-LL-NT. Confluent, barrier forming, iPSC BMEC-like cells on Transwell filters were incubated for 45 min at 37 °C with 5 µg/mL antibody 46.1-scFv-Fc-LL-NT, added to the basolateral compartment. Live cells were post-labeled on ice with secondary anti-rabbit AlexaFluor647 (blue) in the apical compartment, and AlexaFluor555 (red) in the basolateral compartment. Both compartments were washed, BMEC-like cells fixed, permeabilized, and incubated with secondary anti-rabbit AlexaFluor488 (green) to visualize the internalized antibody. All three secondary antibodies had distinctive appearances that were not spatially overlapping, indicating the lack of the paracellular diffusion of 46.1-scFv-Fc-LL-NT or any of the secondary antibodies. Of note, the intracellular fraction of 46.1-scFv-Fc-LL-NT was found at the cell–cell contacts as we have previously documented for apical to basolateral transport [9]. Scale bar, 20 µm.

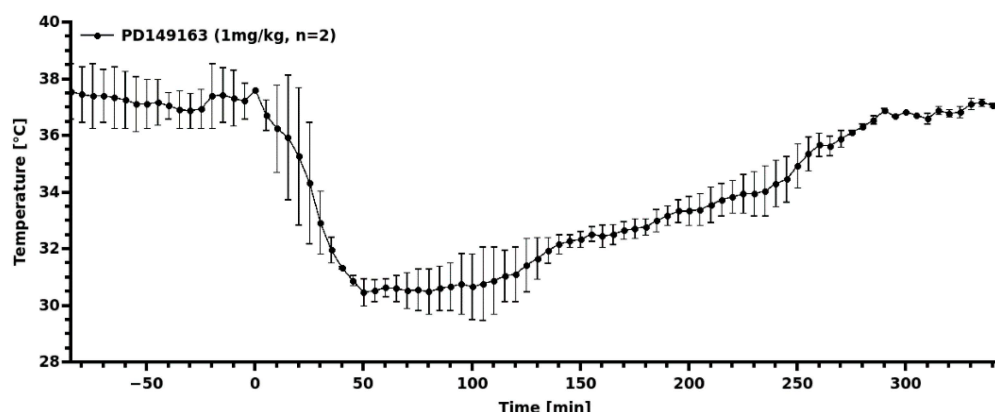


**Figure A3.** Development of hypothermia after tail vein administration of PD149163. Mice (n = 2) were injected at time 0 via the tail vein with 1 mg/kg PD149163, and the temperature recorded with an intraperitoneally-implanted probe as described in the Materials and Methods Section.

## References

1. Pardridge, W.M. Alzheimer's disease drug development and the problem of the blood-brain barrier. *Alzheimer's Dement.* **2009**, *5*, 427–432. [CrossRef] [PubMed]
2. Couch, J.A.; Yu, Y.J.; Zhang, Y.; Tarrant, J.M.; Fuji, R.N.; Meilandt, W.J.; Solanoy, H.; Tong, R.K.; Hoyte, K.; Luk, W.; et al. Addressing safety liabilities of TfR bispecific antibodies that cross the blood-brain barrier. *Sci. Transl. Med.* **2013**, *5*, 183ra57. [CrossRef] [PubMed]
3. Jones, A.R.; Shusta, E.V. Blood-brain barrier transport of therapeutics via receptor-mediation. *Pharm. Res.* **2007**, *24*, 1759–1771. [CrossRef] [PubMed]
4. Pardridge, W.M.; Kang, Y.S.; Buciak, J.L. Transport of human recombinant brain-derived neurotrophic factor ((BDNF)) through the rat blood-brain barrier in vivo using vector-mediated peptide drug delivery. *Pharm. Res.* **1994**, *11*, 738–746. [CrossRef]
5. Pardridge, W.M.; Kang, Y.S.; Buciak, J.L.; Yang, J. Human insulin receptor monoclonal antibody undergoes high affinity binding to human brain capillaries in vitro and rapid transcytosis through the blood-brain barrier in vivo in the primate. *Pharm. Res.* **1995**, *12*, 807–816. [CrossRef]
6. Ullman, J.C.; Arguello, A.; Getz, J.A.; Bhalla, A.; Mahon, C.S.; Wang, J.; Giese, T.; Bedard, C.; Kim, D.J.; Blumenfeld, J.R.; et al. Brain delivery and activity of a lysosomal enzyme using a blood-brain barrier transport vehicle in mice. *Sci. Transl. Med.* **2020**, *12*, eaay1163. [CrossRef]

7. Kariolis, M.S.; Wells, R.C.; Getz, J.A.; Kwan, W.; Mahon, C.S.; Tong, R.; Kim, D.J.; Srivastava, A.; Bedard, C.; Henne, K.R.; et al. Brain delivery of therapeutic proteins using an Fc fragment blood-brain barrier transport vehicle in mice and monkeys. *Sci. Transl. Med.* **2020**, *12*, eaay1359. [CrossRef]
8. Stocki, P.; Szary, J.; Rasmussen, C.L.M.; Demydchuk, M.; Northall, L.; Logan, D.B.; Gauhar, A.; Thei, L.; Moos, T.; Walsh, F.S.; et al. Blood-brain barrier transport using a high affinity, brain-selective VNAR antibody targeting transferrin receptor 1. *FASEB J.* **2021**, *35*, e21172. [CrossRef]
9. Georgieva, J.V.; Goulatis, L.I.; Stutz, C.C.; Canfield, S.G.; Song, H.W.; Gastfriend, B.D.; Shusta, E.V. Antibody screening using a human iPSC-based blood-brain barrier model identifies antibodies that accumulate in the CNS. *FASEB J.* **2020**, *34*, 12549–12564. [CrossRef]
10. Wouters, Y.; Jaspers, T.; De Strooper, B.; Dewilde, M. Identification and in vivo characterization of a brain-penetrating nanobody. *Fluids Barriers CNS* **2020**, *17*, 62. [CrossRef]
11. Demeule, M.; Beaudet, N.; Régina, A.; Besserer-Offroy, É.; Murza, A.; Tétreault, P.; Belleville, K.; Ché, C.; Larocque, A.; Thiot, C.; et al. Conjugation of a brain-penetrant peptide with neurotensin provides antinociceptive properties. *J. Clin. Investig.* **2014**, *124*, 1199–1213. [CrossRef] [PubMed]
12. Ratner, C.; He, Z.; Grunddal, K.V.; Skov, L.J.; Hartmann, B.; Zhang, F.; Feuchtinger, A.; Bjerregaard, A.; Christoffersen, C.; Tschöp, M.H.; et al. Long-acting neurotensin synergizes with liraglutide to reverse obesity through a melanocortin-dependent pathway. *Diabetes* **2019**, *68*, 1329–1340. [CrossRef] [PubMed]
13. Feng, Y.-P.; Wang, J.; Dong, Y.-L.; Wang, Y.-Y.; Li, Y.-Q. The Roles of Neurotensin and its Analogues in Pain. *Curr. Pharm. Des.* **2014**, *21*, 840–848. [CrossRef]
14. Liang, Y.; Boules, M.; Shaw, A.M.; Williams, K.; Fredrickson, P.; Richelson, E. Effect of a novel neurotensin analog, NT69L, on nicotine-induced alterations in monoamine levels in rat brain. *Brain Res.* **2008**, *1231*, 6–15. [CrossRef] [PubMed]
15. Boules, M.; Netz, R.; Fredrickson, P.A.; Richelson, E. A neurotensin analog blocks cocaine-conditioned place preference and reinstatement. *Behav. Pharmacol.* **2016**, *27*, 236–239. [CrossRef]
16. Sharpe, A.L.; Varela, E.; Beckstead, M.J. Systemic PD149163, a neurotensin receptor 1 agonist, decreases methamphetamine self-administration in DBA/2J mice without causing excessive sedation. *PLoS ONE* **2017**, *12*, e0180710. [CrossRef]
17. Binder, E.B.; Kinkead, B.; Owens, M.J.; Nemeroff, C.B. Neurotensin and dopamine interactions. *Pharmacol. Rev.* **2001**, *53*, 453–486.
18. Cáceda, R.; Kinkead, B.; Nemeroff, C.B. Neurotensin: Role in psychiatric and neurological diseases. *Peptides* **2006**, *27*, 2385–2404. [CrossRef]
19. Tabarean, I.V. Neurotensin induces hypothermia by activating both neuronal neurotensin receptor 1 and astrocytic neurotensin receptor 2 in the median preoptic nucleus. *Neuropharmacology* **2020**, *171*, 108069. [CrossRef]
20. Schoch, A.; Thorey, I.S.; Engert, J.; Winter, G.; Emrich, T. Comparison of the lateral tail vein and the retro-orbital venous sinus routes of antibody administration in pharmacokinetic studies. *Lab. Anim.* **2014**, *43*, 95–99. [CrossRef]
21. Foust, K.D.; Nurre, E.; Montgomery, C.L.; Hernandez, A.; Chan, C.M.; Kaspar, B.K. Intravascular AAV9 preferentially targets neonatal neurons and adult astrocytes. *Nat. Biotechnol.* **2009**, *27*, 59–65. [CrossRef] [PubMed]
22. Gruntman, A.M.; Su, L.; Flotte, T.R. Retro-Orbital Venous Sinus Delivery of rAAV9 Mediates High-Level Transduction of Brain and Retina Compared with Temporal Vein Delivery in Neonatal Mouse Pups. *Hum. Gene Ther.* **2017**, *28*, 228–230. [CrossRef] [PubMed]
23. Liguore, W.A.; Domire, J.S.; Button, D.; Wang, Y.; Dufour, B.D.; Srinivasan, S.; McBride, J.L. AAV-PHPB Administration Results in a Differential Pattern of CNS Biodistribution in Non-human Primates Compared with Mice. *Mol. Ther.* **2019**, *27*, 2018–2037. [CrossRef] [PubMed]
24. Harris, F.S.; Rhoton, A.L. Anatomy of the cavernous sinus. A microsurgical study. *J. Neurosurg.* **1976**, *45*, 169–180. [CrossRef]
25. Yang, W.J.; Wong, K.S.; Chen, X.Y. Intracranial atherosclerosis: From microscopy to high-resolution magnetic resonance imaging. *J. Stroke* **2017**, *19*, 249–262. [CrossRef]
26. Masuoka, T.; Hayashi, N.; Hori, E.; Kuwayama, N.; Ohtani, O.; Endo, S. Distribution of internal elastic lamina and external elastic lamina in the internal carotid artery: Possible relationship with atherosclerosis. *Neurol. Med. Chir.* **2010**, *50*, 179–182. [CrossRef]
27. Lippmann, E.S.; Azarin, S.M.; Kay, J.E.; Nessler, R.A.; Wilson, H.K.; Al-Ahmad, A.; Palecek, S.P.; Shusta, E. V Derivation of blood-brain barrier endothelial cells from human pluripotent stem cells. *Nat. Biotechnol.* **2012**, *30*, 783–791. [CrossRef]
28. Lippmann, E.S.; Al-Ahmad, A.; Azarin, S.M.; Palecek, S.P.; Shusta, E.V. A retinoic acid-enhanced, multicellular human blood-brain barrier model derived from stem cell sources. *Sci. Rep.* **2014**, *4*, 4160. [CrossRef]
29. Westfall, P.H.; Johnson, W.O.; Utts, J.M. A bayesian perspective on the bonferroni adjustment. *Biometrika* **1997**, *84*, 419–427. [CrossRef]
30. Bissette, G.; Nemeroff, C.B.; Loosen, P.T.; Prange, A.J.; Lipton, M.A. Hypothermia and intolerance to cold induced by intracisternal administration of the hypothalamic peptide neurotensin. *Nature* **1976**, *262*, 607–609. [CrossRef]
31. Han, B.W.; Herrin, B.R.; Cooper, M.D.; Wilson, I.A. Antigen recognition by variable lymphocyte receptors. *Science* **2008**, *321*, 1834–1837. [CrossRef] [PubMed]
32. Li, Z.; Boules, M.; Williams, K.; Peris, J.; Richelson, E. The novel neurotensin analog NT69L blocks phencyclidine (PCP)-induced increases in locomotor activity and PCP-induced increases in monoamine and amino acids levels in the medial prefrontal cortex. *Brain Res.* **2010**, *1311*, 28–36. [CrossRef] [PubMed]

33. Chou, S.; Davis, C.; Jones, S.; Li, M. Repeated effects of the neurotensin receptor agonist PD149163 in three animal tests of antipsychotic activity: Assessing for tolerance and cross-tolerance to clozapine. *Pharmacol. Biochem. Behav.* **2014**, *128*, 78–88. [CrossRef]
34. Ervin, G.N.; Birkemo, L.S.; Nemeroff, C.B.; Prange, A.J. Neurotensin blocks certain amphetamine-induced behaviours. *Nature* **1981**, *291*, 73–76. [CrossRef] [PubMed]
35. Kalivas, P.W.; Nemeroff, C.B.; Prange, A.J. Neurotensin microinjection into the nucleus accumbens antagonizes dopamine-induced increase in locomotion and rearing. *Neuroscience* **1984**, *11*, 919–930. [CrossRef]
36. Sarhan, S.; Hitchcock, J.M.; Grauffel, C.A.; Wettstein, J.G. Comparative antipsychotic profiles of neurotensin and a related systemically active peptide agonist. *Peptides* **1997**, *18*, 1223–1227. [CrossRef]
37. Hackler, E.A.; Byun, N.E.; Jones, C.K.; Williams, J.M.; Baheza, R.; Sengupta, S.; Grier, M.D.; Avison, M.; Conn, P.J.; Gore, J.C. Selective potentiation of the metabotropic glutamate receptor subtype 2 blocks phencyclidine-induced hyperlocomotion and brain activation. *Neuroscience* **2010**, *168*, 209–218. [CrossRef]
38. Lee, M.D.; Wagenmakers, E.J. *Bayesian Cognitive Modeling: A Practical Course*; Cambridge University Press: Cambridge, UK, 2014; ISBN 9781139087759.
39. Krzymowski, T.; Stefanczyk-Krzymowska, S. New facts and the concept of physiological regulation of the dopaminergic system function and its disorders. *J. Physiol. Pharmacol.* **2015**, *66*, 331–341.
40. Socher, M.; Kuntz, J.; Sawall, S.; Bartling, S.; Kachelrieß, M. The retrobulbar sinus is superior to the lateral tail vein for the injection of contrast media in small animal cardiac imaging. *Lab. Anim.* **2014**, *48*, 105–113. [CrossRef]
41. Petrie, K.A.; Bubser, M.; Casey, C.D.; Davis, M.D.; Roth, B.L.; Deutch, A.Y. The neurotensin agonist PD149163 increases fos expression in the prefrontal cortex of the rat. *Neuropsychopharmacology* **2004**, *29*, 1878–1888. [CrossRef]
42. Gene Erwin, V.; Jones, B.C. Comparison of neurotensin levels, receptors and actions in LS/lbg and SS/lbg mice. *Peptides* **1989**, *10*, 435–440. [CrossRef]
43. Einer-Jensen, N.; Larsen, L. Transfer of tritiated water, tyrosine, and propanol from the nasal cavity to cranial arterial blood in rats. *Exp. Brain Res.* **2000**, *130*, 216–220. [CrossRef] [PubMed]
44. Einer-Jensen, N.; Larsen, L. Local transfer of diazepam, but not of cocaine, from the nasal cavities to the brain arterial blood in rats. *Pharmacol. Toxicol.* **2000**, *87*, 276–278. [CrossRef]
45. Muszak, J.; Krzymowski, T.; Gilun, P.; Stefanczyk-Krzymowska, S. Countercurrent transfer of dopamine from venous blood in the cavernous sinus to the arterial blood supplying the brain—The perfused rabbit head as an experimental model. *J. Physiol. Pharmacol.* **2014**, *65*, 641–648.
46. Wolak, D.J.; Pizzo, M.E.; Thorne, R.G. Probing the extracellular diffusion of antibodies in brain using in vivo integrative optical imaging and ex vivo fluorescence imaging. *J. Control. Release* **2015**, *197*, 78–86. [CrossRef] [PubMed]
47. Dye, J.; Duckwiler, G.; Gonzalez, N.; Kaneko, N.; Goldberg, R.; Rootman, D.; Jahan, R.; Tateshima, S.; Szeder, V. Endovascular approaches to the cavernous sinus in the setting of dural arteriovenous fistula. *Brain Sci.* **2020**, *10*, 554. [CrossRef]
48. Teramoto, A.; Nemoto, S.; Takakura, K.; Sasaki, Y.; Machida, T. Selective venous sampling directly from cavernous sinus in cushing's syndrome. *J. Clin. Endocrinol. Metab.* **1993**, *76*, 637–641. [CrossRef]
49. Wahl, A.S.; Correa, D.; Imobersteg, S.; Maurer, M.A.; Kaiser, J.; Augath, M.A.; Schwab, M.E. Targeting Therapeutic Antibodies to the CNS: A Comparative Study of Intrathecal, Intravenous, and Subcutaneous Anti-Nogo A Antibody Treatment after Stroke in Rats. *Neurotherapeutics* **2020**, *17*, 1153–1159. [CrossRef]
50. Doyle, T.D.; Anand, S.; Edens, M.A. *Scalp Catheterization*; StatPearls Publishing: Treasure Island, FL, USA, 2021.
51. Takaku, A.; Suzuki, J. A new method of orbital and cavernous sinus venography. Technical note. *J. Neurosurg.* **1969**, *30*, 200–205. [CrossRef]
52. Hoy, S.M. Onasemnogene A bepavovec: First Global Approval. *Drugs* **2019**, *79*, 1255–1262. [CrossRef]



Review

# Peptide Shuttles for Blood–Brain Barrier Drug Delivery

Macarena Sánchez-Navarro <sup>1,\*</sup> and Ernest Giralt <sup>2,3,\*</sup>

<sup>1</sup> Department of Molecular Biology, Instituto de Parasitología y Biomedicina “López Neyra” (CSIC), 18016 Granada, Spain

<sup>2</sup> Institute for Research in Biomedicine (IRB Barcelona), Barcelona Institute of Science and Technology (BIST), Baldiri Reixac 10, 08028 Barcelona, Spain

<sup>3</sup> Department of Inorganic and Organic Chemistry, University of Barcelona, Martí i Franquès 1-11, 08028 Barcelona, Spain

\* Correspondence: macarena.sanchez@irbbarcelona.org (M.S.-N.); ernest.giralt@irbbarcelona.org (E.G.)

**Abstract:** The blood–brain barrier (BBB) limits the delivery of therapeutics to the brain but also represents the main gate for nutrient entrance. Targeting the natural transport mechanisms of the BBB offers an attractive route for brain drug delivery. Peptide shuttles are able to use these mechanisms to increase the transport of compounds that cannot cross the BBB unaided. As peptides are a group of biomolecules with unique physicochemical and structural properties, the field of peptide shuttles has substantially evolved in the last few years. In this review, we analyze the main classifications of BBB–peptide shuttles and the leading sources used to discover them.

**Keywords:** blood–brain barrier; BBB–peptide shuttle; brain delivery

**Citation:** Sánchez-Navarro, M.; Giralt, E. Peptide Shuttles for Blood–Brain Barrier Drug Delivery. *Pharmaceutics* **2022**, *14*, 1874. <https://doi.org/10.3390/pharmaceutics14091874>

Academic Editor: William M. Pardridge

Received: 20 July 2022

Accepted: 28 August 2022

Published: 5 September 2022

**Publisher’s Note:** MDPI stays neutral with regard to jurisdictional claims in published maps and institutional affiliations.



**Copyright:** © 2022 by the authors. Licensee MDPI, Basel, Switzerland. This article is an open access article distributed under the terms and conditions of the Creative Commons Attribution (CC BY) license (<https://creativecommons.org/licenses/by/4.0/>).

## 1. Introduction

Neurological-related disorders, such as glioblastoma, and other central nervous system (CNS) tumors, Parkinson’s disease (PD), migraine or stroke, to name a few, are a major cause of death and disability worldwide, being the second most common cause of death after cardiovascular diseases [1]. Despite the efforts to treat those diseases and to improve the quality of lives of patients and families, there are not yet any efficient treatments available. The main limitation in the development of such treatments is the presence of the blood–brain barrier (BBB) [2]. The BBB isolates and protects the brain from harmful blood-borne substances and is the main gate for nutrient entrance [3].

The early idea of a BBB shuttle was developed by Pardridge, who thought the natural transport mechanism of certain peptides and proteins could be explored to deliver pharmaceuticals to the brain [4]. Since then, several types of compounds able to hijack the natural transport mechanism at the BBB have been developed [5–8]. Monoclonal antibodies targeting the receptors and transporters present at the BBB have been established to deliver a wide variety of biotherapeutics [9–12]. For instance, a monoclonal antibody against the human insulin receptor conjugated to the enzyme  $\alpha$ -L-iduronidase is being evaluated in a clinical trial (NCT03053089 and NCT03071341) to treat mucopolysaccharidosis I [13]. However, antibodies display a very high affinity for their targets, which may hamper the dissociation from the receptor, leading to vesicle entrapment and inefficient transport across the BBB [10].

In 1999, Schwarce et al. proved that a cell-penetrating peptide, TAT, delivered an active enzyme to the brain parenchyma [14]. The delivery was not selective, but this result opened a field of investigation. Since then, more than 40 peptides have been described as able to cross the BBB carrying compounds that cannot transverse this membrane alone [8,15]. In this paper, we discuss the main families of BBB–peptide shuttle as well as the most explored sources to discover them.



## 2. The Blood–Brain Barrier

The presence of the BBB ensures brain homeostasis. This highly metabolic and physical barrier allows the passage of only a selected group of nutrients, such as sugars or amino acids, restricting the entrance of harmful substances. The natural transport mechanisms present at the BBB that tightly control the access of nutrients to the brain can be divided into passive and active according to their energy requirements (Figure 1). Passive transport mechanisms embrace transcellular passive diffusion and paracellular diffusion, while active transport mechanisms include receptor- and transporter-mediated transcytosis and adsorptive-mediated transcytosis. The main physiological characteristic of the BBB is that its constitutive endothelial cells are tightly bound by the presence of tight and adherens junction proteins that limit the paracellular transport of substances. In addition, this barrier has reduced vesicular transport, bearing high proteolytic activity and presenting efflux pumps at its abluminal side that force the exit of potentially toxic substances. However, the high vascularization of the brain offers a unique platform for the delivery of therapeutics [16]. Each neuron has a capillary of less than 20  $\mu\text{m}$  [17]. If a compound is able to undergo transcytosis after interacting with a receptor at the BBB, it would be homogeneously distributed along the brain. This unique feature has prompted the study of several types of ligands targeting receptors at the luminal side of the BBB. Antibodies against the transferrin (Tf), insulin, or low-density protein-1 (LRP1) receptors have been widely studied with varying degrees of success [13–18].

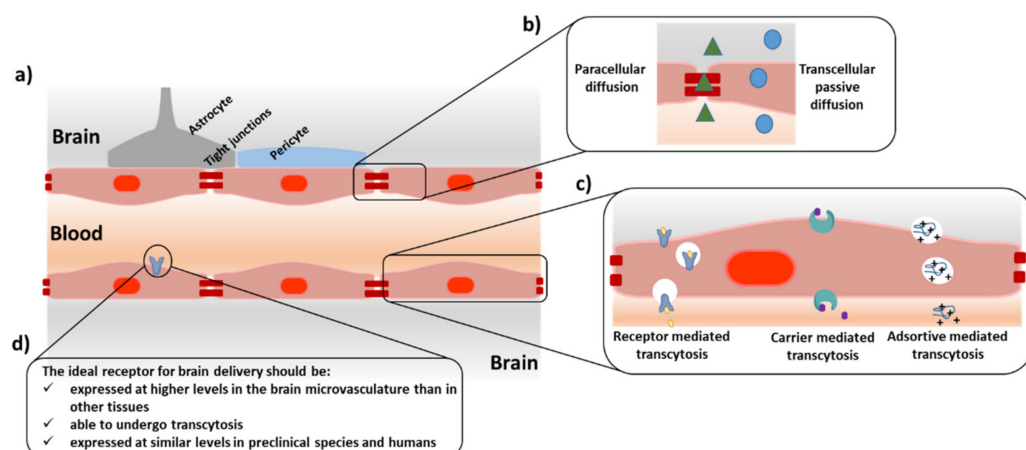


**Figure 1.** Schematic representation of the blood–brain barrier structure (BBB). (a) The blood–brain barrier comprises a monolayer of endothelial cells in intimate contact with astrocytes’ end-feet and pericytes. The endothelial cells are strongly bound by tight junction (TJs) proteins. (b) Passive transport mechanisms are divided into paracellular diffusion and transcellular passive diffusion; (c) active transport mechanisms include transcytosis mediated by receptors and transporters and adsorptive-mediated; (d) minimal requirements of a receptor for targeted brain delivery.

In order to exploit the natural transport mechanisms present at the BBB for the delivery of therapeutics, several BBB peptide shuttles, able to increase the transport of compounds of interest, have been developed [5–8]. On the one hand, small lipophilic peptides, such as diketopiperazines (DKPs) [19], N-methyl phenylalanines [20], or phenyl prolines [21] have been evaluated as carriers of small drugs by targeting passive transport mechanisms. On the other hand, cell-penetrating peptides or peptides targeting receptors have been proposed for the brain delivery of drugs by targeting active transport mechanisms.

## 3. Peptides Designed to Increase Passive Transport of Drugs

Transcellular and paracellular passive diffusion has traditionally been envisaged as a strategy for the delivery of small lipophilic compounds. The use of small peptides that cross by this mechanism has been explored for the delivery of small drugs. One of the most representative examples is the use of diketopiperazines (DKPs) [19], highly stable cyclic

dipeptides that are able to increase the transport of two small compounds with therapeutic interest, L-dopa and baicalin, by means of passive diffusion, as proved by the PAMPA assay, the gold standard model used to evaluate this mechanism. In addition, this family of compounds was used to deliver a hexapeptide, able to inhibit Tau aggregation *in vivo* in mice [22].

Passive diffusion passage is governed by the physicochemical properties of the compounds. For instance, the number of hydrogen acceptors and donors is an important parameter to optimize. In general, the higher the lipophilicity, the higher the transport, but if a compound is too hydrophobic, it can be retained at the lipid membrane. Modifications such as *N*-methylation [23] or halogenation [20,24] have been used as powerful tools to modulate the lipophilicity of small peptides. To this end, a family of BBB shuttle peptides composed of *N*-methylated tetrapeptides was proposed as efficient vectors to increase the transport of small drugs such as L-dopa [23]. Importantly, this chemical modification also increases the stability of the peptide shuttle to serum proteases. The potential *N*-methyl phenylalanines based shuttles have been explored through modifications to its structure with amino acids with different stereochemistry and a different number of halogenated atoms, yielding optimized peptide shuttles with an ideal structure for given cargoes [20]. For instance, when comparing how di-peptides-based *N*-methyl phenylalanines increase the transport of 3,4-dihydroxy-*L*-phenylalanine, 4-aminobutyric acid, and nipecotic acid as cargoes, the authors found that the first, which is more polar, was better transported by *N*-methylated peptide shuttles, while the last two were better transported by chlorinated-*N*-methylated peptide shuttles [20]. This work suggested that slight modifications of the structural properties of a given peptide shuttle for a given cargo can lead to optimized transport. The main drawback of this family of compounds is their limited solubility, which can be overcome using phenylproline-based peptides [21].

Another strategy, which has lately been gaining attention, is the use of peptides able to increase the porosity of the tight junctions, thus enabling the delivery of compounds. To this end, peptides derived from claudin-5 [25], E-cadherin [26], or occluding [27], which have been proved to interact with the proteins that form the tight junctions, are able to modulate the protein-protein interactions that hold these protein connections. For instance, HAV6 (Ac-SHAVSS-NH<sub>2</sub>) derived from the C-1 domain of E-cadherin, is able to increase the paracellular transport of anticancer drugs, magnetic resonance imaging (MRI) contrast agents, or near-infrared dyes [26–28]. More recently, this peptide has been compared with ADT5 (Ac-C(&)DTPPVC(&)-NH<sub>2</sub>) [29], another E-cadherin-derived peptide, for the delivery of proteins [28]. Lysozyme, albumin, IgG mAb, and fibronectin with 15, 65, 150 and 220 kDa, respectively, were intravenously co-administered in mice. ADT5 increased the transport of lysozyme, albumin, and an IgG mAb but not fibronectin, while HAV6 only improved the delivery of lysozyme [28]. Mechanistic studies revealed that these peptides are able to promote the formation of pores within the protein tight junctions of enough size to allow the transport of proteins. The authors proposed that the formed pores are of different sizes, with the largest being the least stable. Thus, depending on the duration of the effect caused by the peptide modulator, the transport of big proteins will be limited [28]. This work demonstrated that tight junction modulation can be used for the delivery of therapeutic proteins, although important factors such as the size of the protein to delivery must be considered. It might be necessary to adapt the selected tight junction modulator to the size of the protein cargo to avoid the passage of bigger proteins that could have undesired effects [29]. Despite the potential of this strategy, significant concerns about its safety must be considered. Precise control of the duration of the effect, to limit the passage of toxic substances, for instance, is of utmost importance.

Other families of peptides, such as membrane-active peptides [30,31], are able to promote the transient opening of the BBB. Melittin, a venom-derived peptide, was recently shown to promote reversible BBB opening during 24 h at neurologically safe sub-toxic concentrations [31].

#### 4. Peptides Designed to Increase Active Transport of Drugs

Targeting the active transport mechanisms of the BBB represents another attractive option for brain delivery. However, the search for an efficient receptor for the delivery of therapeutics directed to the CNS is challenging. Such a receptor should be expressed at higher levels in the brain microvasculature than in the peripheral tissues or in the brain parenchyma. As such, the risk of off-target effects would be minimized. In addition, the receptor must be able to undergo transcytosis at a reasonable rate, allowing for the passage of the selected cargo from the blood to the brain. To identify such a receptor, several proteomic and transcriptomic works have been carried out [31–33]. Importantly, these studies allow for comparison of the level of expression of a given receptor between preclinical species, such as mice or rats, and humans because the difference in expression patterns can hamper the development of delivery agents [33]. As an example, TfR, which has been widely used as a model receptor for brain delivery, is expressed five-fold higher in mice brain microvasculature than in that of humans [34]. Another important fact to consider is that the sole enrichment of the mRNA of a receptor at the brain microvasculature does not make it suitable as a target for brain delivery. For instance, Tam et al. identified Ldlrad3 and CD320 [35] as possible targets for brain delivery, but evaluation of the transport of monoclonal antibodies against these two receptors indicated that they did not have preferred brain uptake, showing similar levels to control IgG [34].

Several peptides have been shown to increase the transport of drugs by targeting the active transport mechanism of the BBB, mainly through targeting the low-density lipoprotein (LDL) and transferrin receptors [8,15]. For instance, Angiopep-2, which was proven to interact with the LRP-1 [36], has been used to modify nanoparticles of different nature [37,38], peptides [39,40], proteins [41,42], and small molecules [43,44], increasing their transport in several *in vivo* and *in vitro* models. Another example is THR, which was discovered through phage display against cells overexpressing the human transferrin receptor [45], and it was shown to deliver gold nanoparticles to the brain parenchyma of mice [8].

#### 5. Sources of BBB Shuttles

##### 5.1. Natural Proteins

Natural proteins have served as an inspiration for developing new brain-targeting peptides (Table 1). For instance, peptides based on apolipoproteins have been widely explored. Apolipoproteins are involved in lipid and cholesterol trafficking and interact with the LDLRs that are present at the BBB. Peptides based on ApoE and ApoB proteins have been used to modify various enzymes to develop new therapies for enzyme replacement therapy [46–48]. The most successful example of a BBB shuttle inspired by natural sources is angiopep-2, a 19-mer peptide derived from the alignment of the Kunitz domain of human proteins that interact with the LRP-1 [35]. Remarkably, angiopep-2 modified with three molecules of paclitaxel (ANG1005) has been evaluated in various clinical trials, showing good safety, tolerability, pharmacokinetics, and efficacy in patients with advanced solid tumors (NCT02048059), high-grade glioma (NCT01967810) [49,50], and leptomeningeal carcinomatosis and brain metastasis from breast cancer (NCT01480583 and NCT02048059) [50]. In the near future, a new trial (NCT03613181) will evaluate the effect of ANG1005 in HER2-negative breast cancer patients with the newly diagnosed leptomeningeal disease and previously treated brain metastases (source: [www.clinicaltrials.gov](http://www.clinicaltrials.gov), accessed on 1 July 2022).

Melanotransferrin (MTf), or p97, is an 80 kDa protein able to bind iron to transport it across the central nervous system [51]. Its soluble form was shown to undergo transcytosis across the BBB [52]. The potential of this protein as a shuttle has been explored in the transport of small molecules or antibodies [53,54]. A 12-mer peptide derived from MTf was described upon evaluation of the tryptic mixture of this protein in a BBB cell-based model [55]. The selected peptide, DSSHAFTLDELRL, preserves the capacity of MTf for crossing the BBB and is found in neurons, astrocytes, and microglia.

**Table 1.** Brain-targeting peptides obtained from natural sources.

Peptide	Origin	Target	Ref
(LRKLRKLL) <sub>2</sub>	ApoE (Aa 141–149) <sub>2</sub>	LDLR	[46,47]
TEELRVRLASHLRKLRKLLRDA	ApoE (Aa 130–152)	LDLR	[47]
SVIDALQYKLEGTRTLTRKRGLKLATALSLSNKFVEGS	ApoB (Aa 3371–3409)	LDLR	[47]
TFFYGGSRGKRNNFKTEEY	Sequence alignment of human Kunitz domains	LRP1	[36]
DSSHAFTLDELRL	MTf (Aa 441–452)	LDLR	[56]
YTIWMPENPRPGTPCDIFTNSRGKRASNG	RVG glycoprotein (Aa 175–203)	AchR	[57]
VQQLTKRFSL	DEN2C <sup>[a]</sup> (Aa 26–35)	None	[58]
KLFMALVAFLRFLT	DEN2C (Aa 45–59)	None	[58]
AGILKRW	DEN2C (Aa 63–69)	None	[58]
KSKAINVLRGFRKEIGRMLNILN	DEN2C (Aa 74–97)	None	[58]
[Dap](&)KAPETALD(&) <sup>[b]</sup>	Apamin	Unknown	[59]
[Dap](&)YGPQD(&)	Chlorotoxin	Unknown	[60]

<sup>[a]</sup> DEN2C: Dengue virus type 2 capsid protein. <sup>[b]</sup> [Dap] is the three-letter code for L-2,3-diaminopropionic acid; (&) refers to cyclic peptides [8].

The rabies virus has clear CNS tropism [61]. The protein responsible for virus internalization is the trimeric glycoprotein known as RVG, which was shown to interact with the  $\alpha$  subunit of AchR. Lentz et al. [62] compared the sequence of RVG with some snake venom toxins that interact with AchR and defined the region between amino acids 175 and 203 of the RVG protein as the most efficient for binding. The peptide RVG29 comprises a nonimmunogenic region of the RVG protein, which made it interesting as a BBB-shuttle peptide. Since the first seminal work where an RVG29 nanosystem was used to deliver small-interfering RNA in vivo in mice [57], several researchers have explored the use of this peptide [63]. Most of the studies modified RVG29 with several arginines in order to enhance the complexation of nucleic acids. The use of this extension may alter the internalization mechanism of the RVG29 peptide.

The dengue virus capsid protein has served as a scaffold for the design of various BBB peptide shuttles [58], which have recently been used to modify an Fc domain of IgG without affecting its binding properties to the FcR [64] or to modify porphyrins to yield peptide–porphyrin conjugates that can be used as antiviral drugs [65].

Venoms are a privileged source of bioactive compounds [66,67]. One of their major components is peptides of complex structure, which are characterized by a rich content on disulfide bridges that confer them high metabolic stability. Currently, there are 11 compounds derived from venoms approved by the FDA [67]. Some venoms affect the CNS, serving as motivation for researchers to search for CNS active compounds. To this end, two BBB-shuttle peptides derived from venoms have been described: MiniAp-4 and miniCTX3 [59,60]. MiniAp-4 is a minimized version of apamin, which is the main component of bee venom. This highly stable peptidomimetic was shown to be able to deliver a fluorophore in vivo in mice [59]. MiniCTX3 corresponds to a minimized version of chlorotoxin [60], a disulfide-rich peptide from the venom of the Israeli scorpion *Leiurus quinquestriatus* [68]. MiniCTX3-modified gold nanoparticles translocated across a human-cell-based BBB model.

### 5.2. Phage Display

Phage display is a potent source of bioactive peptides that have been widely used to obtain BBB-shuttle peptide candidates [69]. It consists of the evaluation against a target of interest of a library of bacteriophages, where each one is genetically modified to display a given peptide or protein on its coat protein. Phage display libraries have been evaluated against isolated receptors or proteins [70–72], cellular models [45,73–75], an even living animals [76–87]. A list of BBB shuttle peptides discovered by phage display is summarized in Table 2.

**Table 2.** Brain -targeting peptides discovered by phage display.

Peptide	Target	Panned Against	Ref
C(&)LSSRLDAC(&)	Brain	BALB/c mice	[76]
GHKAKGPRK	hTfR	hTfR	[70]
THRPPMWSPVWP	TfR	hTfR (chicken fibroblast)	[45]
HLNILSTLWKYR	GM1	Trisialoganglioside (GT1b)	[71]
C(&)AGALC(&Y	Brain endothelium	BALB/c, FVB/N, and C57BL mice	[77]
GLAHSFSDFARDFV	Brain endothelium	C57Bl/6 and BALB/c mice	[80]
GYRPVHNIRGHWAPG	Brain endothelium	C57Bl/6 and BALB/c mice	[80]
TGNYKALHPHNG	Brain	ICR mice	[81]
C(&)RTIGPSVC(&)	Apo-TfR	BALB/c mice	[82]
C(&)TSTSAPYC(&)	Brain	ICR mice	[83]
C(&)SYTSSTMC(&)	Brain	Sprague-Dawley rats	[84]
DSGLC(&)MPRLRGC(&)DPR	LDLR	hLDLR	[72]
TPSYDTYAAELR	Brain through the BCSFB	Sprague-Dawley rats	[85]
RLSSVSDLSGC	BBB/BCSFB	Wistar rats	[86]
SGVYKVAYDWQH	Brain endothelium	Human BBB cellular model	[73]
TFYGGRPKRNNFLRGIRSRGD	BBB/BTB	BALB/c mice	[87]
C(&)SLSHSPQC(&)	Brain endothelium	hCMEC/D3 cell monolayers	[74]
VAARTGEIYVPW	Brain endothelium	Primary endothelial rat cellular model	[75]
GLHTSATNLYLH	Brain endothelium	Primary endothelial rat cellular model	[75]
C(&)SLSHSPQC(&)	Brain endothelium	hCMEC/D3 cell monolayers	[74]
C(&)RGGKRSSC(&)	CNS	Ex vivo and in vivo EAE <sup>[a]</sup> mice	[79]
QFAALPVRAHYG	Brain	C57BL/6J mice	[78]

<sup>[a]</sup> EAE: experimental autoimmune encephalomyelitis.

The validation of the selected targets is of great importance because several factors, such as the affinity for albumin or plastic, can affect the replication of a given phage, biasing the results. To this end, several target-unrelated peptides (TUPs) have been described [69]. For instance, HAIYPRH, which was initially discovered as a transferrin receptor binder [45], has been found in more than 30 phage display experiments against more than 20 different targets (source: Biopanning Data Bank (BDB) [88]). A combination of in vitro and in vivo screening methods is suggested as a way to minimize the discovery of TUPs [69]. However, some peptides can interact in a nonspecific manner with various receptors or cell membrane components and can be useful for more than one application, although their promiscuity would need to be assessed in each case.

### 5.3. Chemical Libraries

High-throughput screening techniques have sped up the development of therapeutics during the last few decades [89]. In the field of peptide drug discovery, phage display is the main example, although it has some limitations, such as the restricted possibilities for including nonproteinogenic amino acids. The use of DNA- or mRNA-encoded libraries [90,91] or one-bead-one compound (OBOC) [92] libraries overcome this restriction. This last technology has been used to discover new protease-resistant BBB-shuttle peptides. Guixer et al. [93] evaluated for the first time an all-D OBOC library against a BBB cell-based model. Detection of the peptides able to transverse the cell monolayer was performed by mass spectrometry analysis. More recently [94], an OBOC library also composed of D amino acids was used to discover brevicin-targeting peptides. Brevican is an extracellular matrix protein located in the CNS and overexpressed in glioma cells. One of the peptides discovered was found to cross the BBB in vivo in mice [94] and to shuttle the insoluble drug camptothecin in an orthotopic mice model [95].

### 5.4. Optimization

Protease liability is one of the major concerns in the development of therapeutic peptides. To overcome this limitation, several strategies have been applied, such as the use of non-natural amino acids, cyclisation, or chemical modifications [96]. In the field of BBB

shuttles, one of the most common methods is the use of the retro-enantio or retro-inverso approach, which consists of the preparation of a given peptide using D amino acids and reversing the order of the sequence. To this end, the topological properties of the parent peptide and its retro-enantio counterpart will be very similar (Figure 2). Thus, this strategy has been applied to angiopep-2 [97], THR [98], CDX [99], and to a minimized version of RVG [100]. In all the cases, the newly designed peptides displayed higher stability to serum proteases and proved to be more efficient in the transport of various cargoes across the BBB, both in vitro and in vivo. In addition, it was demonstrated that retro-enantio/inverso peptides are less immunogenic than the original peptides, making them very attractive for their development as therapeutics [101]. For instance, THRre was recently used to efficiently deliver amphiphilic polymeric nanoparticles loaded with a cytotoxic drug in a diffuse intrinsic pontine glioma model [102].

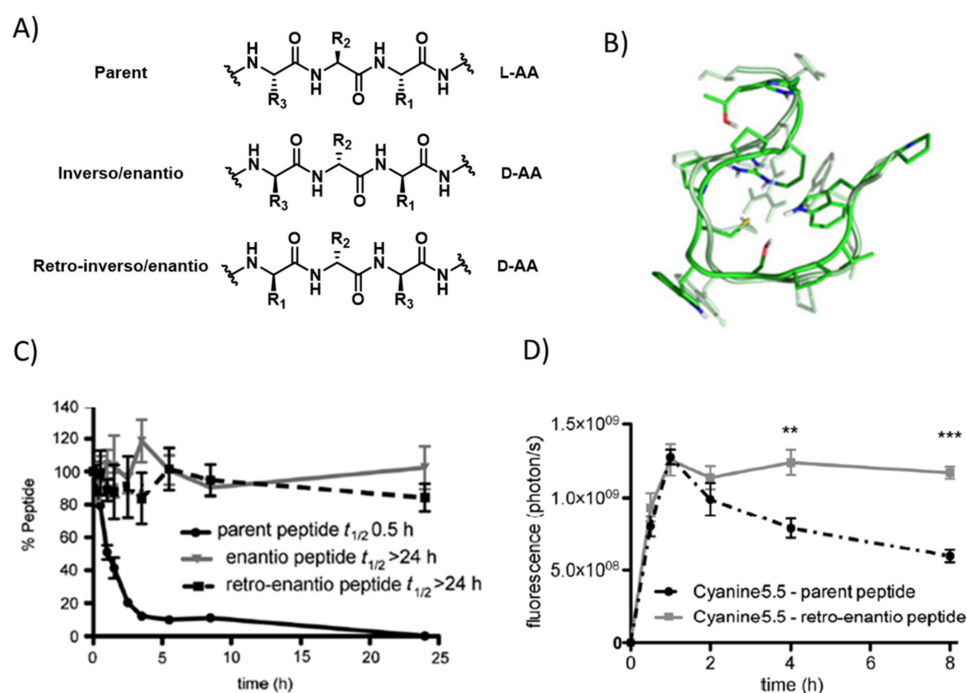


**Figure 2.** (A) Structure of a natural peptide and its retro and retro-enantio/inverso counterparts; (B) three-dimensional superposition of one pairing obtained from the cross-RMSD matrix of THR and THR retro-enantio [101]; (C) percentage of peptide versus incubation time in human serum obtained for THR and its protease-resistant enantio, and retro-enantio analogues [98]; (D) in vivo fluorescence quantification measured in a preclinical IVIS spectrum in vivo imaging system (IVIS-200) at 0.5, 1, 2, 4, and 8 h after injection of cyanine 5,5-THR and cyanine 5,5-THR retro-enantio [98] Error bars correspond to standard error mean (s.e.m.). Unpaired t student test: \*\*  $p < 0.01$ , \*\*\*  $p < 0.001$ .

### 5.5. Computational Prediction

The use of computational methods to predict the BBB permeability of peptides is very attractive due to their low cost and the rapid evolution of the field [103]. These methods use chemoinformatic filters, molecular dynamic simulations, statistical models, and/or artificial intelligence algorithms [103]. Pioneering work was conducted by Giralt et al., who worked on the design of genetic algorithms to decipher the key features necessary for a peptide to cross the BBB [104,105]. Since then, several predictors have been developed, such as the sequence-based predictor BBPpred [106]; B3predict, which is based on machine-learning models [107]; and the online tool BBPpredict [108]. In addition, databases such as B3Pdb [109] and Brainpeps [110] hold relevant information about already described BBB-shuttle peptides.

Despite the increasing number of predictors and the impressive evolution of the field, there are still a few issues that remain to be resolved. The prediction of BBB permeability

based on the physicochemical properties, such as topological polar surface area or the number of hydrogen bond acceptors, among others, only considers passive transport mechanisms across the lipid bilayer, neglecting the active transport mechanisms such as a receptor- or adsorptive-mediated transcytosis. Additionally, machine learning models are limited by the amount and quality of the currently available data [103].

More sophisticated methods are needed to find good BBB-shuttle peptides by computational prediction. For instance, molecular dynamic simulations are time-consuming, both in computing and processing time [103]. Current efforts to overcome these limitations are directed to reduce the computational cost by implementing more realistic membrane compositions, which will also allow for the evaluation of different species and new sampling techniques [111,112].

## 6. Conclusions

The development of peptides as therapeutic entities is in a golden era [113,114]. Peptides have great properties, such as low immunogenicity and biocompatibility. In addition, the advances in synthetic methodologies as well as in the strategies to increase their circulation time and stability to proteases have helped to overcome their main drawbacks. As a consequence, there are more than 150 peptides in clinical development [115]. In this context, the field of peptide shuttles for brain delivery has notably evolved, with a few candidates in clinical development.

Despite the evolution of the field, a better understanding of BBB properties and composition is needed to develop new and more efficient BBB-shuttle peptides. In this way, the discovery of new receptors may be accomplished by studies based on proteomic and transcriptomic approaches [32–34]. In addition, strategies to efficiently characterize the different transport mechanisms undertaken by a given peptide shuttle have to be further developed. Then, nonbiased strategies to discover BBB-shuttle peptides, such as in vivo phage display or in vivo screening of synthetic libraries, can be applied to the discovery of new peptides without missing information about the mechanism used.

**Funding:** This work was funded by MCIN/AEI/10.13039/501100011033 (PID2020-119810RB-I00) and by L'Association Française de l'Ataxie de Friedreich (AFAF2021). We thank ASOGAF for support.

**Conflicts of Interest:** The authors declare no conflict of interest.

## References

1. Feigin, V.L.; Nichols, E.; Alam, T.; Bannick, M.S.; Beghi, E.; Blake, N.; Culpepper, W.J.; Dorsey, E.R.; Elbaz, A.; Ellenbogen, R.G.; et al. Global, Regional, and National Burden of Neurological Disorders, 1990–2016: A Systematic Analysis for the Global Burden of Disease Study 2016. *Lancet Neurol.* **2019**, *18*, 459–480. [CrossRef]
2. Pardridge, W.M. The blood-brain barrier: Bottleneck in brain drug development. *NeuroRX* **2005**, *2*, 3–14. [CrossRef] [PubMed]
3. Daneman, R.; Prat, A. The Blood–Brain Barrier. *Cold Spring Harb. Perspect. Biol.* **2015**, *7*, a020412. [CrossRef] [PubMed]
4. Pardridge, W.M. Receptor-Mediated Peptide Transport through the Blood-Brain Barrier. *Endocr. Rev.* **1986**, *7*, 314–330. [CrossRef]
5. Terstappen, G.C.; Meyer, A.H.; Bell, R.D.; Zhang, W. Strategies for delivering therapeutics across the blood–brain barrier. *Nat. Rev. Drug Discov.* **2021**, *20*, 362–383. [CrossRef] [PubMed]
6. Bors, L.A.; Erdő, F. Overcoming the Blood–Brain Barrier. Challenges and Tricks for CNS Drug Delivery. *Sci. Pharm.* **2019**, *87*, 6. [CrossRef]
7. Puris, E.; Fricker, G.; Gynther, M. Targeting Transporters for Drug Delivery to the Brain: Can We Do Better? *Pharm. Res.* **2022**, *39*, 1415–1455. [CrossRef] [PubMed]
8. Oller-Salvia, B.; Sánchez-Navarro, M.; Giralt, E.; Teixidó, M. Blood–brain barrier shuttle peptides: An emerging paradigm for brain delivery. *Chem. Soc. Rev.* **2016**, *45*, 4690–4707. [CrossRef]
9. Abulrob, A.; Zhang, J.; Tanha, J.; MacKenzie, R.; Stanimirovic, D. Single domain antibodies as blood–brain barrier delivery vectors. *Int. Congr. Ser.* **2005**, *1277*, 212–223. [CrossRef]
10. Niewoehner, J.; Bohrmann, B.; Collin, L.; Urich, E.; Sade, H.; Maier, P.; Rueger, P.; Stracke, J.O.; Lau, W.; Tissot, A.C.; et al. Increased Brain Penetration and Potency of a Therapeutic Antibody Using a Monovalent Molecular Shuttle. *Neuron* **2014**, *81*, 49–60. [CrossRef]
11. Pardridge, W.M. Blood-Brain Barrier and Delivery of Protein and Gene Therapeutics to Brain. *Front. Aging Neurosci.* **2020**, *11*, 373. [CrossRef]

12. Pardridge, W.M. Kinetics of Blood–Brain Barrier Transport of Monoclonal Antibodies Targeting the Insulin Receptor and the Transferrin Receptor. *Pharmaceutics* **2022**, *15*, 3. [CrossRef]
13. Giugliani, R.; Giugliani, L.; de Oliveira Poswar, F.; Donis, K.C.; Corte, A.D.; Schmidt, M.; Boado, R.J.; Nestrasil, I.; Nguyen, C.; Chen, S.; et al. Neurocognitive and somatic stabilization in pediatric patients with severe Mucopolysaccharidosis Type I after 52 weeks of intravenous brain-penetrating insulin receptor antibody-iduronidase fusion protein (valanafusp alpha): An open label phase 1-2 trial. *Orphanet J. Rare Dis.* **2018**, *13*, 110. [CrossRef]
14. Schwarze, S.R.; Ho, A.; Vocero-Akbani, A.; Dowdy, S.F. In Vivo Protein Transduction: Delivery of a Biologically Active Protein into the Mouse. *Science* **1999**, *285*, 1569–1572. [CrossRef]
15. Sánchez-Navarro, M.; Giralt, E.; Teixidó, M. Blood–brain barrier peptide shuttles. *Curr. Opin. Chem. Biol.* **2017**, *38*, 134–140. [CrossRef]
16. Abbott, N.J.; Patabendige, A.A.K.; Dolman, D.E.M.; Yusof, S.R.; Begley, D.J. Structure and function of the blood-brain barrier. *Neurobiol. Dis.* **2010**, *37*, 13–25. [CrossRef]
17. Nagpal, K.; Singh, S.K.; Mishra, D.N. Drug targeting to brain: A systematic approach to study the factors, parameters and approaches for prediction of permeability of drugs across BBB. *Expert Opin. Drug Deliv.* **2013**, *10*, 927–955. [CrossRef]
18. Okuyama, T.; Eto, Y.; Sakai, N.; Minami, K.; Yamamoto, T.; Sonoda, H.; Yamaoka, M.; Tachibana, K.; Hirato, T.; Sato, Y. Iduronate-2-Sulfatase with Anti-human Transferrin Receptor Antibody for Neuropathic Mucopolysaccharidosis II: A Phase 1/2 Trial. *Mol. Ther.* **2019**, *27*, 456–464. [CrossRef]
19. Teixidó, M.; Zurita, E.; Malakoutikhah, M.; Tarragó, A.T.; Giralt, E. Diketopiperazines as a Tool for the Study of Transport across the Blood–Brain Barrier (BBB) and Their Potential Use as BBB-Shuttles. *J. Am. Chem. Soc.* **2007**, *129*, 11802–11813. [CrossRef]
20. Malakoutikhah, M.; Guixer, B.; Arranz-Gibert, P.; Teixidó, M.; Giralt, E. ‘À la Carte’ Peptide Shuttles: Tools to Increase Their Passage across the Blood-Brain Barrier. *ChemMedChem* **2014**, *9*, 1594–1601. [CrossRef]
21. Arranz-Gibert, P.; Guixer, B.; Malakoutikhah, M.; Muttenthaler, M.; Guzmán, F.; Teixidó, M.; Giralt, E. Lipid Bilayer Crossing—The Gate of Symmetry. Water-Soluble Phenylproline-Based Blood-Brain Barrier Shuttles. *J. Am. Chem. Soc.* **2015**, *137*, 7357–7364. [CrossRef] [PubMed]
22. Virgone-Carlotta, A.; Dufour, E.; Bacot, S.; Ahmadi, M.; Cornou, M.; Moni, L.; Garcia, J.; Chierici, S.; Garin, D.; Marti-Batlle, D.; et al. New diketopiperazines as vectors for peptide protection and brain delivery: Synthesis and biological evaluation. *J. Label. Compd. Radiopharm.* **2016**, *59*, 517–530. [CrossRef]
23. Malakoutikhah, M.; Teixido, M.; Giralt, E. Toward an Optimal Blood–Brain Barrier Shuttle by Synthesis and Evaluation of Peptide Libraries. *J. Med. Chem.* **2008**, *51*, 4881–4889. [CrossRef]
24. Fadzen, C.M.; Wolfe, J.M.; Cho, C.-F.; Chiocca, E.A.; Lawler, S.E.; Pentelute, B.L. Perfluoroarene–Based Peptide Macrocycles to Enhance Penetration Across the Blood–Brain Barrier. *J. Am. Chem. Soc.* **2017**, *139*, 15628–15631. [CrossRef]
25. Dithmer, S.; Staat, C.; Müller, C.; Ku, M.-C.; Pohlmann, A.; Niendorf, T.; Gehne, N.; Fallier-Becker, P.; Kittel, Á.; Walter, F.R.; et al. Claudin peptidomimetics modulate tissue barriers for enhanced drug delivery. *Ann. N. Y. Acad. Sci.* **2017**, *1397*, 169–184. [CrossRef]
26. Kiptoo, P.; Sinaga, E.; Calcagno, A.M.; Zhao, H.; Kobayashi, N.; Tambunan, U.S.F.; Siahaan, T.J. Enhancement of Drug Absorption through the Blood–Brain Barrier and Inhibition of Intercellular Tight Junction Resealing by E-Cadherin Peptides. *Mol. Pharm.* **2011**, *8*, 239–249. [CrossRef]
27. Wong, V.; Gumbiner, B.M. A Synthetic Peptide Corresponding to the Extracellular Domain of Occludin Perturbs the Tight Junction Permeability Barrier. *J. Cell Biol.* **1997**, *136*, 399–409. [CrossRef]
28. On, N.H.; Kiptoo, P.; Siahaan, T.J.; Miller, D.W. Modulation of Blood–Brain Barrier Permeability in Mice Using Synthetic E-Cadherin Peptide. *Mol. Pharm.* **2014**, *11*, 974–981. [CrossRef]
29. Ulapane, K.R.; Kopec, B.M.; Siahaan, T.J. In Vivo Brain Delivery and Brain Deposition of Proteins with Various Sizes. *Mol. Pharm.* **2019**, *16*, 4878–4889. [CrossRef]
30. Aasen, S.N.; Espedal, H.; Holte, C.F.; Keunen, O.; Karlsen, T.V.; Tenstad, O.; Maheraly, Z.; Miletic, H.; Hoang, T.; Eikeland, A.V.; et al. Improved Drug Delivery to Brain Metastases by Peptide-Mediated Permeabilization of the Blood–Brain Barrier. *Mol. Cancer Ther.* **2019**, *18*, 2171–2181. [CrossRef]
31. Linville, R.M.; Komin, A.; Lan, X.; DeStefano, J.G.; Chu, C.; Liu, G.; Walczak, P.; Hristova, K.; Searson, P.C. Reversible blood-brain barrier opening utilizing the membrane active peptide melittin in vitro and in vivo. *Biomaterials* **2021**, *275*, 120942. [CrossRef] [PubMed]
32. Uchida, Y.; Ohtsuki, S.; Katsukura, Y.; Ikeda, C.; Suzuki, T.; Kamiie, J.; Terasaki, T. Quantitative targeted absolute proteomics of human blood-brain barrier transporters and receptors. *J. Neurochem.* **2011**, *117*, 333–345. [CrossRef] [PubMed]
33. Zuchero, Y.J.Y.; Chen, X.; Bien-Ly, N.; Bumbaca, D.; Tong, R.K.; Gao, X.; Zhang, S.; Hoyte, K.; Luk, W.; Huntley, M.A.; et al. Discovery of Novel Blood-Brain Barrier Targets to Enhance Brain Uptake of Therapeutic Antibodies. *Neuron* **2016**, *89*, 70–82. [CrossRef]
34. Zhang, W.; Liu, Q.Y.; Haqqani, A.S.; Leclerc, S.; Liu, Z.; Fauteux, F.; Baumann, E.; Delaney, C.E.; Ly, D.; Star, A.T.; et al. Differential expression of receptors mediating receptor-mediated transcytosis (RMT) in brain microvessels, brain parenchyma and peripheral tissues of the mouse and the human. *Fluids Barriers CNS* **2020**, *17*, 47. [CrossRef] [PubMed]



35. Tam, S.J.; Richmond, D.L.; Kaminker, J.S.; Modrusan, Z.; Martin-McNulty, B.; Cao, T.C.; Weimer, R.M.; Carano, R.A.; van Bruggen, N.; Watts, R.J. Death Receptors DR6 and TROY Regulate Brain Vascular Development. *Dev. Cell* **2012**, *22*, 403–417. [CrossRef]
36. Demeule, M.; Régina, A.; Ché, C.; Poirier, J.; Nguyen, T.; Gabathuler, R.; Castaigne, J.-P.; Béliveau, R. Identification and Design of Peptides as a New Drug Delivery System for the Brain. *J. Pharmacol. Exp. Ther.* **2008**, *324*, 1064–1072. [CrossRef]
37. Shen, J.; Zhan, C.; Xie, C.; Meng, Q.; Gu, B.; Li, C.; Zhang, Y.; Lu, W. Poly(ethylene glycol)-block-poly(D,L-lactide acid) micelles anchored with angiopep-2 for brain-targeting delivery. *J. Drug Target.* **2011**, *19*, 197–203. [CrossRef]
38. Velasco-Aguirre, C.; Morales-Zavala, F.; Salas-Huenuleo, E.; Gallardo-Toledo, E.; Andonie, O.; Muñoz, L.; Rojas, X.; Acosta, G.; Sánchez-Navarro, M.; Giralt, E.; et al. Improving gold nanorod delivery to the central nervous system by conjugation to the shuttle Angiopep-2. *Nanomedicine* **2017**, *12*, 2503–2517. [CrossRef]
39. Thiot, C.; et al. Conjugation of a brain-penetrant peptide with neurotensin provides antinociceptive properties. *J. Clin. Investig.* **2014**, *124*, 1199–1213. [CrossRef]
40. Eiselt, E.; Otis, V.; Belleville, K.; Yang, G.; Larocque, A.; Regina, A.; Demeule, M.; Sarret, P.; Gendron, L. Use of a Noninvasive Brain-Penetrating Peptide-Drug Conjugate Strategy to Improve the Delivery of Opioid Pain Relief Medications to the Brain. *J. Pharmacol. Exp. Ther.* **2020**, *374*, 52–61. [CrossRef]
41. Regina, A.; Demeule, M.; Tripathy, S.; Lord-Dufour, S.; Currie, J.-C.; Iddir, M.; Annabi, B.; Castaigne, J.-P.; Lachowicz, J.E. ANG4043, a Novel Brain-Penetrant Peptide–mAb Conjugate, Is Efficacious against HER2-Positive Intracranial Tumors in Mice. *Mol. Cancer Ther.* **2015**, *14*, 129–140. [CrossRef] [PubMed]
42. Anami, Y.; Xiong, W.; Yamaguchi, A.; Yamazaki, C.M.; Zhang, N.; An, Z.; Tsuchikama, K. Homogeneous antibody–angiopep 2 conjugates for effective brain targeting. *RSC Adv.* **2022**, *12*, 3359–3364. [CrossRef]
43. Régina, A.; Demeule, M.; Ché, C.; Lavallée, I.; Poirier, J.; Gabathuler, R.; Béliveau, R.; Castaigne, J.-P. Antitumour activity of ANG1005, a conjugate between paclitaxel and the new brain delivery vector Angiopep-2. *Br. J. Pharmacol.* **2008**, *155*, 185–197. [CrossRef] [PubMed]
44. Ché, C.; Yang, G.; Thiot, C.; Lacoste, M.-C.; Currie, J.-C.; Demeule, M.; Régina, A.; Béliveau, R.; Castaigne, J.-P. New Angiopep-Modified Doxorubicin (ANG1007) and Etoposide (ANG1009) Chemotherapeutics With Increased Brain Penetration. *J. Med. Chem.* **2010**, *53*, 2814–2824. [CrossRef] [PubMed]
45. Lee, J.H.; Engler, J.A.; Collawn, J.F.; Moore, B.A. Receptor mediated uptake of peptides that bind the human transferrin receptor. *Eur. J. Biochem.* **2001**, *268*, 2004–2012. [CrossRef] [PubMed]
46. Wang, D.; El-Amouri, S.S.; Dai, M.; Kuan, C.-Y.; Hui, D.Y.; Brady, R.O.; Pan, D. Engineering a lysosomal enzyme with a derivative of receptor-binding domain of apoE enables delivery across the blood–brain barrier. *Proc. Natl. Acad. Sci. USA* **2013**, *110*, 2999–3004. [CrossRef]
47. Böckenhoff, A.; Cramer, S.; Wölte, P.; Knieling, S.; Wohlenberg, C.; Gieselmann, V.; Galla, H.-J.; Matzner, U. Comparison of Five Peptide Vectors for Improved Brain Delivery of the Lysosomal Enzyme Arylsulfatase A. *J. Neurosci.* **2014**, *34*, 3122–3129. [CrossRef]
48. Meng, Y.; Wiseman, J.A.; Nemtsova, Y.; Moore, D.F.; Guevarra, J.; Reuhl, K.; Banks, W.A.; Daneman, R.; Sleat, D.E.; Lobel, P. A Basic ApoE-Based Peptide Mediator to Deliver Proteins across the Blood-Brain Barrier: Long-Term Efficacy, Toxicity, and Mechanism. *Mol. Ther.* **2017**, *25*, 1531–1543. [CrossRef]
49. Kurzrock, R.; Gabrail, N.; Chandhasin, C.; Moulder, S.; Smith, C.; Brenner, A.; Sankhala, K.; Mita, A.; Elian, K.; Bouchard, D.; et al. Safety, Pharmacokinetics, and Activity of GRN1005, a Novel Conjugate of Angiopep-2, a Peptide Facilitating Brain Penetration, and Paclitaxel, in Patients with Advanced Solid Tumors. *Mol. Cancer Ther.* **2012**, *11*, 308–316. [CrossRef]
50. Drappatz, J.; Brenner, A.; Wong, E.T.; Eichler, A.; Schiff, D.; Groves, M.D.; Mikkelsen, T.; Rosenfeld, S.; Sarantopoulos, J.; Meyers, C.A.; et al. Phase I Study of GRN1005 in Recurrent Malignant Glioma. *Clin. Cancer Res.* **2013**, *19*, 1567–1576. [CrossRef]
51. Moroo, I.; Ujiie, M.; Walker, B.L.; Tiong, J.W.; Vitalis, T.Z.; Karkan, D.; Gabathuler, R.; Moise, A.R.; Jefferies, W.A. Identification of a Novel Route of Iron Transcytosis across the Mammalian Blood-Brain Barrier. *Microcirculation* **2003**, *10*, 457–462. [CrossRef] [PubMed]
52. Demeule, M.; Poirier, J.; Jodoin, J.; Bertrand, Y.; Desrosiers, R.R.; Dagenais, C.; Nguyen, T.; Lanthier, J.; Gabathuler, R.; Kennard, M.; et al. High transcytosis of melanotransferrin (P97) across the blood-brain barrier. *J. Neurochem.* **2002**, *83*, 924–933. [CrossRef] [PubMed]
53. Karkan, D.; Pfeifer, C.; Vitalis, T.Z.; Arthur, G.; Ujiie, M.; Chen, Q.; Tsai, S.; Koliatis, G.; Gabathuler, R.; Jefferies, W.A. A Unique Carrier for Delivery of Therapeutic Compounds beyond the Blood-Brain Barrier. *PLoS ONE* **2008**, *3*, e2469. [CrossRef]
54. Nounou, M.I.; Adkins, C.E.; Rubinchik, E.; Terrell-Hall, T.B.; Afroz, M.; Vitalis, T.; Gabathuler, R.; Tian, M.M.; Lockman, P.R. Anti-cancer Antibody Trastuzumab-Melanotransferrin Conjugate (BT2111) for the Treatment of Metastatic HER2+ Breast Cancer Tumors in the Brain: An In-Vivo Study. *Pharm. Res.* **2016**, *33*, 2930–2942. [CrossRef] [PubMed]
55. Singh, C.S.B.; Eyford, B.A.; Abraham, T.; Munro, L.; Choi, K.B.; Okon, M.; Vitalis, T.Z.; Gabathuler, R.; Lu, C.-J.; Pfeifer, C.G.; et al. Discovery of a Highly Conserved Peptide in the Iron Transporter Melanotransferrin that Traverses an Intact Blood Brain Barrier and Localized in Neural Cells. *Front. Neurosci.* **2021**, *15*, 473. [CrossRef]

56. Thom, G.; Tian, M.-M.; Hatcher, J.P.; Rodrigo, N.; Burrell, M.; Gurrell, I.; Vitalis, T.Z.; Abraham, T.; Jefferies, W.A.; I Webster, C.; et al. A peptide derived from melanotransferrin delivers a protein-based interleukin 1 receptor antagonist across the BBB and ameliorates neuropathic pain in a preclinical model. *J. Cereb. Blood Flow Metab.* **2018**, *39*, 2074–2088. [CrossRef]
57. Kumar, P.; Wu, H.; McBride, J.L.; Jung, K.-E.; Kim, M.H.; Davidson, B.; Lee, S.K.; Shankar, P.; Manjunath, N. Transvascular delivery of small interfering RNA to the central nervous system. *Nature* **2007**, *448*, 39–43. [CrossRef]
58. Neves, V.; Aires-Da-Silva, F.; Morais, M.; Gano, L.; Ribeiro, E.; Pinto, A.; Aguiar, S.; Gaspar, D.; Fernandes, C.; Correia, J.D.G.; et al. Novel Peptides Derived from Dengue Virus Capsid Protein Translocate Reversibly the Blood–Brain Barrier through a Receptor-Free Mechanism. *ACS Chem. Biol.* **2017**, *12*, 1257–1268. [CrossRef]
59. Oller-Salvia, B.; Sánchez-Navarro, M.; Ciudad, S.; Guiu, M.; Arranz-Gibert, P.; Garcia, C.; Gomis, R.R.; Cecchelli, R.; García, J.; Giralt, E.; et al. MiniAp-4: A Venom-Inspired Peptidomimetic for Brain Delivery. *Angew. Chem. Int. Ed.* **2016**, *55*, 572–575. [CrossRef]
60. Diaz-Perlas, C.; Varese, M.; Guardiola, S.; García, J.; Sánchez-Navarro, M.; Giralt, E.; Teixidó, M. From venoms to BBB-shuttles. MiniCTX3: A molecular vector derived from scorpion venom. *Chem. Commun.* **2018**, *54*, 12738–12741. [CrossRef]
61. Salinas, S.; Schiavo, G.; Kremer, E. A hitchhiker's guide to the nervous system: The complex journey of viruses and toxins. *Nat. Rev. Microbiol.* **2010**, *8*, 645–655. [CrossRef] [PubMed]
62. Lentz, T.L.; Hawrot, E.; Wilson, P.T. Synthetic peptides corresponding to sequences of snake venom neurotoxins and rabies virus glycoprotein bind to the nicotinic acetylcholine receptor. *Proteins Struct. Funct. Bioinform.* **1987**, *2*, 298–307. [CrossRef]
63. Oswald, M.; Geissler, S.; Goepferich, A. Targeting the Central Nervous System (CNS): A Review of Rabies Virus-Targeting Strategies. *Mol. Pharm.* **2017**, *14*, 2177–2196. [CrossRef] [PubMed]
64. Cavaco, M.; Frutos, S.; Oliete, P.; Valle, J.; Andreu, D.; Castanho, M.A.R.B.; Vila-Perelló, M.; Neves, V. Conjugation of a Blood Brain Barrier Peptide Shuttle to an Fc Domain for Brain Delivery of Therapeutic Biomolecules. *ACS Med. Chem. Lett.* **2021**, *12*, 1663–1668. [CrossRef]
65. Mendonça, D.A.; Bakker, M.; Cruz-Oliveira, C.; Neves, V.; Jiménez, M.A.; Defaus, S.; Cavaco, M.; Veiga, A.S.; Cadima-Couto, I.; Castanho, M.A.R.B.; et al. Penetrating the Blood-Brain Barrier with New Peptide–Porphyrin Conjugates Having anti-HIV Activity. *Bioconj. Chem.* **2021**, *32*, 1067–1077. [CrossRef] [PubMed]
66. King, G.F. Venoms as a platform for human drugs: Translating toxins into therapeutics. *Expert Opin. Biol. Ther.* **2011**, *11*, 1469–1484. [CrossRef] [PubMed]
67. De Castro Figueiredo Bordon, K.; Cologna, C.T.; Fornari-Baldo, E.C.; Pinheiro-Júnior, E.L.; Cerni, F.A.; Amorim, F.G.; Anjolette, F.A.P.; Cordeiro, F.A.; Wiesel, G.A.; Cardoso, I.A.; et al. From Animal Poisons and Venoms to Medicines: Achievements, Challenges and Perspectives in Drug Discovery. *Front. Pharmacol.* **2020**, *11*, 1132. [CrossRef]
68. Ojeda, P.G.; Wang, C.; Craik, D.J. Chlorotoxin: Structure, activity, and potential uses in cancer therapy. *Pept. Sci.* **2015**, *106*, 25–36. [CrossRef]
69. Andrieu, J.; Re, F.; Russo, L.; Nicotra, F. Phage-displayed peptides targeting specific tissues and organs. *J. Drug Target.* **2019**, *27*, 555–565. [CrossRef]
70. Xia, H.; Anderson, B.; Mao, Q.; Davidson, B.L. Recombinant Human Adenovirus: Targeting to the Human Transferrin Receptor Improves Gene Transfer to Brain Microcapillary Endothelium. *J. Virol.* **2000**, *74*, 11359–11366. [CrossRef]
71. Liu, J.K.; Teng, Q.; Garrity-Moses, M.; Federici, T.; Tanase, D.; Imperiale, M.J.; Boulis, N.M. A novel peptide defined through phage display for therapeutic protein and vector neuronal targeting. *Neurobiol. Dis.* **2005**, *19*, 407–418. [CrossRef] [PubMed]
72. Malcor, J.-D.; Payrot, N.; David, M.; Faucon, A.; Abouzid, K.; Jacquot, G.; Floquet, N.; Debarbieux, F.; Rougon, G.; Martinez, J.; et al. Chemical Optimization of New Ligands of the Low-Density Lipoprotein Receptor as Potential Vectors for Central Nervous System Targeting. *J. Med. Chem.* **2012**, *55*, 2227–2241. [CrossRef] [PubMed]
73. Díaz-Perlas, C.; Sánchez-Navarro, M.; Oller-Salvia, B.; Moreno, M.; Teixidó, M.; Giralt, E. Phage display as a tool to discover blood-brain barrier (BBB)-shuttle peptides: Panning against a human BBB cellular model. *Biopolymers* **2017**, *108*, e22928. [CrossRef] [PubMed]
74. Yamaguchi, S.; Ito, S.; Masuda, T.; Couraud, P.-O.; Ohtsuki, S. Novel cyclic peptides facilitating transcellular blood-brain barrier transport of macromolecules in vitro and in vivo. *J. Control. Release* **2020**, *321*, 744–755. [CrossRef]
75. Majerova, P.; Hanes, J.; Olesova, D.; Sinsky, J.; Pilipcinec, E.; Kovac, A. Novel Blood–Brain Barrier Shuttle Peptides Discovered through the Phage Display Method. *Molecules* **2020**, *25*, 874. [CrossRef] [PubMed]
76. Pasqualini, R.; Ruoslahti, E. Organ targeting In vivo using phage display peptide libraries. *Nature* **1996**, *380*, 364–366. [CrossRef]
77. Fan, X.; Venegas, R.; Fey, R.; van der Heyde, H.; Bernard, M.A.; Lazarides, E.; Woods, C.M. An In Vivo Approach to Structure Activity Relationship Analysis of Peptide Ligands. *Pharm. Res.* **2007**, *24*, 868–879. [CrossRef] [PubMed]
78. Zhang, X.; Chai, Z.; Dobbins, A.L.; Itano, M.S.; Askew, C.; Miao, Z.; Niu, H.; Samulski, R.J.; Li, C. Customized blood-brain barrier shuttle peptide to increase AAV9 vector crossing the BBB and augment transduction in the brain. *Biomaterials* **2022**, *281*, 121340. [CrossRef]
79. Acharya, B.; Meka, R.R.; Venkatesha, S.H.; Lees, J.R.; Teesalu, T.; Moudgil, K.D. A novel CNS-homing peptide for targeting neuroinflammatory lesions in experimental autoimmune encephalomyelitis. *Mol. Cell. Probes* **2020**, *51*, 101530. [CrossRef]
80. van Rooy, I.; Cakir-Tascioglu, S.; Couraud, P.-O.; Romero, I.; Weksler, B.; Storm, G.; Hennink, W.E.; Schiffelers, R.; Mastrobattista, E. Identification of Peptide Ligands for Targeting to the Blood-Brain Barrier. *Pharm. Res.* **2010**, *27*, 673–682. [CrossRef]




81. Li, J.; Feng, L.; Fan, L.; Zha, Y.; Guo, L.; Zhang, Q.; Chen, J.; Pang, Z.; Wang, Y.; Jiang, X.; et al. Targeting the brain with PEG–PLGA nanoparticles modified with phage-displayed peptides. *Biomaterials* **2011**, *32*, 4943–4950. [CrossRef] [PubMed]
82. Staquicini, F.I.; Ozawa, M.G.; Moya, C.A.; Driessen, W.H.; Barbu, E.M.; Nishimori, H.; Soghomonyan, S.; Flores, L.G.; Liang, X.; Paolillo, V.; et al. Systemic combinatorial peptide selection yields a non-canonical iron-mimicry mechanism for targeting tumors in a mouse model of human glioblastoma. *J. Clin. Investig.* **2011**, *121*, 161–173. [CrossRef]
83. Li, J.; Zhang, Q.; Pang, Z.; Wang, Y.; Liu, Q.; Guo, L.; Jiang, X. Identification of peptide sequences that target to the brain using in vivo phage display. *Amino Acids* **2012**, *42*, 2373–2381. [CrossRef]
84. Smith, M.W.; Al-Jayyousi, G.; Gumbleton, M. Peptide sequences mediating tropism to intact blood–brain barrier: An in vivo biodistribution study using phage display. *Peptides* **2012**, *38*, 172–180. [CrossRef] [PubMed]
85. Li, J.; Feng, L.; Jiang, X. In vivo phage display screen for peptide sequences that cross the blood–cerebrospinal-fluid barrier. *Amino Acids* **2015**, *47*, 401–405. [CrossRef]
86. Urich, E.; Schmucki, R.; Ruderisch, N.; Kitas, E.; Certa, U.; Jacobsen, H.; Schweitzer, C.; Bergadano, A.; Ebeling, M.; Loetscher, H.; et al. Cargo Delivery into the Brain by in vivo identified Transport Peptides. *Sci. Rep.* **2015**, *5*, 14104. [CrossRef] [PubMed]
87. Chen, L.; Zeng, D.; Xu, N.; Li, C.; Zhang, W.; Zhu, X.-J.; Gao, Y.; Chen, P.R.; Lin, J. Blood–Brain Barrier- and Blood–Brain Tumor Barrier-Penetrating Peptide-Derived Targeted Therapeutics for Glioma and Malignant Tumor Brain Metastases. *ACS Appl. Mater. Interfaces* **2019**, *11*, 41889–41897. [CrossRef]
88. He, B.; Chai, G.; Duan, Y.; Yan, Z.; Qiu, L.; Zhang, H.; Liu, Z.; He, Q.; Han, K.; Ru, B.; et al. BDB: Biopanning data bank. *Nucleic Acids Res.* **2016**, *44*, D1127–D1132. [CrossRef]
89. Macarron, R.; Banks, M.N.; Bojanic, D.; Burns, D.J.; Cirovic, D.A.; Garyantes, T.; Green, D.V.S.; Hertzberg, R.P.; Janzen, W.P.; Paslay, J.W.; et al. Impact of high-throughput screening in biomedical research. *Nat. Rev. Drug Discov.* **2011**, *10*, 188–195. [CrossRef]
90. Cai, B.; Kim, D.; Akhand, S.; Sun, Y.; Cassell, R.J.; Alpsy, A.; Dykhuizen, E.C.; Van Rijn, R.M.; Wendt, M.K.; Krusemark, C.J. Selection of DNA-Encoded Libraries to Protein Targets within and on Living Cells. *J. Am. Chem. Soc.* **2019**, *141*, 17057–17061. [CrossRef]
91. Goto, Y.; Suga, H. The RaPID Platform for the Discovery of Pseudo-Natural Macrocyclic Peptides. *Acc. Chem. Res.* **2021**, *54*, 3604–3617. [CrossRef] [PubMed]
92. Lam, K.S.; Salmon, S.E.; Hersh, E.M.; Hruby, V.J.; Kazmierski, W.M.; Knapp, R.J. A new type of synthetic peptide library for identifying ligand-binding activity. *Nature* **1991**, *354*, 82–84. [CrossRef]
93. Guixer, B.; Arroyo, X.; Belda, I.; Sabidó, E.; Teixidó, M.; Giralt, E. Chemically synthesized peptide libraries as a new source of BBB shuttles. Use of mass spectrometry for peptide identification. *J. Pept. Sci.* **2016**, *22*, 577–591. [CrossRef] [PubMed]
94. Spreckelsen, N.; Fadzen, C.M.; Hartrampf, N.; Ghotmi, Y.; Wolfe, J.M.; Dubey, S.; Yang, B.Y.; Kijewski, M.F.; Wang, S.; Farquhar, C.; et al. Targeting Glioblastoma Using a Novel Peptide Specific to a Deglycosylated Isoform of Brevican. *Adv. Ther.* **2021**, *4*, 2000244. [CrossRef] [PubMed]
95. Cho, C.-F.; Farquhar, C.E.; Fadzen, C.M.; Scott, B.; Zhuang, P.; von Spreckelsen, N.; Loas, A.; Hartrampf, N.; Pentelute, B.L.; Lawler, S.E. A Tumor-Homing Peptide Platform Enhances Drug Solubility, Improves Blood–Brain Barrier Permeability and Targets Glioblastoma. *Cancers* **2022**, *14*, 2207. [CrossRef]
96. Lucana, M.C.; Arruga, Y.; Petrachi, E.; Roig, A.; Lucchi, R.; Oller-Salvia, B. Protease-Resistant Peptides for Targeting and Intracellular Delivery of Therapeutics. *Pharmaceutics* **2021**, *13*, 2065. [CrossRef]
97. Wei, X.; Zhan, C.; Chen, X.; Hou, J.; Xie, C.; Lu, W. Retro-Inverso Isomer of Angiopep-2: A Stable d-Peptide Ligand Inspires Brain-Targeted Drug Delivery. *Mol. Pharm.* **2014**, *11*, 3261–3268. [CrossRef]
98. Prades, R.; Oller-Salvia, B.; Schwarzmaier, S.M.; Selva, J.; Moros, M.; Balbi, M.; Grazú, V.; de la Fuente, J.M.; Egea, G.; Plesnila, N.; et al. Applying the Retro-Enantio Approach To Obtain a Peptide Capable of Overcoming the Blood-Brain Barrier. *Angew. Chem. Int. Ed.* **2015**, *54*, 3967–3972. [CrossRef]
99. Wei, X.; Zhan, C.; Shen, Q.; Fu, W.; Xie, C.; Gao, J.; Peng, C.; Zheng, P.; Lu, W. AD-Peptide Ligand of Nicotine Acetylcholine Receptors for Brain-Targeted Drug Delivery. *Angew. Chem. Int. Ed.* **2015**, *54*, 3023–3027. [CrossRef]
100. Javed, H.; Menon, S.A.; Al-Mansoori, K.M.; Al-Wandi, A.; Majbour, N.K.; Ardah, M.T.; Varghese, S.; Vaikath, N.N.; Haque, M.E.; Azzouz, M.; et al. Development of Nonviral Vectors Targeting the Brain as a Therapeutic Approach For Parkinson’s Disease and Other Brain Disorders. *Mol. Ther.* **2016**, *24*, 746–758. [CrossRef]
101. Arranz-Gibert, P.; Ciudad, S.; Seco, J.; García, J.; Giralt, E.; Teixidó, M. Immunosilencing peptides by stereochemical inversion and sequence reversal: Retro-D-peptides. *Sci. Rep.* **2018**, *8*, 6446. [CrossRef] [PubMed]
102. Bukchin, A.; Sanchez-Navarro, M.; Carrera, A.; Resa-Pares, C.; Castillo-Ecija, H.; Balaguer-Lluna, L.; Teixidó, M.; Olaciregui, N.G.; Giralt, E.; Carcaboso, A.M.; et al. Amphiphilic Polymeric Nanoparticles Modified with a Protease-Resistant Peptide Shuttle for the Delivery of SN-38 in Diffuse Intrinsic Pontine Glioma. *ACS Appl. Nano Mater.* **2021**, *4*, 1314–1329. [CrossRef]
103. de Oliveira, E.C.L.; da Costa, K.S.; Taube, P.S.; Lima, A.H.; Junior, C.D.S.D.S. Biological Membrane-Penetrating Peptides: Computational Prediction and Applications. *Front. Cell. Infect. Microbiol.* **2022**, *12*, 276. [CrossRef] [PubMed]
104. Teixidó, M.; Belda, I.; Roselló, X.; González, S.; Fabre, M.; Llorá, X.; Bacardit, J.; Garrell, J.M.; Vilaró, S.; Albericio, F.; et al. Development of a Genetic Algorithm to Design and Identify Peptides that can Cross the Blood-Brain Barrier. *QSAR Comb. Sci.* **2003**, *22*, 745–753. [CrossRef]

105. Belda, I.; Madurga, S.; Tarragó, T.; Llorà, X.; Giralt, E. Evolutionary computation and multimodal search: A good combination to tackle molecular diversity in the field of peptide design. *Mol. Divers.* **2006**, *11*, 7–21. [CrossRef]
106. Dai, R.; Zhang, W.; Tang, W.; Wynendaele, E.; Zhu, Q.; Bin, Y.; De Spiegeleer, B.; Xia, J. BBPpred: Sequence-Based Prediction of Blood-Brain Barrier Peptides with Feature Representation Learning and Logistic Regression. *J. Chem. Inf. Model.* **2021**, *61*, 525–534. [CrossRef]
107. Kumar, V.; Patiyal, S.; Dhall, A.; Sharma, N.; Raghava, G.P.S. B3Pred: A Random-Forest-Based Method for Predicting and Designing Blood–Brain Barrier Penetrating Peptides. *Pharmaceutics* **2021**, *13*, 1237. [CrossRef]
108. Chen, X.; Zhang, Q.; Li, B.; Lu, C.; Yang, S.; Long, J.; He, B.; Chen, H.; Huang, J. BBPpredict: A Web Service for Identifying Blood-Brain Barrier Penetrating Peptides. *Front. Genet.* **2022**, *13*, 916. [CrossRef]
109. Kumar, V.; Patiyal, S.; Kumar, R.; Sahai, S.; Kaur, D.; Lathwal, A.; Raghava, G.P.S. B3Pdb: An archive of blood–brain barrier-penetrating peptides. *Brain Struct. Funct.* **2021**, *226*, 2489–2495. [CrossRef]
110. Van Dorpe, S.; Bronselaer, A.; Nielandt, J.; Stalmans, S.; Wynendaele, E.; Audenaert, K.; De Spiegeleer, B. Brainpeps: The blood-brain barrier peptide database. *Brain Struct. Funct.* **2012**, *217*, 687–718. [CrossRef]
111. Marrink, S.J.; Risselada, H.J.; Yefimov, S.; Tieleman, D.P.; de Vries, A.H. The MARTINI force field: Coarse grained model for biomolecular simulations. *J. Phys. Chem. B* **2007**, *111*, 7812–7824. [CrossRef] [PubMed]
112. Sugita, M.; Sugiyama, S.; Fujie, T.; Yoshikawa, Y.; Yanagisawa, K.; Ohue, M.; Akiyama, Y. Large-Scale Membrane Permeability Prediction of Cyclic Peptides Crossing a Lipid Bilayer Based on Enhanced Sampling Molecular Dynamics Simulations. *J. Chem. Inf. Model.* **2021**, *61*, 3681–3695. [CrossRef] [PubMed]
113. Guidotti, G.; Brambilla, L.; Rossi, D. Peptides in clinical development for the treatment of brain tumors. *Curr. Opin. Pharmacol.* **2019**, *47*, 102–109. [CrossRef] [PubMed]
114. Cabri, W.; Cantelmi, P.; Corbisiero, D.; Fantoni, T.; Ferrazzano, L.; Martelli, G.; Mattellone, A.; Tolomelli, A. Therapeutic Peptides Targeting PPI in Clinical Development: Overview, Mechanism of Action and Perspectives. *Front. Mol. Biosci.* **2021**, *8*, 697586. [CrossRef]
115. Lau, J.L.; Dunn, M.K. Therapeutic peptides: Historical perspectives, current development trends, and future directions. *Bioorg. Med. Chem.* **2018**, *26*, 2700–2707. [CrossRef]



Review

# Increased/Targeted Brain (Pro)Drug Delivery via Utilization of Solute Carriers (SLCs)

Johanna Huttunen<sup>1</sup>, Santosh Kumar Adla<sup>1,2</sup> , Magdalena Markowicz-Piasecka<sup>3</sup>   
and Kristiina M. Huttunen<sup>1,\*</sup> 

<sup>1</sup> School of Pharmacy, Faculty of Health Sciences, University of Eastern Finland, P.O. Box 1627, FI-70211 Kuopio, Finland; johanna.huttunen@uef.fi (J.H.); santosh.adla@uef.fi (S.K.A.)

<sup>2</sup> Institute of Organic Chemistry and Biochemistry (IOCB), Czech Academy of Sciences, Flemingovo Namesti 542/2, 160 00 Prague, Czech Republic

<sup>3</sup> Department of Pharmaceutical Chemistry, Drug Analysis and Radiopharmacy, Medical University of Lodz, ul. Muszyńskiego 1, 90-151 Lodz, Poland; magdalena.markowicz@umed.lodz.pl

\* Correspondence: kristiina.huttunen@uef.fi

**Abstract:** Membrane transporters have a crucial role in compounds' brain drug delivery. They allow not only the penetration of a wide variety of different compounds to cross the endothelial cells of the blood–brain barrier (BBB), but also the accumulation of them into the brain parenchymal cells. Solute carriers (SLCs), with nearly 500 family members, are the largest group of membrane transporters. Unfortunately, not all SLCs are fully characterized and used in rational drug design. However, if the structural features for transporter interactions (binding and translocation) are known, a prodrug approach can be utilized to temporarily change the pharmacokinetics and brain delivery properties of almost any compound. In this review, main transporter subtypes that are participating in brain drug disposition or have been used to improve brain drug delivery across the BBB via the prodrug approach, are introduced. Moreover, the ability of selected transporters to be utilized in intrabrain drug delivery is discussed. Thus, this comprehensive review will give insights into the methods, such as computational drug design, that should be utilized more effectively to understand the detailed transport mechanisms. Moreover, factors, such as transporter expression modulation pathways in diseases that should be taken into account in rational (pro)drug development, are considered to achieve successful clinical applications in the future.

**Keywords:** blood–brain barrier (BBB); brain drug delivery; prodrugs; solute carriers (SLCs)

**Citation:** Huttunen, J.; Adla, S.K.; Markowicz-Piasecka, M.; Huttunen, K.M. Increased/Targeted Brain (Pro)Drug Delivery via Utilization of Solute Carriers (SLCs). *Pharmaceutics* **2022**, *14*, 1234. <https://doi.org/10.3390/pharmaceutics14061234>

Academic Editor: William M. Pardridge

Received: 25 May 2022

Accepted: 7 June 2022

Published: 10 June 2022

**Publisher's Note:** MDPI stays neutral with regard to jurisdictional claims in published maps and institutional affiliations.



**Copyright:** © 2022 by the authors. Licensee MDPI, Basel, Switzerland. This article is an open access article distributed under the terms and conditions of the Creative Commons Attribution (CC BY) license (<https://creativecommons.org/licenses/by/4.0/>).

## 1. Introduction

Diseases of the central nervous system (CNS), including neurodegenerative and neurodevelopmental diseases, are one of the greatest threats to public health. According to the World Health Organization, these diseases account for 12% of deaths worldwide and the economic burden of direct and indirect healthcare costs are substantial [1]. To make matters worse, these numbers are expected to increase as the population ages [2]. Most brain diseases lack effective drug therapies, since the brain is protected by multiple mechanisms that block drugs from entering and reaching their target sites [3,4]. Firstly, the majority of drugs are unable to cross the blood–brain barrier (BBB), which is made of capillary endothelial cells that are connected very closely by tight junctions. The endothelial cells of the BBB are also metabolically very active in protecting the brain tissue from various xenobiotics and microbes and effluxing them back to the bloodstream at the luminal membranes of the BBB via numerous ATP-binding cassette (ABC) transporters, including P-glycoprotein (P-gp, *ABCB1*), multidrug resistance proteins 2 (MRP2, *ABCC2*) and 4 (MRP4, *ABCC4*), and breast cancer resistance protein (BCRP, *ABCG2*) [5]. It has been estimated that 98% of all current drugs do not cross the BBB at sufficiently high amounts to therapeutically treat CNS diseases [6]. However, the brain drug disposition is highly regulated not only by

the BBB but also by neurons and glial cells that can serve as a secondary barrier to brain drug exposure [7,8]. Surprisingly, the inability of drugs to cross the cellular membranes of brain parenchymal cells has been less studied in the past, although many of the novel CNS targets are intracellular proteins.

Endogenous solute carriers (SLCs) transport essential substances and xenobiotics across the cell membranes and, e.g., across the BBB but also into the brain parenchyma. In the brain, their primary role is to regulate the supply of essential nutrients, such as amino acids, sugars, vitamins, nucleosides, and electrolytes for the endothelial and parenchymal cells. However, transporters can also carry various drugs and toxins, and thus, they are major determinants of CNS drug/toxin exposure [6,8]. Although SLCs, nearly 500 transporters overall, present promising drug carriers as well as drug targets in the brain, they are still poorly characterized and utilized in rational drug research and development today [9,10]. So far, the expression and function of many SLCs in brain microvascular endothelial cells have been extensively described [5]; however, less is known about SLCs' roles in drug disposition, response, and drug–drug interactions in the parenchymal cells. Nevertheless, carrier-mediated transport via SLCs to improve brain drug disposition can be achieved, if structural features required for the interactions with the selected transporter are known. Unfortunately, the recent focus has been paid to only a selected number of transporters.

Prodrugs are compounds with little or no pharmacological activity of their own. They are designed to be bioconverted to active drugs either chemically or enzymatically, which releases the active parent drug and the promoiety [11,12]. The prodrug approach is used to overcome pharmaceutical and/or pharmacokinetic limitations that are preventing the successful clinical use of the parent drugs. Moreover, by creating transporters' substrate mimicking prodrugs, improved or even targeted drug delivery resulting in enhanced clinical outcomes, can be achieved. This is often the most feasible method to retain the pharmacological potency of a potential drug candidate while changing its structural features into ones that can improve the drug delivery to the target site. Curiously, it has been estimated that approximately 10% of all worldwide approved drugs are currently prodrugs and 11% of new small molecular entities approved by the Food and Drug Administration (FDA) during the years 2008–2018 were prodrugs [13].

However, successful prodrug design and development requires a deeper understanding of the structure and transport mechanisms, which is a dynamic process with conformational changes [14,15]. To date, these so-called “moving barriers” are better understood due to the invasion of cryo-electron microscopic (cryo-EM) structural analyses of different conformations of these proteins. Moreover, improved computational power and more sophisticated methods, such as molecular dynamics simulations (MDS), have enabled us to put these conformational changes in order and describe the detailed mechanisms of the transport process [16,17]. In this comprehensive review, the expression and major functions of several known brain drug carriers belonging to the SLC family are presented. Moreover, their possible utilization for the brain (pro)drug delivery and intrabrain drug targeting are discussed. Most importantly, the effects of transport mechanisms aiding in (pro)drug design and the significance of the transporters' expression/function changes in specific diseases are considered.

## 2. Glutamate and Neutral Amino Acid Transporter Family (SLC1A)

The SLC1A family consists of seven members divided into two groups, namely, excitatory amino acid transporters (EAATs) and alanine, serine, and cystine transporters (ASCT1 and 2). EAATs are high-affinity L-glutamate (and L-aspartate) transporters, while ASCTs facilitate the transfer of several neutral amino acids across the cell membranes (Table 1). EAATs are mainly localized in the brain, particularly in glutamatergic synapses, where they have a fundamental role in maintaining normal glutamate homeostasis [18]. In addition to the abluminal side of the BBB, EAAT1 and 2 (*SLC1A3* and *SLC1A2*) are mainly localized in glial cells, while EAAT3 (*SLC1A1*) is mainly expressed in neurons (Figure 1a) [5,19–21]. Other members of this family, EAAT4 and 5 (*SLC1A6* and *SLC1A7*), are also found in

the Purkinje cells of the cerebellum and retina, respectively; however, their function in glutamate-gated chloride conductance (stronger with EAAT4–5 compared to EAAT1–3) is not well understood today [18]. L-Glutamate uptake via EAATs requires simultaneous cotransport of three Na<sup>+</sup> ions and countertransport of one K<sup>+</sup> ion across the cell membrane. The K<sup>+</sup> countertransport has been proposed to be an independent step of the L-glutamate translocation process.

**Table 1.** Tissue distribution, substrates, inhibitors, and expression/function modulators of EAAT1–3 and ASCT1–2.

Transporter	Gene Name	Tissue Distribution (Expression)	Substrates	Inhibitors	Expression Modulation/Transport Capacity Changes
EAAT1	<i>SLC1A3</i>	Brain: BBB (abluminal), astrocytes	L-Glu, L-Asp	L-Serine- <i>O</i> -sulfate (L-SOS), ( <i>R,S</i> )-2-amino-3-(1-hydroxy-1,2,3-triazol-5-yl)propionate, ( <i>4R</i> )-4-methylglutamate (4-Me-Glu), UCPH-101, UCPH-102	EAAT1 expression ↑ by adenylate cyclase-activating polypeptide (PACAP), transforming growth factor α (TGFα), epidermal growth factor (EGF), estrogen, tamoxifen, raloxifen
EAAT2	<i>SLC1A2</i>	Brain: BBB (abluminal), astrocytes	L-Glu, L-Asp	Dihydrokainic acid, WAY-213613	EAAT2 expression ↑ by adenylate cyclase-activating polypeptide (PACAP), transforming growth factor α (TGFα), epidermal growth factor (EGF), estrogen, tamoxifen, raloxifen, glucocorticoids, ceftriaxone
EAAT3	<i>SLC1A1</i>	Brain: neurons	L-Glu, L-Asp	2-(Furan-2-yl)-8-methyl-N-( <i>o</i> -tolyl)imidazo[1,2- <i>a</i> ]pyridin-3-amine	Amphetamine induces EAAT3 internalization
ASCT1	<i>SLC1A4</i>	Ubiquitous, Brain: luminal and abluminal membranes of BBB, neurons, and astrocytes	L-Ala, L-Ser, L-Cys, L-Gly, L-Met, L-Val, L-Leu, L-Ile, L-Thr, D-Ser; L-Glu (efflux)	Phenylglycine analogs	ASCT1 expression ↓ results in neurodevelopmental alterations
ASCT2	<i>SLC1A5</i>	Ubiquitous, Brain: BBB (abluminal), neurons, and astrocytes	L-Ala, L-Ser, L-Gly, L-Met, L-Val, L-Leu, L-Ile, L-Thr; L-Glu (efflux)	<i>O</i> -Benzyl-L-serine, <i>S</i> -benzyl-cysteine, phenylglycine analogs	ASCT2 expression ↑ in highly proliferative cells, such as cancer cells

↑ (arrow up) represents upregulation of the protein; ↓ (arrow down) represents downregulation of the protein.



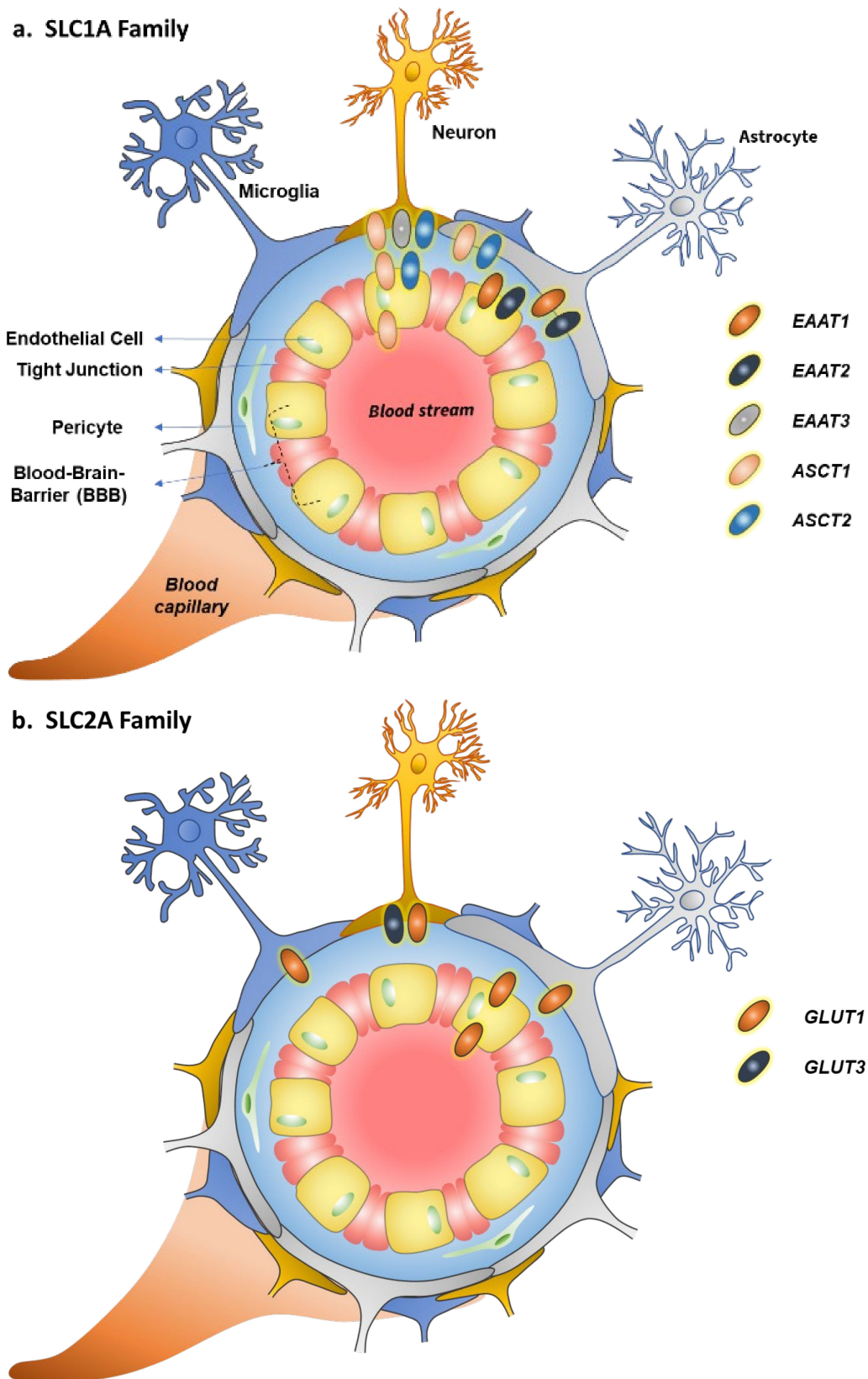


Figure 1. Cont.

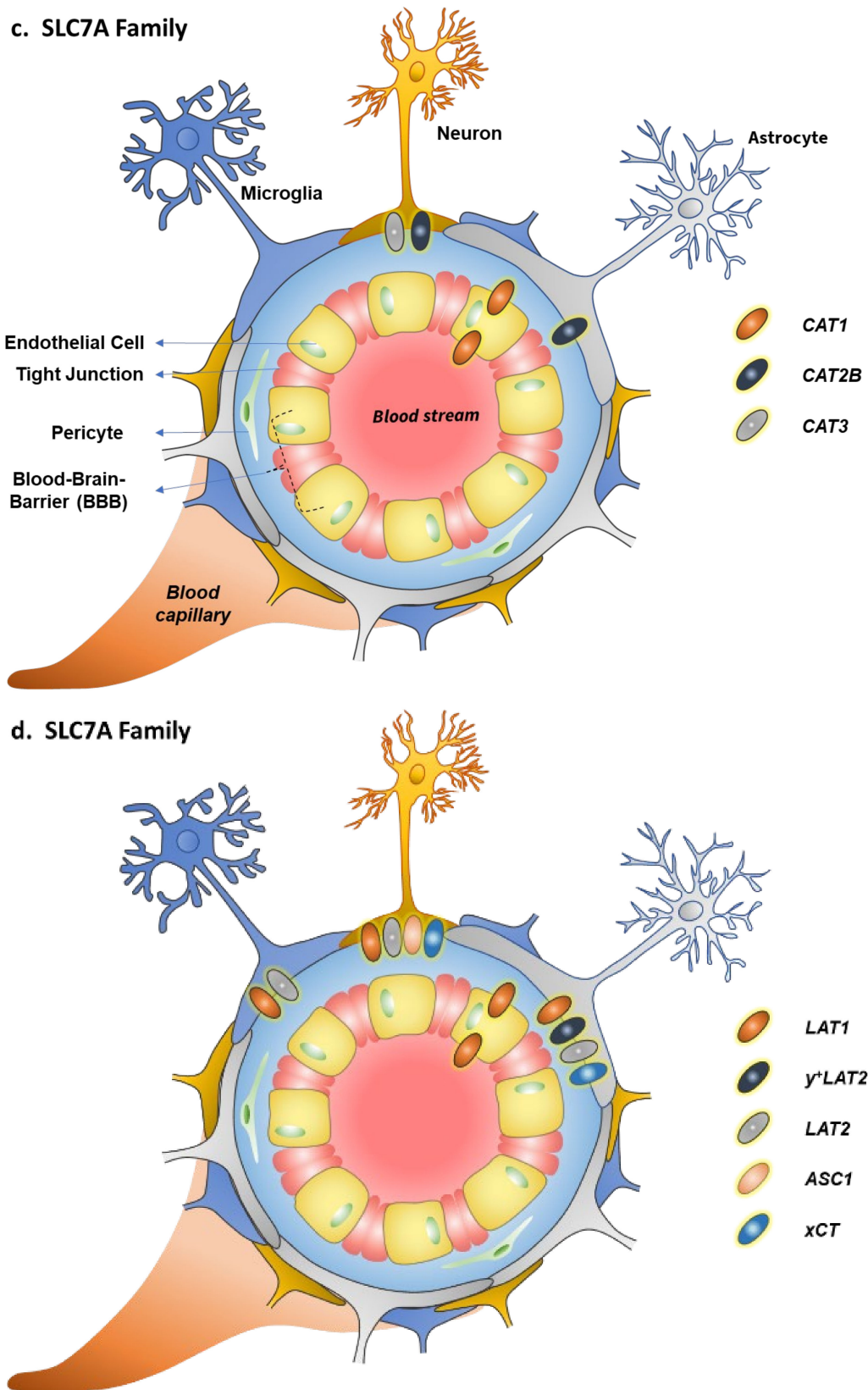


Figure 1. Cont.

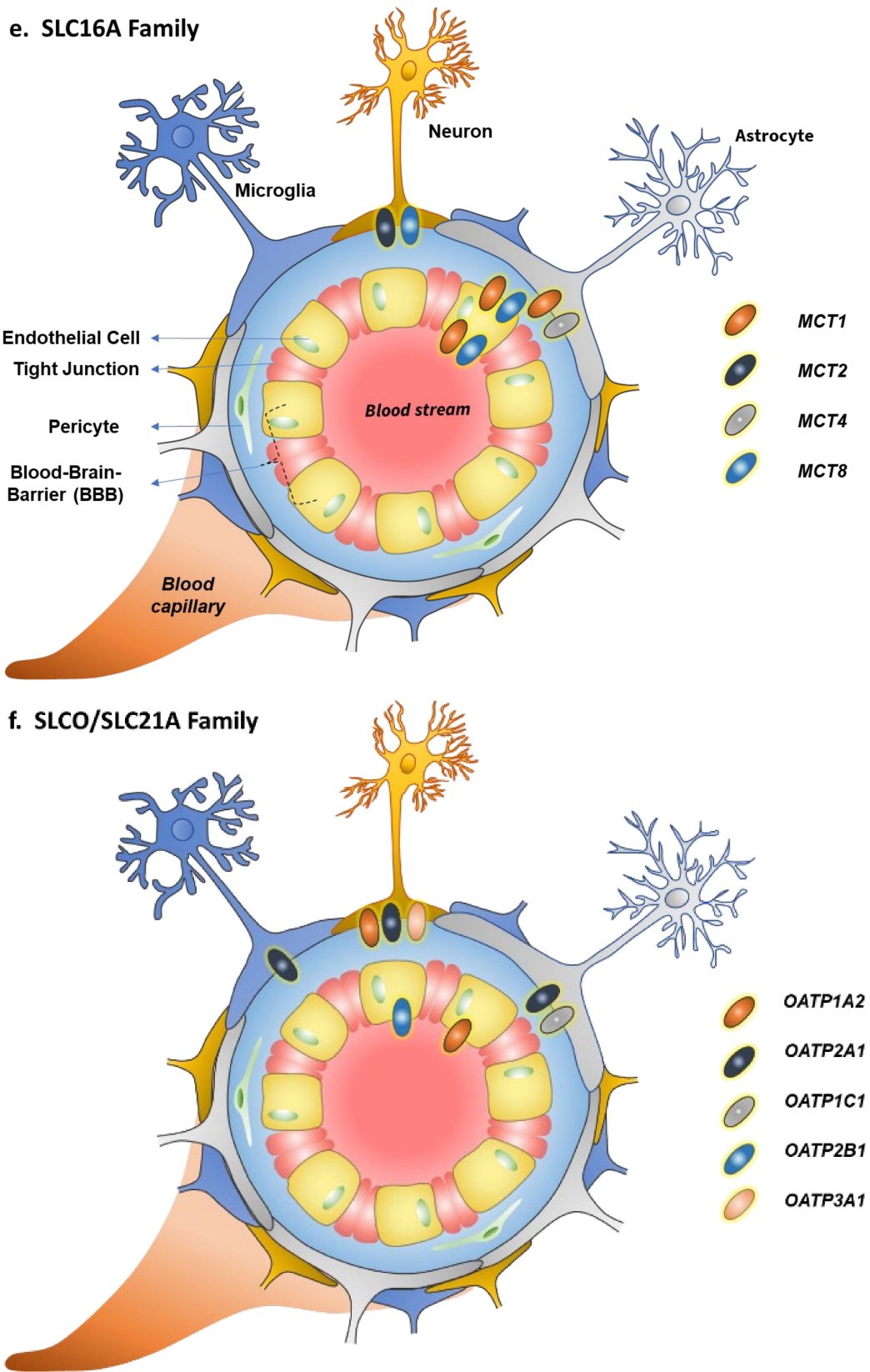
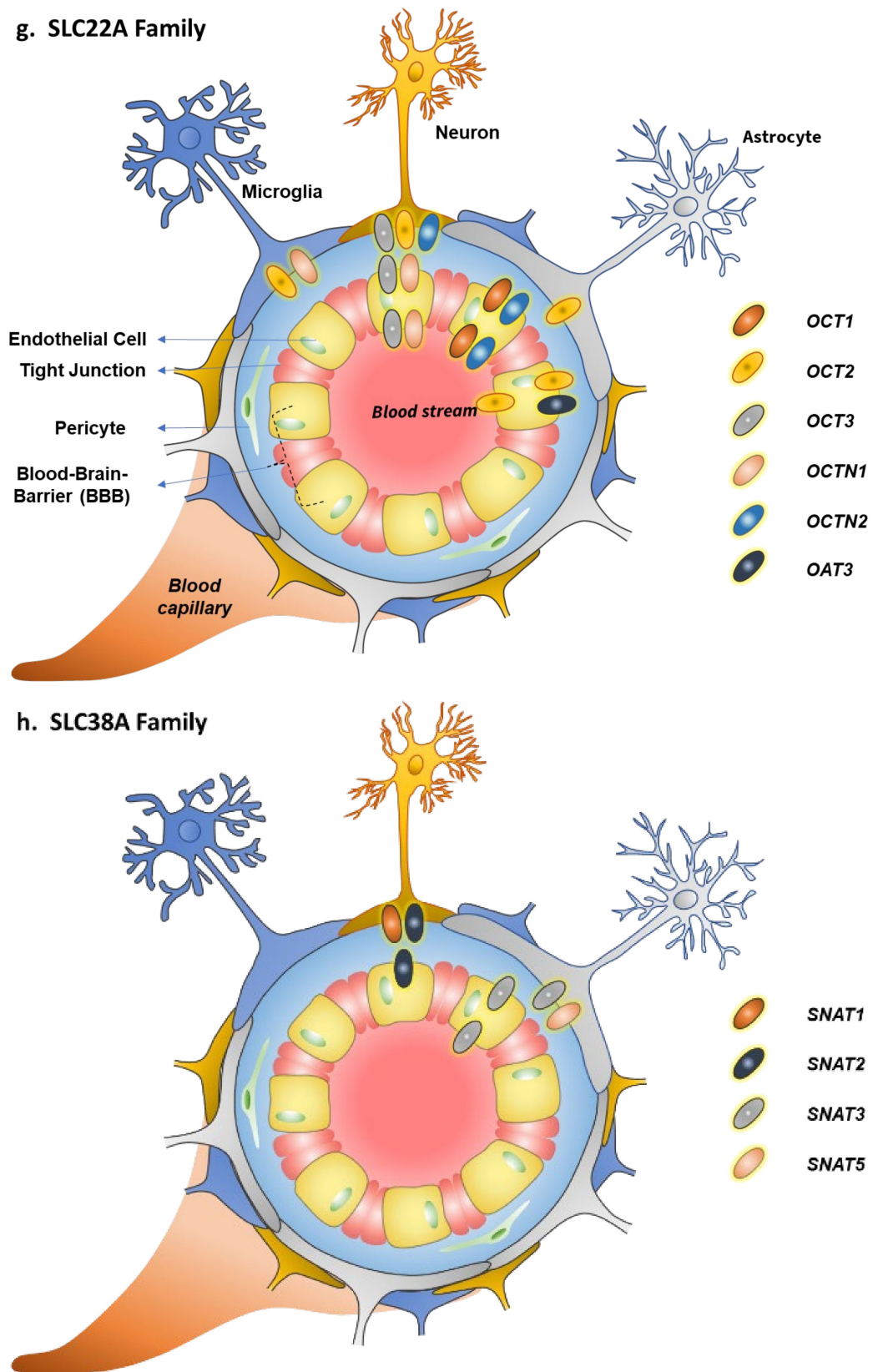
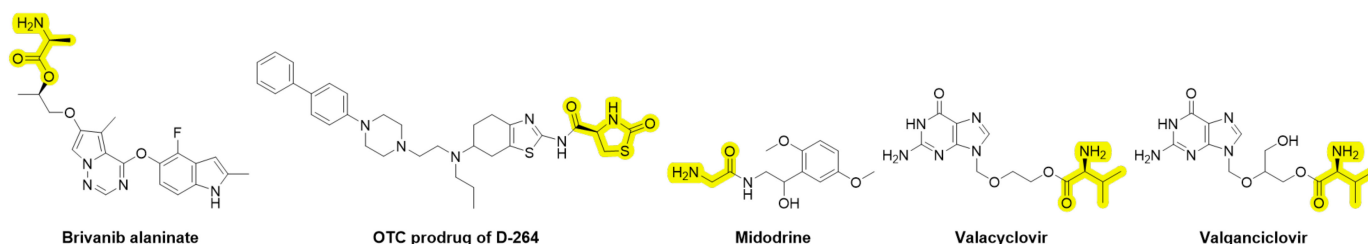


Figure 1. Cont.



**Figure 1.** Neuro-glia vascular units illustrating transporter expression/localization of (a) of SLC1A-, (b) SLC2A-, (c,d) SLC7A-, (e) SLC16A-, (f) SLC21A-, (g) SLC22A-, and (h) SLC38A-families in different cell types. The transporters are illustrated with round-shaped objects with different colors.

Due to the relevance of EAATs in excitatory neurotransmission, they are the key players in preventing neurons from glutamate excitotoxicity induced by pathological conditions and injuries such as neurological disorders and stroke [18,22]. Moreover, EAATs have been acknowledged to have a major role in antioxidant defense balance, since L-glutamate is a precursor for the endogenous antioxidant, tripeptide glutathione (GSH). Since the expression of EAATs in the brain is downregulated in many CNS diseases, including epilepsy, Alzheimer's disease (AD), Parkinson's disease (PD), Huntington's disease (HD), amyotrophic lateral sclerosis (ALS), and ischemic stroke to name a few, the endogenous regulation of their expression levels is extensively studied (Table 1). For example, EAAT1 and 2 are upregulated via adenylate cyclase-activating polypeptide (PACAP), transforming growth factor  $\alpha$  (TGF $\alpha$ ), epidermal growth factor (EGF), estrogen and estrogen receptor modulators tamoxifen and raloxifene [22]. Some drugs, such as  $\beta$ -lactam antibiotic ceftriaxone have also been reported to upregulate EAAT2 expression via stimulated nuclear translocation of p65 and initiation of the transcription nuclear factor  $\kappa$ B (NF- $\kappa$ B) [23,24], while amphetamine is known to modulate EAAT3 plasma membrane expression via induced endocytosis in dopamine neurons [25]. Although EAATs have not been mainly considered drug carriers, several selective inhibitors of EAAT1, EAAT2, and EAAT3 have been reported (Table 1) [26–28]. Furthermore, it has been speculated if L-cystine derivatives, like L-2-oxothiazolidine-4-carboxylic acid (OTC), could have interactions with EAATs and, thus, be used as selective promoieties to carry parent drugs in a prodrug form, like in the case of D-264, a neuroprotective agent that has been studied in the treatment of PD (Figure 2) [29].



**Figure 2.** Molecular structures of proposed SLC1A prodrugs with the promoieties highlighted with yellow color.

Although ASCT1 (*SLC1A4*) and ASCT2 (*SLC1A5*) are ubiquitously expressed throughout the body, they are also found in the brain; mainly in neurons and astrocytes, but also to some extent at the BBB (Table 1) [5,30–34]. Both ASCT1s mediate sodium- and pH-dependent transport of several neutral amino acid substrates, not only L-alanine, L-serine, and L-cystine (ASCT1 only), but also L-glycine, L-methionine, L-valine, L-leucine, L-isoleucine, and L-threonine. Bidirectionally, they can also mediate the efflux of glutamate (ASCT1) or glutamine (ASCT2) out of the cells. Mutations in ASCT1 have been associated with neurodevelopmental deficits, such as alterations in motor function, spatial learning, and affective behavior [35], while expression levels of ASCT2 have been reported to be increased in several cancers, including brain, colon, pancreas, liver, and lung cancer [36,37]. Therefore, ASCT2 has been widely studied as a pharmacological target to inhibit cancer cell growth and development, although ASCT2 expression modulation could also be utilized in neurodevelopmental disorders.

It would be tempting to think that amino acid conjugates, like those attached to L-alanine, would serve as potential ASCT-utilizing prodrugs. However, as proved by several prodrugs, including tumorigenic drug brivanib alaninate (BMS-582664; a selective dual inhibitor of vascular endothelial growth factor receptor 2 (VEGFR-2) and fibroblast growth factor receptor 1 (FGFR-1)), vasopressor/antihypotensive agent midodrine (ProAmatine<sup>®</sup>, Gutron<sup>®</sup>); a glycine prodrug of desglymidodrine (DMAE), a selective  $\alpha$ 1-receptor agonist, and antiviral agents valacyclovir (Valtrex<sup>®</sup>) and valganciclovir (Valcyte<sup>®</sup>)

(Figure 2), their oral absorption is mediated via either intestinal proton-coupled peptide transporter 1 (PepT1, *SLC15A1*) or sodium-dependent neutral amino acid transporter ( $ATB^{0,+}$ , *SLC6A14*) [38]. However, the interactions and brain exposure via ASCTs of these compounds have not been well studied in the past, mainly since all these prodrugs are relatively rapidly bioconverted during the first-pass metabolism by ubiquitous hydrolyzing enzymes. Moreover, all these exemplary prodrugs have been attached to the amino acids via the carboxylic acid group, which may be required to be left untouched and the parent drugs should be attached to the side chain of the amino acids to attain sufficient interactions with ASCTs. Therefore, more detailed structural studies are warranted to develop successful brain-delivered ASCT-utilizing compounds.

ASCT1 and 2 share 58% sequence identity and together with EAATs the whole family shares only 21% sequence identity [39]. Both EAATs and ASCTs are formed from eight transmembrane helices, and their amino acid transport mechanism is well understood. Curiously, all SLC1A family members function with a one-gate elevator mechanism, in which the substrate is occluded in the transport domain that subsequently performs a large movement from the extracellular site to the intracellular site (Figure 3). The binding sites of ASCT1 and 2 are relatively well known today and they differ from each other [40,41]. For example, ASCT1 recognizes also D-amino acids and it has been proposed to have a major role in the brain exposure of D-serine, *N*-methyl-D-aspartate (NMDA) receptor co-agonist (Table 1), thereby, remarkably affecting the brain disorders, such as schizophrenia [35,42]. Although ASCT1 has not been utilized as a drug carrier for a rational drug design, a lot of interest has been laid in ASCT2, particularly, in the development of selective ASCT2 inhibitors, as mentioned above. From these, *O*-benzyl-L-serine and *S*-benzyl-cysteine are well-known examples [43]. Later on, other amino acid analogs, such as proline-, serine-, and glutamine-mimetics have also been developed as ASCT2-selective inhibitors [44–46]. Both ASCT1 and 2 have also been noticed to be inhibited by phenylglycine analogs [42]. However, as with ASCT1, it would be great to see in the future if ASCT2 could be utilized more extensively as a (pro)drug carrier, e.g., in cancer-targeted applications. Nevertheless, the elevator mechanisms may be the determinant of the drug delivery efficiency and exclude the transport of larger compounds. Hence, other SLCs with different mechanisms may be more feasible (pro)drug carriers for brain-targeted purposes than the presented SLC1A-family members.

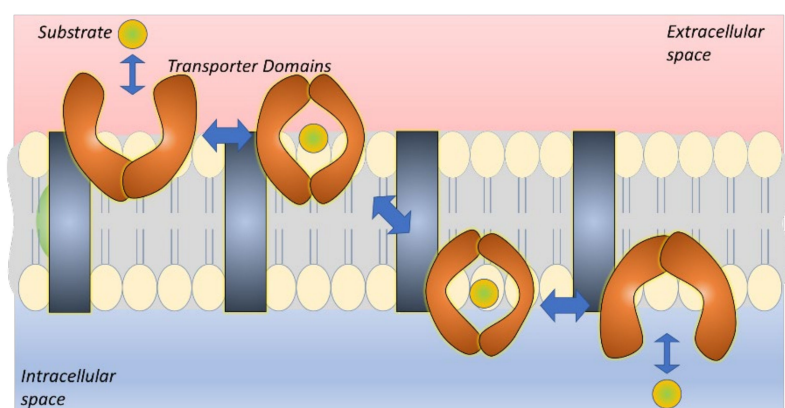


**Figure 3.** The elevator-type transport mechanism of EAATs and ASCTs. The substrate (green ball-shape) is bound to the transporter on the extracellular side of the plasma membrane. The conformational movements of the transporting domains (orange banana-shapes) close the “gate”, which is followed by vertical translocation of this complex in relation to the static domain (blue). Finally, the second conformational movement opens the “gate” and releases the substrate into the cytosolic side.

### 3. Glucose Transporter Family (SLC2A)

Glucose transporters provide basal glucose levels for energy production in many tissues and cell types, from red blood cells, muscles, and adipose tissue to the brain and neurons. The main glucose transporters in the brain are glucose transporter 1 (GLUT1, *SLC2A1*) and 3 (GLUT3, *SLC2A3*) (Table 2) [5,47]. Ubiquitously localized GLUT1 has been found at the BBB in heavily glycosylated form (55 kDa), both at the luminal and abluminal sides of the endothelial cells. A less glycosylated form (45 kDa) is in turn found in the astrocytes and to a lesser extent also in the neurons and microglia (Figure 1b). Contrarily, GLUT3 has been historically called “a neuronal glucose transporter”, as it is almost exclusively expressed in the neurons. In addition, among the classified 14 glucose transporters, GLUT2 and GLUT4–8 have been identified from the brain, either from the BBB or parenchymal cells, although with much smaller expression levels than GLUT1 and 3 [47]. Moreover, their physiological roles in the brain are not yet fully understood.

**Table 2.** Tissue distribution, substrates, inhibitors, and expression/function modulators of GLUT1 and GLUT3.

Transporter	Gene Name	Tissue Distribution (Expression)	Substrates	Inhibitors	Expression Modulation/Transport Capacity Changes
GLUT1	<i>SLC2A1</i>	Ubiquitous, Brain: luminal and abluminal membranes of BBB, astrocytes, (neurons, microglia)	Glucose, galactose, mannose, 2-deoxy-D-glucose, 2-deoxy-2-[ <sup>18</sup> F]-D-glucose, glucosamine and dehydroascorbic acid (vitamin C)	Cytochalasin B, forskolin, phloretin and other flavonoids, WZB117, BAY-876, STF-31, fasentin, apigenin	GLUT1 expression ↑ in numerous cancers and ischemia with poor survival of patients: via hypoxia, p53, PI3K-Akt pathways, Ras or c-Myc oncogenes; GLUT1 expression ↓ in Alzheimer’s disease and GLUT1 deficiency syndrome (G1DS) due to mutations
GLUT3	<i>SLC2A3</i>	Brain: neurons	D-Glucose, D-galactose, D-mannose, D-xylose, 2-deoxy-D-glucose	Cytochalasin B, forskolin, phloretin, quercetin and other flavonoids, glycogen synthase kinase-3 (GSK-3) inhibitors	GLUT3 expression ↑ in various cancers with poor survival of patients: via hypoxia, p53, PI3K-Akt pathway

↑ (arrow up) represents upregulation of the protein; ↓ (arrow down) represents downregulation of the protein.

The preferred substrates for both GLUT1 and GLUT3 are hexoses and pentoses, in pyranose conformation, such as D-glucose, D-galactose, and D-mannose (Table 2). They also carry glucose analogs such as 2-deoxy-D-glucose, and their transport is described as high affinity–high capacity. GLUT1 transports specifically glucosamine and dehydroascorbic acid (vitamin C), as well as 2-deoxy-2-[<sup>18</sup>F]-D-glucose that has been used as a radiolabeled marker in positron emission tomography (PET) for the diagnosis and monitoring of different diseases [48]. GLUT1/3-mediated transport is inhibited by cytochalasin B, forskolin, phloretin, and other flavonoids. GLUT1 can also be selectively inhibited by WZB117, BAY-876, STF-31, fasentin, apigenin, while glycogen synthase kinase-3 (GSK-3) inhibitors have been reported to selectively inhibit GLUT3 [49].

Overexpressions of GLUT1 and 3 have been found with a variety of human carcinomas and this phenomenon has been associated with aggressiveness and poor survival rate (Table 2) [50–52]. The phosphatidylinositol 3-kinase (PI3K)-Akt pathway, hypoxia-inducible factor-1 (HIF-1), and p53 are known to upregulate both GLUT1 and 3 on a transcriptional level, while Ras and c-Myc oncogenes have been associated only to GLUT1 upregulation [52]. In addition, hypoglycemia (low blood glucose caused by starvation,

liver/kidney diseases, or infections) and hypoxic condition related to cerebral ischemia can also upregulate brain GLUT1 and GLUT3 expressions [47]. In turn, in hyperglycemia (high blood glucose due to untreated diabetes or pancreatitis) as well as at the early onset of AD have been demonstrated to downregulate the GLUT1 and GLUT3 levels in the brain. Moreover, mutations of GLUT1 that are inherited in an autosomal dominant or autosomal recessive manner causes GLUT1 deficiency syndrome (G1DS) with severe effects on neural functions and brain development. Curiously, several drugs and alcohol consumption have been associated with brain expression or activity modulation of GLUT1/3. Therefore, drug treatments that are related to these GLUTs or utilize GLUTs for their delivery should be carefully and profoundly evaluated during the preclinical phase. However, GLUT expression modulation can also be an important therapeutic target, e.g., in AD, GLUT1/3 upregulation may prevent the disease progression, and in stroke, GLUT1/3 upregulating treatment may have the potential to improve the final outcome faster. As a cancer treatment, selective GLUT1/3 downregulation could be used to inhibit increased glycolysis and, thus, cell growth.

From all glucose transporters, GLUT1 has been mostly utilized for brain-targeted drug delivery by a prodrug approach and the first brain-targeted GLUT1-utilizing prodrugs were reported already 20 years ago. These include, for example,  $\beta$ -D-glucosyl and  $\beta$ -D-galactosyl derivatives of 7-chlorokynurenic acid to improve NMDA receptor-mediated seizures, and  $\beta$ -D-glucosyl derivatives of dopamine and L-dopa to improve reserpine- or morphine-induced locomotion (Figure 4) [53–55]. In addition,  $\beta$ -D-glucose has also been attached to alkylating agent, chlorambucil to improve delivery into brain tumors, and to neuroactive peptide, enkephalin to improve analgesic effects [56,57]. Later on, the  $\beta$ -D-glucosyl promoiety has also been used with non-steroidal anti-inflammatory drugs (NSAIDs), and at least GLUT1-mediated brain uptake of ketoprofen and indomethacin prodrugs has been reported [58]. However, the benefits of the approach to improve clinical outcomes have remained unclear so far. Interestingly, novel brain-targeted GLUT1-utilizing prodrugs have not been reported recently, despite their early discovery. Instead, the approach has been used more extensively for cancer-targeting purposes.

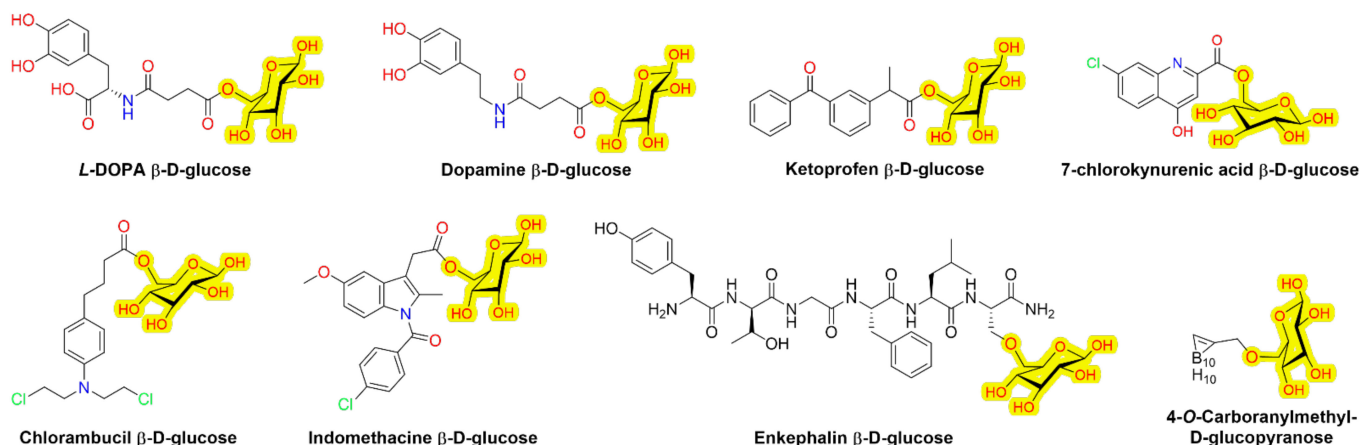


**Figure 4.** Molecular structures of GLUT1-utilizing prodrugs with promoieties highlighted with yellow color.

Notably, most of the reported glyco-prodrugs are esters and relatively unstable during the first-pass metabolism, which most likely limits their use for brain-targeting purposes. Many of the glucose, galactose, or glucuronic acid prodrugs are bioconverted by either  $\beta$ -glucosidase,  $\beta$ -galactosidase, or  $\beta$ -glucuronidase, respectively. These enzymes are relatively ubiquitously expressed in peripheral tissues as well as in the brain, and curiously, they are also over-expressed in many different types of cancer cells [59,60]. There are also a few examples of more stable amide and ether prodrug bond-containing glyco-derivatives



(chlorambucil and enkephalin derivatives) [56,57]. However, these compounds may be enzymatically too stable in the brain and, thus, they may require to be active on their own, without releasing the active parent drug. Thus, utilizing GLUTs for brain-targeting purposes may be more suitable for compounds that are not prodrugs and, therefore, do not require the bioconversion step. A great example is brain tumor-targeted boron ( $^{10}\text{B}$ ) compounds (Figure 4) used in the boron neutron capture therapy (BNCT), in which a low energy thermal neutron beam initiates a fission reaction of  $^{10}\text{B}$  that is selectively accumulated into the cancer cells via GLUT1. This produces high-energy  $\alpha$ -particles ( $^4\text{He}$ ) and  $^7\text{Li}$  atoms that ultimately destroy the cancer cells without affecting non-boron-containing healthy cells [61–63].

The glucose transporters are sodium-independent bidirectional and they commonly have 12 putative transmembrane-spanning  $\alpha$ -helices and a single site for *N*-linked glycosylation. The transport mechanism of GLUT1 and GLUT3 is well known and they follow a model called a “rocker switch”, This mechanism has four distinct states; (1) outward-open state, in which the ligand binds to the transporter causing the outer gate to close, (2) outward-occluded state, in which a rocker-switch takes place forming (3) inward-occluded state that is followed by the opening of the inner gate, and finally (4) inward-open state, from which the ligand is released (Figure 5) [14,15,64]. Today, it is well known which interactions can result in conformational changes in GLUT1 and, thus, induce the translocation of glucose derivatives in the cavity [65–67]. Thus, molecular modeling can be a really helpful tool for designing GLUT1 substrates that are truly transported through the protein cavity and not only bind to the protein on the plasma membrane. However, it would be great to see in the future if this is applicable also for GLUT3 and if neuron-targeted drug delivery can be achieved by utilizing GLUT3.

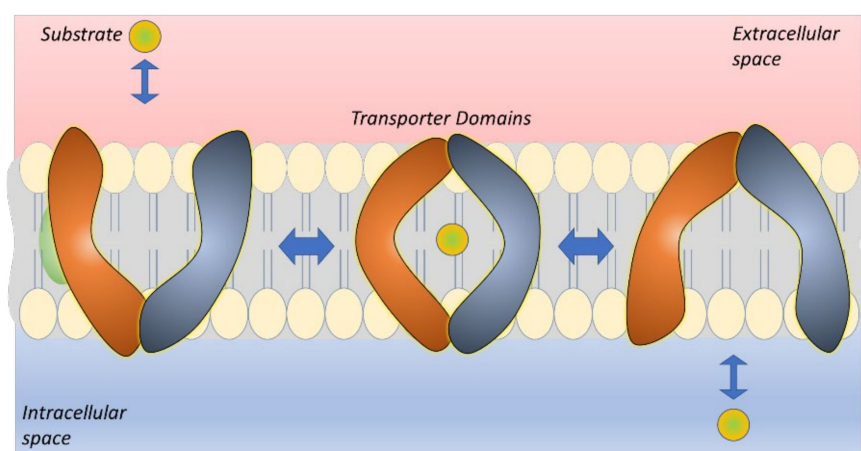


**Figure 5.** The rocker switch transport mechanism of GLUT1 and 3. The substrate (green ball-shape) is bound to the V-shaped transporter (outward-open state) on the extracellular side of the plasma membrane. The conformational movements of the transporter domains (orange and blue banana-shapes) trigger outward-occluded and inward-occluded states (only one state is showing). Finally, the substrate is released from V-shaped inward-open conformation to the cytosolic side.

#### 4. Cationic and Neutral Amino Acid Transporter Family (SLC7A)

The SLC7A family contains cationic amino acid transporters (CATs) and heterodimeric amino acid transporters (HATs). CATs are relatively ubiquitously localized in the body; however, in the brain CAT1 (*SLC7A1*) is mainly found at the luminal and abluminal sides of the BBB [5,68], while, CAT3 (*SLC7A3*) has been identified as a neuron-specific transporter (Table 3, Figure 1c) [69]. CAT2 (*SLC7A2*) has been found in two splicing variants, CAT2A, low affinity, not localized in the brain, and CAT2B, high affinity, localized in neurons and oligodendrocytes and induced in astrocytes [70,71]. In addition to CAT1–3, CAT4 (*SLC7A4*) and an orphan *SLC7A14* have been identified from the brain, although their functions and roles as carriers are not well characterized yet.

**Table 3.** Tissue distribution, substrates, inhibitors, and expression/function modulators of CAT1–3 and LAT1–2, y+LAT2, Asc-1, and xCT.

Transporter	Gene Name	Tissue Distribution (Expression)	Substrates	Inhibitors	Expression Modulation/Transport Capacity Changes
CAT1	<i>SLC7A1</i>	Ubiquitous, Brain: luminal and abluminal membranes of BBB	L-Arg, L-Lys, and L-Orn	Not known	CAT1 expression ↓ via NMDA receptor activation; CAT1 expression ↑ in colorectal and breast cancers, hepatitis B virus-induced hepatocellular carcinoma, and lymphocytic leukemia
CAT2B	<i>SLC7A2</i>	Brain: neurons, oligo-dendrocytes, induced astrocytes	L-Arg, L-Lys, and L-Orn	Not known	CAT2B expression ↑ in different breast cancer cell lines
CAT3	<i>SLC7A3</i>	Placenta, Brain: neurons	L-Arg, L-Lys, and L-Orn	Not known	CAT3 expression ↓ via NMDA receptor activation:
LAT1	<i>SLC7A5</i>	Widely distributed, Brain: luminal and abluminal membranes of BBB, neurons, astrocytes, microglia	L-Leu, L-Phe, L-Tyr, L-Trp, L-His, L-Met, L-Ile, L-Val; triiodothyronine (T3) and thyroxine (T4), L-dopa, melphalan, baclofen, gabapentin, pregabalin	JPH203 (unselective)	LAT1 expression ↑ in numerous cancers with poor survival of patients: via hypoxia/HIF-2α, c-Myc or RAS-MEK-ERK pathways
y+LAT2	<i>SLC7A6</i>	Ubiquitous, Brain: astrocytes	L-Arg, L-Leu, L-glu (efflux)	No specific inhibitor reported	y+LAT2 expression ↑ in the presence of NH <sub>4</sub> <sup>+</sup> : via NF-κB pathway
LAT2	<i>SLC7A8</i>	Ubiquitous, Brain: microglia > neurons > astrocytes	L-Tyr, L-Phe, L-Trp, L-Thr, L-Asn, L-Ile, L-Cys, L-Ser, L-Leu, L-Val, L-Gln, L-His, L-Ala, L-Met; triiodothyronine (T3), 3,3'-diiodothyronine	No specific inhibitor reported	LAT2 expression ↑ in highly proliferative cells, such as cancer cells
Asc-1	<i>SLC7A10</i>	Adipose tissue, Brain: neurons	L-glycine, L-alanine, D-/L-serine, L-threonine, L-cysteine, α-aminobutyric acid, and β-alanine	Several structures have been proposed, requires more studies	Asc-1 downregulation associated with tremors, ataxia, and seizures
xCT	<i>SLC7A11</i>	Macrophages, Brain: astrocytes, neurons	Cystine (extracellular)/glutamate (intracellular) exchange	S-4-carboxy-3-hydroxy-phenylglycine, erastatin, sorafenib, sulfasalazine	xCT is upregulated in several cancers and its dysfunction is associated with epileptic seizures, neurodegeneration, and brain edema

↑ (arrow up) represents upregulation of the protein; ↓ (arrow down) represents downregulation of the protein.

According to their name, the primary substrates of CATs are cationic amino acids, such as L-arginine, L-lysine, and L-ornithine, which are transported in a proton-coupled, sodium-independent manner (Table 3). Since L-arginine is a precursor for both L-ornithine and nitric oxide (NO) synthesis, CATs have a crucial role in regulating different homeostatic and proliferating actions in the brain (and in the peripheral tissues) [72]. Curiously, it has been reported that the expression of CATs is downregulated by NMDA receptor activation and they regulate neuronal processes via the mammalian target of rapamycin (mTOR) pathway [73]. In turn, CAT1 has been found to promote cell growth, proliferation, and metastasis, and it is upregulated in colorectal and breast cancers as well as in hepatitis B virus-induced hepatocellular carcinoma and lymphocytic leukemia [74–77]. In addition, CAT2A and 2B have been detected in different breast cancer cell lines.

The transport mechanism of CATs has not yet been resolved; however, some mechanistic insights and differences to HATs have been recognized [78]. To date, CATs have been recognized neither as potential drug carriers nor drug targets, and therefore, rationally developed substrates or inhibitors have not been reported yet (Table 3). However, CAT1 could be harnessed for increased brain drug delivery and together with CAT3-utilizing compounds, neuronal targeting could be achieved. As an example, L-arginine, L-lysine, and L-ornithine could be utilized as promoieties in the prodrug design. However, more details on the interactions between these promoieties and CATs are required in order to attach the parent drug to the correct functional group of the amino acid and, thus, to prepare successful prodrug candidates.

HATs consist of two subunits: a heavy subunit from the SLC3A family and a light subunit from the SLC7A family that are linked together via a disulfide bond. Two members of SLC3A family are rBAT (*SLC3A1*) and 4F2hc (*SLC3A2*) and these heavy subunits are N-glycosylated [79]. Their primary role is more regulatory, e.g., they traffic the holotransporter to the plasma membrane. However, recently there has been some evidence that heavy subunits may also participate in the ligand recognition process. Furthermore, 4F2hc has been found to mediate integrin-dependent tumorigenesis, and therefore, it is also overexpressed in some types of cancers [80,81]. Contrarily, several mutations in rBAT are found to affect the b<sup>0+</sup> transport, causing cystinuria. Nevertheless, the light subunits catalyze the transport function of HATs. L-Type amino acid transporter 1 (LAT1; *SLC7A5*) is probably the most studied transporter of the SLC7A-family in brain delivery applications, although other members, including  $\gamma$ +L-type amino acid transporter 2 ( $\gamma$ +LAT2; *SLC7A6*), L-type amino acid transporter 2 (LAT2; *SLC7A8*), alanine–serine–cysteine transporter 1 (Asc-1; *SLC7A10*), and cystine/glutamate transporter (xCT, *SLC7A11*), are also expressed in the brain and could be utilized in the brain drug delivery (Table 3).

LAT1 coupled to 4F2hc is a sodium- and pH-independent transporter carrying large, neutral, aromatic, or branched L-amino acids (L-leucine, L-phenylalanine, L-tyrosine, L-tryptophan, L-histidine, L-methionine, and L-valine) into the cells [82,83]. LAT1 is distributed throughout the body, and it is highly expressed in tissues that require a high amino acid supply, such as the brain, placenta, and bone marrow [84,85]. In the brain, LAT1 is localized not only at the luminal and abluminal membranes of BBB, but also in the parenchymal cells, neurons astrocytes, and microglia (Figure 1d) [5,86,87]. Moreover, LAT1 is upregulated in a variety of cancers and their metastases [88–90]. High LAT1 expression has been associated with significantly shorter survival of patients and poorer prognosis of breast and prostate cancers [91,92], and with metastasis of different cancer cell types [93]. The regulation mechanisms are still not well understood; however, hypoxia and HIF-2 $\alpha$ , c-MYC, and RAS-MEK-ERK pathways have been proposed to be involved [90]. Curiously, mutations of LAT1 at the BBB have been associated with decreased LAT1 function in autism spectrum disorders (ASD) [94]. Thus, LAT1 expression modulation could be a potential target in neurodevelopmental diseases, such as ASD.

LAT1 catalyzes the transport of the thyroid hormones triiodothyronine (T3) and thyroxine (T4), but also amino-acid-mimicking drugs, such as the antiparkinsonian drug L-dopa, anti-cancer agent melphalan, muscle relaxer baclofen, and anticonvulsants gabapentin and

pregabalin (Table 3). Due to the intensive research, the binding and translocation of ligands through LAT1 is relatively well known today [95–98]. The definite structural requirements include the presence of amino and carboxylic acid functional groups and a large neutral or aromatic side group. It has been long thought that LAT1 is stereoselective, preferring only L-amino acids; however, recently, it has been proven that LAT1 can also carry some D-enantiomers [99,100]. LAT1 also operates with a rocking-bundle mechanism, in which the “bundle domain” goes through conformational changes from the outward-open state to the inward-open state (Figure 6) [14,15,101]. It is highly likely that this transport mechanism tolerates larger compounds than, e.g., the elevator-type mechanism used by EAATs and ASCTs.

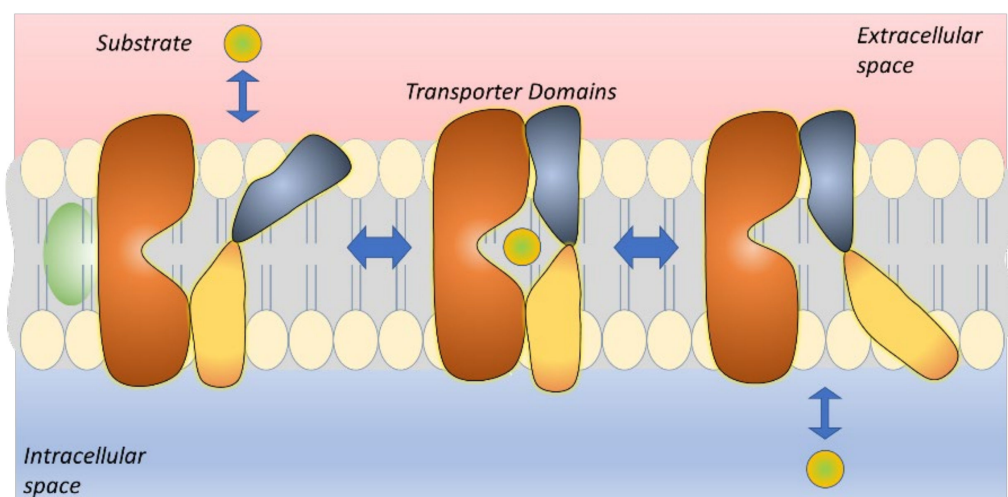


**Figure 6.** The rocking bundle transport mechanism of LAT1. The substrate (green ball-shape) is bound to the K-shaped transporter (outward-open state) on the extracellular side of the plasma membrane. The subsequent conformational movements of the transporter domains (first blue and then yellow shapes) result in the release of the substrate at the cytosolic side (inward-open state).

Utilization of LAT1 for brain drug delivery has been proven not only by serendipitously discovered clinically used LAT1-substrates mentioned above, but also by rationally designed prodrugs, including drugs such as anti-inflammatories, antioxidants, antiepileptics, antiparkinsonians, immunosuppressants, and neuroprotective NMDA receptor antagonists (Figure 7) [102–108]. The greatest challenge with brain-targeted LAT1-utilizing prodrugs is to achieve the balance in bioconversion; not to have a too extensive premature release of the parent drug before crossing the BBB and, on the other hand, to gain an efficient bioconversion rate in the brain. The lack of knowledge on brain-specific prodrug bioconverting enzymes seems to be the greatest hurdle today; however, it is still an attainable goal. The crucial role of LAT1 in cancer has also increased the interest in developing LAT1-inhibitors as potential anticancer agents, such as JPH203, which has already advanced into clinical trials in Japan to treat solid tumors [109].

LAT2 and  $\gamma$ -LAT2 have broader tissue distribution than LAT1, which makes brain-targeting of drugs more challenging (Table 3). LAT2 mediates sodium-independent efflux of many neutral amino acids (L-enantiomers of tyrosine, phenylalanine, tryptophan, threonine, asparagine, isoleucine, cysteine, serine, leucine, valine, glutamine, histidine, alanine, and methionine), while  $\gamma$ -LAT2 mainly carries sodium-dependent exchange of L-arginine or L-leucine to L-glutamine (and  $\text{Na}^+$ ) [110–112]. LAT2 is also an exchanger with lower intracellular substrate affinities compared to extracellular substrate affinities, and similarly to LAT1, it functions with 1:1 stoichiometry [113]. LAT2 expression seems to be highest in microglia, although it is also expressed to some extent in the neurons and astrocytes (Figure 1d) [114]. Thus, this intra-brain selective expression could be utilized in microglia-targeted drug delivery of compounds. However, less is known about  $\gamma$ -LAT2-

specific localization in the brain, it has been reported to be expressed in the astrocytes and upregulated in the presence of ammonia ( $\text{NH}_4^+$ ) [115,116].

#### LAT1-Utilizing Prodrugs of

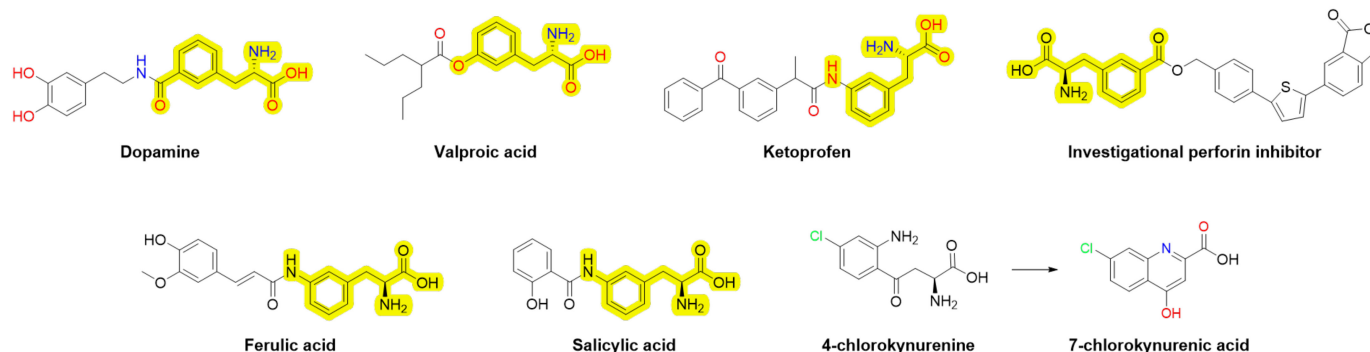


**Figure 7.** Molecular structures of prodrugs that can utilize LAT1 with promoieties highlighted with yellow color, excluding 4-chlorokynurenine, which undergoes internal cyclization to produce 7-chlorokynurenic acid.

Curiously, LAT2 can also carry thyroid hormones (T3 and 3,3'-diiodothyronine [117,118], the neurotransmitter precursor L-DOPA [119,120], although contribution to the overall transport of these compounds has been estimated to be minor compared to LAT1 and monocarboxylate transporters (MCT8/10). To date, no specific LAT2-inhibitor has been reported. LAT2 stimulates the mTOR pathway similarly to LAT1 and, thus, its overexpression has been reported in different types of cancers [120,121]. The transport mechanism of LAT2 and  $\gamma$ -LAT2 resembles LAT1 and differs only with acidic and non-acidic residues in the binding pocket, which explains the substrate preferences of each transporter [122]. Thus, recent advances in structural and computational biology have enabled today's successful design of LAT2- and  $\gamma$ -LAT2-utilizing compounds. However, their minor expression in the brain compared to other transporters as well as wider distribution elsewhere in the body makes them less attractive carriers for brain-targeting purposes.

Asc-1 mediates a sodium-independent uptake of small amino acids, such as L-glycine, L-alanine, L-serine, L-threonine, L-cysteine,  $\alpha$ -aminobutyric acid, and  $\beta$ -alanine, but it also carries D-isomers, such as D-serine [123,124]. Although Asc-1 facilitates the diffusion of small amino acids, it primarily functions as an exchanger (Table 3). Similarly, xCT is a sodium-independent exchanger of extracellular anionic cystine and intracellular glutamate (with a 1:1 stoichiometry) [125,126]. Asc-1 is a neuronal transporter and due to its ability to carry L-glycine and D-serine in synapses, it has been considered a regulator of NMDA receptors [127,128]. Curiously, Asc-1 is mainly localized in those brain areas that are responsible for cognitive functions. Moreover, a lack of Acs-1 has been reported to cause tremors, ataxia, and seizures [129]. xCT has, in turn, been found in the brain from astrocytes and neurons, in addition to macrophages [130,131].

xCT functions together with EAATs, it counter-carries the intracellular L-glutamine that EAATs have carried into the cells [132]. Similarly, it functions together with cysteine transporters, such as ASCTs, and counterbalances intracellular L-cysteine levels that xCT has provided to the cells. Therefore, xCT has a major role in health and diseases, e.g., downregulation of xCT impairs cell growth and survival. Furthermore, xCT mediates the protection of oxidative stress (cystine is a source of reduced glutathione, an endogenous antioxidant) and, therefore, it is upregulated in several different cancers [133,134]. Due to its role in both excitotoxicity (L-glutamine export) and oxidative stress (L-cysteine import), changes in xCT expression (both upregulation and downregulation) can have deleterious effects in the brain and, therefore, results in animal models of epilepsy and neurodegenerative diseases has been controversial [132]. Although several inhibitors have been developed for both of these transporters [135,136], less is known about the possibility

of utilizing Acs-1 and xCT as drug carriers in the brain. Lack or minor expression of these transporters at the BBB, is the first challenge; however, their selective brain localization may offer some advantages in the intrabrain targeting. Therefore, more studies are definitely needed on these transporters in the future.

### 5. Monocarboxylate Transporter Family (SLC16A)

Monocarboxylate transporters (MCTs), members of the SLC16A family, facilitate rapid proton-dependent transport of monocarboxylates, such as lactate, pyruvate, and other metabolic products and energy substances in their anionic forms under physiological conditions [137]. The transportation across the cell membranes by MCTs is an electroneutral co-transport of monocarboxylates along with protons with a stoichiometric ratio of 1:1. The most important transporters of this family in the brain are MCT1 (*SLC16A1*), MCT2 (*SLC16A7*), MCT4 (*SLC16A3*), and MCT8 (*SLC16A2*) (Table 4), although other orphan MCTs, including MCT6 (*SLC16A5*), MCT7 (*SLC16A6*), MCT9 (*SLC16A9*), and MCT14 (*SLC16A14*) have also been found in the brain [138]. Ubiquitous MCT1 is expressed, e.g., in the epithelia of the small intestine and colon, but also in the muscles and particularly on the luminal and abluminal membranes of brain capillary endothelial cells [5,139]. In the brain, MCT1 is also expressed in the astrocytes of gray and white matter (Figure 1e) [140].

At the BBB, MCT1 has been proposed to be functioning bidirectionally to maintain brain homeostasis [141]. The efflux of compounds out of the brain back to the systemic circulation by MCT1 may also limit the brain drug disposition, like has been proposed in the case of probenecid and 6-mercaptopurine (Table 4) [142,143]. Curiously, a controlled substance  $\gamma$ -hydroxy butyric acid (GHB) that has been used clinically to treat insomnia, cataplexy, and narcolepsy is also an MCT1-substrate. Its CNS-related side effects, including respiratory depression, seizure, and loss of consciousness that may even result in coma and death, are predominantly arising from the variable MCT1-mediated transport of GHB across the BBB [144]. 4-Phenylbutyrate (4-PBA), a salt of an aromatic short-chain fatty acid and potential neuroprotective agent against excitotoxicity, oxidative stress, endoplasmic reticulum (ER) stress, apoptosis, and inflammation in several neurodegenerative disease models, such as PD, AD, and HD, has also been found to utilize MCT1 for its brain uptake [145]. MCT1 has also been proposed to be responsible for the transportation of salicylic acid, valproic acid, nicotinic acid, and some antibiotic  $\beta$ -lactams [146,147].

MCT8, in turn, is a specific thyroid hormone transporter mainly expressed in thyroid and adrenal glands, and other peripheral tissues, such as the liver and kidneys [148]. However, it is also highly expressed at the BBB and in neurons, and to some extent on the apical side of the choroid plexus [5,149,150]. MCT8 mediates the cellular uptake but also the efflux of thyroid hormones T3 and T4 (Table 4) [148,151], although the precise mechanism of their transport is still unknown. Studies in potential substrates and inhibitors of MCT8 suggest that the transporter is specific for the L-enantiomers of thyroid hormones. Amino and carboxyl groups of the alanine side-chain of thyroid hormones and at least one iodine atom in each iodothyronine ring are also required. Moreover, several drugs and natural compounds, including desipramine, dexamethasone, buspirone, desethylamiodarone, dronedarone, tyrosine kinase inhibitors, and silychristin have been reported to inhibit MCT8-mediated transport, either non-competitively or competitively [152].

**Table 4.** Tissue distribution, substrates, inhibitors, and expression/function modulators of MCT1–4 and MCT8.

Transporter	Gene Name	Tissue Distribution (Expression)	Substrates	Inhibitors	Expression Modulation/Transport Capacity Changes
MCT1	<i>SLC16A1</i>	Ubiquitous, Brain: luminal and abluminal membranes of BBB, astrocytes	Lactate, pyruvate, ketone bodies; probenecid, 6-mercapto-purine, 4-phenyl-butyrate salicylic acid, nicotinic acid, valproic acid, $\beta$ -lactams, XP13512, $\gamma$ -hydroxy butyric acid	4-Chloro- $\alpha$ -cyanocinnamic acid (non-specific), AZD3965	MCT1 expression $\uparrow$ in numerous cancers, at the BBB of ADHD children, and metabolic active tissues of obese individuals: via MYC, p53
MCT2	<i>SLC16A7</i>	Liver, kidneys, Brain: neurons	Lactate, pyruvate, ketone bodies	4-Chloro- $\alpha$ -cyanocinnamic acid (non-specific), AZD3965	MCT2 expression $\uparrow$ in numerous cancers and metabolic active tissues of obese individuals: via demethylation and hyper-methylation of DNA; MCT2 expression $\downarrow$ in hippocampus and cerebral cortex with pathologic progression of Alzheimer's disease (via reduced energy metabolism?)
MCT3	<i>SLC16A8</i>	Retinal pigment epithelium, choroid plexus	Lactate	Not reported	MCT3 expression $\downarrow$ in retinal pigment epithelium impairs visual functions and wound healing and in smooth muscle cells induces atherosclerosis via DNA methylation
MCT4	<i>SLC16A3</i>	Skeletal muscles, intestine, kidneys, heart, Brain: astrocytes	Lactate, pyruvate, ketone bodies; fluvastatin, atorvastatin, lovastatin, simvastatin, cerivastatin in their acid form	4-Chloro- $\alpha$ -cyanocinnamic acid (non-specific)	MCT4 expression $\uparrow$ in numerous cancers and in muscles of obese individuals: via hypoxia/HIF-1 $\alpha$
MCT8	<i>SLC16A2</i>	Liver, endocrine tissues, Brain: luminal and abluminal membranes of BBB, neurons	Thyroid hormones (T3 and T4)	Possibly desipramine, dexamethasone, buspirone, desethyl-amiodarone, dronedarone, tyrosine kinase inhibitors, and silychristin	MCT8 expression $\downarrow$ in Allan–Herndon–Dudley syndrome and during the inflammation

$\uparrow$  (arrow up) represents upregulation of the protein;  $\downarrow$  (arrow down) represents downregulation of the protein.

The other members of the MCT family are expressed relatively selectively in the brain. MCT2 is the main MCT found in the neurons; it has been found on highly oxidative cells and cell bodies, including dendrites, dendritic spines, and axons of neurons, although there may be species differences (Figure 1e) [153,154]. MCT2 is also ubiquitously expressed in the peripheral tissues [155], making it challenging to utilize for intra-brain targeted drug delivery avoiding peripheral exposure. In turn, MCT3 (*SLC16A8*) is predominantly expressed in the choroid plexus epithelial cells, in addition to retinal epithelial cells [156], and MCT4 is predominantly expressed in astrocytes at least in rodents [153] (Table 4). It has been proposed that lipophilic statins, such as fluvastatin, atorvastatin, lovastatin, simvastatin, and cerivastatin in their acid form, can interact with MCT4 [157]. MCT4 is also known to be involved in the efflux transport of lactate in a pH-dependent manner and thus preventing its intracellular accumulation that could inhibit glycolysis in the cells [158]. Moreover, neurons can accumulate the effluxed lactate from astrocytes (cross-talk between MCT4 and MCT2) and utilize it as a secondary energy source [159].

Lactate is also highly produced in glycolytic cancer cells due to their higher energy demand, leading to intracellular acidification, unless removed from the cells. Therefore, MCT1, MCT2, and MCT4 are over-expressed in many different types of cancers and tumors, and, thus, targeting MCT-mediated lactate efflux could serve as a promising treatment or adjuvant therapy to other chemotherapeutics [160,161]. For example, an MCT1/2-selective inhibitor, AZD3965, has already been studied in phase I clinical trials against hematological cancers [162,163]. Furthermore, AZD3965 has been reported to be more effective than classical non-specific MCT inhibitor, 4-chloro- $\alpha$ -cyanocinnamic acid ( $\alpha$ -CHCA) in the breast tumor model [164]. Curiously, MCT1 expression is increased at the BBB of children with attention-deficit/hyperactivity disorder (ADHD) [165], and expression changes of MCT1, 2, and 4 are related to metabolic states (obese and fasting individuals) in metabolic active tissues [166]. The expression of MCT1 is regulated mainly by transcriptional factors, such as MYC, and p53, while the expression of MCT2 has been associated with selective demethylation of an internal promoter region in the gene locus and reciprocal hyper-methylation of an upstream promoter region [167]. Contrarily, MCT4 is upregulated by hypoxia through a HIF-1 $\alpha$ -dependent mechanism [141,168]. Mutations of MCT1 have also been reported to cause fatigue syndrome (muscle cramping and pain due to the impaired lactate removal after intense exercise) and MCT1 deficiency has been associated with recurrent ketoacidosis in children having a moderate intellectual disability, epilepsy, or migraine [166]. In turn, downregulation of MCT2 in the hippocampus and cerebral cortex has been associated with the pathologic progression of AD, possibly via reduced energy metabolism [169]. Furthermore, the absence of MCT3 expression in retinal pigment epithelium impairs visual functions and wound healing [170,171], and downregulation of MCT3 in smooth muscle cells via DNA methylation can induce the development of atherosclerosis [172]. A rare neurological disorder called Allan–Herndon–Dudley syndrome (AHDS) is a consequence of mutations in the MCT8 gene, leading to increased serum thyroid hormone levels and severe mental retardation and neurological dysfunctions [173–175]. In addition, inflammation has been reported to downregulate MCT8 [176]. Therefore, expression modulation of distinct MCTs in different diseases may have therapeutical potential.

To date, MCT1-utilizing prodrugs have only been reported being used to improve oral bioavailability of compounds, such as 5-fluorouracil (5-FU), gemcitabine, and gabapentin by attaching mono-carboxylic acids with an ester or amide bonds (5-FU and gemcitabine), or shielding the free amino group with a polar acyloxyalkyl side chain with a carbamate bond (XP13512/GSK1838262, gabapentin enacarbil) (Figure 8) [177–180]. However, reports of utilizing MCTs for targeted or improved brain drug delivery via rationally designed prodrugs are less reported. Thus, it remains to be explored how well the reported MCT1-utilizing prodrugs of 5-FU and gemcitabine are transported into the brain, or into the specific brain cell types. Gabapentin enacarbil is already approved in the USA (Horizant<sup>®</sup>) and Japan (Regnite<sup>®</sup>) for the treatment of restless legs syndrome (RLS; moderate to severe)



and the reported adverse effects have been related to CNS; most commonly severity, sedation, and dizziness [181]. Therefore, it is likely that gabapentin enacarbil has also improved brain drug delivery and exposure due to the increased MCT1-mediated transport (low affinity–high capacity transporter) across the BBB than its parent drug gabapentin, which is a LAT1-substrate (high affinity–low capacity transporter).

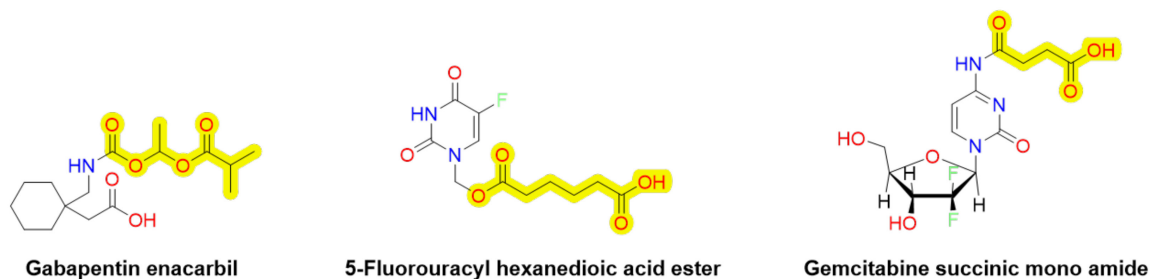


**Figure 8.** Molecular structures of prodrugs that can utilize MCT1 with promoieties highlighted with yellow color.

One challenge with MCTs is the bidirectional transport, which may be difficult to predict and control. Moreover, there are overlapping substrate specificities among MCTs. All the family SLC16A-members are known to have 12 transmembrane domains (TMDs) and an intracellular loop between TMDs 6 and 7. Furthermore, it has been proposed that MCTs facilitate a rocker switch transport mechanism, the same as GLUTs mediate (Figure 5) [64,182]. Structural-based analyses of the transport functions have provided some insights into the structure–activity relationship (SARs) of MCT1, MCT4, and MCT8 [183–192]. However, to develop successful MCT-utilizing prodrugs with improved brain drug delivery, more knowledge is required of the interactions that can affect the transport direction, particularly via MCT1 and MCT8 at the BBB, and MCT2 and MCT1/4 in neurons and astrocytes, respectively. Therefore, utilization of more sophisticated computational methods, such as molecular dynamics simulations (MDS) should be used in the future to reveal structural features of the prodrugs that can induce the conformational changes of the protein resulting in the translocation into the cells.

## 6. Organic Anion Transporting Family (SLCO/SLC21A)

The family of organic anion transporting polypeptides (OATPs) has had an inconsistent nomenclature in the past (OATP-A, OATP-B, OATP-C, etc.), and it was only in 2004 when this superfamily was standardized and renamed as an *SLCO*-family [193]. Another complicating factor with this family is that there are several gene duplicates and divergence between humans and rodents, e.g., OATP1A2 has five rodent orthologues, Oatp1a1, Oatp1a3, Oatps 1a4, Oatp1a5, and Oatp1a6; OATP1B1 and OATP1B3 have a single rodent orthologue (Oatp1a2); and OATP5A1 and OATP6A1 have three rodent orthologues (Oatp6b1, Oatp6c1, Oatp6d1), while other human OATPs have a name matching rodent orthologues [194]. Moreover, OATPs can be both ubiquitously distributed within the body, and very selectively expressed in certain tissues and there are species differences in these expression patterns. From the 11 members of this family that share approximately 40% amino acid sequence identity, at least OATP1A2 (*SLCO1A2*), OATP1C1 (*SLCO1C1*), OATP2A1 (*SLCO2A1*), OATP2B1 (*SLCO2B1*), and OATP3A1 (*SLCO3A1*) have been detected in the brain [194,195]. In addition, OATP4A1, OATP5A1, and OATP6A1 have been proposed to be expressed in the brain; however, these transporters are more or less orphans, i.e., whose functions are less well understood and, thus, these latter ones are not discussed in this review. More specifically, OATP1A2 and OATP2B1 are expressed at the BBB (luminal side), OATP1A2, OATP3A1 are neuronal transporters, OATP1C1 is an astrocytic transporter, and OATP2A1 is evenly distributed among neurons, astrocytes, and neurons (Figure 1f; Table 5) [5,196–200]. Curiously, OATP3A1 has two splice variants (OATP3A1\_v1

and OATP3A1\_v2) that are expressed in the brain in a dissimilar manner in neurons and choroid plexus.

**Table 5.** Tissue distribution, substrates, inhibitors, and expression/function modulators of selected members of the OATP-family.

Transporter	Gene Name	Tissue Distribution (Expression)	Substrates	Inhibitors	Expression Modulation/Transport Capacity Changes
OATP1A2	<i>SLCO1A2</i>	Ubiquitous, Brain: luminal membranes of BBB, neurons	Anionic, cationic, and neutral amphiphilic compounds of large size with different affinities among the transporters	Fruit juices that contain polyphenols and their conjugates, such as hesperidin, naringin, and avicularin; rifampicin, verapamil, elacridar, tariquidar, and zosuquidar (possibly competing substrates)	11 single-nucleotide polymorphisms (SNPs): transport activity ↓ (substrate-specific); OATP1A2 expression ↑ in several cancers: possible involvement of hypoxia/reoxygenation in the upregulation at the BBB
OATP1C1	<i>SLCO1C1</i>	Testis Brain: astrocytes, choroid plexus	Endogenous substrates, such as bile acids (cholate), steroids (estrone-3-sulfate), thyroid hormones (T3 and T4), prosta-glandins (PGE <sub>2</sub> );	NSAIDs, (fenamates), phenytoin (competing substrates exhibiting mutual inhibition function)	OATP1C1 expression ↓ during the inflammation
OATP2A1	<i>SLCO2A1</i>	Ubiquitous, Brain: neurons, astrocytes, and microglia	Exogenous substrates, such as statins (fluvastatin), β-blockers (atenolol), and anticancer drugs (methotrexate)	Polycyclic aromatic compounds, such as suramin, pranlukast, zafirlukast, olmesartan, losartan, non-steroidal anti-inflammatories	OATP2A1 expression ↓ in AD brain parenchymal cells; OATP2A1 expression ↑ in cancers: via PI3K/AKT/mTOR pathway
OATP2B1	<i>SLCO2B1</i>	Ubiquitous, Brain: luminal membranes of BBB		Some of the substrates are also reported as inhibitors due to the drug–drug interactions	11 single-nucleotide polymorphisms (SNPs): transport activity ↓ with 6 SNPs OATP2B1 expression ↑ in several cancers
OATP3A1	<i>SLCO3A1</i>	Ubiquitous, Brain: neurons			OATP3A1 expression ↑ in cholestasis: via TNF-α-activated NF-κB-p65 and ERK-SP1 signaling

↑ (arrow up) represents upregulation of the protein; ↓ (arrow down) represents downregulation of the protein.

Most of the OATPs transport a wide variety of compounds, both endogenous substrates, such as bile acids (e.g., cholate), steroids (e.g., estrone-3-sulfate), thyroid hormones (e.g., T3 and T4), and prostaglandins (e.g., PGE<sub>2</sub>), as well as exogenous substrates, such as hydroxymethylglutaryl-coenzyme A-CoA reductase inhibitors (statins), β-blockers (e.g., atenolol), and anticancer drugs (e.g., methotrexate), to name a few [194,195]. The main substrates of OATPs are anions; however, they can also carry neutral and cationic compounds (Table 5). In addition, many of their substrates are amphiphilic, having hydrophilic polar features and lipophilic proportions and they are relatively large (> 350 mol/g). In general,

the substrate specificities of distinct OATPs overlap; however, some of them have also very narrow and precise substrate specificities. The transport via OATPs is sodium independent, but it can be affected by the pH. In an acidic environment, the transport activity, of at least some OATP subtypes, can be increased due to the increased substrate affinity via protonation of a conserved histidine residue at the extracellular end of TM3 [201]. The substrates of OATP1A2 and OATP2B1 overlap significantly with other OATPs as well as other transporters, and, therefore, specific structural features that would favor either OATP1A2- or OATP2B1-selective transport are relatively challenging to find [202,203]. A specific feature of OATP1C1 is the transport of thyroid hormones (T3, T4) and their derivatives [204]. Contrarily, OATP2A1 is known as a prostaglandin transporter, since it can transport, in addition to PGE<sub>2</sub>, several other prostaglandins (e.g., PGE<sub>1</sub>, PGE<sub>3</sub>, PGF<sub>2α</sub>, PGH<sub>2</sub>, and PGD<sub>2</sub>) that other OATPs are not able to carry, and it has a higher affinity for PGE<sub>2</sub> compared to other OATP-subtypes [194,205]. Specific to OATP3A1 is the transport of arachidonic acid, and similar to OATP1C1 and OATP2A1, it has more discrete substrate specificity and perhaps also narrowed to endogenous compounds [194,195]. However, it needs to be remembered that the lack of reported drug substrate and inhibitors may also be due to the limited number of studies that have been carried out with less studied OATP subtypes [206].

OATP1A2 is known to be inhibited by apple, orange, cranberry, and grapefruit juices that contain polyphenols and their conjugates, such as hesperidin, naringin, and avicularin (Table 5) [207,208]. In addition, rifampicin and verapamil as well as the third generation P-glycoprotein (P-gp) inhibitors, elacridar, tariquidar, and zosuquidar, have been classified as OATP1A2 inhibitors [209,210]. Avicularin has also been reported to inhibit OATP2B1, which in turn, does not have selective inhibitors. However, many drugs and food additives have been reported to interfere with OATP2B1 function [211,212]. Therefore, both OATP1A2 and 2B1 are susceptible to drug–drug and drug–food interactions, already in the gastrointestinal tract, exemplified by well-known interactions with statins, fexofenadine (antihistamine), and aliskiren (renin inhibitor, used in the treatment of hypertension) [213,214]. Most likely, a similar interaction could occur also at the BBB. It has already been reported that prostaglandin transport via OATP2A1 is inhibited by polycyclic aromatic compounds, such as suramin (antiviral/antibacterial), pranlukast and zafirlukast (antiallergic/antiasthmatic), olmesartan and losartan (antihypertensive), and non-steroidal anti-inflammatories (NSAIDs; profens > anthranilates or fenamates), which can have huge effects on eicosanoid disposition [215]. Similarly, NSAIDs, particularly fenamates in addition to phenytoin (anti-seizure) can also inhibit OATP1C1-mediated transport and, thus, have a major impact on thyroid hormone brain disposition [204]. However, these compounds are more likely to be competing substrates rather than inhibitors of OATP1C1.

To date, 11 OATP1A2 single-nucleotide polymorphisms (SNPs) have been identified, some of them having reduced transport capacity of the substrates and some other SNPs having substrate-dependent changes in transport activity overall [216,217]. Therefore, OATP1A2 has a significant role in inter-individual differences in drug disposition in addition to drug–drug interactions (DDIs) (Table 5). Notably, it has been reported that the rodent orthologue *Oatp1a4* is upregulated in hypoxia/reoxygenation via transforming growth factor-β (TGF-β)/activin receptor-like kinase 5 (ALK5) inhibition in the brain, which may offer an opportunity to optimize the CNS drug delivery, e.g., of statins [218]. For OATP2B1, only three missense SNPs have been identified to date, from which only one SNP has shown some effect on the transport capacity of selected probe drugs [219,220]. Since OATP1A2 and 2B1 carry many chemotherapeutics with relatively narrow therapeutic indices, the polymorphism of these OATPs can have dramatic effects on the efficacy and safety of these anti-cancer drugs. However, many OATPs, including 1A2 and 2B1, are overexpressed in many types of cancers, particularly in those which are highly dependent on the transport of steroid hormones required for cell proliferation, and thus affecting the exposure of their substrate drugs [221]. Curiously, OATP2A1 is downregulated in AD

brain parenchymal cells [199], but upregulated in cancers, such as lung cancer via the PI3K/AKTmTOR pathway [222].

On the other hand, OATP1C1 has been reported to be downregulated together with another thyroid hormone transporter, MCT8, during the inflammation [176]. Moreover, Oatp1c1-deficiency and resulting hypothyroidism, have been proposed to cause neurological and behavioral alterations despite the presence of other thyroid hormone transporters, such as Mct8, in animal models [223,224]. Contrarily, OATP3A1 is upregulated in cholestasis (a liver disease where the flow of bile from the liver is reduced or blocked) via TNF- $\alpha$ -activated NF- $\kappa$ B-p65 and ERK-SP1 signaling pathways [225]. Overall, although OATP expressions are mainly regulated on the transcriptional level and as a response to their substrate levels, OATP localization and internalization from the plasma membrane can be affected by phosphorylation and preceding activation of protein kinases [226]. However, the expression modulation particular OATPs in selected conditions/diseases may have the potential to improve clinical outcomes, similar to MCTs.

OATPs have 12 TMDs with both termini located intracellularly. The large fifth extracellular loop has many conserved cysteine residues that can form disulfide bonds, and both the second and fifth extracellular loops contain several *N*-glycosylation sites [227]. It has been proposed that all OATP facilitate the translocation of their substrates through a positively charged pore in a rocker switch type of mechanism, similarly to GLUTs (Figure 5) [228]. Moreover, several amino acid residues that may have crucial roles in the OATP-mediated transport have been identified. However, due to the multiple binding sites of OATPs, the detailed interactions have remained controversial and, therefore, more efforts and additional computational experiments should be directed to understanding the exact translocation interactions of OATP substrates. This would also enable the rational design of OATP subtype-specific (pro)drug design and more efficient utilization of OATPs for brain drug delivery in the future, which has not been studied actively in the past. However, one great challenge with OATPs in brain drug delivery applications is their peripheral expression and overlapping substrate specificities, which may impair the targeting efficacy. Nevertheless, many of the already known substrates could be used as a starting point for the prodrug syntheses, e.g., thyroid hormone conjugates would be expected to be relatively specific for OATP1C1 among OATPs, but on the other hand, they could also be substrates of MCT8 and LAT1.

## 7. Organic Cation/Anion/Zwitterion Transporter Family (SLC22A)

The SLC22A family consists of organic cation transporters (OCTs) and organic anion transporters (OATs) carrying anions, cations, or zwitterions. OCT1 (*SLC22A1*), OCT2 (*SLC22A2*), and OCT3 (*SLC22A3*) are expressed most likely both at the luminal and abluminal sides of the BBB endothelial cells, although more evidence of the exact localizations is needed [229]. Furthermore, OCT2–3 has been identified in neurons and OCT2 in microglia and astrocytes (Table 6, Figure 1g). Similarly, OCTN1 (*SLC22A4*) and OCTN2 (*SLC22A5*) are most likely expressed at the BBB to some extent, but they are also found in parenchymal cells; OCTN1 in microglia and OCTN2 in neurons [229,230]. However, both OCTs and OCTNs are also expressed throughout the body, particularly in the kidneys and liver [194].

**Table 6.** Tissue distribution, substrates, inhibitors, and expression/function modulators of OCT1–3, OCTN1–2, and OAT1–3.

Transporter	Gene Name	Tissue Distribution (Expression)	Substrates	Inhibitors	Expression Modulation/Transport Capacity Changes
OCT1	SLC22A1	Liver and other peripheral tissues, Brain: BBB	Organic cations with different affinities among the transporters Endogenous substrates: catecholamines, monoamine neurotransmitters Drugs: several cytostatic, antiviral, antibiotic, antioxidant, psycho-stimulant, anti-hypertensive, antiemetic, antidepressant, antidiabetic agents	Transported substrates of the OCTs exhibit mutual inhibition function  Cytochalasin B, forskolin, phloretin, quercetin and other flavonoids, glycogen synthase kinase-3 (GSK-3) inhibitors	18 single-nucleotide polymorphisms (SNPs): transport activity ↓ with 6 SNPs  See more information below (OATs)
OCT2	SLC22A2	Kidneys and other peripheral tissues, Brain: BBB, neurons, microglia, astrocytes			10 transporter variants with altered substrate selectivity and transport capacity
OCT3	SLC22A3	Abundant, Brain: BBB, neurons			5 SNPs: transport activity ↓ with 3 SNPs
OCTN1	SLC22A4	Abundant, Brain: BBB, microglia	Acetylcholine, ergothioneine, L-carnitine, TEA, quinidine, pyrilamine, and verapamil	Transported substrates of the OCTNs exhibit mutual inhibition function	OCTN1 variant L503F: familial/ sporadic inflammatory bowel disease
OCTN2	SLC22A5	Abundant Brain: BBB, neurons	Acetyl-L- carnitine, D-/L-carnitine, TEA, quinidine, pyrilamine, and verapamil	Transported substrates of the OCTNs exhibit mutual inhibition function	Multiple OCTN2 variants: systemic carnitine deficiency
OAT1	SLC22A6	Kidneys, Brain: choroid plexus	Overlapping substrate specificities, although not identical, transports several drugs Endogenous substrates: α-ketoglutarate, <i>para</i> -amino-hippuric acid, benzoyl penicillins, indoxyl sulfate, and homovanillic acid, and prostaglandins	Probenecid (inhibitor/ substrate)	Multiple SNPs: decreased function can be compensated with other transporters in the family due to the overlapping substrate specificities; NOTE! OCTs and OATs are all regulated in transcriptional level as well as by post-translational phosphorylation via several protein kinases
OAT3	SLC22A8	abluminal side of the BBB, choroid plexus			

↓ (arrow down) represents downregulation of the protein.

OCT1, OCT2, and OCT3 facilitate sodium and pH-independent transport of a broad range of endogenous and exogenous organic cations down their electro-chemical gradients, in both directions [194,231]. However, the affinity of OCT-ligands can depend on the degree of ionization, and therefore increased transport has been reported at lower pH [232]. Substrates of OCTs include a wide variety of structurally unrelated small organic cations for which they have different affinities (Table 6). These include commonly used probe-substrates, 1-methyl-4-phenylpyridinium (MPP) and tetraethylammonium (TEA), as well as endogenous compounds, such as choline, acetylcholine, dopamine, norepinephrine, epinephrine, serotonin, histamine, and agmatine, as well as drugs, such as quinidine, quinine, aciclovir, ganciclovir and metformin, amantadine, memantine, cimetidine, famotidine and ranitidine, cisplatin, debrisoquine, phenylcyclidine, clonidine, diphenylhydramine, atropine, procainamide, and cocaine, to name a few [231].

Noteworthy, the substrate and inhibitor specificities of OCT1, OCT2, and OCT3 overlap, and, therefore, some cations are transported by one OCT subtype and non-transported but bound (inhibitor) by another OCT subtype. Moreover, the degree and type of inhibition by a high concentration of a given inhibitory substrate may be total or partial [231]. In turn, the transport of OCTN1 and 2 can be sodium and pH-dependent or -independent, depending on the substrate. They are considered to be carnitine transporters; however, OCTN1 can selectively transport ergothioneine. OCTN1 and 2 are also known to carry, e.g., TEA, quinidine, pyrilamine, and verapamil [231].

OCT1 has been found to have 25 SNPs, while OCT3 has only five SNPs [233,234]. However, none of them are associated with human pathologies. Three SNPs of OCT1 and three SNPs of OCT3 are known to have reduced transport activity. Contrarily, OCT2 has ten transporter variants, which all are highly functional, but may have slightly altered substrate selectivity and transport capacity [231]. Nevertheless, the greatest risks with OCTs are related to DDIs, similar to OATPs [235]. Mutations in the OCTN gene, in turn, are directly linked to human autoimmune diseases; OCTN1 variant L503F is related to familial and sporadic inflammatory bowel disease, and multiple nonsense and missense mutations of OCTN2 are related to systemic carnitine deficiency [236,237].

From the OAT family, only OAT1 (*SLC22A6*) and OAT3 (*SLC22A8*) have been found in the brain, although they are highly expressed in the kidneys [194,238]. At the BBB, OAT3 is expressed on the abluminal side, but it has also a crucial role on the apical side of the choroid plexus, similarly to OAT1 (Table 6, Figure 1g) [239,240]. OATs function as anion exchangers and OAT3 has been proposed to participate in the efflux transport of organic anions, such as  $\alpha$ -ketoglutarate, *para*-aminohippuric acid (PAH), benzylpenicillin, indoxyl sulfate, and homovanillic acid at the BBB (Table 6), carrying its substrates from the brain to blood. Although OAT1 and 3 can carry several endogenous and exogenous compounds, such as prostaglandins, non-steroidal anti-inflammatories (NSAIDs), antivirals, antibiotics ( $\beta$  lactams), diuretics, antidiabetics, and anticancer drugs [241], the efflux transport direction makes them less suitable candidates for brain-targeted drug delivery. The uricosuric drug, probenecid, has been regarded as a potent inhibitor of OAT1 and 3, although it has also been referred to as OAT1/-3 substrate [194]. Therefore, with a concomitant administration of probenecid (or similar specific OAT1/-3 inhibitor), the OAT-mediated efflux of selected therapeutics (OAT1/-3 substrates) at the BBB could be avoided [242].

Due to the broad substrate specificity, OATs are related to several DDIs and currently, the U.S. Food and Drug Administration (FDA) and European Medicines Agency (EMA) recommend the evaluation of new chemical entities (NCEs) for their interactions with OAT1 and 3 [243,244]. For OAT1 and 3, several SNPs have been identified, some of which have decreased transporter function, while others do not have any effects [241]. However, due to the overlapping substrate specificities, other OAT members can replace the unfunctional transporter and, thus, mutations of OATs have been thought to have less significance for the clinical outcome.

OCTs and OATs have 12 TMDs with intracellular amino and carboxy-termini [194]. It has been shown that the extracellular loops between TMDs 1 and 2 are relatively large

containing potential *N*-glycosylation sites, while the intracellular loops between 6 and 7 and the C-terminus have putative phosphorylation sites. These sites are prone to protein and tyrosine kinases and, therefore, activation of these kinases affects also the activity of the SLC22A-family transporters [245,246]. In addition, these transporters can be regulated at the transcriptional level. Since OCTs' and OATs' regulation varies a lot among the transporters, species, and tissue localization, more studies are warranted to better understand their life cycle.

Curiously, the exact transport mechanisms of the transporters in the SLC22A family are still unknown. Moreover, although OCTs and OATs are relatively well-explored transporters due to their crucial role in drug–drug interactions, less is known about their capability to carry drugs into the brain across the BBB, or inside the brain. Furthermore, the high hepato-renal expression of OCTs and OATs compared to the brain makes the brain-targeted drug delivery via them relatively challenging. However, since OCTs are responsible for carrying multiple drugs into the brain [238,247–249], and most likely more compounds will be discovered to utilize OCTs for their brain drug delivery, more efforts should be paid to the rational design of OCT-utilizing (pro)drugs in the future. Moreover, the overlapping substrate specificities may offer benefits of concomitant transport across the BBB and, thus, increase the overall brain drug disposition. Although, at the same time it will be at the expense of intra-brain selectivity, which is not likely to be achieved if a drug utilizes several OCTs. Nevertheless, all known drug carriers, including OATPs, OCTs, and OATs have the potential to be used as brain-targeted prodrug carriers. Many of their already known drug substrates could be used as starting point promoieties. Moreover, dual-drug targeting would have advantages in many complex neurodegenerative diseases, such as AD, since multiple targets could be hit with a double-prodrug at the same time. However, it should also be kept in mind that many natural substrates of other transporters, such as L-glutamine, L-cystine (GSH precursors), and L-arginine (precursors of L-ornithine and NO synthesis) that could be utilized as promoieties may also have additional beneficial effects in the brain.

#### 8. Sodium-Coupled Neutral Amino Acid (System N/A) Transporter Family (SLC38A)

The family of SLC38 has eight sodium-coupled neutral amino acid transporters (SNATs) and three additional orphan transporters. From these SNAT1 (*SLC38A1*), SNAT2 (*SLC38A2*), SNAT3 (*SLC38A3*), SNAT5 (*SLC38A5*), SNAT6 (*SLC38A6*), SNAT7 (*SLC38A7*), SNAT8 (*SLC38A8*), and thus excluding SNAT4 (*SLC38A4*), are expressed in the brain [250–252]. These transporters are further classified into system A and system N depending on their functional properties and patterns of substrate recognition. System A transporters (SNAT1 and SNAT2, also referred to as ATA1/SAT1 and ATA2/SAT2, respectively) recognize a broader range of aliphatic amino acids (L-proline, L-asparagine, L-cysteine, L-glutamine, L-glycine, L-methionine, and L-serine), whereas system N transporters (SNAT3 and SNAT5, also referred to as SN1 and SN2, respectively) have a rather narrow substrate profile (L-glutamine, L-histidine, and L-asparagine) (Table 7).

The expression of SNAT1 and SNAT2 is ubiquitous; however, they are also expressed in the brain, preferably in glutamatergic, GABAergic, and dopaminergic neurons but also to some extent in astrocytes (Figure 1h) [250,253–256]. In addition, SNAT2 has been found at the abluminal side of the BBB [5]. The transport of system A carriers (SNAT1 and 2) is sodium-dependent and highly pH-sensitive, and they exchange small and aliphatic amino acids for sodium with 1:1 stoichiometry. SNAT1 and 2 can be inhibited at low extracellular pH, but also by 2-methylamino-isobutyric acid (MeAIB), which is most likely a competing substrate of SNATs rather than an inhibitor (Table 7) [250,251].

**Table 7.** Tissue distribution, substrates, inhibitors, and expression/function modulators of SNAT1–2 (system A) and SNAT3 and 5 (system N).

Transporter	Gene Name	Tissue Distribution (Expression)	Substrates	Inhibitors	Expression Modulation/Transport Capacity Changes
SNAT1	<i>SLC38A1</i>	Ubiquitous, Brain: neurons (astrocytes)	L-proline, L-asparagine, L-cysteine, L-glutamine, L-glycine, L-methionine, and L-serine	2-Methylamino- isobutyric acid (MeAIB, competing substrate); low pH	SNAT1 expression ↑: via protein kinase A (PKA) activation; SNAT1 expression ↓: via inflammation; SNAT1 expression ↑ in many types of cancers
SNAT2	<i>SLC38A2</i>	Ubiquitous, Brain: abluminal side of the BBB, neurons (astrocytes)	L-proline, L-asparagine, L-cysteine, L-glutamine, L-glycine, and L-serine	2-Methylamino- isobutyric acid (MeAIB; competing substrate); low pH	Stable SNAT2 expression requires an active mTOR-signaling; SNAT2 expression ↑ in many types of cancers
SNAT3	<i>SLC38A3</i>	Liver, kidney, muscles, eye, Brain: luminal and abluminal sides of the BBB, astrocytes	L-glutamine, L-histidine, and L-asparagine	Not reported	SNAT3 expression ↓ by insulin: via an mTOR pathway; SNAT3 expression ↑ by calorie restriction: via increased protein kinase C (PKC) activity(?); SNAT3 expression ↑ in many types of cancers
SNAT5	<i>SLC38A5</i>	Intestinal tract, kidney, retina, lung, Brain: astrocytes	L-glutamine, L-histidine, and L-asparagine	Glutamic acid-γ-hydroxamic acid (GluγHA)	Less studied

↑ (arrow up) represents upregulation of the protein; ↓ (arrow down) represents downregulation of the protein.

System N transporters (SNAT3 and 5) are more tissue-specific, but in the brain, they have been suggested to be the major mediators of L-glutamine release from astrocytes (Table 7) and, thus, have a crucial role in the glutamate–GABA–glutamine cycle in the CNS together with system A transporters [250,257,258]. Distinctively, SNAT3, in addition to astrocytes, is also expressed in the luminal and abluminal sides of the BBB [5]. Similar to system A transporters, SNAT3 and 5 are also pH- and sodium-dependent; however, these transporters also accept Li<sup>+</sup> substitution for Na<sup>+</sup>. Curiously, their transport activity can be enhanced by increasing the pH from 6 to 8 and they can function bidirectionally [258]. To date, no SNAT3-selective inhibitors have been reported, although glutamic acid-γ-hydroxamic acid (GluγHA) has been proposed as a SNAT5-selective inhibitor [259].

Transporters 6, 7, and 8 are yet unclassified according to the N/A-system and their role, particularly in the brain, is currently less well understood. SNAT6 is expressed exclusively in excitatory neurons, while SNAT7 and SNAT8 are expressed in the axons of the majority of neurons [260–262]. Therefore, these SNATs may also be important transporters in sustaining the glutamate neurotransmitter pool in the brain. It has been proposed that SNAT7 has similarities with system N, while SNAT8 resembles more of the system A. However, even less is known of SNAT6 function in relation to other SNATs [263].

At least SNAT1, SNAT2, and SNAT3 are upregulated in several different cancers, particularly in response to nutritional stress to compensate for the higher consumption of amino acids by the cancer cells [252]. In addition, SNAT2 has been found to be regulated by amino acids in neurons [256]. SNAT1 expression upregulation, in turn, has been linked to activated protein kinase A (PKA) signaling and SNAT1 expression down-



regulation to lipopolysaccharide-induced inflammation in astrocytes, but not in neurons (Table 7) [264,265]. The stable SNAT2 expression has been suggested to require an active mTOR-signaling, at least in placental trophoblast cells [266]. SNAT3 expression is regulated by insulin in hepatocytes; the calorie restriction upregulates its expression, while a chronic insulin treatment downregulates the expression via an mTOR pathway [267]. Moreover, increased protein kinase C (PKC) activity has been interlinked with SNAT3 internalization and expression downregulation [268]. SNAT5 expression regulation is less studied and understood.

The structure of SNATs is complex and heterogenic, although they all seem to contain 11 TMDs. SNAT1 has been proposed to have a long cytosolic N-terminus and a short extracellular C-terminus and a large glycosylated loop between TMD5 and 6, while SNAT2 most likely has an extracellular C-terminus and putative intracellular loops between TMD6 and 7 as well as 10 and 11 [250]. However, the transport mechanism of SNATs and how amino acids are involved in the pH-sensitivity of SNATs have remained unclear to date [252]. The SLC38A family has been structurally found to resemble a bacterial neurotransmitter-sodium symporter, LeuT and a proton-dependent amino acid transport ApcT, which facilitate the rocking bundle mechanism, similarly to LAT1 (Figure 6) [251]. Therefore, it is highly likely that SNATs could mediate the rocking bundle mechanism; however, more detailed insights into the mechanism from higher resolution structures and MD studies are required. They are also highly needed to enable rational SNAT-utilizing (pro)drug design and to reveal the transport direction. It would be crucial to understand how structural features can affect the transport direction, particularly at the BBB to ensure efficient SNAT-mediated delivery to the target sites. Moreover, with SNATs, there is a great potential to achieve intrabrain selective drug delivery, by utilizing system A transporters for neuronal accumulation and system N carriers for astrocytal accumulation.

## 9. Other Transporters in Discrete Families

Vitamin transporters that belong to different families, such as sodium-dependent multivitamin transporter, SMVT (*SLC5A6*) and sodium-vitamin C co-transporter 2, SVCT2 (*SLC23A2*), are also highly expressed in the brain. SMVT has been primarily found at the BBB while SVCT2 is more of a neuronal transporter; however, it has also been found in reactive astrocytes [269–271]. Some attempts to utilize these transporters for targeted drug delivery have been reported in the past, but overall, only little is known of the interactions of these transporters and their substrates. Well-known substrates of SMVT include biotin, pantothenic acid, and lipoic acid, while only L-ascorbic acid (AA) has been reported as an SVCT2 substrate [272,273]. Notably, the oxidized form, dehydroascorbic acid (DHA), is not only an SVCT2-substrate, it has also been proposed to be transported via GLUT1 and GLUT3. Therefore, it has been suggested that SVCT2 is a part of the AA recycling mechanism within the brain, where DHA is uptake at the BBB and by astrocytes via GLUT1, reduced to AA and released from the astrocytes, and re-uptaken into the neurons via SVCT2 [270,271,273]. Although both transporters are expressed in peripheral tissues too, only SVCT2 has been utilized for brain-targeted purposes by using a prodrug technology. NSAIDs, such as naproxen and ibuprofen, have been conjugated with AA and glucose, and shown improved brain accumulation [274–276]. However, their transport mechanism remains to be solved, whether it is mediated via GLUT1 or SVCT2. So far, SMVT has been utilized only to improve the oral bioavailability and topical ocular delivery of antivirals, saquinavir, and acyclovir [277,278], and their delivery into the brain has remained unknown.

In the SLC5A-family, there is also a choline transporter, CHT (*SLC5A7*), that has a crucial role in the brain, particularly in cholinergic neurons [279–281]. However, CHT is not the only choline transporter, also OCT1–3 (discussed above) and choline transporter-like proteins 1–5 (CTL1–5, *SLC44A1–5*) participate in choline homeostasis. From the latter ones at least, CTL1, CLT2, and CTL5 have been found in the brain, CTL1 and CLT2, particularly at the BBB, but CLT1 also in neurons and glial cells [279,282,283]. Unfortunately, CHT

and CLTs and their roles in the brain are not yet well understood. It has been proposed that they may be involved in the pathogenesis of neurodegenerative diseases, such as AD, and, therefore, their expression modulation could have therapeutical potential [282]. Nevertheless, more studies are also needed to reveal if these transporters could be harnessed for rational prodrug design. Their function is known to be inhibited by several cationic drugs [279], and, therefore, it is likely that they could carry also drugs, in addition to choline.

Curiously, members of the SLC2A-family (GLUTs) are not the only glucose carriers, also sodium-glucose cotransporters, SGLTs (*SLC5A1–12*), have been recognized as sodium-dependent unidirectional sugar carriers [47,49]. From these carriers, at least SGLT1 and 2 have been detected in the brain, although also with smaller expression compared to GLUT1 and 3. Therefore, it is not likely that higher brain drug disposition can be achieved by utilizing the SGLT-transporters; however, in the cases where GLUTs are downregulated, like in AD, additional glucose transporters may have a more critical role in the transport of gluco-conjugates. Some inhibitors of SGLTs (gluco-conjugates and others) have been reported to maintain stable plasma glucose in type 2 diabetic patients, mainly due to the inhibition in the intestine and renal proximal tubules [284–286]. Nevertheless, more structural and functional details overall are required from all the above-mentioned transporters in order to deploy them for rational (pro)drug design in brain-targeted applications.

In addition, there are also several nucleotide transporters expressed in the brain, such as sodium-independent equilibrative nucleoside transporters 1–4 (ENT1–4, *SLC29A1–4*) and to a lesser extent sodium-dependent concentrative nucleoside transporters 1–3 (CNT1–3; *SLC28A1–3*) [287–290]. These transporters can carry not only endogenous nucleosides but also synthetic nucleoside analogs, including anticancer drugs such as 5-fluorouracil, 6-mercaptopurine, cladribine, gemcitabine, fludarabine, and cytarabine, antiviral drugs, such as ribavirin, zalcitabine, and zidovudine. Therefore, purine and pyrimidine nucleosides could be used as promoieties in the prodrug design. Thus, there are also other possibilities and several transporters that could be utilized in the brain-targeted transporter-utilizing prodrug approach in the future.

## 10. Conclusions and Future Prospects

Targeting drugs into the brain or improving the brain drug delivery to the therapeutically relevant levels has remained an unanswerable challenge until today. However, we have come a long way from thinking that increased lipophilicity would increase the passive permeation across the BBB, although, there is still a huge task to increase our understanding of the roles of dozens or hundreds of orphan transporters and to utilize transporters more broadly in therapeutical applications [291–294]. Unfortunately, in science, we tend to focus on hot topics; thus, only a limited number of transporters are very well characterized for different purposes. However, it is hoped that this review encourages particularly young scientists to explore the transporter field even more broadly and without any prejudice in the future.

As presented above, there are several different transporters expressed at the BBB and/or selectively expressed in brain parenchymal cells that are relatively well-characterized and to some extent also utilized for brain-targeted and intrabrain-targeted drug delivery, respectively. Some of the brain-delivered therapeutics are drugs acting as such; however, in many cases a prodrug approach is needed to be utilized in order to temporarily change the pharmacokinetic properties of potent drugs. This requires not only selective transporter-mediated cellular uptake but also a biotransformation step to release the active parent drug, which in many cases, has been the most challenging part of brain-targeted prodrug applications. Therefore, there are not so many clinically used brain-targeted prodrugs available these days despite the success of the prodrug approach for other purposes, such as increasing the solubility of oral absorption [11–13]. L-Dopa, a LAT1-substrate, is one of the few examples as it undergoes enzymatic decarboxylation to release dopamine.

The majority of prodrugs have hydrolyzable bonds, such as ester bonds, which predisposes the prodrugs to premature first-pass metabolism before they reach the brain. On

the other hand, more stable amide prodrug bonds have not released their parent drugs at a sufficient rate in the brain. Moreover, transporters are not the only ones with a great expression variety among the species as well as between the patients. Additionally, enzyme expression levels can vary, which complicates not only the translation from preclinical data to the clinical situation, but also affects the efficacy and safety of the treatments of a particular patient. Compared to transporters, even less is known about the roles of different enzymes in the brain. As mentioned many times in this review, computational methods should be utilized more extensively to understand the exact translocation mechanisms of substrates and transport direction across the transporter cavities, which would increase our success in drug development. However, computational methods should also be used more extensively to design extended-release prodrugs and to find binding and mechanistic catalytic differences among hydrolyzing enzymes in the brain vs. peripheral tissues.

Overall, more efforts should be paid to the brain drug delivery of already used marketed compounds to increase our understanding. Curiously, statins (OATP-substrates) are cyclized lactones that are hydrolyzed to their acid form and they have effects also in the brain [295]. Thus, they could be considered brain-delivered prodrugs. In addition, many OCT-substrates seem to have effects in the brain as such (not prodrugs), including memantine, fluoxetine, and ketamine [229]. Therefore, in addition to already extensively studied LAT1, OATPs and OCTs could be utilized for brain drug delivery in the future. Of course, with these suggested transporters, the targeting efficacy into the brain can be a challenge due to their expression in other tissues. On the other hand, LAT1 successfully delivers L-dopa into the brain, although it is also expressed in many other peripheral tissues. Thus, the expression intensities in different tissues have a great impact on targeting potential. Based on this fact, GLUT1, CAT1, and MCT1 with high BBB expression profiles, should also be considered suitable brain-targeted carriers in the future.

Nevertheless, it needs to be remembered that carrier-mediated drug delivery is only one option and most likely, it is not suitable for all therapeutical agents. Biological drugs are becoming more and more common, and as macromolecules, they are most likely to be delivered into the brain via other routes, like receptor-mediated transport. In addition, other administration routes, such as trans-nasal administration, are still under extensive research. Therefore, more efforts should be paid also to those delivery mechanisms and how they could be utilized more effectively for the brain-targeted as well as intrabrain-targeted purposes.

It is obvious that there will never be 100% brain-targeting avoiding other tissues or cells completely by any developed delivery method, since transporters and receptors are also expressed in other tissues and cells. However, if we can increase the concentration at the target site to the therapeutically relevant level and simultaneously decrease the concentrations in off-target cells, it may have an enormous impact on the clinical outcome. Nevertheless, the protein expression intensity and localization is not the only determinant when targeting compounds, the overlapping substrate specificities of transporters and receptors have also a huge impact on the compounds' distributions. It is more than likely that a single compound is able to utilize more than one transport mechanism. Therefore, if the target transporter or receptor expression or function is downregulated due to the disease condition or polymorphism, there can be additional carriers or mechanisms that can completely change the pharmacokinetic profile of the selected compound. This can have both, negative and targeting minimizing effects, as well as positive and targeting increasing effects. Therefore, more efforts should be paid to secondary interactions with other proteins in the future, in order to obtain successful CNS drugs for clinical use.

Thus, to summarize, in brain-targeted approaches, it is all about finding the right balance. In a transporter-utilizing prodrug approach, it would be a balance among transporter expression profiles and tissue-specific localization, a balance with transporter selectivity and substrate specificities, and a balance between bioconversion rate in peripheral tissues and at the CNS to gain appropriate delivery and targeting of pharmacologically active compounds.

**Author Contributions:** Conceptualization, K.M.H.; data curation, J.H., M.M.-P. and K.M.H.; writing—original draft preparation, J.H. and K.M.H.; writing—review and editing, J.H., M.M.-P., S.K.A. and K.M.H.; visualization, S.K.A.; project administration, K.M.H.; funding acquisition. All authors have read and agreed to the published version of the manuscript.

**Funding:** This research was funded by the Academy of Finland, ProFi6 grant and Sigrid Juselius Foundation.

**Institutional Review Board Statement:** Not applicable.

**Informed Consent Statement:** Not applicable.

**Data Availability Statement:** Not applicable.

**Conflicts of Interest:** The authors declare no conflict of interest.

## References

1. Deuschl, G.; Beghi, E.; Fazekas, F.; Varga, T.; Christoforidi, A.K.; Sipido, E.; Bassetti, C.L.; Vos, T.; Feigin, V.L. The burden of neurological diseases in Europe: An analysis for the Global Burden of Disease Study 2017. *Lancet Public Health* **2020**, *5*, e551–e567. [CrossRef]
2. Olesen, J.; Gustavsson, A.; Svensson, M.; Wittchen, H.-U.; Jönsson, B. The economic cost of brain disorders in Europe. *Eur. J. Neurol.* **2012**, *19*, 155–162. [CrossRef]
3. Pankevich, D.E.; Altevogt, B.M.; Dunlop, J.; Gage, F.H.; Hyman, S.E. Improving and Accelerating Drug Development for Nervous System Disorders. *Neuron* **2014**, *84*, 546–553. [CrossRef]
4. Gribkoff, V.K.; Kaczmarek, L.K. The need for new approaches in CNS drug discovery: Why drugs have failed, and what can be done to improve outcomes. *Neuropharmacology* **2016**, *120*, 11–19. [CrossRef]
5. Uchida, Y.; Yagi, Y.; Takao, M.; Tano, M.; Umetsu, M.; Hirano, S.; Usui, T.; Tachikawa, M.; Terasaki, T. Comparison of Absolute Protein Abundances of Transporters and Receptors among Blood–Brain Barriers at Different Cerebral Regions and the Blood–Spinal Cord Barrier in Humans and Rats. *Mol. Pharm.* **2020**, *17*, 2006–2020. [CrossRef]
6. Pardridge, W.M. Drug Transport across the Blood–Brain Barrier. *J. Cereb. Blood Flow Metab.* **2012**, *32*, 1959–1972. [CrossRef]
7. Dragunow, M. The adult human brain in preclinical drug development. *Nat. Rev. Drug Discov.* **2008**, *7*, 659–666. [CrossRef]
8. Lee, G.; Dallas, S.; Hong, M.; Bendayan, R. Drug transporters in the central nervous system: Brain barriers and brain parenchyma considerations. *Pharmacol. Rev.* **2001**, *53*, 569–596. [CrossRef]
9. Banks, W.A. From blood–brain barrier to blood–brain interface: New opportunities for CNS drug delivery. *Nat. Rev. Drug Discov.* **2016**, *15*, 275–292. [CrossRef]
10. Lin, L.; Yee, S.W.; Kim, R.B.; Giacomini, K.M. SLC transporters as therapeutic targets: Emerging opportunities. *Nat. Rev. Drug Discov.* **2015**, *14*, 543–560. [CrossRef]
11. Huttunen, K.M.; Raunio, H.; Rautio, J. Prodrugs—From Serendipity to Rational Design. *Pharmacol. Rev.* **2011**, *63*, 750–771. [CrossRef]
12. Rautio, J.; Meanwell, N.; Di, L.; Hageman, M.J. The expanding role of prodrugs in contemporary drug design and development. *Nat. Rev. Drug Discov.* **2018**, *17*, 559–587. [CrossRef]
13. Rautio, J.; Kärkkäinen, J.; Sloan, K.B. Prodrugs—Recent approvals and a glimpse of the pipeline. *Eur. J. Pharm. Sci.* **2017**, *109*, 146–161. [CrossRef]
14. Colas, C.; Ung, P.M.-U.; Schlessinger, A. SLC transporters: Structure, function, and drug discovery. *MedChemComm* **2016**, *7*, 1069–1081. [CrossRef]
15. Majumder, P.; Mallela, A.K.; Penmatsa, A. Transporters Through the Looking Glass: An Insight into the Mechanisms of Ion-Coupled Transport and Methods That Help Reveal Them. *J. Indian Inst. Sci.* **2018**, *98*, 283–300. [CrossRef]
16. Janulienė, D.; Moeller, A. Cryo-EM of ABC transporters: An ice-cold solution to everything? *FEBS Lett.* **2020**, *594*, 3776–3789. [CrossRef]
17. Schlessinger, A.; Welch, M.A.; Van Vlijmen, H.; Korzekwa, K.; Swaan, P.W.; Matsson, P. Molecular Modeling of Drug-Transporter Interactions—An International Transporter Consortium Perspective. *Clin. Pharmacol. Ther.* **2018**, *104*, 818–835. [CrossRef]
18. Magi, S.; Piccirillo, S.; Amoroso, S.; Lariccia, V. Excitatory Amino Acid Transporters (EAATs): Glutamate Transport and Beyond. *Int. J. Mol. Sci.* **2019**, *20*, 5674. [CrossRef]
19. O’Kane, R.L.; Martínez-López, I.; DeJoseph, M.R.; Viña, J.R.; Hawkins, R.A. Na(+)-dependent glutamate transporters (EAAT1, EAAT2, and EAAT3) of the blood-brain barrier. A mechanism for glutamate removal. *J. Biol. Chem.* **1999**, *274*, 31891–31895. [CrossRef]
20. Rothstein, J.D.; Martin, L.; Levey, A.I.; Dykes-Hoberg, M.; Jin, L.; Wu, D.; Nash, N.; Kuncl, R.W. Localization of neuronal and glial glutamate transporters. *Neuron* **1994**, *13*, 713–725. [CrossRef]
21. Danbolt, N.C. Glutamate uptake. *Prog. Neurobiol.* **2001**, *65*, 1–105. [CrossRef]
22. Malik, A.R.; Willnow, T.E. Excitatory Amino Acid Transporters in Physiology and Disorders of the Central Nervous System. *Int. J. Mol. Sci.* **2019**, *20*, 5671. [CrossRef]

23. Lee, S.-G.; Su, Z.-Z.; Emdad, L.; Gupta, P.; Sarkar, D.; Borjabad, A.; Volsky, D.J.; Fisher, P.B. Mechanism of Ceftriaxone Induction of Excitatory Amino Acid Transporter-2 Expression and Glutamate Uptake in Primary Human Astrocytes. *J. Biol. Chem.* **2008**, *283*, 13116–13123. [CrossRef]
24. Rothstein, J.D.; Patel, S.; Regan, M.R.; Haenggeli, C.; Huang, Y.H.; Bergles, D.E.; Jin, L.; Hoberg, M.D.; Vidensky, S.; Chung, D.S.; et al. Beta-lactam antibiotics offer neuroprotection by increasing glutamate transporter expression. *Nature* **2005**, *433*, 73–77. [CrossRef]
25. Underhill, S.M.; Wheeler, D.S.; Li, M.; Watts, S.D.; Ingram, S.L.; Amara, S. Amphetamine Modulates Excitatory Neurotransmission through Endocytosis of the Glutamate Transporter EAAT3 in Dopamine Neurons. *Neuron* **2014**, *83*, 404–416. [CrossRef]
26. Jensen, A.A.; Erichsen, M.N.; Nielsen, C.W.; Stensbøl, T.B.; Kehler, J.; Bunch, L. Discovery of the First Selective Inhibitor of Excitatory Amino Acid Transporter Subtype 1. *J. Med. Chem.* **2009**, *52*, 912–915. [CrossRef]
27. Dunlop, J.; McIlvain, H.B.; Carrick, T.A.; Jow, B.; Lu, Q.; Kowal, D.; Lin, S.; Greenfield, A.; Grosanu, C.; Fan, K.; et al. Characterization of Novel Aryl-Ether, Biaryl, and Fluorene Aspartic Acid and Diaminopropionic Acid Analogs as Potent Inhibitors of the High-Affinity Glutamate Transporter EAAT2. *Mol. Pharmacol.* **2005**, *68*, 974–982. [CrossRef]
28. Wu, P.; Bjørn-Yoshimoto, W.E.; Staudt, M.; Jensen, A.A.; Bunch, L. Identification and Structure-Activity Relationship Study of Imidazo[1,2-a]pyridine-3-amines as First Selective Inhibitors of Excitatory Amino Acid Transporter Subtype 3 (EAAT3). *ACS Chem. Neurosci.* **2019**, *10*, 4414–4429. [CrossRef]
29. Dholkawala, F.; Voshavar, C.; Dutta, A.K. Synthesis and characterization of brain penetrant prodrug of neuroprotective D-264: Potential therapeutic application in the treatment of Parkinson's disease. *Eur. J. Pharm. Biopharm.* **2016**, *103*, 62–70. [CrossRef]
30. Weiss, M.D.; Rossignol, C.; Sumners, C.; Anderson, K.J. A pH-dependent increase in neuronal glutamate efflux in vitro: Possible involvement of ASCT1. *Brain Res.* **2005**, *1056*, 105–112. [CrossRef]
31. Bröer, A.; Brookes, N.; Ganapathy, V.; Dimmer, K.S.; Wagner, C.A.; Lang, F.; Bröer, S. The astroglial ASCT2 amino acid transporter as a mediator of glutamine efflux. *J. Neurochem.* **1999**, *73*, 2184–2194. [CrossRef]
32. Gliddon, C.M.; Shao, Z.; LeMaistre, J.L.; Anderson, C.M. Cellular distribution of the neutral amino acid transporter subtype ASCT2 in mouse brain. *J. Neurochem.* **2009**, *108*, 372–383. [CrossRef]
33. Weiss, M.D.; Derazi, S.; Kilberg, M.S.; Anderson, K.J. Ontogeny and localization of the neutral amino acid transporter ASCT1 in rat brain. *Dev. Brain Res.* **2001**, *130*, 183–190. [CrossRef]
34. Sakai, K.; Shimizu, H.; Koike, T.; Furuya, S.; Watanabe, M. Neutral Amino Acid Transporter ASCT1 Is Preferentially Expressed in l-Ser-Synthetic/Storing Glial Cells in the Mouse Brain with Transient Expression in Developing Capillaries. *J. Neurosci.* **2003**, *23*, 550–560. [CrossRef]
35. Kaplan, E.; Zubedat, S.; Radzishewsky, I.; Valenta, A.C.; Rechnitz, O.; Sason, H.; Sajrawi, C.; Bodner, O.; Konno, K.; Esaki, K.; et al. ASCT1 (Slc1a4) transporter is a physiologic regulator of brain d-serine and neurodevelopment. *Proc. Natl. Acad. Sci. USA* **2018**, *115*, 9628–9633. [CrossRef]
36. Fuchs, B.C.; Bode, B.P. Amino acid transporters ASCT2 and LAT1 in cancer: Partners in crime? *Semin. Cancer Biol.* **2005**, *15*, 254–266. [CrossRef]
37. Scalise, M.; Pochini, L.; Console, L.; Losso, M.A.; Indiveri, C. The Human SLC1A5 (ASCT2) Amino Acid Transporter: From Function to Structure and Role in Cell Biology. *Front. Cell Dev. Biol.* **2018**, *6*, 96. [CrossRef]
38. Vig, B.S.; Huttunen, K.M.; Laine, K.; Rautio, J. Amino acids as pro-moieties in prodrug design and development. *Adv. Drug Deliv. Rev.* **2013**, *65*, 1370–1385. [CrossRef]
39. Scalise, M.; Console, L.; Cosco, J.; Pochini, L.; Galluccio, M.; Indiveri, C. ASCT1 and ASCT2: Brother and Sister? *SLAS Discov.* **2021**, *26*, 1148–1163. [CrossRef]
40. Scopelliti, A.J.; Font, J.; Vandenberg, R.J.; Boudker, O.; Ryan, R.M. Structural characterisation reveals insights into substrate recognition by the glutamine transporter ASCT2/SLC1A5. *Nat. Commun.* **2018**, *9*, 38. [CrossRef]
41. Scopelliti, A.J.; Ryan, R.; Vandenberg, R.J. Molecular Determinants for Functional Differences between Alanine-Serine-Cysteine Transporter 1 and Other Glutamate Transporter Family Members. *J. Biol. Chem.* **2013**, *288*, 8250–8257. [CrossRef]
42. Li, Y.-X.; Yang, J.-Y.; Alcantara, M.; Abelian, G.; Kulkarni, A.; Staubli, U.; Foster, A.C. Inhibitors of the Neutral Amino Acid Transporters ASCT1 and ASCT2 Are Effective in In Vivo Models of Schizophrenia and Visual Dysfunction. *J. Pharmacol. Exp. Ther.* **2018**, *367*, 292–301. [CrossRef]
43. Grewer, C.; Grabsch, E. New inhibitors for the neutral amino acid transporter ASCT2 reveal its Na<sup>+</sup>-dependent anion leak. *J. Physiol.* **2004**, *557*, 747–759. [CrossRef]
44. Albers, T.; Marsiglia, W.; Thomas, T.; Gameiro, A.; Grewer, C. Defining Substrate and Blocker Activity of Alanine-Serine-Cysteine Transporter 2 (ASCT2) Ligands with Novel Serine Analogs. *Mol. Pharmacol.* **2011**, *81*, 356–365. [CrossRef]
45. Esslinger, C.S.; Cybulski, K.A.; Rhoderick, J.F. Ngamma-aryl glutamine analogues as probes of the ASCT2 neutral amino acid transporter binding site. *Bioorg. Med. Chem.* **2005**, *13*, 1111–1118. [CrossRef]
46. Singh, K.; Tanui, R.; Gameiro, A.; Eisenberg, G.; Colas, C.; Schlessinger, A.; Grewer, C. Structure activity relationships of benzylproline-derived inhibitors of the glutamine transporter ASCT2. *Bioorganic Med. Chem. Lett.* **2016**, *27*, 398–402. [CrossRef]
47. Patching, S.G. Glucose Transporters at the Blood-Brain Barrier: Function, Regulation and Gateways for Drug Delivery. *Mol. Neurobiol.* **2016**, *54*, 1046–1077. [CrossRef]
48. Buck, A.; Schirrmeister, H.; Mattfeldt, T.; Reske, S.N. Biological characterisation of breast cancer by means of PET. *Eur. J. Pediatr.* **2004**, *31*, S80–S87. [CrossRef]

49. Pliszka, M.; Szablewski, L. Glucose Transporters as a Target for Anticancer Therapy. *Cancers* **2021**, *13*, 4184. [CrossRef]
50. Younes, M.; Lechago, L.V.; Somoano, J.R.; Mosharaf, M.; Lechago, J. Wide expression of the human erythrocyte glucose transporter Glut1 in human cancers. *Cancer Res.* **1996**, *56*, 1164–1167.
51. Macheda, M.L.; Rogers, S.; Best, J. Molecular and cellular regulation of glucose transporter (GLUT) proteins in cancer. *J. Cell. Physiol.* **2004**, *202*, 654–662. [CrossRef]
52. Barron, C.C.; Bilan, P.J.; Tsakiridis, T.; Tsiani, E. Facilitative glucose transporters: Implications for cancer detection, prognosis and treatment. *Metabolism* **2015**, *65*, 124–139. [CrossRef]
53. Bonina, F.P.; Arenare, L.; Ippolito, R.; Boatto, G.; Battaglia, G.; Bruno, V.; de Caprariis, P. Synthesis, pharmacokinetics and anticonvulsant activity of 7-chlorokynurenic acid prodrugs. *Int. J. Pharm.* **2000**, *202*, 79–88. [CrossRef]
54. Bonina, F.; Puglia, C.; Rimoli, M.G.; Melisi, D.; Boatto, G.; Nieddu, M.; Calignano, A.; Rana, G.L.; Caprariis, P. Glycosyl derivatives of dopamine and L-dopa as anti-Parkinson prodrugs: Synthesis, pharmacological activity and in vitro stability studies. *J. Drug Target.* **2003**, *11*, 25–36. [CrossRef]
55. Fernández, C.; Nieto, O.; Fontenla, J.A.; Rivas, E.; de Ceballos, M.L.; Fernández-Mayoralas, A. Synthesis of glycosyl derivatives as dopamine prodrugs: Interaction with glucose carrier GLUT-1. *Org. Biomol. Chem.* **2003**, *1*, 767–771. [CrossRef]
56. Halmos, T.; Santarromana, M.; Antonakis, K.; Scherman, D. Synthesis of glucose-chlorambucil derivatives and their recognition by the human GLUT1 glucose transporter. *Eur. J. Pharmacol.* **1996**, *318*, 477–484. [CrossRef]
57. Bilsky, E.J.; Egleton, R.D.; Mitchell, S.A.; Palian, M.M.; Davis, P.; Huber, J.D.; Jones, H.; Yamamura, H.I.; Janders, J.; Davis, T.P.; et al. Enkephalin Glycopeptide Analogues Produce Analgesia with Reduced Dependence Liability. *J. Med. Chem.* **2000**, *43*, 2586–2590. [CrossRef]
58. Gynther, M.; Ropponen, J.; Laine, K.; Leppänen, J.; Haapakoski, P.; Peura, L.; Järvinen, T.; Rautio, J. Glucose Promoiety Enables Glucose Transporter Mediated Brain Uptake of Ketoprofen and Indomethacin Prodrugs in Rats. *J. Med. Chem.* **2009**, *52*, 3348–3353. [CrossRef]
59. Leenders, R.G.G.; Damen, E.W.P.; Bijsterveld, E.J.A.; Scheeren, H.W.; Houba, P.H.J.; Meulen-Muileman, I.H.; Boven, E.; Haisma, H.J. Novel anthracycline-spacer-beta-glucuronide,-beta-glucoside, and -beta-galactoside prodrugs for application in selective chemotherapy. *Bioorg. Med. Chem.* **1999**, *7*, 1597–1610. [CrossRef]
60. Tranoy-Opalinski, I.; Legigan, T.; Barat, R.; Clarhaut, J.; Thomas, M.; Renoux, B.; Papot, S.  $\beta$ -Glucuronidase-responsive prodrugs for selective cancer chemotherapy: An update. *Eur. J. Med. Chem.* **2014**, *74*, 302–313. [CrossRef]
61. Matović, J.; Järvinen, J.; Sokka, I.K.; Imlimhan, S.; Raitanen, J.-E.; Montaser, A.; Maaheimo, H.; Huttunen, K.M.; Peräniemi, S.; Airaksinen, A.J.; et al. Exploring the Biochemical Foundations of a Successful GLUT1-Targeting Strategy to BNCT: Chemical Synthesis and *In Vitro* Evaluation of the Entire Positional Isomer Library of *ortho*-Carboranyl-methyl-Bearing Glucoconjugates. *Mol. Pharm.* **2020**, *18*, 285–304. [CrossRef]
62. Zhang, K.; Xu, P.; Sowers, J.L.; Machuca, D.F.; Mirfattah, B.; Herring, J.; Tang, H.; Chen, Y.; Tian, B.; Brasier, A.R.; et al. Proteome Analysis of Hypoxic Glioblastoma Cells Reveals Sequential Metabolic Adaptation of One-Carbon Metabolic Pathways. *Mol. Cell. Proteom.* **2017**, *16*, 1906–1921. [CrossRef]
63. Ohnishi, K.; Misawa, M.; Sikano, N.; Nakai, K.; Suzuki, M. Enhancement of Cancer Cell-Killing Effects of Boron Neutron Capture Therapy by Manipulating the Expression of L-Type Amino Acid Transporter 1. *Radiat. Res.* **2021**, *196*, 17–22. [CrossRef]
64. Drew, D.; North, R.A.; Nagarathinam, K.; Tanabe, M. Structures and General Transport Mechanisms by the Major Facilitator Superfamily (MFS). *Chem. Rev.* **2021**, *121*, 5289–5335. [CrossRef]
65. Galochkina, T.; Chong, M.N.F.; Challali, L.; Abbar, S.; Etchebest, C. New insights into GluT1 mechanics during glucose transfer. *Sci. Rep.* **2019**, *9*, 998. [CrossRef]
66. Gonzalez-Resines, S.; Quinn, P.J.; Naftalin, R.J.; Domene, C. Multiple Interactions of Glucose with the Extra-Membranous Loops of GLUT1 Aid Transport. *J. Chem. Inf. Model.* **2021**, *61*, 3559–3570. [CrossRef]
67. Park, M.-S. Molecular Dynamics Simulations of the Human Glucose Transporter GLUT1. *PLoS ONE* **2015**, *10*, e0125361. [CrossRef]
68. Tachikawa, M.; Hirose, S.; Akanuma, S.-I.; Matsuyama, R.; Hosoya, K.-I. Developmental changes of l-arginine transport at the blood-brain barrier in rats. *Microvasc. Res.* **2018**, *117*, 16–21. [CrossRef]
69. Hosokawa, H.; Ninomiya, H.; Sawamura, T.; Sugimoto, Y.; Ichikawa, A.; Fujiwara, K.; Masaki, T. Neuron-specific expression of cationic amino acid transporter 3 in the adult rat brain. *Brain Res.* **1999**, *838*, 158–165. [CrossRef]
70. Braissant, O.; Gotoh, T.; Loup, M.; Mori, M.; Bachmann, C. Differential expression of the cationic amino acid transporter 2(B) in the adult rat brain. *Mol. Brain Res.* **2001**, *91*, 189–195. [CrossRef]
71. Stevens, B.R.; Kakuda, D.K.; Yu, K.; Waters, M.; Vo, C.B.; Raizada, M.K. Induced Nitric Oxide Synthesis Is Dependent on Induced Alternatively Spliced CAT-2 Encoding L-Arginine Transport in Brain Astrocytes. *J. Biol. Chem.* **1996**, *271*, 24017–24022. [CrossRef]
72. Zaragoza, R. Transport of Amino Acids Across the Blood-Brain Barrier. *Front. Physiol.* **2020**, *11*, 973. [CrossRef]
73. Huang, Y.; Kang, B.N.; Tian, J.; Liu, Y.; Luo, H.R.; Hester, L.; Snyder, S.H. The Cationic Amino Acid Transporters CAT1 and CAT3 Mediate NMDA Receptor Activation-Dependent Changes in Elaboration of Neuronal Processes via the Mammalian Target of Rapamycin mTOR Pathway. *J. Neurosci.* **2007**, *27*, 449–458. [CrossRef]
74. Dai, R.; Peng, F.; Xiao, X.; Gong, X.; Jiang, Y.; Zhang, M.; Tian, Y.; Xu, Y.; Ma, J.; Li, M.; et al. Hepatitis B virus X protein-induced upregulation of CAT-1 stimulates proliferation and inhibits apoptosis in hepatocellular carcinoma cells. *Oncotarget* **2017**, *8*, 60962–60974. [CrossRef]

75. Abdelmagid, S.A.; Rickard, J.A.; McDonald, W.J.; Thomas, L.N.; Too, C.K. CAT-1-mediated arginine uptake and regulation of nitric oxide synthases for the survival of human breast cancer cell lines. *J. Cell. Biochem.* **2011**, *112*, 1084–1092. [CrossRef]
76. Lu, Y.; Wang, W.; Wang, J.; Yang, C.; Mao, H.; Fu, X.; Wu, Y.; Cai, J.; Han, J.; Xu, Z.; et al. Overexpression of Arginine Transporter CAT-1 Is Associated with Accumulation of L-Arginine and Cell Growth in Human Colorectal Cancer Tissue. *PLoS ONE* **2013**, *8*, e73866. [CrossRef]
77. Werner, A.; Pieh, D.; Echchannaoui, H.; Rupp, J.; Rajalingam, K.; Theobald, M.; Closs, E.I.; Munder, M. Cationic Amino Acid Transporter-1-Mediated Arginine Uptake Is Essential for Chronic Lymphocytic Leukemia Cell Proliferation and Viability. *Front. Oncol.* **2019**, *9*, 1268. [CrossRef]
78. Jungnickel, K.E.J.; Parker, J.; Newstead, S. Structural basis for amino acid transport by the CAT family of SLC7 transporters. *Nat. Commun.* **2018**, *9*, 550. [CrossRef]
79. Fort, J.; Nicolàs-Aragó, A.; Palacín, M. The Ectodomains of rBAT and 4F2hc Are Fake or Orphan  $\alpha$ -Glucosidases. *Molecules* **2021**, *26*, 6231. [CrossRef]
80. Estrach, S.; Lee, S.-A.; Boulter, E.; Pisano, S.; Errante, A.; Tissot, F.S.; Cailleteau, L.; Pons, C.; Ginsberg, M.H.; Féral, C.C. CD98hc (SLC3A2) Loss Protects Against Ras-Driven Tumorigenesis by Modulating Integrin-Mediated Mechanotransduction. *Cancer Res.* **2014**, *74*, 6878–6889. [CrossRef]
81. Feral, C.C.; Nishiya, N.; Fenczik, C.A.; Stuhlmann, H.; Slepak, M.; Ginsberg, M.H. CD98hc (SLC3A2) mediates integrin signaling. *Proc. Natl. Acad. Sci. USA* **2004**, *102*, 355–360. [CrossRef]
82. Kanai, Y.; Segawa, H.; Miyamoto, K.-I.; Uchino, H.; Takeda, E.; Endou, H. Expression Cloning and Characterization of a Transporter for Large Neutral Amino Acids Activated by the Heavy Chain of 4F2 Antigen (CD98). *J. Biol. Chem.* **1998**, *273*, 23629–23632. [CrossRef]
83. Prasad, P.D.; Wang, H.; Huang, W.; Kekuda, R.; Rajan, D.P.; Leibach, F.H.; Ganapathy, V. Human LAT1, a Subunit of System L Amino Acid Transporter: Molecular Cloning and Transport Function. *Biochem. Biophys. Res. Commun.* **1999**, *255*, 283–288. [CrossRef]
84. Boado, R.J.; Li, J.Y.; Nagaya, M.; Zhang, C.; Pardridge, W.M. Selective expression of the large neutral amino acid transporter at the blood–brain barrier. *Proc. Natl. Acad. Sci. USA* **1999**, *96*, 12079–12084. [CrossRef]
85. Scalise, M.; Galluccio, M.; Console, L.; Pochini, L.; Indiveri, C. The Human SLC7A5 (LAT1): The Intriguing Histidine/Large Neutral Amino Acid Transporter and Its Relevance to Human Health. *Front. Chem.* **2018**, *6*, 243. [CrossRef]
86. Huttunen, J.; Peltokangas, S.; Gynther, M.; Natunen, T.; Hiltunen, M.; Auriola, S.; Ruponen, M.; Vellonen, K.-S.; Huttunen, K.M. L-Type Amino Acid Transporter 1 (LAT1/Lat1)-Utilizing Prodrugs Can Improve the Delivery of Drugs into Neurons, Astrocytes and Microglia. *Sci. Rep.* **2019**, *9*, 12860. [CrossRef]
87. Duelli, R.; Enerson, B.E.; Gerhart, D.Z.; Drewes, L.R. Expression of Large Amino Acid Transporter LAT1 in Rat Brain Endothelium. *J. Cereb. Blood Flow Metab.* **2000**, *20*, 1557–1562. [CrossRef]
88. Yanagida, O.; Kanai, Y.; Chairoungdua, A.; Kim, D.K.; Segawa, H.; Nii, T.; Cha, S.H.; Matsuo, H.; Fukushima, J.-I.; Fukasawa, Y.; et al. Human L-type amino acid transporter 1 (LAT1): Characterization of function and expression in tumor cell lines. *Biochim. Biophys. Acta Biomembr.* **2001**, *1514*, 291–302. [CrossRef]
89. Wang, Q.; Holst, J. L-type amino acid transport and cancer: Targeting the mTORC1 pathway to inhibit neoplasia. *Am. J. Cancer Res.* **2015**, *5*, 1281–1294.
90. Häfliger, P.; Charles, R.-P. The L-Type Amino Acid Transporter LAT1—An Emerging Target in Cancer. *Int. J. Mol. Sci.* **2019**, *20*, 2428. [CrossRef]
91. Furuya, M.; Horiguchi, J.; Nakajima, H.; Kanai, Y.; Oyama, T. Correlation of L-type amino acid transporter 1 and CD98 expression with triple negative breast cancer prognosis. *Cancer Sci.* **2011**, *103*, 382–389. [CrossRef]
92. Sakata, T.; Ferdous, G.; Tsuruta, T.; Satoh, T.; Baba, S.; Muto, T.; Ueno, A.; Kanai, Y.; Endou, H.; Okayasu, I. L-type amino-acid transporter 1 as a novel biomarker for high-grade malignancy in prostate cancer. *Pathol. Int.* **2009**, *59*, 7–18. [CrossRef]
93. Hayashi, K.; Anzai, N. Novel therapeutic approaches targeting L-type amino acid transporters for cancer treatment. *World J. Gastrointest. Oncol.* **2017**, *9*, 21–29. [CrossRef]
94. Tärklungeanu, D.C.; Deliu, E.; Dotter, C.P.; Kara, M.; Janiesch, P.C.; Scalise, M.; Galluccio, M.; Tesulov, M.; Morelli, E.; Sonmez, F.M.; et al. Impaired Amino Acid Transport at the Blood Brain Barrier Is a Cause of Autism Spectrum Disorder. *Cell* **2016**, *167*, 1481–1494. [CrossRef]
95. Kärkkäinen, J.; Gynther, M.; Kokkola, T.; Petsalo, A.; Auriola, S.; Lahtela-Kakkonen, M.; Laine, K.; Rautio, J.; Huttunen, K.M. Structural properties for selective and efficient l-type amino acid transporter 1 (LAT1) mediated cellular uptake. *Int. J. Pharm.* **2018**, *544*, 91–99. [CrossRef]
96. Kärkkäinen, J.; Laitinen, T.; Markowicz-Piasecka, M.; Montaser, A.; Lehtonen, M.; Rautio, J.; Gynther, M.; Poso, A.; Huttunen, K.M. Molecular characteristics supporting l-Type amino acid transporter 1 (LAT1)-mediated translocation. *Bioorganic Chem.* **2021**, *112*, 104921. [CrossRef]
97. Lee, Y.; Wiriyasermkul, P.; Jin, C.; Quan, L.; Ohgaki, R.; Okuda, S.; Kusakizako, T.; Nishizawa, T.; Oda, K.; Ishitani, R.; et al. Cryo-EM structure of the human L-type amino acid transporter 1 in complex with glycoprotein CD98hc. *Nat. Struct. Mol. Biol.* **2019**, *26*, 510–517. [CrossRef]
98. Yan, R.; Zhao, X.; Lei, J.; Zhou, Q. Structure of the human LAT1–4F2hc heteromeric amino acid transporter complex. *Nature* **2019**, *568*, 127–130. [CrossRef]

99. Chien, H.-C.; Colas, C.; Finke, K.; Springer, S.; Stoner, L.; Zur, A.A.; Venteicher, B.; Campbell, J.; Hall, C.; Flint, A.; et al. Reevaluating the Substrate Specificity of the L-Type Amino Acid Transporter (LAT1). *J. Med. Chem.* **2018**, *61*, 7358–7373. [CrossRef]
100. Tampio, J.; Löffler, S.; Guillon, M.; Hügele, A.; Huttunen, J.; Huttunen, K.M. Improved L-Type amino acid transporter 1 (LAT1)-mediated delivery of anti-inflammatory drugs into astrocytes and microglia with reduced prostaglandin production. *Int. J. Pharm.* **2021**, *601*, 120565. [CrossRef]
101. Forrest, L.; Rudnick, G. The Rocking Bundle: A Mechanism for Ion-Coupled Solute Flux by Symmetrical Transporters. *Physiology* **2009**, *24*, 377–386. [CrossRef]
102. Gynther, M.; Peura, L.; Vernerová, M.; Leppänen, J.; Kärkkäinen, J.; Lehtonen, M.; Rautio, J.; Huttunen, K.M. Amino Acid Promoiety Alters Valproic Acid Pharmacokinetics and Enables Extended Brain Exposure. *Neurochem. Res.* **2016**, *41*, 2797–2809. [CrossRef]
103. Gynther, M.; Pickering, D.S.; Spicer, J.A.; Denny, W.A.; Huttunen, K.M. Systemic and Brain Pharmacokinetics of Perforin Inhibitor Prodrugs. *Mol. Pharm.* **2016**, *13*, 2484–2491. [CrossRef]
104. Montaser, A.B.; Järvinen, J.; Löffler, S.; Huttunen, J.; Auriola, S.; Lehtonen, M.; Jalkanen, A.; Huttunen, K.M. L-Type Amino Acid Transporter 1 Enables the Efficient Brain Delivery of Small-Sized Prodrug across the Blood–Brain Barrier and into Human and Mouse Brain Parenchymal Cells. *ACS Chem. Neurosci.* **2020**, *11*, 4301–4315. [CrossRef]
105. Peura, L.; Malmioja, K.; Huttunen, K.; Leppänen, J.; Hämäläinen, M.; Forsberg, M.M.; Rautio, J.; Laine, K. Design, Synthesis and Brain Uptake of LAT1-Targeted Amino Acid Prodrugs of Dopamine. *Pharm. Res.* **2013**, *30*, 2523–2537. [CrossRef]
106. Puris, E.; Gynther, M.; Huttunen, J.; Petsalo, A.; Huttunen, K.M. L-type amino acid transporter 1 utilizing prodrugs: How to achieve effective brain delivery and low systemic exposure of drugs. *J. Control. Release* **2017**, *261*, 93–104. [CrossRef]
107. Puris, E.; Gynther, M.; Huttunen, J.; Auriola, S.; Huttunen, K.M. L-type amino acid transporter 1 utilizing prodrugs of ferulic acid revealed structural features supporting the design of prodrugs for brain delivery. *Eur. J. Pharm. Sci.* **2019**, *129*, 99–109. [CrossRef]
108. Hokari, M.; Wu, H.-Q.; Schwarcz, R.; Smith, Q.R. Facilitated brain uptake of 4-chlorokynurenine and conversion to 7-chlorokynurenic acid. *NeuroReport* **1996**, *8*, 15–18. [CrossRef]
109. Okano, N.; Naruge, D.; Kawai, K.; Kobayashi, T.; Nagashima, F.; Endou, H.; Furuse, J. First-in-human phase I study of JPH203, an L-type amino acid transporter 1 inhibitor, in patients with advanced solid tumors. *Investig. New Drugs* **2020**, *38*, 1495–1506. [CrossRef]
110. Segawa, H.; Fukasawa, Y.; Miyamoto, K.-I.; Takeda, E.; Endou, H.; Kanai, Y. Identification and Functional Characterization of a Na<sup>+</sup>-independent Neutral Amino Acid Transporter with Broad Substrate Selectivity. *J. Biol. Chem.* **1999**, *274*, 19745–19751. [CrossRef]
111. Pineda, M.; Fernández, E.; Torrents, D.; Estevez, R.; López, C.; Camps, M.; Lloberas, J.; Zorzano, A.; Palacín, M. Identification of a Membrane Protein, LAT-2, That Co-expresses with 4F2 Heavy Chain, an L-type Amino Acid Transport Activity with Broad Specificity for Small and Large Zwitterionic Amino Acids. *J. Biol. Chem.* **1999**, *274*, 19738–19744. [CrossRef]
112. Bröer, A.; Wagner, C.A.; Lang, F.; Bröer, S. The heterodimeric amino acid transporter 4F2hc/y+LAT2 mediates arginine efflux in exchange with glutamine. *Biochem. J.* **2000**, *349*, 787–795. [CrossRef]
113. Meier, C.; Ristic, Z.; Klausner, S.; Verrey, F. Activation of system L heterodimeric amino acid exchangers by intracellular substrates. *EMBO J.* **2002**, *21*, 580–589. [CrossRef]
114. Braun, D.; Kinne, A.; Bräuer, A.U.; Sapin, R.; Klein, M.O.; Köhrle, J.; Wirth, E.K.; Schweizer, U. Developmental and cell type-specific expression of thyroid hormone transporters in the mouse brain and in primary brain cells. *Glia* **2010**, *59*, 463–471. [CrossRef]
115. Milewski, K.; Bogacińska-Karaś, M.; Fręsko, I.; Hilgier, W.; Jaźwiec, R.; Albrecht, J.; Zielińska, M. Ammonia Reduces Intracellular Asymmetric Dimethylarginine in Cultured Astrocytes Stimulating Its y+LAT2 Carrier-Mediated Loss. *Int. J. Mol. Sci.* **2017**, *18*, 2308. [CrossRef]
116. Zielińska, M.; Milewski, K.; Skowrońska, M.; Gajos, A.; Zieminska, E.; Beresewicz, A.; Albrecht, J.K. Induction of inducible nitric oxide synthase expression in ammonia-exposed cultured astrocytes is coupled to increased arginine transport by upregulated y+LAT2 transporter. *J. Neurochem.* **2015**, *135*, 1272–1281. [CrossRef]
117. Kinne, A.; Wittner, M.; Wirth, E.K.; Hinz, K.M.; Schüle, R.; Köhrle, J.; Krause, G. Involvement of the L-Type Amino Acid Transporter Lat2 in the Transport of 3,3'-Diiodothyronine across the Plasma Membrane. *Eur. Thyroid J.* **2015**, *4*, 42–50. [CrossRef]
118. Zevenbergen, C.; Meima, M.E.; Lima de Souza, E.C.; Peeters, R.P.; Kinne, A.; Krause, G.; Visser, W.E.; Visser, T.J. Transport of Iodothyronines by Human L-Type Amino Acid Transporters. *Endocrinology* **2015**, *156*, 4345–4355. [CrossRef]
119. Pinto, V.; Pinho, M.J.; Soares-Da-Silva, P. Renal amino acid transport systems and essential hypertension. *FASEB J.* **2013**, *27*, 2927–2938. [CrossRef]
120. Barollo, S.; Bertazza, L.; Fernando, S.W.; Censi, S.; Cavedon, E.; Galuppini, F.; Pennelli, G.; Fassina, A.; Citton, M.; Rubin, B.; et al. Overexpression of L-Type Amino Acid Transporter 1 (LAT1) and 2 (LAT2): Novel Markers of Neuroendocrine Tumors. *PLoS ONE* **2016**, *11*, e0156044. [CrossRef]
121. Feng, M.; Xiong, G.; Cao, Z.; Yang, G.; Zheng, S.; Qiu, J.; You, L.; Zheng, L.; Zhang, T.; Zhao, Y. LAT2 regulates glutamine-dependent mTOR activation to promote glycolysis and chemoresistance in pancreatic cancer. *J. Exp. Clin. Cancer Res.* **2018**, *37*, 274. [CrossRef]



122. Yan, R.; Zhou, J.; Li, Y.; Lei, J.; Zhou, Q. Structural insight into the substrate recognition and transport mechanism of the human LAT2–4F2hc complex. *Cell Discov.* **2020**, *6*, 82. [CrossRef]
123. Nakauchi, J.; Matsuo, H.; Kim, D.K.; Goto, A.; Chairoungdua, A.; Cha, S.H.; Inatomi, J.; Shiokawa, Y.; Yamaguchi, K.; Saito, I.; et al. Cloning and characterization of a human brain Na<sup>+</sup>-independent transporter for small neutral amino acids that transports d-serine with high affinity. *Neurosci. Lett.* **2000**, *287*, 231–235. [CrossRef]
124. Fukasawa, Y.; Segawa, H.; Kim, J.Y.; Chairoungdua, A.; Kim, D.K.; Matsuo, H.; Cha, S.H.; Endou, H.; Kanai, Y. Identification and Characterization of a Na<sup>+</sup>-independent Neutral Amino Acid Transporter That Associates with the 4F2 Heavy Chain and Exhibits Substrate Selectivity for Small Neutral d- and l-Amino Acids. *J. Biol. Chem.* **2000**, *275*, 9690–9698. [CrossRef]
125. Bassi, M.; Gasol, E.; Manzoni, M.; Pineda, M.; Riboni, M.; Martín, R.; Zorzano, A.; Borsani, G.; Palacín, M. Identification and characterisation of human xCT that co-expresses, with 4F2 heavy chain, the amino acid transport activity system x<sup>c-</sup>. *Pflug. Arch.* **2001**, *442*, 286–296. [CrossRef]
126. Sato, H.; Tamba, M.; Ishii, T.; Bannai, S. Cloning and Expression of a Plasma Membrane Cystine/Glutamate Exchange Transporter Composed of Two Distinct Proteins. *J. Biol. Chem.* **1999**, *274*, 11455–11458. [CrossRef]
127. Rutter, A.R.; Fradley, R.L.; Garrett, E.M.; Chapman, K.L.; Lawrence, J.M.; Rosahl, T.W.; Patel, S. Evidence from gene knockout studies implicates Asc-1 as the primary transporter mediating d-serine reuptake in the mouse CNS. *Eur. J. Neurosci.* **2007**, *25*, 1757–1766. [CrossRef]
128. Helboe, L.; Egebjerg, J.; Møller, M.; Thomsen, C. Distribution and pharmacology of alanine-serine-cysteine transporter 1 (asc-1) in rodent brain. *Eur. J. Neurosci.* **2003**, *18*, 2227–2238. [CrossRef]
129. Xie, X.; Dumas, T.; Tang, L.; Brennan, T.; Reeder, T.; Thomas, W.; Klein, R.D.; Flores, J.; O'Hara, B.F.; Heller, H.C.; et al. Lack of the alanine-serine-cysteine transporter 1 causes tremors, seizures, and early postnatal death in mice. *Brain Res.* **2005**, *1052*, 212–221. [CrossRef]
130. Seib, T.M.; Patel, S.A.; Bridges, R.J. Regulation of the System x<sup>-</sup>C cystine/glutamate exchanger by intracellular glutathione levels in rat astrocyte primary cultures. *Glia* **2011**, *59*, 1387–1401. [CrossRef]
131. Lewerenz, J.; Maher, P.; Methner, A. Regulation of xCT expression and system x<sup>(c)</sup> (-) function in neuronal cells. *Amino Acids* **2012**, *42*, 171–179. [CrossRef]
132. Lewerenz, J.; Hewett, S.J.; Huang, Y.; Lambros, M.; Gout, P.W.; Kalivas, P.W.; Massie, A.; Smolders, I.; Methner, A.; Pergande, M.; et al. The cystine/glutamate antiporter system x<sup>(c)</sup>(-) in health and disease: From molecular mechanisms to novel therapeutic opportunities. *Antioxid. Redox Signal.* **2013**, *18*, 522–555. [CrossRef]
133. Sato, M.; Onuma, K.; Domon, M.; Hasegawa, S.; Suzuki, A.; Kusumi, R.; Hino, R.; Kakihara, N.; Kanda, Y.; Osaki, M.; et al. Loss of the cystine/glutamate antiporter in melanoma abrogates tumor metastasis and markedly increases survival rates of mice. *Int. J. Cancer* **2020**, *147*, 3224–3235. [CrossRef]
134. Conrad, M.; Sato, H. The oxidative stress-inducible cystine/glutamate antiporter, system x<sup>(c)</sup> (-): Cystine supplier and beyond. *Amino Acids* **2012**, *42*, 231–246. [CrossRef]
135. Kutchukian, P.S.; Warren, L.; Magliaro, B.C.; Amoss, A.; Cassaday, J.A.; O'Donnell, G.; Squadroni, B.; Zuck, P.; Pascarella, D.; Culberson, J.C.; et al. Iterative Focused Screening with Biological Fingerprints Identifies Selective Asc-1 Inhibitors Distinct from Traditional High Throughput Screening. *ACS Chem. Biol.* **2017**, *12*, 519–527. [CrossRef]
136. Patel, D.; Kharkar, P.S.; Gandhi, N.S.; Kaur, E.; Dutt, S.; Nandave, M. Novel analogs of sulfasalazine as system x<sup>(c)</sup> (-) antiporter inhibitors: Insights from the molecular modeling studies. *Drug Dev. Res.* **2019**, *80*, 758–777. [CrossRef]
137. Halestrap, A.P. The monocarboxylate transporter family—Structure and functional characterization. *IUBMB Life* **2011**, *64*, 1–9. [CrossRef]
138. Halestrap, A.P. The SLC16 gene family—Structure, role and regulation in health and disease. *Mol. Asp. Med.* **2013**, *34*, 337–349. [CrossRef]
139. Halestrap, A.P.; Meredith, D. The SLC16 gene family?from monocarboxylate transporters (MCTs) to aromatic amino acid transporters and beyond. *Pflug. Arch.* **2003**, *447*, 619–628. [CrossRef]
140. Chiry, O.; Pellerin, L.; Monnet-Tschudi, F.; Fishbein, W.N.; Merezinskaya, N.; Magistretti, P.J.; Clarke, S. Expression of the monocarboxylate transporter MCT1 in the adult human brain cortex. *Brain Res.* **2006**, *1070*, 65–70. [CrossRef]
141. Halestrap, A.P.; Wilson, M.C. The monocarboxylate transporter family—Role and regulation. *IUBMB Life* **2011**, *64*, 109–119. [CrossRef] [PubMed]
142. Deguchi, Y.; Nozawa, K.; Yamada, S.; Yokoyama, Y.; Kimura, R. Quantitative evaluation of brain distribution and blood-brain barrier efflux transport of probenecid in rats by microdialysis: Possible involvement of the monocarboxylic acid transport system. *J. Pharmacol. Exp. Ther.* **1997**, *280*, 551–560. [PubMed]
143. Deguchi, Y.; Yokoyama, Y.; Sakamoto, T.; Hayashi, H.; Naito, T.; Yamada, S.; Kimura, R. Brain distribution of 6-mercaptopurine is regulated by the efflux transport system in the blood-brain barrier 1. *Life Sci.* **2000**, *66*, 649–662. [CrossRef]
144. Felmler, M.A.; Morse, B.L.; Morris, M.E.  $\gamma$ -Hydroxybutyric Acid: Pharmacokinetics, Pharmacodynamics, and Toxicology. *AAPS J.* **2021**, *23*, 22. [CrossRef] [PubMed]
145. Lee, N.-Y.; Kang, Y.-S. In Vivo and In Vitro Evidence for Brain Uptake of 4-Phenylbutyrate by the Monocarboxylate Transporter 1 (MCT1). *Pharm. Res.* **2016**, *33*, 1711–1722. [CrossRef] [PubMed]
146. Kang, Y.; Terasaki, T.; Tsuji, A. Acidic drug transport in vivo through the blood-brain barrier. A role of the transport carrier for monocarboxylic acids. *J. Pharm. Dyn.* **1990**, *13*, 158–163. [CrossRef]

147. Terasaki, T.; Takakuwa, S.; Moritani, S.; Tsuji, A. Transport of monocarboxylic acids at the blood-brain barrier: Studies with monolayers of primary cultured bovine brain capillary endothelial cells. *J. Pharmacol. Exp. Ther.* **1991**, *258*, 932–937.
148. Friesema, E.C.H.; Ganguly, S.; Abdalla, A.; Manning Fox, J.E.; Halestrap, A.P.; Visser, T.J. Identification of Monocarboxylate Transporter 8 as a Specific Thyroid Hormone Transporter. *J. Biol. Chem.* **2003**, *278*, 40128–40135. [CrossRef]
149. Roberts, L.M.; Woodford, K.; Zhou, M.; Black, D.S.; Haggerty, J.E.; Tate, E.H.; Grindstaff, K.K.; Mengesha, W.; Raman, C.; Zerangue, N. Expression of the Thyroid Hormone Transporters Monocarboxylate Transporter-8 (SLC16A2) and Organic Ion Transporter-14 (SLCO1C1) at the Blood-Brain Barrier. *Endocrinology* **2008**, *149*, 6251–6261. [CrossRef]
150. Heuer, H.; Maier, M.K.; Iden, S.; Mittag, J.; Friesema, E.C.H.; Visser, T.J.; Bauer, K. The Monocarboxylate Transporter 8 Linked to Human Psychomotor Retardation Is Highly Expressed in Thyroid Hormone-Sensitive Neuron Populations. *Endocrinology* **2005**, *146*, 1701–1706. [CrossRef]
151. Groeneweg, S.; Geest, F.S.; Peeters, R.P.; Heuer, H.; Visser, W.E. Thyroid Hormone Transporters. *Endocr. Rev.* **2020**, *41*, 146–201. [CrossRef] [PubMed]
152. Di Cosmo, C.; De Marco, G.; Agretti, P.; Ferrarini, E.; Dimida, A.; Falcetta, P.; Benvenga, S.; Vitti, P.; Tonacchera, M. Screening for drugs potentially interfering with MCT8-mediated T3 transport in vitro identifies dexamethasone and some commonly used drugs as inhibitors of MCT8 activity. *J. Endocrinol. Investig.* **2021**, *45*, 803–814. [CrossRef] [PubMed]
153. Bergersen, L.H. Lactate Transport and Signaling in the Brain: Potential Therapeutic Targets and Roles in Body–Brain Interaction. *J. Cereb. Blood Flow Metab.* **2014**, *35*, 176–185. [CrossRef] [PubMed]
154. Bröer, S.; Rahman, B.; Pellegrini, G.; Pellerin, L.; Martin, J.-L.; Verleysdonk, S.; Hamprecht, B.; Magistretti, P.J. Comparison of Lactate Transport in Astroglial Cells and Monocarboxylate Transporter 1 (MCT 1) Expressing *Xenopus laevis* Oocytes. *J. Biol. Chem.* **1997**, *272*, 30096–30102. [CrossRef] [PubMed]
155. Lin, R.-Y.; Vera, J.C.; Chaganti, R.S.K.; Golde, D.W. Human Monocarboxylate Transporter 2 (MCT2) Is a High Affinity Pyruvate Transporter. *J. Biol. Chem.* **1998**, *273*, 28959–28965. [CrossRef] [PubMed]
156. Philp, N.J.; Wang, D.; Yoon, H.; Hjelmeland, L.M. Polarized Expression of Monocarboxylate Transporters in Human Retinal Pigment Epithelium and ARPE-19 Cells. *Investig. Ophthalmol. Vis. Sci.* **2003**, *44*, 1716–1721. [CrossRef] [PubMed]
157. Kobayashi, M.; Otsuka, Y.; Itagaki, S.; Hirano, T.; Iseki, K. Inhibitory effects of statins on human monocarboxylate transporter 4. *Int. J. Pharm.* **2006**, *317*, 19–25. [CrossRef]
158. Dimmer, K.S.; Friedrich, B.; Lang, F.; Deitmer, J.W.; Bröer, S. The low-affinity monocarboxylate transporter MCT4 is adapted to the export of lactate in highly glycolytic cells. *Biochem. J.* **2000**, *350*, 219–227. [CrossRef]
159. Gandhi, G.K.; Cruz, N.F.; Ball, K.K.; Dienel, G.A. Astrocytes are poised for lactate trafficking and release from activated brain and for supply of glucose to neurons. *J. Neurochem.* **2009**, *111*, 522–536. [CrossRef]
160. Cheng, C.; Edin, N.F.J.; Lauritzen, K.H.; Aspmo, I.; Christoffersen, S.; Jian, L.; Rasmussen, L.J.; Pettersen, E.O.; Xiaoqun, G.; Bergersen, L.H. Alterations of monocarboxylate transporter densities during hypoxia in brain and breast tumour cells. *Cell. Oncol.* **2012**, *35*, 217–227. [CrossRef]
161. Pinheiro, C.; Longatto-Filho, A.; Azevedo-Silva, J.; Casal, M.; Schmitt, F.C.; Baltazar, F. Role of monocarboxylate transporters in human cancers: State of the art. *J. Bioenerg. Biomembr.* **2012**, *44*, 127–139. [CrossRef] [PubMed]
162. Curtis, N.J.; Mooney, L.; Hopcroft, L.; Michopoulos, F.; Whalley, N.; Zhong, H.; Murray, C.; Logie, A.; Revill, M.; Byth, K.F.; et al. Pre-clinical pharmacology of AZD3965, a selective inhibitor of MCT1: DLBCL, NHL and Burkitt's lymphoma anti-tumor activity. *Oncotarget* **2017**, *8*, 69219–69236. [CrossRef] [PubMed]
163. Felmler, M.A.; Jones, R.S.; Rodriguez-Cruz, V.; Follman, K.E.; Morris, M.E. Monocarboxylate Transporters (SLC16): Function, Regulation, and Role in Health and Disease. *Pharmacol. Rev.* **2020**, *72*, 466–485. [CrossRef] [PubMed]
164. Guan, X.; Morris, M.E. In Vitro and In Vivo Efficacy of AZD3965 and Alpha-Cyano-4-Hydroxycinnamic Acid in the Murine 4T1 Breast Tumor Model. *AAPS J.* **2020**, *22*, 84. [CrossRef]
165. Medin, T.; Medin, H.; Hefte, M.B.; Storm-Mathisen, J.; Bergersen, L.H. Upregulation of the lactate transporter monocarboxylate transporter 1 at the blood-brain barrier in a rat model of attention-deficit/hyperactivity disorder suggests hyperactivity could be a form of self-treatment. *Behav. Brain Res.* **2018**, *360*, 279–285. [CrossRef] [PubMed]
166. Fisel, P.; Schaeffeler, E.; Schwab, M. Clinical and Functional Relevance of the Monocarboxylate Transporter Family in Disease Pathophysiology and Drug Therapy. *Clin. Transl. Sci.* **2018**, *11*, 352–364. [CrossRef] [PubMed]
167. Pertega-Gomes, N.; Vizcaíno, J.R.; Felisbino, S.; Warren, A.Y.; Shaw, G.; Kay, J.; Whitaker, H.; Lynch, A.G.; Fryer, L.; Neal, D.E.; et al. Epigenetic and oncogenic regulation of SLC16A7 (MCT2) results in protein over-expression, impacting on signalling and cellular phenotypes in prostate cancer. *Oncotarget* **2015**, *6*, 21675–21684. [CrossRef]
168. Ullah, M.S.; Davies, A.J.; Halestrap, A.P. The plasma membrane lactate transporter MCT4, but not MCT1, is up-regulated by hypoxia through a HIF-1 $\alpha$ -dependent mechanism. *J. Biol. Chem.* **2006**, *281*, 9030–9037. [CrossRef]
169. Lu, W.; Huang, J.; Sun, S.; Huang, S.; Gan, S.; Xu, J.; Yang, M.; Xu, S.; Jiang, X. Changes in lactate content and monocarboxylate transporter 2 expression in A $\beta$ <sub>25–35</sub>-treated rat model of Alzheimer's disease. *Neurol. Sci.* **2015**, *36*, 871–876. [CrossRef]
170. Daniele, L.L.; Sauer, B.; Gallagher, S.M.; Pugh, E.N., Jr.; Philp, N.J. Altered visual function in monocarboxylate transporter 3 (Slc16a8) knockout mice. *Am. J. Physiol. Cell Physiol.* **2008**, *295*, C451–C457. [CrossRef]
171. Gallagher-Colombo, S.; Maminishkis, A.; Tate, S.; Grunwald, G.B.; Philp, N.J. Modulation of MCT3 Expression during Wound Healing of the Retinal Pigment Epithelium. *Investig. Ophthalmol. Vis. Sci.* **2010**, *51*, 5343–5350. [CrossRef] [PubMed]

172. Zhu, S.; Goldschmidt-Clermont, P.J.; Dong, C. Inactivation of monocarboxylate transporter MCT3 by DNA methylation in atherosclerosis. *Circulation* **2005**, *112*, 1353–1361. [CrossRef] [PubMed]
173. Friesema, E.C.; Grueters, A.; Biebermann, H.; Krude, H.; Moers, A.; Reeser, M.; Barrett, T.G.; Mancilla, E.E.; Svensson, J.; Kester, M.H.A.; et al. Association between mutations in a thyroid hormone transporter and severe X-linked psychomotor retardation. *Lancet* **2004**, *364*, 1435–1437. [CrossRef]
174. Kersseboom, S.; Kremers, G.-J.; Friesema, E.C.H.; Visser, W.E.; Klootwijk, W.; Peeters, R.P.; Visser, T.J. Mutations in MCT8 in Patients with Allan-Herndon-Dudley-Syndrome Affecting Its Cellular Distribution. *Mol. Endocrinol.* **2013**, *27*, 801–813. [CrossRef]
175. Maranduba, C.M.C.; Friesema, E.C.H.; Kok, F.; Kester, M.H.A.; Jansen, J.; Sertie, A.; Passos-Bueno, M.R.; Visser, T.J. Decreased cellular uptake and metabolism in Allan-Herndon-Dudley syndrome (AHDS) due to a novel mutation in the MCT8 thyroid hormone transporter. *J. Med. Genet.* **2005**, *43*, 457–460. [CrossRef]
176. Wittmann, G.; Szabon, J.; Mohácsik, P.; Nouriel, S.S.; Gereben, B.; Fekete, C.; Lechan, R.M. Parallel Regulation of Thyroid Hormone Transporters OATP1c1 and MCT8 During and After Endotoxemia at the Blood-Brain Barrier of Male Rodents. *Endocrinology* **2015**, *156*, 1552–1564. [CrossRef]
177. Sun, Y.; Zhao, D.; Wang, G.; Jiang, Q.; Guo, M.; Kan, Q.; He, Z.; Sun, J. A novel oral prodrug-targeting transporter MCT 1: 5-fluorouracil-dicarboxylate monoester conjugates. *Asian J. Pharm. Sci.* **2019**, *14*, 631–639. [CrossRef]
178. Cundy, K.C.; Branch, R.; Chernov-Rogan, T.; Dias, T.; Estrada, T.; Hold, K.; Koller, K.; Liu, X.; Mann, A.; Panuwat, M.; et al. XP13512 [(+/-)-1-((alpha-isobutanoyloxyethoxy)carbonyl) aminomethyl)-1-cyclohexane acetic acid], a novel gabapentin prodrug: I. Design, synthesis, enzymatic conversion to gabapentin, and transport by intestinal solute transporters. *J. Pharmacol. Exp. Ther.* **2004**, *311*, 315–323. [CrossRef]
179. Cundy, K.C.; Annamalai, T.; Bu, L.; Vera, J.D.; Estrela, J.; Luo, W.; Shirsat, P.; Torneros, A.; Yao, F.; Zou, J.; et al. XP13512 [(+/-)-1-((alpha-isobutanoyloxyethoxy)carbonyl) aminomethyl)-1-cyclohexane acetic acid], a novel gabapentin prodrug: II. Improved oral bioavailability, dose proportionality, and colonic absorption compared with gabapentin in rats and monkeys. *J. Pharmacol. Exp. Ther.* **2004**, *311*, 324–333. [CrossRef]
180. Wang, Y.; Wang, G.; Chen, H.; Sun, Y.; Sun, M.; Liu, X.; Jian, W.; He, Z.; Sun, J. A facile di-acid mono-amidation strategy to prepare cyclization-activating mono-carboxylate transporter 1-targeting gemcitabine prodrugs for enhanced oral delivery. *Int. J. Pharm.* **2019**, *573*, 118718. [CrossRef]
181. Kim, E.S.; Deeks, E.D. Gabapentin Enacarbil: A Review in Restless Legs Syndrome. *Drugs* **2016**, *76*, 879–887. [CrossRef] [PubMed]
182. Schweizer, U.; Johannes, J.; Bayer, D.; Braun, D. Structure and Function of Thyroid Hormone Plasma Membrane Transporters. *Eur. Thyroid J.* **2014**, *3*, 143–153. [CrossRef] [PubMed]
183. Bosshart, P.D.; Kalbermatter, D.; Bonetti, S.; Fotiadis, D. Mechanistic basis of L-lactate transport in the SLC16 solute carrier family. *Nat. Commun.* **2019**, *10*, 2649. [CrossRef] [PubMed]
184. Wilson, M.C.; Meredith, D.; Bunnun, C.; Sessions, R.B.; Halestrap, A.P. Studies on the DIDS-binding Site of Monocarboxylate Transporter 1 Suggest a Homology Model of the Open Conformation and a Plausible Translocation Cycle. *J. Biol. Chem.* **2009**, *284*, 20011–20021. [CrossRef] [PubMed]
185. Yamaguchi, A.; Futagi, Y.; Kobayashi, M.; Narumi, K.; Furugen, A.; Iseki, K. Extracellular lysine 38 plays a crucial role in pH-dependent transport via human monocarboxylate transporter 1. *Biochim. Biophys. Acta Biomembr.* **2020**, *1862*, 183068. [CrossRef] [PubMed]
186. Futagi, Y.; Kobayashi, M.; Narumi, K.; Furugen, A.; Iseki, K. Homology modeling and site-directed mutagenesis identify amino acid residues underlying the substrate selection mechanism of human monocarboxylate transporters 1 (hMCT1) and 4 (hMCT4). *Cell. Mol. Life Sci.* **2019**, *76*, 4905–4921. [CrossRef] [PubMed]
187. Rahman, B.; Schneider, H.-P.; Bröer, A.; Deitmer, J.W.; Bröer, S. Helix 8 and Helix 10 Are Involved in Substrate Recognition in the Rat Monocarboxylate Transporter MCT1. *Biochemistry* **1999**, *38*, 11577–11584. [CrossRef]
188. Galić, S.; Schneider, H.-P.; Bröer, A.; Deitmer, J.W.; Bröer, S. The loop between helix 4 and helix 5 in the monocarboxylate transporter MCT1 is important for substrate selection and protein stability. *Biochem. J.* **2003**, *376*, 413–422. [CrossRef]
189. Wang, N.; Jiang, X.; Zhang, S.; Zhu, A.; Yuan, Y.; Xu, H.; Lei, J.; Yan, C. Structural basis of human monocarboxylate transporter 1 inhibition by anti-cancer drug candidates. *Cell* **2020**, *184*, 370–383. [CrossRef]
190. Groeneweg, S.; De Souza, E.C.L.; Meima, M.E.; Peeters, R.P.; Visser, W.E.; Visser, T.J. Outward-Open Model of Thyroid Hormone Transporter Monocarboxylate Transporter 8 Provides Novel Structural and Functional Insights. *Endocrinology* **2017**, *158*, 3292–3306. [CrossRef]
191. Protze, J.; Braun, D.; Hinz, K.M.; Bayer-Kusch, D.; Schweizer, U.; Krause, G. Membrane-traversing mechanism of thyroid hormone transport by monocarboxylate transporter 8. *Cell Mol. Life Sci.* **2017**, *74*, 2299–2318. [CrossRef] [PubMed]
192. Kinne, A.; Kleinau, G.; Hoefig, C.S.; Grüters, A.; Köhrle, J.; Krause, G.; Schweizer, U. Essential Molecular Determinants for Thyroid Hormone Transport and First Structural Implications for Monocarboxylate Transporter 8. *J. Biol. Chem.* **2010**, *285*, 28054–28063. [CrossRef] [PubMed]
193. Hagenbuch, B.; Meier, P.J. Organic anion transporting polypeptides of the OATP/SLC21 family: Phylogenetic classification as OATP/SLCO superfamily, new nomenclature and molecular/functional properties. *Pflüg. Arch.* **2004**, *447*, 653–665. [CrossRef] [PubMed]
194. Roth, M.; Obaidat, A.; Hagenbuch, B. OATPs, OATs and OCTs: The organic anion and cation transporters of the SLCO and SLC22A gene superfamilies. *J. Cereb. Blood Flow Metab.* **2012**, *165*, 1260–1287. [CrossRef]

195. Ronaldson, P.T.; Davis, T.P. Targeted Drug Delivery to Treat Pain and Cerebral Hypoxia. *Pharmacol. Rev.* **2013**, *65*, 291–314. [CrossRef]
196. Gao, B.; Vavricka, S.R.; Meier, P.J.; Stieger, B. Differential cellular expression of organic anion transporting peptides OATP1A2 and OATP2B1 in the human retina and brain: Implications for carrier-mediated transport of neuropeptides and neurosteroids in the CNS. *Eur. J. Physiol.* **2014**, *467*, 1481–1493. [CrossRef]
197. Schnell, C.; Shahmoradi, A.; Wichert, S.P.; Mayerl, S.; Hagos, Y.; Heuer, H.; Rossner, M.J.; Hülsmann, S. The multispecific thyroid hormone transporter OATP1C1 mediates cell-specific sulforhodamine 101-labeling of hippocampal astrocytes. *Anat. Embryol.* **2013**, *220*, 193–203. [CrossRef]
198. Schäfer, A.; zu Schwabedissen, H.M.; Grube, M. Expression and Function of Organic Anion Transporting Polypeptides in the Human Brain: Physiological and Pharmacological Implications. *Pharmaceutics* **2021**, *13*, 834. [CrossRef]
199. Choi, K.; Zhuang, H.; Crain, B.; Doré, S. Expression and localization of prostaglandin transporter in Alzheimer disease brains and age-matched controls. *J. Neuroimmunol.* **2008**, *195*, 81–87. [CrossRef]
200. Huber, R.D.; Gao, B.; Pfändler, M.-A.S.; Zhang-Fu, W.; Leuthold, S.; Hagenbuch, B.; Folkers, G.; Meier, P.J.; Stieger, B. Characterization of two splice variants of human organic anion transporting polypeptide 3A1 isolated from human brain. *Am. J. Physiol. Physiol.* **2007**, *292*, C795–C806. [CrossRef]
201. Leuthold, S.; Hagenbuch, B.; Mohebbi, N.; Wagner, C.A.; Meier, P.J.; Stieger, B. Mechanisms of pH-gradient driven transport mediated by organic anion polypeptide transporters. *Am. J. Physiol. Cell Physiol.* **2009**, *296*, C570–C582. [CrossRef]
202. Kinzi, J.; Grube, M.; Schwabedissen, H.E.M.Z. OATP2B1—The underrated member of the organic anion transporting polypeptide family of drug transporters? *Biochem. Pharmacol.* **2021**, *188*, 114534. [CrossRef] [PubMed]
203. Franke, R.M.; Scherckenbach, L.A.; Sparreboom, A. Pharmacogenetics of the organic anion transporting polypeptide 1A2. *Pharmacogenomics* **2009**, *10*, 339–344. [CrossRef]
204. Westholm, D.E.; Salo, D.R.; Viken, K.; Rumbley, J.N.; Anderson, G.W. The Blood-Brain Barrier Thyroxine Transporter Organic Anion-Transporting Polypeptide 1c1 Displays Atypical Transport Kinetics. *Endocrinology* **2009**, *150*, 5153–5162. [CrossRef]
205. Gose, T.; Nakanishi, T.; Kamo, S.; Shimada, H.; Otake, K.; Tamai, I. Prostaglandin transporter (OATP2A1/SLCO2A1) contributes to local disposition of eicosapentaenoic acid-derived PGE3. *Prostaglandins Other Lipid Mediat.* **2016**, *122*, 10–17. [CrossRef]
206. Bakos, E.; Tusnády, G.E.; Németh, O.; Patik, I.; Magyar, C.; Németh, K.; Kele, P.; Özvegy-Laczka, C. Synergistic transport of a fluorescent coumarin probe marks coumarins as pharmacological modulators of Organic anion-transporting polypeptide, OATP3A1. *Biochem. Pharmacol.* **2020**, *182*, 114250. [CrossRef]
207. Bailey, D.G.; Dresser, G.K.; Leake, B.F.; Kim, R.B. Naringin is a Major and Selective Clinical Inhibitor of Organic Anion-Transporting Polypeptide 1A2 (OATP1A2) in Grapefruit Juice. *Clin. Pharmacol. Ther.* **2007**, *81*, 495–502. [CrossRef]
208. Morita, T.; Akiyoshi, T.; Tsuchitani, T.; Kataoka, H.; Araki, N.; Yajima, K.; Katayama, K.; Imaoka, A.; Ohtani, H. Inhibitory Effects of Cranberry Juice and Its Components on Intestinal OATP1A2 and OATP2B1: Identification of Avicularin as a Novel Inhibitor. *J. Agric. Food Chem.* **2022**, *70*, 3310–3320. [CrossRef]
209. Kalliokoski, A.; Niemi, M. Impact of OATP transporters on pharmacokinetics. *J. Cereb. Blood Flow Metab.* **2009**, *158*, 693–705. [CrossRef]
210. Bakos, É.; Németh, O.; Patik, I.; Kucsma, N.; Várady, G.; Szakács, G.; Özvegy-Laczka, C. A novel fluorescence-based functional assay for human OATP1A2 and OATP1C1 identifies interaction between third-generation P-gp inhibitors and OATP1A2. *FEBS J.* **2019**, *287*, 2468–2485. [CrossRef]
211. Tikkanen, A.; Pierrot, E.; Deng, F.; Sánchez, V.B.; Hagström, M.; Koenderink, J.B.; Kidron, H. Food Additives as Inhibitors of Intestinal Drug Transporter OATP2B1. *Mol. Pharm.* **2020**, *17*, 3748–3758. [CrossRef]
212. Unger, M.S.; Mudunuru, J.; Schwab, M.; Hopf, C.; Drewes, G.; Nies, A.T.; Zamek-Gliszczynski, M.J.; Reinhard, F. Clinically Relevant OATP2B1 Inhibitors in Marketed Drug Space. *Mol. Pharm.* **2019**, *17*, 488–498. [CrossRef]
213. Chen, M.; Hu, S.; Li, Y.; Gibson, A.A.; Fu, Q.; Baker, S.D.; Sparreboom, A. Role of Oatp2b1 in Drug Absorption and Drug-Drug Interactions. *Drug Metab. Dispos.* **2020**, *48*, 420–426. [CrossRef]
214. Rebello, S.; Zhao, S.; Hariry, S.; Dahlke, M.; Alexander, N.; Vapurcuyan, A.; Hanna, I.; Jarugula, V. Intestinal OATP1A2 inhibition as a potential mechanism for the effect of grapefruit juice on aliskiren pharmacokinetics in healthy subjects. *Eur. J. Clin. Pharmacol.* **2011**, *68*, 697–708. [CrossRef]
215. Kamo, S.; Nakanishi, T.; Aotani, R.; Nakamura, Y.; Gose, T.; Tamai, I. Impact of FDA-Approved Drugs on the Prostaglandin Transporter OATP2A1/SLCO2A1. *J. Pharm. Sci.* **2017**, *106*, 2483–2490. [CrossRef]
216. Lee, W.; Glaeser, H.; Smith, H.; Roberts, R.L.; Moeckel, G.W.; Gervasini, G.; Leake, B.F.; Kim, R.B. Polymorphisms in human organic anion-transporting polypeptide 1A2 (OATP1A2): Implications for altered drug disposition and central nervous system drug entry. *J. Biol. Chem.* **2005**, *280*, 9610–9617. [CrossRef]
217. Zhou, F.; Zheng, J.; Zhu, L.; Jodal, A.; Cui, P.H.; Wong, M.; Gurney, H.; Church, W.; Murray, M. Functional Analysis of Novel Polymorphisms in the Human SLCO1A2 Gene that Encodes the Transporter OATP1A2. *AAPS J.* **2013**, *15*, 1099–1108. [CrossRef]
218. Thompson, B.J.; Sanchez-Covarrubias, L.; Slosky, L.M.; Zhang, Y.; Laracuente, M.-L.; Ronaldson, P.T. Hypoxia/Reoxygenation Stress Signals an Increase in Organic Anion Transporting polypeptide 1a4 (Oatp1a4) at the Blood–Brain Barrier: Relevance to CNS Drug Delivery. *J. Cereb. Blood Flow Metab.* **2014**, *34*, 699–707. [CrossRef]

219. Nies, A.T.; Niemi, M.; Burk, O.; Winter, S.; Zanger, U.M.; Stieger, B.; Schwab, M.; Schaeffeler, E. Genetics is a major determinant of expression of the human hepatic uptake transporter OATP1B1, but not of OATP1B3 and OATP2B1. *Genome Med.* **2013**, *5*, 1. [CrossRef]
220. Tapaninen, T.; Karonen, T.; Backman, J.T.; Neuvonen, P.J.; Niemi, M. SLCO2B1 c.935G>A single nucleotide polymorphism has no effect on the pharmacokinetics of montelukast and aliskiren. *Pharm. Genom.* **2013**, *23*, 19–24. [CrossRef]
221. Schulte, R.R.; Ho, R.H. Organic Anion Transporting Polypeptides: Emerging Roles in Cancer Pharmacology. *Mol. Pharmacol.* **2019**, *95*, 490–506. [CrossRef]
222. Zhu, Q.; Liang, X.; Dai, J.; Guan, X. Prostaglandin transporter, SLCO2A1, mediates the invasion and apoptosis of lung cancer cells via PI3K/AKT/mTOR pathway. *Int. J. Clin. Exp. Pathol.* **2015**, *8*, 9175–9181.
223. Mayerl, S.; Visser, T.J.; Darras, V.M.; Horn, S.; Heuer, H. Impact of Oatp1c1 Deficiency on Thyroid Hormone Metabolism and Action in the Mouse Brain. *Endocrinology* **2012**, *153*, 1528–1537. [CrossRef]
224. Admati, I.; Wasserman-Bartov, T.; Tovim, A.; Rozenblat, R.; Blitz, E.; Zada, D.; Lerer-Goldshtein, T.; Appelbaum, L. Neural Alterations and Hyperactivity of the Hypothalamic–Pituitary–Thyroid Axis in Oatp1c1 Deficiency. *Thyroid* **2020**, *30*, 161–174. [CrossRef]
225. Li, M.; Wang, W.; Cheng, Y.; Zhang, X.; Zhao, N.; Tan, Y.; Xie, Q.; Chai, J.; Pan, Q. Tumor necrosis factor  $\alpha$  upregulates the bile acid efflux transporter OATP3A1 via multiple signaling pathways in cholestasis. *J. Biol. Chem.* **2021**, *298*. [CrossRef]
226. Choi, J.H.; Murray, J.W.; Wolkoff, A.W. PDZK1 binding and serine phosphorylation regulate subcellular trafficking of organic anion transport protein 1a1. *Am. J. Physiol. Liver Physiol.* **2011**, *300*, G384–G393. [CrossRef]
227. Hänggi, E.; Grundschober, A.F.; Leuthold, S.; Meier, P.J.; St-Pierre, M.V. Functional Analysis of the Extracellular Cysteine Residues in the Human Organic Anion Transporting Polypeptide, OATP2B1. *Mol. Pharmacol.* **2006**, *70*, 806–817. [CrossRef]
228. Meier-Abt, F.; Mokrab, Y.; Mizuguchi, K. Organic anion transporting polypeptides of the OATP/SLCO superfamily: Identification of new members in nonmammalian species, comparative modeling and a potential transport mode. *J. Membr. Biol.* **2005**, *208*, 213–227. [CrossRef]
229. Betterton, R.D.; Davis, T.P.; Ronaldson, P.T. Organic Cation Transporter (OCT/OCTN) Expression at Brain Barrier Sites: Focus on CNS Drug Delivery. *Handb. Exp. Pharmacol.* **2021**, *266*, 301–328. [CrossRef]
230. Pochini, L.; Galluccio, M.; Scalise, M.; Console, L.; Indiveri, C. OCTN: A Small Transporter Subfamily with Great Relevance to Human Pathophysiology, Drug Discovery, and Diagnostics. *SLAS Discov. Adv. Sci. Drug Discov.* **2018**, *24*, 89–110. [CrossRef]
231. Koepsell, H.; Lips, K.; Volk, C. Polyspecific Organic Cation Transporters: Structure, Function, Physiological Roles, and Biopharmaceutical Implications. *Pharm. Res.* **2007**, *24*, 1227–1251. [CrossRef] [PubMed]
232. Barendt, W.M.; Wright, S.H. The Human Organic Cation Transporter (hOCT2) Recognizes the Degree of Substrate Ionization. *J. Biol. Chem.* **2002**, *277*, 22491–22496. [CrossRef] [PubMed]
233. Sakata, T.; Anzai, N.; Kimura, T.; Miura, D.; Fukutomi, T.; Takeda, M.; Sakurai, H.; Endou, H. Functional Analysis of Human Organic Cation Transporter OCT3 (SLC22A3) Polymorphisms. *J. Pharmacol. Sci.* **2010**, *113*, 263–266. [CrossRef] [PubMed]
234. Kerb, R.; Brinkmann, U.; Chatskaia, N.; Gorbunov, D.; Gorboulev, V.; Mornhinweg, E.; Keil, A.; Eichelbaum, M.; Koepsell, H. Identification of genetic variations of the human organic cation transporter hOCT1 and their functional consequences. *Pharmacogenetics* **2002**, *12*, 591–595. [CrossRef]
235. Fahrmyr, C.; Fromm, M.F.; König, J. Hepatic OATP and OCT uptake transporters: Their role for drug–drug interactions and pharmacogenetic aspects. *Drug Metab. Rev.* **2010**, *42*, 380–401. [CrossRef]
236. Lin, Z.; Nelson, L.; Franke, A.; Poritz, L.; Li, T.-Y.; Wu, R.; Wang, Y.; MacNeill, C.; Thomas, N.J.; Schreiber, S.; et al. OCTN1 variant L503F is associated with familial and sporadic inflammatory bowel disease. *J. Crohn's Colitis* **2010**, *4*, 132–138. [CrossRef]
237. Lahjouji, K.; Mitchell, G.A.; Qureshi, I.A. Carnitine Transport by Organic Cation Transporters and Systemic Carnitine Deficiency. *Mol. Genet. Metab.* **2001**, *73*, 287–297. [CrossRef]
238. Tsuji, A. Small molecular drug transfer across the blood–brain barrier via carrier-mediated transport systems. *NeuroRx* **2005**, *2*, 54–62. [CrossRef]
239. Nagle, M.A.; Wu, W.; Eraly, S.A.; Nigam, S.K. Organic anion transport pathways in antiviral handling in choroid plexus in Oat1 (Slc22a6) and Oat3 (Slc22a8) deficient tissue. *Neurosci. Lett.* **2013**, *534*, 133–138. [CrossRef]
240. Saidijam, M.; Dermami, F.K.; Sohrobi, S.; Patching, S.G. Efflux proteins at the blood–brain barrier: Review and bioinformatics analysis. *Xenobiotica* **2017**, *48*, 506–532. [CrossRef]
241. Burckhardt, G. Drug transport by Organic Anion Transporters (OATs). *Pharmacol. Ther.* **2012**, *136*, 106–130. [CrossRef]
242. Montaser, A.; Markowicz-Piasecka, M.; Sikora, J.; Jalkanen, A.; Huttunen, K.M. L-type amino acid transporter 1 (LAT1)-utilizing efflux transporter inhibitors can improve the brain uptake and apoptosis-inducing effects of vinblastine in cancer cells. *Int. J. Pharm.* **2020**, *586*, 119585. [CrossRef] [PubMed]
243. U.S. FDA. In Vitro Drug Interaction Studies, Cytochrome P450 Enzyme- and Transporter-Mediated Drug Interactions, Guidance for Industry. 2020. Available online: <https://www.fda.gov/media/134582/download> (accessed on 5 April 2022).
244. EMA. Guideline on the Investigation of Drug Interactions. 2012. Available online: [https://www.ema.europa.eu/en/documents/scientific-guideline/guideline-investigation-drug-interactions-revision-1\\_en.pdf](https://www.ema.europa.eu/en/documents/scientific-guideline/guideline-investigation-drug-interactions-revision-1_en.pdf) (accessed on 5 April 2022).
245. VanWert, A.L.; Gionfriddo, M.; Sweet, D.H. Organic anion transporters: Discovery, pharmacology, regulation and roles in pathophysiology. *Biopharm. Drug Dispos.* **2009**, *31*, 1–71. [CrossRef]

246. Ciarimboli, G. Regulation Mechanisms of Expression and Function of Organic Cation Transporter 1. *Front. Pharmacol.* **2021**, *11*, 2234. [CrossRef]
247. Dickens, D.; Owen, A.; Alfirevic, A.; Giannoudis, A.; Davies, A.; Weksler, B.; Romero, I.; Couraud, P.-O.; Pirmohamed, M. Lamotrigine is a substrate for OCT1 in brain endothelial cells. *Biochem. Pharmacol.* **2012**, *83*, 805–814. [CrossRef]
248. Sekhar, G.N.; Georgian, A.R.; Sanderson, L.; Vizcay-Barrena, G.; Brown, R.C.; Muresan, P.; Fleck, R.; Thomas, S.A. Organic cation transporter 1 (OCT1) is involved in pentamidine transport at the human and mouse blood-brain barrier (BBB). *PLoS ONE* **2017**, *12*, e0173474. [CrossRef]
249. Dos Santos Pereira, J.N.; Tadjerpisheh, S.; Abu Abed, M.; Saadatmand, A.R.; Weksler, B.; Romero, I.; Couraud, P.-O.; Brockmüller, J.; Tzvetkov, M.V. The Poorly Membrane Permeable Antipsychotic Drugs Amisulpride and Sulpiride Are Substrates of the Organic Cation Transporters from the SLC22 Family. *AAPS J.* **2014**, *16*, 1247–1258. [CrossRef]
250. MacKenzie, B.; Erickson, J.D. Sodium-coupled neutral amino acid (System N/A) transporters of the SLC38 gene family. *Pflug. Arch.* **2004**, *447*, 784–795. [CrossRef]
251. Bröer, S. The SLC38 family of sodium–amino acid co-transporters. *Pflug. Arch.* **2014**, *466*, 155–172. [CrossRef]
252. Schiöth, H.B.; Roshanbin, S.; Hägglund, M.G.; Fredriksson, R. Evolutionary origin of amino acid transporter families SLC32, SLC36 and SLC38 and physiological, pathological and therapeutic aspects. *Mol. Asp. Med.* **2013**, *34*, 571–585. [CrossRef]
253. Solbu, T.T.; Bjørkmo, M.; Berghuis, P.; Harkany, T.; Chaudhry, F.A. SAT1, a glutamine transporter, is preferentially expressed in GABAergic neurons. *Front. Neuroanat.* **2010**, *4*, 10. [CrossRef] [PubMed]
254. González-González, I.; Cubelos, B.; Giménez, C.; Zafra, F. Immunohistochemical localization of the amino acid transporter SNAT2 in the rat brain. *Neuroscience* **2005**, *130*, 61–73. [CrossRef] [PubMed]
255. Melone, M.; Quagliano, F.; Barbaresi, P.; Varoqui, H.; Erickson, J.D.; Conti, F. Localization of the Glutamine Transporter SNAT1 in Rat Cerebral Cortex and Neighboring Structures, With a Note on its Localization in Human Cortex. *Cereb. Cortex* **2004**, *14*, 562–574. [CrossRef] [PubMed]
256. Grewal, S.; Defamie, N.; Zhang, X.; Gois, S.D.; Shawki, A.; Mackenzie, B.; Chen, C.; Varoqui, H.; Erickson, J.D. SNAT2 amino acid transporter is regulated by amino acids of the SLC6 gamma-aminobutyric acid transporter subfamily in neocortical neurons and may play no role in delivering glutamine for glutamatergic transmission. *J. Biol. Chem.* **2009**, *284*, 11224–11236. [CrossRef]
257. Cubelos, B.; González-González, I.M.; Giménez, C.; Zafra, F. Amino acid transporter SNAT5 localizes to glial cells in the rat brain. *Glia* **2004**, *49*, 230–244. [CrossRef]
258. Rubio-Aliaga, I.; Wagner, C.A. Regulation and function of the SLC38A3/SNAT3 glutamine transporter. *Channels* **2016**, *10*, 440–452. [CrossRef]
259. Low, S.Y.; Taylor, P.M.; Ahmed, A.; Pogson, C.I.; Rennie, M.J. Substrate-specificity of glutamine transporters in membrane vesicles from rat liver and skeletal muscle investigated using amino acid analogues. *Biochem. J.* **1991**, *278*, 105–111. [CrossRef]
260. Hägglund, M.G.; Hellsten, S.V.; Bagchi, S.; Philippot, G.; Löfqvist, E.; Nilsson, V.C.; Almkvist, I.; Karlsson, E.; Sreedharan, S.; Tafreshiha, A.; et al. Transport of l-Glutamine, l-Alanine, l-Arginine and l-Histidine by the Neuron-Specific Slc38a8 (SNAT8) in CNS. *J. Mol. Biol.* **2015**, *427*, 1495–1512. [CrossRef]
261. Hägglund, M.G.; Sreedharan, S.; Nilsson, V.C.; Shaik, J.H.; Almkvist, I.M.; Bäcklin, S.; Wränge, Ö.; Fredriksson, R. Identification of SLC38A7 (SNAT7) Protein as a Glutamine Transporter Expressed in Neurons. *J. Biol. Chem.* **2011**, *286*, 20500–20511. [CrossRef]
262. Bagchi, S.; Baomar, H.A.; Al-Walai, S.; Al-Sadi, S.; Fredriksson, R. Histological Analysis of SLC38A6 (SNAT6) Expression in Mouse Brain Shows Selective Expression in Excitatory Neurons with High Expression in the Synapses. *PLoS ONE* **2014**, *9*, e95438. [CrossRef]
263. Gandasi, N.; Arapi, V.; Mickael, M.; Belekar, P.; Granlund, L.; Kothegala, L.; Fredriksson, R.; Bagchi, S. Glutamine Uptake via SNAT6 and Caveolin Regulates Glutamine–Glutamate Cycle. *Int. J. Mol. Sci.* **2021**, *22*, 1167. [CrossRef] [PubMed]
264. Ogura, M.; Taniura, H.; Nakamichi, N.; Yoneda, Y. Upregulation of the glutamine transporter through transactivation mediated by camp/protein kinase a signals toward exacerbation of vulnerability to oxidative stress in rat neocortical astrocytes. *J. Cell. Physiol.* **2007**, *212*, 375–385. [CrossRef] [PubMed]
265. Ogura, M.; Nakamichi, N.; Takano, K.; Oikawa, H.; Kambe, Y.; Ohno, Y.; Taniura, H.; Yoneda, Y. Functional expression of A glutamine transporter responsive to down-regulation by lipopolysaccharide through reduced promoter activity in cultured rat neocortical astrocytes. *J. Neurosci. Res.* **2006**, *83*, 1447–1460. [CrossRef] [PubMed]
266. Rosario, F.J.; Kanai, Y.; Powell, T.L.; Jansson, T. Mammalian target of rapamycin signalling modulates amino acid uptake by regulating transporter cell surface abundance in primary human trophoblast cells. *J. Physiol.* **2013**, *591*, 609–625. [CrossRef]
267. Gu, S.; Villegas, C.J.; Jiang, J.X. Differential Regulation of Amino Acid Transporter SNAT3 by Insulin in Hepatocytes. *J. Biol. Chem.* **2005**, *280*, 26055–26062. [CrossRef]
268. Nissen-Meyer, L.S.H.; Chaudhry, F.A. Protein Kinase C Phosphorylates the System N Glutamine Transporter SN1 (Slc38a3) and Regulates Its Membrane Trafficking and Degradation. *Front. Endocrinol.* **2013**, *4*, 138. [CrossRef]
269. Uchida, Y.; Ito, K.; Ohtsuki, S.; Kubo, Y.; Suzuki, T.; Terasaki, T. Major involvement of Na(+)-dependent multivitamin transporter (SLC5A6/SMVT) in uptake of biotin and pantothenic acid by human brain capillary endothelial cells. *J. Neurochem.* **2015**, *134*, 97–112. [CrossRef]
270. Salazar, K.; Martínez, F.; Pérez-Martín, M.; Cifuentes, M.; Trigueros, L.; Ferrada, L.; Espinoza, F.; Saldivia, N.; Bertinat, R.; Forman, K.; et al. SVCT2 Expression and Function in Reactive Astrocytes Is a Common Event in Different Brain Pathologies. *Mol. Neurobiol.* **2017**, *55*, 5439–5452. [CrossRef]

271. Castro, M.; Caprile, T.; Astuya-Villalón, A.; Millán, C.; Reinicke, K.; Vera, J.C.; Vásquez, O.; Aguayo, L.G.; Nualart, F. High-affinity sodium-vitamin C co-transporters (SVCT) expression in embryonic mouse neurons. *J. Neurochem.* **2001**, *78*, 815–823. [CrossRef]
272. Prasad, P.D.; Wang, H.; Kekuda, R.; Fujita, T.; Fei, Y.-J.; Devoe, L.D.; Leibach, F.H.; Ganapathy, V. Cloning and Functional Expression of a cDNA Encoding a Mammalian Sodium-dependent Vitamin Transporter Mediating the Uptake of Pantothenate, Biotin, and Lipoate. *J. Biol. Chem.* **1998**, *273*, 7501–7506. [CrossRef]
273. Nualart, F.; Mack, L.; Garcia, A.; Cisternas, P.; Bongarzone, E.R.; Heitzer, M.; Jara, N.; Martinez, F.; Ferrada, L.; Espinoza, F.; et al. Vitamin C Transporters, Recycling and the Bystander Effect in the Nervous System: SVCT2 versus Gluts. *J. Stem. Cell Res. Ther.* **2014**, *4*, 209. [CrossRef]
274. Zhao, Y.; Qu, B.; Wu, X.; Li, X.; Liu, Q.; Jin, X.; Guo, L.; Hai, L.; Wu, Y. Design, synthesis and biological evaluation of brain targeting l-ascorbic acid prodrugs of ibuprofen with “lock-in” function. *Eur. J. Med. Chem.* **2014**, *82*, 314–323. [CrossRef]
275. Yue, Q.; Peng, Y.; Zhao, Y.; Lu, R.; Fu, Q.; Chen, Y.; Yang, Y.; Hai, L.; Guo, L.; Wu, Y. Dual-targeting for brain-specific drug delivery: Synthesis and biological evaluation. *Drug Deliv.* **2018**, *25*, 426–434. [CrossRef] [PubMed]
276. Wang, L.; Zhang, L.; Zhao, Y.; Fu, Q.; Xiao, W.; Lu, R.; Hai, L.; Guo, L.; Wu, Y. Design, synthesis, and neuroprotective effects of dual-brain targeting naproxen prodrug. *Arch. Pharm.* **2018**, *351*, e1700382. [CrossRef]
277. Alam, K.; Crowe, A.; Wang, X.; Zhang, P.; Ding, K.; Li, L.; Yue, W. Regulation of Organic Anion Transporting Polypeptides (OATP) 1B1- and OATP1B3-Mediated Transport: An Updated Review in the Context of OATP-Mediated Drug-Drug Interactions. *Int. J. Mol. Sci.* **2018**, *19*, 855. [CrossRef]
278. Luo, S.; Kansara, V.S.; Zhu, X.; Mandava, N.K.; Pal, D.; Mitra, A.K. Functional Characterization of Sodium-Dependent Multivitamin Transporter in MDCK-MDR1 Cells and Its Utilization as a Target for Drug Delivery. *Mol. Pharm.* **2006**, *3*, 329–339. [CrossRef]
279. Inazu, M. Functional Expression of Choline Transporters in the Blood–Brain Barrier. *Nutrients* **2019**, *11*, 2265. [CrossRef]
280. Haga, T. Molecular properties of the high-affinity choline transporter CHT1. *J. Biochem.* **2014**, *156*, 181–194. [CrossRef]
281. Okuda, T.; Haga, T.; Kanai, Y.; Endou, H.; Ishihara, T.; Katsura, I. Identification and characterization of the high-affinity choline transporter. *Nat. Neurosci.* **2000**, *3*, 120–125. [CrossRef]
282. Traiffort, E.; O’Regan, S.; Ruat, M. The choline transporter-like family SLC44: Properties and roles in human diseases. *Mol. Asp. Med.* **2013**, *34*, 646–654. [CrossRef]
283. Iwao, B.; Yara, M.; Hara, N.; Kawai, Y.; Yamanaka, T.; Nishihara, H.; Inoue, T.; Inazu, M. Functional expression of choline transporter like-protein 1 (CTL1) and CTL2 in human brain microvascular endothelial cells. *Neurochem. Int.* **2015**, *93*, 40–50. [CrossRef] [PubMed]
284. Hirayama, B.A.; Díez-Sampedro, A.; Wright, E.M. Common mechanisms of inhibition for the Na<sup>+</sup>/glucose (hSGLT1) and Na<sup>+</sup>/Cl<sup>-</sup>/GABA (hGAT1) cotransporters. *Br. J. Pharmacol.* **2001**, *134*, 484–495. [CrossRef] [PubMed]
285. Otto, C.; Friedrich, A.; Madunić, I.V.; Baumeier, C.; Schwenk, R.W.; Karaica, D.; Germer, C.-T.; Schürmann, A.; Sabolić, I.; Koepsell, H. Antidiabetic Effects of a Tripeptide That Decreases Abundance of Na<sup>+</sup>-d-glucose Cotransporter SGLT1 in the Brush-Border Membrane of the Small Intestine. *ACS Omega* **2020**, *5*, 29127–29139. [CrossRef]
286. Tahrani, A.; Barnett, A.H.; Bailey, C.J. SGLT inhibitors in management of diabetes. *Lancet Diabetes Endocrinol.* **2013**, *1*, 140–151. [CrossRef]
287. Boswell-Casteel, R.C.; Hays, F.A. Equilibrative nucleoside transporters—A review. *Nucleosides Nucleotides Nucleic Acids* **2016**, *36*, 7–30. [CrossRef]
288. Arcas, M.M.; Trigueros-Motos, L.; Casado, F.J.; Anglada, M.P. Physiological and Pharmacological Roles of Nucleoside Transporter Proteins. *Nucleosides Nucleotides Nucleic Acids* **2008**, *27*, 769–778. [CrossRef]
289. Chang, C.; Swaan, P.W.; Ngo, L.Y.; Lum, P.Y.; Patil, S.D.; Unadkat, J.D. Molecular Requirements of the Human Nucleoside Transporters hCNT1, hCNT2, and hENT1. *Mol. Pharmacol.* **2004**, *65*, 558–570. [CrossRef]
290. Young, J.D.; Yao, S.Y.; Baldwin, J.M.; Cass, C.E.; Baldwin, S.A. The human concentrative and equilibrative nucleoside transporter families, SLC28 and SLC29. *Mol. Asp. Med.* **2013**, *34*, 529–547. [CrossRef]
291. Kell, D.B.; Dobson, P.D.; Oliver, S.G. Pharmaceutical drug transport: The issues and the implications that it is essentially carrier-mediated only. *Drug Discov. Today* **2011**, *16*, 704–714. [CrossRef]
292. Kell, D.B. Hitchhiking into the cell. *Nat. Chem. Biol.* **2020**, *16*, 367–368. [CrossRef]
293. Superti-Furga, G.; Superti-Furga, G.; Lackner, D.; Wiedmer, T.; Ingles-Prieto, A.; Barbosa, B.; Girardi, E.; Goldmann, U.; Gürtl, B.; Klavins, K.; et al. The RESOLUTE consortium: Unlocking SLC transporters for drug discovery. *Nat. Rev. Drug Discov.* **2020**, *19*, 429–430. [CrossRef] [PubMed]
294. Van de Waterbeemd, H.; Smith, D.A.; Jones, B.C. Lipophilicity in PK design: Methyl, ethyl, futile. *J. Comput. Aided Mol. Des.* **2001**, *15*, 273–286. [CrossRef] [PubMed]
295. Fracassi, A.; Marangoni, M.; Rosso, P.; Pallottini, V.; Fioramonti, M.; Siteni, S.; Segatto, M. Statins and the Brain: More than Lipid Lowering Agents? *Curr. Neuropharmacol.* **2019**, *17*, 59–83. [CrossRef] [PubMed]

Review

# Blood–Brain Barrier Solute Carrier Transporters and Motor Neuron Disease

Sana Latif and Young-Sook Kang \* 

Research Institute of Pharmaceutical Sciences, College of Pharmacy, Sookmyung Women's University,  
100 Cheongpa-ro 47-gil, Yongsan-gu, Seoul 04310, Korea

\* Correspondence: yskang@sm.ac.kr; Tel.: +82-2-710-9562

**Abstract:** Defective solute carrier (SLC) transporters are responsible for neurotransmitter dysregulation, resulting in neurodegenerative diseases such as amyotrophic lateral sclerosis (ALS). We provided the role and kinetic parameters of transporters such as ASCTs, Taut, LAT1, CAT1, MCTs, OCTNs, CHT, and CTL1, which are mainly responsible for the transport of essential nutrients, acidic, and basic drugs in blood–brain barrier (BBB) and motor neuron disease. The affinity for LAT1 was higher in the BBB than in the ALS model cell line, whereas the capacity was higher in the NSC-34 cell lines than in the BBB. Affinity for MCTs was lower in the BBB than in the NSC-34 cell lines. CHT in BBB showed two affinity sites, whereas no expression was observed in ALS cell lines. CTL1 was the main transporter for choline in ALS cell lines. The half maximal inhibitory concentration (IC<sub>50</sub>) analysis of [<sup>3</sup>H]choline uptake indicated that choline is sensitive in TR-BBB cells, whereas amiloride is most sensitive in ALS cell lines. Knowledge of the transport systems in the BBB and motor neurons will help to deliver drugs to the brain and develop the therapeutic strategy for treating CNS and neurological diseases.

**Keywords:** solute carrier (SLC) transporters; blood–brain barrier (BBB); amyotrophic lateral sclerosis (ALS); NSC-34 cell lines; taurine transporter (Taut); large amino acid transporter 1 (LAT1); monocarboxylate transporters (MCTs); organic cation transporters (OCTNs); choline transporter-like protein-1 (CTL1)

**Citation:** Latif, S.; Kang, Y.-S. Blood–Brain Barrier Solute Carrier Transporters and Motor Neuron Disease. *Pharmaceutics* **2022**, *14*, 2167. <https://doi.org/10.3390/pharmaceutics14102167>

Academic Editor: Inge S. Zuhorn

Received: 21 July 2022

Accepted: 4 October 2022

Published: 11 October 2022

**Publisher's Note:** MDPI stays neutral with regard to jurisdictional claims in published maps and institutional affiliations.



**Copyright:** © 2022 by the authors. Licensee MDPI, Basel, Switzerland. This article is an open access article distributed under the terms and conditions of the Creative Commons Attribution (CC BY) license (<https://creativecommons.org/licenses/by/4.0/>).

## 1. Introduction

The solute carrier (SLC) superfamily constitutes more than 65 families and over 400 genes responsible for the influx and efflux of a wide range of molecules such as organic and inorganic ions, sugars, and amino acids across membranes [1]. These transporters are mainly facilitative or depend on ion gradient for the transport of substrates [2]. Specifically for substrates like amino acids, which are building blocks for proteins, the main transporters involved belong to SLC1, 3 SLC6, 7, and SLC25, 36 subfamilies [3]. The range of specificity differs even within the family [4], and mutations in about 71 SLC genes are related to brain diseases. Various SLC transporters have contributed to the identification of diseases and participate in the specific delivery of drugs and are therefore focused as the major targets for drug delivery in the treatment of diseases [5]. Brain homeostasis is maintained with the aid of the blood–brain barrier (BBB) and cerebrospinal fluid (CSF). The BBB has a complex structure that is made of endothelial cells with tight junctions. Brain capillaries are responsible for regulating the transport of metabolites and nutrients across the BBB [6]. About 287 SLC genes have been identified in the brain [7]. SLCs expressed in the BBB [8] protect the brain from toxins and aid the absorption of essential nutrients from the blood [9]. In addition, SLCs present in the glia and neurons play important roles in regulating drug response and brain homeostasis [8]. Hence, attention should be focused on targeting SLCs for treating brain diseases by targeting the modulation of SLCs for drug transport, specifically the movement of prodrugs and drugs from the blood to the brain [10].



Neurodegeneration is a major disorder caused by various factors, including genetic and environmental aspects such as nutrients [11]. Alteration in SLC polymorphism results in neurodegeneration by irregularities in the expression of transporters and abnormal neurotransmission. The SLC families are important targets for the therapeutic drugs used to treat CNS diseases [12]. Dysfunctions of neurotransmitters are mainly involved in neurodegenerative diseases. For instance, glutamate in amyotrophic lateral sclerosis (ALS), gamma-aminobutyric acid (GABA) in schizophrenia and epilepsy, and serotonin in Parkinson's disease (PD).

Among motor neuron diseases, ALS is considered to be the most prevalent disorder resulting in muscle paralysis [13]. ALS cases are mostly sporadic, accounting for 90%, whereas familial cases are about 5–10% [14]. Mutation in the superoxide dismutase -1 gene (SOD1), TAR-DNA binding, chromosome 9 open reading frame 72, and fused sarcoma are the main causes of familial ALS [15]. Pathophysiological processes in ALS involve glutamate excitotoxicity, mitochondrial and axonal transport dysfunction, and increased oxidative stress. For the treatment of ALS, riluzole, an FDA-approved drug, works by reducing glutamate release, which is proposed to be mediated by an increase in the transporter SLC1A3, which removes glutamate from synapses, resulting in decreased glutamate levels [16,17]. In addition to this, in astroglial cells, riluzole has been shown to enhance the uptake of glutamate through elevating the SLC1A1 levels, which is an excitatory amino acid transporter [12]. Further earlier reports have shown that glutamate levels were decreased via decrease in the glutamate receptors GLT1 isoform in sensory and motor cortex in sporadic ALS patients [18]. A member of mitochondrial carrier family SLC25A20 has a role in transportation across the mitochondrial inner membrane, and the possible mechanisms in ALS are reported as maintaining calcium homeostasis, ATP production and mitochondrial apoptosis regulation [19].

The exact mechanism of the ALS is unknown, therefore a set of in vitro and in vivo experimental models are being used to validate how the mutation in the SOD1 gene leads to injury of the motor neuron [20]. In ALS mice, altered levels of amino acids have been shown in the spinal cord (lumber) in comparison with the control type (WT) mice [21]. Therefore, we conducted a series of research works to find the alteration in the transport of amino acids and acidic and basic drugs in ALS model cell lines, and find out the main transporters involved for the transport of those compounds. In our previously published work, we have used NSC-34 cell lines, which are also known as hybrid cell lines produced by the fusion of motor neurons in the spinal cord and neuroblastoma [22]. NSC-34/SOD1<sup>G93A</sup>, a mutant cell line (MT), has an overexpression of human SOD1 gene mutation due to the substitution at the 93 position of glycine with alanine [23]. NSC-34/SOD1<sup>WT</sup> wild type (WT) is considered as the control. In our research work, we have compared the MT cell line with the WT cell line and together referred to them as ALS model cell lines. The procedure for the uptake in NSC-34 cells has been described in earlier studies [24,25]. Another cell model used in our previous research work is a BBB in vitro model. Various compounds have different structural properties [26], therefore it is of prime importance to study the transporters, which are able to mediate the permeability of drugs across blood to the brain [27]. BBB dysregulation causes increased permeability and leads to disease like Alzheimer's disease (AD), ischemia and epilepsy. It is still unknown how the dysregulated BBB affects these various disorders. Animals served as the subject of early research on the BBB's function in neurological illness and method for allowing the entry of medicinal substances [28]. Parallel artificial membrane permeability assay (PAMPA), which was developed by Kansy et al., has been studied for the transport of drugs to the brain [29]. However, PAMPA offers information regarding only passive diffusion, whereas it remains unaffected by the mechanisms including metabolism and active transport [30]. In our study, we have selected conditionally immortalized rat brain capillary endothelial cell lines (TR-BBB cells), which were established by harboring large T-antigen (temperature sensitive simian virus 40) from the transgenic rats [27]. The advantage of TR-BBB cell lines that possess the solute carrier transporters is that they help in determining the active delivery

of drugs. The procedure for the culture and uptake the study has been described earlier [31]. In addition, primary and immortalized brain microvascular endothelial cell lines (BMECs) have also been commonly used models for the study of drug delivery to brain [32].

Transporters for the amino acids have potential importance in the uptake of nutrients, signaling of cells, recycling of neurotransmitters, and expression of genes and maintain cell homeostasis [33]. The scope of the SLC transporters in brain and neurodegenerative diseases is broad, and beyond the scope of this paper; however, in this study, we intend to provide the overview of different transporters involved in the transport of amino acids, essential nutrients, and acidic and basic drugs in ALS model cell lines and TR-BBB cells. In this review, we have selected small amino acids such as alanine-serine-cysteine-threonine 1 (ASCT-1/Slc1a4) and alanine-serine-cysteine-threonine 2 (ASCT-2/Slc1a5) for the transport of L and D serine, respectively, taurine transporter (TauT/Slc6a6), large amino acid transporter 1 (LAT1/Slc7a5) for the transport of neutral amino acids for instance, and citrulline and cationic amino acid transporter (CAT1/Slc7a1) for the transport of basic amino acids such as arginine. In addition, we gave insight into the monocarboxylate transporters 1 (MCT1/Slc16a1) in the BBB, sodium-coupled monocarboxylate transporters (SMCT1/Slc5a7) in ALS for the transport of acidic drugs such as 4-phenylbutyrate (PBA), organic cationic transporters (OCTN1/Slc22a4 and OCTN2/Slc22a5) for the transport of carnitine in ALS cell lines, and OCTN2 for the transport of acetyl-L-carnitine (ALCAR) in TR-BBB cells. Choline transporter 1 (CHT/Slc5a8) and choline transporter-like protein-1 (CTL1/Slc44a1) in the BBB and ALS cell lines. Further, we have mentioned the effect of the inhibition of therapeutic drugs for ALS on the uptake rate of citrulline/LAT1 or valproic acid/SMCT1 transporters.

## 2. Slc1a4/ASCT1 and Slc1a5/ASCT2 Transporter in Motor Neuron Disease

As reported by an earlier study, ASCT1 is a potential transporter for L- and D- serine in astrocytes; in addition, it also acts as a shuttle for the transport of serine along the neuron and glia [34]. ASCT1 is marked as the obligatory exchange transporter and has advanced kinetics in comparison to the one-directional transporters for amino acids [35]. ASCT2, which is known as the transporter for neutral amino acids, also belongs to the SLC1 family, and it is found in numerous body sites localized in the plasma membrane [36]. An N-methyl-D-aspartate (NMDA) receptor co-agonist [37], D-serine, plays a role in several pathophysiological activities including neurotoxicity, neurotransmission and the formation of memory [38]. The relation between the D-serine and ALS was revealed by the findings of abnormal concentration levels of D-serine, which were shown in the mutant SOD1<sup>G93A</sup> mouse and sporadic form of ALS [39,40]. The possible mechanism for the alteration in the level of serine has been reported as perhaps being deletion or mutation of the D-amino acid oxidase (DAO) gene [41]. For a clear understanding, the serine uptake in ALS model cell lines has been studied by Lee et al., 2017, and the findings suggest that the uptake of [<sup>3</sup>H]D-serine was markedly higher in the MT cells, whereas [<sup>3</sup>H]L-serine was higher in the WT cells. The kinetics parameters also elucidate the altered affinity and capacity. In case of [<sup>3</sup>H]D-serine, the affinity was higher in the MT cells as compared to WT; however, the affinity for [<sup>3</sup>H]L-serine in WT cells were two times lower in MT cells as compared to WT cells (Table 1). From the same study, it was revealed that ASCT1 was involved in the transport of [<sup>3</sup>H]L-serine, whereas ASCT2 transporter was involved for the transport of [<sup>3</sup>H]D-serine [42]. The altered levels of transporters were found via immunoblots in the transgenic ALS mice as compared to the non-transgenic mice [43].

**Table 1.** Kinetic parameters analysis of various transporters in BBB and ALS model cell lines.

Transporters (Substrate)	Affinity (mM)			Velocity (nmol/mg Protein/min)		
	BBB	WT	MT	BBB	WT	MT
ASCT1 ( <sub>L</sub> -Serine) <sup>a</sup>	–	0.061 ± 0.004	0.0308 ± 0.0021	–	1.94 ± 0.01	1.69 ± 0.07
ASCT2 ( <sub>D</sub> -Serine) <sup>a</sup>	–	11.3 ± 1.3	21.1 ± 3.0	–	39.5 ± 1.4	41.5 ± 2.0
LAT1 (Citrulline) <sup>b,c</sup>	0.031 ± 0.001 0.0017 ± 0.0004	1.48 ± 0.21 –	0.670 ± 0.050 –	0.185 0.0032	18.3 ± 2.9 –	10.9 ± 0.8 –
CAT1 (Arginine) <sup>d</sup>	–	0.013 ± 0.005 3.51 ± 1.73	0.30 ± 0.11 *** 1.98 ± 1.10	–	0.012 ± 0.006 3.30 ± 1.62	0.47 ± 0.15 ** 1.42 ± 1.30
MCT1 (PBA) <sup>e</sup>	13.4 ± 2.9	–	–	4.16 ± 0.55	–	–
SMCT1 (PBA) <sup>f</sup>	–	0.514 ± 0.068 2.66 ± 0.19	0.314 ± 0.031 7.69 ± 0.44	–	0.562 ± 0.035 2.66 ± 0.19	0.109 ± 0.046 4.17 ± 1.38
OCTN2 (ALCAR) <sup>g</sup>	0.054 ± 0.009	–	–	1.07 ± 0.05	–	–
OCTN1/2 (Carnitine) <sup>h</sup>	–	0.0019 ± 0.0003 0.994 ± 0.034	0.0020 ± 0.0003 0.374 ± 0.089 ***	–	0.00030 ± 0.0001 0.259 ± 0.009	0.00019 ± 0.00003 0.062 ± 0.013 ***
CHT (Choline) <sup>i</sup>	0.020 0.210	– –	– –	0.019 0.167	– –	– –

The kinetic parameters of various transporters in the BBB and ALS model cell lines. <sup>a,b,c,d,e,f,g,h,i</sup> These data points were retrieved from the previously published articles [25,42,44–50]. In front of each transporter, the upper row shows the high affinity site, and the lower row represents the low affinity site, respectively. \*\*  $p < 0.01$ , and \*\*\*  $p < 0.001$  represent significant differences from the respective WT.

### 3. Slc6a6/TauT Transporter in the BBB and ALS

Taurine transporter (TauT), a member of the SLC 6 family, and a sodium and chloride dependent transporter, Slc6a6, play an important role in taurine transport [51]. Taurine possesses osmoregulatory and antioxidant effects that help maintain homeostasis [52]. The brain controls the neuronal release of taurine in response to ischemia [53]. A previous study reported elevated taurine levels in the hippocampal slices under conditions of hypoglycemia and ischemia [54]. Our earlier study demonstrated that taurine transport activity at the BBB was reduced in hypertensive rats compared to the normotensive control rats [55]. Previous research has also shown that taurine, a sulfur-containing  $\beta$ -amino acid, plays an important role as a neuromodulator and neuroprotective agent against excitotoxicity and oxidative stress. Radiolabeled [<sup>3</sup>H]taurine is transported by TauT/Slc6a6 in rat brain capillary endothelial cells (TR-BBB13) [56]. Another research has shown that Slc6a6 uses GABA as a substrate, and this transport system seems to be present at the inner blood–retinal barrier [51]. The kinetic parameters of taurine have been studied in cultured bovine brain capillary endothelial cells (BCECs), and the [<sup>3</sup>H]taurine uptake has shown the activity of transporters at both membranes luminal and antiluminal of BCECs. Saturable taurine transport showed high affinity and low capacity systems, Michaelis-Menten constant ( $K_m$ , affinity);  $12.1 \pm 0.5 \mu\text{M}$  and velocity ( $V_{\text{max}}$ );  $4.32 \pm 0.05 \text{ nmol}/30 \text{ min}/\text{mg}$  protein, for the luminal uptake, whereas,  $K_m$ ;  $13.6 \pm 2.4 \mu\text{M}$  and  $V_{\text{max}}$ ;  $2.81 \pm 0.02 \text{ nmol}/30 \text{ min}/\text{mg}$  protein, for antiluminal uptake of [<sup>3</sup>H]taurine [57].

The role of taurine in ALS has been demonstrated in a previous study. The immune reactivity of TauT was increased in the spinal cord of transgenic ALS mice (Male transgenic ALS mice are the MT SOD1 (G93A) expressing H1 high strain mice) in a pattern similar to that of the motor neurons of ALS patients [58]. Due to the increase in the taurine and TauT levels in the motor neurons of ALS, it was hypothesized it might be due to an increase in the uptake of taurine by the neurons. Therefore, the uptake study was performed in ALS model cell lines, and the data showed a time-dependent uptake of [<sup>3</sup>H]taurine, where the uptake was markedly higher in the MT cell line as compared to the WT cell (Figure 1). Further, the mRNA expression of TauT was higher in the MT cell line in comparison to WT [21].

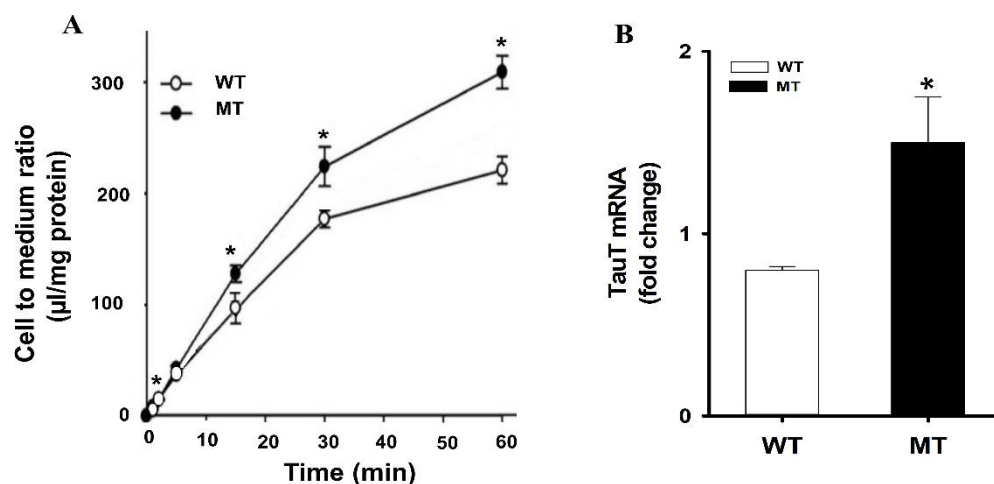


**Figure 1.** Reproduced from Jung et al., *Molecular Neurobiology*, 2013 [21]. (A) Uptake of [ $^3\text{H}$ ]taurine in a time dependent manner. Uptake was carried at temperature 37 °C. (B) Relative expressions of TauT transporter in ALS model cell lines. mRNA expression levels were determined using quantitative RT-PCR analysis and normalized to the internal control GAPDH in ALS model cell lines. Each value represents the mean  $\pm$  SEM. ( $n = 3\text{--}4$ ). \*  $p < 0.05$  indicates a significant difference with respect to the WT control.

Heat shock factor-1 (HSF1) mediated expression of TauT showed a compensatory effect against oxidative stress, which is considered the key factor in ALS pathogenesis. It has been concluded that TauT is one of the key markers for diagnosing stress in motor neurons, and the regulation of Slc6a6 may slow the process of neurodegeneration [21]. Additionally, the role of taurine was also studied against glutamate neurotoxicity, and the results showed that taurine protected the neurons from glutamate-induced injury; hence, taurine was considered valuable for use in ALS clinical trials [59].

#### 4. Slc7a5/LAT1 Transporter in the BBB and ALS

The SLC7 family includes 15 members; two are pseudogenes, and the remaining 13 are divided into subgroups—the cationic amino acid transporters (CATs) and light subunits of LATs [60]. LAT1, associated with the SLC7 family, belongs to the amino acid-polyamine-organo cation (APC) superfamily [61]. SLC7a5 is responsible for the transport of amino acids and forms a heterodimer with glycoprotein SLC3A2 via a disulfide bond [62]. LAT1 is one of the important proteins responsible for the growth and development of cells because of its key role in the distribution of essential amino acids, especially in the placenta and BBB [63]. Neutral amino acids such as citrulline, a precursor of L-arginine [64], have been found to protect and prevent neuronal death and cerebrovascular injury. The role of citrulline in preventing cerebrovascular injury in the hippocampus was due to the regulation of endothelial nitric oxide (eNOS) [65]. Citrulline is transported in various cells such as neural cells [66], intestinal cells, macrophages [67], and bovine aortic smooth muscle cells [68] by different transport systems [44]. Citrulline delivery to the brain by LAT1 provides neuroprotection against cerebrovascular diseases. In the TR-BBB, the transport of [ $^{14}\text{C}$ ]citrulline through the BBB was carried by Slc7a5/LAT1 [44]. In addition, a previous study on ALS model cell lines reported that [ $^{14}\text{C}$ ]citrulline was mediated by Slc7a5/LAT1 transporter. In a similar manner, the roles of essential amino acids such as tryptophan in both the BBB and ALS model cell lines have been studied, and the findings suggested that LAT1 was also involved in the transport of [ $^3\text{H}$ ]tryptophan [69].

A previous study on [ $^{14}\text{C}$ ]citrulline transport in the BBB showed that two saturable processes are involved in the transport, and the results showed that at high affinity site, higher affinity and capacity, whereas at a low affinity site, there was a lower affinity and capacity in the TR-BBB cell lines [44]. Another study has reported that in the BBB, LAT1 exhibits  $K_m$  values 1–10  $\mu\text{M}$  for high affinity and 10–100  $\mu\text{M}$  for low affinity [70]. Similarly,

the kinetic parameters of [<sup>14</sup>C]citrulline in ALS have also been studied. The data showed that the high affinity and low capacity transport systems were involved in the MT compared to the WT [45]. These results are summarized in Table 1 and show that two affinity sites were involved in the BBB, whereas a single saturable process was involved in the ALS model cell line.

Reportedly, the hallmarks of ALS include oxidative stress and glutamate excitotoxicity [71]. Riluzole acts as a glutamate inhibitor and drug for the treatment of ALS. In addition, edaravone, known for its antioxidant effect, has recently been approved for ALS treatment [72]. Therefore, we aimed to compare the inhibitory effects of drugs on the SLC transporters such as LAT1 and SMCT1 substrate uptake from our previously published articles. In the ALS model cell lines, riluzole inhibited the uptake of [<sup>14</sup>C]L-citrulline in a concentration-dependent manner. A previous study reported no inhibition at 0.2 mM, whereas a significant inhibition was observed at 0.5 mM in both NSC-34 cell lines [45] (Table 2). Additionally, L-dopa, an L-system substrate and drug used for Parkinson's disease, significantly inhibited citrulline uptake, showing the involvement of the LAT1 transporter in the transport of L-dopa in ALS cell lines. Furthermore, a previous study has shown in the Lineweaver–Burk plot analysis the competitive inhibition of citrulline with L-dopa. These findings indicated that L-dopa and citrulline compete for the same binding site, LAT1 [45].

**Table 2.** Inhibition effect of therapeutics of ALS on the uptake rate of transporters substrate in ALS model cell lines.

Drugs (% of Control)	Conc. (mM)	LAT1 ( <sup>14</sup> C-Citrulline) <sup>a</sup>		SMCT1 ( <sup>3</sup> H-VPA) <sup>b</sup>	
		WT	MT	WT	MT
+L-Dopa	0.5	32.8 ± 2.7 ***	36.8 ± 12.0 ***	–	–
+Riluzole	0.5	72.6 ± 3.4 **	80.0 ± 1.2 **	–	–
+Ibuprofen	10	–	–	22.3 ± 1.5 ***	33.5 ± 1.0 ***
+PBA	10	–	–	43.1 ± 2.2 ***	56.6 ± 3.0 ***
+Edaravone	10	–	–	67.3 ± 7.6 **	68.6 ± 6.3 **

The percentage of inhibition on each transporter substrate uptake of drugs in NSC-34 cell lines. <sup>a,b</sup> Data points were taken from our earlier published articles [45,73]. \*\*  $p < 0.01$ , and \*\*\*  $p < 0.001$  represent significant difference from the respective control. VPA (valproic acid), PBA (4-phenylbutyric acid).

## 5. Slc7a1/CAT1 Transporter in Motor Neuron Disease

The SLC7 family is subdivided as LATs and cationic amino acid transporters (CATs) [74]. For the transport of basic amino acids including lysine, arginine, and histidine Slc7a1 (CAT1) is mainly involved. Arginine has shown its potential role in the ALS by increasing the flow of blood resulting in the synthesis of protein and generation of  $\alpha$ -ketoglutarate [75]. The scarcity of arginine makes neurons prone to excitotoxicity, and the addition of arginine has shown motor neuron protection against glutamate excitotoxicity [14]. A previous study on the transport of [<sup>3</sup>H]L-lysine has shown that CAT1 (system y+) was responsible for the transport of lysine in the ALS model cell line [24] and also across the BBB [76]. L-Arginine, a cationic amino acid, has important role in the pathogenesis of ALS [75] and has shown a potential role in enhancing the skeletal muscle growth and improving the glucose metabolic dysfunction [77]. The uptake of [<sup>3</sup>H]L-arginine was found to be concentration-dependent in ALS model cell lines, and the kinetics revealed that in the MT cell line, the affinity was lower and capacity was higher at a high affinity site, whereas at a low affinity site there was no significant difference between WT and MT cell lines, as shown in Table 1. According to the differential relative contribution study, it was shown that the system y+ (CAT1) mainly mediates the transport of [<sup>3</sup>H]arginine in ALS cell lines [46]. Similar patterns of results were shown in the inner blood–retinal barrier, showing the transport of arginine by carrier-mediated transporters [78]. Furthermore, the basic drugs, including quinidine, which is known for its antiarrhythmic actions, and verapamil, a calcium channel blocker, have shown the inhibitory effect of the transport of arginine in ALS model cell

lines. Quinidine showed competitive inhibition with the  $K_i$  value of 0.64 mM in the disease model of ALS, showing that it competes with arginine for the same binding site and shared the same transporter, i.e., CAT1 in ALS model [46].

## 6. Slc16a1/MCT1 and Slc5a8/SMCT1 Transporters in BBB and ALS

MCTs play a vital role in cellular metabolism and energy pathways in several tissues [79]. The SLC16 family, which expands over 14 sub-members, is widely expressed in various organs such as the kidneys, heart, liver, adipose tissue, and brain [80]. In pathology and physiology, the commonly expressed and well-characterized members of the SLC16 family are Slc16a1/MCT1, responsible for the transport of pyruvates, ketones, and lactates, and Slc16a7/MCT2 and Slc16a3/MCT4 [81]. Genetic and metabolic studies have been linked to Slc16a1, and various mouse models have been developed to study the link between disease and transporter functions [82]. PBA, a short-chain fatty acid and histone deacetylase inhibitor, is involved in the treatment of various diseases [47]. Our previous study on the BBB has indicated the expression of MCTs, including rMCT1, 2, and 4. However, we observed that MCT1/Slc16a1 was the main transporter in [ $^{14}\text{C}$ ]PBA transport to the brain across the BBB [47]. Additionally, [ $^{14}\text{C}$ ]PBA transport characteristics and transporters involved have been studied in ALS cell lines, and the results indicated that sodium-coupled MCT1 (SMCT1/Slc5a8) and MCT1 both help [ $^{14}\text{C}$ ]PBA transport to NSC-34 cell lines [48].

[ $^{14}\text{C}$ ]PBA transport by TR-BBB showed that the transport was concentration-dependent, and the Michaelis–Menten constant demonstrated that the carrier-mediated transport of PBA was pH-dependent, with the  $K_m$  four times higher at pH 7.4 than the  $K_m$  at pH 6.0. In contrast,  $V_{\max}$  was five times lower at pH 7.4 than pH 6.0 (Table 1) [47]. In addition, transport kinetics of [ $^{14}\text{C}$ ]PBA in ALS model cell lines showed the two affinity sites with altered affinity and capacity. At the high-affinity site, the capacity was five times lower in the MT than in the WT, whereas, at the low-affinity site, affinity was three times lower in the MT than in the WT [48] (Table 1).

Conversely, our previous study on valproic acid (VPA) has shown the neuroprotective effects of VPA in the ALS disease model. The study data suggested that the transporter SMCT1 was commonly involved in mediating the transport of VPA in NSC-34 cell lines [73]. Transport of [ $^3\text{H}$ ]VPA in ALS cell lines was concentration-dependent, and the saturation kinetic parameters demonstrated two affinity sites. MT possessed significantly higher affinity and capacity than the WT at the high-affinity site, whereas, at the low-affinity site, MT showed lower capacity than WT. In the brain endothelial and intestinal epithelium the affinity for VPA ranged between 0.6–0.8 mM [83], that is likewise the  $K_m$  value in NSC-34 cell lines. Other SMCT carried monocarboxylates exhibited the  $K_m$  value between 0.07–6.5 mM that is also comparable to motor neuronal cell lines [84]. Ibuprofen, a strong inhibitor of SMCT1 and an anti-inflammatory agent, significantly inhibited [ $^3\text{H}$ ]VPA uptake at the concentration of 10 mM in WT and MT (Table 2). In addition, PBA, a substrate of SMCT1, also strongly inhibited the transport of VPA in ALS cell lines, suggesting that they both utilize the same transporter system, SMCT1. Furthermore, edaravone, an organic anion transporter (OAT) substrate and a drug for ALS treatment, significantly inhibited [ $^3\text{H}$ ]VPA uptake up to about 68% inhibition at 10 mM in both cell lines [73] (Table 2). A previous study on half maximal inhibitory concentration ( $\text{IC}_{50}$ ) analysis in MT revealed that high edaravone concentration is required to reach 50% inhibition [73]. These results indicated that drugs like ibuprofen, PBA, and edaravone possibly use the transporter SMCT1 and inhibit [ $^3\text{H}$ ]VPA uptake.

## 7. Slc22a4/OCTN1 and Slc22a5/OCTN2 in BBB and ALS

Lee et al., 2012, have studied the transport properties of acetyl-L-carnitine (ALCAR) in the BBB [49]. In the brain, kidney, liver and intestine, ALCAR is produced from carnitine and acetyl coenzyme A. Various physiological effects of ALCAR have been studied in the brain mainly, where ALCAR helps in the transmission of numerous neurotransmitters,

morphology of synapsis, brain energy modulation and as a neurotrophic factor [85]. It has been shown that [<sup>3</sup>H]ALCAR transport in TR-BBB cells was carried by OCTN2. Expression of OCTN2 in the cells confirm the involvement of OCTN2 in TR-BBB cells. Another study has reported that OCTN2 in the brain and astrocytes are responsible for the transport of ALCAR and L-carnitine [86]. The kinetic parameters from the concentration dependent uptake study in TR-BBB cells showed that a single transport system is involved for the uptake of ALCAR (Table 1). Earlier research on L-carnitine has shown the involvement of both OCTN1 and OCTN2 in the transport of carnitine in motor neuron NSC-34 cell lines [25]. Another study has shown that the administration of the energy metabolizing entity L-carnitine to neuronal cells in human has increased neuronal mitochondrial functions and thus has a role in preventing the pathological conditions related to ALS disease [87]. The concentration-dependent uptake of [<sup>3</sup>H]L-carnitine in ALS model cell lines exhibits saturable processes and two affinity sites. The data shown in Table 1 indicated that in MT, the cell affinity is higher and the capacity is lower, which is significantly different from the WT cell line at a low affinity site [25]. An animal study of juvenile visceral steatosis (JVS) disease mice has shown the reduced transporter activity due to the reduced capacity, which supports the findings in NSC-34 cell lines [88]. Additionally, the study in neural cells have shown the high affinity for carnitine transporters [89]. From Table 1, it is concluded that ALCAR exhibit a single affinity site in TR-BBB cells, whereas L-carnitine possesses two affinity sites in ALS model cell lines. Additionally, various pharmacological compounds such as quinidine, pyrilamine, diphenhydramine (DPH) and metformin have shown the significant inhibitory effect of the uptake of carnitine in ALS model cell lines. The organic cationic compounds showed competitive inhibition with L-carnitine, showing they compete for the same binding sites [25]. In addition, it has been reported that the OCTN2 transporter showed a high affinity, whereas OCTN1 showed a low affinity for the carnitine [90]. A human study has shown that the mutations in OCTN2 results in a deficiency of carnitine and resulted in muscle weakness and cardiomyopathy [91]. Furthermore, L-carnitine showed significant inhibition on the uptake of [<sup>3</sup>H]paeonol in ALS model cell lines. The OCTN1 and PMAT transporters showed altered behavior in the disease model of ALS in the uptake of paeonol [92].

#### 8. Slc5a7/CHT in the BBB and Slc44a1/CTL1 in Motor Neuron Disease

Choline is an essential nutrient and hydrophilic cationic compound for plasma cell membrane synthesis [93]. It is an important neurotransmitter for cholinergic neurons that release acetylcholine (ACh) for the sympathetic and parasympathetic systems [94]. For the uptake of choline, various transport systems are involved depending on the affinity of choline. A high affinity, hemicholinium-3, and sodium dependent choline transporter (CHT1) has the rate limiting role for the synthesis of ACh [95]. Mutations in this transporter result in neurological diseases including depression and AD [96]. Another intermediate affinity transporter include choline-like transporters (CTLs). CTL1 is a member of the broader Slc44a1-5 family [97]. Choline transport for membrane phospholipids synthesis is carried by CTL1/Cdw92/Slc44a1 and is considered a major contributor to the family [98]. Reportedly, the homologous CTL1 genes were found in rats, mice, and humans [99–101]. In the mitochondria and plasma membrane, CTL1 is a choline /H<sup>+</sup> antiporter [102]. The exact role and function of CTL2/Slc44a2 are not well known; however, it is indirectly involved in phosphatidylcholine synthesis [103]. Choline scarcity affects various processes, including the expression of genes involved in cell differentiation, apoptosis, and proliferation. In addition, low affinity organic transporters (OCTs) are also responsible for the transport of choline [104]. Research has shown that OCT1 as well as OCT3 expression increases the uptake of choline in in *Xenopus* oocytes [105]. The abnormal metabolism and transportation of choline are involved in neurodegenerative disorders like PD and AD [98]. In hypertensive rats, the alteration in the function of the choline transport system has been reported, and the change in choline transport activity is of prime physiological importance as the brain is incapable of producing choline de novo [104].

A previous *in vivo* choline study via a carotid artery injection and isolated brain capillaries via an *in vitro* technique has shown that choline transport was implicated by a carrier-mediated system in the BBB. Our previous study in the rat conditionally immortalized syncytiotrophoblast cell line (TR-TBT) provided an analysis of the various choline transporters, and the results demonstrated CTL1 expression in TR-TBT cells. In addition, CHT and CTL1 were expressed in the rat brain and placenta (Figure 2A) [93].

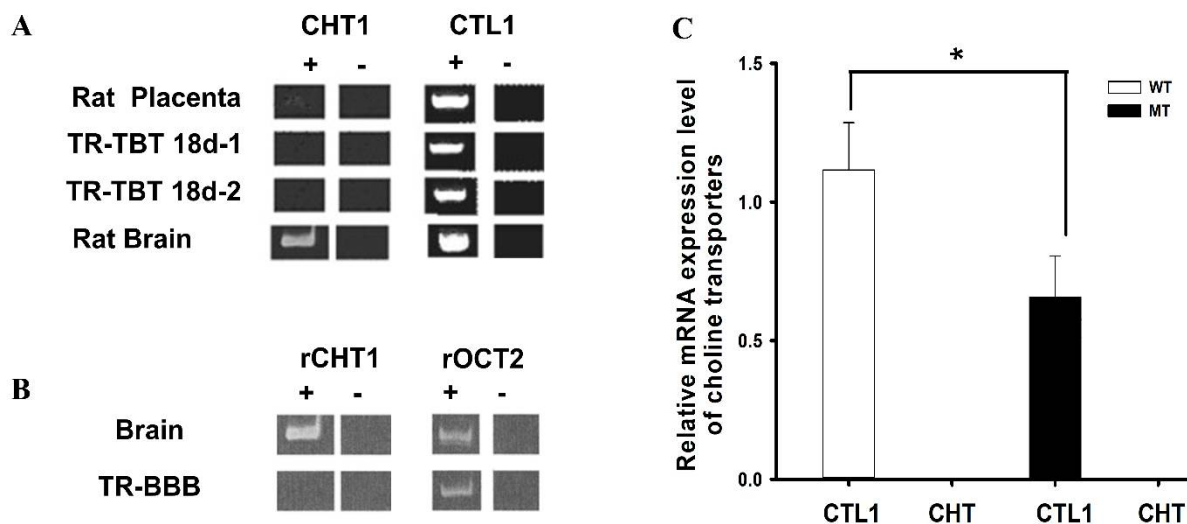


**Figure 2.** Relative expressions of transporters in ALS model cell lines. The data in (A) was retrieved and analyzed from the earlier published study by Lee et al., Placenta, 2009 [93]. (B) Determination of rCHT1 and rOCT2 in TR-BBB cells. This data is retrieved from our previous research by Kang et al., Archives of Pharmacal Research, 2005 [106]. (C) CTL1 mRNA expression levels were determined using quantitative RT-PCR analysis and normalized to the internal control GAPDH in ALS model cell lines. Each value represents the mean  $\pm$  SEM. ( $n = 3-4$ ). \*  $p < 0.05$  indicates a significant difference with respect to the WT control.

Further, in our previous study on TR-BBB cell lines, CHT1 was expressed in the brain, whereas OCT2 was expressed in the brain and TR-BBB (Figure 2B) [50]. CTL is the main transporter for the transport of choline in ALS model cell lines and showing the relative lower expression of CTL1 in MT as compared to WT. Additional studies have reported that choline transport was carried by CTL1 in the mouse neurons primary cultures and rat astrocytes and carcinoma lung cells [106,107].

Reportedly, choline uptake varies due to the differences in the transporter family involved and its sodium dependency and distribution in tissues [108]. Further, the kinetic parameters of [ $^3$ H]choline transport in the BBB were retrieved from our previously published article. The data presented in Table 1 indicated that carrier-mediated saturable processes are involved in the uptake rate of choline in the BBB. At the high affinity site, the affinity was higher and the capacity was lower as compared to the lower affinity site (Table 1) [109]. In TR-BBB cell lines, *in vitro* [ $^3$ H]choline uptake was concentration-dependent, and the Eadie–Hofstee plot showed a straight line, indicating a single saturable process with  $K_m$  (26.2  $\mu$ M) and  $V_{max}$  (397 pmol/mg protein/min) [50]. In addition, another study demonstrated that choline transport in the brain and spinal cord was carried by CHT1 in a sodium-dependent manner and possessed  $K_m$  ranging from 0.5 to 3  $\mu$ M [110]. Furthermore, an organic cation, choline, in multiple tissues has been reported to be transported by CTL1 in a sodium-independent manner, and the  $K_m$  values varied from 10–50  $\mu$ M [111].

A previous study on the transport of choline through TR-BBB cell lines has illustrated the inhibitory effect of basic drugs, including choline, hemicholinium-3, a choline analog, and  $\alpha$ -phenyl-*n*-butyl nitron (PBN); the study results showed that these drugs inhibited choline uptake in TR-BBB cells and exhibited  $IC_{50}$  of 9.40  $\mu$ M, 37.2  $\mu$ M, and 1.20 mM,



respectively (Figure 3A). In ALS model cell lines, the inhibitory effect of pharmacological drugs, including amiloride and DPH, was studied.  $IC_{50}$  was calculated as 1.04  $\mu$ M for amiloride, and 61.0  $\mu$ M for DPH. These drugs showed inhibition in a dose–response manner in the MT cell line (Figure 3B).

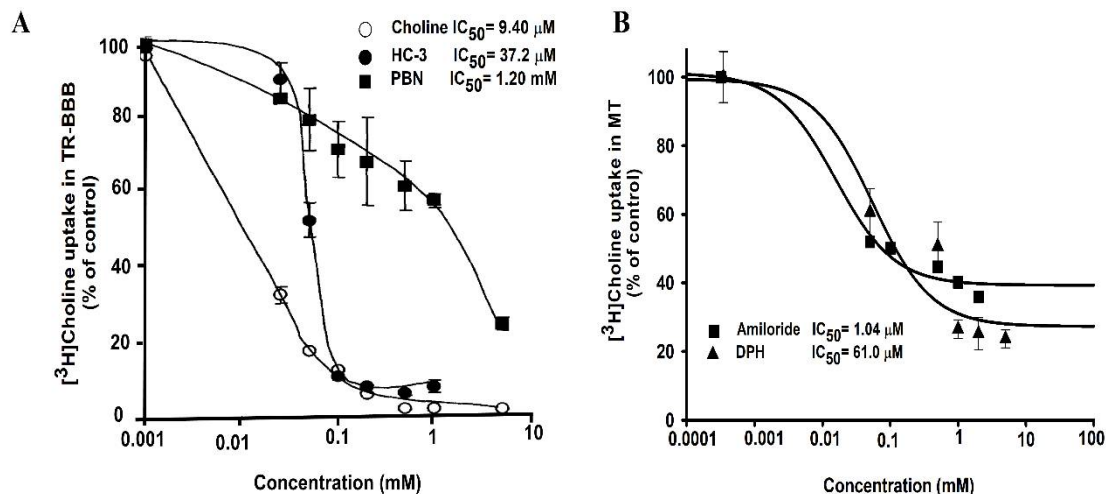


**Figure 3.** Inhibitory effect of drugs in a dose–response manner. (A) Inhibition of choline uptake inhibition by choline, hemicholinium-3, and  $\alpha$ -phenyl-*n*-butyl nitron (PBN) in TR-BBB cells. These data were retrieved and analyzed from the earlier published study by Kang et al., Archives of Pharmacol Research, 2005 [106]. (B) Half inhibitory concentrations ( $IC_{50}$ ) were analyzed either in the presence or absence of diphenhydramine (DPH), and amiloride at concentrations of 0–2 mM at pH 7.4 and 37  $^{\circ}$ C on [ $^3H$ ]choline uptake in the ALS disease model cell line (MT). Data are represented as the mean  $\pm$  S.E.M ( $n = 3$ –4).

Lower concentrations varying from 0.001 to 3 mM of these drugs were required to show inhibition of [ $^3H$ ]choline uptake by half in the ALS disease model cell lines. Amiloride was the most sensitive drug in the ALS model cell line to achieve the maximal half concentration, whereas choline inhibition showed the most sensitivity in the TR-BBB cell line. A previous study on muscle cell lines involving the H1 receptor antagonist, DPH, showed the inhibition of histamine receptors, and the estimated  $IC_{50}$  value, 1.01  $\mu$ M, helped control the intracellular calcium [112]. Another study reported the  $IC_{50}$  of amiloride for the inhibition of calcium channels as 30  $\mu$ mol/L in the mouse neuroblastoma [113]. It must be noted that the inhibitory concentrations varied according to the cell type and concentrations.

## 9. Concluding Remarks

Overall, in this review, the representative transporters, which are related with the transport of amino acids including small amino acid, large neutral amino acids, basic amino acids, as well as acidic drugs including PBA and VPA and essential nutrients such as choline and carnitine in BBB and ALS model cell lines. Affinity and capacity plays important role in understanding the transport ability of compounds into the cells. Therefore, we compared the kinetic parameters obtained in BBB and ALS cell lines. In the BBB, affinity of LAT1 is very high, but capacity is very lower than ALS cell lines. L-Arginine transported by CAT1 in ALS cell lines, showed low affinity and higher capacity in MT cell line. Taurine levels were altered in the transgenic ALS mice, in addition to this, the uptake of [ $^3H$ ]taurine was higher in the disease model as compared to the control. It was concluded that increase in the levels of taurine might be due to increase in the TauT levels in the disease model cell line. TauT modulation might delay the neurodegeneration and is considered to be a novel biomarker for ALS. PBA was transported across the BBB by MCT1; however, in addition to MCT1, PBA transport in ALS cell lines was mediated by SMCT. L-Carnitine was transported by

OCTN1/2 in ALS cell lines whereas its acetylated form ALCAR transport was mediated by OCTN2 in TR-BBB cells. CHT1 was the main transport for choline across the BBB; however, no CHT1 expression was observed in ALS cell lines. CTL1 is responsible for choline transport in NSC-34 cell lines. In addition, IC<sub>50</sub> evaluation of basic drugs showed that choline in BBB and amiloride were the most sensitive in ALS cell lines. Additionally, it is shown that the therapeutics for ALS such as riluzole and edaravone can be transported by LAT1 or SMCT1, respectively, in ALS cell lines. In conclusion, ALS is a devastating neuronal disease and need of hour is to find the possibilities to cure and alleviate the symptoms related to ALS. Hence, adequate knowledge of transporter involvement will be beneficial in delivering novel drugs in ALS. Comprehending the concept of SLC transporters involved in the transport of compounds will aid the development of new drugs and their delivery in brain and motor neuron diseases.

**Author Contributions:** Conceptualization, funding acquisition, Y.-S.K.; investigation, Y.-S.K. and S.L.; analysis, data curation, and interpretation S.L. and Y.-S.K.; supervision and visualization, Y.-S.K.; writing—original draft, S.L.; writing—review and editing, Y.-S.K. All authors have read and agreed to the published version of the manuscript.

**Funding:** This study was supported by the National Research Foundation of Korea (NRF), Korea Government (No. 2019R1F1A1044048) granted to YSK.

**Informed Consent Statement:** Not applicable.

**Data Availability Statement:** All data were included in this study.

**Conflicts of Interest:** The authors declare no conflict of interest.

## References

- Hediger, M.A.; Romero, M.F.; Peng, J.-B.; Rolfs, A.; Takanaga, H.; Bruford, E.A. The ABCs of solute carriers: Physiological, pathological and therapeutic implications of human membrane transport proteins. *Pflug. Arch. Eur. J. Physiol.* **2004**, *447*, 465–468. [CrossRef] [PubMed]
- Lin, L.; Yee, S.W.; Kim, R.B.; Giacomini, K.M. SLC transporters as therapeutic targets: Emerging opportunities. *Nat. Rev. Drug Discov.* **2015**, *14*, 543–560. [CrossRef]
- Bröer, S. Apical transporters for neutral amino acids: Physiology and pathophysiology. *Physiology* **2008**, *23*, 95–103. [CrossRef] [PubMed]
- Fotiadis, D.; Kanai, Y.; Palacín, M. The SLC3 and SLC7 families of amino acid transporters. *Mol. Asp. Med.* **2013**, *34*, 139–158. [CrossRef] [PubMed]
- Hopkins, A.L.; Groom, C.R. The druggable genome. *Nat. Rev. Drug Discov.* **2002**, *1*, 727–730. [CrossRef]
- Zaragozá, R. Transport of amino acids across the blood-brain barrier. *Front. Physiol.* **2020**, *11*, 973. [CrossRef] [PubMed]
- Hu, C.; Tao, L.; Cao, X.; Chen, L. The solute carrier transporters and the brain: Physiological and pharmacological implications. *Asian J. Pharm. Sci.* **2020**, *15*, 131–144. [CrossRef] [PubMed]
- Li, Q.; Zhou, T.; Wu, F.; Li, N.; Wang, R.; Zhao, Q.; Ma, Y.M.; Zhang, J.Q.; Ma, B.L. Subcellular drug distribution: Mechanisms and roles in drug efficacy, toxicity, resistance, and targeted delivery. *Drug Metab. Rev.* **2018**, *50*, 430–447. [CrossRef]
- Nałecz, K.A. Solute Carriers in the Blood–Brain Barrier: Safety in Abundance. *Neurochem. Res.* **2017**, *42*, 795–809. [CrossRef] [PubMed]
- Patching, S.G. Glucose Transporters at the Blood-Brain Barrier: Function, Regulation and Gateways for Drug Delivery. *Mol. Neurobiol.* **2017**, *54*, 1046–1077. [CrossRef] [PubMed]
- Bekdash, R.A. Choline, the brain and neurodegeneration: Insights from epigenetics. *Front. Biosci.-Landmark* **2018**, *23*, 1113–1143. [CrossRef] [PubMed]
- Aykaç, A.; Şehirli, A.Ö. The role of the SLC transporters protein in the neurodegenerative disorders. *Clin. Psychopharmacol. Neurosci.* **2020**, *18*, 174–187. [CrossRef] [PubMed]
- Paez-Colasante, X.; Figueroa-Romero, C.; Sakowski, S.A.; Goutman, S.A.; Feldman, E.L. Amyotrophic lateral sclerosis: Mechanisms and therapeutics in the epigenomic era. *Nat. Rev. Neurol.* **2015**, *11*, 266–279. [CrossRef] [PubMed]
- Lee, J.; Ryu, H.; Kowall, N.W. Motor neuronal protection by l-arginine prolongs survival of mutant SOD1 (G93A) ALS mice. *Biochem. Biophys. Res. Commun.* **2009**, *384*, 524–529. [CrossRef]
- Barber, S.C.; Shaw, P.J. Oxidative stress in ALS: Key role in motor neuron injury and therapeutic target. *Free Radic. Biol. Med.* **2010**, *48*, 629–641. [CrossRef] [PubMed]
- Carbone, M.; Duty, S.; Rattray, M. Riluzole elevates GLT-1 activity and levels in striatal astrocytes. *Neurochem. Int.* **2012**, *60*, 31–38. [CrossRef] [PubMed]

17. Dall'Igna, O.P.; Bobermin, L.D.; Souza, D.O.; Quincozes-Santos, A. Riluzole increases glutamate uptake by cultured C6 astroglial cells. *Int. J. Dev. Neurosci.* **2013**, *31*, 482–486. [CrossRef] [PubMed]
18. Kanai, Y.; Hediger, M.A. The glutamate and neutral amino acid transporter family: Physiological and pharmacological implications. *Eur. J. Pharmacol.* **2003**, *479*, 237–247. [CrossRef] [PubMed]
19. Wong, P.C.; Pardo, C.A.; Borchelt, D.R.; Lee, M.K.; Copeland, N.G.; Jenkins, N.A.; Sisodia, S.S.; Cleveland, D.W.; Price, D.L. An adverse property of a familial ALS-linked SOD1 mutation causes motor neuron disease characterized by vacuolar degeneration of mitochondria. *Neuron* **1995**, *14*, 1105–1116. [CrossRef]
20. Ferraiuolo, L.; Higginbottom, A.; Heath, P.R.; Barber, S.; Greenald, D.; Kirby, J.; Shaw, P.J. Dysregulation of astrocyte-motoneuron cross-talk in mutant superoxide dismutase 1-related amyotrophic lateral sclerosis. *Brain* **2011**, *134*, 2627–2641. [CrossRef] [PubMed]
21. Jung, M.K.; Kim, K.Y.; Lee, N.Y.; Kang, Y.S.; Hwang, Y.J.; Kim, Y.; Sung, J.J.; McKee, A.; Kowall, N.; Lee, J.; et al. Expression of taurine transporter (TauT) is modulated by heat shock factor 1 (HSF1) in motor neurons of ALS. *Mol. Neurobiol.* **2013**, *47*, 699–710. [CrossRef] [PubMed]
22. Cashman, N.R.; Durham, H.D.; Blusztajn, J.K.; Oda, K.; Tabira, T.; Shaw, I.T.; Dahrouge, S.; Antel, J.P. Neuroblastoma × spinal cord (NSC) hybrid cell lines resemble developing motor neurons. *Dev. Dyn.* **1992**, *194*, 209–221. [CrossRef] [PubMed]
23. Gomes, C.H. *Amyotrophic Lateral Sclerosis: Mammalian Cell Models, Copper-Zinc Superoxide Dismutase and Biological Characteristics*; Universidade NOVA de Lisboa (Portugal) ProQuest Dissertations Publishing: Lisbon, Portugal, 2015; ISBN 9781073982288.
24. Latif, S.; Kang, Y. Change in cationic amino acid transport system and effect of lysine pretreatment on inflammatory state in amyotrophic lateral sclerosis cell model. *Biomol. Ther.* **2021**, *29*, 498–505. [CrossRef] [PubMed]
25. Gyawali, A.; Hyeon, S.J.; Ryu, H.; Kang, Y.S. The alteration of l-carnitine transport and pretreatment effect under glutamate cytotoxicity on motor neuron-like NSC-34 lines. *Pharmaceutics* **2021**, *13*, 551. [CrossRef]
26. Ohtsuki, S.; Terasaki, T. Contribution of carrier-mediated transport systems to the blood-brain barrier as a supporting and protecting interface for the brain; importance for CNS drug discovery and development. *Pharm. Res.* **2007**, *24*, 1745–1758. [CrossRef]
27. Hosoya, K.I.; Takashima, T.; Tetsuka, K.; Nagura, T.; Ohtsuki, S.; Takanaga, H.; Ueda, M.; Yanai, N.; Obinata, M.; Terasaki, T. mRNA expression and transport characterization of conditionally immortalized rat brain capillary endothelial cell lines; a new in vitro BBB model for drug targeting. *J. Drug Target.* **2000**, *8*, 357–370. [CrossRef]
28. Simões Da Gama, C.; Morin-Brureau, M. Study of BBB Dysregulation in Neuropathogenicity Using Integrative Human Model of Blood–Brain Barrier. *Front. Cell. Neurosci.* **2022**, *16*, 863836. [CrossRef]
29. Kansy, M.; Senner, F.; Gubernator, K. Physicochemical high throughput screening: Parallel artificial membrane permeation assay in the description of passive absorption processes. *J. Med. Chem.* **1998**, *41*, 1007–1010. [CrossRef]
30. Avdeef, A. The rise of PAMPA. *Expert Opin. Drug Metab. Toxicol.* **2005**, *1*, 325–342. [CrossRef]
31. Lee, K.-E.; Kang, Y.-S. l-Citrulline restores nitric oxide level and cellular uptake at the brain capillary endothelial cell line (TR-BBB cells) with glutamate cytotoxicity. *Microvasc. Res.* **2018**, *120*, 29–35. [CrossRef]
32. Linville, R.M.; Searson, P.C. Next-generation in vitro blood–brain barrier models: Benchmarking and improving model accuracy. *Fluids Barriers CNS* **2021**, *18*, 56. [CrossRef]
33. Yahyaoui, R.; Pérez-Frías, J. Amino acid transport defects in human inherited metabolic disorders. *Int. J. Mol. Sci.* **2020**, *21*, 119. [CrossRef] [PubMed]
34. Kaplan, E.; Zubedat, S.; Radzishhevsky, I.; Valenta, A.C.; Rechnitz, O.; Sason, H.; Sajrawi, C.; Bodner, O.; Konno, K.; Esaki, K.; et al. ASCT1 (Slc1a4) transporter is a physiologic regulator of brain D-serine and neurodevelopment. *Proc. Natl. Acad. Sci. USA* **2018**, *115*, 9628–9633. [CrossRef]
35. Bröer, S.; Bröer, A. Amino acid homeostasis and signalling in mammalian cells and organisms. *Biochem. J.* **2017**, *474*, 1935–1963. [CrossRef]
36. Scalise, M.; Pochini, L.; Console, L.; Losso, M.A.; Indiveri, C. The Human SLC1A5 (ASCT2) amino acid transporter: From function to structure and role in cell biology. *Front. Cell Dev. Biol.* **2018**, *6*, 96. [CrossRef]
37. Mothet, J.P.; Parent, A.T.; Wolosker, H.; Brady, R.O.; Linden, D.J.; Ferris, C.D.; Rogawski, M.A.; Snyder, S.H. D-serine is an endogenous ligand for the glycine site of the N-methyl-D-aspartate receptor. *Proc. Natl. Acad. Sci. USA* **2000**, *97*, 4926–4931. [CrossRef]
38. Rezvani, A.H. Involvement of the NMDA System in Learning and Memory. In *Animal Models of Cognitive Impairment*; Levin, E.D., Buccafusco, J.J., Eds.; CRC Press/Taylor & Francis: Boca Raton, FL, USA, 2019; pp. 1–9.
39. Sasabe, J.; Chiba, T.; Yamada, M.; Okamoto, K.; Nishimoto, I.; Matsuoka, M.; Aiso, S. D-Serine is a key determinant of glutamate toxicity in amyotrophic lateral sclerosis. *EMBO J.* **2007**, *26*, 4149–4159. [CrossRef] [PubMed]
40. Sasabe, J.; Miyoshi, Y.; Suzuki, M.; Mita, M.; Konno, R.; Matsuoka, M.; Hamase, K.; Aiso, S. D-Amino acid oxidase controls motoneuron degeneration through D-serine. *Proc. Natl. Acad. Sci. USA* **2012**, *109*, 627–632. [CrossRef]
41. Paul, P.; De Belleruche, J. The role of D-amino acids in amyotrophic lateral sclerosis pathogenesis: A review. *Amino Acids* **2012**, *43*, 1823–1831. [CrossRef] [PubMed]
42. Lee, N.Y.; Kim, Y.; Ryu, H.; Kang, Y.S. The alteration of serine transporter activity in a cell line model of amyotrophic lateral sclerosis (ALS). *Biochem. Biophys. Res. Commun.* **2017**, *483*, 135–141. [CrossRef] [PubMed]

43. Thompson, M.; Marecki, J.C.; Marinesco, S.; Labrie, V.; Roder, J.C.; Barger, S.W.; Crow, J.P. Paradoxical roles of serine racemase and d-serine in the G93A mSOD1 mouse model of amyotrophic lateral sclerosis. *J. Neurochem.* **2012**, *120*, 598–610. [CrossRef] [PubMed]
44. Lee, K.E.; Kang, Y.S. Characteristics of L-citrulline transport through blood-brain barrier in the brain capillary endothelial cell line (TR-BBB cells). *J. Biomed. Sci.* **2017**, *24*, 28. [CrossRef] [PubMed]
45. Gyawali, A.; Gautam, S.; Hyeon, S.J.; Ryu, H.; Kang, Y.S. L-Citrulline level and transporter activity are altered in experimental models of amyotrophic lateral sclerosis. *Mol. Neurobiol.* **2021**, *58*, 647–657. [CrossRef] [PubMed]
46. Latif, S.; Kang, Y.S. Differences of transport activity of arginine and regulation on neuronal nitric oxide synthase and oxidative stress in amyotrophic lateral sclerosis model cell lines. *Cells* **2021**, *10*, 3554. [CrossRef] [PubMed]
47. Lee, N.Y.; Kang, Y.S. In Vivo and In Vitro Evidence for Brain Uptake of 4-Phenylbutyrate by the Monocarboxylate Transporter 1 (MCT1). *Pharm. Res.* **2016**, *33*, 1711–1722. [CrossRef]
48. Gyawali, A.; Kang, Y.S. Transport alteration of 4-phenyl butyric acid mediated by a sodium- and proton-coupled monocarboxylic acid transporter system in ALS model cell lines (NSC-34) under inflammatory states. *J. Pharm. Sci.* **2021**, *110*, 1374–1384. [CrossRef] [PubMed]
49. Lee, N.Y.; Choi, H.O.; Kang, Y.S. The acetylcholinesterase inhibitors competitively inhibited an acetyl L-carnitine transport through the blood-brain barrier. *Neurochem. Res.* **2012**, *37*, 1499–1507. [CrossRef] [PubMed]
50. Kang, Y.S.; Terasaki, T.; Ohnishi, T.; Tsuji, A. In vivo and in vitro evidence for a common carrier mediated transport of choline and basic drugs through the blood-brain barrier. *J. Pharm.* **1990**, *6*, 353–360. [CrossRef] [PubMed]
51. Tomi, M.; Tajima, A.; Tachikawa, M.; Hosoya, K. Function of taurine transporter (Slc6a6/TauT) as a GABA transporting protein and its relevance to GABA transport in rat retinal capillary endothelial cells. *Biochim. Biophys. Acta-Biomembr.* **2008**, *1778*, 2138–2142. [CrossRef] [PubMed]
52. Baliou, S.; Kyriakopoulos, A.M.; Goulielmaki, M.; Panayiotidis, M.I.; Spandidos, D.A.; Zoumpourlis, V. Significance of taurine transporter (TauT) in homeostasis and its layers of regulation (review). *Mol. Med. Rep.* **2020**, *22*, 2163–2173. [CrossRef] [PubMed]
53. Kusaka, T.; Matsuura, S.; Fujikawa, Y.; Okubo, K.; Kawada, K.; Namba, M.; Okada, H.; Imai, T.; Isobe, K.; Itoh, S. Relationship between cerebral interstitial levels of amino acids and phosphorylation potential during secondary energy failure in hypoxic-ischemic newborn piglets. *Pediatr. Res.* **2004**, *55*, 273–279. [CrossRef]
54. Saransaari, P.; Oja, S.S. Taurine and neural cell damage Review Article. *Amino Acids* **2000**, *19*, 509–526. [CrossRef] [PubMed]
55. Kang, Y.S. Taurine transport mechanism through the blood-brain barrier in spontaneously hypertensive rats. *Adv. Exp. Med. Biol.* **2000**, *483*, 321–324. [CrossRef] [PubMed]
56. Kang, Y.S.; Ohtsuki, S.; Takanaga, H.; Tomi, M.; Hosoya, K.-I.; Terasaki, T. Regulation of taurine transport at the blood-brain barrier by tumor necrosis factor- $\alpha$ , taurine and hypertonicity. *J. Neurochem.* **2002**, *83*, 1188–1195. [CrossRef] [PubMed]
57. Tamai, I.; Senmaru, M.; Terasaki, T.; Tsuji, A. Na<sup>+</sup>- and Cl<sup>-</sup>-Dependent transport of taurine at the blood-brain barrier. *Biochem. Pharmacol.* **1995**, *50*, 1783–1793. [CrossRef]
58. Julien, J.P.; Kriz, J. Transgenic mouse models of amyotrophic lateral sclerosis. *Biochim. Biophys. Acta-Mol. Basis Dis.* **2006**, *1762*, 1013–1024. [CrossRef] [PubMed]
59. Lee, N.Y.; Kang, Y.S. Taurine protects glutamate neurotoxicity in motor neuron cells. *Adv. Exp. Med. Biol.* **2017**, *975*, 887–895. [CrossRef] [PubMed]
60. Verrey, F.; Closs, E.I.; Wagner, C.A.; Palacin, M.; Endou, H.; Kanai, Y. CATs and HATs: The SLC7 family of amino acid transporters. *Pflug. Arch. Eur. J. Physiol.* **2004**, *447*, 532–542. [CrossRef] [PubMed]
61. Christensen, H.N. Role of amino acid transport and countertransport in nutrition and metabolism. *Physiol. Rev.* **1990**, *70*, 43–77. [CrossRef]
62. Scalise, M.; Galluccio, M.; Console, L.; Pochini, L.; Indiveri, C. The human SLC7A5 (LAT1): The intriguing histidine/large neutral amino acid transporter and its relevance to human health. *Front. Chem.* **2018**, *6*, 1–12. [CrossRef] [PubMed]
63. Zhang, J.; Xu, Y.; Li, D.; Fu, L.; Zhang, X.; Bao, Y.; Zheng, L. Review of the Correlation of LAT1 With Diseases: Mechanism and Treatment. *Front. Chem.* **2020**, *8*, 564809. [CrossRef]
64. Bahri, S.; Curis, E.; El Wafi, F.Z.; Aussel, C.; Chaumeil, J.C.; Cynober, L.; Zerrouk, N. Mechanisms and kinetics of citrulline uptake in a model of human intestinal epithelial cells. *Clin. Nutr.* **2008**, *27*, 872–880. [CrossRef]
65. Yabuki, Y.; Shioda, N.; Yamamoto, Y.; Shigano, M.; Kumagai, K.; Morita, M.; Fukunaga, K. Oral L-Citrulline administration improves memory deficits following transient brain ischemia through cerebrovascular protection. *Brain Res.* **2013**, *1520*, 157–167. [CrossRef] [PubMed]
66. Schmidlin, A.; Fischer, S.; Wiesinger, H. Transport of L-citrulline in neural cell cultures. *Dev. Neurosci.* **2000**, *22*, 393–398. [CrossRef] [PubMed]
67. Baydoun, A.R.; Bogle, R.G.; Pearson, J.D.; Mann, G.E. Discrimination between citrulline and arginine transport in activated murine macrophages: Inefficient synthesis of NO from recycling of citrulline to arginine. *Br. J. Pharmacol.* **1994**, *112*, 487–492. [CrossRef] [PubMed]
68. Lambden, S. Bench to bedside review: Therapeutic modulation of nitric oxide in sepsis—An update. *Intensive Care Med. Exp.* **2019**, *7*, 64. [CrossRef] [PubMed]
69. Gyawali, A.; Kang, Y.S. Pretreatment effect of inflammatory stimuli and characteristics of tryptophan transport on brain capillary endothelial (Tr-BBB) and motor neuron like (NSC-34) cell lines. *Biomedicines* **2021**, *9*, 9. [CrossRef] [PubMed]

70. Matsuo, H.; Tsukada, S.; Nakata, T.; Chairoungdua, A.; Kim, D.K.; Cha, S.H.; Inatomi, J.; Yorifuji, H.; Fukuda, J.; Endou, H.; et al. Expression of a system L neutral amino acid transporter at the blood-brain barrier. *Neuroreport* **2000**, *11*, 3507–3511. [CrossRef] [PubMed]
71. Van Damme, P.; Dewil, M.; Robberecht, W.; Van Den Bosch, L. Excitotoxicity and amyotrophic lateral sclerosis. *Neurodegener. Dis.* **2006**, *2*, 147–159. [CrossRef]
72. Jaiswal, M.K. Riluzole and edaravone: A tale of two amyotrophic lateral sclerosis drugs. *Med. Res. Rev.* **2019**, *39*, 733–748. [CrossRef] [PubMed]
73. Gyawali, A.; Latif, S.; Choi, S.-H.; Hyeon, S.J.; Ryu, H.; Kang, Y.-S. Monocarboxylate transporter functions and neuroprotective effects of valproic acid in experimental models of amyotrophic lateral sclerosis. *J. Biomed. Sci.* **2022**, *29*, 2. [CrossRef] [PubMed]
74. Jungnickel, K.E.J.; Parker, J.L.; Newstead, S. Structural basis for amino acid transport by the CAT family of SLC7 transporters. *Nat. Commun.* **2018**, *9*, 550. [CrossRef] [PubMed]
75. Ngo, S.; Mi, J.D.; Henderson, R.; McCombe, P.A.; Steyn, F. Exploring targets and therapies for amyotrophic lateral sclerosis: Current insights into dietary interventions. *Degener. Neurol. Neuromuscul. Dis.* **2017**, *7*, 95–108. [CrossRef] [PubMed]
76. O’Kane, R.L.; Viña, J.R.; Simpson, I.; Zaragoza, R.; Mokashi, A.; Hawkins, R.A. Cationic amino acid transport across the blood-brain barrier is mediated exclusively by system y<sup>+</sup>. *Am. J. Physiol.-Endocrinol. Metab.* **2006**, *291*, 412–419. [CrossRef] [PubMed]
77. Palamiuc, L.; Schlagowski, A.; Ngo, S.T.; Vernay, A.; Dirrig-Grosch, S.; Henriques, A.; Boutillier, A.; Zoll, J.; Echaniz-Laguna, A.; Loeffler, J.; et al. A metabolic switch toward lipid use in glycolytic muscle is an early pathologic event in a mouse model of amyotrophic lateral sclerosis. *EMBO Mol. Med.* **2015**, *7*, 526–546. [CrossRef] [PubMed]
78. Tomi, M.; Kitade, N.; Hirose, S.; Yokota, N.; Akanuma, S.I.; Tachikawa, M.; Hosoya, K.I. Cationic amino acid transporter 1-mediated l-arginine transport at the inner blood-retinal barrier. *J. Neurochem.* **2009**, *111*, 716–725. [CrossRef]
79. Halestrap, A.P.; Meredith, D. The SLC16 gene family—From monocarboxylate transporters (MCTs) to aromatic amino acid transporters and beyond. *Pflug. Arch. Eur. J. Physiol.* **2004**, *447*, 619–628. [CrossRef] [PubMed]
80. Halestrap, A.P. The monocarboxylate transporter family—Structure and functional characterization. *IUBMB Life* **2012**, *64*, 1–9. [CrossRef] [PubMed]
81. Pearl, P.L.; Keith, H.; Chiles, J.; McGavin, C.L.; Yu, Y.; Taylor, D. Partial Pyridoxine Responsiveness in PNPO Deficiency. *JIMD Rep.* **2012**, *4*, 113–116. [CrossRef]
82. Halestrap, A.P. The SLC16 gene family—Structure, role and regulation in health and disease. *Mol. Asp. Med.* **2013**, *34*, 337–349. [CrossRef] [PubMed]
83. Fischer, W.; Praetor, K.; Metzner, L.; Neubert, R.H.H.; Brandsch, M. Transport of valproate at intestinal epithelial (Caco-2) and brain endothelial (RBE4) cells: Mechanism and substrate specificity. *Eur. J. Pharm. Biopharm.* **2008**, *70*, 486–492. [CrossRef] [PubMed]
84. Ganapathy, V.; Thangaraju, M.; Gopal, E.; Martin, P.M.; Itagaki, S.; Miyauchi, S.; Prasad, P.D. Sodium-coupled monocarboxylate transporters in normal tissues and in cancer. *AAPS J.* **2008**, *10*, 193–199. [CrossRef]
85. Pettegrew, J.W.; Levine, J.; McClure, R.J. Acetyl-L-carnitine physical-chemical, metabolic, and therapeutic properties: Relevance for its mode of action in Alzheimer’s disease and geriatric depression. *Mol. Psychiatry* **2000**, *5*, 616–632. [CrossRef]
86. Inazu, M.; Takeda, H.; Maehara, K.; Miyashita, K.; Tomoda, A.; Matsumiya, T. Functional expression of the organic cation/carnitine transporter 2 in rat astrocytes. *J. Neurochem.* **2006**, *97*, 424–434. [CrossRef] [PubMed]
87. Geier, D.A.; Geier, M.R. L-carnitine exposure and mitochondrial function in human neuronal cells. *Neurochem. Res.* **2013**, *38*, 2336–2341. [CrossRef]
88. Hashimoto, N.; Suzuki, F.; Tamai, I.; Nikaido, H.; Kuwajima, M.; Hayakawa, J.I.; Tsuji, A. Gene-dose effect on carnitine transport activity in embryonic fibroblasts of JVS mice as a model of human carnitine transporter deficiency. *Biochem. Pharmacol.* **1998**, *55*, 1729–1732. [CrossRef]
89. Januszewicz, E.; Bekisz, M.; Mozrzymas, J.W.; Nałecz, K.A. High affinity carnitine transporters from OCTN family in neural cells. *Neurochem. Res.* **2010**, *35*, 743–748. [CrossRef]
90. Rodríguez, C.M.; Labus, J.C.; Hinton, B.T. Organic cation/carnitine transporter, OCTN2, is differentially expressed in the adult rat epididymis. *Biol. Reprod.* **2002**, *67*, 314–319. [CrossRef]
91. Lamhonwah, A.M.; Tein, I. Carnitine uptake defect: Frameshift mutations in the human plasmalemmal carnitine transporter gene. *Biochem. Biophys. Res. Commun.* **1998**, *252*, 396–401. [CrossRef]
92. Latif, S.; Choi, S.; Gyawali, A.; Hyeon, S.J.; Kang, Y.; Ryu, H. Antioxidant and neuroprotective effects of paeonol against oxidative stress and altered carrier-mediated transport system on NSC-34 cell lines. *Antioxidants* **2022**, *11*, 1392. [CrossRef]
93. Lee, N.Y.; Choi, H.M.; Kang, Y.S. Choline transport via choline transporter-like protein 1 in conditionally immortalized rat syncytiotrophoblast cell lines TR-TBT. *Placenta* **2009**, *30*, 368–374. [CrossRef] [PubMed]
94. Iwamoto, H.; Blakely, R.D.; De Felice, L.J. Na<sup>+</sup>, Cl<sup>−</sup>, and pH dependence of the human choline transporter (hCHT) in *Xenopus* oocytes: The proton inactivation hypothesis of hCHT in synaptic vesicles. *J. Neurosci.* **2006**, *26*, 9851–9859. [CrossRef] [PubMed]
95. Koshy Cherian, A.; Parikh, V.; Wu, Q.; Mao-Draayer, Y.; Wang, Q.; Blakely, R.D.; Sarter, M. Hemicholinium-3 sensitive choline transport in human T lymphocytes: Evidence for use as a proxy for brain choline transporter (CHT) capacity. *Neurochem. Int.* **2017**, *108*, 410–416. [CrossRef] [PubMed]

96. Ojiakor, O.A.; Rylett, R.J. Modulation of sodium-coupled choline transporter CHT function in health and disease. *Neurochem. Int.* **2020**, *140*, 104810. [CrossRef]
97. Hedtke, V.; Bakovic, M. Choline transport for phospholipid synthesis: An emerging role of choline transporter-like protein 1. *Exp. Biol. Med.* **2019**, *244*, 655–662. [CrossRef]
98. Michel, V.; Yuan, Z.; Ramsuibir, S.; Bakovic, M. Choline transport for phospholipid synthesis. *Exp. Biol. Med.* **2006**, *231*, 490–504. [CrossRef]
99. O'Regan, S.; Traiffort, E.; Ruat, M.; Cha, N.; Compaoré, D.; Meunier, F.M. An electric lobe suppressor for a yeast choline transport mutation belongs to a new family of transporter-like proteins. *Proc. Natl. Acad. Sci. USA* **2000**, *97*, 1835–1840. [CrossRef] [PubMed]
100. Yuan, Z.; Wagner, L.; Poloumienko, A.; Bakovic, M. Identification and expression of a mouse muscle-specific CTL1 gene. *Gene* **2004**, *341*, 305–312. [CrossRef] [PubMed]
101. Wille, S.; Szekeres, A.; Majdic, O.; Prager, E.; Staffler, G.; Stöckl, J.; Kunthalert, D.; Prieschl, E.E.; Baumruker, T.; Burtscher, H.; et al. Characterization of CDw92 as a Member of the choline transporter-like protein family regulated specifically on dendritic cells. *J. Immunol.* **2001**, *167*, 5795–5804. [CrossRef] [PubMed]
102. Michel, V.; Bakovic, M. The solute carrier 44A1 is a mitochondrial protein and mediates choline transport. *EASEB J.* **2009**, *23*, 2749–2758. [CrossRef] [PubMed]
103. Taylor, A.; Grapentine, S.; Ichhpuniani, J.; Bakovic, M. Choline transporter-like proteins 1 and 2 are newly identified plasma membrane and mitochondrial ethanolamine transporters. *J. Biol. Chem.* **2021**, *296*, 100604. [CrossRef] [PubMed]
104. Sweet, D.H.; Miller, D.S.; Pritchard, J.B. Ventricular choline transport: A role for organic cation transporter 2 expressed in choroid plexus. *J. Biol. Chem.* **2001**, *276*, 41611–41619. [CrossRef] [PubMed]
105. Wong, A.D.; Ye, M.; Levy, A.F.; Rothstein, J.D.; Bergles, D.E.; Searson, P.C. The blood-brain barrier: An engineering perspective. *Front. Neuroeng.* **2013**, *6*, 7. [CrossRef] [PubMed]
106. Kang, Y.; Lee, K.; Lee, N.; Terasakp, T. Donepezil, Tacrine and  $\alpha$ -Phenyl-n-tert-Butyl Nitron (PBN) Inhibit Choline Transport by Conditionally Immortalized Rat. *Arch. Pharm. Res.* **2005**, *28*, 443–450. [CrossRef] [PubMed]
107. Inazu, M.; Takeda, H.; Matsumiya, T. Molecular and functional characterization of an  $\text{Na}^+$ -independent choline transporter in rat astrocytes. *J. Neurochem.* **2005**, *94*, 1427–1437. [CrossRef] [PubMed]
108. Wang, T.; Li, J.; Chen, F.; Zhao, Y.; He, X.; Wan, D.; Gu, J. Choline transporters in human lung adenocarcinoma: Expression and functional implications. *Acta Biochim. Biophys. Sin.* **2007**, *39*, 668–674. [CrossRef]
109. Okuda, T.; Haga, T.; Kanai, Y.; Endou, H.; Ishihara, T.; Katsura, I. Identification and characterization of the high-affinity choline transporter. *Nat. Am. Inc.* **2000**, *299*, 351. [CrossRef] [PubMed]
110. Haga, T. Molecular properties of the high-affinity choline transporter CHT1. *J. Biochem.* **2014**, *156*, 181–194. [CrossRef]
111. Inazu, M. Functional expression of choline transporters in the blood-brain barrier. *Nutrients* **2019**, *11*, 2265. [CrossRef] [PubMed]
112. Brown, R.D.; Prendiville, P.; Cain, C. Alpha 1-adrenergic and H1-histamine receptor control of intracellular  $\text{Ca}^{2+}$  in a muscle cell line: The influence of prior agonist exposure on receptor responsiveness. *Mol. Pharmacol.* **1986**, *29*, 531–539. [CrossRef] [PubMed]
113. Guan, Z.; Pollock, J.S.; Cook, A.K.; Hobbs, J.L.; Inscho, E.W. Effect of epithelial sodium channel blockade on the myogenic response of rat juxtamedullary afferent arterioles. *Hypertension* **2009**, *54*, 1062–1069. [CrossRef] [PubMed]



## Article

# Proteomics-Based Transporter Identification by the PICK Method: Involvement of TM7SF3 and LHFPL6 in Proton-Coupled Organic Cation Antiport at the Blood–Brain Barrier

Toshiki Kurosawa <sup>1,†</sup>, Yuma Tega <sup>1,2,†</sup> , Yasuo Uchida <sup>3,\*,†,‡</sup> , Kei Higuchi <sup>4,†</sup>, Hidetsugu Tabata <sup>5</sup>, Takaaki Sumiyoshi <sup>6</sup>, Yoshiyuki Kubo <sup>1</sup> , Tetsuya Terasaki <sup>3,§</sup>  and Yoshiharu Deguchi <sup>1,\*,||</sup> 

- <sup>1</sup> Laboratory of Drug Disposition and Pharmacokinetics, Faculty of Pharma-Sciences, Teikyo University, Tokyo 173-8605, Japan
- <sup>2</sup> Department of Pharmaceutical Sciences, College of Pharmacy, University of Kentucky, Lexington, KY 40536, USA
- <sup>3</sup> Division of Membrane Transport and Drug Targeting, Graduate School of Pharmaceutical Sciences, Tohoku University, Sendai 980-8578, Japan
- <sup>4</sup> Department of Biopharmaceutics, School of Pharmacy, Tokyo University of Pharmacy and Life Sciences, Tokyo 192-0392, Japan
- <sup>5</sup> Laboratory of Medicinal Chemistry, Faculty of Pharma-Sciences, Teikyo University, Tokyo 173-8605, Japan
- <sup>6</sup> Department of Life Science and Biotechnology, Faculty of Chemistry, Materials and Bioengineering, Kansai University, Osaka 564-8680, Japan
- \* Correspondence: yasuo.uchida.c8@tohoku.ac.jp (Y.U.); deguchi@pharm.teikyo-u.ac.jp (Y.D.); Tel.: +81-22-795-6832 (Y.U.); +81-3-3964-8246 (Y.D.)
- † These authors contributed equally to this work.
- ‡ Correspondence for the PICK method.
- § Present address: School of Pharmacy, Faculty of Health Sciences, University of Eastern Finland, FI-70210 Kuopio, Finland.
- || Correspondence for the principal.

**Citation:** Kurosawa, T.; Tega, Y.; Uchida, Y.; Higuchi, K.; Tabata, H.; Sumiyoshi, T.; Kubo, Y.; Terasaki, T.; Deguchi, Y. Proteomics-Based Transporter Identification by the PICK Method: Involvement of TM7SF3 and LHFPL6 in Proton-Coupled Organic Cation Antiport at the Blood–Brain Barrier. *Pharmaceutics* **2022**, *14*, 1683. <https://doi.org/10.3390/pharmaceutics14081683>

Academic Editor: William M. Pardridge

Received: 21 June 2022

Accepted: 9 August 2022

Published: 12 August 2022

**Publisher's Note:** MDPI stays neutral with regard to jurisdictional claims in published maps and institutional affiliations.

**Abstract:** A proton-coupled organic cation ( $H^+$ /OC) antiporter working at the blood–brain barrier (BBB) in humans and rodents is thought to be a promising candidate for the efficient delivery of cationic drugs to the brain. Therefore, it is important to identify the molecular entity that exhibits this activity. Here, for this purpose, we established the Proteomics-based Identification of transporter by Crosslinking substrate in Keyhole (PICK) method, which combines photo-affinity labeling with comprehensive proteomics analysis using SWATH-MS. Using preselected criteria, the PICK method generated sixteen candidate proteins. From these, knockdown screening in hCMEC/D3 cells, an in vitro BBB model, identified two proteins, TM7SF3 and LHFPL6, as candidates for the  $H^+$ /OC antiporter. We synthesized a novel  $H^+$ /OC antiporter substrate for functional analysis of TM7SF3 and LHFPL6 in hCMEC/D3 cells and HEK293 cells. The results suggested that both TM7SF3 and LHFPL6 are components of the  $H^+$ /OC antiporter.

**Keywords:** proton-coupled organic cation antiporter; blood–brain barrier; photo-affinity labeling; proteomics; SWATH-MS (sequential window acquisition of all theoretical-mass spectra)



**Copyright:** © 2022 by the authors. Licensee MDPI, Basel, Switzerland. This article is an open access article distributed under the terms and conditions of the Creative Commons Attribution (CC BY) license (<https://creativecommons.org/licenses/by/4.0/>).

## 1. Introduction

The pyrilamine (PYR)-sensitive proton-coupled organic cation ( $H^+$ /OC) antiporter working at the blood–brain barrier (BBB) in humans and rodents is thought to be a promising candidate for drug delivery, since various psychotropic drugs have cationic forms at physiological pH, and carrier-mediated transport of such drugs across the BBB is inhibited by lipophilic cationic drugs, such as diphenhydramine (DPH) and imipramine [1]. Furthermore, in vivo brain microdialysis studies of DPH and oxycodone (OXY) revealed three- to five-fold higher unbound concentrations in the brain interstitial fluid (ISF) than in

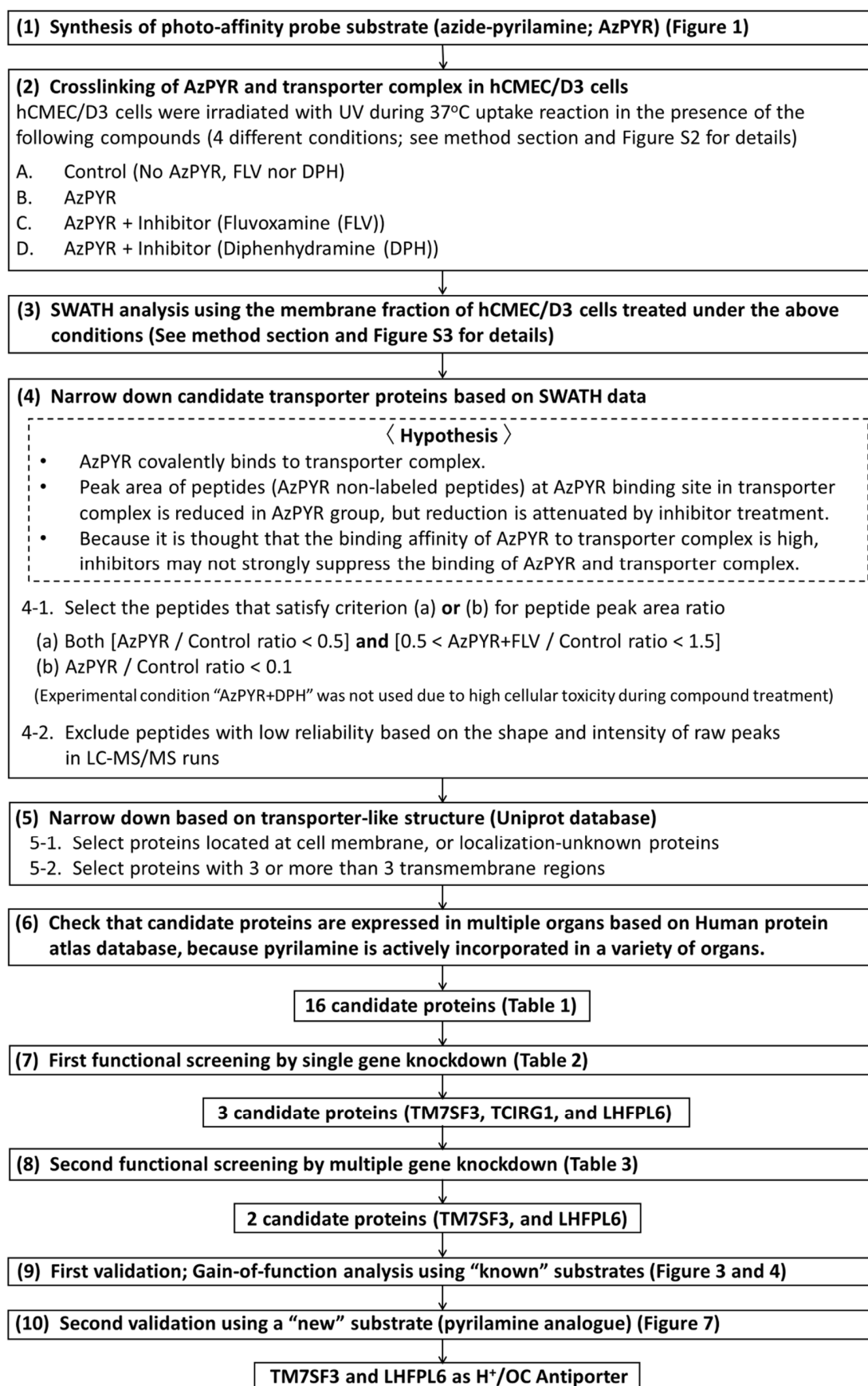


blood [2,3]. A similar influx transport system was found in an in situ mouse brain perfusion study of nicotine and clonidine (CLO) [4,5], as well as an in vivo study on the transport of cationic drugs at the blood–retinal barrier (BRB) and in the liver [6,7]. Possible involvement of a proton-coupled organic cation ( $H^+$ /OC) antiporter was supported by studies using hCMEC/D3 cells, an in vitro model cell line of human BBB, as well as conditionally immortalized capillary endothelial cells of rat brain and retina [8–10]. The pharmacological significance of the  $H^+$ /OC antiporter was also supported by a pharmacophore model study designed to predict inhibitors [11]. Interestingly, hybrid molecules constructed by combining a histone deacetylase (HDAC) inhibitor or non-steroidal anti-inflammatory drug (NSAID) with an  $H^+$ /OC antiporter substrate showed increased blood–brain barrier (BBB) permeability [12,13].

Thus, although the molecular identity of the  $H^+$ /OC antiporter at the BBB remains unclear, it appears to be a promising candidate for the efficient delivery of central nervous system (CNS)-active drugs into the brain [9,14–17]. Various organic cation transporters, including organic cation transporters (OCTs), organic cation/carnitine transporters (OCTNs) and multidrug and toxin extrusion proteins (MATEs), have been identified, molecularly cloned and characterized [18], but none of these molecules has transport properties consistent with those of the  $H^+$ /OC antiporter. The molecular nature of the  $H^+$ /OC antiporter at the BBB has remained elusive for at least 30 years. A possible explanation for this would be that the  $H^+$ /OC antiporter is a protein complex, not a single protein, and thus might not be amenable to identification by conventional methods such as the gene level approach with loss or gain of function.

Since 2000, proteomics technology has been developed and used in a variety of scientific fields [19], including the identification of receptors by the application of sophisticated crosslinkers [20]. The application of this crosslinking-based proteomics approach to substrate–transporter interactions have the potential to efficiently identify multiple constituent molecules of the transporter complex. The photoreactive azide group (one of the crosslinkers) is small, and therefore, azide modification to the substrate of transporter would not significantly change the structure of the substrate, making it easier to enter the transporter’s binding site. Hence, a strategy that combines the use of azide-modified substrates and proteomic techniques with excellent coverage and accuracy would be useful for identification of the  $H^+$ /OC antiporter. We have devised a transporter identification method based on the strategy in Scheme 1 and named it the “PICK” (Proteomics-based Identification of transporter by Crosslinking substrate in Keyhole) method. This combines the use of azide-modified transporter substrates with a proteomic technique that affords excellent coverage and accuracy, and also utilizes inhibitors to increase the specificity/accuracy of transporter identification.

In the present study, the PICK method was applied for the molecular identification of the  $H^+$ /OC antiporter, using azide-pyrimidine (AzPYR) as a photo-affinity probe [21,22]. Candidate proteins selected by the PICK method were taken forward for functional studies utilizing single and multiple gene knockdown analyses. For final confirmation, we used cell lines stably expressing the putative transporter components, together with a newly synthesized  $H^+$ /OC antiporter substrate, which was confirmed to have appropriate membrane permeability.



**Scheme 1.** Strategy for identification of transporter complex by PICK (Proteomics-based Identification of transporter by Crosslinking substrate in Keyhole) method.

## 2. Materials and Methods

### 2.1. Reagents

Reagents used in this study were purchased from Fujifilm Wako Pure Chemical Industries (Osaka, Japan) and Sigma-Aldrich Company (St. Louis, MO, USA), unless otherwise specified. Varenicline tartrate and fluvoxamine maleate were purchased from Abcam (Cambridge, MA, USA) and Tokyo Chemical Industry (Tokyo, Japan), respectively.

### 2.2. Cell Culture

hCMEC/D3 cells were kindly provided by Dr. Pierre-Oliver Couraud (Institut Cochin, Paris, France) under license from INSERM and cultured on rat collagen type I-coated dishes in EBM-2 medium (Lonza, Basel, Switzerland). HEK293 cells were cultured on poly-D-lysine-coated dishes in Dulbecco's modified Eagle's medium (D-MEM, high glucose; Thermo Fisher Scientific, Waltham, MA, USA) supplemented with 10% fetal bovine serum, 1% penicillin-streptomycin and  $\text{NaHCO}_3$  (final concentration; 1.5 g/L). These cells were maintained in an atmosphere of 95% air and 5%  $\text{CO}_2$ . For details of cell culture conditions and medium composition, see the Supplementary Materials.

### 2.3. Uptake Study

Uptake studies with hCMEC/D3 cells and HEK293 cells were performed in accordance with previous reports [16,17]. Briefly, we seeded hCMEC/D3 cells in collagen I-coated 24-well plates (BD Biosciences, Franklin Lakes, NJ, USA) and HEK293 cells in poly-D-lysine (Thermo Fisher Scientific)-coated 24-well plates at a density of  $4.0 \times 10^4$  cells/cm<sup>2</sup>. Uptake studies were performed after 3 days. The cells were washed in uptake buffer and preincubated in fresh uptake buffer for 20 min at 37 °C, and then uptake of the compound was measured at the designated times. Uptake in each experiment was evaluated by calculating the cell-to-medium (C/M) ratio ( $\mu\text{L}/\text{mg}$  protein). The amount of protein in each well was determined with a Micro BCA protein assay kit (Thermo Fisher Scientific). The drugs and compounds were quantified by an LC-MS/MS system consisting of a Nexera XR HPLC system (Shimadzu, Kyoto, Japan) and a Qtrap 4500 (AB Sciex, Foster City, CA, USA) mass spectrometer with an electrospray ionization interface in positive ion mode. Details of the measurement methods and ionization conditions for each drug and compound are given in the Supplementary Materials.

### 2.4. Design, Synthesis and Evaluation of Photo-Affinity Probe (Azide-Pyrimidine; AzPYR)

In our program to identify the  $\text{H}^+/\text{OC}$  antiporter, we designed AzPYR as a photo-affinity probe (Figure 1A). Based on the idea that histone deacetylase inhibitor **1** (Figure 1A) is a relatively slow-reacting  $\text{H}^+/\text{OC}$  antiporter substrate [12], we introduced an azide moiety at the phenyl group of compound **1**. UV irradiation (<300 nm) of AzPYR generated an active phenyl nitrene that binds covalently with the  $\text{H}^+/\text{OC}$  antiporter (Figure 1B). According to the reported procedure for converting an aniline moiety to phenyl azide [23], we synthesized AzPYR from compound **1** using 2-azido-1,3-dimethylimidazolium hexafluorophosphate (Figure S1, see Supplementary Materials).

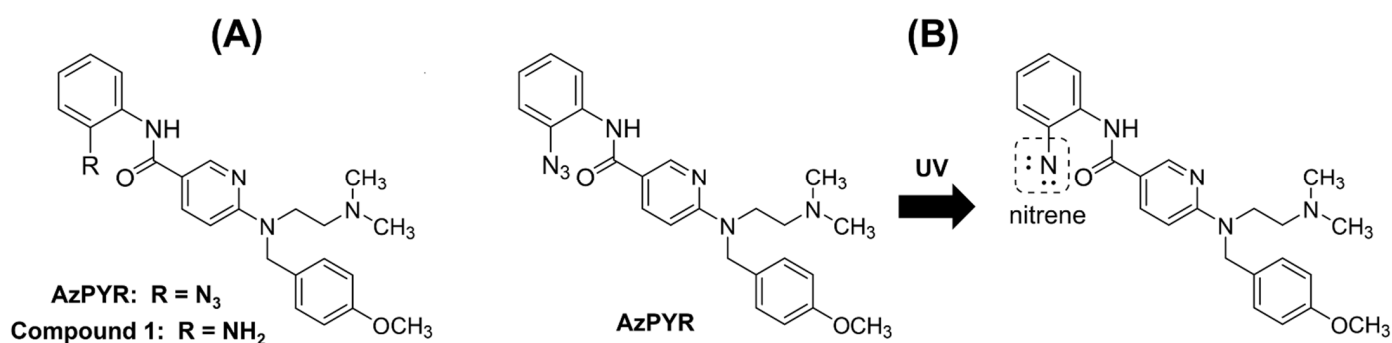


**Figure 1.** (A) Chemical structures of AzPYR and compound 1. (B) Production of the phenyl nitrene moiety, which forms a covalent bond with the H<sup>+</sup>/OC antiporter.

To test the binding ability of AzPYR to the H<sup>+</sup>/OC antiporter, we examined the inhibitory effect of AzPYR on the antiporter-mediated uptake activity. The uptakes of DPH (at 1 μM) and PYR (at 5 μM) by hCMEC/D3 cells for 0.5 min were measured at 37 °C in the presence or absence of 0.4 mM AzPYR. For the photo-crosslinking reaction, the cells were pretreated with AzPYR under UV light for 5 min at 37 °C. Unreacted AzPYR was removed by incubation in the buffer.

### 2.5. Crosslinking of AzPYR and Transporter Complex in hCMEC/D3 Cells

hCMEC/D3 cells were seeded on plastic dishes. After reaching confluence, the cells were preincubated in the buffer with or without an H<sup>+</sup>/OC antiporter inhibitor (fluvoxamine (FLV) or DPH). The cells were treated with 0.1 mM AzPYR in the presence and absence of inhibitor (0.5 mM FLV or 0.5 mM DPH) for 5 min at 37 °C under UV light (302 nm) generated by a benchtop trans-illuminator (Analytik Jena AG, Jena, Germany), then washed twice with ice-cold buffer and transferred into PBS (-) with a cell scraper. Cells irradiated with UV in the absence of AzPYR and inhibitor were also collected as a control. The cell suspensions were centrifuged at 1000 × g for 5 min at 4 °C, and the supernatants were removed. The cell pellets were stored at −80 °C until SWATH-MS (Sequential Window Acquisition of all Theoretical fragment ion spectra-Mass Spectra) analysis. Photoaffinity labeling of the H<sup>+</sup>/OC antiporter using hCMEC/D3 cells is illustrated schematically in the Supplementary Materials (Figure S2).

### 2.6. SWATH Analysis to “PICK” Candidate Transporter Proteins

The membrane fractions were isolated from the hCMEC/D3 cells treated as described above by using a Minute Plasma Membrane Protein Isolation Kit<sup>®</sup> (Invent Biotechnologies). Trypsin digestion of membrane fractions and C18 clean-up were conducted as described previously [24]. The cleaned peptide samples were injected into a NanoLC 425 system (Eksigent Technologies, Dublin, CA, USA) coupled with an electrospray-ionization Triple TOF 5600 mass spectrometer (SCIEX, Framingham, MA, USA) set up for a single direct injection. SWATH-MS data were acquired as previously described [25]. Data extraction from the SWATH chromatogram were processed using the SWATH Processing Micro App in Peakview (SCIEX) with a 10% false discovery rate threshold as previously described [26]. Unreliable peaks and peptides were removed as described [27]. Briefly, transitions with a peak area of more than 1000 counts in the control group were extracted. Transitions whose peak area was >10-fold different between two replicates were removed. Then, peptides with only one or two transitions were removed. Furthermore, nonspecific and unreliable peptides were removed by applying *in silico* peptide selection criteria [27]. For the remaining peptides, the peak areas at the peptide level were calculated as the average values after normalizing differences in signal intensity between the different transitions. Subsequently, the candidate transporter proteins were narrowed down according to steps 4, 5, and 6 shown in the flowchart (Scheme 1). The detailed workflow of the SWATH analysis is shown in the Supplementary Materials (Figure S3).

### 2.7. Functional Screening by Single or Multiple Gene Knockdown

hCMEC/D3 cells were seeded on 24-well plates at a density of  $2.75 \times 10^4$  cells/well on the day before siRNA treatment. They were incubated in Opti-MEM I reduced serum medium (Thermo Fisher Scientific, Waltham, MA, USA) including Lipofectamine RNAi MAX (Millipore-Sigma, Burlington, NJ, USA) and two kinds of siRNA for one target gene, each at a final concentration of 5 nM, for 24 h. Then, the medium was changed to EBM-2 medium, and the cells were cultured for a further 48 h without siRNA. As a control group, the cells were incubated with the same amount of negative control siRNA (Qiagen, Venlo, The Netherlands) instead of target-specific siRNA. Product information for targeted siRNA and negative control siRNA is provided in the Supplementary Materials (Table S2).

To confirm knockdown of target genes, total RNA extraction from hCMEC/D3 cells was performed using NucleoSpin RNA Plus (Macherey-Nagel, Düren, Germany) according to the supplied manual. Reverse transcription reactions from total RNA to cDNA were performed with the combination of SuperScript III Reverse Transcriptase (Thermo Fisher Scientific) and Ribonuclease Inhibitor (TaKaRa Biomedicals, Shiga, Japan). Briefly, 1 µg of total RNA was mixed with 250 ng of random primer and the supplied dNTPs and incubated at 65 °C for 5 min. The mixture was then mixed with a defined volume of SuperScript III and Ribonuclease Inhibitor and incubated at 50 °C for 60 min and 70 °C for 15 min. PCR was performed using a mixture of 10 ng of cDNA, 5 pmol of sense/antisense primers and SYBR Select Master Mix (Thermo Fisher Scientific) on a 7500 Fast Real-Time PCR System (Applied Biosystems) according to the following thermocycling program: 1 cycle of holding stage at 50 °C for 2 min and 95 °C for 2 min, 40 cycles of PCR reaction stage at 95 °C for 3 s and 60 °C for 0.5 min, and 1 cycle of melt curve stage at 95 °C for 0.25 min, 60 °C for 1 min and 95 °C for 0.5 min. Primer sequences are listed in Supplementary Materials (Table S3). Relative mRNA expression of each target protein was calculated by the  $\Delta C_t$  method, corrected for the mRNA expression of TATA-binding protein (TBP; a house-keeping gene).

### 2.8. First Validation; Gain-of-Function Analysis Using “Known” Substrates

HEK293 cells expressing transmembrane 7 superfamily member 3 (TM7SF3) and/or LHFPL tetraspan subfamily member 6 protein (LHFPL6) were generated to assess the involvement of these molecules in the transport of H<sup>+</sup>/OC antiporter substrates. pcDNA TM3.1 (+) vector and pcDNA TM3.1/Zeo (+) vector containing the coding region of TM7SF3 (GenBank accession number: NM\_016551.3) or LHFPL6 (GenBank accession number: NM\_005780.3), respectively, were purchased from Genscript (Piscataway, NJ, USA). The cells were incubated in Opti-MEM I reduced serum medium (Thermo Fisher Scientific) with the vector and Lipofectamine 3000 (Thermo Fisher Scientific) for 6 h. The medium was subsequently changed to D-MEM without antibiotics. For transient expression, the cells were incubated for a further 48 h and used for the uptake experiment. To obtain stably expressing cells, incubation was continued for another 24 h, and then the cells were cultured in the medium with antibiotics (400 µg/mL Zeocin and G418) to obtain resistant cells. These were proliferated, cloned and used for uptake experiments. The mRNA expression of TM7SF3 and LHFPL6 in HEK293 cells was measured by the quantitative PCR method described above.

### 2.9. Second Validation Using a “New” Substrate (Pyrilamine Analogue)

Commercially available 4-bromonicotinate (**1**) was treated with *N,N*-dimethylethylenediamine in pyridine to obtain the secondary amine (**2**) [28,29]. Benzyl derivative (**3**) [12] was obtained by *N*-alkylation of **2** with 4-methoxybenzyl chloride, then hydrolyzed and amidated with ethyl 4-aminobutyrate to obtain **4**. The methods and the properties of each compound are given in the Supplementary Materials (Figure S4). The uptake mechanism of the pyrilamine analogue was analyzed by uptake study in hCMEC/D3 cells. To examine the effects of sodium ions and membrane potential on the uptake, NaCl in the uptake buffer was replaced with LiCl/cholineCl or KCl, respectively. Furthermore, the effect of metabolic

energy on uptake was evaluated by replacing glucose in the uptake buffer with non-metabolizable 3-O-methyl-glucose and adding 0.1% NaN<sub>3</sub>. The influence of intracellular pH was evaluated by adding 30 mM NH<sub>4</sub>Cl to the uptake buffer. For acidification of intracellular pH, NH<sub>4</sub>Cl was included from the preincubation stage; for alkalinization, NH<sub>4</sub>Cl was added simultaneously with the pyrilamine analogue. The composition of the uptake buffer in each experiment is given in the Supplementary Materials. To evaluate the inhibition profile of the pyrilamine analogue in hCMEC/D3 cells, various inhibitors (1 mM) were added simultaneously with the pyrilamine analogue. The inhibitors used were PYR, DPH, CLO, memantine (MEM), varenicline (VAR), tramadol (TRA), naltrexone (NAL) (a substrate and inhibitor of the H<sup>+</sup>/OC antiporter), 1-methyl-4-phenylpyridinium (MPP<sup>+</sup>, a substrate and inhibitor of OCTs and plasma membrane monoamine transporter (PMAT)), p-aminohippuric acid (PAH, a substrate and inhibitor of OATs and organic anion transporting polypeptides (OATPs)), tetraethylammonium (TEA, a substrate and inhibitor of OCTs and MATE1) and L-carnitine (a substrate of OCTN2). In order to calculate kinetic parameters in hCMEC/D3 cells, the uptake of pyrilamine analogue was analyzed by preparing Michaelis–Menten plots based on the following equation (parameters are defined in the Supplementary Materials).

$$V = (V_{\max} \times S)/(K_m + S) + (K_d \times S) \quad (1)$$

The involvement of TM7SF3 and LHFPL6 in the uptake of the pyrilamine analogue was evaluated using knockdown hCMEC/D3 cells and TM7SF3- and/or LHFPL6-expressing HEK293 cells, generated as described above.

### 2.10. Statistical Analysis

All values are presented as the mean ± standard error. Statistical analysis of the data was performed with Student's *t*-test and one-way ANOVA followed by Dunnett's test for single and multiple comparisons, respectively. Values of *p* < 0.05 and 0.01 were considered to represent statistically significant differences. Unless otherwise specified in the figure legend, a significant difference analysis with the Dunnett's test was performed.

## 3. Results

### 3.1. Binding of AzPYR to H<sup>+</sup>/OC Antiporter

The inhibitory effects of AzPYR on H<sup>+</sup>/OC antiporter-mediated uptakes of PYR and DPH, which are representative substrates, was examined using hCMEC/D3 cells in order to confirm the binding of AzPYR to the antiporter. AzPYR at 0.4 mM significantly reduced the uptakes of PYR and DPH (Figure 2A). Pretreatment of hCMEC/D3 cells with AzPYR under UV light caused a significant and irreversible reduction in the uptakes of PYR and DPH, whereas pretreatment under room light caused a moderate and reversible reduction (Figure 2B). These results suggest that the synthesized AzPYR binds to the H<sup>+</sup>/OC antiporter and efficiently photo-labels it.

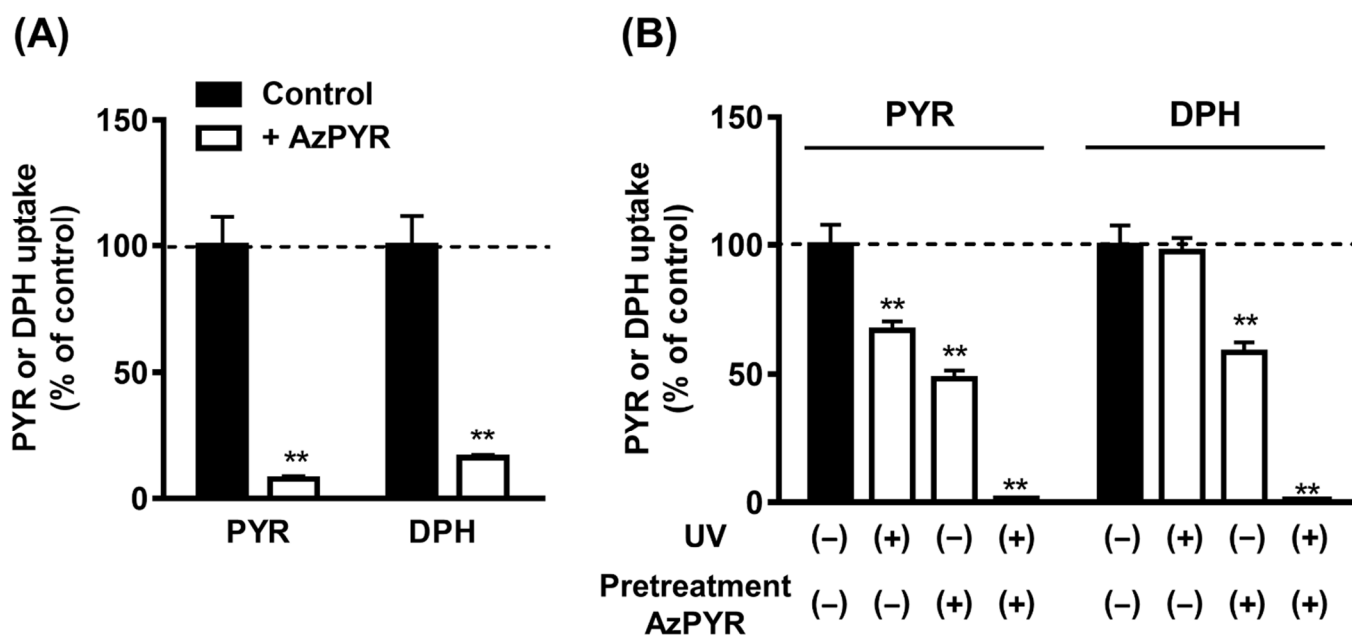


**Figure 2.** (A) Inhibitory effect of AzPYR on  $H^+/OC$  antiporter-mediated uptake. The uptakes of PYR and DPH by hCMEC/D3 cells were measured in presence or absence of AzPYR at 0.4 mM under room light. (B) Effect of photo-cross-linking reaction on  $H^+/OC$  antiporter activity. hCMEC/D3 cells were pretreated in the buffer with or without AzPYR under UV light or room light for 5 min at 37 °C. The treated cells were washed and further incubated in buffer to remove the unreacted AzPYR, and then the uptakes of PYR and DPH were measured. Each point represents the mean  $\pm$  standard error ( $n = 3-4$ ). \*\*  $p < 0.01$  compared to the corresponding control uptake or non-treatment uptake. Significant difference in Figure 2A was examined with  $t$ -test.

### 3.2. SWATH-Based Screening of $H^+/OC$ Antiporter

Our strategy for the identification of the  $H^+/OC$  antiporter is shown in Scheme 1. We assumed that AzPYR covalently binds to the substrate-binding site of the  $H^+/OC$  antiporter upon UV irradiation, and that inhibitors suppress AzPYR binding to the transporter. To distinguish the specific binding of AzPYR to the antiporter, we used DPH and FLV, which have been reported to be the inhibitors of the antiporter [30,31]. However, we finally abandoned the use of DPH because the DPH treatment at 1 mM resulted in lower attachment of hCMEC/D3 cells to the dishes under the conditions used for UV irradiation. In SWATH analysis, membrane fractions are digested with trypsin and measured by LC-MS/MS, so the individual tryptic peptides are separately quantified. We assumed that if the AzPYR/control ratio was smaller than 0.5 and the (AzPYR+FLV)/control ratio was in the range 0.5 to 1.5, the peptide was derived from a candidate transporter (Scheme 1). Furthermore, a peptide with an AzPYR/control ratio  $< 0.1$  (regardless of the value of the (AzPYR+FLV)/control ratio) was also assumed to be derived from a candidate transporter, because if the affinity of AzPYR for the transporter was high, binding may not be strongly suppressed by the inhibitor (Scheme 1). Among the proteins meeting these criteria, we selected 16 that (1) are expressed at the cell membrane; (2) contain 3 or more transmembrane regions; (3) are expressed in multiple organs (Table 1).

**Table 1.** Sixteen proteins selected as H<sup>+</sup>/OC antiporter candidates.

Protein Names	Subcellular Location	Abundance Ratio AzPYR-Unbound Peptide			Number of Transmembrane Domains
		AzPYR /Control	(AzPYR+FLV) /Control	(AzPYR+DPH) /Control	
Magnesium transporter protein 1 (MAGT1)	Cell membrane	0.385	0.626	0.499	4
CD9 antigen (CD9)	Cell membrane	0.182	0.957	1.566	4
Cytochrome b reductase 1 (CYBRD1)	Unknown	0.401	0.975	0.925	6
Sodium/potassium-transporting ATPase subunit alpha-1 (ATP1A1)	Cell membrane	0.365	0.809	1.075	10
Cleft lip and palate transmembrane protein 1 (CLPTM1)	Cell membrane	0.266	0.658	0.692	5
V-type proton ATPase 116 kDa subunit 3 (TCIRG1)	Unknown	0.144	0.84	0.551	8
V-type proton ATPase 116 kDa subunit 1 (ATP6V0A1)	Unknown	0.319	0.739	— <sup>(a)</sup>	8
LHFPL tetraspan subfamily member 6 protein (LHFPL6)	Unknown	0.0326	0.993	0.879	3
PRA1 family protein 3 (ARL6IP5)	Cell membrane	0.0891	0.0732	0.404	4
Solute carrier family 43 member 3 (SLC43A3)	Unknown	0.0725	0.0795	1	12
Transmembrane protein 65 (TMEM65)	Cell membrane	0.28	0.622	0.238	3
Transmembrane 7 superfamily member 3 (TM7SF3)	Cell membrane	0.451	0.681	— <sup>(a)</sup>	7
Sodium/hydrogen exchanger 1 (SLC9A1)	Cell membrane	0.442	1.44	1.09	12
Solute carrier family 12 member 5 (SLC12A5)	Unknown	0.189	0.964	0.977	12
CD63 antigen (CD63)	Cell membrane	0.0906	0.172	0.413	4
Aquaporin-3 (AQP3)	Cell membrane	0.0561	0.494	0.0525	6

SWATH analysis was performed using the membrane fractions of hCMEC/D3 cells treated under the following four conditions: A, neither AzPYR nor inhibitor (control); B, AzPYR without inhibitor (AzPYR); C, AzPYR with FLV (AzPYR+FLV); D, AzPYR with DPH (AzPYR+DPH). The 16 proteins that were narrowed down through steps 1 to 6 (Scheme 1) are listed in this table. The subcellular location is taken from the Uniprot database. Abundance ratio for AzPYR-unbound peptide was calculated using the peptide peak area in SWATH analysis. The number of transmembrane domains was taken from the Uniprot database. AzPYR, azide-pyrimidine; FLV, fluvoxamine; DPH, diphenhydramine. Note that the experimental condition “AzPYR+DPH” was not used due to high cellular toxicity. <sup>(a)</sup> Values were not calculated due to poor data accuracy.



For LHFPL tetraspan subfamily member 6 protein, PRA1 family protein 3, solute carrier family 43 member 3 (SLC43A3), CD63 antigen, and aquaporin-3, the AzPYR/control ratio was smaller than 0.1. The other 11 proteins were selected as molecules with AzPYR/control ratio  $< 0.5$  and  $0.5 < (\text{AzPYR}+\text{FLV})/\text{control ratio} < 1.5$  (Table 1). Note that the value of “AzPYR+DPH” was not used as a criterion due to low cell attachment during DPH treatment. However, as reference data, the values of (AzPYR+DPH)/control ratios are also listed for these 16 proteins in Table 1.

### 3.3. First Functional Screening by Single Gene Knockdown

As a first functional screening, we assessed the effect of single gene knockdown on the uptake of  $\text{H}^+$ /OC antiporter substrates and a non-substrate, gabapentin, by hCMEC/D3 cells. The mRNA reductions resulting from siRNA treatment are shown in Figure S5. All targeted mRNA levels were decreased by more than 71% except for SLC12A5, SLC43A3, and aquaporin-3. Further, TCIRG1 knockdown decreased PYR, TRA, and DPH uptakes by 50, 43, and 16%, respectively (Table 2), although the differences were not statistically significant. In addition, TM7SF3 and LHFPL6 knockdown reduced the uptakes of  $\text{H}^+$ /OC antiporter substrates by more than 30% and 25%, respectively. On the other hand, these gene knockdowns did not decrease gabapentin uptake, suggesting that the effect is specific to  $\text{H}^+$ /OC antiporter substrates. CD9 knockdown decreased the PYR, TRA, and DPH uptakes, but the cell morphology was markedly changed (Figure S6). Hence, we focused on TCIRG1, TM7SF3, and LHFPL6 as candidate molecules.

**Table 2.** First functional screening by single gene knockdown.

Target Gene	Relative Uptake (% of Control)			
	Pyrilamine	Tramadol	Diphenhydramine	Gabapentin
Control	100 ± 12	100 ± 10	100 ± 15	100 ± 7
MAGT1	109 ± 11	104 ± 8	118 ± 11	110 ± 5
CD9	26.0 ± 7.3	56.5 ± 7.1	83.4 ± 12.0	148 ± 17
CYBRD1	96.7 ± 19.0	114 ± 12	121 ± 23	165 ± 22 **
ATP1A1	130 ± 21	129 ± 22	132 ± 12	161 ± 17 **
CLPTM1	128 ± 19	133 ± 17	132 ± 7	169 ± 14 **
TCIRG1	50.2 ± 14.6	67.0 ± 11.7	83.9 ± 9.7	119 ± 5
SLC12A5	95.9 ± 7.6	87.2 ± 5.3	107 ± 9	92.8 ± 5.6
LHFPL6	46.1 ± 20.3	74.8 ± 13.9	68.9 ± 9.2	134 ± 14
ARL6IP5	174 ± 16	149 ± 2	134 ± 5	146 ± 14
SLC43A3	52.0 ± 16.0	122 ± 13	127 ± 21	143 ± 9
TMEM65	120 ± 19	170 ± 17 **	144 ± 16	130 ± 6
TM7SF3	69.5 ± 11.4	76.8 ± 5.5	68.7 ± 8.7	145 ± 8
SLC9A1	68.4 ± 16.3	76.8 ± 2.3	96.5 ± 8.7	87.3 ± 8.6
ATP6V0A1	116 ± 15	119 ± 3	107 ± 9	118 ± 7
CD63	105 ± 6	118 ± 8	97.7 ± 20.2	144 ± 14
AQP3	148 ± 45	114 ± 21	146 ± 25	90.8 ± 11.3

The uptakes of  $\text{H}^+$ /OC antiporter substrates (pyrilamine, tramadol, and diphenhydramine) and a non-substrate (gabapentin) were assessed at 37 °C for 1 min in siRNA-transduced hCMEC/D3 cells. Each value represents the mean ± standard error ( $n = 4$ ). \*\*  $p < 0.01$ , significantly different from the control.

### 3.4. Second Functional Screening by Multiple Gene Knockdown

We postulated that the  $\text{H}^+$ /OC antiporter might be composed of more than one protein. Therefore, we assessed the effect of multiple gene knockdown on the uptake of  $\text{H}^+$ /OC antiporter substrates by hCMEC/D3 cells as a second screening (Table 3). As shown in Figure S5, mRNA levels were decreased by more than 60% in the siRNA-treated groups. TCIRG1 and LHFPL6 knockdown decreased OXY and VAR uptakes by 25 and 39%, respectively, but had little effect on PYR and TRA uptakes. TCIRG1 and TM7SF3 siRNA treatment had an effect similar to that of TCIRG1 and LHFPL6 knockdown. However, TM7SF3 and LHFPL6 siRNA treatment resulted in an over 31% decrease in the uptakes of

all H<sup>+</sup>/OC antiporter substrates, suggesting that the combination of TM7SF3 and LHFPL6 reduction could be critical for H<sup>+</sup>/OC antiporter-mediated uptake.

**Table 3.** Second functional screening by multiple gene knockdown.

	Relative Uptake (% of Control)				
	Pyrilamine	Tramadol	Oxycodone	Varenicline	Gabapentin
Control	100 ± 9	100 ± 6	100 ± 7	100 ± 14	100 ± 5
TCIRG1 + LHFPL6	104 ± 2	112 ± 4	74.6 ± 1.8 *	61.0 ± 8.0	89.5 ± 6.1
TM7SF3 + LHFPL6	68.2 ± 5.7 *	64.8 ± 4.3 **	66.6 ± 3.0 **	67.7 ± 7.9	121 ± 6
TCIRG1 + TM7SF3	87.6 ± 9.0	93.0 ± 6.5	74.6 ± 7.6 *	59.6 ± 13.6	99.7 ± 6.9
Control	100 ± 4	100 ± 5	100 ± 6	100 ± 24	100 ± 3
TCIRG1 + TM7SF3 + LHFPL6	93.6 ± 5.5	101 ± 4	92.0 ± 4.1	76.0 ± 8.0	122 ± 5 *

The uptakes of H<sup>+</sup>/OC antiporter substrates (pyrilamine, tramadol, oxycodone, and varenicline) and a non-substrate (gabapentin) were evaluated at 37 °C for 1 min in hCMEC/D3 cells transfected with siRNA for multiple targets. Each value represents the mean ± standard error ( $n = 4$ ). \*  $p < 0.05$  and \*\*  $p < 0.01$ , significantly different from the control.

### 3.5. First Validation; Gain-of-Function Analysis Using “Known” Substrates

For validation of the involvement of TM7SF3 and LHFPL6 in H<sup>+</sup>/OC antiporter-mediated uptake, we conducted a gain-of-function analysis with HEK293 cells. As shown in Figure 3, there was no difference in uptake of H<sup>+</sup>/OC antiporter substrates between mock and transiently LHFPL6-expressing cells. On the other hand, PYR, TRA, and VAR uptakes were increased by 21–34% in cells transiently expressing TM7SF3, although the differences were not statistically significant. In addition, cells overexpressing both TM7SF3 and LHFPL6 showed increases in PYR and TRA uptakes by 43 and 40%, respectively. Again, these were not statistically significant, but OXY and VAR uptakes were also increased by 31 and 97%, respectively. To further study the transport function, we generated stably expressing HEK293 cells. These cells showed a time-dependent increase in uptakes of H<sup>+</sup>/OC antiporter substrates (Figure 4). Stably TM7SF3-expressing cells showed significantly higher TRA uptakes at 1 and 5 min and VAR uptakes at 0.25, 1, and 5 min compared with mock cells. The uptake of H<sup>+</sup>/OC antiporter substrates by stably TM7SF3 and LHFPL6-expressing cells as well as by TM7SF3-expressing cells tended to be increased at 5 min compared to mock cells. In contrast to transiently expressing cells, the effect of TM7SF3 and LHFPL6 co-expression was not additive in the stably expressing cells. The uptake of antipyrine, a passive diffusion marker, was not altered in these cells (Figure S7).

### 3.6. Second Validation Using a “New” Substrate (Pyrilamine Analogue)

For second validation, we synthesized a new cell membrane-permeable substrate, a pyrilamine analogue, to further examine whether TM7SF3 and LHFPL6 are involved in the function of the H<sup>+</sup>/OC antiporter (Figure 5). We confirmed that the pyrilamine analogue is a substrate of the H<sup>+</sup>/OC antiporter in hCMEC/D3 cells. The C/M ratio of the pyrilamine analogue increased linearly from 0.5 to 5 min (Figure 6A), and the initial uptake rate (up to 5 min) was calculated to be 9.71 μL/mg protein/min. Furthermore, this uptake was reduced by approximately 90% at 4 °C. The uptake of pyrilamine analogue showed a  $K_m$  of  $8.85 \pm 2.15$  μM and a  $V_{max}$  of  $0.487 \pm 0.052$  nmol/mg protein/min for the saturable component and a  $K_d$  of  $0.467 \pm 0.260$  μL/mg protein/min for the non-saturable component (Figure 6B). The uptake was significantly inhibited (to <16.7%) by PYR, MEM, DPH, CLO, VAR, NAL, and TRA, which are substrates and/or inhibitors of the H<sup>+</sup>/OC antiporter, but was not inhibited by MPP<sup>+</sup>, PAH, TEA, and L-carnitine, which are not substrates or inhibitors of the H<sup>+</sup>/OC antiporter (Figure 6C). The C/M ratio was increased to 165% or decreased to 46%, respectively, by intracellular acidification and alkalinization (Figure 6D). The uptake of the pyrilamine analogue was also reduced by NaN<sub>3</sub>, an energy-depleting agent, but was not affected by replacement of extracellular sodium ions with lithium,

choline, or potassium ions (Figure 6E). Thus, the transport characteristics of the pyrilamine analogue are consistent with those of reported substrates of the H<sup>+</sup>/OC antiporter.

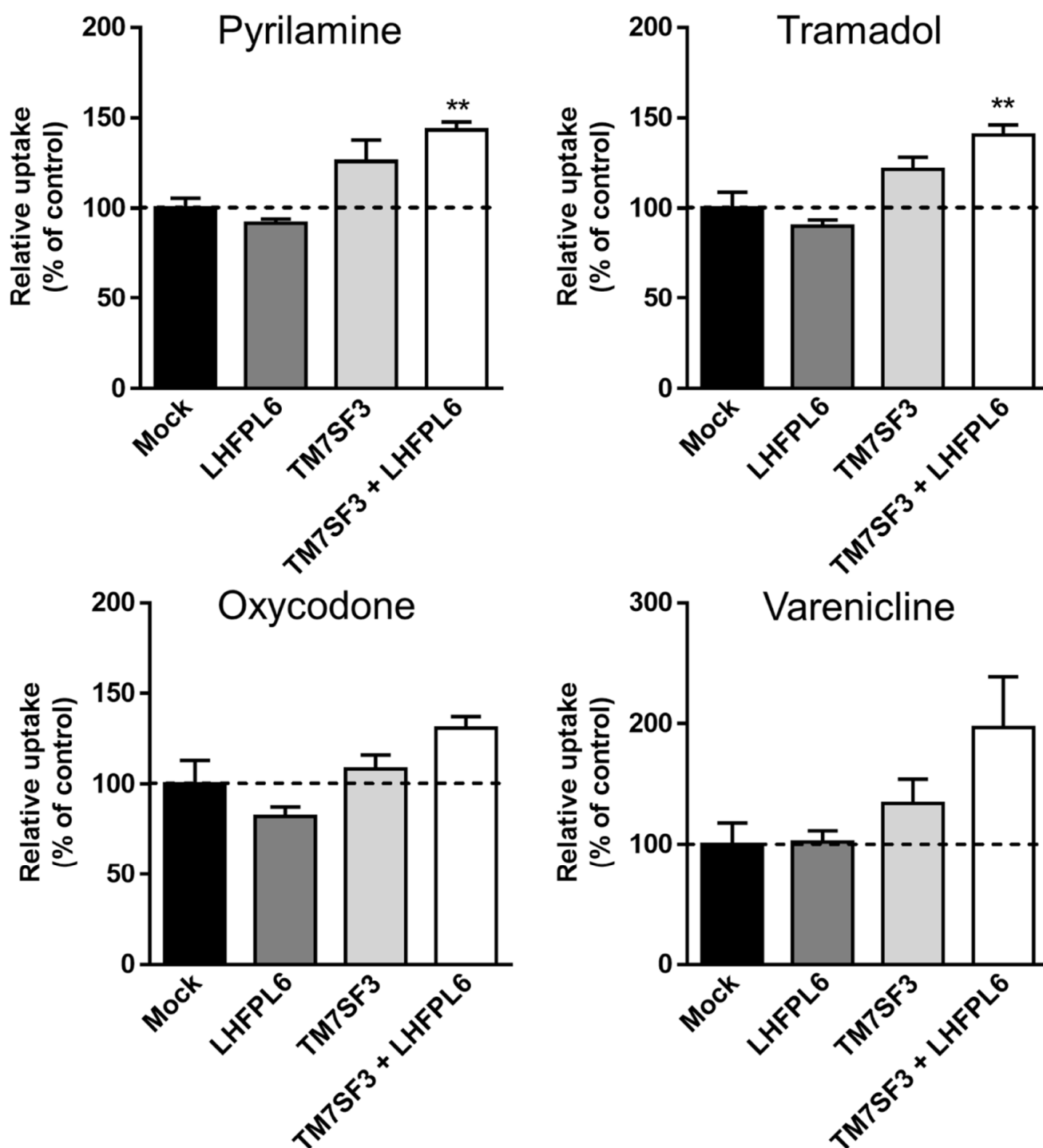


**Figure 3.** Uptakes of H<sup>+</sup>/OC antiporter substrates by HEK293 cells transiently transfected with LHFPL6 and/or TM7SF3. The uptake study was performed at 37 °C for 1 min in HEK293 cells transiently transfected with LHFPL6 and/or TM7SF3. Each column represents the mean ± standard error ( $n = 4$ ). \*\*  $p < 0.01$ , significantly different from the uptake by mock cells.

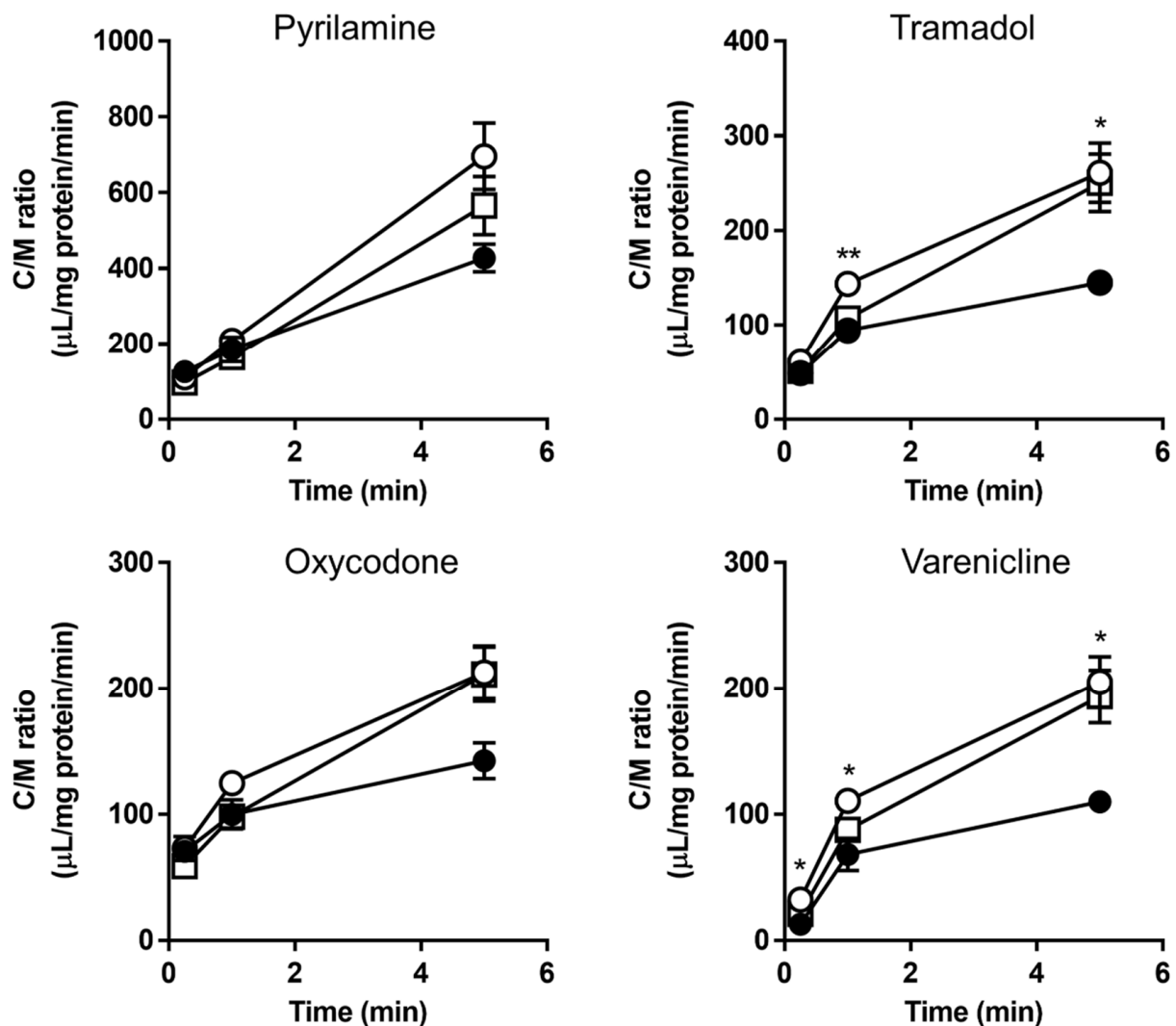


**Figure 4.** Uptake of H<sup>+</sup>/OC antiporter substrates by HEK293 cells stably double-transfected with LHFPL6 and TM7SF3. The time-courses of uptake were assessed at 37 °C in mock (closed circle) and HEK293 cells stably transfected with TM7SF3 (open circle) or both LHFPL6 and TM7SF3 (open square). Each point represents the mean ± standard error (*n* = 3). \* *p* < 0.05 and \*\* *p* < 0.01 indicate significant differences in the uptakes by mock and TM7SF3-transfected cells.

To evaluate the contribution of TM7SF3 and LHFPL6 to the uptake of the pyrilamine analogue, we used hCMEC/D3 cells in which these genes were knocked down with siRNA. Transfection with siRNA blocked the expression of each of TM7SF3 and LHFPL6 by more than 80% (Figure 7B). Similar results were also obtained in the double knockdown of TM7SF3 and LHFPL6. The uptakes of pyrilamine analogue at 0.5 to 5 min were reduced by 23.6, 23.7 and 40.4% at 0.5 min, 38.5, 36.8 and 58.1% at 1 min and 62.7, 27.6 and 33.9% at 5 min in cells with knockdown of TM7SF3, LHFPL6, and TM7SF3 + LHFPL6, respectively, compared to the negative control (Figure 7A). The C/M ratio in these cells was significantly reduced at 30 min to 61.9%, 56.2%, and 70.5%, respectively, but the effects of knockdown declined time-dependently. In addition, the effects of gain-of-function were evaluated using HEK293 cells stably expressing TM7SF3 and LHFPL6 (Figure 4). The C/M ratio of the pyrilamine analogue at 0.5 min was increased to 321% and 181% in TM7SF3-expressing cells and TM7SF3 + LHFPL6-expressing cells, respectively (Figure 7C). Again, the increase in C/M ratio was attenuated with prolonged uptake time. The mRNA expression levels in these cells showed a more than 40-fold increase in TM7SF3 and a 15-fold increase in LHFPL6 (Figure 7D).

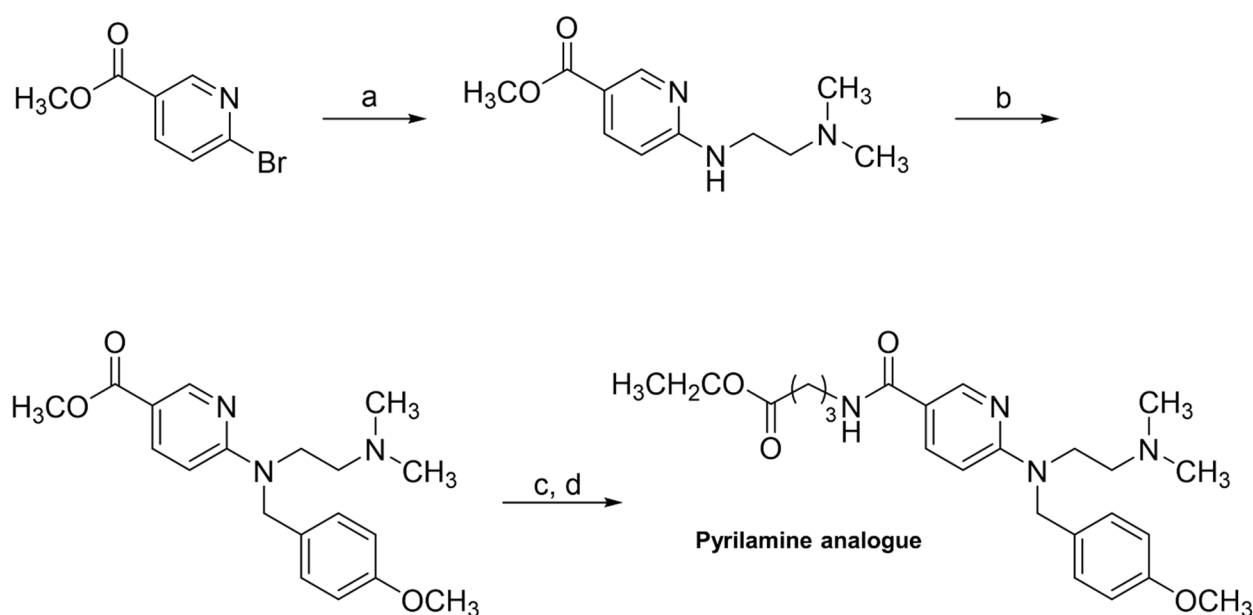


**Figure 5.** Synthesis of pyrilamine analogue as a new  $H^+$ /OC antiporter substrate. (a) *N,N*-Dimethylethylenediamine, pyridine, 120 °C; (b) 4-methoxybenzyl chloride, NaH, THF rt; (c) aq. NaOH,  $CH_3OH$ , 100 °C; (d) ethyl 4-aminobutyrate hydrochloride, ethyl-3-(3-dimethylaminopropyl) carbodiimide hydrochloride, 1-hydroxybenzotriazole, DIPEA, DMF, rt.

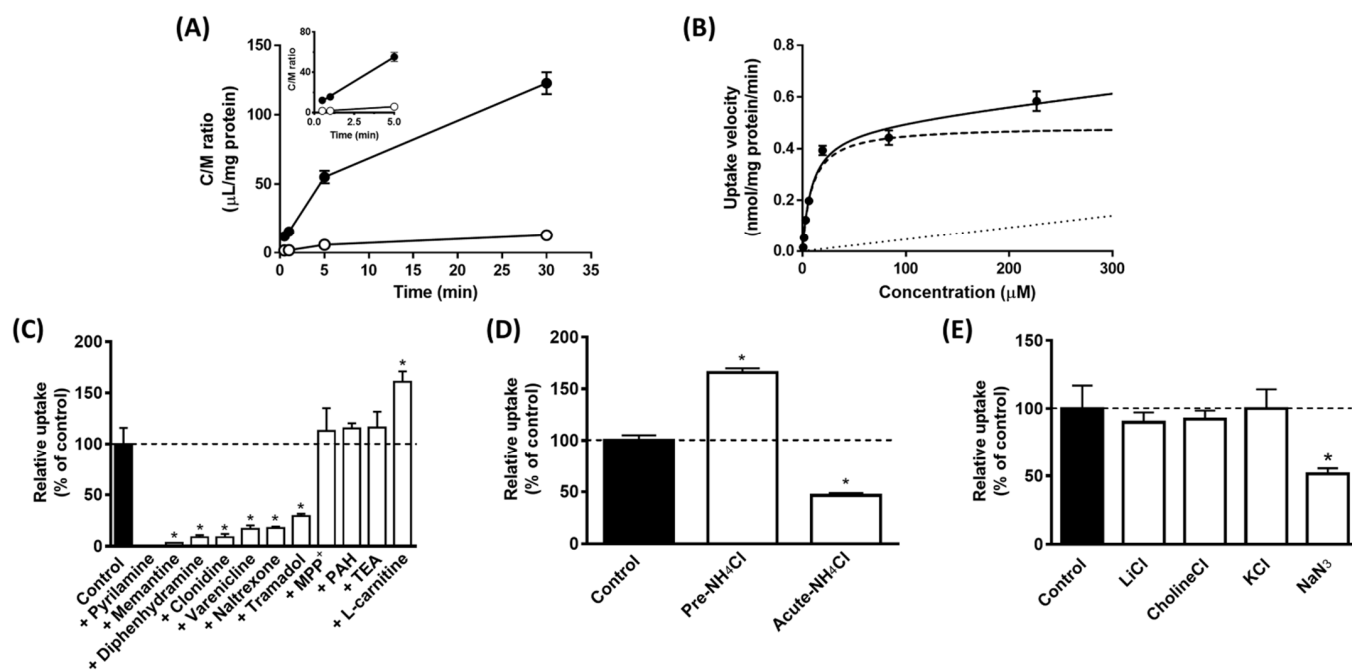


**Figure 6.** Transport characteristics of pyrilamine analogue in hCMEC/D3 cells. (A) Time- and temperature-dependent uptake experiments were performed at 37 °C (closed circles) and 4 °C (open circles) for up to 30 min. (B) The concentration-dependent uptake experiments were performed at 37 °C for 1 min (solid line). The dashed and dotted lines represent the saturable and non-saturable uptake components, respectively. (C) Inhibition experiments were performed at 37 °C for 1 min in the absence and presence of several inhibitors (1 mM). The black and white columns indicate inhibitory effects as percent of the control. (D,E) Effects of intracellular pH, extracellular  $Na^+$ , membrane potential and metabolic energy on pyrilamine analogue uptake by hCMEC/D3 cells. Cellular uptake in the C-E is shown as percent of the control. Each value and column represent the mean  $\pm$  standard error ( $n = 4$ ). \*  $p < 0.05$  indicates a significant difference versus the control.

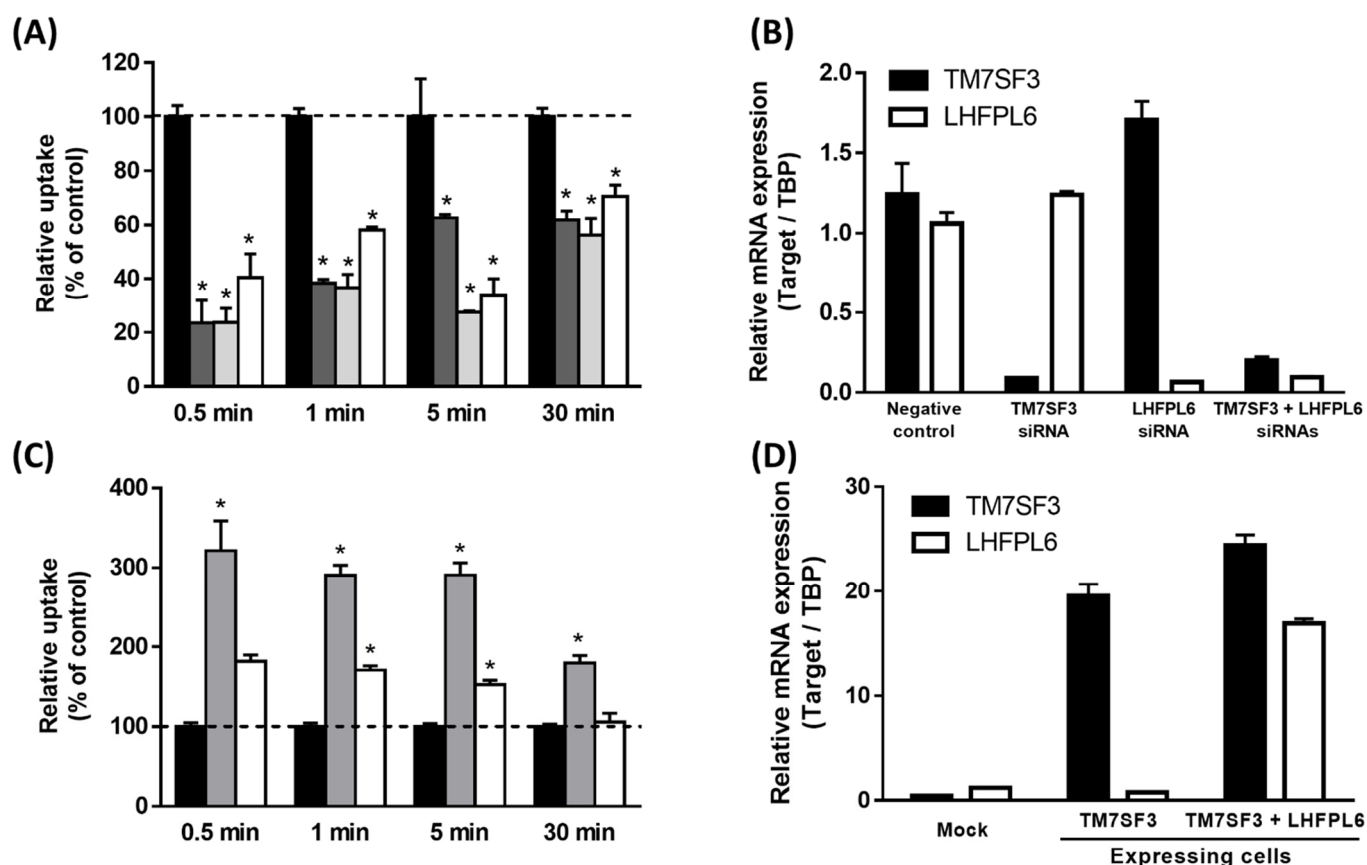


**Figure 7.** Effects of TM7SF3 and LHFPL6 on the cellular uptake of pyrilamine analogue. **(A)** Intracellular uptake of pyrilamine analogue in TM7SF3 or/and LHFPL6 knockdown hCMC/D3 cells was measured at 37 °C, for 0.5, 1, 5 and 30 min. The black, dark gray, light gray and white columns represent the negative control, TM7SF3 knockdown, LHFPL6 knockdown, and their double knockdown cells, respectively. **(B)** The mRNA expression of TM7SF3 and LHFPL6 in hCMC/D3 cells treated with the respective siRNAs. **(C)** Uptake of pyrilamine analogue in HEK293 cells stably expressing TM7SF3 or both TM7SF3 and LHFPL6 was evaluated at 37 °C. The black, gray, and white columns show the results for mock, TM7SF3-expressing, and TM7SF3 + LHFPL6-expressing cells, respectively. **(D)** The mRNA expression in HEK293 cells stably overexpressing TM7SF3 and LHFPL6 was measured by qPCR and normalized to that of TBP. Cellular uptake in A and C is shown as percent of the control. Each column represents the mean  $\pm$  standard error ( $n = 4$ ). \*  $p < 0.05$  indicates a significant difference versus the negative control.

#### 4. Discussion

The present study was designed to establish the molecular identity of the  $H^+/OC$  antiporter at the BBB, using a combination of the PICK method and functional analyses with a cell-permeable pyrilamine analogue. The results indicated that both TM7SF3 and LHFPL6 are involved in the antiporter activity.

Screening of transporters using photoreactive azide compounds had been performed in the 1980s and 1990s. For example, this approach was used to study the rabbit small-intestinal  $Na^+$ , D-glucose membrane transporter [32] and ATP transporter of rat liver rough endoplasmic reticulum [33]. It is considered that such crosslinking has relatively little effect on the substrate structure or substrate recognition of the target transporter, because of the small size of the azide group. Therefore, the PICK method was devised as a transporter identification method based on the strategy in Scheme 1. To our knowledge, this is the first successful application of the SWATH method for the molecular identification of a functional protein. The PICK method combines the use of azide-modified transporter substrates with the SWATH proteomic technique that affords excellent coverage and accuracy, and also

utilizes inhibitors to increase the specificity/accuracy of transporter identification. In this method, it is important to avoid non-specific binding as much as possible, which is achieved by using several different types of inhibitors in combination and by keeping the reaction time between the photoreactive substrate and the cell very short. In principle, within the transporter complex, the proteins that bind to the substrate are likely, and the surrounding subunits are less likely, to be easily identified. Because the labeling reaction with azide is not sufficiently specific, we also introduced an additional criterion for SWATH analysis: inhibition by FLV, an inhibitor of the H<sup>+</sup>/OC antiporter. AzPYR shows affinity for the PYR-binding pocket of the antiporter (Figure 2A), and UV irradiation causes irreversible reaction of the azide group with the antiporter (Figure 2B). SWATH-MS was also carried out for samples under control (neither AzPYR nor FLV), AzPYR, and AzPYR+FLV conditions, finally affording sixteen candidate proteins (Table 1) based on the criteria shown in Scheme 1.

In the first functional screening of candidate proteins generated by the PICK method, TCIRG1, TM7SF3 and LHFPL6 were selected, since knockdown of these proteins affected H<sup>+</sup>/OC antiporter substrate transport (Table 2). Noting that the L-type amino acid transporter is a complex of LAT1 (SLC7A5) and 4F2hc (SLC3A2/CD98) [34], we hypothesized that two or all three candidates might be involved in H<sup>+</sup>/OC antiporter activity. It has been reported that TM7SF3, with seven putative transmembrane domains, inhibits the cytokine-induced death of pancreatic beta cells and promotes their insulin secretion [35]. TM7SF3 is a downstream transcriptional target of p53/TP53, and acts as a pro-survival homeostatic factor that attenuates the development of ER stress [36]. In addition, LHFPL6, with three putative transmembrane domains, is a candidate prognostic biomarker and therapeutic target for gastric cancer [37]. These two proteins have been reported to be expressed in diverse tissues and also in CNS cells [38–43]. Examination of the roles of these proteins in the CNS may provide important insights into the pharmacological effects of drugs and therapeutic strategies, but in the present work we chose to focus on the involvement of TM7SF3 and LHFPL6 in the H<sup>+</sup>/OC antiporter at the BBB, because the BBB protects the physiological function of the entire brain and significantly influences drug efficacy in the CNS. Interestingly, the mRNA expression levels of TM7SF3 and LHFPL6 in brain capillary endothelial cells are comparable to those of other transporters at the BBB (Figure S8) [44]. Indeed, in mice, TM7SF3 expression is greater than that of BCRP, which contributes to drug efflux at the BBB (Figure S8). In humans, LHFPL6 is more highly expressed than GLUT1 and LAT1 (Figure S8). Thus, TM7SF3 and LHFPL6 could contribute to transport at the BBB. TCIRG1 is a subunit of V-ATPase, which is responsible for acidifying and maintaining the pH of intracellular compartments in some cell types, and is also targeted to the plasma membrane, where it acidifies the extracellular environment [45]. In the second functional screening, the combination of TM7SF3 and LHFPL6 knockdown caused the greatest decrease in the uptake of H<sup>+</sup>/OC antiporter substrates, whereas TCIRG1 knockdown had a relatively weak effect (Table 3), strongly suggesting the involvement of TM7SF3 and LHFPL6 in the H<sup>+</sup>/OC antiporter activity.

In the gain-of-function analysis, the HEK293 expression system was used to investigate the contributions of TM7SF3 and LHFPL6 to the uptake of H<sup>+</sup>/OC antiporter substrates. Both transient and stable expression of TM7SF3 tended to increase the substrate uptake, whereas the expression of LHFPL6 had little impact (Figures 3 and 4). In particular, the expression of TM7SF3 and LHFPL6 in HEK293 cells had little effect on the initial uptake. However, an increase in initial uptake of VAR, a relatively hydrophilic substrate, by TM7SF3-expressing cells (Figure 4) was observed.

Drug permeation through biological membranes is affected by the unstirred water layer surrounding the membrane, the plasma membrane, and intracellular binding. Therefore, to detect phenomena on the plasma membrane where the H<sup>+</sup>/OC antiporter is present, it is important to use a compound for which plasma membrane permeability is rate-limiting. Here, we synthesized a new compound, pyrilamine analogue (Figures 5 and S4). The initial uptake rate of pyrilamine analogue was calculated to be 9.71 μL/mg protein/min, which

was approximately 50-fold slower than PYR (Figure S9), implying that the plasma membrane permeability is rate-limiting in the initial uptake rate. In addition, it was proven in the present study to contain enough characteristics as a substrate of the H<sup>+</sup>/OC antiporter (Figure 6). This suggests that pyrilamine analogue would be suitable for clarifying the function of TM7SF3 and LHFPL6. Indeed, its uptake was significantly reduced by knockdown of TM7SF3 and/or LHFPL6 at any time from 0.5 to 30 min (Figure 7A). On the other hand, TM7SF3 and LHFPL6 knockdown did not affect gabapentin uptake (a substrate of LAT1) (Figure S10). Furthermore, the uptake of the pyrilamine analogue showed a 3.2-fold increase at 0.5 min in TM7SF3-stably expressing HEK293 cells (Figure 7C). All of these results suggest that TM7SF3 and LHFPL6 could be components of the H<sup>+</sup>/OC antiporter.

## 5. Conclusions

We developed the PICK method, which combines photo-affinity labeling and comprehensive proteomic analysis using SWATH-MS, to identify the molecular components of the H<sup>+</sup>/OC antiporter, which is responsible for the transport of various CNS drugs at the BBB. Sixteen candidate proteins were picked up based on predefined criteria. The results of knockdown and inhibitor studies in hCMEC/D3 cells, as well as uptake studies with overexpressing cells, indicated that TM7SF3 and LHFPL6 are H<sup>+</sup>/OC antiporter components. This information is expected to promote the development of effective CNS drugs and novel drug delivery systems. We anticipate that the PICK method will be useful for the identification of various transporters. When screening to identify the responsible transporters for compounds of interest, researchers frequently focus on known ABC, SLC and MFS transporters, and consequently may miss transporters that do not belong to these families. Furthermore, transporter complexes consisting of multiple proteins are difficult to identify. The PICK method can overcome these limitations and is expected to accelerate transporter discovery.

**Supplementary Materials:** The following supporting information can be downloaded at: <https://www.mdpi.com/article/10.3390/pharmaceutics14081683/s1>, Detailed experimental methods, composition of media and buffers, and additional data are provided in the Supplementary Materials. Table S1: MRM transitions of test compounds, Table S2: siRNA and negative control siRNA information, Table S3: Sequences of sense and antisense primers (5' to 3') used for qPCR, Figure S1: Synthetic route of AzPYR from compound 1, Figure S2: Detailed scheme of photoaffinity labeling for H<sup>+</sup>/OC antiporter using hCMEC/D3 cells, Figure S3: The detailed workflow for the SWATH analysis (step [3] in Scheme 1), Figure S4: Information on each compound in the synthetic route of pyrilamine analogue, Figure S5: mRNA expression in functional screening after single (A) or multiple (B) knockdown, Figure S6: Alteration of cell morphology by CD9 siRNA, Figure S7: Antipyrine uptake by HEK293 cells stably double-transfected with LHFPL6 and TM7SF3, Figure S8: Reported mRNA expression levels of TM7SF3, LHFPL6 and BBB transporters in human and mouse brain endothelial cells, Figure S9: Uptake study of pyrilamine in hCMEC/D3 cells, Figure S10: Uptake of gabapentin in hCMEC/D3 cells transfected with siRNA.

**Author Contributions:** Conceptualization, Y.U., T.T. and Y.D.; Methodology, T.K., Y.T., Y.U., K.H., H.T. and T.S.; Investigation, T.K., Y.T., Y.U. and K.H.; Data Curation, T.K., Y.T., Y.U. and K.H.; Writing—Original Draft Preparation, T.K., Y.T., Y.U., K.H., H.T. and T.S.; Writing—Review and Editing, Y.U., Y.K., T.T. and Y.D.; Supervision, T.T. and Y.D. All authors have read and agreed to the published version of the manuscript.

**Funding:** This study was supported by a Grant-in-Aid from the Japan Society for the Promotion of Science (JSPS) KAKENHI (Grant Number: 20H03399 to Y.U., 19K07008 to T.S. and 16K08381 to Y.D.), and Fostering Joint International Research KAKENHI (Grant Number: 18KK0446 to Y.U.).

**Institutional Review Board Statement:** Not applicable.

**Informed Consent Statement:** Not applicable.

**Data Availability Statement:** The data of this study are available from the corresponding author upon reasonable request.



**Acknowledgments:** We thank Pierre-Oliver Couraud (Institut Cochin, Paris, France) for supplying hCMEC/D3 cells under license from INSERM.

**Conflicts of Interest:** The authors report no conflict of interest in this work.

## References


1. Yamazaki, M.; Terasaki, T.; Yoshioka, K.; Nagata, O.; Kato, H.; Ito, Y.; Tsuji, A. Carrier-mediated transport of H1-antagonist at the blood-brain barrier: A common transport system of H1-antagonists and lipophilic basic drugs. *Pharm. Res.* **1994**, *11*, 1516–1518. [CrossRef] [PubMed]
2. Sadiq, M.W.; Borgs, A.; Okura, T.; Shimomura, K.; Kato, S.; Deguchi, Y.; Jansson, B.; Björkman, S.; Terasaki, T.; Hammarlund-Udenaes, M. Diphenhydramine active uptake at the blood-brain barrier and its interaction with oxycodone in vitro and in vivo. *J. Pharm. Sci.* **2011**, *100*, 3912–3923. [CrossRef] [PubMed]
3. Boström, E.; Simonsson, U.S.; Hammarlund-Udenaes, M. In vivo blood-brain barrier transport of oxycodone in the rat: Indications for active influx and implications for pharmacokinetics/pharmacodynamics. *Drug Metab. Dispos.* **2006**, *34*, 1624–1631. [CrossRef]
4. Cisternino, S.; Chapy, H.; André, P.; Smirnova, M.; Debray, M.; Scherrmann, J.M. Coexistence of passive and proton antiporter-mediated processes in nicotine transport at the mouse blood-brain barrier. *AAPS J.* **2013**, *15*, 299–307. [CrossRef]
5. André, P.; Debray, M.; Scherrmann, J.M.; Cisternino, S. Clonidine transport at the mouse blood-brain barrier by a new H<sup>+</sup> antiporter that interacts with addictive drugs. *J. Cereb. Blood Flow Metab.* **2009**, *29*, 1293–1304. [CrossRef] [PubMed]
6. Kubo, Y.; Kusagawa, Y.; Tachikawa, M.; Akanuma, S.; Hosoya, K. Involvement of a novel organic cation transporter in verapamil transport across the inner blood-retinal barrier. *Pharm. Res.* **2013**, *30*, 847–856. [CrossRef] [PubMed]
7. Tega, Y.; Akanuma, S.; Kubo, Y.; Hosoya, K. Involvement of the H<sup>+</sup> / organic cation antiporter in nicotine transport in rat liver. *Drug Metab. Dispos.* **2015**, *43*, 89–92. [CrossRef] [PubMed]
8. Shimomura, K.; Okura, T.; Kato, S.; Couraud, P.O.; Scherrmann, J.M.; Terasaki, T.; Deguchi, Y. Functional expression of a proton-coupled organic cation (H<sup>+</sup> / OC) antiporter in human brain capillary endothelial cell line hCMEC/D3, a human blood-brain barrier model. *Fluids Barriers CNS* **2013**, *10*, 8. [CrossRef] [PubMed]
9. Okura, T.; Hattori, A.; Takano, Y.; Sato, T.; Hammarlund-Udenaes, M.; Terasaki, T.; Deguchi, Y. Involvement of the pyrilamine transporter, a putative organic cation transporter, in blood-brain barrier transport of oxycodone. *Drug Metab. Dispos.* **2008**, *36*, 2005–2013. [CrossRef] [PubMed]
10. Shinozaki, Y.; Akanuma, S.; Mori, Y.; Kubo, Y.; Hosoya, K. Comprehensive Evidence of Carrier-Mediated Distribution of Amantadine to the Retina across the Blood-Retinal Barrier in Rats. *Pharmaceutics* **2021**, *13*, 1339. [CrossRef] [PubMed]
11. Chapy, H.; Goracci, L.; Vayer, P.; Parmentier, Y.; Carrupt, P.A.; Declèves, X.; Scherrmann, J.M.; Cisternino, S.; Cruciani, G. Pharmacophore-based discovery of inhibitors of a novel drug/proton antiporter in human brain endothelial hCMEC/D3 cell line. *Br. J. Pharmacol.* **2015**, *172*, 4888–4904. [CrossRef]
12. Hiranaka, S.; Tega, Y.; Higuchi, K.; Kurosawa, T.; Deguchi, Y.; Arata, M.; Ito, A.; Yoshida, M.; Nagaoka, Y.; Sumiyoshi, T. Design, Synthesis, and Blood-Brain Barrier Transport Study of Pyrilamine Derivatives as Histone Deacetylase Inhibitors. *ACS Med. Chem. Lett.* **2018**, *9*, 884–888. [CrossRef] [PubMed]
13. Wang, X.; Qi, B.; Su, H.; Li, J.; Sun, X.; He, Q.; Fu, Y.; Zhang, Z. Pyrilamine-sensitive proton-coupled organic cation (H<sup>+</sup> / OC) antiporter for brain-specific drug delivery. *J. Control. Release* **2017**, *254*, 34–43. [CrossRef] [PubMed]
14. Okura, T.; Higuchi, K.; Kitamura, A.; Deguchi, Y. Proton-coupled organic cation antiporter-mediated uptake of apomorphine enantiomers in human brain capillary endothelial cell line hCMEC/D3. *Biol. Pharm. Bull.* **2014**, *37*, 286–291. [CrossRef] [PubMed]
15. Kitamura, A.; Higuchi, K.; Okura, T.; Deguchi, Y. Transport characteristics of tramadol in the blood-brain barrier. *J. Pharm. Sci.* **2014**, *103*, 3335–3341. [CrossRef]
16. Higuchi, K.; Kitamura, A.; Okura, T.; Deguchi, Y. Memantine transport by a proton-coupled organic cation antiporter in hCMEC/D3 cells, an in vitro human blood-brain barrier model. *Drug Metab. Pharmacokinet.* **2015**, *30*, 182–187. [CrossRef] [PubMed]
17. Kurosawa, T.; Higuchi, K.; Okura, T.; Kobayashi, K.; Kusuhara, H.; Deguchi, Y. Involvement of Proton-Coupled Organic Cation Antiporter in Varenicline Transport at Blood-Brain Barrier of Rats and in Human Brain Capillary Endothelial Cells. *J. Pharm. Sci.* **2017**, *106*, 2576–2582. [CrossRef]
18. Sweet, D.H. Organic Cation Transporter Expression and Function in the CNS. *Handb. Exp. Pharmacol.* **2021**, *266*, 41–80. [PubMed]
19. Alexovič, M.; Urban, P.L.; Tabani, H.; Sabo, J. Recent advances in robotic protein sample preparation for clinical analysis and other biomedical applications. *Clin. Chim. Acta* **2020**, *507*, 104–116. [CrossRef] [PubMed]
20. Frei, A.P.; Moest, H.; Novy, K.; Wollscheid, B. Ligand-based receptor identification on living cells and tissues using TRICEPS. *Nat. Protoc.* **2013**, *8*, 1321–1336. [CrossRef] [PubMed]
21. Sumranjit, J.; Chung, S.J. Recent advances in target characterization and identification by photoaffinity probes. *Molecules* **2013**, *18*, 10425–10451. [CrossRef] [PubMed]
22. Patterson, D.M.; Nazarova, L.A.; Prescher, J.A. Finding the right (bioorthogonal) chemistry. *ACS Chem. Biol.* **2014**, *9*, 592–605. [CrossRef] [PubMed]
23. Kitamura, M.; Yano, M.; Tashiro, N.; Miyagawa, S.; Sando, M.; Okauchi, T. Direct Synthesis of Organic Azides from Primary Amines with 2-Azido-1,3-dimethylimidazolium Hexafluorophosphate. *Eur. J. Org. Chem.* **2011**, *2011*, 458–462. [CrossRef]

24. Tezuka, K.; Suzuki, M.; Sato, R.; Kawarada, S.; Terasaki, T.; Uchida, Y. Activation of Annexin A2 signaling at the blood-brain barrier in a mouse model of multiple sclerosis. *J. Neurochem.* **2022**, *160*, 662–674. [CrossRef] [PubMed]
25. Uchida, Y.; Sasaki, H.; Terasaki, T. Establishment and validation of highly accurate formalin-fixed paraffin-embedded quantitative proteomics by heat-compatible pressure cycling technology using phase-transfer surfactant and SWATH-MS. *Sci. Rep.* **2020**, *10*, 11271. [CrossRef]
26. Sato, R.; Ohmori, K.; Umetsu, M.; Takao, M.; Tano, M.; Grant, G.; Porter, B.; Bet, A.; Terasaki, T.; Uchida, Y. An Atlas of the Quantitative Protein Expression of Anti-Epileptic-Drug Transporters, Metabolizing Enzymes and Tight Junctions at the Blood-Brain Barrier in Epileptic Patients. *Pharmaceutics* **2021**, *13*, 2122. [CrossRef] [PubMed]
27. Uchida, Y.; Higuchi, T.; Shiota, M.; Kagami, S.; Saigusa, D.; Koshihara, S.; Yasuda, J.; Tamiya, G.; Kuriyama, S.; Kinoshita, K.; et al. Identification and Validation of Combination Plasma Biomarker of Afamin, Fibronectin and Sex Hormone-Binding Globulin to Predict Pre-eclampsia. *Biol. Pharm. Bull.* **2021**, *44*, 804–815. [CrossRef]
28. Sadek, B.; Alisch, R.; Buschauer, A.; Elz, S. Synthesis and dual histamine H<sub>1</sub> and H<sub>2</sub> receptor antagonist activity of cyanoguanidine derivatives. *Molecules* **2013**, *18*, 14186–14202. [CrossRef] [PubMed]
29. Takamuro, I.; Sekine, Y.; Tsuboi, Y.; Nogi, K.; Taniguchi, H. A Pyrazolopyrimidine Compound and a Process for Preparing the Same. WO2004064721 A2, 5 August 2004.
30. Yamazaki, M.; Fukuoka, H.; Nagata, O.; Kato, H.; Ito, Y.; Terasaki, T.; Tsuji, A. Transport mechanism of an H<sub>1</sub>-antagonist at the blood-brain barrier: Transport mechanism of mepyramine using the carotid injection technique. *Biol. Pharm. Bull.* **1994**, *17*, 676–679. [CrossRef] [PubMed]
31. Nakazawa, Y.; Okura, T.; Shimomura, K.; Terasaki, T.; Deguchi, Y. Drug-drug interaction between oxycodone and adjuvant analgesics in blood-brain barrier transport and antinociceptive effect. *J. Pharm. Sci.* **2010**, *99*, 467–474. [CrossRef] [PubMed]
32. Hosang, M.; Gibbs, E.M.; Diedrich, D.F.; Semenza, G. Photoaffinity labeling and identification of (a component of) the small-intestinal Na<sup>+</sup>,D-glucose transporter using 4-azidophlorizin. *FEBS Lett.* **1981**, *130*, 244–248. [CrossRef]
33. Kim, S.H.; Shin, S.J.; Park, J.S. Identification of the ATP transporter of rat liver rough endoplasmic reticulum via photoaffinity labeling and partial purification. *Biochemistry* **1996**, *35*, 5418–5425. [CrossRef] [PubMed]
34. Fotiadis, D.; Kanai, Y.; Palacín, M. The SLC3 and SLC7 families of amino acid transporters. *Mol. Asp. Med.* **2013**, *34*, 139–158. [CrossRef]
35. Beck, A.; Isaac, R.; Lavelin, I.; Hart, Y.; Volberg, T.; Shatz-Azoulay, H.; Geiger, B.; Zick, Y. An siRNA screen identifies transmembrane 7 superfamily member 3 (TM7SF3), a seven transmembrane orphan receptor, as an inhibitor of cytokine-induced death of pancreatic beta cells. *Diabetologia* **2011**, *54*, 2845–2855. [CrossRef] [PubMed]
36. Isaac, R.; Goldstein, I.; Furth, N.; Zilber, N.; Streim, S.; Boura-Halfon, S.; Elhanany, E.; Rotter, V.; Oren, M.; Zick, Y. TM7SF3, a novel p53-regulated homeostatic factor, attenuates cellular stress and the subsequent induction of the unfolded protein response. *Cell Death Differ.* **2017**, *24*, 132–143. [CrossRef]
37. Liu, Y.J.; Yin, S.Y.; Zeng, S.H.; Hu, Y.D.; Wang, M.Q.; Huang, P.; Li, J.P. Prognostic Value of LHFPL Tetraspan Subfamily Member 6 (LHFPL6) in Gastric Cancer: A Study Based on Bioinformatics Analysis and Experimental Validation. *Pharmgenomics Pers. Med.* **2021**, *14*, 1483–1504. [CrossRef] [PubMed]
38. Whillans, D.W.; Adams, G.E. Electron transfer oxidation of DNA radicals by paranitroacetophenone. *Int. J. Radiat. Biol. Relat. Stud. Phys. Chem. Med.* **1975**, *28*, 501–510. [CrossRef] [PubMed]
39. Petit, M.M.; Schoenmakers, E.F.; Huysmans, C.; Geurts, J.M.; Mandahl, N.; Van de Ven, W.J. LHFP, a novel translocation partner gene of HMGIC in a lipoma, is a member of a new family of LHFP-like genes. *Genomics* **1999**, *57*, 438–441. [CrossRef]
40. Hirano, S.; Goto, R.; Uchida, Y. SWATH-Based Comprehensive Determination of the Localization of Apical and Basolateral Membrane Proteins Using Mouse Liver as a Model Tissue. *Biomedicines* **2022**, *10*, 383. [CrossRef] [PubMed]
41. Usoskin, D.; Furlan, A.; Islam, S.; Abdo, H.; Lönnerberg, P.; Lou, D.; Hjerling-Leffler, J.; Haeggström, J.; Kharchenko, O.; Kharchenko, P.V.; et al. Unbiased classification of sensory neuron types by large-scale single-cell RNA sequencing. *Nat. Neurosci.* **2015**, *18*, 145–153. [CrossRef]
42. Hodge, R.D.; Bakken, T.E.; Miller, J.A.; Smith, K.A.; Barkan, E.R.; Graybuck, L.T.; Close, J.L.; Long, B.; Johansen, N.; Penn, O.; et al. Conserved cell types with divergent features in human versus mouse cortex. *Nature* **2019**, *573*, 61–68. [CrossRef] [PubMed]
43. Smajčić, S.; Prada-Medina, C.A.; Landoulsi, Z.; Ghelfi, J.; Delcambre, S.; Dietrich, C.; Jarazo, J.; Henck, J.; Balachandran, S.; Pachchek, S.; et al. Single-cell sequencing of human midbrain reveals glial activation and a Parkinson-specific neuronal state. *Brain* **2022**, *145*, 964–978. [CrossRef]
44. Yang, A.C.; Vest, R.T.; Kern, F.; Lee, D.P.; Agam, M.; Maat, C.A.; Losada, P.M.; Chen, M.B.; Schaum, N.; Khoury, N.; et al. A human brain vascular atlas reveals diverse mediators of Alzheimer’s risk. *Nature* **2022**, *603*, 885–892. [CrossRef]
45. Bronckers, A.L.; Lyaruu, D.M.; Bervoets, T.J.; Medina, J.F.; DenBesten, P.; Richter, J.; Everts, V. Murine ameloblasts are immunonegative for Tcigr1, the v-H-ATPase subunit essential for the osteoclast plasma proton pump. *Bone* **2012**, *50*, 901–908. [CrossRef] [PubMed]



Review

# Transport Mechanisms at the Blood–Brain Barrier and in Cellular Compartments of the Neurovascular Unit: Focus on CNS Delivery of Small Molecule Drugs

Patrick T. Ronaldson \* and Thomas P. Davis 

Department of Pharmacology, College of Medicine, University of Arizona, Tucson, AZ 85724-5050, USA; davistp@arizona.edu

\* Correspondence: pronald@arizona.edu; Tel.: +1-520-626-2173

**Abstract:** Ischemic stroke is a primary origin of morbidity and mortality in the United States and around the world. Indeed, several research projects have attempted to discover new drugs or repurpose existing therapeutics to advance stroke pharmacotherapy. Many of these preclinical stroke studies have reported positive results for neuroprotective agents; however, only one compound (3K3A-activated protein C (3K3A-APC)) has advanced to Phase III clinical trial evaluation. One reason for these many failures is the lack of consideration of transport mechanisms at the blood–brain barrier (BBB) and neurovascular unit (NVU). These endogenous transport processes function as a “gateway” that is a primary determinant of efficacious brain concentrations for centrally acting drugs. Despite the knowledge that some neuroprotective agents (i.e., statins and memantine) are substrates for these endogenous BBB transporters, preclinical stroke studies have largely ignored the role of transporters in CNS drug disposition. Here, we review the current knowledge on specific BBB transporters that either limit drug uptake into the brain (i.e., ATP-binding cassette (ABC) transporters) or can be targeted for optimized drug delivery (i.e., solute carrier (SLC) transporters). Additionally, we highlight the current knowledge on transporter expression in astrocytes, microglia, pericytes, and neurons with an emphasis on transport mechanisms in these cell types that can influence drug distribution within the brain.

**Keywords:** ATP-binding cassette transporters; blood–brain barrier; drug delivery; ischemic stroke; SLC transporters

**Citation:** Ronaldson, P.T.; Davis, T.P. Transport Mechanisms at the Blood–Brain Barrier and in Cellular Compartments of the Neurovascular Unit: Focus on CNS Delivery of Small Molecule Drugs. *Pharmaceutics* **2022**, *14*, 1501. <https://doi.org/10.3390/pharmaceutics14071501>

Academic Editor: Ken-ichi Hosoya

Received: 6 June 2022

Accepted: 15 July 2022

Published: 20 July 2022

**Publisher’s Note:** MDPI stays neutral with regard to jurisdictional claims in published maps and institutional affiliations.



**Copyright:** © 2022 by the authors. Licensee MDPI, Basel, Switzerland. This article is an open access article distributed under the terms and conditions of the Creative Commons Attribution (CC BY) license (<https://creativecommons.org/licenses/by/4.0/>).

## 1. Introduction

A primary goal of neuropharmacology is optimal delivery of effective free drug concentrations to specific molecular targets in the brain. Over the past several years, researchers have attempted to exploit the physiology of the blood–brain barrier (BBB) to achieve this objective. For large molecule therapeutics such as proteins, targeting receptor-mediated transcytosis mechanisms (i.e., transferrin receptors (TfRs) and insulin receptors) has resulted in many successful preclinical studies [1–5]. For example, Chang and colleagues demonstrated that an erythropoietin-TfR antibody fusion protein (cTfRMAB-EPO) could cross the BBB, decrease amyloid peptide load in the hippocampus, and improve spatial memory in male APP/PS1 mice aged 5.5 months [3]. More recently, a BBB transport vehicle engineered to bind to the TfR apical domain was shown to successfully deliver an anti- $\beta$ -secretase cargo peptide to the brain and produce a sustained pharmacodynamic effect both in human TfR-expressing C57BL6 mice and in cynomolgus monkeys [5]. While research on the blood-to-brain transport of large molecules is rapidly progressing, there have been few paradigm-shifting studies that have presented new delivery approaches for small molecules. In fact, such strategies for small molecule therapeutics remain focused on optimization of passive transcellular diffusion. This is often reflected by the continued

application of Lipinski's "Rule of 5", which relates the BBB passive permeability to molecular weight, lipophilicity, polar surface area, hydrogen bonding capacity, and charge [6]. Using rational medicinal chemistry approaches, the "Rule of 5" guides drug design toward molecules that are less than 500 Da, possess  $\text{clogP}$  values between 1.5 and 2.5, have polar surface areas with an upper limit of  $90 \text{ \AA}^2$ , have fewer than five hydrogen bond donors and ten hydrogen bond acceptors, and are primarily uncharged at physiological pH [6]. Indeed, many efficacious CNS small molecule drugs possess these physicochemical properties [7,8]; however, passive diffusion is a non-selective process that does not provide the capability of precisely controlling drug delivery into brain tissue. This suggests that many detailed studies are required to identify transport mechanisms that can enable selective drug uptake across the BBB. Success in this area will lead to safer and more effective pharmacological treatments for neurological diseases.

Over the past several years, endogenous BBB transporters have been evaluated due to their importance as determinants of CNS drug disposition and drug efficacy. Most of the published research on BBB transporters has focused on those proteins that restrict therapeutic uptake into brain tissue (i.e., efflux transporters). The panel of efflux transporters that are known to be functionally expressed in brain microvascular endothelial cells include members of the ATP-binding cassette (ABC) superfamily, such as P-glycoprotein (P-gp), breast cancer resistance protein (BCRP in humans; Bcrp in rodents), and multidrug resistance proteins (MRPs in humans; Mrps in rodents) [9,10]. This is primarily due to the concept that efflux transporter liability, particularly with respect to P-gp, is a discriminating factor between centrally active drugs and non-CNS drugs [7]. Hence, it was hypothesized that blockade of BBB efflux transporters could result in improvement in brain penetration for drugs, particularly those with low passive permeability and moderate-to-high P-gp transport liability. Problematically, clinical trials targeting P-gp with pharmacological inhibitors (i.e., verapamil, cyclosporine A, and valsopodar) have failed due to inhibitor toxicity and/or the enhanced penetration of drugs into non-CNS tissues [9,11,12]. P-gp is ubiquitously expressed throughout the human body. Epithelial tissues that functionally express P-gp include the colon, small intestine, renal proximal tubules, and bile canaliculi. This is an important consideration because blocking P-gp at the BBB using pharmacological antagonists will also block its activity in these other tissues, resulting in increased systemic drug disposition and an enhanced probability of off-target effects and/or dose-limiting toxicities [12,13]. A more rational approach for effective CNS drug delivery involves targeting transport mechanisms with the directionality to move substrates out of the systemic circulation, across the endothelial cell, and into brain parenchyma. To achieve this goal, a detailed evaluation of solute carrier (SLC) transporters that include centrally acting drugs amongst their substrate profile (i.e., organic anion-transporting polypeptides (OATPs in humans; Oatps in rodents), organic cation transporters (OCTs in humans; Octs in rodents), and multidrug and toxin extrusion transporters (MATEs in humans; Mates in rodents)) is necessary. Understanding the dynamics of CNS drug delivery also requires an appreciation that both efflux and influx transporters are expressed in other brain cellular compartments (i.e., glial cells, pericytes, and neurons). Such transporters play a critical role in brain drug distribution and, therefore, can have profound effects on the treatment of neurological disorders. In this review, we summarize the current knowledge on the localization and functional expression of those ABC and SLC transporters relevant to CNS drug delivery and drug distribution. Our focus will include both the BBB and brain parenchyma to emphasize how the rigorous comprehension of transporter function in the brain can lead to the optimization of blood-to-brain drug transport and the improved treatment of neurological diseases. We will use the example of ischemic stroke to demonstrate this critical concept.

## 2. Overview of ATP-Binding Cassette (ABC) and Solute Carrier (SLC) Transporters at the Blood–Brain Barrier (BBB)

For many centrally acting drugs, selective uptake into the brain and efflux from the brain is mediated by transport proteins. To date, several transport systems have been identified at the BBB. These include members of the ABC and SLC superfamilies, which function to determine the types of molecules that can access the brain while simultaneously restricting the CNS accumulation of others. Below, we provide an overview of these transport systems and their relevance to CNS drug delivery.

### 2.1. ABC Transporters

The ABC transporter superfamily is among the largest and most ubiquitously expressed protein families that have been discovered. These transporters are grouped into seven distinct subfamilies (i.e., ABCA-ABCG) based upon the sequence homology of their nucleotide-binding domains and transmembrane domains, gene structure, and domain order [14]. ABC transporters are involved in various physiological processes, including lipid bilayer maintenance, peptide transport, and sterol transport. The most clinically relevant role of ABC transporters is their direct contribution to the development of the multidrug resistance (MDR) phenotype [15]. In the seminal work published by Michael Gottesman, the MDR phenotype was defined as the simultaneous resistance to several structurally unrelated compounds that do not result from independent genetic mutations that confer resistance to a single therapeutic agent [16]. Perhaps the most well-studied ABC transporter is P-gp, a principal contributor to the MDR phenotype and a clinically relevant impediment to drug permeation across the BBB. Other ABC transporters that are known to be involved in CNS drug disposition include BCRP/Bcrp (also known as ABCG2) and MRP/Mrp isoforms. The localization of critical ABC transporters that are expressed at the brain microvascular endothelium is depicted in Figure 1.

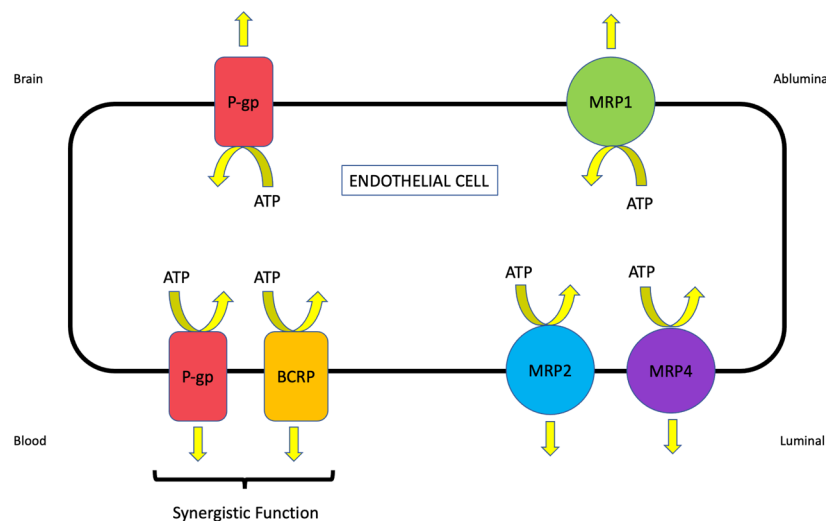


**Figure 1.** Localization of ABC Transporters in Brain Microvessel Endothelial Cells. Adapted with permission from Nilles et al. ref. [17]. 2022. Copyright 2022 by the authors.

#### 2.1.1. P-glycoprotein (P-gp)

P-gp was first discovered by Dr. Victor Ling at the University of Toronto via the identification and characterization of a novel subclone of Chinese hamster ovary cells that displayed reduced cellular permeability and subsequent chemoresistance to the anti-gout drug colchicine [18]. Since this paradigm-shifting observation, P-gp has been shown to be a 170 kDa transmembrane glycoprotein that possesses two homologous halves, each with an intracellular ATP-binding site [19]. The efflux transport of drugs by P-gp requires ATP hydrolysis, which indicates that this protein functions as a primary active transporter. This transporter is encoded by the *MDR/mdr* gene, which has two isoforms

in humans (i.e., *MDR1* and *MDR2*) and three isoforms in rodents (i.e., *mdr1a*, *mdr1b*, and *mdr2*). *MDR2* and *mdr2* are primarily expressed in the liver and are involved in transport of phosphatidylcholine into the bile. P-gp encoded by *MDR1/mdr1a/mdr1b* has evolved as a protective mechanism that prevents the CNS uptake of potentially toxic xenobiotics, a function that is highlighted by observations obtained using P-gp null (i.e., *mdr1a/mdr1b* (-/-)) mice. In rat and human brain tissue, P-gp has been shown to be localized at both the luminal and abluminal plasma membrane of microvascular endothelial cells [20]. While P-gp functional expression at the luminal plasma membrane is well-established to restrict xenobiotic uptake into brain tissue, its role at the abluminal membrane is less clear. Interestingly, immunogold cytochemistry revealed that the density of P-gp antigenic sites at the abluminal plasma membrane was 1.4-fold greater than at the luminal membrane [20]. This may reflect a role for P-gp in directing substances toward brain interstitial fluid to maintain their CNS concentrations. In the presence of ivermectin (i.e., a neurotoxic pesticide), P-gp null mice exhibit a 100-fold increase in brain accumulation as compared to wild-type controls [21]. Furthermore, P-gp null mice treated with ivermectin present with neurological symptoms that reflect central toxicity, including tremors, paralysis, coma, and death [21]. More recently, positron emission tomography (PET) technology has enabled the real-time study of P-gp function in experimental animals. For example, administration of the competitive P-gp inhibitor tariquidar resulted in increased CNS distribution of [<sup>11</sup>C]metoclopramide and [<sup>11</sup>C]verapamil by 2.1-fold and 2.4-fold, respectively [22]. P-gp expression has been demonstrated in cultured human vascular endothelial cells [23–25], in human brain cortical microvessels [26–29], and at the BBB in human cerebral tissue fixed in situ [20]. The advent of PET technology for the study of drug transport mechanisms has also enabled the evaluation of P-gp activity in living human subjects. For example, tariquidar was shown to increase the distribution volume and influx rate constants for [<sup>11</sup>C]verapamil in five healthy human volunteers [30]. An important caveat to this study was that P-gp inhibition at the BBB was reported to be “far from complete” as compared to peripheral P-gp inhibition [30], an observation that adds to the body of literature describing challenges associated with the blocking P-gp function for the enhancement of CNS drug uptake. Similar results were obtained by Muzi and colleagues, where increased cerebral blood flow-corrected brain uptake of [<sup>11</sup>C]verapamil was demonstrated in the presence of the P-gp inhibitory drug cyclosporine A [31]. Therapeutic concentrations of quinidine, a competitive P-gp inhibitor, were also shown to increase CNS delivery of [<sup>11</sup>C]verapamil by PET imaging; however, the P-gp inducer rifampin did not affect P-gp activity at clinically relevant concentrations [32]. These observations should not be interpreted to imply that induction of P-gp transport activity does not occur at the human BBB. Rather, these data point toward a need to test other drugs that have been shown to modulate P-gp transport activity in preclinical studies so that a detailed understanding of this critical transporter can be obtained.

P-gp has a vast substrate profile that renders it a formidable obstacle to CNS drug delivery. In fact, the number of compounds known to be P-gp substrates is continuously expanding in direct correlation with the advancement of the BBB field. Most P-gp transport substrates are non-polar, weakly amphipathic compounds. Indeed, P-gp can recognize and transport drugs with varying structures and sizes that range from 250 to 1202 Da [9,33]. The list of known substrate categories includes, but is not limited to, antibiotics, calcium channel blockers, cardiac glycosides, chemotherapeutics, immunosuppressants, anti-epileptics, anti-depressants, opioid analgesic drugs, statins (i.e., HMG CoA reductase inhibitors), and HIV-1 protease inhibitors [9,10,15]. For example, uptake of atorvastatin and rosuvastatin by human umbilical vein endothelial cells (HUVECs) was shown to be increased in the presence of pharmacological P-gp inhibitors (i.e., cyclosporine A, PSC833), a “mixed” P-gp/Bcrp inhibitor (i.e., GF120918), and metabolic inhibitors (i.e., sodium azide and dinitrophenol), suggesting that these two statins are substrates for P-gp [25]. Additionally, P-gp has been shown to be a critical determinant of brain penetration for morphine [34] and experimental opioid analgesic peptides such as D-Pen<sup>2</sup>,D-Pen<sup>5</sup>]enkephalin (DPDPE) [35].

The brain distribution of the currently marketed catechol-O-methyltransferase (COMT) inhibitor tolcapone and a novel COMT inhibitor (i.e., BIA 9-1079) were demonstrated to be increased in the presence of the P-gp inhibitor drug elacridar [36], suggesting that P-gp is also an important determinant of blood-to-brain transport for this class of centrally acting drugs.

### 2.1.2. Breast Cancer Resistance Protein (BCRP/Bcrp)

BCRP was originally identified in the MCF-7/AdrVp breast cancer cell line that was generated to study novel pharmacological approaches to circumvent the MDR phenotype [37]. Despite the lack of expression of P-gp or MRP1 in these cells, ATP-dependent efflux transport of adriamycin and rhodamine 123 was observed, indicating the presence of a novel transporter protein [38,39]. This novel transporter was later cloned from MCF-7/AdrVp cells and termed “breast cancer resistance protein [40]”. Bcrp is comprised of 655 amino acids and has a molecular weight of approximately 72 kDa. As such, it is often referred to as a “half-transporter” that must form homo- or heterodimers to efflux drugs [41,42]. At the BBB, BCRP/Bcrp has been shown to be expressed at the luminal plasma membrane of brain microvascular endothelial cells [43–45]. Using absolute quantitative targeted proteomics, BCRP was detected at quantifiable levels in a human brain microvessel endothelial cell line (hCMEC/d3) [46] and in human brain microvessels [47]. The substrate profile of BCRP/Bcrp often overlaps with that of P-gp, thereby enabling these two transporters to function in synergy to limit the CNS uptake of selected drugs [25,36,48–51]. For example, rosuvastatin is a transport substrate for both P-gp and Bcrp, a fact that greatly affects its CNS distribution [25,49]. Using triple knockout mice (i.e., *mdr1a/b*(−/−); *Bcrp*(−/−)), Laramy and colleagues demonstrated that the total and free brain-to-plasma concentration ratios for the anti-cancer drug ponatinib were 15 times higher in the knockouts as compared to the wild-type controls, an observation that experimentally emphasizes the synergistic interplay between these two critical efflux transporters [51]. Similar results have been reported in the literature for vemurafenib [52] and sorafenib [53]. Additionally, the HIV-1 protease integrase inhibitor raltegravir was reported to be transported by both P-gp and BCRP in the hCMEC/d3 cell line, suggesting a potential synergistic effect of these ABC transporters [54]. In contrast, CNS uptake of many opioid analgesic drugs is limited by P-gp but not Bcrp [10]. Therefore, it is imperative that these critical efflux transporters be studied together to determine whether synergistic efflux transport involving P-gp and Bcrp exists for individual compounds and how such an effect can modulate CNS drug disposition and/or efficacy. In addition to therapeutic agents, the substrate profile for Bcrp includes endogenous and/or natural product substances such as steroids [55], glutathione [56], folate [57], and phenethyl isothiocyanate (PEITC) [58].

### 2.1.3. Multidrug Resistance Proteins (MRPs/Mrps)

The primary role of Mrps is to extrude substances from cells, thereby providing additional transporter contributors to the development of the MDR phenotype. MRPs/Mrps differ from P-gp in that their substrate profile is restricted to organic anions and their glucuronidated, sulfated, and glutathione-conjugated metabolites [15]. Delineating specific properties and functional significance of individual MRP/Mrp isoforms is challenging due to the existence of multiple homologues with overlapping substrate profiles. At the BBB, the functional expression of Mrp1, 2, 4, and 5 has been confirmed and Mrp3 and 6 may also contribute to brain-to-blood drug transport at the microvascular endothelium [59]. The presence of MRP/Mrp homologues at the luminal side of the BBB is likely a critical determinant in controlling the delivery of drugs to the brain. For example, Mrp downregulation at the BBB was shown to result in the enhanced analgesic potency of morphine following systemic administration [60]. Using Mrp4(−/−) mice, Kanamitsu and colleagues demonstrated that this ATP-dependent efflux transporter was a critical determinant of brain penetration for therapeutic agents such as ochratoxin A, pitavastatin, raltitrexed, pravastatin, and cyclophosphamide [61]. Additionally, the ability of Mrp1, Mrp2, and



Mrp4 to actively efflux the endogenous antioxidant glutathione may have implications in neurological diseases that feature an oxidative stress component. Glutathione is responsible for maintenance of cellular redox balance and antioxidant defense in the brain. It has been previously shown that Mrp functional expression is upregulated in response to oxidative stress conditions, an effect that promotes cellular glutathione extrusion [62]. The enhanced functional expression of Mrp isoforms at the BBB can cause reduced brain and/or endothelial cell concentrations of glutathione, altered cellular redox status, and increased potential for cellular injury and death. Prostaglandin D<sub>2</sub> (PGD<sub>2</sub>), an eicosanoid mediator involved in the exacerbation and progression of neuroinflammation, has also been identified as an endogenous transport substrate for Mrp4 [63]. This was demonstrated by the observation that Mrp4 inhibitors (i.e., probenecid, benzylpenicillin, and cefmetazole) reduced the brain efflux index (BEI) of [<sup>3</sup>H]PGD<sub>2</sub> following intracerebral injection in male Wistar rats [63].

## 2.2. Solute Carrier (SLC) Transporters

A previous publication by the International Transporter Consortium provided a comprehensive analysis of the literature and suggested that effective clinical modulation of BBB efflux transporters using competitive inhibitors is highly unlikely [64]. This article came to this conclusion following a detailed review and analysis of multiple published preclinical studies and predicted that the maximal enhancement in drug uptake possible by blocking P-gp and BCRP will not exceed 2-fold [64]. This determination was based on the assumption that 100% of P-gp and BCRP transporters at the brain microvascular endothelium would need to be inhibited, an impossible goal given the highest clinical doses of efflux transporter inhibitors that could ever be administered to a patient [64]. This hypothesis has profound implications for CNS drug delivery as it suggests that blocking transporters that move substrates out of the brain is not a viable translational strategy to optimize the quantity of drug that gets into the brain. Inhibitor toxicity and increased drug penetration into systemic organs and tissues are additional obstacles that have prevented the advent of efflux transporter inhibition in the clinic. Therefore, our laboratory has proposed that a more rational strategy is to target those transporters that function to move their substrates in the blood-to-brain direction (i.e., uptake transporters). Indeed, selective CNS accumulation of many circulating substances requires SLC transporters. More than 400 SLC transporters that have been shown to be important for functions such as ion and nutrient uptake into the cell and drug absorption, distribution, metabolism, and excretion (ADME) have been identified in human cells/tissues [65,66]. Transport mechanisms for SLC transporters include facilitated diffusion (i.e., transport in the direction of substrate electrochemical gradient) or secondary/tertiary active transport (i.e., substrate transport that is dependent upon ion/solute gradients established by primary or secondary active transporters) [67]. SLC family members exhibit different specificities and affinities for transport substrates [68,69]. In this section, we will focus on OATPs/Oatps and OCTs/Octs, two types of SLC transporters that can be effectively targeted for drug delivery to the brain. The localization of critical OATP/Oatp and OCT/Oct transporters that are expressed in brain microvessel endothelial cells are presented in Figure 2.

### 2.2.1. Organic Anion-Transporting Polypeptides (Oatps)

Due to their capabilities for efficient blood-to-brain delivery of small molecule drugs, our laboratory has extensively studied the protein expression and transport activity of OATPs/Oatps at the BBB. We have focused much of our work on Oatp1a4, the primary Oatp isoform responsible for drug transport at the BBB in rats [35,68,70–73]. Immunohistochemistry, confocal microscopy, and Western blot analysis have confirmed the localization and/or protein expression of Oatp1a4 at the cerebral microvasculature [35,74–76]. Of note, double-labeling immunohistochemistry studies with antibodies targeted against Oatp1a4 and glial fibrillary acidic protein (GFAP), a protein marker of astrocytes, demonstrated Oatp1a4 localization at the plasma membrane in brain capillary endothelial cells [77]. OATP1A2 is the human orthologue of Oatp1a4 and its expression has been reported in



OCT1 ( $0.54 \pm 0.06$ – $0.58 \pm 0.11$  pmol/mg total protein) and OCT3 ( $0.62 \pm 0.08$  pmol/mg total protein) in microvessels derived from healthy postmortem human brain tissue [27]. In contrast, quantitative targeted proteomics has not been able to detect abundant quantities for OCT1 or OCT2 at the BBB in hippocampal Brodmann Areas 17 and 39 [28]. When these proteomics studies are rigorously compared, the disagreements between data sets imply differences in the BBB localization/expression for OCT transporters across different brain regions. Therefore, it is essential that such results be confirmed by molecular analyses and functional studies.

The translocation of cationic solutes across polarized epithelial/endothelial cell layers involves a two-step process involving different transporters that work in a cooperative manner. A pertinent example is found in epithelial cells of the renal proximal tubule, where synergy between two transporters (i.e., OCT2 and MATE1) is required for the efficient secretion of cationic substances [88]. While OCT2 is involved in the initial uptake at the plasma membrane, MATE1 functions to ensure the cationic substrate efflux into urinary filtrate. At the BBB, it has been reported that OCTs/Octs are expressed at the luminal plasma membrane of microvascular endothelial cells, an observation that is consistent with their role as the first step in blood-to-brain transport of cationic substances [69]. The OCT1/Oct1- and OCT2/Oct2-mediated uptake of N-methyl-4-phenyl-1,2,3,6-tetrahydropyridine (MPTP) has been shown in brain endothelial cells, evidence for the functional expression of these transporters at the BBB [87]. The fact that MPTP can efficiently permeate the BBB by an OCT/Oct-dependent mechanism implies that MATEs may also be functionally expressed at the level of the microvascular endothelium. Mate1 and Mate2 protein expression was detected at the BBB in C57BL6/129 mice [86] and Mate1 mRNA and protein expression was detected in brain capillaries isolated from male ddY mice [89]. More recently, Mate1 gene expression was shown in brain capillaries from various mouse strains, including Swiss, FVB, and C57BL6/JRj [90]. With respect to human endothelial cells, studies in the hCMEC/d3 cell line resulted in detection of MATE1 and MATE2 protein expression [86]. Additionally, the Western blot analysis of human brain tissue demonstrated MATE1 and MATE2 expression in the frontal cortex, caudate nucleus, and putamen [86]. In contrast, Chaves and colleagues were unable to show MATE expression in microvasculature derived from human glioma tissue [90]. Indeed, pathophysiological factors associated with cancer progression and/or pharmacological treatment with antineoplastic drugs could explain the variability in results between the work of Chaves and colleagues and other studies examining MATE expression at the BBB. Nonetheless, these discordant observations in the BBB expression of MATE/Mate isoforms suggests that detailed experiments are necessary to clarify the role of OCTs/Octs and MATEs/Mates in CNS drug delivery. Overall, the Oct/Mate system provides an excellent opportunity to deliver cationic therapeutics to the brain. Examples of such drugs include memantine, amantadine, metformin, pramipexole, selegiline, varenicline, and amisulpride [17,86,88,91,92].

### 3. Case Study on Transport at the Blood–Brain Barrier (BBB)—Ischemic Stroke

As reported by the Global Burden of Disease Study in 2019, there are approximately 12.2 million cases of stroke worldwide, which have resulted in the death of 6.55 million individuals [93]. Approximately 87% of all strokes are ischemic [94] and are characterized by pathophysiology resulting from vascular occlusion and subsequent reduction in oxygen and glucose supply to the affected brain region. This process leads to necrotic cell death of neural tissue in the infarction core and substantial injury to tissue surrounding the core (i.e., the ischemic penumbra) [95,96]. The penumbra is a primary target for drug treatment due to slower cell degradation [67,97,98]. Current FDA-approved treatments for ischemic stroke are either pharmacological (i.e., recombinant tissue plasminogen activator (r-tPA; alteplase)) or mechanical/surgical (i.e., endovascular thrombectomy (EVT)). Pharmacotherapy with r-tPA has many limitations, including a short therapeutic window (i.e., 4.5 h) and/or an enhanced risk for intracerebral hemorrhage [97]. In fact, the National Institute of Neurological Disorders and Stroke (NINDS) of the National Institutes of Health

(NIH) reported that the risk of clinically significant bleeding in patients that were dosed with r-tPA was 6.4% as compared to 0.6% for patients given placebo [99]. Risk factors for intracerebral hemorrhage following treatment with thrombolytic drugs include stroke severity, hyperglycemia, time from onset of stroke symptoms to treatment, elevated systolic blood pressure, thrombocytopenia, and advanced chronological age [100]. Mechanical EVT has been an important surgical advancement in the treatment of ischemic stroke by providing improved cerebral reperfusion to stroke patients [101,102]; however, the advent of EVT has not completely prevented post-stroke disability [102–104]. It is important to consider that EVT, as well as the administration of r-tPA, involves the restoration of blood flow to ischemic brain tissue (i.e., recanalization). Paradoxically, recanalization is known to be associated with the exacerbation of neuronal damage. CNS injury following recanalization ranges in severity from infarction progression to the development of vasogenic edema or fatal hemorrhaging, factors that are associated with ischemia/reperfusion (I/R) injury [98]. I/R injury is associated with increased BBB permeability (i.e., paracellular “leak”), the activation of pathological mechanisms associated with cell death (i.e., apoptosis, autophagy, and necrosis), enhanced neuroinflammation, and the production of elevated levels of reactive oxygen species (i.e., oxidative stress) [96,105–108].

The routine application of r-tPA and EVT for acute ischemic stroke treatment suggests that therapeutic approaches capable of protecting neuronal tissue against injury and/or promoting repair following I/R injury are urgently required. Preclinical studies have attempted to address this need through evaluation of currently marketed drugs and experimental therapeutics using in vivo stroke models. Many of these studies have reported positive results demarcated by neuroprotection, prevention of cerebral infarction expansion, and/or improved functional neurocognitive performance. In fact, approximately 95% of studies published in the scientific literature between 1990 and 2018 have reported such outcomes [102]; however, only a single investigational drug (i.e., 3K3A-activated protein C (3K3A-APC)) has advanced to a multi-center Phase III clinical trial [109]. There are several reasons for the poor translation from animal models to successful clinical trials, including (i) the paucity of well-designed experiments to measure cognitive and motor outcomes; (ii) the use of doses in animal studies that are not consistent with those that would be able to be administered to human subjects; and (iii) the use of healthy young animals that are not representative of the vast majority of ischemic stroke patients who tend to be older and frequently present with at least one comorbid condition (i.e., diabetes mellitus, obesity, tobacco smoking, hypertension, and atrial fibrillation) [102,110]. An additional consideration is that studies examining drug efficacy in experimental ischemic stroke have not evaluated the role of endogenous BBB transporters in determining the blood-to-brain uptake of therapeutic agents.

Cerebral ischemia has been previously shown to be associated with altered expression and activity of the critical BBB efflux transporter P-gp. Of particular significance, Spudich and colleagues demonstrated that P-gp protein expression is elevated at the BBB as early as 3 h following transient middle cerebral artery occlusion (MCAO) [111]. Additionally, immunoblot analyses showed increased P-gp protein expression in the cerebral microvasculature following MCAO (90 min) as well as in cultured rat brain endothelial cells subjected to hypoxia/aglycemia [112]. Altered functional expression of P-gp, as well as other BBB transporters that are determinants of CNS drug delivery, can have profound implications for brain disposition and therapeutic effectiveness of drugs designed to treat ischemic stroke. Indeed, several drugs with neuroprotective properties are established substrates of P-gp. For example, P-gp is involved in the brain uptake and distribution of tanshinone IIA, a natural product compound that has shown potential in preclinical studies to protect against I/R injury [113]. More recently, in vitro studies in human umbilical vein endothelial cells (HUVECs) have identified the commonly prescribed statin drugs atorvastatin and rosuvastatin as P-gp transport substrates [25]. In contrast to P-gp, little is known as to how I/R injury affects BCRP/Bcrp. A single study where bovine brain endothelial cells were co-cultured with rat astrocytes showed decreased *Abcg2* mRNA in response to oxygen/glucose

deprivation (OGD) conditions [114]. Interestingly, this reduction in transporter gene expression occurred as early as 4 h post-OGD treatment, but the *ABCG2* transcript expression returned to control levels after 24 h reoxygenation [114]. Since BCRP functions in synergy with P-gp to restrict the BBB permeability of stroke therapeutics such as statins [49], it is critical that this finding be validated using in vivo models of experimental ischemic stroke.

Despite the functional expression of efflux transporters at the BBB, SLC transporters represent a therapeutic opportunity to optimize the blood-to-brain uptake of drugs. Our laboratory has identified that OATPs/Oatps are critical transporters that enable the penetration of statins into the CNS. The chemical structures of currently marketed statins are shown in Figure 3. This mechanism is essential for these drugs to exert positive effects in the ischemic brain. Several in vivo studies performed by our group have provided evidence for BBB statin transport involving Oatps. For example, Thompson and colleagues reported that brain uptake of atorvastatin is mediated by Oatp1a4 in female Sprague-Dawley rats subjected to global hypoxia/reoxygenation stress (i.e., 6% O<sub>2</sub> for 1 h followed by reoxygenation with 21% O<sub>2</sub> for 10 min) [70]. Our results have demonstrated that both lipophilic statins (i.e., atorvastatin) and hydrophilic statins (i.e., pravastatin) can be transported by Oatp1a4 [71]. Interestingly, the Oatp-mediated transport of atorvastatin was at least 4-fold higher in female Sprague-Dawley rats as compared to their age-matched male counterparts [73], a study that provided the first evidence for sex differences of an endogenously expressed BBB transporter for drugs. These studies are congruent with previous observations from Oatp1a4(−/−) mice where the brain uptake of statin drugs (i.e., pitavastatin and rosuvastatin) was lower than that measured in the wild-type controls [115]. The evaluation of Oatp-mediated drug transport at the BBB in preclinical models requires the appreciation that species differences in drug transport properties can exist between rodents and human cells and/or tissues. An excellent example is the observation that OATP/Oatp transport properties for triptans, a class of medications designed to ease the symptoms of migraine or cluster headache, are dramatically unlike between humans and rodents [116]. Specifically, uptake transport for multiple triptan drugs (i.e., almotriptan, naratriptan, sumatriptan, rizatriptan, and zolmitriptan) was similar between Oatp1a4 null mice and wild-type controls, which implies that these drugs do not utilize an Oatp1a4-mediated transport mechanism to accumulate in the brain parenchyma [116]. In contrast, zolmitriptan was shown to be a substrate for OATP1A2, suggesting an OATP-mediated component of blood-to-brain uptake transport for this triptan drug [116]. This observation was confirmed in OATP1A2 knock-in mice where the CNS uptake of zolmitriptan was 1.6-fold higher as compared to age-matched wild-type controls [117]. In vitro studies in transfected Madin-Darby canine kidney (MDCK) II cells [116] and in HUVECs [25] showed that multiple statin drugs (i.e., atorvastatin, pravastatin, and rosuvastatin) are transport substrates for OATP1A2. These results emphasize the translational utility of using preclinical rodent models to study the transport of stroke drugs at the BBB if comparable properties between rodent transporters and their human orthologues have been demonstrated. Other OATP/Oatp transport substrates that may be effective as stroke therapeutics include opioid analgesic peptides. Using human-induced pluripotent stem cell-derived brain microvascular endothelial cells (iPSC-BMECs), Albekairi and colleagues showed that the cellular accumulation of the experimental opioid receptor peptide biphalin was decreased following exposure to estrone-3-sulfate, a known OATP inhibitor [118]. Both perinuclear and membranous expression of OATP1A2 was confirmed in iPSC-BMEC cells using fluorescent immunocytochemistry and flow cytometry [118]. Opioid receptor agonists such as biphalin have been demonstrated to exert neuroprotective effects in preclinical stroke models [119–125]. For example, Nozohouri and colleagues showed that biphalin can increase glutamate uptake in cultured mouse astrocytes and protect against BBB dysfunction in mice subjected to MCAO [125]. Therefore, targeting BBB OATP transporters represents a viable approach that can facilitate the delivery of potentially efficacious neuroprotective drugs to ischemic brain tissue.

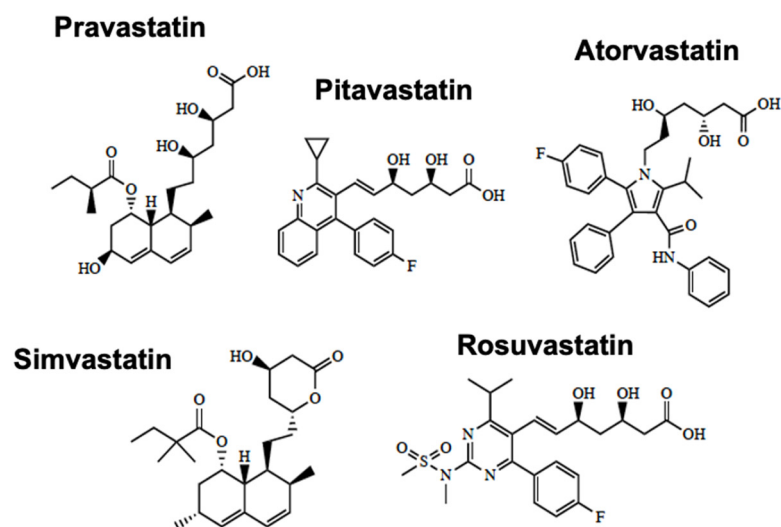


**Figure 3.** Chemical Structures of Currently Marketed Statin Drugs.

The diversity of SLC transporters that are expressed at the BBB provides multiple opportunities to develop approaches for the improvement of CNS drug delivery. Memantine (Figure 4) is a known substrate for OCTs/Oct and, therefore, provides a useful tool to study the potential of targeting BBB transporters for cationic compounds. In terms of its mechanism of action, memantine functions as an antagonist of N-methyl-D-aspartate receptors (NMDARs). Reduced cerebral concentrations of oxygen and glucose following an ischemic insult can lead to an increased influx of calcium into neurons, a process that stimulates the release of the prototypical excitatory neurotransmitter glutamate. The excessive accumulation of glutamate within the synapse (i.e., excitotoxicity) is a primary cause of neuronal injury and/or death in the setting of ischemic stroke. The pharmacological inhibition of NMDARs protects against neuronal injury caused by excitotoxicity, which is the scientific premise for pharmaceutical development of memantine as a neuroprotective drug. At physiological pH, the majority of memantine molecules will carry a positive charge [92], a physicochemical property that indicates that a selective membrane transport mechanism is required for this small molecule drug to cross the BBB. Indeed, memantine has been shown to be transported by a specific system for cationic solutes in brain microvascular endothelial cells [92]. Studies in *Xenopus laevis* oocytes transfected with OCT2 mRNA demonstrated that memantine uptake was dependent upon a saturable transport mechanism ( $K_m = 34 \pm 5 \mu\text{M}$ ) [126]. Using memantine, we have shown for the first time that BBB transport is absolutely required for this drug to be efficacious in the setting of ischemic stroke [127]. Specifically, we report that memantine can improve functional neurological outcomes, reduce cerebral infarction progression, and decrease cerebral edema when administered as a single dose (5 mg/kg, i.v.) in male Sprague-Dawley rats subjected to MCAO [127]. Interestingly, the Oct transport inhibitor cimetidine attenuated all positive effects in our MCAO model [127], suggesting that Oct1/Oct2 transport is a primary mechanism for the neuroprotective effects of memantine. This is the first time that an endogenous BBB transport system has been shown to be required for a stroke drug to be effective, a concept that is depicted in Figure 5.

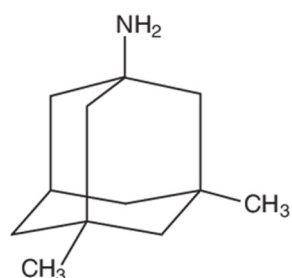


Figure 4. Chemical Structure of Memantine.

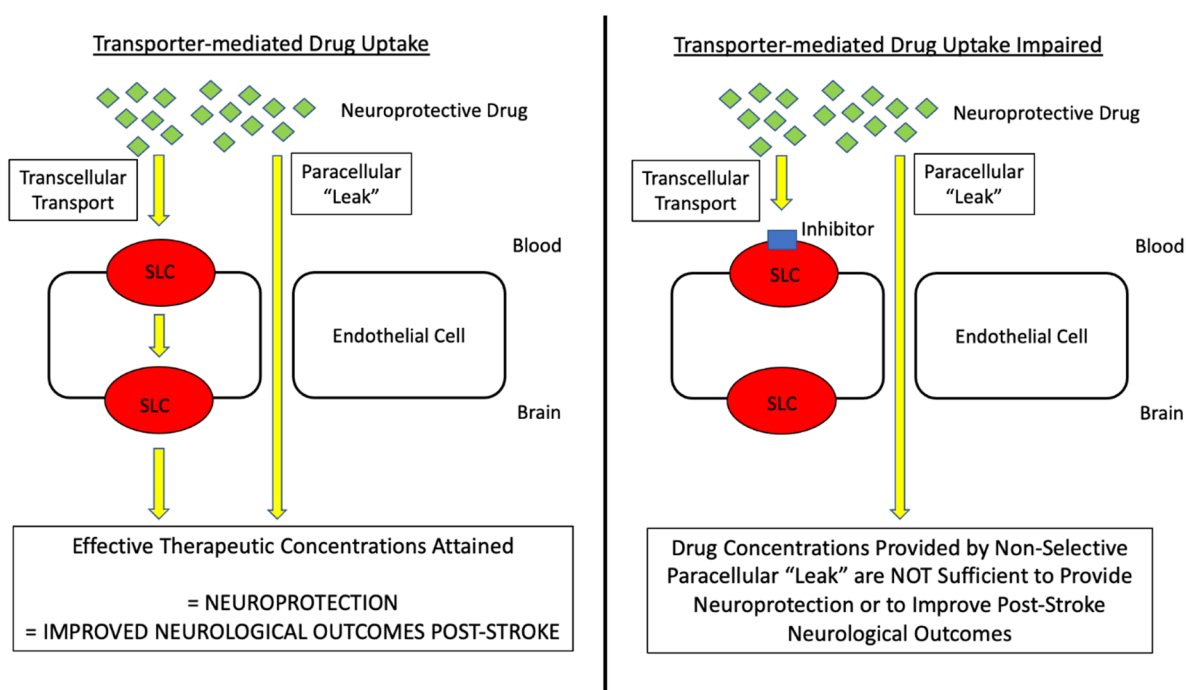


Figure 5. Interplay between SLC Transporter-Mediated Drug Uptake and Passive Paracellular Diffusion as Transport Mechanisms for Neuroprotective Drugs in Ischemic Stroke. Our data with memantine demonstrate that drugs that are transport substrates for SLC transporters such as Oct1/Oct2 require transporter-mediated blood-to-brain uptake to achieve efficacious concentrations following acute ischemic stroke. This leads to effective neuroprotection and an improvement in functional neurological performance during the acute phase of post-stroke recovery. When SLC transporter-mediated uptake is impaired, neuroprotective effects are attenuated despite the presence of “leak” into the brain via paracellular diffusion across the injured BBB.

In the context of ischemic stroke, the role of transporters in cerebral microvasculature must be understood in conjunction with the knowledge that BBB dysfunction occurs 4–6 h following ischemic injury [96]. This pathological event is known to involve changes in localization and expression of transmembrane and intracellular proteins that comprise the tight junction. The modulation of tight junction complexes is manifested as the reorganization of oligomeric protein assemblies, which can lead to profound changes in BBB permeability and the exacerbation of ischemic injury to the brain [128–130]. For example, the decreased expression of claudin-3 and occludin (i.e., transmembrane proteins that are known components of tight junction protein complexes) was reported at the BBB in mice subjected to MCAO, an effect that led to the progression of a cortical infarction and the onset of cerebral edema [131]. The dysregulation of claudin-5 and ZO-1 via the siRNA knock-down of A-kinase anchor protein 12 (AKAP12) was shown to cause enhanced endothelial cell monolayer permeability to fluorescein isothiocyanate-labeled dextran (40 kDa) under

in vitro OGD conditions [132]. Similar results were obtained in vivo where the conditional knockdown of NB-3 at the BBB resulted in the reduced protein expression of claudin-5, occludin, and ZO-1 and the subsequent enhancement in Evan's blue-albumin extravasation [133]. Additionally, reduced dimerization and/or oligomerization of occludin was observed in rat brain microvessels in an in vivo model of hypoxia/reoxygenation stress, a component of stroke pathogenesis [129]. The result of the occludin movement away from the tight junction is increased paracellular diffusion (i.e., "leak") of [<sup>14</sup>C]-sucrose, a vascular tracer with a molecular weight of 342 Da [129]. Under normal physiological conditions, tight junctions are responsible for the formation of a "physical barrier" between adjacent endothelial cells as evidenced by the restriction of paracellular diffusion to small molecule solutes as well as water [96,134,135]. This function requires the presence of transmembrane proteins (i.e., claudins, occludin) that can interact with each other to form a "seal" across the paracellular space that exists between apposing endothelial cells. Perhaps the most critical transmembrane tight junction protein is claudin-5 [130,136,137], whose essential role at the BBB is emphasized by the fact that claudin-5 knockout mice die within 10 h following birth [138]. The precise mechanism that causes death in these claudin-5 knockout mice is associated with the reduced control of a vascular "leak" in the cerebral microvasculature as evidenced by the increased extravasation of small molecule tracers (i.e., gadolinium and Hoechst 33258) that do not typically permeate the BBB [138]. In addition to claudin-5, brain microvascular integrity is maintained by transmembrane tight junction proteins such as occludin [128,129,139], tricellulin [140,141], and junctional adhesion molecules [142,143]. Intracellular accessory proteins such as ZO proteins, which are members of the membrane-associated guanylate kinase-like (MAGUK) protein family, interact with transmembrane tight junction proteins to facilitate linkage to the actin cytoskeleton. There are multiple publications that have shown the altered ZO-1 expression and/or localization and subsequent enhancement in BBB permeability following exposure to a pathophysiological stressor [144–146]. These observations imply that ZO-1 is essential to the maintenance of tight junction stability and function.

Despite the knowledge that disruption of the tight junction can increase a non-selective paracellular "leak" at the BBB, proteins that facilitate the selective transport of small molecules can overcome these changes in microvascular integrity. This enables endogenous BBB transporters to remain as primary determinants of CNS drug disposition despite marked tight junction protein complex dysfunction. Relevant to ischemic stroke, our recent study with memantine shows that cimetidine can block its brain uptake in ipsilateral and contralateral cerebral cortices from both MCAO animals and Sham-operated controls; however, the magnitude of memantine uptake in the ipsilateral cortex was greater than that measured in the contralateral cortex under MCAO conditions [127]. This finding suggests that a component of blood-to-brain memantine uptake results from non-selective paracellular diffusion (i.e., "leak"). Indeed, we demonstrated increased brain uptake of sucrose, a small molecule vascular tracer that does not permeate the intact BBB [137], following MCAO in whole brain tissue and in the ipsilateral cerebral cortex [127]. It must be emphasized that cimetidine treatment blocked the ability of memantine to improve neurological performance and to limit the progression of cerebral infarction and brain edema [127]. Our laboratory has previously demonstrated this concept in another disease state (i.e.,  $\lambda$ -carrageenan-induced inflammatory pain (CIP)). Using the CIP model [34], we have shown that tight junction protein complex integrity is disrupted and paracellular permeability to sucrose is enhanced following plantar injection of  $\lambda$ -carrageenan [139,147–149]; however, we also demonstrated that brain accumulation of morphine (i.e., a transport substrate for P-gp) in saline-treated animals and in  $\lambda$ -carrageenan-injected animals could only be increased in the presence of a competitive P-gp inhibitory drug (i.e., cyclosporine A) [34]. Taken together, these novel results imply that selective transport across microvascular endothelial cells (i.e., transcellular transport) remains a critical determinant of blood-to-brain drug delivery despite the opening of a non-selective paracellular diffusion route between



adjacent BBB endothelial cells (Figure 5). In short, it can no longer be assumed that the BBB is “open” following a pathological insult such as ischemia/reperfusion injury.

#### 4. Transport Mechanisms in Other Cell Types of the Neurovascular Unit

The BBB exists at the level of the brain microvascular endothelium. A central concept in BBB physiology is that endothelial cells cannot form barrier characteristics without coordinated communication networks with other CNS cell types [96,150,151]. Such networks gave rise to the concept of the “neurovascular unit (NVU)” that was formally defined by the National Institutes of Neurological Diseases and Stroke (NINDS) Stroke Progress Review Group in 2001 [152]. By emphasizing the co-operativity of cell–cell interactions between endothelial cells, glial cells (i.e., astrocytes, microglia), pericytes, and neurons as well as contributions from enzymes and proteins that comprise the extracellular matrix, the adoption of the NVU concept by the BBB field resulted in meaningful changes in the way that neurological diseases were studied [152]. It is now understood that glial cells and other CNS cellular constituents interact directly with brain microvascular endothelial cells to enable the development of a distinct barrier phenotype and to allow for rapid and dynamic responses to pathological and pharmacological stressors. This close relationship between neural and vascular function (i.e., neurovascular coupling) ensures that the brain receives an appropriate supply of oxygen and glucose and regulates other critical processes such as proteostasis, immune cell trafficking, temperature control, metabolic waste removal, and neurogenesis [153]. It is also important to note that transport proteins have been identified in these NVU cellular components. The isoforms of transporters in glial cells, pericytes, and neurons may differ from those expressed in endothelial cells; however, it is highly probable that these proteins work in concert with BBB transporters to control drug distribution within the CNS. Therefore, the functional expression of transporters in cellular compartments of the NVU requires more extensive evaluation in the setting of neurological diseases due to their potential role in modulating free drug concentrations at discrete molecular targets and, by extension, therapeutic effectiveness.

##### 4.1. Astrocytes

Astrocytes are the most numerous CNS cell type and play an essential role in the development and maintenance of the BBB phenotype [154–156]. They are localized between neuronal cell bodies and endothelial cells and cover more than 99% of brain microvasculature with their end-feet [151]. The seminal work by Janzer and Raff in 1987 indicated that astrocytes may be the CNS cell type that is primarily responsible for preventing paracellular “leak” at the BBB [157]. Since this study was published, many others have demonstrated the central involvement of astrocytes in the regulation of the BBB. For example, the injection of a toxic chemical (i.e., 3-chloropropanediol) in male Fisher F344 rats resulted in focal astrocyte loss and a subsequent reduction in tight junction protein expression (i.e., claudin-5, occludin, ZO-1) and increased paracellular permeability to 10 kDa dextran [158]. In vitro, porcine brain endothelial cells showed improved BBB properties when co-cultured in the presence of an immortalized rat astrocyte cell line (CTX TNA2), suggesting that astrocytes produce and secrete trophic factors that stimulate the development of the BBB phenotype [155]. More recently, human iPSC-derived astrocytes were observed to reduce paracellular “leak” and improve the integrity of the tight junction protein complexes continuity when co-cultured with endothelial cells also generated from iPSCs [156]. More recently, imaging modalities such as two-photon microscopy have provided critical information on the anatomical relationship between astrocytes and microvascular endothelial cells at the NVU [159]. In addition to their role in the maintenance of the BBB phenotype, astrocytes are involved in the regulation of water and ion transport across the brain microvascular endothelium [160,161] and control of neurotransmitter (i.e., glutamate) concentrations in the synapse [151]. Additionally, astrocytes are known to express volume-regulated anion channels (VRACs). These channels release excitatory amino acids such as glutamate in

a calcium-independent manner under pathological conditions that can lead to cellular swelling such as cerebral hypoxia [162] and ischemic stroke [163].

ABC transporters that are known to be expressed in astrocytes include P-gp [20,164,165], Bcrp [166], and MRP/Mrp isoforms [62,167,168]. Various MRP and OATP isoforms (i.e., OATP1A2, OATP1C1, OATP2B1, and OATP4A1) have been detected at the gene (i.e., mRNA) level in human glioma tissue [75]. Gao and colleagues observed that Oatp1a4 immunoreactivity did not colocalize with GFAP, suggesting that this transporter is not expressed in rat astrocytes [78]. In contrast, Oatp3a1 protein expression was detected in rat astrocytes, which implies a mechanism for prostaglandin and thyroxine transport in glial cells [169]. Several isoforms of organic cation transporters, including OCT3/Oct3, novel organic cation transporters (OCTNs in humans; Octns in rodents), and the plasma membrane monoamine transporter (PMAT in humans; Pmat in rodents) have been reported to be expressed in astrocytes [170]. The expression of these transporters in astrocytes suggests that these glial cells can play a critical role in the regulation of CNS drug distribution. That is, the complement of transporters in astrocytes may either sequester drugs within the cytoplasm (thereby preventing compounds from reaching their molecular target in the brain) or concentrate drugs in the brain extracellular fluid. The current knowledge in the field, as described by the glymphatic hypothesis, indicates that solutes are cleared from brain parenchyma by fluid flow mechanisms [171]. Supporters of the glymphatic hypothesis believe that this occurs via perivenous flow, a perception that is supported by the observation that tracer molecules entering the brain parenchyma via CSF or directly injected into the brain parenchyma will eventually distribute to the walls of large veins [171]. Opponents note that the fluid flow required to allow solutes to diffuse to the perivenous spaces is much greater than that supplied by CSF flow [171]. While we still do not have an adequate understanding of the mechanisms involved in the solute clearance from brain extracellular fluid, it is possible that passive diffusion and active transport processes are also involved. Additionally, it has been proposed that astrocyte cellular volume can fluctuate in response to physiological processes such as the sleep–wake transition, an effect that can lead to considerable changes in brain interstitial fluid volume [172]. Indeed, the release of fluid from astrocytes into the brain extracellular spaces can dilute drug concentrations and potentially affect the rate of transport by cellular compartments of brain parenchyma such as astrocytes. As such, the effect of astrocyte volume changes on drug transport and/or distribution in the brain requires further study.

#### 4.2. Microglia

Microglia are the innate immune cells of the brain and comprise 10–15% of all cell types in the CNS [173]. Microglia belong to the myeloid lineage, which also includes monocytes/macrophages, neutrophils, and platelets [174]. The pathophysiological functions of microglia are best exemplified in the setting of cerebral ischemia where they participate in the initiation and maintenance of neuroinflammation but also post-stroke neural repair and inflammatory dampening [174–176]. In the context of normal physiology, microglia exist in a quiescent state and are not capable of endocytotic and/or phagocytotic functions. Morphologically, these resting microglia are ramified as demarcated by a small (5–10  $\mu\text{m}$ ) cell body and possess multiple thin radial processes [175]. The role of microglial processes under resting conditions are to sense the presence of pathological mediators and/or potentially toxic substances in the brain extracellular space [175]. The ability to employ state-of-the-art technologies such as two-photon microscopy imaging has enabled the visualization of radial processes while microglia are in a resting state [177]. Under pathophysiological conditions, microglia can quickly shift to an activated phenotype. The level of microglial activation is strongly correlated with the type and severity of the CNS disease state. Activated microglia are routinely described as existing in two functional states that are designated as M1-like and M2-like. M1-like microglia perform pro-inflammatory and pro-killing functions and are often perceived to be deleterious to neuronal integrity [176]. In contrast, M2-like microglia are involved in the regulation of the central immunity, in-

flammatory control, and repair/injury resolution [176]. It is important to point out that M2-like microglia are also capable of phagocytosis, which provides a unique ability for these cells to clear cellular debris in the brain and contribute to neural repair [178]. The M1/M2 classification system is imperfect and there are several exceptions as has been shown in several studies on neurological disease states where substantial heterogeneity in microglial phenotypes have been demonstrated [179,180]. Indeed, microglial activation is strongly correlated with BBB dysfunction, which is an early event in neurological diseases, including ischemic stroke [96], Alzheimer's disease [181], and epilepsy [182].

Although previous studies have shown that microglia express ABC transporters, including P-gp, Mrp1, Mrp4, and Mrp5 [183–185], there are no published data outlining the expression of OATP/Oatp isoforms in microglia. In contrast, the uptake of ergothioneine was shown to be reduced in microglia isolated from Octn1 knockout mice, an observation that provides evidence for functional organic cation transporters in these glial cells [186]. Similar to astrocytes, the dynamic expression profile of transporters in microglia points toward a critical role in the regulation of drug distribution in the brain parenchyma. Clearly, more detailed studies on transporter functional expression in microglia are necessary to assess the ability of these cells to contribute to drug permeation and/or distribution in the CNS.

#### 4.3. Pericytes

In addition to glial cells, pericytes play a fundamental role in the control of BBB homeostasis [187–189]. Pericytes are flat, contractile mural cells that are localized to the basement membrane of small blood vessels in the CNS [190,191]. Pericytes maintain direct contact with endothelial cells as demonstrated by pericyte ablation experiments, which result in morphological changes in adjacent pericytes [192]. Specifically, these cells will stretch to provide coverage to “open” areas of the microvascular endothelium where pericytes no longer exist [192]. Several contractile and cytoskeletal proteins, including  $\alpha$ -smooth muscle actin ( $\alpha$ -SMA), neural/glial antigen-2 (NG-2), vimentin, desmin, myosin, and nestin, are expressed by pericytes, observations that support the contractile nature of these cells [190,193]. It is important to point out that  $\alpha$ -SMA content differs amongst pericytes, which suggests the existence of multiple pericyte populations (i.e., ensheathing pericytes, mesh pericytes, and thin-strand pericytes) which possess dissimilar characteristics [191]. Pericytes can be identified based on their expression of cell surface antigens, including the platelet-derived growth factor receptor- $\beta$ , aminopeptidases N and alanyl aminopeptidase (CD13), regulator of G-protein signaling-5 (RGS5), and melanoma cell adhesion molecule (MCAM; also known as CD146) [190]. The role of pericytes in the maintenance of BBB properties is believed to involve the secretion of angiopoietin, which induces the expression of the critical tight junction protein occludin [194]. Using genetically modified mice that exhibit a decreased mural cell density, Armulik and colleagues showed that the magnitude of microvascular pericyte coverage is inversely proportional to the paracellular permeability at the BBB [195]. Specifically, increased endothelial pericyte coverage resulted in decreased extravasation (i.e., “leak”) of large molecular weight tracers, such as Evan's blue-albumin, BSA-Alexa Fluor-555, IgG-DyLight 549, and horseradish peroxidase [195]. Enhanced BBB paracellular diffusion in response to pericyte loss differs across brain regions and the greatest permeability changes observed in the hippocampus, striatum, and cerebral cortex [196]. Although this study indicated that regional differences in the BBB leak did not result from dysfunction of tight junction protein complexes, a comprehensive examination of tight junction protein expression, localization, or dimerization/oligomerization in the pericyte-deficient *Pdgfr-b<sup>ret/ret</sup>* mouse model was not conducted [196]. Furthermore, BBB permeability was only measured using the large molecule tracer IgG, and smaller molecular weight indicators of BBB permeability were not incorporated into the study design. Therefore, data presented in the study by Villasenor and colleagues are not sufficient to conclude that reduced pericyte coverage at the BBB did not cause tight junction dysfunction.

To date, data on the localization and functional expression of transporters in pericytes is limited. P-gp has been localized to the plasma membrane of pericytes in rat and human brain tissue fixed in situ [20]. It is also noteworthy that pericytes have been shown to induce the expression of P-gp in brain microvascular endothelial cells [189,197], further emphasizing their role in the maintenance of the BBB phenotype. The expression of Mrp1, Mrp4, and Mrp5 mRNA has also been reported in pericytes isolated from bovine brain tissue [198]. P-gp and MRP1 have also been detected at the protein level in postmortem brain tissue samples [199]. While the exact role of these transporters in pericytes has not yet been elucidated, it is highly possible that the functional expression of ABC transporters in this NVU cell type can contribute to the barrier properties of cerebral microvasculature by restricting the blood-to-brain uptake of drugs. Despite these intriguing findings with respect to ABC transporters, there are no published studies that describe the expression and/or function of OATPs/Oatps or OCTs/Octs in pericytes. This suggests a critical knowledge gap that must be addressed to fully understand the dynamics of the drug transport mechanism at the NVU.

#### 4.4. Neurons

Neurons form the basic structural and functional component of the CNS. The primary function of neurons is to respond to stimuli by conducting electrical signals along conductive processes (i.e., axons). The conduction of electrical impulses results in the release of neurotransmitters that further regulate (positively and negatively) nearby neural responses [200]. This enables the brain to maintain a highly complex communication network. A few studies have reported expression of Oatp1a5 and Oatp2b1 in neurons isolated from rat and mouse brain [201]. The neuronal expression of Oatp2b1 is particularly compelling because many of its transport substrates (i.e., prostaglandins and leukotriene C<sub>4</sub>) are involved in inflammatory signaling and regulation [201]. Because neuroinflammation is a central component of multiple disease states, neuronal Oatp2b1 may represent a viable molecular target for the treatment of CNS diseases. Additionally, Oatp1a5 and/or Oatp2b1 may be involved in neurotoxicity due to their ability to transport cytotoxic microcystins [202]. Confocal microscopy imaging of human frontal cortical tissue demonstrated the expression of OATP3A1 in neurons at both the cell body and axon [169]. In vivo studies have shown that murine neurons express high levels of Oatp2a1 [203]. Additionally, OCT2 has been detected in human neurons [126], while Oct2 has been observed in murine neurons from the amygdala, dorsal raphe, frontal cortex, hippocampus, thalamus, median eminence, and pituitary gland [204,205]. In terms of efflux transporters, P-gp expression has been reported to be negligible in neurons but can be induced in response to pathological stressors [206–208]. In contrast, Mrp1 has been detected in primary cultures of murine prefrontal cortical neurons [209]. While these studies provide evidence for neuronal transporter expression, their role in CNS drug distribution and the effects on treatment effectiveness for neurological diseases requires more extensive evaluation. Such studies are warranted given the possible role of neuronal transporters in controlling drug distribution in the brain parenchyma and/or the access of therapeutic agents to their site of action.

## 5. Summary and Conclusions

The challenges of CNS drug delivery are best exemplified by ischemic stroke, which continues to be a significant cause of death and disability in the United States and worldwide. Since FDA-approved pharmacotherapy for ischemic stroke remains restricted to fibrinolytic therapy (i.e., r-tPA), safe and effective neuroprotective drugs are urgently needed. The application of these new chemical entities to the population of stroke patients is highly dependent upon transport across the BBB. Previous research by our laboratory has revealed several endogenous transporters with considerable potential to be targeted for optimization of CNS drug delivery; however, there are few studies in the preclinical stroke literature that describe the need to consider BBB transport mechanisms during therapeutic development. It is striking that statins and memantine, drugs that have shown varying

degrees of success in stroke, are substrates for uptake transporters that are expressed at the human brain microvascular endothelium (i.e., OATP1A2 for statins; OCT1/OCT2 for memantine) while other compounds (i.e., disufenton sodium) that are not transported at the BBB have failed in the clinic [98]. Our laboratory has undertaken important studies to address this critical issue. In the case of memantine, we have been successful by demonstrating that membrane transport mediated by Oct1/Oct2 is a critical step that enables this drug to function as a neuroprotectant in the setting of ischemic stroke [127]. Our work has revealed that the BBB does not simply remain “open” and “leaky” following stroke. Rather, endogenous transporters are still capable of providing selective delivery of their solutes to ischemic brain tissue despite the existence of a route for paracellular diffusion. It is also important to consider that CNS disposition of a single drug is often determined by the combined activity of many different transporters that can move their substrates in opposite directions. Understanding the “multi-transporter environment”, both at the BBB and in cellular compartments of the NVU, is essential to moving the field forward by performing detailed and translational preclinical studies that can be developed into effective treatments for neurological diseases. This concept is emphasized by our recent publication where we rigorously evaluated the combined effects of Oatp1a4, P-gp, and Bcrp on the disposition of statin drugs (i.e., atorvastatin, pravastatin, and rosuvastatin) in the brain [49]. Taken together, these findings will facilitate the discovery of treatment strategies where small molecule neuroprotective drugs can be delivered safely and efficiently. Continued research in this area will enable preclinical stroke research to take a “giant step forward” via incorporation of drug transporter experiments into in vivo models of experimental stroke to understand how therapeutics can attain efficacious concentrations in the brain. The future discovery of new chemical entities and/or the development of neuroprotective treatment strategies for ischemic stroke will greatly depend upon obtaining a rigorous understanding of BBB transport mechanisms. Success in this area will also depend upon expansion of transporter studies to include other cell types of the NVU. Indeed, transport mechanisms in astrocytes, microglia, pericytes, and neurons can play a key role in determining drug distribution in the brain parenchyma and, by extension, the capability of a therapeutic agent to reach its site of action. Overall, endogenous transporters at the BBB/NVU represent an untapped opportunity that must be pursued to accelerate the development of pharmacological strategies for the treatment of neurological diseases such as ischemic stroke.

**Author Contributions:** P.T.R. and T.P.D. wrote and edited the original draft of the manuscript. All authors have read and agreed to the published version of the manuscript.

**Funding:** This work is funded by grants from the National Institutes of Neurological Diseases and Stroke (NINDS; R01 NS084941) and the American Heart Association (19TPA34910113) to PTR and by a grant from the National Institute on Drug Abuse (NIDA; R01 DA051812) to TPD and PTR.

**Institutional Review Board Statement:** Not applicable.

**Informed Consent Statement:** Not applicable.

**Data Availability Statement:** Not applicable.

**Conflicts of Interest:** The authors do not have any conflict to declare.

## References

1. Boado, R.J.; Ka-Wai Hui, E.; Zhiqiang Lu, J.; Pardridge, W.M. Insulin receptor antibody-iduronate 2-sulfatase fusion protein: Pharmacokinetics, anti-drug antibody, and safety pharmacology in Rhesus monkeys. *Biotechnol. Bioeng.* **2014**, *111*, 2317–2325. [CrossRef] [PubMed]
2. Pardridge, W.M. Delivery of Biologics Across the Blood-Brain Barrier with Molecular Trojan Horse Technology. *BioDrugs* **2017**, *31*, 503–519. [CrossRef] [PubMed]
3. Chang, R.; Al Maghribi, A.; Vanderpoel, V.; Vasilevko, V.; Cribbs, D.H.; Boado, R.; Pardridge, W.M.; Sumbria, R.K. Brain Penetrating Bifunctional Erythropoietin-Transferrin Receptor Antibody Fusion Protein for Alzheimer’s Disease. *Mol. Pharm.* **2018**, *15*, 4963–4973. [CrossRef] [PubMed]

4. Haqqani, A.S.; Delaney, C.E.; Brunette, E.; Baumann, E.; Farrington, G.K.; Sisk, W.; Eldredge, J.; Ding, W.; Tremblay, T.L.; Stanimirovic, D.B. Endosomal trafficking regulates receptor-mediated transcytosis of antibodies across the blood brain barrier. *J. Cereb Blood Flow Metab.* **2018**, *38*, 727–740. [CrossRef] [PubMed]
5. Kariolis, M.S.; Wells, R.C.; Getz, J.A.; Kwan, W.; Mahon, C.S.; Tong, R.; Kim, D.J.; Srivastava, A.; Bedard, C.; Henne, K.R.; et al. Brain delivery of therapeutic proteins using an Fc fragment blood-brain barrier transport vehicle in mice and monkeys. *Sci. Transl. Med.* **2020**, *12*, eaay1359. [CrossRef] [PubMed]
6. Mikitsh, J.L.; Chacko, A.M. Pathways for small molecule delivery to the central nervous system across the blood-brain barrier. *Perspect Medicin. Chem.* **2014**, *6*, 11–24. [CrossRef]
7. Mahar Doan, K.M.; Humphreys, J.E.; Webster, L.O.; Wring, S.A.; Shampine, L.J.; Serabjit-Singh, C.J.; Adkison, K.K.; Polli, J.W. Passive permeability and P-glycoprotein-mediated efflux differentiate central nervous system (CNS) and non-CNS marketed drugs. *J. Pharmacol. Exp. Ther.* **2002**, *303*, 1029–1037. [CrossRef]
8. Banks, W.A. Characteristics of compounds that cross the blood-brain barrier. *BMC Neurol* **2009**, *9* (Suppl. S1), S3. [CrossRef]
9. Abdullahi, W.; Davis, T.P.; Ronaldson, P.T. Functional Expression of P-glycoprotein and Organic Anion Transporting Polypeptides at the Blood-Brain Barrier: Understanding Transport Mechanisms for Improved CNS Drug Delivery? *AAPS J.* **2017**, *19*, 931–939. [CrossRef]
10. Yang, J.; Reilly, B.G.; Davis, T.P.; Ronaldson, P.T. Modulation of Opioid Transport at the Blood-Brain Barrier by Altered ATP-Binding Cassette (ABC) Transporter Expression and Activity. *Pharmaceutics* **2018**, *10*, 192. [CrossRef]
11. Potschka, H. Modulating P-glycoprotein regulation: Future perspectives for pharmacoresistant epilepsies? *Epilepsia* **2010**, *51*, 1333–1347. [CrossRef] [PubMed]
12. Palmeira, A.; Sousa, E.; Vasconcelos, M.H.; Pinto, M.M. Three decades of P-gp inhibitors: Skimming through several generations and scaffolds. *Curr. Med. Chem.* **2012**, *19*, 1946–2025. [CrossRef] [PubMed]
13. Binkhathlan, Z.; Lavasanifar, A. P-glycoprotein inhibition as a therapeutic approach for overcoming multidrug resistance in cancer: Current status and future perspectives. *Curr. Cancer Drug Targets* **2013**, *13*, 326–346. [CrossRef] [PubMed]
14. Thomas, C.; Aller, S.G.; Beis, K.; Carpenter, E.P.; Chang, G.; Chen, L.; Dassa, E.; Dean, M.; Duong Van Hoa, F.; Ekiert, D.; et al. Structural and functional diversity calls for a new classification of ABC transporters. *FEBS Lett.* **2020**, *594*, 3767–3775. [CrossRef]
15. Sanchez-Covarrubias, L.; Slosky, L.M.; Thompson, B.J.; Davis, T.P.; Ronaldson, P.T. Transporters at CNS barrier sites: Obstacles or opportunities for drug delivery? *Curr. Pharm. Des.* **2014**, *20*, 1422–1449. [CrossRef]
16. Gottesman, M.M.; Hrycyna, C.A.; Schoenlein, P.V.; Germann, U.A.; Pastan, I. Genetic analysis of the multidrug transporter. *Annu. Rev. Genet.* **1995**, *29*, 607–649. [CrossRef]
17. Nilles, K.L.; Williams, E.I.; Betterton, R.D.; Davis, T.P.; Ronaldson, P.T. Blood-Brain Barrier Transporters: Opportunities for Therapeutic Development in Ischemic Stroke. *Int. J. Mol. Sci.* **2022**, *23*, 1898. [CrossRef]
18. Ling, V.; Thompson, L.H. Reduced permeability in CHO cells as a mechanism of resistance to colchicine. *J. Cell Physiol.* **1974**, *83*, 103–116. [CrossRef]
19. Beaulieu, E.; Demeule, M.; Ghitescu, L.; Beliveau, R. P-glycoprotein is strongly expressed in the luminal membranes of the endothelium of blood vessels in the brain. *Biochem. J.* **1997**, *326*, 539–544. [CrossRef]
20. Bendayan, R.; Ronaldson, P.T.; Gingras, D.; Bendayan, M. In situ localization of P-glycoprotein (ABCB1) in human and rat brain. *J. Histochem. Cytochem.* **2006**, *54*, 1159–1167. [CrossRef]
21. Schinkel, A.H.; Smit, J.J.; van Tellingen, O.; Beijnen, J.H.; Wagenaar, E.; van Deemter, L.; Mol, C.A.; van der Valk, M.A.; Robanus-Maandag, E.C.; te Riele, H.P.; et al. Disruption of the mouse mdr1a P-glycoprotein gene leads to a deficiency in the blood-brain barrier and to increased sensitivity to drugs. *Cell* **1994**, *77*, 491–502. [CrossRef]
22. Breuil, L.; Marie, S.; Goutal, S.; Auvity, S.; Truillet, C.; Saba, W.; Langer, O.; Caille, F.; Tournier, N. Comparative vulnerability of PET radioligands to partial inhibition of P-glycoprotein at the blood-brain barrier: A criterion of choice? *J. Cereb. Blood Flow Metab.* **2022**, *42*, 175–185. [CrossRef] [PubMed]
23. Dauchy, S.; Miller, F.; Couraud, P.O.; Weaver, R.J.; Weksler, B.; Romero, I.A.; Scherrmann, J.M.; De Waziers, I.; Declèves, X. Expression and transcriptional regulation of ABC transporters and cytochromes P450 in hCMEC/D3 human cerebral microvascular endothelial cells. *Biochem. Pharmacol.* **2009**, *77*, 897–909. [CrossRef] [PubMed]
24. McInerney, M.P.; Volitakis, I.; Bush, A.I.; Banks, W.A.; Short, J.L.; Nicolazzo, J.A. Ionophore and Biometal Modulation of P-glycoprotein Expression and Function in Human Brain Microvascular Endothelial Cells. *Pharm. Res.* **2018**, *35*, 83. [CrossRef] [PubMed]
25. Ronaldson, P.T.; Brzica, H.; Abdullahi, W.; Reilly, B.G.; Davis, T.P. Transport Properties of Statins by Organic Anion Transporting Polypeptide 1A2 and Regulation by Transforming Growth Factor-beta Signaling in Human Endothelial Cells. *J. Pharmacol. Exp. Ther.* **2021**, *376*, 148–160. [CrossRef] [PubMed]
26. Virgintino, D.; Robertson, D.; Errede, M.; Benagiano, V.; Girolamo, F.; Maiorano, E.; Roncali, L.; Bertossi, M. Expression of P-glycoprotein in human cerebral cortex microvessels. *J. Histochem. Cytochem.* **2002**, *50*, 1671–1676. [CrossRef]
27. Al-Majdoub, Z.M.; Al Feteisi, H.; Achour, B.; Warwood, S.; Neuhoff, S.; Rostami-Hodjegan, A.; Barber, J. Proteomic Quantification of Human Blood-Brain Barrier SLC and ABC Transporters in Healthy Individuals and Dementia Patients. *Mol. Pharm.* **2019**, *16*, 1220–1233. [CrossRef]

28. Billington, S.; Salphati, L.; Hop, C.; Chu, X.; Evers, R.; Burdette, D.; Rowbottom, C.; Lai, Y.; Xiao, G.; Humphreys, W.G.; et al. Interindividual and Regional Variability in Drug Transporter Abundance at the Human Blood-Brain Barrier Measured by Quantitative Targeted Proteomics. *Clin. Pharmacol. Ther.* **2019**, *106*, 228–237. [CrossRef]
29. Storelli, F.; Billington, S.; Kumar, A.R.; Unadkat, J.D. Abundance of P-Glycoprotein and Other Drug Transporters at the Human Blood-Brain Barrier in Alzheimer's Disease: A Quantitative Targeted Proteomic Study. *Clin. Pharmacol. Ther.* **2021**, *109*, 667–675. [CrossRef]
30. Wagner, C.C.; Bauer, M.; Karch, R.; Feurstein, T.; Kopp, S.; Chiba, P.; Kletter, K.; Loscher, W.; Muller, M.; Zeitlinger, M.; et al. A pilot study to assess the efficacy of tariquidar to inhibit P-glycoprotein at the human blood-brain barrier with (R)-11C-verapamil and PET. *J. Nucl. Med.* **2009**, *50*, 1954–1961. [CrossRef]
31. Muzi, M.; Mankoff, D.A.; Link, J.M.; Shoner, S.; Collier, A.C.; Sasongko, L.; Unadkat, J.D. Imaging of cyclosporine inhibition of P-glycoprotein activity using 11C-verapamil in the brain: Studies of healthy humans. *J. Nucl. Med.* **2009**, *50*, 1267–1275. [CrossRef]
32. Liu, L.; Collier, A.C.; Link, J.M.; Domino, K.B.; Mankoff, D.A.; Eary, J.F.; Spiekerman, C.F.; Hsiao, P.; Deo, A.K.; Unadkat, J.D. Modulation of P-glycoprotein at the Human Blood-Brain Barrier by Quinidine or Rifampin Treatment: A Positron Emission Tomography Imaging Study. *Drug Metab. Dispos.* **2015**, *43*, 1795–1804. [CrossRef] [PubMed]
33. Amin, M.L. P-glycoprotein Inhibition for Optimal Drug Delivery. *Drug Target Insights* **2013**, *7*, 27–34. [CrossRef] [PubMed]
34. Seelbach, M.J.; Brooks, T.A.; Egleton, R.D.; Davis, T.P. Peripheral inflammatory hyperalgesia modulates morphine delivery to the brain: A role for P-glycoprotein. *J. Neurochem.* **2007**, *102*, 1677–1690. [CrossRef] [PubMed]
35. Ronaldson, P.T.; Finch, J.D.; Demarco, K.M.; Quigley, C.E.; Davis, T.P. Inflammatory pain signals an increase in functional expression of organic anion transporting polypeptide 1a4 at the blood-brain barrier. *J. Pharmacol. Exp. Ther.* **2011**, *336*, 827–839. [CrossRef] [PubMed]
36. Bicker, J.; Fortuna, A.; Alves, G.; Soares-da-Silva, P.; Falcao, A. Elucidation of the Impact of P-glycoprotein and Breast Cancer Resistance Protein on the Brain Distribution of Catechol-O-Methyltransferase Inhibitors. *Drug Metab. Dispos.* **2017**, *45*, 1282–1291. [CrossRef]
37. Chen, Y.N.; Mickley, L.A.; Schwartz, A.M.; Acton, E.M.; Hwang, J.L.; Fojo, A.T. Characterization of adriamycin-resistant human breast cancer cells which display overexpression of a novel resistance-related membrane protein. *J. Biol. Chem.* **1990**, *265*, 10073–10080. [CrossRef]
38. Nakagawa, M.; Schneider, E.; Dixon, K.H.; Horton, J.; Kelley, K.; Morrow, C.; Cowan, K.H. Reduced intracellular drug accumulation in the absence of P-glycoprotein (mdr1) overexpression in mitoxantrone-resistant human MCF-7 breast cancer cells. *Cancer Res.* **1992**, *52*, 6175–6181.
39. Lee, J.S.; Scala, S.; Matsumoto, Y.; Dickstein, B.; Robey, R.; Zhan, Z.; Altenberg, G.; Bates, S.E. Reduced drug accumulation and multidrug resistance in human breast cancer cells without associated P-glycoprotein or MRP overexpression. *J. Cell Biochem.* **1997**, *65*, 513–526. [CrossRef]
40. Doyle, L.A.; Yang, W.; Abruzzo, L.V.; Krognmann, T.; Gao, Y.; Rishi, A.K.; Ross, D.D. A multidrug resistance transporter from human MCF-7 breast cancer cells. *Proc. Natl. Acad. Sci. USA* **1998**, *95*, 15665–15670. [CrossRef]
41. Graf, G.A.; Yu, L.; Li, W.P.; Gerard, R.; Tuma, P.L.; Cohen, J.C.; Hobbs, H.H. ABCG5 and ABCG8 are obligate heterodimers for protein trafficking and biliary cholesterol excretion. *J. Biol. Chem.* **2003**, *278*, 48275–48282. [CrossRef] [PubMed]
42. Graf, G.A.; Li, W.P.; Gerard, R.D.; Gelissen, I.; White, A.; Cohen, J.C.; Hobbs, H.H. Coexpression of ATP-binding cassette proteins ABCG5 and ABCG8 permits their transport to the apical surface. *J. Clin. Investig.* **2002**, *110*, 659–669. [CrossRef] [PubMed]
43. Eisenblatter, T.; Huwel, S.; Galla, H.J. Characterisation of the brain multidrug resistance protein (BMDP/ABCG2/BCRP) expressed at the blood-brain barrier. *Brain Res.* **2003**, *971*, 221–231. [CrossRef]
44. Zhang, W.; Mojsilovic-Petrovic, J.; Andrade, M.F.; Zhang, H.; Ball, M.; Stanimirovic, D.B. The expression and functional characterization of ABCG2 in brain endothelial cells and vessels. *FASEB J.* **2003**, *17*, 2085–2087. [CrossRef] [PubMed]
45. Aronica, E.; Gorter, J.A.; Redeker, S.; van Vliet, E.A.; Ramkema, M.; Scheffer, G.L.; Scheper, R.J.; van der Valk, P.; Leenstra, S.; Baayen, J.C.; et al. Localization of breast cancer resistance protein (BCRP) in microvessel endothelium of human control and epileptic brain. *Epilepsia* **2005**, *46*, 849–857. [CrossRef]
46. Ohtsuki, S.; Ikeda, C.; Uchida, Y.; Sakamoto, Y.; Miller, F.; Glacial, F.; Decleves, X.; Scherrmann, J.M.; Couraud, P.O.; Kubo, Y.; et al. Quantitative targeted absolute proteomic analysis of transporters, receptors and junction proteins for validation of human cerebral microvascular endothelial cell line hCMEC/D3 as a human blood-brain barrier model. *Mol. Pharm.* **2013**, *10*, 289–296. [CrossRef]
47. Uchida, Y.; Ohtsuki, S.; Katsukura, Y.; Ikeda, C.; Suzuki, T.; Kamiie, J.; Terasaki, T. Quantitative targeted absolute proteomics of human blood-brain barrier transporters and receptors. *J. Neurochem.* **2011**, *117*, 333–345. [CrossRef]
48. Polli, J.W.; Olson, K.L.; Chism, J.P.; John-Williams, L.S.; Yeager, R.L.; Woodard, S.M.; Otto, V.; Castellino, S.; Demby, V.E. An unexpected synergist role of P-glycoprotein and breast cancer resistance protein on the central nervous system penetration of the tyrosine kinase inhibitor lapatinib (N-{3-chloro-4-[(3-fluorobenzoyloxy)phenyl]-6-[5-([2-(methylsulfonyl)ethyl]amino)methyl]-2-furyl]-4-quinazolinamine; GW572016). *Drug Metab. Dispos.* **2009**, *37*, 439–442. [CrossRef]
49. Betterton, R.D.; Abdullahi, W.; Williams, E.I.; Lochhead, J.L.; Brzica, H.; Stanton, J.A.; Reddell, E.; Ogonnaya, C.; Davis, T.P.; Ronaldson, P.T. Regulation of Blood-Brain Barrier Transporters by Transforming Growth Factor-beta / Activin Receptor-Like Kinase 1 (TGF-beta / ALK1) Signaling: Relevance to the Brain Disposition of 3-Hydroxy-3-Methylglutaryl Coenzyme A (HMG-CoA) Reductase Inhibitors (i.e., Statins). *Drug Metab. Dispos.* **2022**, *50*, 942–956. [CrossRef]

50. Agarwal, S.; Hartz, A.M.; Elmquist, W.F.; Bauer, B. Breast cancer resistance protein and P-glycoprotein in brain cancer: Two gatekeepers team up. *Curr. Pharm. Des.* **2011**, *17*, 2793–2802. [CrossRef]
51. Laramy, J.K.; Kim, M.; Parrish, K.E.; Sarkaria, J.N.; Elmquist, W.F. Pharmacokinetic Assessment of Cooperative Efflux of the Multitargeted Kinase Inhibitor Ponatinib Across the Blood-Brain Barrier. *J. Pharmacol. Exp. Ther.* **2018**, *365*, 249–261. [CrossRef] [PubMed]
52. Mittapalli, R.K.; Vaidhyanathan, S.; Sane, R.; Elmquist, W.F. Impact of P-glycoprotein (ABCB1) and breast cancer resistance protein (ABCG2) on the brain distribution of a novel BRAF inhibitor: Vemurafenib (PLX4032). *J. Pharmacol. Exp. Ther.* **2012**, *342*, 33–40. [CrossRef] [PubMed]
53. Agarwal, S.; Elmquist, W.F. Insight into the cooperation of P-glycoprotein (ABCB1) and breast cancer resistance protein (ABCG2) at the blood-brain barrier: A case study examining sorafenib efflux clearance. *Mol. Pharm.* **2012**, *9*, 678–684. [CrossRef] [PubMed]
54. Hoque, M.T.; Kis, O.; De Rosa, M.F.; Bendayan, R. Raltegravir permeability across blood-tissue barriers and the potential role of drug efflux transporters. *Antimicrob. Agents Chemother.* **2015**, *59*, 2572–2582. [CrossRef] [PubMed]
55. Helms, H.C.; Hersom, M.; Kuhlmann, L.B.; Badolo, L.; Nielsen, C.U.; Brodin, B. An electrically tight in vitro blood-brain barrier model displays net brain-to-blood efflux of substrates for the ABC transporters, P-gp, Bcrp and Mrp-1. *AAPS J.* **2014**, *16*, 1046–1055. [CrossRef] [PubMed]
56. Brechbuhl, H.M.; Gould, N.; Kachadourian, R.; Riekhof, W.R.; Voelker, D.R.; Day, B.J. Glutathione transport is a unique function of the ATP-binding cassette protein ABCG2. *J. Biol. Chem.* **2010**, *285*, 16582–16587. [CrossRef]
57. Ifergan, I.; Shafran, A.; Jansen, G.; Hooijberg, J.H.; Scheffer, G.L.; Assaraf, Y.G. Folate deprivation results in the loss of breast cancer resistance protein (BCRP/ABCG2) expression. A role for BCRP in cellular folate homeostasis. *J. Biol. Chem.* **2004**, *279*, 25527–25534. [CrossRef]
58. Ji, Y.; Morris, M.E. Membrane transport of dietary phenethyl isothiocyanate by ABCG2 (breast cancer resistance protein). *Mol. Pharm.* **2005**, *2*, 414–419. [CrossRef]
59. Kadry, H.; Noorani, B.; Cucullo, L. A blood-brain barrier overview on structure, function, impairment, and biomarkers of integrity. *Fluids Barriers CNS* **2020**, *17*, 69. [CrossRef]
60. Su, W.; Pasternak, G.W. The role of multidrug resistance-associated protein in the blood-brain barrier and opioid analgesia. *Synapse* **2013**, *67*, 609–619. [CrossRef]
61. Kanamitsu, K.; Kusuhara, H.; Schuetz, J.D.; Takeuchi, K.; Sugiyama, Y. Investigation of the Importance of Multidrug Resistance-Associated Protein 4 (Mrp4/Abcc4) in the Active Efflux of Anionic Drugs Across the Blood-Brain Barrier. *J. Pharm. Sci.* **2017**, *106*, 2566–2575. [CrossRef] [PubMed]
62. Ronaldson, P.T.; Bendayan, R. HIV-1 viral envelope glycoprotein gp120 produces oxidative stress and regulates the functional expression of multidrug resistance protein-1 (Mrp1) in glial cells. *J. Neurochem.* **2008**, *106*, 1298–1313. [CrossRef] [PubMed]
63. Akanuma, S.I.; Hashimoto, K.; Yoshida, Y.; Kubo, Y.; Hosoya, K.I. Inflammation-Induced Attenuation of Prostaglandin D2 Elimination across Rat Blood-Brain Barrier: Involvement of the Downregulation of Organic Anion Transporter 3 and Multidrug Resistance-Associated Protein 4. *Biol. Pharm. Bull.* **2020**, *43*, 1669–1677. [CrossRef] [PubMed]
64. Kalvass, J.C.; Polli, J.W.; Bourdet, D.L.; Feng, B.; Huang, S.M.; Liu, X.; Smith, Q.R.; Zhang, L.K.; Zamek-Gliszczynski, M.J.; International Transporter, C. Why clinical modulation of efflux transport at the human blood-brain barrier is unlikely: The ITC evidence-based position. *Clin. Pharmacol. Ther.* **2013**, *94*, 80–94. [CrossRef] [PubMed]
65. Colas, C.; Ung, P.M.; Schlessinger, A. SLC Transporters: Structure, Function, and Drug Discovery. *Medchemcomm* **2016**, *7*, 1069–1081. [CrossRef]
66. Schumann, T.; Konig, J.; Henke, C.; Willmes, D.M.; Bornstein, S.R.; Jordan, J.; Fromm, M.F.; Birkenfeld, A.L. Solute Carrier Transporters as Potential Targets for the Treatment of Metabolic Disease. *Pharmacol. Rev.* **2020**, *72*, 343–379. [CrossRef]
67. Brzica, H.; Abdullahi, W.; Ibbotson, K.; Ronaldson, P.T. Role of Transporters in Central Nervous System Drug Delivery and Blood-Brain Barrier Protection: Relevance to Treatment of Stroke. *J. Cent. Nerv. Syst. Dis.* **2017**, *9*, 1179573517693802. [CrossRef]
68. Ronaldson, P.T.; Davis, T.P. Targeted drug delivery to treat pain and cerebral hypoxia. *Pharmacol. Rev.* **2013**, *65*, 291–314. [CrossRef]
69. Betterton, R.D.; Davis, T.P.; Ronaldson, P.T. Organic Cation Transporter (OCT/OCTN) Expression at Brain Barrier Sites: Focus on CNS Drug Delivery. *Handb. Exp. Pharmacol.* **2021**, *266*, 301–328. [CrossRef]
70. Thompson, B.J.; Sanchez-Covarrubias, L.; Slosky, L.M.; Zhang, Y.; Laracuenta, M.L.; Ronaldson, P.T. Hypoxia/reoxygenation stress signals an increase in organic anion transporting polypeptide 1a4 (Oatp1a4) at the blood-brain barrier: Relevance to CNS drug delivery. *J. Cereb. Blood Flow Metab.* **2014**, *34*, 699–707. [CrossRef]
71. Abdullahi, W.; Brzica, H.; Hirsch, N.A.; Reilly, B.G.; Ronaldson, P.T. Functional Expression of Organic Anion Transporting Polypeptide 1a4 Is Regulated by Transforming Growth Factor-beta/Activin Receptor-like Kinase 1 Signaling at the Blood-Brain Barrier. *Mol. Pharmacol.* **2018**, *94*, 1321–1333. [CrossRef] [PubMed]
72. Abdullahi, W.; Brzica, H.; Ibbotson, K.; Davis, T.P.; Ronaldson, P.T. Bone morphogenetic protein-9 increases the functional expression of organic anion transporting polypeptide 1a4 at the blood-brain barrier via the activin receptor-like kinase-1 receptor. *J. Cereb. Blood Flow Metab.* **2017**, *37*, 2340–2345. [CrossRef] [PubMed]
73. Brzica, H.; Abdullahi, W.; Reilly, B.G.; Ronaldson, P.T. Sex-specific differences in organic anion transporting polypeptide 1a4 (Oatp1a4) functional expression at the blood-brain barrier in Sprague-Dawley rats. *Fluids Barriers CNS* **2018**, *15*, 25. [CrossRef] [PubMed]



74. Lee, W.; Glaeser, H.; Smith, L.H.; Roberts, R.L.; Moeckel, G.W.; Gervasini, G.; Leake, B.F.; Kim, R.B. Polymorphisms in human organic anion-transporting polypeptide 1A2 (OATP1A2): Implications for altered drug disposition and central nervous system drug entry. *J. Biol. Chem.* **2005**, *280*, 9610–9617. [CrossRef]
75. Bronger, H.; Konig, J.; Kopplow, K.; Steiner, H.H.; Ahmadi, R.; Herold-Mende, C.; Keppler, D.; Nies, A.T. ABCC drug efflux pumps and organic anion uptake transporters in human gliomas and the blood-tumor barrier. *Cancer Res.* **2005**, *65*, 11419–11428. [CrossRef]
76. Roberts, L.M.; Black, D.S.; Raman, C.; Woodford, K.; Zhou, M.; Haggerty, J.E.; Yan, A.T.; Cwirla, S.E.; Grindstaff, K.K. Subcellular localization of transporters along the rat blood-brain barrier and blood-cerebral-spinal fluid barrier by in vivo biotinylation. *Neuroscience* **2008**, *155*, 423–438. [CrossRef]
77. Gao, B.; Stieger, B.; Noe, B.; Fritschy, J.M.; Meier, P.J. Localization of the organic anion transporting polypeptide 2 (Oatp2) in capillary endothelium and choroid plexus epithelium of rat brain. *J. Histochem. Cytochem.* **1999**, *47*, 1255–1264. [CrossRef]
78. Gao, B.; Hagenbuch, B.; Kullak-Ublick, G.A.; Benke, D.; Aguzzi, A.; Meier, P.J. Organic anion-transporting polypeptides mediate transport of opioid peptides across blood-brain barrier. *J. Pharmacol. Exp. Ther.* **2000**, *294*, 73–79.
79. Gao, B.; Vavricka, S.R.; Meier, P.J.; Stieger, B. Differential cellular expression of organic anion transporting peptides OATP1A2 and OATP2B1 in the human retina and brain: Implications for carrier-mediated transport of neuropeptides and neurosteroids in the CNS. *Pflugers Arch.* **2015**, *467*, 1481–1493. [CrossRef]
80. Schafer, A.M.; Meyer Zu Schwabedissen, H.E.; Bien-Moller, S.; Hubeny, A.; Vogelgesang, S.; Oswald, S.; Grube, M. OATP1A2 and OATP2B1 Are Interacting with Dopamine-Receptor Agonists and Antagonists. *Mol. Pharm.* **2020**, *17*, 1987–1995. [CrossRef]
81. Schafer, A.M.; Meyer Zu Schwabedissen, H.E.; Grube, M. Expression and Function of Organic Anion Transporting Polypeptides in the Human Brain: Physiological and Pharmacological Implications. *Pharmaceutics* **2021**, *13*, 834. [CrossRef] [PubMed]
82. Klaassen, C.D.; Aleksunes, L.M. Xenobiotic, bile acid, and cholesterol transporters: Function and regulation. *Pharmacol. Rev.* **2010**, *62*, 1–96. [CrossRef] [PubMed]
83. Grube, M.; Hagen, P.; Jedlitschky, G. Neurosteroid Transport in the Brain: Role of ABC and SLC Transporters. *Front. Pharmacol.* **2018**, *9*, 354. [CrossRef]
84. Sung, J.H.; Yu, K.H.; Park, J.S.; Tsuruo, T.; Kim, D.D.; Shim, C.K.; Chung, S.J. Saturable distribution of tacrine into the striatal extracellular fluid of the rat: Evidence of involvement of multiple organic cation transporters in the transport. *Drug Metab. Dispos.* **2005**, *33*, 440–448. [CrossRef] [PubMed]
85. Wu, K.C.; Lu, Y.H.; Peng, Y.H.; Tsai, T.F.; Kao, Y.H.; Yang, H.T.; Lin, C.J. Decreased expression of organic cation transporters, Oct1 and Oct2, in brain microvessels and its implication to MPTP-induced dopaminergic toxicity in aged mice. *J. Cereb. Blood Flow Metab.* **2015**, *35*, 37–47. [CrossRef]
86. Sekhar, G.N.; Georgian, A.R.; Sanderson, L.; Vizcay-Barrena, G.; Brown, R.C.; Muresan, P.; Fleck, R.A.; Thomas, S.A. Organic cation transporter 1 (OCT1) is involved in pentamidine transport at the human and mouse blood-brain barrier (BBB). *PLoS ONE* **2017**, *12*, e0173474. [CrossRef]
87. Lin, C.J.; Tai, Y.; Huang, M.T.; Tsai, Y.F.; Hsu, H.J.; Tzen, K.Y.; Liou, H.H. Cellular localization of the organic cation transporters, OCT1 and OCT2, in brain microvessel endothelial cells and its implication for MPTP transport across the blood-brain barrier and MPTP-induced dopaminergic toxicity in rodents. *J. Neurochem.* **2010**, *114*, 717–727. [CrossRef]
88. Sandoval, P.J.; Zorn, K.M.; Clark, A.M.; Ekins, S.; Wright, S.H. Assessment of Substrate-Dependent Ligand Interactions at the Organic Cation Transporter OCT2 Using Six Model Substrates. *Mol. Pharmacol.* **2018**, *94*, 1057–1068. [CrossRef]
89. Hiasa, M.; Matsumoto, T.; Komatsu, T.; Moriyama, Y. Wide variety of locations for rodent MATE1, a transporter protein that mediates the final excretion step for toxic organic cations. *Am. J. Physiol. Cell Physiol.* **2006**, *291*, C678–C686. [CrossRef]
90. Chaves, C.; Campanelli, F.; Chapy, H.; Gomez-Zepeda, D.; Glacial, F.; Smirnova, M.; Taghi, M.; Pallud, J.; Perriere, N.; Declèves, X.; et al. An Interspecies Molecular and Functional Study of Organic Cation Transporters at the Blood-Brain Barrier: From Rodents to Humans. *Pharmaceutics* **2020**, *12*, 308. [CrossRef]
91. Goralski, K.B.; Lou, G.; Prowse, M.T.; Gorboulev, V.; Volk, C.; Koepsell, H.; Sitar, D.S. The cation transporters rOCT1 and rOCT2 interact with bicarbonate but play only a minor role for amantadine uptake into rat renal proximal tubules. *J. Pharmacol. Exp. Ther.* **2002**, *303*, 959–968. [CrossRef] [PubMed]
92. Mehta, D.C.; Short, J.L.; Nicolazzo, J.A. Memantine Transport across the Mouse Blood-Brain Barrier Is Mediated by a Cationic Influx H<sup>+</sup> Antiporter. *Mol. Pharm.* **2013**, *10*, 4491–4498. [CrossRef] [PubMed]
93. GBD 2019 Stroke Collaborators. Global, regional, and national burden of stroke and its risk factors, 1990–2019: A systematic analysis for the Global Burden of Disease Study 2019. *Lancet Neurol.* **2021**, *20*, 795–820. [CrossRef]
94. Tsao, C.W.; Aday, A.W.; Almarazgoq, Z.I.; Alonso, A.; Beaton, A.Z.; Bittencourt, M.S.; Boehme, A.K.; Buxton, A.E.; Carson, A.P.; Commodore-Mensah, Y.; et al. Heart Disease and Stroke Statistics-2022 Update: A Report From the American Heart Association. *Circulation* **2022**, *145*, e153–e639. [CrossRef]
95. Liu, S.; Levine, S.R.; Winn, H.R. Targeting ischemic penumbra: Part I—from pathophysiology to therapeutic strategy. *J. Exp. Stroke Transl. Med.* **2010**, *3*, 47–55. [CrossRef]
96. Abdullahi, W.; Tripathi, D.; Ronaldson, P.T. Blood-brain barrier dysfunction in ischemic stroke: Targeting tight junctions and transporters for vascular protection. *Am. J. Physiol. Cell Physiol.* **2018**, *315*, C343–C356. [CrossRef]
97. Manning, N.W.; Campbell, B.C.; Oxley, T.J.; Chapot, R. Acute ischemic stroke: Time, penumbra, and reperfusion. *Stroke* **2014**, *45*, 640–644. [CrossRef]

98. Williams, E.I.; Betterton, R.D.; Davis, T.P.; Ronaldson, P.T. Transporter-Mediated Delivery of Small Molecule Drugs to the Brain: A Critical Mechanism That Can Advance Therapeutic Development for Ischemic Stroke. *Pharmaceutics* **2020**, *12*, 154. [CrossRef]
99. National Institute of Neurological, D.; Stroke rt, P.A.S.S.G. Tissue plasminogen activator for acute ischemic stroke. *N. Engl. J. Med.* **1995**, *333*, 1581–1587. [CrossRef]
100. O'Carroll, C.B.; Rubin, M.N.; Chong, B.W. What is the Role for Intra-Arterial Therapy in Acute Stroke Intervention? *Neurohospitalist* **2015**, *5*, 122–132. [CrossRef]
101. Tymianski, M. Combining Neuroprotection With Endovascular Treatment of Acute Stroke: Is There Hope? *Stroke* **2017**, *48*, 1700–1705. [CrossRef] [PubMed]
102. Shi, L.; Rocha, M.; Leak, R.K.; Zhao, J.; Bhatia, T.N.; Mu, H.; Wei, Z.; Yu, F.; Weiner, S.L.; Ma, F.; et al. A new era for stroke therapy: Integrating neurovascular protection with optimal reperfusion. *J. Cereb. Blood Flow Metab.* **2018**, *38*, 2073–2091. [CrossRef] [PubMed]
103. Goyal, M.; Menon, B.K.; van Zwam, W.H.; Dippel, D.W.; Mitchell, P.J.; Demchuk, A.M.; Davalos, A.; Majoie, C.B.; van der Lugt, A.; de Miquel, M.A.; et al. Endovascular thrombectomy after large-vessel ischaemic stroke: A meta-analysis of individual patient data from five randomised trials. *Lancet* **2016**, *387*, 1723–1731. [CrossRef]
104. Nogueira, R.G.; Jadhav, A.P.; Haussen, D.C.; Bonafe, A.; Budzik, R.F.; Bhuva, P.; Yavagal, D.R.; Ribo, M.; Cognard, C.; Hanel, R.A.; et al. Thrombectomy 6 to 24 Hours after Stroke with a Mismatch between Deficit and Infarct. *N. Engl. J. Med.* **2018**, *378*, 11–21. [CrossRef]
105. Pan, J.; Konstas, A.A.; Bateman, B.; Ortolano, G.A.; Pile-Spellman, J. Reperfusion injury following cerebral ischemia: Pathophysiology, MR imaging, and potential therapies. *Neuroradiology* **2007**, *49*, 93–102. [CrossRef]
106. Candelario-Jalil, E. Injury and repair mechanisms in ischemic stroke: Considerations for the development of novel neurotherapeutics. *Curr. Opin. Investig. Drugs* **2009**, *10*, 644–654.
107. Eltzschig, H.K.; Eckle, T. Ischemia and reperfusion—from mechanism to translation. *Nat. Med.* **2011**, *17*, 1391–1401. [CrossRef]
108. Nour, M.; Scalzo, F.; Liebeskind, D.S. Ischemia-reperfusion injury in stroke. *Interv. Neurol.* **2013**, *1*, 185–199. [CrossRef]
109. Lyden, P.; Pryor, K.E.; Coffey, C.S.; Cudkowicz, M.; Conwit, R.; Jadhav, A.; Sawyer, R.N., Jr.; Claassen, J.; Adeoye, O.; Song, S.; et al. Final Results of the RHAPSODY Trial: A Multi-Center, Phase 2 Trial Using a Continual Reassessment Method to Determine the Safety and Tolerability of 3K3A-APC, A Recombinant Variant of Human Activated Protein C, in Combination with Tissue Plasminogen Activator, Mechanical Thrombectomy or both in Moderate to Severe Acute Ischemic Stroke. *Ann. Neurol.* **2019**, *85*, 125–136. [CrossRef]
110. Turner, R.C.; Lucke-Wold, B.; Lucke-Wold, N.; Elliott, A.S.; Logsdon, A.F.; Rosen, C.L.; Huber, J.D. Neuroprotection for ischemic stroke: Moving past shortcomings and identifying promising directions. *Int. J. Mol. Sci.* **2013**, *14*, 1890–1917. [CrossRef]
111. Spudich, A.; Kilic, E.; Xing, H.; Kilic, U.; Rentsch, K.M.; Wunderli-Allenspach, H.; Bassetti, C.L.; Hermann, D.M. Inhibition of multidrug resistance transporter-1 facilitates neuroprotective therapies after focal cerebral ischemia. *Nat. Neurosci.* **2006**, *9*, 487–488. [CrossRef] [PubMed]
112. DeMars, K.M.; Yang, C.; Hawkins, K.E.; McCrea, A.O.; Siwarski, D.M.; Candelario-Jalil, E. Spatiotemporal Changes in P-glycoprotein Levels in Brain and Peripheral Tissues Following Ischemic Stroke in Rats. *J. Exp. Neurosci.* **2017**, *11*, 1179069517701741. [CrossRef] [PubMed]
113. Chen, X.; Zhou, Z.W.; Xue, C.C.; Li, X.X.; Zhou, S.F. Role of P-glycoprotein in restricting the brain penetration of tanshinone IIA, a major active constituent from the root of *Salvia miltiorrhiza* Bunge, across the blood-brain barrier. *Xenobiotica* **2007**, *37*, 635–678. [CrossRef] [PubMed]
114. Tornabene, E.; Helms, H.C.C.; Pedersen, S.F.; Brodin, B. Effects of oxygen-glucose deprivation (OGD) on barrier properties and mRNA transcript levels of selected marker proteins in brain endothelial cells/astrocyte co-cultures. *PLoS ONE* **2019**, *14*, e0221103. [CrossRef]
115. Ose, A.; Kusuhara, H.; Endo, C.; Tohyama, K.; Miyajima, M.; Kitamura, S.; Sugiyama, Y. Functional characterization of mouse organic anion transporting peptide 1a4 in the uptake and efflux of drugs across the blood-brain barrier. *Drug Metab. Dispos.* **2010**, *38*, 168–176. [CrossRef]
116. Liu, H.; Yu, N.; Lu, S.; Ito, S.; Zhang, X.; Prasad, B.; He, E.; Lu, X.; Li, Y.; Wang, F.; et al. Solute Carrier Family of the Organic Anion-Transporting Polypeptides 1A2- Madin-Darby Canine Kidney II: A Promising In Vitro System to Understand the Role of Organic Anion-Transporting Polypeptide 1A2 in Blood-Brain Barrier Drug Penetration. *Drug Metab. Dispos.* **2015**, *43*, 1008–1018. [CrossRef]
117. Sano, Y.; Mizuno, T.; Mochizuki, T.; Uchida, Y.; Umetsu, M.; Terasaki, T.; Kusuhara, H. Evaluation of Organic Anion Transporter 1A2-knock-in Mice as a Model of Human Blood-brain Barrier. *Drug Metab. Dispos.* **2018**, *46*, 1767–1775. [CrossRef]
118. Albekairi, T.H.; Vaidya, B.; Patel, R.; Nozohouri, S.; Villalba, H.; Zhang, Y.; Lee, Y.S.; Al-Ahmad, A.; Abbruscato, T.J. Brain Delivery of a Potent Opioid Receptor Agonist, Biphalin during Ischemic Stroke: Role of Organic Anion Transporting Polypeptide (OATP). *Pharmaceutics* **2019**, *11*, 467. [CrossRef]
119. Yang, L.; Islam, M.R.; Karamyan, V.T.; Abbruscato, T.J. In vitro and in vivo efficacy of a potent opioid receptor agonist, biphalin, compared to subtype-selective opioid receptor agonists for stroke treatment. *Brain Res.* **2015**, *1609*, 1–11. [CrossRef]
120. Yang, L.; Shah, K.; Wang, H.; Karamyan, V.T.; Abbruscato, T.J. Characterization of neuroprotective effects of biphalin, an opioid receptor agonist, in a model of focal brain ischemia. *J. Pharmacol. Exp. Ther.* **2011**, *339*, 499–508. [CrossRef]

121. Yang, L.; Wang, H.; Shah, K.; Karamyan, V.T.; Abbruscato, T.J. Opioid receptor agonists reduce brain edema in stroke. *Brain Res.* **2011**, *1383*, 307–316. [CrossRef] [PubMed]
122. Islam, M.R.; Yang, L.; Lee, Y.S.; Hruby, V.J.; Karamyan, V.T.; Abbruscato, T.J. Enkephalin-Fentanyl Multifunctional Opioids as Potential Neuroprotectants for Ischemic Stroke Treatment. *Curr. Pharm. Des.* **2016**, *22*, 6459–6468. [CrossRef] [PubMed]
123. Fang, S.; Xu, H.; Lu, J.; Zhu, Y.; Jiang, H. Neuroprotection by the kappa-opioid receptor agonist, BRL52537, is mediated via up-regulating phosphorylated signal transducer and activator of transcription-3 in cerebral ischemia/reperfusion injury in rats. *Neurochem. Res.* **2013**, *38*, 2305–2312. [CrossRef]
124. Eftekhari-Vaghefi, S.; Esmaeili-Mahani, S.; Elyasi, L.; Abbasnejad, M. Involvement of Mu Opioid Receptor Signaling in the Protective Effect of Opioid against 6-Hydroxydopamine-Induced SH-SY5Y Human Neuroblastoma Cells Apoptosis. *Basic Clin. Neurosci.* **2015**, *6*, 171–178. [PubMed]
125. Nozohouri, S.; Zhang, Y.; Albekairi, T.H.; Vaidya, B.; Abbruscato, T.J. Glutamate Buffering Capacity and Blood-Brain Barrier Protection of Opioid Receptor Agonists Buprenorphine and Nociceptin. *J. Pharmacol. Exp. Ther.* **2021**, *379*, 260–269. [CrossRef]
126. Busch, A.E.; Karbach, U.; Miska, D.; Gorboulev, V.; Akhoundova, A.; Volk, C.; Arndt, P.; Ulzheimer, J.C.; Sonders, M.S.; Baumann, C.; et al. Human neurons express the polyspecific cation transporter hOCT2, which translocates monoamine neurotransmitters, amantadine, and memantine. *Mol. Pharmacol.* **1998**, *54*, 342–352. [CrossRef]
127. Stanton, J.A.; Williams, E.I.; Betterton, R.D.; Davis, T.P.; Ronaldson, P.T. Targeting Organic Cation Transporters at the Blood-Brain Barrier To Treat Ischemic Stroke in Rats. *Exp. Neurol.* **2022**, in press.
128. McCaffrey, G.; Willis, C.L.; Staatz, W.D.; Nametz, N.; Quigley, C.A.; Hom, S.; Lochhead, J.J.; Davis, T.P. Occludin oligomeric assemblies at tight junctions of the blood-brain barrier are altered by hypoxia and reoxygenation stress. *J. Neurochem.* **2009**, *110*, 58–71. [CrossRef]
129. Lochhead, J.J.; McCaffrey, G.; Quigley, C.E.; Finch, J.; DeMarco, K.M.; Nametz, N.; Davis, T.P. Oxidative stress increases blood-brain barrier permeability and induces alterations in occludin during hypoxia-reoxygenation. *J. Cereb. Blood Flow Metab.* **2010**, *30*, 1625–1636. [CrossRef]
130. Hashimoto, Y.; Campbell, M.; Tachibana, K.; Okada, Y.; Kondoh, M. Claudin-5: A Pharmacological Target to Modify the Permeability of the Blood-Brain Barrier. *Biol. Pharm. Bull.* **2021**, *44*, 1380–1390. [CrossRef]
131. Winkler, L.; Blasig, R.; Breitkreuz-Korff, O.; Berndt, P.; Dithmer, S.; Helms, H.C.; Puchkov, D.; Devraj, K.; Kaya, M.; Qin, Z.; et al. Tight junctions in the blood-brain barrier promote edema formation and infarct size in stroke—Ambivalent effects of sealing proteins. *J. Cereb. Blood Flow Metab.* **2021**, *41*, 132–145. [CrossRef]
132. Seo, J.H.; Maki, T.; Miyamoto, N.; Choi, Y.K.; Chung, K.K.; Hamanaka, G.; Park, J.H.; Mandeville, E.T.; Takase, H.; Hayakawa, K.; et al. AKAP12 Supports Blood-Brain Barrier Integrity against Ischemic Stroke. *Int. J. Mol. Sci.* **2020**, *21*, 9078. [CrossRef] [PubMed]
133. Zhou, Y.; Yan, F.; Han, X.; Huang, X.; Cheng, X.; Geng, Y.; Jiang, X.; Han, Y.; Zhao, M.; Zhu, L. NB-3 expression in endothelial cells contributes to the maintenance of blood brain barrier integrity in a mouse high-altitude cerebral edema model. *Exp. Neurol.* **2022**, *354*, 114116. [CrossRef]
134. Hashimoto, Y.; Campbell, M. Tight junction modulation at the blood-brain barrier: Current and future perspectives. *Biochim. et Biophys. Acta (BBA)-Biomembr.* **2020**, *1862*, 183298. [CrossRef] [PubMed]
135. Abbott, N.J.; Patabendige, A.A.K.; Dolman, D.E.M.; Yusof, S.R.; Begley, D.J. Structure and function of the blood-brain barrier. *Neurobiol. Dis.* **2010**, *37*, 13–25. [CrossRef] [PubMed]
136. Greene, C.; Hanley, N.; Campbell, M. Claudin-5: Gatekeeper of neurological function. *Fluids Barriers CNS* **2019**, *16*, 3. [CrossRef]
137. Lochhead, J.J.; Yang, J.; Ronaldson, P.T.; Davis, T.P. Structure, Function, and Regulation of the Blood-Brain Barrier Tight Junction in Central Nervous System Disorders. *Front. Physiol.* **2020**, *11*, 914. [CrossRef]
138. Nitta, T.; Hata, M.; Gotoh, S.; Seo, Y.; Sasaki, H.; Hashimoto, N.; Furuse, M.; Tsukita, S. Size-selective loosening of the blood-brain barrier in claudin-5-deficient mice. *J. Cell Biol.* **2003**, *161*, 653–660. [CrossRef]
139. McCaffrey, G.; Seelbach, M.J.; Staatz, W.D.; Nametz, N.; Quigley, C.; Campos, C.R.; Brooks, T.A.; Davis, T.P. Occludin oligomeric assembly at tight junctions of the blood-brain barrier is disrupted by peripheral inflammatory hyperalgesia. *J. Neurochem.* **2008**, *106*, 2395–2409. [CrossRef]
140. Haseloff, R.F.; Dithmer, S.; Winkler, L.; Wolburg, H.; Blasig, I.E. Transmembrane proteins of the tight junctions at the blood-brain barrier: Structural and functional aspects. *Semin. Cell Dev. Biol.* **2015**, *38*, 16–25. [CrossRef]
141. Zeniya, S.; Kuwahara, H.; Daizo, K.; Watari, A.; Kondoh, M.; Yoshida-Tanaka, K.; Kaburagi, H.; Asada, K.; Nagata, T.; Nagahama, M.; et al. Angubindin-1 opens the blood-brain barrier in vivo for delivery of antisense oligonucleotide to the central nervous system. *J. Control Release* **2018**, *283*, 126–134. [CrossRef]
142. Kakogiannos, N.; Ferrari, L.; Giampietro, C.; Scalise, A.A.; Maderna, C.; Rava, M.; Taddei, A.; Lampugnani, M.G.; Pisati, F.; Malinverno, M.; et al. JAM-A Acts via C/EBP-alpha to Promote Claudin-5 Expression and Enhance Endothelial Barrier Function. *Circ. Res.* **2020**, *127*, 1056–1073. [CrossRef] [PubMed]
143. Pu, Y.; Qian, F.; Guo, J.; Sha, Y.; Qian, Y. Selegiline Protects Against Lipopolysaccharide (LPS)-Induced Impairment of the Blood-Brain Barrier Through Regulating the NF-kappaB/MLCK/p-MLC Signaling Pathway. *Neurotox. Res.* **2022**, *40*, 267–275. [CrossRef] [PubMed]
144. Pan, J.; Qu, M.; Li, Y.; Wang, L.; Zhang, L.; Wang, Y.; Tang, Y.; Tian, H.L.; Zhang, Z.; Yang, G.Y. MicroRNA-126-3p/-5p Overexpression Attenuates Blood-Brain Barrier Disruption in a Mouse Model of Middle Cerebral Artery Occlusion. *Stroke* **2020**, *51*, 619–627. [CrossRef] [PubMed]

145. Bhowmick, S.; D'Mello, V.; Caruso, D.; Wallerstein, A.; Abdul-Muneer, P.M. Impairment of pericyte-endothelium crosstalk leads to blood-brain barrier dysfunction following traumatic brain injury. *Exp. Neurol.* **2019**, *317*, 260–270. [CrossRef] [PubMed]
146. Xia, Y.P.; He, Q.W.; Li, Y.N.; Chen, S.C.; Huang, M.; Wang, Y.; Gao, Y.; Huang, Y.; Wang, M.D.; Mao, L.; et al. Recombinant human sonic hedgehog protein regulates the expression of ZO-1 and occludin by activating angiopoietin-1 in stroke damage. *PLoS ONE* **2013**, *8*, e68891. [CrossRef]
147. Huber, J.D.; Witt, K.A.; Hom, S.; Egleton, R.D.; Mark, K.S.; Davis, T.P. Inflammatory pain alters blood-brain barrier permeability and tight junctional protein expression. *Am. J. Physiol. Heart Circ. Physiol.* **2001**, *280*, H1241–H1248. [CrossRef]
148. Campos, C.R.; Ocheltree, S.M.; Hom, S.; Egleton, R.D.; Davis, T.P. Nociceptive inhibition prevents inflammatory pain induced changes in the blood-brain barrier. *Brain Res.* **2008**, *1221*, 6–13. [CrossRef]
149. Ronaldson, P.T.; Demarco, K.M.; Sanchez-Covarrubias, L.; Solinsky, C.M.; Davis, T.P. Transforming growth factor-beta signaling alters substrate permeability and tight junction protein expression at the blood-brain barrier during inflammatory pain. *J. Cereb. Blood Flow Metab.* **2009**, *29*, 1084–1098. [CrossRef]
150. Daneman, R.; Prat, A. The blood-brain barrier. *Cold Spring Harb. Perspect Biol.* **2015**, *7*, a020412. [CrossRef]
151. Ronaldson, P.T.; Davis, T. Blood-Brain Barrier Integrity and Glial Support: Mechanisms that can be Targeted for Novel Therapeutic Approaches in Stroke. *Curr. Pharm. Des.* **2012**, *18*, 3624–3644. [CrossRef]
152. Iadecola, C. The Neurovascular Unit Coming of Age: A Journey through Neurovascular Coupling in Health and Disease. *Neuron* **2017**, *96*, 17–42. [CrossRef] [PubMed]
153. Schaeffer, S.; Iadecola, C. Revisiting the neurovascular unit. *Nat. Neurosci.* **2021**, *24*, 1198–1209. [CrossRef] [PubMed]
154. Willis, C.L.; Nolan, C.C.; Reith, S.N.; Lister, T.; Prior, M.J.; Guerin, C.J.; Mavroudis, G.; Ray, D.E. Focal astrocyte loss is followed by microvascular damage, with subsequent repair of the blood-brain barrier in the apparent absence of direct astrocytic contact. *Glia* **2004**, *45*, 325–337. [CrossRef] [PubMed]
155. Cantrill, C.A.; Skinner, R.A.; Rothwell, N.J.; Penny, J.I. An immortalised astrocyte cell line maintains the in vivo phenotype of a primary porcine in vitro blood-brain barrier model. *Brain Res.* **2012**, *1479*, 17–30. [CrossRef]
156. Canfield, S.G.; Stebbins, M.J.; Morales, B.S.; Asai, S.W.; Vatine, G.D.; Svendsen, C.N.; Palecek, S.P.; Shusta, E.V. An isogenic blood-brain barrier model comprising brain endothelial cells, astrocytes, and neurons derived from human induced pluripotent stem cells. *J. Neurochem.* **2017**, *140*, 874–888. [CrossRef]
157. Janzer, R.C.; Raff, M.C. Astrocytes induce blood-brain barrier properties in endothelial cells. *Nature* **1987**, *325*, 253–257. [CrossRef]
158. Willis, C.L.; Leach, L.; Clarke, G.J.; Nolan, C.C.; Ray, D.E. Reversible disruption of tight junction complexes in the rat blood-brain barrier, following transitory focal astrocyte loss. *Glia* **2004**, *48*, 1–13. [CrossRef]
159. Kucharz, K.; Kutuzov, N.; Zhukov, O.; Mathiesen Janiurek, M.; Lauritzen, M. Shedding Light on the Blood-Brain Barrier Transport with Two-Photon Microscopy In Vivo. *Pharm. Res.* **2022**, *39*, 1457–1468. [CrossRef]
160. Mathiisen, T.M.; Lehre, K.P.; Danbolt, N.C.; Ottersen, O.P. The perivascular astroglial sheath provides a complete covering of the brain microvessels: An electron microscopic 3D reconstruction. *Glia* **2010**, *58*, 1094–1103. [CrossRef]
161. Ren, Z.; Iliff, J.J.; Yang, L.; Yang, J.; Chen, X.; Chen, M.J.; Giese, R.N.; Wang, B.; Shi, X.; Nedergaard, M. 'Hit & Run' model of closed-skull traumatic brain injury (TBI) reveals complex patterns of post-traumatic AQP4 dysregulation. *J. Cereb. Blood Flow Metab.* **2013**, *33*, 834–845. [CrossRef]
162. Kimelberg, H.K.; Goderie, S.K.; Higman, S.; Pang, S.; Waniewski, R.A. Swelling-induced release of glutamate, aspartate, and taurine from astrocyte cultures. *J. Neurosci.* **1990**, *10*, 1583–1591. [CrossRef] [PubMed]
163. Wilson, C.S.; Bach, M.D.; Ashkavand, Z.; Norman, K.R.; Martino, N.; Adam, A.P.; Mongin, A.A. Metabolic constraints of swelling-activated glutamate release in astrocytes and their implication for ischemic tissue damage. *J. Neurochem.* **2019**, *151*, 255–272. [CrossRef] [PubMed]
164. Schlachetzki, F.; Pardridge, W.M. P-glycoprotein and caveolin-1 $\alpha$  in endothelium and astrocytes of primate brain. *NeuroReport* **2003**, *14*, 2041–2046. [CrossRef] [PubMed]
165. Ronaldson, P.T.; Bendayan, M.; Gingras, D.; Piquette-Miller, M.; Bendayan, R. Cellular localization and functional expression of P-glycoprotein in rat astrocyte cultures. *J. Neurochem.* **2004**, *89*, 788–800. [CrossRef]
166. van Vliet, E.A.; Iyer, A.M.; Mesarosova, L.; Colakoglu, H.; Anink, J.J.; van Tellingen, O.; Maragakis, N.J.; Shefner, J.; Bunt, T.; Aronica, E. Expression and Cellular Distribution of P-Glycoprotein and Breast Cancer Resistance Protein in Amyotrophic Lateral Sclerosis Patients. *J. Neuropathol. Exp. Neurol.* **2020**, *79*, 266–276. [CrossRef]
167. Nies, A.; Jedlitschky, G.; König, J.; Herold-Mende, C.; Steiner, H.; Schmitt, H.-P.; Keppler, D. Expression and immunolocalization of the multidrug resistance proteins, MRP1–MRP6 (ABCC1–ABCC6), in human brain. *Neuroscience* **2004**, *129*, 349–360. [CrossRef]
168. Jördens, M.S.; Keitel, V.; Karababa, A.; Zemtsova, I.; Bronger, H.; Häussinger, D.; Görg, B. Multidrug resistance-associated protein 4 expression in ammonia-treated cultured rat astrocytes and cerebral cortex of cirrhotic patients with hepatic encephalopathy. *Glia* **2015**, *63*, 2092–2105. [CrossRef]
169. Huber, R.D.; Gao, B.; Sidler Pfandler, M.A.; Zhang-Fu, W.; Leuthold, S.; Hagenbuch, B.; Folkers, G.; Meier, P.J.; Stieger, B. Characterization of two splice variants of human organic anion transporting polypeptide 3A1 isolated from human brain. *Am. J. Physiol. Cell Physiol.* **2007**, *292*, C795–C806. [CrossRef]
170. Sweet, D.H. Organic Cation Transporter Expression and Function in the CNS. *Handb. Exp. Pharmacol.* **2021**, *266*, 41–80. [CrossRef]
171. Hladky, S.B.; Barrand, M.A. The glymphatic hypothesis: The theory and the evidence. *Fluids Barriers CNS* **2022**, *19*, 9. [CrossRef]

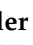

172. Thomas, J.H. Theoretical analysis of wake/sleep changes in brain solute transport suggests a flow of interstitial fluid. *Fluids Barriers CNS* **2022**, *19*, 30. [CrossRef] [PubMed]
173. Salter, M.W.; Stevens, B. Microglia emerge as central players in brain disease. *Nat. Med.* **2017**, *23*, 1018–1027. [CrossRef] [PubMed]
174. Garcia-Culebras, A.; Duran-Laforet, V.; Pena-Martinez, C.; Ballesteros, I.; Pradillo, J.M.; Diaz-Guzman, J.; Lizasoain, I.; Moro, M.A. Myeloid cells as therapeutic targets in neuroinflammation after stroke: Specific roles of neutrophils and neutrophil-platelet interactions. *J. Cereb. Blood Flow Metab.* **2018**, *38*, 2150–2164. [CrossRef] [PubMed]
175. Subramaniam, S.R.; Federoff, H.J. Targeting Microglial Activation States as a Therapeutic Avenue in Parkinson's Disease. *Front. Aging Neurosci.* **2017**, *9*, 176. [CrossRef]
176. Ronaldson, P.T.; Davis, T.P. Regulation of blood-brain barrier integrity by microglia in health and disease: A therapeutic opportunity. *J. Cereb. Blood Flow Metab.* **2020**, *40*, S6–S24. [CrossRef]
177. Nimmerjahn, A.; Kirchhoff, F.; Helmchen, F. Resting microglial cells are highly dynamic surveillants of brain parenchyma in vivo. *Science* **2005**, *308*, 1314–1318. [CrossRef]
178. Akhmetzyanova, E.; Kletenkov, K.; Mukhamedshina, Y.; Rizvanov, A. Different Approaches to Modulation of Microglia Phenotypes After Spinal Cord Injury. *Front. Syst. Neurosci.* **2019**, *13*, 37. [CrossRef]
179. Bachiller, S.; Jimenez-Ferrer, I.; Paulus, A.; Yang, Y.; Swanberg, M.; Deierborg, T.; Boza-Serrano, A. Microglia in Neurological Diseases: A Road Map to Brain-Disease Dependent-Inflammatory Response. *Front. Cell Neurosci.* **2018**, *12*, 488. [CrossRef]
180. Lee, J.; Hamanaka, G.; Lo, E.H.; Arai, K. Heterogeneity of microglia and their differential roles in white matter pathology. *CNS Neurosci. Ther.* **2019**, *25*, 1290–1298. [CrossRef]
181. Barisano, G.; Montagne, A.; Kisler, K.; Schneider, J.A.; Wardlaw, J.M.; Zlokovic, B.V. Blood-brain barrier link to human cognitive impairment and Alzheimer's Disease. *Nat. Cardiovasc. Res.* **2022**, *1*, 108–115. [CrossRef]
182. Bankstahl, M.; Breuer, H.; Leiter, I.; Markel, M.; Bascunana, P.; Michalski, D.; Bengel, F.M.; Loscher, W.; Meier, M.; Bankstahl, J.P.; et al. Blood-Brain Barrier Leakage during Early Epileptogenesis Is Associated with Rapid Remodeling of the Neurovascular Unit. *eNeuro* **2018**, *5*, ENEURO.0123-18.2018. [CrossRef] [PubMed]
183. Lee, G.; Schlichter, L.; Bendayan, M.; Bendayan, R. Functional expression of P-glycoprotein in rat brain microglia. *J. Pharmacol. Exp. Ther.* **2001**, *299*, 204–212. [PubMed]
184. Dallas, S.; Zhu, X.; Baruchel, S.; Schlichter, L.; Bendayan, R. Functional expression of the multidrug resistance protein 1 in microglia. *J. Pharmacol. Exp. Ther.* **2003**, *307*, 282–290. [CrossRef] [PubMed]
185. Dallas, S.; Schlichter, L.; Bendayan, R. Multidrug resistance protein (MRP) 4- and MRP 5-mediated efflux of 9-(2-phosphonylmethoxyethyl)adenine by microglia. *J. Pharmacol. Exp. Ther.* **2004**, *309*, 1221–1229. [CrossRef]
186. Ishimoto, T.; Nakamichi, N.; Nishijima, H.; Masuo, Y.; Kato, Y. Carnitine/Organic Cation Transporter OCTN1 Negatively Regulates Activation in Murine Cultured Microglial Cells. *Neurochem. Res.* **2018**, *43*, 116–128. [CrossRef]
187. Dore-Duffy, P.; Cleary, K. Morphology and properties of pericytes. *Methods Mol. Biol.* **2011**, *686*, 49–68. [CrossRef]
188. Halliday, M.R.; Rege, S.V.; Ma, Q.; Zhao, Z.; Miller, C.A.; Winkler, E.A.; Zlokovic, B.V. Accelerated pericyte degeneration and blood-brain barrier breakdown in apolipoprotein E4 carriers with Alzheimer's disease. *J. Cereb. Blood Flow Metab.* **2016**, *36*, 216–227. [CrossRef]
189. Daneman, R.; Zhou, L.; Kebede, A.A.; Barres, B.A. Pericytes are required for blood-brain barrier integrity during embryogenesis. *Nature* **2010**, *468*, 562–566. [CrossRef]
190. Sweeney, M.D.; Ayyadurai, S.; Zlokovic, B.V. Pericytes of the neurovascular unit: Key functions and signaling pathways. *Nat. Neurosci.* **2016**, *19*, 771–783. [CrossRef]
191. Grant, R.I.; Hartmann, D.A.; Underly, R.G.; Berthiaume, A.A.; Bhat, N.R.; Shih, A.Y. Organizational hierarchy and structural diversity of microvascular pericytes in adult mouse cortex. *J. Cereb. Blood Flow Metab.* **2019**, *39*, 411–425. [CrossRef]
192. Berthiaume, A.A.; Grant, R.I.; McDowell, K.P.; Underly, R.G.; Hartmann, D.A.; Levy, M.; Bhat, N.R.; Shih, A.Y. Dynamic Remodeling of Pericytes In Vivo Maintains Capillary Coverage in the Adult Mouse Brain. *Cell. Rep.* **2018**, *22*, 8–16. [CrossRef] [PubMed]
193. Dore-Duffy, P.; Katychew, A.; Wang, X.; Van Buren, E. CNS microvascular pericytes exhibit multipotential stem cell activity. *J. Cereb. Blood Flow Metab.* **2006**, *26*, 613–624. [CrossRef] [PubMed]
194. Hori, S.; Ohtsuki, S.; Hosoya, K.; Nakashima, E.; Terasaki, T. A pericyte-derived angiopoietin-1 multimeric complex induces occludin gene expression in brain capillary endothelial cells through Tie-2 activation in vitro. *J. Neurochem.* **2004**, *89*, 503–513. [CrossRef] [PubMed]
195. Armulik, A.; Genove, G.; Mae, M.; Nisancioglu, M.H.; Wallgard, E.; Niaudet, C.; He, L.; Norlin, J.; Lindblom, P.; Strittmatter, K.; et al. Pericytes regulate the blood-brain barrier. *Nature* **2010**, *468*, 557–561. [CrossRef] [PubMed]
196. Villasenor, R.; Kuennecke, B.; Ozmen, L.; Ammann, M.; Kugler, C.; Gruninger, F.; Loetscher, H.; Freskgard, P.O.; Collin, L. Region-specific permeability of the blood-brain barrier upon pericyte loss. *J. Cereb. Blood Flow Metab.* **2017**, *37*, 3683–3694. [CrossRef]
197. Dohgu, S.; Takata, F.; Yamauchi, A.; Nakagawa, S.; Egawa, T.; Naito, M.; Tsuruo, T.; Sawada, Y.; Niwa, M.; Kataoka, Y. Brain pericytes contribute to the induction and up-regulation of blood-brain barrier functions through transforming growth factor-beta production. *Brain Res.* **2005**, *1038*, 208–215. [CrossRef] [PubMed]

198. Berezowski, V.; Landry, C.; Dehouck, M.P.; Cecchelli, R.; Fenart, L. Contribution of glial cells and pericytes to the mRNA profiles of P-glycoprotein and multidrug resistance-associated proteins in an in vitro model of the blood-brain barrier. *Brain Res.* **2004**, *1018*, 1–9. [CrossRef] [PubMed]
199. Bernstein, H.G.; Holzl, G.; Dobrowolny, H.; Hildebrandt, J.; Trubner, K.; Krohn, M.; Bogerts, B.; Pahnke, J. Vascular and extravascular distribution of the ATP-binding cassette transporters ABCB1 and ABCC1 in aged human brain and pituitary. *Mech. Ageing Dev.* **2014**, *141–142*, 12–21. [CrossRef] [PubMed]
200. Ludwig, M.; Pittman, Q.J. Talking back: Dendritic neurotransmitter release. *Trends Neurosci.* **2003**, *26*, 255–261. [CrossRef]
201. Nishio, T.; Adachi, H.; Nakagomi, R.; Tokui, T.; Sato, E.; Tanemoto, M.; Fujiwara, K.; Okabe, M.; Onogawa, T.; Suzuki, T.; et al. Molecular identification of a rat novel organic anion transporter moat1, which transports prostaglandin D(2), leukotriene C(4), and taurocholate. *Biochem. Biophys. Res. Commun.* **2000**, *275*, 831–838. [CrossRef] [PubMed]
202. Feurstein, D.; Kleinteich, J.; Heussner, A.H.; Stemmer, K.; Dietrich, D.R. Investigation of microcystin congener-dependent uptake into primary murine neurons. *Environ. Health Perspect* **2010**, *118*, 1370–1375. [CrossRef] [PubMed]
203. Scafidi, S.; Douglas, R.M.; Farahani, R.; Banasiak, K.J.; Haddad, G.G. Prostaglandin transporter expression in mouse brain during development and in response to hypoxia. *Neuroscience* **2007**, *146*, 1150–1157. [CrossRef] [PubMed]
204. Courousse, T.; Bacq, A.; Belzung, C.; Guiard, B.; Balasse, L.; Louis, F.; Le Guisquet, A.M.; Gardier, A.M.; Schinkel, A.H.; Giros, B.; et al. Brain organic cation transporter 2 controls response and vulnerability to stress and GSK3beta signaling. *Mol. Psychiatry* **2015**, *20*, 889–900. [CrossRef] [PubMed]
205. Bacq, A.; Balasse, L.; Biala, G.; Guiard, B.; Gardier, A.M.; Schinkel, A.; Louis, F.; Vialou, V.; Martres, M.P.; Chevarin, C.; et al. Organic cation transporter 2 controls brain norepinephrine and serotonin clearance and antidepressant response. *Mol. Psychiatry* **2012**, *17*, 926–939. [CrossRef]
206. Lazarowski, A.; Caltana, L.; Merelli, A.; Rubio, M.D.; Ramos, A.J.; Brusco, A. Neuronal mdr-1 gene expression after experimental focal hypoxia: A new obstacle for neuroprotection? *J. Neurol. Sci.* **2007**, *258*, 84–92. [CrossRef]
207. Merelli, A.; Ramos, A.J.; Lazarowski, A.; Auzmendi, J. Convulsive Stress Mimics Brain Hypoxia and Promotes the P-Glycoprotein (P-gp) and Erythropoietin Receptor Overexpression. Recombinant Human Erythropoietin Effect on P-gp Activity. *Front. Neurosci.* **2019**, *13*, 750. [CrossRef]
208. Fonseca-Barriendos, D.; Perez-Perez, D.; Fuentes-Mejia, M.; Orozco-Suarez, S.; Alonso-Vanegas, M.; Martinez-Juarez, I.E.; Guevara-Guzman, R.; Castaneda-Cabral, J.L.; Rocha, L. Protein expression of P-glycoprotein in neocortex from patients with frontal lobe epilepsy. *Epilepsy Res.* **2022**, *181*, 106892. [CrossRef]
209. Chen, L.; Chen, H.; Xing, Y.; Li, J. ABCC1 regulates cocaine-associated memory, spine plasticity and GluA1 and GluA2 surface expression. *Neuroreport* **2021**, *32*, 833–839. [CrossRef]



Review

# Blood–Brain Barrier Transport of Transferrin Receptor-Targeted Nanoparticles

Maj Schneider Thomsen <sup>1</sup>, Kasper Bendix Johnsen <sup>1,2,3</sup>, Krzysztof Kucharz <sup>4</sup>, Martin Lauritzen <sup>4</sup> and Torben Moos <sup>1,\*</sup>

<sup>1</sup> Neurobiology Research and Drug Delivery, Department of Health Science and Technology, Aalborg University, 9220 Aalborg, Denmark

<sup>2</sup> Department of Health Technology, Technical University of Denmark, 2800 Kgs. Lyngby, Denmark

<sup>3</sup> Division for Science & Ethics, Danish National Center for Ethics, 2750 Ballerup, Denmark

<sup>4</sup> Department of Neuroscience, Faculty of Health Sciences, University of Copenhagen, 2100 Copenhagen, Denmark

\* Correspondence: tmoos@hst.aau.dk; Tel.: +45-9944-2420

**Abstract:** The blood–brain barrier (BBB), built by brain endothelial cells (BECs), is impermeable to biologics. Liposomes and other nanoparticles are good candidates for the delivery of biologics across the BECs, as they can encapsulate numerous molecules of interest in an omnipotent manner. The liposomes need attachment of a targeting molecule, as BECs unfortunately are virtually incapable of uptake of non-targeted liposomes from the circulation. Experiments of independent research groups have qualified antibodies targeting the transferrin receptor as superior for targeted delivery of nanoparticles to BECs. Functionalization of nanoparticles via conjugation with anti-transferrin receptor antibodies leads to nanoparticle uptake by endothelial cells of both brain capillaries and post-capillary venules. Reducing the density of transferrin receptor-targeted antibodies conjugated to liposomes limits uptake in BECs. Opposing the transport of nanoparticles conjugated to high-affine anti-transferrin receptor antibodies, lowering the affinity of the targeting antibodies or implementing monovalent antibodies increase uptake by BECs and allows for further transport across the BBB. The novel demonstration of transport of targeted liposomes in post-capillary venules from blood to the brain is interesting and clearly warrants further mechanistic pursuit. The recent evidence for passing targeted nanoparticles through the BBB shows great promise for future drug delivery of biologics to the brain.

**Keywords:** antibody; blood–brain barrier; endosomal; liposome; nanoparticle; targeting; transferrin

**Citation:** Thomsen, M.S.; Johnsen, K.B.; Kucharz, K.; Lauritzen, M.; Moos, T. Blood–Brain Barrier Transport of Transferrin Receptor-Targeted Nanoparticles. *Pharmaceutics* **2022**, *14*, 2237. <https://doi.org/10.3390/pharmaceutics14102237>

Academic Editor: William M. Pardridge

Received: 24 September 2022

Accepted: 14 October 2022

Published: 19 October 2022

**Publisher's Note:** MDPI stays neutral with regard to jurisdictional claims in published maps and institutional affiliations.



**Copyright:** © 2022 by the authors. Licensee MDPI, Basel, Switzerland. This article is an open access article distributed under the terms and conditions of the Creative Commons Attribution (CC BY) license (<https://creativecommons.org/licenses/by/4.0/>).

## 1. Introduction

The brain harbors a vascular barrier system consisting of the blood–brain barrier (BBB) and the blood–cerebrospinal fluid (CSF) barrier. Together, they limit the passage from the bloodstream into the brain parenchyma of virtually any drug unless highly lipophilic or smaller than approximately 70 Daltons [1–4]. This is preferable from a physiological perspective, as it allows to sustain integrity and maintain stable extracellular concentrations of solutes in the brain with minimal influence from fluctuations in blood. It is also advantageous from a toxicologic perspective, as the vascular barriers form a strong defense that prevents the entry of unwanted exogenous substances and pathogens [1–4].

However, the presence of the brain barrier system is inconvenient from a pharmacological perspective as many of the existing and forthcoming drug candidates, e.g., polypeptides, or genetic material-based pharmaceuticals like siRNA or cDNA, are unable to pass the brain barriers [5]. This is unfortunate as research of recent years has identified several targets putatively amendable for the treatment of CNS diseases, providing that such biologic therapeutics (“biologics”) can enter the brain [6,7]. Consequently, current therapeutics



attempting to treat neurodegenerative disorders like Alzheimer's and Parkinson's disease, and psychiatric diseases, e.g., schizophrenia and endogenous depression, where the vascular barriers are supposedly intact [8], are pharmacologically restricted.

The discovery of the selective expression of targetable proteins by brain endothelial cells (BECs) has changed the scene and provides new optimism, as several biologics conjugated to targeting antibodies are now amenable for uptake and transport across the BECs [2,5,6]. The use of targeted antibody-conjugated nanoparticles for drug delivery to the brain denotes an interesting alternative to the use of biologics conjugated directly to antibodies [9,10]. A major advantage of nanoparticles is their omnipotence to encapsulate potentially any drug of interest with minimal restraints on their size [9,10]. From the first studies on BBB transport performed more than two decades ago [11–13], the exploration of targeted liposomes and other types of nanoparticles, e.g., polymeric nanoparticles, gold nanoparticles, and magnetic nanoparticles, has progressively continued [9]. A recent peak in this discovery was the identification of transport of transferrin receptor-targeted liposomes into the brain, recently reported using real-time two-photon microscopy *in vivo*. Interestingly, transferrin receptor-targeted liposomes were found to mainly undergo transport into the brain via an unexpected route, i.e., across endothelial cells of post-capillary venules, and not via brain capillaries [14].

Here, we review the most successful attempts made to enable targeted uptake and transport of nanoparticles across the BBB. As most studies target the transferrin receptor, our delineation of the existing literature mainly addresses this receptor. We describe how specific proteins expressed by BECs enhance the binding and uptake of antibodies from the circulation. Next, we cover how targeted nanoparticles can undergo specific binding and uptake, when conjugated with antibodies weakened in affinity or avidity. We also discuss the therapeutic use of targeted nanoparticles in conditions with brain pathology.

## 2. Passaging of Large Molecules through the Blood–Brain and Blood–CSF Barriers

The BBB proper consists of endothelial cells connected by tight junctions. The blood–CSF barrier is formed by choroid plexus epithelial cells also connected by tight junctions, but opposed to the BBB; the capillaries of the blood–CSF barrier are leaky, meaning that solutes of the plasma diffuse into the extracellular space of the choroid plexus where the epithelial cells selectively transport molecules to the CSF [2,3,14]. From a quantitative drug delivery perspective, passaging across the BBB is by far the most important as the brain microvasculature has a surface area thousand-fold higher than that of the choroid plexus. This allows drugs to enter the entire brain while transport across the blood–CSF barrier is restricted to the ventricular system [2,3,15].

The BBB prevents large molecules and particles in blood plasma from entering the brain (Figure 1). This includes entry via the paracellular space between the endothelial cells where tight junctions limit diffusion from blood to brain [1,2,9]. To enable nutrient uptake while preventing the influx of unwanted substances, the BECs express nutrient transporters for, e.g., amino and fatty acids, monosaccharides, vitamins, and essential ions and metals [1–4]. In contrast, the transport of large molecules of the plasma, like albumin and IgG, is diminutive, e.g., intravenous injection of non-immune IgG in the adult rat is limited to as little as 0.03% of the injected dose, which can be surpassed more than ten-fold by injecting anti-rat transferrin receptor-targeted IgG (OX26) [16]. This can also be observed at the ultrastructural level, where a limited number of transporting vesicles occurs in the cytosol of the BECs compared to endothelial cells of other non-fenestrated capillaries, e.g., those of skeletal muscles. For the same reason, the chances of obtaining transport through the brain endothelium of large constituents like nanoparticles are also predictably low, unless nanoparticles are made targetable to nutrient transporters (see next paragraph).

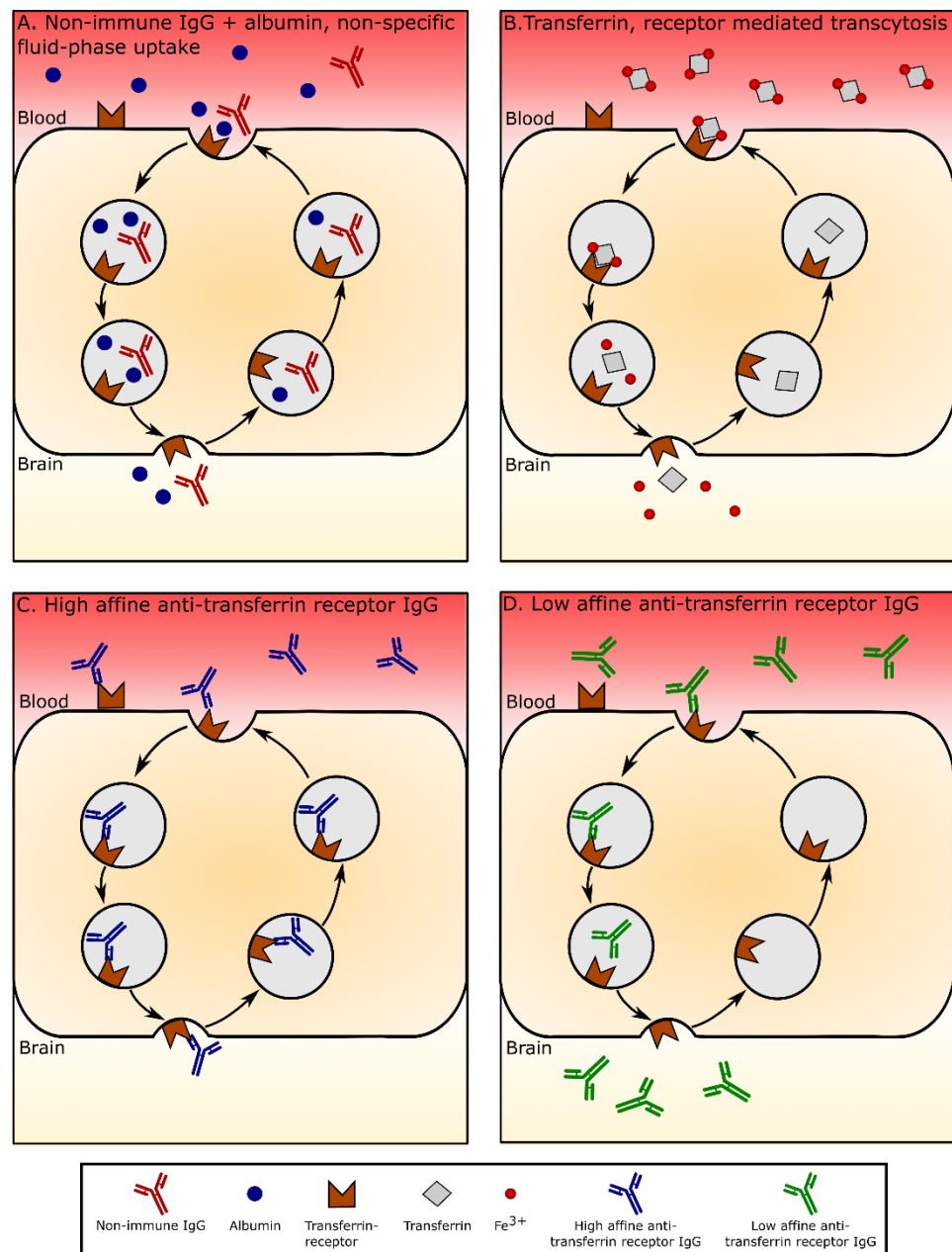


**Figure 1.** Illustration of transport of the three major plasma proteins and targeted anti-transferrin receptor antibodies within brain capillary endothelial cells (BECs). **(A)** Albumin and non-immune IgG enter the BEC non-specifically by fluid-phase uptake. They may undergo release from the BEC at the abluminal side, although the quantitative evidence is scarce and clearly shows that this mean for entry of albumin and non-immune IgG to the brain is negligible. **(B)** Similarly, the transcytotic transport of iron-containing (holo-transferrin) is also negligible and opposed by the release of iron from transferrin due to the lower pH of the endocytosis vesicle. Transport through the BECs may occur to a higher extent in the developing brain where transferrin receptor expression by BECs is far-fold higher than in the adult brain (see body text). **(C)** Transport of high-affine IgG targeted to the transferrin receptor. Transport of this antibody through BECs is negligible. **(D)** Transport of low-affine IgG targeted to the transferrin receptor. Transport of this antibody through BECs is enabled by the detachment of the antibody from the transferrin receptor in late endosomes, which enables this antibody to undergo transport into the brain. Modified from [15].

### 3. The Transferrin Receptor as Target for Drug Delivery

The first indicator of specific uptake and transport of a plasma protein came from observations showing that the brain has a high binding capacity for transferrin, the transporter of the essential metal iron [17]. Later, the identification of a specific binding protein for transferrin, the transferrin receptor (a.k.a. transferrin receptor 1), was identified on BECs [18]. Except for a few other organs, e.g., gonadal cells, the expression of the transferrin receptor by BECs is different from capillaries of organs elsewhere in the body, which do not express this receptor [18–23].

Among the large proteins present in blood plasma, transferrin stands out because of its potential for binding to the transferrin receptor of the BECs [9,24]. The quantitative uptake of iron-containing transferrin by the receptor was first addressed thirty years ago in seminal studies by Morgan and co-workers, who co-examined brain uptake of radiolabeled iron together with iodine-labeled transferrin (reviewed in [24]). This allowed for accurate measures of uptake of both iron and transferrin by the brain and, importantly, showed that the transport of radioactive iron through the BBB by far exceeded that of transferrin even a few hours after injection into the peripheral blood. Similar observations were made independently by another research group [25]. This led to the conclusion that iron-containing transferrin is taken up by receptor-mediated endocytosis at the luminal membrane of brain capillaries. In the brain, iron dissociates from transferrin within the slightly acidic environment in the endosomal compartment [26], and iron is transported across the abluminal lipid bilayer of the BECs to the brain, whereas iron-free transferrin is retro-endocytosed back to the luminal membrane [9,24,27].

Counteracting the notion of receptor-mediated endocytosis and retro-endocytosis of transferrin at the BBB, other studies suggested that the iron-containing transferrin may be transferred across the BECs [28,29]. A caveat, in the relevance of these data for understanding iron and transferrin transport at the BBB, shows only transferrin was detected in the brain, hence leaving out the possibility of interpreting the simultaneous transport of iron. However, supporting that transendothelial transport of iron-containing transferrin may occur, observations made on iron and transferrin uptake combined in other studies do not exclude that a minority of iron–transferrin may pass through the BBB, hence simulating transcytosis at the brain endothelium [24].

The expression of transferrin receptor by BECs varies throughout development, with transferrin transport into the brain being higher in the developing brain than at later ages [30–32]. Interestingly, although magnitudes lower than that of iron, the transport of transferrin across the BBB is significantly higher than that of albumin [28–30], which may be due to higher transcellular trafficking of transferrin. Many more vesicles, typically sized about 70 nm in diameter, are present in BECs of the developing brain [33], so even if only a limited fraction of these vesicles fuse with the abluminal membrane, there would a priori be more vesicles emptying their content into the brain during ontogenesis than in adulthood. Endocytic clathrin-coated vesicles are formed as part of transferrin receptor docking at the luminal side of the BECs. The resulting vesicle forming due to the transferrin attachment will likely also capture fluids from the extracellular space of the luminal side in a non-specific manner, which may explain why albumin also gets transferred through the BBB to a higher degree in the developing brain (Figure 1).

Returning to the attempts to enable transport through the choroid plexus, it should not be overlooked that there is strong morphological and physiological evidence for vesicular transport by transcytosis through this epithelium. Ultrastructurally, tracer studies using peroxidases demonstrate that the choroid plexus epithelium can take up large molecules like horseradish peroxidase (HRP) with transfer from the basolateral to the luminal side eventually leading to release into the ventricles [15,34,35]. The choroid plexus, contrary to the brain endothelium, also contains vesicular structures with albumin, IgG, and transferrin. This is corroborated by the concentration of these proteins being many times higher in the ventricular CSF compared to the interstitial fluid of the brain in the CSF (c.f. [15]). The transport of large plasma proteins could theoretically qualify the blood–CSF barrier

as a feasible route for nanoparticles to enter the brain. Counteracting this consideration, CSF of the ventricular system purely distributes substances to the ventricular system and subarachnoid space and excludes the possibility of targeted transport of antibodies and nanoparticles into the brain via transport across the choroid plexus [2].

#### **4. Specific Proteins Expressed by Brain Endothelial Cells Enhance the Binding and Uptake of Antibodies from the Circulation**

The functional capacity of the brain endothelium to bind and internalize antibodies targeted to the transferrin receptor [18] spawned the idea of using transferrin receptor antibodies to target the brain endothelium, as this would allow conjugated therapeutic molecules to enter the brain [19,21,36,37]. The rationale for injecting transferrin receptor-targeting antibodies is that exogenous transferrin needs to compete with endogenous transferrin of blood plasma, which significantly reduces the likelihood for binding transferrin receptors [36,37]. This is not the case when using transferrin receptor targeting antibodies, which bind to epitopes at the transferrin receptor without interfering with endogenous transferrin. This is advantageous from the physiological point of view, as the brain delivery of iron is not hampered by antibody-targeting of the transferrin receptor [36,37].

The injection of antibodies targeted to the transferrin receptor dramatically increases the brain uptake as compared to non-targeted antibodies [11,36,37]. Noteworthy, injecting antibodies targeting the insulin receptor, also expressed by BECs, similarly allowed for higher uptake in BECs [11,13,19,38]. However, the internalization did not guarantee successful passage across the endothelium. It was later shown that although transferrin receptor-targeted antibodies were internalized in the BECs by receptor-targeting, the antibodies fell short in their capability to pass to the brain parenchyma [16,39]. This observation was explained by antibodies forming covalent binding to the transferrin receptors sufficient to prevent the antibodies from detaching from the receptor. Later, biotechnological advances created the basis for synthesizing mono-specific antibodies lowered with low affinity, and bi-specific antibodies with low avidity. Such antibodies can be constructed by replacement of a single Fab fragment of a monospecific, high-affine, divalent antibody with a Fab fragment able to bind a different molecule. The properties of the modified antibodies counteracted the permeability restraints of the BBB and enabled both uptake and higher transport of transferrin receptor-targeted antibodies into the brain, as verified from their engagement with neurons and proteins deposited extracellularly in the brain [40,41]. Subsequently, these approaches inspired the generation of a plethora of differently designed transferrin receptor-targeting antibodies, all able to transport conjugated biologics across the BBB [41–47]. Together, they have provided new optimism on how to achieve delivery of therapeutics to the brain, with transferrin receptor-targeted antibodies being now amendable for clinical use in conjugation with enzymes needed for treatment of lysosomal deficiency or being tested in clinical trials against amyloid deposition in Alzheimer's disease (ClinicalTrials.gov Identifier: NCT05371613; NCT04639050; NCT04573023).

While the development of antibodies entering the brain was generated using antibodies targeting the transferrin receptor and the insulin receptor, it should not be overlooked that targeting other proteins of the brain endothelium has been pursued. The large amino acid transporter (CD98hc), glucose transporter 1 (GLUT1), and basigin (CD147) are particularly rich in their selective expression by the BECs compared to capillaries in the periphery, e.g., lung and liver, and are alternatives for targeting the brain endothelium [19,38,48,49].

#### **5. Specific Proteins Expressed by the Brain Endothelium also Facilitate the Binding and Uptake of Targeted Nanoparticles**

The plethora of *in vivo* studies on nanoparticle transport typically omit to characterize the pharmacokinetics that leads to transport through the BBB. They rather focus on pharmacodynamics or therapeutic effects after the particles have undergone transport into the brain. Often the evidence for the latter is scarce and is extrapolated from pharmacological studies, where improvement in behavioral tasks of experimental animals treated with nanoparticles is used as evidence for BBB transport. Many studies determine fluorescent

nanoparticles using whole-brain imaging, which prevents the distinction of nanoparticles in BECs versus neurons or glia. Other studies determine changes in protein or gene expression by neurons and glia in dissected brain preparations without taking the expression levels in BECs into consideration, e.g., by analyses of brain capillaries isolated and separated from the remaining brain tissue [50].

In spite of the limited number of studies dealing with the uptake and transport kinetics by BEC, a common observation is that the uptake of nanoparticles, e.g., liposomes, gold nanoparticles, or quantum dots, from the circulation is significantly enhanced when conjugated to the transferrin receptor targeted antibodies [51–55]. Comparing the uptake of stealth liposomes in the mouse brain with or without conjugation to proteins putatively targeting BECs, only antibodies targeting the transferrin receptor (clone RI7217) enhanced the liposomal binding and uptake by the brain endothelium [52]. The uptake of RI7217-conjugated liposomes was almost two-fold higher compared to binding with endogenous transferrin or un-conjugated liposomes in brain capillaries isolated from the brain 12 h post injection [52]. Independent studies in the rat [51,53] and mouse [54,55] also concluded that targeting the transferrin receptor using high-affine anti-transferrin receptor antibodies leads to preferential accumulation of liposomes within BECs (Figure 2). Given this evidence, it stands out as somewhat puzzling that reports continuously occur addressing targeting attempts to the transferrin receptor at BECs using only transferrin and not the antibody.

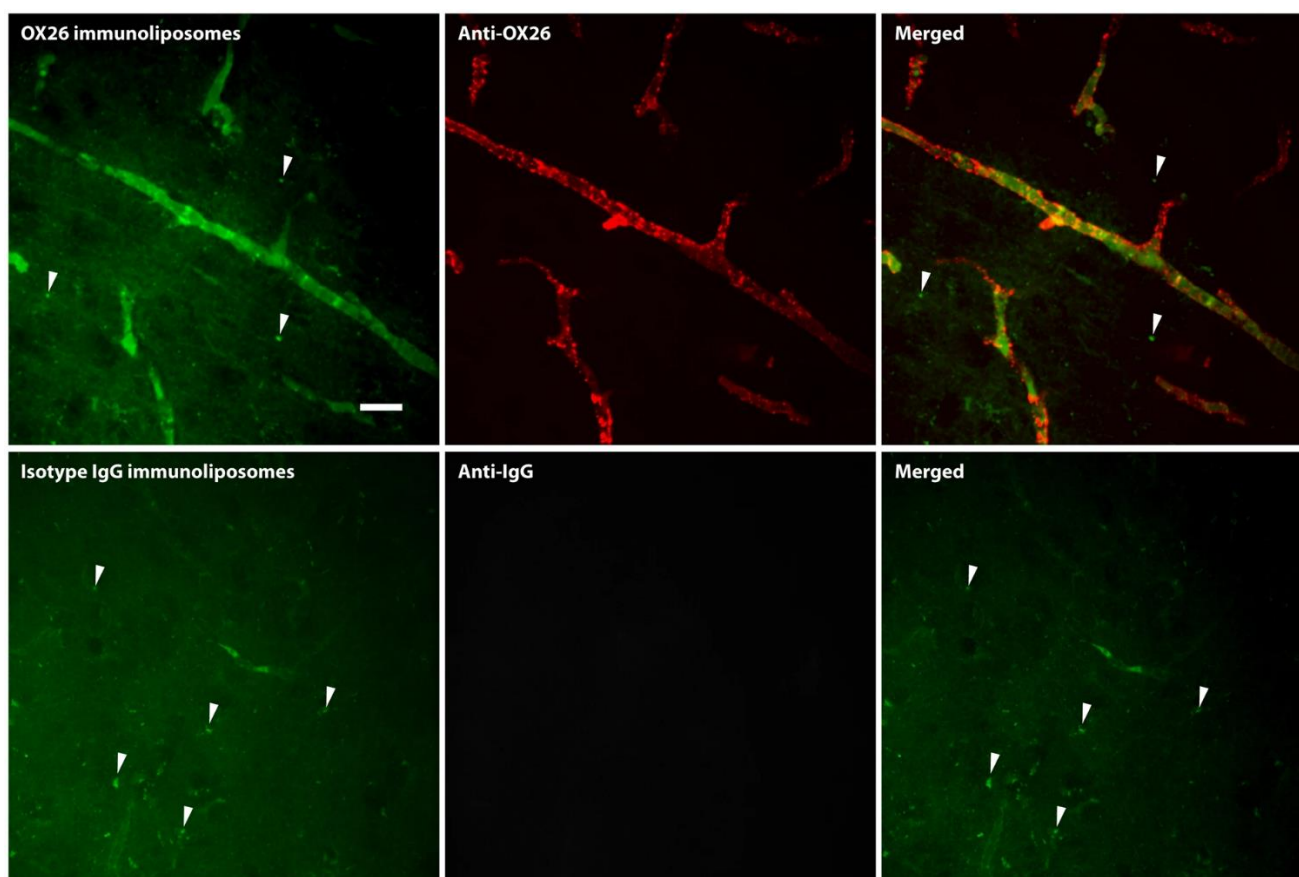


**Figure 2.** Uptake of fluorescently labeled immunoliposomes conjugated with high-affine IgG targeted to the transferrin receptor (OX26) in brain capillaries in vivo in the rat as revealed using spinning disk confocal microscopy. The OX26 immunoliposomes associate to brain microvessels. Immunohistochemical detection of the OX26 of the immunoliposome similarly reveals that the immunoliposome and its binding antibody accumulate in the brain capillaries. Scale bar = 20  $\mu$ m. Modified from [53].

The uptake of RI7217-conjugated liposomes at the BBB is significantly higher compared to stealth liposomes conjugated with non-immune IgG [52]. In contrast, liposomes conjugated to proteins putatively capable of targeting BECs, e.g., (i) cross-reacting material (CRM) with affinity for an endogenous diphtheria toxin receptor; (ii) angiopep-2 with affinity for LRP-1; (iii) COG133 with affinity for apolipoprotein E, all failed to exhibit higher uptake compared to non-immune IgG-conjugated liposomes [52]. In particular, the observations made on liposomes targeting the diphtheria toxin receptor, LRP-1, or apolipoprotein E were discouraging [52], although earlier studies indicated that these targets were relevant for nanoparticle uptake in BECs [56–58]. Studies using unconjugated antibodies targeting LRP-1 also failed to prove that LRP-1 was a viable target for specific uptake by the brain endothelium [19]. It is feasible that the widespread expression of the aforementioned targets in peripheral vasculature may reduce the extent of liposome availability for uptake at BECs.

The number of antibodies present on the surface of antibody-functionalized gold nanoparticles and cargo-loaded stealth liposomes influenced the targeting to BECs in vivo. Hence, the highest density out of a selection of different densities ( $0.15$ ,  $0.3$ , and  $0.6 \times 10^3$  antibodies/ $\mu\text{m}^2$ ) led to the highest binding and uptake [59]. Using gold nanoparticles conjugated with targeting antibodies with different affinity for the transferrin receptor [40], or lowering the avidity inversely led to higher uptake of targeted nanoparticles both in vivo in the adult mouse and in vitro in isolated primary mouse BECs from adult mice [54] (Figure 3). Examining the influence of the avidity of the targeting antibodies, using bispecific antibodies targeting both the transferrin receptor and amyloid beta (i.e., mono-valent binding to the transferrin receptor, this approach resulted in higher binding and uptake when compared to low-affine, bivalent monospecific antibodies both in vivo and in vitro [54].

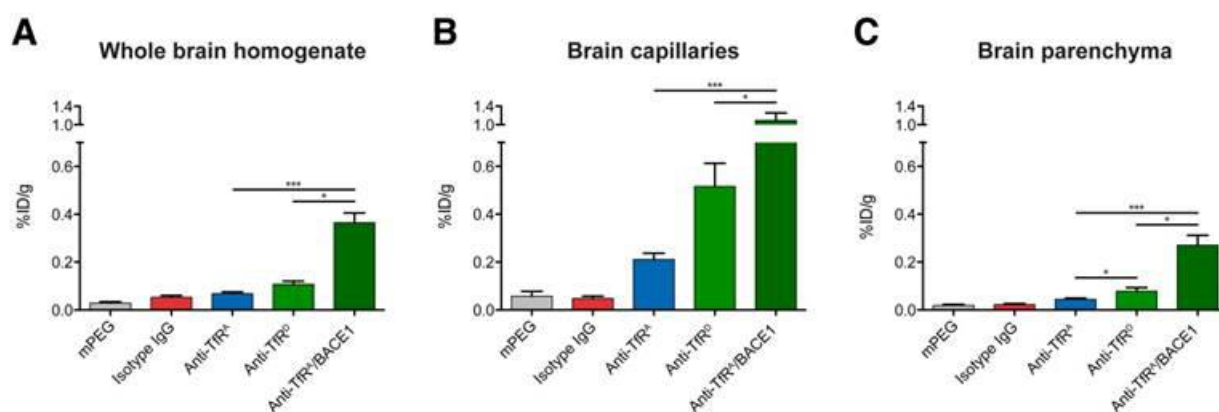


**Figure 3.** Uptake in the adult mouse brain of gold-labeled nanoparticles (AuNPs) targeted to the BBB by anti-transferrin receptor antibodies varying in affinity. Identical antibodies were studied prior for BBB transport without conjugation [44]. (A) In whole brain homogenates, there is a clear distinction between the different transferrin receptor (TfR)-targeted variants with respect to their accumulation. (B) The TfR-targeted AuNPs accumulate in the capillary fraction with  $0.2$ ,  $0.5$ , and  $1.1\%$  ID/g for anti-TfR<sup>A</sup>, anti-TfR<sup>D</sup>, and anti-TfR<sup>A</sup>/BACE1. (C) In fractions containing brain parenchyma, detection of AuNPs indicates transport across the BBB. Accumulation is mainly seen for the low-affinity anti-TfR<sup>D</sup> compared to the high-affinity anti-TfR<sup>A</sup> variant AuNPs. Anti-TfR<sup>A</sup>/BACE1 AuNPs are superior to the other TfR-targeted variant AuNPs with a mean parenchymal accumulation of  $0.23\%$  ID/g compared to  $0.04$  and  $0.08\%$  ID/g for anti-TfR<sup>A</sup> and anti-TfR<sup>D</sup>, respectively. Modified from [54]. Data are presented as mean  $\pm$  SEM ( $n = 7$ – $8$ , Kruskal-Wallis test with Dunn’s multiple comparisons post hoc test) with \*  $p < 0.05$  and \*\*\*  $p < 0.001$ . %ID/g: percentage of injected dose per gram.

The uptake of nanoparticles may be further enhanced by changing the shape of nanoparticles, provided they are constructed by a relevant material [60,61]. In vitro studies showed that rod-shaped polymeric nanoparticles targeted to the transferrin receptor underwent seven-fold higher uptake compared to spherical particles [60], clearly war-

ranting further pursuit *in vivo*. The nanoparticles' zeta potential is also important with slightly negative potential being optimal for uptake [11–13]. When present in blood plasma, nanoparticles tend to absorb blood-circulating proteins forming a so-called protein corona so significant that it may sterically block for binding of the targeting protein to its receptor [61]. Previous research on the liposomal protein corona may have suffered from significant methodological limitations making this issue too problematic as justified in more controlled experiments, showing that contaminating proteins may have interfered with the analysis of the protein corona [62–64]. To prevent a potential unwanted influence of protein corona on the targeting potential of the nanoparticles, the nanoparticles can be conjugated to their targeting antibody bridged in-between by PEG molecules, which simultaneously will limit their likelihood of being taken up in the reticuloendothelial system (RES) [9,10].

The possibility of using the transferrin receptor for targeting nanoparticles to the BECs has also been pursued in studies using dual targeting approaches in which transferrin is linked to the surface of nanoparticles in conjunction with other peptides. Studies were mainly performed *in vitro*, with additional biodistribution studies *in vivo* using nanoparticles conjugated with transferrin and cell-penetrating peptides (CPPs), or rabies virus glycoprotein (RVG) [65–67]. Although these approaches bear great potential, they warrant direct comparisons with antibodies targeting the transferrin receptor for efficient drug delivery to the brain. Other strategies examined the transferrin receptor targeting peptide T7 (aka T7-LS) bound to the surface of liposomes containing the chemotherapeutic vincristine and reported a significantly higher pharmacological effect compared to the targeting of liposomes bound to other transferrin receptor targeting peptides B6 and T12 [68].

Despite being available for experimental use for more than three decades, the transferrin receptor is by far still considered the most relevant target for nanoparticle drug delivery. It is only a few other candidates, such as CD98, GLUT1, basigin (CD147), and the insulin receptor that were being taken into consideration as an alternative, but other than the insulin receptor, these receptors remain unexploited for their targetability to BECs with regard to nanoparticles [19].

## **6. Anti-Transferrin Receptor Antibodies Weakened in Affinity or Lowered in Avidity Facilitate Nanoparticle Transport through BECs**

Anti-transferrin receptor-targeted monoclonal antibodies weakened in affinity for the receptor readily undergo transport across the BBB in a dose-dependent manner, becoming detectable in neurons [40]. Bispecific antibodies, with one domain targeting the transferrin receptor at high affinity and the other domain directed towards a putative therapeutic target relevant for treating Alzheimer's disease, *i.e.*, beta-secretase 1, lead to reduction of amyloidogenic peptide formation in the brain [41]. Unfortunately, studies have not yet been performed to examine the efficacy of targeted nanoparticles with respect to repeated or chronic dosing regimens. Such evaluations would help to understand the amounts of therapeutics encapsulated within nanoparticles that can be accumulated inside the brain.

Antibodies with low affinity for the transferrin receptor seem to follow a cellular route identical to that of high-affine antibodies, as prior exposure to high-affine antibodies leads to reduced transport of low-affine antibodies across the BBB both *in vivo* and *in vitro* [69]. The two different antibodies differ in that antibodies with low affinity are not directed towards lysosomes to the same extent as antibodies with high affinity [69]. Further information on intracellular transport relying on anti-transferrin receptor antibodies comes from the study on the subcellular distribution of anti-transferrin receptor antibody-conjugated gold nanoparticles [54] (Figure 4). This revealed gold particles in BECs, and when conjugated with low-affine or low-avidity antibodies, the gold particles were also detected in neurons, further arguing for transport across BECs. The targeted gold nanoparticles were apparent in BECs in clearly identifiable vesicular structures, which might represent sorting endosomes and lysosomes. The study did not identify gold nanoparticles fusing with the abluminal membrane, but this does not exclude the transcellular transport of the nanoparticles through the BBB. This uncertainty comes from the observation of a low number of sequestered

particles, and that the electron microscopy data were collected from thin sections, typically less than 100 nm. In turn, isolated mouse BECs arranged in hanging cell culture inserts with defined BBB properties revealed transcellular transport of gold nanoparticles when conjugated with low-affine or low-avidity antibodies, which supports the observation of nanoparticle transport across the BBB. Notably, the electron microscopy studies did not show signs of obstructive accumulation of the gold nanoparticles sized approximately 75 nm near the basement membrane, which may be a major restraint for nanoparticle trafficking in the brain's extracellular volume after release at the abluminal side of the BECs [9].

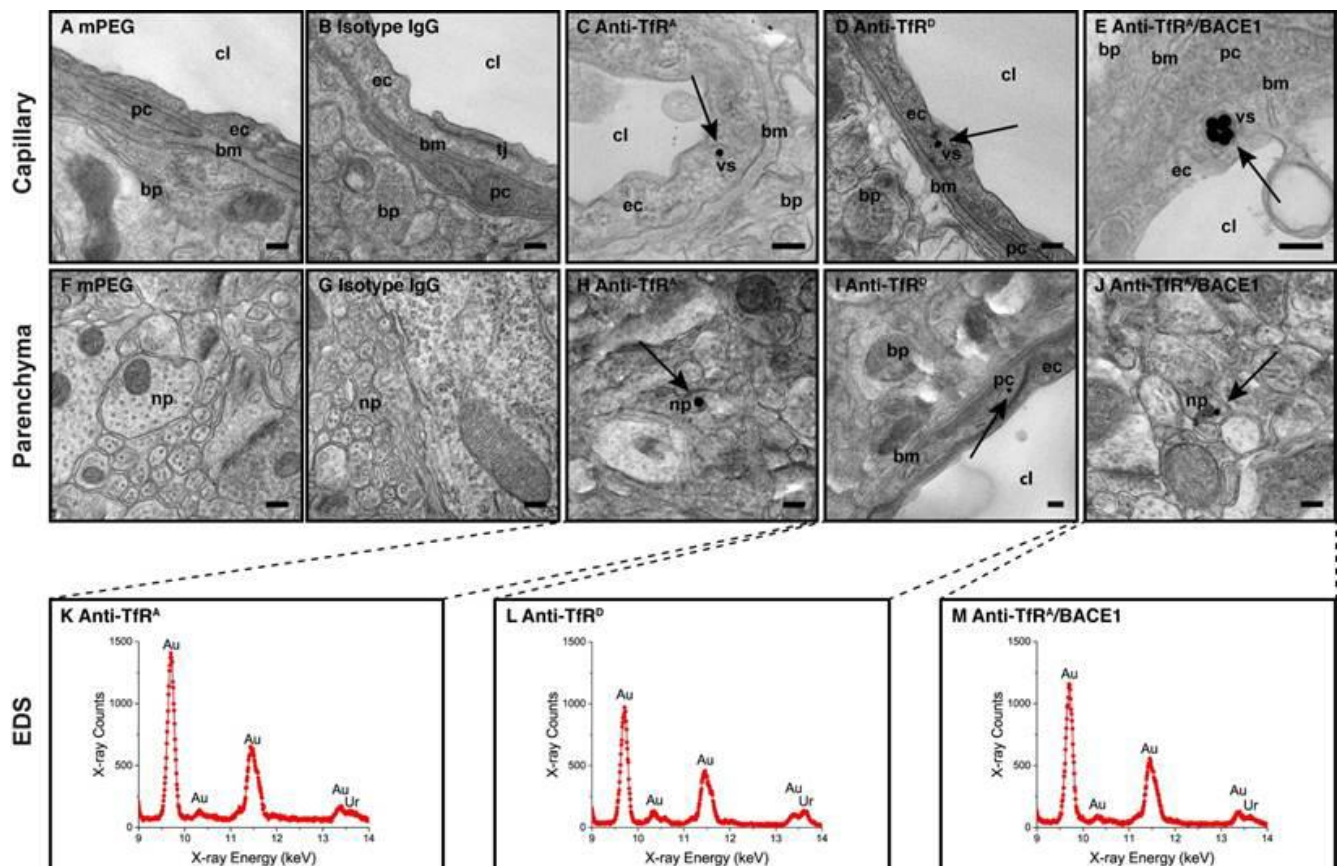


**Figure 4.** Detection of anti-transferrin receptor IgG conjugated gold-labeled nanoparticles (AuNPs) using transmission electron microscopy (TEM) in a normal adult mouse brain. Anti-transferrin receptor antibodies vary in affinity. (A,B) AuNPs are not detected in brain capillaries of mice in the mPEG (no IgG added) or isotype (non-immune) IgG groups. (C–E) In contrast, the AuNPs targeted with anti-transferrin receptor IgG are found in BECs (arrows). The AuNPs are detected in BECs confined to vesicular structures, suggesting receptor-mediated endocytosis as the uptake mechanism. (F,G) In brain parenchyma, AuNPs are not detected in mice in the mPEG or isotype (non-immune) IgG groups. (H–J) AuNPs are seen in brain parenchyma of mice treated with all transferrin receptor (TfR)-targeted variants, among which they are most easily detected in the anti-TfR<sup>A</sup>/BACE1 group (J). The sites for transport of the AuNPs may derive from transport across either BECs or post-capillary venules (see text body). All AuNPs detected in the brain parenchyma were analyzed using energy-dispersive X-ray spectroscopy (EDS) to validate the true presence of gold in the electron-dense points (K–M). Scale bars depict 200 nm. bp: brain parenchyma; bm: basement membrane; cl: capillary lumen; ec: endothelial cell; np: neural process; pc: pericyte; tj: tight junction; vs: vesicular structure. Modified from [54].



## 7. A Mechanistic Approach to an Understanding of Trafficking of Transferrin Receptor-Targeting Liposomes Based on Studies of Iron-Transferrin and Unconjugated Anti-Transferrin Receptor Antibody Trafficking in BECs

The paucity of studies examining intracellular trafficking of nanoparticles in BECs *in vivo* limits the available information about their transport mechanisms. Some lessons may be learned from comparison of endogenous transferrin and unconjugated, targeted anti-transferrin receptor antibodies. Although this difference obviously should be taken into account, the low-affinity antibodies and low-affinity antibodies conjugated to PEGylated liposomes share great similarities in transport through the BBB with unconjugated low-affinity and low-affinity anti-transferrin receptor antibodies [40,54].

### 7.1. Blood to Endothelium Transport

Endogenous transferrin enters the BECs after the interaction with the transferrin receptor on the luminal surface, facilitating subsequent formation of clathrin-coated pits, and eventually, formation of endosomes [9,16,24]. The endosomes have a slightly acidic pH, which promotes detaching iron from transferrin [9,16]. Consequently, the unbound iron can cross the endosomal membrane via divalent metal transporter 1 (DMT1), which makes the iron available in the cytosol [9,25]. In parallel, the iron-depleted apo-transferrin residing inside the endosome loses its affinity for the transferrin receptor, and is thought to undergo retro-endocytosis to the luminal surface of the endothelial cell [9,16].

### 7.2. Endothelium to Brain Transport

Whereas the docking and endosomal formation relate to the affinity of the transferrin receptor, it can be argued that the intracellular trafficking of the endosomes follow routes that occur independently of the luminal receptor internalization [9,16,51]. BECs contain RAB4 and RAB7 proteins specific for early and later sorting endosomes [70,71]. The abluminal membrane of the BECs also contains the protein TSG101 (tumor susceptibility gene 101), which takes part in exocytosis. This suggests that BECs contain organelles fully capable of handling transferrin receptor-containing vesicles that present themselves initially as early forming endosomes with the capacity to fuse with late endosomes, eventually leading to fusion with the abluminal membrane and exocytosis [72]. Therefore, the process of sorting transferrin receptor-containing vesicles is likely to be in two ways: Both morphological and pharmacological studies favor receptor-mediated endocytosis taking place at the luminal side leading to formation of early endosomes. This is followed by a vaguely understood trafficking of late endosomes directed towards fusion with the abluminal surface [9,16].

A morphological approach to detect transferrin at the ultrastructural level in rats subjected to the brain *in situ* perfusion failed to detect HRP-conjugated iron-transferrin near the abluminal side, which, in turn, was outnumbered by the presence of HRP-transferrin in multiple vesicular-like structures near the luminal side of the BECs [58]. However, as mentioned earlier, in the developing brain BECs are enriched in vesicles involved in transcellular trafficking. This, together with the observation that the developing brains have relatively higher expression of transferrin receptors [30,31], could account for directed transcellular trafficking of iron-transferrin-containing vesicles through the BECs. Interestingly, intracarotid perfusion with OX26-conjugated colloidal gold enabled detection at the abluminal side of the brain endothelium [58]. Although this study did not quantify the transport of the gold-labeled OX26, the appearance near the abluminal side may represent transferrin receptor-containing vesicles available for fusion at the abluminal side. A conclusion may be that as only a minor fraction of iron-transferrin within the transferrin-containing vesicles moves towards the abluminal side of the BEC, only a minor fraction of such vesicles including their content are released at the abluminal side of the BECs.

The binding to high-affine anti-transferrin receptor antibodies also leads to the formation of endocytotic vesicles that mainly localize near the luminal membrane [9,16]. The uptake and transport of high-affine, anti-transferrin receptor antibodies within the BECs are likely to follow the same route as that of iron-transferrin. However, differences may

occur, as the binding of the high-affine antibody to the transferrin receptor is thought not to be reversible, leading to accumulation of the antibody within the endosomal-lysosomal compartment [16]. Noteworthy, later studies addressing the fate of the anti-transferrin receptor antibodies showed that the complexes are incorporated in lysosomes rather than being directed towards release at the abluminal membrane [69]. A study in a mouse model with human transferrin receptors revealed that high-affine anti-transferrin receptor antibodies could undergo transport across the BBB [43]. However, it is very difficult to compare the consequences of binding affinity of anti-transferrin receptor antibodies between species concerning the capability to undergo transport at the BBB. The mechanisms that enable high-affine and low-affine antibodies to detach from the transferrin receptor within the endosome is poorly understood, but possibly, the acidic environment in the endosome facilitates the detachment of antibodies from the receptor. Even if a minor fraction of antibodies bound to the transferrin receptor is released in the acidic endosomal environment, a fraction of the high-affinity antibody would be released and would move further into the brain's extracellular space.

It goes beyond doubt that the optimal transport of targeted nanoparticles at the BBB depends on the binding of anti-transferrin receptor antibodies to the endothelial surface [68]. The transport of nanoparticles through BECs appears to depend on the affinity or low avidity of the anti-transferrin receptor antibody. Nanoparticles, therefore, may undergo transport through BECs similar to therapeutically active molecules like enzymes or other proteins directly conjugated to anti-transferrin receptor antibodies [73] (Figure 5).

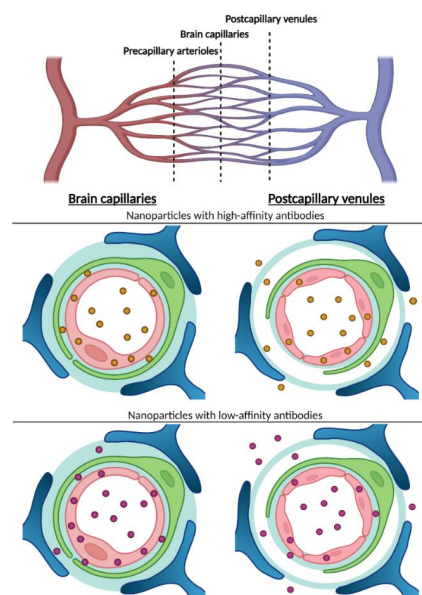


**Figure 5.** Working model of transcytosis-mediated nanoparticle delivery to the brain. Recent study provides evidence that high-affine anti-transferrin receptor IgG conjugated to liposomes mainly undergo transport into the brain at the site of post-capillary venules [14]. This observation counteracts that of unconjugated antibodies that passes the BBB at the site of brain capillaries when designed to be low in affinity or avidity [42]. Targeting the latter antibodies to gold nanoparticles leads to capillary transport in vitro using isolated brain capillaries [58] suggesting that accumulation of targeted nanoparticles in brain parenchyma in vivo may occur via transport across capillaries as well. Studies concerning transport into brain across post-capillary venules using transferrin receptor-targeted low-affine antibodies (lower right) have not been performed but can be stipulated to lead to enhanced transport compared to the use of corresponding antibodies with high affinity. Red bullets: high-affine anti-transferrin receptor IgG conjugated liposomes. Yellow bullets: low-affine or low-avidity anti-transferrin receptor IgG conjugated to liposomes. Drawing created with BioRender, inspired and modified from [14].

## 8. Post-Capillary Venules Denote an Alternate Route for Transport

The use of 2-photon microscopy (2PM) for *in vivo* studies has revolutionized the concept of how the brain works and has recently entered the field of the BBB research [74]. 2 PM visualizes fluorescently labeled molecules in the brain with a sub-micron spatial resolution and allows for visualization of individual nanoparticles in blood vessels to a depth of 600  $\mu\text{m}$  below the pial surface *in vivo* [74]. Recent studies using 2PM on the transferrin receptor-targeted liposomes demonstrated how endothelial cells of both brain capillaries and post-capillary venules in contrast to arterioles handle transferrin receptor-targeted liposomes at the level of a single nanoparticle [14] (Figure 6). The major finding was that the liposomes targeted with high-affine RI7217 were released to the brain almost exclusively from endothelial cells of the post-capillary venules, with negligible results.

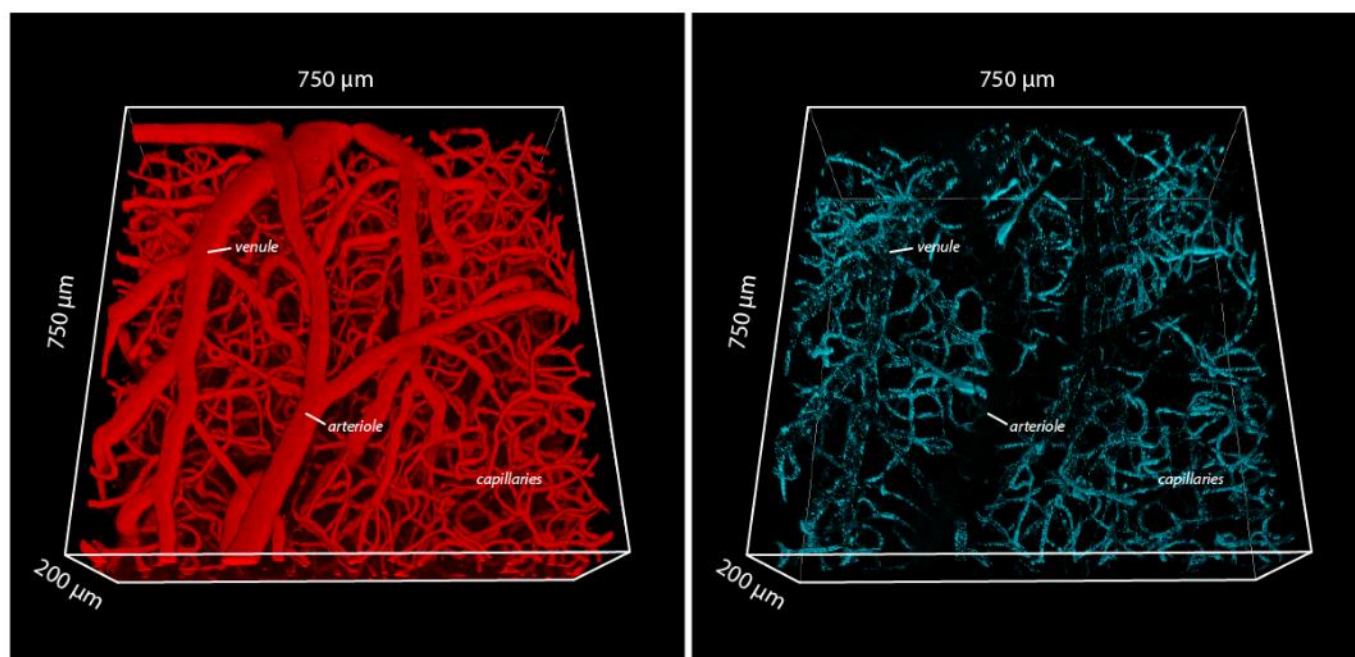


**Figure 6.** Example of *in vivo* 2PM data, showing three-dimensional reconstruction of cortical microvasculature (**left**), and the distribution of intravenously-injected transferrin receptor-targeted liposomes residing at the BBB interface (**right**). The transferrin receptor-targeted liposomes associate primarily to capillaries, then venules, but are absent in arterioles. The images were collected 2 h post injection. Modified from [14].

One study showed the contribution of endothelium at capillaries [14], which is scientifically provocative, considering previous investigations using this antibody to study transport across the brain endothelium. The release of the liposomes from the post-capillary venules is surprising, and the mechanisms and explanation for this observation will need further study. The barrier formed by the endothelial cells of the post-capillary venules is less tight at the venous side with respect to the number of tight junctions compared to BECs [75]. This could principally allow nanoparticles to enter the brain via paracellular transport, but counteracting this notion, the targeted nanoparticles were clearly taken up by the endothelial cells of the post-capillary venules before entering the brain on the abluminal side, verifying transendothelial transport of the targeted liposomes. In all, the density of transferrin receptor-targeted nanoparticles, being highest in capillaries, did not translate to efficient transport of nanoparticles to the brain. Thus, the BBB is highly heterogeneous regarding transport mechanisms, and, in particular, the ability to transcytose large constructs across the BBB [14].

The study of Kucharz et al. [14] clearly opens for novel considerations on the transport of targeted nanoparticles to the brain. An interesting consideration related to prior studies

demonstrating targeted liposomes within the brain [11–13,54] is that they could also have passed into the brain via this hitherto overseen route at post-capillary venules.

### 9. Targeting Nanoparticles to the Brain Endothelium in Pathological Conditions

The use of targeting approaches to promote enhanced drug delivery to the brain in pathology is only coming of age. Targeting approaches in conditions with cerebral pathology can roughly be separated into attempts to treat the brain in acute and chronic conditions. In acute conditions, e.g., ischemic stroke and traumatic brain injury, liposomes are advantageous among nanoparticles because they can be formulated to contain degradable lipids with enzymes like matrix metalloproteinases and phospholipases known to be increased in expression and released from the brain in acute pathology [76–79]. In terms of delivery to the brain, the liposomes will easily enter the affected brain regions as the vasculature is deteriorating, leading to the opening of the BBB. The liposomes are expected to start to degrade once they enter areas of the brain with a raised expression of, e.g., matrix metalloproteinases. This approach does not demand the liposomes to be functionalized by conjugation to a targeting antibody, but the targeting approach could allow for more widespread uptake of the liposomes in the surrounding areas of a central pathology, e.g., in ischemic stroke, the penumbra zone, where the BBB often remains intact [80]. Targeting to the BECs could enhance the liposomal delivery, which might allow, e.g., enhanced pharmacological preconditioning using focused ultrasound and microbubble treatment [81]. However, it should be noted that many acute conditions are also associated with obstructed blood flow due to pericyte-mediated constriction of capillaries, as observed, e.g., post stroke [82,83]. As such, the obstructed blood flow may limit the ability of the blood circulation to deliver the liposomes to the relevant, damaged areas in the brain.

Recent efforts aim to utilize a dual targeting approach using antibodies targeting the transferrin receptor and intercellular adhesion molecule-1 (ICAM1), both conjugated to liposomes. This resulted in higher binding compared to liposomes targeted to only transferrin receptor or ICAM1 antibodies alone [84]. This approach led to enhanced delivery of liposomes encapsulating the anti-inflammatory cytokine TNF-alpha in a model of acute brain inflammation [84].

In chronic brain disorders, like Alzheimer's disease and Parkinson's disease, the brain does not increase the expression of liposome-degradable enzymes like metalloproteinases and phospholipases to the same extent as seen in acute neuropathology, and therefore, the strategy of substrate degradable liposomes may not apply. Instead, it may be advantageous that the BEC expression of the transferrin receptor remains unchanged in Alzheimer's disease [85], which further justifies attempts to target transferrin receptors expressed by BECs in the neurodegenerative brain expected to have a near intact BBB.

### 10. Conclusions

BECs are practically incapable of uptake of native liposomes from the blood, which requires the addition of targeted molecules. Experience gained from different targeting approaches justifies the choice of antibodies targeting the transferrin receptor for targeted delivery of nanoparticles to BECs. Liposomes functionalized by conjugated anti-transferrin receptor antibodies are taken up by endothelial cells at both brain capillaries and post-capillary venules. Modulating the number of transferrin receptor-targeted antibodies shows that limiting the number of targeting antibodies conjugated to liposomes reduces uptake in BECs. In comparison, lowering the affinity of the targeting antibodies or implementing bispecific antibodies with low avidity increases transport by BECs into the brain parenchyma. With increasing evidence of successful preclinical trials and advances in biochemical and analytical approaches, the transferrin receptor-targeted nanoparticles have great promise for future use in drug delivery as they evidently pass the BBB.

**Author Contributions:** Conceptualization, M.S.T. and T.M.; Writing—original draft preparation, M.S.T. and T.M.; Writing—review and editing, K.B.J., K.K. and M.L. All authors have read and agreed to the published version of the manuscript.

**Funding:** Parts of the data by the authors presented in this manuscript were obtained by generous support from the Lundbeck foundation and by a grant from Agnes og Poul Friis Fond to Martin Lauritzen and Krzysztof Kucharz.

**Institutional Review Board Statement:** Not applicable.

**Informed Consent Statement:** Not applicable.

**Data Availability Statement:** None.

**Conflicts of Interest:** The authors have no conflict of interest to declare.

### Abbreviations

**2PM:** 2-photon microscopy; **BBB:** blood–brain barrier; **BECs:** brain endothelial cells; **CRM:** cross-reacting material; **CSF:** cerebrospinal fluid barrier; **GLUT1:** glucose transporter 1.

### References

- Abbott, N.J.; Patabendige, A.A.K.; Dolman, D.E.M.; Yusof, S.R.; Begley, D.J. Structure and Function of the Blood-Brain Barrier. *Neurobiol. Dis.* **2010**, *37*, 13–25. [CrossRef] [PubMed]
- Pardridge, W.M. CSF, Blood-Brain Barrier, and Brain Drug Delivery. *Expert Opin. Drug Deliv.* **2016**, *13*, 963–975. [CrossRef] [PubMed]
- Pardridge, W.M. A Historical Review of Brain Drug Delivery. *Pharmaceutics* **2022**, *14*, 1283. [CrossRef] [PubMed]
- Profaci, C.P.; Munji, R.N.; Pulido, R.S.; Daneman, R. The Blood–Brain Barrier in Health and Disease: Important Unanswered Questions. *J. Exp. Med.* **2020**, *217*, e20190062. [CrossRef]
- Lichota, J.; Skjorringe, T.; Thomsen, L.B.; Moos, T. Macromolecular Drug Transport into the Brain Using Targeted Therapy. *J. Neurochem.* **2010**, *113*, 1–13. [CrossRef]
- Lajoie, J.M.; Shusta, E.V. Targeting Receptor-Mediated Transport for Delivery of Biologics across the Blood-Brain Barrier. *Annu. Rev. Pharmacol. Toxicol.* **2015**, *55*, 613–631. [CrossRef]
- Boado, R.J. IgG Fusion Proteins for Brain Delivery of Biologics via Blood-Brain Barrier Receptor-Mediated Transport. *Pharmaceutics* **2022**, *14*, 1476. [CrossRef]
- Futtrup, J.; Margolinsky, R.; Benros, M.E.; Moos, T.; Routhe, L.J.; Rungby, J.; Krogh, J. Blood-Brain Barrier Pathology in Patients with Severe Mental Disorders: A Systematic Review and Meta-Analysis of Biomarkers in Case-Control Studies. *Brain Behav. Immun.-Health* **2020**, *6*, 100102. [CrossRef]
- Johnsen, K.B.; Burkhart, A.; Thomsen, L.B.; Andresen, T.L.; Moos, T. Targeting the Transferrin Receptor for Brain Drug Delivery. *Prog. Neurobiol.* **2019**, *181*, 101665. [CrossRef]
- Saraiva, C.; Praça, C.; Ferreira, R.; Santos, T.; Ferreira, L.; Bernardino, L. Nanoparticle-Mediated Brain Drug Delivery: Overcoming Blood-Brain Barrier to Treat Neurodegenerative Diseases. *J. Control. Release* **2016**, *235*, 34–47. [CrossRef]
- Shi, N.; Pardridge, W.M. Noninvasive Gene Targeting to the Brain. *Proc. Natl. Acad. Sci. USA* **2000**, *97*, 7567–7572. [CrossRef]
- Shi, N.; Zhang, Y.; Zhu, C.; Boado, R.J.; Pardridge, W.M. Brain-Specific Expression of an Exogenous Gene after i.v. Administration. *Proc. Natl. Acad. Sci. USA* **2001**, *98*, 12754–12759. [CrossRef]
- Zhang, Y.; Schlachetzki, F.; Pardridge, W.M. Global Non-Viral Gene Transfer to the Primate Brain Following Intravenous Administration. *Mol. Ther.* **2003**, *7*, 11–18. [CrossRef]
- Kucharz, K.; Kristensen, K.; Johnsen, K.B.; Lund, M.A.; Lønstrup, M.; Moos, T.; Andresen, T.L.; Lauritzen, M.J. Post-Capillary Venules Are the Key Locus for Transcytosis-Mediated Brain Delivery of Therapeutic Nanoparticles. *Nat. Commun.* **2021**, *12*, 4121. [CrossRef]
- Routhe, L.J.; Thomsen, M.S.; Moos, T. The significance of the choroid plexus for cerebral iron homeostasis. In *Role of the Choroid Plexus in Health and Disease*; Springer: New York, NY, USA, 2020; pp. 125–148. [CrossRef]
- Moos, T.; Morgan, E.H. Restricted Transport of Anti-Transferrin Receptor Antibody (OX26) through the Blood-Brain Barrier in the Rat. *J. Neurochem.* **2001**, *79*, 119–129. [CrossRef]
- Angelova-Gateva, P. Iron Transferrin Receptors in Rat and Human Cerebrum. *Agressologie* **1980**, *1*, 27–30.
- Jefferies, W.A.; Brandon, M.R.; Hunt, S.V.; Williams, A.F.; Gatter, K.C.; Mason, D.Y. Transferrin Receptor on Endothelium of Brain Capillaries. *Nature* **1984**, *312*, 162–163. [CrossRef]
- Zuchero, Y.J.Y.; Chen, X.; Bien-Ly, N.; Bumbaca, D.; Tong, R.K.; Gao, X.; Zhang, S.; Hoyte, K.; Luk, W.; Huntley, M.A.; et al. Discovery of Novel Blood-Brain Barrier Targets to Enhance Brain Uptake of Therapeutic Antibodies. *Neuron* **2016**, *89*, 70–82. [CrossRef]
- Hoyes, K.P.; Morris, I.D.; Hendry, J.H.; Sharma, H.L. Transferrin-Mediated Uptake of Radionuclides by the Testis. *J. Nucl. Med.* **1996**, *37*, 336–340.
- Pardridge, W.M.; Buciak, J.L.; Friden, P.M. Selective Transport of an Anti-Transferrin Receptor Antibody through the Blood-Brain Barrier in Vivo. *J. Pharmacol. Exp. Ther.* **1991**, *259*, 66–70.

22. Vanlandewijck, M.; He, L.; Mäe, M.A.; Andrae, J.; Ando, K.; Del Gaudio, F.; Nahar, K.; Lebouvier, T.; Laviña, B.; Gouveia, L.; et al. A Molecular Atlas of Cell Types and Zonation in the Brain Vasculature. *Nature* **2018**, *554*, 475–480. [CrossRef]
23. He, L.; Vanlandewijck, M.; Mäe, M.A.; Andrae, J.; Ando, K.; Del Gaudio, F.; Nahar, K.; Lebouvier, T.; Laviña, B.; Gouveia, L.; et al. Single-Cell RNA Sequencing of Mouse Brain and Lung Vascular and Vessel-Associated Cell Types. *Sci. Data* **2018**, *5*, 180160. [CrossRef]
24. Moos, T.; Morgan, E.H. Transferrin and Transferrin Receptor Function in Brain Barrier Systems. *Cell. Mol. Neurobiol.* **2000**, *20*, 77–95. [CrossRef]
25. Morris, C.M.; Keith, A.B.; Edwardson, J.A.; Pullen, R.G.L. Uptake and Distribution of Iron and Transferrin in the Adult Rat Brain. *J. Neurochem.* **1992**, *59*, 300–306. [CrossRef]
26. Hu, Y.B.; Dammer, E.B.; Ren, R.J.; Wang, G. The Endosomal-Lysosomal System: From Acidification and Cargo Sorting to Neurodegeneration. *Transl. Neurodegener.* **2015**, *4*, 18. [CrossRef]
27. Burkhart, A.; Skjorringe, T.; Johnsen, K.B.; Siupka, P.; Thomsen, L.B.; Nielsen, M.S.; Thomsen, L.L.; Moos, T. Expression of Iron-Related Proteins at the Neurovascular Unit Supports Reduction and Reoxidation of Iron for Transport Through the Blood-Brain Barrier. *Mol Neurobiol* **2015**, *53*, 7237–7253. [CrossRef]
28. Fishman, J.B.; Rubin, J.B.; Handrahan, J.V.; Connor, J.R.; Fine, R.E. Receptor-Mediated Transcytosis of Transferrin across the Blood-Brain Barrier. *J. Neurosci. Res.* **1987**, *18*, 299–304. [CrossRef]
29. Skarlatos, S.; Yoshikawa, T.; Pardridge, W.M. Transport of [125I]Transferrin through the Rat Blood-Brain Barrier. *Brain Res.* **1995**, *683*, 164–171. [CrossRef]
30. Taylor, E.M.; Morgan, E.H. Developmental Changes in Transferrin and Iron Uptake by the Brain in the Rat. *Brain Res. Dev. Brain Res.* **1990**, *55*, 35–42. [CrossRef]
31. Morgan, E.H.; Moos, T. Mechanism and Developmental Changes in Iron Transport across the Blood-Brain Barrier. *Dev. Neurosci.* **2002**, *24*, 106–113. [CrossRef]
32. Moos, T.; Morgan, E.H. A Morphological Study of the Developmentally Regulated Transport of Iron into the Brain. *Dev. Neurosci.* **2002**, *24*, 99–105. [CrossRef] [PubMed]
33. Kniessel, U.; Risau, W.; Wolburg, H. Development of Blood-Brain Barrier Tight Junctions in the Rat Cortex. *Brain Res. Dev. Brain Res.* **1996**, *96*, 229–240. [CrossRef]
34. Banks, W.A.; Broadwell, R.D. Blood to Brain and Brain to Blood Passage of Native Horseradish Peroxidase, Wheat Germ Agglutinin, and Albumin: Pharmacokinetic and Morphological Assessments. *J. Neurochem.* **1994**, *62*, 2404–2419. [CrossRef]
35. Balin, B.J.; Broadwell, R.D. Transcytosis of Protein through the Mammalian Cerebral Epithelium and Endothelium. I. Choroid Plexus and the Blood-Cerebrospinal Fluid Barrier. *J. Neurocytol.* **1988**, *17*, 809–826. [CrossRef] [PubMed]
36. Friden, P.M.; Walus, L.R.; Musso, G.F.; Taylor, M.A.; Malfroy, B.; Starzyk, R.M. Anti-Transferrin Receptor Antibody and Antibody-Drug Conjugates Cross the Blood-Brain Barrier. *Proc. Natl. Acad. Sci. USA* **1991**, *88*, 4771–4775. [CrossRef] [PubMed]
37. Shin, S.U.; Friden, P.; Moran, M.; Olson, T.; Kang, Y.S.; Pardridge, W.M.; Morrison, S.L. Transferrin-Antibody Fusion Proteins Are Effective in Brain Targeting. *Proc. Natl. Acad. Sci. USA* **1995**, *92*, 2820–2824. [CrossRef]
38. Frank, H.J.L.; Pardridge, W.M. A Direct in Vitro Demonstration of Insulin Binding to Isolated Brain Microvessels. *Diabetes* **1981**, *30*, 757–761. [CrossRef]
39. Paris-Robidas, S.; Emond, V.; Tremblay, C.; Soulet, D.; Calon, F. In Vivo Labeling of Brain Capillary Endothelial Cells after Intravenous Injection of Monoclonal Antibodies Targeting the Transferrin Receptor. *Mol. Pharmacol.* **2011**, *80*, 32–39. [CrossRef]
40. Yu, Y.J.; Zhang, Y.; Kenrick, M.; Hoyte, K.; Luk, W.; Lu, Y.; Atwal, J.; Elliott, J.M.; Prabhu, S.; Watts, R.J.; et al. Boosting Brain Uptake of a Therapeutic Antibody by Reducing Its Affinity for a Transcytosis Target. *Sci. Transl. Med.* **2011**, *3*, 84ra44. [CrossRef]
41. Niewoehner, J.; Bohrmann, B.; Collin, L.; Urich, E.; Sade, H.; Maier, P.; Rueger, P.; Stracke, J.O.; Lau, W.; Tissot, A.C.; et al. Increased Brain Penetration and Potency of a Therapeutic Antibody Using a Monovalent Molecular Shuttle. *Neuron* **2014**, *81*, 49–60. [CrossRef]
42. Kariolis, M.S.; Wells, R.C.; Getz, J.A.; Kwan, W.; Mahon, C.S.; Tong, R.; Kim, D.J.; Srivastava, A.; Bedard, C.; Henne, K.R.; et al. Brain Delivery of Therapeutic Proteins Using an Fc Fragment Blood-Brain Barrier Transport Vehicle in Mice and Monkeys. *Sci. Transl. Med.* **2020**, *12*, eaay1359. [CrossRef]
43. Sonoda, H.; Morimoto, H.; Yoden, E.; Koshimura, Y.; Kinoshita, M.; Golovina, G.; Takagi, H.; Yamamoto, R.; Minami, K.; Mizoguchi, A.; et al. A Blood-Brain-Barrier-Penetrating Anti-Human Transferrin Receptor Antibody Fusion Protein for Neurodegenerative Mucopolysaccharidosis II. *Mol. Ther.* **2018**, *26*, 1366–1374. [CrossRef]
44. Sehlin, D.; Fang, X.T.; Cato, L.; Antoni, G.; Lannfelt, L.; Syvänen, S. Antibody-Based PET Imaging of Amyloid Beta in Mouse Models of Alzheimer’s Disease. *Nat. Commun.* **2016**, *7*, 10759. [CrossRef]
45. Hultqvist, G.; Syvänen, S.; Fang, X.T.; Lannfelt, L.; Sehlin, D. Bivalent Brain Shuttle Increases Antibody Uptake by Monovalent Binding to the Transferrin Receptor. *Theranostics* **2017**, *7*, 308–318. [CrossRef]
46. Stocki, P.; Szary, J.; Rasmussen, C.L.M.; Demydchuk, M.; Northall, L.; Logan, D.B.; Gauhar, A.; Thei, L.; Moos, T.; Walsh, F.S.; et al. Blood-Brain Barrier Transport Using a High Affinity, Brain-Selective VNAR Antibody Targeting Transferrin Receptor 1. *FASEB J.* **2021**, *35*, e21172. [CrossRef]
47. Arguello, A.; Mahon, C.S.; Calvert, M.E.K.; Chan, D.; Dugas, J.C.; Pizzo, M.E.; Thomsen, E.R.; Chau, R.; Damo, L.A.; Duque, J.; et al. Molecular Architecture Determines Brain Delivery of a Transferrin Receptor-Targeted Lysosomal Enzyme. *J. Exp. Med.* **2022**, *219*, e20211057. [CrossRef]

48. Boado, R.J.; Li, J.Y.; Nagaya, M.; Zhang, C.; Pardridge, W.M. Selective Expression of the Large Neutral Amino Acid Transporter at the Blood-Brain Barrier. *Proc. Natl. Acad. Sci. USA* **1999**, *96*, 12079–12084. [CrossRef]
49. Pardridge, W.M.; Boado, R.J.; Farrell, C.R. Brain-Type Glucose Transporter (GLUT-1) Is Selectively Localized to the Blood-Brain Barrier. Studies with Quantitative Western Blotting and in Situ Hybridization. *J. Biol. Chem.* **1990**, *265*, 18035–18040. [CrossRef]
50. Pardridge, W.M. The Isolated Brain Microvessel: A Versatile Experimental Model of the Blood-Brain Barrier. *Front. Physiol.* **2020**, *11*, 398. [CrossRef]
51. Gosk, S.; Vermehren, C.; Storm, G.; Moos, T. Targeting Anti-Transferrin Receptor Antibody (OX26) and OX26-Conjugated Liposomes to Brain Capillary Endothelial Cells Using in Situ Perfusion. *J. Cereb. Blood Flow Metab.* **2004**, *24*, 1193–1204. [CrossRef]
52. Van Rooy, I.; Mastrobattista, E.; Storm, G.; Hennink, W.E.; Schiffelers, R.M. Comparison of Five Different Targeting Ligands to Enhance Accumulation of Liposomes into the Brain. *J. Control. Release* **2011**, *150*, 30–36. [CrossRef] [PubMed]
53. Johnsen, K.B.; Burkhart, A.; Melander, F.; Kempen, P.J.; Vejlebo, J.B.; Siupka, P.; Nielsen, M.S.; Andresen, T.L.; Moos, T. Targeting Transferrin Receptors at the Blood-Brain Barrier Improves the Uptake of Immunoliposomes and Subsequent Cargo Transport into the Brain Parenchyma. *Sci. Rep.* **2017**, *7*, 10396. [CrossRef] [PubMed]
54. Johnsen, K.B.; Bak, M.; Kempen, P.J.; Melander, F.; Burkhart, A.; Thomsen, M.S.; Nielsen, M.S.; Moos, T.; Andresen, T.L. Antibody Affinity and Valency Impact Brain Uptake of Transferrin Receptor-Targeted Gold Nanoparticles. *Theranostics* **2018**, *8*, 3416–3436. [CrossRef] [PubMed]
55. Paris-Robidas, S.; Brouard, D.; Emond, V.; Parent, M.; Calon, F. Internalization of Targeted Quantum Dots by Brain Capillary Endothelial Cells in Vivo. *J. Cereb. Blood Flow Metab.* **2016**, *36*, 731–742. [CrossRef]
56. Michaelis, K.; Hoffmann, M.M.; Dreis, S.; Herbert, E.; Alyautdin, R.N.; Michaelis, M.; Kreuter, J.; Langer, K. Covalent Linkage of Apolipoprotein e to Albumin Nanoparticles Strongly Enhances Drug Transport into the Brain. *J. Pharmacol. Exp. Ther.* **2006**, *317*, 1246–1253. [CrossRef]
57. Gaillard, P.J.; Visser, C.C.; de Boer, A.G. Targeted Delivery across the Blood-Brain Barrier. *Expert Opin. Drug Deliv.* **2005**, *2*, 299–309. [CrossRef]
58. Shao, K.; Huang, R.; Li, J.; Han, L.; Ye, L.; Lou, J.; Jiang, C. Angiopep-2 Modified PE-PEG Based Polymeric Micelles for Amphotericin B Delivery Targeted to the Brain. *J. Control. Release* **2010**, *147*, 118–126. [CrossRef]
59. Johnsen, K.B.; Bak, M.; Melander, F.; Thomsen, M.S.; Burkhart, A.; Kempen, P.J.; Andresen, T.L.; Moos, T. Modulating the Antibody Density Changes the Uptake and Transport at the Blood-Brain Barrier of Both Transferrin Receptor-Targeted Gold Nanoparticles and Liposomal Cargo. *J. Control. Release* **2019**, *295*, 237–249. [CrossRef]
60. Kolhar, P.; Anselmo, A.C.; Gupta, V.; Pant, K.; Prabhakarpandian, B.; Ruoslahti, E.; Mitragotri, S. Using Shape Effects to Target Antibody-Coated Nanoparticles to Lung and Brain Endothelium. *Proc. Natl. Acad. Sci. USA* **2013**, *110*, 10753–10758. [CrossRef]
61. Sepand, M.R.; Ghavami, M.; Zanganeh, S.; Stacks, S.; Ghasemi, F.; Montazeri, H.; Corbo, C.; Derakhshankhah, H.; Ostad, S.N.; Ghahremani, M.H.; et al. Impact of Plasma Concentration of Transferrin on Targeting Capacity of Nanoparticles. *Nanoscale* **2020**, *12*, 4935–4944. [CrossRef]
62. Kristensen, K.; Münter, R.; Kempen, P.J.; Thomsen, M.E.; Stensballe, A.; Andresen, T.L. Isolation Methods Commonly Used to Study the Liposomal Protein Corona Suffer from Contamination Issues. *Acta Biomater.* **2021**, *130*, 460–472. [CrossRef]
63. Kristensen, K.; Urquhart, A.J.; Thormann, E.; Andresen, T.L. Binding of Human Serum Albumin to PEGylated Liposomes: Insights into Binding Numbers and Dynamics by Fluorescence Correlation Spectroscopy. *Nanoscale* **2016**, *8*, 19726–19736. [CrossRef]
64. Kristensen, K.; Engel, T.B.; Stensballe, A.; Simonsen, J.B.; Andresen, T.L. The Hard Protein Corona of Stealth Liposomes Is Sparse. *J. Control. Release* **2019**, *307*, 1–15. [CrossRef]
65. Dos Santos Rodrigues, B.; Lakkadwala, S.; Kanekiyo, T.; Singh, J. Dual-Modified Liposome for Targeted and Enhanced Gene Delivery into Mice Brain. *J. Pharmacol. Exp. Ther.* **2020**, *374*, 354–365. [CrossRef]
66. Dos Santos Rodrigues, B.; Arora, S.; Kanekiyo, T.; Singh, J. Efficient Neuronal Targeting and Transfection Using RVG and Transferrin-Conjugated Liposomes. *Brain Res.* **2020**, *1734*, 146738. [CrossRef]
67. Dos Santos Rodrigues, B.; Kanekiyo, T.; Singh, J. In Vitro and in Vivo Characterization of CPP and Transferrin Modified Liposomes Encapsulating PDNA. *Nanomedicine* **2020**, *28*, 102225. [CrossRef]
68. Mojarad-Jabali, S.; Farshbaf, M.; Hemmati, S.; Sarfraz, M.; Motasadizadeh, H.; Shahbazi Mojarrad, J.; Atyabi, F.; Zakeri-Milani, P.; Valizadeh, H. Comparison of Three Synthetic Transferrin Mimetic Small Peptides to Promote the Blood-Brain Barrier Penetration of Vincristine Liposomes for Improved Glioma Targeted Therapy. *Int. J. Pharm.* **2022**, *613*, 121395. [CrossRef]
69. Bien-Ly, N.; Yu, Y.J.; Bumbaca, D.; Elstrott, J.; Boswell, C.A.; Zhang, Y.; Luk, W.; Lu, Y.; Dennis, M.S.; Weimer, R.M.; et al. Transferrin Receptor (TfR) Trafficking Determines Brain Uptake of TfR Antibody Affinity Variants. *J. Exp. Med.* **2014**, *211*, 233–244. [CrossRef]
70. Toth, A.E.; Holst, M.R.; Nielsen, M.S. Vesicular Transport Machinery in Brain Endothelial Cells: What We Know and What We Do Not. *Curr. Pharm. Des.* **2020**, *26*, 1405–1416. [CrossRef]
71. Haqqani, A.S.; Delaney, C.E.; Brunette, E.; Baumann, E.; Farrington, G.K.; Sisk, W.; Eldredge, J.; Ding, W.; Tremblay, T.L.; Stanimirovic, D.B. Endosomal Trafficking Regulates Receptor-Mediated Transcytosis of Antibodies across the Blood Brain Barrier. *J. Cereb. Blood Flow Metab.* **2018**, *38*, 727–740. [CrossRef]
72. Haqqani, A.S.; Delaney, C.E.; Tremblay, T.L.; Sodja, C.; Sandhu, J.K.; Stanimirovic, D.B. Method for Isolation and Molecular Characterization of Extracellular Microvesicles Released from Brain Endothelial Cells. *Fluids Barriers CNS* **2013**, *10*, 4. [CrossRef]



73. Moos, T.; Gudbergsson, J.M.; Johnsen, K.B. Transport of Transferrin Receptor-Targeted Antibodies through the Blood-Brain Barrier for Drug Delivery to the Brain. *AAPS Adv. Pharm. Sci. Ser.* **2022**, *33*, 527–549. [CrossRef]
74. Kucharz, K.; Kutuzov, N.; Zhukov, O.; Mathiesen Janiurek, M.; Lauritzen, M. Shedding Light on the Blood-Brain Barrier Transport with Two-Photon Microscopy In Vivo. *Pharm. Res.* **2022**, *39*, 1457–1468. [CrossRef]
75. Nagy, Z.; Peters, H.; Huttner, I. Fracture Faces of Cell Junctions in Cerebral Endothelium during Normal and Hyperosmotic Conditions. *Lab. Investig.* **1984**, *50*, 313–322.
76. Elegbede, A.I.; Banerjee, J.; Hanson, A.J.; Tobwala, S.; Ganguli, B.; Wang, R.; Lu, X.; Srivastava, D.K.; Mallik, S. Mechanistic Studies of the Triggered Release of Liposomal Contents by Matrix Metalloproteinase-9. *J. Am. Chem. Soc.* **2008**, *130*, 10633–10642. [CrossRef]
77. Zhao, B.Q.; Wang, S.; Kim, H.Y.; Storrie, H.; Rosen, B.R.; Mooney, D.J.; Wang, X.; Lo, E.H. Role of Matrix Metalloproteinases in Delayed Cortical Responses after Stroke. *Nat. Med.* **2006**, *12*, 441–445. [CrossRef]
78. Bruch, G.E.; Fernandes, L.F.; Bassi, B.L.T.; Alves, M.T.R.; Pereira, I.O.; Frézard, F.; Massensini, A.R. Liposomes for Drug Delivery in Stroke. *Brain Res. Bull.* **2019**, *152*, 246–256. [CrossRef]
79. Muralikrishna Adibhatla, R.; Hatcher, J.F.; Dempsey, R.J. Phospholipase A2, Hydroxyl Radicals, and Lipid Peroxidation in Transient Cerebral Ischemia. *Antioxid. Redox Signal.* **2003**, *5*, 647–654. [CrossRef]
80. Heidari, P.; Blayney, S.; Butler, J.; Hitomi, E.; Luby, M.; Leigh, R. The Relationship Between Penumbra Tissue and Blood-Brain Barrier Disruption in Acute Stroke Patients Presenting in an Extended Time Window. *Front. Neurol.* **2020**, *11*, 582994. [CrossRef]
81. Olsman, M.; Sereti, V.; Mühlenpfordt, M.; Johnsen, K.B.; Andresen, T.L.; Urquhart, A.J.; de Lange Davies, C. Focused Ultrasound and Microbubble Treatment Increases Delivery of Transferrin Receptor-Targeting Liposomes to the Brain. *Ultrasound Med. Biol.* **2021**, *47*, 1343–1355. [CrossRef]
82. Hall, C.N.; Reynell, C.; Gesslein, B.; Hamilton, N.B.; Mishra, A.; Sutherland, B.A.; O’Farrell, F.M.; Buchan, A.M.; Lauritzen, M.; Attwell, D. Capillary Pericytes Regulate Cerebral Blood Flow in Health and Disease. *Nature* **2014**, *508*, 55–60. [CrossRef] [PubMed]
83. Grubb, S.; Lauritzen, M.; Aalkjær, C. Brain Capillary Pericytes and Neurovascular Coupling. *Comp. Biochem. Physiol. Part A Mol. Integr. Physiol.* **2021**, *254*, 110893. [CrossRef] [PubMed]
84. Marcos-Contreras, O.A.; Greineder, C.F.; Kiseleva, R.Y.; Parhiz, H.; Walsh, L.R.; Zuluaga-Ramirez, V.; Myerson, J.W.; Hood, E.D.; Villa, C.H.; Tombacz, I.; et al. Selective Targeting of Nanomedicine to Inflamed Cerebral Vasculature to Enhance the Blood–Brain Barrier. *Proc. Natl. Acad. Sci. USA* **2020**, *117*, 3405–3414. [CrossRef] [PubMed]
85. Bourassa, P.; Alata, W.; Tremblay, C.; Paris-Robidas, S.; Calon, F. Transferrin Receptor-Mediated Uptake at the Blood-Brain Barrier Is Not Impaired by Alzheimer’s Disease Neuropathology. *Mol. Pharm.* **2019**, *16*, 583–594. [CrossRef]





## Article

# pH-Responsive Lipid Nanoparticles Achieve Efficient mRNA Transfection in Brain Capillary Endothelial Cells

Yu Sakurai <sup>1,\*</sup>,<sup>†</sup> , Himeka Watanabe <sup>1,†</sup>, Kazuma Nishio <sup>1,†</sup>, Kohei Hashimoto <sup>1,†</sup>, Atsuki Harada <sup>1,†</sup>, Masaki Gomi <sup>2</sup>, Masayoshi Suzuki <sup>1</sup>, Ryotaro Oyama <sup>2</sup>, Takumi Handa <sup>1</sup>, Risa Sato <sup>1</sup>, Hina Takeuchi <sup>1</sup>, Ryoga Taira <sup>1</sup>, Kenta Tezuka <sup>1</sup>, Kota Tange <sup>3</sup>, Yuta Nakai <sup>3</sup>, Hidetaka Akita <sup>1,\*</sup> and Yasuo Uchida <sup>1,\*</sup> 

- <sup>1</sup> Laboratory of DDS Design and Drug Disposition, Graduate School of Pharmaceutical Sciences, Tohoku University, 6-3 Aoba, Aramaki, Aoba-ku, Sendai 980-8578, Japan; himeka.watanabe.q7@dc.tohoku.ac.jp (H.W.); kazuma.nishio.t7@dc.tohoku.ac.jp (K.N.); kohei.hashimoto.t7@dc.tohoku.ac.jp (K.H.); atsuki.harada.s3@dc.tohoku.ac.jp (A.H.); masayoshi.suzuki.s8@dc.tohoku.ac.jp (M.S.); takumi.handa.q2@dc.tohoku.ac.jp (T.H.); risa.sato.t8@dc.tohoku.ac.jp (R.S.); hina.takeuchi.t5@dc.tohoku.ac.jp (H.T.); ryoga.taira.q2@dc.tohoku.ac.jp (R.T.); kenta.tezuka.r5@dc.tohoku.ac.jp (K.T.)
- <sup>2</sup> Laboratory of DDS Design and Drug Disposition, Graduate School of Pharmaceutical Sciences, Chiba University, 1-8-1 Inohana, Chuo-ku, Chiba 260-0856, Japan; gomi.masaki.t6@dc.tohoku.ac.jp (M.G.); oyama.ryotaro.p3@dc.tohoku.ac.jp (R.O.)
- <sup>3</sup> DDS Research Laboratory, NOF CORPORATION, 3-3 Chidori-cho, Kawasaki-ku, Kawasaki 210-0865, Japan; kota\_tange@nof.co.jp (K.T.); yuta\_nakai@nof.co.jp (Y.N.)
- \* Correspondence: yu.sakurai.e7@tohoku.ac.jp (Y.S.); hidetaka.akita.a4@tohoku.ac.jp (H.A.); yasuo.uchida.c8@tohoku.ac.jp (Y.U.); Tel.: +81-22-795-6833 (Y.S.); +81-22-795-6831 (H.A.); +81-22-795-6832 (Y.U.)
- † These authors contributed equally to this work.

**Citation:** Sakurai, Y.; Watanabe, H.; Nishio, K.; Hashimoto, K.; Harada, A.; Gomi, M.; Suzuki, M.; Oyama, R.; Handa, T.; Sato, R.; et al. pH-Responsive Lipid Nanoparticles Achieve Efficient mRNA Transfection in Brain Capillary Endothelial Cells. *Pharmaceutics* **2022**, *14*, 1560. <https://doi.org/10.3390/pharmaceutics14081560>

Academic Editors: William M. Pardridge, Patrick T. Ronaldson and Inge S. Zuhorn

Received: 23 May 2022

Accepted: 24 July 2022

Published: 27 July 2022

**Publisher's Note:** MDPI stays neutral with regard to jurisdictional claims in published maps and institutional affiliations.

**Abstract:** The blood–brain barrier (BBB), which is comprised of brain capillary endothelial cells, plays a pivotal role in the transport of drugs from the blood to the brain. Therefore, an analysis of proteins in the endothelial cells, such as transporters and tight junction proteins, which contribute to BBB function, is important for the development of therapeutics for the treatment of brain diseases. However, gene transfection into the vascular endothelial cells of the BBB is fraught with difficulties, even in vitro. We report herein on the development of lipid nanoparticles (LNPs), in which mRNA is encapsulated in a nano-sized capsule composed of a pH-activated and reductive environment-responsive lipid-like material (ssPalm). We evaluated the efficiency of mRNA delivery into non-polarized human brain capillary endothelial cells, hCMEC/D3 cells. The ssPalm LNPs permitted marker genes (GFP) to be transferred into nearly 100% of the cells, with low toxicity in higher concentration. A proteomic analysis indicated that the ssPalm-LNP had less effect on global cell signaling pathways than a Lipofectamine MessengerMAX/GFP-encoding mRNA complex (LFN), a commercially available transfection reagent, even at higher mRNA concentrations.

**Keywords:** lipid nanoparticle; ssPalm; mRNA transfection; blood–brain barrier; hCMEC/D3 cells; cell toxicity; SWATH-MS; translation; chaperonin-containing TCP-1



**Copyright:** © 2022 by the authors. Licensee MDPI, Basel, Switzerland. This article is an open access article distributed under the terms and conditions of the Creative Commons Attribution (CC BY) license (<https://creativecommons.org/licenses/by/4.0/>).

## 1. Introduction

Various cells are currently available as in vitro models for the BBB model. However, none of them completely reflect in vivo brain capillary endothelial cells. One example, a human brain capillary endothelial cell line (hCMEC/D3), has a smaller claudin-5 expression than isolated brain capillaries and therefore results in the formulation of weaker tight junctions [1]. Another example, human-induced pluripotent stem cell-derived brain microvascular endothelial cells (hiPS-BMECs), show significantly lower expression levels of the multidrug resistance protein (MDR1/P-gp), and therefore, they lack drug efflux activity [2]. Therefore, the transfection of genes that can complement the protein to the

level of that in the in vitro model cells would be a powerful tool for establishing a more valid BBB model that can mimic in vivo. However, the transfection of brain capillary endothelial cells has been reported to be difficult in some studies. It has been reported that, in primary cerebral vascular endothelial cells, less than 5% of the cells are transfected with plasmid DNA when a commercially available transfection reagent, LyoVec is used [3]. Such a low transfection efficiency has also been reported for hCMEC/D3 cells. For example, when hCMEC/D3 cells were transduced with a P-gp fusion gene and the green fluorescent protein (GFP) using the Lentivirus vector, the transfection efficiency was only approximately 10% [4]. One of the reasons for the low transfection efficiency is attributed to poor cellular uptake. In fact, it has been reported that the percentage of cells that took up double-stranded DNA as an agonist of the toll-like receptor was less than half that of hepatocytes and macrophages using a cationic polymer [5]. While there is no doubt that hCMEC/D3 cells are potentially useful as an in vitro BBB model, a reliable method for introducing specific genes remains to be developed. Lipofectamine is widely used, but a major drawback to its use is that the cationic liposomes contained in it produce unintended cytotoxicity. In human endothelium-derived cells (HUVECs), lipofectamine 2000 has been reported to inhibit cell proliferation, reduce the expression of various proteins, and cause an unfolded protein response (UPR) [6]. We here hypothesize that the use of an uncharged neutral nanoparticle would be more feasible for use in conjunction with endothelial cells.

To achieve a more efficient gene delivery into human brain capillary endothelial cells, hCMEC/D3, we developed lipid nanoparticles (LNPs) that contain encapsulated mRNA [7]. This LNP was designed to satisfy two fundamental properties, namely, high biocompatibility and high intracellular auto-degradability. To achieve this, we developed an ss-cleavable pH-activated lipid-like material (ssPalm), which was equipped with tertiary amines that develops a positive charge in response to the acidic pH and a disulfide-bonded unit that undergoes molecular disintegration in the intracellular reductive environment (Figure S1). When the ssPalm molecules are reconstituted into the LNPs (ssPalm-LNPs), the entire LNP had an apparent acid dissociation constant ( $pK_a$ ) of around 6.3. Therefore, under physiological conditions, the ssPalm-LNP would behave as a neutral nanoparticle. However, in the acidic environment of endosomes, they would become positively charged and then fuse with the negatively charged cell membrane. The fusion between LNP and cell membrane in acidic endosome led to membrane disruption and subsequent endosomal escape of LNP to cytosol. The ssPalm also reacts with reducing agents such as the glutathione present in the cell and disintegrates, thus releasing the loaded nucleic acid into the cytoplasm [7]. Controlling the intracellular dynamics of encapsulated nucleic acids through such multi-step actions of these functional units enabled mRNA to be efficiently introduced into cells that are generally considered to be relatively resistant to transfection [8]. In this study, we attempted to apply the ssPalm-LNP for the transfection of mRNA into hCMEC/D3 cells, for which introducing genes has been difficult.

Regarding the evaluation of adverse effects after the transfection, a comprehensive analysis of the protein expression level would be useful. The SWATH-MS (sequential window acquisition of all theoretical fragment ion spectra mass spectrometry) method is one of the recently developed quantitative proteomics methods, whose quantitative accuracy is higher than previous comprehensive proteomics technology [9]. Using this methodology, we compared the variation in the level of protein expression after the transfection with the ssPalm-LNP.

Based on these analyses, we report herein on the advantage of using the ssPalm-LNP in terms of achieving a high mRNA transfection to the non-polarized human brain capillary cells, hCMEC/D3, with low adverse effects.

## 2. Materials and Methods

### 2.1. Cell Culture

The detail in the hCMEC/D3 culture procedure was almost the same as previously reported but slightly modified [1,10,11]. The hCMEC/D3 cells were cultured in Endo-GRO

complete Media Kit (Merck-Millipore, Burlington, MA, USA) on the plate coated with Cultrex Rat type-I collagen (R&D Systems, Minneapolis, MN, USA) at 37 °C under a 5% CO<sub>2</sub> atmosphere for 3–4 days, and maintained until used for mRNA transfection.

### 2.2. Preparation of ssPalm-LNP Encapsulating GFP-Encoding mRNA

The GFP-encoding mRNA modified with 5-methoxyuridine was obtained from TriLink Biotech (San Diego, CA, USA). The ssPalm-LNP using SS-OP (provided by NOF CORPORATION), 1,2-dioleoyol-*sn*-glycerophosphocholine (DOPC, NOF CORPORATION), cholesterol (Chol, Sigma-Aldrich, Burlington, MA, USA) and poly(ethylene) glycol (average molecular weight 2000)-1,2-dimyristoyl-*sn*-glycerol (PEG-DMG, NOF CORPORATION) was prepared as previously [12,13]. The structures of these lipids are depicted in Figure S1. We formulated mRNA into LNP using ethanol dilution methods, in which lipid molecules/mRNA was spontaneously assembled by gradual decrease in ethanol concentration, based on previously published methodology [14]. Briefly, 3 µg of GFP-encoding mRNA, dissolved in 45 µL of 25 mM malic buffer (30 mM NaCl, pH 3.0), was gradually added to the lipid mixture (total 131.5 nmol (SS-OP/DOPC/Chol 52.5/7.5/35.0) with 3.95 nmol PEG-DMG) in 30.26 µL of ethanol. The solution was then further diluted with 1 mL of 20 mM 2-(*N*-morpholino)ethanesulfonic acid (MES) buffer (pH 5.5, 30 mM NaCl) under vigorous mixing with a vortex mixer. The resulting mixture was diluted with 3 mL of MES buffer and then ultrafiltered with an Amicon Ultra-4 (Merck-Millipore, molecular weight cut off: 100 kDa). The concentrate was again ultrafiltered after the dilution with phosphate-buffered saline without Mg<sup>2+</sup> and Ca<sup>2+</sup> (PBS). The obtained LNP was characterized using a ZetaSizer Pro (Malvern Panalytical, Malvern, UK). The recovery rate and the encapsulation efficiency of the mRNA were determined by a RiboGreen assay, as previously reported [12,13]. To label the LNP with near-infrared fluorescence, 1,1'-dioctadecyl-3,3,3',3'-tetramethylindodicarbocyanine (DiD) was added to the lipid mixture at 0.5 mol% to total lipid moles before mixing it with the mRNA solution.

### 2.3. Preparation of Lipofectamine/GFP-Encoding mRNA Complex (LFN)

Lipofectamine MessengerMAX (ThermoFisher Scientific, Waltham, CA, USA) was used as a control. According to the manufacturers' protocol, 1.5 µL of Lipofectamine Messenger MAX was incubated with 1000 ng of GFP-encoding mRNA for 10 min.

### 2.4. Flow Cytometry Analysis of Cellular Uptake and Gene Expression

hCMEC/D3 cells were plated on a 12-well plate at a density of  $7.5 \times 10^4$  cells/well 24 h before the addition of the ssPalm LNP and LFN. The cells were incubated with the DiD-labeled ssPalm-LNP at a dose of 300 ng mRNA in 750 µL of culture medium with 5% fetal bovine serum (0.4 µg/mL) for 2 h (cellular uptake) at 37 °C. To prepare the DiD-labeled LFN, DiD was first mixed with the Lipofectamine MessengerMAX solution so that the final fluorescence intensity in the LFN solution was the same as that for the ssPalm-LNP solution.

To measure GFP expression, the cells were exposed to the ssPalm-LNP solution that had been diluted with a culture medium at an mRNA concentration of 300 ng in 750 µL (0.4 µg/mL) for 16 h. The dilution volume of the ssPalm-LNP was adjusted based on the mRNA recovery ratio measured by the RiboGreen assay result in each experiment. As a control, the LFN was then added to cells cultured in a 12-well plate and incubated for 16 h. The incubated cells were then washed twice with 1.0 mL of PBS and then trypsinized. The obtained cells were suspended in PBS with 0.5% bovine serum albumin and 0.1% sodium azide and analyzed using a NovoCyte (Agilent Technology, Santa Clara, CA, USA).

### 2.5. Observation of Cellular Uptake and Gene Expression with Con-Focal Laser Scanning Microscopy

hCMEC/D3 cells were plated onto a glass-based 8-well chamber plate, which had been pre-coated with type-I collagen, at a density of 500 cells/well 48 h before the addition of

the ssPalm-LNP or LFN. The cells were incubated with the ssPalm-LNP at a concentration of 300 ng/200  $\mu$ L (0.4  $\mu$ g/mL) for 48 h at 37 °C in the presence of 5% fetal bovine serum. As a control treatment, cells were exposed to LFN at the same dose as the ssPalm LNP. Both the ssPalm-LNP and the LFN complex were first diluted in 200  $\mu$ L of culture medium. Nuclei were stained by a 10-min incubation in 1.0  $\mu$ g/mL Hoechst33342. After washing with 200  $\mu$ L of PBS, cells were observed by a Nikon C1 confocal laser scanning microscope system (Nikon, Tokyo, Japan).

#### 2.6. Evaluation of Cytotoxicity in mRNA Transfection Using ssPalm-LNP and LFN in hCMEC/D3 Cells

The hCMEC/D3 cells were treated with the ssPalm-LNP containing GFP-encoding mRNA, and the LFN with 1250, 2500, and 6250 ng of GFP-mRNA in 1 mL (1.25, 2.5, and 6.25  $\mu$ g/mL) for 48 h at 37 °C in 5% CO<sub>2</sub> in the presence of 5% fetal bovine serum, and observed under a microscope.

#### 2.7. SWATH-MS Analysis in hCMEC/D3 Cells Treated with ssPalm LNP and LFN

The ssPalm-LNP and the LFN were treated with hCMEC/D3 cells at a concentration of 2.5  $\mu$ g/mL for 48 h at 37 °C in 5% CO<sub>2</sub>. The SWATH-MS analysis was then performed for the whole cell lysate of hCMEC/D3 cells, as previously described [15,16]. Briefly, after a 48-h treatment, 6 well plates of cells were placed on ice, and the cell surface was immediately washed with ice-cold PBS. A denaturing buffer (7 M guanidium hydrochloride, 0.5 M Tris-HCl (pH 8.5), 10 mM EDTA) was directly added to the cell surface in order to prepare a whole cell lysate. The dissolved cells were subjected to up-and-down strokes in a 27G  $\times$  1/2 syringe (Terumo, Tokyo, Japan) to completely lyse the cells. The protein concentration of the whole cell lysate was determined by a BCA assay (Thermo Fisher Scientific Inc., Waltham, MA, USA). A 50  $\mu$ g sample of protein in the whole cell lysate was reduced, S-carboxymethylated, and purified by methanol-chloroform precipitation. The precipitate was solubilized in a urea buffer containing 0.05% ProteaseMax surfactant (Promega, Madison, WI, USA), and the proteins were digested with lysyl endopeptidase (Lys-C, Wako Pure Chemical Industries, Osaka, Japan) at an enzyme/substrate ratio of 1:100 for 3 h at 30 °C. The resulting Lys-C digested proteins were then digested with TPCK-treated trypsin (Promega, Madison, WI, USA) at an enzyme/substrate ratio of 1:100 for 16 h at 37 °C. After a C18 clean-up, the digested protein sample was injected into a NanoLC Ultra system (Eksigent Technologies, Dublin, CA, USA) coupled with an electrospray-ionization Triple TOF 5600 mass spectrometer (SCIEX, Framingham, MA, USA), which was set up for single direct injection, and analyzed by SWATH-MS acquisition. The details of measurement and subsequent data analysis have been described previously [17,18]. Finally, the relative expression levels among the control, ssPalm-LNP-treated, and LFN-treated groups were determined for all the quantified proteins. Benjamini-Hochberg adjusted *p* values were calculated, and based on a cutoff of 0.05, the issue of whether there is a significant difference in protein expression level between the groups was determined.

### 3. Results

#### 3.1. The mRNA Introduced by the ssPalm-LNP Is Homogeneously Translated in hCMEC/D3 Cells

The ssPalm-LNPs that were manually prepared by the vortex method had an average particle size of 106.0  $\pm$  15.0 nm, and polydispersity index was 0.09  $\pm$  0.02 in PBS. The  $\zeta$ -potential of  $-1.5 \pm 1.0$  mV in 10 mM HEPES buffer (pH 7.4). The distribution in particle size is shown in Figure S2A and indicates that particles with homogenous size distribution were successfully prepared. The mRNA recovery rate was 91.7  $\pm$  12.8%, and the encapsulation efficiency was 86.5  $\pm$  6.1%. This was comparable to a previous report using in vitro a transcribed mRNA encoding luciferase [12]. Considering LFN, size distribution is also homogenous (polydispersity index 0.17  $\pm$  0.03) but slightly large (diameter 340.5  $\pm$  2.5 nm) in PBS (Figure S2B), indicating colloidal formulation of LFN/mRNA complex is also stable even in an isotonic condition.

GFP expression was initially observed by microscopy (Figure 1). Most of the cells treated with the ssPalm-LNPs expressed GFP (Figure 1 left), while only a small fraction of cells was positive in the LFN-treated group (Figure 1 right). To quantitatively evaluate the heterogeneity in gene expression, GFP fluorescence was analyzed by flow cytometry (Figure 2). The mean for the GFP fluorescence intensity in the ssPalm-LNP-treated cells was significantly higher than that in the LFN-treated cells. Of note, the ssPalm-LNP induced GFP expression in a majority (95.0 ± 2.1%) of the cells (Figure 2C), consistent with the microscopic observations. On the other hand, the LFN treatment resulted in the GFP expression in a small fraction of cells (0.43 ± 0.27%). In conclusion, the ssPalm-LNPs showed a drastically higher transfection in hCMEC/D3 cells compared to LFN.

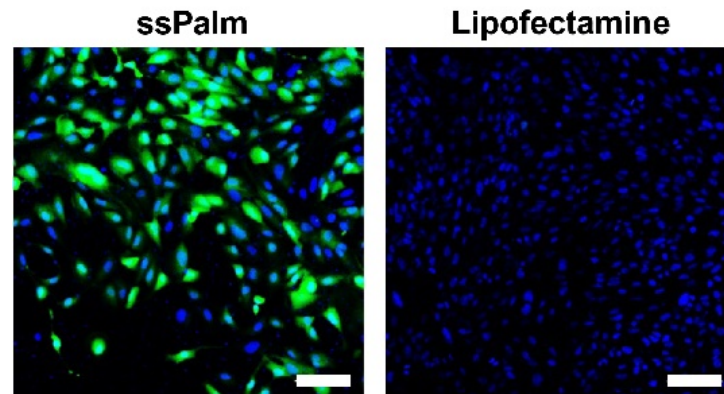


**Figure 1.** GFP expression by mRNA transfection using the ssPalm LNP or LFN. The GFP expression in hCMEC/D3 observed after mRNA transfection at a concentration of 0.4 µg/mL. Nuclei (Hoechst33342) and GFP were depicted in blue and green, respectively. Scale bars: 100 µm.

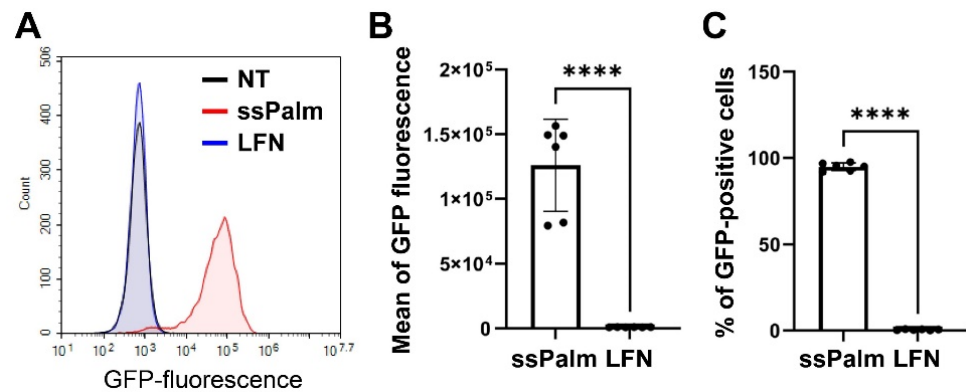


**Figure 2.** Flow cytometry analysis of GFP expression after mRNA transfection by the ssPalm-LNP or LFN. The GFP expression in hCMEC/D3 cells after mRNA transfection at a concentration of 0.4 µg/mL. (A) The representative histogram of the GFP expression in hCMEC/D3 cells. Black, blue, and red lines indicate non-treatment (NT), LFN treatment, and ssPalm-LNP treatment, respectively. (B,C) The mean GFP fluorescence intensity (B) and the percentage of GFP-positive hCMEC/D3 cells (C) were analyzed in several independent experiments. Data represent the mean ± standard deviation. Student's t-test was performed between ssPalm and LFN. \*\*\*\*:  $p$  value < 0.001.

### 3.2. Higher Amount of the ssPalm-LNP Internalizes hCMEC/D3 Cells Than LFN

Cellular uptake was also evaluated to determine the reasons for the ssPalm-LNPs being highly expressed in hCMEC/D3 cells. We found that the more homogenous the particles (Figure 3A), the higher the uptake of the ssPalm-LNPs (Figure 3B) in comparison with LFN (Figure 3B). Additionally, the % of DiD-positive cells were also higher in ssPalm-LNP treatment group (Figure 3C).

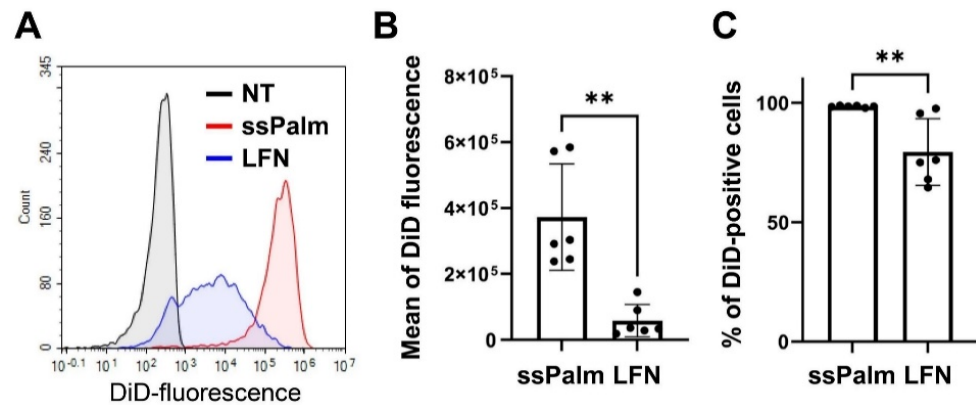


**Figure 3.** Cellular uptake of the ssPalm LNP or LFN. The cellular uptake of the ssPalm-LNP and LFN by hCMEC/D3 cells was measured by flow cytometry. (A) Representative histogram of the uptake of DiD-labeled ssPalm-LNP and LFN by hCMEC/D3 cells at a concentration of 0.4  $\mu\text{g}/\text{mL}$ . Black, blue, and red lines indicate the non-treated (NT), the LFN-treated, and the ssPalm-LNP-treated group, respectively. (B,C) The mean of DiD fluorescence intensity (B) and the percentage of DiD-positive hCMEC/D3 cells (C) were calculated in several independent experiments. Data represent mean  $\pm$  standard deviation. Student's *t*-test was performed between ssPalm and LFN. \*\*: *p* value < 0.01.

### 3.3. mRNA Transfection into hCMEC/D3 Cells by ssPalm-LNP Is Significantly Less Cytotoxic Than LFN

To observe the cytotoxicity of the ssPalm-LNP and LFN, hCMEC/D3 cells were observed after treatment at a higher concentration than the above concentrations that were used in these gene expression experiments. In the LFN-treated group, some cells were detached at higher concentrations (Figure 4). The morphology of the cells also differed from that of non-treated cells. At an mRNA concentration of 6.25  $\mu\text{g}/\text{mL}$ , these morphological changes were more prominent. In contrast, in the ssPalm-LNP treatment, no change in cell morphology and no detachment of cells were observed, even at the highest concentration (Figure 4).

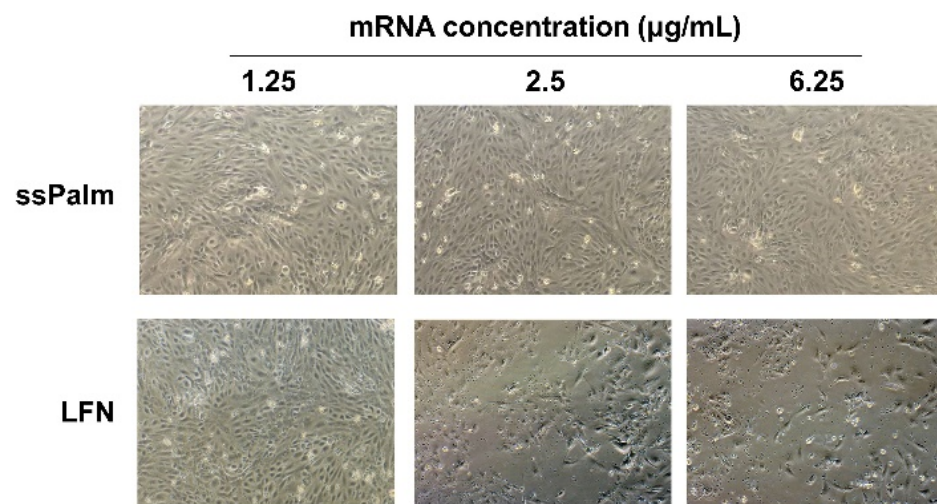


**Figure 4.** Microscopic observation of hCMEC/D3 cells after the treatment with ssPalm-LNP and LFN. The ssPalm-LNP and the LFN were treated with hCMEC/D3 cells for 48 h at the indicated concentrations.

### 3.4. ssPalm LNP Has Significantly Fewer Adverse Effects than LFN

To evaluate possible effects on off-target proteins, hCMEC/D3 cells were analyzed after being exposed to a higher concentration of the ssPalm-LNP and LFN than used in

the gene transfection experiment. A total of 1899 proteins were quantified by SWATH-MS analysis in the control, ssPalm-LNP-, and LFN-treated groups (Table S1). The levels of expression of four typical proteins in cerebral vascular endothelial cells (PECAM1, GLUT1, MDR1, and ZO-1) were unchanged among these three groups (Figure S3). Out of 1899 proteins, the significantly up- and down-regulated proteins in the ssPalm-LNP-treated group against the control group were 14 and 26 molecules, respectively (Figure 5). In contrast, the proteins that were significantly up- and down-regulated in the LFN-treated group compared to the control group were 7 and 77 molecules, respectively (Figure 5). This suggests that the LFN treatment results in a more prominent perturbation (mainly decreased) in protein expression, whereas this was minimal in the case of the ssPalm-LNP treatment.

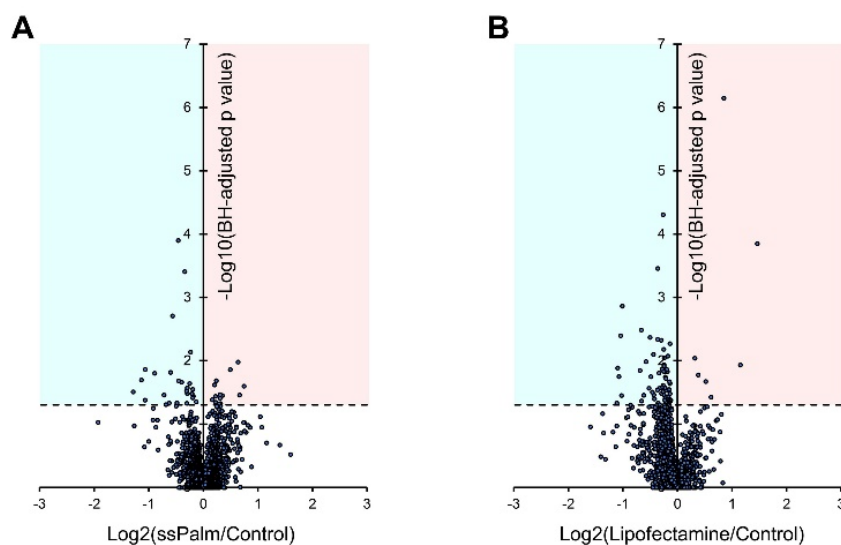


**Figure 5.** Volcano plot representation for the protein expression levels of all the quantified proteins by SWATH-MS analysis. The ssPalm-LNP (A) and LFN (B) were treated with hCMEC/D3 cells for 48 h at a concentration of 2.5  $\mu\text{g}/\text{mL}$ . Then, the SWATH-MS analysis was performed for the whole cell lysate of hCMEC/D3 cells. The levels of expression of all the quantified proteins were compared with those in the control group ( $n = 5-9$ ). X-axis represents the log2 values for the fold changes in protein expression levels compared with the control group. Y-axis represents the minus log10 values of the Benjamini–Hochberg (BH) adjusted  $p$  values for the differences between two groups. Blue and red areas represent the down- and up-regulated proteins with  $p$  values less than 0.05.

In the above experiments, unlike LFN, the ssPalm-LNPs did not cause cytotoxicity. To understand the molecular mechanisms that are involved in this difference, proteins with significant differences in expression between the LFN and control groups, but not between the ssPalm and control groups, were extracted. As a result, 67 proteins were extracted (Table S2). These were analyzed by a “String functional protein association network” analysis, and as the top two clusters, translation-related proteins and chaperonin-containing TCP-1 (CCT) (Figure 6) were then identified. As translation-related proteins, the levels of expression of RPS3, RPL11, RPL27, EIF2S3, EIF3F, EFTUD2, and HSPD1 proteins were significantly decreased by the LFN treatment by 1.17-, 1.17-, 1.28-, 1.20-, 1.27-, 1.10-, and 1.12-fold, respectively, whereas no significant reduction was observed in ssPalm-LNP-treated group (Figure 6). As CCTs, the levels of expression of the TCP1, CCT2, CCT3, and CCT4 proteins were significantly reduced by the LFN treatment by 1.15-, 1.13-, 1.10-, and 1.16-fold, respectively, but not significantly in the ssPalm-LNP-treated group (Figure 6).



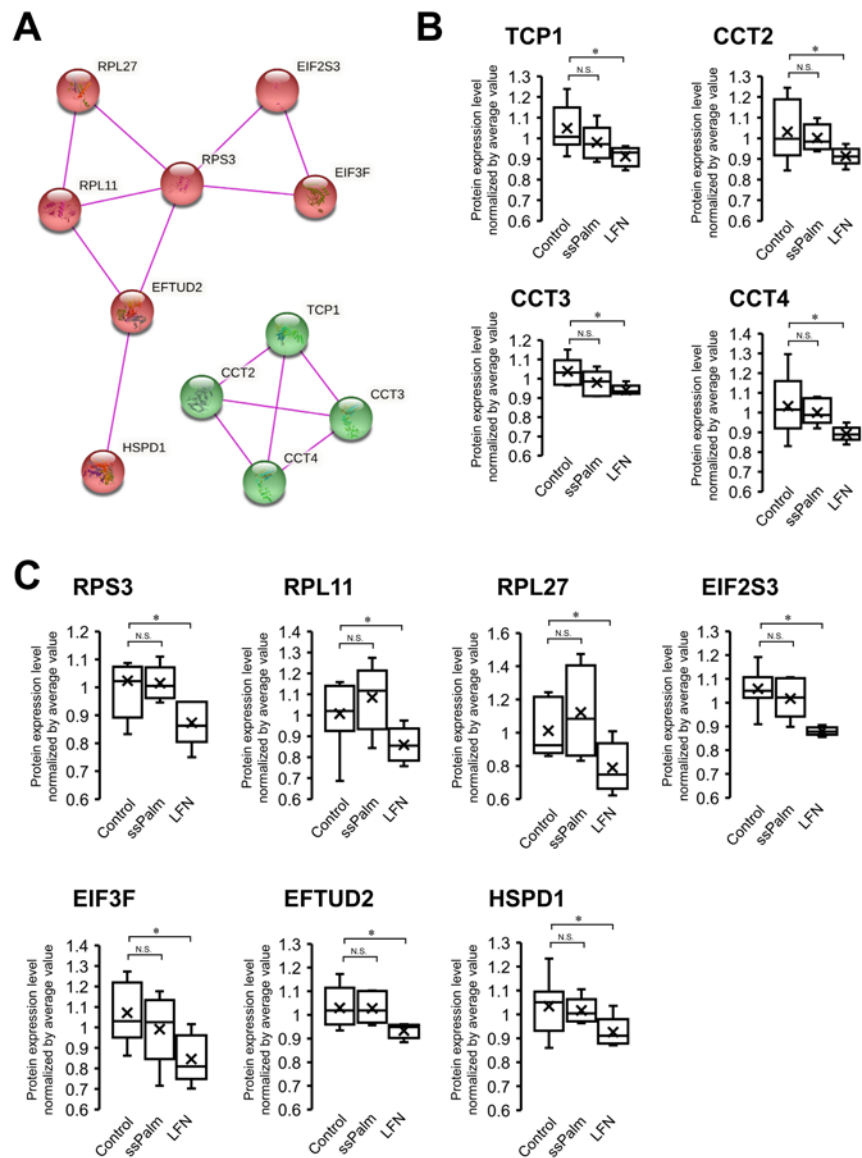


**Figure 6.** Top 2 clusters that are down-regulated in the LFN group but not in the ssPalm group. (A) 67 proteins whose expression levels were significantly changed in the LFN-treated group but not in the ssPalm-LNP-treated group (Table S2 analyzed using the STRING Database (<https://string-db.org/> accessed on 2 May 2022)) to visualize functional protein association networks [19] with an MCL clustering mode based exclusively on experimentally determined interactions. For the top 2 clusters, the interaction maps obtained on the String website are shown in this figure. The first cluster consists of translation-related proteins (red-colored nodes), and the second cluster consists of chaperonin-containing TCP-1 (CCT) proteins (green-colored nodes). (B,C) the levels of expression of CCT (B) and translation-related proteins (C) were compared among the control, ssPalm-LNP-treated group, and LFN-treated groups ( $n = 5-9$ ). The band inside the box represents the median, and the bottom and top of the box indicate the first and third quartiles, respectively. Whiskers indicate the minimum and maximum values of the protein levels. X plots show the average in each group. \* the Benjamini–Hochberg adjusted  $p$  value  $< 0.05$  was significantly down-regulated compared to control group. N.S.—not significantly different (Benjamini–Hochberg adjusted  $p$  value  $> 0.05$ ).

#### 4. Discussion

In the present study, we reported that mRNA-loaded ssPalm-LNPs can be used to efficiently transfect hCMEC/D3 cells with a marker gene GFP without any obvious toxicity. Although previous reports have not provided a clear reason for the low transfection

efficiency in BBB-derived endothelial cells, the present results suggest that one major factor is the low uptake of cationic substrates (Figure 3). Commonly used cancer cells and mouse embryo fibroblasts exhibited a much higher uptake of cationic nanoparticles compared to neutral ones [7,20,21]. This high uptake of cationic substances is thought to be, at least in part, due to interactions with negatively charged proteoglycans on the outer surface of the cell membrane [22]. Although the exact mechanism is unclear, it is possible that this uptake pathway might not be available in hCMEC/D3 cells. On the other hand, the uptake of neutral LNPs, including ssPalm-LNPs, is attributed to the formation of complexes of LNPs with Apoproteins (Apos) in the culture medium or in the biological fluid, and apolipoprotein receptors such as low-density lipoprotein receptors (LDLR) subsequently recognize these complexes [23–25]; it has been reported that LDLR and low-density lipoprotein receptor-related protein (LRP), a receptor for Apos, are expressed in BMEC [26,27]. The current SWATH-MS results showed the expression of LRP2, LRP8, and various apoproteins such as apoproteins A-I, B, E, and L3 (Table S1), although the amounts are not currently known. Taken together, the uptake of ssPalm-LNP may have been much higher than that of LFN due to the interaction of these receptors in hCMEC/D3 with medium-derived Apos that are adsorbed on the LNPs. In addition, it should be noted that the mRNA localization and whole structure of these nanoparticles were completely different: mRNA would be encapsulated into lipid molecules (LNP), or mRNA would be attached to the cationic surface of liposomes (LFN). Actually, the size of the ssPalm LNP was smaller than LFN (106.0 nm vs. 340.5 nm). The effect of the difference in the size and structure on the gene transfection efficacy should be taken into account.

The ssPalm-LNPs did not alter the morphology of the hCMEC/D3 cells (Figure 4), even though cells were treated with the ssPalm-LNP at 15.6-fold higher concentrations than that for the controls where >95% of the cells were transfected (Figures 1 and 2). Furthermore, compared to the LFN, the ssPalm-LNPs had less adverse effects on cellular protein expression (Figure 5). These data suggest that the ssPalm-LNPs developed in this study are superior for mRNA delivery to brain capillary endothelial cells in terms of cytotoxicity and off-target effects. It should also be noted that the levels of expression of many proteins were significantly down-regulated as the result of the LFN treatment (Figure 5). This is consistent with a report showing that the expression of various proteins was reduced in Lipofectamine 2000-treated HUVEC cells [6]. This may be attributed to the significant reduction in protein translation, such as ribosomal proteins and chaperonin (HSPD1/HSP60 and CCT/TRiC) in the LFN-treatment group (Figure 6).

When misfolded proteins accumulate in the cell, the unfolded protein response (UPR) is activated at the endoplasmic reticulum (ER) to reduce the accumulation of misfolded proteins. If the UPR fails to restore the ER to normality, ER stress can promote apoptosis [6]. In HUVEC cells, lipofectamine 2000 causes UPR and suppresses cell proliferation [6]. CCT/TRiC and HSPD1/HSP60 are two important chaperonins that interact with misfolded proteins to prevent misfolding and aggregation and facilitate correct folding. These levels of expression of these proteins were reduced in the case of the LFN treatment in hCMEC/D3 cells (Figure 6). This may have resulted in an over-accumulation of misfolded proteins in the cells, causing cell death. Since ssPalm-LNPs do not adversely affect the expression of molecules that are involved in protein translation and chaperonins (HSPD1/HSP60 and CCT/TRiC), they would be expected to be safe materials for future in vivo gene delivery to brain capillary endothelial cells.

The currently reported mRNA transfection technology could be applied to the expression of various genes. We demonstrated the successful encapsulation of mRNA molecules ranging from 850 bases to more than 4.5 kilobases regardless of the presence or absence of chemical modification (i.e., N1-Methylpseudouridine) [7]. Additionally, the introducible proteins are not limited to cytosolic proteins such as GFP: membrane proteins such as transporters and tight junction-related proteins can also be expressed. Further, although we demonstrate herein the efficient gene transfection with monocultured, non-polarized brain capillary endothelial cells, the mRNA transfection by the ssPalm-LNP is expected

to be applied for multiplexed culture (endothelial cells, astrocytes, pericytes, and related cells), which are currently used as in vivo BBB model [28,29] since the LNP can transfect mRNA even in complete medium containing serum.

## 5. Conclusions

We report herein that the ssPalm-LNP is a promising carrier for efficiently transporting mRNA into the non-polarized human brain capillary endothelial cells, hCMEC/D3. The transfection efficiency of the ssPalm LNP was found to be much higher than that of a commercially available transfection reagent Lipofectamine MessengerMAX. Treatment with high concentrations of the ssPalm-LNP did not induce cytotoxicity in comparison with LFN. Further, a SWATH-MS analysis revealed that the exposure of hCMEC/D3 cells to the ssPalm-LNP had only minimal effects on cellular proteins. These results indicate that the ssPalm-LNP represents a potent tool for elucidating the functional, biological characteristics of the brain endothelium by the transfection of a gene of interest.

**Supplementary Materials:** The following supporting information can be downloaded at: <https://www.mdpi.com/article/10.3390/pharmaceutics14081560/s1>, Figure S1: The structures of lipid molecules used in the ssPalm LNP; Figure S2: The particle size distribution of ssPalm LNP; Figure S3: Protein expression levels of BBB marker proteins in hCMEC/D3 cells treated with ssPalm LNP and Lipofectamine; Table S1: Relative protein expression levels of all the proteins quantified by SWATH-MS analysis among control, ssPalm LNP, and lipofectamine groups; Table S2: The proteins whose expression levels were significantly changed in Lipofectamine group but not changed in ssPalm group.

**Author Contributions:** Conceptualization, Y.S., H.A. and Y.U.; methodology, Y.S., M.G., M.S., R.O. and Y.U.; software, Y.S., M.G., M.S., R.O. and Y.U.; validation, H.W., K.N., K.H., A.H., M.G. and M.S.; formal analysis, H.W., K.N., K.H. and A.H.; investigation, H.W., K.N., K.H., A.H., T.H., R.S., H.T., R.T. and K.T. (Kenta Tezuka); resources, K.T. (Kota Tange) and Y.N.; data curation, H.W., K.N., K.H., A.H., M.S. and Y.U.; writing—original draft preparation, Y.S. and Y.U.; writing—review and editing, Y.S., H.A. and Y.U.; visualization, Y.S. and Y.U.; supervision, Y.S., H.A. and Y.U.; project administration, Y.S. and Y.U.; funding acquisition, Y.S., H.A. and Y.U. All authors have read and agreed to the published version of the manuscript.

**Funding:** The study was supported, in part, by the JST core research for evolutionary science and technology (crest) grant (grant number: JPMJCR17H1), the JSPS KAKENHI Grant-in-Aid for Scientific Research (B) (grant number: 20H03399), a Grant-in-Aid for Young Scientists (grant number: 20K20195), the MEXT KAKENHI Grant-in-Aid for Scientific Research on Innovative Areas (grant number: 22H04798).

**Institutional Review Board Statement:** Not applicable.

**Informed Consent Statement:** Not applicable.

**Data Availability Statement:** The data presented in this study are available from the corresponding authors on reasonable request.

**Acknowledgments:** The authors wish to thank Pierre-Olivier Couraud for generously providing the hCMEC/D3 cell line (Institut Cochin, France) and Milton S Feather (a scientific editor in the United States of America) for English proofreading of the entire manuscript.

**Conflicts of Interest:** This research was conducted as joint research between Tohoku University and NOF CORPORATION. The other funders had no role in the design of the study; in the collection, analyses, or interpretation of data; in the writing of the manuscript, or in the decision to publish the results.

## References

- Ohtsuki, S.; Ikeda, C.; Uchida, Y.; Sakamoto, Y.; Miller, F.; Glacial, F.; Decleves, X.; Scherrmann, J.M.; Couraud, P.O.; Kubo, Y.; et al. Quantitative targeted absolute proteomic analysis of transporters, receptors and junction proteins for validation of human cerebral microvascular endothelial cell line hCMEC/D3 as a human blood-brain barrier model. *Mol. Pharm.* **2013**, *10*, 289–296. [CrossRef] [PubMed]
- Kurosawa, T.; Sako, D.; Tega, Y.; Debori, Y.; Tomihara, Y.; Aoyama, K.; Kubo, Y.; Amano, N.; Deguchi, Y. Construction and Functional Evaluation of a Three-Dimensional Blood-Brain Barrier Model Equipped with Human Induced Pluripotent Stem Cell-Derived Brain Microvascular Endothelial Cells. *Pharm. Res.* **2022**, *39*, 1535–1547. [CrossRef] [PubMed]
- Burkhart, A.; Thomsen, L.B.; Thomsen, M.S.; Lichota, J.; Fazakas, C.; Krizbai, I.; Moos, T. Transfection of brain capillary endothelial cells in primary culture with defined blood-brain barrier properties. *Fluids Barriers CNS* **2015**, *12*, 19. [CrossRef]
- Huber, O.; Brunner, A.; Maier, P.; Kaufmann, R.; Couraud, P.O.; Cremer, C.; Fricker, G. Localization microscopy (SPDM) reveals clustered formations of P-glycoprotein in a human blood-brain barrier model. *PLoS ONE* **2012**, *7*, e44776. [CrossRef] [PubMed]
- Zhou, Y.; Guo, M.; Wang, X.; Li, J.; Wang, Y.; Ye, L.; Dai, M.; Zhou, L.; Persidsky, Y.; Ho, W. TLR3 activation efficiency by high or low molecular mass poly I:C. *Innate Immun.* **2013**, *19*, 184–192. [CrossRef]
- Li, Z.; Zhang, C.; Wang, Z.; Shen, J.; Xiang, P.; Chen, X.; Nan, J.; Lin, Y. Lipofectamine 2000/siRNA complexes cause endoplasmic reticulum unfolded protein response in human endothelial cells. *J. Cell. Physiol.* **2019**, *234*, 21166–21181. [CrossRef]
- Tanaka, H.; Sakurai, Y.; Anindita, J.; Akita, H. Development of lipid-like materials for RNA delivery based on intracellular environment-responsive membrane destabilization and spontaneous collapse. *Adv. Drug Deliv. Rev.* **2020**, *154–155*, 210–226. [CrossRef]
- Tanaka, H.; Miyama, R.; Sakurai, Y.; Tamagawa, S.; Nakai, Y.; Tange, K.; Yoshioka, H.; Akita, H. Improvement of mRNA Delivery Efficiency to a T Cell Line by Modulating PEG-Lipid Content and Phospholipid Components of Lipid Nanoparticles. *Pharmaceutics* **2021**, *13*, 2097. [CrossRef]
- Gillet, L.C.; Navarro, P.; Tate, S.; Rost, H.; Selevsek, N.; Reiter, L.; Bonner, R.; Aebersold, R. Targeted data extraction of the MS/MS spectra generated by data-independent acquisition: A new concept for consistent and accurate proteome analysis. *Mol. Cell. Proteomics* **2012**, *11*, O111.016717. [CrossRef]
- Shimomura, K.; Okura, T.; Kato, S.; Couraud, P.O.; Scherrmann, J.M.; Terasaki, T.; Deguchi, Y. Functional expression of a proton-coupled organic cation (H<sup>+</sup>/OC) antiporter in human brain capillary endothelial cell line hCMEC/D3, a human blood-brain barrier model. *Fluids Barriers CNS* **2013**, *10*, 8. [CrossRef]
- Weksler, B.B.; Subileau, E.A.; Perriere, N.; Charneau, P.; Holloway, K.; Leveque, M.; Tricoire-Leignel, H.; Nicotra, A.; Bourdoulous, S.; Turowski, P.; et al. Blood-brain barrier-specific properties of a human adult brain endothelial cell line. *FASEB J.* **2005**, *19*, 1872–1874. [CrossRef]
- Tanaka, H.; Nakatani, T.; Furihata, T.; Tange, K.; Nakai, Y.; Yoshioka, H.; Harashima, H.; Akita, H. In Vivo Introduction of mRNA Encapsulated in Lipid Nanoparticles to Brain Neuronal Cells and Astrocytes via Intracerebroventricular Administration. *Mol. Pharm.* **2018**, *15*, 2060–2067. [CrossRef] [PubMed]
- Tanaka, H.; Takahashi, T.; Konishi, M.; Takata, N.; Gomi, M.; Shirane, D.; Miyama, R.; Hagiwara, S.; Yamasaki, Y.; Sakurai, Y.; et al. Self-Degradable Lipid-Like Materials Based on “Hydrolysis accelerated by the intra-Particle Enrichment of Reactant (HyPER)” for Messenger RNA Delivery. *Adv. Funct. Mater.* **2020**, *30*, 1910575. [CrossRef]
- Jefts, L.B.; Palmer, L.R.; Ambegia, E.G.; Giesbrecht, C.; Ewanick, S.; MacLachlan, I. A scalable, extrusion-free method for efficient liposomal encapsulation of plasmid DNA. *Pharm. Res.* **2005**, *22*, 362–372. [CrossRef]
- Sato, R.; Ohmori, K.; Umetsu, M.; Takao, M.; Tano, M.; Grant, G.; Porter, B.; Bet, A.; Terasaki, T.; Uchida, Y. An Atlas of the Quantitative Protein Expression of Anti-Epileptic-Drug Transporters, Metabolizing Enzymes and Tight Junctions at the Blood-Brain Barrier in Epileptic Patients. *Pharmaceutics* **2021**, *13*, 2122. [CrossRef]
- Tezuka, K.; Suzuki, M.; Sato, R.; Kawarada, S.; Terasaki, T.; Uchida, Y. Activation of Annexin A2 signaling at the blood-brain barrier in a mouse model of multiple sclerosis. *J. Neurochem.* **2022**, *160*, 662–674. [CrossRef] [PubMed]
- Uchida, Y.; Sasaki, H.; Terasaki, T. Establishment and validation of highly accurate formalin-fixed paraffin-embedded quantitative proteomics by heat-compatible pressure cycling technology using phase-transfer surfactant and SWATH-MS. *Sci. Rep.* **2020**, *10*, 11271. [CrossRef]
- Uchida, Y.; Higuchi, T.; Shiota, M.; Kagami, S.; Saigusa, D.; Koshiha, S.; Yasuda, J.; Tamiya, G.; Kuriyama, S.; Kinoshita, K.; et al. Identification and Validation of Combination Plasma Biomarker of Afamin, Fibronectin and Sex Hormone-Binding Globulin to Predict Pre-eclampsia. *Biol. Pharm. Bull.* **2021**, *44*, 804–815. [CrossRef]
- Szklarczyk, D.; Gable, A.L.; Nastou, K.C.; Lyon, D.; Kirsch, R.; Pyysalo, S.; Doncheva, N.T.; Legeay, M.; Fang, T.; Bork, P.; et al. The STRING database in 2021: Customizable protein-protein networks, and functional characterization of user-uploaded gene/measurement sets. *Nucleic Acids Res.* **2021**, *49*, D605–D612. [CrossRef]
- Sakurai, Y.; Kato, A.; Hida, Y.; Hamada, J.; Maishi, N.; Hida, K.; Harashima, H. Synergistic Enhancement of Cellular Uptake with CD44-Expressing Malignant Pleural Mesothelioma by Combining Cationic Liposome and Hyaluronic Acid-Lipid Conjugate. *J. Pharm. Sci.* **2019**, *108*, 3218–3224. [CrossRef]
- Li, Y.; Wang, J.; Gao, Y.; Zhu, J.; Wientjes, M.G.; Au, J.L. Relationships between liposome properties, cell membrane binding, intracellular processing, and intracellular bioavailability. *AAPS J.* **2011**, *13*, 585–597. [CrossRef]

22. Mounkes, L.C.; Zhong, W.; Cipres-Palacin, G.; Heath, T.D.; Debs, R.J. Proteoglycans mediate cationic liposome-DNA complex-based gene delivery in vitro and in vivo. *J. Biol. Chem.* **1998**, *273*, 26164–26170. [CrossRef] [PubMed]
23. Akinc, A.; Querbes, W.; De, S.; Qin, J.; Frank-Kamenetsky, M.; Jayaprakash, K.N.; Jayaraman, M.; Rajeev, K.G.; Cantley, W.L.; Dorkin, J.R.; et al. Targeted delivery of RNAi therapeutics with endogenous and exogenous ligand-based mechanisms. *Mol. Ther.* **2010**, *18*, 1357–1364. [CrossRef] [PubMed]
24. Sato, Y.; Hatakeyama, H.; Sakurai, Y.; Hyodo, M.; Akita, H.; Harashima, H. A pH-sensitive cationic lipid facilitates the delivery of liposomal siRNA and gene silencing activity in vitro and in vivo. *J. Control. Release* **2012**, *163*, 267–276. [CrossRef]
25. Akita, H.; Noguchi, Y.; Hatakeyama, H.; Sato, Y.; Tange, K.; Nakai, Y.; Harashima, H. Molecular Tuning of a Vitamin E-Scaffold pH-Sensitive and Reductive Cleavable Lipid-like Material for Accelerated In Vivo Hepatic siRNA Delivery. *ACS Biomater. Sci. Eng.* **2015**, *1*, 834–844. [CrossRef]
26. Ribocco-Lutkiewicz, M.; Sodja, C.; Haukenfrers, J.; Haqqani, A.S.; Ly, D.; Zachar, P.; Baumann, E.; Ball, M.; Huang, J.; Rukhlova, M.; et al. A novel human induced pluripotent stem cell blood-brain barrier model: Applicability to study antibody-triggered receptor-mediated transcytosis. *Sci. Rep.* **2018**, *8*, 1873. [CrossRef] [PubMed]
27. Molino, Y.; David, M.; Varini, K.; Jabes, F.; Gaudin, N.; Fortoul, A.; Bakloul, K.; Masse, M.; Bernard, A.; Drobecq, L.; et al. Use of LDL receptor-targeting peptide vectors for in vitro and in vivo cargo transport across the blood-brain barrier. *FASEB J.* **2017**, *31*, 1807–1827. [CrossRef]
28. Hanafy, A.S.; Dietrich, D.; Fricker, G.; Lamprecht, A. Blood-brain barrier models: Rationale for selection. *Adv. Drug Deliv. Rev.* **2021**, *176*, 113859. [CrossRef]
29. Jagtiani, E.; Yeolekar, M.; Naik, S.; Patravale, V. In vitro blood brain barrier models: An overview. *J. Control. Release* **2022**, *343*, 13–30. [CrossRef]

Review

# Modeling Blood–Brain Barrier Permeability to Solutes and Drugs In Vivo

Ulrich Bickel <sup>1,2</sup> 

<sup>1</sup> Department of Pharmaceutical Sciences, Jerry H. Hodge School of Pharmacy, Texas Tech University Health Sciences Center, Amarillo, TX 79106, USA; ulrich.bickel@ttuhsc.edu; Tel.: +1-806-414-9236; Fax: +1-806-356-4034

<sup>2</sup> Center for Blood-Brain Barrier Research, Jerry H. Hodge School of Pharmacy, Texas Tech University Health Sciences Center, Amarillo, TX 79106, USA

**Abstract:** Our understanding of the pharmacokinetic principles governing the uptake of endogenous substances, xenobiotics, and biologicals across the blood–brain barrier (BBB) has advanced significantly over the past few decades. There is now a spectrum of experimental techniques available in experimental animals and humans which, together with pharmacokinetic models of low to high complexity, can be applied to describe the transport processes at the BBB of low molecular weight agents and macromolecules. This review provides an overview of the models in current use, from initial rate uptake studies over compartmental models to physiologically based models and points out the advantages and shortcomings associated with the different methods. A comprehensive pharmacokinetic profile of a compound with respect to brain exposure requires the knowledge of BBB uptake clearance, intra-brain distribution, and extent of equilibration across the BBB. The application of proper pharmacokinetic analysis and suitable models is a requirement not only in the drug development process, but in all of the studies where the brain uptake of drugs or markers is used to make statements about the function or integrity of the BBB.

**Keywords:** pharmacokinetics; blood–brain barrier; compartmental models; physiologically based PK models

**Citation:** Bickel, U. Modeling Blood–Brain Barrier Permeability to Solutes and Drugs In Vivo. *Pharmaceutics* **2022**, *14*, 1696. <https://doi.org/10.3390/pharmaceutics14081696>

Academic Editor: Paul Chi Lui Ho

Received: 8 July 2022

Accepted: 10 August 2022

Published: 15 August 2022

**Publisher's Note:** MDPI stays neutral with regard to jurisdictional claims in published maps and institutional affiliations.



**Copyright:** © 2022 by the author. Licensee MDPI, Basel, Switzerland. This article is an open access article distributed under the terms and conditions of the Creative Commons Attribution (CC BY) license (<https://creativecommons.org/licenses/by/4.0/>).

## 1. Introduction

It has been over 120 years since the earliest publications on the distinct features of the brain vasculature compared to other organs, which over time gave rise to the concept of a “blood–brain barrier” (BBB). As recently reviewed [1], there have been many misconceptions along the way about its structure and function. It is now established that the physical and biochemical BBB is formed by the endothelial cells of the brain microvasculature, which are connected by tight junctions (Figure 1). The barrier function is induced or modulated by other elements of the “neurovascular unit” [2], including pericytes, astrocytes, neurons, and microglial cells. Some misunderstandings linger to this day in parts of the literature. One area concerns the methods of measuring the brain uptake of drugs and the proper evaluation and interpretation. The present review will provide an overview of the development and application of modeling approaches to describe the pharmacokinetics (PK) of brain uptake of low molecular weight drug-like solutes and macromolecules. We will not attempt to include all of the aspects of the extensive and rapidly growing literature in this field, but aim to focus on practical applicability with some examples.

The purpose of the PK models covers a range from the evaluation and the fitting of sets of experimental data that are as good as possible to simulations and predictions based on few or no experimental data, to employing complex physiologically based pharmacokinetic (PBPK) models with parameter values obtained from *in silico*, *in vitro*, and *in vivo* studies. Which model is appropriate also depends on the experimental design in each case and

the physicochemical characteristics of the agent to be evaluated. Macromolecules differ greatly in kinetic behavior from small molecule drugs and studying poorly permeable substances requires a different experimental design and PK evaluation approaches than highly permeable drugs. From an experimental perspective, it is feasible in preclinical studies to obtain blood and (brain) tissue samples at multiple time points, while clinical studies are typically limited to blood sampling, and occasionally CSF sampling, and noninvasive imaging modalities (MRI, SPECT, PET), if applicable. Finally, a distinction can be made, based on whether the parameter of primary interest is the uptake rate across the BBB or the brain exposure (fraction of a dose, or extent). These models will be presented, from the simple to the more complex.

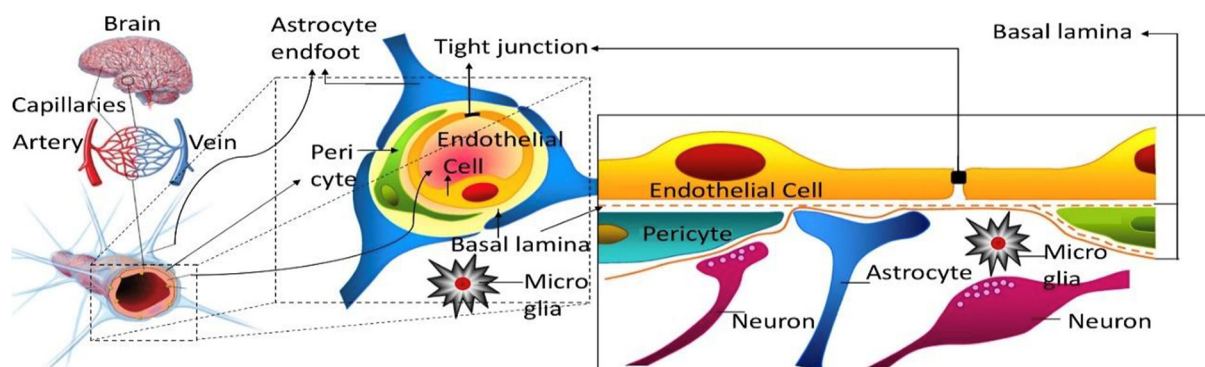


**Figure 1.** Scheme of the BBB: The endothelial cells of the capillaries are connected by tight junctions and form a physical and biochemical barrier. The pericytes and astrocytes play critical roles in the induction and maintenance of the endothelial barrier properties. Microglial cells and neurons also secrete signals, which can influence the endothelial cells. The diameter of the capillaries is on the order of 7–10  $\mu\text{m}$ . Figure adapted from Reference [3] with permission. Copyright 2010, Elsevier.

## 2. Models Assuming Unidirectional Brain Uptake

As the name implies, unidirectional organ uptake models are based on the concept that for the duration of the experiment, a drug or tracer diffuses (or is undergoing transport) only from the blood side (luminal) to the brain side (abluminal) across the BBB. Provided that there is no significant backflux, it allows the determination of the initial rate of brain uptake. The approach can be most readily illustrated considering the examples of carotid injection and carotid artery brain perfusion techniques.

### 2.1. Brain Uptake Index (BUI)

The technique, as introduced by Oldendorf [4,5], uses radiotracers labeled with different isotopes and measures the brain tissue-extraction ratio (brain concentration: injectate concentration) of a compound during a single pass through the cerebral vasculature after bolus injection into the carotid artery under anesthesia. BUI (as a percentage) is then estimated from the brain extraction ratio of the test substance ( $E_{test}$ ), relative to that of a permeable reference substance ( $E_{refp}$ ) with a known, near total extraction:

$$BUI = \frac{E_{test}}{E_{refp}} \times 100 = \frac{C_{test\text{ in brain}} / C_{test\text{ in injectate}}}{C_{refp\text{ in brain}} / C_{refp\text{ in injectate}}} \times 100 \quad (1)$$

where  $C_{test}$  refers to the concentrations of the test substance and  $C_{refp}$  refers to the concentrations of the permeable reference. The examples of highly permeable substances with a complete (100%) extraction include iodoamphetamine [6] and diazepam [7]. In order to correct for brain intravascular volume, an additional reference substance was introduced, which is assumed to show no tissue uptake during the single passage.

BUI in percent is then calculated as the ratio:

$$BUI = 100 \times (E_{test} - E_{refV}) / E_{refP} \quad (2)$$

where  $E_{refV}$  is the apparent “extraction” of the vascular marker (non-permeant reference).  $E_{test}$  can then be used to calculate the permeability surface area product (PS), applying a rearranged Renkin–Crone equation:

$$PS = -F \ln(1 - E) \quad (3)$$

where  $F$  is the tissue perfusion flow rate. The BUI method allows wide flexibility in the composition of the injectate and the concentrations of the test substance. In the BUI technique, the brain tissue is treated as one compartment. It has been successfully applied to study, in particular, the BBB transport of nutrients, including the characterization of saturable transport by applying Michaelis–Menten kinetics [8]. A limitation of the technique is its low sensitivity for poorly permeable solutes. For example, the brain uptake of the classical CNS-active drug, morphine could not be distinguished from [ $^{14}\text{C}$ ]sucrose, which behaves as a vascular marker in a single-pass experiment [9].

## 2.2. In Situ Brain Perfusion

These techniques perfuse the brain in anesthetized animals with oxygenated buffer solutions via the carotid artery. Similar methods have been established in the rat [7], guinea pig [10], and mouse [11,12] and are in widespread use. The pharmacokinetic principle is analogous to the BUI method, in the assumption that the initial rate of brain uptake can be measured as long as the effective tissue concentrations are much lower than the perfusate concentration and unidirectional transport prevails. The evaluation is based on a plot of the apparent volume of distribution ( $V_D$ ) in the brain compartment against perfusion time ( $T$ ), where  $V_D$  is the ratio of the amount of the test substance in the brain per unit weight,  $A_{br}$  (e.g., nmol/g brain) over the perfusate concentration ( $C_{perf}$ ) of the analyte (e.g., nmol/mL), with  $C_{perf}$  being constant. With a unidirectional uptake, this results in a linear increase, and the slope of a linear regression line represents the unidirectional transfer constant,  $K_{in}$ , from the perfusate fluid into the brain compartment, which is a clearance parameter, e.g., in units of [mL/min]:

$$V_D = \frac{A_{br}}{C_{perf}} = K_{in}T + V_i \quad (4)$$

The y-intercept of the regression line represents an “initial” volume of distribution,  $V_i$ . It corresponds to the sum of the intravascular volume,  $V_0$ , which in rodents typically is in a range of 8–10  $\mu\text{L/g}$  [13], and a potential residual volume, which is physiologically difficult to characterize, e.g., caused by nonspecific binding to the vascular wall, or associated with cellular components of the BBB. In cases where substantially higher values of  $V_i$  are observed, the inclusion of a marker substance, such as albumin or inulin, which is expected to undergo negligible transport across the BBB, can be applied to experimentally measure the intravascular space.  $K_{in}$  approaches the value of the PS product at the BBB within 10% for conditions of permeability-limited transport (low E), when flow  $F$  is greater than  $5 \times PS$ . Depending on the test compound, in situ perfusions are typically conducted over a few seconds up to several minutes. Similar to BUI, the experimental advantages are that the perfusate compositions and concentrations of the test substance can be controlled within wide limits, outside of the conditions tolerated in the whole animal with systemic administration. On the other hand, the sensitivity for accurate permeability measurements of analytes with low permeability is superior to the single-pass technique, but is still limited. The extended perfusion times (e.g., 10–20 min) require the inclusion of oxygen carriers, such as washed erythrocytes in the perfusate, to avoid hypoxic conditions [10].



### 2.3. Intravenous Injection

The most physiological technique for the analysis of BBB transport is the intravenous administration (as a bolus or infusion), followed by the analysis of the concentration time course in blood and brain. To obtain reliable and correct measurements, several conditions have to be met in such studies. First, considering the free drug hypothesis [14], the free fraction in plasma needs to be determined by microdialysis *in vivo*, or by *ex vivo* techniques, such as ultrafiltration. This will be discussed in more detail below in Section 4. Second, if metabolism occurs, the analytical method used must be able to measure the intact substance in the plasma and tissue.

#### 2.3.1. Multiple Time Point Analysis

Depending on the experimental design, different options for the pharmacokinetic evaluation of brain uptake are available. With a series of brain and plasma samples taken at different time points, the multiple time-point graphical evaluation, also known as a Patlak plot, is frequently used [15–17]. In its original form, it modeled the brain tissue as consisting of several reversible compartments and one irreversible compartment [17]. A practical example is the intracellular entrapment of tracers, such as deoxy-glucose or  $\alpha$ -amino-isobutyric acid. Under the condition that the reversible compartments are in rapid exchange with the plasma compartment, Patlak and colleagues showed that the unidirectional brain uptake can be analyzed by plotting the time-dependent apparent volume of distribution against the ratio of the plasma area under the curve (AUC) from time zero to time T and terminal plasma concentration at time T:

$$\frac{A_{br}(T)}{C_p(T)} = K_{in} \frac{\int_0^T C_p(t) dt}{C_p(T)} + V_i \quad (5)$$

where  $C_p(T)$  is the plasma concentration at sampling time T; and  $V_i$  is the initial volume of distribution, as introduced above. The term  $[AUC_0^T/C_p(T)]$  gives a value in units of time. It is, however, distinct from the experimental time in all of the cases where plasma concentrations are not constant, and is labeled “effective time” or “stretch time”. After the initial phase of rapid equilibration of  $V_i$ , a phase of linear increase in the plotted data is expected, as long as the unidirectional uptake into the brain compartment occurs. This linear phase allows for an analysis by linear regression, yielding  $K_{in}$  as the slope of the regression line as described above for the *in situ* perfusion technique. The intravascular content may be experimentally accounted for by the inclusion of a vascular marker injected shortly before the terminal experimental time and tissue sampling, or by a vascular wash procedure to clear out the intravascular content from the tissue. Both options, if appropriately applied, yield equivalent corrections, as recently demonstrated [13].

#### 2.3.2. Single Time Point Analysis

This evaluation only requires one terminal brain sample and sufficient blood samples obtained over the experimental period to accurately describe the plasma concentration time-course of the test substance. The calculation of the brain uptake clearance is then performed, utilizing a version of Equation (5) re-arranged as follows:

$$K_{in} = \frac{(V_D - V_0)C_p(t)}{AUC_0^t} \quad (6)$$

where  $V_D$  corresponds to the apparent brain volume of distribution ( $A_{br}/C_{pT}$ ); and  $V_0$  is the intravascular volume. The latter needs to be either measured experimentally, using a vascular marker, taken from the literature, or eliminated by a buffer wash through the left heart ventricle. When serial blood samples can be taken from one animal, the single time-point method has the advantage of reducing the number of experimental animals. The disadvantage is that it is challenging to select the best terminal sampling time, up

to which the unidirectional BBB transport can be expected. There is a trade-off between sensitivity for the analysis of low permeability substances in the brain tissue and the risk of violating the initial rate condition (see also the next section). At short experimental times, when the tissue concentrations beyond the BBB are relatively low and the intravascular concentrations are still high, minor errors in correction for vascular content may have outsized effects on the apparent  $K_{in}$ .

#### 2.4. Caveats Associated with Unidirectional Uptake Models

While the original Patlak model was developed assuming an irreversible brain compartment, the multiple-time graphical method has found widespread application in the analysis of the uptake of compounds, which are unbound or reversibly bound by brain tissue beyond the BBB. In these scenarios, a deviation from the linearity at later time points, when the backflux cannot be neglected, is theoretically expected. Applying a linear regression analysis should then result in a systematic underestimation of the apparent value of  $K_{in}$  and an overestimation of  $V_i$ . Unfortunately, it is difficult to identify such errors in practice from the output of linear regression of the experimental data, which are also inherently associated with error. The dilemma has been explored with the example of an in situ brain perfusion study of [ $^{14}\text{C}$ ]iodoacetamide, a moderately lipophilic test substance [18]. The data acquired experimentally, up to 40 s perfusion time, were corrected for vascular content by [ $^3\text{H}$ ]inulin. Within the experimental period, the [ $^{14}\text{C}$ ]iodoacetamide reached an apparent  $V_D$  in brain of 0.15–0.2 mL/g, indicating quite rapid BBB transport. A linear regression of the Patlak plot (after vascular correction) gave a value of  $4.39 \pm 0.33 \times 10^{-3}$  mL/s/g and a  $V_i$  not significantly different from zero, as predicted. The same data were fitted to a two-compartment model, allowing for backflux from the brain, resulting in a slightly higher  $K_{in}$  of  $5.08 \pm 0.14 \times 10^{-3}$  mL/s/g. When the parameters of the two-compartment model were applied to simulate the later data points from 60 up to 240 s, the Patlak analysis still showed an  $r^2$  coefficient of 0.973 in support of linearity. However, the  $K_{in}$  estimate dropped more than half to  $2.06 \pm 0.24 \times 10^{-3}$  mL/s/g and the  $V_i$  increased to 0.15 mL/g. Therefore, the assumption of linearity based on the  $r^2$  values close to one cannot be taken as proof of an accurate estimate of  $K_{in}$ . Importantly, this conclusion not only applies to the compounds with moderate or high permeability, but also to poorly permeable substances, such as the hydrophilic markers [ $^{13}\text{C}$ ]sucrose and [ $^{13}\text{C}$ ]mannitol. A recent study was performed with IV bolus injections of these compounds in awake mice, followed by the sampling of blood and brains, with terminal sampling time points between 30 min and 480 min [19]. Separate Patlak analyses were conducted, using multiple-time point graphical analysis for data covering experimental periods either up to 30, 60, 120, 240, or 480 min (Figure 2). Analogous to the simulation scenario with [ $^{14}\text{C}$ ]iodoacetamide, the inclusion of the late experimental time points resulted in a substantial underestimation of  $K_{in}$ , with values for both mannitol and sucrose decreasing at 120 min by 40–50% and by 480 min around 70% from the estimates obtained, with 30 min as the terminal sampling time. When the same dataset was analyzed using the single time technique, there was a similar gradual decline in the apparent  $K_{in}$  calculated from the late terminal time points of brain tissue sampling (Figure 3), while the mannitol and sucrose values compared at each time point remained significantly different. The figure also reveals that the variability coefficient of the  $K_{in}$  estimates at the earliest time point (15 min) is highest, likely due to the argument outlined above, about the impact of the intravascular content.

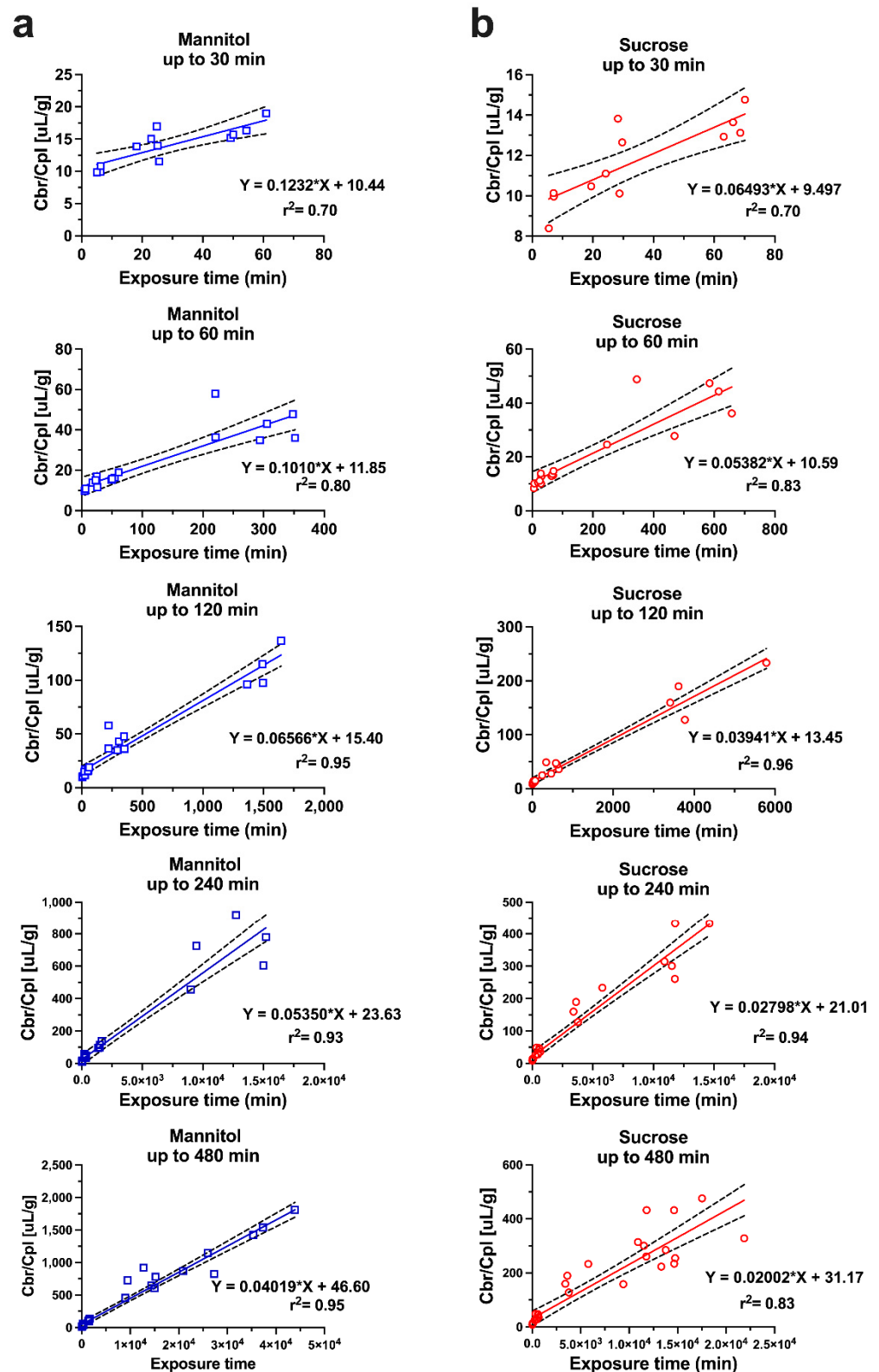


**Figure 2.** Multiple time point-analysis covering different sampling time points up to 480 min for (a) mannitol and (b) sucrose. Dashed lines represent the 95% confidence intervals.  $n = 4-7$  animals per marker per time point. Reprinted with permission from Reference [19]. Copyright 2022, Springer Nature.

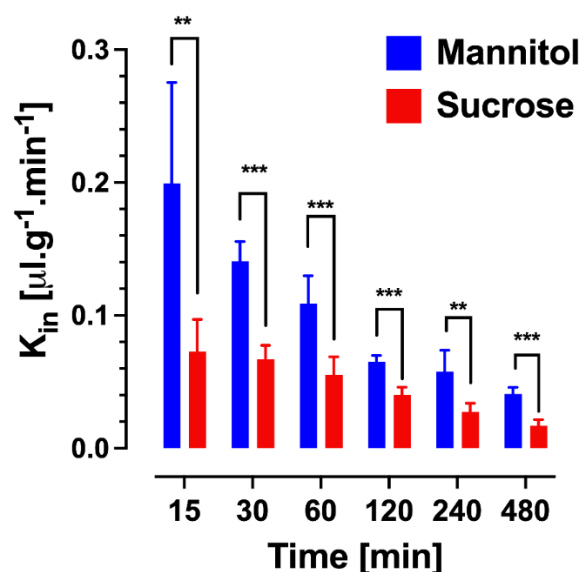


**Figure 3.** Single time point analysis of sucrose and mannitol brain uptake clearance values ( $K_{in}$ ) at different time points from 15 to 480 min ( $n = 4\text{--}7$  animals per marker per time point). Sucrose and mannitol values at each time point were compared by  $t$ -test. \*\*  $p < 0.01$ , \*\*\*  $p < 0.001$ . Reprinted with permission from Reference [19]. Copyright 2022, Springer Nature.

### 2.5. PK Analysis in Brain Imaging Techniques

Notwithstanding the limitations of the standard version of the Patlak analysis, the graphical evaluation technique is widely used in the fields of PET imaging and MRI, where a time series can be acquired of the regional brain uptake and from the regions over large arteries, as reference measurements of the input function. Patlak and Blasberg presented a generalized, non-linear version of their original approach, which allowed for the loss of the test substance from the brain [16]. The modified equation:

$$\frac{A_{br}(T)}{C_p(T)} = K_{in} \frac{\int_0^T e^{-k_b(T-t)} C_p(t) dt}{C_p(T)} + (fV_e + V_p) \quad (7)$$

includes a rate constant  $k_b$  for the test substance leaving the brain tissue, where it is assumed that  $k_b \ll K_{in}$ . The term  $fV_e$  denotes a fraction of the extravascular distribution volume in brain tissue, and  $V_p$  is brain plasma space. The non-linear generalized Patlak equation is used in the evaluation of preclinical and clinical PET and MRI data [20–22]. In addition, for the PET imaging of radioligands showing reversible binding to receptors or enzymes in the brain, Logan et al. proposed a graphical analysis to estimate the steady state volume of the distribution of a tracer from the slope of a linear segment of the plot [23]. Subsequently, a number of variations of the “Logan plot” were introduced in an effort to reduce the bias for the underestimation of  $V_D$ , caused by noisy data in the original version [24]. Due to their non-invasiveness, advanced imaging modalities such as dynamic-contrast enhanced MRI (DCE-MRI) and fluid-attenuated inversion recovery MRI (FLAIR MRI) are in widespread clinical use. The regional BBB dysfunctions can be detected and quantified in multiple disease states, ranging from neuroinflammatory diseases, such as multiple sclerosis [25] and brain tumors [26], to ischemic brain diseases [27]. The enhanced sensitivity for the detection of subtle BBB leakage in patients could recently be shown under high field strength (7T) MRI [28].

### 3. Compartmental Models of Brain Uptake

The methods discussed in the previous sections are based on the presence of at least one central compartment representing the input source for brain uptake, and possibly additional compartments, which can determine the characteristic concentration–time course of a

drug in the circulation after systemic administration, and one or more brain compartments. However, the determination of the initial rate of uptake  $K_{in}$  from the intravascular space across the BBB does not require analytic or numerical solutions of intercompartmental transfer rates. The plasma AUC in Equations (5) and (6) may be readily calculated by a non-compartmental trapezoidal approach. The unidirectional clearance transfers the analyte from the intravascular fluid into brain tissue, which is reduced to a single compartment, represented by an apparent volume of distribution. However, to analyze the exchange in both directions across the BBB, and the potential transport between additional compartments within the tissues of the central nervous system, compartmental PK models or PKPB models are required.

The analysis of this type of model is based on the law of mass action for mass transfer between compartments, for which a series of corresponding differential equations can be formulated. To enable the fitting of model parameters to the data and to obtain values describing the rates and extent of tissue distribution, a compartmental model should not be over-parameterized, i.e., be only as complex as necessary. This may be illustrated by our recent approach to describe the PK behavior of the hydrophilic solutes presented above, [ $^{13}\text{C}$ ]sucrose and [ $^{13}\text{C}$ ]mannitol, using a three-compartment model. The model (Figure 4) consists of central and peripheral compartments, in addition to a brain compartment. The clearance rates across the BBB in either direction ( $CL_{13}$ , Figure 4) are equal and based on passive diffusion for both the mannitol and sucrose, which are not substrates of known transporters and are metabolically stable in tissues. However, a PK model based only on symmetrical exchange across the BBB failed to adequately describe the time course in the brain. An additional term was required for clearance from the brain ( $CL_{31}$ ). This resulted in an extension of the two-compartment model used by Rapoport's group for the description of the brain uptake of small nonelectrolytes [29]. The model (Figure 4) is expressed by the following mass transfer equations:

$$dA_1/dt = -CL_{10} \cdot \frac{A_1}{V_1} - CL_{12} \cdot \frac{A_1}{V_1} + CL_{12} \cdot \frac{A_2}{V_2} - CL_{13} \cdot \frac{A_1}{V_1} + ((CL_{13} + CL_{31}) \cdot A_3) / (V_e \cdot W_{\text{brain}}) \quad (8)$$

$$dA_2/dt = CL_{12} \cdot A_1 / V_1 - CL_{12} \cdot A_2 / V_2 \quad (9)$$

$$dA_3/dt = CL_{13} \cdot A_1 / V_1 - ((CL_{13} + CL_{31}) \cdot A_3) / (V_e \cdot W_{\text{brain}}) \quad (10)$$

where,

$$C_1 = A_1 / V_1$$

$$C_2 = A_2 / V_2$$

$$C_3 = A_3 / W_{\text{brain}}$$

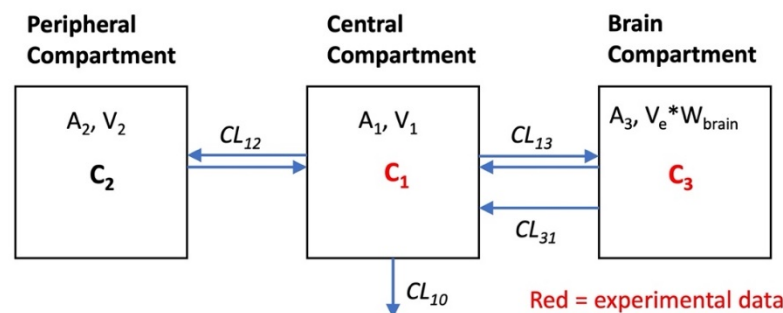


**Figure 4.** Schematic of a three-compartment semi-physiologic model for the pharmacokinetic study. Parameter definitions are given in the methods above.  $A_1, V_1, C_1$  are the amount, the volume, and the concentration in the central compartment 1, analogous in the peripheral compartment 2.  $A_3$  is the amount in brain tissue;  $V_e$  the volume fraction of brain ISF (mL/g);  $W_{\text{brain}}$  is brain weight; and  $C_3$  the concentration in brain tissue after correction for the intravascular content. Reprinted with permission from Reference [19]. Copyright 2022, Springer Nature.

$A_1$  and  $A_2$  denote the amount of analytes in the central and peripheral compartment, respectively.  $V_1$  and  $V_2$  are the volumes of these compartments.  $A_3$  is the amount in the brain compartment,  $V_e$  is equal to the volume of distribution of sucrose and mannitol in the brain tissue, expressed as a dimensionless volume fraction (assuming  $\text{mL/g} \approx \text{mL/mL}$ ).  $W_{\text{brain}}$  equals the brain weight.  $C_1$ ,  $C_2$ , and  $C_3$  in Figure 4 are the concentrations. The clearance parameter  $CL_{31}$  denotes an efflux mechanism, which likely represents the bulk flow from the brain interstitial fluid, based on physiological considerations. The model parameters were fitted to the data by numerical solution of the differential equations using WinNonlin.  $V_e$  was fixed at 0.2, corresponding to the literature values of the extracellular volume fraction [30].

The estimates of the model parameters fitted to the data for mannitol and sucrose are listed in Table 1, and the plots of plasma and brain concentrations of the marker are shown in Figure 5. The parameter estimate for  $CL_{13}$  is the brain uptake clearance and is equivalent to  $K_{in}$ . The fitted  $CL_{13}$  values for mannitol and sucrose (Table 1) are close to the  $K_{in}$  values obtained by the Patlak analysis over a 30 min period, and to the values of single time point analysis up to 30 min terminal sampling time (Figures 2 and 3). The  $CL_{13}$  of mannitol is twice as high compared to sucrose ( $1.46 \pm 0.02 \mu\text{L}\cdot\text{min}^{-1}\cdot\text{g}^{-1}$  vs.  $0.68 \pm 0.005 \mu\text{L}\cdot\text{min}^{-1}\cdot\text{g}^{-1}$ ). It is noteworthy that the  $CL_{31}$  estimates of both of the markers are not different ( $0.881 \pm 0.20 \mu\text{L}\cdot\text{min}^{-1}\cdot\text{g}^{-1}$  and  $0.693 \pm 0.106 \mu\text{L}\cdot\text{min}^{-1}\cdot\text{g}^{-1}$ ). The same efflux value, despite differences in molecular weight, size, and octanol/water partition coefficient, is consistent with the bulk flow. This efflux clearance mechanism can be separated from diffusional exchange across the BBB because of the very low passive permeability of mannitol and sucrose. Therefore, the bulk flow clearance should have a significant impact on the brain kinetics of any endogenous substance or xenobiotic with similar physicochemical characteristics (low passive permeability, not a substrate of influx or efflux transport), and needs to be considered in the PK models used for analysis. The previous experimental estimates of the bulk flow in the brain typically relied on invasive techniques, such as ventriculo-cisternal perfusion or stereotaxic injection of tracers or dyes into the brain tissue [30–32]. The estimates of bulk flow in rodents range from 0.56 to  $1.2 \mu\text{L}\cdot\text{min}^{-1}\cdot\text{g}^{-1}$ , as compiled in a recent review [33]. The above case study with sucrose and mannitol illustrates how relatively simple semi-physiological compartmental PK models can describe the PK behavior of extracellular markers, based on the measurement of whole tissue concentrations. The plots of plasma and brain concentration–time profiles of these markers after IV bolus injection (Figure 5) reveal that a model of BBB transport assuming unidirectional uptake cannot be applied for any time point beyond 30 min, because the brain concentrations already declined. This is consistent with the progressively decreasing  $K_{in}$  estimates discussed above (Figures 2 and 3).

More complex compartmental models have been described in the literature, beginning with the distributed model introduced by Fenstermacher, Patlak, and Blasberg [34] and later by Collins and Dedrick [35], which considers the exchange between the plasma compartment, the brain tissue, and the cerebrospinal fluid. Deeper insights into the PK characteristics of analytes can be gained when the experimental data are acquired from the additional tissue compartments. Of particular relevance in this regard is the *in vivo* microdialysis technique, which has been in use for drug analysis in brain interstitial fluid (ISF) since the 1990s [36–38]. Its value in brain uptake studies can be readily illustrated with the recent comparison of two isotopically labeled versions of sucrose [39]. A radiolabeled version, [ $^{14}\text{C}$ ]sucrose, accumulated in the whole brain tissue to about four-fold higher concentrations than the stable isotope labeled [ $^{13}\text{C}$ ]sucrose, while the brain ISF concentrations, measured in microdialysate from the striatum, were comparable. The discrepancy could be explained by the presence of a low amount of contaminants in the [ $^{14}\text{C}$ ]sucrose tracer solution [40], which are more lipophilic, more BBB permeable, and able to distribute into brain cells.

**Table 1.** Parameters of the 3 compartmental semi-physiologic model for fitting [ $^{13}\text{C}_{12}$ ] sucrose and [ $^{13}\text{C}_6$ ] mannitol plasma and brain uptake data simultaneously in adult male mice.

Parameters	Units	$^{13}\text{C}_{12}$ Sucrose			$^{13}\text{C}_6$ Mannitol		
		Value	SE	CV %	Value	SE	CV%
$V_1$	mL	4.97 <sup>a</sup>	0.326	6.56	6.06	0.34	5.6
$V_2$	mL	14.1 <sup>b</sup>	8.28	58.6	3.22	0.63	19.7
$V_e$ (fixed)	mL/g		0.2		0.2		
$\text{CL}_{10}$	mL/min	0.226 <sup>c</sup>	0.011	4.84	0.212	0.008	3.86
$\text{CL}_{12}$	mL/min	0.019 <sup>d</sup>	0.005	23.2	0.010	0.001	9.94
$\text{CL}_{13}/W_{\text{brain}}$	$\mu\text{L}/(\text{min} \times \text{g})$	0.068 <sup>e</sup>	0.005	7.73	0.146	0.020	9.64
$\text{CL}_{31}/W_{\text{brain}}$	$\mu\text{L}/(\text{min} \times \text{g})$	0.693 <sup>f</sup>	0.106	15.4	0.881	0.20	22.5
$W_{\text{brain}}$ (fixed)	g		0.4		0.4		

Parameter definition as in Figure 4. Reprinted with permission from Reference [19]. Copyright 2022, Springer Nature. <sup>a</sup>  $p < 0.05$  (Z-test value 2.31) compared to mannitol  $V_1$ ; <sup>b</sup> not significant (Z-test value 1.31) compared to mannitol  $V_2$ ; <sup>c</sup> not significant (Z-test value 1.03) compared to mannitol  $\text{CL}_{10}$ ; <sup>d</sup> not significant (Z-test value 1.77) compared to mannitol  $\text{CL}_{12}$ ; <sup>e</sup>  $p < 0.01$  (Z-test value 3.85) compared to mannitol  $\text{CL}_{13}/W_{\text{brain}}$ ; <sup>f</sup> not significant (Z-test value 0.8) compared to mannitol  $\text{CL}_{31}/W_{\text{brain}}$ .

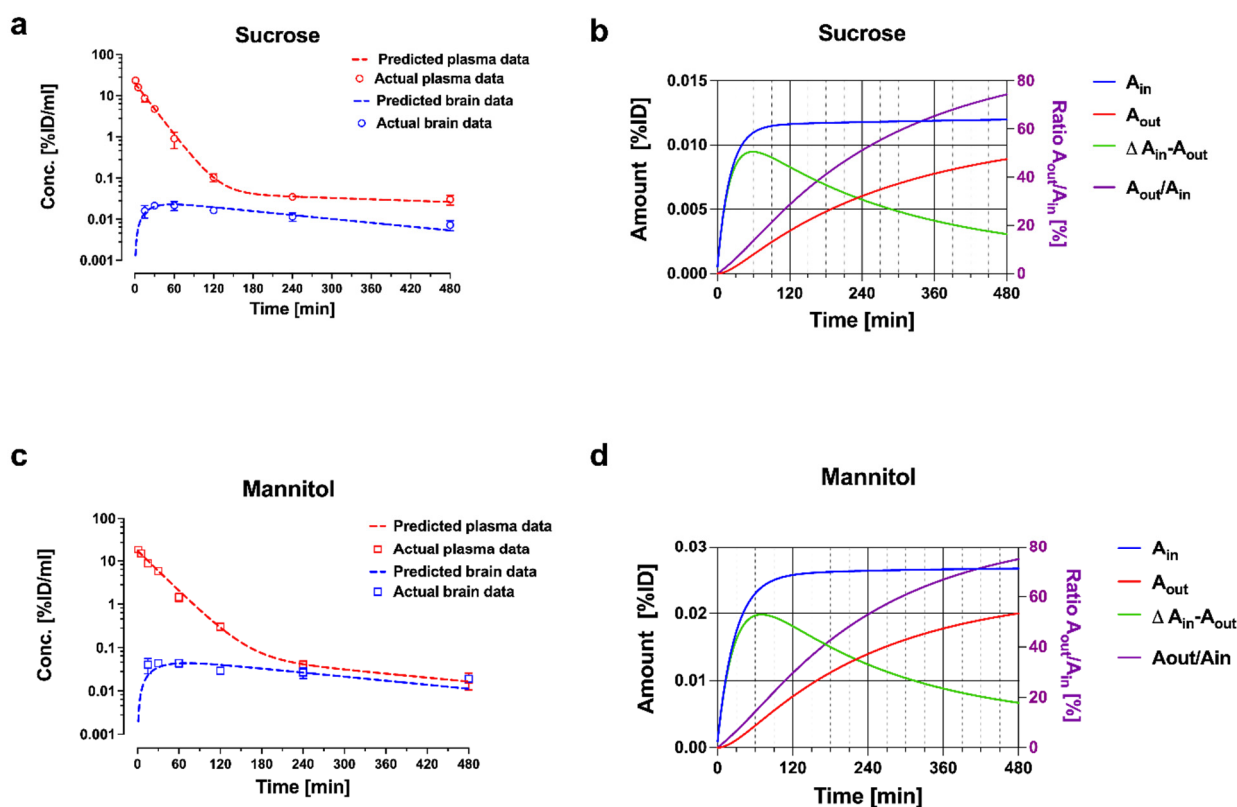


**Figure 5.** Plasma and brain pharmacokinetic data with model fitting for (a) sucrose and (c) mannitol. Plasma and brain concentrations are expressed in percent of injected dose (%ID/mL). Panels (b) and (d) depict cumulative amounts of sucrose and mannitol entering ( $A_{\text{in}}$ ) and leaving ( $A_{\text{out}}$ ) the brain compartment, and the ratio of  $A_{\text{out}}/A_{\text{in}}$  over time. Reprinted with permission from Reference [19]. Copyright 2022, Springer Nature.

#### Choice of Permeability Markers

While it is beyond the scope of this paper to broadly cover the range of markers used in the studies of the BBB, which have been discussed in several recent reviews [41,42], a comment is appropriate, considering the potential impact of technical issues on the results

and interpretation of brain uptake studies. Evidently, any markers allowing only qualitative or semiquantitative analysis in blood and tissue cannot be reasonably used in PK models. The examples include horseradish peroxidase, (unlabeled) IgG, fibrinogen and dextrans, Trypan blue, and Evans blue [42]. Radiolabeled markers (e.g., radiolabeled forms of sucrose, mannitol, or inulin) can yield quantitative data, but careful chromatographic analysis of the integrity of the labeled substance in blood and tissue is required, as first pointed out decades ago [43], and illustrated in the preceding paragraph. Stable isotope-labeled and metabolically stable solutes, such as [<sup>13</sup>C] sucrose or [<sup>13</sup>C] mannitol, which lack affinity to transporter proteins appear as superior choices, because LC-MS/MS analysis is highly specific and sensitive [40,44], and the handling of radioisotopes is avoided. Fluorescein remains among the most frequently used permeability markers in the literature [42]. Typically, the total plasma and tissue concentrations are measured in plate readers, although it has been demonstrated that a seemingly higher brain uptake can be caused by altered plasma protein binding, especially under pathophysiological conditions, without actual changes in the BBB permeability [45]. Therefore, free fluorescein concentrations should be analyzed after ultrafiltration by sensitive chromatographic techniques. An additional caveat with fluorescein is that reports have implicated it as a substrate of probenecid sensitive efflux transporters for organic anions at the BBB [46,47]. Another drug initially considered to represent a hydrophilic marker suitable for PK studies of passive BBB permeability is S-atenolol, which was subsequently shown to be subject to efflux at the BBB [48].

#### 4. Extent of Brain Drug Exposure

The majority of small molecule drugs will distribute to some degree into the cells or bind to the cell membranes, and this also applies to the brain tissue after passage of the BBB. The knowledge of the value of BBB uptake clearance alone is therefore insufficient. In addition, depending on the location of the drug target (e.g., membrane receptors vs. intracellular) the relevance of the total tissue concentrations is limited. Based on these considerations and on the free drug hypothesis, the group of Hammarlund-Udenaes developed a concept to describe the brain exposure, using a newly defined parameter, the unbound brain-to-plasma partition coefficient,  $K_{p,uu,brain}$  [49,50]:

$$K_{p,uu,brain} = \frac{AUC_{u,brainISF}}{AUC_{u,plasma}} \quad (11)$$

With  $AUC_{u,brainISF}$  denoting the AUC of the unbound concentrations in the brain interstitial fluid (ISF), and  $AUC_{u,plasma}$  denoting the AUC of the free drug in the plasma. This parameter has been widely adopted, in particular in industrial CNS-drug development programs, and has largely supplanted the previously prevalent brain tissue to plasma partition coefficients, which represented the ratio between the total brain concentration and the total plasma concentration ( $K_p$ ) or the free plasma concentration ( $K_{p,u}$ ).  $K_{p,uu,brain}$  is experimentally obtained from measurements of the brain extracellular fluid-drug concentrations by intracerebral microdialysis. The unbound plasma concentrations can also be determined by an indwelling microdialysis probe, or by ultrafiltration of the plasma samples *ex vivo*. As is evident from Equation (11), the determination of  $K_{p,uu,brain}$  is independent of any specific compartmental model and can be performed after IV, bolus administration, or infusion. In practice, it is often based on a constant rate infusion schedule with a sufficiently long infusion time to achieve steady state conditions. At a steady state, the ratio of AUCs in Equation (11) can be replaced by the ratio of the free drug concentrations in the brain ISF and plasma.  $K_{p,uu,brain}$  does not depend on partitioning processes inside the brain tissue between the ISF and cells. Further, because at steady state (*ss*) there is no net exchange between the drug in the brain ISF and plasma, the amounts,  $A$ , of drug influx into the brain and efflux from the brain are equal. With:

$$\frac{dA_{in}}{dt} = CL_{in} \times C_{u,ss,plasma} = \frac{dA_{out}}{dt} = CL_{out} \times C_{u,ss,brainISF} \quad (12)$$



$$K_{p,uu,brain} = \frac{C_{u,ss,brainISF}}{C_{u,ss,plasma}} = \frac{CL_{in}}{CL_{out}} \quad (13)$$

Therefore,  $K_{p,uu,brain}$  can also be expressed as the ratio of the clearances  $CL_{in}/CL_{out}$ , where  $CL_{in}$  comprises the sum of all of the passive and active influx clearances, and  $CL_{out}$  represents the sum of all of the elimination clearances from the brain, i.e., passive and active BBB transport, metabolism in the brain, and bulk flow clearance [50]. If passive processes dominate the transport across the BBB, a value near unity would be expected. Correspondingly, if active influx is prevalent,  $K_{p,uu,brain}$  is larger than unity, and if active efflux prevails,  $K_{p,uu,brain}$  is less than one. This ratio provides, therefore, a powerful and simple tool to identify the principal transport mechanism of a drug at the BBB. It also follows from Equation (13) that the absolute clearance values cannot be assessed from this type of analysis. An estimate for  $CL_{in}$  can be provided as complementary information from the measurement of the total brain concentrations, as discussed in the previous sections.

Another relevant parameter, the unbound drug volume of distribution,  $V_{u,brain}$ , can be calculated from the measurement of microdialysate concentration and total brain tissue concentration at steady state:

$$V_{u,brain} = \frac{A_{brain}}{C_{u,brainISF}} \quad (14)$$

where  $A_{brain}$  is the amount in the brain per unit weight, after correction for the intravascular content. This parameter may also be estimated from an in vitro assay, the brain slice technique [51].  $V_{u,brain}$  provides information on the drug distribution inside the brain tissue between ISF and cells [50]. Importantly,  $V_{u,brain}$ , according to Equation (14), is distinct from the apparent brain volume of distribution as used in the multiple time graphical analysis, which puts the plasma concentration in the denominator (see Equation (5)).

The synopsis of the plasma data, brain microdialysate sampling and whole tissue analysis provides unique pharmacokinetic insights, exemplified by a series of studies with morphine [52], its glucuronide metabolites [53–56], and the opioids, codeine and oxycodone [57,58]. The following conclusions can be derived from the comparison of these CNS-active drugs, as discussed before [50]: There is a vast range of BBB permeabilities, for example 167-fold in favor of oxycodone over morphine, and 1,150 fold over morphine-6-glucuronide. The  $K_p$  and  $K_{p,u}$  values also show differences of two log orders, because more lipophilic drugs tend to have a high affinity with brain tissue, which results in high values of  $V_{u,brain}$ . In contrast, the  $K_{p,uu,brain}$  values among these opioids differ only by a factor of about 10, between about 0.3 (morphine, morphine-6-glucuronide) and 3 (oxycodone). As explained above, these differences in  $K_{p,uu,brain}$  can be attributed to the properties of the drugs as either a substrate of efflux transport (by P-gp and MRPs in case of morphine, morphine-6-glucuronide), of active uptake (oxycodone), or being a non-substrate (codeine) [52,56–59]. The impact of the transporters on the PK of opioids and its clinical implications have been discussed in a recent review [60]. Based on the relations outlined above, it can be argued that a complete picture of the delivery of CNS-active drugs requires knowledge of: (i) BBB permeability clearance; (ii) intra-brain distribution; and (iii) extent of equilibrium across the BBB. The appreciation of this concept is important in the decision processes for drug development.

## 5. Physiologically Based Pharmacokinetic Models

As a concept, PBPK dates back to the beginnings of the PK field [61,62]. Physiologically based models aim to describe the organism in terms of the compartments based on actual organs and their associated blood flow rates, with differential equations for mass transfer, tissue binding, and metabolic activity. In the classical compartmental models and semi-physiological models presented in the previous sections, all or part of the compartments were hypothetical spaces, defined by the apparent volumes of distribution, which were calculated from the plasma concentrations. While the compartmental and semi-physiologic models require fewer parameters, values for all or the majority of parameters can be obtained by fitting the models to experimental data (blood or plasma concentrations, and

organ concentrations when available). A limitation of the compartmental models is that they cannot be readily scaled from one experimental species to another. In addition, the invasive nature of the animal experiments used in generating the input data for the models discussed above implies that a direct translation to the human condition is limited, which is one of the main drivers of the growing interest in PBPK models.

While there is no convincing evidence for major species' differences in passive BBB permeability, the active transporters show marked differences among species. The recent advances in tandem mass spectrometry have enabled quantitative proteomics studies of transporter protein expression in animal and human brain microvessels [63]. Striking examples of species differences between a model organism and humans include the expression levels of the breast cancer-resistance protein, which is 1.85-fold higher expressed at the human BBB than in mice, and of p-glycoprotein (MDR), which is less expressed at the human BBB by a factor of 2.33 compared to *mdr1a* in mice. These quantitative data are now being utilized in the new field of pharmacoproteomics, to predict the  $K_{p,uu,brain}$  in humans from the data in experimental animals [64]. This will be beneficial in addressing the issue in PBPK involving the numerous parameters that these cannot be all determined by fitting to the available, sparse experimental data. Many of the parameters need to be fixed to the values from independent *in vitro* or *in vivo* studies, which are typically taken from the literature. The better estimates of transporter activity based on proteomics plugged into PBPK models would then facilitate interspecies scaling beyond the usage of the known values of organ weights, blood flow, and metabolic capacity, among others. The simulations with PBPK models have, in recent years, gained popularity as tools in drug development in industry and with regulatory agencies. The potential pitfalls in the widespread use of complex PBPK models due to over-parameterization and parameter optimization are under debate [65].

In the BBB field, different academic groups proposed PBPK models aimed at predicting drug concentrations at the target sites, taking into account the different brain compartments, e.g., ISF and CSF, and eventually down to the level of intracellular vs. extracellular distribution and subcellular compartments, e.g., lysosomes [66–68]. Figure 6 depicts the scheme of such a model, which also includes different, connected CSF compartments, and asymmetry factors derived from the  $K_{p,uu}$  values to account for the net effect of the influx and efflux transporters between compartments. An extensive list of published parameter values taken from experimental animals, human data, and *in vitro* studies has been compiled in a recent review [69]. Running simulations with this model for 10 diverse small molecule drugs with the published data on plasma kinetics, brain, and CSF concentrations, resulted in a less than two-fold prediction error of the concentration–time course in plasma, brain ISF, and two CSF sites (lateral ventricle and cisterna magna) [66].

The PBPK modeling is also increasingly applied to biotherapeutics, in particular monoclonal antibodies. An early example is the study of the distribution into tumor xenografts and organs of mice of an antibody targeting colon cancer [70]. Besides the specific target affinity, the later PBPK models also considered the role of the neonatal Fc receptor (FcRn) in the organ distribution and kinetics in plasma [71,72]. While the brain as a target organ had been previously ignored, in recent years the PBPK models have been proposed for the analysis of data generated with antibodies, which are under development as drug delivery vehicles, including antibodies targeted to the transferrin receptor (TfR) and insulin receptor [73–75]. The PBPK studies with TfR antibodies, in particular, benefit from a considerable body of published experimental data with full length antibodies, antibody fragments, bispecific antibodies, as well as antibody variants covering a wide range of target affinities, from low nanomolar to micromolar  $K_D$  values, over a range of doses. Two recent papers presented for the prediction of the brain disposition of TfR antibodies put an emphasis on the partially different sets of model parameters [73,75]. For example, in the model put forward by Pardridge and Chow, the binding kinetics and trafficking inside the BBB endothelial cells of the endogenous receptor ligand, transferrin, play major roles [75]. On the other hand, the model by Chang et al. did not consider transferrin-binding kinetics

relevant with respect to the trafficking of TfR antibodies, but rather included the parameters for binding to FcRn and to TfR expressed on brain cells beyond the BBB [73]. Therefore, the output of simulations generated by these different models cannot be readily compared.

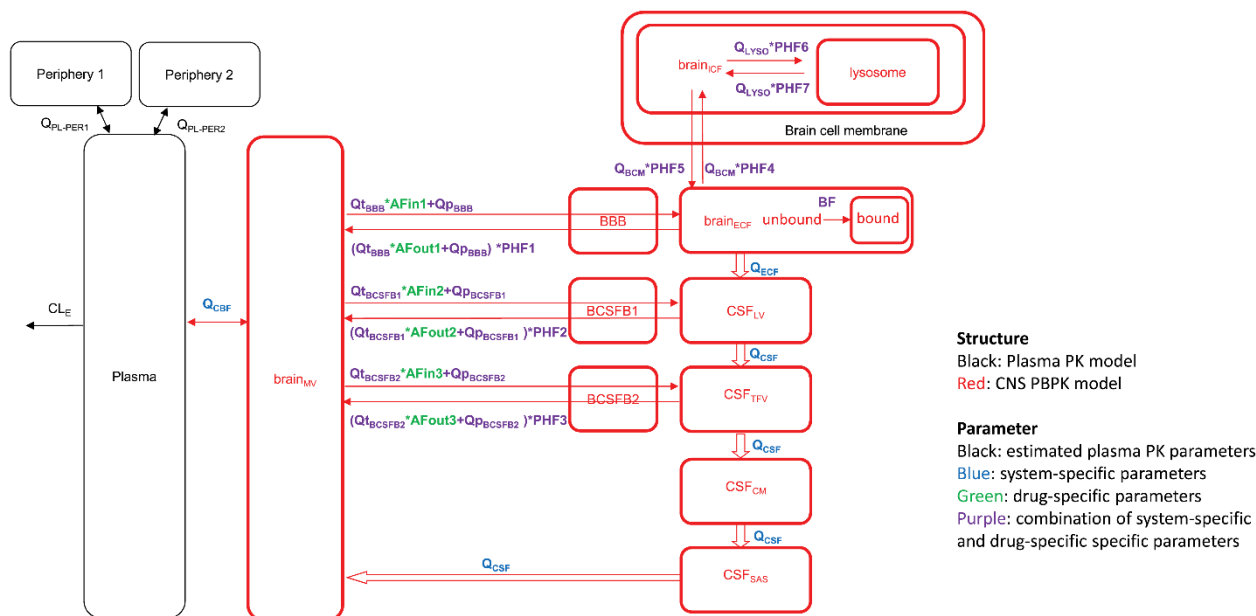


**Figure 6.** The model consists of a plasma pharmacokinetic (PK) model and a central nervous system (CNS) physiologically based pharmacokinetic (PBPK) model with estimated plasma PK parameters, and system-specific and drug-specific parameters (colors) for CNS. Peripheral compartments 1 and 2 are used when required to describe the plasma data adequately by a plasma PK model. AFin1–3, asymmetry factor into the CNS compartments 1–3; AFout1–3, asymmetry factor out from the CNS compartments 1–3; BBB, blood-brain barrier; BCSFB, blood-cerebrospinal fluid barrier; BF, binding factor; brain<sub>ECF</sub>, brain extracellular fluid; brain<sub>ICF</sub>, brain intracellular fluid; brain<sub>MV</sub>, brain microvascular; CSF<sub>CM</sub>, cerebrospinal fluid in the cisterna magna; CSF<sub>LV</sub>, cerebrospinal fluid in the lateral ventricle; CSF<sub>SAS</sub>, cerebrospinal fluid in the subarachnoid space; CSF<sub>TFV</sub>, cerebrospinal fluid in the third and fourth ventricle; PHF1–7, pH-dependent factor 1–7; Q<sub>BCM</sub>, passive diffusion clearance at the brain cell membrane; Q<sub>CBF</sub>, cerebral blood flow; Q<sub>CSF</sub>, cerebrospinal fluid flow; Q<sub>ECF</sub>, brain<sub>ECF</sub> flow; Q<sub>LYSO</sub>, passive diffusion clearance at the lysosomal membrane; Q<sub>PBB</sub>, paracellular diffusion clearance at the BBB; Q<sub>PBCSFB1</sub>, paracellular diffusion clearance at the BCSFB1; Q<sub>PBCSFB2</sub>, paracellular diffusion clearance at the BCSFB2; Q<sub>tBBB</sub>, transcellular diffusion clearance at the BBB; Q<sub>tBCSFB1</sub>, transcellular diffusion clearance at the BCSFB1; Q<sub>tBCSFB2</sub>, transcellular diffusion clearance at the BCSFB2. From ref. [66] with permission under Creative Commons Attribution-NonCommercial-NoDerivs License.

## 6. Conclusions and Perspectives

A selection of models is now at the disposal of investigators to evaluate pharmacokinetics and brain uptake in vivo in animal models and humans. The initial uptake rate measurements appear superficially straight forward, but they have associated caveats, which need to be considered. A full appreciation of the brain exposure of known compounds and of drug candidates requires knowledge of the uptake rate, the distribution in brain tissue, and the extent of equilibration across the BBB. The semi-physiological models, and complex PBPK models introduced in recent years, rely to a varying degree on the availability of the values for some of the parameters taken from independent in vitro or in vivo studies. The progress of quantitative pharmacoproteomics in experimental species and humans, which allows for interspecies adjustments and the scaling of the PK effect of transporter activities, as discussed in Section 5, is expected to enhance the predictive accuracy of the PBPK models. At this stage of maturation of the PK field, efforts should

also be undertaken by the BBB PK expert community to push towards an improved quality of the host of studies being conducted in the neuroscience field, in which the measurement of the BBB permeability of drugs or markers serves only an ancillary purpose. In particular with respect to studies in disease models, the claims of altered permeability are often based on inadequate kinetic approaches, as pointed out for the use of markers viewed as imperfect by today's standards (e.g., Evans Blue [42]), or neglecting the role of protein binding in plasma [45], or the common case of measurements at a single time point in brain tissue only, without considering the plasma kinetics as input.

**Funding:** This research received no external funding.

**Institutional Review Board Statement:** Not applicable.

**Informed Consent Statement:** Not applicable.

**Data Availability Statement:** Not applicable.

**Conflicts of Interest:** The author declares no conflict of interest.

## References

1. Saunders, N.R.; Dreifuss, J.J.; Dziegielewska, K.M.; Johansson, P.A.; Habgood, M.D.; Mollgard, K.; Bauer, H.C. The rights and wrongs of blood-brain barrier permeability studies: A walk through 100 years of history. *Front. Neurosci.* **2014**, *8*, 404. [CrossRef]
2. Iadecola, C. The Neurovascular Unit Coming of Age: A Journey through Neurovascular Coupling in Health and Disease. *Neuron* **2017**, *96*, 17–42. [CrossRef] [PubMed]
3. Abbott, N.J.; Patabendige, A.A.; Dolman, D.E.; Yusof, S.R.; Begley, D.J. Structure and function of the blood-brain barrier. *Neurobiol. Dis.* **2010**, *37*, 13–25. [CrossRef] [PubMed]
4. Oldendorf, W.H. Clearance of Radiolabeled Substances by Brain after Arterial Injection Using a Diffusible Internal Standard. In *Research Methods in Neurochemistry*; Springer: Boston, MA, USA, 1981; Volume 5, pp. 91–112.
5. Oldendorf, W.H. Measurement of brain uptake of radiolabeled substances using a tritiated water internal standard. *Brain Res.* **1970**, *24*, 372–376. [CrossRef]
6. Pardridge, W.M.; Fierer, G. Blood-brain barrier transport of butanol and water relative to N-isopropyl-p-iodoamphetamine as the internal reference. *J. Cereb. Blood Flow Metab.* **1985**, *5*, 275–281. [CrossRef]
7. Takasato, Y.; Rapoport, S.I.; Smith, Q.R. An in situ brain perfusion technique to study cerebrovascular transport in the rat. *Am. J. Physiol.* **1984**, *247*, H484–H493. [CrossRef]
8. Pardridge, W.M. Blood-brain barrier carrier-mediated transport and brain metabolism of amino acids. *Neurochem. Res.* **1998**, *23*, 635–644. [CrossRef] [PubMed]
9. Oldendorf, W.H.; Hyman, S.; Braun, L.; Oldendorf, S.Z. Blood-brain barrier: Penetration of morphine, codeine, heroin, and methadone after carotid injection. *Science* **1972**, *178*, 984–986. [CrossRef] [PubMed]
10. Zlokovic, B.V.; Lipovac, M.N.; Begley, D.J.; Davson, H.; Rakic, L. Transport of leucine-enkephalin across the blood-brain barrier in the perfused guinea pig brain. *J. Neurochem.* **1987**, *49*, 310–315. [CrossRef]
11. Dagenais, C.; Rousselle, C.; Pollack, G.M.; Scherrmann, J.M. Development of an in situ mouse brain perfusion model and its application to mdr1a P-glycoprotein-deficient mice. *J. Cereb. Blood Flow Metab.* **2000**, *20*, 381–386. [CrossRef]
12. Murakami, H.; Takanaga, H.; Matsuo, H.; Ohtani, H.; Sawada, Y. Comparison of blood-brain barrier permeability in mice and rats using in situ brain perfusion technique. *Am. J. Physiol. Heart Circ. Physiol.* **2000**, *279*, H1022–H1028. [CrossRef]
13. Chowdhury, E.A.; Alqahtani, F.; Bhattacharya, R.; Mehvar, R.; Bickel, U. Simultaneous UPLC–MS/MS analysis of two stable isotope labeled versions of sucrose in mouse plasma and brain samples as markers of blood-brain barrier permeability and brain vascular space. *J. Chromatogr. B* **2018**, *1073*, 19–26. [CrossRef]
14. Summerfield, S.G.; Yates, J.W.T.; Fairman, D.A. Free Drug Theory—No Longer Just a Hypothesis? *Pharm. Res.* **2022**, *39*, 213–222. [CrossRef]
15. Blasberg, R.G.; Fenstermacher, J.D.; Patlak, C.S. Transport of alpha-aminoisobutyric acid across brain capillary and cellular membranes. *J. Cereb. Blood Flow Metab.* **1983**, *3*, 8–32. [CrossRef]
16. Patlak, C.S.; Blasberg, R.G. Graphical evaluation of blood-to-brain transfer constants from multiple-time uptake data. Generalizations. *J. Cereb. Blood Flow Metab.* **1985**, *5*, 584–590. [CrossRef]
17. Patlak, C.S.; Blasberg, R.G.; Fenstermacher, J.D. Graphical evaluation of blood-to-brain transfer constants from multiple-time uptake data. *J. Cereb. Blood Flow Metab.* **1983**, *3*, 1–7. [CrossRef]
18. Smith, Q.R. A review of blood-brain barrier transport techniques. *Methods Mol. Med.* **2003**, *89*, 193–208.
19. Noorani, B.; Chowdhury, E.A.; Alqahtani, F.; Sajib, M.S.; Ahn, Y.; Nozohouri, E.; Patel, D.; Mikelis, C.; Mehvar, R.; Bickel, U. A Semi-Physiological Three-Compartment Model Describes Brain Uptake Clearance and Efflux of Sucrose and Mannitol after IV Injection in Awake Mice. *Pharm. Res.* **2022**, *39*, 251–261. [CrossRef]

20. Ewing, J.R.; Brown, S.L.; Lu, M.; Panda, S.; Ding, G.; Knight, R.A.; Cao, Y.; Jiang, Q.; Nagaraja, T.N.; Churchman, J.L.; et al. Model selection in magnetic resonance imaging measurements of vascular permeability: Gadomer in a 9L model of rat cerebral tumor. *J. Cereb. Blood Flow Metab.* **2006**, *26*, 310–320. [CrossRef]
21. Karakatsanis, N.A.; Zhou, Y.; Lodge, M.A.; Casey, M.E.; Wahl, R.L.; Zaidi, H.; Rahmim, A. Generalized whole-body Patlak parametric imaging for enhanced quantification in clinical PET. *Phys. Med. Biol.* **2015**, *60*, 8643–8673. [CrossRef]
22. Tofts, P.S.; Brix, G.; Buckley, D.L.; Evelhoch, J.L.; Henderson, E.; Knopp, M.V.; Larsson, H.B.; Lee, T.Y.; Mayr, N.A.; Parker, G.J.; et al. Estimating kinetic parameters from dynamic contrast-enhanced T(1)-weighted MRI of a diffusible tracer: Standardized quantities and symbols. *J. Magn. Reson. Imaging* **1999**, *10*, 223–232. [CrossRef]
23. Logan, J.; Fowler, J.S.; Volkow, N.D.; Wolf, A.P.; Dewey, S.L.; Schlyer, D.J.; MacGregor, R.R.; Hitzemann, R.; Bendriem, B.; Gatley, S.J.; et al. Graphical analysis of reversible radioligand binding from time-activity measurements applied to [N-11C-methyl]-(-)-cocaine PET studies in human subjects. *J. Cereb. Blood Flow Metab.* **1990**, *10*, 740–747. [CrossRef]
24. Logan, J.; Alexoff, D.; Fowler, J.S. The use of alternative forms of graphical analysis to balance bias and precision in PET images. *J. Cereb. Blood Flow Metab.* **2011**, *31*, 535–546. [CrossRef]
25. Absinta, M.; Sati, P.; Reich, D.S. Advanced MRI and staging of multiple sclerosis lesions. *Nat. Rev. Neurol.* **2016**, *12*, 358–368. [CrossRef]
26. Guo, Y.; Lebel, R.M.; Zhu, Y.; Lingala, S.G.; Shiroishi, M.S.; Law, M.; Nayak, K. High-resolution whole-brain DCE-MRI using constrained reconstruction: Prospective clinical evaluation in brain tumor patients. *Med. Phys.* **2016**, *43*, 2013. [CrossRef]
27. Candelario-Jalil, E.; Dijkhuizen, R.M.; Magnus, T. Neuroinflammation, Stroke, Blood-Brain Barrier Dysfunction, and Imaging Modalities. *Stroke* **2022**, *53*, 1473–1486. [CrossRef]
28. Canjels, L.P.W.; Jansen, J.F.A.; van den Kerkhof, M.; Alers, R.J.; Poser, B.A.; Wiggins, C.J.; Schiffer, V.; van de Ven, V.; Rouhl, R.P.W.; Palm, W.M.; et al. 7T dynamic contrast-enhanced MRI for the detection of subtle blood-brain barrier leakage. *J. Neuroimaging* **2021**, *31*, 902–911. [CrossRef]
29. Ohno, K.; Pettigrew, K.D.; Rapoport, S.I. Lower limits of cerebrovascular permeability to nonelectrolytes in the conscious rat. *Am. J. Physiol.* **1978**, *235*, H299–H307. [CrossRef]
30. Nicholson, C.; Hrabetova, S. Brain Extracellular Space: The Final Frontier of Neuroscience. *Biophys. J.* **2017**, *113*, 2133–2142. [CrossRef]
31. Cserr, H.F.; Cooper, D.N.; Suri, P.K.; Patlak, C.S. Efflux of radiolabeled polyethylene glycols and albumin from rat brain. *Am. J. Physiol.* **1981**, *240*, F319–F328. [CrossRef]
32. Groothuis, D.R.; Vavra, M.W.; Schlageter, K.E.; Kang, E.W.; Itskovich, A.C.; Hertzler, S.; Allen, C.V.; Lipton, H.L. Efflux of drugs and solutes from brain: The interactive roles of diffusional transcapillary transport, bulk flow and capillary transporters. *J. Cereb. Blood Flow Metab.* **2007**, *27*, 43–56. [CrossRef] [PubMed]
33. Hladky, S.B.; Barrand, M.A. Elimination of substances from the brain parenchyma: Efflux via perivascular pathways and via the blood-brain barrier. *Fluids Barriers CNS* **2018**, *15*, 30. [CrossRef] [PubMed]
34. Fenstermacher, J.D.; Patlak, C.S.; Blasberg, R.G. Transport of material between brain extracellular fluid, brain cells and blood. *Fed. Proc.* **1974**, *33*, 2070–2074.
35. Collins, J.M.; Dedrick, R.L. Distributed model for drug delivery to CSF and brain tissue. *Am. J. Physiol.* **1983**, *245*, R303–R310. [CrossRef] [PubMed]
36. De Lange, E.C.; Danhof, M.; de Boer, A.G.; Breimer, D.D. Critical factors of intracerebral microdialysis as a technique to determine the pharmacokinetics of drugs in rat brain. *Brain Res.* **1994**, *666*, 1–8. [CrossRef]
37. Elmquist, W.F.; Sawchuk, R.J. Application of microdialysis in pharmacokinetic studies. *Pharm. Res.* **1997**, *14*, 267–288. [CrossRef] [PubMed]
38. Hammarlund-Udenaes, M.; Paalzow, L.K.; de Lange, E.C. Drug equilibration across the blood-brain barrier—pharmacokinetic considerations based on the microdialysis method. *Pharm. Res.* **1997**, *14*, 128–134. [CrossRef]
39. Alqahtani, F.; Chowdhury, E.A.; Bhattacharya, R.; Noorani, B.; Mehvar, R.; Bickel, U. Brain Uptake of [<sup>13</sup>C] and [<sup>14</sup>C]Sucrose Quantified by Microdialysis and Whole Tissue Analysis in Mice. *Drug Metab. Dispos.* **2018**, *46*, 1514–1518. [CrossRef] [PubMed]
40. Miah, M.K.; Chowdhury, E.A.; Bickel, U.; Mehvar, R. Evaluation of [<sup>14</sup>C] and [<sup>13</sup>C]Sucrose as Blood-Brain Barrier Permeability Markers. *J. Pharm. Sci.* **2017**, *106*, 1659–1669. [CrossRef] [PubMed]
41. Chowdhury, E.A.; Noorani, B.; Alqahtani, F.; Bhalerao, A.; Raut, S.; Sivandzade, F.; Cucullo, L. Understanding the brain uptake and permeability of small molecules through the BBB: A technical overview. *J. Cereb. Blood Flow Metab.* **2021**, *41*, 1797–1820. [CrossRef]
42. Saunders, N.R.; Dziegielewska, K.M.; Mollgard, K.; Habgood, M.D. Markers for blood-brain barrier integrity: How appropriate is Evans blue in the twenty-first century and what are the alternatives? *Front. Neurosci.* **2015**, *9*, 385. [CrossRef] [PubMed]
43. Preston, E.; Haas, N. Defining the lower limits of blood-brain barrier permeability: Factors affecting the magnitude and interpretation of permeability-area products. *J. Neurosci. Res.* **1986**, *16*, 709–719. [CrossRef]
44. Noorani, B.; Chowdhury, E.A.; Alqahtani, F.; Ahn, Y.; Patel, D.; Al-Ahmad, A.; Mehvar, R.; Bickel, U. LC-MS/MS-based in vitro and in vivo investigation of blood-brain barrier integrity by simultaneous quantitation of mannitol and sucrose. *Fluids Barriers CNS* **2020**, *17*, 61. [CrossRef]
45. Shaik, I.H.; Miah, M.K.; Bickel, U.; Mehvar, R. Effects of short-term portacaval anastomosis on the peripheral and brain disposition of the blood-brain barrier permeability marker sodium fluorescein in rats. *Brain Res.* **2013**, *1531*, 84–93. [CrossRef] [PubMed]

46. Hawkins, B.T.; Ocheltree, S.M.; Norwood, K.M.; Egleton, R.D. Decreased blood-brain barrier permeability to fluorescein in streptozotocin-treated rats. *Neurosci. Lett.* **2007**, *411*, 1–5. [CrossRef] [PubMed]
47. Sun, H.; Johnson, D.R.; Finch, R.A.; Sartorelli, A.C.; Miller, D.W.; Elmquist, W.F. Transport of fluorescein in MDCKII-MRP1 transfected cells and mrp1-knockout mice. *Biochem. Biophys. Res. Commun.* **2001**, *284*, 863–869. [CrossRef] [PubMed]
48. Chen, X.; Slattengren, T.; de Lange, E.C.M.; Smith, D.E.; Hammarlund-Udenaes, M. Revisiting atenolol as a low passive permeability marker. *Fluids Barriers CNS* **2017**, *14*, 30. [CrossRef]
49. Gupta, A.; Chatelain, P.; Massingham, R.; Jonsson, E.N.; Hammarlund-Udenaes, M. Brain distribution of cetirizine enantiomers: Comparison of three different tissue-to-plasma partition coefficients:  $K(p)$ ,  $K(p,u)$ , and  $K(p,uu)$ . *Drug Metab. Dispos.* **2006**, *34*, 318–323. [CrossRef]
50. Hammarlund-Udenaes, M.; Friden, M.; Syvanen, S.; Gupta, A. On the rate and extent of drug delivery to the brain. *Pharm. Res.* **2008**, *25*, 1737–1750. [CrossRef]
51. Becker, S.; Liu, X. Evaluation of the utility of brain slice methods to study brain penetration. *Drug Metab. Dispos.* **2006**, *34*, 855–861. [CrossRef] [PubMed]
52. Tunblad, K.; Jonsson, E.N.; Hammarlund-Udenaes, M. Morphine blood-brain barrier transport is influenced by probenecid co-administration. *Pharm. Res.* **2003**, *20*, 618–623. [CrossRef] [PubMed]
53. Bickel, U.; Schumacher, O.P.; Kang, Y.S.; Voigt, K. Poor permeability of morphine 3-glucuronide and morphine 6-glucuronide through the blood-brain barrier in the rat. *J. Pharmacol. Exp. Ther.* **1996**, *278*, 107–113. [PubMed]
54. Stain-Textier, F.; Boschi, G.; Sandouk, P.; Scherrmann, J.M. Elevated concentrations of morphine 6-beta-D-glucuronide in brain extracellular fluid despite low blood-brain barrier permeability. *Br. J. Pharmacol.* **1999**, *128*, 917–924. [CrossRef] [PubMed]
55. Wu, D.; Kang, Y.S.; Bickel, U.; Pardridge, W.M. Blood-brain barrier permeability to morphine-6-glucuronide is markedly reduced compared with morphine. *Drug Metab. Dispos.* **1997**, *25*, 768–771. [PubMed]
56. Xie, R.; Bouw, M.R.; Hammarlund-Udenaes, M. Modelling of the blood-brain barrier transport of morphine-3-glucuronide studied using microdialysis in the rat: Involvement of probenecid-sensitive transport. *Br. J. Pharmacol.* **2000**, *131*, 1784–1792. [CrossRef]
57. Bostrom, E.; Simonsson, U.; Hammarlund-Udenaes, M. In vivo blood-brain barrier transport of oxycodone in the rat—Indications for active influx and implications for PK/PD. *Drug Metab. Dispos.* **2006**, *34*, 1624–1631. [CrossRef] [PubMed]
58. Xie, R.; Hammarlund-Udenaes, M. Blood-brain barrier equilibration of codeine in rats studied with microdialysis. *Pharm. Res.* **1998**, *15*, 570–575. [CrossRef]
59. Tunblad, K.; Hammarlund-Udenaes, M.; Jonsson, E.N. Influence of probenecid on the delivery of morphine-6-glucuronide to the brain. *Eur. J. Pharm. Sci.* **2005**, *24*, 49–57. [CrossRef]
60. Yang, J.; Reilly, B.G.; Davis, T.P.; Ronaldson, P.T. Modulation of Opioid Transport at the Blood-Brain Barrier by Altered ATP-Binding Cassette (ABC) Transporter Expression and Activity. *Pharmaceutics* **2018**, *10*, 192. [CrossRef]
61. Bischoff, K.B.; Dedrick, R.L. Thiopental pharmacokinetics. *J. Pharm. Sci.* **1968**, *57*, 1346–1351. [CrossRef]
62. Teorell, T. Kinetics of distribution of substances administered to the body. I. The extravascular modes of administration. *Arch. Int. Pharmacodyn. Ther.* **1937**, *57*, 205–225.
63. Uchida, Y.; Ohtsuki, S.; Katsukura, Y.; Ikeda, C.; Suzuki, T.; Kamiie, J.; Terasaki, T. Quantitative Targeted Absolute Proteomics of Human Blood-Brain Barrier Transporters and Receptors. *J. Neurochem.* **2011**, *117*, 333–345. [CrossRef]
64. Huttunen, K.M.; Terasaki, T.; Urtti, A.; Montaser, A.B.; Uchida, Y. Pharmacoproteomics of Brain Barrier Transporters and Substrate Design for the Brain Targeted Drug Delivery. *Pharm. Res.* **2022**, *39*, 1363–1392. [CrossRef]
65. Sugano, K. Lost in modelling and simulation? *ADMET DMPK* **2021**, *9*, 75–109. [CrossRef]
66. Yamamoto, Y.; Valitalo, P.A.; Huntjens, D.R.; Proost, J.H.; Vermeulen, A.; Krauwinkel, W.; Beukers, M.W.; van den Berg, D.J.; Hartman, R.; Wong, Y.C.; et al. Predicting Drug Concentration-Time Profiles in Multiple CNS Compartments Using a Comprehensive Physiologically-Based Pharmacokinetic Model. *CPT Pharmacomet. Syst. Pharmacol.* **2017**, *6*, 765–777. [CrossRef]
67. De Lange, E.C. The mastermind approach to CNS drug therapy: Translational prediction of human brain distribution, target site kinetics, and therapeutic effects. *Fluids Barriers CNS* **2013**, *10*, 12. [CrossRef]
68. Ball, K.; Bouzom, F.; Scherrmann, J.M.; Walther, B.; Declèves, X. Development of a physiologically based pharmacokinetic model for the rat central nervous system and determination of an in vitro-in vivo scaling methodology for the blood-brain barrier permeability of two transporter substrates, morphine and oxycodone. *J. Pharm. Sci.* **2012**, *101*, 4277–4292. [CrossRef]
69. Vendel, E.; Rottschäfer, V.; de Lange, E.C.M. The need for mathematical modelling of spatial drug distribution within the brain. *Fluids Barriers CNS* **2019**, *16*, 12. [CrossRef]
70. Baxter, L.T.; Zhu, H.; Mackensen, D.G.; Jain, R.K. Physiologically based pharmacokinetic model for specific and nonspecific monoclonal antibodies and fragments in normal tissues and human tumor xenografts in nude mice. *Cancer Res.* **1994**, *54*, 1517–1528.
71. Ferl, G.Z.; Wu, A.M.; DiStefano, J.J., III. A predictive model of therapeutic monoclonal antibody dynamics and regulation by the neonatal Fc receptor (FcRn). *Ann. Biomed. Eng.* **2005**, *33*, 1640–1652. [CrossRef]
72. Garg, A.; Balthasar, J.P. Physiologically-based pharmacokinetic (PBPK) model to predict IgG tissue kinetics in wild-type and FcRn-knockout mice. *J. Pharmacokinet. Pharmacodyn.* **2007**, *34*, 687–709. [CrossRef] [PubMed]

73. Chang, H.Y.; Wu, S.; Chowdhury, E.A.; Shah, D.K. Towards a translational physiologically-based pharmacokinetic (PBPK) model for receptor-mediated transcytosis of anti-transferrin receptor monoclonal antibodies in the central nervous system. *J. Pharmacokinet. Pharmacodyn.* **2022**, *49*, 337–362. [CrossRef] [PubMed]
74. Gadkar, K.; Yadav, D.B.; Zuchero, J.Y.; Couch, J.A.; Kanodia, J.; Kenrick, M.K.; Atwal, J.K.; Dennis, M.S.; Prabhu, S.; Watts, R.J.; et al. Mathematical PKPD and safety model of bispecific TfR/BACE1 antibodies for the optimization of antibody uptake in brain. *Eur. J. Pharm. Biopharm.* **2016**, *101*, 53–61. [CrossRef] [PubMed]
75. Pardridge, W.M.; Chou, T. Mathematical Models of Blood-Brain Barrier Transport of Monoclonal Antibodies Targeting the Transferrin Receptor and the Insulin Receptor. *Pharmaceutics* **2021**, *14*, 535. [CrossRef]

MDPI  
St. Alban-Anlage 66  
4052 Basel  
Switzerland  
Tel. +41 61 683 77 34  
Fax +41 61 302 89 18  
[www.mdpi.com](http://www.mdpi.com)

*Pharmaceutics* Editorial Office  
E-mail: [pharmaceutics@mdpi.com](mailto:pharmaceutics@mdpi.com)  
[www.mdpi.com/journal/pharmaceutics](http://www.mdpi.com/journal/pharmaceutics)







MDPI  
St. Alban-Anlage 66  
4052 Basel  
Switzerland

Tel: +41 61 683 77 34  
Fax: +41 61 302 89 18

[www.mdpi.com](http://www.mdpi.com)



ISBN 978-3-0365-6416-6